RADIOCHEMOTHERAPY IN MULTIMODAL CANCER THERAPY

EDITED BY: Benjamin Frey, Anne Vehlow and Iris Eke
PUBLISHED IN: Frontiers in Oncology and Frontiers in Immunology

frontiers Research Topics

About Frontiers

Frontiers is more than just an open-access publisher of scholarly articles: it is a pioneering approach to the world of academia, radically improving the way scholarly research is managed. The grand vision of Frontiers is a world where all people have an equal opportunity to seek, share and generate knowledge. Frontiers provides immediate and permanent online open access to all its publications, but this alone is not enough to realize our grand goals.

Frontiers Journal Series

The Frontiers Journal Series is a multi-tier and interdisciplinary set of open-access, online journals, promising a paradigm shift from the current review, selection and dissemination processes in academic publishing. All Frontiers journals are driven by researchers for researchers; therefore, they constitute a service to the scholarly community. At the same time, the Frontiers Journal Series operates on a revolutionary invention, the tiered publishing system, initially addressing specific communities of scholars, and gradually climbing up to broader public understanding, thus serving the interests of the lay society, too.

Dedication to Quality

Each Frontiers article is a landmark of thfee highest quality, thanks to genuinely collaborative interactions between authors and review editors, who include some of the world's best academicians. Research must be certified by peers before entering a stream of knowledge that may eventually reach the public - and shape society; therefore, Frontiers only applies the most rigorous and unbiased reviews.
Frontiers revolutionizes research publishing by freely delivering the most outstanding research, evaluated with no bias from both the academic and social point of view. By applying the most advanced information technologies, Frontiers is catapulting scholarly publishing into a new generation.

What are Frontiers Research Topics?

Frontiers Research Topics are very popular trademarks of the Frontiers Journals Series: they are collections of at least ten articles, all centered on a particular subject. With their unique mix of varied contributions from Original Research to Review Articles, Frontiers Research Topics unify the most influential researchers, the latest key findings and historical advances in a hot research area! Find out more on how to host your own Frontiers Research Topic or contribute to one as an author by contacting the Frontiers Editorial Office: frontiersin.org/about/contact

RADIOCHEMOTHERAPY IN MULTIMODAL CANCER THERAPY

Topic Editors:
Benjamin Frey, University Hospital Erlangen, Germany
Anne Vehlow, Technical University Dresden, Germany
Iris Eke, Stanford University, United States

Table of Contents

Check for updates

Peptide Vaccine Combined Adjuvants Modulate Anti-tumor Effects of Radiation in Glioblastoma Mouse Model

Thi-Anh-Thuy Tran[1], Young-Hee Kim[1], Thi-Hoang-Oanh Duong[1], Shin Jung[1,2],
In-Young Kim[1,2], Kyung-Sub Moon[1,2], Woo-Youl Jang[1,2], Hyun-Ju Lee[3], Je-Jung Lee[3,4] and
Tae-Young Jung[1,2]*

[1] Brain Tumor Research Laboratory, Chonnam National University Medical School and Hwasun Hospital, Chonnam National University, Hwasun, South Korea, [2] Department of Neurosurgery, Chonnam National University Medical School and Hwasun Hospital, Chonnam National University, Hwasun, South Korea, [3] Research Center for Cancer Immunotherapy, Chonnam National University Medical School and Hwasun Hospital, Chonnam National University, Hwasun, South Korea, [4] Department of Internal Medicine, Chonnam National University Medical School and Hwasun Hospital, Chonnam National University, Hwasun, South Korea

Glioblastoma, the most common aggressive cancer, has a poor prognosis. Among the current standard treatment strategies, radiation therapy is the most commonly recommended. However, it is often unsuccessful at completely eliminating the cancer from the brain. A combination of radiation with other treatment methods should therefore be considered. It has been reported that radiotherapy in combination with immunotherapy might show a synergistic effect; however, this still needs to be investigated. In the current study, a "branched multipeptide and peptide adjuvants [such as pan DR epitope (PADRE) and polyinosinic-polycytidylic acid—stabilized with polylysine and carboxymethylcellulose—(poly-ICLC)]," namely vaccine and anti-PD1, were used as components of immunotherapy to assist in the anti-tumor effects of radiotherapy against glioblastomas. With regard to experimental design, immunological characterization of GL261 cells was performed and the effects of radiation on this cell line were also evaluated. An intracranial GL261 mouse glioma model was established, and therapeutic effects were observed based on tumor size and survival time. The distribution of effector immune cells in the spleen, based on cytotoxic T lymphocyte (CTL) and natural killer (NK) cell function, was determined. The pro-inflammatory and anti-inflammatory cytokine production from re-stimulated splenocytes and single tumor cells were also evaluated. As GL261 cells demonstrated both immunological characteristics and radiation sensitivity, they were found to be promising candidates for testing this combination treatment. Combinatorial treatment with radiation, vaccine, and anti-PD1 prolonged mouse survival by delaying tumor growth. Although this combination treatment led to an increase in the functional activity of both CTLs and NK cells, as evidenced by the increased percentage of these cells in the spleen, there was a greater shift toward CTL rather than NK cell activity. Moreover, the released cytokines from re-stimulated splenocytes

and single tumor cells also showed a shift toward the pro-inflammatory response. This study suggests that immunotherapy comprising a branched multipeptide plus PADRE, poly-ICLC, and anti-PD1 could potentially enhance the anti-tumor effects of radiotherapy in a glioblastoma mouse model.

INTRODUCTION

Glioblastoma (GBM) is the most malignant tumor of the central nervous system and is associated with poor prognosis and low survival. The survival rates of GBM patients have not demonstrated notable improvements over the last few decades (1). Therefore, a combination of several treatment methods is essential to overcome this type of cancer. Radiation therapy (RT) is commonly used to treat GBM; $\sim$60% of patients with solid tumors are administered radiation as part of their treatment (2). RT involves the breakdown of double-stranded DNA, thereby affecting cancer cell survival and proliferation. It also enhances immunological aspects, such as tumor antigen presentation and immunomodulation, by exposing tumor antigens and making them visible to the immune surveillance machinery (3, 4). Preclinical evidence suggests that RT can prime the immune system to enhance the efficiency of immunotherapy and that a combination of RT with immunotherapy is more effective than monotherapy (5).

Developments in the field of immunotherapy have recently provided new options for the treatment of GBM. Although the brain is an immunologically distinct organ, the immune microenvironment offers sufficient opportunities to promote immune cell responses and modify the "cold" tumor status of GBM (6). Although vaccination appears to be a promising treatment strategy for improving the clinical outcomes of GBM patients, no successful result has been reported in phase III clinical trials of vaccines against GBM to date; moreover, vaccine therapy faces many challenges. Combinations of different therapy methods, such as various vaccination strategies, vaccinations with immune checkpoint inhibitors, or surgical resection with chemotherapy, radiotherapy, and immunotherapy, are potential future directions for GBM treatment (7, 8).

To enhance the function of vaccines, immune adjuvants have also been developed. Immune adjuvants are defined as compounds that act to accelerate, prolong, and enhance the antigen-specific immune response, thereby allowing the use of smaller antigen doses and fewer immunizations (9). Among the available peptide vaccine adjuvants, pan DR epitope (PADRE) is a synthetic epitope-based vaccine adjuvant that is used as a T-helper peptide that induces Th1 cell polarization. PADRE is derived from HLA-DR epitopes and a tetanus toxin fragment. The PADRE peptide can bind to many different types of MHC-II alleles to boost immune responses, leading to the enhanced anti-tumor efficacy of vaccines (10, 11). Previous clinical trials reported that a polyinosinic-polycytidylic acid—stabilized with polylysine and carboxymethylcellulose—(poly-ICLC)-combined tumor antigen-specific vaccine is effective at achieving a higher therapeutic index (12). Poly-ICLC stimulates the Th1-polarizing dendritic cells and microglia-expressed toll-like receptor 3 (TLR3), resulting in the anti-tumor immune response. In addition, poly-ICLC serves as a simple and low-cost pathogen-associated molecular pattern (PAMP) that can trigger the immune response against solid cancers. Phase II clinical trials have been initiated for poly-ICLC (13).

Although anti-PD1 has been approved for the treatment of multiple cancer types, the effects of anti-PD1 monotherapy are still uncommon and unpredictable in GBM treatment. Only a small subset of patients have shown beneficial effects in response to anti-PD1 monotherapy; therefore, this requires further evaluation (14). However, the efficacy of immune checkpoint blockade has been demonstrated in combination with RT and a peptide-based vaccine. In particular, the combination of anti-PD1 and localized RT was shown to result in long-term survival in orthotopic GBM mouse models (15). Moreover, combinatorial treatment with peptide-based vaccines and immune checkpoint inhibitors was demonstrated to prolong the survival of tumor-bearing mice via enhanced vaccine-induced immune responses and tumor-infiltrating CD8$^+$ T cell counts, leading to delayed tumor growth (16).

Therefore, in this study, we aimed to determine the role of immunotherapy in modulating the anti-tumor effects of RT against GBM. For immunotherapy, branched multipeptide constructs based on the epidermal growth factor receptor 2 (ErbB2) and Wilms tumor gene 1 (WT1) peptides were used to stimulate antigen-specific cytotoxic T lymphocytes (CTLs). A combination of this branched multipeptide with peptide adjuvants, such as PADRE and poly-ICLC, was considered a component of the vaccine. We found that this vaccine, in combination with or without anti-PD1, modulated the anti-tumor effects of RT in a mouse GBM model.

MATERIALS AND METHODS

Animals and Cell Lines

Six- to eight- week-old female C57BL/6 mice (H2b, IAb) were purchased from Orient Bio (Iksan, Republic of Korea). Mice were raised under specific-pathogen-free conditions. All animal care, experiments, and euthanasia were performed after obtaining approval from the Chonnam National University Animal Research Committee.

Mouse glioblastoma cell lines (GL261: H2b and IAb, Gibco-BRL, Gaithersburg, MD, USA), and mouse lymphoma cell lines (YAC-1, ATCC, Rockville, MD, USA), sensitive to the cytotoxic activity of natural killer (NK) cells in mice, were used for cell culture. GL261 cells were maintained in Dulbecco's

Modified Eagle's Medium (DMEM) and YAC-1 cells were grown in Roswell Park Memorial Institute (RPMI) 1640 medium supplemented with 10% fetal bovine serum (FBS) and 1% penicillin-streptomycin (P/S) at 37°C in an atmosphere of 5% CO_2.

Peptide Synthesis and Antibodies

All peptides were commercially synthesized by the Peptron Company (Daejeon, Republic of Korea) with a purity >95% as assessed by reverse phase high-performance liquid chromatography. The branched multipeptide was synthesized by incorporating two single peptides, mouse modified 9-mer WT1 peptide (H2b-restricted $WT1_{235-243}$: CYTWNQMNL) and the mouse 9-mer epidermal growth factor receptor 2 peptide (H2b-restricted $ErbB2_{63-71}$: TYLPANASL) (predicted binding scores from SYFPEITHI: http://www.syfpeithi.de). Mini-polyethylene glycol (mini-PEG) spacers were used to synthesize the corresponding branched multipeptide, which was designated as CYTWNQMNL-miniPEG2-K (TYLPANASL-miniPEG2) shown in **Figure S1**. A pan HLA-DR binding epitope (IAb-restricted PADRE, ak-Cha-VAAWTLKAAa-Z-C) was also synthesized (17). All peptides were dissolved in dimethyl sulfoxide (DMSO) and diluted with phosphate buffered saline (PBS). Mouse anti-PD1 (clone J43) was used for flow cytometry and mouse anti-PD1 (clone RMP1-14) was used for *in vivo* blockade. All antibodies were purchased from BioXcell (West Lebanon, NH, USA).

Western Blotting

The expression of ErbB2, WT1, and programmed death ligand 1 (PDL1) in the GL261 cells before and after radiation was confirmed by western blotting. In general, the cells were exposed to 2, 4, or 6 Gy of radiation and cultured. The cells were harvested after the indicated time periods (0 and 24 h) for western blot analysis. The bicinchoninic acid (BCA) Protein Assay Kit (Thermo Scientific, USA) was used to measure protein concentration. Thereafter, SDS-PAGE was used to separate the proteins of interest, which were then transferred to a polyvinylidene difluoride (PVDF) membrane and soaked in a blocking solution [5% non-fat dry milk in TBST (tris-buffered saline, Tween 20)] for 1 h. The membrane was probed overnight with primary antibodies against WT1 (Abcam, Cambridge, UK), ErbB2 (Cell Signaling, Danvers, MA, USA), PDL1 (Santa Cruz Biotechnology, Santa Cruz, CA, USA), and β-Actin (Santa Cruz Biotechnology) at 4°C, and then incubated with horseradish peroxidase-conjugated goat anti-rabbit or anti-mouse polyclonal IgG secondary antibodies (Ab Frontier, Seoul, Republic of Korea). Chemiluminescent detection was performed using Immobilon Western Chemiluminescent HRP Substrate (Millipore Corporation, Billerica, MA, USA). β-Actin was used as an internal control. The expression of WT1, ErbB2, and PDL1 was determined using Amersham Imager 600 (GE Healthcare, Marlborough, MA, USA).

Clonogenic Long-Term Survival Assay

Stable GL261 cells were harvested and irradiated at different doses (2, 4, and 6 Gy). Thereafter, GL261 cells (5×10^2 cells/well)

were reseeded in 6-well culture dishes and incubated at 37°C in an atmosphere of 5% CO_2 for 14 d. The cells were fixed in methanol for 5 min and stained with toluidine blue (0.1%, Sigma, St. Louis, MO, USA) for 15 min. Dishes were washed with distilled water and dried at room temperature. Colony counting was performed on the following day. Colonies containing at least 50 cells were counted. The number of colonies in the irradiated wells was compared to the corresponding number in the non-irradiated wells. Plating efficiency was calculated as plating efficiency = [number of colonies counted/number of cells plated] × 100. Finally, the percentage survival fraction was calculated as survival fraction = [plating efficiency of treated sample/plating efficiency of control] × 100.

MTT Assay

The effects of radiation on the proliferation of GL261 cells was estimated using the MTT assay. Briefly, after radiation with 2, 4, or 6 Gy, the cells (2.5×10^3 cells/well) were seeded in 96-well plates and cultured with DMEM media supplemented with 10% FBS and 1% P/S at 37°C in an atmosphere of 5% CO_2. Subsequently, the cells were stained every 24 h incubation until day 5 with 3-(4,5-dimethylthiazol-2-yl)-2,5-diphenyltetrazolium bromide (MTT; Sigma). For staining, the plates were washed with PBS, and MTT (0.5 mg/mL) was added to each well. The MTT solution was removed from each well after 4 h of incubation. MTT formazan was then solubilized using isopropanol (Merck, Darmstadt, Germany), and the optical density was read at 570 nm.

Intracranial Glioma Mouse Model and Treatment Schedule

To establish the mouse intracranial model, we stereotactically injected 1×10^5 GL261 cells in 5 μL PBS into the right striatum of the mice at a rate of 1 μL/min. Injection sites were estimated using the following coordinates: 2 mm anterior, 2 mm lateral from bregma, and 4 mm deep from the cortical surface (18). The mice was randomly allocated to the treatment arms. For treatment, the mice was divided into the following four treatment groups: (1) control; (2) RT only; (3) RT plus vaccine; and (4) RT plus vaccine and anti-PD1. On day 13 after injection, the mice were irradiated (6 Gy). Thereafter, branched multipeptide (150 μg/injection) and PADRE (50 μg/injection) were subcutaneously administrated on days 14 and 18. Poly-ICLC (Hiltonol, Oncovir Inc.) (50 μg/injection) was intramuscularly injected on the same day with peptide treatment (12, 19). The mice were also administered intraperitoneal injections of *in vivo* MAb anti-mouse PD1 (200 μg/injection) every other day (day 14, 16, and 18). Overall survival was quantified. The mice was euthanized on day 20 after injection to assess tumor size and immunological parameters in the spleen and tumor.

Hematoxylin and Eosin (H&E) Staining of the Brain

Mouse brains were collected and fixed in formaldehyde. Thereafter, brains were sectioned into 4-mm thick slices at the injection site. Brain slices were stored in 5% paraformaldehyde, embedded in paraffin, and sectioned into 4-μm coronal sections

using a microtome. For tumor size confirmation, H&E staining was performed. Briefly, hematoxylin was used to completely cover the tissue section in 5 min. After rinsing twice with distilled water to remove any excess stain, a bluing reagent was applied to the tissue for 1 min. Thereafter, slides were washed with distilled water and dipped in absolute alcohol. Finally, slides were incubated in eosin solution for 3 min, rinsed in distilled water, and dehydrated with absolute alcohol. Slides were then cleared and mounted using Histomount (National Diagnostics, USA). Tumor slides were scanned using the Aperio Scan Scope System (Aperio, Technology; Vista, CA, USA), and cross-section areas (mm^2) of different treatment groups were confirmed using Aperio ImageScope software (Aperio). Data were summarized using bar charts.

Isolation of Splenocytes and Single Tumor Cells

Splenocytes and single tumor cells were isolated directly from the spleen and tumor of non-vaccinated and vaccinated mice. For the isolation of splenocytes, the spleen was collected and washed with DMEM media supplemented with 10% FBS and 1% P/S. Then, a 1-mL syringe plunger was used to gently press the spleen through a 100-μm cell strainer (BD Falcon, Becton Dickinson, NJ, USA) while continuously adding media. After filtering through a 40-μm cell strainer (Falcon), erythrocytes were removed using 0.83% (w/v) NH_4Cl (Sigma) (red blood cell lysis buffer). Cells were collected and washed with media. For the isolation of single tumor cells, the tumor was collected and washed with DMEM media supplemented with 10% FBS and 1% P/S. Subsequently, the tumor was minced into 3 to 4-mm pieces using a sterile scalpel. Tumor pieces were incubated with collagenase type IV (0.25%; Gibco-BRL) at 37°C in an atmosphere of 5% CO_2 for 2 h. Samples were observed and suspended at 15-min intervals. Cells were filtered using 100- and 40-μm cell strainers (Falcon), and single tumor cells were collected. Erythrocytes were removed using the red blood cell lysis buffer.

Flow Cytometry

For *in vitro* experiments, the expression of MHC I and PDL1 on GL261 cells before and after radiation was confirmed by flow cytometry. The cells were exposed to 2, 4, or 6 Gy radiation and cultured for the indicated time periods for flow cytometric analysis. Generally, the cells were stained with FITC-conjugated H-2Kb (BD Biosciences, San Jose, CA, USA) or PE-conjugated PDL1 (BD Biosciences) at the 0 and 24 h time points. Data were acquired on a BD FACS Calibur.

For the *in vivo* experiments, splenocytes, re-stimulated splenocytes, and tumor single cells were stained to confirm the immune cells. For cell surface staining, the cells (1 × 10^6 cells) were stained with Pacific blue-conjugated CD45, PE-conjugated CD4 and CD8, PE-cy7-conjugated CD8, APC-conjugated CD44, APC-cy7-conjugated CD44, FITC-conjugated CD62L, FITC-conjugated CD69, PE-conjugated CD49b, FITC-conjugated CD279 (PD1), or PE-conjugated CD274 (PDL1) for 30 min at 4°C. For intracellular staining, the cells (1 × 10^6 cells) were stained with PE-conjugated CD4, PE-cy7-conjugated CD8, or FITC-conjugated CD25 for 30 min at 4°C. The cells were

then washed and permeabilized with FACS™ Permeabilizing Solution 2 (BD Biosciences) for 30 min at room temperature. After washing twice with permeabilization buffer, the cells were stained with Alexa Fluor-conjugated Foxp3 or FITC-conjugated IFN-γ for 30 min at 4°C. For IFN-γ intracellular staining, the Protein Transport Inhibitor containing Brefeldin A (BD Golgi Plug™) at 1 μL/1 × 10^6 cell/well was added at the final 5 h of re-stimulation time. All antibodies were purchased from BD Biosciences. All samples were processed on a BD FACs Canto II (Becton Dickinson, Mountain View, CA, USA). Cell debris was eliminated by forward and side-scatter gating. All data were analyzed using FlowJo v10 software (TreeStar, San Carlos, CA, USA). Mean fluorescence intensity (MFI) ratio was calculated by dividing the median fluorescence intensity (MFI) of the positive cells (stained cell population) by that of the negative cells (unstained cell population).

Splenocyte Re-stimulation and Single Tumor Cell Culture *ex vivo*

Splenocytes were re-stimulated according to the manufacturer's protocol. Splenocytes isolated from non-vaccinated and vaccinated mice after the final immunization (day 20) were cultured in 24-well plates (1 × 10^6 cells/well) and re-stimulated with branched multipeptide (20 μg/mL) and PADRE (3 μg/mL) for 5 d in RPMI-1640 (Gibco-BRL) prepared in 10% FBS with 1% P/S supplementation and recombinant mouse (rm) IL-2 (20 ng/mL) (R&D systems). Anti-PD1 (10 μg/mL) was added during incubation. After re-stimulation, the supernatant and cells were collected and used for checking immune cell function. For IFN-γ intracellular staining, the splenocytes were re-stimulated and IFN-γ intracellular staining was performed or IFN-γ in the supernatant was estimated after 24-h incubation.

Single tumor cells from tumor were cultured in 6-well plates (1 × 10^6 cells/well) for 24 h in 37°C in an atmosphere of 5% CO_2, and the supernatant was collected for pro-inflammatory and anti-inflammatory cytokine determination by enzyme-linked immunosorbent assay (ELISA).

IFN-γ Release Enzyme-Linked Immunospot (ELISPOT) Assay

The IFN-γ secreted by re-stimulated splenocytes against target cancer cells was examined using an IFN-γ ELISPOT assay kit (BD Biosciences). Ninety-six well PVDF membrane ELISPOT plates (Millipore, USA) were coated with the capture-purified anti-mouse IFN-γ antibody overnight at 4°C. Then, RPMI medium supplemented with 10% FBS was added to saturate the treated antibody. The re-stimulated splenocytes from the immunized mice were co-cultured with the target cells (GL261 and YAC-1 cell line) at a 10:1 ratio. Co-cultured cells were incubated in 10% FBS-RPMI medium for 24 h at 37°C in an atmosphere of 5% CO_2. Subsequently, the plates were incubated for 2 h with the biotinylated detection anti-mouse IFN-γ antibody and then for 1 h with streptavidin-HRP. After washing, spots were revealed using an AEC substrate reagent set (BD Bioscience) and measured on an automatic CTL Immunospot Analyzer (Cellular Technology Ltd., Shaker Heights, OH, USA).

Lactate Dehydrogenase (LDH) Release Cytotoxicity Assay

CytoTox 96 non-radioactive cytotoxicity assay (CytoTox 96, Promega, Madison, WI, USA) was performed to analyze the killing effects of the re-stimulated splenocyte effector cells against target cancer cells according to the manufacturer's instructions. GL261 and YAC-1 cell lines (2×10^5 cells/well) were used as the target cells. The re-stimulated splenocytes were co-cultured with the target cells at a 10:1 ratio in Costar 96-well plates (Corning, Inc., Corning, NY, USA) for 4 h in 37°C and an atmosphere of 5% CO_2. Then, supernatants were collected for determining the LDH concentration. The mean percentage of specific lysis was calculated as follows:

$$\%Cyotoxicity = \frac{(Experimental - Effector\ Spontaneous - Target\ Spontaneous)}{(Target\ Maximum - Target\ Spontaneous)} \times 100$$

Enzyme-Linked Immunosorbent Assay (ELISA)

ELISA was performed to measure the levels of pro-inflammatory and anti-inflammatory cytokines released into the culture media of re-stimulated splenocytes or single tumor cells from non-vaccinated and vaccinated mice using the OptEIA ELISA set (BD Bioscience) following the manufacturer's instructions. Culture media from re-stimulated splenocytes isolated from vaccinated mice were analyzed for changes in the levels of the pro-inflammatory (IL-12p70 and IFN-γ) and anti-inflammatory (IL-10) cytokines, whereas the culture media of single tumor cells were analyzed for changes in the levels of the pro-inflammatory (IFN-γ) and anti-inflammatory [transforming growth factor-beta (TGF-β) and IL-10] cytokines.

Statistical Analysis

All statistical analyses were performed using SPSS 20.0 for Windows (SPSS Inc., Chicago, IL, USA). One-way analysis of variance (ANOVA) was performed for analyses across multiple groups. The log-rank test was performed on survival data, and $p < 0.05$ was considered statistically significant. The results are represented as the means ± SD.

RESULTS

Immunological Characteristics and Effects of Radiation on the GL261 Cell Line

To determine whether the tumor-associated antigens that were used for the synthesis of the branched multipeptide were indeed present on GL261 cells, we estimated the expression of the two tumor-associated antigens (ErbB2 and WT1) on GL261 cells. Our data indicated that GL261 cells have strong expression of both ErbB2 and WT1, and it is thus feasible to construct a branched multipeptide based on these antigens. Moreover, the high expression of MHC I and PDL1 on GL261 cells was also verified to confirm the efficiency of the treatment. Overall, GL261 cells showed immunological characteristics for immunotherapy.

The short-term effects of radiation on GL261 cells were also determined. As shown in **Figures 1A,B**, the levels of ErbB2, WT1 expression were enhanced after treatment with the different radiation doses at 0 h and were reduced after 24 h. However, no differences were observed, except with regard to the expression of ErbB2. In particular, ErbB2 expression was reduced in all radiation groups treated with 2 Gy ($p = 0.029$), 4 Gy ($p = 0.032$), and 6 Gy ($p = 0.013$) compared with that in the no-radiation control group. Additionally, the effects of radiation on MHC I and PDL1 expression on GL261 cells was also confirmed at 0 and 24 h. The expression of MHC I and PDL1 on GL261 cells after irradiation (2, 4, and 6 Gy) is shown in **Figures 1C–E**; most GL261 cells showed strong surface expression of MHC I and PDL1 with no differences before and after radiation at 0 and 24 h, which paralleled the total PDL1 protein expression on GL261 cells. These results showed that the effects of radiation on GL261 cells after a short-term 24-h period only altered the expression of ErbB-2.

To investigate the long-term effects of radiation, we evaluated the viability and proliferation of GL261 cells after radiation with different doses (2, 4, and 6 Gy). The percentage survival fraction of GL261 cells after radiation was determined based on the results of the clonogenic assay. As shown in **Figure 1F**, GL261 cells showed reduced survival upon irradiation. Particularly, the survival fraction of GL261 cells was reduced to 58.17% with 2 Gy ($p < 0.001$), 92.37% with 4 Gy ($p < 0.001$), and 98.69% with 6 Gy ($p < 0.001$), compared with that of the no-radiation control. Moreover, the survival fraction of GL261 cells exposed to 4 and 6 Gy was also reduced compared with that of 2 Gy (34.2 and 40.5%, respectively, both $p < 0.001$). The effects of radiation on GL261 cell proliferation were also estimated. As shown in **Figure 1G**, irradiated GL261 cells showed a delayed proliferation as evidenced by the lower OD values in the MTT assay compared with that in the no-radiation control from day 3 after treatment. In particular, GL261 cells treated with 4 and 6 Gy radiation showed delayed proliferation compared with the no-radiation GL261 cells ($p = 0.037$ and $p = 0.047$, respectively) at day 3. Similarly, GL261 cells treated with 4 and 6 Gy radiation showed more delayed proliferation than the no-radiation GL261 cells ($p = 0.000$ and $p = 0.000$, respectively) on day 4. On day 5, GL261 cells treated with 2, 4, and 6 Gy radiation showed delayed proliferation compared with the no-radiation GL261 cells ($p = 0.000$, $p = 0.000$, and $p = 0.000$, respectively). Moreover, GL261 cells treated with 4 Gy radiation also had delayed proliferation compared with the 2 Gy-treated GL261 cells ($p = 0.001$), and GL261 cells treated with 6 Gy radiation had delayed proliferation compared with the 2 and 4 Gy-treated GL261 cells ($p = 0.000$ and $p = 0.007$, respectively). Overall, radiation affected the long-term survival and proliferation of GL261 cells *in vitro*.
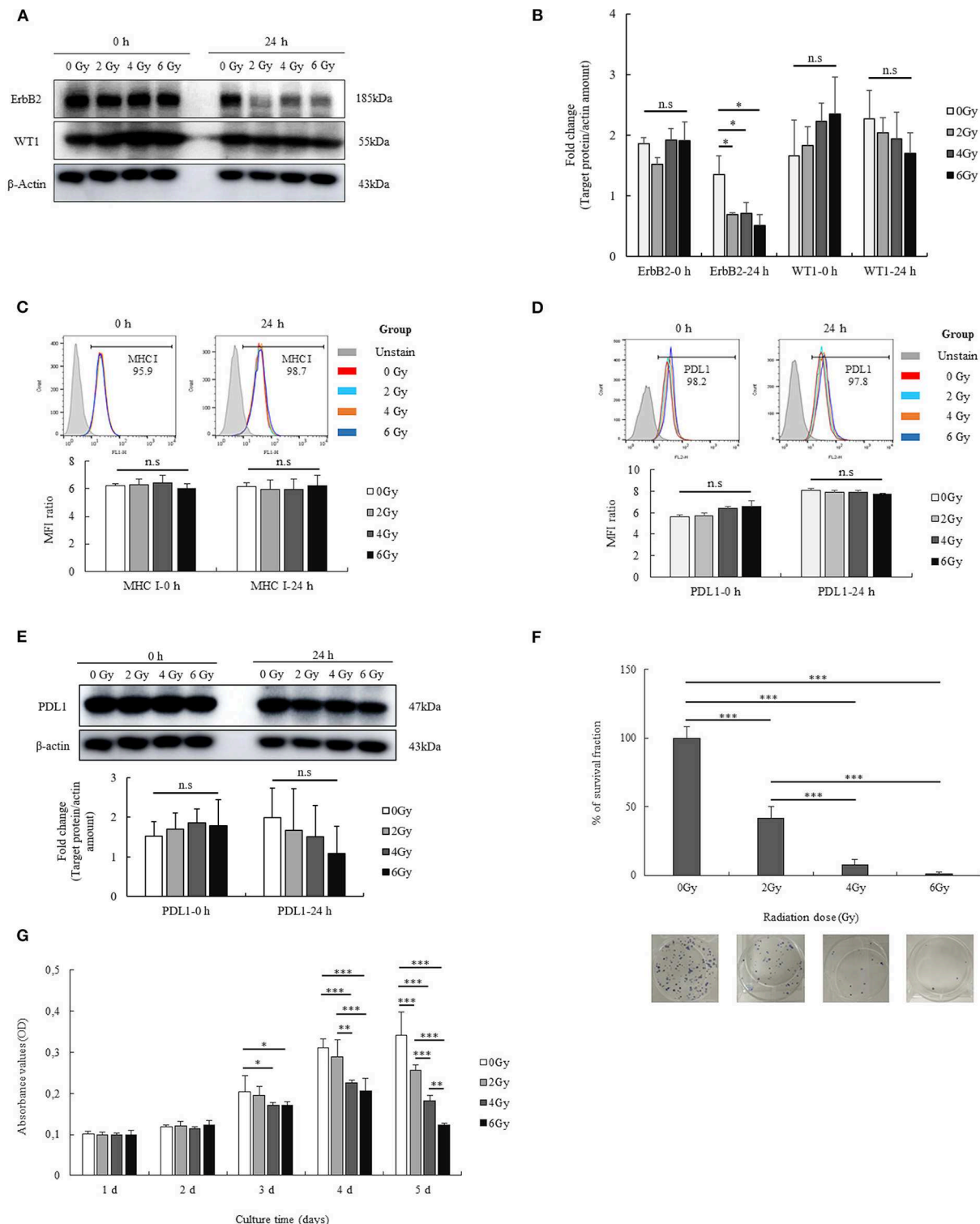
FIGURE 1 | Immunological characterization of the GL261 cell line, and the effects of radiation. The expression of two tumor-associated antigens (ErbB2 and WT1) on GL261 cells and the short-term effects of radiation on the expression of these proteins were confirmed by western blot analysis **(A)**. Fold changes in protein signals are summarized by bar charts **(B)**. The expression of MHC I on GL261 cells and the short-term effects of radiation on this expression were also confirmed by flow cytometry **(C)**. The surface expression and total protein expression of PDL1 on GL261 was estimated by flow cytometry and western blot **(D,E)**. Moreover, the effects of radiation (2, 4, and 6 Gy) on the viability and proliferation of GL261 cells were also clarified by clonogenic assay and MTT assay **(F,G)**. Data is summarized by bar charts as the mean ± standard deviation (SD). All data are represented as the mean of two independent experiments. β-Actin was used as an internal control, and the figure is composed of multiple gel images. Full-length blots are presented in **Figure S2**. GL261, mouse glioblastoma cell line; H-2Kb, MHC class I expression in mice. *$p < 0.05$; **$p < 0.01$; and ***$p < 0.001$; n.s., no significant difference.

Therapeutic Effects of Radiation Combined With Vaccine and Anti-PD1 on the GBM Mouse Model

The treatment schedule described in **Figure 2A** was followed. First, the radiation dose was screened in the mouse GBM model, and the optimal dose was selected for the subsequent *in vivo* experiments. On day 13, after transplantation, the mice were irradiated at different doses (4, 5, and 6 Gy). Thereafter, the mice were euthanized on day 20 to determine the tumor size; additionally, the tumor was also subjected to H&E staining. Tumor cross-sections at different radiation doses (4, 5, and 6 Gy) were studied (**Figure 2B**). In the 4 Gy-treated mice, no significant difference was noted in the cross-sectioned areas of the tumor compared to the control. However, the 5 and 6 Gy-treated mice showed smaller cross-sectioned areas than the no-radiation control ($p = 0.001$ and $p = 0.000$, respectively). Furthermore, 5 and 6 Gy-treated mice exhibited lower tumor sizes than the 4 Gy-treated mice ($p = 0.014$ and $p = 0.000$, respectively). Between 5 and 6 Gy-treated mice, the latter showed a greater effect on tumor proliferation that resulted in delayed tumor growth ($p = 0.022$). Radiation with 6 Gy on day 13 was chosen for the subsequent experiments.

After treatment with radiation plus vaccine and anti-PD1, the size of the brain tumor on day 20 and survival were investigated in the different treatment groups. The size of the brain tumor at the injection site before and after treatment was confirmed by H&E staining (**Figure 2C**). The tumor size before treatment was confirmed on day 13. On day 20, the tumor size was also compared between the control and treatment groups. A significant difference was noted in the cross-sectioned areas between the treatment groups and the control group. In particular, the control group showed larger cross-sectioned areas than in RT ($p = 0.000$), RT plus vaccine ($p = 0.000$), and RT plus vaccine and anti-PD1 ($p = 0.000$) groups. Although there was no significant difference between RT and RT plus vaccine or RT plus vaccine and RT plus vaccine and anti-PD1, RT plus vaccine and anti-PD1 showed smaller cross-sectioned areas than the RT group ($p = 0.043$). These data correspond with the results of mouse survival (**Figure 2D**). Mice exhibited prolonged survival following radiation treatment. In particular, RT enhanced survival from ∼25.8 ± 2.2 days in the control to 31.5 ± 5.7 days in the RT group ($p = 0.003$), 38.3 ± 6.2 days in the RT plus vaccine ($p < 0.001$), and 40 ± 6.5 days in the RT plus vaccine and anti-PD1 group ($p < 0.001$). Although the RT plus vaccine and anti-PD1 group showed no significant difference from the RT plus vaccine group, the former exhibited prolonger survival than the RT only group ($p = 0.022$). Therefore, RT combined vaccine and anti-PD1 showed a prolonged mouse survival according to delay in tumor growth in GBM model.

The Expression of PD1 on T Lymphocytes and That of PDL1 on Single Tumor Cells After Treatment

The expression of the PD1 receptor on CD8$^+$ and CD4$^+$ T cells in the splenocytes and single tumor cells was confirmed by flow cytometry. The percentages of CD8$^+$PD1$^+$ cells and CD4$^+$PD1$^+$

cells in the splenocytes are shown in **Figures 3A,B**; RT only enhanced the expression of PD1 on CD8$^+$ T cells, whereas RT plus vaccine enhanced the expression of PD1 on both CD8$^+$ and CD4$^+$ T cells. Notably, the percentage of CD8$^+$PD1$^+$ T cells was higher in the RT group (4.8%; $p = 0.005$) and in the RT plus vaccine group (5.7%; $p = 0.003$) than in the control group. The percentage of CD4$^+$PD1$^+$ T cells in the RT plus vaccine group was higher (by 6.08%) than that in the control group ($p = 0.038$). Moreover, the percentages of tumor-infiltrating CD8$^+$PD1$^+$ T cells on the single tumor cells were also confirmed. Although the RT plus vaccine group showed a slightly lower percentage of tumor-infiltrating CD8$^+$PD1$^+$ T cells than the control or RT only group, there was no difference between the RT plus vaccine group compared to RT only group or control group with regard to single tumor cells (**Figures 3C,D**).

The expression of PDL1 on the single tumor cells was also estimated. As shown in **Figures 3E,F**, there was no significant difference between the control, RT only, and RT plus vaccine group. However, the addition of anti-PD1 to the RT plus vaccine group led greater PDL1 expression in the single tumor cells than in the control group ($p = 0.049$). Therefore, anti-PD1 may lead to an increase in the expression of PDL1 in the tumor.

The Distribution of Immune Cells in the Splenocytes and Single Tumor Cells

In the splenocytes, both activated CD8$^+$ and CD4$^+$ T cells were enhanced in response to the combination treatment. Although the number of CD8$^+$CD44$^+$ T cells was not significantly different between the control and treatment groups, CD8$^+$CD44^{high} T cells were increased in the RT plus vaccine and anti-PD1 group (**Figures 4A–C**). In particular, the RT plus vaccine and anti-PD1 group exhibited a higher percentage of CD8$^+$CD44^{high} T cells compared with that in the control (5.2%, $p = 0.025$) and the RT only group (4.37%, $p = 0.043$). Similarly, CD4$^+$CD44$^+$ T cells showed a reduction in response to the RT plus vaccine or RT plus vaccine and anti-PD1 treatments, whereas CD4$^+$CD44^{high} T cells showed an increase in response to these treatments (**Figures 4D–F**). In particular, RT plus vaccine reduced the percentage of CD4$^+$CD44$^+$ T cells compared with that in the control (4.85%, $p = 0.012$) and the RT only group (5.65%, $p = 0.007$). Moreover, RT plus vaccine and anti-PD1 reduced CD4$^+$CD44$^+$ T cells compared with that in the control (8.35%, $p = 0.002$), the RT only (9.15%, $p = 0.001$), and the RT plus vaccine group (3.5%, $p = 0.034$). However, RT plus vaccine enhanced CD4$^+$CD44^{high} T cells compared with that in the control group (2.1%, $p = 0.011$) and the RT only group (1.63%, $p = 0.017$). In addition, RT plus vaccine and anti-PD1 enhanced CD4$^+$CD44^{high} T cells compared with that in the control group (2.98%, $p = 0.003$) and the RT only group (2.52%, $p = 0.004$).

Moreover, RT plus vaccine or RT plus vaccine and anti-PD1 also enhanced the effector memory T cell counts in the splenocytes (**Figures 4G,H**). In particular, the RT plus vaccine group has a higher percentages of CD44^{high}CD62L$^-$ T cells than the control group (2.17%; $p = 0.021$), whereas the RT plus vaccine and anti-PD1 group had a higher percentage of CD44^{high}CD62L$^-$ T cells than the control group (3.66%; $p =$

FIGURE 2 | Experimental treatment schedule, and therapeutic effects of combination treatment. Schema outlining treatments used in the experiments **(A)**. Brain tumor size with and without radiation relative to the different radiation dose treatment (4, 5, and 6 Gy) was estimated with H&E staining **(B)**. The brain tumor sizes before (day 13) and after treatment (day 20) with different combinations, such as RT, RT plus vaccine, and RT plus vaccine and anti-PD1, were confirmed by H&E staining **(C)**. The Kaplan-Meier survival curves used to estimate the survival of the mouse tumor model according to the different treatment combinations in GL261 glioma-bearing mice, such as RT ($n = 8$), RT plus vaccine ($n = 8$), and RT plus vaccine and anti-PD1 ($n = 8$), compared with the untreated control ($n = 20$) **(D)**. Data are summarized by bar charts as the mean ± standard deviation (SD). All data are represented as the mean of two independent experiments. Control: no treatment group; RT, radiation therapy; vaccine, branched multipeptide plus PADRE and poly-ICLC; $*p < 0.05$; $**p < 0.01$; and $***p < 0.001$.

0.003) and the RT only group (2.52%; $p = 0.013$). Similarly, the percentages of activated NK cells ($CD49b^+CD69^+$) in the splenocytes also showed an increase in the RT plus vaccine or RT plus vaccine and anti-PD1 groups (**Figures 4I,J**). In particular, the RT plus vaccine group had higher percentages of $CD69^+CD49b^+$ NK cells compared with that in the control (3.02%; $p = 0.018$) and the RT only group (2.72%; $p = 0.026$). Moreover, RT plus vaccine and anti-PD1 group had higher percentages of $CD69^+CD49b^+$ NK cell levels than the control (2.89%; $p = 0.021$) and the RT only group (2.6%; $p = 0.03$).

The treatment groups showed increased percentages of not only activated T cells and NK cells but also regulatory T cells (Tregs) in the splenocytes. The addition of anti-PD1 to the RT plus vaccine group resulted in an increased percentage of $CD4^+CD25^+Foxp3^+$ Tregs (**Figures 4K,L**). Notably, RT plus vaccine and anti-PD1 treatment lead to higher $CD4^+CD25^+Foxp3^+$ Treg cell counts than the control group (7.32%; $p = 0.02$) and the RT only group (6.26%; $p = 0.033$).

The percentages of tumor-infiltrating $CD8^+CD44^+$ T cells were also confirmed by flow cytometry. As shown in **Figures 4M,N**, there was a small amount of tumor-infiltrating $CD45^+CD3^+$ cells were detected and no significant difference between the tumor-infiltrating $CD8^+CD44^+$ cells gated from $CD45^+CD3^+$ cells in all the treatment groups compared with the control group. Moreover, tumor-infiltrating $CD4^+CD44^+$ cells

gated from $CD45^+CD3^+$ cells were not detected in our study (data not shown).

Pro-inflammatory and Anti-inflammatory Cytokine Production From Re-stimulated Splenocytes

For pro-inflammatory cytokines, IL-12p70 and IFN-γ were investigated. There was an increase in the IL-12p70 levels in response to the treatments; however, there was no significant difference between the treatments, except for the RT plus vaccine and anti-PD1 group (**Figure 5A**). In particular, the RT plus vaccine and anti-PD1 group showed a significant difference in the IL-12p70 levels compared with the control group ($p = 0.044$). With regard to IFN-γ, only the RT group showed no significant difference compared with the control; the RT plus vaccine or RT plus vaccine and anti-PD1 groups showed increase compared with the control and RT group (**Figure 5B**). In particular, RT plus vaccine group exhibited higher IFN-γ levels than the control ($p < 0.001$) and RT groups ($p < 0.001$), whereas the RT plus vaccine and anti-PD1 group showed the highest levels compared with the control ($p < 0.001$), RT ($p < 0.001$), and RT plus vaccine groups ($p < 0.001$). The anti-inflammatory cytokine IL-10 levels were enhanced in response to treatment (**Figure 5C**). Although RT alone showed no significant difference compared with the control
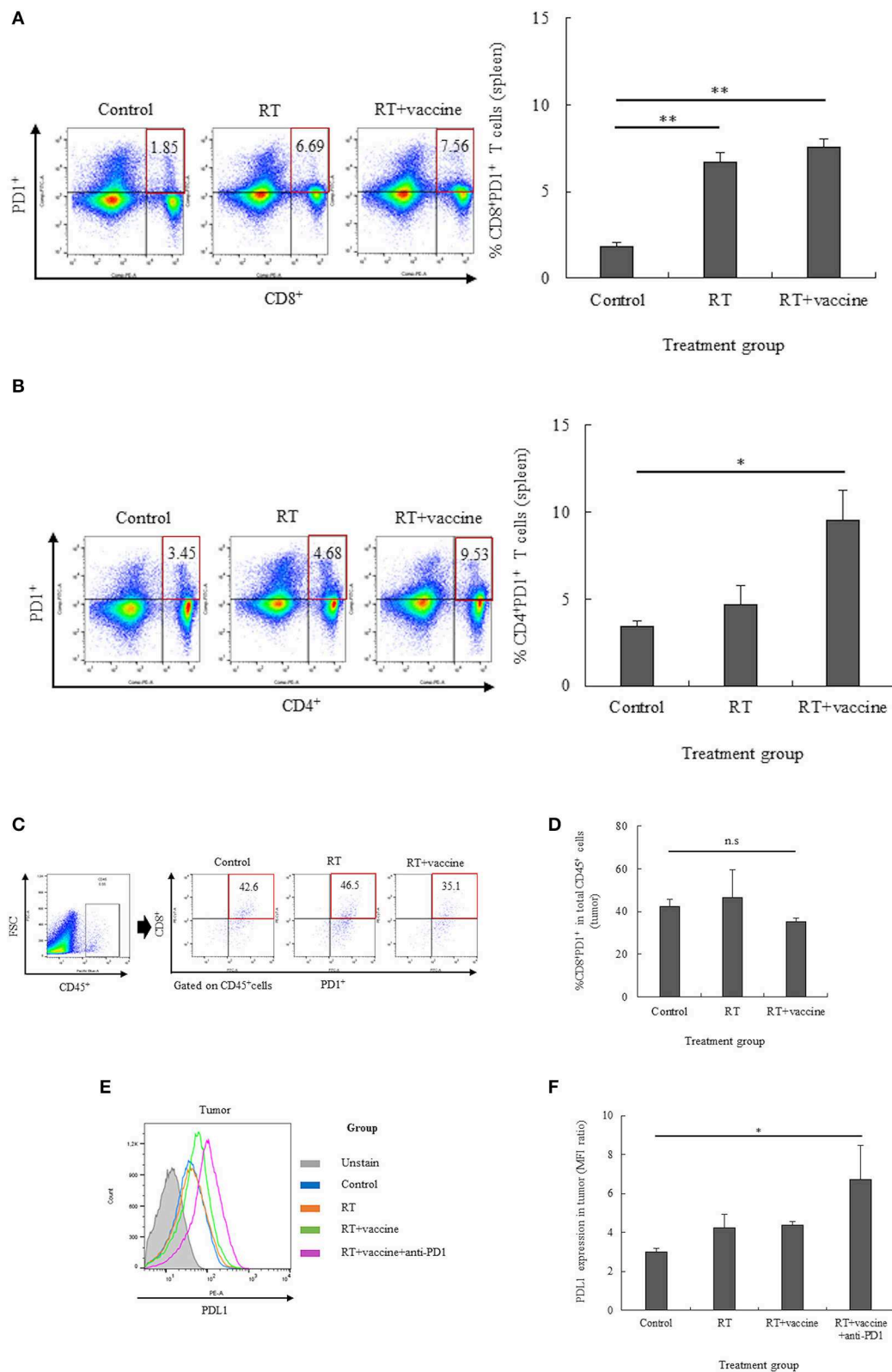
FIGURE 3 | The expression of PD1 on T lymphocytes in the spleen and tumor and that of PDL1 on the tumor were estimated by flow cytometry. The expression of PD1 on the T lymphocyte population was estimated, and percentages of CD8$^+$PD1$^+$ T cells or CD4$^+$PD1$^+$ T cells in the spleen and CD8$^+$PD1$^+$ T cells in the tumor were determined **(A–D)**. The expression of PDL1 in the tumor was also clarified **(E,F)**. Data are summarized by bar charts as the mean $\pm$ standard deviation (SD). All data are represented as the mean of two independent experiments. Control, no treatment group; RT, radiation therapy; vaccine, branched multipeptide plus PADRE and poly-ICLC; *$p < 0.05$; **$p < 0.01$; and n.s., no significant difference.
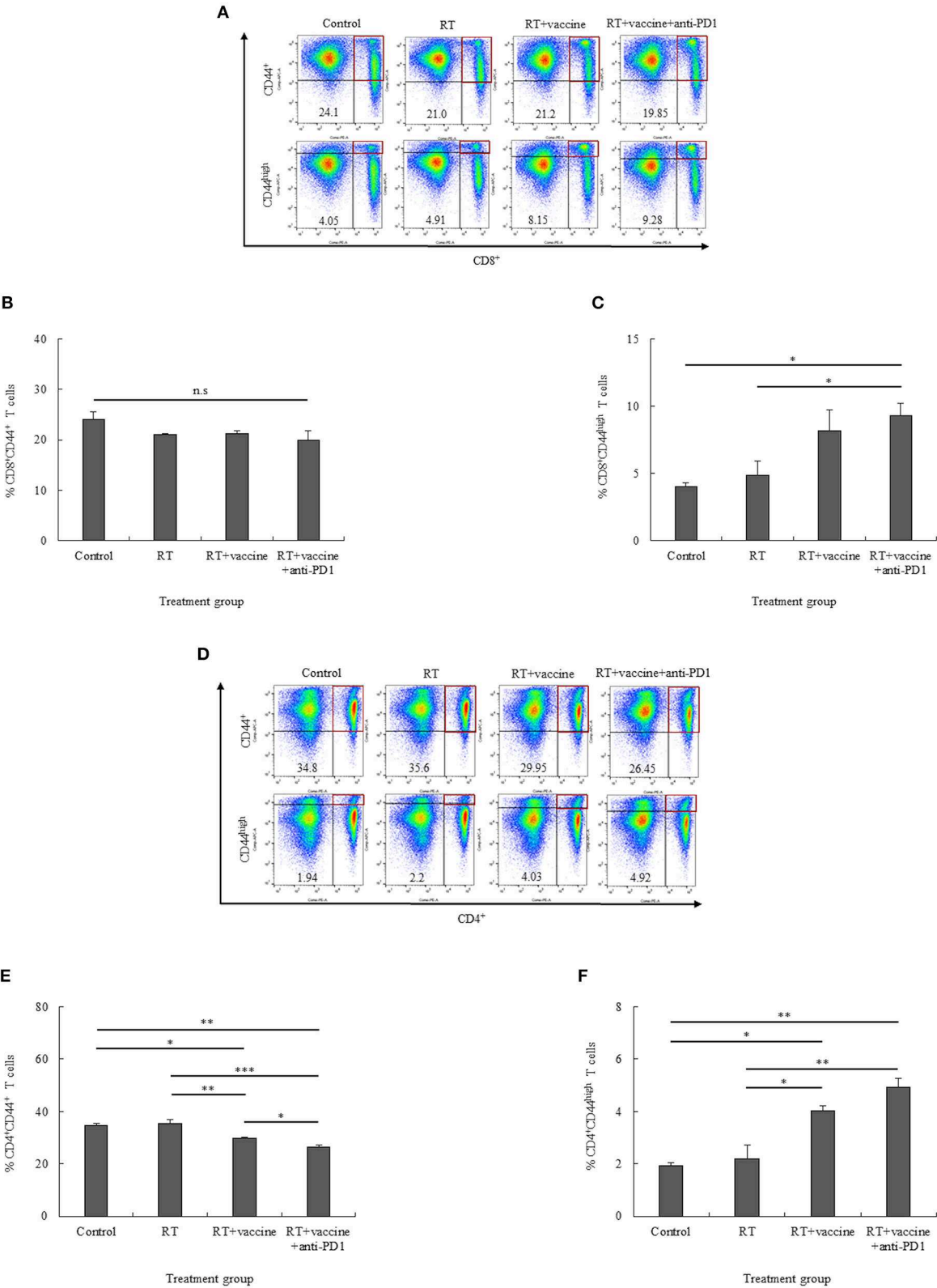
FIGURE 4 | Continued
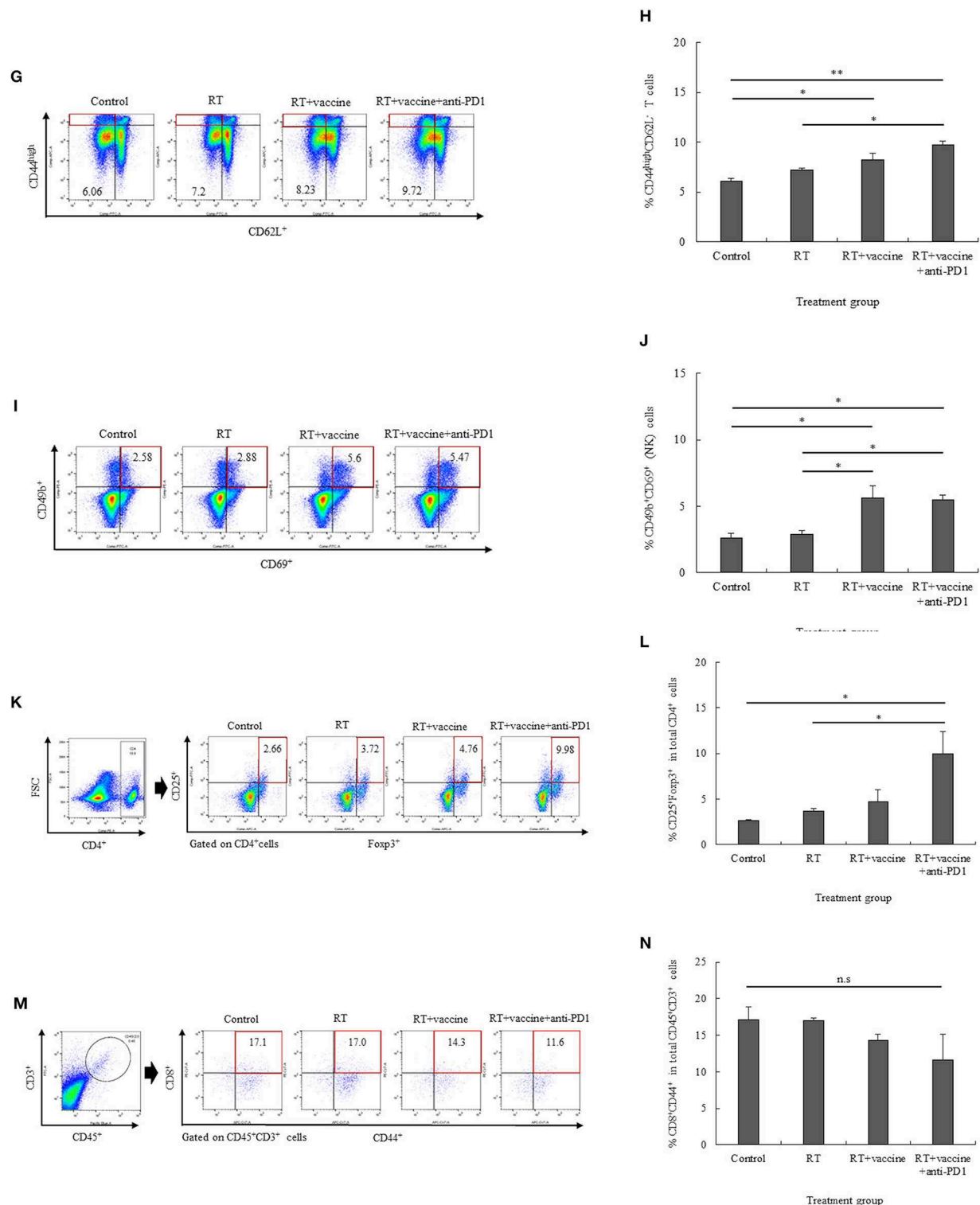
FIGURE 4 | The distribution of immune cells in the spleen and tumor was confirmed by flow cytometry. The presentation of activated $CD8^+CD44^+$ T cells and high activated $CD8^+CD44^{high}$ effector T cells **(A–C)**, activated $CD4^+CD44^+$ T cells and high activated $CD4^+CD44^{high}$ effector T cells **(D–F)**, high activated $CD44^{high}CD62L^-$ effector memory T cells **(G,H),** $CD49b^+CD69^+$ natural killer (NK) effector cells **(I,J)**, and $CD4^+CD25^+Foxp3^+$ regulatory T cells **(K,L)** in the splenocytes of non-vaccinated and vaccinated mice was estimated. Moreover, the presentation of activated $CD8^+CD44^+$ T cells in the tumor was also confirmed **(M,N)**. Data are summarized by bar charts as the mean ± standard deviation (SD). All data are represented as the mean of two independent experiments. Control, no treatment group; RT, radiation therapy; vaccine, branched multipeptide plus PADRE and poly-ICLC; *$p < 0.05$; **$p < 0.01$; and ***$p < 0.001$; n.s., no significant difference.

group in terms of IL-10 levels, the RT plus vaccine or RT plus vaccine and anti-PD1 groups showed higher IL-10 levels than the control and RT groups. In particular, the RT plus vaccine group showed higher IL-10 levels than the control ($p < 0.001$) and RT only groups ($p < 0.001$). Moreover, the RT plus vaccine and anti-PD1 group had higher IL-10 production than the control ($p < 0.001$) and RT only groups ($p < 0.001$).

The expression of IFN-γ on CD8$^+$ and CD4$^+$ T cells was also clarified. As shown in **Figures 5D–F**, the percentages of CD8$^+$IFN-γ$^+$ cells were higher in the RT plus vaccine or RT plus vaccine and anti-PD1 groups than in the control and RT only groups. Particularly, RT plus vaccine enhanced compared with the control group (4.39%, $p = 0.004$) and the RT only group (3.34%, $p = 0.012$). Similarly, RT plus vaccine and anti-PD1 increased compared the control group (4.6%, $p = 0.004$) and the RT only group (3.55%, $p = 0.009$). There was no difference between the RT only and control or RT plus vaccine and RT plus vaccine and anti-PD1 groups. In contrast, although there was a slightly higher percentage of CD4$^+$IFN-γ$^+$ cells in the RT plus vaccine with or without anti-PD1 groups than in the RT only or control groups, there was no significant difference between all the treatment groups was found. The IFN-γ released in the supernatant after blocking for IFN-γ intracellular staining was also examined; IFN-γ in supernatant showed low levels, and no significant differences between the treatment groups were detected after blocking before intracellular staining (**Figure S3**). Our data showed that the RT plus vaccine and anti-PD1 group exhibited the pro-inflammatory cytokine IFN-γ mainly secreted by CD8$^+$ cells in the re-stimulated splenocytes, which play an important role in stimulating the immune response.

CTL and NK Cell Function of the Re-stimulated Splenocytes

The CTL- and NK cell-mediated immune responses of the re-stimulated splenocytes from non-vaccinated and vaccinated mice were elucidated. IFN-γ secretion by the re-stimulated splenocytes after co-culture with target cancer cells was investigated for the anti-tumor effect of combination treatment in a murine GBM model. Re-stimulated splenocytes from non-treated and treated mice were prepared for IFN-γ ELISPOT assays. GL261 and YAC-1 cells were used as target cancer cells for investigating the CTL and NK cell activity, respectively. As shown in **Figures 6A,B**, mice treated with RT only showed an enhanced level of IFN-γ-secreting splenocytes against GL261 target cells whereas the RT plus vaccine- or RT plus vaccine and anti-PD1-treated mice showed an increase in the IFN-γ-secreting splenocytes against both GL261 and YAC-1 target cells. In particular, the RT plus vaccine group showed a higher level of IFN-γ-secreting splenocytes against GL261 and YAC-1 cells than the control ($p < 0.001$ and $p = 0.003$, respectively). Moreover, the RT plus vaccine and anti-PD1 group showed a higher level of IFN-γ-secreting splenocytes against GL261 and YAC-1 target cells than the control, RT only, and RT plus vaccine (all $p < 0.001$). However, there was no significant difference between the

RT only and the RT plus vaccine groups with regard to the IFN-γ-secreting splenocytes.

The specific lysis of the re-stimulated splenocytes against target cancer cells was also confirmed. As shown in **Figures 6C,D**, RT plus vaccine and anti-PD1 enhanced the specific lysis of the re-stimulated splenocytes against both GL261 and YAC-1 cells. Particularly, with GL261 target cells, the RT plus vaccine and anti-PD1 group showed higher specific lysis than the control group (29%, $p = 0.001$), the RT only group (18.28%, $p = 0.013$), and the RT plus vaccine group (16.31%, $p = 0.023$). Similarly, with YAC-1 target cells, the RT plus vaccine and anti-PD1 group showed higher specific lysis than the control group (15.68%, $p = 0.003$), the RT only group (9.84%, $p = 0.038$), and the RT plus vaccine group (11.2%, $p = 0.021$). There was no significant difference in the percentages of specific lysis between the RT only or RT plus vaccine groups compared with the control group against GL261 and YAC-1 cells.

Although there was a higher number of IFN-γ-secreting splenocytes in the RT only, RT plus vaccine, or RT plus vaccine and anti-PD1 groups than in the control group, only the RT plus vaccine and anti-PD1 group showed highest percentages of specific lysis against GL261 and YAC-1 target cells than the control group. Moreover, these data showed an enhanced function in both CTL and NK cell activity. However, CTL activity in the re-stimulated splenocytes showed a greater shift than NK activity (**Figures S4A,B**). In particular, with IFN-γ-secreting splenocytes, the CTL activity was higher than the NK activity in the RT group ($p = 0.029$), RT plus vaccine group ($p = 0.000$), and RT plus vaccine and anti-PD1 group ($p = 0.002$). Similarly, the percentage of specific lysis of re-stimulated splenocytes against GL261 cells was also higher than that against YAC-1 cells in the RT plus vaccine and anti-PD1 group ($p = 0.003$).

Pro-inflammatory and Anti-inflammatory Cytokines From the Single Tumor Cells

IL-10 and TFG-β have been identified as key factors that mediate inhibitory action, whereas IFN-γ has been shown to be a pro-inflammatory cytokine in tumors. Culture media from single tumor cells during 24-h incubation were used to estimate the levels of the cytokines IFN-γ, IL-10, and TFG-β. As shown in **Figure 7A**, although single tumor cells present low levels of IFN-γ, these levels were higher in all the treatment groups than in the control. In particular, the RT only group had higher levels than the control ($p < 0.001$). Moreover, the RT plus vaccine group had higher IFN-γ levels than the control ($p < 0.001$) and RT only ($p = 0.002$) groups. Although RT plus vaccine and anti-PD1 showed higher IFN-γ levels than the control ($p < 0.001$) and RT plus vaccine ($p < 0.001$) groups, there was no difference between the RT plus vaccine and RT plus vaccine and anti-PD1 groups.

While TGF-β levels showed no difference between all treatment groups and the control, IL-10 showed different cytokine levels according to the various treatments administered. In particular, although TGF-β was increased in the RT plus vaccine and anti-PD1 group, there was no significant difference between the RT plus vaccine and anti-PD1 group compared with other groups (**Figure 7B**). In **Figure 7C**, whereas the IL-10 level
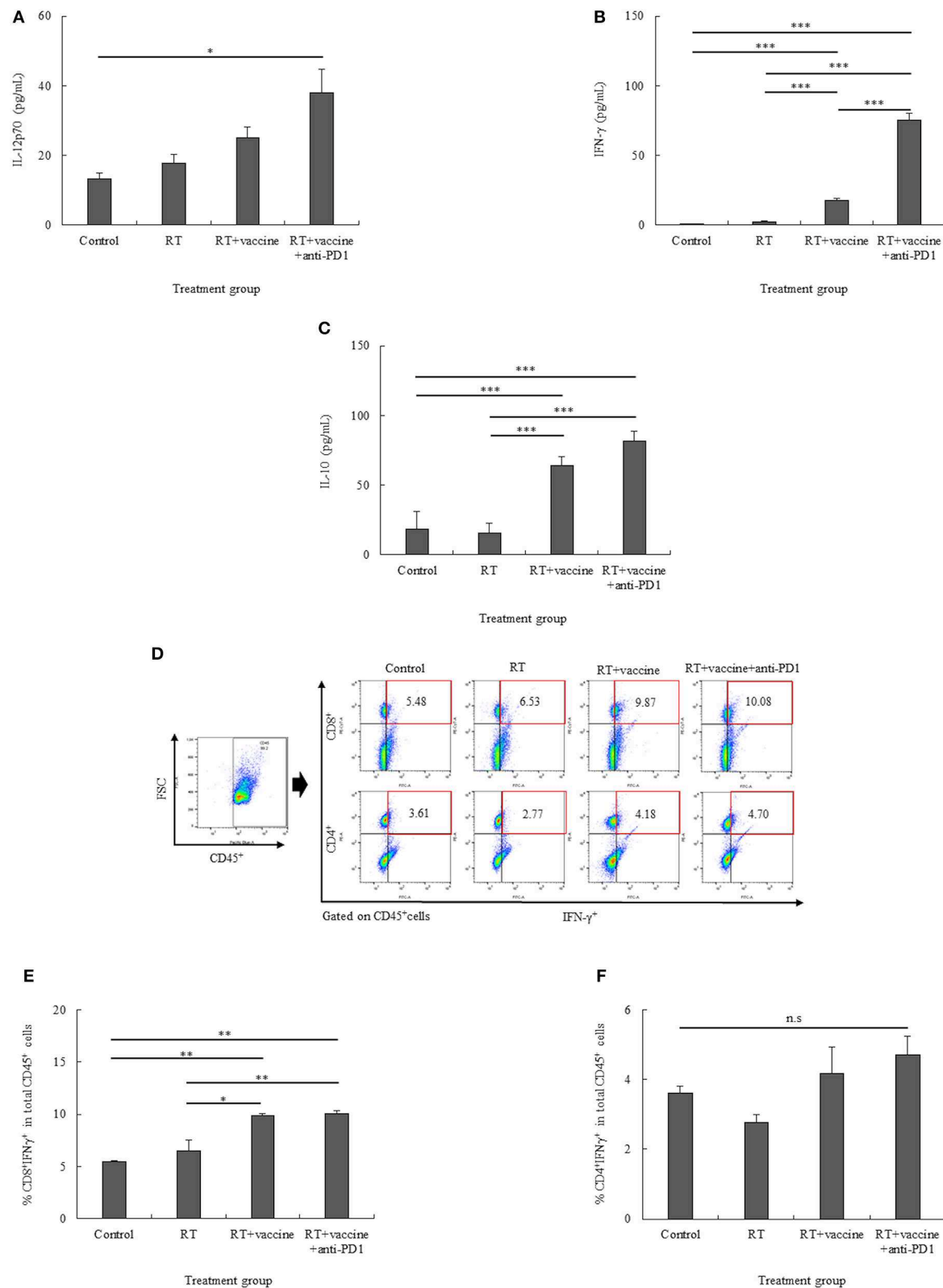
FIGURE 5 | The pro-inflammatory (IL-12p70 and IFN-γ) and anti-inflammatory (IL-10) cytokine levels in the re-stimulated splenocytes were determined using ELISA **(A–C)**. The percentages of CD8$^+$IFN-γ$^+$ cells and CD4$^+$IFN-γ$^+$ cells in the re-stimulated splenocytes were also confirmed **(D–F)**. Data are summarized by bar charts as the mean ± standard deviation (SD). All data are represented as the mean of two independent experiments with total 5 mouse per group. Control, no treatment group; RT, radiation therapy; vaccine, branched multipeptide plus PADRE and poly-ICLC; *$p < 0.05$; **$p < 0.01$; and ***$p < 0.001$.

FIGURE 6 | The cytotoxic T lymphocyte (CTL)- and natural killer (NK) cell-mediated immune response of re-stimulated splenocytes from vaccinated mice. The IFN-γ secreted by re-stimulated splenocytes when co-cultured with target cancer cells was measured using the IFN-γ ELISPOT assay **(A,B)**. The specific killing effects of re-stimulated splenocytes against target cancer cells was confirmed using the LDH assay **(C,D)**. The GL261 and YAC-1 cell lines were used as target cells for CTL and NK cell sensitivity, respectively. All data are represented as the mean of two independent experiments. GL261, mouse glioblastoma cell line; YAC-1, mouse lymphoma cell lines sensitive to the cytotoxic activity of naturally occurring killer cells in mice; Control, no treatment group; RT, radiation therapy; vaccine, branched multipeptide plus PADRE and poly-ICLC; *$p < 0.05$; **$p < 0.01$; and ***$p < 0.001$.

was higher in the RT only group than in the control group ($p < 0.001$); the RT plus vaccine group showed lower levels of IL-10 than the control ($p < 0.001$) and RT only ($p < 0.001$) groups. Moreover, adding anti-PD1 to the RT plus vaccine group led to the recovery of the IL-10 levels in the single tumor cells. However, this IL-10 level was lower than that observed with RT only ($p < 0.001$). Therefore, combination treatment with RT along with the vaccine and anti-PD1 showed potential to produce pro-inflammatory response in the tumor.

DISCUSSION

ErbB2 and WT1 are not only tumor associated antigens for immunological targeting (20, 21) but also biomarkers of cancer cell proliferation and survival, especially GBM (22–25). In this study, a branched multipeptide was synthesized on the basis of the high expression of tumor-associated antigens on GL261 cells. Moreover, RT also showed short- and long-term effects on the GL261 cell line *in vitro*. In particular, radiation affects GL261 cells by reducing ErbB2 expression after a short (24 h) period as evidenced by the decrease in the long-term survival and proliferation of GL261 cells *in vitro*. These data showed that GL261 cells have both immunological characteristics and radiosensitive activity. Moreover, radiation also resulted in delayed tumor growth in the mouse model. This was expected,

since the main therapeutic function is from radiation during early treatment stages. After a 24-h period, radiation starts to cause a delay in tumor proliferation and tumor cell death, resulting in the release of tumor-associated antigens for further immune response stimulation. The combination of RT with vaccines may bring about optimal results to further enhance the immune response in later treatment stages, when cancer cells recover and function normally.

The effectiveness of immune checkpoint blockade is hypothesized to require the expression of PDL1 on tumor cells and PD1 on peritumoral CTLs (26). In the present study, the expression of PD1 on T cell populations from splenocytes and single tumor cells and that of PDL1 on glioblastoma target cells and single tumor cells were confirmed to verify the efficiency of anti-PD1 treatment. Previous studies showed that the presence of the cytokine IFN-γ leads to enhanced PDL1 expression on tumors as a mechanism by which cancer cells protect themselves from T cell-mediated destruction (27–29). In the present study, anti-PD1 combined with RT plus vaccine also enhanced the levels of IFN-γ, which led to enhanced PDL1 expression in single tumor cells. Although our data showed enhanced IFN-γ levels in single tumor cells, this level was quite low; we are yet to clarify the source of the IFN-γ released by the tumor-infiltrating immune cells. The percentages of tumor-infiltrating CD45+CD3+ cells as well as tumor-infiltrating CD8+CD44+ T cells gated from CD45+CD3+ cells were quite low in this study.

FIGURE 7 | Pro-inflammatory and anti-inflammatory cytokine production in the culture media of single tumor cells was confirmed using ELISA. Pro-inflammatory cytokines such as IFN-γ **(A)** and anti-inflammatory cytokines such as IL-10 and TGF-β **(B,C)** were identified. While IFN-γ showed an increase, TGF-β was stable in all the treatment groups, and IL-10 showed different levels according to the different treatments. Data are summarized by bar charts as the mean ± standard deviation (SD). All data are represented as the mean of two independent experiments. Control, no treatment group; RT, radiation; vaccine, branched multipeptide plus PADRE and poly-ICLC; **$p < 0.01$; and ***$p < 0.001$; n.s., no significant difference.

There was no difference in the percentages of tumor-infiltrating $CD8^+CD44^+$ T cells observed between the different treatment groups, and no tumor-infiltrating $CD4^+CD44^+$ T cells gated from $CD45^+CD3^+$ cells were detected in our study (data not shown). The distribution of lymphoid lineage cells in lymph nodes and myeloid lineage cells was not clarified in this study. Therefore, these immune cells should be investigated in greater detail in future studies.

While PD1 blockade enhanced the cytotoxic efficacy of $CD8^+$ CTLs, it also enhanced the proliferation and immunosuppressive activity of Tregs in humans and mice (30, 31). Similarly, in our study, the addition of 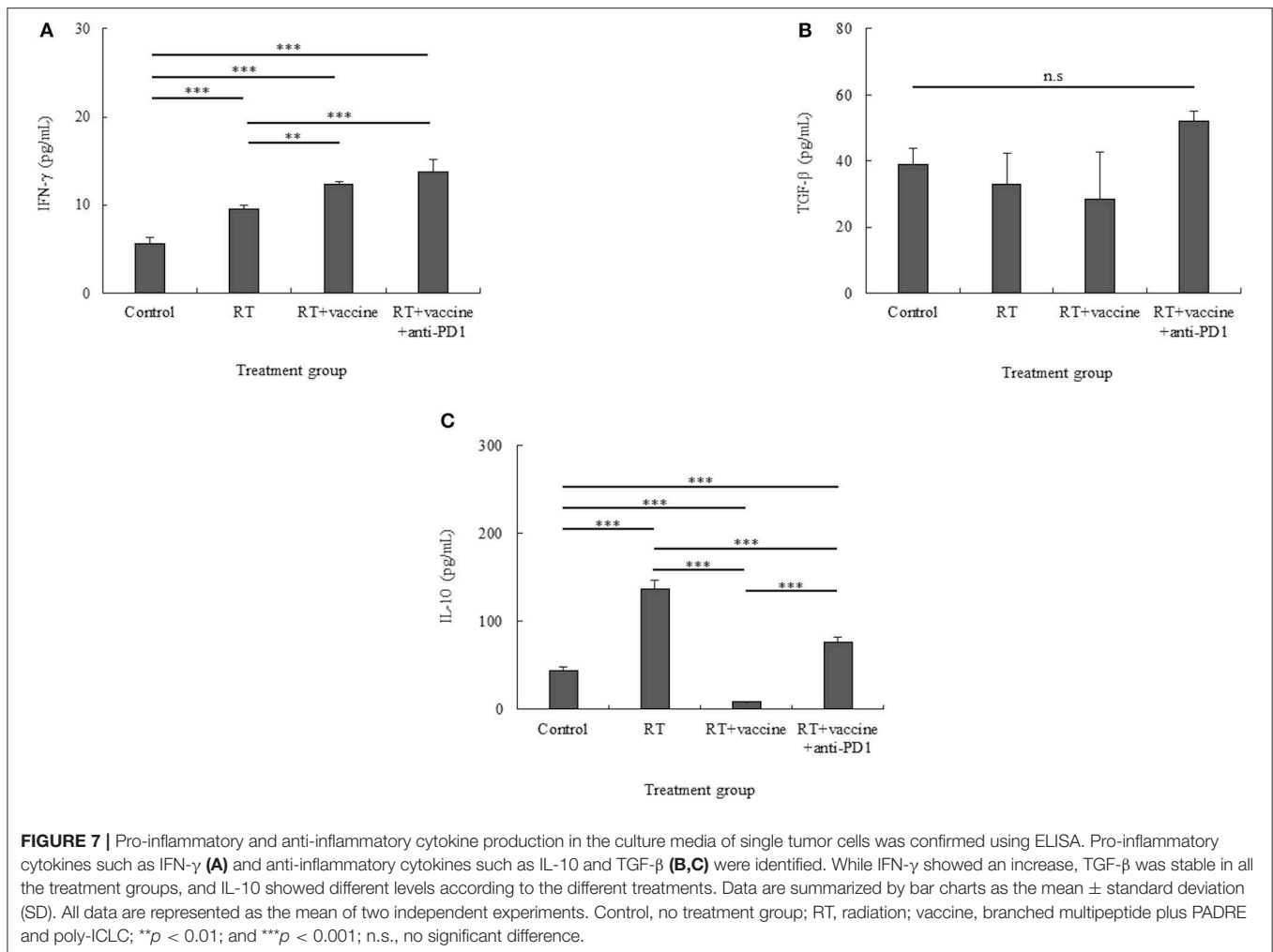anti-PD1 into the RT plus vaccine group also led to an increase in both the activated effector cells ($CD8^+$ T cells, $CD4^+$ T cells, NK cells, and memory T cells) and suppressor immune cells (Tregs) in the splenocytes. Although the percentages of Tregs were also enhanced by the addition of anti-PD1 in the RT plus vaccine group, RT plus vaccine and anti-PD1 therapy still showed a shift to effector immune cell function. In particular, the RT plus vaccine and anti-PD1 group showed the highest CTL and NK cell-mediated tumor cell-targeting immune response following prolonged mouse survival compared with the other treatment groups. In contrast, dendritic

cells were responsible for the uptake of tumor-associated antigens from the treated peptide vaccine or dying tumor cells induced by radiation. This led to DC maturation, which stimulated both the innate and adaptive immune systems. Mature DCs not only activate CTLs to target tumors but are also capable of activating NK cells by enhancing their cytotoxicity, IFN-γ production, and the crosstalk of NK cells; DCs also play an important role in the induction of the tumor-specific immune response against cancer (32, 33). Although our data showed an increase in both CTL and NK cell function targeting tumor cells, our results mainly support a shift in CTL activity rather than NK activity.

Cytokines play an important role in mediating and regulating the immune response. Examining both pro-inflammatory and anti-inflammatory cytokine levels is important while verifying cancer treatment effects (34, 35). In our data, although there were high levels of pro-inflammatory cytokines in the re-stimulated splenocytes (IL-12p70 and IFN-γ) and single tumor cells (IFN-γ), the levels of anti-inflammatory cytokines (IL-10) in the re-stimulated splenocytes and single tumor cells were also increased. We found that the IFN-γ released in the re-stimulated splenocytes mainly originated from $CD8^+$ T cells. Particularly,

the increase in IL-10 paralleled the increased percentage of Tregs in the re-stimulated splenocytes. Both TGF-β and IL-10 cytokines are known to be suppressive cytokines mainly released by Tregs, which may directly suppress effector T cells in the tumor microenvironment (36). While no difference in TGF-β was observed between all the treatment groups, IL-10 showed an increased level in single tumor cells. Similar patterns may occur in single tumor cells, whereby enhanced IL-10 increases the percentage of Tregs. However, Tregs in single tumor cells were not examined in our study. This supports the notion that enhanced Tregs may be related to enhanced IL-10, which subsequently resulted in no significant difference between RT plus vaccine and RT plus vaccine and anti-PD1. However, more experiments should be conducted to clarify this issue.

It is well-known that GBM has an unfavorable prognosis, mainly owing to its high propensity for tumor recurrence: more than 90% of patients show recurrence at the original tumor location and 5% develop multiple lesions after treatment (37). Enhanced effector memory T cell with RT plus vaccine and anti-PD1 have the potential to prevent GBM recurrence after treatment. RT plus vaccine and anti-PD1 is preferable in GBM treatment. However, the results of our study did not fully elucidate the exact manner in which this combination affected glioblastoma recurrence.

CONCLUSION

In this study, a branched multipeptide and adjuvants, such as PADRE and poly-ICLC, were used as components of a vaccine. Our study suggests that immunotherapy using this vaccine combined with anti-PD1 could be helpful for improving RT effects in a GBM mouse model.

DATA AVAILABILITY STATEMENT

The datasets generated in this study are available on request from the corresponding author.

ETHICS STATEMENT

This animal study was reviewed and approved by Chonnam National University Animal Research Committee.

AUTHOR CONTRIBUTIONS

T-A-TT, Y-HK, and T-YJ designed and performed the experiment. T-A-TT, Y-HK, and T-H-OD analyzed the data. T-A-TT and T-YJ wrote the article. SJ, I-YK, K-SM, W-YJ, H-JL, J-JL, and T-YJ contributed intellectually to the research.

SUPPLEMENTARY MATERIAL

The Supplementary Material for this article can be found online at: https://www.frontiersin.org/articles/10.3389/fimmu.2020.01165/full#supplementary-material

Figure S1 | Construction of the branched multipeptide. The branched multipeptide was designed by combining two single peptides (ErbB2$_{aa63-71}$ and WT1$_{aa235-243}$) that were restricted to H-2b. Mini-polyethylene glycol (mini-PEGs) spacers were used to create the corresponding branched multipeptide by incorporating two single MHC I peptides. These were designated as CYTWNQMNL-miniPEG2-K (TYLPANASL-miniPEG2) for the *in vivo* experiment.

Figure S2 | Specific antibodies against ErbB2, WT1, and PDL1 in the mouse GL261 cell line. Protein marker molecular weights are given in kDa. Full gel expression of ErbB2, WT1, and PDL1 against mouse GL261 cells was confirmed by western blot analysis **(A–D)**. Changes in the expression of these proteins before and after radiation with 2, 4, and 6 Gy was confirmed at 0 and 24 h. The estimated band was cut and presented **(E,F)**. β-Actin was used as an internal control in all the western blot experiments. GL261, mouse glioblastoma cell line.

Figure S3 | IFN-γ in the supernatant after membrane blocking for IFN-γ intracellular staining was confirmed using ELISA. Data are summarized by bar charts as the mean ± standard deviation (SD). All data are represented as the mean of two independent experiments. Control: no treatment group; RT: radiation; vaccine: branched multipeptide plus PADRE and poly-ICLC; n.s., no significant difference.

Figure S4 | The cytotoxic T lymphocyte (CTL)- and natural killer (NK) cell-mediated immune response of re-stimulated splenocytes from vaccinated mice. The IFN-γ secreted by re-stimulated splenocytes when co-cultured with target cancer cells was measured using the IFN-γ ELISPOT assay **(A)**, and the specific killing effects of re-stimulated splenocytes against target cells was estimated by the LDH assay **(B)**. The GL261 and YAC-1 cell lines were used as target cells for CTL and NK cell sensitivity, respectively. All data are represented as the mean of two independent experiments. Control, no treatment group; GL261, mouse glioblastoma cell line; YAC-1, mouse lymphoma cell lines sensitive to the cytotoxic activity of naturally occurring killer cells in mice; RT, radiation therapy; vaccine, branched multipeptide plus PADRE and poly-ICLC; *$p < 0.05$; **$p < 0.01$; and ***$p < 0.001$.

REFERENCES

1. Tamimi AF, Juweid M. Epidemiology and outcome of glioblastoma. In: De Vleeschouwer S, editor. *Glioblastoma*. Brisbane, QLD: Codon Publications (2017). doi: 10.15586/codon.glioblastoma.2017.ch8
2. Orth M, Lauber K, Niyazi M, Friedl AA, Li M, Maihöfer C, et al. Current concepts in clinical radiation oncology. *Radiat Environm Biophys*. (2014) 53:1–29. doi: 10.1007/s00411-013-0497-2
3. Ahmed MM, Hodge JW, Guha C, Bernhard EJ, Vikram B, Coleman CN. Harnessing the potential of radiation-induced immune modulation for cancer therapy. *Cancer Immunol Res*. (2013) 1:280–4. doi: 10.1158/2326-6066.CIR-13-0141
4. Ahmed MM, Guha C, Hodge JW, Jaffee E. Immunobiology of radiotherapy: new paradigms. *Radiat Res*. (2014) 182:123–5. doi: 10.1667/RR13849.1
5. Reznik E, Smith AW, Taube S, Mann J, Yondorf MZ, Parashar B, et al. Radiation and immunotherapy in high-grade gliomas where do we

stand? *Am J Clin Oncol*. (2018) 41:197–212. doi: 10.1097/COC.00000000000 00406

6. Chen ZH, Hambardzumyan D. Immune microenvironment in glioblastoma subtypes. *Front Immunol*. (2018) 9:1004. doi: 10.3389/fimmu.2018.01004

7. Kong ZR, Wang Y, Ma WB. Vaccination in the immunotherapy of glioblastoma. *Hum Vaccines Immunother*. (2018) 14:255–68. doi: 10.1080/21645515.2017.1388481

8. Cuoco JA, Benko MJ, Busch CM, Rogers CM, Prickett JT, Marvin EA. Vaccine-based immunotherapeutics for the treatment of glioblastoma: advances, challenges, and future perspectives. *World Neurosurg*. (2018) 120: 302–15. doi: 10.1016/j.wneu.2018.08.202

9. Coffman RL, Sher A, Seder RA. Vaccine adjuvants: putting innate immunity to work. *Immunity*. (2010) 33:492–503. doi: 10.1016/j.immuni.2010.10.002

10. Nezafat N, Ghasemi Y, Javadi G, Khoshnoud MJ, Omidinia E. A novel multi-epitope peptide vaccine against cancer: an *in silico* approach. *J Theor Biol*. (2014) 349:121–34. doi: 10.1016/j.jtbi.2014.01.018

11. Nezafat N, Sadraeian M, Rahbar MR, Khoshnoud MJ, Mohkam M, Gholami A, et al. Production of a novel multi-epitope peptide vaccine for cancer immunotherapy in TC-1 tumor-bearing mice. *Biologicals*. (2015) 43:11–7. doi: 10.1016/j.biologicals.2014.11.001

12. Zhu X, Nishimura F, Sasaki K, Fujita M, Dusak JE, Eguchi J, et al. Toll like receptor-3 ligand poly-ICLC promotes the efficacy of peripheral vaccinations with tumor antigen-derived peptide epitopes in murine CNS tumor models. *J Transl Med*. (2007) 5:10. doi: 10.1186/1479-5876-5-10

13. Salazar AM, Erlich RB, Mark A, Bhardwaj N, Herberman RB. Therapeutic in situ autovaccination against solid cancers with intratumoral poly-ICLC: case report, hypothesis, and clinical trial. *Cancer Immunol Res*. (2014) 2:720–4. doi: 10.1158/2326-6066.CIR-14-0024

14. Zhao J, Chen AX, Gartrell RD, Silverman AM, Aparicio L, Chu T, et al. Immune and genomic correlates of response to anti-PD-1 immunotherapy in glioblastoma. *Nat Med*. (2019) 25:462–9. doi: 10.1038/s41591-019-0449-8

15. Zeng J, See AP, Phallen J, Jackson CM, Belcaid Z, Ruzevick J, et al. Anti-PD-1 blockade and stereotactic radiation produce long-term survival in mice with intracranial gliomas. *Int J Radiat Oncol Biol Phys*. (2013) 86:343–9. doi: 10.1016/j.ijrobp.2012.12.025

16. Karyampudi L, Lamichhane P, Scheid AD, Kalli KR, Shreeder B, Krempski JW, et al. Accumulation of memory precursor CD8 T cells in regressing tumors following combination therapy with vaccine and anti-PD-1 antibody. *Cancer Res*. (2014) 74:2974–85. doi: 10.1158/0008-5472.CAN-13-2564

17. Okada H, Kalinski P, Ueda R, Hoji A, Kohanbash G, Donegan TE, et al. Induction of CD8+ T-cell responses against novel glioma-associated antigen peptides and clinical activity by vaccinations with {alpha}-type 1 polarized dendritic cells and polyinosinic-polycytidylic acid stabilized by lysine and carboxymethylcellulose in patients with recurrent malignant glioma. *J Clin Oncol*. (2011) 29:330–6. doi: 10.1200/JCO.2010. 30.7744

18. Sonabend AM, Velicu S, Ulasov IV, Han Y, Tyler B, Brem H, et al. A safety and efficacy study of local delivery of interleukin-12 transgene by PPC polymer in a model of experimental glioma. *Anticancer Drugs*. (2008) 19:133–42. doi: 10.1097/CAD.0b013e3282f24017

19. Zhu X, Fallert-Junecko BA, Fujita M, Ueda R, Kohanbash G, Kastenhuber ER, et al. Poly-ICLC promotes the infiltration of effector T cells into intracranial gliomas via induction of CXCL10 in IFN-alpha and IFN-gamma dependent manners. *Cancer Immunol Immunother*. (2010) 59:1401–9. doi: 10.1007/s00262-010-0876-3

20. Zhang C, Burger MC, Jennewein L, Genßler S, Schönfeld K, Zeiner P, et al. ErbB2/HER2-Specific NK Cells for targeted therapy of glioblastoma. *J Natl Cancer Inst*. (2016) 108:djv375. doi: 10.1093/jnci/djv375

21. Hashimoto N, Tsuboi A, Kagawa N, Chiba Y, Izumoto S, Kinoshita M, et al. Wilms tumor 1 peptide vaccination combined with temozolomide against newly diagnosed glioblastoma: safety and impact on immunological response. *Cancer Immunol Immunother*. (2015) 64:707–16. doi: 10.1007/s00262-015-1674-8

22. Clark PA, Iida M, Treisman DM, Kalluri H, Ezhilan S, Zorniak M, et al. Activation of multiple erbb family receptors mediates glioblastoma cancer stem-like cell resistance to EGFR-targeted inhibition. *Neoplasia*. (2012) 14:420–8. doi: 10.1596/neo.12432

23. Clark AJ, et al. Effect of WT1 gene silencing on the tumorigenicity of human glioblastoma multiforme cells laboratory investigation. *J Neurosurg*. (2010) 112:18–25. doi: 10.3171/2008.11.JNS08368

24. Iqbal N, Iqbal N. Human epidermal growth factor receptor 2 (HER2) in cancers: overexpression and therapeutic implications. *Mol Biol Int*. (2014) 2014:852748. doi: 10.1155/2014/852748

25. Kijima N, Hosen N, Kagawa N, Hashimoto N, Kinoshita M, Oji Y, et al. Wilms' tumor 1 is involved in tumorigenicity of glioblastoma by regulating cell proliferation and apoptosis. *Anticancer Res*. (2014) 34:61–7. Retrieved from http://ar.iiarjournals.org/content/34/1/61.full

26. Berghoff AS, Kiesel B, Widhalm G, Rajky O, Ricken G, Wöhrer A, et al. Programmed death ligand 1 expression and tumor-infiltrating lymphocytes in glioblastoma. *Neuro Oncol*. (2015) 17:1064–75. doi: 10.1093/neuonc/n ou307

27. Ribas A. Adaptive immune resistance: how cancer protects from immune attack. *Cancer Discov*. (2015) 5:915–9. doi: 10.1158/2159-8290.CD-15-0563

28. Pardoll DM. The blockade of immune checkpoints in cancer immunotherapy. *Nat Rev Cancer*. (2012) 12:252–64. doi: 10.1038/nrc3239

29. Benci JL, Xu B, Qiu Y, Wu TJ, Dada H, Twyman-Saint Victor C, et al. Tumor interferon signaling regulates a multigenic resistance program to immune checkpoint blockade. *Cell*. (2016) 167:1540–54. e12. doi: 10.1016/j.cell.2016.11.022

30. Kumar R, Yu F, Zhen YH, Li B, Wang J, Yang Y, et al. PD-1 blockade restores impaired function of *ex vivo* expanded CD8+T cells and enhances apoptosis in mismatch repair deficient EpCACAM+PD-L1+cancer cells. *Onco Targets Ther*. (2017) 10:3453–65. doi: 10.2147/OTT.S130131

31. Kamada T, Togashi Y, Tay C, Ha D, Sasaki A, Nakamura Y, et al. PD-1(+) regulatory T cells amplified by PD-1 blockade promote hyperprogression of cancer. *Proc Natl Acad Sci USA*. (2019) 116:9999–10008. doi: 10.1073/pnas.1822001116

32. Jacobs B, Ullrich E. The interaction of NK cells and dendritic cells in the tumor environment: how to enforce NK cell & DC action under immunosuppressive conditions? *Curr Med Chem*. (2012) 19:1771–9. doi: 10.2174/092986712800099857

33. Harizi H. Reciprocal crosstalk between dendritic cells and natural killer cells under the effects of PGE2 in immunity and immunopathology. *Cell Mol Immunol*. (2013) 10:213–21. doi: 10.1038/cmi.2013.1

34. Grivennikov SI, Greten FR, Karin M. Immunity, inflammation, and cancer. *Cell*. (2010) 140:883–99. doi: 10.1016/j.cell.2010.01.025

35. Qu X, Tang Y, Hua S. Immunological approaches towards cancer and inflammation: a cross talk. *Front Immunol*. (2018) 9:563. doi: 10.3389/fimmu.2018.00563

36. Munn DH, Bronte V. Immune suppressive mechanisms in the tumor microenvironment. *Curr Opin Immunol*. (2016) 39:1–6. doi: 10.1016/j.coi.2015.10.009

37. Roy S, Lahiri D, Maji T, Biswas J. Recurrent glioblastoma: where we stand. *South Asian J Cancer*. (2015) 4:163–73. doi: 10.4103/2278-330X.175953

Long-Term Survival of Patients With Chemotherapy-Naïve Metastatic Nasopharyngeal Carcinoma Receiving Cetuximab Plus Docetaxel and Cisplatin Regimen

Mengping Zhang [1,2†], He Huang [1†], Xueying Li [1,3†], Ying Huang [4†], Chunyan Chen [4], Xiaojie Fang [1], Zhao Wang [1], Chengcheng Guo [1], Sioteng Lam [1,5], Xiaohong Fu [1,6], Huangming Hong [1], Ying Tian [1], Taixiang Lu [4] and Tongyu Lin [1*]

[1] State Key Laboratory of Oncology in South China, Collaborative Innovation Center for Cancer Medicine, Department of Medical Oncology, Sun Yat-sen University Cancer Center, Guangzhou, China, [2] Department of Oncology, The First Affiliated Hospital of Sun Yat-sen University, Guangzhou, China, [3] Department of Medical Oncology, The Seventh Affiliated Hospital, Sun Yat-sen University, Shenzhen, China, [4] State Key Laboratory of Oncology in South China, Collaborative Innovation Center for Cancer Medicine, Department of Radiation Oncology, Sun Yat-sen University Cancer Center, Guangzhou, China, [5] Centro Hospitalar Conde de Sáo Januário, Macau, China, [6] Department of Oncology, Shenzhen Nanshan Hospital, Shenzhen, China

Purpose: Metastatic nasopharyngeal carcinoma (mNPC) remains incurable. This prospective study aimed to investigate whether adding cetuximab to cisplatin-based induction therapy could improve efficacy and survival for chemotherapy-naïve mNPC patients.

Patients and Methods: Eligible chemotherapy-naïve mNPC patients were enrolled, including those initially diagnosed with mNPC (IM) and those with first-relapse metastases after radiotherapy (RM). Patients all received induction chemotherapy (IC) including docetaxel and cisplatin plus cetuximab. Those who obtained objective remission after IC would continue to receive radiotherapy concurrent with cetuximab and cisplatin, and further capecitabine as maintenance. Contemporaneous patients who received conventional therapy served as controls.

Results: Forty-three patients were enrolled, including 17 IM and 26 RM patients. Thirty-nine (90.7%) patients had WHO III subtype. The overall response and complete response (CR) rates were, respectively, 79.1 and 34.9% after induction therapy and 76.7 and 46.5% after chemoradiotherapy. The 5-year overall survival (OS) and progression-free survival (PFS) rates reached 34.9 and 30%, respectively. Subgroup analysis showed that compared with RM patients, IM patients had a higher 5-year OS (58.8 vs. 19.2%) and PFS (52.9 vs. 19.2%). The IM group had a higher CR rate of induction treatment than the RM group (52.9 vs. 23.1%). No treatment-related death was observed. Twelve patients (27.9%) remained alive with disease-free survival times from 60+ to 135+ months. Control patients showed a substantially lower survival rate (5-year OS, 10.9%) and few long-term survivors.

Conclusions: This regimen resulted in significantly improved efficacy and survival, which indicates a potentially curative role for chemotherapy-naïve mNPC, especially in newly diagnosed patients. A phase III clinical trial (NCT02633176) is ongoing for confirmation.

Keywords: survival, chemotherapy, metastatic nasopharyngeal carcinoma, cetuximab, induction therapy

INTRODUCTION

Nasopharyngeal carcinoma (NPC) is epidemic in southern China and Southeast Asia (1). Additionally, ~25–30% of NPC patients exhibit metastatic disease (2), and 15% of all NPC patients present with distant metastases at primary diagnosis (3). The outcomes of patients with metastatic NPC (mNPC) are heterogeneous, and long-term survival is possible in very few patients (4). On the basis of high-level evidence, patients with recurrent or primary mNPC generally have very poor survival, with a median overall survival of 11.5–15 months reported 10 years ago (5, 6) and a median survival of 29.1 months reported in 2016 (7). Generally, mNPC is recognized as an incurable disease, as few patients survive beyond 5 years.

Platinum-containing doublet regimens or concurrent chemoradiotherapy (CCRT) alone or induction chemotherapy followed by chemoradiotherapy continue to be regarded as standard first-line treatments for patients with recurrent or metastatic NPC. Gemcitabine, capecitabine, paclitaxel, and docetaxel have also been combined with cisplatin and yield similar survival (8, 9). However, no randomized trials have defined the optimum regimens.

Cetuximab is an IgG1 monoclonal antibody that inhibits ligand binding to the epidermal growth factor receptor (EGFR) (10). EGFR expression is reported in more than 85% of undifferentiated NPCs and is associated with a poor clinical outcome (11). Radiotherapy and platinum-based chemotherapy plus cetuximab have enhanced activity against head and neck cancer, with improved overall survival (OS) (12, 13). Although distinct differences exist between NPC and other head and neck cancers, despite originating from a similar cell or tissue lineage, we speculated that adding an EGFR inhibitor to platinum-based chemotherapy and CCRT could be beneficial for mNPC. Moreover, a phase 2 study of cetuximab in combination with a cytotoxic agent showed clinical activity and an acceptable safety profile in heavily pretreated patients with mNPC (14).

A meta-analysis of 11 randomized trials showed that longer first-line chemotherapy is associated with longer OS (15). However, prolongation of docetaxel or cisplatin exposure until disease progression is unrealistic because of cumulative toxic effects. Therefore, switching to a more tolerable chemotherapy, such as capecitabine, as a maintenance regimen might be a more effective treatment strategy.

We therefore conducted this single-center, prospective study of an epidermal growth factor receptor antibody (cetuximab)-containing induction therapy and chemoradiotherapy regimen to investigate whether it would significantly improve survival outcomes while maintaining tolerability in mNPC patients without prior systemic therapy and would alter the therapeutic modality from conventional palliative to curative treatment.

METHODS

Study Design and Patients

We performed an investigator-initiated, open-label, single arm, single center, phase 2 trial at Sun Yat-sen University Cancer Center, Guangzhou, China. Eligible participants were 18 to 65 years of age and had histologically confirmed mNPC, including initial diagnosed NPC with metastases (IM) and first-relapse metastases after curative radiotherapy without neoadjuvant or adjuvant chemotherapy (RM). Pretreatment staging and metastases were confirmed via positron emission tomography/computerized tomography scans (PET/CT). Eligible patients had a type II or III histological subtype according to the WHO classification. Other eligibility criteria were as follows: patients had not received any previous systemic chemotherapy for recurrent or metastatic disease; had an Eastern Cooperative Oncology Group (ECOG) performance status of 0 or 1; had not received previous treatment with any investigational drug, surgery, irradiation or other anticancer therapies within the prior 4 weeks; had no known brain metastases; had adequate organ function as defined by adequate bone marrow function (hemoglobin$\geq$90 g/L, WBC count$\geq$3 $\times$ 10^9/L, platelet count$\geq$100 $\times$ 10^9/L), renal function (serum creatinine$\leq$140 μmol/L or calculated creatinine clearance$\geq$40 mL/min), and liver function (ALT or AST$\leq$3$\times$ the upper limit of normal, bilirubin$\leq$2$\times$ the upper limit of normal); had no uncontrolled cardiac or other disease with life expectancy of 3 months or more; provided written informed consent; and was amenable for regular follow-up. The study protocol was approved by the ethics committee of Sun Yat-sen University Cancer Center.

Procedures

The induction chemotherapy regimen was repeated every 3 weeks and comprised the following: intravenous docetaxel 75 mg/m^2 day 1; cisplatin at 25 mg/m^2 on days 1, 2, and 3; and cetuximab at 250 mg/m^2 on days 0, 7, and 14 with an initial dose of 400 mg/m^2. This induction regimen was followed by CCRT consisting of intensity-modulated radiotherapy (IMRT) plus concomitant cetuximab (250 mg/m^2/week for 6 cycles) and cisplatin (75 mg/m^2/3 weeks for 2 cycles). IMRT was given at 68–70 Gy over 30 daily fractions over 6 weeks to the planning target volume of the existing primary tumor in IM patients, or 64–66 Gy in RM patients with previous radiotherapy, with additional radiotherapy of 62–66 Gy over 30 fractions to metastatic regional neck nodes if indicated. After CCRT, capecitabine was continued

as maintenance therapy (cycles were repeated every 21 days with 1,000 mg/m^2 twice daily, days 1 through 14).

Patients received this induction therapy regimen for a maximum of six cycles or until disease progression, death, intolerable toxicities, or patient request to stop. Furthermore, only patients who obtained complete or partial responses (CR or PR) after induction therapy could receive CCRT. For patients with locoregional metastatic bone lesions, additional radiotherapy with 30–40 Gy in 10–20 fractions to these sites of lesions was performed. Patients with other residual metastatic foci in lung, liver, and non-cervical lymph nodes after induction therapy that was amenable to local therapy were offered surgery or radiofrequency ablation before CCRT. For patients who exhibited a CR after CCRT, maintenance therapy was continued for up to 3 years or until unacceptable toxicity, disease progression, or death.

Treatment-emergent adverse events (AEs) were assessed with the Common Terminology Criteria for Adverse Events version

3.0 and were noted separately for the induction, CCRT, and maintenance treatment. The indications for cetuximab dose adjustment or interruption were described previously (14). The chemotherapy was continued independent of any temporary interruption of cetuximab. Cetuximab was not withheld for chemotherapy-related toxicities, unless the patient developed a concomitant illness that, in the opinion of the investigator, mandated interruption of therapy.

Tumor response was assessed by CT imaging according to RECIST version 1.1 by the independent image committee every two cycles during induction therapy and every 3 weeks during CCRT. CR and PR were defined, respectively, as 100% or at least 30% decrease in the sum of the longest diameters of target lesions compared with baseline. Follow-up was performed at the outpatient clinic every 1–3 months for the first year, every 3 months for the second year, every 6 months for the third to fifth years, and annually thereafter.

Outcomes

The primary objective was to determine progression-free survival (PFS), which was defined as the time from treatment initiation

TABLE 1 | Demographic and clinical characteristics.

Characteristics	NO. (%)
NO.	43
Gender	
Female	7 (16.3)
Male	36 (83.7)
Age, years*	
Median	43
Range	23-63
ECOG performance status	
0	14 (32.6)
1	29 (67.4)
Histology	
WHO type 2	4 (9.3)
WHO type 3	39 (90.7)
EBV-DNA status	
Positive*	32 (74.4)
Negative	11 (25.6)
Number of metastatic organs	
1	27 (62.8)
2	8 (18.6)
≥3	8 (18.6)
Sites of disease at registration	
Distant lymph node	7 (16.3)
Bone	32 (74.4)
Liver	14 (32.6)
Lung	11 (25.6)
Others	6 (14.0)
Prior radiotherapy	
Yes	26 (60.5)
No	17 (39.5)

Data are presented as a number (percentage) unless otherwise indicated. *Positive: EBV-DNA copies $\geq 10^3$ copies/mL.

TABLE 2 | Antitumor efficacy.

Variable	IM (n = 17)	RM (n = 26)	Overall (n = 43)
Response after induction chemotherapy, n (%)			
Complete response	9 (52.9)	6 (23.1)	15 (34.9)
Partial response	7 (41.2)	12 (46.2)	19 (44.2)
Stable disease	0 (0)	6 (23.1)	6 (14.0)
Progressive disease	1 (5.9)	2 (7.7)	3 (7.0)
Overall response, % [95% CI])	94.1 [82.9–100]	69.2 [51.5–87]	79.1 [66.9–91.2]
Disease control	94.1 [82.9–100]	92.3 [82.1–100]	93 [85.4–100]
Response after chemoradiotherapy, n (%)			
Complete response	12 (70.6)	8 (30.8)	20 (46.5)
Partial response	4 (23.5)	9 (34.6)	13 (30.2)
Stable disease	0 (0)	6 (23.1)	6 (14.0)
Progressive disease	1 (5.9)	3 (11.5)	4 (9.3)
Overall survival			
Median, months [95% CI]	Unreached*	20.3 [13.3–37.6]	32.9 [18.2–47.5]
2-year rate, %	88.2	42.3	60.5
5-year rate, %	58.8	19.2	34.9
Progression-free survival			
Median, months [95% CI]	Unreached*	12.5 [7.9–17.1]	18.3 [10.6–26.0]
2-year rate, %	58.8	30.8	41.9
5-year rate, %	52.9	19.2	30.0

*Indicates that the IM subgroup significantly differed from RM subgroup; CI, confidence interval.

to disease progression or death from any cause, whichever came first. Secondary endpoints included the proportion of patients who had a confirmed overall response (OR) (defined as CR or PR lasting at least 4 weeks according to the RECIST 1.1), OS (defined as the time from treatment initiation to the date of death or last follow-up), and AEs. Patients were considered long-term survivors if they were disease-free for a period of more than 60 months without any treatment except maintenance treatment after a CR.

Statistical Analyses

The asymptotic distribution, provided in Lachin [(16), p. 409–411] was used to calculate the sample size for this single arm trial. The justification for the sample size is explained below. The two-sides Type I error rate was set at 5%, and the type II error rate set at 20%, giving 80% power. The accrual period was set at 1 year, and the total study period was set at 2 years. The OS rate at 1 year, based upon a previous study (17), is as high as 60% among patients treated with platinum-based therapy. Among patients receiving the novel regimen, the 1-year OS rate was expected to increase to 80%. This difference of 20% equates to a hazard ratio of 0.44. The sample size calculation, given the above information, estimates that 12 events were needed. Finally, it was estimated that 25 patients were required to achieve this number of events allowing for a 10% loss to follow-up/non-adherence rate.

PFS and OS were estimated using the Kaplan-Meier method. Hazard ratios were calculated by the use of the Cox proportional-hazards model. The response rate and its 95% CI (using the method of Pearson and Clopper) were calculated. We performed subgroup analyses among subgroups between mNPC patients with IM and RM for OS and PFS and response rate. We performed *post-hoc* subgroup analyses for OS and PFS, focusing on CR after induction therapy. We calculated the median follow-up time as the median of all enrolled patients, irrespective of whether the patients had died (18). Descriptive statistics were used for safety evaluations. All statistical testing was two-sided
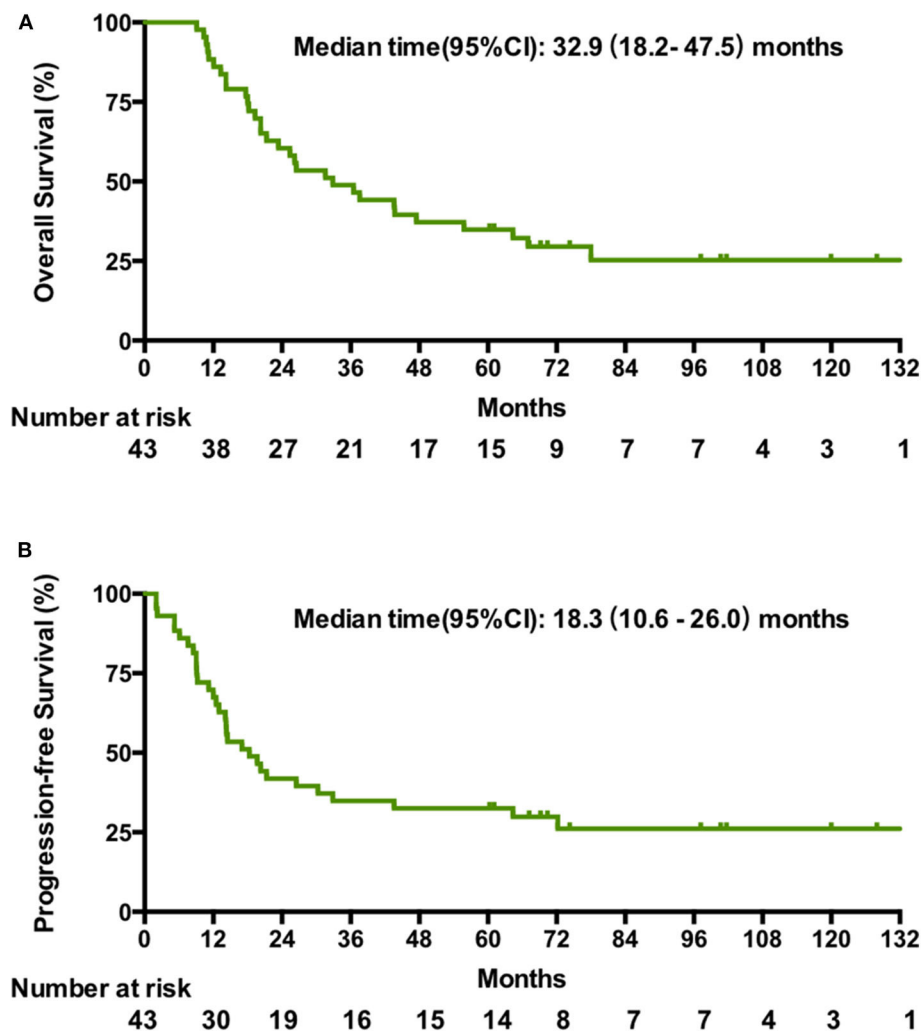

FIGURE 1 | Kaplan-Meier estimates of the overall OS **(A)** and PFS **(B)** in patients treated with the novel regimen.

at the nominal 5% significance level. All analyses were performed with SPSS 13.0.

RESULTS

Between July 2006 and December 2014, we enrolled 43 patients, 17 (39.5%) with initial diagnosis of NPC with metastases (IM) and 26 (60.5%) with first-relapse metastases (RM). All patients had evidence of EGFR-positive NPC. **Table 1** summarizes the baseline characteristics of all 43 enrolled patients.

After the completion of induction chemotherapy, median cycles given to patients were 5 cycles (IQR 4–6). The OR rate was 79.1%, and 15 of 43 patients (34.9%) had a CR at all disease sites. Cetuximab was interrupted in 5 patients (11.6%) due to grade 3 acneiform skin rash. Six (13.9%) required a dose reduction of cisplatin or docetaxel during induction therapy due to serious myelosuppressive toxicity. Thirty-four patients obtained a CR or PR after induction chemotherapy, including 16 IM patients and 18 RM patients, and went on to receive CCRT; the OR and CR rates after CCRT were 76.7 and 46.5%, respectively (**Table 2**). Due to drug-related toxicity or patient refusal, only 15 patients received capecitabine as maintenance following CR after CCRT, among which 5 patients had disease progression during this period.

The cutoff date for survival analysis was July 30, 2018. The median follow-up time for survival was 89 months (range, 32–135). During follow-up, 31 patients had disease progression and finally died. After documented SD or PD during treatment or follow-up period, patients received second-line or third-line chemotherapy or palliative radiotherapy or did not receive any antitumor therapy. The median OS was 32.9 months (95% CI, 18.2–47.5). Kaplan-Meier estimated OS rates at 6 months, 1, 2, 3, and 5 years were 100, 86, 60.5, 46.4, and 34.9% respectively (**Figure 1A**). The median PFS was 18.3 months (95% CI, 10.6–26 months). The PFS at 6 months, 1, 2, 3, and 5 years was 86, 67.4,

41.9, 34.9, and 30% respectively (**Figure 1B**). Contemporaneous patients in the same hospital received conventional regimen showed poorer survival: for OS, median OS, 21 mo, 95% CI, 17.8–24.0, HR = 2.1, 95% CI, 1.3–3.3; for PFS, median PFS, 8 mo, 95% CI, 6.4–9.6 mo, HR = 3.3, 95% CI, 2.1–5.3 (**Supplement Figure 1**). The baseline data of the two groups were comparable which were showed in the **Supplement Table 1**.

With regard to the cutoff date, there were 15 long-term survivors who were disease-free for more than 60 months without treatment after obtaining a CR during the novel treatment. Among these 15 patients, 12 patients were still alive with no evidence of disease after treatment with a disease-free survival time from 60+ to 135+ months, as shown in **Table 3** and **Figure 2**; two patients died of disease progression while in CR at 64 and 72 months after treatment; and one patient died of acute leukemia at 64 months after treatment.

AEs are shown in **Table 4**. During induction therapy, the most common AEs ≥ grade 3 were leucopenia (39.5%), acne-like rash (11.6%), febrile neutropenia (14%), and thrombocytopenia (9.3%). Frequent grade 3/4 toxicities exceeded 10% of patients during CCRT, including oral mucositis (39.1%), dermatitis (in-field) (26.1%), leukopenia (17.4%), acne-like rash (13%), and thrombocytopenia (13%). Severe (i.e., grade 3/4) toxicities during maintenance treatment were rare, including hand-foot skin reactions in one patient and hyperbilirubinemia in one patient, and these 2 patients discontinued treatment because of the toxic effects. No patients died during treatment or within 30 days of completion of CCRT. Except for some acne-like rash in patients with the novel regimen but not in patients with conventional regimens, the novel regimen did not result in increased AEs according to the toxicities grade classification.

The median OS was unreached (95% CI undefined; eight events) in patients with IM and was 20.3 months (95% CI, 13.8–26.8; 23 events) in patients with RM (HR, 3.4; 95% CI, 1.6–6.6, p = 0.0013; **Figure 3A**). In patients with IM, the median PFS was more than 44 months (eight events; [51.5% of deaths were in 44

TABLE 3 | Characters and survival outcome of long-term disease-free survivors.

Patient	Gender	Age	Group	Metastatic sites	EBV status	Response of introduction treatment	Disease-free survival time (months)
1	Male	63	IM	Bone	Negative	CR	102
2	Female	48	IM	Bone, liver, lung	Positive	CR	120
3	Female	43	IM	Lung	Negative	CR	61
4	Female	63	IM	Bone, distant lymph node, pelvic	Positive	CR	70
5	Female	46	IM	Bone	Negative	CR	69
6	Male	46	IM	Bone	Positive	CR	67
7	Male	43	IM	Bone	Negative	CR	60
8	Male	45	IM	Bone	Negative	PR	74
9	Male	23	RM	Bone, lung	Positive	CR	128
10	Male	36	RM	Bone, lung, pleura	Negative	CR	101
11	Male	43	RM	Lung	Negative	CR	97
12	Male	40	IM	Liver, lung	Negative	CR	135
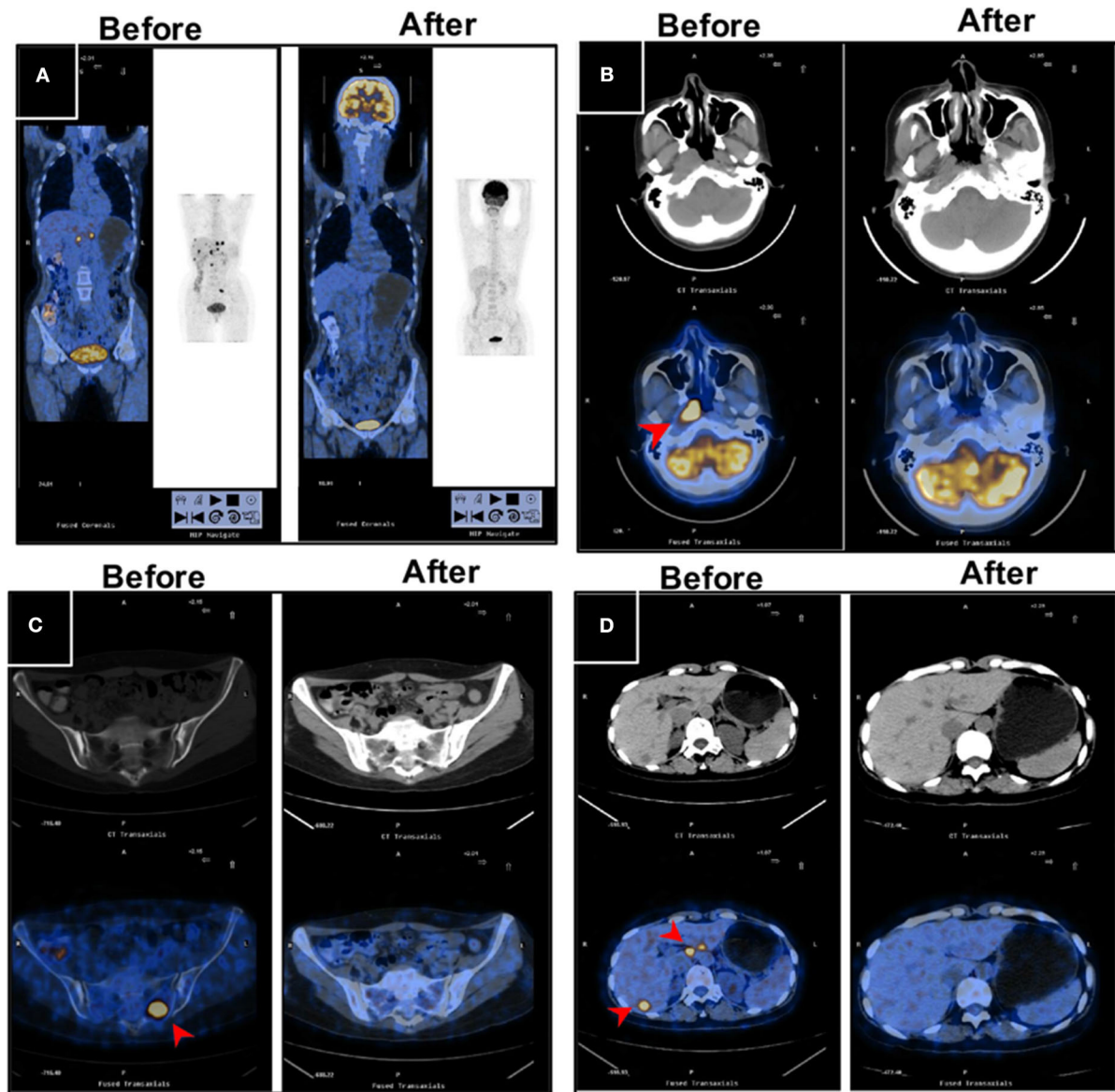
FIGURE 2 | PET/CT images for a long-term disease-free patient before and after the novel regimen. The female patient, 48 years of age, with an initial diagnosis of nasopharyngeal carcinoma with bone and liver metastases, EBV+, survived without disease for more than 120 months. **(A)** The systemic lesions, **(B)** the primary nasopharyngeal tumors, **(C)** the bone metastases, and **(D)** the liver metastases disappeared or decreased after treatment compared with before treatment.

mo]) vs. 12.5 months (95% CI, 11.2–17.0; 23 events) in patients with RM (HR, 2.7, 95% CI, 1.3–5.2; $p = 0.009$; **Figure 3B**).

Post-hoc analysis showed that the IM group had a higher CR rate (9/17, 52.9%; 95% CI, 29.2–76.7%) compared with 23.1% (6/26; 95% CI, 6.9–39.3%) in RM patients ($p = 0.045$). Indeed, the 15 patients with a CR had a significant longer OS than these patients without a CR after induction chemotherapy (median OS, undefined vs. 20.3 months [95% CI, 15–25.6], $p < 0.001$), with a better OS at 2 years (93.3 vs. 42.9%) and 5 years (82.2 vs. 7.1%) and a lower risk of death (HR, 8.3, 95% CI, 3.5–14.5, $p < 0.000$; **Figure 4A**). Correspondingly, these patients also exhibited a better PFS (median PFS, undefined vs. 14.1 months

[95% CI 11.8–16.4], HR 7.1, 95% CI, 2.7–10.9, $p < 0.0001$) and a higher 2-year PFS (80 vs. 21.4%) and 5-year PFS (80 vs. 7.1%) (**Figure 4B**).

DISCUSSION

Despite advances in radiotherapy and effective systemic agents during the past decade, the long-term survival of patients with mNPC remains poor. The standard first-line treatment of platinum-containing doublet regimens for mNPC is essentially palliative therapy. This new therapeutic strategy in our study

TABLE 4 | Adverse events during different periods of treatment in the study group.

Toxicity	Induction (N = 43)		CCRT (N = 34)		Maintenance (N = 15)	
	Any grade	Grade ≥ 3	Any grade	Grade ≥ 3	Any grade	Grade ≥ 3
Leukopenia	31 (72.1)	17 (39.5)	16 (47.1)	6 (17.6)	1 (6.0)	0
Acne-like rash	19 (44.2)	5 (11.6)	10 (29.4)	4 (11.8)	2 (13.3)	0
Dermatitis (in-field)	0	0	20 (58.8)	8 (23.5)	0	0
Nausea	18 (41.9)	0	6 (17.6)	3 (8.8)	2 (13.3)	0
Vomiting	6 (14.0)	0	3 (8.8)	2 (5.9)	1 (6.0)	0
Oral mucositis	8 (18.6)	0	22 (64.7)	13 (38.2)	2 (13.3)	0
Febrile neutropenia	6 (14.0)	6 (14.0)	4 (11.8)	3 (8.8)	0	0
Hyperbilirubinemia	3 (7.0)	0	2 (5.9)	0	2 (13.3)	1 (6.0)
Infusion reaction	3 (7.0)	0	0	0	0	0
Infection	2 (4.7)	0	6 (17.6)	2 (5.9)	0	0
Diarrhea	4 (9.3)	0	3 (8.8)	0	1 (6.0)	0
Premature heartbeat	1 (2.3)	0	1 (2.9)	0	0	0
Alopecia	10 (23.3)	0	5 (14.7)	1 (2.9)	0	0
Thrombocytopenia	5 (11.6)	4 (9.3)	6 (17.6)	4 (11.8)	0	0
Transaminitis	2 (4.7)	0	4 (11.8)	0	1 (6.0)	0
Anemia	3 (7.0)	1 (2.3)	6 (17.6)	3 (8.8)	0	0
Hypokalemia	2 (4.7)	0	2 (5.9)	1 (2.9)	1 (6.0)	0
Peripheral neuropathy	0	0	17 (50.0)	1 (2.9)	1 (6.0)	0
Hand-foot skin reaction	0	0	0	0	4 (26.7)	1 (6.0)
Dysphagia	0	0	12 (35.3%)	7 (20.6)		

yielded significantly long durations of OS and PFS (5-year OS, 33.2%; 5-year PFS, 29%). Moreover, further subgroup analyses suggested that patients who were not pretreated with radiotherapy achieved better outcomes than radiotherapy-pretreated patients. The 5-year OS and PFS were 54.4 and 51.5% in initially diagnosed mNPC patients, respectively. This finding may be associated with the history of radiotherapy. Previous ionizing radiation may increase chemotherapy resistance, as confirmed in prostate cancer and chronic myeloid leukemia (19, 20). A low survival rate in the contemporaneous controls was observed in our center (5-year OS, 10.9%; 5-year PFS, 0%), which was in accordance with previous reports. The favorable outcome of the novel regimen indicates the possible opportunity to completely cure chemotherapy-naïve mNPC, especially in patients with IM.

A long survival time is particularly prominent for patients who achieve a CR or PR of metastatic lesions after systemic chemotherapy (21). One study analyzed these different treatment combinations (induction, concurrent, and maintenance chemotherapy) and found that only induction-based chemotherapy was associated with significantly improved survival (22). In our study, the OR and CR rates after induction chemotherapy were 79.1 and 34.9%, respectively. Furthermore, 94% of patients with IMs achieved objective remission, and more than half of them exhibited CR after induction chemotherapy. Induction therapy consisting of cetuximab plus cisplatin and docetaxel in the regimen conferred a significant improvement in the response rate, especially the CR rate, vs. historic controls (OR rate, 60–74%; CR rate, 3–7%) (9) and contemporaneous controls

(OR rate, 47%; CR rate, 3%) in our center. These results imply that adding cetuximab to induction chemotherapy improved chemotherapy outcomes. In fact, anti-EGFR monoclonal antibody therapy can improve the effect of chemotherapy or reverse resistance to the chemotherapy agent. Cetuximab was shown in a previous study to circumvent irinotecan resistance in irinotecan-refractory colorectal cancer (23). In metastatic/recurrent head and neck squamous-cell carcinoma (HNSCC) or squamous-cell lung cancer, the addition of these molecular-targeted agents, such as cetuximab, nimotuzumab, panitumumab, necitumumab, to platinum-based chemotherapy also improves the response rate and survival (13, 24–27). Chan et al. found a dose-dependent additive enhanced antitumor activity when cetuximab was combined with cisplatin or taxanes in NPC cell lines (28) and then confirmed its clinical activity in combination with carboplatin in heavily pretreated patients with mNPC (14).

Several studies have shown that radiotherapy to the primary tumor site combined with active systematic therapy can improve the survival of patients with stage IVc NPC (29, 30). Anti-EGFR-targeted agents have been demonstrated to improve the effect of chemoradiotherapy or to reverse radiotherapy resistance (12, 31, 32). The multicenter ENCORE study (33) and a phase 2 study (31) in Hong Kong Prince of Wales Hospital both showed prolonged 2-year PFS beyond 85% compared with historic data in patients with locoregional advanced NPC who received cetuximab-added chemoradiotherapy. During our study, among 34 patients who attained an objective response after induction therapy and continued to receive CCRT, 33
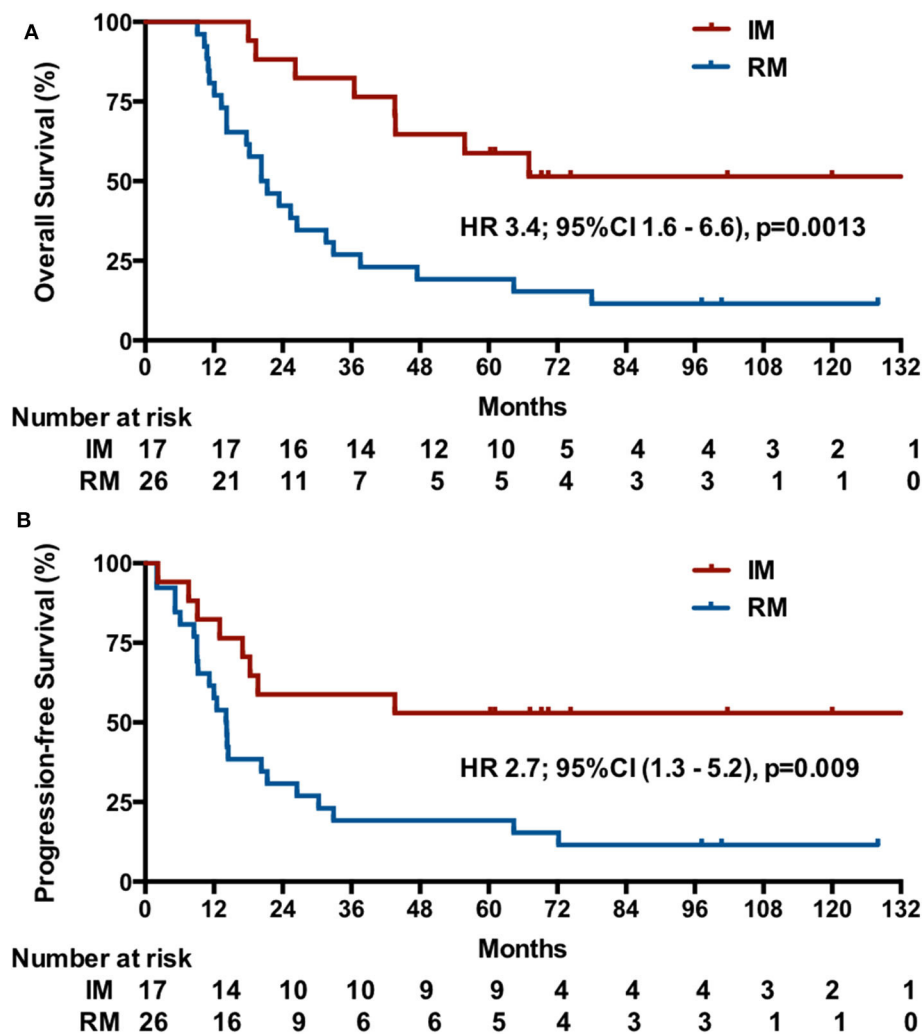
FIGURE 3 | Kaplan-Meier estimates of OS **(A)** and PFS **(B)** among patients initially diagnosed with mNPC (IM) or NPC patients with first-relapse metastases after radiotherapy (RM).

achieved further remission, and one case exhibited PD. Another anti-EGFR humanized antibody, nimotuzumab, also provided survival benefit when used concurrently with chemoradiotherapy in HNSCC (34, 35). Nevertheless, the addition of panitumumab to CCRT did not confer any benefit in HNSCC (36). The role of these EGFR antagonists in mNPC needs to be assessed in the future. The investigations in the studies above have demonstrated the safety and tolerability of cetuximab in patients with locoregionally advanced or recurrent and/or metastatic NPC. However, our study is the first to explore the addition of cetuximab to two processes of one regimen, i.e., induction and chemoradiation. There were few grade 3 skin reactions and no treatment-related mortalities or discontinuations of therapy reported during the entire treatment period. Importantly, in the last years local therapy of oligometastatic disease shows improvement of overall survival in several types of cancer. In

our study patients also underwent local therapy of metastatic disease whenever possible. Therefore, not only systemic therapy but also local therapy may improve the overall survival. However, it required a further study to confirm the function of local therapy for residual metastatic foci after induction therapy.

In the present study we selected capecitabine but not cetuximab as maintenance therapy based on the following reasons: first, at present, fluorouracil or capecitabine plus cisplatin is one of the widely used regimens in patients with recurrent or metastatic NPC. Moreover, single-agent capecitabine as a maintenance treatment has already shown a favorable safety profile in other metastatic cancers (37, 38). Second, based on our clinical trial initiated by investigator rather than a company-sponsored study, it is difficult for most patients to afford the high cost of cetuximab for a long maintenance therapy. Last, capecitabine is more convenient for
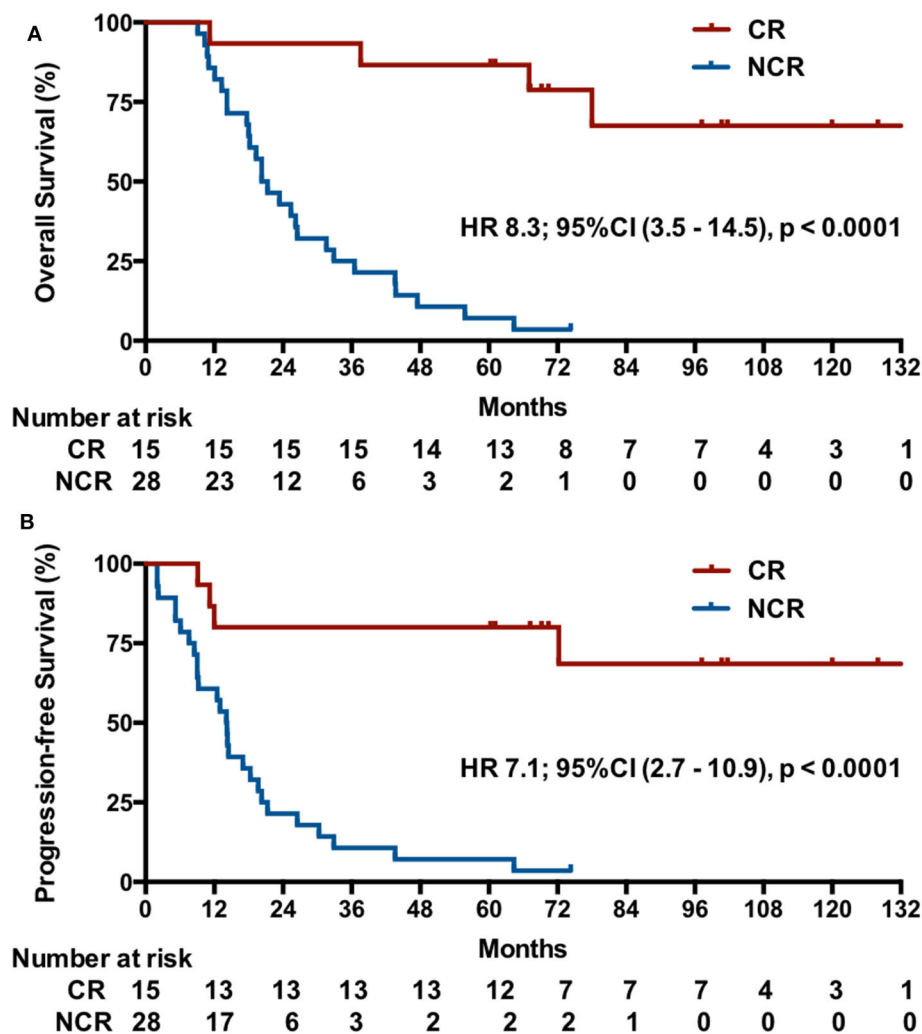
FIGURE 4 | Kaplan-Meier estimates of the OS **(A)** and PFS **(B)** by CR after induction chemotherapy.

oral administration, which does not require weekly intravenous injection like cetuximab. However, our data showed that one-third of patients had PD during the oral administration of capecitabine as maintenance treatment, suggesting the need for further exploration of the role of this strategy. In addition, anti-PD-1 antibodies (39, 40) have shown promising antitumor activity (OR rate>20%) for multiply pretreated mNPC, which may be considered as another choice for maintenance therapy.

Our regimen was derived from this above evidence and showed good outcomes. Metastatic NPC appears to be incurable from the current literature. Few studies have reported the 5-year OS for mNPC, while patients with mNPC at initial diagnosis obtained a 54.4% 5-year OS rate in our study. Although few long-term survivors after various aggressive treatments were presented in a retrospective study (4), currently, no prospective study has reported a definite regimen that could result in a considerable long-term survival rate for mNPC. In our study, 15 patients (34.9%) who achieved long-term survival (>60 months), among

whom, 12 were still alive with no evidence of disease at the 60 to 135-month follow-ups. Our data suggest a potential curative role for chemotherapy-naïve mNPC when the novel regimen is applied. To the best of our knowledge, this study is the first report of a series of long-term survivors with mNPC. Although this study was a non-randomized and single-armed phase II study trial, we have to realize that the novel study regime at the time of 2006 is a very bold, new and high-intensity scheme with the attempt to achieve an expected long survival. Considering this limitation, we have currently initiated a randomized multi-center phase 3 trial (NCT02633176) in 2015 to further investigate this topic.

DATA AVAILABILITY STATEMENT

The datasets generated for this study are available on request to the corresponding author.

ETHICS STATEMENT

The studies involving human participants were reviewed and approved by the ethics committee of Sun Yat-sen University Cancer Center. The patients/participants provided their written informed consent to participate in this study.

AUTHOR CONTRIBUTIONS

TLi: conception and design. HHu, YH, SL, and TLi: development of methodology. MZ, HHu, XL, YH, CC, XFa, SL, and HHo: acquisition of data. MZ, HHu, XL, ZW, CG, SL, XFu, TLu, and TLi: analysis and interpretation of data. MZ, TLi, HHu, and XL: writing, review and/or revision of the manuscript. HHu, YT, and TLu: administrative, technical, or material support. TLi and TLu: study supervision. All authors contributed to the article and approved the submitted version.

SUPPLEMENTARY MATERIAL

The Supplementary Material for this article can be found online at: https://www.frontiersin.org/articles/10.3389/fonc.2020.01011/full#supplementary-material

Supplement Figure 1 | Kaplan-Meier estimates of the OS **(A)** and PFS **(B)** among patients receiving the novel regimen or conventional treatment.

Supplement Table 1 | Demographic and clinical characteristics of the patients receiving novel regimen and conventional regimen.

REFERENCES

1. Ferlay J, Soerjomataram I, Dikshit R, Eser S, Mathers C, Rebelo M, et al. Cancer incidence and mortality worldwide: sources, methods and major patterns in GLOBOCAN 2012. *Int J Cancer.* (2015) 136:E359–86. doi: 10.1002/ijc.29210

2. Perez CA, Devineni VR, Marcial-Vega V, Marks JE, Simpson JR, Kucik N. Carcinoma of the nasopharynx: factors affecting prognosis. *Int J Radiat Oncol Biol Phys.* (1992) 23:271–80. doi: 10.1016/0360-3016(92)90741-Y

3. Tang L-Q, Chen Q-Y, Fan W, Liu H, Zhang L, Guo L, et al. Prospective study of tailoring whole-body dual-modality [18F]fluorodeoxyglucose positron emission tomography/computed tomography with plasma Epstein-Barr virus DNA for detecting distant metastasis in endemic nasopharyngeal carcinoma at initial staging. *J Clin Oncol.* (2013) 31:2861–9. doi: 10.1200/JCO.2012.46.0816

4. Fandi A, Bachouchi M, Azli N, Taamma A, Boussen H, Wibault P, et al. Long-term disease-free survivors in metastatic undifferentiated carcinoma of nasopharyngeal type. *J Clin Oncol.* (2000) 18:1324–30. doi: 10.1200/JCO.2000.18.6.1324

5. Chua DTT, Sham JST, Au GKH. A phase II study of docetaxel and cisplatin as first-line chemotherapy in patients with metastatic nasopharyngeal carcinoma. *Oral Oncol.* (2005) 41:589–95. doi: 10.1016/j.oraloncology.2005.01.008

6. Li YH, Wang FH, Jiang WQ, Xiang XJ, Deng YM, Hu GQ, et al. Phase II study of capecitabine and cisplatin combination as first-line chemotherapy in Chinese patients with metastatic nasopharyngeal carcinoma. *Cancer Chemother Pharmacol.* (2008) 62:539–44. doi: 10.1007/s00280-007-0641-2

7. Zhang L, Huang Y, Hong S, Yang Y, Yu G, Jia J, et al. Gemcitabine plus cisplatin versus fluorouracil plus cisplatin in recurrent or metastatic nasopharyngeal carcinoma: a multicentre, randomised, open-label, phase 3 trial. *Lancet.* (2016) 388:1883–92. doi: 10.1016/S0140-6736(16)31388-5

8. Chua MLK, Wee JTS, Hui EP, Chan ATC. Nasopharyngeal carcinoma. *Lancet.* (2016) 387:1012–24. doi: 10.1016/S0140-6736(15)00055-0

9. Jin Y, Shi YX, Cai XY, Xia XY, Cai YC, Cao Y, et al. Comparison of five cisplatin-based regimens frequently used as the first-line protocols in metastatic nasopharyngeal carcinoma. *J Cancer Res Clin Oncol.* (2012) 138:1717–25. doi: 10.1007/s00432-012-1219-x

10. Kimura H, Sakai K, Arao T, Shimoyama T, Tamura T, Nishio K. Antibody-dependent cellular cytotoxicity of cetuximab against tumor cells with wild-type or mutant epidermal growth factor receptor. *Cancer Sci.* (2007) 98:1275–80. doi: 10.1111/j.1349-7006.2007.00510.x

11. Ma BBY, Poon TCW, To KF, Zee B, Mo FKF, Chan CML, et al. Prognostic significance of tumor angiogenesis, Ki 67, p53 oncoprotein, epidermal growth factor receptor and HER2 receptor protein expression in undifferentiated nasopharyngeal carcinoma–a prospective study. *Head Neck.* (2003) 25:864–72. doi: 10.1002/hed.10307

12. Bonner JA, Harari PM, Giralt J, Azarnia N, Shin DM, Cohen RB, et al. Radiotherapy plus cetuximab for squamous-cell carcinoma of the head and neck. *N Engl J Med.* (2006) 354:567–78. doi: 10.1056/NEJMoa053422

13. Vermorken JB, Mesia R, Rivera F, Remenar E, Kawecki A, Rottey S, et al. Platinum-based chemotherapy plus cetuximab in head and neck cancer. *N Engl J Med.* (2008) 359:1116–27. doi: 10.1056/NEJMoa0802656

14. Chan ATC, Hsu M-M, Goh BC, Hui EP, Liu T-W, Millward MJ, et al. Multicenter, phase II study of cetuximab in combination with carboplatin in patients with recurrent or metastatic nasopharyngeal carcinoma. *J Clin Oncol.* (2005) 23:3568–76. doi: 10.1200/JCO.2005.02.147

15. Gennari A, Stockler M, Puntoni M, Sormani M, Nanni O, Amadori D, et al. Duration of chemotherapy for metastatic breast cancer: a systematic review and meta-analysis of randomized clinical trials. *J Clin Oncol.* (2011) 29:2144–9. doi: 10.1200/JCO.2010.31.5374

16. Lachin JM. *Biostatistical Methods: The Assessment of Relative Risks.* New York, NY: John Wiley & Sons. (2000). doi: 10.1002/9780470317051

17. Ngan RKC, Yiu HHY, Lau WH, Yau S, Cheung FY, Chan TM, et al. Combination gemcitabine and cisplatin chemotherapy for metastatic or recurrent nasopharyngeal carcinoma: report of a phase II study. *Ann Oncol.* (2002) 13:1252–8. doi: 10.1093/annonc/mdf200

18. Shuster JJ. Median follow-up in clinical trials. *J Clin Oncol.* (1991) 9:191–2. doi: 10.1200/JCO.1991.9.1.191

19. Dmytrenko IV, Fedorenko VG, Shlyakhtychenko TY, Sholoyko VV, Lyubarets TF, Malinkina TV, et al. The efficiency of tyrosine kinase inhibitor therapy in patients with chronic myeloid leukemia exposed to ionizing radiation due to the Chornobyl nuclear power plant accident. *Probl Radiac Med Radiobiol.* (2014) 19:241–55.

20. Spratt DE, Evans MJ, Davis BJ, Doran MG, Lee MX, Shah N, et al. Androgen receptor upregulation mediates radioresistance after ionizing radiation. *Cancer Res.* (2015) 75:4688–96. doi: 10.1158/0008-5472.CAN-15-0892

21. Zeng L, Tian YM, Huang Y, Sun XM, Wang FH, Deng XW, et al. Retrospective analysis of 234 nasopharyngeal carcinoma patients with distant metastasis at initial diagnosis: therapeutic approaches and prognostic factors. *PLoS ONE.* (2014) 9:e108070. doi: 10.1371/journal.pone.0108070

22. Chen MY, Jiang R, Guo L, Zou X, Liu Q, Sun R, et al. Locoregional radiotherapy in patients with distant metastases of nasopharyngeal carcinoma at diagnosis. *Chin J Cancer.* (2013) 32:604–13. doi: 10.5732/cjc.013.10148

23. Cunningham D, Humblet Y, Siena S, Khayat D, Bleiberg H, Santoro A, et al. Cetuximab monotherapy and cetuximab plus irinotecan in irinotecan-refractory metastatic colorectal cancer. *N Engl J Med.* (2004) 351:337–45. doi: 10.1056/NEJMoa033025

24. Meng J, Gu QP, Meng QF, Zhang J, Li ZP, Si YM, et al. Efficacy of nimotuzumab combined with docetaxel-cisplatin-fluorouracil regimen in treatment of advanced oral carcinoma. *Cell Biochem Biophys.* (2014) 68:181–4. doi: 10.1007/s12013-013-9686-5

25. Vermorken JB, Stöhlmacher-Williams J, Davidenko I, Licitra L, Winquist E, Villanueva C, et al. Cisplatin and fluorouracil with or without panitumumab in patients with recurrent or metastatic squamous-cell carcinoma of the head and neck (SPECTRUM): an open-label phase 3 randomised trial. *Lancet Oncol.* (2013) 14:697–710. doi: 10.1016/S1470-2045(13)70181-5

26. Thatcher N, Hirsch FR, Luft AV, Szczesna A, Ciuleanu TE, Dediu M, et al. Necitumumab plus gemcitabine and cisplatin versus gemcitabine and cisplatin alone as first-line therapy in patients with stage IV squamous non-small-cell lung cancer (SQUIRE): an open-label, randomised, controlled phase 3 trial. *Lancet Oncol.* (2015) 16:763–74. doi: 10.1016/S1470-2045(15)00021-2

27. Burtness B, Goldwasser MA, Flood W, Mattar B, Forastiere AA, Eastern Cooperative Oncology Group. Phase III randomized trial of cisplatin plus placebo compared with cisplatin plus cetuximab in metastatic/recurrent head and neck cancer: an eastern cooperative Oncology Group study. *J Clin Oncol.* (2005). 23:8646–54. doi: 10.1200/JCO.2005.02.4646

28. Sung FL, Poon TCW, Hui EP, Ma BBY, Liong E, To KF, et al. Antitumor effect and enhancement of cytotoxic drug activity by cetuximab in nasopharyngeal carcinoma cells. *In Vivo.* (2005) 19:237–45.

29. Yeh SA, Tang Y, Lui CC, Huang EY. Treatment outcomes of patients with AJCC stage IVC nasopharyngeal carcinoma: benefits of primary radiotherapy. *JPN J Clin Oncol.* (2006) 36:132–6. doi: 10.1093/jjco/hyi245

30. Lin S, Tham IWK, Pan J, Han L, Chen Q, Lu JJ. Combined high-dose radiation therapy and systemic chemotherapy improves survival in patients with newly diagnosed metastatic nasopharyngeal cancer. *Am J Clin Oncol.* (2012) 35:474–9. doi: 10.1097/COC.0b013e31821a9452

31. Ma BBY, Kam MKM, Leung SF, Hui EP, King AD, Chan SL, et al. A phase II study of concurrent cetuximab-cisplatin and intensity-modulated radiotherapy in locoregionally advanced nasopharyngeal carcinoma. *Ann Oncol.* (2012) 23:1287–92. doi: 10.1093/annonc/mdr401

32. Bonner JA, Harari PM, Giralt J, Cohen RB, Jones CU, Sur RK, et al. Radiotherapy plus cetuximab for locoregionally advanced head and neck cancer: 5-year survival data from a phase 3 randomised trial, and relation between cetuximab-induced rash and survival. *Lancet Oncol.* (2010) 11:21–8. doi: 10.1016/S1470-2045(09)70311-0

33. Lin T, Zhao C, Gao L, Lang JY, Pan JJ, Hu CS, et al. 8558 POSTER an open, multicenter clinical study of cetuximab combined With intensity modulated radiotherapy plus concurrent chemotherapy in locally advanced nasopharyngeal carcinoma. *Eur J Cancer.* (2011). 47:S561. doi: 10.1016/S0959-8049(11)72200-6

34. Basavaraj C, Sierra P, Shivu J, Melarkode R, Montero E, Nair P. Nimotuzumab with chemoradiation confers a survival advantage in treatment-naïve head and neck tumors over expressing EGFR. *Cancer Biol Ther.* (2010) 10:673–81. doi: 10.4161/cbt.10.7.12793

35. Rodríguez MO, Rivero TC, del Castillo Bahi R, Muchuli CR, Bilbao MA, Vinageras EN, et al. Nimotuzumab plus radiotherapy for unresectable squamous-cell carcinoma of the head and neck. *Cancer Biol Ther.* (2010) 9:343–9. doi: 10.4161/cbt.9.5.10981

36. Mesía R, Henke M, Fortin A, Minn H, Yunes Ancona AC, Cmelak A, et al. Chemoradiotherapy with or without panitumumab in patients with unresected, locally advanced squamous-cell carcinoma of the head and neck (CONCERT-1): a randomised, controlled, open-label phase 2 trial. *Lancet Oncol.* (2015) 16:208–20. doi: 10.1016/S1470-2045(14)71198-2

37. Zhang Y, Sun M, Huang G, Yin L, Lai Q, Yang Y, et al. Maintenance of antiangiogenic and antitumor effects by orally active low-dose capecitabine for long-term cancer therapy. *Proc Natl Acad Sci USA.* (2017) 114:E5226–35. doi: 10.1073/pnas.1705066114

38. Cremolini C, Moretto R, Masi G, Falcone A. Safety profile of capecitabine as maintenance treatment after induction with XELOX or FOLFOX in metastatic colorectal cancer patients. *Ann Oncol.* (2016) 27:1810. doi: 10.1093/annonc/mdw208

39. Hsu C, Lee SH, Ejadi S, Even C, Cohen RB, Le Tourneau C, et al. Safety and antitumor activity of pembrolizumab in patients with programmed death-ligand 1-positive nasopharyngeal carcinoma: results of the KEYNOTE-028 study. *J Clin Oncol.* (2017) 35:4050–6. doi: 10.1200/JCO.2017.73.3675

40. Ma BBY, Lim W-T, Goh B-C, Hui EP, Lo K-W, Pettinger A, et al. Antitumor activity of nivolumab in recurrent and metastatic nasopharyngeal carcinoma: an international, multicenter study of the mayo clinic phase 2 consortium (NCI-9742). *J Clin Oncol.* (2018) 36:1412–8. doi: 10.1200/JCO.2017.77.0388

Improving the Efficacy of Tumor Radiosensitization Through Combined Molecular Targeting

Katharina Hintelmann [1,2], Malte Kriegs [1], Kai Rothkamm [1] and Thorsten Rieckmann [1,2*]

[1] Laboratory of Radiobiology & Experimental Radiation Oncology, University Medical Center Hamburg Eppendorf, Hamburg, Germany, [2] Department of Otolaryngology and Head and Neck Surgery, University Medical Center Hamburg Eppendorf, Hamburg, Germany

Chemoradiation, either alone or in combination with surgery or induction chemotherapy, is the current standard of care for most locally advanced solid tumors. Though chemoradiation is usually performed at the maximum tolerated doses of both chemotherapy and radiation, current cure rates are not satisfactory for many tumor entities, since tumor heterogeneity and plasticity result in chemo- and radioresistance. Advances in the understanding of tumor biology, a rapidly growing number of molecular targeting agents and novel technologies enabling the in-depth characterization of individual tumors, have fuelled the hope of entering an era of precision oncology, where each tumor will be treated according to its individual characteristics and weaknesses. At present though, molecular targeting approaches in combination with radiotherapy or chemoradiation have not yet proven to be beneficial over standard chemoradiation treatment in the clinical setting. A promising approach to improve efficacy is the combined usage of two targeting agents in order to inhibit backup pathways or achieve a more complete pathway inhibition. Here we review preclinical attempts to utilize such dual targeting strategies for future tumor radiosensitization.

Keywords: radiotherapy, radioresistance, radiosensitization, combined molecular targeting, dual inhibition

INTRODUCTION

Chemoradiation is a current standard of care for the curative treatment of most locally advanced solid malignancies. Both modalities are generally administered at the maximum-tolerated doses to achieve best possible cure rates, which for many entities such as lung, brain, colorectal, bladder, or human Papillomavirus (HPV)-negative head and neck cancer, are still far from satisfactory. Due to the intense treatment regimes a considerable fraction of patients suffer from severe acute as well as late and partly irreversible side effects that can seriously impact quality of life. For example in head and neck squamous cell carcinoma (HNSCC) the addition of platin-based chemotherapy to radiotherapy increases 5-year overall survival by about 10% (1, 2) at the cost of increases in the rate of severe adverse events, such as grade 3 mucositis, anemia and nephro- and ototoxicity, which can result in lifetime renal insufficiency and hearing loss (3).

Combining radiotherapy with molecular targeting agents may offer an alternative to chemoradiation with potentially less severe side effects, provided the tumor cells are more dependent on the specific target than normal tissue. To be effective, the targeting agent needs to be directly toxic for the tumor and/or has to induce a meaningful radiosensitization. Despite a plethora of promising preclinical data, the results achieved in the clinic are so far exceedingly disappointing. The only currently approved molecular targeting agent for the combination with radiotherapy is the anti-epidermal growth factor receptor (EGFR)-antibody cetuximab in HNSCC. The combination was approved on the basis of the IMC 9815 phase III clinical trial, which demonstrated superiority over radiation alone in a range similar to the addition of cisplatin to radiotherapy (4). However, after a considerable number of subsequent publications it has to be seriously called into question whether the addition of cetuximab to radiotherapy is a viable alternative for cisplatin (5–7) and cetuximab also failed to enhance survival when added to chemoradiation (8). Recently, cetuximab-radiation was directly shown to be inferior to cisplatin-based chemoradiation in HPV-positive oropharyngeal cancer in two prospective phase III trials (9, 10) although this entity had shown the greatest benefit from cetuximab in the IMC 9815 trial (11).

A general limitation for the effective use of molecular targeted agents is the current lack of biomarkers that could predict a possible oncogenic addiction to a given druggable target or a possible role of the target in radiation resistance. Also in the case of cetuximab in HNSCC, no predictive biomarker has been established. In order to fully exploit the potential of precision medicine, such biomarkers are mandatory to select the best agents for a given tumor. Sequencing individual tumors for druggable driver mutations is one way forward. However, to what extent the targeting of such potential oncogenic driver proteins will also result in an enhanced sensitivity toward radiotherapy is currently unknown.

Another important concern is therapy resistance due to backup pathways or incomplete inhibition. In such cases, combined molecular targeting approaches may be an effective way to increase efficacy. Combined targeting often follows three main strategies: (1) blocking of potential alternative pathways, (2) dual targeting of the same pathway to achieve a more complete inhibition or (3) targeting of two distinct pathways whose dual inhibition will result in synthetic lethality or synergistic radiosensitization (12).

Here we review preclinical attempts to utilize such dual targeting strategies for future tumor radiosensitization.

METHODS

A PubMed search based on the key words "agent*, radiosensiti*, radiotherapy, molecular targeted therapy, combined molecular targeting" was conducted and the results were screened for use of combined molecular targeting for radiosensitization in the preclinical setting. In addition, because titles and abstracts do not follow any regular pattern, references from identified articles were further screened for suitable publications and PubMed was additionally screened for publications from the last/senior authors of identified articles (**Figure 1**).

Publications dealing with immunotherapy, e.g., using immune checkpoint inhibitors were not included, since they do not represent radiosensitization in the narrow sense. Publications of combined usage of molecular targeting and chemotherapy to achieve radiosensitization were also not included. Further, it was not always possible to discriminate between the intentional combined inhibition of two defined molecular targets and the less well-defined usage of somewhat unspecific agents with two or more targets. The latter were considered when reflecting the basic idea of the combined targeting approaches for radiosensitization, i.e., the intended selection of two targets whose inhibition should achieve at least additive or even synergistic effects.
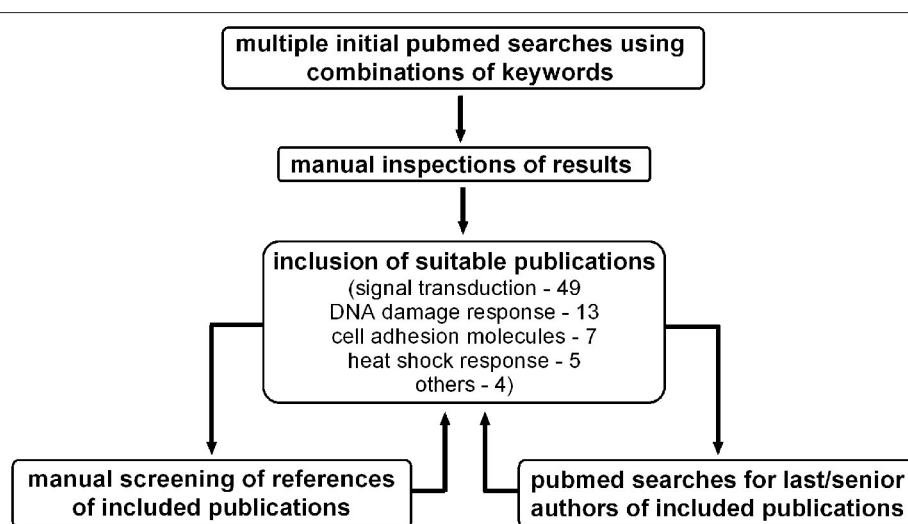
FIGURE 1 | Screening process for preclinical publications utilizing combined molecular targeting approaches for tumor radiosensitization.

Regarding clinical trials with published results, we performed a PubMed search with the respective targeting agents found in preclinical studies plus the terms "radiation" or "radiotherapy." Since the focus of this review is on preclinical approaches, we only present a selection of the most important clinical trials.

RESULTS

The vast majority of publications reporting experimental dual targeting approaches in combination with ionizing radiation fall into four categories: (1) growth factor receptor signaling, (2) DNA damage response and cell cycle checkpoints, (3) cell adhesion molecules, and (4) the heat shock response. From these categories targeting growth factor receptor signaling currently represents the by far most extensively studied dual targeting approach. In some of the identified papers inhibitors belonging to two of these categories were combined. These papers will only be presented in one section. Studies using a single substance with dual specificity were considered when its use was based on a rational selection of targets whose inhibition should achieve at least an additive or a synergistic effect.

Targeting Growth Factor Receptor Signaling

The most frequently used approach of radiosensitization through dual molecular targeting is the inhibition of growth factor receptor tyrosine kinases and their related signaling pathways. Growth factor receptor signaling can contribute to radioresistance, because it stimulates proliferation, inhibits apoptosis and has been described to increase the repair of radiation-induced DNA-damage, which makes it an attractive molecular target for radiosensitization (13, 14). Combined targeting approaches were further fuelled by the approval of the anti-EGFR monoclonal antibody (mAb) cetuximab in the curative treatment of HNSCC and by the desire to increase efficacy and repress by-pass signaling and resistance, which pose a potential risk to all signaling inhibition approaches (15). **Figure 2** provides an overview of the inhibited signaling pathways and proteins described in this section.

The HER Family

The HER sub-family of receptor tyrosine kinases (RTK) includes the members EGFR (also termed HER1 or ErbB1), Her2 (ErbB2),

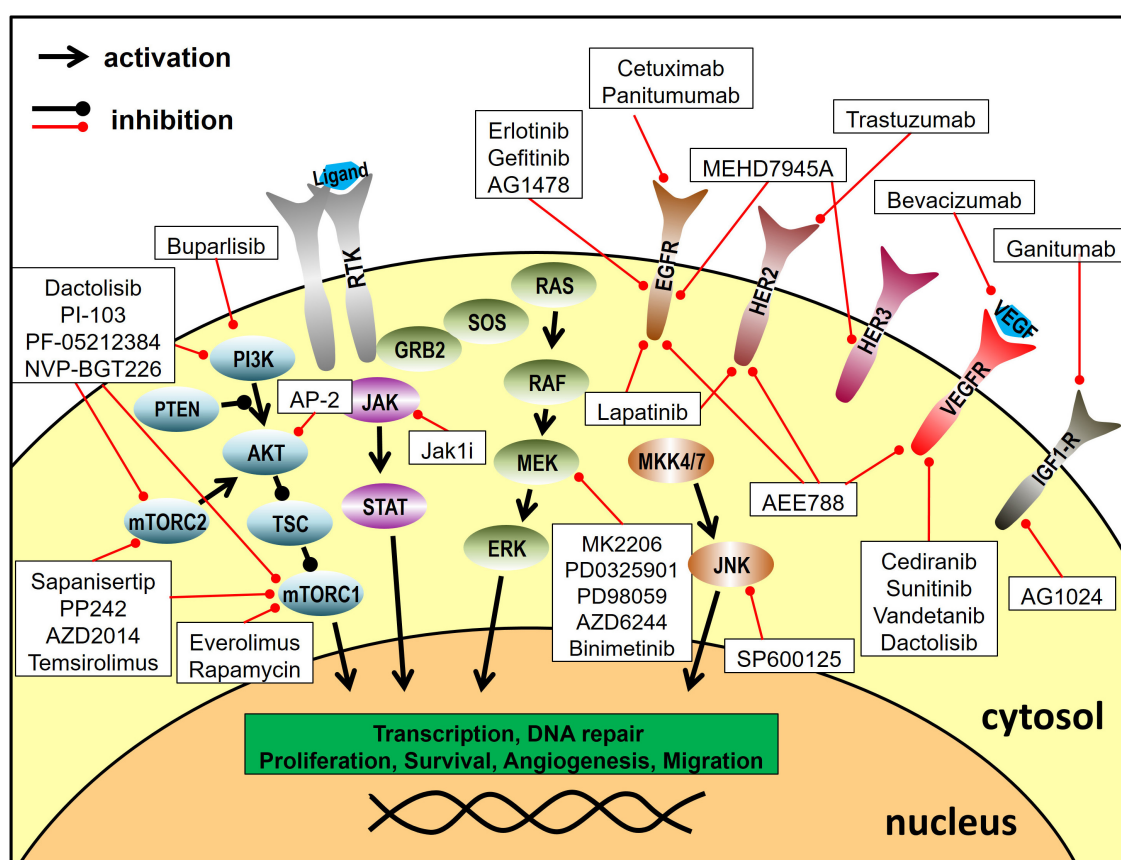**FIGURE 2 |** Targeting of signal transduction pathways. Depicted are the inhibitors utilized for combined molecular targeting approaches for tumor radiosensitization and their respective target proteins. Reported inhibitor combinations for radiosensitization are described in the text and are listed in **Table 1**. RTK, receptor tyrosine kinase.

HER3 (ErbB3), and HER4 (ErbB4). These transmembrane receptors are located at the cell surface, harbor an intrinsic protein kinase domain and regulate proliferation, migration, cell fate determination and apoptosis via diverse downstream signaling pathways such as MAPK and AKT signaling [16]. EGFR is expressed in normal epithelial cells of the skin, hair follicles or the gastro intestinal tract, but it is also detected in many tumor entities. Furthermore, EGFR gene amplifications or mutations are found in e.g., HNSCC, lung cancer or glioblastoma (GBM), driving carcinogenesis and tumor progression [17, 18]. Consequently, targeting EGFR with mAbs or tyrosine kinase inhibitors (TKI) has been established in cancer therapy in e.g. NSCLC, colorectal cancer, head and neck cancer, or pancreatic cancer but therapy resistance occurs frequently and compromises outcome [19]. Usually, ligand-binding leads to ErbB receptor homodimerization but can also result in the formation of heterodimers consisting of different sub-family members. Due to these interactions and possible functional redundancies co-targeting of different sub-family members has been investigated in several pre-clinical studies.

HER/HER targeting

Combined inhibition of different members of the HER sub-family indeed showed promising results in terms of radiosensitization. For example in first studies Fukutome et al. combined the EGFR inhibitor gefitinib (TKI) and the anti-HER2 antibody trastuzumab. Both inhibitors induced radiosensitization on their own and their combination resulted in a synergistic sensitization in vulvar squamous cell carcinoma cells expressing EGFR and HER2 [20].

Also EGFR/HER-2 inhibition by the dual inhibitor lapatinib resulted in enhanced radiosensitivity in cancer cells of various entities, such as bladder cancer, peripheral nerve sheath tumors, pancreatic or breast cancer. This sensitization was shown to be partly dependent on the expression of the specific targets (HER2, EGFR) and to be inhibited through the constitutive activation of downstream signaling factors, such as Ras & Raf mutations [21–27].

To inhibit EGFR and HER3 Huang et al. used the dual inhibitor MEHD7945A. They demonstrated that MEHD7945A inhibits growth in cetuximab (EGFR mAb) and erlotinib (EGFR TKI) resistant cells with a significant PI3K and MAPK pathway inhibition. In a xenograft model, MEHD7945A reduced the growth of tumors resistant to mono-EGFR-targeting, and, in contrast to cetuximab, the combination with radiation resulted in a more pronounced growth inhibition than either modality alone. EGFR and HER3 are both activated upon radiation and the blockade of one receptor may be compensated by the other. Treatment with MEHD7945A but not with cetuximab reduced survival signaling and DNA repair [28]. The same group could substantiate the evidence for a radiosensitizing effect of MEHD7945A using human lung and head and neck cancer cells as well as xenografts further supporting the clinical implementation of this EGFR/HER3 combined targeting approach [29].

HER/IGF-1R targeting

In addition to the formation of heterodimers within the HER-family there is also a cross talk between EGFR and other receptor tyrosine kinases such as the insulin like growth factor 1 receptor (IGF-1R), which is also involved in tumor development and progression [30]. In this context Matsumoto et al. compared individual and dual targeting of EGFR and IGF-1R in an HNSCC xenograft model using the mAbs ganitumab (anti-IGF-1R) and panitumumab (anti-EGFR). They observed the strongest growth arrest and significantly fewer recurrences upon combined inhibition plus radiation [31]. Wang et al. also showed a radiosensitizing effect of combined inhibition of EGFR through erlotinib and the IGF-1R inhibitor AG1024 in prostate cancer cells, suggesting a suppression of homologous recombination repair as a possible underlying mechanism [32]. Using two breast cancer cell lines with similarly high expression of IGF-1R but differential expression of EGFR, Li et al. observed radiosensitization through IGF-1R-inhibition (AG1024) in both strains. The EGFR inhibitor AG1478, however, only radiosensitized the cell line with high EGFR-expression both alone and when added to IGF-1R-inhibition. Radiosensitization through combined targeting was further validated in a xenograft model [33].

HER/downstream targeting

The HER receptors transduce their signals through several downstream pathways including the Ras-Raf-MAPK, the PI3K-Akt and the JAK/STAT pathway [19, 34]. Alterations within these pathways might affect the efficacy of HER inhibition as demonstrated by the importance of the Ras mutation status in colorectal cancer where patients carrying such mutations do not benefit from cetuximab treatment [35, 36]. Therefore, another strategy to increase efficacy is to combine the inhibition of the receptors and relevant downstream targets.

In this context Bonner et al. assessed the effect of combined treatment of head and neck cancer cells with cetuximab and the JAK inhibitor JAK1i. STAT3 is a downstream protein activated by JAK (among others) protecting cells from apoptosis. The authors observed enhanced anti-proliferative and apoptotic effects upon dual inhibition plus radiation. Dual inhibition was accompanied by a more complete inhibition of STAT3-phosphorylation and, in contrast to single inhibition, resulted in radiosensitization in colony formation assays [37].

Eke et al. identified the activation of c-Jun N-terminal kinase 2 (JNK2) via the scaffold protein JNK-interacting protein 4 (JIP-4) as a possible signaling bypass after EGFR targeting. The authors knocked down JIP4 or JNK2 via siRNA and used the JNK2 inhibitor SP600125 in addition to cetuximab treatment and achieved enhanced tumor cell radiosensitization in an additive manner as compared to single inhibition [38].

Activation of the PI3K/Akt/mTOR pathway was demonstrated by Zhuang et al. in lung adenocarcinoma cells as another resistance mechanism against EGFR targeting. They could demonstrate that mTOR inhibition with everolimus enhanced radiation sensitivity when added to erlotinib in vitro and in a xenograft model [39].

HER/VEGF(R) targeting

The family of vascular endothelial growth factors (VEGFs) and their specific receptors (VEGFRs) are frequently targeted in cancer therapy, e.g., in lung, breast, kidney, ovarian and cervix cancer. A fundamental difference in this therapeutic strategy is that, although the inhibition of tumor cell signaling is also of relevance, the main target of VEGF(R)-inhibition is tumor angiogenesis. VEGFs and VEGFRs are critical factors in the formation and maintenance of new vasculature in both normal tissues and solid tumors (40, 41). Their inhibition can indeed follow two contrary intentions: (1) a complete inhibition resulting in depletion of tumor nutrient and oxygen supply, or (2) a partial inhibition that results in normalization of tumor vasculature, enhances oxygenation and decreases hypoxia-based radiation resistance. Some rationales have been described for combining VEGF and EGFR inhibition. Amongst others, EGFR is also involved in angiogenesis and it has been described that EGFR inhibitor resistance may be associated with VEGF up-regulation and angiogenesis (42, 43).

In this context Bozec et al. demonstrated promising results using the VEGFR inhibitor cediranib (AZD2171) (targeting VEGFR1/2/3) concurrent with the EGFR inhibitor gefitinib and radiotherapy in a VEGF secreting HNSCC xenograft model. Combined treatment plus radiation clearly inhibited tumor growth more effectively than dual or single inhibition or radiotherapy alone. Dual inhibition was associated with decreased vessel density and dual inhibition plus irradiation showed the highest decrease in proliferation as assessed by Ki67 staining (44). The group could confirm the radiosensitizing effects in further studies when treating the same VEGF-secreting HNSCC model as orthotopic xenografts using alternative, but functionally equivalent agents, namely the anti-VEGF monoclonal antibody bevacizumab combined with the EGFR TKI erlotinib or using the combination of the VEGFR TKI sunitinib and the EGFR mAb cetuximab (45, 46). Due to an observed tumor re-growth associated with AKT/mTOR signaling activation, they further investigated the triple-targeting approach of cetuximab, bevacizumab, and the mTOR inhibitor temsirolimus in combination with irradiation. Adding the third inhibitor they indeed achieved the most sustained growth inhibition (47). In previous studies the same group had combined ZD6126, an antivascular tubulin-binding agent, with the EGFR TKI inhibitor gefitinib and irradiation. In contrast to the results described above, and although the combined targeting was moderately more effective than single targeting, the addition of radiation to dual targeting did not result in a further reduction of tumor growth (48).

Radiosensitiziation could also be induced in a lung cancer model by vandetanib, an inhibitor of VEGFR2 and EGFR but also of RET and other receptors. In human lung adenocarcinoma vandetanib treatment added to radiotherapy resulted in a dose enhancement ratio of 1.32 and markedly inhibited sublethal damage repair as assessed by a split dose recovery assay. *In vivo* the combination with irradiation showed enhanced tumor growth inhibition as compared to single treatment (49). Oehler et al. tested the effect of AEE788, an inhibitor of EGFR, HER2

and VEGFR, plus irradiation in a spontaneously growing murine mammary carcinoma model and in tumor allografts derived from murine mammary carcinoma cells. AEE788 alone as well as in combination with radiation improved tumor oxygenation in both models and the combined treatment resulted in an at least additive tumor response. Using specific inhibitors, the improvement of oxygenation could be assigned to the EGFR/HER2 inhibition (50).

In U87 GBM cell lines with or without ectopic EGFR expression vandetanib as well as cediranib failed to induce radiosensitization in clonogenic assays indicating no effect on DNA repair. In the respective xenograft models only the combination of vandetanib plus irradiation reduced tumor growth more strongly than irradiation alone, and only in the EGFR expressing substrain. In line with reduced tumor growth in this model system, vandetanib but not cediranib suppressed the expression levels of pAkt, survivin, and Ki67 as well as VEGF secretion (51).

The PI3K-AKT-mTOR Pathway

The stimulation of various growth factor receptors leads to the activation of the PI3K-AKT-mTOR signaling pathway, which can cause resistance to apoptosis and radiation. Elevated activity of the PI3K-AKT-mTOR pathway is observed in a broad range of tumor entities and associated with poor outcome, which makes this pathway a promising target for inhibitory strategies (52–55).

mTORC1/mTORC2

Inhibition of the PI3K-AKT-mTOR pathway is usually achieved by mTOR inhibitors, such as rapamycin or everolimus. However, these inhibitors block the mTOR Complex1 (mTORC1), which often results in the up-regulation of the mTOR Complex 2. Therefore, combined inhibition of mTOR Complex 1 and 2 has been studied using dual inhibitors. Sapanisertib is an ATP-competitive mTORC1 and mTORC2 inhibitor. Miyahara et al. demonstrated an enhanced inhibition of proliferation and induction of apoptosis when combining the dual inhibitor and radiation in diffuse intrinsic pontine glioma cells (56). Liu et al. also showed a radiosensitizing effect of sapanisertib in breast cancer cells, which was associated with G2/M cell-cycle arrest and an inhibition of DNA double-strand break (DSB) repair (57).

Hayman et al. compared the radiosensitization through the mTORC1-inhibitor rapamycin and the dual mTORC1/mTORC2 inhibitor PP242 in breast cancer cell lines and only observed a radiosensitizing effect using the dual inhibitor. As a normal tissue cell control, lung fibroblasts were not radiosensitized through PP242 treatment. *In vivo* PP242 alone had no impact on tumor growth but enhanced the radiation-induced growth reduction (58). The same group also tested an alternative mTORC1/mTORC2 inhibitor, AZD2014, which induced radiosensitization in glioblastoma stem-like cells *in vitro* and *in vivo*. A delay in the dispersal of radiation-induced γH2AX foci suggests that this effect involves the inhibition of DNA repair (59).

PI3K/mTOR targeting

In addition to dual targeting of mTORC1 and mTORC2 the combination of inhibitors targeting different players of the PI3K-AKT-mTOR pathway are under highly intensive investigation. In this context Yu et al. examined the effect of the dual PI3K/mTOR inhibitor dactolisib (NVP-BEZ235) in patient-derived and in radioresistant oral squamous cell carcinoma cells *in vitro* and in an *in vivo* tumor model. They observed radiosensitization *in vitro*, associated with G1 phase arrest by the downregulation of cyclin D1/CDK4 complex as a consequence of the PI3K/mTOR signaling inhibition. Tumor shrinkage was more pronounced upon the combination of dactolisib and radiation as compared to radiation alone (60). Dactolisib was further shown to reduce the activity of the central DNA repair factors DNA-PKcs and ATM and, as a consequence, to efficiently block the repair of IR-induced DSBs. Consequently, an effective radiosensitization could be demonstrated in glioblastoma cells *in vitro* and *in vivo* (61, 62).

Aberrant activation of the PI3K/AKT/mTOR pathway by Ras mutations is an important factor in Ras-driven tumorigenesis (63). Using dactolisib, Konstantinidou et al. could demonstrate a more effective radiosensitization of K-ras mutant NSCLC cells as compared to the single inhibition of PI3K (LY294002) or mTOR (rapamycin). *In vivo* dactolisib alone had little effect on tumor growth but profoundly enhanced the effect of irradiation (64). Substantiating this data, Chen et al. also targeted PI3K and mTOR with dactolisib using K-ras mutant and wild type colorectal cancer cells. Dactolisib had a radiosensitizing effect in both cases. They further demonstrated the same effect in a xenograft tumor model and suggested inefficient DNA repair, possibly due to impaired activation of ATM and DNAPKcs upon dactolisib treatment (65). In glioblastoma cell lines the radiosensitizing effect of dactolisib was shown to be dependent on the scheduling of drug and radiation. A 24 h preincubation period and wash out of the drug right before irradiation and seeding failed to sensitize the cells, while the addition of the drug shortly (1 h) before radiation with subsequent incubation for 24 h before seeding was highly effective. In line with the colony formation data, only the latter schedule showed reduced levels of P-AKT and P-mTOR without and 30 min after irradiation (66). Potiron et al. used dactolisib *in vitro* and *in vivo* in prostate cancer cell lines under normoxic and hypoxic conditions. They found a radiosensitizing effect in all cases and observed a reduction in DSB repair associated with an enhanced G2 cell cycle arrest (67). Comparable results in prostate cancer cell lines were reported in two further studies, supporting the theory of an impaired DNA repair capacity (68, 69). Schötz et al. observed radiosensitization in HNSCC cell lines, regardless of HPV-status. A DNA-repair defect was more apparent in the G1 than G2 phase and reporter gene assays pointed toward inhibition of non-homologous endjoining (NHEJ), but not homologous recombination (HR) (70). Chang et al. also tested an alternative dual PI3K/mTOR inhibitor, PI-103, which caused radiosensitization comparable to dactolisib. They suggested a novel mechanism of radiosensitization based on a reduced expression of NHEJ (Ku70/80), as well as HR (BRCA1/2, Rad51) factors upon PI3K/mTOR inhibition and radiation (69). Along

the same line Jang et al. reported a severely reduced BRCA1 expression upon PI-103 treatment and a radiosensitzation that could be further augmented by PARP-inhibition through olaparib. PI-103 failed to induce radiosensitization after a preceeding siRNA-mediated knockdown of BRCA1 suggesting that BRCA1/HR is the most relevant target in this regard (71). PI-103 was also shown to radiosensitize colon cancer cells with activated AKT through inhibition of DSB repair (72).

Leiker et al. analyzed a third ATP-competitive dual PI3K-mTOR inhibitor, PF-05212384. Using HNSCC cells they demonstrated delayed γH2AX foci resolution and a significant radiosensitization *in vivo* and *in vitro*. Since the effect was more pronounced in tumor cells compared to normal fibroblasts the results indicate some degree of tumor specificity (73). A differential response in two HNSCC cell lines toward the PI3K-mTOR inhibitor, PF-04691502 was described by Tonlaar et al. While one strain was sensitized, the other failed to respond, in line with an increased constitutive activity of PI3K, AKT, and mTOR and an inability to inhibit key phosphorylation events upon treatment (74).

Following a concept of PI3K/mTOR inhibition different from the ones described above, Fokas et al. used dactolisib as an alternative to VEGFR-inhibition in order to induce vascular normalization and improved oxygen supply. *In vivo* they observed a reduction in tumor hypoxia and an increase in perfusion. Using different schedules of drug treatment and irradiation that did or did not provide adequate time for vascular remodeling, they observed differences in tumor growth delay and concluded that dactolisib is capable of both, radiosensitization through vasculature normalization and in a direct manner (75). The same group further characterized this direct effect in a panel of different tumor and endothelial cells using dactolisib and another dual PI3K/mTOR inhibitor, NVP-BGT226. They observed PI3K pathway inhibition and enhanced residual γH2AX foci and G2-arrest after irradiation. Human endothelial and dermal microvascular cells were also sensitized, which suggests possible effects on tumor vasculature but may also indicate sensitization of normal tissue cells, which urges caution, when progressing to clinical trials (76).

AKT/mTOR

Another possibility for highly effective targeting of the PI3K-AKT-mTOR pathway is the combined inhibition of AKT and mTOR. Upon treatment with the mTOR-inhibitor rapamycin, Holler et al. observed an activation of Akt in cell lines that showed no or little radiosensitization. Since this activation was not present in responsive cells, they combined rapamycin with the Akt-inhibitor MK2206 and observed radiosensitization and an enhanced number of residual DSBs (77).

Combined inhibition of the PI3K/AKT/mTOR and Ras/Raf/Mek/MAPK pathways

Since there is crosstalk between the PI3K/AKT/mTOR pathway and the Ras/Raf/MAPK pathway with compensatory potential, dual targeting of these two pathways is also an option. Williams et al. investigated the inhibition of both pathways in K-ras mutated pancreatic cancer cells and xenografts. While sole MEK

inhibition by PD0325901 already resulted in radiosensitization and apoptosis, both effects were further enhanced by a dose of the Akt-inhibitor API-2 that was not effective on its own. Dual inhibition plus radiation also showed the most pronounced growth inhibition in a corresponding xenograft model (78). Toulany et al. demonstrated radiosensitization in K-ras mutated NSCLC cells upon PI-103 treatment but prolonged inhibition resulted in K-ras/Raf/MAPK-dependent Akt activation and loss of radiosensitization. Combining PI3K/mTOR inhibition with the MEK inhibitor PD98059 prevented the reactivation of K-ras/Raf/MAPK-dependent Akt signaling upon long-term PI-103 incubation and resulted in inhibition of DSB repair and radiosensitization (79). Using the MEK inhibitor AZD6244, Kuger et al. investigated whether additional inhibition of the MAPK pathway further enhances the radiosensitization induced by dactolisib treatment. They consistently found a radiosensitizing effect through PI3K/mTOR inhibition in lung and glioblastoma cancer cells that, however, was not increased through additional MEK inhibiton (80). Lastly, Blas et al. combined the PI3K family inhibitor buparlisib with the MEK1/2 inhibitor binimetinib in HNSCC cells. *In vitro*, both inhibitors showed a dose dependent inhibition of proliferation/viability without additional effects upon combination. None of the inhibitors, nor the combination induced radiosensitization, partly even induced radioprotection in UT-SCC-15 cells. *In vivo*, combining both inhibitors did not show any benefit in combination with irradiation and in UT-SCC-15 cells even diminished the growth delay compared to radiotherapy with either agent alone (81).

TABLE 1 | Combined targeting of growth factor receptor signaling.

Targets	Inhibitor(s)	Entity	References
EGFR/HER2	Gefitinib**,*** Trastuzumab**,***	Vulvar squamous cell carcinoma	(20)
EGFR/HER2	Lapatinib**,***	Breast cancer	(21, 22, 24)
		Breast cancer (HER2+)	(25)
		K- pancreatic cancer (K-ras wt)	(23)
		NF2 associated peripheral nerve sheath tumor	(26)
		Bladder cancer	(27)
EGFR/HER3	MEHD7945A*	NSCLC, HNSCC	(28, 29)
EGFR/IGF-1R	Panitumumab**,*** Ganitumab*	HNSCC	(31)
	Erlotinib**,*** AG1024 exp	Prostate cancer	(32)
	AG1478exp AG1024 exp	Breast cancer	(33)
EGFR/JAK/ STAT-3	Cetuximab**,*** JAK1i exp	HNSCC	(37)
EGFR/JNK2/ JIP-4	Cetuximab**,*** SP600125 exp	HNSCC/VSCC	(38)

(Continued)

TABLE 1 | Continued

Targets	Inhibitor(s)	Entity	References
EGFR/mTOR	Erlotinib**,*** Everolimus**,***	NSCLC?	(39)
EGFR/VEGFR	Gefitinib**,*** ZD6126* (sus)	HNSCC	(48)
	Gefitinib**,*** AZD2171 (Cediranib)**	HNSCC	(44)
	Erlotinib**,*** Bevacizumab**,***	HNSCC	(45)
	Cetuximab**,*** Sunitinib**,***	HNSCC	(46)
	Cetuximab**,*** Bevacizumab**,*** Temsirolimus**,***	HNSCC	(47)
	Vandetanib**,***	NSCLC	(49)
	Vandetanib**,***	GBM	(51)
EGFR/VEGFR/ HER2	AEE788*(disc)	Mammary carcinoma (murine)	(50)
mTOR1C/mTOR2C	Sapanisertib*	Pontine Glioma	(56)
		Breast Cancer	(57)
	PP242exp	Breast Cancer	(58)
	AZD2014 (Vistusertib)*	Glioblastoma	(59)
PI3K/mTOR [(ATM/DNAPKCS)]	Dactolisib*	Oral SCC	(60)
		HNSCC	(70)
		Glioblastoma	(61, 62, 66)
		NSCLC	(64)
		Colorectal cancer	(65)
		Prostate cancer	(67, 68)
		Fibrosarcoma, HNSCC	(75)
	Dactolisib* NVP-BGT226 *(disc)	HNSCC, bladder cancer, endothelial cells	(76)
	Dactolisib* PI-103 exp	Prostate cancer	(69)
PI3K/mTOR	PI-103exp	Colon cancer	(72)
	PF-05212384 (Gedatolisib)*	HNSCC	(73)
	PF-04691502* (disc)	HNSCC	(74)
PI3K/mTOR/PARP	PI-103exp Olaparib**,***	TNBC	(71)
mTOR/Akt	Rapamycin**,*** MK2206*	NSCLC, breast cancer	(77)
MEK/Akt	PD0325901* API-2 (=Triciribine)*	Pancreatic cancer (K-ras mut.)	(78)
PI3K/mTOR/MEK	PI-103exp PD98059 exp	K-ras mut. NSCLC	(79)
	Dactolisib* AZD6244 (Selumentinib)**,***	Lung cancer, Glioblastoma	(80)
PI3K/MEK	Buparlisib** Binimetinib**,***	HNSCC	(81)

*Tested in clinical trials.
**Tested in clinical trials in combination with radiotherapy.
***Approved (any clinical setting).
exp, experimental; disc, discontinued; sus, suspended.
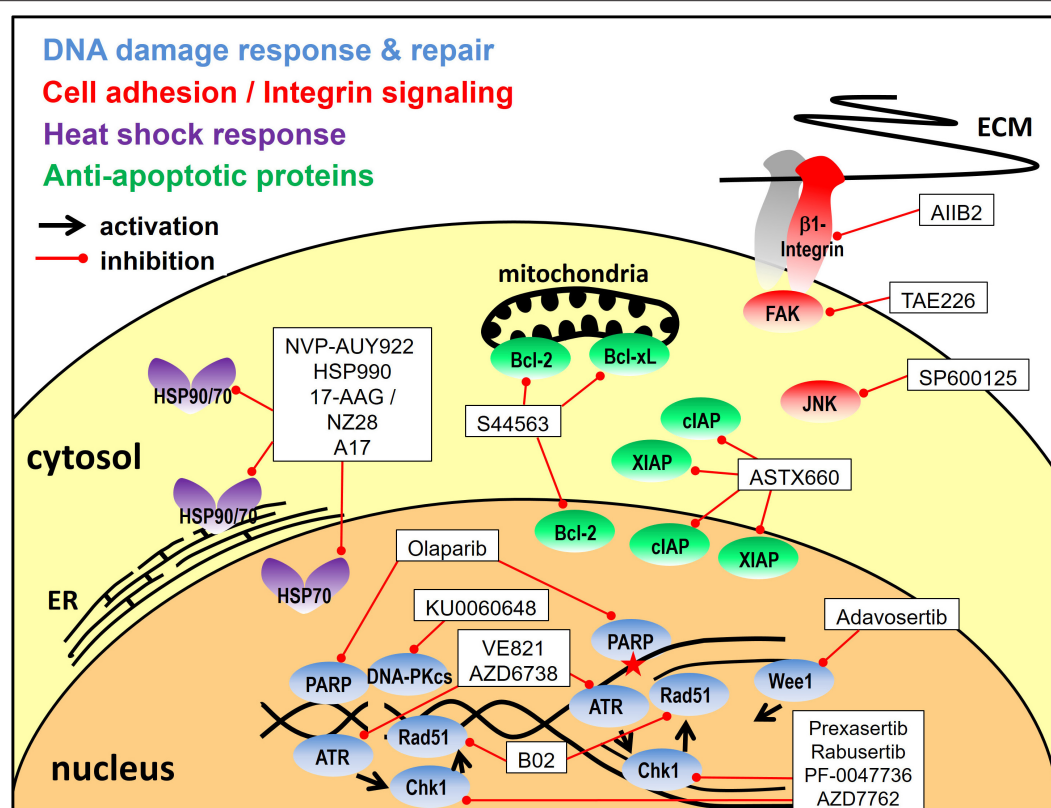
FIGURE 3 | Targeting approaches other than signal transduction pathways. Depicted are the inhibitors utilized for combined molecular targeting of the DNA damage response, integrin signaling, the heat shock response or apoptosis for tumor radiosensitization and the respective target proteins. Reported inhibitor combinations are described in the text and are listed in **Tables 2**, **3**, **4**. ECM, extracellular matrix; ER, endoplasmatic reticulum.

Apart from the inhibition of signal transduction pathways a number of other strategies have been developed for tumor radiosensitization through combined molecular targeting. These include the targeting of the DNA damage response, cell adhesion molecules, the heat shock response or apoptosis, as detailed below and outlined in **Figure 3**.

Targeting the DNA Damage Response

Ionizing radiation causes DNA lesions, such as base damages, single-strand breaks, and double-strand breaks with the latter being largely responsible for cell inactivation (82). Therefore, the most obvious approach for radiosensitization is the direct targeting of the DNA damage response (DDR) and DSB repair. An integral part of the DDR are the damage induced cell cycle checkpoints in the G1, S or G2 phase, which allow additional time for DNA repair before the critical passage through mitosis where mis- or unrepaired DSBs can result in cell death due to failure in chromosome segregation (83). One of the most frequent transforming events in human cancerogenesis is the inactivation of p53. p53 mutations, the overactivation of the MDM2-controlled regulatory pathway or p53 degradation through viral oncoproteins represent the underlying mechanisms (84, 85). As p53 is essential for G1 checkpoint activation its deficiency renders affected tumor cells more dependent on S/G2

cell cycle checkpoint activation (83). Upon DNA damage these checkpoints are activated through checkpoint kinase 1 (Chk1), which is further involved in DNA repair through HR and has an impact on the stabilization of stalled replication forks and other responses to genotoxic stress during the S-phase (86). Upon activation through phosphorylation it inactivates members of the Cdc25 phosphatase family which leads to the inactivation of the cyclin-dependent kinases (CDKs) 1/2 and arrests cells in the G2 phase in response to DNA damage (87). Another kinase necessary for S and G2 checkpoint activation as well as for normal cell cycle progression is Wee1. As the direct counterpart of CDC25 phosphatases it constitutively inactivates CDK1/2 through phosphorylation and is also involved in homologous recombination (88, 89). Targeting the S- and G2-checkpoints through the inhibition of Chk1 and partly of Wee1 has been a frequently used approach for preclinical radio- or chemosensitization and was recently combined with PARP-inhibitors. The rationale is that the inhibition of PARP causes additional DNA damage especially in the S- and G2-phase through the inhibition of single-strand break (SSB) repair and PARP trapping on damaged DNA and through the subsequent collision of single strand lesions with replication forks (90–92). PARP-inhibition further impairs the alternative end-joining pathway which is also preferentially active in S- and G2 (93).

These mechanisms additionally enhance the dependence on the S- and G2-checkpoints and the well described synthetic lethality of PARP-inhibition and HR deficiency (94) may further increase radiosensitization.

Chk1/Wee1

Focusing on cell-cycle checkpoint inhibition, Busch et al. tested the combined targeting of Chk1 (LY2603618) and Wee1 (adavosertib; AZD1775) in HPV-positive HNSCC cells because they had observed an activation of Chk1 upon Wee1 inhibition that may in part counteract the effects of sole Wee1 targeting. Analyzing proliferation, inhibition of G2 arrest and radiosensitization, they found dual targeting to be effective at profoundly reduced concentrations as compared to single agent usage. Additionally, they observed only minimal radiosensitization in p53 proficient normal human fibroblasts, thus demonstrating tumor specificity (95).

PARP1/Chk1

Vance et al. combined the inhibition of PARP1 through olaparib and Chk1 through AZD7762 in p53 mutant pancreatic cancer cells and observed an additive radiosensitization. The authors observed G2 checkpoint abrogation, inhibition of HR and a persistent γH2AX signal after combined inhibition of the two targets. There was no significant radiosensitization in G1-checkpoint-proficient intestinal epithelial cells, backing up the hypothesis that tumor cells harboring aberrations in p53 or other DNA damage response pathways are more selectively sensitized (96). In line with these data, Güster et al. demonstrated radiosensitization of p53 deficient HPV-positive HNSCC cells through olaparib and the Chk1-inhibitor PF-0047736, with the extent of sensitization being highest upon combined inhibition (97).

PARP/Wee1

Karnak et al. investigated the radiosensitizing effect of the combined inhibition of PARP1 and Wee1 through olaparib and adavosertib in pancreatic cancer cells. This dual-targeted approach is highly similar to combined PARP/Chk1-inhibition and was also associated with G2 checkpoint abrogation, inhibition of HR and persistent DNA damage. *In vitro* the combination of both inhibitors caused enhanced radiosensitization as compared to single inhibition. In *vivo*, there was no radiosensitization with olaparib alone and a moderate effect of adavosertib. Combined targeting, however, demonstrated highly significant radiosensitization (98). The same group further assessed this dual-targeting approach in hepatocellular carcinoma cells and K-ras mutant NSCLC cells, also showing an increased radiosensitization *in vitro* and *in vivo* compared to either agent alone. The authors suggested that trapping of PARP to chromatin by olaparib as well as replication stress induced through this inhibitor combination contribute to radiosensitization (99, 100). Molkentine et al. compared PARP-inhibition through niraparib plus either Wee1-inhibition through adavosertib or Chk1-inhibition through MK-8776 in an HPV-positive and an HPV-negative cell line. While both ways of S/G2-checkpoint-inhibition enhanced the radiosensitization

through sole PARP-inhibition, the addition of Chk1-inhibition was more effective in the HPV-positive and of Wee1-inhibition in the HPV-negative strain. Whether these differences are generally valid for the two subentities remains to be shown in future studies (101).

PARP/ATR

Carruthers et al. had reported that glioblastoma stem-like cells are characterized by intrinsic replication stress, which activates the DDR and leads to radiation resistance. Ataxia telangiectasia and Rad3-related protein (ATR) is a key DDR kinase acting directly upstream of Chk1. Through Chk1 activation but also partly independent from Chk1, ATR is critically involved in replication processes, such as the stabilization of stalled replication forks, and in DSB repair pathways (102, 103). Targeting the replication stress response by a combination of olaparib and the ATR inhibitor VE821 resulted in cytotoxicity and synergistic radiosensitization, completely abolishing radioresistance (104). These data confirm results from a previous report by the same group, where the same combination resulted in greater radiosensitization than ATM inhibition in primary glioblastoma cell cultures. Radiosensitization was higher when the cells were cultured under conditions enriching the fraction of stem-like cells as compared to conditions favoring their depletion and a more differentiated state (105).

PARP/Rad51

Olaparib was further combined with the Rad51 inhibitor B02 and X- as well as proton-irradiation with the intention to induce HR deficiency that would synergize with PARP inhibition. Lung and pancreatic cancer cell lines were radiosensitized by the inhibitors, with the strongest effect for dual inhibition, similarly for both types of irradiation. Radiosensitization was found to be dependent on the proliferation rate, as serum deprivation reduced the effectiveness of dual targeting and in slowly proliferating PANC1 cells the combination was even less effective than sole PARP-inhibition (106).

Chk1/2/EGFR

The addition of the Chk1/2 inhibitor prexasertib to cetuximab and irradiation was investigated by Zeng et al. in HPV-positive and HPV-negative HNSCC cell lines. Prexasertib caused an accumulation of cells in the S-phase, the triple combination partly resulted in decreased proliferation and increased apoptosis as compared to single or double treatment (107).

ATR/DNA-PK

DNA-dependent protein kinase, catalytic subunit (DNA-PKcs) is well known as an essential component of the classical NHEJ pathway but is further associated with genomic stability, hypoxia, inflammatory responses, metabolism and regulation of transcription (108, 109). Hafsi et al. used combined ATR and DNA-PKcs inhibition (AZD6738, KU0060648) to radiosensitize HNSCC cells and observed an at least additive effect. A key element in this approach is that ATR inhibition interferes with cell cycle arrest and HR, whereas DNA-PKcs inhibition inhibits NHEJ. This combination therefore leaves few options for the cells

to repair the radiation-induced damage in any cell cycle phase and curbs the development of resistance mechanisms. It may, however, come at the cost of tumor specificity (110).

Targeting Cell Adhesion Molecules

Cell matrix interaction by integrins was shown to be a modulator of tumor progression, invasion, metastasis and response to therapy. β1-integrin, a member of the integrin family of cell adhesion molecules is significantly involved in tumor survival and proliferation and is associated with radio- or chemotherapy resistance (111). β1-integrin overexpression was shown in many tumor entities and its molecular targeting was found to be an effective means of radiosensitization. Integrins recruit signaling molecules to their cytoplasmic domain, mainly focal adhesion kinase (FAK) but also components of the EGFR signaling pathway, such as Erk and Akt (112). FAK is involved in proliferation, cell motility and radiation response and was found to be overexpressed or hyperphosphorylated in e.g., liver, head, and neck or breast cancer cells.

β1 Integrin or FAK/EGFR

Eke et al. investigated the effect of concurrent β1 integrin and EGFR targeting using the monoclonal inhibitory antibodies AIIB2 and cetuximab, respectively in head and neck cancer cells. They observed enhanced cytotoxicity and radiosensitization upon combined inhibition in 8 out of 10 cell lines and, in line

with that, enhanced survival in a xenograft model of a responder cell line (113). FAK was shown to mediate the effects of β1 integrin targeting in line with previous reports of the same group that had shown dual inhibition of EGFR (cetuximab, siRNA) and FAK (TAE226, siRNA) to achieve a stronger radiosensitizing effect in HNSCCs than either inhibitor alone (114). Zscheppang et al. further investigated single and dual β1-integrin/EGFR targeting using AIIB2 & cetuximab in sphere-forming HNSCC cells based on the concept that tumor initiating cells are enriched in spheres. Sphere-forming cells were found to be resistant to this targeting approach and future work is warranted to understand the mechanisms and relevance of this finding (115). In another report, the same dual β1-integrin/EGFR inhibition approach, as well as KRAS or BRAF depletion and 5-FU-treatment failed to modulate the radiosensitivity of colorectal carcinoma cells (116).

Recently, a screen for predictive biomarkers for the dual β1-integrin/EGFR targeting approach showed different mutational profiles of responding and non-responding cells and suggested some proteins as potential resistance factors. Using an RNAi screen and pharmacological inhibition (ML334, everolimus) Kelch like ECH associated protein 1 (KEAP1) and mTOR were identified as druggable targets for radiosensitization in combination with β1-integrin/EGFR targeting (117).

β1-Integrin/c-Abl

C-Abl is a tyrosine kinase found to be hyperphosphorylated upon β1-integrin inhibition. Therefore, dual β1-integrin (AIIB2) and c-Abl (imatinib) targeting was tested in a panel of tumor cell lines from various entities, where a cell line dependent cytotoxicity and enhancement or induction of radiosensitivity was observed as compared to single treatment in a subgroup of the panel. Radiosensitization was accompanied by altered expression of DSB repair proteins KU70 and NBS1 and was associated with reduced DSB repair (118).

TABLE 2 | Dual targeting of DNA damage response factors.

Targets	Inhibitor(s)	Entity	References
Chk1/Wee1	LY2603618 (Rabusertib) *(disc) Adavosertib**	HNSCC (HPV+)	(95)
PARP1/ Chk1	Olaparib**,*** AZD7762* (disc)	Pancreatic cancer (p53 mut)	(96)
	Olaparib**,*** PF-0047736* (disc)	HNSCC (HPV+)	(97)
		HNSCC	(101)
PARP1/Wee1	Olaparib**,*** Adavosertib**	Pancreatic cancer	(98)
		Hepatocellular carcinoma	(99)
		NSCLC (K-ras mut)	(100)
		HNSCC	(101)
PARP1/ATR	Olaparib**,*** VE821 exp	GBM	(104, 105)
PARP1/RAD51	Olaparib*,*** B02 exp	NSCLC, Pancreatic cancer	(106)
Chk1/2/EGFR	Prexasertib** Cetuximab**,***	HNSCC	(107)
ATR/DNA-PK	AZD6738 (Ceralasertib)* KU0060648 exp	HNSCC, Colon cancer	(110)

*Tested in clinical trials.
**Tested in clinical trials in combination with radiotherapy.
***Approved (any clinical setting).
exp, experimental; disc, discontinued.

TABLE 3 | Combined targeting approaches involving cell adhesion molecules.

Targets	Inhibitor(s)	Entity	References
β1-integrin/ EGFR	AIIB2 exp Cetuximab**,***	HNSCC	(113)
		HNSCC	(115)
		Colorectal Cancer	(116)
β1-integrin/ EGFR/KEAP1/ mTOR	AIIB2 exp Cetuximab**,*** Everolimus**,*** ML334 exp	HNSCC	(117)
FAK/EGFR	TAE226 exp Cetuximab**,***	HNSCC	(114)
β1-integrin/ c-Abl	AIIB2 exp Imatinib***	various	(118)
β1-integrin/ JNK	AIIB2 exp SP600125 exp	Glioblastoma	(119)

**Tested in clinical trials in combination with radiotherapy.
***Approved (any clinical setting).
exp, experimental.

β1-Integrin/JNK

Vehlow et al. identified the c-Jun N-terminal kinase (JNK), a known stress mediator, to mediate bypass signaling after β1-integrin-inhibition in established glioblastoma cell lines, as well as stem-like and patient-derived glioblastoma cells. Dual β1-integrin/JNK inhibition through AIIB2 and the JNK inhibitor SP600125 *in vitro* and *in vivo* resulted in a superior effect when combined with radiation as compared to single inhibition, i.e., increasing the median survival of orthotopic, radiochemotherapy-treated GBM mice. *In vitro* the authors observed defects in DNA repair associated with chromatin changes, enhanced ATM phosphorylation, and prolonged G2/M cell cycle arrest as the underlying mechanism of radiosensitization [119].

Targeting the Heat-Shock Response

Heat shock proteins (HSPs) are a group of proteins with enhanced expression in response to various kinds of stresses, such as hyperthermia, infections, heavy metals, or oxidative stress [120]. As molecular chaperones they assist their substrate proteins, termed clients, in acquiring or recovering their functional three dimensional fold, a process especially important under stressed conditions. Furthermore they assist the binding of ligands to their targets and the assembly of multiprotein complexes and they are potent inhibitors of apoptosis [121, 122]. HSP70 and HSP90 proteins represent two important, druggable HSP families with actually hundreds of client proteins making their molecular targeting a biologically complex approach with numerous possible subsequent effects. The inhibition of both HSP70 and HSP90 are being tested for cancer therapy because of their especially high expression levels in tumors. Enhanced expression is believed to be necessary because in tumor cells proteostasis is permanently challenged by tumor cell metabolism, oxidative stress, dysregulated protein expression and the expression of mutant (onco) proteins, which may be less stable and require more assistance from the chaperone machinery [123]. A prominent example for the latter is the stabilization of mutant, gain of function p53 variants through HSP90 [124].

HSP90/HSP70

It was shown that the inhibition of Hsp90 compromises DNA repair after irradiation and enhances tumor cell radiosensitivity [125, 126]. However, HSP90 inhibition also leads to the activation of the transcription factor Heat Shock Factor 1 (HSF 1). HSF-1 is inactivated when bound by HSPs and becomes active upon release, e.g., upon HSP-inhibition or under stressed conditions, in order to adjust the HSP-expression level to the chaperone demand of the cell [120]. Therefore, targeting HSP90 can enhance the expression of Hsp70, which may partly antagonize the effects of HSP90-inhibition. This led to the dual targeting approach of Schilling et al. in which HSP70 inhibition through the peptide aptamer A17 failed to significantly radiosensitize lung and breast cancer cells on its own but augmented the radiosensitizing effect of the Hsp90 inhibitor NVP-AUY922. The authors suggested that increased levels of DNA double-strand breaks and enhanced G2/M arrest are involved in cell death after combined treatment and radiation [127]. In a previous work the

same group had already shown similar results in which addition of NVP-AUY922 allowed for a reduction in the concentration of the HSP70 inhibitor NZ28 to 1/10 to 1/20 to still achieve the same radiosensitization [128].

HSP90/PI3K/mTOR

Following the same concept as dual HSP70/90-inhibition the PI3K/mTOR inhibitor PI-103, which had previously been shown to suppress the up-regulation of Hsp70 [129], was combined with Hsp90-inhibition through NVP-AUY922. Adding both inhibitors 3 h prior to irradiation followed by 24 h of culture moderately enhanced the radiosensitizing effect. The authors supposed a down regulation of PI3K and ERK pathways, increased DNA damage, and a pronounced G2/M arrest as possible causative factors. Interestingly, using another treatment schedule, adding the inhibitor 24 h before irradiation slightly reduces the radiosensitizing effect of the HSP90 inhibitor. They considered a reactivation of the PI3K/MAPK pro-survival pathway and an increased G1 arrest at the moment of irradiation and better DNA repair to cause these controversial observations. These findings underline the importance of IR-drug scheduling [130].

In human glioma cells Wachsberger et al. combined the PI3K inhibitor Buparlisib (BKM120) with the HSP90 inhibitor HSP990, which resulted in downregulation of the AKT pathway and induction of apoptosis. *In vitro* from a panel of four cell lines only U373MG showed a profound radiosensitization after dual targeting as compared to single inhibition. Still, *in vivo,* U87MG showed a more pronounced tumor growth delay compared to single inhibition with and without the combination with irradiation [131].

HSP90/PARP1

Also targeting human glioma cells Dungey et al. combined the inhibition of PARP through olaparib with the Hsp90 inhibitor 17-AAG. The rationale behind is that Hsp90-inhibition

TABLE 4 | Combined targeting approaches involving the heat shock response.

Targets	Inhibitor(s)	Entity	References
HSP90/HSP70	NVP-AUY922 (Luminespib)[exp] NZ28 [exp]	Lung and breast cancer	[128]
	NVP-AUY922[exp] A17 (peptide aptamer) [exp]	Lung and breast cancer	[127]
HSP90/PI3K/mTOR	NVP-AUY922[exp] PI-103 [exp]	Glioblastoma, colon cancer	[130]
HSP90/PI3K	HSP990*[(disc)] Buparlisib**	Glioma	[131]
HSP90/PARP	17-AAG (Tanespimycin)*[(disc)] Olaparib**,***	Glioma	[132]

*Tested in clinical trials.
**Tested in clinical trials in combination with radiotherapy.
***Approved (any clinical setting).
exp, experimental; disc, discontinued.

decreases HR, which is needed to repair replication-associated DSB generated through PARP inhibition. They observed a downregulation of Rad51 and BRCA2 protein levels and inhibition of HR upon HSP90 inhibition. Combined treatment resulted in additive radiosensitization in proliferating cells. Since the authors did not observe radiosensitization through HSP90 inhibition in non-tumor control cells and had previously described olaparib-mediated radiosensitization to be replication-dependent, they expect an enhancement of the therapeutic ratio by taking advantage of the non-dividing state of normal brain tissue (132).

Other Approaches
MEK/Cyclin Dependent Kinases (CDKs)

Tao et al. observed that in Kras-mutant NSCLC cells, the inhibition of MEK through trametinib resulted in p16 expression and reduced phosphorylation and therefore activation of the tumorsuppressor RB in the cell line most sensitive toward both sole MEK-inhibition and MEK-inhibition induced radiosensitization. Likewise, activation of RB through CDK4/6-inhibition through palbociclib sensitized the more resistant cells to MEK-inhibition and resulted in enhanced radiation sensitivity as compared to single treatment. Dual targeting plus irradiation was also most effective in a xenograft model (133).

Targeting Histone Deacetylases/HER Family Receptors

Histone deacetylase inhibitors are a heterogeneous group of epigenetic therapeutics, which a.o. interfere with DNA damage signaling and repair (134). Moertl et al. have compared the radiosensitization of pancreatic cancer cells through the HDAC inhibitor SAHA and the multi target inhibitor CUDC-101, which, besides HDAC, also targets EGFR and HER2 (135). They observed reduced proliferation and clonogenic survival and increased apoptosis with reduced expression of the antiapoptotic proteins XIAP and survivin with both inhibitors. While the multi target inhibitor was identified as the more potent radiosensitizer, no clues can presently be drawn regarding a synergistic mechanism of HDAC and EGFR/HER2 targeting since no combined treatment of SAHA and HER family receptor inhibition was performed.

Targeting Anti-apoptotic Proteins

We further identified two studies, which followed a strategy of inhibiting two anti-apoptotic proteins. In the first study, Bcl-2 and Bcl-XL, two members of the anti-apoptotic fraction of the Bcl-2 family of mitochondrial membrane proteins, were inhibited using the dual inhibitor S44563. Upon targeting plus irradiation the authors observed an enhanced sub-G1 fraction and caspase 3 cleavage as compared to single treatment. In clonogenic assays they further observed radiosensitization and a slight growth delay in xenograft models upon inhibition plus radiation. Interestingly, treatment was most effective when the inhibitor was added after completion of fractionated radiation, highlighting the importance of the optimal sequence of modalities (136). Another approach utilized a novel antagonist

of the E3 ubiquitin ligases cIAP and XIAP (cellular inhibitor of apoptosis protein, X-linked inhibitor of apoptosis protein), ASTX660. *In vitro*, the inhibitor sensitized subsets of HPV-negative and HPV-positive HNSCC cell lines to TNF family death ligands TNFα and TRAIL, which involved a reactivation of p53 in the HPV-positive strains. In HPV-positive and -negative human HNSCC xenografts the authors observed significantly delayed growth when the dual inhibitor was combined with radiation, which was attenuated by anti-TNFα pretreatment blockade (137).

TABLE 5 | Various combined targeting approaches.

Targets	Inhibitor(s)	Entity	References
MEK/CDK4/6	Trametinib**, *** Palbociclib**, ***	NSCLC (K-ras mut.)	(133)
HDAC/EGFR/ HER2	CUDC-101*	Pancreatic Cancer	(135)
Bcl-2/Bcl-XL	S44563[exp]	SCLC	(136)
cIAP (BIRC2)/XIAP	ASTX660**	HNSCC	(137)

*Tested in clinical trials.
**Tested in clinical trials.
***Approved (any clinical setting).

CLINICAL TRIALS

Despite a plethora of positive preclinical data, molecular targeting for tumor radiosensitization is not yet a valid treatment option in the clinic, but a considerable number of clinical trials is testing targeting approaches in combination with (chemo)radiation. However, when searching for trials with combined molecular targeting for radiosensitization in the narrow sense, we only found two running studies combining two inhibitors with sole radiotherapy, both in HNSCC. One trial is testing the combination of cetuximab and the CDK4/6 inhibitor palbociclib, a combination, for which we did not find a preceding preclinical evaluation but only a similar approach combining MEK-inhibition plus palbociclib (133) (NCT03024489). The other trial compares the dual targeting of EGFR and Chk1 through cetuximab and prexasertib vs. the combination of cisplatin and prexasertib (NCT02555644). Since this design does not include single inhibition or standard treatment but uses the non-approved inhibitor prexasertib in both arms, it may become difficult to finally estimate to what extent this dual targeting approach may increase radiation sensitivity.

In the following we present a selection of relevant publications reporting results from clinical trials using combined molecular targeting and (mostly chemo-)radiation. A common approach is the combination of chemoradiation, inhibition of signal transduction pathways and VEGFR-inhibition. However, while these combined inhibitor approaches clearly cover anticipated effectiveness through dual targeting, the purpose of radiosensitization is less in focus than the idea of achieving

additive effects through repression of angiogenesis. Especially the combination of chemoradiation, EGFR-inhibition and the anti-VEGF antibody bevacizumab has been tested in different entities but efficacy so far appears limited: In HNSCC, the addition of bevacizumab to radiation, cetuximab and pemetrexed was reported to increase toxicity without an apparent improvement in efficacy (138). Similarly, the combination of (chemo)radiation, bevacizumab and erlotinib did not result in a survival benefit but demonstrated targeted-agent specific toxicity in esophageal cancer (139). Along the same line, adding erlotinib to chemoradiation and bevacizumab did not show efficacy but induced esophageal toxicity in NSCLC (140) and the addition of the EGFR/VEGFR inhibitor vandetanib did not prolong survival in a phase II study of glioblastoma (141). In contrast to these clearly negative results, encouraging responses have been reported for the addition of erlotinib to neoadjuvant chemoradiation plus bevacizumab in phase I trials of rectal cancer, which warrant further investigation in larger studies (142, 143). Clinical results have also been reported for the inhibition of EGFR and HER2 in HNSCC through lapatinib. Addition to primary chemoradiation plus lapatinib maintenance resulted in increased 6-month complete response rates and progression-free survival as compared to placebo in a phase II study (144). However, in a similar design in the setting of adjuvant chemoradiation after surgery, lapatinib did not result in any efficacy benefits but additional toxicity in a large phase III trial of 688 patients (145).

At present, molecular targeting is often added to current chemoradiation regimes to increase efficacy and trials are mostly in early clinical development. It is therefore not surprising that combined targeting approaches are still quite rare and often based on dual specific inhibitors, which may be easier to implement than inhibitor combinations for which toxicity data may still be lacking, even without radiotherapy.

DISCUSSION

Molecular targeting approaches for tumor radiosensitization have been investigated for two decades (146–149), but their implementation into the clinic has proven extremely difficult. As outlined above, the only molecular targeting agent that is approved in the curative setting in combination with radiotherapy is the anti-EGFR-antibody cetuximab in HNSCC, and considerable doubts exist regarding its efficacy (150). The various approaches described in this review aimed to achieve a meaningful radiosensitization through combined inhibition of two or more targets, mostly with the aim of a more complete pathway inhibition or the suppression of compensatory mechanisms, partly with similarities to the concept of synthetic lethality (**Supplementary Figure 1**). The diversity of the approaches reflects the heterogeneity of radiosensitization strategies although some additional emerging concepts, such as interference with NAD^+-, glucose- or mitochondrial metabolism (151, 152) or the eradication of cancer stem cells (153, 154) were not identified in our search for combined targeting approaches. While molecular targeting is

also increasingly being considered as a strategy to enhance the efficacy of particle irradiation (155), we only identified one such publication, which reported the effect of PARP and Rad51 inhibition when added to proton (and photon) irradiation (106).

With 49 identified publications, the combined targeting of classical kinase dependent signal transduction pathways, such as EGFR, MAPK, or PI3K/AKT/mTOR signaling is the most exhaustively studied approach. The underlying rationale is that tumor cells often rely on the hyperactivation of these kinases to drive key mechanisms such as proliferation, survival and, to some extent, DNA repair ("oncogene addiction"). This should make them more sensitive to kinase inhibitors than normal tissue, providing some tumor specificity. What remains a major challenge is the choice of pathway inhibition for individual tumors, which requires reliable biomarkers. Unfortunately, the commonly analyzed kinase expression level is a poor surrogate for actual kinase activity, as we have recently demonstrated for EGFR activation in HNSCC (156). Keeping this in mind, it will be crucial to establish robust markers of aberrantly high activity, e.g., the detection of activating mutations, protein phosphorylation levels, or functional measurements. Given the identification of an overactive pathway, dual inhibition may be an appropriate way to achieve highly effective inhibition or to avoid bypass signaling through compensatory pathways or mutations of downstream pathway members. To what extent and in which setting a more effective inhibition of signal transduction pathways will subsequently also translate into a clinically meaningful radiosensitization and finally enhanced patient survival remains to be shown.

A major advantage for the targeting of DDR components is their direct involvement in radiation-induced DNA repair. On one hand, this makes it likely that a majority of tumors will be affected. On the other hand, specificity can be a major issue, as normal cells utilize the same pathways for DNA damage recognition, processing and repair. Nine of the 13 studies identified in this field combined PARP- and S/G2 phase checkpoint-inhibition. This approach is partly based on the model of synthetic lethality (see **Supplementary Figure 1**), which has been described for PARP inhibition and HR deficiency (157), as the inhibition of Chk1, Wee1, and ATR was reported to compromise HR (89, 158–160). The same concept applies to the direct targeting of the central HR factor Rad51 combined with PARP inhibition (106) and in part HSP90 inhibition plus PARP inhibition (132). As HR is only active in the S/G2 phase, some degree of tumor specificity can be expected because normal tissue cells mostly do not proliferate and, in contrast to the majority of tumor cells, are p53 proficient and therefore able to arrest in the G1 phase after irradiation. Additional S/G2 phase-derived DNA damage through PARP inhibition is likely to further increase the dependence on S/G2 arrest, which may further be fostered by oncogenic replication stress.

Similar characteristics, i.e., high pathway activity and tumor cells' reliance also motivate the targeting of adhesion molecules [e.g., high expression of focal adhesion signaling receptors (112)] or the heat shock response [e.g., proteostatic control of instable mutants (123)] in order to achieve

tumor specificity. Again, the additional inhibition of compensatory factors provides a main rationale for dual targeting approaches.

The tailored use of molecular targeting agents based on individual tumor characteristics is referred to as precision oncology. Apart from enhancing efficacy and thereby cure rates, molecular targeting is also expected to reduce toxicity, in case it can replace chemotherapy. It has to be noted, however, that the use of targeting agents can result in considerable side effects, which can of course be more severe and difficult to predict when agents are combined and added to (chemo-) radiotherapy. For example, EGFR inhibition frequently causes skin rash and diarrhea (161), which can be especially severe in the radiation field, when the effects add up with (chemo-) radiation induced erythema/mucositis (162). In a phase 3 study for HNSCC the addition of cetuximab to cisplatin-based chemoradiation resulted in considerably more grade 3/4 mucositis and rash and hence higher rates of interruptions in radiation therapy without achieving any clinical benefit (8). As further examples, combining bevacizumab with concomitant radiotherapy can lead to decreased wound healing (163, 164) and, in patients with lung cancer, to fistula formation (165), and the Chk1 inhibitors LY2603618 and ADZ7762 increased the risk of severe thromboembolic events (166) and cardiac side effects (167), respectively, in part when combined with chemotherapy. At present, preclinical data on tumor radiosensitization hardly ever contain thorough *in vivo* analyses of side effects other than weight loss and inspection of the skin/mucosa in the radiation field. Future approaches should therefore not only focus on the identification of the most efficacious radiosensitization but also more deeply on the safety of a possible clinical translation. Detailed *in vivo* studies on systemic as well as in-field toxicity may help design the most promising clinical trials and achieve better clinical outcomes.

In conclusion, dual targeting for tumor radiosensitization has shown promising results in pre-clinical studies. The way to proceed toward a substantial future clinical benefit requires convincing *in vitro* mechanistic studies that should ideally include predictive biomarkers, with the results substantiated in a relevant number of adequate model systems, such as cell lines and (patient derived) xenografts, but possibly also tumor stem cell cultures as well as *ex vivo* cultured tumor tissues. The most promising combined targeting approaches should be thoroughly inspected for treatment efficacy and safety based on normal tissue toxicity *in vivo*. Such a concept should lead to the identification of effective targeting strategies for subsets of tumors, based on reliable predictive biomarkers to provide the best possible preclinical rationale to allow clinicians to implement the most appropriate combined targeting strategies in well-designed clinical trials.

AUTHOR CONTRIBUTIONS

KH and TR: idea, literature search, and preparation of tables and figures. All authors were involved in the preparation of the manuscript.

FUNDING

SUPPLEMENTARY MATERIAL

The Supplementary Material for this article can be found online at: https://www.frontiersin.org/articles/10.3389/fonc.2020.01260/full#supplementary-material

REFERENCES

1. Blanchard P, Baujat B, Holostenco V, Bourredjem A, Baey C, Bourhis J, et al. Meta-analysis of chemotherapy in head and neck cancer (MACH-NC): a comprehensive analysis by tumour site. *Radiother Oncol.* (2011) 100:33–40. doi: 10.1016/j.radonc.2011.05.036

2. Bourhis J, Sire C, Graff P, Gregoire V, Maingon P, Calais G, et al. Concomitant chemoradiotherapy versus acceleration of radiotherapy with or without concomitant chemotherapy in locally advanced head and neck carcinoma (GORTEC 99-02): an open-label phase 3 randomised trial. *Lancet Oncol.* (2012) 13:145–53. doi: 10.1016/S1470-2045(11)70346-1

3. Dasari S, Tchounwou PB. Cisplatin in cancer therapy: molecular mechanisms of action. *Eur J Pharmacol.* (2014) 740:364–78. doi: 10.1016/j.ejphar.2014.07.025

4. Bonner JA, Harari PM, Giralt J, Azarnia N, Shin DM, Cohen RB, et al. Radiotherapy plus cetuximab for squamous-cell carcinoma of the head and neck. *N Engl J Med.* (2006) 354:567–78. doi: 10.1056/NEJMoa053422

5. Petrelli F, Coinu A, Riboldi V, Borgonovo K, Ghilardi M, Cabiddu M, et al. Concomitant platinum-based chemotherapy or cetuximab with radiotherapy for locally advanced head and neck cancer: a systematic review and meta-analysis of published studies. *Oral Oncol.* (2014) 50:1041–8. doi: 10.1016/j.oraloncology.2014.08.005

6. Magrini SM, Buglione M, Corvo R, Pirtoli L, Paiar F, Ponticelli P, et al. Cetuximab and radiotherapy versus cisplatin and radiotherapy for locally advanced head and neck cancer: a randomized phase II trial. *J Clin Oncol.* (2016) 34:427–35. doi: 10.1200/JCO.2015.63.1671

7. Beckham TH, Barney C, Healy E, Wolfe AR, Branstetter A, Yaney A, et al. Platinum-based regimens versus cetuximab in definitive chemoradiation for human papillomavirus-unrelated head and neck cancer. *Int J Cancer.* (2019) 147:107–15. doi: 10.1002/ijc.32736

8. Ang KK, Zhang Q, Rosenthal DI, Nguyen-Tan PF, Sherman EJ, Weber RS, et al. Randomized phase III trial of concurrent accelerated radiation plus cisplatin with or without cetuximab for stage III to IV head and neck carcinoma: RTOG 0522. *J Clin Oncol.* (2014) 32:2940–50. doi: 10.1200/JCO.2013.53.5633

9. Gillison ML, Trotti AM, Harris J, Eisbruch A, Harari PM, Adelstein DJ, et al. Radiotherapy plus cetuximab or cisplatin in human papillomavirus-positive oropharyngeal cancer. (NRG Oncology RTOG 1016): a randomised, multicentre, non-inferiority trial. *Lancet.* (2019) 393:40–50. doi: 10.1016/S0140-6736(18)32779-X

10. Mehanna H, Robinson M, Hartley A, Kong A, Foran B, Fulton-Lieuw T, et al. Radiotherapy plus cisplatin or cetuximab in low-risk human papillomavirus-positive oropharyngeal cancer. (De-ESCALaTE HPV): an open-label randomised controlled phase

3 trial. *Lancet*. (2019) 393:51–60. doi: 10.1016/S0140-6736(18)3 2752-1

11. Rosenthal DI, Harari PM, Giralt J, Bell D, Raben D, Liu J, et al. Association of human papillomavirus and p16 status with outcomes in the IMCL-9815 phase III registration trial for patients with locoregionally advanced oropharyngeal squamous cell carcinoma of the head and neck treated with radiotherapy with or without cetuximab. *J Clin Oncol*. (2016) 34:1300–8. doi: 10.1200/JCO.2015.62.5970

12. Morgan MA, Parsels LA, Maybaum J, Lawrence TS. Improving the efficacy of chemoradiation with targeted agents. *Cancer Discov*. (2014) 4:280–91. doi: 10.1158/2159-8290.CD-13-0337

13. Meyn RE, Munshi A, Haymach JV, Milas L, Ang KK. Receptor signaling as a regulatory mechanism of DNA repair. *Radiother Oncol*. (2009) 92:316–22. doi: 10.1016/j.radonc.2009.06.031

14. Toulany M. Targeting DNA double-strand break repair pathways to improve radiotherapy response. *Genes*. (2019) 10:25. doi: 10.3390/genes10010025

15. Liu Q, Yu S, Zhao W, Qin S, Chu Q, Wu K. EGFR-TKIs resistance via EGFR-independent signaling pathways. *Mol Cancer*. (2018) 17:53. doi: 10.1186/s12943-018-0793-1

16. Bogdan S, Klambt C. Epidermal growth factor receptor signaling. *Curr Biol*. (2001) 11:R292–5. doi: 10.1016/S0960-9822(01)00167-1

17. Normanno N, De Luca A, Bianco C, Strizzi L, Mancino M, Maiello MR, et al. Epidermal growth factor receptor. (EGFR) signaling in cancer. *Gene*. (2006) 366:2–16. doi: 10.1016/j.gene.2005.10.018

18. Bianco R, Gelardi T, Damiano V, Ciardiello F, Tortora G. Rational bases for the development of EGFR inhibitors for cancer treatment. *Int J Biochem Cell Biol*. (2007) 39:1416–31. doi: 10.1016/j.biocel.2007.05.008

19. Mendelsohn J, Baselga J. Epidermal growth factor receptor targeting in cancer. *Semin Oncol*. (2006) 33:369–85. doi: 10.1053/j.seminoncol.2006.04.003

20. Fukutome M, Maebayashi K, Nasu S, Seki K, Mitsuhashi N. Enhancement of radiosensitivity by dual inhibition of the HER family with ZD1839. ("Iressa") and trastuzumab. ("Herceptin"). *Int J Radiat Oncol Biol Phys*. (2006) 66:528–36. doi: 10.1016/j.ijrobp.2006.05.036

21. Zhou H, Kim YS, Peletier A, Mccall W, Earp HS, Sartor CI. Effects of the EGFR/HER2 kinase inhibitor GW572016 on EGFR- and HER2-overexpressing breast cancer cell line proliferation, radiosensitization, and resistance. *Int J Radiat Oncol Biol Phys*. (2004) 58:344–52. doi: 10.1016/j.ijrobp.2003.09.046

22. Sambade MJ, Camp JT, Kimple RJ, Sartor CI, Shields JM. Mechanism of lapatinib-mediated radiosensitization of breast cancer cells is primarily by inhibition of the Raf>MEK>ERK mitogen-activated protein kinase cascade and radiosensitization of lapatinib-resistant cells restored by direct inhibition of MEK. *Radiother Oncol*. (2009) 93:639–44. doi: 10.1016/j.radonc.2009.09.006

23. Kimple RJ, Vaseva AV, Cox AD, Baerman KM, Calvo BF, Tepper JE, et al. Radiosensitization of epidermal growth factor receptor/HER2-positive pancreatic cancer is mediated by inhibition of Akt independent of ras mutational status. *Clin Cancer Res*. (2010) 16:912–23. doi: 10.1158/1078-0432.CCR-09-1324

24. Sambade MJ, Kimple RJ, Camp JT, Peters E, Livasy CA, Sartor CI, et al. Lapatinib in combination with radiation diminishes tumor regrowth in HER2+ and basal-like/EGFR+ breast tumor xenografts. *Int J Radiat Oncol Biol Phys*. (2010) 77:575–81. doi: 10.1016/j.ijrobp.2009.12.063

25. Yu T, Cho BJ, Choi EJ, Park JM, Kim DH, Kim IA. Radiosensitizing effect of lapatinib in human epidermal growth factor receptor 2-positive breast cancer cells. *Oncotarget*. (2016) 7:79089–100. doi: 10.18632/oncotarget.12597

26. Paldor I, Abbadi S, Bonne N, Ye X, Rodriguez FJ, Rowshanshad D, et al. The efficacy of lapatinib and nilotinib in combination with radiation therapy in a model of NF2 associated peripheral schwannoma. *J Neurooncol*. (2017) 135:47–56. doi: 10.1007/s11060-017-2567-9

27. Mu Y, Sun D. Lapatinib, a dual inhibitor of epidermal growth factor receptor (EGFR) and HER-2, enhances radiosensitivity in mouse bladder tumor line-2 (MBT-2) cells *in vitro* and *in vivo*. *Med Sci Monit*. (2018) 24:5811–9. doi: 10.12659/MSM.909865

28. Huang S, Li C, Armstrong EA, Peet CR, Saker J, Amler LC, et al. Dual targeting of EGFR and HER3 with MEHD7945A overcomes acquired

29. Li C, Huang S, Armstrong EA, Francis DM, Werner LR, Sliwkowski MX, et al. Antitumor effects of MEHD7945A, a dual-specific antibody against EGFR and HER3, in combination with radiation in lung and head and neck cancers. *Mol Cancer Ther*. (2015) 14:2049–59. doi: 10.1158/1535-7163.MCT-15-0155

30. Van Der Veeken J, Oliveira S, Schiffelers RM, Storm G, Van Bergen En Henegouwen PM, Roovers RC. Crosstalk between epidermal growth factor receptor- and insulin-like growth factor-1 receptor signaling: implications for cancer therapy. *Curr Cancer Drug Targets*. (2009) 9:748–60. doi: 10.2174/156800909789271495

31. Matsumoto F, Valdecanas DN, Mason KA, Milas L, Ang KK, Raju U. The impact of timing of EGFR and IGF-1R inhibition for sensitizing head and neck cancer to radiation. *Anticancer Res*. (2012) 32:3029–35.

32. Wang Y, Yuan JL, Zhang YT, Ma JJ, Xu P, Shi CH, et al. Inhibition of both EGFR and IGF1R sensitized prostate cancer cells to radiation by synergistic suppression of DNA homologous recombination repair. *PLoS ONE*. (2013) 8:e68784. doi: 10.1371/journal.pone.0068784

33. Li P, Veldwijk MR, Zhang Q, Li ZB, Xu WC, Fu S. Co-inhibition of epidermal growth factor receptor and insulin-like growth factor receptor 1 enhances radiosensitivity in human breast cancer cells. *BMC Cancer*. (2013) 13:297. doi: 10.1186/1471-2407-13-297

34. Benavente S, Huang S, Armstrong EA, Chi A, Hsu KT, Wheeler DL, et al. Establishment and characterization of a model of acquired resistance to epidermal growth factor receptor targeting agents in human cancer cells. *Clin Cancer Res*. (2009) 15:1585–92. doi: 10.1158/1078-0432.CCR-08-2068

35. Karapetis CS, Khambata-Ford S, Jonker DJ, O'callaghan CJ, Tu D, Tebbutt NC, et al. K-ras mutations and benefit from cetuximab in advanced colorectal cancer. *N Engl J Med*. (2008) 359:1757–65. doi: 10.1056/NEJMoa0804385

36. Bokemeyer C, Bondarenko I, Hartmann JT, De Braud F, Schuch G, Zubel A, et al. Efficacy according to biomarker status of cetuximab plus FOLFOX-4 as first-line treatment for metastatic colorectal cancer: the OPUS study. *Ann Oncol*. (2011) 22:1535–46. doi: 10.1093/annonc/mdq632

37. Bonner JA, Trummell HQ, Bonner AB, Willey CD, Bredel M, Yang ES. Enhancement of Cetuximab-Induced Radiosensitization by JAK-1 Inhibition. *BMC Cancer*. (2015) 15:673. doi: 10.1186/s12885-015-1679-x

38. Eke I, Schneider L, Forster C, Zips D, Kunz-Schughart LA, Cordes N. EGFR/JIP-4/JNK2 signaling attenuates cetuximab-mediated radiosensitization of squamous cell carcinoma cells. *Cancer Res*. (2013) 73:297–306. doi: 10.1158/0008-5472.CAN-12-2021

39. Zhuang H, Bai J, Chang JY, Yuan Z, Wang P. MTOR inhibition reversed drug resistance after combination radiation with erlotinib in lung adenocarcinoma. *Oncotarget*. (2016) 7:84688–94. doi: 10.18632/oncotarget.12423

40. Ellis LM, Hicklin DJ. VEGF-targeted therapy: mechanisms of anti-tumour activity. *Nat Rev Cancer*. (2008) 8:579–91. doi: 10.1038/nrc2403

41. Goel HL, Mercurio AM. VEGF targets the tumour cell. *Nat Rev Cancer*. (2013) 13:871–82. doi: 10.1038/nrc3627

42. Huang SM, Harari PM. Modulation of radiation response after epidermal growth factor receptor blockade in squamous cell carcinomas: inhibition of damage repair, cell cycle kinetics, and tumor angiogenesis. *Clin Cancer Res*. (2000) 6:2166–74.

43. Tabernero J. The role of VEGF and EGFR inhibition: implications for combining anti-VEGF and anti-EGFR agents. *Mol Cancer Res*. (2007) 5:203–20. doi: 10.1158/1541-7786.MCR-06-0404

44. Bozec A, Formento P, Lassalle S, Lippens C, Hofman P, Milano G. Dual inhibition of EGFR and VEGFR pathways in combination with irradiation: antitumour supra-additive effects on human head and neck cancer xenografts. *Br J Cancer*. (2007) 97:65–72. doi: 10.1038/sj.bjc.6603791

45. Bozec A, Sudaka A, Fischel JL, Brunstein MC, Etienne-Grimaldi MC, Milano G. Combined effects of bevacizumab with erlotinib and irradiation: a preclinical study on a head and neck cancer orthotopic model. *Br J Cancer*. (2008) 99:93–9. doi: 10.1038/sj.bjc.6604429

46. Bozec A, Sudaka A, Toussan N, Fischel JL, Etienne-Grimaldi MC, Milano G. Combination of sunitinib, cetuximab and irradiation in an

orthotopic head and neck cancer model. *Ann Oncol.* (2009) 20:1703–7. doi: 10.1093/annonc/mdp070

47. Bozec A, Etienne-Grimaldi MC, Fischel JL, Sudaka A, Toussan N, Formento P, et al. The mTOR-targeting drug temsirolimus enhances the growth-inhibiting effects of the cetuximab-bevacizumab-irradiation combination on head and neck cancer xenografts. *Oral Oncol.* (2011) 47:340–4. doi: 10.1016/j.oraloncology.2011.02.020

48. Bozec A, Lassalle S, Gugenheim J, Fischel JL, Formento P, Hofman P, et al. Enhanced tumour antiangiogenic effects when combining gefitinib with the antivascular agent ZD6126. *Br J Cancer.* (2006) 95:722–8. doi: 10.1038/sj.bjc.6603308

49. Shibuya K, Komaki R, Shintani T, Itasaka S, Ryan A, Jurgensmeier JM, et al. Targeted therapy against VEGFR and EGFR with ZD6474 enhances the therapeutic efficacy of irradiation in an orthotopic model of human non-small-cell lung cancer. *Int J Radiat Oncol Biol Phys.* (2007) 69:1534–43. doi: 10.1016/j.ijrobp.2007.07.2350

50. Oehler-Janne C, Jochum W, Riesterer O, Broggini-Tenzer A, Caravatti G, Vuong V, et al. Hypoxia modulation and radiosensitization by the novel dual EGFR and VEGFR inhibitor AEE788 in spontaneous and related allograft tumor models. *Mol Cancer Ther.* (2007) 6:2496–504. doi: 10.1158/1535-7163.MCT-07-0253

51. Wachsberger PR, Lawrence YR, Liu Y, Daroczi B, Xu X, Dicker AP. Epidermal growth factor receptor expression modulates antitumor efficacy of vandetanib or cediranib combined with radiotherapy in human glioblastoma xenografts. *Int J Radiat Oncol Biol Phys.* (2012) 82:483–91. doi: 10.1016/j.ijrobp.2010.09.019

52. Horn D, Hess J, Freier K, Hoffmann J, Freudlsperger C. Targeting EGFR-PI3K-AKT-mTOR signaling enhances radiosensitivity in head and neck squamous cell carcinoma. *Expert Opin Ther Targets.* (2015) 19:795–805. doi: 10.1517/14728222.2015.1012157

53. Wise HM, Hermida MA, Leslie NR. Prostate cancer, PI3K, PTEN and prognosis. *Clin Sci.* (2017) 131:197–210. doi: 10.1042/CS20160026

54. Sobhani N, Roviello G, Corona SP, Scaltriti M, Ianza A, Bortul M, et al. The prognostic value of PI3K mutational status in breast cancer: a meta-analysis. *J Cell Biochem.* (2018) 119:4287–92. doi: 10.1002/jcb.26687

55. Marquard FE, Jücker M. PI3K/AKT/mTOR signaling as a molecular target in head and neck cancer. *Biochem Pharmacol.* (2019) 172:113729. doi: 10.1016/j.bcp.2019.113729

56. Miyahara H, Yadavilli S, Natsumeda M, Rubens JA, Rodgers L, Kambhampati M, et al. The dual mTOR kinase inhibitor TAK228 inhibits tumorigenicity and enhances radiosensitization in diffuse intrinsic pontine glioma. *Cancer Lett.* (2017) 400:110–6. doi: 10.1016/j.canlet.2017.04.019

57. Liu ZG, Tang J, Chen Z, Zhang H, Wang H, Yang J, et al. The novel mTORC1/2 dual inhibitor INK128 enhances radiosensitivity of breast cancer cell line MCF-7. *Int J Oncol.* (2016) 49:1039–45. doi: 10.3892/ijo.2016.3604

58. Hayman TJ, Kramp T, Kahn J, Jamal M, Camphausen K, Tofilon PJ. Competitive but not allosteric mTOR kinase inhibition enhances tumor cell radiosensitivity. *Transl Oncol.* (2013) 6:355–62. doi: 10.1593/tlo.13163

59. Kahn J, Hayman TJ, Jamal M, Rath BH, Kramp T, Camphausen K, et al. The mTORC1/mTORC2 inhibitor AZD2014 enhances the radiosensitivity of glioblastoma stem-like cells. *Neuro Oncol.* (2014) 16:29–37. doi: 10.1093/neuonc/not139

60. Yu CC, Hung SK, Lin HY, Chiou WY, Lee MS, Liao HF, et al. Targeting the PI3K/AKT/mTOR signaling pathway as an effectively radiosensitizing strategy for treating human oral squamous cell carcinoma *in vitro* and *in vivo*. *Oncotarget.* (2017) 8:68641–53. doi: 10.18632/oncotarget.19817

61. Mukherjee B, Tomimatsu N, Amancherla K, Camacho CV, Pichamoorthy N, Burma S. The dual PI3K/mTOR inhibitor NVP-BEZ235 is a potent inhibitor of ATM- and DNA-PKcs-mediated DNA damage responses. *Neoplasia.* (2012) 14:34–43. doi: 10.1593/neo.111512

62. Gil Del Alcazar CR, Hardebeck MC, Mukherjee B, Tomimatsu N, Gao X, Yan J, et al. Inhibition of DNA double-strand break repair by the dual PI3K/mTOR inhibitor NVP-BEZ235 as a strategy for radiosensitization of glioblastoma. *Clin Cancer Res.* (2014) 20:1235–48. doi: 10.1158/1078-0432.CCR-13-1607

63. Gupta S, Ramjaun AR, Haiko P, Wang Y, Warne PH, Nicke B, et al. Binding of ras to phosphoinositide 3-kinase p110alpha is

64. required for ras-driven tumorigenesis in mice. *Cell.* (2007) 129:957–68. doi: 10.1016/j.cell.2007.03.051

64. Konstantinidou G, Bey EA, Rabellino A, Schuster K, Maira MS, Gazdar AF, et al. Dual phosphoinositide 3-kinase/mammalian target of rapamycin blockade is an effective radiosensitizing strategy for the treatment of non-small cell lung cancer harboring K-RAS mutations. *Cancer Res.* (2009) 69:7644–52. doi: 10.1158/0008-5472.CAN-09-0823

65. Chen YH, Wei MF, Wang CW, Lee HW, Pan SL, Gao M, et al. Dual phosphoinositide 3-kinase/mammalian target of rapamycin inhibitor is an effective radiosensitizer for colorectal cancer. *Cancer Lett.* (2015) 357:582–90. doi: 10.1016/j.canlet.2014.12.015

66. Kuger S, Graus D, Brendtke R, Gunther N, Katzer A, Lutyj P, et al. Radiosensitization of glioblastoma cell lines by the dual PI3K and mTOR Inhibitor NVP-BEZ235 depends on drug-irradiation schedule. *Transl Oncol.* (2013) 6:169–79. doi: 10.1593/tlo.12364

67. Potiron VA, Abderrahmani R, Giang E, Chiavassa S, Di Tomaso E, Maira SM, et al. Radiosensitization of prostate cancer cells by the dual PI3K/mTOR inhibitor BEZ235 under normoxic and hypoxic conditions. *Radiother Oncol.* (2013) 106:138–46. doi: 10.1016/j.radonc.2012.11.014

68. Zhu W, Fu W, Hu L. NVP-BEZ235, dual phosphatidylinositol 3-kinase/mammalian target of rapamycin inhibitor, prominently enhances radiosensitivity of prostate cancer cell line PC-3. *Cancer Biother Radiopharm.* (2013) 28:665–73. doi: 10.1089/cbr.2012.1443

69. Chang L, Graham PH, Hao J, Ni J, Bucci J, Cozzi PJ, et al. PI3K/Akt/mTOR pathway inhibitors enhance radiosensitivity in radioresistant prostate cancer cells through inducing apoptosis, reducing autophagy, suppressing NHEJ and HR repair pathways. *Cell Death Dis.* (2014) 5:e1437. doi: 10.1038/cddis.2014.415

70. Schötz U, Balzer V, Brandt FW, Frank Ziemann F, Subtil FSB, Rieckmann T, et al. Dual PI3K/mTOR inhibitor NVP-BEZ235 enhances radiosensitivity of head and neck squamous cell carcinoma (HNSCC) cell lines due to suppressed double-strand break (DSB) repair by non-homologous end joining. *Cancers.* (2020) 12:467. doi: 10.3390/cancers12020467

71. Jang NY, Kim DH, Cho BJ, Choi EJ, Lee JS, Wu HG, et al. Radiosensitization with combined use of olaparib and PI-103 in triple-negative breast cancer. *BMC Cancer.* (2015) 15:89. doi: 10.1186/s12885-015-1090-7

72. Prevo R, Deutsch E, Sampson O, Diplexcito J, Cengel K, Harper J, et al. Class I PI3 kinase inhibition by the pyridinylfuranopyrimidine inhibitor PI-103 enhances tumor radiosensitivity. *Cancer Res.* (2008) 68:5915–23. doi: 10.1158/0008-5472.CAN-08-0757

73. Leiker AJ, Degraff W, Choudhuri R, Sowers AL, Thetford A, Cook JA, et al. Radiation enhancement of head and neck squamous cell carcinoma by the dual PI3K/mTOR inhibitor PF-05212384. *Clin Cancer Res.* (2015) 21:2792–801. doi: 10.1158/1078-0432.CCR-14-3279

74. Tonlaar N, Galoforo S, Thibodeau BJ, Ahmed S, Wilson TG, Yumpo Cardenas P, et al. Antitumor activity of the dual PI3K/MTOR inhibitor, PF-04691502, in combination with radiation in head and neck cancer. *Radiother Oncol.* (2017) 124:504–12. doi: 10.1016/j.radonc.2017.08.001

75. Fokas E, Im JH, Hill S, Yameen S, Stratford M, Beech J, et al. Dual inhibition of the PI3K/mTOR pathway increases tumor radiosensitivity by normalizing tumor vasculature. *Cancer Res.* (2012) 72:239–48. doi: 10.1158/0008-5472.CAN-11-2263

76. Fokas E, Yoshimura M, Prevo R, Higgins G, Hackl W, Maira SM, et al. NVP-BEZ235 and NVP-BGT226, dual phosphatidylinositol 3-kinase/mammalian target of rapamycin inhibitors, enhance tumor and endothelial cell radiosensitivity. *Radiat Oncol.* (2012) 7:48. doi: 10.1186/1748-717X-7-48

77. Holler M, Grottke A, Mueck K, Manes J, Jucker M, Rodemann HP, et al. Dual targeting of Akt and mTORC1 impairs repair of DNA double-strand breaks and increases radiation sensitivity of human tumor cells. *PLoS ONE.* (2016) 11:e0154745. doi: 10.1371/journal.pone.0154745

78. Williams TM, Flecha AR, Keller P, Ram A, Karnak D, Galban S, et al. Cotargeting MAPK and PI3K signaling with concurrent radiotherapy as a strategy for the treatment of pancreatic cancer. *Mol Cancer Ther.* (2012) 11:1193–202. doi: 10.1158/1535-7163.MCT-12-0098

79. Toulany M, Iida M, Keinath S, Iyi FF, Mueck K, Fehrenbacher B, et al. Dual targeting of PI3K and MEK enhances the radiation response of K-RAS mutated non-small cell lung cancer. *Oncotarget.* (2016) 7:43746–61. doi: 10.18632/oncotarget.9670

80. Kuger S, Flentje M, Djuzenova CS. Simultaneous perturbation of the MAPK and the PI3K/mTOR pathways does not lead to increased radiosensitization. *Radiat Oncol.* (2015) 10:214. doi: 10.1186/s13014-015-0514-5

81. Blas K, Wilson TG, Tonlaar N, Galoforo S, Hana A, Marples B, et al. Dual blockade of PI3K and MEK in combination with radiation in head and neck cancer. *Clin Transl Radiat Oncol.* (2018) 11:1–10. doi: 10.1016/j.ctro.2018.04.003

82. Carrano AV. Chromosome aberrations and radiation-induced cell death II Predicted and observed cell survival. *Mutat Res.* (1973) 17:355–66. doi: 10.1016/0027-5107(73)90007-9

83. Dillon MT, Good JS, Harrington KJ. Selective targeting of the G2/M cell cycle checkpoint to improve the therapeutic index of radiotherapy. *Clin Oncol.* (2014) 26:257–65. doi: 10.1016/j.clon.2014.01.009

84. Moore PS, Chang Y. Why do viruses cause cancer? Highlights of the first century of human tumour virology. *Nat Rev Cancer.* (2010) 10:878–89. doi: 10.1038/nrc2961

85. Joerger AC, Fersht AR. The p53 pathway: origins, inactivation in cancer, and emerging therapeutic approaches. *Annu Rev Biochem.* (2016) 85:375–404. doi: 10.1146/annurev-biochem-060815-014710

86. Qiu Z, Oleinick NL, Zhang J. ATR/CHK1 inhibitors and cancer therapy. *Radiother Oncol.* (2018) 126:450–64. doi: 10.1016/j.radonc.2017.09.043

87. Zhang Y, Hunter T. Roles of Chk1 in cell biology and cancer therapy. *Int J Cancer.* (2014) 134:1013–23. doi: 10.1002/ijc.28226

88. Watanabe N, Broome M, Hunter T. Regulation of the human WEE1Hu CDK tyrosine 15-kinase during the cell cycle. *EMBO J.* (1995) 14:1878–91. doi: 10.1002/j.1460-2075.1995.tb07180.x

89. Krajewska M, Heijink AM, Bisselink YJ, Seinstra RI, Sillje HH, De Vries EG, et al. Forced activation of Cdk1 via wee1 inhibition impairs homologous recombination. *Oncogene.* (2013) 32:3001–8. doi: 10.1038/onc.2012.296

90. Godon C, Cordelieres FP, Biard D, Giocanti N, Megnin-Chanet F, Hall J, et al. PARP inhibition versus PARP-1 silencing: different outcomes in terms of single-strand break repair and radiation susceptibility. *Nucleic Acids Res.* (2008) 36:4454–64. doi: 10.1093/nar/gkn403

91. Helleday T. The underlying mechanism for the PARP and BRCA synthetic lethality: clearing up the misunderstandings. *Mol Oncol.* (2011) 5:387–93. doi: 10.1016/j.molonc.2011.07.001

92. Murai J, Huang SY, Das BB, Renaud A, Zhang Y, Doroshow JH, et al. Trapping of PARP1 and PARP2 by Clinical PARP Inhibitors. *Cancer Res.* (2012) 72:5588–99. doi: 10.1158/0008-5472.CAN-12-2753

93. Iliakis G. Backup pathways of NHEJ in cells of higher eukaryotes: cell cycle dependence. *Radiother Oncol.* (2009) 92:310–5. doi: 10.1016/j.radonc.2009.06.024

94. Bryant HE, Schultz N, Thomas HD, Parker KM, Flower D, Lopez E, et al. Specific killing of BRCA2-deficient tumours with inhibitors of poly(ADP-ribose) polymerase. *Nature.* (2005) 434:913–7. doi: 10.1038/nature03443

95. Busch CJ, Kroger MS, Jensen J, Kriegs M, Gatzemeier F, Petersen C, et al. G2-checkpoint targeting and radiosensitization of HPV/p16-positive HNSCC cells through the inhibition of Chk1 and Wee1. *Radiother Oncol.* (2017) 122:260–6. doi: 10.1016/j.radonc.2016.11.017

96. Vance S, Liu E, Zhao L, Parsels JD, Parsels LA, Brown JL, et al. Selective radiosensitization of p53 mutant pancreatic cancer cells by combined inhibition of Chk1 and PARP1. *Cell Cycle.* (2011) 10:4321–9. doi: 10.4161/cc.10.24.18661

97. Guster JD, Weissleder SV, Busch CJ, Kriegs M, Petersen C, Knecht R, et al. The inhibition of PARP but not EGFR results in the radiosensitization of HPV/p16-positive HNSCC cell lines. *Radiother Oncol.* (2014) 113:345–51. doi: 10.1016/j.radonc.2014.10.011

98. Karnak D, Engelke CG, Parsels LA, Kausar T, Wei D, Robertson JR, et al. Combined inhibition of Wee1 and PARP1/2 for radiosensitization in pancreatic cancer. *Clin Cancer Res.* (2014) 20:5085–96. doi: 10.1158/1078-0432.CCR-14-1038

99. Cuneo KC, Morgan MA, Davis MA, Parcels LA, Parcels J, Karnak D, et al. Wee1 kinase inhibitor AZD1775 radiosensitizes hepatocellular carcinoma regardless of TP53 mutational status through induction of replication stress. *Int J Radiat Oncol Biol Phys.* (2016) 95:782–90. doi: 10.1016/j.ijrobp.2016.01.028

100. Parsels LA, Karnak D, Parsels JD, Zhang Q, Velez-Padilla J, Reichert ZR, et al. PARP1 trapping and DNA replication stress enhance radiosensitization with combined WEE1 and PARP inhibitors. *Mol Cancer Res.* (2018) 16:222–32. doi: 10.1158/1541-7786.MCR-17-0455

101. Molkentine JM, Molkentine DP, Bridges KA, Xie T, Yang L, Sheth A, et al. Targeting DNA damage response in head and neck cancers through abrogation of cell cycle checkpoints. *Int J Radiat Biol.* 25:1–8. doi: 10.1080/09553002.2020.1730014

102. Cimprich KA, Cortez D. ATR: an essential regulator of genome integrity. *Nat Rev Mol Cell Biol.* (2008) 9:616–27. doi: 10.1038/nrm2450

103. Fokas E, Prevo R, Hammond EM, Brunner TB, Mckenna WG, Muschel RJ. Targeting ATR in DNA damage response and cancer therapeutics. *Cancer Treat Rev.* (2014) 40:109–17. doi: 10.1016/j.ctrv.2013.03.002

104. Carruthers RD, Ahmed SU, Ramachandran S, Strathdee K, Kurian KM, Hedley A, et al. Replication stress drives constitutive activation of the DNA damage response and radioresistance in glioblastoma stem-like cells. *Cancer Res.* (2018) 78:5060–71. doi: 10.1158/0008-5472.CAN-18-0569

105. Ahmed SU, Carruthers R, Gilmour L, Yildirim S, Watts C, Chalmers AJ. Selective inhibition of parallel DNA damage response pathways optimizes radiosensitization of glioblastoma stem-like cells. *Cancer Res.* (2015) 75:4416–28. doi: 10.1158/0008-5472.CAN-14-3790

106. Wera AC, Lobbens A, Stoyanov M, Lucas S, Michiels C. Radiation-induced synthetic lethality: combination of poly(ADP-ribose) polymerase and RAD51 inhibitors to sensitize cells to proton irradiation. *Cell Cycle.* (2019) 18:1770–83. doi: 10.1080/15384101.2019.1632640

107. Zeng L, Beggs RR, Cooper TS, Weaver AN, Yang ES. Combining Chk1/2 inhibition with cetuximab and radiation enhances *in vitro* and *in vivo* cytotoxicity in head and neck squamous cell carcinoma. *Mol Cancer Ther.* (2017) 16:591–600. doi: 10.1158/1535-7163.MCT-16-0352

108. Mahaney BL, Meek K, Lees-Miller SP. Repair of ionizing radiation-induced DNA double-strand breaks by non-homologous end-joining. *Biochem J.* (2009) 417:639–50. doi: 10.1042/BJ20080413

109. Goodwin JF, Knudsen KE. Beyond DNA repair: DNA-PK function in cancer. *Cancer Discov.* (2014) 4:1126–39. doi: 10.1158/2159-8290.CD-14-0358

110. Hafsi H, Dillon MT, Barker HE, Kyula JN, Schick U, Paget JT, et al. Combined ATR and DNA-PK inhibition radiosensitizes tumor cells independently of their p53 status. *Front Oncol.* (2018) 8:245. doi: 10.3389/fonc.2018.00245

111. Blandin AF, Renner G, Lehmann M, Lelong-Rebel I, Martin S, Dontenwill M. beta1 integrins as therapeutic targets to disrupt hallmarks of cancer. *Front Pharmacol.* (2015) 6:279. doi: 10.3389/fphar.2015.00279

112. Eke I, Cordes N. Focal adhesion signaling and therapy resistance in cancer. *Semin Cancer Biol.* (2015) 31:65–75. doi: 10.1016/j.semcancer.2014.07.009

113. Eke I, Zscheppang K, Dickreuter E, Hickmann L, Mazzeo E, Unger K, et al. Simultaneous beta1 integrin-EGFR targeting and radiosensitization of human head and neck cancer. *J Natl Cancer Inst.* (2015) 107. doi: 10.1093/jnci/dju419

114. Eke I, Cordes N. Dual targeting of EGFR and focal adhesion kinase in 3D grown HNSCC cell cultures. *Radiother Oncol.* (2011) 99:279–86. doi: 10.1016/j.radonc.2011.06.006

115. Zscheppang K, Kurth I, Wachtel N, Dubrovska A, Kunz-Schughart LA, Cordes N. Efficacy of beta1 integrin and EGFR targeting in sphere-forming human head and neck cancer cells. *J Cancer.* (2016) 7:736–45. doi: 10.7150/jca.14232

116. Poschau M, Dickreuter E, Singh-Muller J, Zscheppang K, Eke I, Liersch T, et al. EGFR and beta1-integrin targeting differentially affect colorectal carcinoma cell radiosensitivity and invasion. *Radiother Oncol.* (2015) 116:510–6. doi: 10.1016/j.radonc.2015.06.005

117. Klapproth E, Dickreuter E, Zakrzewski F, Seifert M, Petzold A, Dahl A, et al. Whole exome sequencing identifies mTOR and KEAP1 as potential targets for radiosensitization of HNSCC cells refractory to EGFR and beta1 integrin inhibition. *Oncotarget.* (2018) 9:18099–114. doi: 10.18632/oncotarget.24266

118. Koppenhagen P, Dickreuter E, Cordes N. Head and neck cancer cell radiosensitization upon dual targeting of c-Abl and beta1-integrin. *Radiother Oncol.* (2017) 124:370–8. doi: 10.1016/j.radonc.2017.05.011

119. Vehlow A, Klapproth E, Storch K, Dickreuter E, Seifert M, Dietrich A, et al. Adhesion- and stress-related adaptation of glioma radiochemoresistance is circumvented by beta1 integrin/JNK co-targeting. *Oncotarget.* (2017) 8:49224–37. doi: 10.18632/oncotarget.17480

120. Morimoto RI. Cells in stress: transcriptional activation of heat shock genes. *Science*. (1993) 259:1409–10. doi: 10.1126/science.8451637

121. Jego G, Hazoume A, Seigneuric R, Garrido C. Targeting heat shock proteins in cancer. *Cancer Lett*. (2013) 332:275–85. doi: 10.1016/j.canlet.2010.10.014

122. Schopf FH, Biebl MM, Buchner J. The HSP90 chaperone machinery. *Nat Rev Mol Cell Biol*. (2017) 18:345–60. doi: 10.1038/nrm.2017.20

123. Dai C, Sampson SB. HSF1: guardian of proteostasis in cancer. *Trends Cell Biol*. (2016) 26:17–28. doi: 10.1016/j.tcb.2015.10.011

124. Alexandrova EM, Marchenko ND. Mutant p53 - heat shock response oncogenic cooperation: a new mechanism of cancer cell survival. *Front Endocrinol*. (2015) 6:53. doi: 10.3389/fendo.2015.00053

125. Dote H, Burgan WE, Camphausen K, Tofilon PJ. Inhibition of hsp90 compromises the DNA damage response to radiation. *Cancer Res*. (2006) 66:9211–20. doi: 10.1158/0008-5472.CAN-06-2181

126. Elaimy AL, Ahsan A, Marsh K, Pratt WB, Ray D, Lawrence TS, et al. ATM is the primary kinase responsible for phosphorylation of Hsp90alpha after ionizing radiation. *Oncotarget*. (2016) 7:82450–7. doi: 10.18632/oncotarget.12557

127. Schilling D, Garrido C, Combs SE, Multhoff G. The Hsp70 inhibiting peptide aptamer A17 potentiates radiosensitization of tumor cells by Hsp90 inhibition. *Cancer Lett*. (2017) 390:146–52. doi: 10.1016/j.canlet.2017.01.015

128. Schilling D, Kuhnel A, Konrad S, Tetzlaff F, Bayer C, Yaglom J, et al. Sensitizing tumor cells to radiation by targeting the heat shock response. *Cancer Lett*. (2015) 360:294–301. doi: 10.1016/j.canlet.2015.02.033

129. Stuhmer T, Iskandarov K, Gao Z, Bumm T, Grella E, Jensen MR, et al. Preclinical activity of the novel orally bioavailable HSP90 inhibitor NVP-HSP990 against multiple myeloma cells. *Anticancer Res*. (2012) 32:453–62.

130. Djuzenova CS, Fiedler V, Katzer A, Michel K, Deckert S, Zimmermann H, et al. Dual PI3K- and mTOR-inhibitor PI-103 can either enhance or reduce the radiosensitizing effect of the Hsp90 inhibitor NVP-AUY922 in tumor cells: the role of drug-irradiation schedule. *Oncotarget*. (2016) 7:38191–209. doi: 10.18632/oncotarget.9501

131. Wachsberger PR, Lawrence YR, Liu Y, Rice B, Feo N, Leiby B, et al. Hsp90 inhibition enhances PI-3 kinase inhibition and radiosensitivity in glioblastoma. *J Cancer Res Clin Oncol*. (2014) 140:573–82. doi: 10.1007/s00432-014-1594-6

132. Dungey FA, Caldecott KW, Chalmers AJ. Enhanced radiosensitization of human glioma cells by combining inhibition of poly(ADP-ribose) polymerase with inhibition of heat shock protein 90. *Mol Cancer Ther*. (2009) 8:2243–54. doi: 10.1158/1535-7163.MCT-09-0201

133. Tao Z, Le Blanc JM, Wang C, Zhan T, Zhuang H, Wang P, et al. Coadministration of trametinib and palbociclib radiosensitizes KRAS-mutant non-small cell lung cancers *in vitro* and *in vivo*. *Clin Cancer Res*. (2016) 22:122–33. doi: 10.1158/1078-0432.CCR-15-0589

134. Groselj B, Sharma NL, Hamdy FC, Kerr M, Kiltie AE. Histone deacetylase inhibitors as radiosensitisers: effects on DNA damage signalling and repair. *Br J Cancer*. (2013) 108:748–54. doi: 10.1038/bjc.2013.21

135. Moertl S, Payer S, Kell R, Winkler K, Anastasov N, Atkinson MJ. Comparison of radiosensitization by HDAC inhibitors CUDC-101 and SAHA in pancreatic cancer cells. *Int J Mol Sci*. (2019) 20:3259. doi: 10.3390/ijms20133259

136. Loriot Y, Mordant P, Dugue D, Geneste O, Gombos A, Opolon P, et al. Radiosensitization by a novel Bcl-2 and Bcl-XL inhibitor S44563 in small-cell lung cancer. *Cell Death Dis*. (2014) 5:e1423. doi: 10.1038/cddis.2014.365

137. Xiao R, An Y, Ye W, Derakhshan A, Cheng H, Yang X, et al. Dual Antagonist of cIAP/XIAP ASTX660 Sensitizes HPV(-) and HPV(+) Head and neck cancers to TNFalpha, TRAIL, and radiation therapy. *Clin Cancer Res*. (2019) 25:6463–74. doi: 10.1158/1078-0432.CCR-18-3802

138. Argiris A, Bauman JE, Ohr J, Gooding WE, Heron DE, Duvvuri U, et al. Phase II randomized trial of radiation therapy, cetuximab, and pemetrexed with or without bevacizumab in patients with locally advanced head and neck cancer. *Ann Oncol*. (2016) 27:1594–600. doi: 10.1093/annonc/mdw204

139. Bendell JC, Meluch A, Peyton J, Rubin M, Waterhouse D, Webb C, et al. A phase II trial of preoperative concurrent chemotherapy/radiation therapy plus bevacizumab/erlotinib in the treatment of localized esophageal cancer. *Clin Adv Hematol Oncol*. (2012) 10:430–7.

140. Socinski MA, Stinchcombe TE, Moore DT, Gettinger SN, Decker RH, Petty WJ, et al. Incorporating bevacizumab and erlotinib in the combined-modality treatment of stage III non-small-cell lung cancer: results of a phase I/II trial. *J Clin Oncol*. (2012) 30:3953–9. doi: 10.1200/JCO.2012.41.9820

141. Lee EQ, Kaley TJ, Duda DG, Schiff D, Lassman AB, Wong ET, et al. A multicenter, phase II, randomized, noncomparative clinical trial of radiation and temozolomide with or without vandetanib in newly diagnosed glioblastoma patients. *Clin Cancer Res*. (2015) 21:3610–8. doi: 10.1158/1078-0432.CCR-14-3220

142. Blaszkowsky LS, Ryan DP, Szymonifka J, Borger DR, Zhu AX, Clark JW, et al. Phase I/II study of neoadjuvant bevacizumab, erlotinib and 5-fluorouracil with concurrent external beam radiation therapy in locally advanced rectal cancer. *Ann Oncol*. (2014) 25:121–6. doi: 10.1093/annonc/mdt516

143. Das P, Eng C, Rodriguez-Bigas MA, Chang GJ, Skibber JM, You YN, et al. Preoperative radiation therapy with concurrent capecitabine, bevacizumab, and erlotinib for rectal cancer: a phase 1 trial. *Int J Radiat Oncol Biol Phys*. (2014) 88:301–5. doi: 10.1016/j.ijrobp.2013.10.034

144. Harrington K, Berrier A, Robinson M, Remenar E, Housset M, De Mendoza FH, et al. Randomised Phase II study of oral lapatinib combined with chemoradiotherapy in patients with advanced squamous cell carcinoma of the head and neck: rationale for future randomised trials in human papilloma virus-negative disease. *Eur J Cancer*. (2013) 49:1609–18. doi: 10.1016/j.ejca.2012.11.023

145. Harrington K, Temam S, Mehanna H, D'cruz A, Jain M, D'onofrio I, et al. Postoperative adjuvant lapatinib and concurrent chemoradiotherapy followed by maintenance lapatinib monotherapy in high-risk patients with resected squamous cell carcinoma of the head and neck: a phase III, randomized, double-blind, placebo-controlled study. *J Clin Oncol*. (2015) 33:4202–9. doi: 10.1200/JCO.2015.61.4370

146. Chen AY, Okunieff P, Pommier Y, Mitchell JB. Mammalian DNA topoisomerase I mediates the enhancement of radiation cytotoxicity by camptothecin derivatives. *Cancer Res*. (1997) 57:1529–36.

147. Bernhard EJ, Mckenna WG, Hamilton AD, Sebti SM, Qian Y, Wu JM, et al. Inhibiting Ras prenylation increases the radiosensitivity of human tumor cell lines with activating mutations of ras oncogenes. *Cancer Res*. (1998) 58:1754–61.

148. Sartor CI. Biological modifiers as potential radiosensitizers: targeting the epidermal growth factor receptor family. *Semin Oncol*. (2000) 27, 15–20; discussion 92–100. doi: 10.1016/B978-0-12-398342-8.00007-0

149. Harari PM, Huang SM. Epidermal growth factor receptor modulation of radiation response: preclinical and clinical development. *Semin Radiat Oncol*. (2002) 12:21–6. doi: 10.1053/srao.2002.34865

150. Rieckmann T, Kriegs M. The failure of cetuximab-based de-intensified regimes for HPV-positive OPSCC: a radiobiologists perspective. *Clin Transl Radiat Oncol*. (2019) 17:47–50. doi: 10.1016/j.ctro.2019.05.003

151. Tang L, Wei F, Wu Y, He Y, Shi L, Xiong F, et al. Role of metabolism in cancer cell radioresistance and radiosensitization methods. *J Exp Clin Cancer Res*. (2018) 37:87. doi: 10.1186/s13046-018-0758-7

152. Lewis JE, Singh N, Holmila RJ, Sumer BD, Williams NS, Furdui CM, et al. Targeting NAD(+) metabolism to enhance radiation therapy responses. *Semin Radiat Oncol*. (2019) 29:6–15. doi: 10.1016/j.semradonc.2018.10.009

153. Peitzsch C, Kurth I, Ebert N, Dubrovska A, Baumann M. Cancer stem cells in radiation response: current views and future perspectives in radiation oncology. *Int J Radiat Biol*. (2019) 95:900–11. doi: 10.1080/09553002.2019.1589023

154. Shibata M, Hoque MO. Targeting cancer stem cells: a strategy for effective eradication of cancer. *Cancers*. (2019) 11:732. doi: 10.3390/cancers11050732

155. Konings K, Vandevoorde C, Baselet B, Baatout S, Moreels M. Combination therapy with charged particles and molecular targeting: a promising avenue to overcome radioresistance. *Front Oncol*. (2020) 10:128. doi: 10.3389/fonc.2020.00128

156. Kriegs M, Clauditz TS, Hoffer K, Bartels J, Buhs S, Gerull H, et al. Analyzing expression and phosphorylation of the EGF receptor in HNSCC. *Sci Rep*. (2019) 9:13564. doi: 10.1038/s41598-019-49885-5

157. Lord CJ, Ashworth A. PARP inhibitors: synthetic lethality in the clinic. *Science*. (2017) 355:1152–8. doi: 10.1126/science.aam7344

158. Sorensen CS, Hansen LT, Dziegielewski J, Syljuasen RG, Lundin C, Bartek J, et al. The cell-cycle checkpoint kinase Chk1 is required for mammalian homologous recombination repair. *Nat Cell Biol.* (2005) 7:195–201. doi: 10.1038/ncb1212

159. Buisson R, Niraj J, Rodrigue A, Ho CK, Kreuzer J, Foo TK, et al. Coupling of homologous recombination and the checkpoint by ATR. *Mol Cell.* (2017) 65:336–46. doi: 10.1016/j.molcel.2016.12.007

160. Kim D, Liu Y, Oberly S, Freire R, Smolka MB. ATR-mediated proteome remodeling is a major determinant of homologous recombination capacity in cancer cells. *Nucleic Acids Res.* (2018) 46:8311–25. doi: 10.1093/nar/gky625

161. Huang J, Meng L, Yang B, Sun S, Luo Z, Chen H. Safety profile of epidermal growth factor receptor tyrosine kinase inhibitors: a disproportionality analysis of FDA adverse event reporting system. *Sci Rep.* (2020) 10:4803. doi: 10.1038/s41598-020-61571-5

162. Bonomo P, Loi M, Desideri I, Olmetto E, Delli Paoli C, Terziani F, et al. Incidence of skin toxicity in squamous cell carcinoma of the head and neck treated with radiotherapy and cetuximab: a systematic review. *Crit Rev Oncol Hematol.* (2017) 120:98–110. doi: 10.1016/j.critrevonc.2017.10.011

163. Crane CH, Eng C, Feig BW, Das P, Skibber JM, Chang GJ, et al. Phase II trial of neoadjuvant bevacizumab, capecitabine, and radiotherapy for locally advanced rectal cancer. *Int J Radiat Oncol Biol Phys.* (2010) 76:824–30. doi: 10.1016/j.ijrobp.2009.02.037

164. Niyazi M, Ganswindt U, Schwarz SB, Kreth FW, Tonn JC, Geisler J, et al. Irradiation and bevacizumab in high-grade glioma retreatment settings. *Int J Radiat Oncol Biol Phys.* (2012) 82:67–76. doi: 10.1016/j.ijrobp.2010.09.002

165. Spigel DR, Hainsworth JD, Yardley DA, Raefsky E, Patton J, Peacock N, et al. Tracheoesophageal fistula formation in patients with lung cancer treated with chemoradiation and bevacizumab. *J Clin Oncol.* (2010) 28:43–8. doi: 10.1200/JCO.2009.24.7353

166. Wehler T, Thomas M, Schumann C, Bosch-Barrera J, Vinolas Segarra N, Dickgreber NJ, et al. A randomized, phase 2 evaluation of the CHK1 inhibitor, LY2603618, administered in combination with pemetrexed and cisplatin in patients with advanced nonsquamous non-small cell lung cancer. *Lung Cancer.* (2017) 108:212–6. doi: 10.1016/j.lungcan.2017.03.001

167. Sausville E, Lorusso P, Carducci M, Carter J, Quinn MF, Malburg L, et al. Phase I dose-escalation study of AZD7762, a checkpoint kinase inhibitor, in combination with gemcitabine in US patients with advanced solid tumors. *Cancer Chemother Pharmacol.* (2014) 73:539–49. doi: 10.1007/s00280-014-2380-5

Priming of Anti-tumor Immune Mechanisms by Radiotherapy Is Augmented by Inhibition of Heat Shock Protein 90

Anne Ernst[1†‡], Roman Hennel[1‡], Julia Krombach[1], Heidi Kapfhammer[1], Nikko Brix[1], Gabriele Zuchtriegel[2,3], Bernd Uhl[2,3], Christoph A. Reichel[2,3], Benjamin Frey[4], Udo S. Gaipl[4], Nicolas Winssinger[5], Senji Shirasawa[6], Takehiko Sasazuki[7], Markus Sperandio[3,8], Claus Belka[1,9] and Kirsten Lauber[1,9]*

[1] Department of Radiation Oncology, University Hospital, LMU Munich, Munich, Germany, [2] Department of Otorhinolaryngology, University Hospital, LMU Munich, Munich, Germany, [3] Walter Brendel Center for Experimental Medicine, Faculty of Medicine, LMU Munich, Munich, Germany, [4] Department of Radiation Oncology, Universitätsklinikum Erlangen, Friedrich-Alexander-University Erlangen-Nürnberg (FAU), Erlangen, Germany, [5] Department of Organic Chemistry, NCCR Chemical Biology, University of Geneva, Geneva, Switzerland, [6] Department of Cell Biology, Faculty of Medicine Fukuoka University, Fukuoka, Japan, [7] Institute for Advanced Study, Kyushu University, Fukuoka, Japan, [8] Institute of Cardiovascular Physiology and Pathophysiology, Biomedical Center, LMU Munich, Munich, Germany, [9] German Cancer Consortium (DKTK), Partner Site Munich, Heidelberg, Germany

Radiotherapy is an essential part of multi-modal cancer therapy. Nevertheless, for certain cancer entities such as colorectal cancer (CRC) the indications of radiotherapy are limited due to anatomical peculiarities and high radiosensitivity of the surrounding normal tissue. The development of molecularly targeted, combined modality approaches may help to overcome these limitations. Preferably, such strategies should not only enhance radiation-induced tumor cell killing and the abrogation of tumor cell clonogenicity, but should also support the stimulation of anti-tumor immune mechanisms – a phenomenon which moved into the center of interest of preclinical and clinical research in radiation oncology within the last decade. The present study focuses on inhibition of heat shock protein 90 (HSP90) whose combination with radiotherapy has previously been reported to exhibit convincing therapeutic synergism in different preclinical cancer models. By employing *in vitro* and *in vivo* analyses, we examined if this therapeutic synergism also applies to the priming of anti-tumor immune mechanisms in model systems of CRC. Our results indicate that the combination of HSP90 inhibitor treatment and ionizing irradiation induced apoptosis in colorectal cancer cells with accelerated transit into secondary necrosis in a hyperactive Kras-dependent manner. During secondary necrosis, dying cancer cells released different classes of damage-associated molecular patterns (DAMPs) that stimulated migration and recruitment of monocytic cells *in vitro* and *in vivo*. Additionally, these dying cancer cell-derived DAMPs enforced the differentiation of a monocyte-derived antigen presenting cell (APC) phenotype which potently triggered the

priming of allogeneic T cell responses *in vitro*. In summary, HSP90 inhibition – apart from its radiosensitizing potential – obviously enables and supports the initial steps of anti-tumor immune priming upon radiotherapy and thus represents a promising partner for combined modality approaches. The therapeutic performance of such strategies requires further in-depth analyses, especially for but not only limited to CRC.

Keywords: HSP90 inhibition, radiotherapy, anti-tumor immunity, immune priming, colorectal cancer, cancer immunology, DAMPs, secondary necrosis

INTRODUCTION

Radiotherapy is a cornerstone of multi-modal cancer treatment. Its therapeutic efficacy is primarily considered to derive from direct tumor cell killing and the abrogation of tumor cell clonogenicity (1, 2). Additionally, there is growing evidence for a relevant contribution of the immune system to local as well as distant tumor control, and the concept of cancer *in situ* vaccination by radiotherapy is receiving increasing acceptance (3, 4). In this regard, the mode of cancer cell death induced by radiotherapy appears to be of fundamental importance. The priming of anti-tumor immune mechanisms has predominantly been observed in the context of necrotic forms of cell death due to the release of damage-associated molecular patterns (DAMPs) paralleled by the stimulation of an intra-tumoral type I interferon response (5, 6). Yet, the mode of irradiation-induced cell death varies considerably and depends on several factors, including the origin and genetic repertoire of the irradiated cell, the irradiation quality, the fractionation regimen, and the overall dose (4). With photon irradiation, higher single doses or strongly hypofractionated protocols, such as 3×8 Gy, seem to be beneficial for the stimulation of systemic anti-tumor immune mechanisms (7–10). We and others have shown that DAMPs released from irradiated, dying tumor cells stimulate the activation of endothelial cells and the recruitment of antigen presenting cells (APCs) which then crossprime $CD8^+$ T cells in a type I interferon-dependent manner involving the cGAS/STING axis (8, 9, 11–14).

Despite its broad relevance for the treatment of other solid cancer entities, indications of radiotherapy in colorectal cancer (CRC) remain largely confined to malignancies of the rectum (15–17). The increased mobility of the colon and the resulting challenges of treatment volume definition and dose administration, as well as the high degree of radiosensitivity of the surrounding normal tissue limit the application of radiotherapy in colon cancer to high-risk cases receiving adjuvant fractionated (1.8–2 Gy per fraction) or neoadjuvant hypofractionated (5 Gy per fraction) radiotherapy alone or in combination with systemic

chemotherapy, respectively (16, 17). Particularly for these high-risk cases it would be of relevant clinical interest to therapeutically exploit not only the induction of tumor cell death and abrogation of clonogenicity but also the radiotherapy-induced priming of anti-tumor immune mechanisms. To this end, various combined modality approaches with molecularly targeted agents are currently being explored, including inhibition of heat shock protein 90 (HSP90) (18). The chaperone HSP90 is frequently overexpressed in tumors due to high protein turnover and constitutively increased levels of proteotoxic stress (19). It contributes to maintaining the integrity, correct folding, and stability of diverse oncogene products (20, 21). Within the large substrate spectrum, many HSP90 client proteins belong to oncogenic signaling pathways and thus orchestrate the malignant phenotype (22, 23). Hence, interference with HSP90 function appears to be a promising strategy to target cancer cells *via* multiple axes, and several HSP90 inhibitors (HSP90i) showed encouraging preclinical results (24, 25). In contrast however, most clinical trials with HSP90i monotherapy failed due to poor therapeutic efficacy and an unfavorable spectrum of side effects, particularly in terms of hepatotoxicity (26). Nevertheless, since key regulators of the DNA damage response have been reported to be specifically sensitive to HSP90i treatment, even at low inhibitor concentrations, combinations of HSP90i with radio- and/or chemotherapy recently moved into focus. The superordinate aim of these approaches is to improve the therapeutic performance and at the same time reduce the required HSP90i doses and concurrent adverse effects (27–33). For preclinical models of CRC, the radiosensitizing potential of HSP90i treatment has already been demonstrated (34, 35). We have previously shown that the second generation HSP90i NW457 exhibits reduced hepatotoxicity and potently sensitizes CRC cells toward ionizing irradiation *in vitro* and *in vivo* by interfering with the DNA damage response (36–38). The underlying mechanisms of radiation-induced cell death in the presence of HSP90i are currently being dissected (39). However, the immunological potential of HSP90i-mediated radiosensitization has not yet been examined, although seminal data suggest that HSP90i may augment the stimulation of anti-tumor immune mechanisms (19). Accordingly, the present study was designed to elucidate the immunological aspects of HSP90 inhibition in combination with ionizing irradiation in model systems of CRC. We show that the combination of radiotherapy and HSP90i treatment induced apoptosis and accelerated transit into secondary necrosis in CRC cells with concomitant release of DAMPs. These DAMPs mediated migration and recruitment of monocytic cells *in vitro* and *in vivo* and enhanced the

Abbreviations: 7-AAD, 7-amino actinomycin D; APC, antigen presenting cell; AS, autologous serum; Bax, Bcl-2-associated X protein; CFSE, carboxyfluorescein diacetate succinimidyl ester; DAMP, damage-associated molecular pattern; DC, dendritic cell; DMSO, dimethyl sulfoxide; FCS, fetal calf serum; FMI, forward migration index; GM-CSF, granulocyte-macrophage colony-stimulating factor; HMGB1, high mobility group box1; HSP, heat shock protein; HSP90i, HSP90 inhibitor; i.p., intraperitoneal; i.s., intrascrotal; IFN, interferon; IL, interleukin; Kras, Kirsten Rat Sarcoma virus protein; MLR, mixed leukocyte reaction; PI, propidium iodide; PS, penicillin/streptomycin; SDF-1α, stromal cell-derived factor 1α; TLR, toll-like receptor; TNF, tumor necrosis factor; zVAD-fmk, carbobenzoxy-valyl-alanyl-aspartyl-[O-methyl]-fluoromethylketone.

differentiation of a monocyte-derived APC phenotype which potently activated proliferation of allogeneic CD4$^+$ and CD8$^+$ T cells *in vitro*.

MATERIALS AND METHODS

Cells, Animals, and Reagents

The human CRC cell lines HCT116 Kras$^{+/G13D}$ Bax$^{+/+}$ and HCT116 Kras$^{+/G13D}$ Bax$^{-/-}$ were kindly provided by B. Vogelstein (Baltimore, MD, United States) (40), and HCT116 Kras$^{+/-}$ Bax$^{+/+}$ cells (Hke3) were a generous gift from S. Shirasawa and T. Sasazuki (Fukuoka University, Japan) (41). Cells were cultured in McCoy's full medium (McCoy's 5A medium supplemented with 10% heat-inactivated fetal calf serum (FCS) [both from Thermo Fisher Scientific, Dreieich, Germany), 100 units/ml penicillin, and 0.1 mg/ml streptomycin (PS) (Lonza, Cologne, Germany)] at 37°C and 7.5% CO_2. HCT8, HT29, and SW480 CRC cells and monocytic THP-1 cells were obtained from ATCC or DSMZ (Braunschweig, Germany) and were cultivated in DMEM full medium (DMEM (Thermo Fisher Scientific) supplemented with 10% FCS, 100 units/ml penicillin, and 0.1 mg/ml streptomycin (PS) for HCT8 and HT29 cells) at 37°C and 7.5% CO_2 or RPMI 1640 full medium [RPMI 1640 medium (Thermo Fisher Scientific) supplemented with 10% FCS, 100 units/ml penicillin, 0.1 mg/ml streptomycin (PS), and 1% 4-(2-hydroxyethyl)-1-piperazineethanesulfonic acid (HEPES, Lonza) for SW480 and THP-1 cells] at 37°C and 5% CO_2, respectively. Cell line authenticity was confirmed by short tandem repeat typing (service provided by the DSMZ), and absence of mycoplasma contamination was ensured by regular testing (MycoAlert Mycoplasma Detection Kit, Lonza).

Experiments with primary blood cells from healthy volunteers were approved by the ethics committee of the medical faculty of the LMU Munich and were performed upon written informed consent. Primary human monocytes were prepared from heparinized blood from healthy donors as described before (42) and cultured in X-Vivo full medium (X-Vivo 15 medium (Lonza) supplemented with 10% autologous serum (AS) and PS) at 37°C and 5% CO_2. Monocytes were differentiated to dendritic cells with 20 ng/ml GM-CSF and 40 ng/ml IL-4 for up to 5 days (all cytokines from R&D Systems, Wiesbaden, Germany). Naïve T cells were isolated by Biocoll density gradient centrifugation (density 1.077 g/ml, Biochrom AG, Berlin, Germany) from heparinized blood of healthy donors followed by anti-CD3 magnetic bead separation (Miltenyi, Bergisch Gladbach, Germany) according to the manufacturer's recommendations.

All *in vivo* analyses were performed in accordance with the Federation of European Laboratory Animal Science Associations (FELASA) guidelines and with the approval of local government authorities (*Regierung von Oberbayern*). Male C57BL/6 or Balb/c mice were purchased from Charles River (Sulzfeld, Germany). CX$_3$CR-1$^{GFP/+}$ C57BL/6 mice were generated as described previously and backcrossed for 6 to 10 generations to the C57BL/6 background (43). Mice used in the experiments were

10 to 13 weeks old and housed under standard conditions with access to food and water *ad libitum*.

The pochoxime-derived HSP90 inhibitor (HSP90i) NW457 (*epi*-pochoxime F; HSP90i) was described previously (44–46). A 10 mM stock solution was prepared in dimethyl sulfoxide (DMSO) and stored at -20°C as described (37, 38). Calcein-AM was purchased from Merck Millipore (Darmstadt, Germany), carboxyfluorescein diacetate succinimidyl ester (CFSE) from Thermo Fisher Scientific, uridine 5′-diphoshoglucose (UDP-glucose) from Abcam (Cambridge, United Kingdom), and IL-4, GM-CSF, TNF, SDF-1α, and WKYMVm (agonist of formyl-peptide receptors 1, 2, and 3) from R&D Systems. All other reagents were obtained from Sigma-Aldrich (Taufkirchen, Germany), if not stated otherwise.

Radiation Treatment and Preparation of Cell-Free, Conditioned HCT116 Cell Culture Supernatants

Cells (0.9×10^6 cells/well in a 6-well plate) were γ-irradiated with an RS225 X-ray cabinet (Xstrahl Ltd., Camberley, United Kingdom; 200 kV, 10 mA, Thoraeus filter, 1 Gy in 63 s) or with a Mueller RT-250 x-ray tube (200 kV, 10 mA, Thoraeus filter, 1 Gy in 1 min 52 s). Subsequently, full medium was replaced by serum-free medium supplemented with the indicated HSP90i concentrations. Cell-free supernatants were collected by centrifugation ($10,000 \times g$, 5 min, 4°C) at the indicated time points after irradiation and stored at −80°C until further use.

Analysis of DAMPs in HCT116 Cell Culture Supernatants

HSP70, high mobility group box 1 (HMGB1) and UTP levels in cell-free supernatants were measured by ELISA (HSP70, R&D Systems; HMGB1, IBL International, Hamburg, Germany; UTP, USCN, Wuhan, China). ATP levels were analyzed by luciferase tests (ATP Determination Kit, Thermo Fisher Scientific, Waltham, MA, United States) on a Synergy MX plate reader (BioTek, Bad Friedrichshall, Germany).

Transwell Migration Assay

Transwell migration of calcein-labeled THP-1 cells toward cell-free supernatants or positive controls was allowed for 90 min with 96-well Multiscreen-MIC transwell chambers with 5 μm pore size (Merck Millipore, Darmstadt, Germany) as described before (42). Transmigrated THP-1 cells were collected by centrifugation, and transmigration was calculated from the calcein-fluorescence signal measured upon lysis on a Synergy MX plate reader (BioTek, Bad Friedrichshall, Germany) as percentage of total THP-1 cells applied.

For the biochemical characterization of monocyte attraction signals, cell-free supernatants harvested 48 h post treatment and ultracentrifuged at $42,000 \times g$ (143 min, 4°C) were employed. Supernatants were subjected to heat-treatment at 90°C for 40 min, ultrafiltration with VivaSpin2 tubes with an MW cut-off of 10 kDa (Sartorius Stedim Biotech, Göttingen, Germany), or enzymatic digestion with active or heat-inactivated proteinase K

(3 U/ml) or apyrase (50 mU/ml) at 30°C for 30 min (both from New England Biolabs, Frankfurt, Germany), respectively. Culture medium supplemented with either ATP (200 nM) or SDF-1α (200 ng/ml) served as control and was treated analogously to the cell culture supernatants. Migration stimulating capacity of the processed supernatants was assessed in THP-1 cell transwell migration assays and normalized to non-treated supernatants.

Chemotaxis/Chemokinesis Assays

Chemotaxis and chemokinesis of primary human monocytes toward conditioned supernatants or apyrase digested-supernatants were analyzed with IBIDI μ-slide 2D-chemotaxis chambers (IBIDI, Munich, Germany) by live cell tracking for 3 h as described previously (42). Time-lapse video microscopy was performed on an AxioObserver Z1 inverted microscope with a heat stage (37°C, 5% CO$_2$) at 5 × magnification. Cell tracking was performed with ImageJ (National Institutes of Health, Bethesda, MD, United States), and cell tracks (2.5 h time frame) were analyzed with the IBIDI chemotaxis and migration tool to determine accumulated distance, Euclidean distance (linear distance between the start and end position), and forward migration index (FMI, defined as the distance from start to endpoint in gradient direction divided by the total accumulated distance).

Flow Cytometric Analyses of Apoptotic DNA Fragmentation, Plasma Membrane Integrity, and APC Surface Marker Expression

Flow cytometric measurements were performed on an LSRII cytometer (BD Biosciences, Heidelberg, Germany), and data were analyzed with FACSDiva (BD Biosciences) or FlowJo 7.6.5 Software (Tree Star Inc., Ashland, OR, United States), respectively.

Cells (4–8 × 10^4 cells/well in 24-well plate) were irradiated with 0–5 Gy in the presence of 0–625 nM HSP90i. Cells without treatment were used as controls. Time course analyses of apoptosis and necrosis induction were analyzed by flow cytometry as described previously (38). For analyses of secondary necrosis and necroptosis, the poly-caspase inhibitor zVAD-fmk (50 μM; Bachem, Bubendorf, Switzerland) or the necroptosis inhibitor necrostatin-1 (50 μM; Enzo Life Sciences, Loerrach, Germany) were used in addition to irradiation and HSP90i treatment.

For APC surface marker expression analyses, primary human monocytes (0.8–2 × 10^5 cells/well in 24-well plate) were cultured for 5 days in the presence of conditioned HCT116 culture supernatants (1 + 1 in X-Vivo full medium) with or without addition of GM-CSF (20 ng/ml) and IL-4 (40 ng/ml). 100 ng/ml TNF served as positive control. After 5 days, APCs were harvested, and stained for 20 min on ice with the following monoclonal antibodies in FACS stain buffer (BD Biosciences): anti-HLA-DR-Per-CP-Cy5.5, anti-CD86-A700, anti-CD80-PE, anti-CD40-PE-Cy5 or corresponding isotypes (all from BD Biosciences). Following two washing steps, cells were examined by flow cytometry. Expression levels of cell surface markers were calculated as median fluorescence intensities subtracted by corresponding isotype controls and are displayed as x-fold expression values compared to values obtained with HCT116 control supernatants.

Phagocytosis Assays

Phagocytosis experiments were performed as described previously (11). In brief, PKH67-labeled primary human monocytes (10^5 cells/well in a 24-well plate) were differentiated for 4 days into DCs by addition of GM-CSF (20 ng/ml) and IL-4 (40 ng/ml) and were then added to Hoechst-labeled HCT116 cells (ratio 1:2). Adherence was allowed for 4 h, and co-cultures were irradiated with 0 or 5 Gy plus 0–625 nM HSP90i treatment. After 48 h, cells were harvested by trypsinization, stained with 7-amino actinomycin D (7-AAD, BD Biosciences) for exclusion of non-viable phagocytes, and analyzed by flow cytometry. Phagocytosis was determined as percentage of 7-AAD negative, double-positive (PKH67, Hoechst) phagocytes. In order to confirm active prey cell engulfment, labeled DCs were pre-incubated with 10 μM cytochalasin D for 1 h before addition of the prey cells.

Allogeneic Mixed Leukocyte Reaction

Allogeneic mixed leukocyte reactions (MLRs) were carried out as described previously (11). Briefly, naïve CFSE-stained T cells (positively selected on anti-CD3 magnetic beads) were added in a ratio of 10:1 to allogeneic human monocyte-derived DCs (1 × 10^4 cells/well in 96-well plates) that had been differentiated in the presence of conditioned HCT116 culture supernatants in X-Vivo full medium. After 5 days, cells were collected, T cells were stained with anti-CD3-PE-Cy7, anti-CD4-PE, and anti-CD8-APC (all from BD Biosciences), and T cell proliferation was determined by flow cytometry based on the decline in T cell CFSE fluorescence intensity. Results are displayed as x-fold proliferation values normalized on the values obtained with HCT116 control supernatants.

Purinergic P2Y Receptor RT-PCR

Purinergic P2Y receptor (P2RY) expression levels were determined by RT-PCR. Total RNA was isolated from THP-1 cells and primary human monocytes with the NucleoSpin RNA II Kit according to the manufacturer's instructions, and reverse transcription was performed as described before (11). 10 ng of corresponding cDNA were subjected to amplification by PCR [10 min 95°C, 33x (15 s 95°C, 1 s 60°C)] with distinct primer pairs for each P2RY subtype (**Supplementary Table 1**). Human genomic DNA was used as positive and H$_2$O as negative control. Amplification products were analyzed by agarose gel electrophoresis (3% agarose gel).

Peritonitis Assays

In vivo recruitment of myeloid cells by culture supernatants of treated HCT116 cells was determined in peritonitis assays as described previously with minor variations (47–49). In brief, conditioned supernatants were injected intraperitoneally (*i.p.*) into C57BL/6 mice, and peritoneal lavages were collected from

sacrificed mice after 6 h ($n = 4$ per group) or after 6, 12, and 24 h ($n = 2$ per group) for time course analyses, respectively. Total numbers of leukocytes were determined by using a Coulter A C T counter (Beckman Coulter, Krefeld, Germany). Cells were stained on ice for 30 min with the following monoclonal antibodies: anti-CD45-APC-Cy7 (from BD Biosciences), anti-CD11b-FITC, anti-Gr-1-PE, anti-F4/80-eFluor450 (from eBiosciences, San Diego, CA, United States). FACS analyses were performed upon lysis of erythrocytes (Gallios, Beckman Coulter). Monocytic cells and granulocytes were distinguished and quantified within the CD45^{+}/CD11b^{+} myeloid cell population by cell surface expression levels of Gr-1 and F4/80.

M. cremaster Assay and Intravital Microscopy

The single steps of leukocyte trafficking were examined in the *Musculus cremaster* assay by intravital microscopy as described before with minor modifications (48–51). Briefly, two groups of randomly assigned CX$_3$CR1$^{GFP/+}$ mice were injected intrascrotally (i.s.) and stimulated with conditioned supernatants for 6 h ($n = 6$ per group). After surgical preparation of the cremaster muscle, intravital microscopy was performed at an AxioTech-Vario 100 Microscope (Zeiss MicroImaging, Göttingen, Germany) equipped with a Colibiri LED light source (Zeiss MicroImaging) for fluorescence epi-illumination. Images were taken with an AxioCam Hsm digital camera with a 20 × water immersion lens (0.5 NA, Zeiss MicroImaging) and were processed with AxioVision 4.6 software (Zeiss MicroImaging). The region of interest (ROI) was analyzed with ImageJ (National Institutes of Health) for rolling, firm adhesion, and extravasation of leukocytes or CX$_3$CR1$^{GFP/+}$ monocytes, including classical (GFP^{low}) and non-classical monocytes (GFP^{high}), respectively. CX$_3$CR1-expressing DCs were excluded from analyses on the basis of their characteristic stellate morphology.

Statistical Analyses

Statistical analyses were performed using OriginPro 9.1 software (OriginLab Ltd., Northampton, MA, United States). 2-sided exact Wilcoxon Rank tests, or two-way ANOVAs were employed where indicated, and *post hoc* Bonferroni-Holm correction was applied where appropriate. Synergism was analyzed on the basis of combination indices (CIs) according to the Chou-Talalay Method (52). CIs indicate synergism (CI < 1), additivity (CI = 1), or antagonism (CI > 1).

RESULTS

HSP90i Treatment Augments Radiation-Induced Death of Colorectal Cancer Cells and the Release of Monocyte Attracting DAMPs

An initial and essential step in the induction of anti-tumor immune responses is the attraction of monocytic cells and APC precursors by dying tumor cells (53, 54). For detailed analyses of the dynamics of cell death induction and monocyte attraction, HCT116 CRC cells were irradiated at doses of 0–5 Gy in the presence of 0–625 nM HSP90i. Monocyte attraction by cell-free supernatants was measured 24–72 h after irradiation *via* transwell migration assays with the monocytic cell line THP-1. In parallel, induction of apoptosis (determined as the percentage of cells with subG1 DNA content) and necrosis (determined as the percentage of cells with permeable plasma membrane) in treated HCT116 cells was examined by flow cytometry. HSP90i strongly increased irradiation-induced apoptosis and accelerated the transit into necrosis in a dose-dependent manner (**Figure 1A**). Supernatants of dying HCT116 cells stimulated a time- and dose-dependent migratory response in THP-1 cells with a maximum approximately 48 h after treatment. Comprehensive time course analyses confirmed that monocyte attraction was strongest with supernatants harvested 48 h upon treatment with 625 nM HSP90i and 5 Gy irradiation (**Figure 1B**). Therefore, 625 nM HSP90i + 5 Gy was chosen as standard combination treatment for further experiments. Notably, combination indices calculated according to Chou and Talalay (52) revealed a synergistic mode of action for HSP90i and irradiation (CI < 1) regarding the attraction of monocytic cells.

The release of DAMPs is a vital trigger for the attraction of monocytic cells by dying tumor cells (11, 42, 53, 54). Therefore, we measured the concentrations of several established DAMPs, including HMGB1, HSP70, and ATP, in culture supernatants of HCT116 cells upon treatment. The levels of HMGB1 and HSP70 increased over time especially in response to HSP90i and combined treatment with irradiation (**Figure 1C**). Interestingly, the release of ATP into the culture supernatants revealed similar kinetics as the migratory monocyte response in the transwell assays peaking 48 h after treatment with HSP90i plus irradiation (**Figure 1B**) and exhibited also the synergistic mode of action between HSP90i and irradiation. Taken together, in comparison to the monoagent settings, combination of HSP90i and irradiation results in synergistically enhanced DAMP release and monocyte attraction by dying tumor cells.

DAMP Release and Monocyte Attraction Occur During Secondary Necrosis Upon Irradiation in Combination With HSP90i Treatment

The mode of cell death is of central importance for the stimulation of immune responses. Particularly necrotic forms of cell death – primary as well as secondary, post-apoptotic necrosis – are known to be associated with the exposure of potent immunostimulating signals (5, 6, 55). In order to assess if necrosis induction and DAMP release are a common response of CRC cells to the combined treatment of HSP90i and irradiation, we made use of three additional CRC cell lines: HCT8, SW480, and HT29 cells. Whereas HCT8 cells showed a similar response pattern as HCT116 cells, yet with elevated amplitude, neither necrosis induction nor DAMP release were observed in HT29 cells (**Supplementary Figure 1**). SW480 cells revealed an intermediate response pattern. Despite the common colorectal origin, these cell lines differ in their mutational Kras

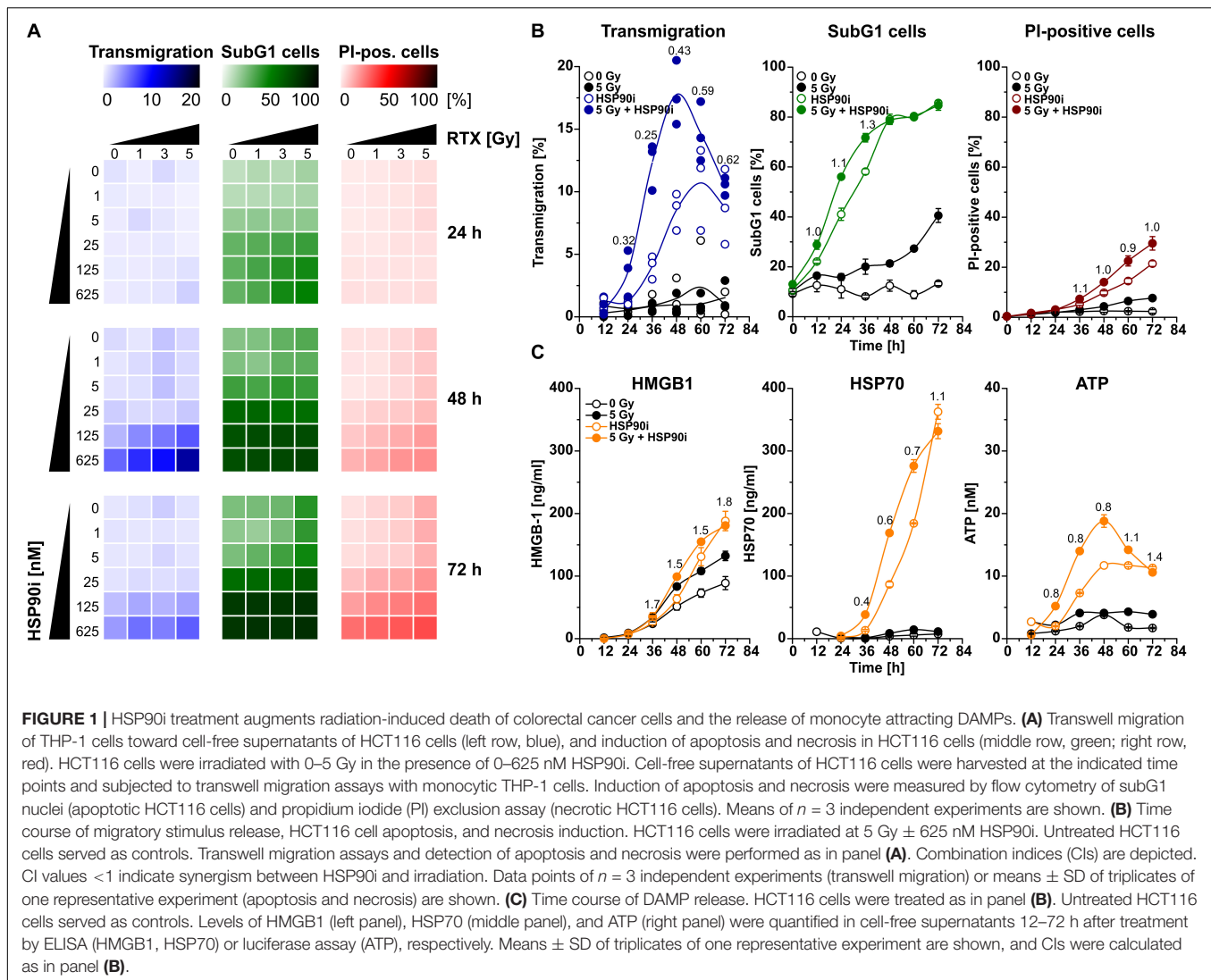**FIGURE 1 |** HSP90i treatment augments radiation-induced death of colorectal cancer cells and the release of monocyte attracting DAMPs. **(A)** Transwell migration of THP-1 cells toward cell-free supernatants of HCT116 cells (left row, blue), and induction of apoptosis and necrosis in HCT116 cells (middle row, green; right row, red). HCT116 cells were irradiated with 0–5 Gy in the presence of 0–625 nM HSP90i. Cell-free supernatants of HCT116 cells were harvested at the indicated time points and subjected to transwell migration assays with monocytic THP-1 cells. Induction of apoptosis and necrosis were measured by flow cytometry of subG1 nuclei (apoptotic HCT116 cells) and propidium iodide (PI) exclusion assay (necrotic HCT116 cells). Means of $n = 3$ independent experiments are shown. **(B)** Time course of migratory stimulus release, HCT116 cell apoptosis, and necrosis induction. HCT116 cells were irradiated at 5 Gy ± 625 nM HSP90i. Untreated HCT116 cells served as controls. Transwell migration assays and detection of apoptosis and necrosis were performed as in panel **(A)**. Combination indices (CIs) are depicted. CI values <1 indicate synergism between HSP90i and irradiation. Data points of $n = 3$ independent experiments (transwell migration) or means ± SD of triplicates of one representative experiment (apoptosis and necrosis) are shown. **(C)** Time course of DAMP release. HCT116 cells were treated as in panel **(B)**. Untreated HCT116 cells served as controls. Levels of HMGB1 (left panel), HSP70 (middle panel), and ATP (right panel) were quantified in cell-free supernatants 12–72 h after treatment by ELISA (HMGB1, HSP70) or luciferase assay (ATP), respectively. Means ± SD of triplicates of one representative experiment are shown, and CIs were calculated as in panel **(B)**.

status. While HCT116 and HCT8 cells are heterozygous for hyperactive Kras^{G13D}, HT29 cells harbor two wildtype Kras alleles, and SW480 are homozygous for Kras^{G12V} which has been shown to be associated with moderate Kras activation (56, 57). Thus, our results point toward an involvement of hyperactive Kras^{G13D} in necrosis induction and DAMP release upon irradiation plus HSP90i treatment. However, since there are further molecular differences between these cell lines, we utilized isogenic subclones of HCT116 cells with genetically manipulated Kras status in order to characterize the mode(s) of cell death responsible for the observed release of monocyte attracting DAMPs in further detail. We also included HCT116 cells with manipulated Bax status to distinguish between apoptosis, primary, and secondary necrosis. So, apart from the established parental cell line HCT116 which is heterozygous for the activating Kras mutation G13D and has functional Bax, we employed HCT116 Kras$^{+/G13D}$ Bax$^{-/-}$ cells with hyperactive Kras lacking functional Bax (40) and HCT116 Kras$^{+/-}$ Bax$^{+/+}$ cells with both normal Bax and normal Kras function (41). All cell lines

were treated with the combination therapy, and induction of apoptosis as well as necrosis, monocyte transwell migration, and DAMP release were monitored 0–72 h after treatment. In HCT116 parental cells, the combined treatment strongly induced apoptosis with subsequent transit into secondary necrosis, paralleled by robust monocyte attraction and release of HSP70 and ATP (**Figure 2A**, upper panel). HCT116 Kras$^{+/G13D}$ Bax$^{-/-}$ cells, lacking the proapoptotic regulator Bax showed considerably reduced levels of apoptosis induction (**Figure 2A**, middle panel), supporting the common notion that ionizing irradiation and HSP90 inhibition stimulate apoptosis mainly *via* the intrinsic apoptosis pathway (37, 58, 59). Without preceding apoptosis, virtually no necrosis was observed in HCT116 Bax$^{-/-}$ cells, indicating that the necrotic phenotype seen in treated parental HCT116 cells was in fact of the secondary, post-apoptotic kind. Cell-free supernatants of treated HCT116 Bax$^{-/-}$ cells failed to attract monocytic cells, and only background levels of HSP70 and ATP were detected. In contrast to HCT116 Bax$^{-/-}$ cells, HCT116 Kras$^{+/-}$ Bax$^{+/+}$ cells showed a strong
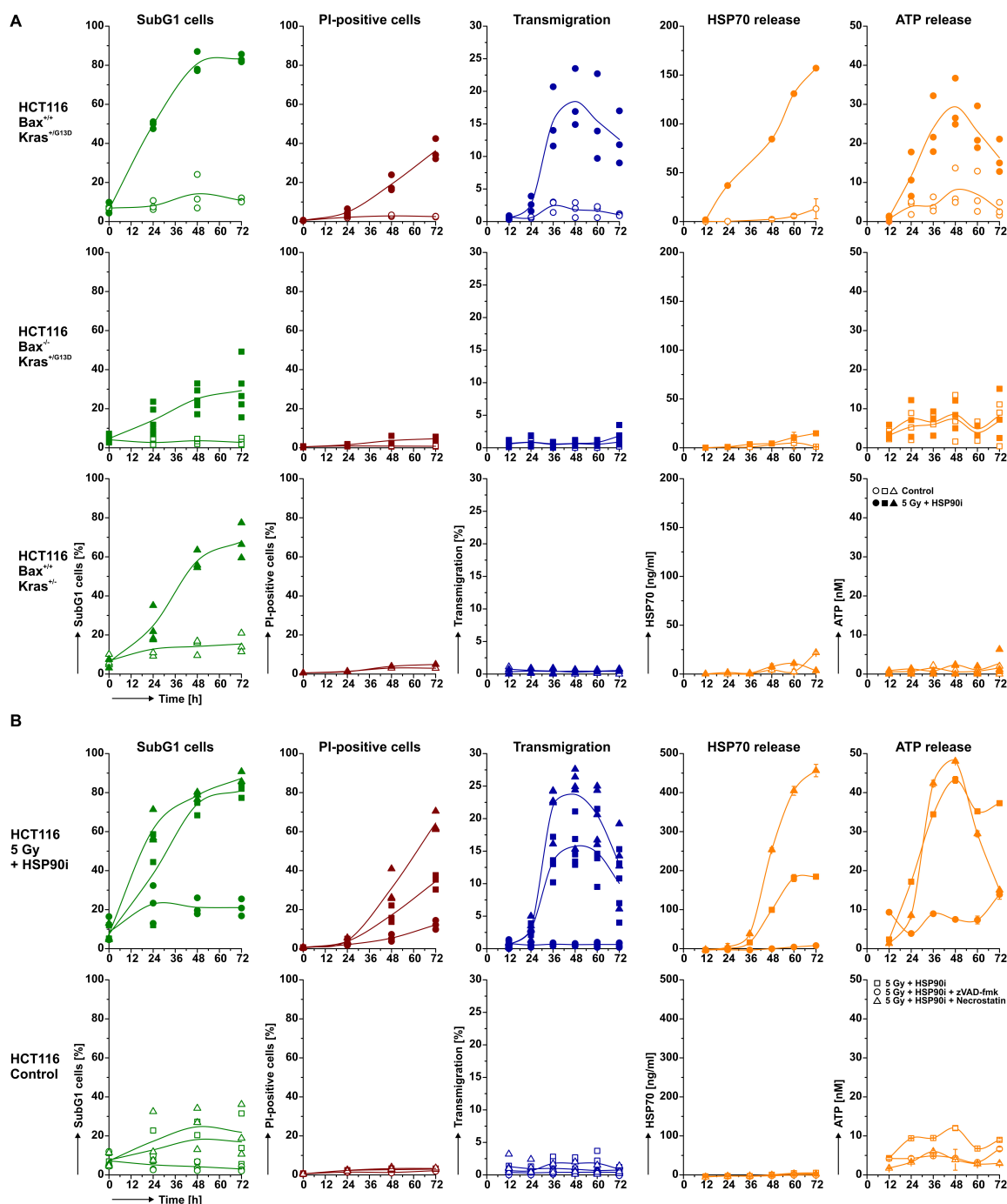
FIGURE 2 | DAMP release and monocyte attraction occur during secondary necrosis upon irradiation in combination with HSP90i treatment. **(A)** Induction of cell death, THP-1 cell attraction, and DAMP release in HCT116 subclones with or without functional Bax and/or hyperactive Kras^{G13D}. Parental HCT116 Kras$^{+/G13D}$ Bax$^{+/+}$ cells (upper row), HCT116 Kras$^{+/G13D}$ Bax$^{-/-}$ cells (middle row), and HCT116 Kras$^{+/-}$ Bax$^{+/+}$ cells (lower panel) were treated with 5 Gy plus 625 nM HSP90i or left untreated. At the indicated time points, induction of apoptosis (first column) and necrosis (second column), THP-1 cell transwell migration (third column), and release of HSP70 (fourth column) and ATP (last column) were measured as in **Figure 1**. Data points of n = 3–5 independent experiments (apoptosis, necrosis, transwell migration, ATP release) or means ± SD of triplicates of one representative experiment (HSP70 release) are shown. **(B)** Impact of different cell death inhibitors on apoptosis and necrosis induction, THP-1 cell attraction, and DAMP release in HCT116 cells upon treatment with radiotherapy and HSP90i. HCT116 cells were treated with 5 Gy plus 625 nM HSP90i in the presence of the poly-caspase inhibitor zVAD-fmk or the necroptosis inhibitor necrostatin-1, respectively (upper panel). Untreated cells served as controls (lower panel). Induction of apoptosis (first column) and necrosis (second column), THP-1 cell transwell migration (third column), and release of HSP70 (fourth column) and ATP (last column) were measured as in **Figure 1**. Data points of n = 3–5 independent experiments (apoptosis, necrosis, transwell migration) or means ± SD of triplicates of one representative experiment (release of HSP70 and ATP) are shown.

induction of apoptosis upon treatment, comparable to the parental cells (**Figure 2A**, lower panel). However, apoptotic HCT116 Kras$^{+/-}$ Bax$^{+/+}$ cells did not transit into secondary necrosis, and neither monocyte attraction nor DAMP release were observed. These results clearly suggest that DAMP release and attraction of monocytic cells after combined treatment with HSP90i and irradiation occur in the phase of post-apoptotic, secondary necrosis.

In order to further prove the causal link between monocyte attraction, DAMP release, and secondary necrosis, we employed the poly-caspase inhibitor carbobenzoxy-valyl-alanyl-aspartyl-[O-methyl]-fluoromethylketone (zVAD-fmk) which interferes with apoptosis induction and necrostatin-1, an inhibitor of receptor-interacting serine/threonine-protein kinase 1 (RIPK1), which blocks necroptosis induction *via* RIPK1 (**Figure 2B**). Addition of zVAD-fmk clearly decreased apoptosis induction in parental HCT116 cells upon treatment, subsequently also preventing transit into secondary necrosis. Consequently, neither monocyte attraction nor DAMP release were observed. In contrast, treatment with necrostatin-1 did not impair but even increased necrosis induction, eventually resulting in elevated monocyte transwell migration and HSP70 release. In summary, these data underline the essential role of secondary necrosis for the release of monocyte attracting DAMPs by dying HCT116 cells upon combined treatment with HSP90i and irradiation. Analogous results obtained with HCT8 and SW480 cells further confirmed the post-apoptotic nature of necrosis induced by irradiation plus HSP90i treatment (**Supplementary Figure 2**).
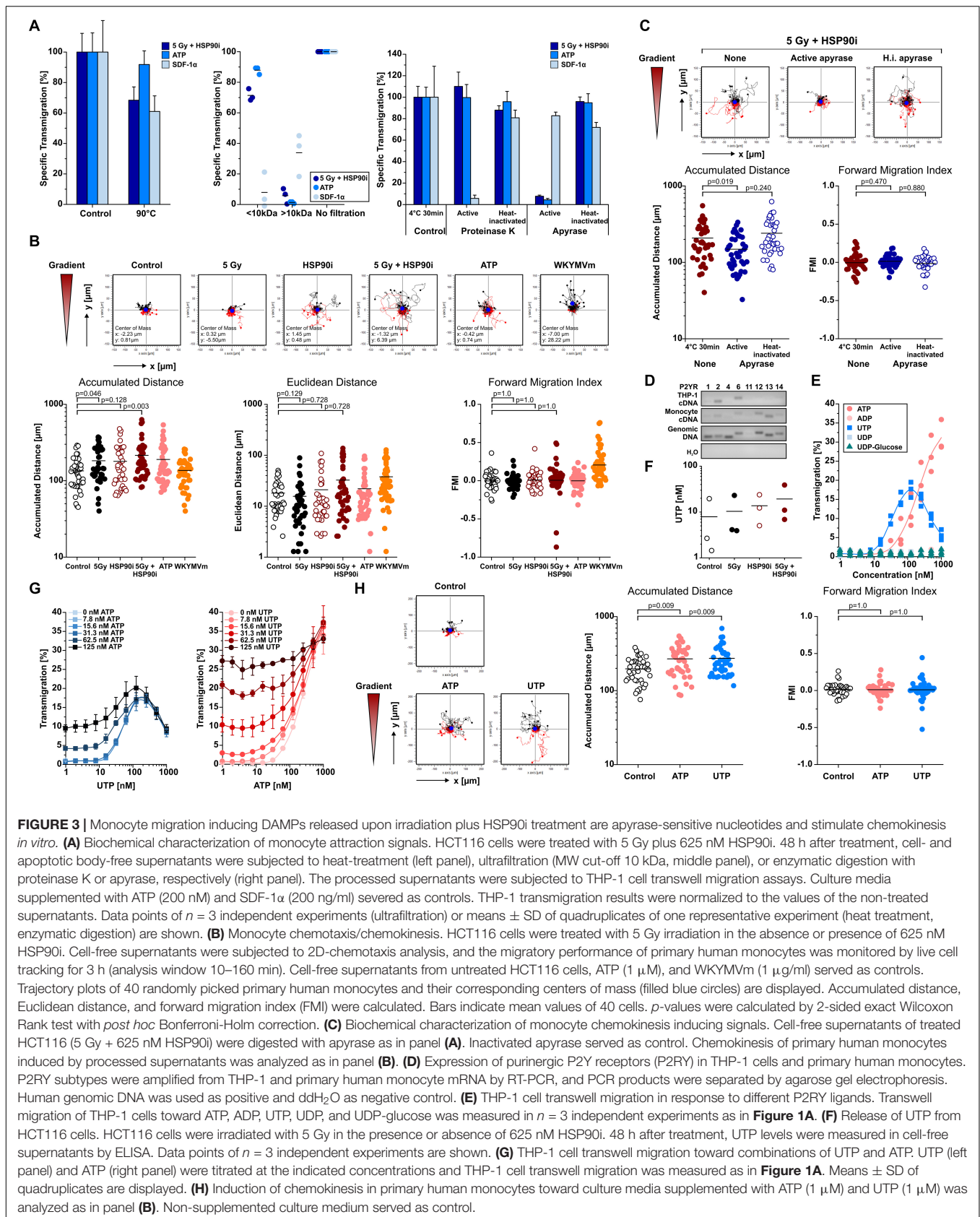
Monocyte Migration Inducing DAMPs Released Upon Irradiation Plus HSP90i Treatment Are Apyrase-Sensitive Nucleotides and Stimulate Chemokinesis *in vitro*

Necrotic cells release several DAMPs that have been reported to contribute to monocyte recruitment, including low molecular weight compounds such as nucleotides and high molecular weight compounds such as HSP70 and HMGB1 (5, 11, 42, 60). As shown in **Figures 1**, **2**, the kinetics of ATP release upon treatment of HCT116 cells with HSP90i and irradiation closely paralleled the kinetics of monocyte transwell migration, thus pointing toward a crucial contribution of nucleotides to monocyte attraction in our model system. Nevertheless, other well-known DAMPs, such as HSP70 and HMGB1, were released at high concentrations as well. In order to dissect the involvement of different molecular classes of DAMPs, the monocyte attracting signals in supernatants of treated HCT116 cells were subjected to biochemical characterization experiments. As such, heat-treatment (90°C, 40 min), ultrafiltration (molecular weight cut-off ≤10 kDa), and enzymatic degradation (nucleoside triphosphate degrading apyrase or protein degrading proteinase K) were applied to culture supernatants of treated HCT116 cells before THP-1 cell transwell migration was analyzed (**Figure 3A**). ATP (MW = 507 Da) and the CXC chemokine stromal cell-derived factor 1 α (SDF-1α) (MW = 11 kDa)

served as controls. In summary, the migration stimulating activity in culture supernatants of HCT116 cells treated with HSP90i and irradiation was observed to be largely heat stable with an apparent molecular weight ≤10 kDa, and sensitive to apyrase treatment. These results indicate that nucleotides released from secondary necrotic HCT116 cells are the key players in this scenario.

Nucleotides have been reported to induce undirected forms of migration (i.e., chemokinesis) and to act as auto- and paracrine amplifiers of other chemotactic stimuli rather than stimulating directed migratory responses in monocytic cells (i.e., chemotaxis) (42, 61, 62). We therefore characterized the mode of migration of primary human monocytes stimulated by supernatants of treated HCT116 cells by live cell imaging in 2D-migration chambers in greater detail (**Figure 3B**). The chemotaxis inducing formyl peptide receptor agonist WKYMVm and chemokinesis inducing ATP were used for comparison. In response to supernatants of HCT116 cells treated with HSP90i plus irradiation, monocyte migration was clearly increased but revealed an undirected pattern as indicated by the trajectory plots and quantified by significantly increased accumulated distance while Euclidean distance and forward migration index remained not significantly different from the controls. Notably, apyrase treatment of the culture supernatants completely abrogated the chemokinetic migration of monocytic cells, thus confirming the crucial role of nucleotides in our model (**Figure 3C**). Since apyrase hydrolyzes various nucleoside triphosphates to diphosphates and monophosphates (63), a more in-depth characterization of the monocyte attracting nucleotides released from treated HCT116 cells was performed.

Migration of monocytes in response to nucleotides is mediated by the family of P2Y receptors (P2RYs) (64). RT-PCR analyses of P2RY family members showed that THP-1 cells mainly express P2RY2 and P2RY6, whereas the spectrum in primary human monocytes was broader and included P2RY2, P2RY6, P2RY12, P2RY13, and P2RY14 (**Figure 3D**). The cognate ligands of these receptors were tested for their monocyte attracting potential. Only ATP and UTP, both ligands of P2RY2, were able to stimulate transwell migration of THP-1 cells and induced chemokinesis in primary human monocytes (**Figures 3E,H**). However, whereas the concentrations of purified nucleotides needed to induce THP-1 cell migration at comparable levels to supernatants of dying HCT116 cells ranged from 125 to 1000 nM for ATP and 30–250 nM for UTP, the measured concentrations of both nucleotides in the supernatants were only in the low nanomolar range (**Figures 1**, **2**, **3F**). To characterize potential interactions between ATP and UTP, monocyte attraction was examined in checkerboard titration experiments with different concentrations of both nucleotides. The combined effects of ATP and UTP on THP-1 cell migration showed additive behavior, without obvious synergism (CI ≈ 1). Still, with mixtures of ATP and UTP in concentrations analogous to the ones measured in the supernatants of treated HCT116 cells (ATP 20–40 nM and UTP 20 nM) THP-1 cell migration reached comparable levels (**Figure 3G**). Accordingly, we conclude that HSP90i plus irradiation stimulates the release of the P2RY2 ligands ATP

FIGURE 3 | Monocyte migration inducing DAMPs released upon irradiation plus HSP90i treatment are apyrase-sensitive nucleotides and stimulate chemokinesis *in vitro*. **(A)** Biochemical characterization of monocyte attraction signals. HCT116 cells were treated with 5 Gy plus 625 nM HSP90i. 48 h after treatment, cell- and apoptotic body-free supernatants were subjected to heat-treatment (left panel), ultrafiltration (MW cut-off 10 kDa, middle panel), or enzymatic digestion with proteinase K or apyrase, respectively (right panel). The processed supernatants were subjected to THP-1 cell transwell migration assays. Culture media supplemented with ATP (200 nM) and SDF-1α (200 ng/ml) severed as controls. THP-1 transmigration results were normalized to the values of the non-treated supernatants. Data points of $n = 3$ independent experiments (ultrafiltration) or means ± SD of quadruplicates of one representative experiment (heat treatment, enzymatic digestion) are shown. **(B)** Monocyte chemotaxis/chemokinesis. HCT116 cells were treated with 5 Gy irradiation in the absence or presence of 625 nM HSP90i. Cell-free supernatants were subjected to 2D-chemotaxis analysis, and the migratory performance of primary human monocytes was monitored by live cell tracking for 3 h (analysis window 10–160 min). Cell-free supernatants from untreated HCT116 cells, ATP (1 µM), and WKYMVm (1 µg/ml) served as controls. Trajectory plots of 40 randomly picked primary human monocytes and their corresponding centers of mass (filled blue circles) are displayed. Accumulated distance, Euclidean distance, and forward migration index (FMI) were calculated. Bars indicate mean values of 40 cells. *p*-values were calculated by 2-sided exact Wilcoxon Rank test with *post hoc* Bonferroni-Holm correction. **(C)** Biochemical characterization of monocyte chemokinesis inducing signals. Cell-free supernatants of treated HCT116 (5 Gy + 625 nM HSP90i) were digested with apyrase as in panel **(A)**. Inactivated apyrase served as control. Chemokinesis of primary human monocytes induced by processed supernatants was analyzed as in panel **(B)**. **(D)** Expression of purinergic P2Y receptors (P2RY) in THP-1 cells and primary human monocytes. P2RY subtypes were amplified from THP-1 and primary human monocyte mRNA by RT-PCR, and PCR products were separated by agarose gel electrophoresis. Human genomic DNA was used as positive and ddH$_2$O as negative control. **(E)** THP-1 cell transwell migration in response to different P2RY ligands. Transwell migration of THP-1 cells toward ATP, ADP, UTP, UDP, and UDP-glucose was measured in $n = 3$ independent experiments as in **Figure 1A**. **(F)** Release of UTP from HCT116 cells. HCT116 cells were irradiated with 5 Gy in the presence or absence of 625 nM HSP90i. 48 h after treatment, UTP levels were measured in cell-free supernatants by ELISA. Data points of $n = 3$ independent experiments are shown. **(G)** THP-1 cell transwell migration toward combinations of UTP and ATP. UTP (left panel) and ATP (right panel) were titrated at the indicated concentrations and THP-1 cell transwell migration was measured as in **Figure 1A**. Means ± SD of quadruplicates are displayed. **(H)** Induction of chemokinesis in primary human monocytes toward culture media supplemented with ATP (1 µM) and UTP (1 µM) was analyzed as in panel **(B)**. Non-supplemented culture medium served as control.

DAMPs Released Upon Irradiation Plus HSP90i Treatment Stimulate Myeloid Cell Recruitment *in vivo*

In vitro, supernatants of HCT116 cells treated with HSP90i and irradiation stimulated undirected monocyte chemokinesis. However, for the priming of anti-tumor immune mechanisms directed recruitment of APCs and their precursors, such as monocytes, is crucial (65). To examine myeloid cell recruitment by dying tumor cell-derived DAMPs *in vivo*, we used the experimental peritonitis model, one of the standard model systems to assess leukocyte trafficking *in vivo*. Culture supernatants of HCT116 cells (treated with irradiation plus HSP90i or left untreated) were injected intraperitoneally into C57BL/6 mice, and after 6 h, recruited myeloid cell populations (CD45$^+$CD11b$^+$) were characterized by FACS analyses of the peritoneal lavage. In comparison to the untreated controls, supernatants of treated HCT116 cells stimulated significantly enhanced infiltration of different myeloid cell subsets. This applied to classical monocytes (Gr-1^{hi}F4/80^{hi} and Gr-1^{hi}F4/80^{int}),

macrophages (Gr-1^{low}F4/80^{hi}), and granulocytes (Gr-1^{hi}F4/80^{low}) (**Figure 4A**). Time course experiments also suggested that recruited classical monocytes subsequently start to differentiate into more macrophagocytic and/or APC-like phenotypes by downregulation of Gr-1 and upregulation of F4/80 (**Figure 4B**).

To further dissect the individual steps of myeloid cell recruitment, we made use of the *M. cremaster* model, a standard microcirculatory observation technique (66). Culture supernatants of HCT116 cells (treated with irradiation plus HSP90i or left untreated) were injected intrascrotally into CX$_3$CR-1$^{GFP/+}$ reporter mice. After 6 hours of stimulation, the trafficking of leukocytes and GFP-positive monocytic cells from postcapillary venules into the parenchyma of the *M. cremaster* tissue was monitored by intravital microscopy. Whereas no significant differences in the initial step of leukocyte rolling were observed, firm adhesion and extravasation were significantly increased in response to supernatants of HSP90i-treated and irradiated HCT116 cells as compared to the controls. These data indicate that the myeloid cell attracting potential of DAMPs released by dying HCT116 as observed *in vitro* also translates into increased transendothelial recruitment and tissue extravasation of different myeloid subsets *in vivo*.
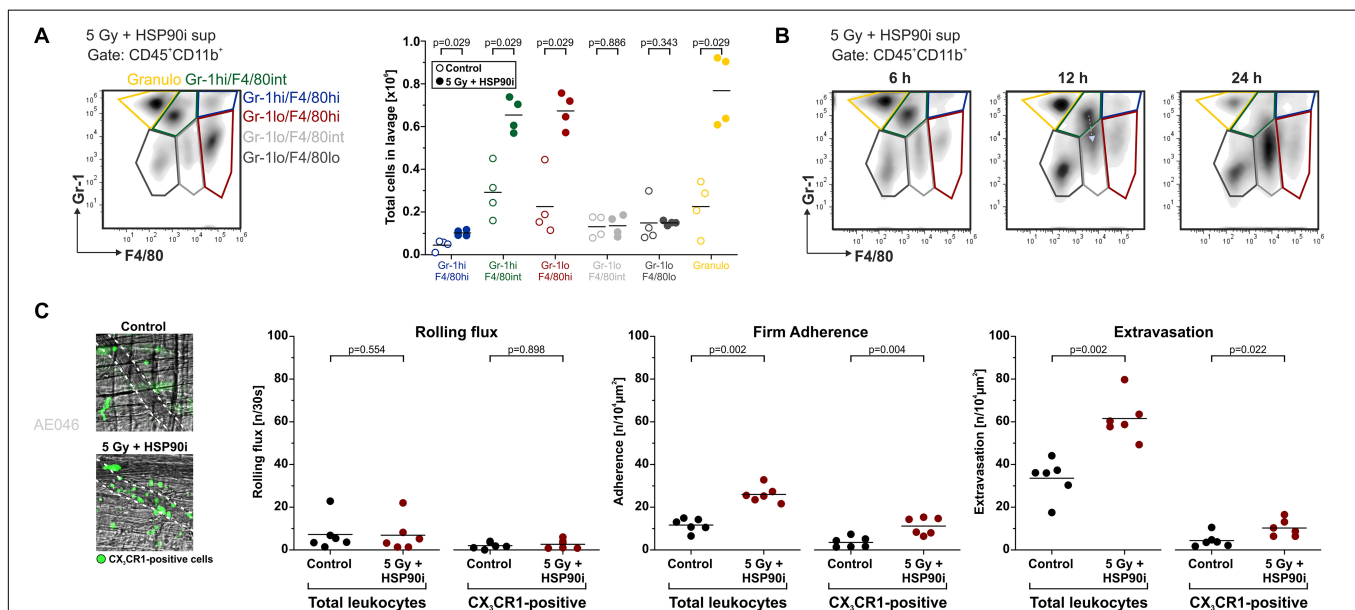

FIGURE 4 | DAMPs released upon irradiation plus HSP90i treatment stimulate myeloid cell recruitment *in vivo*. **(A)** Recruitment of myeloid leukocyte subsets in the peritonitis model. Cell-free supernatants of treated HCT116 cells (5 Gy + 625 nM HSP90i) were harvested after 48 h and injected intraperitoneally (i.p.) into C57BL/6 mice. Supernatants from untreated HCT116 cells served as controls. 6 h after injection, the peritoneal lavage was collected, and myeloid leukocyte subsets were analyzed by flow cytometry. Representative density plots of peritoneal myeloid leukocytes (Gr-1 vs. F4/80 gated on CD45$^+$CD11b$^+$ cells) are shown. Quantification of peritoneal recruitment is depicted for classical monocytes (Gr-1^{hi}F4/80^{hi}, Gr-1^{hi}F4/80^{int}), macrophage-like cells (Gr-1^{low}F4/80^{hi}, Gr-1^{low}F4/80^{int}, Gr-1^{low}F4/80^{low}), and neutrophils (Gr-1^{hi}F4/80^{low}). Bars indicate median values of n = 4 mice per group. p-values were calculated by two-sided exact Wilcoxon Rank test. **(B)** Time course of myeloid cell recruitment. Recruitment of myeloid leukocyte subsets was analyzed 6, 12, and 24 h after supernatant injection as in panel **(A)**. Representative density plots of n = 2 animals are shown. Gray arrow indicates the shift in Gr-1 expression. **(C)** Extravasation of leukocytes in the *M. cremaster* model. Cell-free HCT116 cell supernatants were generated as in panel **(A)** and intrascrotally (i.s.) injected into CX$_3$CR1$^{GFP/+}$ mice. Leukocyte and CX$_3$CR1$^{GFP/+}$ monocyte trafficking in cremasteric venules were monitored by intravital microscopy 6 hours after injection. In representative images CX$_3$CR1$^{GFP/+}$ monocytes are depicted in green. Intravascular rolling, firm adherence, and extravasation was quantified for total leukocytes and CX$_3$CR1$^{GFP/+}$ monocytes. Bars indicate mean values of n = 6 mice per group. p-values were calculated by two-sided exact Wilcoxon Rank test.
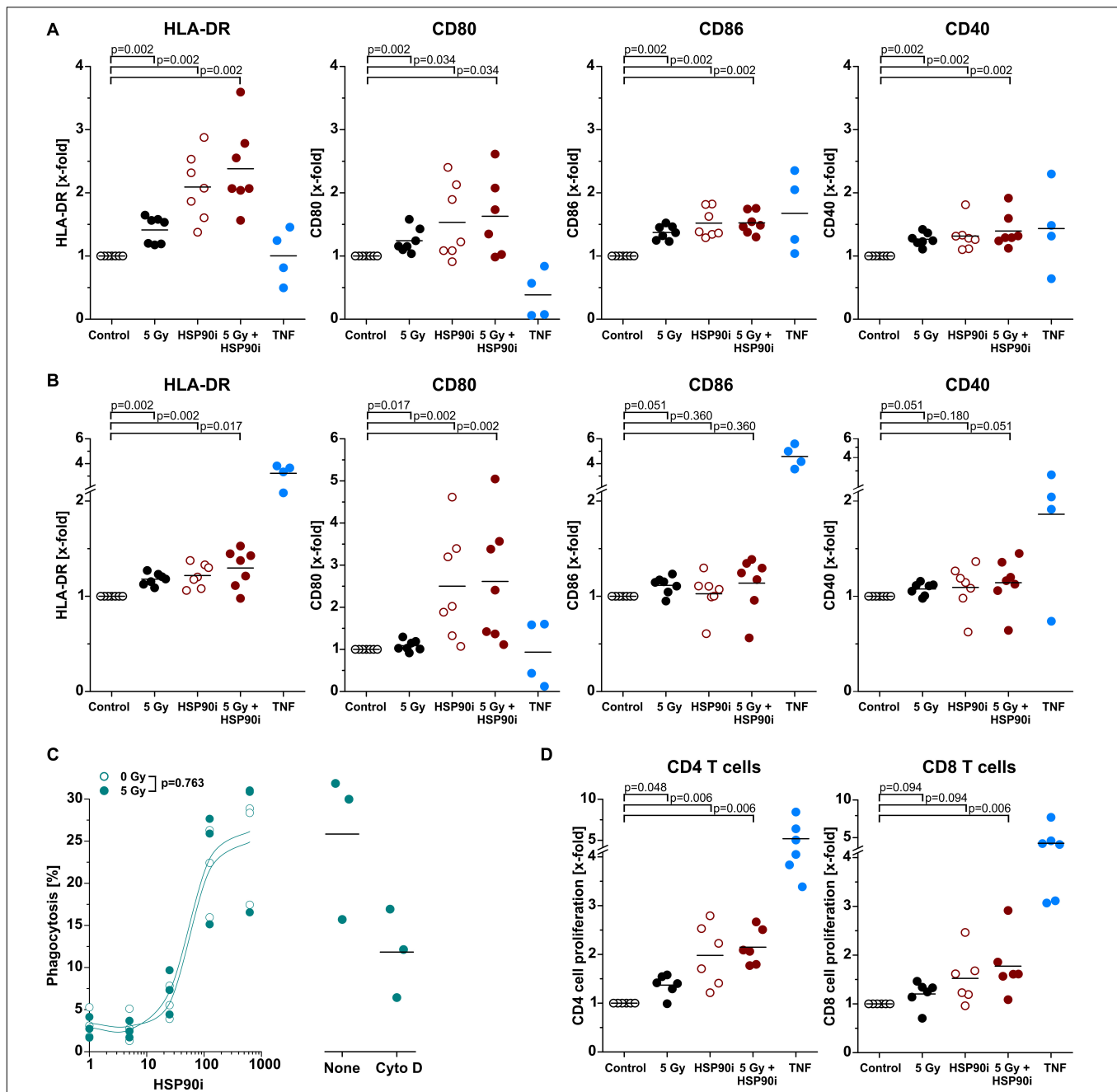
FIGURE 5 | Differentiation and effector functions of antigen presenting cells are enhanced upon contact with DAMPs released from irradiated and HSP90i-treated cancer cells. **(A)** Differentiation of antigen presenting cells from primary human monocytes. HCT116 cells were treated with 5 Gy irradiation ± 625 nM HSP90i. Cell-free supernatants were harvested 48 h after treatment, and primary human monocytes were stimulated with the supernatants (1 + 1 in X-Vivo full medium) for 5 days. Surface expression of HLA-DR, CD80, CD86, and CD40 on monocytes were analyzed by flow cytometry. Supernatants from untreated HCT116 cells and TNF served as controls. Bars indicate mean values of $n = 7$ independent experiments. p-values were calculated by two-sided exact Wilcoxon Rank test with *post hoc* Bonferroni-Holm correction. **(B)** Differentiation of monocyte-derived dendritic cells. Primary human monocytes were differentiated in the presence of GM-CSF (20 ng/ml), IL-4 (40 ng/ml), and HCT116 supernatants (1 + 1 in X-Vivo full medium), and surface marker expression was analyzed as in panel **(A)**. Bars indicate mean values of $n = 7$ independent experiments. p-values were calculated by two-sided exact Wilcoxon Rank test with Bonferroni-Holm correction. **(C)** Phagocytosis of HCT116 cells by DCs. Co-cultures of PKH67-labeled DCs [differentiated for 4 days in the presence of GM-CSF (20 ng/ml) and IL-4 (40 ng/ml)] with Hoechst-labeled dying HCT116 cells (ratio 1:2) were treated with 0 or 5 Gy + 0–625 nM HSP90i. After 48 h, phagocytosis was determined by flow cytometry as the percentage of double-positive phagocytes (left panel). Datapoints for $n = 3$ independent experiments are shown. p-values were calculated by two-way ANOVA. Treatment with 10 μM cytochalasin D was used to confirm prey cell internalization (right panel). **(D)** T cell proliferation in allogeneic mixed leukocyte reactions (MLRs). Monocyte-derived DCs differentiated as in panel **(B)** were co-cultured with CFSE-labeled allogeneic CD3$^+$ human blood T cells (ratio 1:10) for 5 days. The percentage of proliferating T cells was calculated as the percentage of CD3$^+$CFSE^{low}CD4$^+$ or CD3$^+$CFSE^{low}CD8$^+$ on the basis of all CD3$^+$CD4$^+$ or CD3$^+$CD8$^+$ cells, respectively. Bars indicate mean values of $n = 6$ independent experiments. p-values were calculated by two-sided exact Wilcoxon Rank test with Bonferroni-Holm correction.

Differentiation and Effector Functions of Antigen Presenting Cells Are Enhanced Upon Contact With DAMPs Released From Irradiated and HSP90i-Treated Cancer Cells

Upon recruitment of monocytic cells, their differentiation into potent APCs is necessary in order to achieve T cell (cross-)priming for the stimulation of systemic, adaptive anti-tumor immune responses (4, 53). Along these lines, we next exposed primary human monocytes to cell-free supernatants of treated HCT116 cells and analyzed characteristic APC surface markers of the immunological synapse by flow cytometry after 5 days without any further differentiation stimulus. As such, the MHC class II molecule HLA-DR and the co-stimulatory ligands CD80 and CD86 as well as the co-activation marker CD40 were strongly upregulated, particularly upon exposure to supernatants of HCT116 cells treated with HSP90i and irradiation, indicating differentiation into an APC phenotype (**Figure 5A**). The most robust effects were observed for CD80 and HLA-DR, and similar findings were also obtained when IL-4 and GM-CSF were additionally supplemented in order to further support APC maturation (**Figure 5B**). For successful T cell (cross-)priming, tumor antigens need to be engulfed and processed by APCs. However, in contrast to APC surface marker expression, the engulfment of treated HCT116 cells by monocyte-derived dendritic cells was not affected by irradiation and only depended on the HSP90i concentration (**Figure 5C**). Finally, we analyzed the functional relevance of enhanced APC surface marker expression for their T cell (cross-)priming capacity by allogeneic MLR with CFSE-labeled primary T cells. Priming of both, CD4$^+$ and CD8$^+$ T cell proliferation was significantly enhanced by APCs differentiated in the presence of supernatants of HSP90i-treated and irradiated HCT116 cells. Collectively, our results indicate that DAMPs released by dying HCT116 cells upon irradiation plus HSP90i treatment support the recruitment, differentiation, and T cell (cross-)priming functions of APCs, and thus should favor the stimulation of systemic anti-tumor immune responses.

DISCUSSION

Despite its central role in the medical attendance of various cancer entities, indications of radiotherapy in CRC currently remain limited to malignancies of the rectum and high-risk cases of colon cancer receiving adjuvant fractionated (1.8–2 Gy per fraction) or neoadjuvant hypofractionated (5 Gy per fraction) radiotherapy alone or in combination with systemic chemotherapy, respectively (16, 17, 67). Due to the high mobility of the colon and the relevant radiosensitivity of the surrounding normal tissue, treatment planning, target volume delineation, and dose administration remain challenging, and supporting biological approaches for specific radiosensitization of the tumor appear highly attractive. In

this regard, inhibition of HSP90 has been reported to be a promising strategy. Tumor cells show a strong dependence on HSP90 chaperoning function due to their high basal protein turnover and proteotoxic stress, and crucial regulators of the DNA damage response have been identified to be particularly susceptible to HSP90 inhibition (18, 19, 22, 27). Furthermore, HSP90 in tumor cells is largely organized in multi-chaperone complexes which exhibit higher affinity for HSP90i than "normal" HSP90 complexes in non-malignant cells, thus ensuring a relevant degree of tumor specificity for HSP90i-based targeted radiosensitization (68). In this context, we and others have previously shown the synergistic therapeutic efficacy of HSP90 inhibition in combination with radiotherapy in different models of CRC *in vitro* and *in vivo* (34, 37, 39).

Apart from targeted radiosensitization, HSP90 inhibition may also enhance the priming of anti-tumor immune mechanisms that has been observed upon radiotherapy but appears to be restricted to higher single doses and strongly hypofractionated protocols (3 × 8 Gy) (7–11, 42). Improved priming of anti-tumor immune mechanisms would be particularly desirable for patients with high-risk CRC whose tumors are prone to local failure as well as metastasis formation, and who receive radiotherapy in fractions of ≤ 5 Gy – for instance in combination with immunotherapeutic protocols (69–71). Therefore, the primary motivation for our present study was to examine how HSP90 inhibition enhances radiotherapy-induced immune cell priming with the clinical perspective to develop improved treatment options for high-risk cases of colon cancer. Here, we show that HSP90 inhibition in combination with radiotherapy induced apoptosis already at radiation doses ≤ 5 Gy in a Bax-dependent manner and accelerated transit into secondary necrosis *via* mechanisms involving hyperactive Kras in CRC cells. During secondary necrosis, dying tumor cells released different classes of DAMPs which stimulated migration and recruitment of monocytic cells *in vitro* and *in vivo* and induced differentiation of APCs with potent antigen presenting capacity. Thus, HSP90 inhibition obviously enables and supports the initial steps of anti-tumor immune priming upon radiotherapy at radiation doses ≤5 Gy.

Mechanistically, our results together with prior reports reveal that HSP90i-mediated apoptosis induction upon ionizing irradiation derives from targeted disintegration of crucial DNA damage response regulators and is executed *via* the intrinsic apoptosis pathway as indicated by its clear dependence on functional Bax (37, 39). The observed accelerated transit into secondary necrosis interestingly was dependent on hyperactive Kras. Whether this observation stems from the previously reported involvement of Kras in cytoskeletal rearrangements and cell softening (72), in mechanisms of autophagy (73, 74), in metabolic rewiring (75), or so far unknown functions of hyperactive Kras, respectively, requires further investigation. Nevertheless, since a relevant number of CRC cases exhibit oncogenic Kras mutations (16), the combination of HSP90 inhibition with radiotherapy seems particularly interesting for this subgroup of patients.

In the course of secondary necrosis, dying CRC cells released different classes of DAMPs – proteins, such as HMGB1 and HSP70, as well as nucleotides, including ATP and UTP. Whereas ATP and UTP increased the chemokinetic mobility of monocytic cells in a concerted way of action as similarly described in previous studies (11, 42, 61, 62), directed recruitment of myeloid cells *in vivo* may rather rely on protein DAMPs that activate endothelial cells and stimulate the upregulation of adhesion molecules and chemokines (11, 42). Along these lines, our detailed analyses of the recruitment process in postcapillary venules in the *M. cremaster* model revealed that predominantly the steps of firm leukocyte adherence and extravasation were facilitated by DAMPs released from dying CRC cells, whereas the preceding phase of leukocyte rolling remained largely unaffected (76). This kind of activation of vascular endothelial cells allowing improved immune cell recruitment has already been described for HSP90i monotherapy settings (77).

Among the populations of myeloid cells recruited by dying CRC cell-derived DAMPs in our *in vivo* experiments, classical monocytic cells (GR-1^{hi}F4/80^{int-hi}) appear to be of specific interest for the priming of anti-tumor immune mechanisms since they have been shown to prime tumor-specific CD8$^+$ T cell responses *per se* or after intra-tumoral differentiation into potent APCs, respectively (78–80). The time-dependent decline in Gr-1 surface expression as observed in the experimental peritonitis model insinuated the differentiation into APCs (81) and was further confirmed in our *in vitro* differentiation experiments. Indeed, the upregulation of the MHC class II receptor HLA-DR, the co-stimulatory molecules CD80 as well as CD86, and the co-activating receptor CD40 upon stimulation of monocytes with supernatants of treated CRC cells indicates the emergence of a potent APC phenotype which was most pronounced upon exposure to supernatants of CRC cells treated with HSP90i plus radiotherapy. Functionally, this translated into significantly improved activation of allogeneic CD4$^+$ as well as CD8$^+$ T cells. Similar findings were obtained with supernatants of other human CRC cell lines upon irradiation with different fractionation protocols which stimulated activation of *in vitro* differentiated dendritic cells (82).

In our study, we focused on the initial steps of anti-tumor immune priming with particular interest in the release of dying cell-derived DAMPs upon radiotherapy and HSP90i treatment. Nevertheless, it should be noted that HSP90 inhibition has been described to enhance tumor immunogenicity on multiple other levels. As such, HSP90i treatment reportedly increases the expression of MHC class I and MHC class I-related molecules on tumor cells, enlarges the intracellular antigen pool, and improves the recognition of tumor cells by CD8$^+$ T cells (83, 84). Further studies observed improved T cell-dependent killing of poorly immunogenic tumor cells by HSP90 inhibition *via* additional mechanisms involving inactivation of HER2/neu, EphA2, or TCLA1, respectively (85–87). Eventually also immune checkpoint inhibition has been reported to benefit from additional HSP90 inhibition (88). However, also contradictory

results describing immunosuppressive effects of HSP90i have been published (89, 90). If the HSP90i-mediated immunological effects can add to the immunogenic reconditioning of the tumor microenvironment and the stimulation of anti-tumor immunity *in vivo* which have been observed in the context of radiotherapy (91) – ideally in a synergistic manner – requires more in-depth analyses. Apparently, the therapeutic success of such approaches in the clinical situation will depend on sequence and dose of both HSP90i and radiation (4, 19, 92).

In conclusion, our study shows that the therapeutic synergism between radiotherapy and HSP90 inhibition for the treatment of CRC is not only limited to the radiosensitizing effects of HSP90 inhibition but extends also to facilitated priming of anti-tumor immune mechanisms – specifically in case of Kras-driven tumors and at clinically relevant irradiation doses $\leq$ 5 Gy. However, further studies are needed in order to optimize treatment sequence and dose, and additional immune checkpoint inhibition might be considered with the aim of achieving the best therapeutic outcome for CRC patients.

DATA AVAILABILITY STATEMENT

The raw data supporting the conclusions of this article will be made available by the authors, without undue reservation.

ETHICS STATEMENT

The studies involving human participants were reviewed and approved by Ethics Committee of the Medical Faculty of the LMU Munich. The patients/participants provided their written informed consent to participate in this study. The animal study was reviewed and approved by the Regierung von Oberbayern.

AUTHOR CONTRIBUTIONS

KL, CB, AE, RH, CR, BF, UG, NW, and MS conceived and designed the experiments. AE, RH, HK, GZ, BU, and JK performed the experiments and analyzed the data. NW provided the HSP90i NW457. SS and TS provided the HCT116 Kras$^{+/-}$ Bax$^{+/+}$ cells. AE, RH, NB, GZ, BU, and KL wrote the manuscript. All authors discussed the results and commented on the manuscript.

FUNDING

ACKNOWLEDGMENTS

REFERENCES

1. Orth M, Lauber K, Niyazi M, Friedl AA, Li M, Maihofer C, et al. Current concepts in clinical radiation oncology. *Radiat Environ Biophys.* (2014) 53:1–29.
2. Citrin DE. Recent developments in radiotherapy. *N Engl J Med.* (2017) 377:2200–1. doi: 10.1056/nejmc1713349
3. Formenti SC, Demaria S. Radiation therapy to convert the tumor into an in situ vaccine. *Int J Radiat Oncol Biol Phys.* (2012) 84:879–80. doi: 10.1016/j.ijrobp.2012.06.020
4. Brix N, Tiefenthaller A, Anders H, Belka C, Lauber K. Abscopal, immunological effects of radiotherapy: narrowing the gap between clinical and preclinical experiences. *Immunol Rev.* (2017) 280:249–79. doi: 10.1111/imr.12573
5. Lauber K, Ernst A, Orth M, Herrmann M, Belka C. Dying cell clearance and its impact on the outcome of tumor radiotherapy. *Front Oncol.* (2012) 2:116. doi: 10.3389/fonc.2012.00116
6. Galluzzi L, Vitale I, Aaronson SA, Abrams JM, Adam D, Agostinis P, et al. Molecular mechanisms of cell death: recommendations of the nomenclature committee on cell death 2018. *Cell Death Differ.* (2018) 25:486–541.
7. Lee Y, Auh SL, Wang Y, Burnette B, Wang Y, Meng Y, et al. Therapeutic effects of ablative radiation on local tumor require CD8+ T cells: changing strategies for cancer treatment. *Blood.* (2009) 114:589–95. doi: 10.1182/blood-2009-02-206870
8. Lugade AA, Moran JP, Gerber SA, Rose RC, Frelinger JG, Lord EM. Local radiation therapy of B16 melanoma tumors increases the generation of tumor antigen-specific effector cells that traffic to the tumor. *J Immunol.* (2005) 174:7516–23. doi: 10.4049/jimmunol.174.12.7516
9. Lugade AA, Sorensen EW, Gerber SA, Moran JP, Frelinger JG, Lord EM. Radiation-induced IFN-gamma production within the tumor microenvironment influences antitumor immunity. *J Immunol.* (2008) 180:3132–9. doi: 10.4049/jimmunol.180.5.3132
10. Vanpouille-Box C, Alard A, Aryankalayil MJ, Sarfraz Y, Diamond JM, Schneider RJ, et al. DNA exonuclease Trex1 regulates radiotherapy-induced tumour immunogenicity. *Nat Commun.* (2017) 8:15618.
11. Krombach J, Hennel R, Brix N, Orth M, Schoetz U, Ernst A, et al. Priming anti-tumor immunity by radiotherapy: dying tumor cell-derived DAMPs trigger endothelial cell activation and recruitment of myeloid cells. *Oncoimmunology.* (2019) 8:e1523097. doi: 10.1080/2162402x.2018.1523097
12. Burnette BC, Liang H, Lee Y, Chlewicki L, Khodarev NN, Weichselbaum RR, et al. The efficacy of radiotherapy relies upon induction of type i interferon-dependent innate and adaptive immunity. *Cancer Res.* (2011) 71:2488–96. doi: 10.1158/0008-5472.can-10-2820
13. Deng L, Liang H, Xu M, Yang X, Burnette B, Arina A, et al. dna sensing promotes radiation-induced type I interferon-dependent antitumor immunity in immunogenic tumors. *Immunity.* (2014) 41:843–52. doi: 10.1016/j.immuni.2014.10.019
14. Sistigu A, Yamazaki T, Vacchelli E, Chaba K, Enot DP, Adam J, et al. Cancer cell-autonomous contribution of type I interferon signaling to the efficacy of chemotherapy. *Nat Med.* (2014) 20:1301–9.
15. Bray F, Ferlay J, Soerjomataram I, Siegel RL, Torre LA, Jemal A. Global cancer statistics 2018: GLOBOCAN estimates of incidence and mortality worldwide for 36 cancers in 185 countries. *CA Cancer J Clin.* (2018) 68:394–424. doi: 10.3322/caac.21492
16. Binefa G, Rodriguez-Moranta F, Teule A, Medina-Hayas M. Colorectal cancer: from prevention to personalized medicine. *World J Gastroenterol.* (2014) 20:6786–808. doi: 10.3748/wjg.v20.i22.6786
17. van de Velde CJ, Boelens PG, Borras JM, Coebergh JW, Cervantes A, Blomqvist L, et al. EURECCA colorectal: multidisciplinary management: European consensus conference colon & rectum. *Eur J Cancer.* (2014) 50:1.e1–e34.
18. Sveen A, Bruun J, Eide PW, Eilertsen IA, Ramirez L, Murumagi A, et al. Colorectal cancer consensus molecular subtypes translated to preclinical models uncover potentially targetable cancer cell dependencies. *Clin Cancer Res.* (2018) 24:794–806. doi: 10.1158/1078-0432.ccr-17-1234
19. Lauber K, Brix N, Ernst A, Hennel R, Krombach J, Anders H, et al. Targeting the heat shock response in combination with radiotherapy: sensitizing cancer cells to irradiation-induced cell death and heating up their immunogenicity. *Cancer Lett.* (2015) 368:209–29. doi: 10.1016/j.canlet.2015.02.047
20. Jaeger AM, Whitesell L. HSP90: enabler of cancer adaptation. *Annu Rev Cancer Biol.* (2019) 3:275–97. doi: 10.1146/annurev-cancerbio-030518-055533
21. Whitesell L, Lindquist SL. HSP90 and the chaperoning of cancer. *Nat Rev Cancer.* (2005) 5:761–72. doi: 10.1038/nrc1716
22. Trepel J, Mollapour M, Giaccone G, Neckers L. Targeting the dynamic HSP90 complex in cancer. *Nat Rev Cancer.* (2010) 10:537–49. doi: 10.1038/nrc2887
23. Hanahan D, Weinberg RA. Hallmarks of cancer: the next generation. *Cell.* (2011) 144:646–74. doi: 10.1016/j.cell.2011.02.013
24. Rozenberg P, Ziporen L, Gancz D, Saar-Ray M, Fishelson Z. Cooperation between Hsp90 and mortalin/GRP75 in resistance to cell death induced by complement C5b-9. *Cell Death Dis.* (2018) 9:150.
25. Liu K, Chen J, Yang F, Zhou Z, Liu Y, Guo Y, et al. BJ-B11, an Hsp90 inhibitor, constrains the proliferation and invasion of breast cancer cells. *Front Oncol.* (2019) 9:1447. doi: 10.3389/fonc.2019.01447
26. Yuno A, Lee MJ, Lee S, Tomita Y, Rekhtman D, Moore B, et al. Clinical evaluation and biomarker profiling of Hsp90 inhibitors. *Methods Mol Biol.* (2018) 1709:423–41. doi: 10.1007/978-1-4939-7477-1_29
27. Sharma K, Vabulas RM, Macek B, Pinkert S, Cox J, Mann M, et al. Quantitative proteomics reveals that Hsp90 inhibition preferentially targets kinases and the DNA damage response. *Mol Cell Proteomics.* (2012) 11:M111014654.
28. Kryeziu K, Bruun J, Guren TK, Sveen A, Lothe RA. Combination therapies with HSP90 inhibitors against colorectal cancer. *Biochim Biophys Acta Rev Cancer.* (2019) 1871:240–7. doi: 10.1016/j.bbcan.2019.01.002
29. Alexandrova EM, Xu S, Moll UM. Ganetespib synergizes with cyclophosphamide to improve survival of mice with autochthonous tumors in a mutant p53-dependent manner. *Cell Death Dis.* (2017) 8:e2683. doi: 10.1038/cddis.2017.108
30. Subramaniam DS, Liu SV, Crawford J, Kramer J, Thompson J, Wang H, et al. A Phase Ib/II study of ganetespib with doxorubicin in advanced solid tumors including relapsed-refractory small cell lung cancer. *Front Oncol.* (2018) 8:64. doi: 10.3389/fonc.2018.00064
31. Ray-Coquard I, Braicu I, Berger R, Mahner S, Sehouli J, Pujade-Lauraine E, et al. Part I of GANNET53: a European multicenter phase I/II trial of the Hsp90 inhibitor ganetespib combined with weekly paclitaxel in women with high-grade, platinum-resistant epithelial ovarian cancer-a study of the GANNET53 consortium. *Front Oncol.* (2019) 9:832. doi: 10.3389/fonc.2019.00832
32. Nagaraju GP, Zakka KM, Landry JC, Shaib WL, Lesinski GB, El-Rayes BF. Inhibition of HSP90 overcomes resistance to chemotherapy and radiotherapy in pancreatic cancer. *Int J Cancer.* (2019) 145:1529–37. doi: 10.1002/ijc.32227
33. Kuhnel A, Schilling D, Combs SE, Haller B, Schwab M, Multhoff G. Radiosensitization of HSF-1 knockdown lung cancer cells by low concentrations of Hsp90 inhibitor NVP-AUY922. *Cells.* (2019) 8:1166. doi: 10.3390/cells8101166
34. He S, Smith DL, Sequeira M, Sang J, Bates RC, Proia DA. The HSP90 inhibitor ganetespib has chemosensitizer and radiosensitizer activity in colorectal cancer. *Invest New Drugs.* (2014) 32:577–86. doi: 10.1007/s10637-014-0095-4
35. Spiegelberg D, Dascalu A, Mortensen AC, Abramenkovs A, Kuku G, Nestor M, et al. The novel HSP90 inhibitor AT13387 potentiates radiation effects

in squamous cell carcinoma and adenocarcinoma cells. *Oncotarget*. (2015) 6:35652–66. doi: 10.18632/oncotarget.5363

36. Whitesell L, Santagata S, Lin NU. Inhibiting HSP90 to treat cancer: a strategy in evolution. *Curr Mol Med*. (2012) 12:1108–24. doi: 10.2174/156652412803306657

37. Kinzel L, Ernst A, Orth M, Albrecht V, Hennel R, Brix N, et al. A novel HSP90 inhibitor with reduced hepatotoxicity synergizes with radiotherapy to induce apoptosis, abrogate clonogenic survival, and improve tumor control in models of colorectal cancer. *Oncotarget*. (2016) 7:43199–219. doi: 10.18632/oncotarget.9774

38. Ernst A, Anders H, Kapfhammer H, Orth M, Hennel R, Seidl K, et al. HSP90 inhibition as a means of radiosensitizing resistant, aggressive soft tissue sarcomas. *Cancer Lett*. (2015) 365:211–22. doi: 10.1016/j.canlet.2015.05.024

39. Spiegelberg D, Abramenkovs A, Mortensen ACL, Lundsten S, Nestor M, Stenerlow B. The HSP90 inhibitor onalespib exerts synergistic anti-cancer effects when combined with radiotherapy: an in vitro and in vivo approach. *Sci Rep*. (2020) 10:5923.

40. Zhang L, Yu J, Park BH, Kinzler KW, Vogelstein B. Role of BAX in the apoptotic response to anticancer agents. *Science*. (2000) 290:989–92. doi: 10.1126/science.290.5493.989

41. Shirasawa S, Furuse M, Yokoyama N, Sasazuki T. Altered growth of human colon cancer cell lines disrupted at activated Ki-ras. *Science*. (1993) 260:85–8. doi: 10.1126/science.8465203

42. Hennel R, Brix N, Seidl K, Ernst A, Scheithauer H, Belka C, et al. Release of monocyte migration signals by breast cancer cell lines after ablative and fractionated gamma-irradiation. *Radiat Oncol*. (2014) 9:85. doi: 10.1186/1748-717x-9-85

43. Jung S, Aliberti J, Graemmel P, Sunshine MJ, Kreutzberg GW, Sher A, et al. Analysis of fractalkine receptor CX(3)CR1 function by targeted deletion and green fluorescent protein reporter gene insertion. *Mol Cell Biol*. (2000) 20:4106–14. doi: 10.1128/mcb.20.11.4106-4114.2000

44. Barluenga S, Fontaine JG, Wang C, Aouadi K, Chen R, Beebe K, et al. Inhibition of HSP90 with pochoximes: SAR and structure-based insights. *Chembiochem*. (2009) 10:2753–9. doi: 10.1002/cbic.200900494

45. Barluenga S, Wang C, Fontaine JG, Aouadi K, Beebe K, Tsutsumi S, et al. Divergent synthesis of a pochonin library targeting HSP90 and in vivo efficacy of an identified inhibitor. *Angew Chem Int Ed Engl*. (2008) 47:4432–5. doi: 10.1002/anie.200800233

46. Karthikeyan G, Zambaldo C, Barluenga S, Zoete V, Karplus M, Winssinger N. Asymmetric synthesis of pochonin E and F, revision of their proposed structure, and their conversion to potent Hsp90 inhibitors. *Chemistry*. (2012) 18:8978–86. doi: 10.1002/chem.201200546

47. Lerchenberger M, Uhl B, Stark K, Zuchtriegel G, Eckart A, Miller M, et al. Matrix metalloproteinases modulate ameboid-like migration of neutrophils through inflamed interstitial tissue. *Blood*. (2013) 122:770–80. doi: 10.1182/blood-2012-12-472944

48. Uhl B, Zuchtriegel G, Puhr-Westerheide D, Praetner M, Rehberg M, Fabritius M, et al. Tissue plasminogen activator promotes postischemic neutrophil recruitment via its proteolytic and nonproteolytic properties. *Arterioscler Thromb Vasc Biol*. (2014) 34:1495–504. doi: 10.1161/atvbaha.114.303721

49. Zuchtriegel G, Uhl B, Hessenauer ME, Kurz AR, Rehberg M, Lauber K, et al. Spatiotemporal expression dynamics of selectins govern the sequential extravasation of neutrophils and monocytes in the acute inflammatory response. *Arterioscler Thromb Vasc Biol*. (2015) 35:899–910. doi: 10.1161/atvbaha.114.305143

50. Reichel CA, Uhl B, Lerchenberger M, Puhr-Westerheide D, Rehberg M, Liebl J, et al. Urokinase-type plasminogen activator promotes paracellular transmigration of neutrophils via Mac-1, but independently of urokinase-type plasminogen activator receptor. *Circulation*. (2011) 124:1848–59. doi: 10.1161/circulationaha.110.017012

51. Mempel TR, Moser C, Hutter J, Kuebler WM, Krombach F. Visualization of leukocyte transendothelial and interstitial migration using reflected light oblique transillumination in intravital video microscopy. *J Vasc Res*. (2003) 40:435–41. doi: 10.1159/000073902

52. Chou TC. Drug combination studies and their synergy quantification using the Chou-Talalay method. *Cancer Res*. (2010) 70:440–6. doi: 10.1158/0008-5472.can-09-1947

53. Chen DS, Mellman I. Oncology meets immunology: the cancer-immunity cycle. *Immunity*. (2013) 39:1–10. doi: 10.1016/j.immuni.2013.07.012

54. Kroemer G, Galluzzi L, Kepp O, Zitvogel L. Immunogenic cell death in cancer therapy. *Annu Rev Immunol*. (2013) 31:51–72.

55. Silva MT. Secondary necrosis: the natural outcome of the complete apoptotic program. *FEBS Lett*. (2010) 584:4491–9. doi: 10.1016/j.febslet.2010.10.046

56. Stolze B, Reinhart S, Bulllinger L, Frohling S, Scholl C. Comparative analysis of KRAS codon 12, 13, 18, 61, and 117 mutations using human MCF10A isogenic cell lines. *Sci Rep*. (2015) 5:8535.

57. Munoz-Maldonado C, Zimmer Y, Medova M. A comparative analysis of individual RAS mutations in cancer biology. *Front Oncol*. (2019) 9:1088. doi: 10.3389/fonc.2019.01088

58. Rudner J, Belka C, Marini P, Wagner RJ, Faltin H, Lepple-Wienhues A, et al. Radiation sensitivity and apoptosis in human lymphoma cells. *Int J Radiat Biol*. (2001) 77:1–11. doi: 10.1080/095530001453069

59. Eriksson D, Stigbrand T. Radiation-induced cell death mechanisms. *Tumour Biol*. (2010) 31:363–72. doi: 10.1007/s13277-010-0042-8

60. Sachet M, Liang YY, Oehler R. The immune response to secondary necrotic cells. *Apoptosis*. (2017) 22:1189–204. doi: 10.1007/s10495-017-1413-z

61. Isfort K, Ebert F, Bornhorst J, Sargin S, Kardakaris R, Pasparakis M, et al. Real-time imaging reveals that P2Y2 and P2Y12 receptor agonists are not chemoattractants and macrophage chemotaxis to complement C5a is phosphatidylinositol 3-kinase (PI3K)- and p38 mitogen-activated protein kinase (MAPK)-independent. *J Biol Chem*. (2011) 286:44776–87. doi: 10.1074/jbc.m111.289793

62. Kronlage M, Song J, Sorokin L, Isfort K, Schwerdtle T, Leipziger J, et al. Autocrine purinergic receptor signaling is essential for macrophage chemotaxis. *Sci Signal*. (2010) 3:ra55. doi: 10.1126/scisignal.2000588

63. Elliott MR, Chekeni FB, Trampont PC, Lazarowski ER, Kadl A, Walk SF, et al. Nucleotides released by apoptotic cells act as a find-me signal to promote phagocytic clearance. *Nature*. (2009) 461:282–6. doi: 10.1038/nature08296

64. Chen J, Zhao Y, Liu Y. The role of nucleotides and purinergic signaling in apoptotic cell clearance – implications for chronic inflammatory diseases. *Front Immunol*. (2014) 5:656.

65. Deloch L, Derer A, Hartmann J, Frey B, Fietkau R, Gaipl US. Modern radiotherapy concepts and the impact of radiation on immune activation. *Front Oncol*. (2016) 6:141. doi: 10.3389/fonc.2016.00141

66. Baez S. An open cremaster muscle preparation for the study of blood vessels by in vivo microscopy. *Microvasc Res*. (1973) 5:384–94. doi: 10.1016/0026-2862(73)90054-x

67. Hawkins AT, Ford MM, Geiger TM, Hopkins MB, Kachnic LA, Muldoon RL, et al. Neoadjuvant radiation for clinical T4 colon cancer: a potential improvement to overall survival. *Surgery*. (2019) 165:469–75. doi: 10.1016/j.surg.2018.06.015

68. Kamal A, Thao L, Sensintaffar J, Zhang L, Boehm MF, Fritz LC, et al. A high-affinity conformation of Hsp90 confers tumour selectivity on Hsp90 inhibitors. *Nature*. (2003) 425:407–10. doi: 10.1038/nature01913

69. Ghiringhelli F, Fumet JD. Is there a place for immunotherapy for metastatic microsatellite stable colorectal cancer? *Front Immunol*. (2019) 10:1816. doi: 10.3389/fimmu.2019.01816

70. Picard E, Verschoor CP, Ma GW, Pawelec G. Relationships between immune landscapes, genetic subtypes and responses to immunotherapy in colorectal cancer. *Front Immunol*. (2020) 11:369. doi: 10.3389/fimmu.2020.00369

71. Correale P, Botta C, Staropoli N, Nardone V, Pastina P, Ulivieri C, et al. Systemic inflammatory status predict the outcome of k-RAS WT metastatic colorectal cancer patients receiving the thymidylate synthase poly-epitope-peptide anticancer vaccine. *Oncotarget*. (2018) 9:20539–54. doi: 10.18632/oncotarget.24993

72. Rudzka DA, Spennati G, McGarry DJ, Chim YH, Neilson M, Ptak A, et al. Migration through physical constraints is enabled by MAPK-induced cell softening via actin cytoskeleton re-organization. *J Cell Sci*. (2019) 132:jcs224071. doi: 10.1242/jcs.224071

73. Ko A, Kanehisa A, Martins I, Senovilla L, Chargari C, Dugue D, et al. Autophagy inhibition radiosensitizes in vitro, yet reduces radioresponses in vivo due to deficient immunogenic signalling. *Cell Death Differ*. (2014) 21:92–9. doi: 10.1038/cdd.2013.124

74. Yang S, Wang X, Contino G, Liesa M, Sahin E, Ying H, et al. Pancreatic cancers require autophagy for tumor growth. *Genes Dev.* (2011) 25:717–29. doi: 10.1101/gad.2016111

75. Pupo E, Avanzato D, Middonti E, Bussolino F, Lanzetti L. KRAS-driven metabolic rewiring reveals novel actionable targets in cancer. *Front Oncol.* (2019) 9:848. doi: 10.3389/fonc.2019.00848

76. Ley K, Laudanna C, Cybulsky MI, Nourshargh S. Getting to the site of inflammation: the leukocyte adhesion cascade updated. *Nat Rev Immunol.* (2007) 7:678–89. doi: 10.1038/nri2156

77. Rao A, Taylor JL, Chi-Sabins N, Kawabe M, Gooding WE, Storkus WJ. Combination therapy with HSP90 inhibitor 17-DMAG reconditions the tumor microenvironment to improve recruitment of therapeutic T cells. *Cancer Res.* (2012) 72:3196–206. doi: 10.1158/0008-5472.can-12-0538

78. Larson SR, Atif SM, Gibbings SL, Thomas SM, Prabagar MG, Danhorn T, et al. Ly6C(+) monocyte efferocytosis and cross-presentation of cell-associated antigens. *Cell Death Differ.* (2016) 23:997–1003. doi: 10.1038/cdd.2016.24 doi: 10.1038/cdd.2016.24

79. Ma Y, Adjemian S, Mattarollo SR, Yamazaki T, Aymeric L, Yang H, et al. Anticancer chemotherapy-induced intratumoral recruitment and differentiation of antigen-presenting cells. *Immunity.* (2013) 38:729–41. doi: 10.1016/j.immuni.2013.03.003

80. Ma Y, Mattarollo SR, Adjemian S, Yang H, Aymeric L, Hannani D, et al. CCL2/CCR2-dependent recruitment of functional antigen-presenting cells into tumors upon chemotherapy. *Cancer Res.* (2014) 74:436–45. doi: 10.1158/0008-5472.can-13-1265

81. Jakubzick CV, Randolph GJ, Henson PM. Monocyte differentiation and antigen-presenting functions. *Nat Rev Immunol.* (2017) 17:349–62. doi: 10.1038/nri.2017.28

82. Kulzer L, Rubner Y, Deloch L, Allgauer A, Frey B, Fietkau R, et al. Norm- and hypo-fractionated radiotherapy is capable of activating human dendritic cells. *J Immunotoxicol.* (2014) 11:328–36. doi: 10.3109/1547691x.2014.880533

83. Fionda C, Soriani A, Malgarini G, Iannitto ML, Santoni A, Cippitelli M. Heat shock protein-90 inhibitors increase MHC class I-related chain A and B ligand expression on multiple myeloma cells and their ability to trigger NK cell degranulation. *J Immunol.* (2009) 183:4385–94. doi: 10.4049/jimmunol.0901797

84. Haggerty TJ, Dunn IS, Rose LB, Newton EE, Pandolfi F, Kurnick JT. Heat shock protein-90 inhibitors enhance antigen expression on melanomas and increase T cell recognition of tumor cells. *PLoS One.* (2014) 9:e114506. doi: 10.1371/journal.pone.0114506

85. Castilleja A, Ward NE, O'Brian CA, Swearingen B II, Swan E, Gillogly MA, et al. Accelerated HER-2 degradation enhances ovarian tumor recognition by CTL. Implications for tumor immunogenicity. *Mol Cell Biochem.* (2001) 217:21–33.

86. Kawabe M, Mandic M, Taylor JL, Vasquez CA, Wesa AK, Neckers LM, et al. Heat shock protein 90 inhibitor 17-dimethylaminoethylamino-17-demethoxygeldanamycin enhances EphA2+ tumor cell recognition by specific CD8+ T cells. *Cancer Res.* (2009) 69:6995–7003. doi: 10.1158/0008-5472.can-08-4511

87. Song KH, Oh SJ, Kim S, Cho H, Lee HJ, Song JS, et al. HSP90A inhibition promotes anti-tumor immunity by reversing multi-modal resistance and stem-like property of immune-refractory tumors. *Nat Commun.* (2020) 11:562.

88. Mbofung RM, McKenzie JA, Malu S, Zhang M, Peng W, Liu C, et al. HSP90 inhibition enhances cancer immunotherapy by upregulating interferon response genes. *Nat Commun.* (2017) 8:451.

89. Callahan MK, Garg M, Srivastava PK. Heat-shock protein 90 associates with N-terminal extended peptides and is required for direct and indirect antigen presentation. *Proc Natl Acad Sci USA.* (2008) 105:1662–7. doi: 10.1073/pnas.0711365105

90. Tsuji T, Matsuzaki J, Caballero OL, Jungbluth AA, Ritter G, Odunsi K, et al. Heat shock protein 90-mediated peptide-selective presentation of cytosolic tumor antigen for direct recognition of tumors by CD4(+) T cells. *J Immunol.* (2012) 188:3851–8. doi: 10.4049/jimmunol.1103269

91. Filatenkov A, Baker J, Mueller AM, Kenkel J, Ahn GO, Dutt S, et al. Ablative tumor radiation can change the tumor immune cell microenvironment to induce durable complete remissions. *Clin Cancer Res.* (2015) 21:3727–39. doi: 10.1158/1078-0432.ccr-14-2824

92. Jaeger AM, Stopfer L, Lee S, Gaglia G, Sandel D, Santagata S, et al. Rebalancing protein homeostasis enhances tumor antigen presentation. *Clin Cancer Res.* (2019) 25:6392–405. doi: 10.1158/1078-0432.ccr-19-0596

Prospective Evaluation of All-lesion Versus Single-lesion Radiotherapy in Combination With PD-1/PD-L1 Immune Checkpoint Inhibitors

Philipp Schubert[1,2]*, Sandra Rutzner[1,2], Markus Eckstein[2,3], Benjamin Frey[1,2], Claudia Schweizer[1,2], Marlen Haderlein[1,2], Sebastian Lettmaier[1,2], Sabine Semrau[1,2], Antoniu-Oreste Gostian[2,4], Jian-Guo Zhou[1,2,5], Udo S. Gaipl[1,2], Rainer Fietkau[1,2] and Markus Hecht[1,2]

[1] Department of Radiation Oncology, Universitätsklinikum Erlangen, Friedrich-Alexander-Universität Erlangen-Nürnberg, Erlangen, Germany, [2] Comprehensive Cancer Center Erlangen-EMN, Erlangen, Germany, [3] Institute of Pathology, Universitätsklinikum Erlangen, Friedrich-Alexander-Universität Erlangen-Nürnberg, Erlangen, Germany, [4] Department of Otolaryngology—Head & Neck Surgery, Universitätsklinikum Erlangen, Friedrich-Alexander-Universität Erlangen-Nürnberg, Erlangen, Germany, [5] Department of Oncology, The Second Affiliated Hospital of Zunyi Medical University, Zunyi, China

Background: Local ablative treatments improve survival in patients with oligometastatic disease in addition to chemotherapy. The application of immune checkpoint inhibitors prolonged patients' survival in different tumor entities. This raises the question if patients still benefit from intensified local treatments in combination with a more efficient systemic treatment with immune checkpoint inhibitors.

Methods: The prospective non-interventional ST-ICI trial investigates treatment with PD-1/PD-L1 (Programmed cell death protein 1/Programmed cell death 1 ligand 1) immune checkpoint inhibitors and radiotherapy in different tumor entities. Patients who started radiotherapy and immunotherapy concomitantly were included in this interim analysis. In this cohort patients with all-lesion radiotherapy (all tumor lesions irradiated, al-RT) were compared to patients with radiotherapy to only a single of their tumor lesions (single-lesion radiotherapy, sl-RT). Endpoints of the interim analysis were progression-free survival (PFS), overall survival (OS) and time to progression (TTP).

Results: A total of 104 patients were registered between April 2017 and August 2019. Fifty patients started immune checkpoint inhibitor treatment and radiotherapy concomitantly and were included. Most frequent tumor entities were non-small cell lung cancer (62%) followed by head and neck squamous cell cancer (26%). Most frequent location of radiotherapy was lung (34%) and central nervous system (20%). Median duration of follow-up was 8.6 months beginning with first administration of the immune-checkpoint-inhibitor. Median PFS was 9.2 months (95% CI, 5.8 – 12.6) in the al-RT group and 3.0 months (95% CI, 2.5 – 3.5) in the sl-RT group (p<0.001). Median OS was 11.6 months (95% CI, 8.1 - 15.1) in the al-RT group and 4.2 months (95% CI, 3.0 - 5.4) in the sl-RT group (p=0.007). Median TTP was not reached in the al-RT group compared to 4.6 months (95% CI, 1.1–8.0) in the sl-RT group (p=0.028). Univariate Cox regression

analyses computed tumor entity, histology, central nervous system metastases, immunotherapy drug and al-RT as predictors of OS (with an effect p-value of ≤ 0.1). In the multivariable analysis only tumor entity and al-RT remained prognostic factors for OS.

Conclusion: Patients with PD-1/PD-L1 immune checkpoint inhibitor therapy benefit from local radiotherapy to all known lesions compared to single-lesion radiotherapy regarding PFS and OS.

INTRODUCTION

Multi-disciplinary treatment strategies combining local ablative treatments and systemic therapy in patients with limited number of distant metastases, i.e. oligometastatic disease, improved survival in different tumor entities (1, 2). Especially in lung cancer, the combination of local ablative therapy in addition to chemotherapy improved survival (3). During the last years immune checkpoint inhibitors have improved survival compared to classical chemotherapy in several types of metastatic cancer and became first-line treatment (4, 5). However, most data about local ablative treatments in oligometastatic patients origin from the pre-immunotherapy era. Consequently, there is lack of evidence, whether patients still benefit from local treatments if more effective systemic treatment with immune checkpoint inhibitors is available (1, 6).

However, the combination of immune checkpoint inhibitors with radiotherapy might even be more efficient due to local immune-modulatory effects of radiotherapy (7). The expression of PD-L1 increases on the patients' tumor cells after radiotherapy, which is the most important predictive parameter for anti-PD(L)1 inhibitors (8, 9). In preclinical models local radiotherapy in combination with immune checkpoint inhibitors also enhanced immunological effects distant to the irradiated area (10, 11). These systemic immune-modulating effects of local radiotherapy were also found in several clinical retrospective analyses (12–14).

The ST-ICI study was originally conducted to determine the effect of radiotherapy in combination with programmed cell death 1 (PD-1) or PD-L1 immune checkpoint inhibitors. In the current analysis, patients in an oligometastatic situation receiving radiotherapy to all known lesions (al-RT group) were compared to patients with radiotherapy to a fraction of known metastases (sl-RT group) in order to improve current treatment strategies.

MATERIAL AND METHODS

Trial Design and Treatments

ST-ICI is a prospective non-interventional, non-randomized, single-center trial investigating interactions of radiotherapy and immune checkpoint inhibitors. Patients with metastatic non-melanoma solid tumors of several entities and clinical indication for PD-L1/CTLA-4 therapy along with planed

palliative radiotherapy according to clinical standard were included in the study. Patients that are known for substance abuse, not willing to take contraceptive measures, deemed uncooperative, not speaking German language and patients under legal care were not included in the trial. The current exploratory interim analysis focuses on patients with radiotherapy to all present metastases(al-RT) compared to patients receiving radiotherapy only to single of their metastases (single-lesion radiotherapy, sl-RT). The treatment decision was made by treating physicians based on clinical standards and national guidelines. Patients were allocated to the al-RT group, when local radiotherapy to all tumor lesions was possible according to the treating physician. Patients with single symptomatic metastases beyond other metastases received radiotherapy within the sl-RT group. Treatment with any EMA-approved inhibitor PD-1 or PD-L1 was allowed. Dosing and treatment indication of the immune checkpoint inhibitors was according to the European Medicines Agency (EMA) marketing authorizations. Radiotherapy was administered as stereotactic radiosurgery (SRS), stereotactic body radiotherapy (SBRT) or volumetric modulated arc radiotherapy (VMAT). The described total dose as well as dose per fraction was prescribed according local guidelines derived from national and international recommendations.

Patients

Patients were eligible for this interim analysis if they were treated with immune checkpoint inhibitors and radiotherapy. Radiotherapy had to be delivered within a timeframe of ±30 days from the first administration of the immune checkpoint inhibitor. There was no limitation regarding tumor entity. As the trial should represent unselected patients, there were no limitations regarding baseline Eastern Cooperative Oncology Group (ECOG) performance status, pre-existing diseases, tumor entity or baseline blood parameters.

Endpoint and Assessment

The objective in this exploratory interim analysis was to evaluate the efficacy of immune checkpoint inhibitors combined with al-RT compared to sl-RT. The endpoints of this interim analysis were overall survival (OS), progression-free survival (PFS) and time to progression (TTP). Survival analyses were defined from the date of first administration of immune checkpoint inhibitor, to the date of last follow-up, tumor progression or death. Data was collected from patients' electronic health records (EHR) as

well as the radiotherapy planning software (Pinnacle, Philips, USA). Survival data was provided by the Comprehensive Cancer Center Erlangen-EMN (CCC, Friedrich-Alexander University Erlangen-Nuremberg, Erlangen, Germany). Tumor staging was performed with computed tomography (CT) and/or magnetic resonance (MRI) imaging according to clinical standards.

Trial Oversight

The ST-ICI trial was registered with ClinicalTrials.gov (identifier: NCT03453892). The institutional review board at the Friedrich-Alexander-Universität Erlangen-Nürnberg approved the study (number: 2_17 B). The study was performed in accordance with the Declaration of Helsinki. All patients gave written informed consent that comprised a data privacy clause for data collection and analysis for research purpose.

Statistical Analysis

All statistical tests were performed using IBM SPSS Statistics Version 25. Associations between clinical baseline characteristics were evaluated using the Fisher's exact chi- test. Kaplan-Meier method was used to analyze OS and PFS. The log-rank test was used to compare Kaplan-Meier survival curves. A p-value <0.05 was considered to be statistically significant. Cox proportional hazard methods were used to study the association between different baseline factors and OS. During the selection process, all explanatory factors with an effect p-value of <0.1 in the univariate Cox regression analysis were included in the multivariate analysis. A backward selection procedure was applied. Only the parameters with a p-value <0.05 in the backward selection procedure remained in the final model.

RESULTS

Patient Characteristics

A total of 104 patients were registered for the ST-ICI trial between April 2017 and August 2019. Out of these, 50 patients received radiotherapy within a timeframe of ±30 days from the first administration of the immune checkpoint inhibitor and were included in this interim analysis. Baseline characteristics are presented in **Table 1**. Median age was 60 years (range, 37–87 years), 29 patients were male (58%). Radiotherapy of all metastases (al-RT) was performed in 27 (54%) patients, 23 (46%) patients received radiotherapy of only a single metastasis besides others (sl-RT). The mean number of metastases was 1.63 (95% CI, 1.34 – 1.92) in the al-RT group and 6.30 (95% CI, 4.72 – 7.89) in the sl-RT group (p < 0.001). Fourteen patients with one metastases were included in the al-RT group, whereas none in the sl-RT group (not possible). Most frequent tumor entity was non-small cell lung cancer (NSCLC) with 31 patients (62%), head and neck squamous cell cancer (HNSCC) in 13 patients (26%). Additional 3 patients with urothelial cancer (5%), one patient with esophageal cancer, one patient with mixed adenoneuroendocrine carcinoma in the gastric region and one patient with sinonasal-undifferentiated carcinoma were included

in the analysis. PD-L1 expression was <1% in 15 patients (30%) and ≥1% in 33 patients (66). The majority of patients received prior local treatment. Previous treatment consisted of surgery of the primary tumor in 17 patients (34%) and radiotherapy in 39 patients (78%). In the recurrent or metastatic situation 35 patients (70%) received 1 to 2 lines of previous chemotherapy whereas 7 patients have received even more lines of chemotherapy. First line chemotherapy was platinum based in 36 patients (72%).

There were no statistically significant differences of baseline characteristics in the al-RT and sl-RT cohort except the number of metastases.

Treatment

Treatment characteristics are displayed in **Table 2**. The most frequent fractionation of radiotherapy was normal fractionation (single doses between 1.8 and 2.2 Gy) in 25 (50%) patients, followed by 22 (44%) patients receiving hypo-fractionation (single doses between 3 Gy and 6 Gy), three patients (6%) received radiosurgery (18 – 20 Gy). Radiotherapy was delivered to a single lesion in 14 patients (51%) of the al-RT group and 15 patients (65%) of the sl-RT group (p= 0.134). The location of radiotherapy differed significantly in both groups with the most frequent location being lung (51%) in the al-RT group and brain (39%) in the sl-RT group (p<0.001). Conventional fractionation was used more frequently in the al-RT group than in the sl-RT group (60% vs. 40%, p=0.023). The mean total administered dose was higher in the al-RT group than in the sl-RT group (55.3 Gy versus 43.4 Gy, p=0.004). In both cohorts the most frequently used immune checkpoint inhibitor was nivolumab (50%) followed by pembrolizumab (32%). Concomitant chemotherapy was administered in four patients (8%), whereas three were in the al-RT group and one in the sl-RT group

Safety

A total of 15 patients developed immune-related averse events (irAE). The rate of irAE seems increased in the al-RT group (al-RT n=11; sl-RT n=4). The predominant irAE was hypothyroidism (n=6), followed by skin reaction, hepatitis, diarrhea and pneumonitis that appeared in two patients each. The majority of these patients experienced CTCAE grade one or two toxicity (n=13), grade three was observed in two patients. The development of an irAE in a specific organ was not associated with the location of radiotherapy. No relevant radiation toxicity was reported within the follow-up time. Especially in patients with radiotherapy to brain metastases, no case of radionecrosis was reported until the most recent MRI.

Efficacy

The median follow-up of the entire cohort was 8.2 months (95% CI, 0.7–21.8) beginning with initiation of ICI. The median OS in the al-RT group was 11.6 months (95% CI, 8.1–15.1) and significantly longer than 4.2 months (95% CI, 3.0–5.4, p=0.007) in the sl-RT group (**Figure 1A**). After one-year OS was 30% in the al-RT group compared to 13% in the sl-RT group.

TABLE 1 | Baseline Characteristics.

Characteristic	Total (n = 50)	al-RT (n = 27)	sl-RT (n = 23)	p-value
Age, years				1.0
Mean +/- SD	60.9 ± 11.3	59.0 ± 10.5	63.3 ± 11.9	
Sex				0.398
Male	29 (58)	14 (51)	15 (65)	
Female	21 (42)	13 (49)	8 (35)	
Tumor entity				0.454
HNSCC	13 (26)	5 (18)	8 (34)	
NSCLC	31 (62)	18 (66)	13 (56)	
Urothelial cancer	3 (6)	2 (8)	1 (5)	
Others*	3 (6)	2 (8)	1 (5	
No. of Metastasis				<0.001
1	14 (28)	14 (52)	0	
2–5	25 (50)	13 (48)	12 (52)	
6–10	6 (12)	0	6 (26)	
>10	5 (10)	0	5 (22)	
CNS Metastases				0.136
No	34 (68)	21 (77)	13 (55)	
Yes	16 (32)	6 (23)	10 (45)	
No. Previous Chemotherapies in the recurrent/metastatic situation				1.0
0	12 (24)	6 (22)	6 (26)	
1–2	35 (70)	20 (74)	15 (65)	
>2	3 (8)	1 (4)	2 (9)	
No. of previous radiotherapies				0.367
0	4 (8)	3 (11)	1 (4)	
1–2	39 (78)	22 (81)	17 (74)	
>2	7 (14)	2 (8)	5 (22)	
1st line Platin CT				0.251
Yes	36 (72)	21 (77)	15 (65)	
No	14 (28)	6 (23)	8 (35)	
Prior Surgery				0.239
Yes	17 (34)	7 (26)	10 (44)	
No	33 (66)	20 (74)	13 (56)	
PD-L1 Expression Tumor				0.215
<1%	15 (30)	6 (22)	9 (39)	
1–49%	12 (24)	9 (33)	3 (13)	
≥50%	21 (42)	11 (41)	10 (43)	
unknown	2 (4)	1(4)	1(5)	
Histology				0.167
Squamous Cell	19 (38)	9 (34)	10 (43)	
Adeno	20 (40)	14 (51)	6 (27)	
NSCLC NOS	5 (10)	1 (4)	4 (17)	
Urothelial	3 (6)	2 (7)	1 (5)	
Others**	3 (6)	1 (4)	2 (8)	

al-RT, all-lesion radiotherapy; sl-RT, single-lesion radiotherapy; SD, standard deviation; HNSCC, Head and Neck squamous cell carcinoma; NSCLC, non-small cell lung carcinoma; CNS, central nervous system; PD-L1, programmed cell death ligand 1.

*others include one case of esophageal cancer, on case of sinonasal undifferentiated cancer and one mixed adenoneuroendocrine carcinoma.

**Others include one case of mixed-neuroendocrine carcinoma (MANEC), one case of undifferentiated carcinoma (SNUC) and one case of acinic-cell-carcinoma.

The median PFS was 9.2 months (95% CI, 5.8 - 12.6) in the al-RT group and also significantly longer than 3.0 months (CI 95%, 2.5–3.5, p<0.001) in the sl-RT group (**Figure 1B**). The median TTP was not reached in the al-RT group compared to 4.6 months (95% CI, 1.1–8.0, p=0.028) in the sl-RT group (**Figure 1C**).

As the al-RT group contained patients with only one metastasis, which is not possible in the sl-RT group, additional Kaplan-Meier analyses were performed. In the al-RT group both OS and PFS were similar in patients with one metastasis of more metastases in the ST-ICI cohort The same accounts for Kaplan_Meier analyses within the sl-RT group (**Supplementary Figure 1**).

A univariate cox regression analysis was performed to study potentially prognostic factors for OS (**Table 3**). Tumor entity NSCLC, adenocarcinoma histology, absence of brain metastases, immunotherapy drug and treatment group al-RT were associated with lower mortality risk with an effect p-value of ≤ 0.1. These factors were included in the multivariable analysis. Age, sex, PD-L1 and number of previous treatments were not associated at a p-level of ≤ 0.1. In the multivariable analysis only tumor entity (NSCLC compared to HNSCC, HR 1.19, 95% CI, 0.46 – 3.10, p=0.028; other compared to HNSCC, HR 7.25, 95% CI, 1.49–35.28, p=0.028) and al-RT (HR 0.32,

TABLE 2 | Treatment characteristics.

	No. (%) Patients			
Treatment	**Total (n = 50)**	**al-RT (n = 27)**	**sl-RT (n = 23)**	**p-value**
Fractionation of radiotherapy				0.023
Normofract.	25 (50)	16 (60)	9 (40)	
Hypofract.	22 (44)	10 (37)	12 (52)	
SRS	3 (6)	1 (3)	2 (8)	
Total Dose				
Mean (SD)	49.8 ± 17.1 Gy	55.3 ± 16.6 Gy	43.4 ± 15.7 Gy	0.004
Median (range)	48 Gy (16–72)	60 Gy (18–72)	40 Gy (16–72)	
No. of irradiated lesions				0.134
1	29 (58)	14 (51)	15 (65)	
2	15 (30)	9 (34)	6 (26)	
>3*	6 (12)	4 (15)	2 (9)	
Location of radiotherapy				<0.001
Lung	17 (34)	14 (51)	3 (13)	
CNS	10 (20)	1 (5)	9 (39)	
Bone	5 (10)	0	5 (21)	
Other	18 (36)	12 (44)	6 (27)	
Drug				0.038
Nivolumab	25 (50)	11 (40)	14 (60)	
Pembrolizumab	16 (32)	9 (33)	7 (30)	
Other	9 (28)	7 (27)	2 (10)	
Concomitant Chemotherapy				0.614
Yes	4 (8)	3 (10)	1 (5)	
No	46 (92)	24 (90)	22 (95)	
irAE				0.121
any grade	15 (30)	11 (40)	4 (18)	
Grade 1–2	13 (26)	10 (37)	3 (13)	
Grade 3	2 (4)	1 (3)	1 (4)	

al-RT, all-lesion radiotherapy; sl-RT, single-lesion radiotherapy; SD, standard deviation; CNS, central nervous system; irAE, immune-related adverse event.
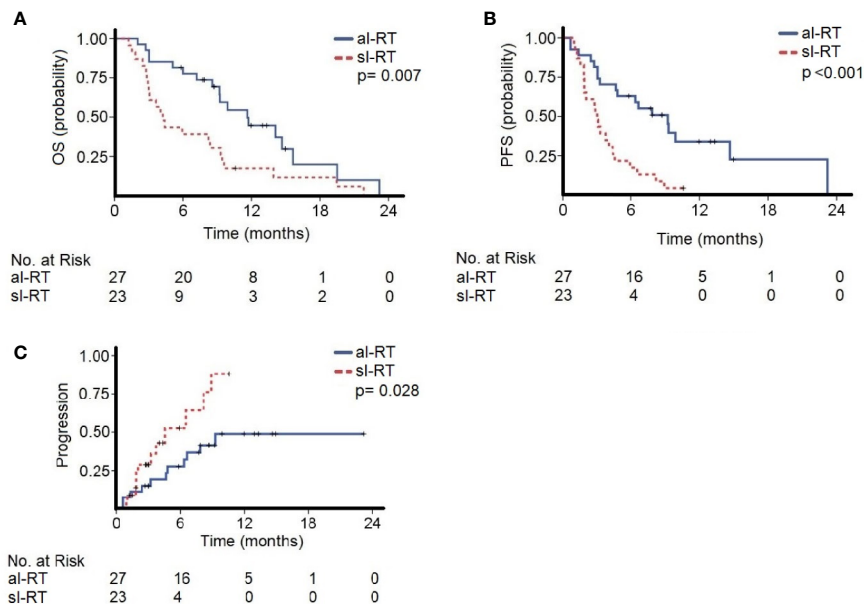*1 patient irradiated on a total of 8 cerebral lesions.

FIGURE 1 | The cohorts with all-lesion radiotherapy (al-RT) and single-lesion radiotherapy (sl-RT) are compared regarding **(A)** overall survival (OS), **(B)** progression-free survival (PFS) and **(C)** time to progression (TTP).

TABLE 3 | Univariate and multivariate Cox proportional hazard models to investigate the association between patient characteristics and overall survival.

Explanatory factors	(N = 50)	Univariate					Multivariate[#]		
		N	Death	HR	95% CI	p-value	HR	95% CI	p-value
Age*	≤60 years	16	11	1		0.748			
	>60 years	34	21	1.12	0.53–2.37				
Sex*	Male	29	21	1		0.833			
	Female	21	11	1.08	0.50–2.334				
Tumor entity	HNSCC	13	10	1		0.064	1		0.028
	NSCLC	31	17	0.42	0.18–0.97		1.19	0.46 - 3.10	
	other	6	5	1.13	0.38–3.31		7.25	1.49 - 35.28	
Histology	SC	19	14	1		0.011			
	Adeno	20	9	0.27	0.10–0.70				
	other	11	9	0.81	0.34–1.92				
PD-L1 tumor cells*	<1%	15	13	1		0.491			
	1–49%	12	6	0.67	0.24–1.82				
	≥50%	21	12	0.62	0.28–1.39				
Brain metastases	no	16	13	1		0.089			
	yes	34	19	1.89	0.92–3.89				
Number of previous treatments*	0–1	32	16	1		0.265			
	≥2	18	16	1.5	0.74–3.05				
Immunotherapy drug	Nivo	25	21	1		0.064			
	Pembro	16	8	0.49	0.22–1.14				
	other	9	3	0.32	0.09–1.09				
Lesions irradiated	al-RT	27	13	1		0.005	1		0.007
	sl-RT	23	19	0.36	0.17–0.74		0.32	0.14 - 0.75	

HR, hazard ratio; CI, confidence interval; HNSCC, head and neck squamous cell cancer; NSCLC, non-small cell lung cancer; SC, squamous cell; Nivo, nivolumab; Pembro, pembrolizumab; al-RT, all-lesion radiotherapy; sl-RT, single-lesion radiotherapy.
*Within the selection process, only explanatory factors with an effect p-value of < 0.1 in the univariate Cox regression analysis were considered (*).
[#]Final Cox regression model after backward selection. Only factors with p < 0.05 remained in the final model.

95% CI, 0.14 – 0.75, p = 0.007) remained prognostic factors for overall survival.

DISCUSSION

Local ablative treatments in an oligometastatic situation gained importance during the past years (1). Particularly in oligometastatic lung cancer the addition of local therapy of all tumor lesions in patients responding to systemic chemotherapy improved OS (3). Recent studies investigated especially the role of stereotactic radiotherapy as local ablative treatment method and found a clinical benefit (15). Furthermore, in a phase II trial a survival benefit for local consolidative radiotherapy of the primary tumor in metastatic NSCLC was also found (11). These studies justify the addition of local treatments to all lesions to classical chemotherapy in patients with oligometastatic cancer.

During the past years, immune checkpoint inhibitors suppressing the PD-1/PD-L1 pathway improved prognosis in different tumor entities significantly and became first line treatment in metastatic melanoma, NSCLC, HNSCC, renal and bladder cancer (4, 5, 16–18). In this new first line treatment setting, the efficacy of treatment to all known metastatic sites has not been studied so far.

In this regard, the ST-ICI study investigates the effects of radiotherapy in combination with PD-1/PD-L1 immune checkpoint inhibitors. The presented analysis shows that patients with oligo-metastatic disease treated with al-RT had superior OS, PFS and TTP compared to patients with sl-RT. This advocates a benefit of local therapy to all tumor lesions also in the era of immune checkpoint inhibitors. In general, the combination of radiotherapy and immunotherapy in the ST-ICI trial seems not increase the frequency or severity of irAEs as they were similar to reports on SCLC and HSNCC treated with anti-PD-1 monotherapy (4, 5). However, the frequency of irAE seems increased in the al-RT compared to the sl-RT cohort. Previous analyses of concomitant radiotherapy and immunotherapy indicated increased toxicity (19). The increased rate of irAE may be partially explained by immune modulating effects of radiotherapy resulting in the activation of tumor-surrounding immune cells (20).

Limitations of the study are based on the inevitable shortcomings due to the missing randomization. Thus, the results of the study need to be interpreted in view of the different tumor entities, number of metastases and minor differences in the PD-L1 status. These partially differing baseline characteristics may have influenced the results of this analysis. A major limitation is the differing number of metastases in both treatment groups. Due to this imbalance additional Kaplan-Meier analyses were performed. Both in the al-RT and sl-RT group the number of metastases did not influence PFS or OS. Regarding radiotherapy treatment the location, dose and fractionation of the two groups differed. Especially the more frequent irradiation of brain metastases in the sl-RT group and lung metastases in the al-RT group may be a bias for survival. However, al-RT was the most important predictor of OS in the multivariate model, which consolidates the findings of this trial.

Especially brain metastases remained no prognostic parameter in the multivariate model. The main advantage of the ST-ICI trial is its prospective design compared to existing analyses.

Prospective data about the combination of radiotherapy and immunotherapy in oligometastatic situations are limited. In a recent single-arm phase two trial patients with oligometastatic NSCLC (up to four metastases) were treated with local ablative treatment (radiotherapy or surgery) followed by pembrolizumab. There was no limitation regarding PD-L1 status. This strategy achieved an impressive median PFS of 19.1 months (21). One analysis studied treatment continuation with pembrolizumab beyond progression in NSCLC patients with PDL1>50% with the addition of local therapy in nine of 18 patients and found a one-year OS of 71% (22).

Besides these clinical findings, there is a strong biological rationale to combine radiotherapy with immune checkpoint inhibitors. Radiotherapy not only kills tumor cells, but also has different immune-modulating effects (7). Locally induced immune-modulating effects of radiotherapy can also enhance tumor directed systemic immune response distant from the irradiated area (10). Mechanisms behind these effects are increase in T-cell infiltration in locally treated tumors and further enhanced T-cell responses out of field (23). These systemic immune responses to local radiotherapy, also called "abscopal effects", have been observed in patients with combined radiotherapy and immune checkpoint inhibitors in numerous case reports (24). Additional retrospective analyses indicated the presence of abscopal effects in up to 25% of melanoma patients treated with PD-1 inhibitors and radiotherapy (25). However, in a prospective single arm trial the combination of Nivolumab with stereotactic body radiation therapy of a single tumor lesion did not increase the response rate in melanoma patients compared to historical controls (26). A trial in metastatic head and neck cancer that combined nivolumab with single lesion stereotactic radiotherapy did also not increase the response rate in non-irradiated lesions (27). The only partially promising prospective trial was in metastatic NSCLC. In this trial stereotactic radiotherapy increased the response rate in non-irradiated lesions from 18% to 36%, whereas this did not reach statistical significance (28). In contrast to these trials, our trial compared the efficacy of single lesion radiotherapy in patients with multiple metastases to radiotherapy of all tumor lesions. Furthermore, we used fractionated radiotherapy compared to stereotactic ablative approaches in the other trials. In our study radiotherapy of all tumor lesions significantly prolonged overall survival. Recently, also a correlation of tumor burden and reduced immune competence was demonstrated (29). Therefore, a maximal reduction of tumor load appears to be beneficial for the effect of immunotherapy. Our findings are in line with another prospective single-arm trial in metastatic NSCLC of stereotactic radiotherapy to all tumor lesions followed by Pembrolizumab maintenance therapy that achieved a median overall survival of 41.6 months (21). The results of these first prospective trials on abscopal effects should induce a discussion on more elaborate treatment concepts (30). In this discussion, our finding of a superiority of radiotherapy to all lesions compared to a single lesion should be addressed. Furthermore, the fractionation of radiotherapy with either conventionally fractionated low doses or high ablative doses has to be discussed. In addition, the treatment sequence of concomitant versus sequential administration of PD-1 inhibitors should be further investigated. And finally, also a biomarker-based patient selection should be an essential point in future trials on combined radio-immunotherapy.

DATA AVAILABILITY STATEMENT

The raw data supporting the conclusions of this article will be made available by the authors on reasonable request, without undue reservation.

ETHICS STATEMENT

The studies involving human participants were reviewed and approved by the ethics committee of Friedrich-Alexander University Erlangen Nürnberg (number: 2_17 B). The patients/participants provided their written informed consent to participate in this study.

AUTHOR CONTRIBUTIONS

ACKNOWLEDGMENTS

SUPPLEMENTARY MATERIAL

The Supplementary Material for this article can be found online at: https://www.frontiersin.org/articles/10.3389/fonc.2020.576643/full#supplementary-material

SUPPLEMENTARY FIGURE 1 | The numbers of metastases of the cohorts all-lesion radiotherapy (al-RT) are compared regarding (A) overall survival (OS) and (B) progression-free survival (PFS). Patients of the single-lesion radiotherapy cohort (sl-RT) were compared concerning (C) overall-survival (OS) and (D) progression-free-survival (PFS).

REFERENCES

1. Guckenberger M, Lievens Y, Bouma AB, Collette L, Dekker A, deSouza NM, et al. Characterisation and classification of oligometastatic disease: a European Society for Radiotherapy and Oncology and European Organisation for Research and Treatment of Cancer consensus recommendation. *Lancet Oncol* (2020) 21(1):e18–28. doi: 10.1016/S1470-2045(19)30718-1

2. Kroeze SGC, Fritz C, Basler L, Gkika E, Brunner TB, Grosu AL, et al. Combination of stereotactic radiotherapy and targeted therapy: patterns-of-care survey in German-speaking countries. *Strahlenther Onkol* (2019) 195(3):199–206. doi: 10.1007/s00066-018-01422-5

3. Gomez DR, Tang C, Zhang J, Blumenschein GRJr., Hernandez M, Lee JJ, et al. Local Consolidative Therapy Vs. Maintenance Therapy or Observation for Patients With Oligometastatic Non-Small-Cell Lung Cancer: Long-Term Results of a Multi-Institutional, Phase II, Randomized Study. *J Clin Oncol* (2019) 37(18):1558–65. doi: 10.1200/JCO.19.00201

4. Burtness B, Harrington KJ, Greil R, Soulieres D, Tahara M, de Castro G Jr., et al. Pembrolizumab alone or with chemotherapy versus cetuximab with chemotherapy for recurrent or metastatic squamous cell carcinoma of the head and neck (KEYNOTE-048): a randomised, open-label, phase 3 study. *Lancet* (2019) 394(10212):1915–28. doi: 10.1016/S0140-6736(19)32591-7

5. Reck M, Rodriguez-Abreu D, Robinson AG, Hui R, Csoszi T, Fulop A, et al. Updated Analysis of KEYNOTE-024: Pembrolizumab Versus Platinum-Based Chemotherapy for Advanced Non-Small-Cell Lung Cancer With PD-L1 Tumor Proportion Score of 50% or Greater. *J Clin Oncol* (2019) 37(7):537–46. doi: 10.1200/JCO.18.00149

6. Weichselbaum RR, Hellman S. Oligometastases revisited. *Nat Rev Clin Oncol* (2011) 8(6):378–82. doi: 10.1038/nrclinonc.2011.44

7. Derer A, Frey B, Fietkau R, Gaipl US. Immune-modulating properties of ionizing radiation: rationale for the treatment of cancer by combination radiotherapy and immune checkpoint inhibitors. *Cancer Immunol Immunother* (2016) 65(7):779–86. doi: 10.1007/s00262-015-1771-8

8. Hecht M, Buttner-Herold M, Erlenbach-Wunsch K, Haderlein M, Croner R, Grutzmann R, et al. PD-L1 is upregulated by radiochemotherapy in rectal adenocarcinoma patients and associated with a favourable prognosis. *Eur J Cancer* (2016) 65:52–60. doi: 10.1016/j.ejca.2016.06.015

9. Ruckert M, Deloch L, Fietkau R, Frey B, Hecht M, Gaipl US. Immune modulatory effects of radiotherapy as basis for well-reasoned radioimmunotherapies. *Strahlenther Onkol* (2018) 194(6):509–19. doi: 10.1007/s00066-018-1287-1

10. Dovedi SJ, Adlard AL, Lipowska-Bhalla G, McKenna C, Jones S, Cheadle EJ, et al. Acquired resistance to fractionated radiotherapy can be overcome by concurrent PD-L1 blockade. *Cancer Res* (2014) 74(19):5458–68. doi: 10.1158/0008-5472.CAN-14-1258

11. Iyengar P, Wardak Z, Gerber DE, Tumati V, Ahn C, Hughes RS, et al. Consolidative Radiotherapy for Limited Metastatic Non-Small-Cell Lung Cancer: A Phase 2 Randomized Clinical Trial. *JAMA Oncol* (2018) 4(1):e173501. doi: 10.1001/jamaoncol.2017.3501

12. Ahmed KA, Stallworth DG, Kim Y, Johnstone PA, Harrison LB, Caudell JJ, et al. Clinical outcomes of melanoma brain metastases treated with stereotactic radiation and anti-PD-1 therapy. *Ann Oncol* (2016) 27(3):434–41. doi: 10.1093/annonc/mdv622

13. Knisely JP, Yu JB, Flanigan J, Sznol M, Kluger HM, Chiang VL. Radiosurgery for melanoma brain metastases in the ipilimumab era and the possibility of longer survival. *J Neurosurg* (2012) 117(2):227–33. doi: 10.3171/2012.5.JNS111929

14. Shaverdian N, Lisberg AE, Bornazyan K, Veruttipong D, Goldman JW, Formenti SC, et al. Previous radiotherapy and the clinical activity and toxicity of pembrolizumab in the treatment of non-small-cell lung cancer: a secondary analysis of the KEYNOTE-001 phase 1 trial. *Lancet Oncol* (2017) 18(7):895–903. doi: 10.1016/S1470-2045(17)30380-7

15. Palma DA, Olson R, Harrow S, Gaede S, Louie AV, Haasbeek C, et al. Stereotactic ablative radiotherapy versus standard of care palliative treatment in patients with oligometastatic cancers (SABR-COMET): a randomised, phase 2, open-label trial. *Lancet* (2019) 393(10185):2051–8. doi: 10.1016/S0140-6736(18)32487-5

16. Cohen EEW, Soulieres D, Le Tourneau C, Dinis J, Licitra L, Ahn MJ, et al. Pembrolizumab versus methotrexate, docetaxel, or cetuximab for recurrent or metastatic head-and-neck squamous cell carcinoma (KEYNOTE-040): a randomised, open-label, phase 3 study. *Lancet* (2019) 393(10167):156–67. doi: 10.1016/S0140-6736(18)31999-8

17. Balar AV, Galsky MD, Rosenberg JE, Powles T, Petrylak DP, Bellmunt J, et al. Atezolizumab as first-line treatment in cisplatin-ineligible patients with locally advanced and metastatic urothelial carcinoma: a single-arm, multicentre, phase 2 trial. *Lancet* (2017) 389(10064):67–76. doi: 10.1016/S0140-6736(16)32455-2

18. Motzer RJ, Tannir NM, McDermott DF, Aren Frontera O, Melichar B, Choueiri TK, et al. Nivolumab plus Ipilimumab versus Sunitinib in Advanced Renal-Cell Carcinoma. *N Engl J Med* (2018) 378(14):1277–90. doi: 10.1056/NEJMoa1712126

19. Louvel G, Bahleda R, Ammari S, Le Pechoux C, Levy A, Massard C, et al. Immunotherapy and pulmonary toxicities: can concomitant immune-checkpoint inhibitors with radiotherapy increase the risk of radiation pneumonitis? *Eur Respir J* (2018) 51(1):1701737. doi: 10.1183/13993003.01737-2017

20. Gordon SR, Maute RL, Dulken BW, Hutter G, George BM, McCracken MN, et al. PD-1 expression by tumour-associated macrophages inhibits phagocytosis and tumour immunity. *Nature* (2017) 545(7655):495–9. doi: 10.1038/nature22396

21. Bauml JM, Mick R, Ciunci C, Aggarwal C, Davis C, Evans T, et al. Pembrolizumab After Completion of Locally Ablative Therapy for Oligometastatic Non-Small Cell Lung Cancer: A Phase 2 Trial. *JAMA Oncol* (2019) 5(9):1283–90. doi: 10.1001/jamaoncol.2019.1449

22. Metro G, Addeo A, Signorelli D, Gili A, Economopoulou P, Roila F, et al. Outcomes from salvage chemotherapy or pembrolizumab beyond progression with or without local ablative therapies for advanced non-small cell lung cancers with PD-L1 >/=50% who progress on first-line immunotherapy: real-world data from a European cohort. *J Thorac Dis* (2019) 11(12):4972–81. doi: 10.21037/jtd.2019.12.23

23. Dovedi SJ, Cheadle EJ, Popple AL, Poon E, Morrow M, Stewart R, et al. Fractionated Radiation Therapy Stimulates Antitumor Immunity Mediated by Both Resident and Infiltrating Polyclonal T-cell Populations when Combined with PD-1 Blockade. *Clin Cancer Res* (2017) 23(18):5514–26. doi: 10.1158/1078-0432.CCR-16-1673

24. Dagoglu N, Karaman S, Caglar HB, Oral EN. Abscopal Effect of Radiotherapy in the Immunotherapy Era: Systematic Review of Reported Cases. *Cureus* (2019) 11(2):e4103. doi: 10.7759/cureus.4103

25. Ribeiro Gomes J, Schmerling RA, Haddad CK, Racy DJ, Ferrigno R, Gil E, et al. Analysis of the Abscopal Effect With Anti-PD1 Therapy in Patients With Metastatic Solid Tumors. *J Immunother* (2016) 39(9):367–72. doi: 10.1097/CJI.0000000000000141

26. Sundahl N, Seremet T, Van Dorpe J, Neyns B, Ferdinande L, Meireson A, et al. Phase 2 Trial of Nivolumab Combined With Stereotactic Body Radiation Therapy in Patients With Metastatic or Locally Advanced Inoperable Melanoma. *Int J Radiat Oncol Biol Phys* (2019) 104(4):828–35. doi: 10.1016/j.ijrobp.2019.03.041

27. McBride S, Sherman E, Tsai CJ, Baxi S, Aghalar J, Eng J, et al. Randomized Phase II Trial of Nivolumab With Stereotactic Body Radiotherapy Versus Nivolumab Alone in Metastatic Head and Neck Squamous Cell Carcinoma. *J Clin Oncol* (2020) JCO2000290. doi: 10.1200/JCO.20.00290

28. Theelen W, Peulen HMU, Lalezari F, van der Noort V, de Vries JF, Aerts J, et al. Effect of Pembrolizumab After Stereotactic Body Radiotherapy vs Pembrolizumab Alone on Tumor Response in Patients With Advanced Non-Small Cell Lung Cancer: Results of the PEMBRO-RT Phase 2 Randomized Clinical Trial. *JAMA Oncol* (2019) 5(9):1276–82. doi: 10.1001/jamaoncol.2019.1478

29. Huang AC, Postow MA, Orlowski RJ, Mick R, Bengsch B, Manne S, et al. T-cell invigoration to tumour burden ratio associated with anti-PD-1 response. *Nature* (2017) 545(7652):60–5. doi: 10.1038/nature22079

30. Seiwert TY, Kiess AP. Time to Debunk an Urban Myth? The "Abscopal Effect" With Radiation and Anti-PD-1. *J Clin Oncol* (2020) JCO2002046. doi: 10.1200/JCO.20.02046

Augmenting Anticancer Immunity Through Combined Targeting of Angiogenic and PD-1/PD-L1 Pathways: Challenges and Opportunities

Stephen P. Hack[1]*, Andrew X. Zhu[2,3] and Yulei Wang[1]

[1] Product Development (Oncology), Genentech, Inc., South San Francisco, CA, United States, [2] Massachusetts General Hospital Cancer Center and Harvard Medical School, Boston, MA, United States, [3] Jiahui International Cancer Center, Jiahui Health, Shanghai, China

Cancer immunotherapy (CIT) with antibodies targeting the programmed cell death 1 protein (PD-1)/programmed cell death 1 ligand 1 (PD-L1) axis have changed the standard of care in multiple cancers. However, durable antitumor responses have been observed in only a minority of patients, indicating the presence of other inhibitory mechanisms that act to restrain anticancer immunity. Therefore, new therapeutic strategies targeted against other immune suppressive mechanisms are needed to enhance anticancer immunity and maximize the clinical benefit of CIT in patients who are resistant to immune checkpoint inhibition. Preclinical and clinical studies have identified abnormalities in the tumor microenvironment (TME) that can negatively impact the efficacy of PD-1/PD-L1 blockade. Angiogenic factors such as vascular endothelial growth factor (VEGF) drive immunosuppression in the TME by inducing vascular abnormalities, suppressing antigen presentation and immune effector cells, or augmenting the immune suppressive activity of regulatory T cells, myeloid-derived suppressor cells, and tumor-associated macrophages. In turn, immunosuppressive cells can drive angiogenesis, thereby creating a vicious cycle of suppressed antitumor immunity. VEGF-mediated immune suppression in the TME and its negative impact on the efficacy of CIT provide a therapeutic rationale to combine PD-1/PD-L1 antibodies with anti-VEGF drugs in order to normalize the TME. A multitude of clinical trials have been initiated to evaluate combinations of a PD-1/PD-L1 antibody with an anti-VEGF in a variety of cancers. Recently, the positive results from five Phase III studies in non-small cell lung cancer (adenocarcinoma), renal cell carcinoma, and hepatocellular carcinoma have shown that combinations of PD-1/PD-L1 antibodies and anti-VEGF agents significantly improved clinical outcomes compared with respective standards of care. Such combinations have been approved by health authorities and are now standard treatment options for renal cell carcinoma, non-small cell lung cancer, and hepatocellular carcinoma. A plethora of other randomized studies of similar combinations are currently ongoing. Here, we discuss the principle mechanisms of VEGF-mediated immunosuppression studied in preclinical models or as part of translational clinical

studies. We also discuss data from recently reported randomized clinical trials. Finally, we discuss how these concepts and approaches can be further incorporated into clinical practice to improve immunotherapy outcomes for patients with cancer.

INTRODUCTION

Over the past decade, cancer immunotherapy (CIT) has dramatically changed the treatment landscape of cancer. This major therapeutic advance was made possible in large part by pioneering preclinical and clinical research focused on immune modulation using antibodies that block immune regulatory checkpoints (1–5).

Immune checkpoints such as cytotoxic T-lymphocyte-associated protein 4 (CTLA-4), programed cell death protein 1 (PD-1), and programed cell death 1 ligand 1 (PD-L1) act to negatively regulate T-cell–mediated immune responses that play a critical role in allowing cancer cells to evade the immune destruction. Immune checkpoint inhibitors (ICIs) are monoclonal antibodies directed against either the PD-1/PD-L1 axis or CTLA-4. ICIs attenuate inhibitory T-cell activation signals, thereby permitting tumor-reactive T cells to overcome regulatory mechanisms in order to mount an effective antitumor response (6). At the time of writing, a total of 10 PD-1/PD-L1 monoclonal antibodies are approved by regulatory authorities either as monotherapy or in combination across different lines of treatment for 19 different types of cancer, including a tissue-agnostic indication (**Supplemental Table 1**). As of September 2019, approximately 3,000 trials involving drugs targeting the PD-1/PD-L1 axis are ongoing across a range of tumors types, with 76% of them evaluating combination regimens (7). Given this rapid pace of clinical development, it is anticipated that more PD-1/PD-L1–based treatments will change the standard of care in many more cancer types.

A hallmark of drugs that inhibit the PD-1/PD-L1 axis is the induction of deep and durable antitumor responses that can translate into a survival benefit in patients with a variety of tumor histologies. Anti–PD-1 treatment has resulted in marked improvements in 5-year survival for patients with advanced melanoma, lung cancer, and renal cancer over previous standards of care (8). However, long-term responses are restricted to a minority of patients and an estimated 87% of patients' cancers for which PD-1/PD-L1 are indicated will fail to respond (9). Most patients experiencing resistance to PD-1/PD-L1 inhibition either never respond to treatment (primary resistance) or relapse after a period of response (acquired resistance). Furthermore, some tumor types such as pancreatic, microsatellite stable (MSS) colorectal, biliary tract, and prostate cancers appear intrinsically resistant to PD-1/PD-L1 axis blockade (10). A major reason accounting for both primary or acquired resistance is the ability of tumors to exploit alternate immune-suppressive mechanisms, thereby circumventing checkpoint blockade (11). Collectively, the tumor microenvironment (TME), tumor immunogenicity, antigen presentation, as well as oncologic signal transduction pathways all play important roles in response and resistance to immune checkpoint blockade (10).

As the molecular mechanisms underlying resistance to ICI are unearthed, actionable therapeutic strategies to prevent or abrogate them are being developed to improve clinical outcomes for patients. Tumor mutation burden (TMB)—which reflects the abundance of immunogenic neoantigens that are identified as foreign by cytotoxic T cells—and expression of inhibitory immune checkpoints such as PD-L1 have been widely studied as biomarkers of response to checkpoint inhibitors (CPIs). However, neither of these markers can fully explain the lack of response to checkpoint blockade observed in the majority of patients (10, 12–16). It is therefore likely that other immunosuppressive mechanisms act to restrain anticancer immunity. Abnormalities within the TME are strongly associated with repressed anticancer immunity, which profoundly impacts the effectiveness of immunotherapy (11, 17–19). Thus, therapeutic reprogramming of specific immune components of the TME with combination treatments, such as immunosuppressive cell types, may overcome TME-induced resistance to checkpoint blockade, thereby enhancing or reinvigorating anticancer immunity (17, 20). ICIs in combination with treatment modalities such as chemotherapy, targeted agents and CTLA-4 antibodies have been successfully developed and further studies are ongoing to evaluate other combination approaches including radiation and immune modulators [recently reviewed by Murciano-Goroff et al. (21)]. Each of these combination partners is thought to modulate anticancer immunity *via* direct and indirect mechanisms (21,

Abbreviations: 5-FU, fluorouracil; ABCP, atezolizumab plus bevacizumab plus carboplatin plus paclitaxel; ALK, ALK receptor tyrosine kinase; BCP, bevacizumab plus carboplatin plus paclitaxel; CIC, cancer-immunity cycle; CIT, cancer immunotherapy; CPI, checkpoint inhibitors; CTLA-4, cytotoxic T-lymphocyte-associated protein 4; DCs, dendritic cells; dMMR, deficient DNA mismatch repair pathways; EGFR, epidermal growth factor receptor; EOC, epithelial ovarian cancer; FDA, US Food and Drug Administration; FOLFOX, leucovorin calcium, fluorouracil, and oxaliplatin; HCC, hepatocellular carcinoma; ICIs, immune checkpoint inhibitors; IFN, interferon; ITT, intention-to-treat; mCRC, metastatic colorectal cancer; MDSCs, myeloid-derived suppressor cells; MEK, mitogen-activated protein kinase kinase; MHC, major histocompatibility complex; MSI-H, high microsatellite instability; MSS, microsatellite stable; NSCLC, non-small cell lung cancer; ORR, objective response rate; OS, overall survival; PD-1, programed cell death protein 1; PD-L1, programed cell death ligand 1; PFS, progression-free survival; pMMR, proficient DNA mismatch repair pathways; RCC, renal cell carcinoma; TAMs, tumor-associated macrophages; TILs, tumor-infiltrating lymphocytes; TKI, tyrosine kinase inhibitor; TME, tumor microenvironment; Treg, regulatory T cells; VEGF, vascular endothelial growth factor; VEGFR, vascular endothelial growth factor receptor.

22). PD-1 inhibitors along with anti-CTLA-4 antibodies have received FDA approvals for a range of cancers and trials involving other inhibitory checkpoints, such as LAG-3 and TIM-3 are ongoing (23–25). Conventional cytotoxic chemotherapies promote anticancer immunity through the release of tumor-associated antigens and/or depletion of immunosuppressive cells (26, 27). Chemotherapy regimens in tandem with ICIs have been extensively studied and have become treatment options for NSCLC, triple-negative breast cancer and urothelial carcinoma (28–31). Similar to chemotherapy, radiation treatment can augment the anticancer immune response through the release of tumor antigens and modulation of the TME (21, 32). Studies of ICIs with radiation are ongoing in a variety of cancers (21, 33). ICIs combined agents targeting components of the MAP-kinase pathway have also been evaluated (21, 34–36). Within the TME, vascular endothelial growth factor (VEGF)–driven angiogenesis is a key driver of tumor-associated immunosuppression. VEGF-mediated immunosuppression has been extensively studied in a variety of preclinical and clinical studies, which collectively have highlighted the mechanisms underpinning combined immune checkpoint blockade and VEGF inhibition in patients with cancer.

In this comprehensive review, we focus on the mechanisms underpinning VEGF-mediated immunosuppression and how these can be therapeutically abrogated by combined VEGF and PD-(L)1 blockade in patients with cancer to augment antitumor immunity. These mechanistic concepts and clinical approaches are very relevant and timely given that combinations of PD-(L)1 inhibitors and antiangiogenic agents are either currently approved or are close to approval for the treatment of a variety of malignancies. We also highlight the opportunities and challenges associated with dual targeting of VEGF and PD-(L)1 pathways.

INTERSECTION BETWEEN ANTICANCER IMMUNITY AND ANGIOGENESIS

Angiogenesis and immune evasion are interdependent processes that often occur in parallel and are considered hallmarks of cancer (37, 38). Both are physiological mechanisms that can be hijacked in cancer, facilitating tumor development and progression (38) (**Figure 1**).

The Cancer-Immunity Cycle

Cancer immunity was characterized by Chen and Mellman as a seven-step, self-propagating, cyclical, multistep process, referred to as the cancer-immunity cycle (CIC) (39). In order for effective antitumor immunity to occur, a series of stepwise events that enable T-cell–mediated tumor cell killing is necessary. The seven steps of the CIC can be grouped into 3 distinct phases (40):

1. Recruitment and activation of immune effector cells (steps 1–3);
2. Trafficking and infiltration of T cells into tumors (steps 4 and 5);
3. Recognition and killing of cancer cells (steps 6 and 7).

In steps 1 through 3 of the CIC, tumor antigens (including neoantigens) liberated from tumor cells are taken up and processed by dendritic cells (DCs) and are then presented to T

cells that results in the priming and activation of T-cells. In step 4, activated effector T cells enter the circulation, are trafficked to the tumor and then infiltrate the tumor bed (step 5), where they attach to and destroy cancer cells (steps 6 and 7). The killing of malignant cells leads to the additional release of tumor-derived antigens and the restarting of the CIC. Tumors are able to co-opt mechanisms to evade immune surveillance by obstructing one or more steps in the CIC, thus rendering tumors safe from immune destruction.

Knowledge of the mechanisms underpinning anticancer immunity has led to the development of classification systems characterizing the TME that help identify patients who are more likely to respond to immunotherapy and also serves as a framework to inform rational combination treatments (12, 41, 42). Current classifications are primarily defined according to the composition of the immune infiltrate and the character of the inflammatory response (43). Histologically, tumors can be broadly categorized as either inflamed ("hot") or noninflamed ("cold") (42). Most data support the idea that patients with hot or inflamed tumors, which harbor markers of preexisting functional antitumor T-cell immunity [e.g., interferon (IFN)-γ signaling, high PD-L1 expression, high prevalence of tumor-infiltrating lymphocytes (TILs), or genomic instability], tend to respond relatively well to PD-1/PD-L1 inhibition (12, 41, 42). Other tumor immune phenotypes with deficits in antitumoral immunity such as those with immune-excluded (immune cells present only in the periphery) and immune-desert (with limited or no infiltration of immune cells in to the tumor)—are not as likely to respond to CPIs, suggesting the existence of other vital immune-suppressive mechanisms in either the tumor or the TME (12, 42). The immune phenotypes described above can be present to varying degrees within a given tumor type and among different cancers (12).

VEGF Immunomodulation

Angiogenesis, defined as new blood vessel formation from the preexisting vasculature, is a complex, multistep process that under physiological conditions is tightly regulated by a plethora of proangiogenic and antiangiogenic factors (44). However, in malignant settings, proliferating tumors tend to activate angiogenesis by shifting the balance of proangiogenic and antiangiogenic mediators toward a proangiogenic outcome (referred to as the "angiogenic switch").

Of all the molecules known to regulate angiogenesis, VEGF and its receptors (VEGFRs) have received the most attention due to VEGF's key role in regulating physiological and pathological angiogenesis (45). VEGF belongs to a family of growth factors that includes VEGFs A to D and placental growth factor. VEGF (VEGF-A) binds to both R1 and R2 VEGFR subtypes as well as the neuropilin 1 receptors (46) (**Figure 1**). The binding of VEGF to VEGFR2 is the primary signaling event in blood endothelial cells triggering angiogenesis (46). VEGF binding to VEGFR initiates various intracellular signaling pathways that regulate processes such as vascular permeability and endothelial cell survival, migration, and proliferation (47). The role played by VEGFR1 is unclear. VEGFR1 binds VEGF-A with a higher affinity than VEGFR2 (approximately 10 times) but possesses
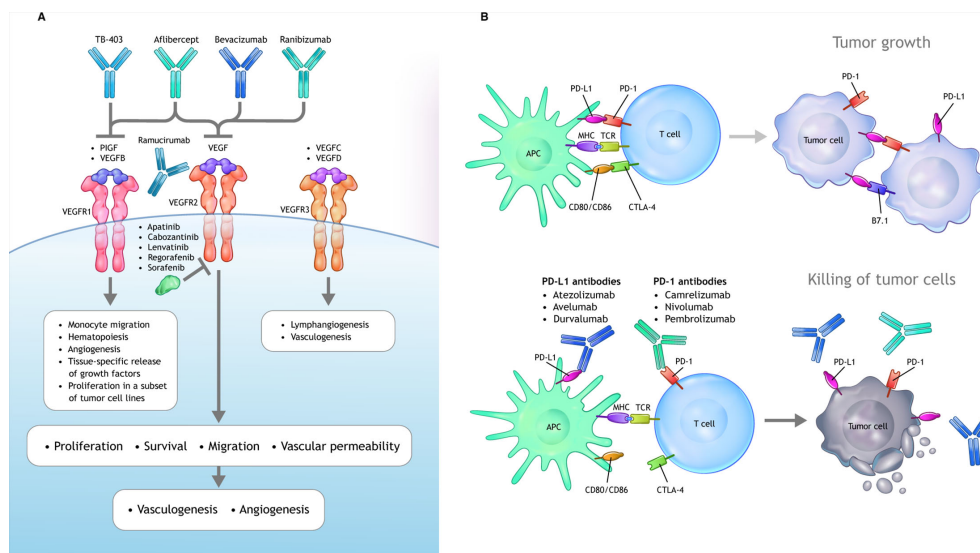
FIGURE 1 | VEGF and PD-1/PD-L1 signaling axes. **(A)** VEGF ligands include VEGF-A, VEGF-B, VEGF-C, VEGF-D, and PlGF, which interact with a combination of various VEGFRs. Canonical VEGF signaling through VEGF-R1/R2 (with R2 being the dominant signaling receptor) regulates the activities of several kinases and ultimately guides cell proliferation, migration, survival, and vascular permeability during vasculogenesis and angiogenesis. Multiple inhibitors block VEGFA-induced signaling. Bevacizumab and ranibizumab bind VEGFA. The soluble chimeric receptor aflibercept binds VEGFA, PlGF, and VEGFB. The VEGFR2-specific monoclonal antibody ramucirumab prevents VEGFR2-dependent signaling. Numerous small molecule TKIs block VEGFR signaling. **(B)** Activated T cells express PD-1, which engages with its specific ligand (PD-L1 or PD-L2) to dampen activation. PD-1 axis blockade through the administration of an anti–PD-1 or anti–PD-L1 antibody prevents this inhibitory interaction and unleashes antitumoral T lymphocyte activity by promoting increased T-cell activation and proliferation, by enhancing their effector functions. APC, antigen-presenting cells; CTL, cytotoxic T lymphocytes; DC, dendritic cell; iDCs, immature dendritic cells; IL, interleukin; iMC, immature myeloid cells; M1, classical macrophages; M2, alternative macrophages; matDCs, mature dendritic cells; MDSC, myeloid-derived suppressor cell; PD-1, programmed cell death 1 protein; PD-L1, programed cell death ligand 1; PlGF, placental growth factor; TAM, tumor associated macrophages; TFG-β, transforming growth factor β; TKI, tyrosine kinase inhibitor; Treg, tumor-associated macrophages; VEGF, vascular endothelial growth factor; VEGFR, vascular endothelial growth factor receptor.

weak kinase activity; it is hypothesized that VEGFR1 may act to sequester VEGF-A away from VEGFR2 (48).

Antiangiogenic drugs can be classified according to three mechanisms of action: monoclonal antibodies that bind and deplete the VEGF ligand, monoclonal antibodies that bind to the VEGFR, and tyrosine kinase inhibitors (TKIs) that block the intracellular domain of the VEGFR. The role of VEGF in oncogenesis and signaling mechanisms and the development of anti-VEGF therapeutics have been reviewed in detail elsewhere (47, 49). A summary of US Food and Drug Administration (FDA)-approved anti-VEGF agents and their indications is provided in **Supplemental Table 2**.

In addition to vascular regulation, emerging and evolving data have implicated VEGF as an important mediator of immunosuppression within the TME (13). VEGF is able to drive a range of immunosuppressive mechanisms impacting the ability to mount an effective anticancer immune response (38, 39) (**Figure 2**).

Overproduction of VEGF in the TME can drive suppress antitumor immunity either directly or indirectly *via* four principle mechanisms (13, 38, 50):

1. Inhibition of DC maturation and antigen presentation;
2. Inhibition of cytotoxic T-cell proliferation, trafficking, and infiltration;
3. Promotion of an aberrant tumor vasculature;

4. Recruitment and proliferation of immunosuppressive cell types, e.g., MDSCs, regulatory T cells (Tregs), and pro-tumor M2-like tumor-associated macrophages.

Here, we describe the mechanistic interplay between VEGF and the CIC (51). Key preclinical studies are summarized in **Table 1**.

Dendritic Cell Maturation (CIC Steps 1, 2, and 3)
Steps 1 through 3 of the CIC refer to the activation and recruitment of immune cells (39, 40). Step 1 encompasses the release and capture of tumor neoantigens by DCs. DCs are antigen-presenting cells that play a critical role in T-cell priming and the activation of anticancer T cells (steps 2 and 3 of the CIC).

T-cell priming and activation of cytotoxic T cells is reliant upon the ability of mature DCs to capture and present tumor antigens to T cells in the lymph nodes (39, 60). However, tumor-associated DCs exist in an immature state and are often unable to properly contribute to initiating a functional anticancer immune response. The ability to inhibit DC maturation, which can result in deficient tumor-antigen presentation and thus in potential immune evasion by tumors, was one of the first-described immunosuppressive functions of VEGF (61). Mature DCs are characterized by increased expression of MHC I and II and other costimulatory molecules on the cell surface that are required for

FIGURE 2 | Mechanisms of VEGF-mediated immunosuppression in the TME. Beyond its ability to mediate immune suppression *via* an abnormal tumor vasculature, increased VEGF levels can lead to immune suppression *via* inhibition of DC maturation, reduction of T-cell tumor infiltration, and promotion of inhibitory cell types in the TME. APC, antigen-presenting cells; CTLA, cytotoxic T lymphocyte associated; DC, dendritic cell; MHC, major histocompatibility complex; PD-1, programmed cell death 1 protein; PD-L1, programed cell death ligand 1; PlGF, placental growth factor; TME, tumor microenvironment; TCR, T-cell receptor; VEGF, vascular endothelial growth factor; VEGFR, vascular endothelial growth factor receptor.

T-cell activation, all of which are under the regulation of the nuclear factor-κB pathway (51). However, in cancers harboring elevated VEGF levels, DC maturation can be impeded through nuclear factor-κB pathway inhibition as a result of VEGF-VEGFR1 binding on DCs. This lack of DC maturation can prevent the upregulation of MHC and other molecules, ultimately resulting in impaired T-cell activation. VEGF, acting through VEGFR2, has also been shown to inhibit the ability of mature DCs to stimulate T cells (62). VEGFR1 and VEGFRs may have differential roles in regulating DC differentiation where VEGFR1 is the principle mediator of VEGF-induced inhibition of DC maturation (63). Neuropilin 1 has also been implicated in VEGF-mediated inhibition of DC maturation (64). Furthermore, by upregulating PD-L1 on DCs, VEGF can further suppress DC function, resulting in suppressed T-cell function and/or expansion (65). High levels of VEGF expression in human cancers have been linked with defective DC function and a reduction in mature DCs, especially in advanced-stage tumors (38, 50).

Data from *in vitro* studies show that VEGF was able to inhibit the differentiation of monocytes into DCs which could be restored with treatment with bevacizumab or sorafenib, a multi–tyrosine kinase VEGFR2 inhibitor (66). Relatedly, bevacizumab treatment has been shown to increase the

number of mature DCs in peripheral blood of cancer patients (67).

A recent study reported that DCs are regulated by PD-L1, and through blocking PD-L1, T-cell priming was augmented by the activation of the PD-L1/B7.1 signaling axis (68). In the same study, patients with either renal cell carcinoma (RCC) or non-small cell lung cancer (NSCLC) harboring a high DC signature before treatment were more prone to respond to PD-L1 inhibition with atezolizumab.

In summary, studies show that DCs are regulated by both the PD-L1 and VEGF signaling axes. Multiple studies demonstrate that VEGF can drive immunosuppression partly through inhibition of DC maturation and can facilitate immune evasion as a result of attenuated T-cell activation and priming which. Taken together, these findings suggest that combined inhibition of PD-1/PD-L1 and VEGF could result in enhanced activation and recruitment of T cells *via* regulation of DC function and maturation.

T-Cell Proliferation, Trafficking, and Infiltration (CIC Steps 4 and 5)

The trafficking of primed and activated T cells from the lymph node to the tumor bed are highlighted in Steps 4 and 5 of the CIC. Anticancer immunity is imparted by both tumor-

TABLE 1 | Selected preclinical studies.

Checkpoint Inhibitor	Antiangiogenic Therapy	Tumor Model	Key Results[a]	Reference
Anti–PD-1 mAb (clone RMP-014)	DC101 (anti-VEGFR2 mAb)	Hepatocellular carcinoma	* Anticancer activity ↑ * Animal survival ↑ * CD8$^+$ T-cell infiltration and activation ↑ * CD4$^+$-mediated vessel normalization * PD-1/PD-L1 expression ↑ with anti-VEGFR2 block (mediated by IFN-γ) * M2 → M1 shift in TAMs * Treg and CCR2$^+$ infiltration ↓	Shigeta et al. (52)
Anti–PD-1 mAb; (clone RMP1-14)	Lenvatinib (TKI targeting VEGFR 1-3, FGFR 1-4, PDGFRα, KIT, and RET)	Hepatocellular carcinoma	* Anticancer activity ↑ * Response rate ↑ * CD8$^+$ T cells ↑ * Macrophages and monocytes ↓	Kimura et al. (53)
Anti–PD-1 mAb (clone RMP-014)	DC101 (anti-VEGFR2 mAb)	Colon cancer	* Anticancer activity ↑ * Animal survival ↑ * TOX-dependent T-cell exhaustion induced by VEGF-A * Reinvigoration of exhausted T cells	Kim et al. (54)
Anti–PD-L1 mAb (clone 6E11)	Anti-VEGF mAb (B20-4.1.1)	SCLC	* Animal PFS and OS ↑ * Rescue of exhausted T-cell phenotype	Meder et al. (55)
Anti–PD-1 mAb (clone RMPI-14)	DC101	Colon cancer	* Angiogenesis ↓ * T-cell infiltration ↑ * Cytokine expression ↑	Yasuda et al. (56)
Anti–PD-1 mAb (clone RMP1-14)	Sunitinib (VEGFR TKI)	Colon cancer	* PD-1$^+$CD8$^+$ T cells ↓ * Anticancer activity ↑	Voron et al. (57)
Anti–PD-L1 mAb (clone 10F.9G2)	DC101	* Pancreatic cancer * Breast cancer * Glioblastoma	* IFNγ-expressing CD8+ and IFNγ-expressing CD4+ T cells ↑ * Anti–PD-L1 enhanced antiangiogenic efficacy in pNET and BC, but not GBM * PD-L1 expression on relapsing tumor cells ↑ * Vessel normalization ↑ by PD-L1 blockade and formation of HEVs ↑ via LTβR	Allen et al. (58)
Anti–PD-1 mAb (clone 29F.1A12	Axitinib	* Lung * Colon	* Mast cells ↓ * TAMs ↓ * T-cell depletion ↓ axitinib antitumor activity and survival * Axitinib induced ↓ checkpoint expression on CD8$^+$ T cells * Axitinib + anti–PD-1 ↑ animal survival	Läubli et al. (59)

↑ indicates increased cell numbers or an improvement in outcome compared with those observed with control treatments. ↓ indicates decreased cell numbers or a decrease in the outcome measured compared with control treatments.

CCR2$^+$, chemokine (C-C motif) receptor 2–positive monocyte; HEVs, high endothelial venules; LTβR, lymphotoxin-β receptor; mAb, monoclonal antibody; MDSCs, myeloid-derived suppressor cells; NA, not applicable; PD-1, programmed cell death protein 1; PD-L1, programmed cell death 1 ligand 1; sVEGFR, soluble VEGF receptor; TAMs, tumor-associated macrophages; TOX, thymocyte selection-associated high mobility group box protein; TKI, tyrosine kinase inhibitor; Treg, regulatory T cell; VEGFR, VEGF receptor.

[a]Comparisons are between combined therapy and monotherapy or control treatments (see references for details).

infiltrating immune cells residing in tissue as well as in the blood (13). Successful blockade of PD-1/PD-L1 is reliant on effective trafficking of tumor-targeted T cells from lymph nodes, through the blood stream, and into the tumor (69). As a result, resistance to PD-1/PD-L1 inhibition is often linked with inadequate T-cell infiltration into the tumor prior to treatment (12, 41, 42). To effectively infiltrate the tumor and integrate into the TME, immune cells must be able to enter the tumor vasculature, attach to the endothelium, and then migrate across the vessel wall (39). The trafficking of primed and activated T cells from the lymph node into circulation and then to the tumor is dependent on a series of steps that includes T-cell rolling and adhesion to the vascular endothelium (69, 70).

VEGF plays a critical role in this process by stimulating abnormal vasculature formation in the tumor, which can negatively impact T-cell migration from lymph nodes into the tumor bed (40, 45, 51). VEGF, as well as other immunosuppressive factors, can attenuate the expression of adhesion molecules (e.g.,

intracellular adhesion molecule 1, vascular adhesion molecule 1, CD34) on the vascular endothelium of the tumor. Reduced expression of adhesion molecules acts to impair the ability of immune cells to adhere to and migrate across the vessel wall, thereby preventing their entry into the tumor (71). Other studies have suggested that VEGF exposure can lead to the abnormal clustering of adhesion molecules on endothelial cells, resulting in reduced T-cell adhesion (72).

Endothelial cells can express a range of molecules that serve to create an impermeable barrier to certain immune cells (13). One such molecule is FAS antigen ligand. In combination with prostaglandin E2 and IL-10, FAS antigen ligand acquired the ability to induce apoptosis of CD8$^+$ T cells but not Tregs (73). Pharmacologic blockade of VEGF-A induced a marked increase in the influx of tumor-rejecting CD8$^+$ T cells over Tregs that was dependent on attenuation of FAS antigen ligand expression and led to CD8-dependent tumor growth suppression (73). Studies in cancer patients have shown links between tumor angiogenesis,

tumor vascular dysfunction, or elevated VEGF-A levels and diminished tumor T-cell infiltration (74).

T-cell exhaustion, characterized by the expression of negative immune checkpoints such as PD-1 receptors that result in a progressive loss of function, is an important mechanism of anticancer immune evasion. Studies in mouse models have shown that increased VEGF-A in the TME can enhance the expression of PD-1—as well as other receptors involved in T-cell exhaustion—on CD8$^+$ T cells, which could be prevented by anti VEGF treatment (57).

In summary, many of the immunosuppressive effects of VEGF are mediated by abnormalities in the tumor vasculature that are driven by VEGF, which can subsequently prevent effective T-cell infiltration and promote tumor immune evasion. Further, pharmacologic blockade of VEGF promotes the infiltration of cytotoxic T cells into tumors.

Vascular Normalization

Aberrant angiogenesis as well as physical compression leads to abnormal vessels and impaired blood perfusion in tumors (45). Abnormal vessels mediate immune escape and can reduce the efficacy of immunotherapy by hampering the delivery of drugs, oxygen, and effector T cells. Abnormal tumor blood vessels are prone to hypoxia and acidosis within the TME, which mediates suppressed anticancer immunity through several mechanisms (13, 45). As a result, alleviating vascular dysfunction—a process referred to as "vascular normalization"—could both improve the delivery and efficacy of anticancer treatments and overcome TME immunosuppression (75). Studies in mice have demonstrated that modulation or normalization of tumor vasculature can result in increased T-cell recruitment and infiltration into tumors (76, 77). In turn, vascular function can also be regulated by immune cells, as shown by a recent study in experimental breast tumors models in which effector CD4$^+$ T cells, introduced by either adoptive transfer or dual PD-1/CTLA4 blockade, were found to both normalize blood vessels and attenuate hypoxia (78). Relatedly, in breast and colon tumor models, anti-PD-1 or anti-CTLA-4 treatment boosted vessel perfusion through the promotion of CD8$^+$ T-cell accumulation and IFN-γ production, suggesting that improved vessel perfusion was contingent on upregulated T-cell immunity induced by checkpoint blockade (79). These data indicate that both vascular and T-cell function are mutually regulated processes in cancer.

Recruitment and Proliferation of Immunosuppressive Cells (CIC Steps 6 and 7)

Steps 6 and 7 of the CIC rely on a permissive TME in which the balance of effector T cells and immune suppressive cells permits the recognition and killing of tumor cells (51). VEGF-mediated immunosuppression is caused by both negative effects on immune effectors and the augmentation of immune suppressive cells such as Tregs, MDSCs, and TAMs with pro-tumor phenotypes (17, 80). In addition to downregulating anticancer immunity, suppressive cells can also drive angiogenesis, thereby creating a vicious cycle of immunosuppression (80). Reprogramming of the TME from immune suppressive to immune permissive may be

possible by blocking VEGF-induced expansion of MDSCs, Tregs and other immune suppressive cells which would lead to activation of antitumor immunity (17, 39).

Myeloid Cells

Myeloid cells include macrophages, neutrophils, and MDSCs. MDSCs play a critical role in regulating anticancer immunity in the TME as well as resistance to PD-1/PD-L1 antibodies. MDSCs are a diverse population of myeloid cells existing in various states of differentiation that display potent immune suppressive functions (81, 82). MDSCs also potentiate angiogenesis *via* different mechanisms (83).

MDSCs facilitate tumor progression *via* two principle mechanisms: (1) immune suppression by perturbation of immune effector function (T cells and natural killer cells) and the induction of Tregs; (2) promotion of angiogenesis (77). MDSCs in the TME are able to suppress the proliferation of tumor-specific T cells and promote Treg development or differentiation, leading to suppressed T-cell immunity. The binding of VEGF to VEGFR on MDSCs activates signaling *via* signal transducer and activator of transcription 3, resulting in their expansion (83). Although the pro-tumoral effects of MSDCs have been ascribed to immune-related parameters, non-immune mechanisms such as promotion of angiogenesis also foster cancer progression and metastasis (84). A recent study reported that PD-1 signaling regulates the lineage fate and functionality of myeloid cells in mice. Specifically, selective PD-1 ablation in myeloid cells was found to be more effective at inhibiting tumor growth than global PD-1 deletion in T cells (85, 86). In addition, targeted ablation of PD-1 on myeloid cells was shown to induce an increase of T-effector memory cells with improved functionality which allowed for effective antitumor protection despite functional PD-1 expression in T cells.

In a RCC mouse model, bevacizumab was shown to reduce the number of MDSCs (87). Sunitinib (a VEGFR TKI) increases TILs and reduced MDSCs in human RCC (88). In a murine model of RCC, sunitinib markedly reduced the infiltration of MDSCs into tumors, as well as reduced MDSCs in the peripheral blood of patients with RCC (89). MDSCs are also implicated in resistance to VEGF blockade in both mouse models as well as patients with cancer (89–91). In a syngeneic murine model of hepatocellular carcinoma (HCC), antibody targeting of tumor-infiltrating MDSCs improved the anticancer activity of sorafenib (90).

Collectively, these data indicate that myeloid cell function is orchestrated by both VEGF and PD-1 pathways, highlighting the rationale for therapeutic PD-1/PD-L1 plus VEGF inhibition in cancers in which myeloid-driven immunosuppression blunts an effective anticancer immune response.

Regulatory T-Cells

Regulatory T-cells (Tregs) are potent mediators of TME immunosuppression (92) and are regulated by several tumor-secreted factors, including VEGF (93, 94). VEGF has been shown to trigger Treg recruitment and proliferation (93). For example, VEGF blockade can lead to decreased numbers of Tregs in the TME

both in CRC mouse models and patients with CRC treated with combination of bevacizumab and chemotherapy (95). Further, the hypoxic conditions that result from VEGF-mediated abnormalities in the tumor vasculature can also induce secretion of chemokine CCL28 from tumor cells that leads to Treg recruitment, and accumulation of immunosuppressive M2 tumor-associated macrophages. Through these actions, excessive VEGF creates an immune suppressive TME that downregulates tumor-specific T-cell function, thereby facilitating tumor immune evasion (13, 17). Anti-VEGF treatment has been shown to reduce tumor-related Tregs in patients with RCC (96).

Other Immunosuppressive Cell Types

MDSCs and Tregs act in concert with other immunosuppressive cell types in the TME that are regulated by VEGF and contribute suppressed antitumor immunity (17). For example, in a murine HCC model dual anti–PD-1/VEGFR2 treatment significantly inhibited primary tumor growth and (52) and successfully reprogrammed the TME through increased CD8+ T-cell infiltration and activation, shifting the M1:M2 ratio of TAMs, and reducing Treg and chemokine receptor 2 infiltration in HCC tissue. In addition, combination treatment induced durable vessel fortification. Similar immunomodulatory effects have been reported with lenvatinib, an anti-VEGFR TKI, combined with an anti–PD-1 antibody in murine HCC models (53, 97).

Data From Clinical Biomarker Studies

Accumulating clinical biomarker data from studies in RCC and HCC have offered mechanistic insights into how VEGF blockade can overcome ICI resistance.

The combination of atezolizumab and bevacizumab was evaluated in two clinical studies of patients with advanced RCC in which immune markers were correlated with clinical efficacy to investigate the mechanisms underpinning PD-L1/VEGF inhibition (98, 99).

In Phase I study, 10 patients with RCC were treated initially with bevacizumab to evaluate the effects of bevacizumab on the TME, followed by combination therapy with atezolizumab (98). Serial biopsies and blood draws were performed at baseline, following bevacizumab, and 4 to 6 weeks after commencing combination treatment. Treatment with bevacizumab alone resulted in upregulation of MHC I staining by immunohistochemistry (IHC). Interestingly, this response was coupled with other favorable effects in the TME such as increased CD8+ T-cell and macrophage infiltration, as well as increased gene signature expression related to T-helper and CD8+ T-effector cells, natural killer cells, and chemokines.

In addition to favorable immune-related changes, bevacizumab alone or bevacizumab plus atezolizumab also induced changes in vascular parameters such as decreases in expression of neovasculature-related genes, staining of vessel-lining endothelial cell marker CD31 in the tumor, and microvascular density (98). Reduced microvascular density was associated with enhanced CD8+ T-cell tumor staining by IHC, suggesting increased T-cell infiltration. Of note, patients treated with atezolizumab and bevacizumab had more CD8+ T-cell tumor infiltration than those treated with bevacizumab alone.

Subsequently, a randomized Phase II trial was undertaken to evaluate the efficacy of atezolizumab with or without bevacizumab compared with sunitinib as a first-line treatment of clear-cell RCC (99). This study included biomarker analysis (high vs. low) to study three biological axes: angiogenesis, preexisting immunity, and myeloid immune suppression. The combination of atezolizumab plus bevacizumab had a marked PFS benefit over sunitinib or atezolizumab monotherapy in patients with tumors harboring elevated expression of a myeloid inflammation signature and T-effector signature, whereas sunitinib had greater efficacy than the combination in patients with tumors with high levels of angiogenesis (99). These exploratory data suggest that myeloid-induced immune suppression might act to restrain antitumor immune responses induced by atezolizumab and that the addition of bevacizumab could act to circumvent this restraint (50).

More recently, a genomic correlative study from a randomized Phase Ib cohort evaluating atezolizumab alone or in combination with bevacizumab in unresectable HCC was presented (100). Similar to the RCC analysis described above (99), this study evaluated immunological biomarker subpopulations defined according to gene signatures (characterized as high vs. low relative to the median). The progression-free survival (PFS) benefit of combination treatment compared with atezolizumab alone was particularly marked in patients with HCC who had high expression of the following biomarkers: VEGFR2 gene (*KDR*), myeloid, Tregs, and triggering receptor expressed on myeloid cells-1 (TREM-1) (**Table 2**). These observations are consistent with mechanisms implicated in preclinical studies in murine HCC models, as well as data showing that VEGF/VEGFR2 blockade can inhibit Treg and MDSC accumulation tumors or blood in human cancers (52, 63, 95, 101). Although these findings require validation, they provide direct evidence that myeloid- and/or Treg-mediated immunosuppression play an important role in mediating resistance to PD-L1 blockade and that these mechanisms can be therapeutically abrogated with anti-VEGF therapy.

It remains to be seen whether the therapeutically relevant immune suppressive mechanisms described in this section are broadly applicable across cancer types or vary depending on tumor histology and tissue-specific immune regulation (102).

TABLE 2 | PFS benefit with atezolizumab plus bevacizumab compared vs. atezolizumab alone in subpopulations of patients by HCC exploratory biomarkers.

Biomarker Subpopulation		Atezolizumab + Bevacizumab vs. Atezolizumab PFS, HR (95% CI)	N per Group (combo, mono)
VEGFR2	VEGFR2high	0.36 (0.16–0.81)	21, 25
	VEGFR2low	0.88 (0.4–1.9)	23, 22
Tregs	Treghigh	0.35 (0.15–0.82)	21, 25
	Treglow	0.82 (0.39–1.7)	23, 22
Myeloid	Myeloidhigh	0.43 (0.19–0.95)	22, 24
	Myeloidlow	0.80 (0.37–1.7)	22, 23
TREM	TREMhigh	0.43 (0.10–0.94)	24, 22
	TREMlow	0.77 (0.36–1.6)	20, 25

HCC, hepatocellular carcinoma; PFS, progression-free survival; Treg, regulatory T cells; TREM, triggering receptor expressed on myeloid cells-1.

ANTI-VEGF AS IMMUNOTHERAPY: EVIDENCE FROM CLINICAL TRIALS

The intriguing preclinical and translational clinical studies highlighting the immunomodulatory effects of VEGF blockade described in the previous section have resulted in a myriad of clinical trials testing the combination of PD-1/PD-L1 antibodies with anti-VEGF drugs (**Tables 3** and **4**) (7). Positive Phase III studies have led to recent approvals by the FDA for dual PD-1/PD-L1 and anti-VEGF combinations in RCC (pembrolizumab plus axitinib, and avelumab plus axitinib), endometrial carcinoma (pembrolizumab plus lenvatinib), non-squamous NSCLC (atezolizumab, bevacizumab and chemotherapy), and HCC, suggesting a potential broad clinical utility of this combination strategy (104, 105, 107, 109–111). Given the number of clinical studies, the following section focuses primarily on randomized trials for which results are available.

Renal Cell Carcinoma

Clear-cell RCCs, which make up approximately 70% of RCC cases, are associated with a hyperangiogenic state that is brought on by VEGF overproduction resulting from inactivation of the von Hippel–Lindau tumor-suppressor gene (112). As a result, multiple VEGF-directed therapies are approved for the treatment of RCC (**Supplemental Table 2**).

As well as being highly angiogenic, RCC is also immunogenic, as evidenced by responsiveness to PD-1/PD-L1 axis blockade (99, 113). These clinical findings, coupled with emerging data regarding the immunomodulatory actions of anti-VEGF drugs, led to multiple studies combining anti-VEGF agents with PD-1/PD-L1 antibodies (114). The combination of ICIs and antiangiogenics has been tested most extensively in patients with advanced RCC.

Early clinical studies in patients with RCC demonstrated encouraging antitumor activity of these combination regimens along with a manageable safety profile (94, 115, 116). However, some combinations involving VEGF TKIs were associated with excessive toxicity that precluded further development and highlighted the need for careful selection of the antiangiogenic agent (117). To date, five Phase III studies have been initiated to evaluate various combinations of VEGF or VEGFR inhibitors plus either PD-1 or PD-L1 antibodies in patients with advanced RCC, of which three have been published (103, 105, 109). Based on the results of JAVELIN 101 and KEYNOTE-426, combination treatment with either pembrolizumab or avelumab plus axitinib is now considered a standard of care in frontline advanced RCC (118, 119).

IMmotion151

IMmotion151 was a randomized Phase III study comparing atezolizumab plus bevacizumab vs. sunitinib in patients with advanced RCC (103). Co-primary endpoints were investigator-assessed PFS in the PD-L1$^+$ population and overall survival (OS) in the intention-to-treat (ITT) population. A total of 915 patients were randomized to receive either atezolizumab plus bevacizumab or sunitinib. Bevacizumab plus atezolizumab significantly improved PFS compared with sunitinib in patients with PD-L1$^+$ tumors (HR, 0.74; P = .02) and in the ITT population (HR, 0.83). In the ITT population, OS did not cross the significance boundary at the interim analysis (HR, 0.93).

Javelin 101

Javelin 101 was a randomized Phase III study comparing avelumab plus axitinib vs. sunitinib in patients with advanced RCC (105). A total of 886 patients were randomized to either avelumab plus axitinib or sunitinib. The combination of axitinib plus avelumab significantly improved PFS compared with sunitinib in patients with PD-L1$^+$ tumors (HR, 0.61; P <.001) and in the ITT population (HR, 0.69; P <.001). PD-L1$^+$ patients had objective response rates (ORRs) of 55.2% vs. 25.5% in favor of axitinib plus avelumab. OS was immature at the time of data cutoff. In the ITT population, axitinib plus avelumab treatment resulted in an ORR of 51% compared with 26% with sunitinib.

KEYNOTE-426

KEYNOTE-426 was a randomized Phase III study comparing pembrolizumab plus axitinib to sunitinib in patients with advanced clear-cell RCC (109). A total of 861 patients were randomized to receive either pembrolizumab plus axitinib or sunitinib. The combination of axitinib plus pembrolizumab significantly improved both OS (HR, 0.53; P < 0.0001) and PFS (HR, 0.69; P < 0.001) compared with sunitinib in the ITT population. Notably, KEYNOTE-426 was the first of the combination studies to demonstrate an OS benefit over sunitinib in RCC. ORR, a secondary endpoint, was also significantly improved with axitinib plus pembrolizumab compared with sunitinib (59.3% vs. 35.7%; P < 0.0001).

Colorectal Cancer

The clinical benefit of ICIs in metastatic colorectal cancer (mCRC) is confined to the 4% to 5% of patients with tumors with deficient DNA mismatch repair pathways (dMMR) or high microsatellite instability (MSI-H) (120, 121). Conversely, PD-(L)1 inhibitors do not show clinically relevant activity in proficient DNA mismatch repair pathways (pMMR) or MSS mCRC (120, 122). The marked response to anti–PD-1 therapy in dMMR/MSI-H mCRC can be explained by high levels of tumor mutation burden (123–125). However, mutation burden alone cannot explain the lack of response to anti–PD-1 treatment in MSS/pMMR mCRC (15, 126). Factors other than mutational burden might therefore account for the lack of response to checkpoint blockade in MSS/pMMR mCRC.

The differential response to CPI in dMMR/MSI-H and MSS/pMMR mCRC is likely due in part to differences in the TME that impact the tumor's ability to mount an effective anticancer immune response (127). VEGF is believed to play a fundamental role in shaping the immune-suppressive TME in MSS CRC. Recent data from a series of *in vitro*, *in vivo*, and *ex vivo* studies demonstrated that severe T-cell exhaustion driven by VEGF-A was highly prominent in MSS CRC tumors compared with MSI-H CRC tumors (54). T-cell exhaustion in MSS CRC tumors was characterized by diminished CD8$^+$ T-cell infiltration at the invasive margin and tumor body, upregulated expression of exhaustion markers such as PD-L1, and reduced IFN-γ release.

TABLE 3 | Ongoing randomized Phase II or Phase III studies of PD-1/PD-L1 antibodies combined with VEGF inhibitors.

Anti-VEGF	PD-1/PD-L1	Other Drugs/Interventions	Tumor Type	Study Phase	n	Primary Endpoint(s)	NCT ID (study name)
Bevacizumab	Atezolizumab	Paclitaxel + carboplatin	Recurrent OC, FTC, or PPC	III	1300	PFS/OS	NCT03038100 (IMagyn050)
Bevacizumab	Atezolizumab	Paclitaxel or pegylated liposomal doxorubicin	Recurrent OC	III	664	PFS/OS	NCT03353831
Bevacizumab	Atezolizumab	Carboplatin + gemcitabine, carboplatin + paclitaxel or carboplatin + pegylated liposomal doxorubicin	OC	III	600	PFS	NCT02891824 (ATALANTE/ENGOT OV29)
Bevacizumab	Atezolizumab	Pegylated liposomal doxorubicin hydrochloride	Recurrent OC, FTC, or PPC	II/III	488	PFS/OS	NCT02839707
Bevacizumab	Atezolizumab	Aspirin	Recurrent platinum-resistant OC, FTC or PPC	II	160	PFS at 6 months	NCT02659384 (EORTC-1508)
Bevacizumab	Durvalumab	Carbo/tax Olaparib	1L OC	III	1056	PFS in BRCA non-mut	NCT03737643 (DUO-O)
Bevacizumab	Atezolizumab	FOLFOX	1L dMMR mCRC	III	347	PFS	NCT02997228 (COMMIT)
Bevacizumab	Atezolizumab	FOLFOXIRI	1L mCRC	II	201	PFS	NCT03721653 (AtezoTRIBE)
Bevacizumab	Nivolumab	N/A	Recurrent GBM	II	90	OS at 12 months	NCT03452579
Bevacizumab	Nivolumab	FOLFOX	1L mCRC	II/III	180	PFS	NCT03414983 (CheckMate 9X8)
Bevacizumab	Atezolizumab	carboplatin and pemetrexed	1L NSCLC (non-squamous)	II	117	PFS	NCT03786692
Bevacizumab	Nivolumab	Carboplatin/paclitaxel	1L NSCLC (non-squamous)	III	530	PFS	NCT03117049 (TASUKI-52)
Bevacizumab	Pembrolizumab	Chemotherapy	1L cervical cancer	III	600	PFS/OS	NCT03635567 (KEYNOTE-826)
Bevacizumab	Atezolizumab	Chemotherapy	1L cervical cancer	III	404	OS	NCT03556839 (BEATcc)
Bevacizumab	Atezolizumab	Carboplatin/pemetrexed	1L pleural mesothelioma	III	320	PFS/OS	NCT03762018 (BEAT-meso)
Bevacizumab	Atezolizumab	N/A	Adjuvant HCC	III	662	RFS	NCT04102098 (IMbrave 050)
Bevacizumab	Durvalumab	N/A	Adjuvant HCC	III	888	RFS	NCT03847428 (EMERALD-2)
Bevacizumab	Durvalumab	TACE	Intermediate-stage HCC	III	600	PFS	NCT03778957 (EMERALD-1)
Bevacizumab	Durvalumab	N/A	1L HCC	II	433	Safety	NCT02519348
Cabozantinib	Atezolizumab	N/A	1L HCC	III	740	PFS/OS	NCT03755791 (COSMIC-312)
Apatinib	SHR-1210	N/A	IL HCC	III	510	PFS/OS	NCT03764293
Lenvatinib	Pembrolizumab	N/A	Recurrent endometrial cancer	III	780	PFS/OS	NCT03517449 (KEYNOTE-775)
Lenvatinib	Pembrolizumab	N/A	1L advanced endometrial cancer	III	720	PFS/OS	NCT03884101 (LEAP-001)
Lenvatinib	Pembrolizumab	N/A	1L HCC	III	750	PFS/OS	NCT03713593 (LEAP 002)
Lenvatinib	Pembrolizumab	N/A	1L RCC	III	1069	PFS	NCT02811861 (CLEAR)
Cabozantinib	Nivolumab	N/A	1L RCC	III	638	PFS	NCT03141177 (CheckMate 9ER)
Cabozantinib	Nivolumab	Ipilimumab	1L RCC	III	1046	OS	NCT03793166 (PDIGREE)
Cabozantinib	Nivolumab	Ipilimumab	1L RCC	III	676	PFS	NCT03937219 (COSMIC-313)

CRC, colorectal carcinoma; dMMR, mismatch repair deficient; ER, estrogen receptor; FTC, fallopian tube cancer; GBM, glioblastoma; HCC, hepatocellular carcinoma; HER2, human epidermal growth factor receptor 2; m, metastatic; MSS, microsatellite stable; N/A, not applicable; NSCLC, non-small cell lung cancer; OC, ovarian cancer; OS, overall survival; PD-1, programmed cell death protein 1; PD-L1, programmed cell death 1 ligand 1; PFS, progression-free survival; pMMR, mismatch repair proficient; PPC, primary peritoneal cancer; RCC, renal cell carcinoma; TACE, transarterial chemoembolization; UC, urothelial carcinoma.

*Studies included in **Table 1** are not included.*

TABLE 4 | Completed randomized studies of PD-1/PD-L1 antibodies combined with VEGF inhibitors in solid tumors.

Experimental Arm(s)	Control Arm	Tumor	Phase	Primary Endpoint(s)	OS	PFS	ORR (vs. control)	NCT ID (study name)	Reference
Bevacizumab + Atezolizumab	Sunitinib	1L RCC	III	PFS (PD-L1+); OS (ITT)	ITT Population OS HR: 0.93; (0.76–1.14; $P = 0.4751$)[a]	PD-L1 HR, 0.74 (95% CI, 0.57–0.96), $P = 0.02$ ITT HR, 0.83 (95% CI: 0.70–0.97)	PD-L1+ 43% vs. 35% ITT 37% vs. 33%	NCT02420821 (IMmotion151)	Rini (103),. *Lancet* 393, 2404–2415.
Bevacizumab + Atezolizumab + chemo	Chemo + bevacizumab	1L NSCLC	III	PFS in ITT-WT; PFS in Teff-high WT; OS in ITT-WT	ITT-WT HR, 0.78 (95% CI, 0.64–0.96; $P = 0.02$)	ITT-WT HR, 0.62 (95% CI, 0.52–0.74; $P < 0.001$)	ITT-WT ORR: 64% vs. 48%	NCT02366143 (IMpower150)	Socinski et al. *N Engl J Med*, (104)
Bevacizumab + Atezolizumab	Sunitinib	1L RCC	II	PFS in ITT and PD-L1+	NR	ITT HR, 1.00 (95% CI, 0.69–1.45) PD-L1+ HR, 0.64 (95% CI, 0.38–1.08)	ITT 32% vs. 29% PD-L1+ 46% vs. 27%	NCT01984242 (IMmotion150)	McDermott et al. *Nat Med* (99)
Axitinib + Pembrolizumab	Sunitinib	1L RCC	III	PFS/OS	HR 0.53; (95% CI, 0.38–0.74; $P < 0.0001$)	HR: 0.69; (95% CI, 0.57–0.84; $P = 0.0001$)	59% vs. 36%; $P < 0.0001$	NCT02853331 (Keynote 426)	Motzer, (105). *N Engl J Med* 380, 1103–1115.
Axitinib + Avelumab	Sunitinib	1L RCC	III	PFS/OS (PD-L1+)	0.82 (95% CI, 0.53–1.28; $P = 0.38$)	0.61 (95% CI, 0.47–0.79; $P < 0.001$)	ORR: 55% vs. 26%	NCT02684006 (Javelin RENAL)	Motzer et al. (105). *N Engl J Med* 380, 1103–1115.
Bevacizumab + Atezolizumab	Atezolizumab	1L HCC	Ib	PFS (Arm F)	NR	PFS HR: 0.55; (80% CI, 0.40–0.74; $P = 0.011$)	ORR: 20% vs. 17%	NCT01633970	Lee et al. (106) *Lancet Oncol* 21, 808–820
Bevacizumab + Atezolizumab	Sorafenib	1L HCC	III	PFS/OS	OS HR: 0.58 (0.42–0.79; $P < 0.001$)	PFS HR: 0.59; (95% CI, 0.47–0.76; $P < 0.001$)	ORR: 27% vs. 12% ($P < 0.001$)	NCT03434379 (IMbrave150)	Finn et al. (107). *N Engl J Med* 382, 1894–1905.
Bevacizumab + Atezolizumab + capecitabine	Capecitabine + bevacizumab	Chemo refractory mCRC	II	PFS	HR 0.94 (0.56–1.56; $P = 0.398$)	HR 0.73 (95% CI, 0.49–1.07; $P = 0.051$)	ORR: 9% vs. 4%	NCT02873195 (BACCI)	Mettu et al. (108) (ESMO)

HCC, hepatocellular carcinoma; HR, hazard ratio; INV, investigator-assessed; ITT, intention-to-treat; NA, not available; NCT ID, ClinicalTrials.gov identifier; NR, not yet reached; NSCLC, non-small cell lung cancer; OS, overall survival; PD-L1, programmed death-ligand 1; PFS, progression-free survival; RCC, renal cell carcinoma; Teff, T-effector gene signature (PD-L1, CXCL9, and interferon-γ); WT, wild-type.
[a]Results did not cross the prespecified significance boundary of α = 0.0009 at the first interim analysis.

The frequency of a wound-healing gene signature characterized by the elevated expression of angiogenic genes was found in 81% of MSS CRC tumors compared with 40% of MSI-H tumors. Furthermore, VEGF expression was markedly higher in MSS vs. MSI-H CRC tumors and VEGF was found to drive T-cell exhaustion as well as reduced T-cell functionality in MSS tumors. Together, these data give mechanistic insights into the role of VEGF-mediated suppression of T-cell immunity in CRC tumors and provide a rational framework to clinically evaluate co-targeting VEGF and PD-1/PD-L1 pathways.

dMMR/MSI-H Colorectal Cancer

MSI-H/dMMR status is a biomarker associated with poor prognosis in mCRC and is predictive for response to immune CPIs (128). Phase II studies demonstrated durable responses of MSI-H/dMMR tumors to PD-1 inhibitors (120, 128, 129). Pembrolizumab was recently shown in a Phase III study to significantly improve PFS vs. chemotherapy as first-line therapy for patients with MSI-H/dMMR mCRC (130).

Despite high levels of response to PD-1 blockade, not all patients with dMMR/MSI-H disease respond or subsequently develop resistance, potentially as a result of mechanisms similar to those observed in other cancers, including VEGF (129). The combination of atezolizumab and bevacizumab was studied in a cohort of 10 patients with heavily pretreated MSI-H mCRC and resulted in an ORR of 30% and a disease control rate of 90% (131).

The immunomodulatory role of VEGF in colon cancer was retrospectively studied in the NSABP C-08 study of adjuvant FOLFOX plus bevacizumab in stage II/III colon cancer (132). In the overall study population, bevacizumab did not significantly improve disease-free survival (HR, 0.89). However, in a *post hoc* analysis of patients harboring either dMMR or pMMR, bevacizumab was associated with improved survival compared with FOLFOX alone in the dMMR subgroup (133). By contrast, no survival benefit was seen in the pMMR subgroup. This result suggests that inhibition of VEGF alone, at least in some groups of patients with CRC and preexisting anticancer immunity, provides an immunostimulatory effect sufficient to augment the anticancer immune response and provides a rationale to combine bevacizumab with a CPI to amplify immunity (38). A Phase III study is ongoing to evaluate the combination of FOLFOX and bevacizumab with or without atezolizumab in first-line mCRC with dMMR (134).

MSS Colorectal Cancer

Unlike dMMR/MSI-H mCRC, patients with MSS mCRC (who account for around 95% of patients) anti–PD-(L)1 therapy has demonstrated limited or no clinical benefit (124, 135–138).

Treatment with chemotherapy and bevacizumab has been shown to induce positive immunological changes (e.g., increase in total lymphocytes, increase in CD4 and CD8 T cells) in the peripheral blood of patients with mCRC (139). However, these favorable changes were largely transient and had dissipated by cycle 6 of treatment. This suggests that amplifying these chemotherapy/anti-VEGF-induced immunomodulatory effects with a CPI could be beneficial.

In a Phase I study of 14 patients with refractory MSS CRC treated with atezolizumab plus bevacizumab, 1 patient (7%) had an objective response and 9 patients (64%) had stable disease (140). In a cohort of 23 patients with first-line mCRC, an ORR of 52% was reported, along with a median PFS of 14.1 months (95% CI, 8.7–17.1) and a median duration of response of 11.4 months (141). Interestingly, a single patient experienced a durable complete radiological response in a liver lesion.

These preliminary Phase I data prompted the initiation of a number of randomized studies evaluating the combination of PD-(L)1 antibodies and anti-VEGF drugs in mCRC. The BACCI study, a placebo-controlled randomized Phase II study, evaluated the addition of atezolizumab to bevacizumab and capecitabine in refractory mCRC (108). Approximately, 86% of randomized patients had MSS mCRC. In the overall study population (n = 133), atezolizumab plus capecitabine/bevacizumab significantly improved PFS compared with capecitabine/bevacizumab (median PFS, 3.3 vs. 4.4 months; HR, 0.73; $P = 0.051$). In patients with MSS tumors, the PFS benefit was more pronounced (HR 0.67). Response rate and OS were not significantly increased (108). Maintenance therapy with atezolizumab following induction treatment with FOLFOX plus bevacizumab in first-line mCRC was evaluated in the MODUL study (142). A total of 696 patients without B-Raf proto-oncogene, serine/threonine kinase (*BRAF*) mutations were randomized to either fluorouracil (5-FU)–bevacizumab plus atezolizumab or 5-FU–bevacizumab (143). The study did not meet its primary PFS endpoint (HR, 0.92; $P = 0.48$). In an updated analysis, the PFS outcome was unchanged and survival was not significantly increased (HR, 0.86; $P = 0.28$).

In an effort to improve the immune recognition of colorectal tumors, atezolizumab was combined with cobimetinib [a mitogen-activated protein kinase kinase (MEK) inhibitor] and bevacizumab in patients with previously treated mCRC in a Phase I trial (144). The rationale for pairing a PD-L1 antibody with a MEK inhibitor was the results of a preclinical study that showed that MEK pathway blockade augmented the antitumor activity of CPIs by increased T-cell infiltration into tumors and increased MHC-1 and PD-L1 expression (145, 146). The combination of atezolizumab, bevacizumab, and cobimetinib had an ORR of 8% in both patients with second-line mCRC and those with refractory mCRC; 92% of patients had MSS disease and 8% had unknown MSI status (144). PFS and OS appeared to be enhanced in patients harboring RAS mutations. Notably, atezolizumab combined with cobimetinib did not improve survival in refractory mCRC compared with standard-of-care regorafenib in a Phase III study (35). Because of the equivocal clinical benefit of the atezolizumab-bevacizumab-cobimetinib combination, further clinical development was halted (144).

The combination of regorafenib and nivolumab was studied in a Phase Ib trial in Japanese patients with refractory CRC or gastric cancer, 98% of whom had MSS disease (147). In 25 patients with heavily pretreated MSS CRC, ORR was 33%. Unlike in the GC cohort, in the limited number of patients with CRC no clear relationship between PD-L1 or TMB and efficacy outcomes was observed, and therefore, additional analysis is necessary to clarify the optimal patient population for this combination.

Taken together, the efficacy of combined PD-(L)1 antibodies plus anti-VEGF in MSS mCRC is inconclusive and may suggest that the combination could be efficacious in as-yet unidentified subgroups of patients. The data also point to the highly immunosuppressed nature of MSS colorectal tumors and the need for novel strategies to circumvent inherent immune resistance. A Phase II/III trial (CheckMate 9X8) is currently ongoing to evaluate nivolumab in combination with bevacizumab and FOLFOX (**Table 3**).

Lung Cancer

NSCLC accounts for 80% to 85% of lung cancers, and adenocarcinoma and squamous cell carcinoma are the most common NSCLC histologic subtypes (148). CPIs have revolutionized the treatment of NSCLC, and most patients with newly diagnosed advanced NSCLC are indicated for treatment with PD-1 or PD-L1 antibodies, either as monotherapy or in combination (149, 150).

The IMpower150 study was designed to evaluate the clinical benefit of PD-L1 blockade with the immunomodulatory effects of chemotherapy and anti-VEGF (17, 28, 151–153). IMpower150 was a Phase III randomized trial comparing atezolizumab plus bevacizumab and chemotherapy (carboplatin and paclitaxel) to standard-of-care chemotherapy plus bevacizumab in patients with stage IV non-squamous NSCLC (104). A total of 1,202 patients were randomized to one of three arms to receive either:

- atezolizumab plus carboplatin-paclitaxel (ACP group)
- atezolizumab plus bevacizumab plus carboplatin-paclitaxel (ABCP group)
- bevacizumab plus carboplatin-paclitaxel (BCP group).

Patients treated with ABCP had improved PFS vs. patients receiving BCP therapy (HR, 0.62; P < .001) as well as improved OS (HR 0.78; P = .02). In addition, ORR (a secondary endpoint) was also increased in patients who received ABCP vs. BCP (64% vs. 48%, respectively). The clinical benefit of ABCP compared with BCP extended across key patient subgroups irrespective of PD-L1 expression levels, presence of baseline liver metastases (unstratified PFS HR, 0.42; unstratified OS HR, 0.54), and EGFR/ALK genetic alterations (unstratified PFS HR, 0.59; unstratified OS HR, 0.54).

In contrast to the OS benefit observed in patients treated with ABCP vs. BCP (HR, 0.76), no survival benefit (HR 0·85) was seen in those receiving ACP compared with the standard-of-care BCP regimen in the ITT population (154). Furthermore, whereas treatment with ABCP markedly improved PFS and OS relative to BCP in patients with activating EGFR mutations or liver metastases, the ACP regimen (without bevacizumab) did not show improved PFS or survival compared with BCP in these important clinical subgroups (154) (**Figure 3**). Relatedly, the lack of efficacy seen with the ACP regimen in IMpower150 in patients with EGFR mutations or baseline liver metastases was also observed in IMpower130, which evaluated atezolizumab in combination with carboplatin plus nab-paclitaxel chemotherapy (29). Together, these data indicate that bevacizumab, *via* restraint of angiogenesis and reversal of VEGF-driven immunosuppression in

the TME, is needed in addition to atezolizumab and chemotherapy to unleash clinically effective anticancer immunity in patients with NSCLC harboring an *EGFR* mutation or liver metastases (50). Liver metastases are discussed further in a subsequent section.

On the basis of these data, carboplatin-paclitaxel in combination with bevacizumab plus atezolizumab is considered a standard-of-care first-line treatment for patients with non-squamous metastatic NSCLC (155). Additional randomized trials evaluating PD-(L)1–VEGF-chemotherapy combinations are currently ongoing in patients with NSCLC (**Table 3**).

Gynecological Cancers

Gynecologic malignancies are among the most prevalent cancers affecting women worldwide. With the exception endometrial cancer, in advanced gynecologic cancers CPIs have demonstrated only limited antitumor activity, highlighting the need for combination strategies to bolster anticancer immunity in these tumors (156).

Endometrial Cancer

Up to 30% of endometrial cancers are MSI-H/dMMR and respond well to anti–PD-(L)1 inhibitors. However, response to PD-(L)1 blockade in MSS/pMMR endometrial tumors is modest, highlighting an unmet need for combination CIT regimens to augment anticancer immunity (157). Dual PD-1 and VEGF inhibition is one such combination that has been evaluated in advanced endometrial cancer.

The combination of pembrolizumab and lenvatinib in advanced primary or recurrent endometrial cancer, independent of MMR status, was studied in a single arm Phase II study (110, 111). In the final efficacy analysis, the ORR (by irRECIST) in 108 previo15usly treated patients was 38% at week 24 per investigator review, with a median PFS of 7.5 months (111). ORR was 64% in patients with MSI-H tumors (n = 11) and 36% in patients with MSS tumors (n = 94) (158). These encouraging preliminary data led to accelerated FDA approval of the combination of lenvatinib with pembrolizumab for the treatment of advanced endometrial cancer that is not MSI-H/dMMR and has progressed following prior therapy (157). The combination of lenvatinib and pembrolizumab is now under study in two ongoing Phase III trials (**Table 3**): lenvatinib with pembrolizumab vs. doxorubicin or weekly paclitaxel in advanced recurrent endometrial cancer (NCT03517449) and frontline lenvatinib with pembrolizumab vs. carboplatin and paclitaxel chemotherapy in advanced endometrial cancer (NCT03884101). There is also an ongoing Phase II single-group study evaluating bevacizumab and atezolizumab in recurrent endometrial cancer (NCT03526432).

Cervical Cancer

The standard treatment for recurrent or metastatic cervical cancer is a combination of chemotherapy and bevacizumab (159–162), but treatment options for recurrent disease are limited. Almost all cervical cancers are mediated by human papillomavirus infection which, when considered alongside relatively high mutation burden and expression of PD-L1,
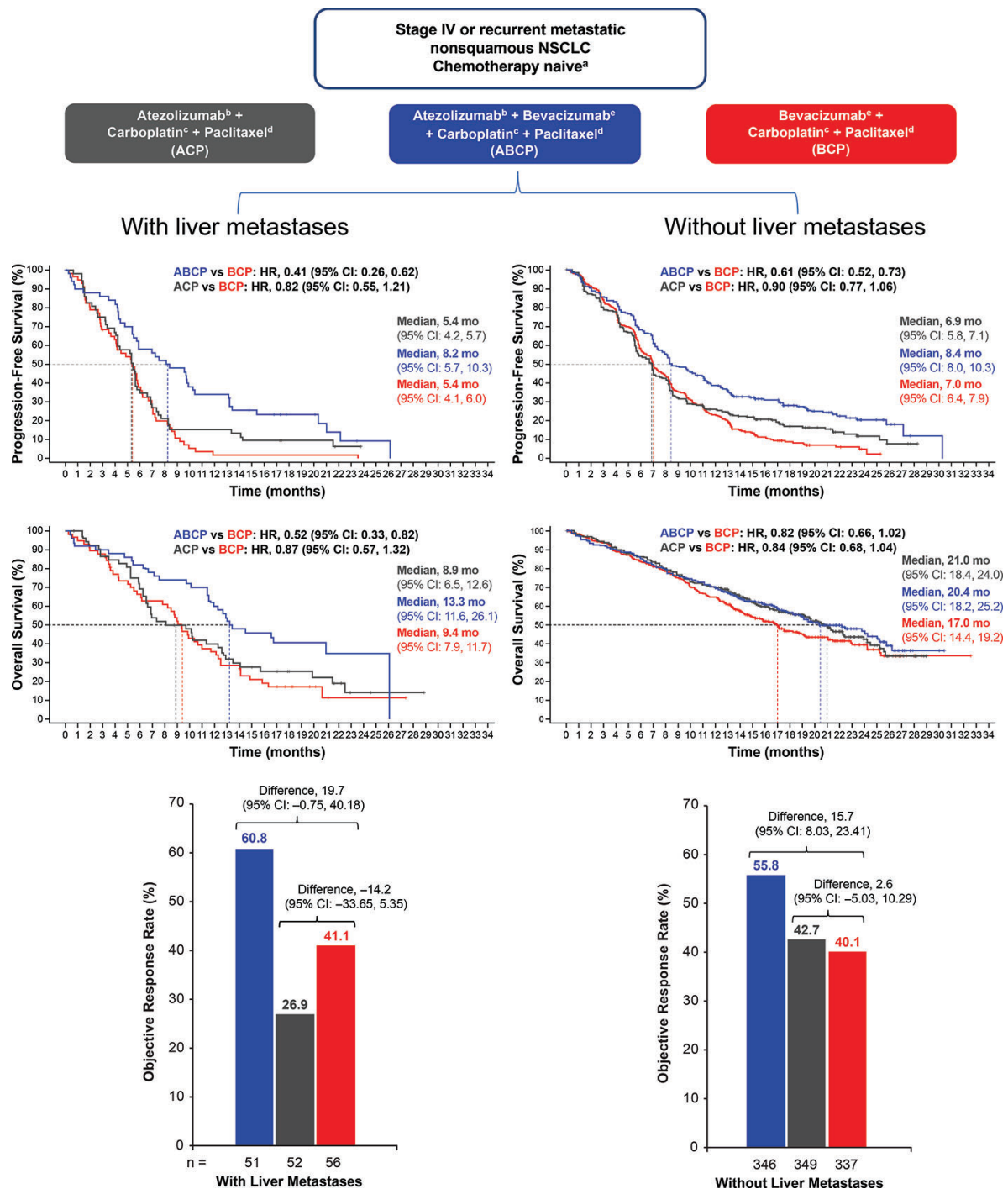
FIGURE 3 | PFS, OS, and ORR in patients with NSCLC with or without baseline liver metastases. Kaplan-Meier estimates of PFS and OS in patients with or without liver metastases at baseline in the intention-to-treat population for the ABCP vs. BCP treatment comparison and the ACP vs. BCP treatment comparison. Adapted from Reck et al. (154). ABCP, atezolizumab plus bevacizumab plus carboplatin plus paclitaxel; ACP, atezolizumab plus carboplatin plus paclitaxel; BCP, bevacizumab plus carboplatin plus paclitaxel; CI, confidence interval; HR, hazard ratio; NSCLC, non-small cell lung cancer; ORR, objective response rate; OS, overall survival; PFS, progression-free survival.

makes immunotherapy a potentially attractive treatment strategy (163, 164).

Despite having favorable immune biology, patients with cervical cancer have seen modest activity with single-agent CPIs (164, 165). The Phase II nonrandomized KEYNOTE-158 study evaluated pembrolizumab in 98 patients with recurrent or metastatic cervical cancer who had progressed on or were intolerant to at least one line of standard therapy and reported an ORR of 12% (166); all responses occurred in PD-L1–positive tumors. On the basis of these data, the FDA granted accelerated approval of pembrolizumab for patients with advanced PD-L1–positive cervical cancer whose disease progressed following first-line chemotherapy.

The modest activity of single-agent CPIs in patients with cervical cancer led to studies evaluating multiple combinations, including of PD-1 and VEGF (156). KEYNOTE-826 and the BEATcc studies are ongoing Phase III studies evaluating the combination of PD-(L)1 and VEGF antibodies on a chemotherapy backbone (167, 168).

Ovarian Cancer

Epithelial ovarian cancer (EOC) accounts for over 95% of cases of ovarian cancer (169). Chemotherapy combined with bevacizumab is a standard of care for patients with newly diagnosed or recurrent disease (170). Despite EOC having favorable immune characteristics (high levels of TILs, neoantigens, and PD-L1 expression), the activity of PD-1/PD-L1 antibodies in EOC is modest, indicating the need for combination approaches to enhance antitumor immunity (171).

Given the pathogenic role of angiogenesis and the clinical utility of bevacizumab in EOC, a rationale exists for combined PD-(L)1–VEGF blockade. Atezolizumab plus bevacizumab was studied in a single-arm Phase II trial of 38 women with relapsed EOC: 18 with platinum-resistant and 20 with platinum-sensitive disease (172). The overall confirmed ORR was 29%; ORR was 40% and 17% in platinum-sensitive and platinum-resistant patients, respectively. A single-arm Phase II trial reported a response rate of 40% in platinum-resistant patients with recurrent EOC with the combination of bevacizumab, pembrolizumab, and metronomic oral cyclophosphamide (173).

Phase III studies in patients with advanced EOC are ongoing. The ATALANTE trial is comparing the combinations of chemotherapy with bevacizumab and atezolizumab vs. chemotherapy and bevacizumab alone in platinum-sensitive relapsed disease, while IMagyn050 is exploring this strategy in first-line treatment of newly diagnosed disease (**Table 3**). Alternative combinations that build on CPI/VEGF blockade are also under study. The emergence of poly (ADP-ribose) polymerase (PARP) inhibition as a treatment for EOC has provided justification to explore triplet therapy with a CPI, anti-VEGF, and PARP inhibitor (174). A Phase III study of durvalumab, bevacizumab, and olaparib is ongoing (175).

Hepatocellular Carcinoma

HCC is highly angiogenic, as evidenced by hypervascularity, marked vascular abnormalities, and frequent overexpression of angiogenic factors such as VEGF (176, 177). Reflecting this vascular biology, most treatments currently approved for advanced HCC are either oral agents that inhibit angiogenic kinases or monoclonal antibodies against VEGFR (176, 178, 179). Despite initially appearing to offer a marked therapeutic advance, antiangiogenic drugs have shown modest survival improvements and low response rates, resulting in limited clinical benefit (176).

HCC is associated with inflammation and a suppressed immune environment, making CIT approaches a rational therapeutic approach (180–183). Encouraging early clinical data from two single-arm trials of pembrolizumab and nivolumab in advanced HCC formed the basis for the accelerated approval by the FDA (184, 185). In patients previously treated with sorafenib, response rates with nivolumab and pembrolizumab were 20% and 17%, respectively (184, 185). Despite these encouraging preliminary data, randomized Phase III trials of anti–PD-1 monotherapy in either first-line (nivolumab vs. sorafenib) or second-line (pembrolizumab vs. placebo) settings did not demonstrate statistically significant improvements in OS (186, 187). CheckMate 459, a Phase III study evaluating nivolumab vs. sorafenib as a first-line treatment in patients with unresectable HCC, did not achieve significance for its primary endpoint of OS (HR, 0.85; $P = 0.075$). Likewise, KEYNOTE-240, a Phase III trial evaluating pembrolizumab in patients who had previously received systemic therapy, did not achieve the prespecified OS boundary for statistical significance (HR, 0.781; $P = 0.0238$). These data likely highlight the strongly immunosuppressive nature of HCC and indicate the critical need for combination strategies to address additional immune defects beyond PD-(L)1.

Co-targeting the PD-(L)1 and VEGF signaling axes is the most extensively studied combination approach for advanced HCC (188, 189). Results from single-arm studies showed that combinations of VEGF and PD-(L)1 inhibitors were associated with a manageable safety profile and promising antitumor activity, with ORRs of 11% to 50% (190–195).

Of these combinations, atezolizumab and bevacizumab has been the most widely studied to date in HCC. A confirmed ORR of 36%—including a complete response rate of 12%—was reported in patients with unresectable HCC treated with atezolizumab and bevacizumab (106). Subsequently, combined atezolizumab and bevacizumab was evaluated in patients with unresectable HCC in two randomized studies, the results of which have been recently reported (106, 107, 196). These studies were designed to determine: (1) does bevacizumab augment the efficacy of atezolizumab treatment; and (2) is atezolizumab in combination with bevacizumab more effective than sorafenib for unresectable HCC?

In Arm F of study GO30140, 119 patients with unresectable HCC were randomly assigned 1:1 to receive either atezolizumab alone or atezolizumab plus bevacizumab (106). The primary endpoint was PFS assessed by an independent review facility. A statistically and clinically significant improvement in PFS was observed with the combination vs. atezolizumab monotherapy (HR, 0.55; $P = 0.0108$), with a median of 5.6 months vs. 3.4 months, respectively. Surprisingly, ORR was not markedly

higher in the combination arm than in the atezolizumab arm (20% vs. 17%); however, the disease control rate was improved in favor of the combination (67% vs. 49%) (106). These data indicate that anti-VEGF treatment significantly enhances the efficacy of PD-L1 inhibition and a combination of PD-L1 and VEGF blockade is likely required to augment anticancer immunity in patients with unresectable HCC.

These encouraging findings led to the several randomized Phase III trials comparing these combination regimens with current standards of care (**Tables 3** and **4**).

IMbrave150 was a randomized Phase III study in which 501 patients with unresectable HCC were randomly assigned, in a 2:1 ratio, to receive either atezolizumab plus bevacizumab or sorafenib (a standard first-line anti-VEGF treatment). Co-primary endpoints were PFS (by blinded independent review) and OS. The results of IMbrave150 showed that atezolizumab plus bevacizumab resulted in a significant improvement in both PFS (HR, 0.59; $P < 0.0001$) and OS (HR, 0.58; $P = 0.0006$) compared with sorafenib (107). Further emphasizing the superior clinical benefit of combination therapy, ORR by central assessment more than doubled with atezolizumab plus bevacizumab compared with sorafenib alone (27% vs. 12%, $P < 0.0001$). Importantly, analysis of patient-reported outcomes showed significant and consistent benefits in quality of life, functioning, and key symptoms with atezolizumab plus bevacizumab compared to sorafenib, further supporting the overall clinical benefit of this combination (197). Based on the results of IMbrave150, the combination of atezolizumab and bevacizumab was recently approved by the FDA for the treatment of unresectable HCC, and it is expected that this combination will become a new standard of care (198, 199).

The clinical benefit of combined anti-VEGFR TKIs and CPIs in HCC remains to be validated in randomized studies. Several Phase III studies are currently ongoing assessing the combination of PD-(L)1 antibodies and VEGFR TKIs, including pembrolizumab combined with lenvatinib, atezolizumab plus cabozantinib, and camrelizumab (SHR-1210) with apatinib in advanced HCC, the results of which will clarify the utility of antiangiogenic TKIs as immunomodulators in conjunction with CPIs (**Table 3**) (190).

Liver Metastases

The liver is a common metastatic site for most gastrointestinal (GI) cancers as well as for some non-GI tumors, such as lung cancer, renal cancer, breast cancer, and melanoma (200, 201). The presence of liver metastases is a negative prognostic factor in patients with lung and other cancers treated with CPIs (8, 202–204).

Differential organ responses in the liver vs. other anatomic sites have been recently reported in subgroup analyses from Phase III trials and retrospective series. Studies of CPIs have shown minimal therapeutic benefit as single agents or in combination with chemotherapy in patients with NSCLC and baseline liver metastases (29, 203, 205). In a subgroup of patients with metastatic melanoma treated with pembrolizumab as part of the KEYNOTE-001 trial, lung metastases were found to have the highest rate of complete response (42%), followed by peritoneal (37%) and liver (24%) metastatic lesions (206). In

90 patients with advanced malignancies (mostly melanoma and GI tumors) treated with CPIs in Phase I trials, the presence of liver metastasis was significantly associated with shorter OS, PFS, and lower rate of clinical benefit (204). In a retrospective review of 75 patients with advanced HCC, ORRs in the liver, lung, lymph node, and other intra-abdominal metastases were 22%, 41%, 26%, and 39%, respectively (207). Together, these clinical data suggest that hepatic metastases may be less responsive to CPIs than extrahepatic lesions.

One possible explanation for these clinical findings could be that secondary liver tumors harbor a more suppressive TME than primary anatomic sites. Consistent with this idea, results of a longitudinal analysis of metastases from a single patient with advanced ovarian cancer showed that each tumor deposit harbored divergent tumor genetics and distinct TMEs that evolved over time (208). Interestingly, progressing metastases were characterized by an immune cell excluded phenotype, whereas shrinking and stable metastases were well infiltrated by effector T cells and exhibited oligoclonal expansion of specific T-cell subsets (208). The presence of liver metastases from CPI-treated patients with NSCLC or melanoma was associated with abrogated CD8$^+$ T-cell infiltration (202). Differential hepatic CPI responses also conceptually align with the idea of organ-specific immunoregulation—or "immunostat"—which hypothesizes that tissue-specific factors within the liver can modulate the sensitivity of metastatic deposits derived from other sites to CPIs (102). This may, in part, be due to the unique immune biology of the liver which acts to promote tolerance and an immunosuppressive TME (183, 209, 210).

Recent clinical data from randomized trials support the notion that CPIs combined with anti-VEGF agents could augment response to CPI treatment in patients with secondary liver tumors. In a pre-specified analysis from IMpower150, atezolizumab combined with bevacizumab and chemotherapy significantly improved OS and PFS in a subgroup of NSCLC patients with liver metastases (**Figure 3**). Conversely, neither atezolizumab plus chemotherapy or bevacizumab combined with chemotherapy did not prolong survival or PFS in patients with liver metastases (154). This indicates that the dual targeting of PD-L1 and VEGF may be needed to induce clinically meaningful antitumor immunity in NSCLC patients with liver metastases. Collectively, these clinical data suggest that the combination of bevacizumab and atezolizumab in patients with primary or secondary liver cancers may thwart the induction of immunosuppressive immune cell types (e.g., MDSCs, Tregs, and TAMs) that are induced by tumor hypoxia, VEGF overexpression, or increased hepatic angiogenesis (50).

CHALLENGES AND FUTURE OPPORTUNITIES: WHERE DO WE GO FROM HERE?

A wealth of preclinical and clinical data supports the critical role that angiogenesis plays in modulating immunity in the TME. Randomized phase III studies have now shown that treatment

combining antiangiogenics with a PD-(L)1 antibody significantly increased survival compared to standard-of-care treatment in RCC, NSCLC, and HCC. Results from ongoing randomized studies will further clarify the clinical benefit of this treatment approach in other types of cancer.

So far, anti-VEGF plus CPI combinations appear particularly effective in tumors for which antiangiogenesis and PD-(L)1 blockade are effective as individual monotherapies. It therefore remains to be seen whether CPI/VEGF combinations are efficacious in diseases such as ovarian cancer and MSS colorectal cancer that are angiogenic but often lack markers of preexisting immunity and respond poorly to PD-(L)1 antibody monotherapy. If randomized studies of CPI/VEGF-inhibitor combinations in poorly immunogenic cancers are positive, we will have compelling clinical evidence that switching or reprograming a cold TME to one that is immunogenic is a realistic clinical proposition.

Combinations of antiangiogenic agents in combination with CPIs have been studied with either anti-VEGF antibodies or TKIs; however, it is not clear whether the efficacy of these two approaches with respect to augmenting antitumor immunity are comparable. A key question is, how important is the choice of antiangiogenic when it is combined with a CPI? Antiangiogenic TKIs inhibit a broad spectrum of tyrosine kinases and do not only inhibit proangiogenic signaling pathways, whereas antibodies are directed against either VEGF-A or VEGFR2. The contribution of non-VEGF angiogenic kinases or other oncogenic pathways to TME immunomodulation remains to be delineated. Relatedly, antiangiogenic TKIs with different target inhibition profiles may possess differential immunomodulatory capacities. On one hand, TKIs may leverage additional immune-promoting mechanisms via a broader biological activity against angiogenesis; on the other hand, differences between TKIs and VEGF antibodies in safety profile and toxicity burden may be important determinants of clinical benefit, treatment duration, or combinability with other treatments. Identification of the optimal dose of antiangiogenic agents for immune modulation is critical for success in the clinic. A recent systematic review of the immune effects of antiangiogenic TKI drugs in preclinical models concluded that low doses were immunostimulatory, whereas higher doses were immunosuppressive (211). This aligns with other preclinical data in tumor models that suggest that antiangiogenic therapies that are high dose, long term, or both can cause excessive vessel pruning and increased immunosuppression (13). The clinical significance of anti-VEGF dose (higher vs. lower) remains to be determined. Notably, data from completed Phase III studies in RCC, NSCLC, and HCC all used standard FDA-approved doses of antiangiogenic agents. The optimal duration of treatment and sequencing of drugs is also an important consideration that will require evaluation in well-controlled clinical studies.

In addition to the choice of anti-VEGF agent, the choice of CPI may also be relevant. No direct head-to-head clinical studies contrasting PD-1 and PD-L1 antibodies are available. Indirect data from systematic reviews or meta-analyses, mostly in NSCLC, are inconsistent with those from some studies showing no difference in efficacy between PD-1 or PD-L1 antibodies and from others indicating improved survival in favor of PD-1 inhibitors (212–214). Differential clinical efficacy of receptor- vs. ligand-based PD-1 blockade may be partially a function the tumor type being treated (214). Recent *in vitro* studies suggest that differences between receptor- vs. ligand-based antagonism may exist and have implications for combination treatments. In a study using a functional T-cell *in vitro* assay, PD-L1 antibodies were found to be more effective than PD-1 antibodies in inhibiting PD-1 signaling (215). A study using *in vivo* murine breast and colon cancer models showed that anti–PD-L1 (but not anti–PD-1) monotherapy was able to deplete CD80 ligand expression on tumor-infiltrating antigen-presenting cells, thereby inhibiting CTLA-4 axis through a Treg-dependent mechanism (216). The role of Tregs in this model is intriguing when considering anti–PD-(L)1/VEGF combinations given the role that Tregs play in VEGF-mediated immunosuppression. The clinical implications of these basic research data remain to be seen, and the results of ongoing trials with different combinations of PD-1/PD-L1 antibodies and anti-VEGF agents will be informative.

The encouraging results from Phase III trials of CPIs combined with anti-VEGF agents and their adoption as standards of care for patients with advanced disease motivates consideration of this approach in earlier, potentially curative, treatment settings. Anti–PD-(L)1 antibodies are currently approved as adjuvant treatment following resection in melanoma and following chemoradiation in NSCLC (217–219). Two Phase III studies are currently ongoing to evaluate anti–PD-L1 antibodies combined with bevacizumab in patients with HCC at high risk of tumor recurrence following potentially curative liver resection or tumor ablation (220, 221). These adjuvant studies are predicated on the hypothesis that dual PD-L1/VEGF blockade may reduce HCC recurrence by creating a more immune-favorable TME (221). PD-L1/VEGF blockade is also under study in a Phase III trial in combination with transarterial chemoembolization in patients with unresectable liver-confined HCC. This combination is based on the potential to amplify antitumor immune mechanisms induced by locoregional treatment (222).

Antiangiogenics combined with PD-1/PD-L1 antibodies are now standard-of-care frontline treatments for NSCLC, RCC, endometrial cancer, and HCC. These successes may represent the tip of the iceberg in efficacious combinations of CPIs and TME-modulating agents. At present, 76% of the almost 3000 PD-1/PD-L1 antibody clinical trials are testing combination regimens (7). This will likely result in continued rapid evolution of cancer treatment algorithms, potentially adding complexity to the processes of personalization and determining the right treatment approach for a patient's specific disease. In the era of combination CIT and modulation of specific facets of the TME, biomarker development is challenging. Unlike molecularly targeted drugs for which diagnostic biomarkers are typically a specific genetic aberration defined as a binary (yes or no) assay, CIT biomarkers are often continuous variables that have a gradation of association with clinical endpoints (12). Data

so far suggest that established CIT biomarkers such as PD-L1 expression or TMB have limited utility for dual CPI/VEGF blockade. Molecular profiling of the TME may represent a useful approach to identify patients with TME immune defects mediated by VEGF (223). For example, exploratory data from randomized studies in patients with RCC or HCC harboring a myeloid gene signature suggest that the use of bevacizumab with atezolizumab may be beneficial. Further translational studies that include either paired serial biopsies or neoadjuvant approaches will be needed to identify mechanisms of response and resistance to CIT treatment. The learnings from these types of trials will enable the rational development of next-generation combinations in which drugs targeting specific immune suppressive mechanisms in the TME are added to a PD-(L1)/ VEGF backbone. The search for predictive biomarkers in order to better select patients for CIT treatment is ongoing, but as yet no biomarkers have been validated for use in clinical practice.

CONCLUSION

Combined blockade of PD-(L)1 and VEGF pathways represents a significant therapeutic advance in cancer treatment. The immunomodulatory role of VEGF, now well described by data from preclinical and translational studies as well as randomized clinical trials, provides a compelling reason to continue the study of anti-VEGF and immune checkpoint therapies across the cancer spectrum. Ongoing trials will continue to discern the immunological mechanisms underpinning this treatment

approach and will further delineate the clinical benefit of this approach for the treatment of cancer.

SUPPLEMENTARY MATERIAL

The Supplementary Material for this article can be found online at: https://www.frontiersin.org/articles/10.3389/fimmu.2020. 598877/full#supplementary-material

REFERENCES

1. Couzin-Frankel J. Cancer Immunotherapy. *Science* (2013) 342(6165):1432. doi: 10.1126/science.342.6165.1432
2. Altmann DM. A Nobel Prize-worthy pursuit: cancer immunology and harnessing immunity to tumour neoantigens. *Immunology* (2018) 155 (3):283–4. doi: 10.1111/imm.13008
3. Rotte A, D'Orazi G, Bhandaru M. Nobel committee honors tumor immunologists. *J Exp Clin Cancer Res* (2018) 37(1):262. doi: 10.1186/ s13046-018-0937-6
4. Wolchok J. Putting the Immunologic Brakes on Cancer. *Cell* (2018) 175 (6):1452–4. doi: 10.1016/j.cell.2018.11.006
5. Waldman AD, Fritz JM, Lenardo MJ. A guide to cancer immunotherapy: from T cell basic science toclinical practice. *Nat Rev Immunol* (2020) 1–18. doi: 10.1038/s41577-020-0306-5
6. Wei SC, Duffy CR, Allison JP. Fundamental Mechanisms of Immune Checkpoint Blockade Therapy. *Cancer Discov* (2018) 8(9):1069. doi: 10.1158/2159-8290.CD-18-0367
7. Xin Yu J, Hodge JP, Oliva C, Neftelinov ST, Hubbard-Lucey VM, Tang J. Trends in clinical development for PD-1/PD-L1 inhibitors. *Nat Rev Drug Discov* (2020) 19(3):163–4. doi: 10.1038/d41573-019-00182-w
8. Topalian SL, Hodi FS, Brahmer JR, Gettinger SN, Smith DC, McDermott DF, et al. Five-Year Survival and Correlates Among Patients With Advanced Melanoma, Renal Cell Carcinoma, or Non–Small Cell Lung Cancer Treated With Nivolumab. *JAMA Oncol* (2019) 5(10):1411–20. doi: 10.1001/ jamaoncol.2019.2187
9. Haslam A, Prasad V. Estimation of the Percentage of US Patients With Cancer Who Are Eligible for and Respond to Checkpoint Inhibitor Immunotherapy Drugs. *JAMA Netw Open* (2019) 2(5):e192535–e. doi: 10.1001/jamanetworkopen.2019.2535

10. Fares CM, Van Allen EM, Drake CG, Allison JP, Hu-Lieskovan S. Mechanisms of Resistance to Immune Checkpoint Blockade: Why Does Checkpoint Inhibitor Immunotherapy Not Work for All Patients? *Am Soc Clin Oncol Educ Book* (2019) (39):147–64. doi: 10.1200/EDBK_240837
11. Sharma P, Hu-Lieskovan S, Wargo JA, Ribas A. Primary, Adaptive, and Acquired Resistance to Cancer Immunotherapy. *Cell* (2017) 168(4):707–23. doi: 10.1016/j.cell.2017.01.017
12. Hegde PS, Chen DS. Top 10 Challenges in Cancer Immunotherapy. *Immunity* (2020) 52(1):17–35. doi: 10.1016/j.immuni.2019.12.011
13. Fukumura D, Kloepper J, Amoozgar Z, Duda DG, Jain RK. Enhancing cancer immunotherapy using antiangiogenics: opportunities and challenges. *Nat Rev Clin Oncol* (2018) 15(5):325–40. doi: 10.1038/nrclinonc.2018.29
14. Topalian SL, Taube JM, Anders RA, Pardoll DM. Mechanism-driven biomarkers to guide immune checkpoint blockade in cancer therapy. *Nat Rev Cancer* (2016) 16(5):275–87. doi: 10.1038/nrc.2016.36
15. Yarchoan M, Hopkins A, Jaffee EM. Tumor Mutational Burden and Response Rate to PD-1 Inhibition. *New Engl J Med* (2017) 377(25):2500–1. doi: 10.1056/ NEJMc1713444
16. Lee JS, Ruppin E. Multiomics Prediction of Response Rates to Therapies to Inhibit Programmed Cell Death 1 and Programmed Cell Death 1 Ligand 1. *JAMA Oncol* (2019) 5(11):1614–8. doi: 10.1001/jamaoncol.2019.2311
17. Datta M, Coussens LM, Nishikawa H, Hodi FS, Jain RK. Reprogramming the Tumor Microenvironment to Improve Immunotherapy: Emerging Strategies and Combination Therapies. *Am Soc Clin Oncol Educ Book* (2019) 39):165–74. doi: 10.1200/EDBK_237987
18. Li X, Song W, Shao C, Shi Y, Han W. Emerging predictors of the response to the blockade of immune checkpoints in cancer therapy. *Cell Mol Immunol* (2019) 16(1):28–39. doi: 10.1038/s41423-018-0086-z
19. Palucka AK, Coussens LM. The Basis of Oncoimmunology. *Cell* (2016) 164 (6):1233–47. doi: 10.1016/j.cell.2016.01.049

20. Zemek RM, Chin WL, Nowak AK, Millward MJ, Lake RA, Lesterhuis WJ. Sensitizing the Tumor Microenvironment to Immune Checkpoint Therapy. *Front Immunol* (2020) 11:223. doi: 10.3389/fimmu.2020.00223

21. Murciano-Goroff YR, Warner AB, Wolchok JD. The future of cancer immunotherapy: microenvironment-targeting combinations. *Cell Res* (2020) 30(6):507–19. doi: 10.1038/s41422-020-0337-2

22. Zappasodi R, Merghoub T, Wolchok JD. Emerging Concepts for Immune Checkpoint Blockade-Based Combination Therapies. *Cancer Cell* (2018) 33(4):581–98. doi: 10.1016/j.ccell.2018.03.005

23. De Sousa Linhares A, Leitner J, Grabmeier-Pfistershammer K, Steinberger P. Not All Immune Checkpoints Are Created Equal. *Front Immunol* (2018) 9:1909. doi: 10.3389/fimmu.2018.01909

24. Lichtenegger FS, Rothe M, Schnorfeil FM, Deiser K, Krupka C, Augsberger C, et al. Targeting LAG-3 and PD-1 to Enhance T Cell Activation by Antigen-Presenting Cells. *Front Immunol* (2018) 9:385. doi: 10.3389/fimmu.2018.00385

25. Wolf Y, Anderson AC, Kuchroo VK. TIM3 comes of age as an inhibitory receptor. *Nat Rev Immunol* (2020) 20(3):173–85. doi: 10.1038/s41577-019-0224-6

26. Bailly C, Thuru X, Quesnel B. Combined cytotoxic chemotherapy and immunotherapy of cancer:moderntimes. *NAR Cancer* (2020) 2(1):1–20. doi: 10.1093/narcan/zcaa002

27. Heinhuis KM, Ros W, Kok M, Steeghs N, Beijnen JH, Schellens JHM. Enhancing antitumor response by combining immune checkpoint inhibitors with chemotherapy in solid tumors. *Ann Oncol* (2019) 30(2):219–35. doi: 10.1093/annonc/mdy551

28. Melosky B, Juergens R, Hirsh V, McLeod D, Leighl N, Tsao M-S, et al. Amplifying Outcomes: Checkpoint Inhibitor Combinations in First-Line Non-Small Cell Lung Cancer. *Oncologist* (2020) 25(1):64–77. doi: 10.1634/theoncologist.2019-0027

29. West H, McCleod M, Hussein M, Morabito A, Rittmeyer A, Conter HJ, et al. Atezolizumab in combination with carboplatin plus nab-paclitaxel chemotherapy compared with chemotherapy alone as first-line treatment for metastatic non-squamous non-small-cell lung cancer (IMpower130): a multicentre, randomised, open-label, phase 3 trial. *Lancet Oncol* (2019) 20(7):924–37. doi: 10.1016/S1470-2045(19)30167-6

30. Schmid P, Adams S, Rugo HS, Schneeweiss A, Barrios CH, Iwata H, et al. Atezolizumab and Nab-Paclitaxel in Advanced Triple-Negative Breast Cancer. *New Engl J Med* (2018) 379(22):2108–21. doi: 10.1056/NEJMoa1809615

31. Galsky MD, Arija JÁA, Bamias A, Davis ID, De Santis M, Kikuchi E, et al. Atezolizumab with or without chemotherapy in metastatic urothelial cancer (IMvigor130): a multicentre, randomised, placebo-controlled phase 3 trial. *Lancet* (2020) 395(10236):1547–57. doi: 10.1016/S0140-6736(20)30230-0

32. Keam S, Gill S, Ebert MA, Nowak AK, Cook AM. Enhancing the efficacy of immunotherapy using radiotherapy. *Clin Transl Immunol* (2020) 9(9):e1169. doi: 10.1002/cti2.1169

33. Hecht M, Gostian A-O, Eckstein M, Rutzner S, von der Grün J, Illmer T, et al. A multicenter phase II trial of the combination cisplatin/docetaxel/durvalumab/tremelimumab as single-cycle induction treatment in locally advanced HNSCC (CheckRad-CD8 trial). *J Clin Oncol* (2020) 38(15_suppl):6519. doi: 10.1200/JCO.2020.38.15_suppl.6519

34. Gutzmer R, Stroyakovskiy D, Gogas H, Robert C, Lewis K, Protsenko S, et al. Atezolizumab, vemurafenib, and cobimetinib as first-line treatment for unresectable advanced BRAFV600 mutation-positive melanoma (IMspire150): primary analysis of the randomised, double-blind, placebo-controlled, phase 3 trial. *Lancet* (2020) 395(10240):1835–44. doi: 10.1016/S0140-6736(20)30934-X

35. Eng C, Kim TW, Bendell J, Argilés G, Tebbutt NC, Di Bartolomeo M, et al. Atezolizumab with or without cobimetinib versus regorafenib inpreviously treated metastatic colorectal cancer (IMblaze370): a multicentre, open-label, phase 3,randomised, controlled trial. *Lancet Oncol* (2019)20(6):849–61. doi: 10.1016/S1470-2045(19)30027-0

36. Arance AM, Gogas H, Dreno B, Flaherty KT, Demidov L, Stroyakovskiy D, et al. Combination treatment with cobimetinib (C) and atezolizumab (A) vs pembrolizumab (P) in previously untreated patients (pts) with BRAFV600 wild type (wt) advanced melanoma: Primary analysis from the phase III IMspire170 trial. *Ann Oncol* (2019) 30:v906. doi: 10.1093/annonc/mdz394.066

37. Hanahan D, Weinberg RA. Hallmarks of Cancer: The Next Generation. *Cell* (2011) 144(5):646–74. doi: 10.1016/j.cell.2011.02.013

38. Khan KA, Kerbel RS. Improving immunotherapy outcomes with anti-angiogenic treatments and vice versa. *Nat Rev Clin Oncol* (2018) 15(5):310–24. doi: 10.1038/nrclinonc.2018.9

39. Chen DS, Mellman I. Oncology Meets Immunology: The Cancer-Immunity Cycle. *Immunity* (2013) 39(1):1–10. doi: 10.1016/j.immuni.2013.07.012

40. Kim JM, Chen DS. Immune escape to PD-L1/PD-1 blockade: seven steps to success (or failure). *Ann Oncol* (2016) 27(8):1492–504. doi: 10.1093/annonc/mdw217

41. Galon J, Bruni D. Approaches to treat immune hot, altered and cold tumours with combination immunotherapies. *Nat Rev Drug Discov* (2019) 18(3):197–218. doi: 10.1038/s41573-018-0007-y

42. Hegde PS, Karanikas V, Evers S. The Where, the When, and the How of Immune Monitoring for Cancer Immunotherapies in the Era of Checkpoint Inhibition. *Clin Cancer Res* (2016) 22(8):1865–74. doi: 10.1158/1078-0432.CCR-15-1507

43. Binnewies M, Roberts EW, Kersten K, Chan V, Fearon DF, Merad M, et al. Understanding the tumor immune microenvironment (TIME) for effective therapy. *Nat Med* (2018) 24(5):541–50. doi: 10.1038/s41591-018-0014-x

44. Lin Z, Zhang Q, Luo W. Angiogenesis inhibitors as therapeutic agents in cancer: Challenges and future directions. *Eur J Pharmacol* (2016) 793:76–81. doi: 10.1016/j.ejphar.2016.10.039

45. Jain RK. Antiangiogenesis Strategies Revisited: From Starving Tumors to Alleviating Hypoxia. *Cancer Cell* (2014) 26(5):605–22. doi: 10.1016/j.ccell.2014.10.006

46. Simons M, Gordon E, Claesson-Welsh L. Mechanisms and regulation of endothelial VEGF receptor signalling. *Nat Rev Mol Cell Biol* (2016) 17(10):611–25. doi: 10.1038/nrm.2016.87

47. Apte RS, Chen DS, Ferrara N. VEGF in Signaling and Disease: Beyond Discovery and Development. *Cell* (2019) 176(6):1248–64. doi: 10.1016/j.cell.2019.01.021

48. Sullivan LA, Brekken RA. The VEGF family in cancer and antibody-based strategies for their inhibition. *MAbs* (2010) 2(2):165–75. doi: 10.4161/mabs.2.2.11360

49. Ferrara N, Adamis AP. Ten years of anti-vascular endothelial growth factor therapy. *Nat Rev Drug Discov* (2016) 15(6):385–403. doi: 10.1038/nrd.2015.17

50. Chen DS, Hurwitz H. Combinations of Bevacizumab With Cancer Immunotherapy. *Cancer J* (2018) 24(4):193. doi: 10.1097/PPO.0000000000000327

51. Hegde PS, Wallin JJ, Mancao C. Predictive markers of anti-VEGF and emerging role of angiogenesis inhibitors as immunotherapeutics. *Semin Cancer Biol* (2018) 52:117–24. doi: 10.1016/j.semcancer.2017.12.002

52. Shigeta K, Datta M, Hato T, Kitahara S, Chen IX, Matsui A, et al. Dual Programmed Death Receptor-1 and Vascular EndothelialGrowthFactor Receptor-2 Blockade Promotes Vascular Normalization and Enhances Antitumor Immune Responsesin Hepatocellular Carcinoma. *Hepatology* (2019) 71:1247–61. doi: 10.1002/hep.30889

53. Kimura T, Kato Y, Ozawa Y, Kodama K, Ito J, Ichikawa K, et al. Immunomodulatory activity of lenvatinib contributes to antitumor activity in the Hepa1-6 hepatocellular carcinoma model. *Cancer Sci* (2018) 109(12):3993–4002. doi: 10.1111/cas.13806

54. Kim CG, Jang M, Kim Y, Leem G, Kim KH, Lee H, et al. VEGF-A drives TOX-dependent T cell exhaustion in anti–PD-1–resistant microsatellite stable colorectal cancers. *Sci Immunol* (2019) 4(41):eaay0555. doi: 10.1126/sciimmunol.aay0555

55. Meder L, Schuldt P, Thelen M, Schmitt A, Dietlein F, Klein S, et al. Combined VEGF and PD-L1 Blockade Displays Synergistic Treatment Effects in an Autochthonous Mouse Model of Small Cell Lung Cancer. *Cancer Res* (2018) 78:4270.

56. Yasuda S, Sho M, Yamato I, Yoshiji H, Wakatsuki K, Nishiwada S, et al. Simultaneous blockade of programmed death 1 and vascular endothelial growth factor receptor 2 (VEGFR2) induces synergistic anti-tumour effect in vivo. *Clin Exp Immunol* (2013) 17:500–6.

57. Voron T, Colussi O, Marcheteau E, Pernot S, Nizard M, Pointet A-L, et al. VEGF-A modulates expression of inhibitory checkpoints on CD8+ T cells in tumors. *J Exp Med* (2015) 212(2):139–48. doi: 10.1084/jem.20140559

58. Allen E, Jabouille A, Rivera LB, Lodewijckx I, Missiaen R, Steri V, et al. Combined antiangiogenic and anti–PD-L1 therapy stimulates tumorimmunity through HEV formation. *Sci Transl Med* (2017) 9:eaak9679.

59. Läubli H, Müller P, D'amico L, Buchi M, Kashyap AS, Zippelius A, et al. The multi-receptor inhibitor axitinib reverses tumor-inducedimmunosuppression and potentiates treatment with immune-modulatory antibodies in preclinical murine models. *Cancer Immunol Immunother* (2018) 67:815–24.

60. Motz GT, Coukos G. Deciphering and Reversing Tumor Immune Suppression. *Immunity* (2013) 39(1):61–73. doi: 10.1016/j.immuni. 2013.07.005

61. Gabrilovich DI, Chen HL, Girgis KR, Cunningham HT, Meny GM, Nadaf S, et al. Production of vascular endothelial growth factor by human tumors inhibits the functional maturation of dendritic cells. *Nat Med* (1996) 2 (10):1096–103. doi: 10.1038/nm1096-1096

62. Mimura K, Kono K, Takahashi A, Kawaguchi Y, Fujii H. Vascular endothelial growth factor inhibits the function of human mature dendritic cells mediated by VEGF receptor-2. *Cancer Immunol Immunother* (2007) 56 (6):761–70. doi: 10.1007/s00262-006-0234-7

63. Dikov MM, Ohm JE, Ray N, Tchekneva EE, Burlison J, Moghanaki D, et al. Differential Roles of Vascular Endothelial Growth Factor Receptors 1 and 2 in Dendritic Cell Differentiation. *J Immunol* (2005) 174(1):215. doi: 10.4049/jimmunol.174.1.215

64. Oussa NAE, Dahmani A, Gomis M, Richaud M, Andreev E, Navab-Daneshmand A-R, et al. VEGF Requires the Receptor NRP-1 To Inhibit Lipopolysaccharide-Dependent Dendritic Cell Maturation. *J Immunol* (2016) 197(10):3927. doi: 10.4049/jimmunol.1601116

65. Curiel TJ, Wei S, Dong H, Alvarez X, Cheng P, Mottram P, et al. Blockade of B7-H1 improves myeloid dendritic cell–mediated antitumor immunity. *Nat Med* (2003) 9(5):562–7. doi: 10.1038/nm863

66. Alfaro C, Suarez N, Gonzalez A, Solano S, Erro L, Dubrot J, et al. Influence of bevacizumab, sunitinib and sorafenib as single agents or in combination on the inhibitory effects of VEGF on human dendritic cell differentiation from monocytes. *Br J Cancer* (2009) 100(7):1111–9. doi: 10.1038/sj.bjc.6604965

67. Osada T, Chong G, Tansik R, Hong T, Spector N, Kumar R, et al. The effect of anti-VEGF therapy on immature myeloid cell and dendritic cells in cancer patients. *Cancer Immunol Immunother* (2008) 57(8):1115–24. doi: 10.1007/s00262-007-0441-x

68. Mayoux M, Roller A, Pulko V, Sammicheli S, Chen S, Sum E, et al. Dendritic cells dictate responses to PD-L1 blockade cancer immunotherapy. *Sci Trans Med* (2020) 12(534):eaav7431. doi: 10.1126/scitranslmed.aav7431

69. Georganaki M, van Hooren L, Dimberg A. Vascular Targeting to Increase the Efficiency of Immune Checkpoint Blockade in Cancer. *Front Immunol* (2018) 9:3081. doi: 10.3389/fimmu.2018.03081

70. Ley K, Laudanna C, Cybulsky MI, Nourshargh S. Getting to the site of inflammation: the leukocyte adhesion cascade updated. *Nat Rev Immunol* (2007) 7(9):678–89. doi: 10.1038/nri2156

71. Munn LL, Jain RK. Vascular regulation of antitumor immunity. *Science* (2019) 365(6453):544. doi: 10.1126/science.aaw7875

72. Bouzin C, Brouet A, De Vriese J, DeWever J, Feron O. Effects of Vascular Endothelial Growth Factor on the Lymphocyte-Endothelium Interactions: Identification of Caveolin-1 and Nitric Oxide as Control Points of Endothelial Cell Anergy. *J Immunol* (2007) 178(3):1505. doi: 10.4049/jimmunol.178.3.1505

73. Motz GT, Santoro SP, Wang L-P, Garrabrant T, Lastra RR, Hagemann IS, et al. Tumor endothelium FasL establishes a selective immune barrier promoting tolerance in tumors. *Nat Med* (2014) 20(6):607–15. doi: 10.1038/nm.3541

74. Zhang L, Conejo-Garcia JR, Katsaros D, Gimotty PA, Massobrio M, Regnani G, et al. Intratumoral T Cells, Recurrence, and Survival in Epithelial Ovarian Cancer. *New Engl J Med* (2003) 348(3):203–13. doi: 10.1056/NEJMoa020177

75. De Palma M, Jain RK. CD4+ T Cell Activation and Vascular Normalization: Two Sides of the Same Coin? *Immunity* (2017) 46(5):773–5. doi: 10.1016/j.immuni.2017.04.015

76. Hamzah J, Jugold M, Kiessling F, Rigby P, Manzur M, Marti HH, et al. Vascular normalization in Rgs5-deficient tumours promotes immune destruction. *Nature* (2008) 453(7193):410–4. doi: 10.1038/nature06868

77. Huang Y, Yuan J, Righi E, Kamoun WS, Ancukiewicz M, Nezivar J, et al. Vascular normalizing doses of antiangiogenic treatment reprogram the immunosuppressive tumor microenvironment and enhance immunotherapy. *Proc Natl Acad Sci* (2012) 109(43):17561. doi: 10.1073/pnas.1215397109

78. Tian L, Goldstein A, Wang H, Ching Lo H, Sun Kim I, Welte T, et al. Mutual regulation of tumour vessel normalization and immunostimulatory reprogramming. *Nature* (2017) 544(7649):250–4. doi: 10.1038/nature21724

79. Zheng X, Fang Z, Liu X, Deng S, Zhou P, Wang X, et al. Increased vessel perfusion predicts the efficacy of immune checkpoint blockade. *J Clin Invest* (2018) 128(5):2104–15. doi: 10.1172/JCI96582

80. Rahma OE, Hodi FS. The Intersection Between Tumor Angiogenesis and ImmuneSuppression. *Clin Cancer Res* (2019) 1543:2018. doi: 10.1158/1078-0432.CCR-18-1543

81. Qu P, Wang L-z, Lin PC. Expansion and functions of myeloid-derived suppressor cells in the tumor microenvironment. *Cancer Lett* (2016) 380 (1):253–6. doi: 10.1016/j.canlet.2015.10.022

82. De Cicco P, Ercolano G, Ianaro A. The New Era of Cancer Immunotherapy: Targeting Myeloid-Derived Suppressor Cells to Overcome Immune Evasion. *Front Immunol* (2020) 11:1680. doi: 10.3389/fimmu.2020.01680

83. Vetsika E-K, Koukos A, Kotsakis A. Myeloid-Derived Suppressor Cells: Major Figures that Shape theImmunosuppressive and Angiogenic Network in Cancer. *Cells* (2019) 8(12):1647. doi: 10.3390/cells8121647

84. Trovato R, Canè S, Petrova V, Sartoris S, Ugel S, De Sanctis F. The Engagement Between MDSCs and Metastases: Partners in Crime. *Front Oncol* (2020) 10:165. doi: 10.3389/fonc.2020.00165

85. Rudd CE. A new perspective in cancer immunotherapy: PD-1 on myeloid cells takes center stage in orchestrating immune checkpoint blockade. *Sci Immunol* (2020) 5(43):eaaz8128. doi: 10.1126/sciimmunol.aaz8128

86. Strauss L, Mahmoud MAA, Weaver JD, Tijaro-Ovalle NM, Christofides A, Wang Q, et al. Targeted deletion of PD-1 in myeloid cells induces antitumor immunity. *Sci Immunol* (2020) 5(43):eaay1863. doi: 10.1126/sciimmunol.aay1863

87. Kusmartsev S, Eruslanov E, Kübler H, Tseng T, Sakai Y, Su Z, et al. Oxidative Stress Regulates Expression of VEGFR1 in Myeloid Cells: Link to Tumor-Induced Immune Suppression in Renal Cell Carcinoma. *J Immunol* (2008) 181(1):346. doi: 10.4049/jimmunol.181.1.346

88. Guislain A, Gadiot J, Kaiser A, Jordanova ES, Broeks A, Sanders J, et al. Sunitinib pretreatment improves tumor-infiltrating lymphocyte expansion by reduction in intratumoral content of myeloid-derived suppressor cells in human renal cell carcinoma. *Cancer Immunol Immunother* (2015) 64 (10):1241–50. doi: 10.1007/s00262-015-1735-z

89. Finke J, Ko J, Rini B, Rayman P, Ireland J, Cohen P. MDSC as a mechanism of tumor escape from sunitinib mediated anti-angiogenic therapy. *Int Immunopharmacol* (2011) 11(7):856–61. doi: 10.1016/j.intimp.2011.01.030

90. Chang C-J, Yang Y-H, Chiu C-J, Lu L-C, Liao C-C, Liang C-W, et al. Targeting tumor-infiltrating Ly6G+ myeloid cells improves sorafenib efficacy in mouse orthotopic hepatocellular carcinoma. *Int J Cancer* (2018) 142(9):1878–89. doi: 10.1002/ijc.31216

91. Shojaei F, Wu X, Malik AK, Zhong C, Baldwin ME, Schanz S, et al. Tumor refractoriness to anti-VEGF treatment is mediated by CD11b+Gr1+ myeloid cells. *Nat Biotechnol* (2007) 25(8):911–20. doi: 10.1038/nbt1323

92. Takeuchi Y, Nishikawa H. Roles of regulatory T cells in cancer immunity. *Int Immunol* (2016) 28(8):401–9. doi: 10.1093/intimm/dxw025

93. Courau T, Nehar-Belaid D, Florez L, Levacher B, Vazquez T, Brimaud F, et al. TGF-β and VEGF cooperatively control the immunotolerant tumorenvironment and the efficacy of cancer immunotherapies. *JCI Insight* (2016) 1(9):e85974. doi: 10.1172/jci.insight.85974

94. Zhu P, Hu C, Hui K, Jiang X. The role and significance of VEGFR2(+) regulatory T cells in tumor immunity. *Onco Targets Ther* (2017) 10:4315–9. doi: 10.2147/OTT.S142085

95. Terme M, Pernot S, Marcheteau E, Sandoval F, Benhamouda N, Colussi O, et al. VEGFA-VEGFR Pathway Blockade Inhibits Tumor-Induced Regulatory T-cell Proliferation in Colorectal Cancer. *Cancer Res* (2013) 73 (2):539. doi: 10.1158/0008-5472.CAN-12-2325

96. Adotevi O, Pere H, Ravel P, Haicheur N, Badoual C, Merillon N, et al. A Decrease of Regulatory T Cells Correlates With Overall SurvivalAfter Sunitinib-based Antiangiogenic Therapy in Metastatic Renal Cancer Patients. *J Immunother* (2010) 33(9):991–8. doi: 10.1097/CJI.0b013e3181f4c208

97. Kato Y, Tabata K, Kimura T, Yachie-Kinoshita A, Ozawa Y, Yamada K, et al. Lenvatinib plus anti-PD-1 antibody combination treatment activates CD8+ T cells through reduction of tumor-associated macrophage and activation of

the interferon pathway. *PloS One* (2019) 14(2):e0212513. doi: 10.1371/journal.pone.0212513

98. Wallin JJ, Bendell JC, Funke R, Sznol M, Korski K, Jones S, et al. Atezolizumab in combination with bevacizumab enhances antigen-specific T-cell migration in metastatic renal cell carcinoma. *Nat Commun* (2016) 7 (1):12624. doi: 10.1038/ncomms12624

99. McDermott DF, Huseni MA, Atkins MB, Motzer RJ, Rini BI, Escudier B, et al. Clinical activity and molecular correlates of response toatezolizumab alone or in combination with bevacizumab versus sunitinib in renal cellcarcinoma. *Nat Med* (2018) 24(6):749–57. doi: 10.1038/s41591-018-0053-3

100. Zhu A, Guan Y, Abbas A, Koeppen H, Lu S, Hsu C-H, et al. Abstract CT044: Genomic correlates of clinical benefits from atezolizumab combined with bevacizumab vs. atezolizumab alone in patients with advanced hepatocellular carcinoma (HCC). *Cancer Res* (2020) 80:CT044.

101. Koinis F, Vetsika EK, Aggouraki D, Skalidaki E, Koutoulaki A, Gkioulmpasani M, et al. Effect of First-Line Treatment on Myeloid-Derived Suppressor Cells' Subpopulations in the Peripheral Blood of Patients with Non–Small Cell Lung Cancer. *J Thorac Oncol* (2016) 11 (8):1263–72. doi: 10.1016/j.jtho.2016.04.026

102. Pao W, Ooi C-H, Birzele F, Ruefli-Brasse A, Cannarile MA, Reis B, et al. Tissue-Specific Immunoregulation: A Call for Better Understanding of the "Immunostat" in the Context of Cancer. *Cancer Discov* (2018) 8(4):395. doi: 10.1158/2159-8290.CD-17-1320

103. Rini BI, Powles T, Atkins MB, Escudier B, McDermott DF, Suarez C, et al. Atezolizumab plus bevacizumab versus sunitinib in patients withpreviously untreated metastatic renal cell carcinoma (IMmotion151): a multicentre, open-label, phase3, randomised controlled trial. *Lancet* (2019) 393 (10189):2404–15. doi: 10.1016/S0140-6736(19)30723-8

104. Socinski MA, Jotte RM, Cappuzzo F, Orlandi F, Stroyakovskiy D, Nogami N, et al. Atezolizumab for First-Line Treatment of Metastatic Nonsquamous NSCLC. *New Engl J Med* (2018) 378(24):2288–301. doi: 10.1056/NEJMoa1716948

105. Motzer RJ, Penkov K, Haanen J, Rini B, Albiges L, Campbell MT, et al. Avelumab plus Axitinib versus Sunitinib for Advanced Renal-Cell Carcinoma. *New Engl J Med* (2019) 380(12):1103–15. doi: 10.1056/NEJMoa1816047

106. Lee MS, Ryoo B-Y, Hsu C-H, Numata K, Stein S, Verret W, et al. Atezolizumab with or without bevacizumab in unresectable hepatocellular carcinoma (GO30140): an open-label, multicentre, phase 1b study. *Lancet Oncol* (2020) 21(6):808–20. doi: 10.1016/S1470-2045(20)30156-X

107. Finn RS, Qin S, Ikeda M, Galle PR, Ducreux M, Kim T-Y, et al. Atezolizumab plus Bevacizumab in Unresectable Hepatocellular Carcinoma. *New Engl J Med* (2020) 382(20):1894–905. doi: 10.1056/NEJMoa1915745

108. Mettu NB, Twohy E, Ou FS, Halfdanarson TR, Lenz HJ, Breakstone R, et al. BACCI: A phase II randomized, double-blind, multicenter, placebo-controlled study of capecitabine (C) bevacizumab (B) plus atezolizumab (A) or placebo (P) in refractory metastatic colorectal cancer (mCRC): An ACCRU network study. *Ann Oncol* (2019) 30:v203. doi: 10.1093/annonc/mdz246.011

109. Rini BI, Plimack ER, Stus V, Gafanov R, Hawkins R, Nosov D, et al. Pembrolizumab plus Axitinib versus Sunitinib for Advanced Renal-Cell Carcinoma. *New Engl J Med* (2019) 380(12):1116–27. doi: 10.1056/NEJMoa1816714

110. Makker V, Rasco D, Vogelzang NJ, Brose MS, Cohn AL, Mier J, et al. Lenvatinib plus pembrolizumab in patients with advanced endometrial cancer: an interim analysis of a multicentre, open-label, single-arm, phase 2 trial. *Lancet Oncol* (2019) 20(5):711–8. doi: 10.1016/S1470-2045(19)30020-8

111. Makker V, Taylor MH, Aghajanian C, Oaknin A, Mier J, Cohn AL, et al. 994O - Lenvatinib (LEN) and pembrolizumab (PEMBRO) in advanced endometrial cancer (EC). *Ann Oncol* (2019) 30:v404–5. doi: 10.1093/annonc/mdz250.002

112. Choueiri TK, Motzer RJ. Systemic Therapy for Metastatic Renal-Cell Carcinoma. *New Engl J Med* (2017) 376(4):354–66. doi: 10.1056/NEJMra1601333

113. Motzer RJ, Escudier B, McDermott DF, George S, Hammers HJ, Srinivas S, et al. Nivolumab versus Everolimus in Advanced Renal-Cell Carcinoma. *New Engl J Med* (2015) 373(19):1803–13. doi: 10.1056/NEJMoa1510665

114. Gao X, McDermott DF, Michaelson MD. Enhancing Antitumor Immunity with Antiangiogenic Therapy: A Clinical Model in Renal Cell Carcinoma? *Oncologist* (2019) 24(6):725–7. doi: 10.1634/theoncologist.2019-0165

115. Atkins MB, Plimack ER, Puzanov I, Fishman MN, McDermott DF, Cho DC, et al. Axitinib in combination with pembrolizumab in patients with advanced renal cell cancer: a non-randomised, open-label, dose-finding, and dose-expansion phase 1b trial. *Lancet Oncol* (2018) 19(3):405–15. doi: 10.1016/S1470-2045(18)30081-0

116. Choueiri TK, Larkin J, Oya M, Thistlethwaite F, Martignoni M, Nathan P, et al. Preliminary results for avelumab plus axitinib as first-line therapy in patients with advanced clear-cell renal-cell carcinoma (JAVELIN Renal 100): an open-label, dose-finding and dose-expansion, phase 1b trial. *Lancet Oncol* (2018) 19(4):451–60. doi: 10.1016/S1470-2045(18)30107-4

117. Amin A, Plimack ER, Ernstoff MS, Lewis LD, Bauer TM, McDermott DF, et al. Safety and efficacy of nivolumab in combination with sunitinib or pazopanib in advanced or metastatic renal cell carcinoma: the CheckMate 016 study. *J ImmunoTher Cancer* (2018) 6(1):109. doi: 10.1186/s40425-018-0420-0

118. Albiges L, Powles T, Staehler M, Bensalah K, Giles RH, Hora M, et al. Updated European Association of Urology Guidelines on Renal Cell Carcinoma: Immune Checkpoint Inhibition Is the New Backbone in First-line Treatment of Metastatic Clear-cell Renal Cell Carcinoma. *Eur Urol* (2019) 76(2):151–6. doi: 10.1016/j.eururo.2019.05.022

119. Huang JJ, Hsieh JJ. The Therapeutic Landscape of Renal Cell Carcinoma: From the Dark Age to the Golden Age. *Semin Nephrol* (2020) 40(1):28–41. doi: 10.1016/j.semnephrol.2019.12.004

120. Overman MJ, Ernstoff MS, Morse MA. Where We Stand With Immunotherapy in Colorectal Cancer: Deficient Mismatch Repair, Proficient Mismatch Repair, and Toxicity Management. *Am Soc Clin Oncol Educ Book* (2018) (38):239–47. doi: 10.1200/EDBK_200821

121. Dekker E, Tanis PJ, Vleugels JLA, Kasi PM, Wallace MB. Colorectal cancer. *Lancet* (2019) 394(10207):1467–80. doi: 10.1016/S0140-6736(19)32319-0

122. Lichtenstern RC, Ngu KR, Shalapour S, Karin M. Immunotherapy, Inflammation and Colorectal Cancer. *Cells* (2020) 9(3):618. doi: 10.3390/cells9030618

123. Le DT, Durham JN, Smith KN, Wang H, Bartlett BR, Aulakh LK, et al. Mismatch repair deficiency predicts response of solid tumors to PD-1blockade. *Science* (2017) 357(6349):409. doi: 10.1126/science.aan6733

124. Le DT, Uram JN, Wang H, Bartlett BR, Kemberling H, Eyring AD, et al. PD-1 Blockade in Tumors with Mismatch-RepairDeficiency. *New Engl J Med* (2015) 372(26):2509–20. doi: 10.1056/NEJMoa1500596

125. Overman MJ, McDermott R, Leach JL, Lonardi S, Lenz H-J, Morse MA, et al. Nivolumab in patients with metastatic DNA mismatch repair-deficient or microsatellite instability-high colorectal cancer (CheckMate 142): an open-label, multicentre, phase 2 study. *Lancet Oncol* (2017) 18(9):1182–91. doi: 10.1016/S1470-2045(17)30422-9

126. Fabrizio DA, George TJ Jr., Dunne RF, Frampton G, Sun J, Gowen K, et al. Beyond microsatellite testing: assessment of tumor mutational burden identifies subsets of colorectal cancer who may respond to immune checkpointinhibition. *J Gastrointest Oncol* (2018) 9:610–7. doi: 10.21037/jgo.2018.05.06

127. Ganesh K, Stadler ZK, Cercek A, Mendelsohn RB, Shia J, Segal NH, et al. Immunotherapy in colorectal cancer: rationale, challenges and potential. *Nat Rev Gastroenterol Hepatol* (2019) 16(6):361–75. doi: 10.1038/s41575-019-0126-x

128. Morse MA, Hochster H, Benson A. Perspectives on Treatment of Metastatic Colorectal Cancer with Immune Checkpoint Inhibitor Therapy. *Oncologist* (2020) 25(1):33–45. doi: 10.1634/theoncologist.2019-0176

129. Thomas J, Leal A, Overman MJ. Clinical Development of Immunotherapy for Deficient Mismatch RepairColorectal Cancer. *Clin Colorectal Cancer* (2020) 19:73–81. doi: 10.1016/j.clcc.2020.02.002

130. Andre T, Shiu K-K, Kim TW, Jensen BV, Jensen LH, Punt CJA, et al. Pembrolizumab versus chemotherapy for microsatellite instability-high/mismatch repair deficient metastatic colorectal cancer: The phase 3 KEYNOTE-177 Study. *J Clin Oncol* (2020) 38(18_suppl):LBA4–LBA. doi: 10.1200/JCO.2020.38.18_suppl.LBA4

131. Hochster HS, Bendell JC, Cleary JM, Foster P, Zhang W, He X, et al. Efficacy and safety of atezolizumab (atezo) and bevacizumab (bev) in a phase Ib study of microsatellite instability (MSI)-high metastatic colorectal cancer (mCRC). *J Clin Oncol* (2017) 35(4_suppl):673. doi: 10.1200/JCO.2017.35.4_suppl.673

132. Allegra CJ, Yothers G, O'Connell MJ, Sharif S, Petrelli NJ, Colangelo LH, et al. Phase III Trial Assessing Bevacizumab in Stages II and III Carcinoma of

the Colon: Results of NSABP Protocol C-08. *J Clin Oncol* (2010) 29(1):11–6. doi: 10.1200/JCO.2010.30.0855

133. Pogue-Geile K, Yothers G, Taniyama Y, Tanaka N, Gavin P, Colangelo L, et al. Defective Mismatch Repair and Benefit from Bevacizumab for Colon Cancer: Findings from NSABP C-08. *JNCI: J Natl Cancer Inst* (2013) 105 (13):989–92. doi: 10.1093/jnci/djt140

134. Lee JJ, Yothers G, Jacobs SA, Sanoff HK, Cohen DJ, Guthrie KA, et al. Colorectal Cancer Metastatic dMMR Immuno-Therapy (COMMIT) study (NRG- GI004/SWOG-S1610): A randomized phase III study of mFOLFOX6/bevacizumab combination chemotherapy with or without atezolizumab or atezolizumab monotherapy in the first-line treatment of patients with deficient DNA mismatch repair (dMMR) metastatic colorectal cancer. *J Clin Oncol* (2018) 36(15_suppl):TPS3615–TPS. doi: 10.1200/JCO.2018.36.15_suppl.TPS3615

135. Overman MJ, Lonardi S, Wong KYM, Lenz H-J, Gelsomino F, Aglietta M, et al. Durable Clinical Benefit With Nivolumab Plus Ipilimumab in DNA Mismatch Repair–Deficient/Microsatellite Instability–High Metastatic Colorectal Cancer. *J Clin Oncol* (2018) 36(8):773–9. doi: 10.1200/JCO.2017.76.9901

136. Chalabi M, Fanchi LF, Van den Berg JG, Beets GL, Lopez-Yurda M, Aalbers AG, et al. LBA37_PR - Neoadjuvant ipilimumab plus nivolumab in early stage colon cancer. *Ann Oncol* (2018) 29:viii731. doi: 10.1093/annonc/mdy424.047

137. Chen EX, Jonker DJ, Kennecke HF, Berry SR, Couture F, Ahmad CE, et al. CCTG CO.26 trial: A phase II randomized study of durvalumab (D) plus tremelimumab (T) and best supportive care (BSC) versus BSC alone in patients (pts) with advanced refractory colorectal carcinoma (rCRC). *J Clin Oncol* (2019) 37(4_suppl):481–. doi: 10.1200/JCO.2019.37.4_suppl.481

138. Chen EX, Jonker DJ, Loree JM, Kennecke HF, Berry SR, Couture F, et al. Effect of Combined Immune Checkpoint Inhibition vs Best SupportiveCare Alone in Patients With Advanced Colorectal Cancer: The Canadian Cancer Trials Group CO.26Study. *JAMA Oncol* (2020) 6:831–8. doi: 10.1001/jamaoncol.2020.0910

139. Manzoni M, Rovati B, Ronzoni M, Loupakis F, Mariucci S, Ricci V, et al. Immunological Effects of Bevacizumab-Based Treatment in Metastatic Colorectal Cancer. *Oncology* (2010) 79(3-4):187–96. doi: 10.1159/000320609

140. Bendell JC, Powderly JD, Lieu CH, Eckhardt SG, Hurwitz H, Hochster HS, et al. Safety and efficacy of MPDL3280A (anti-PDL1) in combination with bevacizumab (bev) and/or FOLFOX in patients (pts) with metastatic colorectal cancer (mCRC). *J Clin Oncol* (2015) 33(3_suppl):704–. doi: 10.1200/jco.2015.33.3_suppl.704

141. Wallin J, Pishvaian MJ, Hernandez G, Yadav M, Jhunjhunwala S, Delamarre L, et al. Abstract 2651: Clinical activity and immune correlates from a phase Ib study evaluating atezolizumab (anti-PDL1) in combination with FOLFOX and bevacizumab (anti-VEGF) in metastatic colorectal carcinoma. *Cancer Res* (2016) 76(14 Supplement):2651. doi: 10.1158/1538-7445.AM2016-2651

142. Schmoll H-J, Arnold D, de Gramont A, Ducreux M, Grothey A, O'Dwyer PJ, et al. MODUL—a multicenter randomized clinical trial of biomarker-driven maintenance therapy following first-line standard induction treatment of metastatic colorectal cancer: an adaptable signal-seeking approach. *J Cancer Res Clin Oncol* (2018) 144(6):1197–204. doi: 10.1007/s00432-018-2632-6

143. Grothey A, Tabernero J, Arnold D, De Gramont A, Ducreux MP, O'Dwyer PJ, et al. Fluoropyrimidine (FP) + bevacizumab (BEV) + atezolizumab vs FP/BEV in BRAFwt metastatic colorectal cancer (mCRC): Findings from Cohort 2 of MODUL – a multicentre, randomized trial of biomarker-driven maintenance treatment following first-line induction therapy. *Ann Oncol* (2018) 29:viii714–viii5. doi: 10.1093/annonc/mdy424.020

144. Bendell J, Lieu C, Raghav KPS, Argilés G, Cubillo A, Qu X, et al. A phase Ib study of the safety and efficacy of atezolizumab (atezo) + bevacizumab (bev) + cobimetinib (cobi) in patients (pts) with metastatic colorectal cancer (mCRC). *Ann Oncol* (2019) 30:v227–v8. doi: 10.1093/annonc/mdz246.080

145. Ebert PJR, Cheung J, Yang Y, McNamara E, Hong R, Moskalenko M, et al. MAP Kinase Inhibition Promotes T Cell and Anti-tumor Activity in Combination with PD-L1 Checkpoint Blockade. *Immunity* (2016) 44 (3):609–21. doi: 10.1016/j.immuni.2016.01.024

146. Liu L, Mayes PA, Eastman S, Shi H, Yadavilli S, Zhang T, et al. and MEK Inhibitors Dabrafenib and Trametinib: Effects on Immune Function and in Combination with Immunomodulatory Antibodies Targeting PD-1, PD-L1,

and CTLA-4. *Clin Cancer Res* (2015) 21(7):1639. doi: 10.1158/1078-0432.CCR-14-2339

147. Fukuoka S, Hara H, Takahashi N, Kojima T, Kawazoe A, Asayama M, et al. Regorafenib Plus Nivolumab in Patients With Advanced Gastric or Colorectal Cancer: An Open-Label, Dose-Escalation, and Dose-Expansion Phase Ib Trial (REGONIVO,EPOC1603). *J Clin Oncol* (2020)38:2053–61. doi: 10.1200/JCO.19.03296

148. Herbst RS, Morgensztern D, Boshoff C. The biology and management of non-small cell lung cancer. *Nature* (2018) 553(7689):446–54. doi: 10.1038/nature25183

149. Arbour KC, Riely GJ. Systemic Therapy for Locally Advanced and Metastatic Non–Small Cell Lung Cancer: A Review. *JAMA* (2019) 322(8):764–74. doi: 10.1001/jama.2019.11058

150. Martinez P, Peters S, Stammers T, Soria J-C. Immunotherapy for the First-Line Treatment of Patients with Metastatic Non–Small Cell Lung Cancer. *Clin Cancer Res* (2019) 25(9):2691. doi: 10.1158/1078-0432.CCR-18-3904

151. Galluzzi L, Buqué A, Kepp O, Zitvogel L, Kroemer G. Immunological Effects of Conventional Chemotherapy and Targeted Anticancer Agents. *Cancer Cell* (2015) 28(6):690–714. doi: 10.1016/j.ccell.2015.10.012

152. Zitvogel L, Galluzzi L, Smyth MJ, Kroemer G. Mechanism of Action of Conventional and Targeted Anticancer Therapies: Reinstating Immunosurveillance. *Immunity* (2013) 39(1):74–88. doi: 10.1016/j.immuni.2013.06.014

153. Wu J, Waxman DJ. Immunogenic chemotherapy: Dose and schedule dependence and combination with immunotherapy. *Cancer Lett* (2018) 419:210–21. doi: 10.1016/j.canlet.2018.01.050

154. Reck M, Mok TSK, Nishio M, Jotte RM, Cappuzzo F, Orlandi F, et al. Atezolizumab plus bevacizumab and chemotherapy in non-small-cell lung cancer (IMpower150): key subgroup analyses of patients with EGFR mutations or baseline liver metastases in a randomised, open-label phase 3 trial. *Lancet Respir Med* (2019) 7(5):387–401. doi: 10.1016/S2213-2600(19)30084-0

155. Ettinger DS, Wood DE, Aggarwal C, Aisner DL, Akerley W, Bauman JR, et al. NCCN Guidelines Insights: Non-Small Cell Lung Cancer, Version1.2020. *J Natl Compr Canc Netw* (2019) 17(12):1464–72. 10.6004/jnccn.2019.0059

156. Rubinstein MM, Makker V. Optimizing immunotherapy for gynecologic cancers.*Curr Opin Obstet Gynecol* (2020) 32(1):1–8. doi: 10.1097/GCO.0000000000000603

157. Green AK, Feinberg J, Makker V. A Review of Immune Checkpoint Blockade Therapy in Endometrial Cancer. *Am Soc Clin Oncol Educ Book* (2020) 40):1–7. doi: 10.1200/EDBK_280503

158. Makker V, Taylor MH, Aghajanian C, Oaknin A, Mier J, Cohn AL, et al. Lenvatinib Plus Pembrolizumab in Patients With Advanced Endometrial Cancer. *J Clin Oncol* (2020) 38:2981–92. doi: 10.1016/S1470-2045(19)30020-8

159. Tewari KS, Sill MW, Long HJ, Penson RT, Huang H, Ramondetta LM, et al. Improved Survival with Bevacizumab in Advanced Cervical Cancer. *New Engl J Med* (2014) 370(8):734–43. doi: 10.1056/NEJMoa1309748

160. Tewari KS, Sill MW, Penson RT, Huang H, Ramondetta LM, Landrum LM, et al. Bevacizumab for advanced cervical cancer: final overall survival and adverse event analysis of a randomised, controlled, open-label, phase 3 trial (Gynecologic Oncology Group 240). *Lancet* (2017) 390(10103):1654–63. doi: 10.1016/S0140-6736(17)31607-0

161. Pfaendler KS, Liu MC, Tewari KS. Bevacizumab in Cervical Cancer: 5 Years After. *Cancer J* (2018) 24(4):187–92. doi: 10.1097/PPO.0000000000000324

162. Cohen PA, Jhingran A, Oaknin A, Denny L. Cervical cancer. *Lancet* (2019) 393(10167):169–82. doi: 10.1016/S0140-6736(18)32470-X

163. Otter SJ, Chatterjee J, Stewart AJ, Michael A. The Role of Biomarkers for the Prediction of Response to Checkpoint Immunotherapy and the Rationale for the Use of Checkpoint Immunotherapy in Cervical Cancer. *Clin Oncol* (2019) 31(12):834–43. doi: 10.1016/j.clon.2019.07.003

164. Tewari KS. Immune Checkpoint Blockade in PD-L1–Positive Platinum-Refractory Cervical Carcinoma. *J Clin Oncol* (2019) 37(17):1449–54. doi: 10.1200/JCO.19.00119

165. Santin AD, Deng W, Frumovitz M, Buza N, Bellone S, Huh W, et al. Phase II evaluation of nivolumab in the treatment of persistent orrecurrent cervical cancer (NCT02257528/NRG-GY002). *Gynecol Oncol* (2020) 157:161–6. doi: 10.1016/j.ygyno.2019.12.034

166. Chung HC, Ros W, Delord J-P, Perets R, Italiano A, Shapira-Frommer R, et al. Efficacy and Safety of Pembrolizumab in Previously Treated Advanced Cervical Cancer: Results From the Phase II KEYNOTE-158 Study. *J Clin Oncol* (2019) 37(17):1470–8. doi: 10.1200/JCO.18.01265

167. Shapira-Frommer R, Alexandre J, Monk B, Fehm TN, Colombo N, Caceres MV, et al. KEYNOTE-826: A phase 3, randomized, double-blind, placebo-controlled study of pembrolizumab plus chemotherapy for first-line treatment of persistent, recurrent, or metastatic cervical cancer. *J Clin Oncol* (2019) 37(15_suppl): TPS5595–TPS. doi: 10.1200/JCO.2019.37.15_suppl.TPS5595

168. Grau JF, Farinas-Madrid L, Oaknin A. A randomized phase III trial of platinum chemotherapy plus paclitaxel with bevacizumab and atezolizumab versus platinum chemotherapy plus paclitaxel and bevacizumab in metastatic (stage IVB), persistent, or recurrent carcinoma of the cervix: the BEATcc study (ENGOT-Cx10/GEICO 68-C/JGOG1084/GOG-3030). *Int J Gynecol Cancer* (2020) 30(1):139. doi: 10.1136/ijgc-2019-000880

169. Lheureux S, Gourley C, Vergote I, Oza AM. Epithelial ovarian cancer. *Lancet* (2019) 393(10177):1240–53. doi: 10.1016/S0140-6736(18)32552-2

170. Pfisterer J, Shannon CM, Baumann K, Rau J, Harter P, Joly F, et al. Bevacizumab and platinum-based combinations for recurrent ovarian cancer: a randomised, open-label, phase 3 trial. *Lancet Oncol* (2020) 21 (5):699–709. doi: 10.1016/S1470-2045(20)30142-X

171. Levinson K, Dorigo O, Rubin K, Moore K. Immunotherapy in Gynecologic Cancers: What We Know Now and Where We Are Headed. *Am Soc Clin Oncol Educ Book* (2019) 39:e126–40. doi: 10.1200/EDBK_237967

172. Liu JF, Herold C, Gray KP, Penson RT, Horowitz N, Konstantinopoulos PA, et al. Assessment of Combined Nivolumab and Bevacizumab in Relapsed Ovarian Cancer: A Phase 2 Clinical Trial. *JAMA Oncol* (2019) 5(12):1731–8. doi: 10.1001/jamaoncol.2019.3343

173. Zsiros E, Frederick PJ, Akers SN, Attwood K, Wang K, Lele SB, et al. A phase II trial of pembrolizumab in combination with bevacizumab and oral metronomic cyclophosphamide for recurrent epithelial ovarian, fallopian tube or primary peritoneal cancer. *Gynecol Oncol* (2019) 154:23. doi: 10.1016/j.ygyno.2019.04.056

174. Zimmer AS, Nichols E, Cimino-Mathews A, Peer C, Cao L, Lee M-J, et al. A phase I study of the PD-L1 inhibitor, durvalumab, in combination with a PARP inhibitor, olaparib, and a VEGFR1–3 inhibitor, cediranib, in recurrent women's cancers with biomarker analyses. *J ImmunoTher Cancer* (2019) 7 (1):197. doi: 10.1186/s40425-019-0680-3

175. Harter P, Bidziński M, Colombo N, Floquet A, Rubio Pérez MJ, Kim J-W, et al. DUO-O: A randomized phase III trial of durvalumab (durva) in combination with chemotherapy and bevacizumab (bev), followed by maintenance durva, bev and olaparib (olap), in newly diagnosed advanced ovarian cancer patients. *J Clin Oncol* (2019) 37(15_suppl):TPS5598–TPS. doi: 10.1200/JCO.2019.37.15_suppl.TPS5598

176. Morse MA, Sun W, Kim R, He AR, Abada PB, Mynderse M, et al. The Role of Angiogenesis in Hepatocellular Carcinoma. *Clin Cancer Res* (2019) 25 (3):912. doi: 10.1158/1078-0432.CCR-18-1254

177. Zhu AX, Duda DG, Sahani DV, Jain RK. HCC and angiogenesis: possible targets and future directions. *Nat Rev Clin Oncol* (2011) 8(5):292–301. doi: 10.1038/nrclinonc.2011.30

178. Llovet JM, Montal R, Sia D, Finn RS. Molecular therapies and precision medicine for hepatocellular carcinoma. *Nat Rev Clin Oncol* (2018) 15 (10):599–616. doi: 10.1038/s41571-018-0073-4

179. Villanueva A. Hepatocellular Carcinoma. *New Engl J Med* (2019) 380 (15):1450–62. doi: 10.1056/NEJMra1713263

180. Ringelhan M, Pfister D, O'Connor T, Pikarsky E, Heikenwalder M. The immunology of hepatocellular carcinoma. *Nat Immunol* (2018) 19(3):222–32. doi: 10.1038/s41590-018-0044-z

181. Wang L, Wang F-S. Clinical immunology and immunotherapy for hepatocellular carcinoma: current progress and challenges. *Hepatol Int* (2019) 13(5):521–33. doi: 10.1007/s12072-019-09967-y

182. Iñarrairaegui M, Melero I, Sangro B. Immunotherapy of Hepatocellular Carcinoma: Facts and Hopes. *Clin Cancer Res* (2018) 24(7):1518. doi: 10.1158/1078-0432.CCR-17-0289

183. Cariani E, Missale G. Immune landscape of hepatocellular carcinoma microenvironment: Implications for prognosis and therapeutic applications. *Liver Int* (2019) 39(9):1608–21. doi: 10.1111/liv.14192

184. El-Khoueiry AB, Sangro B, Yau T, Crocenzi TS, Kudo M, Hsu C, et al. Nivolumab in patients with advanced hepatocellular carcinoma (CheckMate 040): an open-label, non-comparative, phase 1/2 dose escalation and expansion trial. *Lancet* (2017) 389(10088):2492–502. doi: 10.1016/S0140-6736(17)31046-2

185. Zhu AX, Finn RS, Edeline J, Cattan S, Ogasawara S, Palmer D, et al. Pembrolizumab in patients with advanced hepatocellular carcinoma previously treated with sorafenib (KEYNOTE-224): a non-randomised, open-label phase 2trial. *Lancet Oncol* (2018) 19(7):940–52. doi: 10.1016/S1470-2045(18)30351-6

186. Yau T, Park JW, Finn RS, Cheng A-L, Mathurin P, Edeline J, et al. LBA38_PRCheckMate 459: A randomized, multi-center phase III study ofnivolumab (NIVO) vs sorafenib (SOR) as first-line (1L) treatment in patients (pts) with advancedhepatocellular carcinoma (aHCC). *Ann Oncol* (2019) 30(Supplement_5):v874–5. doi: 10.1093/annonc/mdz394.029

187. Finn RS, Ryoo B-Y, Merle P, Kudo M, Bouattour M, Lim HY, et al. Pembrolizumab As Second-Line Therapy in Patients With Advanced Hepatocellular Carcinoma in KEYNOTE-240: A Randomized, Double-Blind, Phase III Trial. *J Clin Oncol* (2019) 38:193–202. doi: 10.1200/JCO.19.01307

188. Cheng A-L, Hsu C, Chan SL, Choo S-P, Kudo M. Challenges of combination therapy with immune checkpoint inhibitors for hepatocellular carcinoma. *J Hepatol* (2020) 72(2):307–19. doi: 10.1016/j.jhep.2019.09.025

189. Kudo M. Combination Cancer Immunotherapy with Molecular Targeted Agents/Anti-CTLA-4 Antibody for Hepatocellular Carcinoma. *Liver Cancer* (2019) 8(1):1–11. doi: 10.1159/000496277

190. Llovet J, Shepard KV, Finn RS, Ikeda M, Sung M, Baron AD, et al. A phase Ib trial of lenvatinib (LEN) plus pembrolizumab (PEMBRO) in unresectable hepatocellular carcinoma (uHCC): Updated results. *Ann Oncol* (2019) 30: v286–7. doi: 10.1093/annonc/mdz247.073

191. Kudo M, Motomura K, Wada Y, Inaba Y, Sakamoto Y, Kurosaki M, et al. First-line avelumab + axitinib in patients with advanced hepatocellular carcinoma: Results from a phase 1b trial (VEGF Liver 100). *J Clin Oncol* (2019) 37(15_suppl):4072–. doi: 10.1200/JCO.2019.37.15_suppl.4072

192. Pishvaian MJ, Lee MS, Ryoo BY, Stein S, Lee KH, Verret W, et al. LBA26 - Updated safety and clinical activity results from a phase Ib study of atezolizumab + bevacizumab in hepatocellular carcinoma (HCC). *Ann Oncol* (2018) 29:viii718–9. doi: 10.1093/annonc/mdy424.028

193. Xu J, Zhang Y, Jia R, Yue C, Chang L, Liu R, et al. Anti-PD-1 Antibody SHR-1210 Combined with Apatinib for Advanced Hepatocellular Carcinoma, Gastric, or Esophagogastric Junction Cancer: An Open-label, Dose Escalation and Expansion Study. *Clin Cancer Res* (2019) 25(2):515. doi: 10.1158/1078-0432.CCR-18-2484

194. Bang Y-J, Golan T, Lin C-C, Dahan L, Fu S, Moreno V, et al. Ramucirumab (Ram) and durvalumab (Durva) treatment of metastatic non-small cell lung cancer (NSCLC), gastric/gastroesophageal junction (G/GEJ) adenocarcinoma, and hepatocellular carcinoma (HCC) following progression on systemic treatment(s). *J Clin Oncol* (2019) 37(15_suppl):2528–. doi: 10.1200/JCO.2019.37.15_suppl.2528

195. Finn RS, Ikeda M, Zhu AX, Sung MW, Baron AD, Kudo M, et al. Phase Ib Study of Lenvatinib Plus Pembrolizumab in Patients WithUnresectable Hepatocellular Carcinoma. *J Clin Oncol* (2020) 38:2960–70. doi: 10.1200/JCO.20.00808

196. Lee M, Ryoo B-Y, Hsu C-H, Numata K, Stein S, Verret W, et al. LBA39Randomised efficacy and safety results for atezolizumab (Atezo)+ bevacizumab (Bev) in patients (pts) with previously untreated, unresectable hepatocellular carcinoma (HCC). *Ann Oncol* (2019) 30(Supplement_5): v875. doi: 10.1093/annonc/mdz394.030

197. Galle PR, Finn RS, Qin S, Ikeda M, Zhu AX, Kim T-Y, et al. Patient-reported outcomes (PROs) from the Phase III IMbrave150 trial of atezolizumab (atezo) + bevacizumab (bev) vs sorafenib (sor) as first-line treatment (tx) for patients (pts) with unresectable hepatocellular carcinoma (HCC). *J Clin Oncol* (2020) 38(4_suppl):476–. doi: 10.1200/JCO.2020.38.4_suppl.476

198. Vogel A, Saborowski A. Current strategies for the treatment of intermediate and advanced hepatocellular carcinoma. *Cancer Treat Rev* (2020) 82:101946. doi: 10.1016/j.ctrv.2019.101946

199. Kelley RK. Atezolizumab plus Bevacizumab — A Landmark in Liver Cancer. *New Engl J Med* (2020) 382(20):1953–5. doi: 10.1056/NEJMe2004851

200. Van den Eynden GG, Majeed AW, Illemann M, Vermeulen PB, Bird NC, Høyer-Hansen G, et al. The Multifaceted Role of the Microenvironment in Liver Metastasis: Biology and Clinical Implications. *Cancer Res* (2013) 73 (7):2031. doi: 10.1158/0008-5472.CAN-12-3931

201. Hess KR, Varadhachary GR, Taylor SH, Wei W, Raber MN, Lenzi R, et al. Metastatic patterns in adenocarcinoma. *Cancer* (2006) 106(7):1624–33. doi: 10.1002/cncr.21778

202. Tumeh PC, Hellmann MD, Hamid O, Tsai KK, Loo KL, Gubens MA, et al. Liver Metastasis and Treatment Outcome with Anti-PD-1 Monoclonal Antibody in Patients with Melanoma and NSCLC. *Cancer Immunol Res* (2017) 5(5):417. doi: 10.1158/2326-6066.CIR-16-0325

203. Kitadai R, Okuma Y, Hakozaki T, Hosomi Y. The efficacy of immune checkpoint inhibitors in advanced non-small-cell lung cancer with liver metastases. *J Cancer Res Clin Oncol* (2020) 146(3):777–85. doi: 10.1007/s00432-019-03104-w

204. Bilen MA, Shabto JM, Martini DJ, Liu Y, Lewis C, Collins H, et al. Sites of metastasis and association with clinical outcome in advanced stage cancer patients treated with immunotherapy. *BMC Cancer* (2019) 19(1):857. doi: 10.1186/s12885-019-6073-7

205. Sridhar S, Paz-Ares L, Liu H, Shen K, Morehouse C, Rizvi N, et al. Prognostic Significance of Liver Metastasis in Durvalumab-Treated Lung Cancer Patients. *Clin Lung Cancer* (2019) 20(6):e601–e8. doi: 10.1016/j.cllc.2019.06.020

206. Khoja L, Kibiro M, Metser U, Gedye C, Hogg D, Butler MO, et al. Patterns of response to anti-PD-1 treatment: an exploratory comparison of four radiological response criteria and associations with overall survival in metastatic melanoma patients. *Br J Cancer* (2016) 115(10):1186–92. doi: 10.1038/bjc.2016.308

207. Lu LC, Hsu C, Shao YY, Chao Y, Yen CJ, Shih IL, et al. Differential Organ-Specific Tumor Response to Immune Checkpoint Inhibitors in Hepatocellular Carcinoma. *Liver Cancer* (2019) 8(6):480–90. doi: 10.1159/000501275

208. Jiménez-Sánchez A, Memon D, Pourpe S, Veeraraghavan H, Li Y, Vargas HA, et al. Heterogeneous Tumor-Immune Microenvironments among DifferentiallyGrowing Metastases in an Ovarian Cancer Patient. *Cell* (2017)170(5):927–38.e20. doi: 10.1016/j.cell.2017.07.025

209. Keenan BP, Fong L, Kelley RK. Immunotherapy in hepatocellular carcinoma: the complex interface between inflammation, fibrosis, and the immune response. *J ImmunoTher Cancer* (2019) 7(1):267. doi: 10.1186/s40425-019-0749-z

210. Tiegs G, Lohse AW. Immune tolerance: What is unique about the liver. *J Autoimmun* (2010) 34(1):1–6. doi: 10.1016/j.jaut.2009.08.008

211. Lin Y-Y, Tan C-T, Chen C-W, Ou D-L, Cheng A-L, Hsu C. Immunomodulatory Effects of Current Targeted Therapies on Hepatocellular Carcinoma: Implication for the Future of Immunotherapy. *Semin Liver Dis* (2018) 38(04):379–88. doi: 10.1055/s-0038-1673621

212. Koneru M, Patnaik A, Liu J, Nanda S, Thomas ZM, Lin J. A meta-analysis to indirectly compare the safety and efficacy of PD-1 and PD-L1 antibodies across solid tumors using a Bayesian hierarchical model. *J Clin Oncol* (2018) 36(15_suppl):3065–. doi: 10.1200/JCO.2018.36.15_suppl.3065

213. Wu Y, Lin L, Shen Y, Wu H. Comparison between PD-1/PD-L1 inhibitors (nivolumab, pembrolizumab, and atezolizumab) in pretreated NSCLC patients: Evidence from a Bayesian network model. *Int J Cancer* (2018) 143(11):3038–40. doi: 10.1002/ijc.31733

214. Duan J, Cui L, Zhao X, Bai H, Cai S, Wang G, et al. Use of Immunotherapy With Programmed Cell Death 1 vs Programmed Cell Death Ligand 1 Inhibitors in Patients With Cancer: A Systematic Review and Meta-analysis. *JAMA Oncol* (2020) 6(3):375–84. doi: 10.1001/jamaoncol.2019.5367

215. De Sousa Linhares A, Battin C, Jutz S, Leitner J, Hafner C, Tobias J, et al. Therapeutic PD-L1 antibodies are more effective than PD-1 antibodies in blocking PD-1/PD-L1 signaling. *Sci Rep* (2019) 9(1):11472. doi: 10.1038/s41598-019-47910-1

216. Zhao Y, Lee CK, Lin C-H, Gassen RB, Xu X, Huang Z, et al. PD-L1:CD80 *Cis*-Heterodimer Triggers the Co-stimulatory Receptor CD28 While Repressing the Inhibitory PD-1 and CTLA-4 Pathways. *Immunity* (2019) 51(6):1059–73.e9. doi: 10.1016/j.immuni.2019.11.003

217. Antonia SJ, Villegas A, Daniel D, Vicente D, Murakami S, Hui R, et al. Durvalumab after Chemoradiotherapy in Stage III Non–Small-Cell Lung Cancer. *New Engl J Med* (2017) 377(20):1919–29. doi: 10.1056/NEJMoa1709937

218. Eggermont AMM, Blank CU, Mandala M, Long GV, Atkinson V, Dalle S, et al. Adjuvant Pembrolizumab versus Placebo in Resected Stage III Melanoma. *New Engl J Med* (2018) 378(19):1789–801. doi: 10.1056/NEJMoa1802357

219. Weber J, Mandala M, Del Vecchio M, Gogas HJ, Arance AM, Cowey CL, et al. Adjuvant Nivolumab versus Ipilimumab in Resected Stage III or IV Melanoma. *New Engl J Med* (2017) 377(19):1824–35. doi: 10.1056/NEJMoa1709030

220. Knox J, Cheng A, Cleary S, Galle P, Kokudo N, Lencioni R, et al. P-217 - A phase 3 study of durvalumab with or without bevacizumab as adjuvant therapy in patients with hepatocellular carcinoma at high risk of recurrence after curative hepatic resection or ablation: EMERALD-2. *Ann Oncol* (2019) 30:v59–60. doi: 10.1093/annonc/mdz155.216

221. Hack SP, Spahn J, Chen M, Cheng A-L, Kaseb A, Kudo M, et al. IMbrave 050: a Phase III trial of atezolizumab plus bevacizumab inhigh-risk hepatocellular carcinoma after curative resection or ablation. *Future Oncol* (2020) 16:975–89. doi: 10.2217/fon-2020-0162

222. Greten TF, Mauda-Havakuk M, Heinrich B, Korangy F, Wood BJ. Combined locoregional-immunotherapy for liver cancer. *J Hepatol* (2019) 70(5):999–1007. doi: 10.1016/j.jhep.2019.01.027

223. Havel JJ, Chowell D, Chan TA. The evolving landscape of biomarkers for checkpoint inhibitor immunotherapy. *Nat Rev Cancer* (2019) 19(3):133–50. doi: 10.1038/s41568-019-0116-x

Tumor Microenvironment Status Predicts the Efficacy of Postoperative Chemotherapy or Radiochemotherapy in Resected Gastric Cancer

Ran Duan [1,2†], Xiaoqin Li [1†], Dongqiang Zeng [3], Xiaofeng Chen [4], Bo Shen [5], Dongqin Zhu [6], Liuqing Zhu [6], Yangyang Yu [7] and Deqiang Wang [1*]

[1] Department of Medical Oncology, Affiliated Hospital of Jiangsu University, Zhenjiang, China, [2] Department of Ultrasonography, Affiliated Hospital of Jiangsu University, Zhenjiang, China, [3] Department of Oncology, Nanfang Hospital, Southern Medical University, Guangzhou, China, [4] Department of Medical Oncology, Jiangsu Province Hospital, Nanjing, China, [5] Department of Medical Oncology, The Affiliated Cancer Hospital of Nanjing Medical University, Nanjing, China, [6] Nanjing Geneseeq Technology Inc., Nanjing, China, [7] The Medical Department, 3D Medicines Inc., Shanghai, China

Purpose: Chemotherapy (CT) and radiochemotherapy (RCT) are currently the standard postoperative treatments for resected gastric cancer (GC). However, owing to a lack of predictive biomarkers, their efficacy is currently suboptimal. As tumor microenvironment (TME) has the potential to determine treatment response, we investigated the association of TME status with the efficacy of fluoropyrimidine (FU)-based postoperative CT/RCT in resected GC.

Methods: Patients with transcriptome data were screened and selected in three independent cohorts. Favorable (fTME) and poor TME (pTME) were defined by a transcriptome-based TME qualification method. Immune infiltration and hypoxia were assessed.

Results: A total of 535 patients were eligible. fTME, indicating the presence of immune activation, was characterized by NK cell rather than CD8+ T cell infiltration. However, postoperative CT/RCT improved overall survival and disease-free survival time more evidently in patients with pTME GC than those with fTME GC. Stratified by stage in fTME GC, stage III patients benefited from postoperative CT/RCT while stage Ib/II patients did not. In comparison, patients with pTME GC benefited from postoperative CT/RCT, regardless of stage. Furthermore, fTME was more hypoxic than pTME, accompanied by a stronger expression of thymidylate synthase (TS)—the target of FU. Stage Ib/II fTME GC was the most hypoxic and had the strongest TS expression across all the subgroups stratified by TME status and stage.

Conclusions: We found that fTME, with the enrichment of NK cells, may predict the lack of postoperative CT/RCT efficacy in stage Ib/II GC, which may be associated with hypoxia and TS expression. Further validations and mechanism researches are needed.

Keywords: tumor microenvironment, chemotherapy, radiochemotherapy, immune infiltration, hypoxia, gastric cancer

INTRODUCTION

Gastric cancer (GC) is characterized by high relapse rates even after curative surgery. Two different postoperative therapeutic strategies—fluoropyrimidine (FU)-based chemotherapy (CT) and radiochemotherapy (RCT)—have been verified for use in improving the curative and survival rates in patients with resected GC (1). Both CT and RCT exert equivalent effects in improving patients' overall survival (OS), while RCT yields superior local control than CT, correlating to better disease-free survival (DFS), especially in stage III GC (2–4). However, regardless of the treatment type, many patients still experience relapse after surgery, independently of the disease stage, suggesting the presence of molecular heterogeneity, in terms of therapy response, among patients.

Currently, there are no validated prognostic or predictive biomarkers for GC patients who receive postoperative CT/RCT. However, recent findings on the molecular mechanisms of GC, obtained using high-throughput methods, may allow for the identification of novel biomarkers. The Cancer Genome Atlas (TCGA) and Asian Cancer Research Group (ACRG) projects—landmarks in the molecular characterization of GC—provide invaluable resources for the development of more comprehensive methods to interpret and combat GC (5, 6).

A large body of evidence, based on the TCGA and ACRG datasets and other Next Generation Sequencing (NGS) data, has recently been obtained. However, few distinct biological targets are found on the tumor cell alone. An increasing amount of attention is now being directed to the tumor microenvironment (TME), considering the significance of tumor-related structures as well as the interaction between tumor cells and other cells in the TME. The clinical relevance of TME-associated biomarkers, which reveal changes in the compositions of resident cell types within the TME during cancer evolution, has been reported for various malignancies (7, 8).

In the current era of widespread immunotherapy use, CT and RCT are still the current cornerstones of GC treatment, especially in the postoperative setting. Gaining further insights into TME may help improve the efficacy of not only immunotherapy but also CT/RCT. A previous study found that cancer-associated fibroblasts, among the immunosuppressive cell types in the TME, can promote irradiated cancer cell recovery and cause radioresistance (9). Another study reported that intratumoral interleukin-17-producing cell infiltration improved the response to CT in GC (10). However, there is still a lack of qualification method for a comprehensive evaluation of the TME status to aid in the prediction of CT/RCT efficacy in GC.

Recently, based on a comprehensive landscape of the TME-associated transcriptome characteristics in ACRG, a methodology for the quantification of TME status—the TMEscore—was established specifically for GC. The TMEscore has been validated as a robust prognostic biomarker in GC (11). However, the association between TMEscore and immune infiltration needs further experimental validation and it remains unknown whether TMEscore is predictive for postoperative CT/RCT efficacy of GC.

Accordingly, in this study we aimed to use the novel TMEscore to investigate the association between TME status and postoperative CT/RCT efficacy in resected GC.

MATERIALS AND METHODS

Patients

This study included three independent cohorts. Patients who were retrospectively screened from GC cases received gastrectomy at the Affiliated Hospital of Jiangsu University (AHJU) composed the AHJU cohort. Informed consent was obtained from all patients and the research protocol was approved by the hospital ethics committee (Grant No: 201750). GC cohorts from the ACRG and TCGA were also analyzed. The enrollment criteria for all patients included: 1) a prior history of gastrectomy; 2) histologically confirmed stages IB–III (≥T2 and/or node-positive and M0) adenocarcinoma of the stomach; 3) available gene expression data for TME status estimation; and 4) a definite treatment history of surgery plus FU-based postoperative CT/RCT or surgery alone. American Joint Committee on Cancer criteria were used for clinical and clinicopathologic classification and staging.

Transcriptome Data

We used the dataset—EGAD00001004164—from the European Genome-phenome Archive, including 34 consecutive patients who underwent GC surgery in 2016 at the AHJU. In brief, total RNA from fresh samples was extracted using Trizol (Invitrogen, USA). Ribosomal RNA was depleted using RNase H followed by library preparation using KAPA Stranded RNA-seq Kit with RiboErase (KAPA Biosystems, USA). The library concentration was determined using KAPA Library Quantification Kit (KAPA Biosystems, USA), and library quality was assessed by the Agilent High Sensitivity DNA kit on Bioanalyzer 2100 (Agilent Technologies, USA), which was then sequenced on Illumina HiSeq4000 NGS platforms (Illumina, USA). Base calling was performed on bcl2fastq v2.16.0.10 (Illumina, USA) for the generation of sequence reads in the FASTQ format

(Illumina 1.8+ encoding). Quality control was performed with Trimmomatic (version 0.33). STAR (version 2.5.3a) was used for transcriptome mapping followed by isoform and gene level quantification, as performed using RSEM (version 1.3.0). ACRG and TCGA GC RNA abundance data were downloaded from the NCBI Gene Expression Omnibus (GSE62254) and University of California Santa Cruz (UCSC) Xena platform (https://xenabrowser.net/datapages/), respectively.

Tumor Microenvironment Assessment

The TMEscore was estimated using principal component analysis (PCA) based on transcriptome data of genes associated with different TME phenotypes and prognoses in GC, as previously described (11), using the R package available in GitHub (https://github.com/DongqiangZeng0808/TMEscore). In brief, the TMEscore construction included: 1) the TME phenotype was determined by transcriptome-based cell abundance deconvolution, unsupervised clustering and consensus clustering; 2) differentially expressed genes associated with TME phenotypes were identified and TME gene signatures were generated after dimension reduction; 3) principal component 1 from PCA was extracted to serve as the score of TME gene signatures; 4) TMEscore was calculated using the signature score whose Cox coefficient for prognosis was positive to subtract the signature score whose Cox coefficient for prognosis was negative. We defined favorable TME (fTME) and poor TME (pTME) based on the contrast immune infiltration status, using the median TMEscore value as a cut-off.

Microsatellite Instability Assay

Genomic DNA was extracted from GC and normal tissues, following which single fluorescent multiplex polymerase chain reaction was performed for the detection of five well-known mononucleotide repeats. Further details on MSI and microsatellite stability (MSS) assay as well as their definitions have been provided elsewhere (6).

RNA-Based Immune Infiltration Quantification and Hypoxia Scoring

Cell, an RNA-based silico tool (12), was used for the quantification of the proportions of the pertinent phenotypes of human immune cells in GC samples. Parametric Gene Set Enrichment Analysis (13), which determines the misregulation of defined gene signatures, was used for the quantification of the degree of tumor hypoxia, based on well-established signatures (14–19).

Immunohistochemistry

Programmed death ligand-1 (PD-L1) staining using Dako PD-L1 IHC 22C3 pharmDx kit (Agilent Technologies) was performed on a Dako Autostainer Link 48 system (Agilent Technologies), and the specimen was then counterstained with hematoxylin and coverslipped, according to the manufacturer's instructions. The PD-L1 expression level was determined using the combined positive score (CPS), which is the percentage of PD-L1-positive cells (tumor cells, lymphocytes, and macrophages) relative to all the viable tumor cells present in the sample, multiplied by 100. PD-L1-positivity was confirmed at a CPS ≥1 (20). Anti-thymidylate synthetase (TS, ab108995, Abcam, UK) and

anti-ERO1A (ab177156) antibodies were used in a two-step IHC protocol. The presence of nuclear and/or cytoplasm tumor cell staining was considered as positive TS expression, irrespective of the proportion or intensity (21). An IHC score ≥8 (median value) was used to define positive ERO1A expression.

Multiplexed Immunohistochemistry and Multispectral Imaging

Immune cell subsets in the TME were identified by mIHC and multispectral imaging. Multiplex immunofluorescence staining was performed using PANO 7-plex IHC kit (Panovue, Beijing, China), according to the manufacturer's instructions. T cells were identified using the CD8 marker. NK cells were identified using the CD56 marker and were divided into two categories according to the intensity of membrane staining for the CD56 protein: CD56dim (weak staining) and CD56bright (strong staining). TAMs were identified by CD68 and HLA-DR and were divided into two categories: type M1 (CD68+ and HLA-DR+) and type M2 (CD68+ and HLA-DR−). Different primary antibodies were sequentially applied, including anti-CD8 (CST70306, Cell Signaling Technology, USA), anti-CD56 (CST3576), anti-panCK (CST4545), anti-CD68 (BX50031, Biolynx, China), anti-HLA-DR (ab92511), and anti-S100 (ab52642). S100 staining was used to define the invasive margin and tumor parenchyma (22). The Mantra System (PerkinElmer, Waltham, Massachusetts, US) was used to scan the stained slides and subsequently build a single stack image. The inForm image analysis software (PerkinElmer, Waltham, Massachusetts, US) was used for the reconstruction of images of sections with autofluorescence removal, based on a spectral library for multispectral unmixing.

Statistical Analysis

First, we used multiple imputation to generate complete datasets for the subsequent analyses in the ACRG, TCGA, and pooled cohorts that included all patients (**Supplementary Data**), according to the multiple imputation guideline (23). Chi-square tests, Fisher's exact probability tests, Student's t tests, Wilcoxon tests, and Mann–Whitney U tests were used for between-group comparisons, as needed. Spearman's correlation was used for pairs of continuous variables. Survival analyses were performed using Kaplan–Meier plots and log-rank tests. Cox proportional hazards regression analysis was used for the evaluation of prognostic factors and calculation of hazard ratios (HRs) along with their 95% confidence intervals (CIs). The HR for each imputed dataset was estimated, and all the estimated HRs were then combined according to Rubin's rules (24). The imputed dataset with the closest HR to the combined HR was selected for survival curve plotting. We used 5% as the significance level for all tests. SPSS (version 19.0, Chicago, IL), R (version 3.6.1), and R Bioconductor packages were used for all the above-mentioned analyses.

RESULTS

Patient Characteristics

A total of 34, 271, and 230 eligible patients were enrolled from the AHJU, ACRG, and TCGA cohorts, respectively (**Table 1**).

TABLE 1 | Patient characteristics according to tumor microenvironment status.

Characteristic*	AHJU cohort (%)			ACRG cohort (%)			TCGA cohort (%)		
	pTME	fTME	P value	pTME	fTME	P value	pTME	fTME	P value
Age (years)									
<65	9 (69.2)	4 (30.8)	0.078	76 (52.4)	69 (47.6)	0.359	49 (51.0)	47 (49.0)	0.789
≥65	8 (38.1)	13 (61.9)		59 (46.8)	67 (53.2)		66 (49.3)	68 (50.7)	
Sex									
Female	9 (69.2)	4 (30.8)	0.078	44 (41.1)	42 (58.9)	0.762	41 (45.1)	50 (54.9)	0.225
Male	8 (38.1)	13 (61.9)		91 (49.2)	94 (50.8)		74 (53.2)	65 (46.8)	
Tumor location									
Non-antrum	11 (47.8)	12 (52.2)	0.714	69 (54.3)	58 (45.7)	0.180	58 (43.0)	77 (57.0)	0.011
Antrum	6 (54.5)	5 (45.5)		66 (46.2)	77 (53.8)		57 (60.0)	38 (40.0)	
Histology grade									
I/II	8 (53.3)	7 (46.7)	0.730	47 (38.5)	75 (61.5)	0.001	41 (45.6)	49 (54.4)	0.280
III	9 (47.4)	10 (52.6)		88 (59.1)	61 (40.9)		74 (52.9)	66 (47.1)	
TNM stage									
IB/II	8 (44.4)	10 (55.6)	0.492	45 (35.7)	81 (64.3)	<0.001	64 (48.1)	69 (51.9)	0.504
III	9 (56.2)	7 (43.8)		90 (62.1)	55 (37.9)		51 (52.6)	46 (47.4)	
MSI status									
MSS	15 (53.6)	13 (46.4)	0.368	126 (61.5)	79 (38.5)	<0.001	103 (57.5)	76 (42.5)	<0.001
MSI	2 (33.3)	4 (66.7)		9 (13.6)	57 (86.4)		12 (23.5)	39 (76.5)	
Postoperative chemotherapy or radiochemotherapy									
Untreated	5 (31.2)	11 (68.8)	0.039	55 (49.5)	56 (50.5)	0.942	77 (53.5)	67 (46.5)	0.173
Treated	12 (66.7)	6 (33.3)		80 (50.0)	80 (50.0)		38 (44.2)	48 (55.8)	

*Unimputed data were shown.

AHJU, Affiliated Hospital of Jiangsu University; TCGA, The Cancer Genome Atlas; ACRG, Asian Cancer Research Group; MSS, microsatellite stability; MSI, microsatellite instability.

MSI GC was more frequently associated with fTME than MSS GC, while about 40% of the MSS cases also showed fTME in each cohort. In terms of the associations between TME status and the other characteristics, differing results were observed across the cohorts, indicating the presence of heterogeneity.

Tumor Microenvironment Status and Immune Infiltration Characteristics

At first, we investigated TMEscore-associated immune infiltration characteristics which need further validation. It is well-known that Th1 cells activate antitumor immunity while fibroblasts suppress it (25, 26). Through transcriptome-based cell type enrichment analysis, we found that the TMEscore positively correlated with the abundance of Th1 cells but negatively correlated with the abundance of fibroblasts in all the cohorts (**Figure 1A**). Moreover, the TMEscore positively correlated with the abundance of NK cells and macrophages M1 in all the cohorts, but negatively correlated with the abundance of CD8+ T cells in the AHJU and ACRG cohorts (**Figure 1A**).

mIHC staining was used to validate the infiltration of selected cells in eight of the AHJU cohort patients that had a sufficient amount of tissue (**Figure 1B**). Compared to pTME GC, fTME GC was associated with higher densities of CD56bright/dim NK cells and macrophages M1 but lower densities of CD8+ T cells and macrophages M2 inside the tumors, despite the significance of these differences were limited by the small sample size (**Figure 1C**). As the mobilization of immune cells from the stromal tumor edge into the tumor parenchyma is crucial for antitumor immunity (22), we next applied the effective infiltration degree (EID: the number of immune cells in tumor parenchyma divided by the total number of immune cells at the stromal tumor edge and in the tumor parenchyma, multiplied by 100%) for the

evaluation of antitumor immunity dynamism. We found that TMEscore positively correlated with the EID of CD56bright/dim NK cells (Spearman r = 0.88, P = 0.007) but negatively correlated with the EID of CD8+ T cells (Spearman r = -0.90, P = 0.005; **Figure 1D**). These results confirmed our transcriptome-based findings.

PD-L1 staining (**Figure 1E**) showed that the only one PD-L1-positive tumor (CPS = 2) from the eight samples had the lowest TMEscore but the highest densities of CD8+ T cells and immunosuppressive macrophages M2 inside the tumors (**Figure 1F**), indicating that the CD8+ T cells inside tumors may be deactivated by PD-L1 signaling and that the TMEscore is a strong indicator of antitumor immunity dynamism.

Tumor Microenvironment Status and Postoperative Chemotherapy/ Radiochemotherapy Efficacy

First, we confirmed that postoperative CT/RCT improved the OS and DFS of patients with resected GC compared to surgery alone, across all the cohorts (**Figure S1**). Then, we showed that the benefit of postoperative CT/RCT was more pronounced in cases with pTME, in terms of both OS (**Figure 2A**) and DFS (**Figure 2B**). In comparison, these benefits were reduced or even disappeared in cases with fTME (**Figures 2A, B**). These findings were further confirmed in the combined cohort with all patients (**Figure 2C**). Moreover, after univariate selection for the prognostic significance of variables, multivariate models were created. Because a requirement of large sample size, this analysis was conducted in the combined cohort. We showed that postoperative CT/RCT was an independent predictor of both OS (HR = 0.32, 0.21–0.48, P < 0.001) and DFS (HR = 0.31, 0.21–0.47, P < 0.001) in pTME GC (**Table 2**).
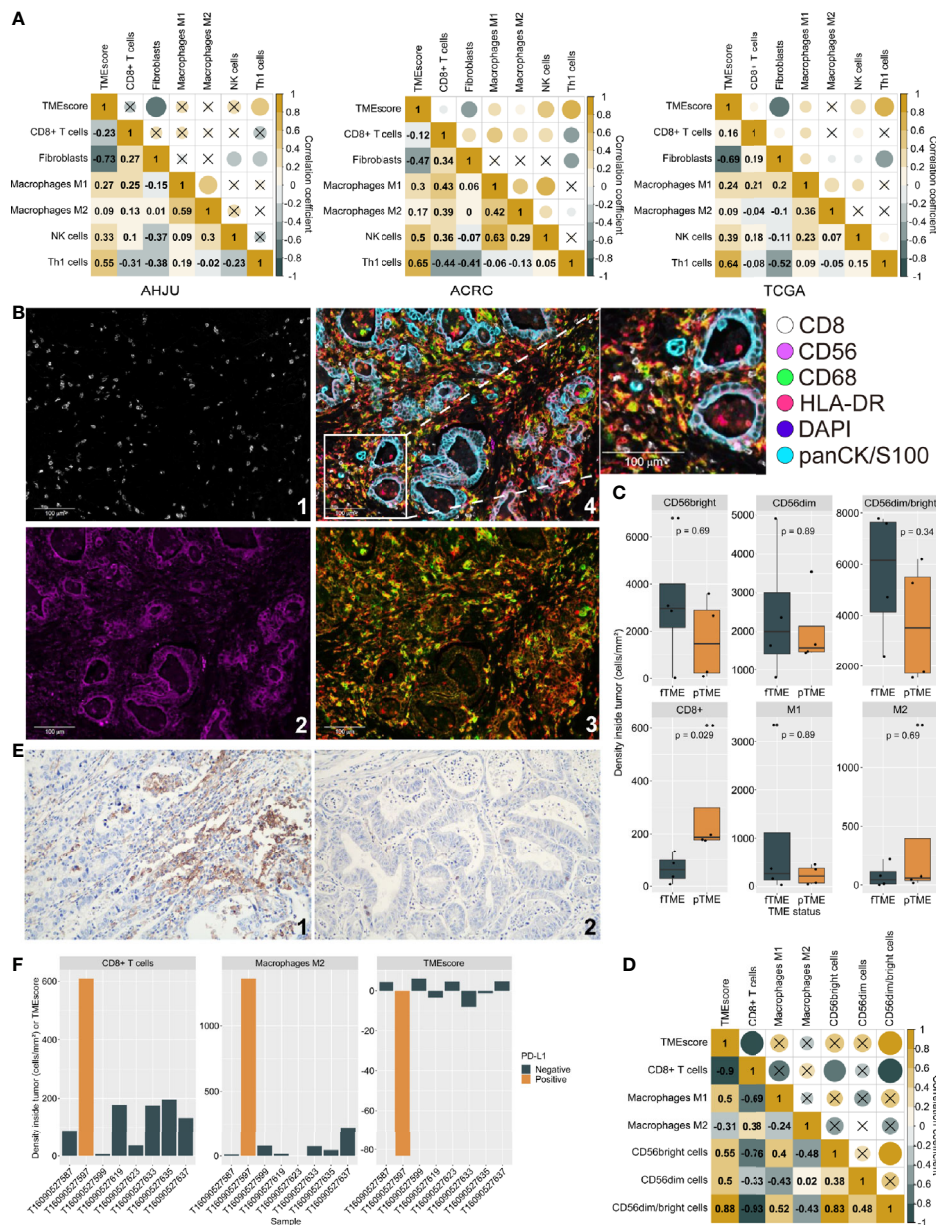
FIGURE 1 | Tumor microenvironment (TME) status and immune infiltration characteristics. **(A)**: Correlation between TMEscore and immune cell abundance based on transcriptome. **(B)**: Typical micrographs of multiplexed IHC and multispectral imaging, at 200× magnification; 1: CD8+; 2: CD56+; 3: CD68+ (green) and HLA-DR (red); 4. Reconstructed image after autofluorescence removal. **(C)**: Cell density inside tumor by TME status. **(D)**: The correlation between TMEscore and the effective infiltration degree of varied immune cells. **(E)**: Typical micrographs of programmed death ligand-1 (PD-L1)-positive (1) and negative (2) tumors, at 200× magnification. **(F)**: TMEscore and densities of CD8+ T cells and macrophages M2 inside tumors by PD-L1 expression. AHJU: Affiliated Hospital of Jiangsu University; ACRG, Asian Cancer Research Group; TCGA, The Cancer Genome Atlas; fTME or pTME, favorable or poor TME.

Tumor Microenvironment Status and Postoperative Chemotherapy/ Radiochemotherapy Efficacy by Stages

As patient selection for postoperative CT/RCT is currently based predominantly on pathological staging, we performed stratified analyses using TNM staging. We found that the OS and DFS benefits of postoperative CT/RCT in fTME GC were limited to patients with stage III disease; these benefits in pTME GC were pronounced in both stage Ib/II and III disease (**Figure 3**), indicating that fTME may predict a lack of postoperative CT/ RCT efficacy in stage Ib/II GC. Besides, patients with pTME GC benefited more evidently from postoperative CT/RCT than patients with fTME GC, even in cases with stage III disease (**Figure 3**).
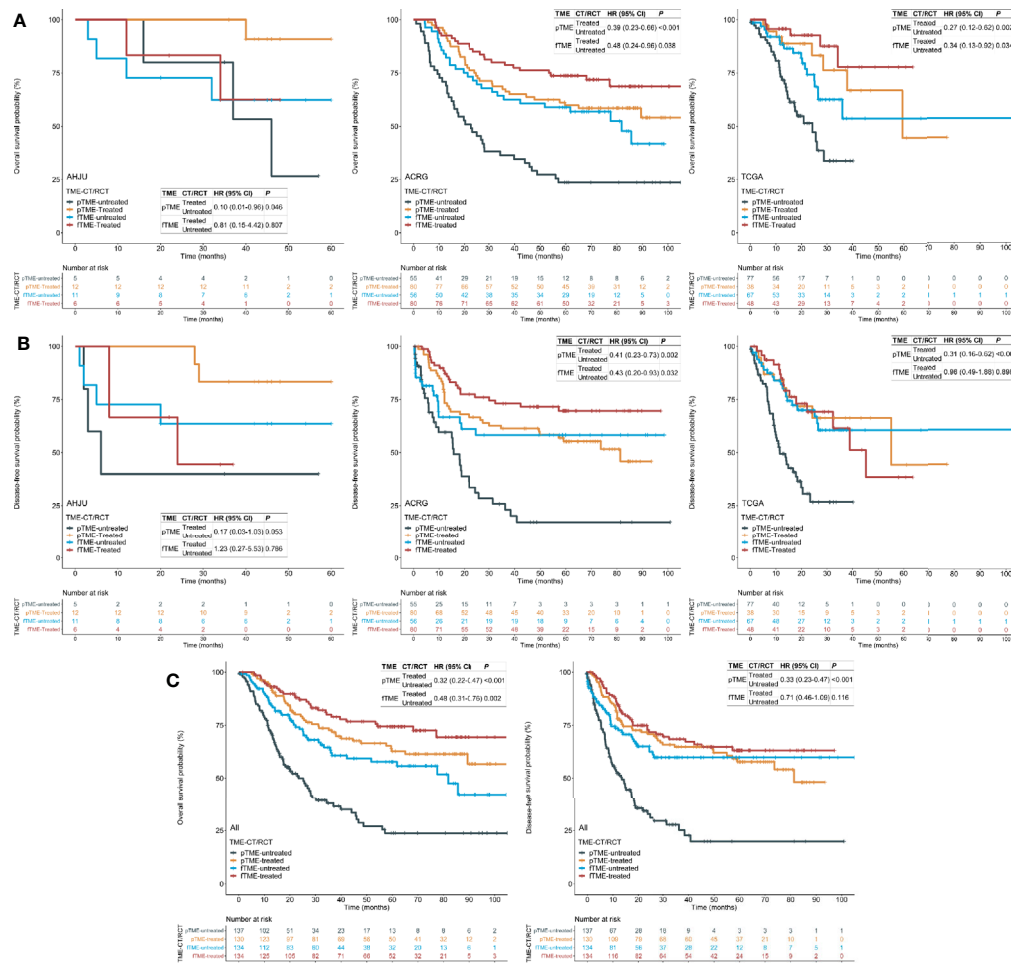
FIGURE 2 | Tumor microenvironment (TME) status and the efficacy of postoperative chemotherapy (CT) or radiochemotherapy (RCT). **(A)** Overall survival (OS) in each cohort; **(B)** disease-free survival (DFS) in each cohort; **(C)** OS and DFS in the pooled cohort. AHJU, Affiliated Hospital of Jiangsu University; ACRG, Asian Cancer Research Group; TCGA, The Cancer Genome Atlas; HR, hazard ratio; CI, confidence interval; fTME or pTME, favorable or poor TME.

TABLE 2 | Univariate and multivariate analyses of variables associated with overall survival and disease-free survival in patients with resected gastric cancer who had poor tumor microenvironment status in the pooled cohort.

Variable	Univariate analysis				Multivariate analysis*			
	Overall survival		Disease-free survival		Overall survival		Disease-free survival	
	HR (95% CI)	P	HR (95% CI)	P	HR (95% CI)	P	HR (95% CI)	P
Age (≥65 vs <65 years)	1.92 (1.33–2.76)	<0.001	1.58 (1.12–2.23)	0.010	1.76 (1.19–2.60)	0.005	1.22 (0.85–1.77)	0.279
Sex (Male vs female)	0.93 (0.64–1.35)	0.700	1.04 (0.72–1.49)	0.846	–		–	
Tumor location (Antrum vs non-antrum)	0.76 (0.53–1.09)	0.131	0.94 (0.67–1.33)	0.737	0.65 (0.45–0.96)	0.031	–	
Histology grade (III vs I/II)	1.51 (1.02–2.23)	0.038	1.45 (0.99–2.13)	0.053	1.52 (1.00–2.30)	0.050	1.30 (0.88–1.93)	0.188
TNM stage (III vs IB/II)	1.89 (1.28–2.79)	0.001	1.62 (1.13–2.33)	0.009	2.06 (1.37–3.10)	<0.001	1.84 (1.26–2.69)	0.002
MSI status (MSI vs MSS)	1.24 (0.68–2.25)	0.481	1.02 (0.55–1.90)	0.944	–		–	
Postoperative CT/RCT (Treated vs untreated)	0.32 (0.22–0.47)	<0.001	0.33 (0.23–0.47)	<0.001	0.32 (0.21–0.48)	<0.001	0.31 (0.21–0.47)	<0.001

*Variables were adopted for their prognostic significance (P < 0.15) by univariate analysis.
HR, hazard ratio; CI, confidence interval; MSI, microsatellite instability; MSS, microsatellite stability; CT, chemotherapy; RCT, radiochemotherapy.
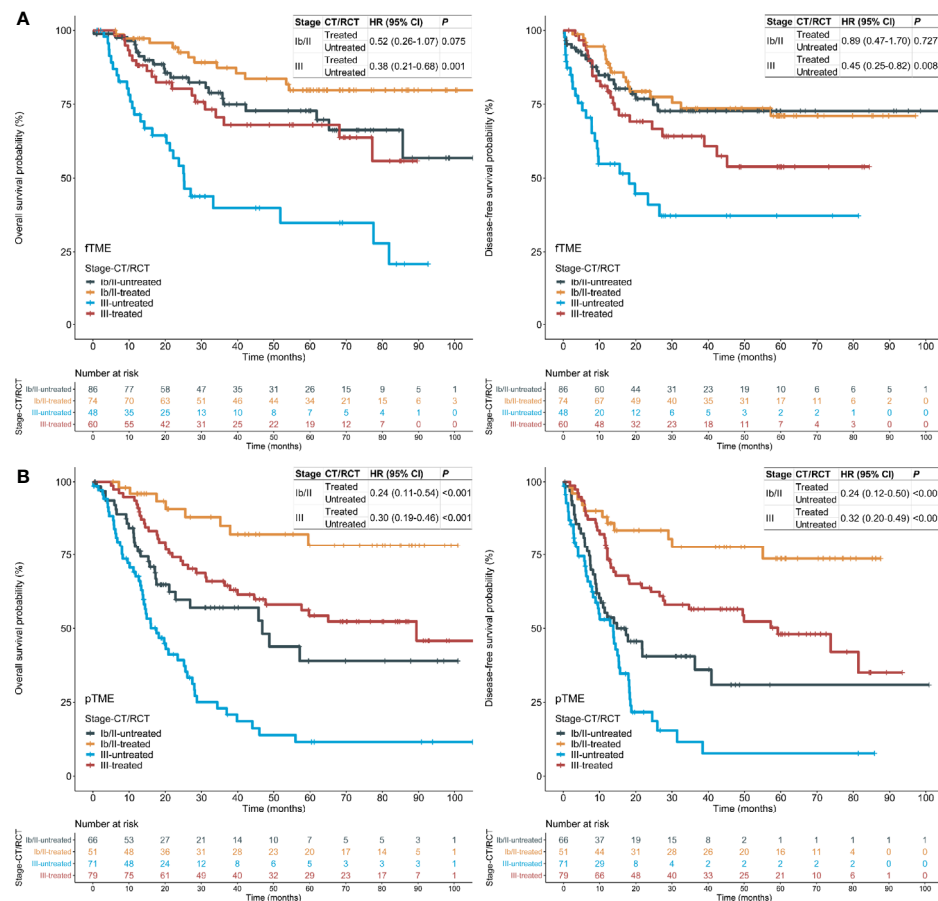
FIGURE 3 | Tumor microenvironment (TME) status and the efficacy of postoperative chemotherapy (CT) or radiochemotherapy (RCT), stratified by stages in the pooled cohort. **(A)** fTME subset; **(B)** pTME subset. HR: hazard ratio; CI: confidence interval; fTME or pTME: favorable or poor TME.

Tumor Microenvironment Status and Hypoxia

As tumor hypoxia induces CT and RCT resistance (27), its association with TME status was analyzed. Surprisingly, TMEscore was positively correlated with the hypoxia scores (**Figure 4A**), suggesting that fTME is related to a greater degree of hypoxia than pTME. On the contrary, the TMEscore was negatively correlated with an RCT response score in association with hypoxia (19) (**Figure 4A**). Moreover, stage Ib/II fTME GC showed the highest mean hypoxia score and lowest RCT response score across all the subgroups in the pooled cohort (**Figure 4B**).

We further validated our findings through a novel endogenous hypoxia marker—ERO1A (28) and observed that the TMEscore was positively correlated with the mRNA expression of ERO1A in all the cohorts (**Figure 4C**). Similar results were found for the mRNA expression of TS (**Figure 4C**)—the target of FU and an indicator of poor CT outcomes—potentially in association with upregulation by hypoxia (21, 29). In addition, stage Ib/II fTME GC was associated with the

strongest ERO1A and TS mRNA expressions across all the subgroups in the pooled cohort (**Figure 4D**).

Further validations were performed using IHC analysis in the AHJU cohort (**Figure 4E**). We found that the positive rates of ERO1A (12/17 *vs* 8/17; P = 0.163) and TS (14/17 *vs* 7/17; P = 0.013) were higher in fTME than pTME. Besides, stage Ib/II fTME GC showed the highest positivity rate for both ERO1A and TS proteins across all the subgroups (**Figure 4F**).

DISCUSSION

The treatment for GC has long been suboptimal, owing to a lack of validated prognostic or predictive biomarkers for therapy strategy optimization. The potential application of immune-associated biomarkers in resected cancers has recently been highlighted. Of them, tumor mutation burden (TMB) is a predictor of response to immune checkpoint inhibitors (30). A retrospective study on resected non-small-cell lung cancer found that a high TMB is correlated with favorable prognoses; however, a pronounced benefit from adjuvant CT was observed with a low
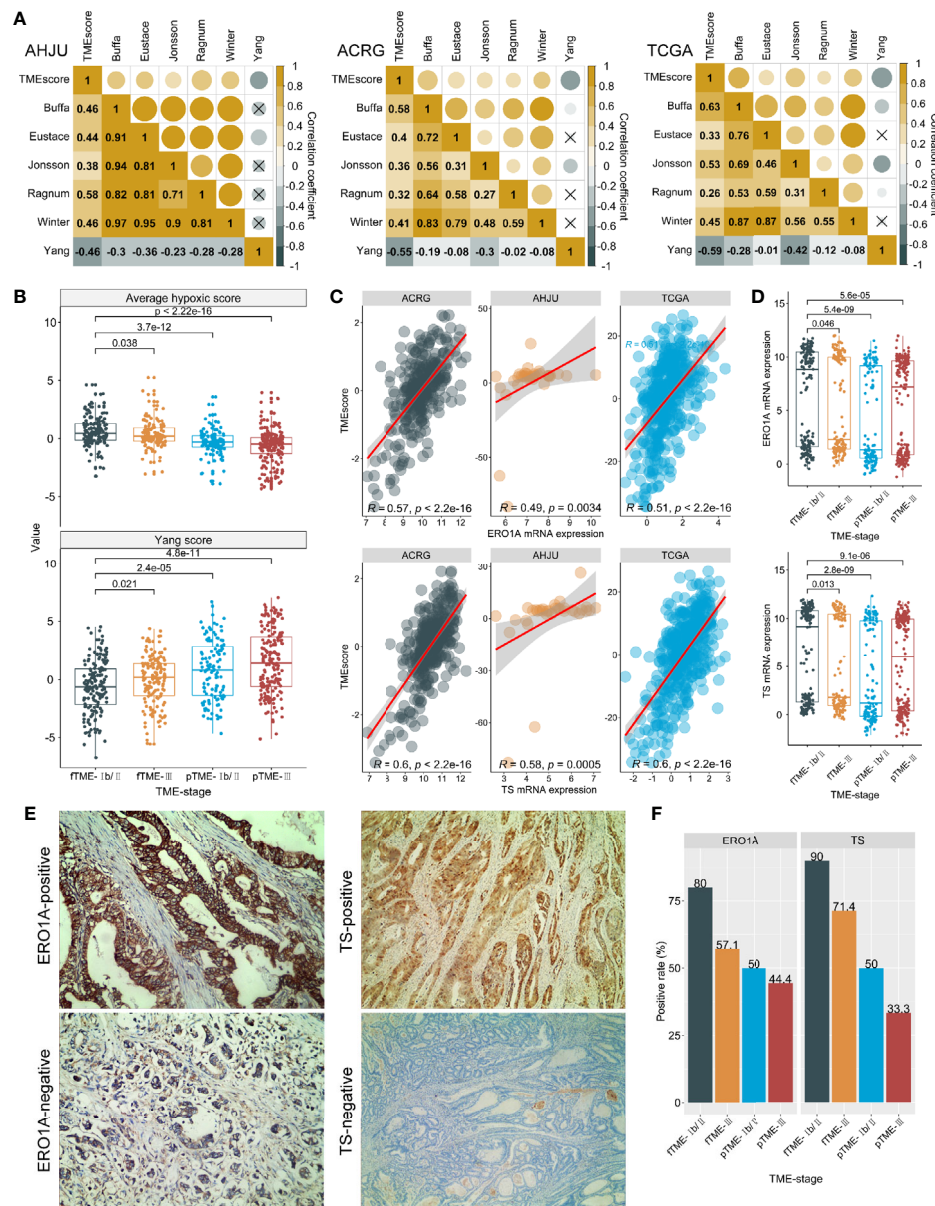
FIGURE 4 | Tumor microenvironment (TME) status and hypoxia. **(A)**: Correlation between TMEscore and hypoxia scores (Authors who develop hypoxia signatures are shown); **(B)**: Average hypoxia score and RCT response score developed by Yang, stratified by TME status and stage. **(C)**: Correlations between TMEscore and ERO1A and thymidylate synthase (TS) mRNA expression. **(D)**: ERO1A and TS mRNA expression, stratified by TME status and stage; **(E)**: Typical micrographs for immunohistochemistry staining of ERO1A and TS proteins, at 200× magnification; **(F)**: Protein expressions of ERO1A and TS, by TME status and stage. AHJU, Affiliated Hospital of Jiangsu University; ACRG, Asian Cancer Research Group; TCGA, The Cancer Genome Atlas; fTME or pTME, favorable or poor TME.

TMB (31). In resected GC, MSI and PD-L1 expression, two other major predictors of immunotherapy efficacy, were found to be independent predictors of favorable prognoses; however, patients with MSI or stromal PD-L1-positive GC did not benefit from adjuvant CT (32). Recently, we also reported that MSI may predict poor response to postoperative RCT in patients with stage Ib/II GC (13). Based on these findings, we sought to investigate the association between TME status and the efficacy of postoperative CT/RCT in resected GC.

This study revealed that patients with pTME GC may benefit to a greater degree from postoperative CT/RCT than those with fTME GC. Specifically, the postoperative CT/RCT benefit was observed regardless of the disease stage in patients with pTME GC, but was limited in stage III fTME GC. These findings indicated that GC patients who are considered for postoperative CT/RCT should have the tumor TME status assessed to inform the likelihood of therapy benefit, which may help improve the outcome of postoperative CT/RCT.

Immune-associated biomarkers are reflective of tumor-host immune interactions (33, 34), partly explaining their clinical relevance in resected tumors. In this study, we validated the positive correlation between TME status and antitumor immunity using both mRNA-based bioinformatics and IHC-based assessment. Specifically, we found that fTME GC was associated with a high level of NK cell infiltration, consistent with the increasing body of evidence on the interaction between TME and NK cells (35, 36). However, fTME GC was related to a lack of CD8+ T cell infiltration. This result may be unsurprising considering the positive correlation between CD8+ T cell infiltration and the key immunosuppressive indicator—PD-L1-positive expression, as previously reported (37, 38) and also indicated in our study. These findings suggest that TME status, as evaluated by the TMEscore, is a specific biomarker of immune activation.

Previously, we reported that stage Ib/II MSI GC was the only subgroup that did not experience the benefits of postoperative RCT (13). In this study, a similar result was found for stage Ib/II fTME GC. Because MSI also correlated with more inflamed tumors, these findings indicate that dynamic immune infiltration may impair CT/RCT response. Similarly, in bladder cancer, a study found that immunotypes characterized by low rather than high levels of immune infiltration derive benefits from adjuvant CT (39).

Hypoxia can determine CT/RCT response (27). Correspondingly, we further revealed that fTME was more hypoxic than pTME. Specifically, stage Ib/II fTME GC showed the highest level of hypoxia, accompanied by the highest TS expression. Interestingly, active immune infiltration in fTME seemed to increase hypoxia level. Recently, elevated hypoxia was also found to be associated with increased TMB across cancer types including GC (40). Because high TMB promotes immune infiltration by producing more novel peptide epitopes or neoantigens (41), this finding indicated again the association between immune infiltration and hypoxia. More studies need to investigate this association.

This study has some limitations. First, we retrieved the patient data from public databases; some important information, including that on the CT/RCT regimens, criteria for CT/RCT decisions, surgical style, and margin status was incomplete and even missing, impacting our results. Second, the patients were not randomly selected in this retrospective study, highlighting the need for randomized prospective validations. Moreover, heterogeneity existed among the study populations in terms of the patients' characteristics, NGS methods, and data processing methods, among others. However, we obtained consistent results among the three independent cohorts, indicating the robustness of our findings.

In conclusion, our results indicate that TME status is correlated with the efficacy of postoperative CT/RCT in resected GC and that fTME may predict a lack of postoperative CT/RCT response in stage Ib/II GC. Therefore, TME evaluation, especially in the setting of stage Ib/II GC, should be considered a clinically useful marker to identify patients who may fail in postoperative CT/RCT, and represents an additional step in individualized GC therapy. Further validations of our findings especially in randomized prospective studies are necessary.

DATA AVAILABILITY STATEMENT

The datasets presented in this study can be found in online repositories. The names of the repository/repositories and accession number(s) can be found in the article/**Supplementary Material**.

ETHICS STATEMENT

The studies involving human participants were reviewed and approved by the Ethics Committee of the Affiliated Hospital of Jiangsu University. The patients/participants provided their written informed consent to participate in this study.

AUTHOR CONTRIBUTIONS

RD, XL, and DW conceived and designed the study. RD, DZe, XC, BS, DZh, LZ, YY, XL, and DW developed the methodology, RD, DZe, XC, BS, DZh, LZ, YY, XL, and DW acquired the data. RD, DZe, XC, BS, DZh, LZ, YY, XL, and DW analyzed and interpreted the data. RD, XL, and DW wrote, reviewed, and/or revised the manuscript. RD, DZe, XC, BS, DZh, LZ, YY, XL, and DW provided administrative, technical, or material support. RD, XL, and DW supervised the study. All authors contributed to the article and approved the submitted version.

FUNDING

ACKNOWLEDGMENTS

SUPPLEMENTARY MATERIAL

The Supplementary Material for this article can be found online at: https://www.frontiersin.org/articles/10.3389/fimmu.2020.609337/full#supplementary-material

SUPPLEMENTARY FIGURE 1 | The efficacy of postoperative chemotherapy (CT) or radiochemotherapy (RCT) in resected gastric cancer. AHJU, Affiliated Hospital of Jiangsu University; ACRG, Asian Cancer Research Group; TCGA, The Cancer Genome Atlas; HR, hazard ratio; CI, confidence interval.

REFERENCES

1. Cai Z, Yin Y, Yin Y, Shen C, Wang J, Yin X, et al. Comparative effectiveness of adjuvant treatments for resected gastric cancer: a network meta-analysis. *Gastric Cancer* (2018) 21:1031–40. doi: 10.1007/s10120-018-0831-0

2. Kim TH, Park SR, Ryu KW, Kim YW, Bae JM, Lee JH, et al. Phase 3 trial of postoperative chemotherapy alone versus chemoradiation therapy in stage III-IV gastric cancer treated with R0 gastrectomy and D2 lymph node dissection. *Int J Radiat Oncol Biol Phys* (2012) 84:e585–92. doi: 10.1016/j.ijrobp.2012.07.2378

3. Park SH, Sohn TS, Lee J, Lim DH, Hong ME, Kim KM, et al. Phase III Trial to Compare Adjuvant Chemotherapy With Capecitabine and Cisplatin Versus Concurrent Chemoradiotherapy in Gastric Cancer: Final Report of the Adjuvant Chemoradiotherapy in Stomach Tumors Trial, Including Survival and Subset Analyses. *J Clin Oncol* (2015) 33:3130–6. doi: 10.1200/JCO.2014.58.3930

4. Matuschek C, Haussmann J, Bölke E, Tamaskovics B, Djiepmo Njanang FJ, Orth K, et al. Adjuvant radiochemotherapy vs. chemotherapy alone in gastric cancer: a meta-analysis. *Strahlenther Onkol* (2019) 195:695–706. doi: 10.1007/s00066-019-01431-y

5. Cancer Genome Atlas Research Network. Comprehensive molecular characterization of gastric adenocarcinoma. *Nature* (2014) 513:202–9. doi: 10.1038/nature13480

6. Cristescu R, Lee J, Nebozhyn M, Kim KM, Ting JC, Wong SS, et al. Molecular analysis of gastric cancer identifies subtypes associated with distinct clinical outcomes. *Nat Med* (2015) 21:449–56. doi: 10.1038/nm.3850

7. Turley SJ, Cremasco V, Astarita JL. Immunological hallmarks of stromal cells in the tumour microenvironment. *Nat Rev Immunol* (2015) 15:669–82. doi: 10.1038/nri3902

8. Fridman WH, Zitvogel L, Sautès-Fridman C, Kroemer G. The immune contexture in cancer prognosis and treatment. *Nat Rev Clin Oncol* (2017) 14:717–34. doi: 10.1038/nrclinonc.2017.101

9. Wang Y, Gan G, Wang B, Wu J, Cao Y, Zhu D, et al. Cancer-associated Fibroblasts Promote Irradiated Cancer Cell Recovery Through Autophagy. *EBioMedicine* (2017) 17:45–56. doi: 10.1016/j.ebiom.2017.02.019

10. Wang JT, Li H, Zhang H, Chen YF, Cao YF, Li RC, et al. Intratumoral IL17-producing cells infiltration correlate with antitumor immune contexture and improved response to adjuvant chemotherapy in gastric cancer. *Ann Oncol* (2019) 30:266–73. doi: 10.1093/annonc/mdy505

11. Zeng D, Li M, Zhou R, Zhang J, Sun H, Shi M, et al. Tumor Microenvironment Characterization in Gastric Cancer Identifies Prognostic and Immunotherapeutically Relevant Gene Signatures. *Cancer Immunol Res* (2019) 7:737–50. doi: 10.1158/2326-6066.CIR-18-0436

12. Aran D, Hu Z, Butte AJ. xCell: digitally portraying the tissue cellular heterogeneity landscape. *Genome Biol* (2017) 18:220. doi: 10.1186/s13059-017-1349-1

13. Dai D, Zhao X, Li X, Shu Y, Shen B, Chen X, et al. Association Between the Microsatellite Instability Status and the Efficacy of Postoperative Adjuvant Chemoradiotherapy in Patients With Gastric Cancer. *Front Oncol* (2019) 9:1452. doi: 10.3389/fonc.2019.01452

14. Buffa FM, Harris AL, West CM, Miller CJ. Large meta-analysis of multiple cancers reveals a common, compact and highly prognostic hypoxia metagene. *Br J Cancer* (2010) 102:428–35. doi: 10.1038/sj.bjc.6605450

15. Eustace A, Mani N, Span PN, Irlam JJ, Taylor J, Betts GN, et al. A 26-gene hypoxia signature predicts benefit from hypoxia-modifying therapy in laryngeal cancer but not bladder cancer. *Clin Cancer Res* (2013) 19:4879–88. doi: 10.1158/1078-0432.CCR-13-0542

16. Jonsson M, Ragnum HB, Julin CH, Yeramian A, Clancy T, Frikstad KM, et al. Hypoxia-independent gene expression signature associated with radiosensitisation of prostate cancer cell lines by histone deacetylase inhibition. *Br J Cancer* (2016) 115:929–39. doi: 10.1038/bjc.2016.278

17. Ragnum HB, Vlatkovic L, Lie AK, Axcrona K, Julin CH, Frikstad KM, et al. The tumour hypoxia marker pimonidazole reflects a transcriptional programme associated with aggressive prostate cancer. *Br J Cancer* (2015) 112:382–90. doi: 10.1038/bjc.2014.604

18. Winter SC, Buffa FM, Silva P, Miller C, Valentine HR, Turley H, et al. Relation of a hypoxia metagene derived from head and neck cancer to prognosis of multiple cancers. *Cancer Res* (2007) 67:3441–9. doi: 10.1158/0008-5472.CAN-06-3322

19. Yang L, Taylor J, Eustace A, Irlam JJ, Denley H, Hoskin PJ, et al. A Gene Signature for Selecting Benefit from Hypoxia Modification of Radiotherapy for High-Risk Bladder Cancer Patients. *Clin Cancer Res* (2017) 23:4761–8. doi: 10.1158/1078-0432.CCR-17-0038

20. Kim ST, Cristescu R, Bass AJ, Kim KM, Odegaard JI, Kim K, et al. Comprehensive molecular characterization of clinical responses to PD-1 inhibition in metastatic gastric cancer. *Nat Med* (2018) 24:1449–58. doi: 10.1038/s41591-018-0101-z

21. Tao Q, Zhu W, Zhao X, Li M, Shu Y, Wang D, et al. Perineural Invasion and Postoperative Adjuvant Chemotherapy Efficacy in Patients With Gastric Cancer. *Front Oncol* (2020) 10:530. doi: 10.3389/fonc.2020.00530

22. Tumeh PC, Harview CL, Yearley JH, Shintaku IP, Taylor EJ, Robert L, et al. PD-1 blockade induces responses by inhibiting adaptive immune resistance. *Nature* (2014) 515:568–71. doi: 10.1038/nature13954

23. White IR, Royston P, Wood AM. Multiple imputation using chained equations: Issues and guidance for practice. *Stat Med* (2011) 30:377–99. doi: 10.1002/sim.4067

24. Rubin DB. *Multiple Imputation for Nonresponse in Surveys*. New York: NY: John Wiley & Sons (2004).

25. Zhang Y, Zhang Y, Gu W, Sun B. TH1/TH2 cell differentiation and molecular signals. *Adv Exp Med Biol* (2014) 841:15–44. doi: 10.1007/978-94-017-9487-9_2

26. Costa A, Kieffer Y, Scholer-Dahirel A, Pelon F, Bourachot B, Cardon M, et al. Fibroblast Heterogeneity and Immunosuppressive Environment in Human Breast Cancer. *Cancer Cell* (2018) 33:463–79.e10. doi: 10.1016/j.ccell.2018.01.011

27. Wilson WR, Hay MP. Targeting hypoxia in cancer therapy. *Nat Rev Cancer* (2011) 11:393–410. doi: 10.1038/nrc3064

28. Takei N, Yoneda A, Kosaka M, Sakai-Sawada K, Tamura Y. ERO1α is a novel endogenous marker of hypoxia in human cancer cell lines. *BMC Cancer* (2019) 19:510. doi: 10.1186/s12885-019-5727-9

29. Pereira MA, Ramos M, Dias AR, Faraj SF, Cirqueira C, de Mello ES, et al. Immunohistochemical expression of thymidylate synthase and prognosis in gastric cancer patients submitted to fluoropyrimidine-based chemotherapy. *Chin J Cancer Res* (2018) 30:526–36. doi: 10.21147/j.issn.1000-9604.2018.05.06

30. Cao D, Xu H, Xu X, Guo T, Ge W. High tumor mutation burden predicts better efficacy of immunotherapy: a pooled analysis of 103078 cancer patients. *Oncoimmunology* (2019) 8:e1629258. doi: 10.1080/2162402X.2019.1629258

31. Devarakonda S, Rotolo F, Tsao MS, Lanc I, Brambilla E, Masood A, et al. Tumor Mutation Burden as a Biomarker in Resected Non-Small-Cell Lung Cancer. *J Clin Oncol* (2018) 36:2995–3006. doi: 10.1200/JCO.2018.78.1963

32. Choi YY, Kim H, Shin SJ, Kim HY, Lee J, Yang HK, et al. Microsatellite Instability and Programmed Cell Death-Ligand 1 Expression in Stage II/III Gastric Cancer: Post Hoc Analysis of the CLASSIC Randomized Controlled study. *Ann Surg* (2018) 270:309–16. doi: 10.1097/SLA.0000000000002803

33. Rosenthal R, Cadieux EL, Salgado R, Bakir MA, Moore DA, Hiley CT, et al. Neoantigen-directed immune escape in lung cancer evolution. *Nature* (2019) 567:479–85. doi: 10.1038/s41586-019-1032-7

34. Lin EM, Gong J, Klempner SJ, Chao J. Advances in immuno-oncology biomarkers for gastroesophageal cancer: Programmed death ligand 1, microsatellite instability, and beyond. *World J Gastroenterol* (2018) 24:2686–97. doi: 10.3748/wjg.v24.i25.2686

35. Terrén I, Orrantia A, Vitallé J, Zenarruzabeitia O, Borrego F. NK Cell Metabolism and Tumor Microenvironment. *Front Immunol* (2019) 10:2278. doi: 10.3389/fimmu.2019.02278

36. Böttcher JP, Bonavita E, Chakravarty P, Blees H, Cabeza-Cabrerizo M, Sammicheli S, et al. NK Cells Stimulate Recruitment of cDC1 into the Tumor Microenvironment Promoting Cancer Immune Control. *Cell* (2018) 172:1022–37.e14. doi: 10.1016/j.cell.2018.01.004

37. Jiang T, Shi J, Dong Z, Hou L, Zhao C, Li X, et al. Genomic landscape and its correlations with tumor mutational burden, PD-L1 expression, and immune cells infiltration in Chinese lung squamous cell carcinoma. *J Hematol Oncol* (2019) 12:75. doi: 10.1186/s13045-019-0762-1

38. Angell HK, Lee J, Kim KM, Kim K, Kim ST, Park SH, et al. PD-L1 and immune infiltrates are differentially expressed in distinct subgroups of gastric

cancer. *Oncoimmunology* (2019) 8:e1544442. doi: 10.1080/2162402X.2018.1 544442

39. Fu H, Zhu Y, Wang Y, Liu Z, Zhang J, Xie H, et al. Identification and Validation of Stromal Immunotype Predict Survival and Benefit from Adjuvant Chemotherapy in Patients with Muscle-Invasive Bladder Cancer. *Clin Cancer Res* (2018) 24:3069–78. doi: 10.1158/1078-0432. CCR-17-2687

40. Bhandari V, Li CH, Bristow RG, Boutros PC. PCAWG Consortium. Divergent mutational processes distinguish hypoxic and normoxic tumours. *Nat Commun* (2020) 11:737. doi: 10.1038/s41467-019-14052-x

41. Rizvi NA, Hellmann MD, Snyder A, Kvistborg P, Makarov V, Havel JJ, et al. Cancer immunology. Mutational landscape determines sensitivity to PD-1 blockade in non-small cell lung cancer. *Science* (2015) 348:124–8. doi: 10.1126/science.aaa1348

Glioma Stem Cells as Immunotherapeutic Targets: Advancements and Challenges

Keenan Piper[1,2†], Lisa DePledge[1,3†], Michael Karsy[4] and Charles Cobbs[1*]

[1] Ben & Catherine Ivy Center for Advanced Brain Tumor Treatment, Swedish Neuroscience Institute, Seattle, WA, United States,
[2] Sidney Kimmel Medical College, Philadelphia, PA, United States, [3] University of Washington School of Medicine, Spokane, WA,
United States, [4] Department of Neurological Surgery, Thomas Jefferson University, Philadelphia, PA, United States

Glioblastoma is the most common and lethal primary brain malignancy. Despite major investments in research into glioblastoma biology and drug development, treatment remains limited and survival has not substantially improved beyond 1–2 years. Cancer stem cells (CSC) or glioma stem cells (GSC) refer to a population of tumor originating cells capable of self-renewal and differentiation. While controversial and challenging to study, evidence suggests that GCSs may result in glioblastoma tumor recurrence and resistance to treatment. Multiple treatment strategies have been suggested at targeting GCSs, including immunotherapy, posttranscriptional regulation, modulation of the tumor microenvironment, and epigenetic modulation. In this review, we discuss recent advances in glioblastoma treatment specifically focused on targeting of GCSs as well as their potential integration into current clinical pathways and trials.

Keywords: glioblastoma stem cells, glioblastoma, cancer vaccination, radioresistance, tumor recurrence, cancer stem cell, brain tumors, immunotherapy

INTRODUCTION

Glioblastoma (GBM), a World Health Organization grade IV astrocytoma, is the most common primary brain malignancy with an incidence of 3.22:100,000 annually in the U.S (1). Despite standard of care treatment with maximal surgical resection, radiotherapy, adjuvant temozolomide (TMZ) chemotherapy, and tumor-treating-fields, median survival is still only 14.6 months (2), and nearly all patients succumb to fatal tumor recurrence and progression, with a <5% 5-year overall survival (OS).

The lack of improvement in GBM outcomes may be attributed, in part, to current therapies' inability to target glioma stem cells (GSCs), a small subpopulation of cells that are implicated in tumor invasiveness, recurrence, and chemo(radio)resistance. The GSC population remains challenging both to define empirically and treat. GSCs are described by their ability to self-renew and differentiate to reform the heterogeneity of GBM (3). Multiple strategies to target GSC are currently under investigation with varying levels of preclinical and clinical development (4). In this review, we discuss the evidence supporting GBM's common stem cell origin and outline the limitations of standard of care treatment for GBM. We then explore immunotherapeutic targeting of GSCs and highlight ongoing clinical trials.

GLIOBLASTOMA AND THE CANCER STEM CELL MODEL

GBM development originally was defined by two divergent but interconnected models, namely, the stochastic model and CSC model. The stochastic or clonal evolution model suggests that all cells have the equal capacity for undergoing transformation based on accumulated mutations and/or epigenetic changes that confer a survival benefit (5). The CSC or hierarchical model suggests that a limited number of stem-like cells with few tumorigenic driver mutations have the capacity to divide symmetrically into identical daughter cells and differentiated progeny resulting in self-renewal and heterogeneous tumor progression (6–9). Bonnet and Dick's seminal discovery of CSCs in leukemia, and subsequent discoveries of CSCs in most hematologic and solid tumor malignancies, including breast, colon, and some skin cancers greatly promoted the acceptance of the model (10–18). While CSCs mirror many of the features of normal stem cells, such as lineage determinization, resistance to apoptosis, neoangiogenesis, and self-renewal, they are distinct entities capable of tumorigenesis defined by few genetic mutations and altered epigenetic regulation (19–21). In the convergence of the stochastic and CSC models (22), differentiated cells can be transformed (23) and subsequently acquire a stem-like state (24), although some cell types such as neurons and their immediate precursors appear to be resistant to such mutations (25).

While the CSC hypothesis provides a compelling model for many cancers, attempts to define CSCs based on a set of genetic markers, epigenetic makeup, or cell state (e.g., quiescent or proliferative) have not reproducibly supported the isolation of fully competent CSCs. Three functional tests that are considered the gold standard for validating CSCs are: 1) self-renewal, 2) tumor initiation upon transplantation, and 3) differentiation into distinct progeny that can recapitulate the initial tumor's heterogeneity upon serial transplantation (3). Regulation of the CSC population *in vitro* has depended on multiple molecular mechanisms, genetics, epigenetics, cellular states, intrinsic cell stimuli, microenvironmental influences, and other factors (7, 11–13). These mechanisms potentially allow the CSC population to transition between CSC and non-CSC states.

GSCs were first studied in 2002 (26), and were found to localize to a vascular niche (27). They are thought to arise from cells of the subventricular zone (SVZ) or differentiated glioma cells (28). Several markers of GSCs, namely, CD133, CD44, and CD15, help to define and enrich these population of cells but are not specific (3) (**Figure 1**). Recent single-cell sequencing studies have revealed that astrocyte-like neural stem cells with driver mutations migrate from the SVZ and lead to the development of high-grade gliomas in distant brain regions (28). This has provided precedent for radiotherapy targeted at high doses at the SVZ (National Clinical Trial [NCT] 02177578, NCT03956706). Another recent study demonstrated, *via* a xenotransplant model, the potential for slow-cycling cells to form rapidly cycling progenitor cells capable of self-maintenance and generation of non-proliferating progeny (29). These results are consistent with the CSC model suggesting that GBM tumor heterogeneity may result from a mono- or polyclonal tumor origin (30–32).
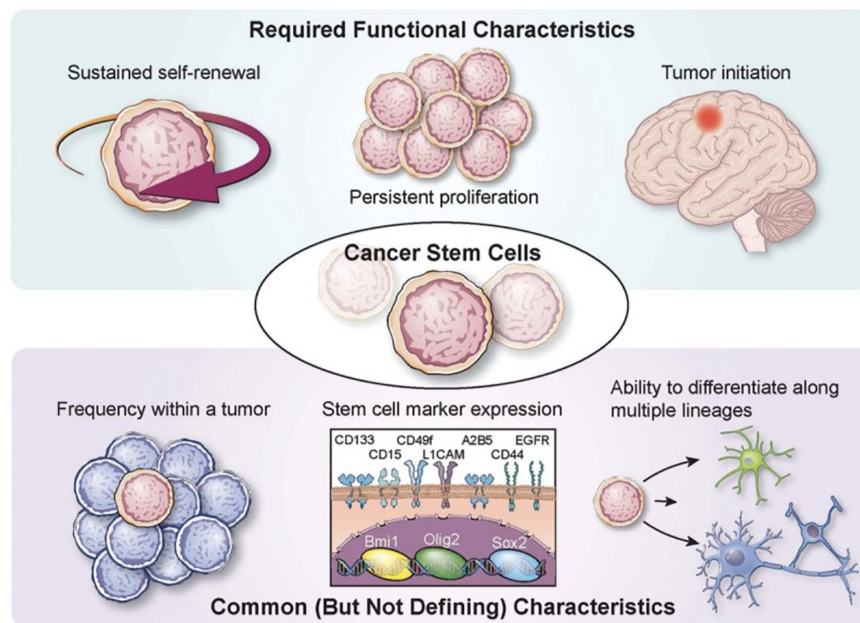

FIGURE 1 | Characterization of glioma stem cells Various required functional characteristics of cancer stem cells (CSCs) and glioma stem cells (GCSs) are shown including self-renewal, proliferation, and initiation. Common characteristics include low frequency within a tumor, stem cell marker expression, and potential for differentiation. Reprinted with permission from Lathia et al. (3).

CONTROVERSY

While there is evidence that supports GSCs involvement in GBM's genesis, progression, and recurrence, there are several roadblocks to studying this cell population. First, stem cells are regulated in a multitude of ways, including genetic and epigenetic modifications, metabolic changes, cell responses to the immune system, microenvironment, and niche factors (3, 4, 33). These regulatory mechanisms result in a highly dynamic pool of cells which are therefore difficult to define and target. Additionally, the stem-like phenotype is mutable and in-vitro techniques may induce differentiation of the cells making them increasingly difficult to study. For the studies that have investigated, there are not consistent methods to define and isolate the physical characteristics of GSCs, so it is difficult to find consensus in the scientific community with regards to their role in GBM. Finally, CSCs in general are rare within the tumor mass (34), casting doubt upon the role they might play in tumor genesis, progression, and recurrence.

Despite the challenges of studying GSCs, there is hope that more advanced techniques, such as single cell sequencing, are elucidating some of the mysteries of these cells. One study by Patel et al. (2014) utilized single cell sequencing technology to investigate 430 cells in each of 5 GBM tumors, and elucidated a stem-like population of cells which existed within a stemness gradient (35). Further, a recent study by Couturier et al. (2020) used single cell RNA sequencing and discovered that in 16 IDHwt glioblastomas there was a GSC cell type with a distinct transcriptomic signature (36). While GSCs have historically been difficult to define, emerging technologies and findings are furthering the hypothesis that GSCs may be a worthy target in researching GBM therapeutics.

LIMITATIONS OF CURRENT GLIOBLASTOMA TREATMENTS

Current therapeutic treatment remains limited for GBM and multiple resistance mechanisms for GCS may partially account for this. Subclonal populations of cells left behind after gross total resection result in tumor recurrence and resistance (31). GSCs have the potential to maintain a quiescent cell cycle phenotype, rendering many chemotherapeutic agents ineffective. GSCs primarily reside within perivascular niches, where components of the extracellular matrix (ECM) modulate GSC survival and function. Several components within the ECM, like hyaluronic acid and the dystrophin–glycoprotein complex (DGC), have been shown to contribute to resistance and promote invasion (37–39). In addition, CSCs overexpress ATP-binding cassette (ABC) transporters that pump foreign toxins out of the cell, conferring multidrug resistance (40). Cells that express CD133, a cell surface marker highly associated with GSCs, have been shown to express O^6-methylguanine-DNA methyltransferase (MGMT) at levels 32–56 times those of CD133(−) cells (41). The high activity of MGMT in these cells helps explain TMZ's

relative ineffectiveness against GSCs (42). By inducing expression of hypoxia-inducible factors, such as HIF1α and HIF2α—itself associated with poor prognosis for glioma patients (42)—TMZ may induce stemness in differentiated glioma cells (43). Resistance to radiation is also seen in GCSs, where a high ratio of GSCs to differentiated tumor cells correlates with increased tumor radioresistance (44), and CD133(+) cells have been reported to be resistant to apoptosis induced by *in vitro* radiotherapy (45). Hypoxic microenvironments preferentially contribute to GCS growth, which can reduce oxidative-stress produced by radiation (46). GSC radioresistance is also conferred by both the hypoxia-mediated activation of DNA damage checkpoint response enzymes Chk 1/2 (47) as well as by induction of autophagy to process and eliminate constituent parts of cells damaged by radiation (48).

TARGETED THERAPY OF GSCS

Scientists have attempted to target GSCs through a multitude of avenues (**Figure 2**). Small molecules which activate or inhibit common, upregulated pathways in this cell population associated with their resilience. Targeted pathways are those that, when disrupted, result in chemo- and radiosensitization, tumor growth inhibition, induction of differentiation, inhibition of multidrug resistance, and promotion of apoptosis. Some of these pathways include STAT3 (49), Notch (50), PI3K/Akt/mTOR (51, 52), and Hedgehog (53). There are many pathways that contribute to the resilience and tumorigenicity of GSCs, and the dominant driver pathways vary from patient to patient. Because of this, finding a "one size fits all" small molecule solution is unlikely. Difficulties associated with chemotherapeutic approaches to treat GBM highlight the need for a new generation of cancer therapy, and immunotherapy presents an alternative that addresses these shortcomings.

IMMUNOTHERAPY: THE FUTURE OF GSC TREATMENT?

The body prevents neoplastic proliferation primarily *via* the immune system. However, GBMs are known to exert immunosuppressive effects systemically and in the tumor microenvironment through a combination of decreased immunogenicity and active suppression of T cells that exceeds the immunosuppressive capacity of non-stem glioma cells (54, 55). Immunotherapy is a highly specific GBM treatment modality that may overcome the immunosuppressive effects of GBM generally, and GSCs in particular, through the introduction of monoclonal antibodies (mAb) or stimulation of the patient's own immune response. These approaches may induce fewer side effects than other oncolytic methods which are less precise in their action.

Cancer immunotherapy approaches can be primarily categorized as passive, active, or adoptive (**Figure 3**). Passive immunotherapy uses antibodies to target tumor specific antigens
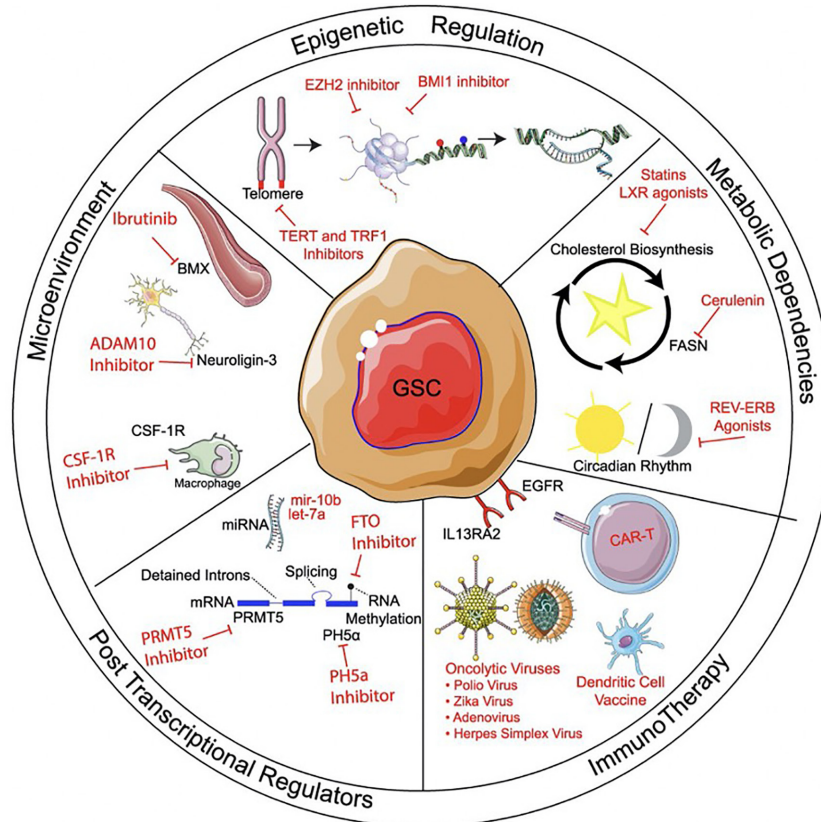
FIGURE 2 | Methods of targeting glioma stem cells. Methods of targeting glioma stem cells (GSCs) can be divided into treatments targeting epigenetic regulation, metabolic pathways, microenvironment, post-transcriptional regulation, and immunotherapy. Within immunotherapy, strategies can include immunomodulatory drugs, oncolytic viral targeting, as well as passive, active, and adoptive immunotherapy approaches. Reprinted with permission from Gimple et al. (4).

and often doesn't require a host immune response to initiate cancer cell death. Active immunotherapy activates the host's immune system against tumor specific antigens, most often utilizing dendritic cells as antigen presenters. In adoptive immunotherapy, immune cells are removed from the patient, selected or genetically engineered for their reactivity against a target of interest, and reintroduced. Finally, many consider virotherapy a form of immunotherapy due to the activation of the immune system. Virotherapy makes use of genetically engineered oncolytic viruses to train the body's immune system against remnant cancer particles following virus-mediated killing.

Radiation therapy used as a complement with immunotherapy is an exciting and promising avenue to explore in the management of GBM. For example, radiation has been shown to cause immunogenic tumor cell death (ICD). ICD induces the translocation of calreticulin to the surface of the tumor cells surface, causing APCs to phagocytose tumor cells. ICD also promotes the release of HMGB1, encouraging dendritic cell maturation and tumor antigen presentation (56). Radiation can also enhance the permeability of the blood-brain barrier, which may allow T-cells to invade the tumor. Furthermore, radiation has

been shown to drastically increase the presence of MHC on the tumor cell surface providing greater density of T-cell targets (57–60). The various potential benefits presented by the combination of radiation and immunotherapy have spurred immense interest in the field.

In this section, we will discuss immunotherapy clinical trials which target GSC-specific and GSC-overexpressed targets with a focus on ongoing clinical trials (**Table 1**).

Passive Immunotherapy

Passive immunotherapy utilizes antibodies to bind to oncomodulatory signaling molecules or target proteins on cancer cells and disrupt cellular function without producing a memory immune response in the patient. The most significant improvement in standard of care treatment in the United States recently has been the addition of the monoclonal antibody bevacizumab, or Avastin, which was granted accelerated approval by the FDA in 2009 (61). Bevacizumab targets vascular endothelial growth factor (VEGF), a signaling molecule that promotes angiogenesis and is secreted in high quantities by GBM cells. While bevacizumab has improved the
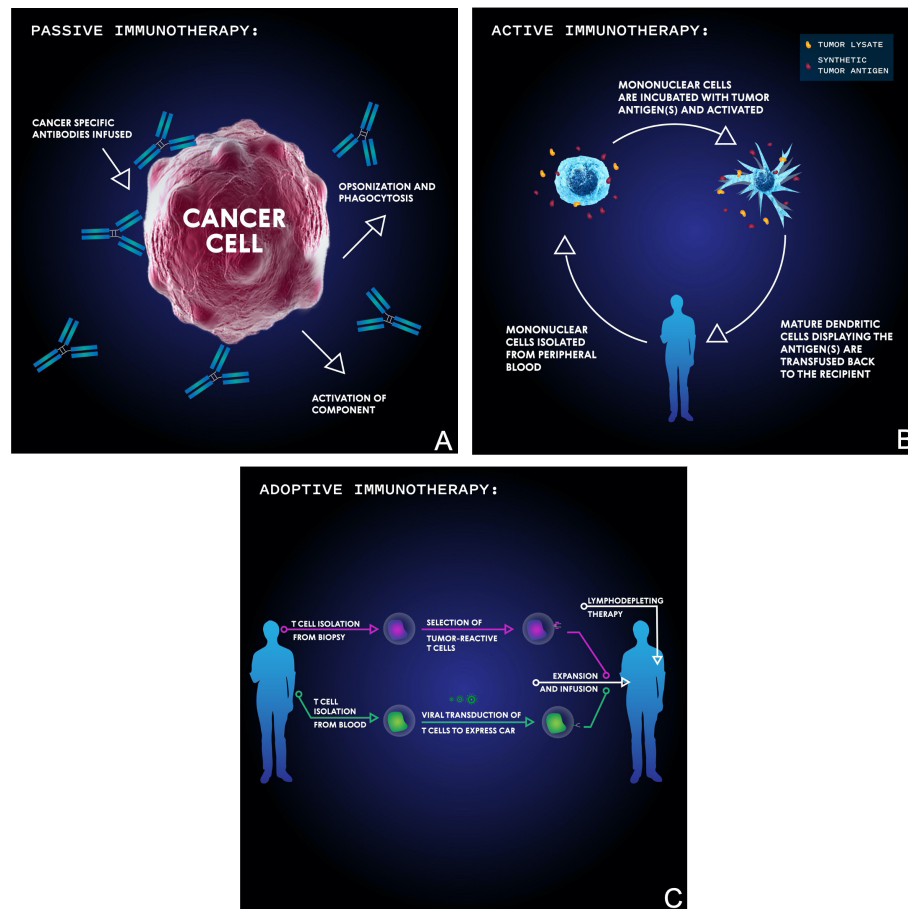
FIGURE 3 | Basic schema of the main immunotherapeutic modalities for targeting malignancies. In passive immunotherapy **(A)**, antibodies are developed which bind specific tumor antigens and induce cellular-mediated phagocytosis or complement membrane attack complex-mediated cell death. In active immunotherapy **(B)**, mononuclear cells are isolated from the patient's blood then incubated with synthetic or biopsy-derived tumor antigens and activated before being transfused back into the patient in order to facilitate an anti-tumor T cell immune response. In adoptive immunotherapy **(C)**, either tumor-infiltrating T cells are isolated from tumor biopsy, selected for their reactivity, and then transfused into a lymphodepleted patient, or T cells are isolated from blood, virally transduced to express a chimeric antigen receptor (CAR), and then transfused into a lymphodepleted patient.

progression free survival (PFS) of patients with GBM, it has failed to improve OS. GSCs are notoriously resistant to hypoxia and may therefore persist despite the additional therapeutic, contributing to inevitable recurrence (62).

Epidermal growth factor receptor (EGFR) is molecular target overexpressed in GSCs which confers chemo- and radioresistance in GBM tumors, resulting in poorer outcomes among GBM patients (63). The EGFR-targeting mAbs nimotuzumab and cetuximab have been shown to reduce the total number of radioresistant CD133(+) cancer stem cells in a murine glioma model (64). Nimotuzumab alone demonstrates antiangiogenic and antiproliferative activity while cetuximab inhibits downstream EGFR signaling, resulting in tumor radiosensitization. The co-administration of these drugs delayed tumor growth, decreased brain tumor sizes, inhibited invasion, and promoted tumor cell apoptosis. The synergistic effects of these monoclonal antibodies makes the case for further investigation of combination therapies,

especially given the well-documented resistance developed by GBM tumors to individual anti-EGFR mAbs which are frequently rendered ineffective by extracellular EGFR mutations (65, 66). This limitation has been evidenced in clinical trials when, used in combination with standard of care treatment, nimotuzumab failed to demonstrate significantly improved PFS or OS in 142 patients with newly diagnosed GBM (NCT00753246) (66). Cetuximab is now being assessed in a phase I/II clinical trial in combination with bevacizumab (NCT01884740). There are currently nearly two dozen trials testing the efficacy of bevacizumab in combination with another treatment against GBM (67).

EGFR variant III (EGFRvIII) is a constitutively active mutated form of EGFR that is highly expressed in many GBM tumors (68). Though not specific to GSCs, it is significantly co-expressed with CD133 (69) and promotes a stem-like phenotype in GBM cells. It has been targeted for antibody therapy in combination with radiation and chemotherapy. Although the anti-EGFRvIII

TABLE 1 | Ongoing immunotherapy clinical trials targeting glioma stem cells (GSCs).

Trial name	Therapy type	Target	Combination	Phase (O-III)	ClinicalTrials.gov Identifier
AVeRT	DC vaccine	pp65	Nivolumab	I	NCT02529072
DENDR-STEM	DC vaccine	Autologous GSCs		I	NCT02820584
IL13Rα2 CAR T cell therapy	CAR T cell	IL13Rα2	Ipilimumab, nivolumab	I	NCT04003649
Allogeneic GSC lysate DC vaccine	DC vaccine	Allogeneic GSC lysate	SOC	I	NCT02010606
HERT-GBM	CAR T cell	HER2, pp65		I	NCT01109095
Autologous GSC lysate DC vaccine	DC vaccine	Autologous GSC lysate	SOC	II	NCT01567202
SurVaxM	Antibody mediated T cell therapy	Survivin	TMZ, GM-CSF	II	NCT02455557
ELEVATE	DC vaccine	pp65	Td, basiliximab, TMZ	II	NCT02366728
ATTAC-II	DC vaccine	pp65	TMZ	II	NCT02465268
AV-GBM-1	DC vaccine	Autologous tumor-initiating cellular antigens		II	NCT03400917
DEN-STEM	DC vaccine	GSC antigens, hTERT, survivin		II/III	NCT03548571

GM-CSF, granulocyte-macrophage colony-stimulating factor; GSC, glioma stem cell; SOC, standard of care; TMZ, temozolomide; Td, tetrodotoxin.

antibody rindopepimut showed promising results in phases I and II (70, 71), its large international phase III trial, ACT IV, was discontinued after interim analysis did not demonstrate survival benefit (72).

While monotherapies have stumbled in clinical studies, bispecific antibodies (bsAb) and novel technologies have shown promise in bolstering the anti-GSC effects of passive immunotherapies. A bispecific antibody against CD133 and EGFRvIII was demonstrated to be highly cytotoxic against GSCs (but not NSCs) and significantly more effective in prolonging OS in mice as compared to CD133 or EGFRvIII mAbs alone (69). Though it has yet to be validated in human studies, these bispecific antibodies' increased specificity may confer greater anti-GSC effects and decreased toxicity than monotherapies (73, 74). Near-infrared photoimmunotherapy (NIR-PIT) is another novel technology that has the potential to improve the anti-GSC effect of monoclonal antibodies. NIR-PIT involves administration of monoclonal antibodies tagged with photoactive molecules (commonly IR700 dye) followed by near-infrared irradiation. Photoactivation of these antibodies results in specific and robust cell death via cellular membrane damage. Jing et al. demonstrated that CD133-targeted NIR-PIT induced rapid cell death of CD133(+) GSCs in vitro and in orthotopic GSC tumor mouse models (75). Importantly, the ability to administer this non-harmful irradiation through the skull suggests that NIR-PIT may present a safe treatment method in humans.

While research into GSC-specific passive immunotherapy is sorely lacking, additional research is warranted given their demonstrated superiority to bulk tumor-targeting mAbs in preclinical applications. New antibodies which can eliminate chemo(radio)resistant GSC populations, such as one against anti-apoptotic protein CD47, are being developed constantly and warrant optimism (74). Given their ability to target a variety of pathways, and their general tolerability in humans, GSC-specific passive immunotherapies may be utilized as safe and effective adjuncts to more aggressive chemo- or immunotherapeutic approaches.

Active Immunotherapy

Both dendritic cell (DC) vaccines and antibody-mediated T cell immunotherapies rely on the activation of host immunity in order to target specific cancer cells. These approaches have demonstrated safety and efficacy for treatment of GBM in both preclinical and clinical trials (76). Given the success of these trials, researchers are utilizing active immunotherapeutic approaches to eliminate chemo (radio)resistant GSC subpopulations. These GSC specific therapies work via two primary mechanisms: 1) promotion of a broad immunity against GSCs by GSC lysate-pulsed DCs and 2) activation of immunity against specific GSC antigens by synthetic peptide/RNA/mRNA-pulsed DCs.

Promoting immunity against GSC lysate trains the immune system against any antigens associated with GSCs. Murine models which utilize this technique have highlighted the potential for anti-GSC DC vaccines and have served as the basis for multiple clinical trials. Dendritic cells pulsed with GSC tumor lysate have shown to be highly effective at preventing viability of murine GBM tumors grown as both neurospheres (which preferences GSC growth) (77), and have elicited specific T cell responses against GSCs and improved OS in xenografted mice (78). Allogenic GSC lysate-loaded DCs are now being tested in multiple clinical trials (NCT02010606 and NCT01567202).

Other groups are utilizing patients' surgical specimens to culture tumor-initiating GSCs and train autologously derived dendritic cells (NCT03400917). Along with GSC lysate, it is also possible to extract mRNA from patient derived GSCs and produce personalized vaccines. One phase I trial, NCT00846456, demonstrated the safety of this approach as well as a nearly three-times longer PFS compared to matched controls (78).

Much effort has been taken over the past three decades to define GSC specific peptides in order to decrease the risk for off-target effects, and numerous clinical studies are now assessing the effectiveness of DC vaccines which target peptides that are highly expressed in GSCs. One phase III clinical trial, NCT02546102, which was suspended in 2017 for inadequate funding showed

significant promise in early phases. DC vaccines were pulsed with 6 synthetic peptides overexpressed in GSCs: HER2, TRP-2, gp100, MAGE-1, IL13Rα2, and AIM-2 and this therapy was given in conjunction with standard of care chemo(radio)therapy. Results from phase I of the trial suggested a powerful therapeutic effect: median PFS in newly diagnosed patients treated with the vaccine was 16.9 months and OS was 38.4 months, noticeably exceeding historical standards (79). Five patients who underwent a second tumor resection also demonstrated a decrease or absence of CD133 expression in tumor tissue, suggesting the therapy may have exerted GSC-selective cell death. Another phase I trial (NCT02049489) demonstrated that a DC vaccine against CD133 was well tolerated in a pilot group of 20 patients (80).

The phosphoprotein pp65, a product of human cytomegalovirus (HCMV), is an interesting DC vaccine target. A large fraction of clinically isolated CD133(+) cells are found to be positive for pp65, and infection of GBM cells with HCMV *in vitro* causes an upregulation of CD133, Notch1, Sox2, Oct4, and Nestin, and promotes the growth of GBM neurospheres, suggesting that pp65 may play a role in stemness (81). The presence of HCMV in GBM is a controversial topic, having been confirmed and denied by various labs (82). Regardless, targeting HCMV products may show promise in clinical trials.

Researchers at Duke University have a number of ongoing clinical trials investigating the effectiveness of a pp65 RNA-pulsed DC vaccine in combination with various other treatments. One addition being tested is that of anti-IL-2Rα antibodies which researchers hope will decrease Treg function and improve the penetration of DC vaccinations. Early research demonstrated that TMZ-induced lymphopenia enhances vaccine responses but dramatically upregulates T-reg function. IL-2Rα therefore diminishes the T-reg response allowing for a more robust anti-tumor effect (83). Interestingly, administration of IL-2Rα antibodies depleted vaccine-induced immune responses in mice without lymphopenia, but acted synergistically with TMZ in mice experiencing TMZ-induced lymphopenia. These results were confirmed in a pilot study with six patients and draw focus to the importance of combination therapies which utilize tumor debulking therapies like TMZ along with targeted therapies like IL-2Rα antibodies and DC vaccines.

In a phase I trial (NCT00626483), the group combined a pp65 DC vaccine with basiliximab, another anti-IL-2Rα antibody (84). Initial results from phase I of the trial demonstrated high tolerability of the combination therapy but survival benefit was not extrapolated at the time of data collection. After demonstrating that pp65 RNA-pulsed DC vaccines with tetanus/diphtheria (Td) toxoid pre-conditioning significantly increased patient PFS and OS in a small pilot study (85), the group is comparing the effectiveness of pp65 vaccine alone, with Td toxoid pre-conditioning, and with both Td toxoid pre-conditioning and basiliximab against newly diagnosed GBM after standard of care treatment (ELEVATE; phase II; NCT02366728). The most promising of the group's trials combines the pp65 DC vaccine with dose-intensified TMZ cycles (ATTAC; NCT00639639). Preliminary results demonstrated more than double the OS and triple the PFS as compared to historical controls (85). Notably,

four patients remained progression-free at 59 to 64 months. Phase II of this trial (NCT02465268) is currently underway. Finally, an ongoing phase I trial (NCT02529072) is evaluating the effectiveness of the pp65 vaccine in combination with the programmed cell death 1 (PD-1) blocking antibody nivolumab. In a fashion similar to anti-IL-2R antibodies, the inclusion of this checkpoint inhibitor will hopefully antagonize GBM's immunosuppressive effects.

Another promising ongoing clinical trial is that of a trivalent GSC-targeting DC vaccine which is now in stage II/III (NCT03548571). Researchers at Oslo University Hospital are targeting GSCs by administering DC vaccines transfected with GSC mRNA along with the anti-apoptotic peptide survivin and human telomerase reverse transcriptase (hTERT). Both survivin and hTERT have been found to increase stemness in GBM and are expressed in high levels in GSCs (86, 87). In a small preliminary study of this therapy, median PFS was nearly three times longer as compared to those receiving standard of care.

Monoclonal and bispecific antibodies are also being investigated for their ability to activate T cell immune responses against GSCs, and once again survivin is a promising target. SurVaxM, a survivin vaccine, is being tested in combination with TMZ and granulocyte-macrophage colony-stimulating factor in a phase II clinical trial (NCT02455557). Initial results warrant optimism: of 55 patients with newly diagnosed GBM treated with the SurVaxM vaccine concomitant with standard of care therapy, 96% were progression free at 6 months and 93% were alive at 12 months, a substantial improvement over historical controls of 43 and 41%, respectively (88). Survivin has also been utilized along with peptides IL13Rα2 and Ephrin-A2, a target highly expressed in GSCs and responsible for self-renewal and tumorigenicity (89). This trivalent vaccine was tested in a phase I/II trial (NCT02078648) against recurrent GBM with or without bevacizumab but demonstrated poor results, with median OS around 11 months in both groups (90).

The recombinant bispecific antibody AC133CD3 targets T cells and the CD133 epitope AC133, redirecting human polyclonal T cells to patient derived AC133(+) GSCs, inducing GSC lysis, and preventing the growth of subcutaneous GBM xenografts (91). In tandem with CD8(+) T cell infusion, this treatment has been demonstrated effective as both a prophylactic and therapeutic treatment for orthotopic GSC-derived brain tumors, while AC133(+) hematopoietic stem cells were virtually unaffected by the therapy.

The successes of endogenous and virus-associated GSC antigen-targeted therapies indicate that GSC antigens may represent promising targets for various therapy modalities. Caution must be taken, however, when considering early clinical victories, particularly with antibody-mediated T cell therapies. Some trials which demonstrated promise in phase I and II have failed in phase III as they could not demonstrate survival benefit. In the context of their established success in recurrent GBM treatment, DC vaccines are a promising GBM immunotherapy approach and preclinical and clinical results of GSC antigen-specific and GSC lysate DC vaccine approaches should motivate further investigation.

Adoptive Immunotherapy

Adoptive immunotherapy utilizes a patient's own immune cells—whether selected or genetically modified for antitumor activity—to combat the growth and spread of neoplasia. Both T cell and natural killer (NK) cell therapies are of growing interest for various cancers and are being utilized to target GSCs. Cytotoxic T lymphocytes (CTL) can be used to target tumor-associated antigens by being drawn from the patient, selected for their existing antitumor specificity, and expanded *ex vivo* before autologous reintroduction. CTL-mediated GSC targeting has demonstrated promise in preclinical applications and small human cohorts, but has yet to be put to test in a large clinical trial. Chimeric antigen receptor (CAR) T cells, in contrast, are genetically engineered to exert their cytotoxic effects against specific antigens and have been extensively studied in the context of targeting tumor-associated antigens in various types of cancer. Though CAR T cell therapies have been successful treating blood cancers—two different therapies were approved by the FDA in 2017 for treatment of acute lymphoblastic leukemia (92) and diffuse large B cell lymphoma (93)—they have shown mixed results in targeting solid cancers. NK cell therapies are less common and represent a promising, but largely theoretical, avenue for targeting GSCs. NK cells broadly recognize transformed cells, do not require activation by particular tumor-bound antigens, and generally leave healthy cells unharmed. Finally, CAR NK cells, like CAR T cells, are genetically modified NK cells which target cancer-specific antigens. Researchers hope to harness these technologies to eliminate chemo(radio)resistant GSC populations while relying on standard of care therapy to debulk tumors.

CAR T cells have been developed to target several GSC-specific antigens. In a preclinical application of CAR T cell therapies targeting GSCs, therapies have been developed against the CD133 epitope AC133 (94). These AC133-specific CAR T cells recognized and eradicated patient-derived AC133 (+) glioma stem cells *in vitro* and in mouse models and improved OS in treated mice.

Non-GSC-specific peptides, which are also upregulated in GSCs, have demonstrated some efficacy in killing GSC populations. IL13Rα2 (95, 96), EGFRvIII (97, 98), and chlorotoxin-based therapies (99) have all been shown to eliminate both GSCs and bulk tumor cells in preclinical experiments. An IL13Rα2 CAR T cell therapy is currently being investigated in a phase I clinical trial alone and in combination with two checkpoint inhibitors (NCT04003649).

Adoptive immunotherapies cannot always be easily subcategorized. Some groups of researchers are investigating technologies which utilize both genetic modification (i.e., CAR) as well as selection of T cells based on reactivity to particular antigens (i.e., CTL). A group at Baylor has an ongoing clinical trial (NCT01109095) aiming to improve the efficacy of a human epidermal growth factor receptor 2 (HER2) CAR T cell therapy by selecting for cytotoxic T cells which recognize the human cytomegalovirus (HCMV) protein pp65. The group has previously demonstrated the efficacy of the HER2-targeted CAR T cells in eliminating GBM cells irrespective of CD133 expression (100).

Their inclusion of the pp65 target in this clinical trial is predicated on the theory that anti-HCMV antibodies are present in most human adults and thus this HCMV protein will cause persistent activation of the CAR T cells. In addition to broadly activating the CAR T cells, it is possible that this treatment preferentially targets GSCs. As previously mentioned, HCMV has been shown to increase stemness of GBM cells, and pp65 is preferentially expressed in GSCs among infected tumors (81). Initial results from the phase I study demonstrate that the approach is safe and potentially effective (101). Eight out of the 16 patients enrolled demonstrated objective response to the treatment. Three of the patients demonstrated stable disease and were still alive 24 to 30 months, and longer, after T cell infusion.

Some groups also are investigating the HCMV protein pp65 as a target for CTL-mediated oncolysis. In one study, HCMV pp65-specific CTLs were comparably cytotoxic against both GSCs and differentiated cells both *in vitro* and in a mouse model (102). Here, all GSC populations were eliminated *in vivo* in an antigen-specific manner, indicating a potentially safe method of attacking GBM. Two phase I/II clinical trials (NCT01205334 and NCT00990496) which utilized pp65-trained CTLs in patients with GBM were stopped due to poor subject recruitment, though other groups are pursuing this approach with promising preliminary results. The Duke group pursuing multiple pp65 DC vaccination trials has also demonstrated that training T cells with pp65-pulsed DCs increases the polyfunctionality of CTLs in a cohort of 11 patients (NCT00693095), increasing OS (103). Another group at MD Anderson is investigating autologous pp65-specific CTLs following lymphodepleting doses of TMZ and found that the therapy was well tolerated in a pilot trial of 12 patients (104). Unfortunately, the group recently released results of their phase I/II trial which demonstrated attenuated T cell functionality and poor PFS (NCT02661282) (105).

Another peptide which is being utilized for CTL-mediated cytolysis is that of SOX6, an immunogenic peptide is involved in inhibition of neuronal cell differentiation and neuronal stem cell maintenance (106, 107). It has been demonstrated that, due to SOX6's immunogenicity and upregulation in GSCs, human leukocyte antigen (HLA)-A2, and -A24 restricted SOX6 derivatives are effective and safe targets for glioma CTL-mediated cytolysis in mouse model (107). This target has yet to be tested in a clinical setting but represents another avenue for CTL therapies targeting GSCs.

Most adoptive GBM immunotherapy research has been devoted to CAR T cell and CTL therapies as early research suggested NK cells were ineffective against GBM (108–110). However, in 2009, Castriconi et al. showed that allogeneic and autologous IL-2 and IL-5-activated NK cells were effective in killing human-derived GSCs (111), opening the door to further investigations into lymphokine-activated NK cell therapy. Recent research supports this finding and suggests that NK cell therapies might be even more effective against GSCs than differentiated cells, as GSCs were significantly more susceptible to NK cell-mediated cytolysis than were cells grown in differentiation-inducing media (112).

Finally, CAR-NK cells have also been explored for their ability to selectively target and eradicate GSCs. In 2015, a group from The Ohio State University demonstrated that CAR-NK cells targeting both EGFR and EGFRvIII effectively killed patient-derived GSCs *in vitro* (113). They also demonstrated that EGFR targeting CAR-NK cells significantly suppressed growth of xenografted human-GSC tumors in mice and yielded double the median lifespan compared to controls. Of note, the EGFR targeting CAR-NK cells were more effective than non-modified NK cells.

Preclinical insights for NK and CTL therapies warrant some optimism, and clinical evidence that utilizing DCs to train CTLs increases the treatment modality's effectiveness supports further research into this strategy. However, in the absence of clinical evidence which demonstrates an improvement in OS or PFS, hope for approaching advancements in adoptive GSC therapies lies primarily with CAR T cells. Even these advancements, though, will take patience. None of the three ongoing CAR T cell clinical trials which target GSCs have yet to reach phase III, and therefore clinical adoption is unlikely for a number of years.

Virus-Mediated Immunotherapy

A broad range of viruses have been explored for treating high grade glioma (114), and the list continues to grow (115). These viruses have demonstrated tropism for tumor cells resulting in tumor cell lysis, recruitment of the immune system, and finally a T cell mediated antiviral and antitumor response. This leads to systemic immunity against the tumor and its recurrence (116). Because of the interaction with the immune system, some have classified the use of oncolytic viral therapies as an immunotherapeutic approach. Clinical trials involving viral immunotherapies against GBM have recently been reviewed (117), and those which target GSCs in addition to bulk tumor cells are listed in **Table 2**. Researchers have focused efforts on fine tuning genetic modifications in viruses to specifically target tumor cells and introduce cytotoxic transgenes. Transgenes generally function by enhancing prodrug activation, inducing apoptosis and immune activation, and in the case of GBM, inhibiting angiogenesis. Investigators have utilized these features to deliver short interfering (si)RNA and short hairpin (sh)RNA in

order to downregulate cancer cell gene expression, or directly kill GSCs. Lentivirus-mediated shRNA inhibition of Chk1/2, the stem cell gene SirT1, and STAT3 have all been found to sensitize GSCs to radiotherapy (45, 47, 118, 119). Clinical trials have had varying success, and like most therapies for GBM, clinical adaptation is slow. To date, there are only two governmentally approved oncolytic virus-mediated immunotherapies on the market, both of which utilize herpes simplex virus vectors (120, 121).

DISCUSSION

The growing body of knowledge regarding GSCs' role in oncogenesis and tumor recurrence necessitates reevaluation of conventional cancer assessment and treatment methods, as lasting remission will likely remain elusive for many GBM patients without the means of reliably detecting and extinguishing GSC populations. Methods of targeting GSCs vary widely, both in terms of the vector used to exert cytolytic effects on this cell population as well as the antigen or cellular pathway targeted by such vectors. Over the past several years, immunotherapy has emerged as a promising method of culling GSC populations in GBM tumors and has increased survival in GBM patients. Nevertheless, immunotherapies targeting malignancies of the immune-privileged central nervous system present a host of unique challenges.

Due to the relative inability of many immunotherapies to penetrate the blood-brain barrier and subsequently localize to GBM, modalities which show promise *in vitro* may stumble in *in vivo* and clinical application. Direct introduction of immunotherapeutic agents into the tumor resection cavity effectively bypasses the blood-brain barrier but runs the risk of causing inflammation in the brain due to a productive immune response. The paradoxical need for a robust immune response with limited inflammatory changes to kill GBM while preserving the patient highlights just one of the complexities of immunotherapy in the context of intracranial neoplasia. Dexamethasone, the current standard of care agent to treat GBM-associated edema, exerts global immunosuppression and may thereby limit the efficacy of some immunotherapies (122). This underscores the importance of

TABLE 2 | Ongoing virotherapy clinical trials targeting glioma stem cells (GSCs).

Virus family	Therapy type	Viral strain	Combination	Phase (O-III)	ClinicalTrials.gov Identifier
ADV	NSC vector oncolytic virus	BM-hMSC-DNX-2401		I	NCT03896568
Reovirus	Oncolytic virus	Wild-type reovirus (reolysin)	Sargamostim (rGM-CSF)	I	NCT02444546
Vaccinia virus	Oncolytic virus	TG6002	5-FC	I	NCT03294486
ADV	Oncolytic virus	DNX-2440		I	NCT03714334
HSV	Oncolytic virus	HSV G207	Low dose radiation	I	NCT03911388
HSV	Oncolytic virus	C134-HSV-1		I	NCT03657576
ADV	Viral vector gene therapy	ADV/HSK-tk	Valacyclovir, SOC	I	NCT03596086
ADV	Viral vector gene therapy	ADV/HSK-tk	Valacyclovir, SOC	I	NCT03603405
ADV	Oncolytic virus	DNX-2401	Pembrolizumab	II	NCT02798406

ADV, adenovirus; HSV, herpes simplex virus; rGM-CSF, recombinant granulocyte-macrophage colony-stimulating factor; 5-FC, flucytosine; SOC, standard of care.

developing safe anti-inflammatory medications to be administered concomitantly with immunotherapy that do not limit the effectiveness of these agents.

Another hurdle for future immunotherapies to clear is the necessity that therapies be highly specific for glioma stem cells, avoiding antigens shared by healthy neural stem cells or other normal stem cell populations throughout the body, in order to mitigate the risk of adversely affecting somatic stem cell function. Even with highly targeted therapies, however, GBM tumors' innate immunosuppressive effects can dampen the benefit of immunotherapies. Although aberrant cell growth results in immune recruitment through production of chemotactic factors, GBMs antagonize this process by secreting other chemokines which recruit T regulatory cells and suppress immune effector cells (123). In GBM, systemic decrease in T cell responsiveness and immunoglobulin levels, as well as an increase in Treg circulation, limits the effectiveness of those immunotherapies which rely on the body's endogenous immune system. Further, immunosuppression in the tumor microenvironment can render ineffective both endogenous and exogenous immunotherapies. Finally, autologous vaccination strategies are both costly and time consuming. Given the rapid progression of GBM and the association between minimal tumor burden and immunotherapy success (124), efforts to expedite vaccine preparation are imperative to the success of this treatment modality.

Though many immunotherapeutic approaches are currently being investigated, some have shown greater promise in clinical application than others. The use of static monotherapies such as single-target antibodies have been repeatedly demonstrated to be ineffective in the long term due to cellular adaptation by GSCs and, in some cases, even differentiated tumor cells. However, the success of bevacizumab in slowing GBM progression and improving quality of life indicates that passive immunotherapies might be viable adjuncts to more aggressive chemo- or immunotherapeutic approaches.

Further, research into the interaction between GSCs and the tumor microenvironment has shown us that stem cell phenotypes vary significantly throughout the tumor and that subpopulations of GSCs may be differentially susceptible to immunotherapeutic approaches (125). These studies provide a basis for pursuing multiple immunotherapeutic modalities based on the relative permissiveness of GSC populations. Currently, the most thoroughly investigated and perhaps most promising form of immunotherapy against GBM is that of DC vaccination. Nearly three dozen clinical trials are currently assessing DC vaccines against high grade gliomas (126). DC vaccines' ability to train cytotoxic T cells to target GSCs without harmful off-target effects is well documented in both preclinical and clinical applications. However, none of these vaccines have yet attained FDA approval. The number of avenues being pursued to target GSCs warrants optimism, but for now agents trained to eliminate this cancer-driving cell population remain inaccessible to many.

AUTHOR CONTRIBUTIONS

FUNDING

ACKNOWLEDGMENTS

REFERENCES

1. Ostrom QT, Cioffi G, Gittleman H, Patil N, Waite K, Kruchko C, et al. CBTRUS Statistical Report: Primary Brain and Other Central Nervous System Tumors Diagnosed in the United States in 2012-2016. *Neuro Oncol* (2019) 21(Suppl 5):v1–v100. doi: 10.1093/neuonc/noz150
2. Stupp R, Mason WP, van den Bent MJ, Weller M, Fisher B, Taphoorn MJ, et al. Radiotherapy plus concomitant and adjuvant temozolomide for glioblastoma. *N Engl J Med* (2005) 352(10):987–96. doi: 10.1056/NEJMoa043330
3. Lathia JD, Mack SC, Mulkearns-Hubert EE, Valentim CL, Rich JN, et al. Cancer stem cells in glioblastoma. *Genes Dev* (2015) 29(12):1203–17. doi: 10.1101/gad.261982.115
4. Gimple RC, Bhargava S, Dixit D, Rich JN. Glioblastoma stem cells: lessons from the tumor hierarchy in a lethal cancer. *Genes Dev* (2019) 33(11-12):591–609. doi: 10.1101/gad.324301.119
5. Nowell PC. The clonal evolution of tumor cell populations. *Science* (1976) 194(4260):23–8. doi: 10.1126/science.959840
6. Gerdes MJ, Sood A, Sevinsky C, Pris AD, Zavodszky MI, Ginty F, et al. Emerging understanding of multiscale tumor heterogeneity. *Front Oncol* (2014) 4:366. doi: 10.3389/fonc.2014.00366

7. Michor F, Polyak K. The origins and implications of intratumor heterogeneity. *Cancer Prev Res (Phila)* (2010) 3(11):1361–4. doi: 10.1158/1940-6207.CAPR-10-0234
8. Plaks V, Kong N, Werb Z. The cancer stem cell niche: how essential is the niche in regulating stemness of tumor cells? *Cell Stem Cell* (2015) 16(3):225–38. doi: 10.1016/j.stem.2015.02.015
9. Meacham CE, Morrison SJ. Tumour heterogeneity and cancer cell plasticity. *Nature* (2013) 501(7467):328–37. doi: 10.1038/nature12624
10. Bonnet D, Dick JE. Human acute myeloid leukemia is organized as a hierarchy that originates from a primitive hematopoietic cell. *Nat Med* (1997) 3(7):730–7. doi: 10.1038/nm0797-730
11. Cleary ML. Regulating the leukaemia stem cell. *Best Pract Res Clin Haematol* (2009) 22(4):483–7. doi: 10.1016/j.beha.2009.08.005
12. Piccirillo SG, Binda E, Fiocco R, Vescovi AL, Shah K. Brain cancer stem cells. *J Mol Med (Berl)* (2009) 87(11):1087–95. doi: 10.1007/s00109-009-0535-3
13. Lawson JC, Blatch GL, Edkins AL. Cancer stem cells in breast cancer and metastasis. *Breast Cancer Res Treat* (2009) 118(2):241–54. doi: 10.1007/s10549-009-0524-9
14. Singh SR. Gastric cancer stem cells: a novel therapeutic target. *Cancer Lett* (2013) 338(1):110–9. doi: 10.1016/j.canlet.2013.03.035

15. Bednar F, Simeone DM. Pancreatic cancer stem cell biology and its therapeutic implications. *J Gastroenterol* (2011) 46(12):1345–52. doi: 10.1007/s00535-011-0494-7

16. Lundin A, Driscoll B. Lung cancer stem cells: progress and prospects. *Cancer Lett* (2013) 338(1):89–93. doi: 10.1016/j.canlet.2012.08.014

17. Hardin H, Montemayor-Garcia C, Lloyd RV. Thyroid cancer stem-like cells and epithelial-mesenchymal transition in thyroid cancers. *Hum Pathol* (2013) 44(9):1707–13. doi: 10.1016/j.humpath.2013.01.009

18. Dalerba P, Dylla SJ, Park IK, Liu R, Wang X, Cho RW, et al. Phenotypic characterization of human colorectal cancer stem cells. *Proc Natl Acad Sci USA* (2007) 104(24):10158–63. doi: 10.1073/pnas.0703478104

19. Saygin C, Matei D, Majeti R, Reizes O, Lathia JD, et al. Targeting Cancer Stemness in the Clinic: From Hype to Hope. *Cell Stem Cell* (2019) 24(1):25–40. doi: 10.1016/j.stem.2018.11.017

20. Wicha MS, Liu S, Dontu G. Cancer stem cells: an old idea–a paradigm shift. *Cancer Res* (2006) 66(4):1883–90. discussion 1895-6. doi: 10.1158/0008-5472.CAN-05-3153

21. Wang Y, Yang J, Zheng H, Tomasek GJ, Zhang P, McKeever PE, et al. Expression of mutant p53 proteins implicates a lineage relationship between neural stem cells and malignant astrocytic glioma in a murine model. *Cancer Cell* (2009) 15(6):514–26. doi: 10.1016/j.ccr.2009.04.001

22. Odoux C, Fohrer H, Hoppo T, Guzik L, Stolz DB, Lewis DW, et al. A stochastic model for cancer stem cell origin in metastatic colon cancer. *Cancer Res* (2008) 68(17):6932–41. doi: 10.1158/0008-5472.CAN-07-5779

23. Hemmati HD, Nakano I, Lazareff JA, Masterman-Smith M, Geschwind DH, Bronner-Fraser M, et al. Cancerous stem cells can arise from pediatric brain tumors. *Proc Natl Acad Sci USA* (2003) 100(25):15178–83. doi: 10.1073/pnas.2036535100

24. Nouri M, Caradec J, Lubik AA, Li N, Hollier BG, Takhar M, et al. Therapy-induced developmental reprogramming of prostate cancer cells and acquired therapy resistance. *Oncotarget* (2017) 8(12):18949–67. doi: 10.18632/oncotarget.14850

25. Alcantara Llaguno S, Sun D, Pedraza AM, Vera E, Wang Z, Burns DK, et al. Cell-of-origin susceptibility to glioblastoma formation declines with neural lineage restriction. *Nat Neurosci* (2019) 22(4):545–55. doi: 10.1038/s41593-018-0333-8

26. Ignatova TN, Kukekov VG, Laywell ED, Suslov ON, Vrionis FD, Steindle DA, et al. Human cortical glial tumors contain neural stem-like cells expressing astroglial and neuronal markers in vitro. *Glia* (2002) 39(3):193–206. doi: 10.1002/glia.10094

27. Gilbertson RJ, Rich JN. Making a tumour's bed: glioblastoma stem cells and the vascular niche. *Nat Rev Cancer* (2007) 7(10):733–6. doi: 10.1038/nrc2246

28. Lee JH, Lee JE, Kahng JY, Kim SH, Park JS, Yoon SJ, et al. Human glioblastoma arises from subventricular zone cells with low-level driver mutations. *Nature* (2018) 560(7717):243–7. doi: 10.1038/s41586-018-0389-3

29. Lan X, Jorg DJ, Cavalli FMG, Richards LM, Nguyen LV, Vanner RJ, et al. Fate mapping of human glioblastoma reveals an invariant stem cell hierarchy. *Nature* (2017) 549(7671):227–32. doi: 10.1038/nature23666

30. Wang J, Cazzato E, Ladewig E, Frattini V, Rosenbloom DI, Zairis S, et al. Clonal evolution of glioblastoma under therapy. *Nat Genet* (2016) 48(7):768–76. doi: 10.1038/ng.3590

31. Johnson BE, Mazor T, Hong C, Barnes M, Aihara K, McLean CY, et al. Mutational analysis reveals the origin and therapy-driven evolution of recurrent glioma. *Science* (2014) 343(6167):189–93. doi: 10.1126/science.1239947

32. Korber V, Yang J, Barah P, Wu Y, Stichel D, Gu Z, et al. Evolutionary Trajectories of IDH(WT) Glioblastomas Reveal a Common Path of Early Tumorigenesis Instigated Years ahead of Initial Diagnosis. *Cancer Cell* (2019) 35(4):692–704.e12. doi: 10.1016/j.ccell.2019.02.007

33. Cheray M, Begaud G, Deluche E, Nivet A, Battu S, Lalloue F, et al. *Glioblastoma* (2017). doi: 10.15586/codon.glioblastoma.2017.ch4

34. Boman BM, Wicha MS. Cancer stem cells: a step toward the cure. *J Clin Oncol* (2008) 26(17):2795–9. doi: 10.1200/JCO.2008.17.7436

35. Patel AP, Tirosh I, Trombetta JJ, Shalek AK, Gillespie SM, Wakimoto H, et al. Single-cell RNA-seq highlights intratumoral heterogeneity in primary glioblastoma. *Science* (2014) 344(6190):1396–401. doi: 10.1126/science.1254257

36. Couturier CP, Ayyadhury S, Le PU, Nadaf J, Monlong J, Riva G, et al. Single-cell RNA-seq reveals that glioblastoma recapitulates a normal neurodevelopmental hierarchy. *Nat Commun* (2020) 11(1):3406. doi: 10.1038/s41467-020-17979-8

37. Roos A, Ding Z, Loftus JC, Tran NL. Molecular and Microenvironmental Determinants of Glioma Stem-Like Cell Survival and Invasion. *Front Oncol* (2017) 7:120. doi: 10.3389/fonc.2017.00120

38. Belousov A, Titov S, Shved N, Garbuz M, Malykin G, Gulaia V, et al. The Extracellular Matrix and Biocompatible Materials in Glioblastoma Treatment. *Front Bioeng Biotechnol* (2019) 7:341. doi: 10.3389/fbioe.2019.00341

39. Day BW, Lathia JD, Bruce ZC, D'Souza RCJ, Baumgartner U, Ensbey KS, et al. The dystroglycan receptor maintains glioma stem cells in the vascular niche. *Acta Neuropathol* (2019) 138(6):1033–52. doi: 10.1007/s00401-019-02069-x

40. Dean M, Fojo T, Bates S. Tumour stem cells and drug resistance. *Nat Rev Cancer* (2005) 5(4):275–84. doi: 10.1038/nrc1590

41. Liu G, Yuan X, Zeng Z, Tunici P, Ng H, Abdulkadir IR, et al. Analysis of gene expression and chemoresistance of CD133+ cancer stem cells in glioblastoma. *Mol Cancer* (2006) 5:67. doi: 10.1186/1476-4598-5-67

42. Li Z, Bao S, Wu Q, Wang H, Eyler C, Sathornsumetee S, et al. Hypoxia-inducible factors regulate tumorigenic capacity of glioma stem cells. *Cancer Cell* (2009) 15(6):501–13. doi: 10.1016/j.ccr.2009.03.018

43. Lee G, Auffinger B, Guo D, Hasan T, Deheeger M, Tobias AL, et al. Dedifferentiation of Glioma Cells to Glioma Stem-like Cells By Therapeutic Stress-induced HIF Signaling in the Recurrent GBM Model. *Mol Cancer Ther* (2016) 15(12):3064–76. doi: 10.1158/1535-7163.MCT-15-0675

44. Carruthers RD, Ahmed SU, Ramachandran S, Strathdee K, Kurian KM, Hedley A, et al. Replication Stress Drives Constitutive Activation of the DNA Damage Response and Radioresistance in Glioblastoma Stem-like Cells. *Cancer Res* (2018) 78(17):5060–71. doi: 10.1158/0008-5472.CAN-18-0569

45. Chang CJ, Hsu CC, Yung MC, Chen KY, Tzao C, Wu WF, et al. Enhanced radiosensitivity and radiation-induced apoptosis in glioma CD133-positive cells by knockdown of SirT1 expression. *Biochem Biophys Res Commun* (2009) 380(2):236–42. doi: 10.1016/j.bbrc.2009.01.040

46. Diehn M, Cho RW, Lobo NA, Kalisky T, Dorie MJ, Kulp AN, et al. Association of reactive oxygen species levels and radioresistance in cancer stem cells. *Nature* (2009) 458(7239):780–3. doi: 10.1038/nature07733

47. Bao S, Wu Q, McLendon RE, Hao Y, Shi Q, Hjelmeland AB, et al. Glioma stem cells promote radioresistance by preferential activation of the DNA damage response. *Nature* (2006) 444(7120):756–60. doi: 10.1038/nature05236

48. Lomonaco SL, Finniss S, Xiang C, Decarvalho A, Umansky F, Kalkanis SN, et al. The induction of autophagy by gamma-radiation contributes to the radioresistance of glioma stem cells. *Int J Cancer* (2009) 125(3):717–22. doi: 10.1002/ijc.24402

49. Swiatek-Machado K, Kaminska B. STAT signaling in glioma cells. *Adv Exp Med Biol* (2013) 986:189–208. doi: 10.1007/978-94-007-4719-7_10

50. Wang J, Wakeman TP, Lathia JD, Hjelmeland AB, Wang XF, White RR, et al. Notch promotes radioresistance of glioma stem cells. *Stem Cells* (2010) 28(1):17–28. doi: 10.1002/stem.542

51. Porta C, Paglino C, Mosca A. Targeting PI3K/Akt/mTOR Signaling in Cancer. *Front Oncol* (2014) 4:64. doi: 10.3389/fonc.2014.00064

52. Bahmad HF, Mouhieddine TH, Chalhoub RM, Assi S, Araji T, Chamaa F, et al. The Akt/mTOR pathway in cancer stem/progenitor cells is a potential therapeutic target for glioblastoma and neuroblastoma. *Oncotarget* (2018) 9(71):33549–61. doi: 10.18632/oncotarget.26088

53. Gupta S, Takebe N, Lorusso P. Targeting the Hedgehog pathway in cancer. *Ther Adv Med Oncol* (2010) 2(4):237–50. doi: 10.1177/1758834010366430

54. Di Tomaso T, Mazzoleni S, Wang E, Sovena G, Clavenna D, Franzin A, et al. Immunobiological characterization of cancer stem cells isolated from glioblastoma patients. *Clin Cancer Res* (2010) 16(3):800–13. doi: 10.1158/1078-0432.CCR-09-2730

55. Wei J, Barr J, Kong LY, Wang Y, Wu A, Sharma AK, et al. Glioblastoma cancer-initiating cells inhibit T-cell proliferation and effector responses by the signal transducers and activators of transcription 3 pathway. *Mol Cancer Ther* (2010) 9(1):67–78. doi: 10.1158/1535-7163.MCT-09-0734

56. Rovere-Querini P, Capobianco A, Scaffidi P, Valentinis B, Catalanotti F, Giazzon M, et al. HMGB1 is an endogenous immune adjuvant released by necrotic cells. *EMBO Rep* (2004) 5(8):825–30. doi: 10.1038/sj.embor.7400205

57. Sharabi AB, Nirschl CJ, Kochel CM, Nirschl TR, Francica BJ, Velarde E, et al. Stereotactic Radiation Therapy Augments Antigen-Specific PD-1-Mediated Antitumor Immune Responses via Cross-Presentation of Tumor Antigen. *Cancer Immunol Res* (2015) 3(4):345–55. doi: 10.1158/2326-6066.CIR-14-0196

58. Hauser SH, Calorini L, Wazer DE, Gattoni-Celli S. Radiation-enhanced expression of major histocompatibility complex class I antigen H-2Db in B16 melanoma cells. *Cancer Res* (1993) 53(8):1952–5.

59. Garnett CT, Palena C, Chakraborty M, Tsang KY, Schlom J, Hodge JW, et al. Sublethal irradiation of human tumor cells modulates phenotype resulting in enhanced killing by cytotoxic T lymphocytes. *Cancer Res* (2004) 64 (21):7985–94. doi: 10.1158/0008-5472.CAN-04-1525

60. Reits EA, Hodge JW, Herberts CA, Groothuis TA, Chakraborty M, Wansley EK, et al. Radiation modulates the peptide repertoire, enhances MHC class I expression, and induces successful antitumor immunotherapy. *J Exp Med* (2006) 203(5):1259–71. doi: 10.1084/jem.20052494

61. Cohen MH, Shen YL, Keegan P, Pazdur R. FDA drug approval summary: bevacizumab (Avastin) as treatment of recurrent glioblastoma multiforme. *Oncologist* (2009) 14(11):1131–8. doi: 10.1634/theoncologist.2009-0121

62. Yang SB, Gao KD, Jiang T, Cheng SJ, Li WB. Bevacizumab combined with chemotherapy for glioblastoma: a meta-analysis of randomized controlled trials. *Oncotarget* (2017) 8(34):57337–44. doi: 10.18632/oncotarget.16924

63. Pang LY, Saunders L, Argyle DJ. Epidermal growth factor receptor activity is elevated in glioma cancer stem cells and is required to maintain chemotherapy and radiation resistance. *Oncotarget* (2017) 8(42):72494–512. doi: 10.18632/oncotarget.19668

64. Diaz Miqueli A, Rolff J, Lemm M, Fichtner I, Perez R, Montero E, et al. Radiosensitisation of U87MG brain tumours by anti-epidermal growth factor receptor monoclonal antibodies. *Br J Cancer* (2009) 100(6):950–8. doi: 10.1038/sj.bjc.6604943

65. Eskilsson E, Rosland GV, Solecki G, Wang Q, Harter PN, Graziani G, et al. EGFR heterogeneity and implications for therapeutic intervention in glioblastoma. *Neuro Oncol* (2018) 20(6):743–52. doi: 10.1093/neuonc/nox191

66. Westphal M, Heese O, Steinbach JP, Schnell O, Schackert G, Mehdorn M, et al. A randomised, open label phase III trial with nimotuzumab, an anti-epidermal growth factor receptor monoclonal antibody in the treatment of newly diagnosed adult glioblastoma. *Eur J Cancer* (2015) 51(4):522–32. doi: 10.1016/j.ejca.2014.12.019

67. Esparza R, Azad TD, Feroze AH, Mitra SS, Cheshier SH. Glioblastoma stem cells and stem cell-targeting immunotherapies. *J Neurooncol* (2015) 123 (3):449–57. doi: 10.1007/s11060-015-1729-x

68. An Z, Aksoy O, Zheng T, Fan QW, Weiss WA. Epidermal growth factor receptor and EGFRvIII in glioblastoma: signaling pathways and targeted therapies. *Oncogene* (2018) 37(12):1561–75. doi: 10.1038/s41388-017-0045-7

69. Emlet DR, Gupta P, Holgado-Madruga M, Del Vecchio CA, Mitra SS, Han SY, et al. Targeting a glioblastoma cancer stem-cell population defined by EGF receptor variant III. *Cancer Res* (2014) 74(4):1238–49. doi: 10.1158/0008-5472.CAN-13-1407

70. Schuster J, Lai RK, Recht LD, Reardon DA, Paleologos NA, Groves MD, et al. A phase II, multicenter trial of rindopepimut (CDX-110) in newly diagnosed glioblastoma: the ACT III study. *Neuro Oncol* (2015) 17(6):854–61. doi: 10.1093/neuonc/nou348

71. Reardon DA, Desjardins A, Vredenburgh JJ, O'Rourke DM, Tran DD, Fink KL, et al. Rindopepimut with Bevacizumab for Patients with Relapsed EGFRvIII-Expressing Glioblastoma (ReACT): Results of a Double-Blind Randomized Phase II Trial. *Clin Cancer Res* (2020) 26(7):1586–94. doi: 10.1158/1078-0432.CCR-18-1140

72. Weller M, Butowski N, Tran DD, Recht LD, Lim M, Hirte H, et al. Rindopepimut with temozolomide for patients with newly diagnosed, EGFRvIII-expressing glioblastoma (ACT IV): a randomised, double-blind, international phase 3 trial. *Lancet Oncol* (2017) 18(10):1373–85. doi: 10.1016/S1470-2045(17)30517-X

73. Zhang M, Hutter G, Kahn SA, Azad TD, Gholamin S, Xu CY, et al. Anti-CD47 Treatment Stimulates Phagocytosis of Glioblastoma by M1 and M2 Polarized Macrophages and Promotes M1 Polarized Macrophages In Vivo. *PloS One* (2016) 11(4):e0153550. doi: 10.1371/journal.pone.0153550

74. Li F, Lv B, Liu Y, Hua T, Han J, Sun C, et al. Blocking the CD47-SIRPalpha axis by delivery of anti-CD47 antibody induces antitumor effects in glioma and glioma stem cells. *Oncoimmunology* (2018) 7(2):e1391973. doi: 10.1080/2162402X.2017.1391973

75. Jing H, Weidensteiner C, Reichardt W, Gaedicke S, Zhu X, Grosu AL, et al. Imaging and Selective Elimination of Glioblastoma Stem Cells with Theranostic Near-Infrared-Labeled CD133-Specific Antibodies. *Theranostics* (2016) 6(6):862–74. doi: 10.7150/thno.12890

76. Liau LM, Ashkan K, Tran DD, Campian JL, Trusheim JE, Cobbs CS, et al. First results on survival from a large Phase 3 clinical trial of an autologous dendritic cell vaccine in newly diagnosed glioblastoma. *J Transl Med* (2018) 16(1):142. doi: 10.1186/s12967-018-1507-6

77. Pellegatta S, Poliani PL, Corno D, Menghi F, Ghielmetti F, Suarez-Merino B, et al. Neurospheres enriched in cancer stem-like cells are highly effective in eliciting a dendritic cell-mediated immune response against malignant gliomas. *Cancer Res* (2006) 66(21):10247–52. doi: 10.1158/0008-5472.CAN-06-2048

78. Vik-Mo EO, Nyakas M, Mikkelsen BV, Moe MC, Due-Tonnesen P, Suso EM, et al. Therapeutic vaccination against autologous cancer stem cells with mRNA-transfected dendritic cells in patients with glioblastoma. *Cancer Immunol Immunother* (2013) 62(9):1499–509. doi: 10.1007/s00262-013-1453-3

79. Phuphanich S, Wheeler CJ, Rudnick JD, Mazer M, Wang H, Nuno MA, et al. Phase I trial of a multi-epitope-pulsed dendritic cell vaccine for patients with newly diagnosed glioblastoma. *Cancer Immunol Immunother* (2013) 62 (1):125–35. doi: 10.1007/s00262-012-1319-0

80. Rudnick JD. Immunological targeting of CD133 in recurrent glioblastoma: A multi-center phase I translational and clinical study of autologous CD133 dendritic cell immunotherapy. *J Clin Oncol* (2017) 35:2059. doi: 10.1200/JCO.2017.35.15_suppl.2059

81. Soroceanu L, Matlaf L, Khan S, Akhavan A, Singer E, Bezrookove V, et al. Cytomegalovirus Immediate-Early Proteins Promote Stemness Properties in Glioblastoma. *Cancer Res* (2015) 75(15):3065–76. doi: 10.1158/0008-5472.CAN-14-3307

82. Foster H, Ulasov IV, Cobbs CS. Human cytomegalovirus-mediated immunomodulation: Effects on glioblastoma progression. *Biochim Biophys Acta Rev Cancer* (2017) 1868(1):273–6. doi: 10.1016/j.bbcan.2017.05.006

83. Mitchell DA, Cui X, Schmittling RJ, Sanchez-Perez L, Snyder DJ, Congdon KL, et al. Monoclonal antibody blockade of IL-2 receptor alpha during lymphopenia selectively depletes regulatory T cells in mice and humans. *Blood* (2011) 118(11):3003–12. doi: 10.1182/blood-2011-02-334565

84. Maes W, Rosas GG, Verbinnen B, Boon L, De Vleeschouwer S, Ceuppens JL, et al. DC vaccination with anti-CD25 treatment leads to long-term immunity against experimental glioma. *Neuro Oncol* (2009) 11(5):529–42. doi: 10.1215/15228517-2009-004

85. Batich KA, Reap EA, Archer GE, Sanchez-Perez L, Nair SK, Schmittling RJ, et al. Long-term Survival in Glioblastoma with Cytomegalovirus pp65-Targeted Vaccination. *Clin Cancer Res* (2017) 23(8):1898–909. doi: 10.1158/1078-0432.CCR-16-2057

86. Guvenc H, Pavlyukov MS, Joshi K, Kurt H, Banasavadi-Siddegowda YK, Mao P, et al. Impairment of glioma stem cell survival and growth by a novel inhibitor for Survivin-Ran protein complex. *Clin Cancer Res* (2013) 19 (3):631–42. doi: 10.1158/1078-0432.CCR-12-0647

87. Beck S, Jin X, Sohn YW, Kim JK, Kim SH, Yin J, et al. Telomerase activity-independent function of TERT allows glioma cells to attain cancer stem cell characteristics by inducing EGFR expression. *Mol Cells* (2011) 31(1):9–15. doi: 10.1007/s10059-011-0008-8

88. Ballman KV, Buckner JC, Brown PD, Giannini C, Flynn PJ, LaPlant BR, et al. The relationship between six-month progression-free survival and 12-month overall survival end points for phase II trials in patients with glioblastoma multiforme. *Neuro Oncol* (2007) 9(1):29–38. doi: 10.1215/15228517-2006-025

89. Binda E, Visioli A, Giani F, Lamorte G, Copetti M, Pitter KL, et al. The EphA2 receptor drives self-renewal and tumorigenicity in stem-like tumor-propagating cells from human glioblastomas. *Cancer Cell* (2012) 22(6):765–80. doi: 10.1016/j.ccr.2012.11.005

90. Reardon D. ATIM-10. Phase 2 Trial of SL-701, a novel immunotherapy comprised of synthetic short peptides against GBM targets IL-12Ralpha2, EphA2, and Survivin, in adults with second-line recurrent GBM. *Neuro-Oncology* (2017) 19:vi28. doi: 10.1093/neuonc/nox168.106

91. Prasad S, Gaedicke S, Machein M, Mittler G, Braun F, Hettich M, et al. Effective Eradication of Glioblastoma Stem Cells by Local Application of an AC133/CD133-Specific T-cell-Engaging Antibody and CD8 T Cells. *Cancer Res* (2015) 75(11):2166–76. doi: 10.1158/0008-5472.CAN-14-2415

92. Maude SL, Laetsch TW, Buechner J, Rives S, Boyer M, Bittencourt H, et al. Tisagenlecleucel in Children and Young Adults with B-Cell Lymphoblastic Leukemia. N Engl J Med (2018) 378(5):439–48. doi: 10.1056/NEJMoa1709866

93. Neelapu SS, Locke FL, Bartlett NL, Lekakis LJ, Miklos DB, Jacobson CA, et al. Axicabtagene Ciloleucel CAR T-Cell Therapy in Refractory Large B-Cell Lymphoma. N Engl J Med (2017) 377(26):2531–44. doi: 10.1056/NEJMoa1707447

94. Zhu X, Prasad S, Gaedicke S, Hettich M, Firat E, Niedermann G, et al. Patient-derived glioblastoma stem cells are killed by CD133-specific CAR T cells but induce the T cell aging marker CD57. Oncotarget (2015) 6(1):171–84. doi: 10.18632/oncotarget.2767

95. Brown CE, Starr R, Aguilar B, Shami AF, Martinez C, D'Apuzzo M, et al. Stem-like tumor-initiating cells isolated from IL13Ralpha2 expressing gliomas are targeted and killed by IL13-zetakine-redirected T Cells. Clin Cancer Res (2012) 18(8):2199–209. doi: 10.1158/1078-0432.CCR-11-1669

96. Brown CE, Badie B, Barish ME, Weng L, Ostberg JR, Chang WC, et al. Bioactivity and Safety of IL13Ralpha2-Redirected Chimeric Antigen Receptor CD8+ T Cells in Patients with Recurrent Glioblastoma. Clin Cancer Res (2015) 21(18):4062–72. doi: 10.1158/1078-0432.CCR-15-0428

97. O'Rourke DM, Nasrallah MP, Desai A, Melenhorst JJ, Mansfield K, Morrissette JJD, et al. A single dose of peripherally infused EGFRvIII-directed CAR T cells mediates antigen loss and induces adaptive resistance in patients with recurrent glioblastoma. Sci Transl Med (2017) 9(399). doi: 10.1126/scitranslmed.aaa0984

98. Goff SL, Morgan RA, Yang JC, Sherry RM, Robbins PF, Restifo NP, et al, et al. Pilot Trial of Adoptive Transfer of Chimeric Antigen Receptor-transduced T Cells Targeting EGFRvIII in Patients With Glioblastoma. J Immunother (2019) 42(4):126–35. doi: 10.1097/CJI.0000000000000260

99. Wang D, Starr R, Chang WC, Aguilar B, Alizadeh D, Wright SL, et al. Chlorotoxin-directed CAR T cells for specific and effective targeting of glioblastoma. Sci Transl Med (2020) 12(533). doi: 10.1126/scitranslmed.aaw2672

100. Ahmed N, Salsman VS, Kew Y, Shaffer D, Powell S, Zhang YJ, et al. HER2-specific T cells target primary glioblastoma stem cells and induce regression of autologous experimental tumors. Clin Cancer Res (2010) 16(2):474–85. doi: 10.1158/1078-0432.CCR-09-1322

101. Ahmed N, Hedge VB,M, Bielamowicz K, Wakefield A, Ghazi A, Ashoori A. Autologous HER2 CMV bispecific CAR T cells are safe and demonstrate clinical benefit for glioblastoma in a Phase I trial. J Immunother Cancer (2015) 3:O11. doi: 10.1186/2051-1426-3-S2-O11

102. Brown CE, Starr R, Martinez C, Aguilar B, D'Apuzzo M, Todorov I, et al. Recognition and killing of brain tumor stem-like initiating cells by CD8+ cytolytic T cells. Cancer Res (2009) 69(23):8886–93. doi: 10.1158/0008-5472.CAN-09-2687

103. Reap EA, Suryadevara CM, Batich KA, Sanchez-Perez L, Archer GE, Schmittling RJ, et al. Dendritic Cells Enhance Polyfunctionality of Adoptively Transferred T Cells That Target Cytomegalovirus in Glioblastoma. Cancer Res (2018) 78(1):256–64. doi: 10.1158/0008-5472.CAN-17-0469

104. Penas-Prado M. ATIM-10. A phase I/II clinical trial of autologous CMV-specific cytotoxic T cells (CMV-TC) for glioblastoma: dose escalation and correlative results. Neuro-Oncology (2018) 20:vi2–3. doi: 10.1093/neuonc/noy148.006

105. Weathers SP, Penas-Prado M, Pei BL, Ling X, Kassab C, Banerjee P, et al. Glioblastoma-mediated Immune Dysfunction Limits CMV-specific T Cells and Therapeutic Responses: Results from a Phase I/II Trial. Clin Cancer Res (2020) 26(14):3565–77. doi: 10.1158/1078-0432.CCR-20-0176

106. Lee KE, Seo J, Shin J, Ji EH, Roh J, Kim JY, et al. Positive feedback loop between Sox2 and Sox6 inhibits neuronal differentiation in the developing central nervous system. Proc Natl Acad Sci USA (2014) 111(7):2794–9. doi: 10.1073/pnas.1308758111

107. Ueda R, Ohkusu-Tsukada K, Fusaki N, Soeda A, Kawase T, Kawakami Y, et al. Identification of HLA-A2- and A24-restricted T-cell epitopes derived from SOX6 expressed in glioma stem cells for immunotherapy. Int J Cancer (2010) 126(4):919–29. doi: 10.1002/ijc.24851

108. Friese MA, Platten M, Lutz SZ, Naumann U, Aulwurm S, Bischof F, et al. MICA/NKG2D-mediated immunogene therapy of experimental gliomas. Cancer Res (2003) 63(24):8996–9006.

109. Wischhusen J, Friese MA, Mittelbronn M, Meyermann R, Weller M. HLA-E protects glioma cells from NKG2D-mediated immune responses in vitro: implications for immune escape in vivo. J Neuropathol Exp Neurol (2005) 64(6):523–8. doi: 10.1093/jnen/64.6.523

110. Wu A, Wiesner S, Xiao J, Ericson K, Chen W, Hall WA, et al. Expression of MHC I and NK ligands on human CD133+ glioma cells: possible targets of immunotherapy. J Neurooncol (2007) 83(2):121–31. doi: 10.1007/s11060-006-9265-3

111. Castriconi R, Daga A, Dondero A, Zona G, Poliani PL, Melotti A, et al. NK cells recognize and kill human glioblastoma cells with stem cell-like properties. J Immunol (2009) 182(6):3530–9. doi: 10.4049/jimmunol.0802845

112. Haspels HN, Rahman MA, Joseph JV, Gras Navarro A, Chekenya M, et al. Glioblastoma Stem-Like Cells Are More Susceptible Than Differentiated Cells to Natural Killer Cell Lysis Mediated Through Killer Immunoglobulin-Like Receptors-Human Leukocyte Antigen Ligand Mismatch and Activation Receptor-Ligand Interactions. Front Immunol (2018) 9:1345. doi: 10.3389/fimmu.2018.01345

113. Han J, Chu J, Keung Chan W, Zhang J, Wang Y, Cohen JB, et al. CAR-Engineered NK Cells Targeting Wild-Type EGFR and EGFRvIII Enhance Killing of Glioblastoma and Patient-Derived Glioblastoma Stem Cells. Sci Rep (2015) 5:11483. doi: 10.1038/srep11483

114. Wollmann G, Ozduman K, van den Pol AN. Oncolytic virus therapy for glioblastoma multiforme: concepts and candidates. Cancer J (2012) 18(1):69–81. doi: 10.1097/PPO.0b013e31824671c9

115. Zhu Z, Gorman MJ, McKenzie LD, Chai JN, Hubert CG, Prager BC, et al. Zika virus has oncolytic activity against glioblastoma stem cells. J Exp Med (2017) 214(10):2843–57. doi: 10.1084/jem.20171093

116. Lawler SE, Chiocca EA. Oncolytic Virus-Mediated Immunotherapy: A Combinatorial Approach for Cancer Treatment. J Clin Oncol (2015) 33(25):2812–4. doi: 10.1200/JCO.2015.62.5244

117. Martikainen M, Essand M. Virus-Based Immunotherapy of Glioblastoma. Cancers (Basel) (2019) 11(2):1–16. doi: 10.3390/cancers11020186

118. Villalva C, Martin-Lannerée S, Cortes U, Dkhissi F, Wager M, Le Corf A, et al. STAT3 is essential for the maintenance of neurosphere-initiating tumor cells in patients with glioblastomas: a potential for targeted therapy? Int J Cancer (2011) 128(4):826–38. doi: 10.1002/ijc.25416

119. Masliantsev K, Pinel B, Balbous A, Guichet PO, Tachon G, Milin S, et al. Impact of STAT3 phosphorylation in glioblastoma stem cells radiosensitization and patient outcome. Oncotarget (2018) 9(3):3968–79. doi: 10.18632/oncotarget.23374

120. Garber K. China approves world's first oncolytic virus therapy for cancer treatment. J Natl Cancer Inst (2006) 98(5):298–300. doi: 10.1093/jnci/djj111

121. Ott PA, Hodi FS. Talimogene Laherparepvec for the Treatment of Advanced Melanoma. Clin Cancer Res (2016) 22(13):3127–31. doi: 10.1158/1078-0432.CCR-15-2709

122. Giles AJ, Hutchinson MND, Sonnemann HM, Jung J, Fecci PE, Ratnam NM, et al. Dexamethasone-induced immunosuppression: mechanisms and implications for immunotherapy. J Immunother Cancer (2018) 6(1):51. doi: 10.1186/s40425-018-0371-5

123. Razavi SM, Lee KE, Jin BE, Aujla PS, Gholamin S, Li G, et al. Immune Evasion Strategies of Glioblastoma. Front Surg (2016) 3:11. doi: 10.3389/fsurg.2016.00011

124. McGranahan T, Therkelsen KE, Ahmad S, Nagpal S. Current State of Immunotherapy for Treatment of Glioblastoma. Curr Treat Options Oncol (2019) 20(3):24. doi: 10.1007/s11864-019-0619-4

125. Prager BC, Xie Q, Bao S, Rich JN. Cancer Stem Cells: The Architects of the Tumor Ecosystem. Cell Stem Cell (2019) 24(1):41–53. doi: 10.1016/j.stem.2018.12.009

126. Eagles ME, Nassiri F, Badhiwala JH, Suppiah S, Almenawer SA, Zadeh G, et al. Dendritic cell vaccines for high-grade gliomas. Ther Clin Risk Manag (2018) 14:1299–313. doi: 10.2147/TCRM.S135865

Metastatic Spread in Prostate Cancer Patients Influencing Radiotherapy Response

Daria Klusa[1,2], Fabian Lohaus[3], Giulia Furesi[4], Martina Rauner[4], Martina Benešová[2], Mechthild Krause[1,2,3,5], Ina Kurth[2] and Claudia Peitzsch[1,2,5*]

[1] National Center for Tumor Diseases (NCT), Dresden, Germany, [2] German Cancer Research Center (DKFZ), Heidelberg, Germany, [3] Faculty of Medicine and University Hospital Carl Gustav Carus, Technische Universität Dresden, Dresden, Germany, [4] Helmholtz-Zentrum Dresden—Rossendorf (HZDR), Dresden, Germany, [5] Department of Radiotherapy and Radiation Oncology, Faculty of Medicine and University Hospital Carl Gustav Carus, Technische Universität Dresden, Dresden, Germany

Radiotherapy and surgery are curative treatment options for localized prostate cancer (PCa) with a 5-year survival rate of nearly 100%. Once PCa cells spread into distant organs, such as bone, the overall survival rate of patients drops dramatically. The metastatic cascade and organotropism of PCa cells are regulated by different cellular subtypes, organ microenvironment, and their interactions. This cross-talk leads to pre-metastatic niche formation that releases chemo-attractive factors enforcing the formation of distant metastasis. Biological characteristics of PCa metastasis impacting on metastatic sites, burden, and latency is of clinical relevance. Therefore, the implementation of modern hybrid imaging technologies into clinical routine increased the sensitivity to detect metastases at earlier stages. This enlarged the number of PCa patients diagnosed with a limited number of metastases, summarized as oligometastatic disease. These patients can be treated with androgen deprivation in combination with local-ablative radiotherapy or radiopharmaceuticals directed to metastatic sites. Unfortunately, the number of patients with disease recurrence is high due to the enormous heterogeneity within the oligometastatic patient population and the lack of available biomarkers with predictive potential for metastasis-directed radiotherapy. Another, so far unmet clinical need is the diagnosis of minimal residual disease before onset of clinical manifestation and/or early relapse after initial therapy. Here, monitoring of circulating and disseminating tumor cells in PCa patients during the course of radiotherapy may give us novel insight into how metastatic spread is influenced by radiotherapy and vice versa. In summary, this review critically compares current clinical concepts for metastatic PCa patients and discuss the implementation of recent preclinical findings improving our understanding of metastatic dissemination and radiotherapy resistance into standard of care.

Keywords: prostate cancer, radiotherapy, metastasis, circulating tumor cells, radiopharmacy

INTRODUCTION

Standard of care for metastatic prostate cancer (PCa) patients is systemic therapy, e.g. androgen deprivation therapy (ADT) or docetaxel-based chemotherapy. First-line therapy for non-metastatic, castration resistant prostate cancer (CRPC) patients is systemic ADT based on second-generation nonsteroidal antiandrogens enzalutamide or apalutamide with a significant benefit in metastasis free survival. At prostate-specific antigen (PSA) recurrence after definitive local therapy, e.g. radical prostatectomy, radiotherapy, or both, prostate-specific membrane antigen-based imaging can identify local recurrence or oligo-metastases (1). This increases the number of diagnosed patients with asymptomatic metastasis and rising PSA level. High-dose external beam radiotherapy can successfully control those lesions in hormone-naïve and even in metastatic CRPC patients (2–4). However, up to 70% of these patients will experience further disease progression. Established methods for stratification of PCa patients into prognostic subgroups are solely based on PSA kinetics (e.g. PSA velocity, PSA doubling time), but not on biological, disease-related differences. Whether the observed differences in response are related to specific biological phenotypes is often hypothesized, but not clinically proven yet. Therefore, the characterization of cellular signatures for radiotherapy response coming from the primary tumor or distant metastasis, e.g. based on liquid biopsy analysis, has the potential to detect underlying resistance and metastasis-initiating mechanisms. Despite the increasing understanding of the cellular and molecular processes underlying the metastatic cascade, there are still key questions to answer: How do metastases differ molecularly and phenotypically from the primary tumor? Is it possible to predict metastatic spread from signatures within the primary tumor? Can the cellular composition and degree of heterogeneity in the metastases be used as signature for patient stratification? How efficient can metastasis-directed therapy be implemented into clinical routine and do PCa patients benefit? To answer the raised questions, this review summarizes the current knowledge about the metastatic cascade in PCa, introduces state-of-the-art imaging modalities to visualize microscopic metastatic lesions, and discusses novel developments in the field of metastasis-directed therapies. Moreover, we introduce the concept of circulating and disseminating tumor cells and discuss their prognostic potential for patient stratification and therapy monitoring.

CHARACTERISTICS OF METASTATIC SITES IN PROSTATE CANCER

Routes of Metastasis in Prostate Cancer

The invasion of tumor cells into the surrounding tissue and the seeding of metastases remains a challenging issue, as it represents the main cause of increased mortality among patients (5, 6). During metastasis formation, tumor cells undergo a complex multi-stage intra- and intercellular remodeling process. The metastatic cascade can be described by five major steps: 1) invasion throughout the basement membrane and migration into the surrounding tissue; 2) intravasation into the vasculature or lymphatic system; 3) survival within the circulation; 4) extravasation from the vasculature into the tissue; and 5) colonization and formation of metastatic lesions at secondary sites (**Figure 1**) (5, 7). Each stage represents enormous environmental pressure and energetically demanding conditions for the cancer cells. The whole process is thought to be extremely inefficient and less than 0.1% of the cancer cells that detach from the primary tumor survive within 24 h (8, 9). Moreover, different tumor entities display a different metastatic pattern depending on cell-intrinsic and extrinsic regulatory mechanisms. The so-called pre-metastatic niches support the adaptation of cancer cells to their new environment and increase the rate of metastases. Despite the circulation of tumor cells is a random process, the metastasis formation follows specific routes. This was already proposed within the seed-and-soil theory by Sir Stephen Paget in 1889 who stated that distant organs provide a specific environment as soil for cancer cells to seed secondary tumors (10). The concept of metastatic organotropism defines tumor entity-specific target organs. Organotropism is regulated by circulation pattern, tumor cell-intrinsic signaling, organ-specific niches, and the communication between tumor cells and the host microenvironment (11). PCa cells preferentially metastasize into bone and lung as secondary site. Within a large autopsy study of 19,000 cancer patients including 1,600 PCa patients, the bone was with 90% the most frequent metastatic site in PCa (12). This was followed by metastasis to the lungs (46%), liver (25%), pleura (21%), and adrenals (13%). Within the bone, metastases were mostly detected at the spine (90%), whereas ribs (18%), long bones (15%), and skull (8%) were less frequently affected. Within the spine, the lumbar spine is affected most (90%), followed by the thoracic (66%) and cervical spine (38%), suggesting that PCa cells follow a venous spread from the prostate to the spine. Besides the hematogenic spread through the blood stream, cancer cells can enter the lymphatic system. As such, PCa cells favor settlement into the paraaortic, pelvic, and mediastinal lymph nodes (12). Of note, there is a strong association between lymphatic and hematogenous spread. Over 84% of the tumors with paraaortic and pelvic lymphatic metastasis also displayed hematogenous metastasis, whereas when paraaortic and pelvic metastasis were absent, only 16% showed hematogenous spread. Finally, the nodal status correlates strongly with the occurrence of distant metastases, and both of them are associated with advanced histological grade and tumor growth, highlighting the importance of the detection of metastasis as a major prognostic factor in PCa. The occurrence of lymph node metastasis in patients with PCa indicates a poor prognosis (13–17) and it is frequently associated with a poor response to radical prostatectomy and radiation therapy. Thus, it is critical to understand the mechanisms underlying lymph node metastasis to improve the care of patients with PCa.

Characteristics of Lymph Node Metastasis

Lymph node metastasis positive PCa patients are at high risk for further disease progression (13–17) and a poor response to
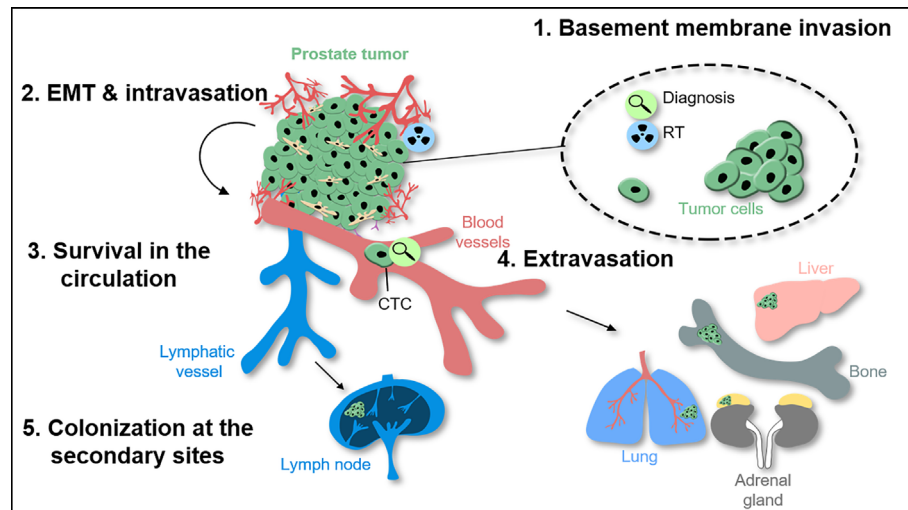
FIGURE 1 | The metastatic cascade in prostate cancer and molecular effects of radiotherapy. During tumor invasion throughout the basement membrane and further migration into surrounding normal tissue, prostate cancer (PCa) cells use epithelial-to-mesenchymal-transition (EMT) as biological program. Intravasation allows tumor cells to enter the circulation including the lymphatic and/or vascular system. To extravasate into distant tissue prostate circulating tumor cells (CTCs) have to attach to the inner vessel wall before leaving the blood system. Once the cells left the circulation they may settle down and colonize secondary organs e.g. within bones as the main metastatic site for PCa patients.

radical prostatectomy and radiation therapy. However, data from randomized clinical studies demonstrated that local therapy in combination with ADT can result in long-term disease control (18, 19). Thus, it is critical to understand the mechanisms underlying lymph node metastasis to improve the care of patients with PCa. PCa cells form a pre-metastatic niche in lymph nodes as tumor-adjacent lymph nodes display changes in the architecture and immune function even before tumor cell dissemination and lymph node colonization. The decreased immune function is reflected by the reduced density of paracortical antigen-presenting dendritic cells and T cells (20, 21), but also by the attraction of immune-suppressive cell types such as myeloid-derived suppressor cells or tumor-associated macrophages (22). This is a critical step to escape recognition and elimination by immune cells in the lymph nodes. Several means of bi-directional pre-metastatic niche communication have been proposed, e.g. that the lymphatics produce factors that attract PCa cells, but also that PCa cells or other cells present in the tumor microenvironment, such as cancer-associated fibroblasts (CAFs), produce growth factors and cytokines that promote lymph-angiogenesis. Recently, the CC-chemokine ligand 21-CC chemokine receptor 7 (CCL21-CCR7) axis has been implicated in PCa migration into the lymph nodes (23). High expression of CCL21 was detected in lymph node metastasis of PCa patients. The tumor necrosis factor α (TNF-α) has been shown to induce CCR7, the receptor for CCL21, and migration of PCa cells. Moreover, the epithelial membrane protein 1 (EMP1) was identified to be induced in PCa cells after contact with stroma cells subsequently promoting cancer progression and metastasis formation in the lymph nodes and lung *via* a Rac1-dependent mechanism (24). These tumor-stroma interactions are facilitated

by the glycoprotein podoplanin and the extracellular matrix protein tenascin-C expressed by CAFs. A high podoplanin and tenascin-C expression in the stroma of PCa biopsies strongly correlates with tumor stage, lymph node metastasis, and poor prognosis (25, 26). Lymph-angiogenesis studies identified the vascular endothelial growth factor receptor 3 (VEGFR3) and its ligands vascular endothelial growth factor (VEGF) -C and -D as critical determinants of lymphatic endothelial cell proliferation and sprouting of lymphatic vessels. In PCa, expression of VEGF-C and VEGFR3 is highly correlated with regional lymph node metastasis and associated with a poor prognosis (27–29). A recent study showed that blocking VEGF-C or VEGFR3 with antibodies or RNA interference reduced lymph node and distant metastasis, while not interfering with the growth of the primary tumor (30). This is in contrast to VEGFR2, whose inhibition reduced metastasis mainly due to the reduction of primary tumor growth by suppressed angiogenesis. Recently, phase I/II clinical trials have been completed to test the safety of VEGFR3 or VEGFR2 inhibition in patients with advanced solid tumors. Despite good tolerability, VEGFR3 or VEGFR2 inhibition showed no benefit in suppressing tumor growth or lymph node metastasis. However, these studies show that VEFGR inhibition is safe paving the way for potential combination therapies (31, 32) (**Figure 2A**).

Taken together, the concept of the pre-metastatic niche also holds true in prostate cancer lymph node metastasis. Identifying key pathways of niche communication may have significant implications for prognostic and therapeutic purposes in prostate cancer, such as targeting the VEGR3-VEGF-C axis to halt the progression of lymph node metastasis and improve the patient´s prognosis.

Characteristics of Bone Metastasis

The propensity of PCa cells to metastasize to the skeleton, and further progression to other organs, is a principal cause of morbidity and mortality among the male population. Although bone metastases can be initially asymptomatic, their consequences are often detrimental due to the occurrence of skeletal-related events such as fractures, bone pain, and spinal cord compression that markedly reduce the quality of life. While most of the solid tumors, such as breast cancer and melanoma, tend to cause osteolytic lesions with excessive bone resorption, bone lesions resulting from PCa are primarily osteoblastic and associated with uncontrolled low-quality bone formation (33).

Similar to lymph node metastasis, one of the crucial steps in the establishment of bone metastases is the formation of the metastatic niche (34). This process relies on the interactions between prostate cancer cells and bone resident cells to create a pro-tumorigenic environment in an otherwise non-permissive site. During the initial phase of bone metastasis, prostate cancer cells target the endosteal niches and compete with hematopoietic stem cells in order to survive and thrive (35). Once in the niche, disseminated prostate cancer cells invade the surrounding tissue by acquiring a bone-like phenotype, also known as osteo-mimicry. In fact, tumor cells modify their molecular signature by releasing factors originally involved in bone formation and maintenance, such as osteocalcin, alkaline phosphatase, and bone morphogenetic proteins (36, 37). This leads to the disruption of physiological bone remodeling and the onset of pathological lesions.

Among all the molecules that actively participate in PCa metastasis, bone-derived-chemokines have been shown to be crucial for a successful colonization of the skeleton. One of the most studied chemokines secreted by bone marrow stromal cells and mature osteoblasts is the C-X-C motif chemokine ligand 12 (CXCL12). Experimental evidence revealed that secretion of osteoblastic CXCL12 triggers dissemination of tumor cells from the bloodstream to the target site by binding the receptor C-X-C chemokine receptor type 4 (CXCR4) located on the tumor cells (38, 39). Inhibition of CXCL12/CXCR4 axis using a CXCR4 antagonist compromised tumor growth by altering the interaction of cancer cells with osteoblast niches (40, 41). However, this treatment failed to reduce already established metastasis (41, 42), suggesting that CXCL12/CXCR4 axis is relevant during the initial colonization phase, but not at the late stage of the disease. In addition, it has been shown that the binding of CXCL12 to its receptor enhances the expression of α5 and β3 integrins in PCa cells, two major glycoproteins involved in tumor progression (43).

Other factors involved in tumor retention within the bone marrow are the adhesion proteins. Huang et al. demonstrated that the expression of cadherin-11 in PCa cells enhances the metastatic spread to bone by providing a physical link to the osteoblastic component (44). In accordance with that, clinical specimens confirmed higher levels of cadherin-11 in metastasis compared to the primary site (45). In addition, gene expression analyses showed that cadherin-11 facilitates PCa migration and invasion through upregulation of invasive-related genes, such as

metalloproteinases (MMP) -7 and -15 (44). Results from studies investigating the role of bone cells for prostate carcinogenesis further revealed that osteoblasts redirect PCa cells toward the endosteal niche by expressing annexin 2, an adhesion molecule involved in osteoclast activation and mineralization (46, 47). Interaction of tumor cells with osteoblasts activates gap junction signaling with a subsequent impairment of the bone matrix structure (48). For example, high expression of the gap junction subunit connexin 43 has been reported to alter osteoblast cytoskeletal organization and enhance migration of tumor cells (49) (**Figure 2B**).

After colonization to the bone, PCa cells adapt to the foreign microenvironment and escape immune surveillance by entering a quiescent phase, also known as dormancy. Dormant tumor cells exhibit a reversible cell cycle arrest in G0-G1 phase, in which they remain viable but do not proliferate. Thus, quiescent cancer cells represent a clinical challenge since they are commonly chemo-resistant. Stroma-derived growth arrest-specific protein 6 (Gas6) has been shown to induce dormancy in PCa cells by binding to the receptor tyrosine kinases family member Tyro3, Axl, and Mer (TAM) and downstream activation of multiple signaling pathways, including MAPK and phosphoinositide 3-kinase (PI3K)-Akt (50). The engagement of annexin 2 on PCa cells stimulate Axl, which contributes to a dormant state and drug resistance in metastatic cells (51). While Axl levels are significantly high in quiescent cells, Tyro3 has been associated with rapid tumor growth, suggesting that a balance between the expression of Axl and Tyro3 might influence the switch of PCa cells from a dormant to proliferative state and vice versa (52). Moreover, Kim et al. found that the binding of PCa cells to osteoblasts in the endosteal niche induces the expression of TANK-binding kinase 1 (TBK1) in tumor cells, which in turn inhibits mTOR signaling pathway and induces cell cycle arrest (53). Finally, recent studies showed that two members of the transforming growth factor beta (TGF-β) superfamily, TGF-β2, and BMP-7, play a crucial role in metastatic dormancy. Specifically, osteoblast-derived TGF-β2 activates TGF-βRIII signaling in PCa cells with a subsequent phosphorylation of p38MAPK and interruption of the cell-cycle in G1-phase through the increase of the cell cycle inhibitor p27 (54). Similarly, stroma-derived BMP-7 suppresses the proliferation of prostate cancer cells through an increased expression of the mitotic inhibitors p21 and p27 (**Figure 2C**). Even though dormancy ensures tumor cell survival within the bone, the formation of detectable metastasis requires the exit of PCa cells from the quiescent state. Reactivation can be achieved by endosteal niche remodeling due to activation of osteoclastogenesis, meaning the differentiation of bone-resorbing osteoclasts from myeloid precursor cells (55). For instance, *in vivo* experiments have shown that induced by castration bone resorption leads to increased bone metastasis, a process that can be prevented using osteoclastic inhibitors, such as bisphosphonates or receptor activator of nuclear factor kappa-B ligand (RANKL) inhibitors (56). Uncontrolled activation of osteoclasts promotes a vicious cycle of growth factor signaling between bone resident cells and cancer cells leading to a final outgrowth of the tumor. From a clinical perspective, several trials have investigated the
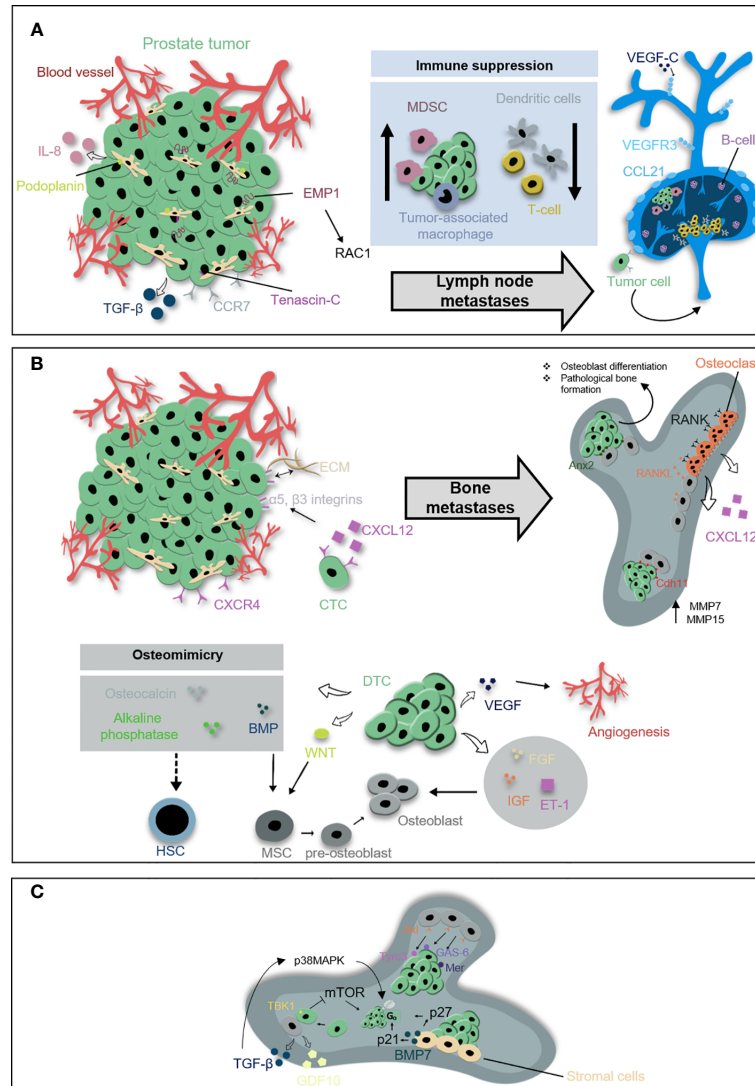
FIGURE 2 | Prostate metastases within lymph nodes and bone. **(A)** Prostate cancer cells form a pre-metastatic niche in lymph nodes prior dissemination and colonization to the lymph nodes. The decreased immune function is reflected by the reduced density of dendritic cells and T cells but also by the attraction of myeloid-derived suppressor cells (MDSCs) or tumor-associated macrophages. PCa cells and surrounded cancer-associated fibroblasts release soluble factors such as tumor necrosis factor α (TNF-α), CC-chemokine ligand 21 (CCL21), and interleukin-8 (IL-8) involved in pre-metastatic niche formation within lymph nodes. CCL21 induces chemokine receptor 7 (CCR7) on PCa cells. Epithelial membrane protein 1 (EMP1) is induced in PCa cells after contact with prostate stromal cells and likely promotes metastasis into the lymph nodes *via* a Rac1-dependent mechanism. Lymph-angiogenesis involves the outgrowth and remodeling of lymphatic vessels and is induced by vascular endothelial growth factor C (VEGF-C) secreted from PCa cells and vascular endothelial growth factor receptor 3 (VEGFR3) on lymphatic vessels. **(B)** Beside lymph nodes, the bone is a major metastatic site for PCa. The C-X-C motif chemokine ligand 12 C-X-C chemokine receptor type 4 (CXCL12-CXCR4) signaling guides disseminating PCa cells into the bone where they colonize within already formed pre-metastatic endosteal niche close to osteoblasts. CXCL12/CXCR4 binding enhances the expression of α5 and β3 integrins in PCa cells and reinforces their adhesion to the extracellular matrix (ECM). Prostate disseminated tumor cells (DTCs) target the endosteal niches and compete with hematopoietic stem cells (HSCs) in order to survive. In the niche, DTCs release factors originally involved in bone formation and maintenance, such as osteocalcin, alkaline phosphatase, and bone morphogenetic proteins (BMP). DTCs support osteoblastic activity through the release of fibroblast growth factors (FGFs), insulin-like growth factors (IGFs), VEGFs, endothelin 1 (ET-1), Wnt pathway-related factors, and BMPs. Moreover, adhesion proteins facilitate the metastatic spread to the bone, including cadherin-11 (Cdh11) upregulating metalloproteinases MMP-7 and MMP-15. Osteoblasts redirect prostate cancer cells toward the endosteal niche by expressing Annexin2 (Anx2). PCa cells and other cells within the bone microenvironment subsequently are co-regulated throughout a vicious cycle e.g., *via* receptor activator of nuclear factor kappa-B ligand (RANKL). **(C)** Tumor cells within a quiescent phase, also known as dormancy, exhibit a reversible cell cycle arrest in G0 phase. Stroma-derived growth arrest-specific protein 6 (GAS-6) induces dormancy by binding the Tyro3, Axl, and Mer receptor tyrosine kinases. Dormancy is also regulated by the expression of TANK-binding kinase 1 (TBK1) induced by osteoblast and PCa cell interactions inhibit mTOR signaling and induce G0 phase. Stroma-derived BMP-7 suppress the proliferation of PCa cells through increased expression of the mitotic inhibitors p21 and p27. Additional regulators of dormancy are GDF10 and TGF-β which phosphorylates p38MAPK.

efficacy of osteoprotective drugs in advanced PCa (57). Administration of bisphosphonates, e.g., zoledronic acid, has consistently shown protection against bone loss in patients receiving endocrine therapy compared with placebo (58, 59). Despite promising results obtained using animal models (56), there is no clear evidence of survival improvement in humans (60, 61). Besides zoledronic acid, denosumab, a RANKL inhibitor has been validated as an effective antiresorptive agent in the treatment of bone metastasis in PCa patients. In a randomized phase III study, denosumab significantly reduced skeletal-related events and improved pain control compared to bisphosphonates (62). However, more long-term follow-up studies are needed to identify potential complications and define the time point for treatment initiation (63, 64).

In summary, despite significant progress into mechanisms of PCa, further analyses need to be addressed in order to unravel the molecular basis of bone metastasis at both early and late stages. This will help to reduce the rate of metastasis formation and eventually develop new molecular targeting strategies for PCa management.

Molecular Characteristics of Metastasis in Comparison to Primary Tumor

The complex metastatic cascade is accompanied by a multitude of molecular and phenotypic changes within tumor cells to enable metastasis formation. When cancer cells leave the primary tumor, cell-autonomous characteristics that promote survival in the circulation and within target organs are extremely important (7). Genetic and epigenetic alterations within the primary tumor and acquired at the metastatic site contribute to phenotypic changes and corresponding host interactions (65). A genetic relationship between the primary tumor and the metastases is rather seen as linear progression whereas genetic divergence is interpreted as parallel development (66). Within a published study in 2009, Li et al. examined copy number variations (CNVs) of multiple metastases within 24 patients and found that a majority of samples had the same CNVs in primary tumor and metastases pointing to a linear progression model with monoclonal origin for metastatic PCa (66, 67). A 17-year longitudinal sampling of lethal PCa cases with subsequent comprehensive genomic and pathologic analysis supported this finding. Haffner et al. traced the lethal metastatic clone back to the specific lesion of origin (68). Surprisingly, the lethal clone, defined by the presence of phosphatase and tensin homolog (PTEN), tumor protein P53 (TP53), and speckle-type POZ protein (SPOP) mutations arose from a tumor region with pathological characteristics of a low-risk area and low Gleason score (68, 69). Primary PCa displays an enormous heterogeneity, which is reflected by distinct molecular subtypes and a wide variety of clinical outcomes (70). A comprehensive molecular analysis of 333 primary PCa samples from The Cancer Genome Atlas (TCGA) defined seven subtypes based on erythroblast transformation specific transcription factors (ETS) fusions or mutations in SPOP, forkhead box A1 (FOXA1), and isocitrate dehydrogenase 1 (IDH1), but demonstrated a substantial epigenetic heterogeneity within the subgroups (70). When comparing sequencing data from primary PCa and metastatic CRPC, it becomes clear that metastases carry significantly more mutations and copy number alterations than primary tumors (65, 71). In particular, metastases show frequent alterations of the androgen receptor (AR), TP53, retinoblastoma-associated protein (RB1), lysine N-methyltransferase KMT2C and KMT2D, DNA repair genes, and members of the phosphoinositide 3-kinases (PI3K) signaling pathway (71). A hallmark of PCa is the dependency on AR signaling pathways for tumor progression illustrated by the increased abundance of AR amplification. Prospective AR diagnostics impact on the clinical choice for AR-specific targeting therapies (71). In a multicenter study, a significantly higher incidence of germline mutations was found in metastatic PCa patients (11.8%) compared to 4.6% in men with localized PCa (72). Mutations were found in 16 genes, including key regulators of DNA-repair such as BRCA2, ATM, CHEK2, BRCA1, RAD51D, and PALB2. These defects in DNA repair may contribute to a further increase of mutational burden. Moreover, they can be accounted as metastasis driver mutations impacting clonal expansion while passenger mutations have no effect on the cancer cell (73). Within the primary tumor, specific genes are selectively mutated at early or later stages during tumor progression enforcing clonal evolution (74).

Clonal Evolution During Metastatic Cascade

Major determinants for metastasis formation are tumor cell adaptability and plasticity to its changing microenvironment during disease progression and therapeutic intervention (75). Early metastatic features are already selected within the primary tumor under immune pressure, within hypoxic areas or at the invasive front (7). In PCa, it appears that individual clones within the primary tumor acquired pro-metastatic properties and the most potent clones are responsible for metastasis formation or re-seeding of the primary tumor-bed e.g., after surgical removal (7, 76). Therefore, PCa cells undergo an epithelial-to-mesenchymal transition (EMT) in response to TGF-β secreted by surrounding stromal cells. EMT is a reversible phenotypic switch where epithelial cancer cells lose their intercellular adhesion and polarization in order to gain motility and invasiveness (77).

Clonal evolution analysis in metastatic PCa patients based on a deep sequencing technique revealed a branching phylogenetic architecture from primary tumor to distant metastasis with stage-specific mutational signatures (76). Interestingly, Hong et al. detected clones from various tumor stages within the blood implying multiple, temporally separated waves of tumor cell dissemination from the primary tumor. This parallel model of prostate metastasis assumes that metastasis-initiating clones may occur already before clinical diagnosis of the primary tumor (65). Another study found that an initial hormone-naïve metastasis clone contained two sub-populations after treatment. One subclone derived from the original clone and the other origined from distant sacral metastasis. This points to the requirement of specific genetic alterations for metastatic colonization that may evolve outside of the primary tumor and describes, for the first time, a pre-requisite for the parallel

progression model (65, 76). For example, the acquisition of *TP53* missense mutations in low-frequency sub-clones inside the primary tumor and their subsequent accumulation in metastasis samples may indicate that *TP53* mutations increase the metastatic potential of tumor clones and are key drivers for PCa metastasis (74, 76). In ten patients with metastatic CRPC, Gundem et al. found evidence for the existence of polyclonal seeding at distant sites. They found that metastases frequently spread from metastasis to metastasis, either by de-novo monoclonal seeding of daughter metastases or through the transfer of multiple tumor clones (5/10 patients, 50%). Within those lesions, they found mutations in tumor suppressor genes occurring as a single event in distinct clones, whereas mutations in AR signaling were detected simultaneously in multiple metastatic clones (78). Additional studies validated this polyclonal seeding based on the genomics analysis (65, 78), which indicates that subclones may cooperate or compete at all steps during metastatic cascade (78). Another study published by Gundem et al. investigated the polyclonal seeding under therapeutical pressure and identified oncogenic alterations associated with ADT resistance such as *MYC* amplification or *CTNNB1* mutation. The authors hypothesize that polyclonal expansion may be driven by distinct resistance mechanisms (78, 79). They also found that multiple metastases were more closely related to each other than to the primary tumor. Phylogenetic trees illustrate the acquisition of mutations in PCa metastases either linear, parallel, or branched (78). It seems that metastatic PCa cells share a common genetic fingerprint and thus may share a common heritage.

To sum up the molecular part, *ETS* fusion and mutations in *FOXA1*, *FLI1*, *SPOP*, and *IDH1* are tumorigenic drivers and the basis for PCa heterogeneity (70). Missense mutations of *TP53* and *PTEN* occur before or at early stages during metastatic cascade (68, 76) determining them as metastasis drivers. One interesting finding is that AR expression, which is altered in >60% of metastatic prostate cancer (80), changes after the occurrence of metastases. Currently, it is unclear whether rare subclones originate from the primary tumor or early metastases harbor AR alterations and promote ADT resistance. It may be also possible that such alterations occur after metastasis formation and ADT (81). Finally, it has been demonstrated that metastatic spread is not unidirectional and metastatic clones may re-seed the original tumor bed (76, 78). This impacts the clinical characteristics of metastatic PCa and therapeutic options.

DIAGNOSTIC IMAGING OF PROSTATE CANCER PATIENTS WITH DISSEMINATED DISEASE

Imaging of Metastasis Status in Prostate Cancer Patients

The screening for PSA level in the serum of patients was introduced in the late 1980s (82) and enabled a dramatic increase in early PCa detection (83). On the other hand, PSA is not solely a PCa-specific biomarker and, as such, leads to overdiagnosis and overtreatment of clinically insignificant cases, representing a significant burden for patients (84). Moreover, absolute PSA level does not always correlate with prognosis (85). Therefore, more specific and sensitive PSA-based values like PSA density (PSAD) (86), PSA velocity (PSAV) (87), free-to-total PSA (F/T PSA) (88), and PSA doubling time (PSADT) (89) are seen as options with stronger predictive value. For example, PSADT is defined as the length of time for two-fold PSA level increase. A PSADT <6 months is strongly associated with metastatic disease, increased PCa mortality (90), and relapse (91). Nonetheless, the reported benefit of PSADT in PCa management did not enter clinical routine and some studies even reported discrepant results indicating that further studies are required to determine the reliability of PSADT and other available biomarkers (92–94).

Recommended diagnostics for men at risk of extra-prostatic cancer spread include computer tomography (CT), skeletal scintigraphy and positron emission tomography (PET) as well as combined imaging modalities like single photon emission computed tomography (SPECT)/CT, PET/CT, and PET/magnetic resonance imaging (MRI). The most promising strategy is represented by radiotracer-based PET imaging which mainly employs changed metabolic activity or specifically overexpressed receptors (95). The choice of a respective radiotracer has to be considered carefully as one single radiotracer is usually not suitable to visualize all clinical stages of PCa. Moreover, its utilization is strongly dependent on the level of malignant tissue, tumor heterogeneity (96), and previously applied treatments (97). The 2-deoxy-2-^{18}F-fluoro-D-glucose (^{18}F-FDG) is the most commonly used radiotracer in clinical PET imaging worldwide. It is seen as limited with rather low overall sensitivity for PCa compared to other malignancies with a higher glycolytic rate (98). In contrast, patients with discordant ^{18}F-FDG-avid metastatic CRPC are usually identified with a poor prognosis and short overall survival (99). Thus, ^{18}F-FDG-PET imaging represents a relevant prognostic indicator correlating with enhanced glucose transporter 1 expression in high-risk PCa patients (100). The androgen receptor (AR) represents a key molecular target for AR-binding 16β-^{18}F-fluoro-5α-dihydrotestosterone (^{18}F-FDHT). ^{18}F-FDHT-PET enables detection of metastatic CRPC with overexpressed AR and indicates a low pharmacological efficacy of ADT (101). Another commonly applied strategy is represented by the utilization of multiple radiolabeled choline derivatives such as ^{11}C-methyl-choline and ^{18}F-fluorocholine (102). Choline is phosphorylated by the choline kinase overexpressed in PCa and necessary for malignant transformation (103). ^{11}C- and ^{18}F-choline-PET demonstrated clinical benefit for the detection of bone and lymph node metastases. However, in the latter case, the sensitivity is strongly dependent on PSA level as demonstrated by detection rates of less than 50% for PCa patients with serum PSA level <2 ng/ml (104). Moreover, anti-1-amino-3-^{18}F-fluorocyclobutane-1-carboxylic acid (^{18}F-FACBC, Axumin®, Blue Earth Diagnostics) was proven to be superior to ^{11}C-

methyl-choline in PET imaging for PCa patients with biochemical relapse after radical prostatectomy (105). Finally, ^{18}F-sodium fluoride (Na^{18}F) is a hydroxyapatite-affine bone-seeker which is incorporated at sites of active bone remodeling adjacent to metastatic foci analogically to 99m-technetium medronic acid (99mTc-MDP) used for skeletal scintigraphy (106). However, ^{18}F-NaF-PET was shown to have a higher sensitivity and specificity for the detection of osseous metastatic disease compared to scintigraphy (107).

Radiopharmaceutical Options

Among all previously mentioned radiotracers for PCa imaging, particular attention is given to radiotracers targeting the peptidase prostate-specific membrane antigen (PSMA) (108). PSMA expression reflects the progression of the disease, with the highest expression level in the late stage of metastatic CRPC, and enables monitoring of disease recurrence (109). Diverse PSMA-directed antibodies, antibody-derivatives, peptides, peptidomimetics, small molecules, and nanoparticles have been designed as capable diagnostic, therapeutic, and/or theranostic constructs for the management of PCa (110–113). As reported by Zippel et al., more than 100 clinical trials utilize PSMA-specific diagnostics or therapeutics currently (114). Until now, it has been shown that ^{68}Ga-PSMA-PET outperforms all standard-of-care imaging within sensitivity and specificity for PCa detection (115). In the randomized proPSMA trial for primary staging of localized high risk prostate cancer, PSMA-based PET imaging showed superior sensitivity and specificity over conventional imaging for accurate diagnosis of nodal and distant metastases {27% (95% CI 23–31) vs. 65% [60–69]; p<0·0001}. Further, ^{18}F-PSMA-PET has a significant impact on PCa patient management as shown by a prospective clinical study (116). The most prominent diagnostic radioligand for the imaging of PSMA-positive PCa is ^{68}Ga-PSMA-11 (117). Comprehensive meta-analysis by Perera et al. demonstrated high PCa detection rates for ^{68}Ga-PSMA-PET with 59% for patients with low PSA levels of 0.5–0.99 ng/ml, 75% for 1–1.99 ng/ml and 95% for PSA values >2 ng/ml (118). In parallel, ^{18}F-labeled PSMA ligands like ^{18}F-DCFPyL (119) and ^{18}F-PSMA-1007 (120) may gain even more clinical importance. For example, ^{18}F-PSMA-PET/CT was able to visualize metastatic lesions in >70% of CRPC patients that were not previously detected (121) and in >67% patients with biochemical recurrence whose conventional imaging has also failed (122). On the other hand, 5%–10% of patients with primary PCa are PSMA-negative and PSMA-targeted diagnosis is not applicable in those patients (123). Additionally, patients who receive long-term ADT demonstrate a significant reduction in PSMA expression (97). In this scenario, other targets such as gastrin-releasing peptide receptor (124), fibroblast activation protein (125), and somatostatin receptor (126) demonstrated clinical potential (**Table 1**).

Imaging and Theranostic of Skeletal Metastasis

The skeletal compartment is the most frequent site of metastases in PCa patients (127). Bone metastases occupy a nutrient-rich niche that enhances the treatment-resistance of disseminated PCa (128). Approved agents for palliative therapy of PCa patients with bone metastasis include beta-emitting particles such as strontium chloride (^{89}Sr-chloride) (129) and samarium-153-ethylene-diamine-tetra-methylene-phosphonate (^{153}Sm-EDTMP) (130). However, both options did not improve overall survival and demonstrated limited tolerability due to side effects on the bone marrow and hematopoietic system. On the other hand, alpha-emitting particles including agents such as radium-223 dichloride (^{223}RaCl2, Xofigo®, Bayer Healthcare) revealed overall survival benefit and reduced symptomatic skeletal events (131). The ALSYMPCA trial reported that the application of ^{223}RaCl2 increases median overall survival from 11.3 to 14.9 months and time to develop skeletal-related events from 9.8 to 15.6 months (132).

The novel concept of theranostic approaches combines diagnostics with therapy. Due to the increased availability of potent PSMA-directed agents, several PSMA-labelled radiopharmaceuticals are used in the late stage of PCa. Meanwhile, beta-particle-emitting ^{177}Lu-PSMA-617 (133–136) and alpha-particle-emitting ^{225}Ac-PSMA-617 (137–139) became the main candidates for PSMA-targeted radioligand therapy of patients with metastatic CRPC. A retrospective multicenter phase I study with 145 patients demonstrated safety and efficacy of ^{177}Lu-PSMA-617. The clinical benefit exceeded those of other third-line systemic therapies and prolonged the overall survival in patients without any other treatment option (134, 140–142). A prospective single center phase II trial validated the high response rate, low toxicity, and improved quality-of-life in additional 50 patients for the ^{177}Lu-PSMA-617-based theranostic (143). The long-term follow-up of this study including re-treatment upon progression demonstrated higher response rates than other third-line therapies, as far as such comparison between different studies is valid (144). A systematic review from von Eyben et al. concluded that ^{177}Lu-PSMA-targeted radioligand therapy decreased PSA level in patients twice as often as chemotherapy (145). Another agent, the ^{225}Ac-PSMA-617, revealed an even higher radiological and biochemical response rate in patients with poor prognosis. However, those patients experienced an increased rate of severe side-effects like irreversible xerostomia (139). The current focus is given to the prospective international multicenter phase-III trial called VISION (NCT03511664) which evaluates ^{177}Lu-PSMA-617 for the treatment of 750 patients with progressive PSMA-positive metastatic CRPC (146). The outcome of this clinical trial might clarify the role and clinical potential of ^{177}Lu-PSMA-targeted radioligand therapy for the management of metastatic CRPC as second-line therapy in the future.

RADIOTHERAPY FOR PATIENTS WITH METASTATIC PROSTATE CANCER

Clinical Potential of Radiotherapy for Metastatic Prostate Cancer Patients

The current standard-of-care for patients with metastatic PCa includes systemic androgen-deprivation therapy with or without

TABLE 1 | Clinical trials applying radiopharmaceutical in PCa patients, including patient characteristics, therapeutics, outcome, study ID.

Compound	Characteristics & number of participants	Patient characteristics	Primary outcome measures	Completion date	Study ID & short name
[68Ga]Ga-PSMA-11 *compared to histopathology*	Diagnostic Phase I/II 173	Patients with newly diagnosed PCa and a high risk for metastasis, scheduled for radical prostatectomy (RP) with extended pelvic lymph node dissection (EPLND).	True positive fraction (TPF) and false positive fraction (FPF) of identified tumor tissue in soft tissue, analyzed separately for prostate gland and pelvic lymph nodes, using histopathology as standard of truth. Frequency of occurrence and severity of abnormal findings in safety investigations.	Jul 2020	NCT03362359
[68Ga]Ga-PSMA-11 *compared with pathology reports and/or routine imaging*	Diagnostic Phase n.d. 1574	Subjects with high risk PCa at initial presentation, with biochemical persistence of PCa following radical prostatectomy, with biochemical recurrence of PCa following initial curative treatment with radical prostatectomy or radiation therapy, with biochemical recurrence of PCa following radical prostatectomy	Sensitivity of [68Ga]Ga-PSMA-11 PET/CT imaging in the assessment of high risk and recurrent PCa. Determination of sensitivity when compared with pathology reports (if available) and routine imaging (CT, MRI, bone scan) if available.	Sep 2028	NCT04484701
[18F]DCFPyL *compared to histopathology*	Diagnostic Phase II/III 385	Patients with at least high risk PCa who are planned for radical prostatectomy with lymphadenectomy (Cohort A) or patients with locally recurrent or metastatic disease willing to undergo biopsy (Cohort B).	Sensitivity and specificity of [18F]DCFPyL PET/CT imaging to detect metastatic PCa within the pelvic lymph nodes relative to histopathology.	Jul 2018	NCT02981368 "OSPREY"
[18F]DCFPyL *followed by biopsy/ surgery, conventional imaging or locoregional RT*	Diagnostic Phase III 208	Patients with suspected recurrence of PCa who have negative or equivocal findings on conventional imaging.	Correct localization rate, defined as % of subjects with a one-to-one correspondence between localization of at least one lesion identified on [18F]DCFPyL PET/CT imaging and the composite truth standard.	Aug 2019	NCT03739684 "CONDOR"
[18F]PSMA-1007 *vs. [18F]fluorocholine*	Diagnostic Phase III 200	Patients with suspected biochemical recurrence of PCa after previous definitive treatment for localized PCa.	Comparison of detection rate of metastatic PCa lesions for [18F]PSMA-1007 versus [18F]fluorocholine.	Sep 2020	NCT04102553
[177Lu]Lu-PSMA-617 *vs. cabazitaxel*	Therapy Phase II 201	Patients with mCRPC who have progressed despite hormonal therapy and chemotherapy.	PSA RR defined as the proportion of participants in each group with a PSA reduction of ≥50% from baseline.	Jan 2021	NCT03392428 "TheraP"
[177Lu]Lu-PSMA-617 *vs. best supportive/ standard care*	Therapy Phase III 750	Patients with progressive PSMA-positive mCRPC who received at least one novel androgen axis drug and were previously treated with one to two taxane regimens.	OS in patients with progressive PSMA-positive mCRPC who receive [177Lu]Lu-PSMA-617 in addition to best supportive and/or standard of care.	Sep 2021	NCT03511664 "VISION"
[177Lu]Lu-PSMA I&T *vs. standard care*	Therapy Phase II 58	Patients with hormone-sensitive oligo-metastatic PCa.	To compare the fraction of patients that have disease progression and meet EOT 1 criteria in a group of patients that are treated with [177Lu]Lu-PSMA I&T and a control group.	Jan 2024	NCT04443062 "Bullseye"
[225Ac]Ac-PSMA-617 *pilot trial for therapy*	Therapy Early phase I 20	Patients with mCRPC who were incapable of 2nd ADT or chemotherapy.	Serum PSA level.	Dec 2021	NCT04225910
[225Ac]Ac-J591 *dose escalation*	Therapy Phase I 42	Patients with documented progressive mCRPC.	Change in the number of subjects with dose limiting toxicities. Estimation of maximum tolerated dose.	Jul 2024	NCT03276572
[225Ac]Ac-J591 *dose escalation*	Therapy Phase I/II 105	Patients with progressive mCRPC.	Change in the number of subjects with dose limiting toxicities. Estimation of cumulative maximum tolerated dose. Assessing the recommended phase II dose (RP2D) of [225Ac]Ac-J591 in fractionated dose and multiple dose regimens (phase I).	Jun 2027	NCT04506567
[131I]-MIP-1095 *with or without enzalutamide*	Therapy Phase II 175	Patients PSMA-avid mCRPC who have progressed on abiraterone and are planned for treatment with enzalutamide. Patients must be chemotherapy-naive and must be ineligible or refuse to receive taxane-based chemotherapy at time of study entry.	The proportion of patients with PSA response according to PCWG3 criteria defined as the first occurrence of a 50% or more decline in PSA from baseline, confirmed by a second measurement at least 3 weeks later.	Dec 2022	NCT03939689 "ARROW"

docetaxel-based chemotherapy. The effects of local radiotherapy for men with metastatic PCa as well as the optimal combination with systemic therapies are currently under debate. In particular, the heterogeneity within PCa patients in terms of tumor volume, metastatic distribution, tumor properties, and clinical symptoms impact tumor progression and therapeutic outcome and need to be further investigated. Several ongoing prospective randomized trials aim to clarify the impact of local radiotherapy in patients with metastatic PCa (NCT01957436, NCT03678025, NCT01751438). The randomized phase 3 trial STAMPEDE compared standard-of-care with external-beam radiotherapy to the prostate in metastatic patients and showed no improved overall survival in the whole cohort (HR 0.92, 0.80–1.06; p=0.266). However, in a pre-specified subgroup analysis of patients with low metastatic burden, the trial demonstrated an improved 3-year overall survival in patients with low metastatic burden (819 of 2061 randomized patients) compared with standard-of- care (81% vs. 73%; HR 0.68, 95% CI 0.52–0.90; p=0.007) (147). Within this study, high-volume metastatic disease was defined as presence of visceral metastases and/or more than four bone metastases with at least one outside of the vertebral column and pelvis. These results are in line with the data obtained within the HORRAD trial, the only published randomized-controlled trial so far that has found a survival benefit in men with low metastatic burden applying local radiotherapy in combination with androgen-deprivation therapy for PCa patients with primary bone metastasis (148). This indicates that patients with few metastases could potentially benefit from local prostate radiotherapy. In both trials, only conventional staging such as bone scan or CT was used. As modern PSMA-PET would be able to detect even smaller metastatic lesions, the method has the potential to precisely define low-volume disease. Furthermore, more patients would be staged as high-volume disease. Therefore, the definition of high-volume disease and the question which of those patients would benefit from local radiotherapy has to be addressed in randomized controlled trials in the future. However, there is an urgent need to clarify the benefit of local radiotherapy on metastatic spread not only from the clinical point of view but also from a better understanding of the underlying molecular and cellular mechanisms.

Clinical Features of Oligometastatic Prostate Cancer Patients

The term oligometastatic cancer refers to a wide range of patients with a low number of metastatic lesions. The occurrence of one to five metastases in those patients leads to a distinct clinical prognosis compared to patients with widespread metastatic disease (149, 150). Oligometastatic patients benefit from local ablative treatment to all visible lesions in terms of a significant clinical benefit for overall survival, time to initiation of systemic therapy, or time to progression (151–156). In general, the prognosis of patients differs when addressing the timepoint of metastatic onset e.g. in patients with oligo-recurrence after initial local therapy, appearance of metastases after local therapy without a local recurrence, or detection of additional metastatic lesions in patients with metastatic disease. It is hypothesized that those differences may be due to primary location and histology, previous treatments, metastasis activity (synchronous metastases

vs. metachronous metastases), and metastasis status (lymph node vs. other sites) at first diagnosis (157). Until now, no clinical data are available evaluating the prognostic differences in PCa patients with oligometastatic disease, underlining an urgent clinical need for the development of biomarkers to stratify this heterogeneous group of oligometastatic PCa patients. Another assumption currently under discussion is whether treating all metastatic lesions with ablative intent using e.g. high dose radiotherapy, surgery, thermal ablation or laser resection may lead to complete tumor response, high cure rates, or long-term disease control in a subgroup of oligometastatic PCa patients. This is supported by clinical trials showing a significant benefit in prolonging time to initiation of androgen-deprivation therapy (13 vs. 21 months) or tumor progression after metastasis-directed therapy (MDT) in comparison to standard of care (158).

Due to the development of novel imaging techniques for PCa patients, as already introduced previously, the detection of metastases is possible even at low PSA serum levels (1–2 ng/ml) (159). PSMA-PET-based staging entered successfully the clinical routine for primary diagnosis in high-risk PCa patients and influenced significantly the choice of treatment (160). Moreover, it is applied for staging of patients with biochemical recurrence after prostatectomy or progression after radiotherapy (161). Detected metastases are typically small and asymptomatic in the lymph node or bone. High precision conformal radiotherapy techniques such as stereotactic body radiotherapy is able to control those lesions without significant normal tissue toxicity (162).

PCa with recurrent disease is usually not accompanied by fast progression into symptomatic stages. Patients with recurrence develop symptomatic metastases within a median time of 8 years and a mean overall survival rate of 5 years upon onset. Only a small subgroup of patients characterized with an initial Gleason score of 8 to 10, biochemical recurrence within 2 years, and a PSA doubling time <10 months show a faster metastatic progression (163). In summary, the prognosis of oligometastatic PCa is heterogeneous as those lesions appear at different disease stages at primary diagnosis and upon different pre-treatment regimens. Stratifying those heterogeneous patient population into several subgroups solely based on PSA level is currently under investigation. Unfortunately, no prognostic biomarker for those patients is available so far. Moreover, the development of predictive biomarkers for metastasis-directed therapy would help to answer the clinical questions, if PCa patients would benefit in all stages of the disease (164).

Metastasis-Directed Radiotherapy

In incurable disease stages, palliative radiotherapy in few fractions is frequently applied to alleviated symptoms including pain, bleeding, or urinary tract problems. The gained improvement of these clinical symptoms, however, does not affect overall survival and metastatic progression at other sites (165). Novel imaging techniques enable the detection of single or few PCa metastases even in patients with low PSA-level and the treatment of those lesions with local ablative radiotherapy (162). Therefore, a growing number of patients are treated with the so-called metastases-directed therapy, including all forms of local treatments (e.g.,

lymph node dissection, thermal ablation, surgery, or high-dose radiotherapy) with the aim of long-term tumor control. Improved radiotherapy planning systems and precise delivery techniques allow metastasis-directed, local ablative radiotherapy with a few high-conformal fractions as stereotactic body radiation therapy (SBRT). Due to the non-invasive nature of SBRT, the treatment can be done without serious side effects. Most retrospective case series [summary in (150)] focus on a local control and disease progression and demonstrated clinical benefit with local control rates of >90% within the first year. However, further biochemical or metastatic progression after 1 year is observed in ~50% of the treated patients. All published data are not comparable, because those cohorts differ within risk group stratification, primary treatment, concurrent medication, diagnostics, and fractionation scheme. To date, only two randomized trials, the STOMP, and ORIOLE study investigated the clinical benefit of metastasis-directed radiotherapy in comparison to observation as standard-of-care in castration-sensitive PCa patients. Within the STOMP study, 5 out of 31 patients received pelvic lymph node resection and showed a significant improvement of androgen deprivation therapy-free survival (21 vs. 13 months). Within the ORIOLE study, SBRT was applied with a fractionation schedule depending on the metastatic site and included 3 to 5 fractions with a total dose of 19.5–48 Gy. The primary clinical endpoint was progression at 6 months from randomization and proofed safety and efficacy of SBRT to all metastases. The results demonstrated in 19% vs. 61% of the patients a metastatic progression favoring the SBRT arm. However, in both trials, a high number of patients showed biochemical or metastatic progression within 2 years upon locally applied metastasis-directed therapy (166, 167). Due to the rapid progression in the majority of the analyzed patients, the impact of other clinically relevant endpoints, e.g., overall survival, time to castration-resistance, or time to symptomatic progression, remains unclear (168, 169) and should be evaluated in future trials. Moreover, there are still several open clinical questions regarding the treatment of patients with hormone-sensitive, metastatic PCa:

1. What is the optimal radiotherapy volume, as retrospective data indicate fewer nodal recurrences with larger pelvic irradiation fields compared to small node fields (170)?
2. What is the clinical effect and duration of concurrent androgen-deprivation therapy since retrospective data demonstrate a benefit in terms of time to biochemical progression (171)?
3. Can "omics" (e.g., based on tissue or imaging) or other biomarkers guide individualized treatment decisions?

Up to now, the clinical utility of metastasis-directed radiotherapy in patients with oligometastatic CRPC was only demonstrated in retrospective studies. These promising results illustrate that PSMA-based imaging can identify oligometastatic disease in up to 75% of patients when applied at low PSA values (172). Moreover, it was shown that local radiotherapy is able to control or induce regression of the detected metastatic lesions (173–176). The clinical aims of metastasis-directed radiotherapy in terms of long-term curation, regression, or time prolongation of symptomatic disease are currently a matter of debate. However, prospective and

randomized clinical data are necessary to demonstrate the clinical benefit of metastasis-directed radiotherapy including clinical endpoints such as velocity of progression, progression of asymptomatic to symptomatic metastases, and overall survival. Nonetheless, the sensitivity and clinical applicability of novel imaging modalities are limited and combination with molecular diagnostics would be necessary in the future for therapy monitoring and early detection of metastatic spread.

CIRCULATING TUMOR CELLS IN PROSTATE CANCER

Biology of Circulating Tumor Cells

Circulating tumor cells (CTCs) are malignant epithelial cells within the blood of cancer patients and origin either from the primary tumor or from distant metastasis (177, 178). They were first described in 1869 by the Australian physician Thomas Ashworth (179). The initiation of tumor cell dissemination from the primary tumor is promoted either actively or passively due to tumor cell shedding into surrounding blood vessels during biopsy, surgery, or brachytherapy. Active dissemination is induced through TGF-β, Wnt, or IL-6 stimulation leading to induction of a partial EMT phenotype (180, 181). Upon leaving the primary tumor, migratory cancer cells can intravasate into the blood stream passively through disorganized and leaky vessels in fast growing tumors, which are formed rapidly upon VEGF-induced neovascularization (182–184). In addition, trans-endothelial migration along a chemoattractant gradient consisting of VEGF-C, VEGF-D, and CCL21 regulates active intravasation. In addition, upon adhesion of cancer cells to endothelial cells they secrete cytokines and growth factors, such as VEGF, angiopoietin 2 (Angpt2), and angiopoietin-like 4 (Angptl4), leading to hyperpermeability of the endothelial wall (185). In prostate CTCs, the G-protein coupled receptor CD97 was identified as key promotor for trans-endothelial migration through platelet activation, ATP release, and lysophosphatidic acid signaling (186). Moreover, these platelet coating shields the major histocompatibility complex class I (MHC I) signal and protects CTCs from T and NK cell-mediated immunity. Other groups could demonstrate that CTCs express programmed death-ligand 1 (PD-L1), a member of the B7/CD28 co-stimulatory receptor family, that mediate immune tolerance upon binding to PD-1 on T cells (187). Even nuclear PD-L1 expression in prostate CTCs was found to be associated with poor overall survival of patients (7). Within the circulation, CTCs travel either alone, as cluster, or covered with platelets, megakaryocytes, or neutrophils. In breast cancer, it was shown that CTCs form clusters through the cell junction component plakoglobin or the glycoprotein CD44. Such oligoclonal CTC clusters are better protected from reactive oxygen species (ROS) and exhibit a significantly increased metastatic potential (188). Most of the CTCs entering the circulation die within 24 h either *via* anoikis or immune attack (8). The mean CTC frequency is assumed to be approximately 1 CTC per 1 billion red blood cells with a determined half-life of

2.5 h for breast CTCs (189). The ExPeCT (Exercise, Prostate Cancer, and Circulating Tumor Cells, NCT02453139) trial analyzed the impact of a structured exercise on metastasis progression in PCa patients including analysis of CTCs, CTC clusters, and platelet-CTC cloaking. So far, there are no study results published, but preliminary analysis demonstrated no relationship between physical exercise and CTC count. However, first indications point to a significant influence of immune crosstalk on metastasis cascade (190). In breast cancer patients, Szczerba et al. analyzed CTC-associated white blood cells and found a connection with neutrophils. CTCs within cluster, together with neutrophils, display differently regulated genes involved in cell cycle progression, cell-cell junction, and cytokine receptor expression, survive better in the blood stream, and exhibit elevated metastatic potential compared to single CTCs (191). Active CTC extravasation is induced by rolling of CTCs along the endothelium mediated by interaction with CD44 and integrin αvβ3 (192). In addition, hemodynamic forces facilitate adhesion of CTCs to the blood vessel wall and induce endothelial remodeling (193). Upon stabilization of CTC-endothelium interaction, CTCs induce extravasation through binding of sialofucosylated proteins, such as podocalyxin or glycosphingolipids with C-type lectin binding, e.g., E-selectin (CD62E), on endothelial cells (194). Besides the above described, TGF-β induced hematogenous dissemination and lymphatic spreading was described for several tumor entities including colorectal cancer (180, 195) (**Figure 3A**). A recently published study demonstrated protective metabolic priming of melanoma cells within the lymph node and increased metastatic potential. The metabolic rewiring is mediated by oleic acid within the lymph node and reduces oxidative stress, lipid oxidation, and ferroptosis when the cancer cells travel through the blood stream (196). It is not known whether this protective metabolic mechanism is also involved during lymphatic spread of PCa.

Within local PCa tumor heterogeneity and cellular plasticity are key regulators for progression, therapy resistance, and metastatic spread (197–199). A population with a high degree of heterogeneity has a higher chance to survive evolutionarily (200, 201). Recent findings indicate that the prostate CTC population is heterogeneous in terms of their genomic alterations, gene expression profile, and cell surface marker expression (202–204). Lack of datasets correlating the impact of CTC heterogeneity and plasticity for metastatic spread and therapy response in PCa patients is a consequence of low CTC number and limited availability of molecular approaches with high sensitivity and specificity (205). This obstacle was tackled by the group of Johann de Bono which isolated prostate CTCs from patients with lethal disease based on apheresis technique. Therapeutic apheresis removes patient's blood followed by the separation of cells-of-interest from other blood cells, e.g., in the mentioned study of EpCAM⁺ CTCs, and reinfusion of the blood. With the application of this method, the group was able to isolate app. 12,500 CTCs per patient within 59.5 ml blood. 185 single CTCs from 14 patients underwent genomic analysis *via* array-based comparative genomic hybridization upon whole genome amplification. The individual copy number alteration

demonstrated complex intra- and interpatient heterogeneity (202). However, all published results analyzing prostate CTCs are not experimentally homogenized according to the isolation procedure and biomarker analysis (206). Therefore, the European cancerID consortium (2014–2019) was aiming to establish clinical utility of liquid biopsy analysis (207, 208). The study by Massard et al. impressively demonstrated how isolation methods affect CTC count and characterization. This group compared two CTC isolation techniques, CellSearch with isolation by size of epithelial tumor cells (ISET) filtration, and found that the CellSearch system is biased to identify CTCs with epithelial phenotype while missing mesenchymal CTCs and CTC cluster. However, detection rate of AR amplification based on downstream fluorescence *in situ* hybridization analysis was higher in CellSearch enriched CTCs compared to ISET (209). Another study published by Scher et al. investigated the heterogeneity of prostate CTCs in 179 patients with metastatic disease and how the degree of CTC heterogeneity can be clinically applied to support decision making either for AR inhibitor-based therapy or taxane-based chemotherapy. They hypothesized that the degree of pre-therapeutic CTC heterogeneity inversely correlates with overall survival upon ADT but not with chemotherapy. Therefore, they analyzed cells within the blood upon red blood cell lysis using automated immunofluorescent analysis for nuclear DAPI, leukocyte marker CD45, epithelial marker cytokeratin (CK), and prostate-specific AR. Upon digital pathology, the Shannon diversity index describes the occurrence of individual CTC clones within the whole CTC population defined as DAPI⁺CD45⁻. Heterogeneity was evaluated based on densitometric, morphometric, and texture patterns of nuclear DAPI, CK, and AR signal. The results validated the relationship between the degree of CTC heterogeneity and overall survival for ADT, but not for taxanes. In addition, genomic profiling of 10 CTCs in 17 patients identified unique driver subclones for ADT resistance (210). Further studies validated the clinical utility of molecular CTC features for clinical decisions. For example, the expression of the AR splice variant 7 (*ARv7*) status in CTCs of metastatic CRPC patients is able to predict the efficacy of ADT (211–213). So far, no published study correlated CTC heterogeneity and dynamics with predictive value for radiotherapy response and metastatic progression in PCa patients.

Clonal Evolution and Dynamics Within Prostate Circulating Tumor Cells

That tumors follow the Darwin's theory of evolution was already proposed by Peter Nowell in 1976. This can be seen in slow growing PCa which is characterized by extensive intra-tumoral heterogeneity and sub-clonal diversity (74, 214). This clonal diversity has a significant impact on therapy response. For example, Beltran et al. analyzed 114 biopsies from 81 patients with metastatic CRPC including specimens with adenocarcinoma (Adeno) or neuroendocrine (NE) features. The differentiation into neuroendocrine morphology includes the downregulation of AR and explains the ADT escape. The genome-wide expression and
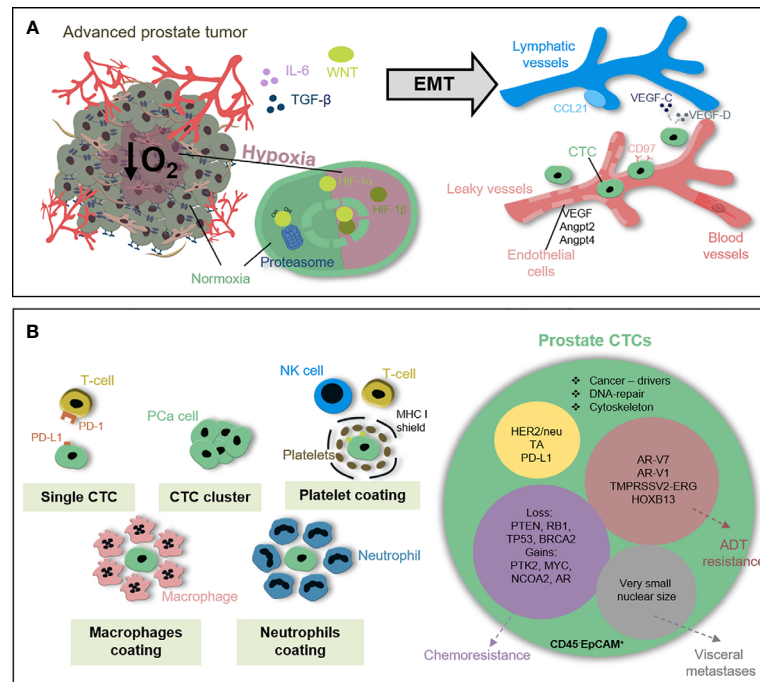
FIGURE 3 | Circulating tumor cells in prostate cancer patients. **(A)** Early metastatic features within PCa cells can be induced under stress conditions e.g. hypoxia, immune attack, or therapeutic pressure. In response to TGF-β, Wnt or IL-6 PCa cells undergo EMT to gain motility and invasiveness. PCa cells intravasate into blood vessels either passively throughout leaky vessel walls or actively *via* trans-endothelial migration. **(B)** Prostate CTCs circulate either as single cells, CTC cluster, or coated with platelets, neutrophils or macrophages shielding immune attack and reducing shear stress. CD45⁻EpCAM⁺ CTCs are a heterogeneous population differing in, e.g. the expression of androgen receptor splice variants, TMPRSS2-ERG status or loss of tumor suppressors PTEN, RB1, and TP53 recapitulating local tumor heterogeneity, influencing metastatic capacity and indicating therapy response.

DNA methylation data of this study demonstrated a high level of clonality, but overall similarity of genomic alterations while epigenetic adaptations were able to distinguish CRPC-Adeno from CRPC-NE subset. Key mechanisms important for the induction and maintenance of the ADT-resistant state base on cell-cell adhesion, EMT and histone methyltransferase EZH2 signaling. These findings support the independent emergence of an AR-insensitive cell state through clonal evolution as major ADT resistance mechanism (214). Several studies demonstrated that this clonal heterogeneity and genomic alteration known from stepwise prostate tumorigenesis could be recapitulated within the CTC population including the detection of tumor suppressor gene loss, e.g. *PTEN*, *RB1*, and *TP53* (215, 216) (**Figure 3B**). Moreover, Mahili et al. determined copy-number alteration in 257 isolated CTCs from 47 patients with aggressive PCa treated with cabazitaxel- and carboplatin-based chemotherapy and found a higher frequency of detectable chromosomal alteration in CTCs compared to match-paired cell-free tumor DNA (73.7% vs. 42.1%). The observed genomic instability in CTCs is independent of the CTC count and associated with chromosomal gains in regions containing the *PTK2*, *MYC*, and *NCOA2* gene increased AR expression, and *BRCA2* loss (217). This opens new preclinical and clinical questions:

1. Does molecular analysis of CTCs have the potential to predict sites and degree of metastatic spread?

2. How does the genetic profile of CTCs overlap with metastases and are CTCs the origin of polyclonal metastatic lesions?
3. Do CTC-based analysis outcompete routine diagnostics such as PSA plasma level, Gleason score or imaging modalities to predict and monitor therapy response in PCa patients, in particular for local or systemic metastasis-directed therapies?

To demonstrate the clinical importance of CTCs for the diagnosis of metastasis, Faugeroux et al. performed whole-exome sequencing analysis from 179 isolated CTCs and matched metastasis biopsies from 11 PCa patients. They found that app. 30%–50% of the mutations are shared between the metastasis and epithelial CTCs. In addition, a CTC exclusive mutation pattern was found in epithelial and non-epithelial CTCs containing known cancer-driver genes and genes involved in cytoskeleton and DNA repair. Based on these data, the group hypothesized that the phenotypically distinct CTC populations found in the patient's blood resemble a phylogenetic relationship rather than offspring from different precursors (218). Another study was able to distinguish three morphologically distinct CTC populations based on nuclear size measurements. Upon analysis of 148 blood samples from 57 PCa patients, they were able to identify patients with visceral metastasis based on the amount of very small nuclear CTCs (219). However, further experimental studies and prospective clinical trials are needed to prove clinical utility of CTC

diagnostics and answer upcoming clinical questions e.g. in terms of decision-making for metastasis-directed therapy, in particular for oligometastatic PCa patients with ablative radiotherapy. Cell-extrinsic pressures, such as environmental forces, immune attack, or lack of nutrients are key drivers for clonal evolution and cellular plasticity influencing the degree of tumor heterogeneity. Therapeutic pressure is another driver for clonal selection and induction of cellular escape mechanisms influencing geno- and phenotype of CTCs. Novel findings indicate that different CTC populations may have different metastatic potential in terms of frequency and site-specificity.

Clinical Application of Circulating Tumor Cell-Based Diagnostics

The detection of ≥5 CTCs per 7.5 ml blood in PCa patients with metastatic disease has a relevant prognostic value and correlates significantly with reduced progression-free survival and overall survival compared to patients with <5 CTCs (220–222). This data led to the approval of CTC-based diagnostics via CellSearch system by the United States Food and Drug Administration (FDA) in 2008 and the implementation into recommendations by international trial groups like Prostate Cancer Working Group (PCWG), Southwest Oncology Group (SWOG by National Cancer Institute) and European Organization for Research and Treatment of Cancer (EORTC). Most of the published studies applied the CellSearch system with a phenotypic definition for prostate CTCs as leukocyte marker CD45-negative and epithelial cell adhesion molecule (EpCAM)-positive. Despite the presence of CTCs in PCa patients can be correlated with prognosis and metastatic status, the predictive value is still under debate. Lowes et al. assessed the presence of prostate CTCs at baseline and several time points after radiotherapy (6, 12, and 24 months) (31). They found no correlation between PSA-level and CTC count. However, the presence of extracapsular extension or seminal vesicle invasion combined with CTC-positive status at baseline was predictive for poor response to radiotherapy. Therefore, determining the number of CTCs during radiotherapy may have the potential to stratify patients that need additional systemic therapy from those with high therapeutic efficacy from local radiotherapy alone. Moreover, neither of the standard parameters such as time to biochemical recurrence, PSA doubling time, and pathological features (e.g. Gleason score or margin status) nor available imaging technologies can provide information about the precise location of upcoming recurrences (223). First clinical indications point to the potential of CTCs to predict metastatic spread even upon therapy and the ability to discriminate different sites of metastasis. Besides promising results for CTC-based diagnostics in PCa patients with metastatic disease (222, 224), the prognostic value of CTC count in localized stages is currently not clear due to low detection rates. Most studies analyzing CTCs in locally-advanced PCa patients applied a reduced cut-off value from five to one CTC per 7.5 ml blood or increased analyzed blood volume. However, the data are controversial and the prognostic values of CTC count within this PCa patient group could not be demonstrated yet (225).

A recently published study analyzed CTCs in treatment-naïve patients with locally advanced high-risk PCa (NCT01800058, n=66) (226). The authors found that the baseline CTC count was associated with conversion into stage T3 and N1, but not with overall survival. Initially, CTC-negative patients became CTC-positive directly upon androgen-deprivation therapy or radiotherapy followed by a consecutive drop in CTC count within 6–12 months. The authors hypothesize that passive mechanisms due to tumor destruction are responsible for the observed increase in CTC count directly upon therapy. Another, still recruiting, phase III trial (SABR-COMET 10, NCT03721341, n=159) aimed to analyze the clinical benefit of stereotactic ablative radiotherapy for oligometastatic PCa patients (227). Besides the primary endpoint analyzing overall survival, it is planned to evaluate translational endpoints, such as CTC count or immune cell composition (228). All in all, these data demonstrate that CTC count can be applied as prognostic marker in metastatic PCa patients, but it is still controversial whether it is an independent predictor for overall survival. In combination with other prognostic markers such as albumin, alkaline phosphatase, hemoglobin, lactate dehydrogenase (LDH), and PSA the CTC count was able to discriminate PCa patients independently on their treatment (NCT00638690; NCT01193244) (229). These findings were validated in another study that analyzed CTC count in combination with LDH measurements. Based on both parameters PCa patients could be stratified into a low-risk (<5 CTCs, LDH independent), intermediate (≥5 CTCs, LDH ≤ 250U/L), and high-risk group (≥5 CTCs, LDH>250U/L) (230).

While EpCAM-based CTC enumeration methods may miss CTC subpopulation with low EpCAM expression, there are attempts to apply additional markers for CTC detection to increase sensitivity and specificity or apply label-free methods such as microfiltration, density gradient centrifugation or dielectrophoretic techniques (231, 232). Putative prostate CTC markers include e.g. EMT phenotype (NCT02025413), the tyrosine kinase cMET (NCT02080650), the immune checkpoint marker PD-L1 (NCT02456571), telomerase activity (SWOG Trial S042) (233, 234) and the TMPRSS2-ERG translocation (NCT00485303, NCT00474383) (235). The applicable additional marker would enable the monitoring of therapy resistance in real-time and may recapitulate tumor heterogeneity within the blood. Another putative prostate CTC marker is the human epidermal growth factor receptor 2 (HER-2/neu), but detection level was demonstrated to be higher in metastatic patients compared to local disease (236). Promising results were also obtained with the cytological ISET test in combination with prostate-specific marker PSA and prostein (P501S). Within this observational study, 20 men with diagnosed PCa were analyzed with a mean CTC count of 6.5 CTCs per 7.5 ml blood (237). Interestingly, in patients without previously diagnosed PCa ISET-CTC-based screening demonstrated a predictive value of 99% compared to 25% with the standard PSA-based test method within patients receiving PSMA-PET-imaging later on.

Another important clinical question is the predictive potential of CTCs and the possibility to monitor acquired therapy resistance

in real-time. As already mentioned above, clinical data for radiotherapy are limited so far. However, the expression of the androgen receptor splice variant 7 (ARv7) in CTCs of patients with metastatic CRPC is able to predict the therapeutic potential of ADT (213, 238, 239). In addition, the predictive value of other AR splice variant transcripts, e.g., AR-V1, AR-V3, AR-V7, and AR-V9, was investigated in comparison to the canonical full-length version in CTCs of metastatic CRPC patients under cabazitaxel treatment (n=118) (CABARESC trial). Although all AR variants were similarly co-expressed at baseline and post-treatment, patients carrying AR-V9-positive CTCs display decreased CTC counts below the threshold. In turn, AR-V1-positive CTCs after cabazitaxel treatment, but not at baseline, was an independent prognostic factor for reduced overall survival (240). The TAXYNERGY trial found an association of AR-V7- and AR-V567-negativity in metastatic CRPC patients before taxane therapy with PSA response and progression-free survival. Within those analyses, the authors compared the sensitivity of digital droplet PCR (ddPCR) in comparison to quantitative PCR-based method and found an increased detection rate of AR-V7 variant with ddPCR (19% to 55%) (241). This method was also applied for prostate CTC detection by Miyamoto et al. and demonstrated that CTC-specific HOXB13 gene expression may identify patients with altered AR-signaling and disease progression under abiraterone therapy (n=27) in patients with localized PCa (n=34) (242). Approximately 50 ongoing clinical studies (20 terminated, 13 with results) worldwide aim to validate the clinical utility of CTC count for PCa patients undergoing radical prostatectomy (16 studies), androgen-deprivation therapy (16 studies) or radiotherapy (28 studies) and implemented CTC-based diagnostics as secondary endpoint (**Table 2**, www.clinicaltrial.gov). In the upcoming years, the results from the running clinical trials may prove the potential of CTC-based diagnostics for patient stratification and therapeutical decision making. Furthermore, CTCs may help to identify patients with a high risk to develop metastasis even at the early stage of the disease and maybe predict the site of metastases occurrence before they are detectable with imaging.

DISSEMINATING TUMOR CELLS AND MINIMAL RESIDUAL DISEASE IN PROSTATE CANCER

Early Prostate Cancer Cell Dissemination and Dormancy

Approximately 35% of PCa patients with local disease will develop a recurrence within 10 years and around 10% of those patients present already bone involvement at the time of diagnosis (127, 243–245). This clinical observation indicates that tumor cell dissemination happens at early phases during tumorigenesis without clinical symptoms for decades. However, it is unknown how often and to what extent early dissemination happens upon cellular transformation and tumor initiation. The vast majority of malignant cells leaving the primary tumor are

eliminated within the surrounding tissue, the blood stream, or the lymph vessels by immune cells (246, 247). It is hypothesized that <0.01% of metastasis-initiating cells survive in the blood stream with inherent properties to initiate distant metastasis. Therefore, disseminated tumor cells (DTCs) have to switch their phenotype and function from mesenchymal state back to epithelial features, the so-called mesenchymal-to-epithelial transition. In addition, they require a supportive niche including activated stroma and immune suppressive environment (4). The phenotype of prostate DTC is not fully identified yet and might be different within different patient subgroups and upon therapeutic pressure. DTC detection methods apply negative markers to exclude immune cells (e.g., CD45, CD34, CD61) and positive selection for the epithelial cell adhesion molecule (EpCAM). Despite the DTC frequency is low and in most of the analyzed patients below detection level, the prognostic value of prostate DTC is of high clinical relevance to identify patients with increased risk for bone progression and the need for therapeutic adaptation. To address this, Morgen et al. analyzed bone marrow aspirates of 569 PCa patient's prior radical prostatectomy and compared the DTC count with biochemical recurrence. Therefore, 10 ml bone marrow from the iliac crest was separated using Ficoll-Isopaque-based density gradient centrifugation followed by exclusion of immune cells via CD45/CD61-dependent magnetic-associated cell separation and EpCAM-based evaluation with immunofluorescence microscopy. The threshold for DTC positivity was set to ≥1 $CD45^-CD61^-$ $EpCAM^+$ cell. In 72% of the analyzed patients DTCs were detected already prior to surgery, but without correlation to pathological stage, Gleason score, or PSA level. However, in 98 patients with no evidence of disease after radical prostatectomy, DTC occurrence had a significant predictive value for biochemical recurrence indicating the importance of dynamic diagnostic sampling (248). For independent validation of the clinical findings, it would be critical to develop uniform and standardized prostate DTC detection methods and nomenclature. Besides the established phenotype combining negative markers to exclude hematopoietic lineages and positive marker for epithelial cells, several studies applied also prostate-specific markers to increase specificity and sensitivity. For example, Chalfin et al. analyzed bone marrow aspirates from 208 PCa patients with local disease and compared different DTC detection methods, including antibody-based enrichment with epithelial (e.g., EpCAM) and prostate-specific (e.g. NKX3.1, AR, PSA) markers and found that epithelial markers are not applicable due to unspecific binding (249). A recently published study analyzed the transcriptome of single $EpCAM^+CD45^-$ bone DTCs from prostate cancer patients (77 cells in 10 patients) and distinguished DTCs according to their gene signatures into no evidence of disease (NED) and advanced disease origin. Prostate specificity was validated by prostate-specific markers including AR, CD63, FOLH1, HOXB13, ID1, NKX3-1, RELB, and XAGE1A and the exclusion of erythroid lineage marker. Unsupervised cluster analysis identified p38 stress response pathway regulating dormancy in NED-associated DTCs, which was not found in DTCs of patients with advanced disease. In addition, the authors

TABLE 2 | Summary of completed clinical trials applying enumeration of circulating tumor cells (CTCs) in PCa patients either as primary or secondary endpoint.

Treatment	CTC detection method	Study type & number of participants	Patient characteristics	CTC-specific endpoint	Completion date	Study ID & short name
Cryosurgery with or without dendritic cells and cytokine-induced killers	Flow cytometry, RT-PCR	Observational (n=60)	PCa patients with stages II, III, IV	CTC count within 6 months	Dec 2015	NCT02450435
–	Filtration system	Observational (n=14	Breast cancer, PCa, colorectal cancer patients and healthy volunteers	CTC count	Jan 2014	NCT01943500
ADT, RT	CellSearch	Observational (n=68)	High-risk PCa	CTC count (before treatment, post ADT, 1–3 months post-RT, 6–12 months post-RT)	Dec 2018	NCT01800058
Sipuleucel-T (Provenge), ADT	CellSearch	Observational (n=38)	mCRPC patients with visceral or high-risk disease, metastatic castration sensitive PCa patients with high tumor volume	Expression of immune checkpoint marker PD-L1, PD-L2, B7-H3, and CTLA-4 on CTCs (baseline, 12 weeks, 14 months)	Jun 2019	NCT02456571
–	Ferrofluid EMT-Based Capture Method (CTC-EMT)	Interventional (n=46)	mCRPC, neuroendocrine prostate cancer (NEPC), metastatic breast cancer	CTC detection using mesenchymal-marker N-cadherin or O-cadherin	Dec 2015	NCT02025413
–	Ferrofluid c-MET-Based Capture Method (CTC-MET)	Interventional (n=62)	Progressive metastatic cancer patients	CTC detection using mesenchymal-marker c-MET	Jul 2016	NCT02080650
Docetaxel/ Cabazitaxel with prednisone	GEDI ddPCR	Interventional Phase II (n=63)	mCRPC	Reduction of nuclear AR from baseline	Aug 2015	NCT01718353 "TAXYNERGY"
Docetaxel, Prednisone Atrasentan	*Parylene-C slot microfilter, qPCR-TRAP	Observational, Phase III (n=263)	mCRPC	Telomerase expression in CTCs	Jan 2010	SWOG Trial S0421
Abiraterone acetate, prednisone	CellSearch	Interventional Phase III (n=1195)	Docetaxel-refractory mCRPC	CTC count in combination with albumin, LDH PSA, hemoglobin, ALK	Oct 2012	NCT00638690
Orteronel, prednisone	CellSearch	Interventional Phase III (n=1560)	Progressive, therapy-naive mCRPC	CTC count in combination with albumin, LDH PSA, hemoglobin, ALK	Apr 2016	NCT01193244
Cabazitaxel, ADT	Gene expression	Interventional Phase II (n=140)	Docetaxel refractory PCa patients without SCPC or NEPC	CTC count 9–12 weeks after start of treatment	Sep 2019	NCT03050866
Doxorubicin-GnRH agonist conjugate AEZS-108	IF	Interventional Phase I/II 108	PCa patients	AEZS-108 internalization and LHRH expression	Feb 2017	NCT01240629
Cabazitaxel, Prednisone, Ciprofloxacin, G-CSF	unknown	Interventional Phase IV (n=45)	Docetaxel-refractory CRPC grade IV	CTC count (days 42, 84, 126, and post-treatment)	Jan 2014	NCT01649635 "PROSPECTA"
Cabazitaxel, budesonide	CellSearch, RT-PCR	Interventional Phase II (n=118)	mCRPC	Predictive value of AR-V3 and AR-V7 vs. AR-FL expression in CTCs (baseline, post-treatment)	Oct 2015	2011-003346-40 "CABARESC"

ADT, androgen deprivation therapy; ddPCR, digital droplet PCR; GEDI, geometrically enhanced differential immunocapture; G-CSF, granulocyte colony-stimulating factor; IF, immunofluorescence; nd, non-defined; NEPC, neuroendocrine prostate cancer; NSCLC, non- small cell lung cancer; RT, radiotherapy; RT-PCR, reverse transcriptase polymerase chain reaction; SCPC, small cell prostate cancer; TRAP, Telomeric repeat amplification protocol.

validated the upregulation of dormancy genes in NED DTCs including ABI1, CDC25B, CDK7, CELF1, and COX7B2 (250). Another study published by Cackowski et al. used fluorescence-activated cell sorting to isolated CD45⁻CD235a⁻AP⁻CD34⁻ EpCAM⁺ DTCs and found in 17% of PCa patients (10 out of 58) with local and in 50% with metastatic disease (4 out of 8) >5 DTCs per 10^6 bone cells. Whole exome sequencing, RNA sequencing, and gene expression analysis identified characteristic single nucleotide polymorphism and gene variants for PCa, but found also a B-lineage-like signature in prostate DTCs indicative

of niche adaptations (251). Several previously published studies demonstrated already that prostate DTCs hijack the hematopoietic stem cell niche within the bone marrow to survive quiescence over decades (252). This was elegantly shown by the group of Russel Taichman using an experimental model based on subcutaneous transplantation of human PCa cell lines PC3 and C4-2B in CD45.1-expressing immunocompromised NOD/SCID mice. Upon surgical removal of the subcutaneous xenograft tumor, transplantation of bone marrow cells origin from CD45.2 mice was performed. The authors found that hematopoietic stem cell

engraftment was decreased in tumor-bearing mice compared to control and that PCa cells occupy the endosteal niche close to Runx2-expressing osteoblasts (253). Once within the niche, tumor cell dormancy is dictated by the environmental niche factors as well as by tumor cell intrinsic features. For example, Yu-Lee et al. demonstrated cellular quiescence of bone-tropic PCa cell line C4-2B upon culture with conditioned media originated from differentiated and undifferentiated osteoblast cultures. Moreover, Axelrod et al. validated in AXL-null and overexpressing prostate cancer cell lines dormancy induction *in vivo* (254, 255). However, they did not find AXL expression in primary or metastatic prostate tissue and it is questionable if AXL is expressed in DTCs. Beside this described cell-extrinsic cues, cell-intrinsic features may impact the dormant state of PCa cells. Within a recently published study, Owen et al. demonstrate that type I interferon (IFN) signaling regulates PCa dormancy and metastatic outgrowth in the bone. Therefore, they injected intracardially murine PCa cell line RM1 labeled with the red-fluorescent dye PKH26 into C57BL/6 mice and isolated red-labeled cells from the bones using fluorescence activated cell sorting. They found that cell intrinsic expression of type I IFN was dynamically regulated on the epigenetic level *via* a histone deacetylase-dependent mechanism. Moreover, they speculate that the observed loss of IFN signaling within the tumor and the suppressed tumor immunogenicity in bone metastases may be an explanation of why current immunotherapeutic strategies fail in patients with metastatic PCa (256). However, certain studies postulate that bone niche and dormancy signaling may be putative therapeutic targets to prevent bone metastasis in PCa patients. These agents include bone homeostasis targeting compounds affecting osteoclast-osteoblast equilibrium e.g., bisphosphonates, the anti-RANKL antibody denosumab, or radiopharmaceuticals such as radium-223. Inhibition of signals within the microenvironment, e.g. *via* ET1 receptor inhibitor, SCR inhibitor (e.g. dasatinib), thalidomide, cabozantinib, or androgen-directed agents demonstrated already clinical benefit in patients with metastatic PCa. However, androgen-deprivation therapy is often associated with bone loss and has a negative impact on the incidence of bone metastases (257). Another possibility to turn dormant DTCs sensitive to chemotherapeutics and to reduce late recurrences would be the re-activation and induction of proliferation. Several studies investigated the underlying molecular mechanisms as putative therapeutic targets. For example, Decker et al. found that the sympathetic nervous system and the neurotransmitter norepinephrine stimulated PCa cell proliferation in the bone niche *via* β2-adrenergic receptors and decreased the secretion of growth arrest specific-6 (Gas6) by osteoblasts (258). However, this strategy is critically discussed due to the risk of further metastasis initiation. Another newly discovered process that might foster tumor growth and metastasis is the so-called tumor self-seeding, a phenomenon where CTCs or re-activated DTCs return to the site of tumor of origin (259, 260). For example, it has been shown that self-seeding CTCs in human osteosarcoma was mediated by interleukin 8-CXCR1/2 axis, resulting in an increased metastatic potential (261). In metastatic PCa, translational and retrospective studies indicate that local treatment to the primary tumor affects metastatic spread and patient outcome. However, the data are controversial, and supportive prospective trials are needed before the implementation of this concept into clinical routine recommendations (262). Data from the STAMPEDE trial shows that radiotherapy to the primary tumors in M1 disease stage improves overall survival of low burden PCa patients by 8% after 3 years [hazard ratio: 0.68, p-value 0.007 (arm H)] (263). However, biomarker research is urgently needed to discriminate metastatic PCa patients profiting from those local therapies. In parallel, experimental and translational studies are necessary to improve our understanding of the underlying molecular and cellular mechanisms regulating early dissemination, metastatic spread, and colonization.

Liquid Biopsy-Based Methods for Detection of Minimal Residual Disease

Besides early dissemination, another clinical obstacle is the monitoring and treatment of PCa patients with minimal residual disease (MRD). This concept describes remaining tumor cells after initial therapy and complete remission. These few malignant cells and/or micro-metastasis cannot be detected by routine diagnostics, e.g. plasma PSA level or PET imaging. It is hypothesized that they persist locally as cancer stem cells (CSC), in the circulation as CTCs, or at distant organs such as the bone marrow as DTCs. The National Cancer Institute defines MDR as one cancer cell among one million normal tissue cells. First evidence for MDR in PCa was published by Murray et al. as prospective data analysis of 321 patients 10 years after initial radical prostatectomy including CTC and DTC count 1 month after therapy. Based on CTC and DTC positivity, the patients could be stratified into 4 subgroups with significant differences in overall survival. The authors found that CTC positivity correlates with early relapse while DTC positivity is associated with late failure. Therefore, they propose the existence of two forms of MRD representing different clinical characteristics (264, 265). This leads to the hypothesis that the dynamics of MRD determines therapy response and patient outcome. MRD can be analyzed through detection of tumor-specific antigens, genetic and epigenetic changes in bone marrow aspirates and/or peripheral blood with highly sensitive multiparameter flow cytometry, digital droplet PCR, or next generation sequencing (NGS)-based methods. Despite the sensitivity and specificity of molecular genetic methods to detect prostate specific gene fusions, transcript variants, or point mutations in cell-free tumor DNA (cfDNA) is higher (1 cell in 10^6 cells) compared to antibody-based detection methods determining DTC/CTC count (1 cell in 10^4 cells), it is cost-intensive and therefore only available for a small subset of patients. Moreover, the mutational load in PCa is compared to other tumor entities relatively low with a somatic mutation rate between 1×10^{-6} and 2×10^{-6}. For example, in primary PCa app. 50% of the patients harbor a *TMPRSS2-ERG* gene fusion (70, 266, 267). In metastatic CRPC the mutational burden is app. 3.8-fold higher compared to the earlier disease stages including an increased frequency of driver mutations such as *AR* (5%–30%), *TP53* (3%–47%), and/or *PTEN* (20%–60%) (268). Wyatt et al. compared the mutational pattern of cfDNA with the primary tumor in 45 patients with metastatic PCa and found 88.9% concordance. 75% of the tested patients showed

a fraction of circulating tumor DNA (ctDNA) >2% of the total cfDNA. In 64.7% of those patients an AR amplification and in 8.8% a *SPOP* mutations were detected (269). Based on these findings, the authors propose that cfDNA assays are sufficient to identify all driver mutations and may guide clinical decision making for metastatic CRPC in the future. Currently, there is no approved clinically test for prostate MRD available. However, the prognostic potential of those assays is demonstrated by the FDA approval of the NGS-based method cloneSEQ to detect MDR in multiple myeloma, B-cell acute lymphoblastic leukemia and chronic lymphocytic leukemia in 2018. Within the same year, the FDA approved the Oncotype DX AR-V7 Nucleus Detect® test for the detection of the splice variant of the androgen receptor *AR-V7* in CTCs for late-stage mCRPC to predict responsiveness to androgen deprivation. On the other hand, the immunophenotype-based detection methods for CTCs and DTCs still need clinical standardization before they may become broadly available. The disadvantage of this method is the dependency on the detection of pre-defined markers e.g., epithelial markers such as EpCAM which are dynamically regulated during tumorigenesis, clonal evolution, metastatic spread and under therapeutic pressure. Therefore, highly sensitive, label-free approaches based on microfluidic devices to discriminate different cell populations based on cell size or cell viscosity are currently under development and in clinical testing, e.g., the Parsortix® system (ANGLE plc.), the DEPArray™ System (Menarini Silicon Biosystems), the ClearCell® FX System or real-time deformability cytometry (270–273). Additionally, non-invasive tests to monitor tumor progression and therapy response in urinary samples of PCa patients, for example, gene expression analysis of urine exosome with the ExoDx (IntelliScore) test (274). If these approaches can be applied for DTC analysis in the bone has to be tested. Moreover, sensitivity, and specificity, as well as clinical applicability, are necessary before proposing MRD positivity to guide treatment planning and individual decision making for metastatic PCa patients. Moreover, at present, there is no experimental or clinical study published investigating DTC counts and MRD upon radiotherapy. Future prospective clinical trials for MRD detection methods may consider novel clinical endpoints such as metastasis-free survival for non-metastatic CRPC (275). However, given the high degree of heterogeneity within PCa and the dormant cell state of DTCs the applicability of MRD diagnostics in PCa might be limited.

Impact of the Immune System on Metastatic Spread

Metastasis-initiating PCa cells use the homing factor CXCL12, which is under physiological conditions a chemoattractant secreted by stromal cells and involved in the regulation of bone marrow homing, retention, and mobilization of hematopoietic stem cells (HSC) (253, 276). Despite PCa cells hijack the HSC homing route and bone niche, upon arrival they often enter a dormancy state induced by GAS6 or DKK1 signaling and thus evade immune attack (277). The connection of cancer progression and chronic inflammation was already described in 1863 by Rudolf Virchow who recognized an increased leukocyte count in tumors (278). Today we

distinguish 'hot' tumors with an inflammatory hallmark based on a high number of infiltrating T cells such as melanoma or lung cancer from 'cold' entities. These tumors are genetically unstable, with high mutational burden and increased production of T cell recognized neoantigens. However, PCa is classified as 'cold' tumor with a low rate of immune infiltration. At the primary site, tumor cells generate an immune suppressive environment through recruitment of myeloid cells and macrophages to escape from $CD8^+$ T cell- and NK cell-mediated cell killing (279). In particular, tumor-associated macrophages (TAMs) are able to switch their phenotype from tumor-suppressive (M1) to tumor promoting (M2) function. M2 TAMs promote migration and environmental adaptations at the metastatic site (280). The interaction of $CD163^+$ M2 macrophages and $FoxP3^+CD4^+$ regulatory T cell (Treg) was investigated by Erlandsson et al. in PCa biopsies from 1367 patients with localized tumors. Within this study, they separated patients with tumor progression and development of metastatic PCa (n=225) from patients with indolent disease (n=367) based on 10-year follow-up data. The authors found that the amount of M2 macrophages and Tregs correlate to each other and that patients with high macrophage numbers (>25 cells within the core) had a 2.05-fold higher risk to progress into lethal disease (281). They conclude that Treg and M2 macrophages have a dominating role to turn the local prostate tumor microenvironment into an immunosuppressive and tumor promoting milieu. Another study published by Di Mitri et al. investigated the same in an experimental PTEN-null prostate-specific conditional (pc−/−) mouse model and identified the CXCL1/CXCL2/CXCL5-CXCR2 signaling as major driver to polarize TAMs into $CD45^+CD11b^+LY6G^-F4/80^+$ macrophages with M2 phenotype. Moreover, they found that CXCR2 blockade leads to TAM re-education into M1, tumor regression, increased T cell response, and decreased vessel size. The TAM reprogramming was associated with increased TNFα secretion and induction of senescence in PCa (282). Macrophages within the bone, so-called osteal macrophages, are located adjacent to osteoclasts and regulate bone formation and skeletal homeostasis under physiological conditions. Metastasis-associated macrophages (MAMs) within metastatic PCa lesions are actively recruited *via* IL-6 secreted by PCa cells and promote bone metastasis formation (283). Another immune regulator responsible for DTC immune evasion is the high TGF-β concentration within bone metastasis that is released either through bone matrix remodeling or secreted by osteoblasts. TGF-β induces polarization of $CD4^+$ T helper into Th17 and Treg lineage and restrains Th1 cells (284). Jiao et al. hypothesize that this mechanism is the key factor that explains the lack of clinical efficiency of immunotherapies in metastatic CRPC patients and indicates the potential of immune checkpoint therapy in combination with TGF-β inhibitors (285, 286). A recently published study demonstrated that the immunosuppressive microenvironment within PCa bone metastasis can be targeted *via* the CCL20-CCR6 axis. Treatment of mice with syngeneic prostate bone metastases with a CCL20-blocking antibody led to T cell exhaustion and significantly prolonged survival (287). However, further studies

are needed to understand the role of immune cell induced and/or regulated DTC dormancy to prevent rapid interruption, re-activation, mobilization and further metastatic progression of novel targeting agents. Another highly interesting research focus with therapeutic potential are investigations of immune signals from the primary tumor to form a pre-metastatic, "primed" niche at a distant site.

CONCLUSION

Elucidation of the molecular and cellular mechanisms that drive tumor cell dissemination and regulate cellular response to radiotherapy is essential for developing novel diagnostic criteria and individualized therapeutic strategies. Today, systemic therapy remains standard of care, even in patients with no or up to three visible metastases. However, PCa patients may benefit from metastasis-directed therapy, e.g., based on stereotactic ablative radiotherapy, in combination with immediate androgen deprivation or extension of systemic therapy. Moreover, PCa patients with oligo-metastatic disease

are a heterogeneous subgroup of patients and urgently need a better stratification system to improve standard of care. Blood-based biomarkers such as circulating tumor cells (CTCs) are a unique non-invasive method with enormous clinical utility for patient stratification and monitoring in particular for patients with metastatic disease.

AUTHOR CONTRIBUTIONS

All authors contributed to the article and approved the submitted version.

FUNDING

REFERENCES

1. Fendler WP, Calais J, Eiber M, Flavell RR, Mishoe A, Feng FY, et al. Assessment of 68Ga-PSMA-11 PET Accuracy in Localizing Recurrent Prostate Cancer: A Prospective Single-Arm Clinical Trial. *JAMA Oncol* (2019) 5(6):856–63. doi: 10.1001/jamaoncol.2019.0096

2. Siva S, Bressel M, Murphy DG, Shaw M, Chander S, Violet J, et al. Stereotactic Abative Body Radiotherapy (SABR) for Oligometastatic Prostate Cancer: A Prospective Clinical Trial. *Eur Urol* (2018) 74:455–62. doi: 10.1016/j.eururo.2018.06.004

3. Lohaus F, Zöphel K, Löck S, Wirth M, Kotzerke J, Krause M, et al. Can Local Ablative Radiotherapy Revert Castration-resistant Prostate Cancer to an Earlier Stage of Disease? *Eur Urol* (2019) 75:548–51. doi: 10.1016/j.eururo.2018.11.050

4. Ost P, Reynders D, Decaestecker K, Fonteyne V, Lumen N, De Bruycker A, et al. Surveillance or Metastasis-Directed Therapy for Oligometastatic Prostate Cancer Recurrence: A Prospective, Randomized, Multicenter Phase II Trial. *JCO* (2017) 36:446–53. doi: 10.1200/JCO.2017.75.4853

5. Fares J, Fares MY, Khachfe HH, Salhab HA, Fares Y. Molecular principles of metastasis: a hallmark of cancer revisited. *Signal Transduct Targeted Ther* (2020) 5:1–17. doi: 10.1038/s41392-020-0134-x

6. Hanahan D, Weinberg RA. Hallmarks of Cancer: The Next Generation. *Cell* (2011) 144:646–74. doi: 10.1016/j.cell.2011.02.013

7. Massagué J, Obenauf AC. Metastatic colonization by circulating tumour cells. *Nature* (2016) 529:298–306. doi: 10.1038/nature17038

8. Fidler IJ. Metastasis: Quantitative Analysis of Distribution and Fate of Tumor Emboli Labeled With 125I-5-Iodo-2′ -deoxyuridine. *J Natl Cancer Inst* (1970) 45:773–82. doi: 10.1093/jnci/45.4.773

9. Hapach LA, Mosier JA, Wang W, Reinhart-King CA. Engineered models to parse apart the metastatic cascade. *NPJ Precis Oncol* (2019) 3:1–8. doi: 10.1038/s41698-019-0092-3

10. Paget S. THE DISTRIBUTION OF SECONDARY GROWTHS IN CANCER OF THE BREAST. *Lancet* (1889) 133:571–3. doi: 10.1016/S0140-6736(00)49915-0

11. Gao Y, Bado I, Wang H, Zhang W, Rosen JM, Zhang XH-F. Metastasis Organotropism: Redefining the Congenial Soil. *Dev Cell* (2019) 49:375–91. doi: 10.1016/j.devcel.2019.04.012

12. Bubendorf L, Schöpfer A, Wagner U, Sauter G, Moch H, Willi N, et al. Metastatic patterns of prostate cancer: An autopsy study of 1,589 patients. *Hum Pathol* (2000) 31:578–83. doi: 10.1053/hp.2000.6698

13. Fleischmann A, Schobinger S, Schumacher M, Thalmann GN, Studer UE. Survival in surgically treated, nodal positive prostate cancer patients is predicted by histopathological characteristics of the primary tumor and its lymph node metastases. *Prostate* (2009) 69:352–62. doi: 10.1002/pros.20889

14. Kadono Y, Nohara T, Ueno S, Izumi K, Kitagawa Y, Konaka H, et al. Validation of TNM classification for metastatic prostatic cancer treated using primary androgen deprivation therapy. *World J Urol* (2016) 34:261–7. doi: 10.1007/s00345-015-1607-3

15. Gandaglia G, Karakiewicz PI, Briganti A, Passoni NM, Schiffmann J, Trudeau V, et al. Impact of the Site of Metastases on Survival in Patients with Metastatic Prostate Cancer. *Eur Urol* (2015) 68:325–34. doi: 10.1016/j.eururo.2014.07.020

16. Da Pozzo LF, Cozzarini C, Briganti A, Suardi N, Salonia A, Bertini R, et al. Long-term follow-up of patients with prostate cancer and nodal metastases treated by pelvic lymphadenectomy and radical prostatectomy: the positive impact of adjuvant radiotherapy. *Eur Urol* (2009) 55:1003–11. doi: 10.1016/j.eururo.2009.01.046

17. Burkhard FC, Studer UE. Regional lymph node staging in prostate cancer: prognostic and therapeutic implications. *Surg Oncol* (2009) 18:213–8. doi: 10.1016/j.suronc.2009.02.008

18. Hanks GE, Pajak TF, Porter A, Grignon D, Brereton H, Venkatesan V, et al. Phase III Trial of Long-Term Adjuvant Androgen Deprivation After Neoadjuvant Hormonal Cytoreduction and Radiotherapy in Locally Advanced Carcinoma of the Prostate: The Radiation Therapy Oncology Group Protocol 92–02. *JCO* (2003) 21:3972–8. doi: 10.1200/JCO.2003.11.023

19. Lawton CA, Winter K, Grignon D, Pilepich MV. Androgen Suppression Plus Radiation Versus Radiation Alone for Patients With Stage D1/Pathologic Node-Positive Adenocarcinoma of the Prostate: Updated Results Based on National Prospective Randomized Trial Radiation Therapy Oncology Group 85-31. *JCO* (2005) 23:800–7. doi: 10.1200/JCO.2005.08.141

20. Cochran AJ, Huang R-R, Lee J, Itakura E, Leong SPL, Essner R. Tumour-induced immune modulation of sentinel lymph nodes. *Nat Rev Immunol* (2006) 6:659–70. doi: 10.1038/nri1919

21. Huang RR, Wen D-R, Guo J, Giuliano AE, Nguyen M, Offodile R, et al. Selective Modulation of Paracortical Dendritic Cells and T-Lymphocytes in Breast Cancer Sentinel Lymph Nodes. *Breast J* (2000) 6:225–32. doi: 10.1046/j.1524-4741.2000.98114.x

22. Sleeman JP. The lymph node pre-metastatic niche. *J Mol Med* (2015) 93:1173–84. doi: 10.1007/s00109-015-1351-6

23. Maolake A, Izumi K, Natsagdorj A, Iwamoto H, Kadomoto S, Makino T, et al. Tumor necrosis factor-α induces prostate cancer cell migration in

lymphatic metastasis through CCR7 upregulation. *Cancer Sci* (2018) 109:1524–31. doi: 10.1111/cas.13586

24. Ahmat Amin MKB, Shimizu A, Zankov DP, Sato A, Kurita S, Ito M, et al. Epithelial membrane protein 1 promotes tumor metastasis by enhancing cell migration via copine-III and Rac1. *Oncogene* (2018) 37:5416–34. doi: 10.1038/s41388-018-0286-0

25. Kitano H, Kageyama S-I, Hewitt SM, Hayashi R, Doki Y, Ozaki Y, et al. Podoplanin expression in cancerous stroma induces lymphangiogenesis and predicts lymphatic spread and patient survival. *Arch Pathol Lab Med* (2010) 134:1520–7. doi: 10.1043/2009-0114-OA.1

26. Ni W-D, Yang Z-T, Cui C-A, Cui Y, Fang L-Y, Xuan Y-H. Tenascin-C is a potential cancer-associated fibroblasts marker and predicts poor prognosis in prostate cancer. *Biochem Biophys Res Commun* (2017) 486:607–12. doi: 10.1016/j.bbrc.2017.03.021

27. Zeng Y, Opeskin K, Baldwin ME, Horvath LG, Achen MG, Stacker SA, et al. Expression of Vascular Endothelial Growth Factor Receptor-3 by Lymphatic Endothelial Cells Is Associated with Lymph Node Metastasis in Prostate Cancer. *Clin Cancer Res* (2004) 10:5137–44. doi: 10.1158/1078-0432.CCR-03-0434

28. Yang J, Wu H-F, Qian L-X, Zhang W, Hua L-X, Yu M-L, et al. Increased expressions of vascular endothelial growth factor (VEGF), VEGF-C and VEGF receptor-3 in prostate cancer tissue are associated with tumor progression. *Asian J Androl* (2006) 8:169–75. doi: 10.1111/j.1745-7262.2006.00120.x

29. Jennbacken K, Vallbo C, Wang W, Damber J-E. Expression of vascular endothelial growth factor C (VEGF-C) and VEGF receptor-3 in human prostate cancer is associated with regional lymph node metastasis. *Prostate* (2005) 65:110–6. doi: 10.1002/pros.20276

30. Burton JB, Priceman SJ, Sung JL, Brakenhielm E, An DS, Pytowski B, et al. Suppression of Prostate Cancer Nodal and Systemic Metastasis by Blockade of the Lymphangiogenic Axis. *Cancer Res* (2008) 68:7828–37. doi: 10.1158/0008-5472.CAN-08-1488

31. Saif MW, Knost JA, Chiorean EG, Kambhampati SRP, Yu D, Pytowski B, et al. Phase 1 study of the anti-vascular endothelial growth factor receptor 3 monoclonal antibody LY3022856/IMC-3C5 in patients with advanced and refractory solid tumors and advanced colorectal cancer. *Cancer Chemother Pharmacol* (2016) 78:815–24. doi: 10.1007/s00280-016-3134-3

32. Maughan BL, Pal SK, Gill D, Boucher K, Martin C, Salgia M, et al. Modulation of Premetastatic Niche by the Vascular Endothelial Growth Factor Receptor Tyrosine Kinase Inhibitor Pazopanib in Localized High-Risk Prostate Cancer Followed by Radical Prostatectomy: A Phase II Randomized Trial. *Oncologist* (2018) 23:1413–e151. doi: 10.1634/theoncologist.2018-0652

33. Roudier MP, Corey E, True LD, Hiagno CS, Ott SM, Vessella RL. "Histological, Immunophenotypic and Histomorphometric Characterization of Prostate Cancer Bone Metastases,". In: ET Keller and LWK Chung, editors. *The Biology of Skeletal Metastases Cancer Treatment and Research*. Boston, MA: Springer US. (2004) p. 311–39. doi: 10.1007/978-1-4419-9129-4_13

34. Celià-Terrassa T, Kang Y. Metastatic niche functions and therapeutic opportunities. *Nat Cell Biol* (2018) 20:868–77. doi: 10.1038/s41556-018-0145-9

35. Cackowski FC, Taichman RS. Parallels between hematopoietic stem cell and prostate cancer disseminated tumor cell regulation. *Bone* (2019) 119:82–6. doi: 10.1016/j.bone.2018.02.025

36. Hagberg Thulin M, Jennbacken K, Damber J-E, Welén K. Osteoblasts stimulate the osteogenic and metastatic progression of castration-resistant prostate cancer in a novel model for in vitro and in vivo studies. *Clin Exp Metastasis* (2014) 31:269–83. doi: 10.1007/s10585-013-9626-1

37. Scimeca M, Urbano N, Bonfiglio R, Mapelli SN, Catapano CV, Carbone GM, et al. Prostate Osteoblast-Like Cells: A Reliable Prognostic Marker of Bone Metastasis in Prostate Cancer Patients. *Contrast Media Mol Imaging* (2018) 2018:9840962. doi: 10.1155/2018/9840962

38. Sun Y-X, Schneider A, Jung Y, Wang J, Dai J, Wang J, et al. Skeletal localization and neutralization of the SDF-1(CXCL12)/CXCR4 axis blocks prostate cancer metastasis and growth in osseous sites in vivo. *J Bone Miner Res* (2005) 20:318–29. doi: 10.1359/JBMR.041109

39. Cojoc M, Peitzsch C, Trautmann F, Polishchuk L, Telegeev GD, Dubrovska A. Emerging targets in cancer management: role of the CXCL12/CXCR4 axis. *Onco Targets Ther* (2013) 6:1347–61. doi: 10.2147/OTT.S36109

40. Domanska UM, Timmer-Bosscha H, Nagengast WB, Oude Munnink TH, Kruizinga RC, Ananias HJ, et al. CXCR4 Inhibition with AMD3100 Sensitizes Prostate Cancer to Docetaxel Chemotherapy. *Neoplasia* (2012) 14:709–18. doi: 10.1593/neo.12324

41. Conley-LaComb MK, Semaan L, Singareddy R, Li Y, Heath EI, Kim S, et al. Pharmacological targeting of CXCL12/CXCR4 signaling in prostate cancer bone metastasis. *Mol Cancer* (2016) 15(1):68. doi: 10.1186/s12943-016-0552-0

42. Wang N, Docherty FE, Brown HK, Reeves KJ, Fowles AC, Ottewell PD, et al. Prostate Cancer Cells Preferentially Home to Osteoblast-rich Areas in the Early Stages of Bone Metastasis: Evidence From In Vivo Models. *J Bone Mineral Res* (2014) 29:2688–96. doi: 10.1002/jbmr.2300

43. Engl T, Relja B, Marian D, Blumenberg C, Müller I, Beecken W-D, et al. CXCR4 Chemokine Receptor Mediates Prostate Tumor Cell Adhesion through α5 and β3 Integrins. *Neoplasia* (2006) 8:290–301. doi: 10.1593/neo.05694

44. Huang C-F, Lira C, Chu K, Bilen MA, Lee Y-C, Ye X, et al. Cadherin-11 increases migration and invasion of prostate cancer cells and enhances their interaction with osteoblasts. *Cancer Res* (2010) 70:4580–9. doi: 10.1158/0008-5472.CAN-09-3016

45. Chu K, Cheng C-J, Ye X, Lee Y-C, Zurita AJ, Chen D-T, et al. Cadherin-11 Promotes the Metastasis of Prostate Cancer Cells to Bone. *Mol Cancer Res* (2008) 6:1259–67. doi: 10.1158/1541-7786.MCR-08-0077

46. Li F, Chung H, Reddy SV, Lu G, Kurihara N, Zhao AZ, et al. Annexin II stimulates RANKL expression through MAPK. *J Bone Miner Res* (2005) 20:1161–7. doi: 10.1359/JBMR.050207

47. Genetos DC, Wong A, Weber TJ, Karin NJ, Yellowley CE. Impaired Osteoblast Differentiation in Annexin A2- and -A5-Deficient Cells. *PloS One* (2014) 9(9):e107482. doi: 10.1371/journal.pone.0107482

48. Wu J-I, Wang L-H. Emerging roles of gap junction proteins connexins in cancer metastasis, chemoresistance and clinical application. *J BioMed Sci* (2019) 26:8. doi: 10.1186/s12929-019-0497-x

49. Zhang A, Hitomi M, Bar-Shain N, Dalimov Z, Ellis L, Velpula KK, et al. Connexin 43 expression is associated with increased malignancy in prostate cancer cell lines and functions to promote migration. *Oncotarget* (2015) 6:11640–51. doi: 10.18632/oncotarget.3449

50. Cummings CT, DeRyckere D, Earp HS, Graham DK. Molecular Pathways: MERTK Signaling in Cancer. *Clin Cancer Res* (2013) 19:5275–80. doi: 10.1158/1078-0432.CCR-12-1451

51. Shiozawa Y, Pedersen EA, Patel LR, Ziegler AM, Havens AM, Jung Y, et al. GAS6/AXL Axis Regulates Prostate Cancer Invasion, Proliferation, and Survival in the Bone Marrow Niche. *Neoplasia* (2010) 12:116–27. doi: 10.1593/neo.91384

52. Taichman RS, Patel LR, Bedenis R, Wang J, Weidner S, Schumann T, et al. GAS6 Receptor Status Is Associated with Dormancy and Bone Metastatic Tumor Formation. *PloS One* (2013) 8:e61873. doi: 10.1371/journal.pone.0061873

53. Kim JK, Jung Y, Wang J, Joseph J, Mishra A, Hill EE, et al. TBK1 Regulates Prostate Cancer Dormancy through mTOR Inhibition. *Neoplasia* (2013) 15:1064–74. doi: 10.1593/neo.13402

54. Yu-Lee L-Y, Yu G, Lee Y-C, Lin S-C, Pan J, Pan T, et al. Osteoblast-Secreted Factors Mediate Dormancy of Metastatic Prostate Cancer in the Bone via Activation of the TGFβRIII-p38MAPK-pS249/T252RB Pathway. *Cancer Res* (2018) 78:2911–24. doi: 10.1158/0008-5472.CAN-17-1051

55. Phan TG, Croucher PI. The dormant cancer cell life cycle. *Nat Rev Cancer* (2020) 20:398–411. doi: 10.1038/s41568-020-0263-0

56. Ottewell PD, Wang N, Meek J, Fowles CA, Croucher PI, Eaton CL, et al. Castration-induced bone loss triggers growth of disseminated prostate cancer cells in bone. *Endocr-Relat Cancer* (2014) 21:769–81. doi: 10.1530/ERC-14-0199

57. Rachner TD, Coleman R, Hadji P, Hofbauer LC. Bone health during endocrine therapy for cancer. *Lancet Diabetes Endocrinol* (2018) 6:901–10. doi: 10.1016/S2213-8587(18)30047-0

58. Israeli RS, Rosenberg SJ, Saltzstein DR, Gottesman JE, Goldstein HR, Hull GW, et al. The effect of zoledronic acid on bone mineral density in patients

undergoing androgen deprivation therapy. *Clin Genitourin Cancer* (2007) 5:271–7. doi: 10.3816/CGC.2007.n.003

59. Nishizawa S, Inagaki T, Iba A, Kikkawa K, Kodama Y, Matsumura N, et al. Zoledronic acid prevents decreases in bone mineral density in patients with prostate cancer undergoing combined androgen blockade. *Springerplus* (2014) 3:586. doi: 10.1186/2193-1801-3-586

60. Vale CL, Burdett S, Rydzewska LHM, Albiges L, Clarke NW, Fisher D, et al. Addition of docetaxel or bisphosphonates to standard of care in men with localised or metastatic, hormone-sensitive prostate cancer: a systematic review and meta-analyses of aggregate data. *Lancet Oncol* (2016) 17:243–56. doi: 10.1016/S1470-2045(15)00489-1

61. James ND, Sydes MR, Clarke NW, Mason MD, Dearnaley DP, Spears MR, et al. Addition of docetaxel, zoledronic acid, or both to first-line long-term hormone therapy in prostate cancer (STAMPEDE): survival results from an adaptive, multiarm, multistage, platform randomised controlled trial. *Lancet* (2016) 387:1163–77. doi: 10.1016/S0140-6736(15)01037-5

62. Fizazi K, Carducci MA, Smith MR, Damião R, Brown JE, Karsh L, et al. A randomized phase III trial of denosumab versus zoledronic acid in patients with bone metastases from castration-resistant prostate cancer. *JCO* (2010) 28:LBA4507–LBA4507. doi: 10.1200/jco.2010.28.18_suppl.lba4507

63. Hegemann M, Bedke J, Stenzl A, Todenhöfer T. Denosumab treatment in the management of patients with advanced prostate cancer: clinical evidence and experience. *Ther Adv Urol* (2017) 9:81–8. doi: 10.1177/1756287216686018

64. Miller K, Steger GG, Niepel D, Lüftner D. Harnessing the potential of therapeutic agents to safeguard bone health in prostate cancer. *Prostate Cancer Prostatic Dis* (2018) 21:461–72. doi: 10.1038/s41391-018-0060-y

65. Turajlic S, Swanton C. Metastasis as an evolutionary process. *Science* (2016) 352:169–75. doi: 10.1126/science.aaf2784

66. Naxerova K, Jain RK. Using tumour phylogenetics to identify the roots of metastasis in humans. *Nat Rev Clin Oncol* (2015) 12:258–72. doi: 10.1038/nrclinonc.2014.238

67. Liu W, Laitinen S, Khan S, Vihinen M, Kowalski J, Yu G, et al. Copy number analysis indicates monoclonal origin of lethal metastatic prostate cancer. *Nat Med* (2009) 15:559–65. doi: 10.1038/nm.1944

68. Haffner MC, Mosbruger T, Esopi DM, Fedor H, Heaphy CM, Walker DA, et al. Tracking the clonal origin of lethal prostate cancer. *J Clin Invest* (2013) 123:4918–22. doi: 10.1172/JCI70354

69. Brannon AR, Sawyers CL. "N of 1" case reports in the era of whole-genome sequencing. *J Clin Invest* (2013) 123:4568–70. doi: 10.1172/JCI70935

70. Abeshouse A, Ahn J, Akbani R, Ally A, Amin S, Andry CD, et al. The Molecular Taxonomy of Primary Prostate Cancer. *Cell* (2015) 163:1011–25. doi: 10.1016/j.cell.2015.10.025

71. Dan R, Van Allen EM, Wu Y-M, Schultz N, Lonigro RJ, Mosquera J-M, et al. Integrative clinical genomics of advanced prostate cancer. *Cell* (2015) 161:1215–28. doi: 10.1016/j.cell.2015.05.001

72. Pritchard CC, Mateo J, Walsh MF, De Sarkar N, Abida W, Beltran H, et al. Inherited DNA-Repair Gene Mutations in Men with Metastatic Prostate Cancer. *New Engl J Med* (2016) 375:443–53. doi: 10.1056/NEJMoa1603144

73. Stratton MR, Campbell PJ, Futreal PA. The cancer genome. *Nature* (2009) 458:719–24. doi: 10.1038/nature07943

74. Espiritu SMG, Liu LY, Rubanova Y, Bhandari V, Holgersen EM, Szyca LM, et al. The Evolutionary Landscape of Localized Prostate Cancers Drives Clinical Aggression. *Cell* (2018) 173:1003–1013.e15. doi: 10.1016/j.cell.2018.03.029

75. Burrell RA, McGranahan N, Bartek J, Swanton C. The causes and consequences of genetic heterogeneity in cancer evolution. *Nature* (2013) 501:338–45. doi: 10.1038/nature12625

76. Hong MKH, Macintyre G, Wedge DC, Van Loo P, Patel K, Lunke S, et al. Tracking the origins and drivers of subclonal metastatic expansion in prostate cancer. *Nat Commun* (2015) 6:6605. doi: 10.1038/ncomms7605

77. Thiery JP, Acloque H, Huang RYJ, Nieto MA. Epithelial-Mesenchymal Transitions in Development and Disease. *Cell* (2009) 139:871–90. doi: 10.1016/j.cell.2009.11.007

78. Gundem G, Van Loo P, Kremeyer B, Alexandrov LB, Tubio JMC, Papaemmanuil E, et al. The evolutionary history of lethal metastatic prostate cancer. *Nature* (2015) 520:353–7. doi: 10.1038/nature14347

79. Ignatiadis M, Lee M, Jeffrey SS. Circulating Tumor Cells and Circulating Tumor DNA: Challenges and Opportunities on the Path to Clinical Utility. *Clin Cancer Res* (2015) 21:4786–800. doi: 10.1158/1078-0432.CCR-14-1190

80. Watson PA, Arora VK, Sawyers CL. Emerging mechanisms of resistance to androgen receptor inhibitors in prostate cancer. *Nat Rev Cancer* (2015) 15:701–11. doi: 10.1038/nrc4016

81. Etten JLV, Dehm SM. Clonal origin and spread of metastatic prostate cancer. *Endocr-Relat Cancer* (2016) 23:R207–17. doi: 10.1530/ERC-16-0049

82. Catalona WJ. History of the discovery and clinical translation of prostate-specific antigen. *Asian J Urol* (2014) 1:12–4. doi: 10.1016/j.ajur.2014.09.008

83. Thompson IM, Ankerst DP. Prostate-specific antigen in the early detection of prostate cancer. *CMAJ: Can Med Assoc J* (2007) 176:1853. doi: 10.1503/cmaj.060955

84. Loeb S, Bjurlin MA, Nicholson J, Tammela TL, Penson DF, Carter HB, et al. Overdiagnosis and overtreatment of prostate cancer. *Eur Urol* (2014) 65:1046–55. doi: 10.1016/j.eururo.2013.12.062

85. Shariat SF, Canto EI, Kattan MW, Slawin KM. Beyond Prostate-Specific Antigen: New Serologic Biomarkers for Improved Diagnosis and Management of Prostate Cancer. *Rev Urol* (2004) 6:58–72.

86. Saidi S, Georgiev V, Stavridis S, Petrovski D, Dohcev S, Lekovski L, et al. Does prostate specific antigen density correlates with aggressiveness of the prostate cancer? *Hippokratia* (2009) 13:232–6.

87. Carter HB, Ferrucci L, Kettermann A, Landis P, Wright EJ, Epstein JI, et al. Detection of life-threatening prostate cancer with prostate-specific antigen velocity during a window of curability. *J Natl Cancer Inst* (2006) 98:1521–7. doi: 10.1093/jnci/djj410

88. Hoffman RM, Clanon DL, Littenberg B, Frank JJ, Peirce JC. Using the Free-to-total Prostate-specific Antigen Ratio to Detect Prostate Cancer in Men with Nonspecific Elevations of Prostate-specific Antigen Levels. *J Gen Intern Med* (2000) 15:739–48. doi: 10.1046/j.1525-1497.2000.90907.x

89. Vickers AJ, Brewster SF. PSA velocity and doubling time in diagnosis and prognosis of prostate cancer. *Br J Med Surg Urol* (2012) 5:162–8. doi: 10.1016/j.bjmsu.2011.08.006

90. Jackson WC, Johnson SB, Li D, Foster C, Foster B, Song Y, et al. A prostate-specific antigen doubling time of <6 months is prognostic for metastasis and prostate cancer-specific death for patients receiving salvage radiation therapy post radical prostatectomy. *Radiat Oncol* (2013) 8:170. doi: 10.1186/1748-717X-8-170

91. Markowski M, Chen Y, Feng Z, Trock B, Cullen J, Suzman D, et al. PSA doubling time (PSADT) and proximal PSA predict metastasis-free survival (MFS) in men with biochemically recurrent prostate cancer (BRPC) after radical prostatectomy (RP): Implications for patient counseling and clinical trial design. *Ann Oncol* (2017) 28:v283–4. doi: 10.1093/annonc/mdx370.035

92. Thomsen FB, Brasso K, Berg KD, Gerds TA, Johansson J-E, Angelsen A, et al. Association between PSA kinetics and cancer-specific mortality in patients with localised prostate cancer: analysis of the placebo arm of the SPCG-6 study. *Ann Oncol* (2016) 27:460–6. doi: 10.1093/annonc/mdv607

93. Takeuchi H, Ohori M, Tachibana M. Clinical significance of the prostate-specific antigen doubling time prior to and following radical prostatectomy to predict the outcome of prostate cancer. *Mol Clin Oncol* (2017) 6:249–54. doi: 10.3892/mco.2016.1116

94. Kohaar I, Petrovics G, Srivastava S. A Rich Array of Prostate Cancer Molecular Biomarkers: Opportunities and Challenges. *Int J Mol Sci* (2019) 20(8):1813. doi: 10.3390/ijms20081813

95. Lau J, Rousseau E, Kwon D, Lin K-S, Bénard F, Chen X. Insight into the Development of PET Radiopharmaceuticals for Oncology. *Cancers* (2020) 12:1312. doi: 10.3390/cancers12051312

96. O'Connor JPB, Rose CJ, Waterton JC, Carano RAD, Parker GJM, Jackson A. Imaging intratumor heterogeneity: role in therapy response, resistance, and clinical outcome. *Clin Cancer Res* (2015) 21:249–57. doi: 10.1158/1078-0432.CCR-14-0990

97. Afshar-Oromieh A, Debus N, Uhrig M, Hope TA, Evans MJ, Holland-Letz T, et al. Impact of long-term androgen deprivation therapy on PSMA ligand PET/CT in patients with castration-sensitive prostate cancer. *Eur J Nucl Med Mol Imaging* (2018) 45:2045–54. doi: 10.1007/s00259-018-4079-z

98. Jadvar H. FDG PET in Prostate Cancer. *PET Clin* (2009) 4:155–61. doi: 10.1016/j.cpet.2009.05.002

99. Iravani A, Violet J, Azad A, Hofman MS. Lutetium-177 prostate-specific membrane antigen (PSMA) theranostics: practical nuances and intricacies. *Prostate Cancer Prostatic Dis* (2020) 23:38–52. doi: 10.1038/s41391-019-0174-x

100. Meziou S, Ringuette Goulet C, Hovington H, Lefebvre V, Lavallée É, Bergeron M, et al. GLUT1 expression in high-risk prostate cancer: correlation with 18 F-FDG-PET/CT and clinical outcome. *Prostate Cancer Prostatic Dis* (2020) 23:441–8. doi: 10.1038/s41391-020-0202-x

101. Dehdashti F, Picus J, Michalski JM, Dence CS, Siegel BA, Katzenellenbogen JA, et al. Positron tomographic assessment of androgen receptors in prostatic carcinoma. *Eur J Nucl Med Mol Imaging* (2005) 32:344–50. doi: 10.1007/s00259-005-1764-5

102. Nitsch S, Hakenberg OW, Heuschkel M, Dräger D, Hildebrandt G, Krause BJ, et al. Evaluation of Prostate Cancer with 11C- and 18F-Choline PET/CT: Diagnosis and Initial Staging. *J Nucl Med* (2016) 57:38S–42S. doi: 10.2967/jnumed.115.169748

103. Kennedy EP, Weiss SB. The function of cytidine coenzymes in the biosynthesis of phospholipides. *J Biol Chem* (1956) 222:193–214. doi: 10.1016/S0021-9258(19)50785-2

104. Krause BJ, Souvatzoglou M, Tuncel M, Herrmann K, Buck AK, Praus C, et al. The detection rate of [11C]choline-PET/CT depends on the serum PSA-value in patients with biochemical recurrence of prostate cancer. *Eur J Nucl Med Mol Imaging* (2008) 35:18–23. doi: 10.1007/s00259-007-0581-4

105. Nanni C, Zanoni L, Pultrone C, Schiavina R, Brunocilla E, Lodi F, et al. (18)F-FACBC (anti1-amino-3-(18)F-fluorocyclobutane-1-carboxylic acid) versus (11)C-choline PET/CT in prostate cancer relapse: results of a prospective trial. *Eur J Nucl Med Mol Imaging* (2016) 43:1601–10. doi: 10.1007/s00259-016-3329-1

106. Jadvar H, Desai B, Conti PS. Sodium 18F-Fluoride PET/CT of Bone, Joint and Other Disorders. *Semin Nucl Med* (2015) 45:58–65. doi: 10.1053/j.semnuclmed.2014.07.008

107. Minamimoto R, Loening A, Jamali M, Barkhodari A, Mosci C, Jackson T, et al. Prospective Comparison of 99mTc-MDP Scintigraphy, Combined 18F-NaF and 18F-FDG PET/CT, and Whole-Body MRI in Patients with Breast and Prostate Cancer. *J Nucl Med* (2015) 56:1862–8. doi: 10.2967/jnumed.115.162610

108. Chang SS. Overview of prostate-specific membrane antigen. *Rev Urol* (2004) 6 Suppl;10:S13–18.

109. Bravaccini S, Puccetti M, Bocchini M, Ravaioli S, Celli M, Scarpi E, et al. PSMA expression: a potential ally for the pathologist in prostate cancer diagnosis. *Sci Rep* (2018) 8:4254. doi: 10.1038/s41598-018-22594-1

110. Kopka K, Benešová M, Bařinka C, Haberkorn U, Babich J. Glu-Ureido-Based Inhibitors of Prostate-Specific Membrane Antigen: Lessons Learned During the Development of a Novel Class of Low-Molecular-Weight Theranostic Radiotracers. *J Nucl Med* (2017) 58:17S–26S. doi: 10.2967/jnumed.116.186775

111. Pandit-Taskar N, O'Donoghue JA, Beylergil V, Lyashchenko S, Ruan S, Solomon SB, et al. 89Zr-huJ591 immuno-PET imaging in patients with advanced metastatic prostate cancer. *Eur J Nucl Med Mol Imaging* (2014) 41:2093–105. doi: 10.1007/s00259-014-2830-7

112. Pandit-Taskar N, O'Donoghue JA, Ruan S, Lyashchenko SK, Carrasquillo JA, Heller G, et al. First-in-Human Imaging with 89Zr-Df-IAB2M Anti-PSMA Minibody in Patients with Metastatic Prostate Cancer: Pharmacokinetics, Biodistribution, Dosimetry, and Lesion Uptake. *J Nucl Med* (2016) 57:1858–64. doi: 10.2967/jnumed.116.176206

113. Mangadlao JD, Wang X, McCleese C, Escamilla M, Ramamurthy G, Wang Z, et al. Prostate-Specific Membrane Antigen Targeted Gold Nanoparticles for Theranostics of Prostate Cancer. *ACS Nano* (2018) 12:3714–25. doi: 10.1021/acsnano.8b00940

114. Zippel C, Ronski SC, Bohnet-Joschko S, Giesel FL, Kopka K. Current Status of PSMA-Radiotracers for Prostate Cancer: Data Analysis of Prospective Trials Listed on ClinicalTrials.gov. *Pharm (Basel)* (2020) 13(1):12. doi: 10.3390/ph13010012

115. Fendler WP, Calais J, Eiber M, Flavell RR, Mishoe A, Feng FY, et al. Assessment of 68Ga-PSMA-11 PET Accuracy in Localizing Recurrent Prostate Cancer: A Prospective Single-Arm Clinical Trial. *JAMA Oncol* (2019) 5:856–63. doi: 10.1001/jamaoncol.2019.0096

116. Rousseau E, Wilson D, Lacroix-Poisson F, Krauze A, Chi K, Gleave M, et al. A Prospective Study on 18F-DCFPyL PSMA PET/CT Imaging in Biochemical Recurrence of Prostate Cancer. *J Nucl Med* (2019) 60:1587–93. doi: 10.2967/jnumed.119.226381

117. Afshar-Oromieh A, Holland-Letz T, Giesel FL, Kratochwil C, Mier W, Haufe S, et al. Diagnostic performance of 68Ga-PSMA-11 (HBED-CC) PET/CT in patients with recurrent prostate cancer: evaluation in 1007 patients. *Eur J Nucl Med Mol Imaging* (2017) 44:1258–68. doi: 10.1007/s00259-017-3711-7

118. Perera M, Papa N, Roberts M, Williams M, Udovicich C, Vela I, et al. Gallium-68 Prostate-specific Membrane Antigen Positron Emission Tomography in Advanced Prostate Cancer-Updated Diagnostic Utility, Sensitivity, Specificity, and Distribution of Prostate-specific Membrane Antigen-avid Lesions: A Systematic Review and Meta-analysis. *Eur Urol* (2020) 77:403–17. doi: 10.1016/j.eururo.2019.01.049

119. Wondergem M, Jansen BHE, van der Zant FM, van der Sluis TM, Knol RJJ, van Kalmthout LWM, et al. Early lesion detection with 18F-DCFPyL PET/CT in 248 patients with biochemically recurrent prostate cancer. *Eur J Nucl Med Mol Imaging* (2019) 46:1911–8. doi: 10.1007/s00259-019-04385-6

120. Giesel FL, Knorr K, Spohn F, Will L, Maurer T, Flechsig P, et al. Detection Efficacy of 18F-PSMA-1007 PET/CT in 251 Patients with Biochemical Recurrence of Prostate Cancer After Radical Prostatectomy. *J Nucl Med* (2019) 60:362–8. doi: 10.2967/jnumed.118.212233

121. Rowe SP, Macura KJ, Mena E, Blackford AL, Nadal R, Antonarakis ES, et al. PSMA-Based [(18)F]DCFPyL PET/CT Is Superior to Conventional Imaging for Lesion Detection in Patients with Metastatic Prostate Cancer. *Mol Imaging Biol* (2016) 18:411–9. doi: 10.1007/s11307-016-0957-6

122. Rowe SP, Campbell SP, Mana-Ay M, Szabo Z, Allaf ME, Pienta KJ, et al. Prospective Evaluation of PSMA-Targeted 18F-DCFPyL PET/CT in Men with Biochemical Failure after Radical Prostatectomy for Prostate Cancer. *J Nucl Med* (2019) 61(1):58–61. doi: 10.2967/jnumed.119.226514. jnumed.119.226514.

123. Ferraro DA, Rüschoff JH, Muehlematter UJ, Kranzbühler B, Müller J, Messerli M, et al. Immunohistochemical PSMA expression patterns of primary prostate cancer tissue are associated with the detection rate of biochemical recurrence with 68Ga-PSMA-11-PET. *Theranostics* (2020) 10:6082–94. doi: 10.7150/thno.44584

124. Cornelio DB, Roesler R, Schwartsmann G. Gastrin-releasing peptide receptor as a molecular target in experimental anticancer therapy. *Ann Oncol* (2007) 18:1457–66. doi: 10.1093/annonc/mdm058

125. Liu R, Li H, Liu L, Yu J, Ren X. Fibroblast activation protein. *Cancer Biol Ther* (2012) 13:123–9. doi: 10.4161/cbt.13.3.18696

126. Barbieri F, Bajetto A, Pattarozzi A, Gatti M, Würth R, Thellung S, et al. Peptide Receptor Targeting in Cancer: The Somatostatin Paradigm. *Int J Peptides* (2013) 2013:e926295. doi: 10.1155/2013/926295

127. Bubendorf L, Schöpfer A, Wagner U, Sauter G, Moch H, Willi N, et al. Metastatic patterns of prostate cancer: an autopsy study of 1,589 patients. *Hum Pathol* (2000) 31:578–83. doi: 10.1053/hp.2000.6698

128. Weilbaecher KN, Guise TA, McCauley LK. Cancer to bone: a fatal attraction. *Nat Rev Cancer* (2011) 11:411–25. doi: 10.1038/nrc3055

129. Furubayashi N, Negishi T, Ura S, Hirai Y, Nakamura M. Palliative effects and adverse events of strontium-89 for prostate cancer patients with bone metastasis. *Mol Clin Oncol* (2015) 3:257–63. doi: 10.3892/mco.2014.449

130. Wilky BA, Loeb DM. Beyond Palliation: Therapeutic Applications of 153Samarium-EDTMP. *Clin Exp Pharmacol* (2013) 3(3):1000131. doi: 10.4172/2161-1459.1000131

131. Deshayes E, Roumiguie M, Thibault C, Beuzeboc P, Cachin F, Hennequin C, et al. Radium 223 dichloride for prostate cancer treatment. *Drug Des Devel Ther* (2017) 11:2643–51. doi: 10.2147/DDDT.S122417

132. Hoskin P, Sartor O, O'Sullivan JM, Johannessen DC, Helle SI, Logue J, et al. Efficacy and safety of radium-223 dichloride in patients with castration-resistant prostate cancer and symptomatic bone metastases, with or without previous docetaxel use: a prespecified subgroup analysis from the randomised, double-blind, phase 3 ALSYMPCA trial. *Lancet Oncol* (2014) 15:1397–406. doi: 10.1016/S1470-2045(14)70474-7

133. Yadav MP, Ballal S, Tripathi M, Damle NA, Sahoo RK, Seth A, et al. 177Lu-DKFZ-PSMA-617 therapy in metastatic castration resistant prostate cancer: safety, efficacy, and quality of life assessment. *Eur J Nucl Med Mol Imaging* (2017) 44:81–91. doi: 10.1007/s00259-016-3481-7

134. Rahbar K, Ahmadzadehfar H, Kratochwil C, Haberkorn U, Schäfers M, Essler M, et al. German Multicenter Study Investigating 177Lu-PSMA-617 Radioligand Therapy in Advanced Prostate Cancer Patients. *J Nucl Med* (2017) 58:85–90. doi: 10.2967/jnumed.116.183194

135. von Eyben FE, Roviello G, Kiljunen T, Uprimny C, Virgolini I, Kairemo K, et al. Third-line treatment and 177Lu-PSMA radioligand therapy of metastatic castration-resistant prostate cancer: a systematic review. *Eur J Nucl Med Mol Imaging* (2018) 45:496–508. doi: 10.1007/s00259-017-3895-x

136. Bräuer A, Grubert LS, Roll W, Schrader AJ, Schäfers M, Bögemann M, et al. 177Lu-PSMA-617 radioligand therapy and outcome in patients with metastasized castration-resistant prostate cancer. *Eur J Nucl Med Mol Imaging* (2017) 44:1663–70. doi: 10.1007/s00259-017-3751-z

137. Kratochwil C, Bruchertseifer F, Rathke H, Hohenfellner M, Giesel FL, Haberkorn U, et al. Targeted α-Therapy of Metastatic Castration-Resistant Prostate Cancer with 225Ac-PSMA-617: Swimmer-Plot Analysis Suggests Efficacy Regarding Duration of Tumor Control. *J Nucl Med* (2018) 59:795–802. doi: 10.2967/jnumed.117.203539

138. Sathekge M, Bruchertseifer F, Vorster M, Lawal IO, Knoesen O, Mahapane J, et al. Predictors of Overall and Disease-Free Survival in Metastatic Castration-Resistant Prostate Cancer Patients Receiving 225Ac-PSMA-617 Radioligand Therapy. *J Nucl Med* (2020) 61:62–9. doi: 10.2967/jnumed.119.229229

139. Kratochwil C, Bruchertseifer F, Giesel FL, Weis M, Verburg FA, Mottaghy F, et al. 225Ac-PSMA-617 for PSMA-Targeted α-Radiation Therapy of Metastatic Castration-Resistant Prostate Cancer. *J Nucl Med* (2016) 57:1941–4. doi: 10.2967/jnumed.116.178673

140. Yordanova A, Becker A, Eppard E, Kürpig S, Fisang C, Feldmann G, et al. The impact of repeated cycles of radioligand therapy using [177Lu]Lu-PSMA-617 on renal function in patients with hormone refractory metastatic prostate cancer. *Eur J Nucl Med Mol Imaging* (2017) 44:1473–9. doi: 10.1007/s00259-017-3681-9

141. von Eyben FE, Singh A, Zhang J, Nipsch K, Meyrick D, Lenzo N, et al. 177Lu-PSMA radioligand therapy of predominant lymph node metastatic prostate cancer. *Oncotarget* (2019) 10:2451–61. doi: 10.18632/oncotarget.26789

142. Ahmadzadehfar H, Wegen S, Yordanova A, Fimmers R, Kürpig S, Eppard E, et al. Overall survival and response pattern of castration-resistant metastatic prostate cancer to multiple cycles of radioligand therapy using [177Lu]Lu-PSMA-617. *Eur J Nucl Med Mol Imaging* (2017) 44:1448–54. doi: 10.1007/s00259-017-3716-2

143. Hofman MS, Violet J, Hicks RJ, Ferdinandus J, Thang SP, Akhurst T, et al. [177Lu]-PSMA-617 radionuclide treatment in patients with metastatic castration-resistant prostate cancer (LuPSMA trial): a single-centre, single-arm, phase 2 study. *Lancet Oncol* (2018) 19:825–33. doi: 10.1016/S1470-2045(18)30198-0

144. Violet J, Sandhu S, Iravani A, Ferdinandus J, Thang S-P, Kong G, et al. Long-Term Follow-up and Outcomes of Retreatment in an Expanded 50-Patient Single-Center Phase II Prospective Trial of 177Lu-PSMA-617 Theranostics in Metastatic Castration-Resistant Prostate Cancer. *J Nucl Med* (2020) 61:857–65. doi: 10.2967/jnumed.119.236414

145. von Eyben FE, Roviello G, Kiljunen T, Uprimny C, Virgolini I, Kairemo K, et al. Third-line treatment and 177Lu-PSMA radioligand therapy of metastatic castration-resistant prostate cancer: a systematic review. *Eur J Nucl Med Mol Imaging* (2018) 45:496–508. doi: 10.1007/s00259-017-3895-x

146. Rahbar K, Bodei L, Morris MJ. Is the Vision of Radioligand Therapy for Prostate Cancer Becoming a Reality? An Overview of the Phase III VISION Trial and Its Importance for the Future of Theranostics. *J Nucl Med* (2019) 60:1504–6. doi: 10.2967/jnumed.119.234054

147. Boeri L, Sharma V, Karnes RJ. Radiotherapy for newly diagnosed oligometastatic prostate cancer. *Lancet* (2018) 392:2327–8. doi: 10.1016/S0140-6736(18)32598-4

148. Boevé LMS, Hulshof MCCM, Vis AN, Zwinderman AH, Twisk JWR, Witjes WPJ, et al. Effect on Survival of Androgen Deprivation Therapy Alone Compared to Androgen Deprivation Therapy Combined with Concurrent Radiation Therapy to the Prostate in Patients with Primary Bone Metastatic Prostate Cancer in a Prospective Randomised Clinical Trial: Data from the HORRAD Trial. *Eur Urol* (2019) 75:410–8. doi: 10.1016/j.eururo.2018.09.008

149. Hellman S, Weichselbaum RR. Oligometastases. *J Clin Oncol* (1995) 13:8–10. doi: 10.1200/jco.1995.13.1.8

150. Foster CC, Weichselbaum RR, Pitroda SP. Oligometastatic prostate cancer: Reality or figment of imagination? *Cancer* (2019) 125:340–52. doi: 10.1002/cncr.31860

151. Iyengar P, Wardak Z, Gerber DE, Tumati V, Ahn C, Hughes RS, et al. Consolidative Radiotherapy for Limited Metastatic Non–Small-Cell Lung Cancer. *JAMA Oncol* (2018) 4:e173501. doi: 10.1001/jamaoncol.2017.3501

152. Bauml JM, Mick R, Ciunci C, Aggarwal C, Davis C, Evans T, et al. Pembrolizumab After Completion of Locally Ablative Therapy for Oligometastatic Non–Small Cell Lung Cancer. *JAMA Oncol* (2019) 5(9):1283–90. doi: 10.1001/jamaoncol.2019.1449

153. Gomez DR, Blumenschein GR, Lee JJ, Hernandez M, Ye R, Camidge DR, et al. Local consolidative therapy versus maintenance therapy or observation for patients with oligometastatic non-small-cell lung cancer without progression after first-line systemic therapy: a multicentre, randomised, controlled, phase 2 study. *Lancet Oncol* (2016) 17:1672–82. doi: 10.1016/S1470-2045(16)30532-0

154. Palma DA, Olson R, Harrow S, Gaede S, Louie AV, Haasbeek C, et al. Stereotactic ablative radiotherapy versus standard of care palliative treatment in patients with oligometastatic cancers (SABR-COMET): a randomised, phase 2, open-label trial. *Lancet* (2019) 393:2051–8. doi: 10.1016/S0140-6736(18)32487-5

155. Gomez DR, Tang C, Zhang J, Blumenschein GR, Hernandez M, Lee JJ, et al. Local Consolidative Therapy Vs. Maintenance Therapy or Observation for Patients With Oligometastatic Non-Small-Cell Lung Cancer: Long-Term Results of a Multi-Institutional, Phase II, Randomized Study. *J Clin Oncol: Off J Am Soc Clin Oncol* (2019) 37:1558–65. doi: 10.1200/JCO.19.00201

156. You R, Liu Y-P, Huang P-Y, Zou X, Sun R, He Y-X, et al. Efficacy and Safety of Locoregional Radiotherapy With Chemotherapy vs Chemotherapy Alone in De Novo Metastatic Nasopharyngeal Carcinoma. *JAMA Oncol* (2020) 6(9):1345–52. doi: 10.1001/jamaoncol.2020.1808

157. Foster CC, Weichselbaum RR, Pitroda SP. Oligometastatic prostate cancer: Reality or figment of imagination? *Cancer* (2019) 125:340–52. doi: 10.1002/cncr.31860

158. Deek MP, Taparra K, Phillips R, Velho PI, Gao RW, Deville C, et al. Metastasis-directed Therapy Prolongs Efficacy of Systemic Therapy and Improves Clinical Outcomes in Oligoprogressive Castration-resistant Prostate Cancer. *Eur Urol Oncol* (2020) S2588-9311(20)30058-4. doi: 10.1016/j.euo.2020.05.004

159. Perera M, Papa N, Christidis D, Wetherell D, Hofman MS, Murphy DG, et al. Sensitivity, Specificity, and Predictors of Positive 68Ga–Prostate-specific Membrane Antigen Positron Emission Tomography in Advanced Prostate Cancer: A Systematic Review and Meta-analysis. *Eur Urol* (2016) 70:926–37. doi: 10.1016/j.eururo.2016.06.021

160. Welsh JW, Tang C, De Groot P, Naing A, Hess KR, Heymach JV, et al. Phase II trial of ipilimumab with stereotactic radiation therapy for metastatic disease: Outcomes, toxicities, and low-dose radiation-related abscopal responses. *Cancer Immunol Res* (2019) 7:1903–9. doi: 10.1158/2326-6066.CIR-18-0793

161. Perera M, Papa N, Roberts M, Williams M, Udovicich C, Vela I, et al. Gallium-68 Prostate-specific Membrane Antigen Positron Emission Tomography in Advanced Prostate Cancer—Updated Diagnostic Utility, Sensitivity, Specificity, and Distribution of Prostate-specific Membrane Antigen-avid Lesions: A Systematic Review and Meta-analysis. *Eur Urol* (2020) 77:403–17. doi: 10.1016/j.eururo.2019.01.049

162. Tree AC, Khoo VS, Eeles RA, Ahmed M, Dearnaley DP, Hawkins MA, et al. Stereotactic body radiotherapy for oligometastases. *Lancet Oncol* (2013) 14:e28–37. doi: 10.1016/S1470-2045(12)70510-7

163. Pound CR, Partin AW, Eisenberger MA, Chan DW, Pearson JD, Walsh PC. Natural History of Progression After PSA Elevation Following Radical Prostatectomy. *JAMA* (1999) 281:1591. doi: 10.1001/jama.281.17.1591

164. Kyriakopoulos CE, Heath EI, Ferrari A, Sperger JM, Singh A, Perlman SB, et al. Exploring Spatial-Temporal Changes in 18F-Sodium Fluoride PET/CT and Circulating Tumor Cells in Metastatic Castration-Resistant Prostate Cancer Treated With Enzalutamide. *J Clin Oncol: Off J Am Soc Clin Oncol* (2020) 38(31):JCO2000348. doi: 10.1200/JCO.20.00348

165. Cameron MG, Kersten C, Vistad I, van Helvoirt R, Weyde K, Undseth C, et al. Palliative pelvic radiotherapy for symptomatic incurable prostate cancer – A prospective multicenter study. *Radiother Oncol* (2015) 115:314–20. doi: 10.1016/j.radonc.2015.05.021

166. Phillips R, Shi WY, Deek M, Radwan N, Lim SJ, Antonarakis ES, et al. Outcomes of Observation vs Stereotactic Ablative Radiation for Oligometastatic Prostate Cancer: The ORIOLE Phase 2 Randomized Clinical Trial. *JAMA Oncol* (2020) 6:650–9. doi: 10.1001/jamaoncol. 2020.0147

167. Ost P, Reynders D, Decaestecker K, Fonteyne V, Lumen N, De Bruycker A, et al. Surveillance or Metastasis-Directed Therapy for Oligometastatic Prostate Cancer Recurrence: A Prospective, Randomized, Multicenter Phase II Trial. *J Clin Oncol: Off J Am Soc Clin Oncol* (2018) 36:446–53. doi: 10.1200/JCO.2017.75.4853

168. Gillessen S, Attard G, Beer TM, Beltran H, Bossi A, Bristow R, et al. Management of Patients with Advanced Prostate Cancer: The Report of the Advanced Prostate Cancer Consensus Conference APCCC 2017. *Eur Urol* (2018) 73:178–211. doi: 10.1016/j.eururo.2017.06.002

169. Scher HI, Morris MJ, Stadler WM, Higano C, Basch E, Fizazi K, et al. Trial Design and Objectives for Castration-Resistant Prostate Cancer: Updated Recommendations From the Prostate Cancer Clinical Trials Working Group 3. *J Clin Oncol: Off J Am Soc Clin Oncol* (2016) 34:1402–18. doi: 10.1200/ JCO.2015.64.2702

170. De Bleser E, Jereczek-Fossa BA, Pasquier D, Zilli T, Van As N, Siva S, et al. Metastasis-directed Therapy in Treating Nodal Oligorecurrent Prostate Cancer: A Multi-institutional Analysis Comparing the Outcome and Toxicity of Stereotactic Body Radiotherapy and Elective Nodal Radiotherapy. *Eur Urol* (2019) 76:732–9. doi: 10.1016/j.eururo.2019.07.009

171. Kroeze SGC, Henkenberens C, Schmidt-Hegemann NS, Vogel MME, Kirste S, Becker J, et al. Prostate-specific Membrane Antigen Positron Emission Tomography–detected Oligorecurrent Prostate Cancer Treated with Metastases-directed Radiotherapy: Role of Addition and Duration of Androgen Deprivation. *Eur Urol Focus* (2019) S2405-4569(19)30270-6. doi: 10.1016/j.euf.2019.08.012

172. Weber M, Kurek CE, Barbato F, Eiber M, Maurer T, Nader M, et al. PSMA-ligand PET for early castration-resistant prostate cancer: a retrospective single-center study. *J Nucl Med* (2020) 62(1):88–91. doi: 10.2967/ jnumed.120.245456. jnumed.120.245456.

173. Deek MP, Taparra K, Phillips R, Velho PI, Gao RW, Deville C, et al. Metastasis-directed Therapy Prolongs Efficacy of Systemic Therapy and Improves Clinical Outcomes in Oligoprogressive Castration-resistant Prostate Cancer. *Eur Urol Oncol* (2020) S2588-9311(20)30058-4. doi: 10.1016/j.euo.2020.05.004

174. Yoshida S, Takahara T, Arita Y, Ishii C, Uchida Y, Nakagawa K, et al. Progressive Site-Directed Therapy for Castration-Resistant Prostate Cancer: Localization of the Progressive Site as a Prognostic Factor. *Int J Radiat Oncol Biol Phys* (2019) 105:376–81. doi: 10.1016/j.ijrobp.2019.06.011

175. Lohaus F, Zöphel K, Löck S, Wirth M, Kotzerke J, Krause M, et al. Can Local Ablative Radiotherapy Revert Castration-resistant Prostate Cancer to an Earlier Stage of Disease? *Eur Urol* (2019) 75:548–51. doi: 10.1016/ j.eururo.2018.11.050

176. Triggiani L, Mazzola R, Magrini SM, Ingrosso G, Borghetti P, Trippa F, et al. Metastasis-directed stereotactic radiotherapy for oligoprogressive castration-resistant prostate cancer: a multicenter study. *World J Urol* (2019) 37:2631–7. doi: 10.1007/s00345-019-02717-7

177. de Wit S, van Dalum G, Terstappen LWMM. Detection of Circulating Tumor Cells. *Scientifica (Cairo)* (2014) 2014:819362. doi: 10.1155/2014/ 819362

178. Alix-Panabières C, Pantel K. Circulating Tumor Cells: Liquid Biopsy of Cancer. *Clin Chem* (2013) 59:110–8. doi: 10.1373/clinchem.2012.194258

179. Ashworth TR. A Case of Cancer in Which Cells Similar to Those in the Tumours Were Seen in the Blood after Death. *Aust Med J* (1869) 14:146.

180. Drake JM, Strohbehn G, Bair TB, Moreland JG, Henry MD. ZEB1 Enhances Transendothelial Migration and Represses the Epithelial Phenotype of Prostate Cancer Cells. *MBoC* (2009) 20:2207–17. doi: 10.1091/mbc.e08-10-1076

181. Smith S, Linehan J, Babilonia G, Mejia R, Amparo C, Smith D, et al. Do Circulating Tumor Cell Numbers Increase in Prostate Cancer Patients after

182. Chiang SPH, Cabrera RM, Segall JE. Tumor cell intravasation. *Am J Physiol Cell Physiol* (2016) 311:C1–C14. doi: 10.1152/ajpcell.00238.2015

183. Conn EM, Botkjaer KA, Kupriyanova TA, Andreasen PA, Deryugina EI, Quigley JP. Comparative analysis of metastasis variants derived from human prostate carcinoma cells: roles in intravasation of VEGF-mediated angiogenesis and uPA-mediated invasion. *Am J Pathol* (2009) 175:1638–52. doi: 10.2353/ajpath.2009.090384

184. Reymond N, d'Água BB, Ridley AJ. Crossing the endothelial barrier during metastasis. *Nat Rev Cancer* (2013) 13:858–70. doi: 10.1038/nrc3628

185. Shenoy AK, Lu J. Cancer cells remodel themselves and vasculature to overcome the endothelial barrier. *Cancer Lett* (2016) 380:534–44. doi: 10.1016/j.canlet.2014.10.031

186. Ward Y, Lake R, Faraji F, Sperger J, Martin P, Gilliard C, et al. Platelets Promote Metastasis via Binding Tumor CD97 Leading to Bidirectional Signaling that Coordinates Transendothelial Migration. *Cell Rep* (2018) 23:808–22. doi: 10.1016/j.celrep.2018.03.092

187. Janning M, Kobus F, Babayan A, Wikman H, Velthaus J-L, Bergmann S, et al. Determination of PD-L1 Expression in Circulating Tumor Cells of NSCLC Patients and Correlation with Response to PD-1/PD-L1 Inhibitors. *Cancers (Basel)* (2019) 11(6):835. doi: 10.3390/cancers11060835

188. Aceto N, Bardia A, Miyamoto DT, Donaldson MC, Wittner BS, Spencer JA, et al. Circulating Tumor Cell Clusters are Oligoclonal Precursors of Breast Cancer Metastasis. *Cell* (2014) 158:1110–22. doi: 10.1016/j.cell.2014.07.013

189. Meng S, Tripathy D, Frenkel EP, Shete S, Naftalis EZ, Huth JF, et al. Circulating Tumor Cells in Patients with Breast Cancer Dormancy. *Clin Cancer Res* (2004) 10:8152–62. doi: 10.1158/1078-0432.CCR-04-1110

190. Brady L, Hayes B, Sheill G, Baird A-M, Guinan EM, Stanfill B, et al. The effect of a structured exercise intervention on CTCs and platelet cloaking in patients with metastatic prostate cancer. *JCO* (2019) 37:243–3. doi: 10.1200/JCO.2019.37.7_suppl.243

191. Szczerba BM, Castro-Giner F, Vetter M, Krol I, Gkountela S, Landin J, et al. Neutrophils escort circulating tumour cells to enable cell cycle progression. *Nature* (2019) 566:553–7. doi: 10.1038/s41586-019-0915-y

192. Osmani N, Follain G, García León MJ, Lefebvre O, Busnelli I, Larnicol A, et al. Metastatic Tumor Cells Exploit Their Adhesion Repertoire to Counteract Shear Forces during Intravascular Arrest. *Cell Rep* (2019) 28:2491–2500.e5. doi: 10.1016/j.celrep.2019.07.102

193. Follain G, Osmani N, Azevedo AS, Allio G, Mercier L, Karreman MA, et al. Hemodynamic Forces Tune the Arrest, Adhesion, and Extravasation of Circulating Tumor Cells. *Dev Cell* (2018) 45:33–52.e12. doi: 10.1016/ j.devcel.2018.02.015

194. Gakhar G, Navarro VN, Jurish M, Lee GY, Tagawa ST, Akhtar NH, et al. Circulating Tumor Cells from Prostate Cancer Patients Interact with E-Selectin under Physiologic Blood Flow. *PloS One* (2013) 8:e85143. doi: 10.1371/journal.pone.0085143

195. Zhang C, Zhang L, Xu T, Xue R, Yu L, Zhu Y, et al. Mapping the spreading routes of lymphatic metastases in human colorectal cancer. *Nat Commun* (2020) 11:1993. doi: 10.1038/s41467-020-15886-6

196. Ubellacker JM, Tasdogan A, Ramesh V, Shen B, Mitchell EC, Martin-Sandoval MS, et al. Lymph protects metastasizing melanoma cells from ferroptosis. *Nature* (2020) 585:113–8. doi: 10.1038/s41586-020-2623-z

197. Carm KT, Hoff AM, Bakken AC, Axcrona U, Axcrona K, Lothe RA, et al. Interfocal heterogeneity challenges the clinical usefulness of molecular classification of primary prostate cancer. *Sci Rep* (2019) 9:13579. doi: 10.1038/s41598-019-49964-7

198. Boyd LK, Mao X, Lu Y-J. The complexity of prostate cancer: genomic alterations and heterogeneity. *Nat Rev Urol* (2012) 9:652–64. doi: 10.1038/ nrurol.2012.185

199. Brastianos H, Murgic J, Salcedo A, Chua MLK, Meng A, Fraser M, et al. The impact of intratumoral heterogeneity on prognostic biomarkers in localized prostate cancer. *JCO* (2019) 37:46–6. doi: 10.1200/JCO.2019.37.7_suppl.46

200. El-Deiry WS, Taylor B, Neal JW. Tumor Evolution, Heterogeneity, and Therapy for Our Patients With Advanced Cancer: How Far Have We Come? *Am Soc Clin Oncol Educ Book* (2017) 37:e8–e15. doi: 10.1200/ EDBK_175524

201. McGranahan N, Swanton C. Clonal Heterogeneity and Tumor Evolution: Past, Present, and the Future. *Cell* (2017) 168:613–28. doi: 10.1016/j.cell.2017.01.018

202. Lambros MB, Seed G, Sumanasuriya S, Gil V, Crespo M, Fontes M, et al. Single-Cell Analyses of Prostate Cancer Liquid Biopsies Acquired by Apheresis. *Clin Cancer Res* (2018) 24:5635–44. doi: 10.1158/1078-0432.CCR-18-0862

203. Markou A, Lazaridou M, Paraskevopoulos P, Chen S, Świerczewska M, Budna J, et al. Multiplex Gene Expression Profiling of In Vivo Isolated Circulating Tumor Cells in High-Risk Prostate Cancer Patients. *Clin Chem* (2018) 64:297–306. doi: 10.1373/clinchem.2017.275503

204. Gorges TM, Kuske A, Röck K, Mauermann O, Müller V, Peine S, et al. Accession of Tumor Heterogeneity by Multiplex Transcriptome Profiling of Single Circulating Tumor Cells. *Clin Chem* (2016) 62:1504–15. doi: 10.1373/clinchem.2016.260299

205. van der Toom EE, Verdone JE, Gorin MA, Pienta KJ. Technical challenges in the isolation and analysis of circulating tumor cells. *Oncotarget* (2016) 7:62754–66. doi: 10.18632/oncotarget.11191

206. Rubis GD, Krishnan SR, Bebawy M. Liquid Biopsies in Cancer Diagnosis, Monitoring, and Prognosis. *Trends Pharmacol Sci* (2019) 40:172–86. doi: 10.1016/j.tips.2019.01.006

207. Siravegna G, Marsoni S, Siena S, Bardelli A. Integrating liquid biopsies into the management of cancer. *Nat Rev Clin Oncol* (2017) 14:531–48. doi: 10.1038/nrclinonc.2017.14

208. Cabel L, Proudhon C, Gortais H, Loirat D, Coussy F, Pierga J-Y, et al. Circulating tumor cells: clinical validity and utility. *Int J Clin Oncol* (2017) 22:421–30. doi: 10.1007/s10147-017-1105-2

209. Massard C, Oulhen M, Le Moulec S, Auger N, Foulon S, Abou-Lovergne A, et al. Phenotypic and genetic heterogeneity of tumor tissue and circulating tumor cells in patients with metastatic castration-resistant prostate cancer: A report from the PETRUS prospective study. *Oncotarget* (2016) 7:55069–82. doi: 10.18632/oncotarget.10396

210. Scher HI, Graf RP, Schreiber NA, McLaughlin B, Jendrisak A, Wang Y, et al. Phenotypic Heterogeneity of Circulating Tumor Cells Informs Clinical Decisions between AR Signaling Inhibitors and Taxanes in Metastatic Prostate Cancer. *Cancer Res* (2017) 77:5687–98. doi: 10.1158/0008-5472.CAN-17-1353

211. Sharp A, Welti JC, Lambros MBK, Dolling D, Rodrigues DN, Pope L, et al. Clinical Utility of Circulating Tumour Cell Androgen Receptor Splice Variant-7 Status in Metastatic Castration-resistant Prostate Cancer. *Eur Urol* (2019) 76:676–85. doi: 10.1016/j.eururo.2019.04.006

212. Strati A, Zavridou M, Bournakis E, Mastoraki S, Lianidou E. Expression pattern of androgen receptors, AR-V7 and AR-567es, in circulating tumor cells and paired plasma-derived extracellular vesicles in metastatic castration resistant prostate cancer. *Analyst* (2019) 144:6671–80. doi: 10.1039/c9an00999j

213. Worroll D, Galletti G, Gjyrezi A, Nanus DM, Tagawa ST, Giannakakou P. Androgen receptor nuclear localization correlates with AR-V7 mRNA expression in circulating tumor cells (CTCs) from metastatic castration resistance prostate cancer patients. *Phys Biol* (2019) 16:036003. doi: 10.1088/1478-3975/ab073a

214. Beltran H, Prandi D, Mosquera JM, Benelli M, Puca L, Cyrta J, et al. Divergent clonal evolution of castration resistant neuroendocrine prostate cancer. *Nat Med* (2016) 22:298–305. doi: 10.1038/nm.4045

215. Jiang R, Lu Y-T, Ho H, Li B, Chen J-F, Lin M, et al. A comparison of isolated circulating tumor cells and tissue biopsies using whole-genome sequencing in prostate cancer. *Oncotarget* (2015) 6:44781–93. doi: 10.18632/oncotarget.6330

216. Lack J, Gillard M, Cam M, Paner GP, VanderWeele DJ. Circulating tumor cells capture disease evolution in advanced prostate cancer. *J Trans Med* (2017) 15:44. doi: 10.1186/s12967-017-1138-3

217. Malihi PD, Graf RP, Rodriguez A, Ramesh N, Lee J, Sutton R, et al. Single-Cell Circulating Tumor Cell Analysis Reveals Genomic Instability as a Distinctive Feature of Aggressive Prostate Cancer. *Clin Cancer Res* (2020) 26:4143–53. doi: 10.1158/1078-0432.CCR-19-4100

218. Faugeroux V, Lefebvre C, Pailler E, Pierron V, Marcaillou C, Tourlet S, et al. An Accessible and Unique Insight into Metastasis Mutational Content Through Whole-exome Sequencing of Circulating Tumor Cells in Metastatic Prostate Cancer. *Eur Urol Oncol* (2020) 3:498–508. doi: 10.1016/j.euo.2018.12.005

219. Chen J-F, Ho H, Lichterman J, Lu Y-T, Zhang Y, Garcia MA, et al. Subclassification of prostate cancer circulating tumor cells by nuclear size reveals very small nuclear circulating tumor cells in patients with visceral metastases. *Cancer* (2015) 121:3240–51. doi: 10.1002/cncr.29455

220. Scher HI, Heller G, Molina A, Attard G, Danila DC, Jia X, et al. Circulating tumor cell biomarker panel as an individual-level surrogate for survival in metastatic castration-resistant prostate cancer. *J Clin Oncol* (2015) 33:1348–55. doi: 10.1200/JCO.2014.55.3487

221. Okunieff P, Casey-Sawicki K, Lockney NA, Hoppe BS, Enderling H, Pinnix C, et al. Report from the SWOG Radiation Oncology Committee: Research Objectives Workshop 2017. *Clin Cancer Res* (2018) 24:3500–9. doi: 10.1158/1078-0432.CCR-17-3202

222. de Bono JS, Scher HI, Montgomery RB, Parker C, Miller MC, Tissing H, et al. Circulating tumor cells predict survival benefit from treatment in metastatic castration-resistant prostate cancer. *Clin Cancer Res* (2008) 14:6302–9. doi: 10.1158/1078-0432.CCR-08-0872

223. Lowes LE, Lock M, Rodrigues G, D'Souza D, Bauman G, Ahmad B, et al. The significance of circulating tumor cells in prostate cancer patients undergoing adjuvant or salvage radiation therapy. *Prostate Cancer Prostatic Dis* (2015) 18:358–64. doi: 10.1038/pcan.2015.36

224. Heller G, McCormack R, Kheoh T, Molina A, Smith MR, Dreicer R, et al. Circulating Tumor Cell Number as a Response Measure of Prolonged Survival for Metastatic Castration-Resistant Prostate Cancer: A Comparison With Prostate-Specific Antigen Across Five Randomized Phase III Clinical Trials. *JCO* (2017) 36:572–80. doi: 10.1200/JCO.2017.75.2998

225. Broncy L, Paterlini-Bréchot P. Clinical Impact of Circulating Tumor Cells in Patients with Localized Prostate Cancer. *Cells* (2019) 8(7):676. doi: 10.3390/cells8070676

226. Zapatero A, Gómez-Caamaño A, Cabeza Rodriguez MÁ, Muinelo-Romay L, Martin de Vidales C, Abalo A, et al. Detection and dynamics of circulating tumor cells in patients with high-risk prostate cancer treated with radiotherapy and hormones: a prospective phase II study. *Radiat Oncol* (2020) 15:137. doi: 10.1186/s13014-020-01577-5

227. Palma DA, Olson R, Harrow S, Correa RJM, Schneiders F, Haasbeek CJA, et al. Stereotactic ablative radiotherapy for the comprehensive treatment of 4-10 oligometastatic tumors (SABR-COMET-10): study protocol for a randomized phase III trial. *BMC Cancer* (2019) 19:816. doi: 10.1186/s12885-019-5977-6

228. Palma DA, Olson R, Harrow S, Correa RJM, Schneiders F, Haasbeek CJA, et al. Stereotactic ablative radiotherapy for the comprehensive treatment of 4-10 oligometastatic tumors (SABR-COMET-10): Study protocol for a randomized phase III trial. *BMC Cancer* (2019) 19:1–15. doi: 10.1186/s12885-019-5977-6

229. Heller G, Fizazi K, McCormack R, Molina A, MacLean D, Webb IJ, et al. The added value of circulating tumor cell enumeration to standard markers in assessing prognosis in a metastatic castration-resistant prostate cancer population. *Clin Cancer Res* (2017) 23:1967–73. doi: 10.1158/1078-0432.CCR-16-1224

230. Scher HI, Heller G, Molina A, Attard G, Danila DC, Jia X, et al. Circulating tumor cell biomarker panel as an individual-level surrogate for survival in metastatic castration-resistant prostate cancer. *J Clin Oncol* (2015) 33:1348–55. doi: 10.1200/JCO.2014.55.3487

231. Armstrong AJ, Marengo MS, Oltean S, Kemeny G, Bitting RL, Turnbull JD, et al. Circulating Tumor Cells from Patients with Advanced Prostate and Breast Cancer Display Both Epithelial and Mesenchymal Markers. *Mol Cancer Res* (2011) 9:997–1007. doi: 10.1158/1541-7786.MCR-10-0490

232. Habli Z, AlChamaa W, Saab R, Kadara H, Khraiche ML. Circulating Tumor Cell Detection Technologies and Clinical Utility: Challenges and Opportunities. *Cancers (Basel)* (2020) 12(7):1930. doi: 10.3390/cancers12071930

233. Goldkorn A, Ely B, Quinn DI, Tangen CM, Fink LM, Xu T, et al. Circulating tumor cell counts are prognostic of overall survival in SWOG S0421: a phase III trial of docetaxel with or without atrasentan for metastatic castration-resistant prostate cancer. *J Clin Oncol* (2014) 32:1136–42. doi: 10.1200/JCO.2013.51.7417

234. Goldkorn A, Ely B, Tangen CM, Tai Y-C, Xu T, Li H, et al. Circulating tumor cell telomerase activity as a prognostic marker for overall survival in SWOG 0421: a phase III metastatic castration resistant prostate cancer trial. *Int J Cancer* (2015) 136:1856–62. doi: 10.1002/ijc.29212

235. Danila DC, Anand A, Sung CC, Heller G, Leversha MA, Cao L, et al. TMPRSS2-ERG Status in circulating tumor cells as a predictive biomarker of sensitivity in castration-resistant prostate cancer patients treated with abiraterone acetate. *Eur Urol* (2011) 60:897–904. doi: 10.1016/j.eururo.2011.07.011

236. Ady N, Morat L, Fizazi K, Soria JC, Mathieu MC, Prapotnich D, et al. Detection of HER-2/neu-positive circulating epithelial cells in prostate cancer patients. *Br J Cancer* (2004) 90:443–8. doi: 10.1038/sj.bjc.6601532

237. Ried K, Tamanna T, Matthews S, Eng P, Sali A. New Screening Test Improves Detection of Prostate Cancer Using Circulating Tumor Cells and Prostate-Specific Markers. *Front Oncol* (2020) 10:582. doi: 10.3389/fonc.2020.00582

238. Sharp A, If TD, Welti JC, If TD, Lambros MBK, If TD, et al. Clinical Utility of Circulating Tumour Cell Androgen Receptor Splice Variant-7 Status in Metastatic Castration-resistant Prostate Cancer. *Eur Urol* (2019) 76:676–85. doi: 10.1016/j.eururo.2019.04.006

239. Strati A, Zavridou M, Bournakis E, Mastoraki S, Lianidou E. Expression pattern of androgen receptors, AR-V7 and AR-567es, in circulating tumor cells and paired plasma-derived extracellular vesicles in metastatic castration resistant prostate cancer. *Analyst* (2019) 144 (22):6671–80. doi: 10.1039/c9an00999j

240. Sieuwerts AM, Onstenk W, Kraan J, Beaufort CM, Van M, De Laere B, et al. AR splice variants in circulating tumor cells of patients with castration-resistant prostate cancer: relation with outcome to cabazitaxel. *Mol Oncol* (2019) 13:1795–807. doi: 10.1002/1878-0261.12529

241. Tagawa ST, Antonarakis ES, Gjyrezi A, Galletti G, Kim S, Worroll D, et al. Expression of AR-V7 and ARV 567Es in circulating tumor cells correlates with outcomes to taxane therapy in men with metastatic prostate cancer treated in taxynergy. *Clin Cancer Res* (2019) 25:1880–8. doi: 10.1158/1078-0432.CCR-18-0320

242. Miyamoto DT, Lee RJ, Kalinich M, LiCausi JA, Zheng Y, Chen T, et al. An RNA-based digital circulating tumor cell signature is predictive of drug response and early dissemination in prostate cancer. *Cancer Discovery* (2018) 8:288–303. doi: 10.1158/2159-8290.CD-16-1406

243. Freedland SJ, Humphreys EB, Mangold LA, Eisenberger M, Dorey FJ, Walsh PC, et al. Risk of prostate cancer-specific mortality following biochemical recurrence after radical prostatectomy. *JAMA* (2005) 294:433–9. doi: 10.1001/jama.294.4.433

244. Gulati R, Psutka SP, Etzioni R. Personalized Risks of Over Diagnosis for Screen Detected Prostate Cancer Incorporating Patient Comorbidities: Estimation and Communication. *J Urol* (2019) 202:936–43. doi: 10.1097/JU.0000000000000346

245. Berruti A, Dogliotti L, Bitossi R, Fasolis G, Gorzegno G, Bellina M, et al. Incidence of skeletal complications in patients with bone metastatic prostate cancer and hormone refractory disease: predictive role of bone resorption and formation markers evaluated at baseline. *J Urol* (2000) 164:1248–53. doi: 10.1016/S0022-5347(05)67149-2

246. Gonzalez H, Robles I, Werb Z. Innate and Acquired Immune Surveillance in the Post-Dissemination Phase of Metastasis. *FEBS J* (2018) 285:654–64. doi: 10.1111/febs.14325

247. Mohme M, Riethdorf S, Pantel K. Circulating and disseminated tumour cells — mechanisms of immune surveillance and escape. *Nat Rev Clin Oncol* (2017) 14:155–67. doi: 10.1038/nrclinonc.2016.144

248. Morgan TM, Lange PH, Porter MP, Lin DW, Ellis WJ, Gallaher IS, et al. Disseminated tumor cells in prostate cancer patients after radical prostatectomy and without evidence of disease predicts biochemical recurrence. *Clin Cancer Res* (2009) 15:677–83. doi: 10.1158/1078-0432.CCR-08-1754

249. Chalfin HJ, Glavaris SA, Malihi PD, Sperger JM, Gorin MA, van der Toom EE, et al. Prostate Cancer Disseminated Tumor Cells are Rarely Detected in the Bone Marrow of Localized Patients Undergoing Radical Prostatectomy Across Multiple Rare Cell Detection Platforms. *J Urol* (2018) 199:1494–501. doi: 10.1016/j.juro.2018.01.033

250. Chéry L, Lam H-M, Coleman I, Lakely B, Coleman R, Larson S, et al. Characterization of single disseminated prostate cancer cells reveals tumor cell heterogeneity and identifies dormancy associated pathways. *Oncotarget* (2014) 5:9939–51. doi: 10.18632/oncotarget.2480

251. Cackowski FC, Wang Y, Decker JT, Sifuentes C, Weindorf S, Jung Y, et al. Detection and isolation of disseminated tumor cells in bone marrow of patients with clinically localized prostate cancer. *Prostate* (2019) 79:1715–27. doi: 10.1002/pros.23896

252. Shiozawa Y, Pienta KJ, Taichman RS. Hematopoietic Stem Cell Niche Is a Potential Therapeutic Target for Bone Metastatic Tumors. *Clin Cancer Res* (2011) 17:5553–8. doi: 10.1158/1078-0432.CCR-10-2505

253. Shiozawa Y, Pedersen EA, Havens AM, Jung Y, Mishra A, Joseph J, et al. Human prostate cancer metastases target the hematopoietic stem cell niche to establish footholds in mouse bone marrow. *J Clin Invest* (2011) 121:1298–312. doi: 10.1172/JCI43414

254. Axelrod HD, Valkenburg KC, Amend SR, Hicks JL, Parsana P, Torga G, et al. AXL Is a Putative Tumor Suppressor and Dormancy Regulator in Prostate Cancer. *Mol Cancer Res* (2019) 17:356–69. doi: 10.1158/1541-7786.MCR-18-0718

255. Yumoto K, Eber MR, Wang J, Cackowski FC, Decker AM, Lee E, et al. Axl is required for TGF-β2-induced dormancy of prostate cancer cells in the bone marrow. *Sci Rep* (2016) 6:36520. doi: 10.1038/srep36520

256. Owen KL, Gearing LJ, Zanker DJ, Brockwell NK, Khoo WH, Roden DL, et al. Prostate cancer cell-intrinsic interferon signaling regulates dormancy and metastatic outgrowth in bone. *EMBO Rep* (2020) 21:e50162. doi: 10.15252/embr.202050162

257. Ottewell PD, Wang N, Meek J, Fowles CA, Croucher PI, Eaton CL, et al. Castration-induced bone loss triggers growth of disseminated prostate cancer cells in bone. *Endocr-Relat Cancer* (2014) 21:769–81. doi: 10.1530/ERC-14-0199

258. Decker AM, Jung Y, Cackowski FC, Yumoto K, Wang J, Taichman RS. Sympathetic Signaling Reactivates Quiescent Disseminated Prostate Cancer Cells in the Bone Marrow. *Mol Cancer Res* (2017) 15:1644–55. doi: 10.1158/1541-7786.MCR-17-0132

259. Kim M-Y, Oskarsson T, Acharyya S, Nguyen DX, Zhang XH-F, Norton L, et al. Tumor self-seeding by circulating cancer cells. *Cell* (2009) 139:1315–26. doi: 10.1016/j.cell.2009.11.025

260. Leung CT, Brugge JS. Tumor Self-Seeding: Bidirectional Flow of Tumor Cells. *Cell* (2009) 139:1226–8. doi: 10.1016/j.cell.2009.12.013

261. Liu T, Ma Q, Zhang Y, Wang X, Xu K, Yan K, et al. Self-seeding circulating tumor cells promote the proliferation and metastasis of human osteosarcoma by upregulating interleukin-8. *Cell Death Dis* (2019) 10:1–13. doi: 10.1038/s41419-019-1795-7

262. Bayne CE, Williams SB, Cooperberg MR, Gleave ME, Graefen M, Montorsi F, et al. Treatment of the Primary Tumor in Metastatic Prostate Cancer: Current Concepts and Future Perspectives. *Eur Urol* (2016) 69:775–87. doi: 10.1016/j.eururo.2015.04.036

263. Parker CC, James ND, Brawley CD, Clarke NW, Hoyle AP, Ali A, et al. Radiotherapy to the primary tumour for newly diagnosed, metastatic prostate cancer (STAMPEDE): a randomised controlled phase 3 trial. *Lancet* (2018) 392:2353–66. doi: 10.1016/S0140-6736(18)32486-3

264. Murray NP, Aedo S, Fuentealba C, Reyes E, Salazar A, Lopez MA, et al. Subtypes of minimal residual disease, association with Gleason score, risk and time to biochemical failure in pT2 prostate cancer treated with radical prostatectomy. *Ecancermedicalscience* (2019) 13:934. doi: 10.3332/ecancer.2019.934

265. Murray NP, Murray NP. Minimal residual disease in prostate cancer patients after primary treatment: theoretical considerations, evidence and possible use in clinical management. *Biol Res* (2018) 51(1):32. doi: 10.1186/s40659-018-0180-9

266. Persi E, Wolf YI, Leiserson MDM, Koonin EV, Ruppin E. Criticality in tumor evolution and clinical outcome. *PNAS* (2018) 115:E11101–10. doi: 10.1073/pnas.1807256115

267. Samstein RM, Lee C-H, Shoushtari AN, Hellmann MD, Shen R, Janjigian YY, et al. Tumor mutational load predicts survival after immunotherapy across multiple cancer types. *Nat Genet* (2019) 51:202–6. doi: 10.1038/s41588-018-0312-8

268. van Dessel LF, van Riet J, Smits M, Zhu Y, Hamberg P, van der Heijden MS, et al. The genomic landscape of metastatic castration-resistant prostate cancers reveals multiple distinct genotypes with potential clinical impact. *Nat Commun* (2019) 10:5251. doi: 10.1038/s41467-019-13084-7

269. Wyatt AW, Annala M, Aggarwal R, Beja K, Feng F, Youngren J, et al. Concordance of Circulating Tumor DNA and Matched Metastatic Tissue Biopsy in Prostate Cancer. *J Natl Cancer Inst* (2017) 109(12):djx118. doi: 10.1093/jnci/djx118

270. Miller MC, Robinson PS, Wagner C, O'Shannessy DJ. The ParsortixTM Cell Separation System-A versatile liquid biopsy platform. *Cytom A* (2018) 93:1234–9. doi: 10.1002/cyto.a.23571

271. Di Trapani M, Manaresi N, Medoro G. DEPArrayTM system: An automatic image-based sorter for isolation of pure circulating tumor cells. *Cytom A* (2018) 93:1260–6. doi: 10.1002/cyto.a.23687

272. Lee Y, Guan G, Bhagat AA. ClearCell® FX, a label-free microfluidics technology for enrichment of viable circulating tumor cells. *Cytom A* (2018) 93:1251–4. doi: 10.1002/cyto.a.23507

273. Otto O, Rosendahl P, Mietke A, Golfier S, Herold C, Klaue D, et al. Real-time deformability cytometry: on-the-fly cell mechanical phenotyping. *Nat Methods* (2015) 12:199–202. doi: 10.1038/nmeth.3281

274. Tutrone R, Donovan MJ, Torkler P, Tadigotla V, McLain T, Noerholm M, et al. Clinical utility of the exosome based ExoDx Prostate(IntelliScore) EPI test in men presenting for initial Biopsy with a PSA 2–10 ng/mL. *Prostate Cancer Prostatic Dis* (2020) 23(4)607–14. doi: 10.1038/s41391-020-0237-z

275. Beaver JA, Kluetz PG, Pazdur R. Metastasis-free Survival — A New End Point in Prostate Cancer Trials. *New Engl J Med* (2018) 378(26):2458–60. doi: 10.1056/NEJMp1805966

276. Jung Y, Wang J, Lee E, McGee S, Berry JE, Yumoto K, et al. Annexin 2–CXCL12 Interactions Regulate Metastatic Cell Targeting and Growth in the Bone Marrow. *Mol Cancer Res* (2015) 13:197–207. doi: 10.1158/1541-7786.MCR-14-0118

277. Malladi S, Macalinao DG, Jin X, He L, Basnet H, Zou Y, et al. Metastatic Latency and Immune Evasion through Autocrine Inhibition of WNT. *Cell* (2016) 165:45–60. doi: 10.1016/j.cell.2016.02.025

278. Balkwill F, Mantovani A. Inflammation and cancer: back to Virchow? *Lancet* (2001) 357:539–45. doi: 10.1016/S0140-6736(00)04046-0

279. Kitamura T, Qian B-Z, Pollard JW. Immune cell promotion of metastasis. *Nat Rev Immunol* (2015) 15:73–86. doi: 10.1038/nri3789

280. Qian B, Pollard JW. Macrophage Diversity Enhances Tumor Progression and Metastasis. *Cell* (2010) 141:39–51. doi: 10.1016/j.cell.2010.03.014

281. Erlandsson A, Carlsson J, Lundholm M, Fält A, Andersson S, Andrén O, et al. M2 macrophages and regulatory T cells in lethal prostate cancer. *Prostate* (2019) 79:363–9. doi: 10.1002/pros.23742

282. Di Mitri D, Mirenda M, Vasilevska J, Calcinotto A, Delaleu N, Revandkar A, et al. Re-education of Tumor-Associated Macrophages by CXCR2 Blockade Drives Senescence and Tumor Inhibition in Advanced Prostate Cancer. *Cell Rep* (2019) 28:2156–2168.e5. doi: 10.1016/j.celrep.2019.07.068

283. Kim SJ, Busby E, Kim JS, Kaya M, He J, Zhang F, et al. Tumor associated macrophages enhance the establishment and growth of prostate cancer bone metastasis. *Cancer Res* (2007) 67:2458–8.

284. Zhang S. The role of transforming growth factor β in T helper 17 differentiation. *Immunology* (2018) 155:24–35. doi: 10.1111/imm.12938

285. Jiao S, Subudhi SK, Aparicio A, Ge Z, Guan B, Miura Y, et al. Differences in Tumor Microenvironment Dictate T Helper Lineage Polarization and Response to Immune Checkpoint Therapy. *Cell* (2019) 179:1177–1190.e13. doi: 10.1016/j.cell.2019.10.029

286. de Almeida DVP, Fong L, Rettig MB, Autio KA. Immune Checkpoint Blockade for Prostate Cancer: Niche Role or Next Breakthrough? *Am Soc Clin Oncol Educ Book* (2020) 40:1–18. doi: 10.1200/EDBK_278853

287. Baryawno N, Kfoury Y, Severe N, Mei S, Gustafsson K, Hirz T, et al. Human prostate cancer bone metastases have an actionable immunosuppressive microenvironment. *Mol Carcinog* (2020) 59(7):822–29. doi: 10.1002/mc.23192. 2020.03.19.998658.

Conflict of Interest: The authors declare that the research was conducted in the absence of any commercial or financial relationships that could be construed as a potential conflict of interest.

Modeling Radioimmune Response— Current Status and Perspectives

Thomas Friedrich [1*], Nicholas Henthorn [2,3] and Marco Durante [1,4]

[1] Biophysics Department, GSI Helmholtz Center for Heavy Ion Research, Darmstadt, Germany, [2] Division of Cancer Sciences, School of Medical Sciences, Faculty of Biology, Medicine and Health, The University of Manchester, Manchester, United Kingdom, [3] The Christie NHS Foundation Trust, Manchester Academic Health Science Centre, Manchester, United Kingdom, [4] Institute for Solid State Physics, Technical University Darmstadt, Darmstadt, Germany

The combination of immune therapy with radiation offers an exciting and promising treatment modality in cancer therapy. It has been hypothesized that radiation induces damage signals within the tumor, making it more detectable for the immune system. In combination with inhibiting immune checkpoints an effective anti-tumor immune response may be established. This inversion from tumor immune evasion raises numerous questions to be solved to support an effective clinical implementation: These include the optimum immune drug and radiation dose time courses, the amount of damage and associated doses required to stimulate an immune response, and the impact of lymphocyte status and dynamics. Biophysical modeling can offer unique insights, providing quantitative information addressing these factors and highlighting mechanisms of action. In this work we review the existing modeling approaches of combined 'radioimmune' response, as well as associated fields of study. We propose modeling attempts that appear relevant for an effective and predictive model. We emphasize the importance of the time course of drug and dose delivery in view to the time course of the triggered biological processes. Special attention is also paid to the dose distribution to circulating blood lymphocytes and the effect this has on immune competence.

Keywords: radiation immunity, immunotherapy, radiation therapy, modeling, radiation effect

INTRODUCTION

Supporting immune therapy with radiotherapy is a promising approach in particular to tackle non immunogenic tumors, where formation of distant metastases is one of the main reason for failure of curative therapy (1–3). An important variant of immune therapy focuses on immune checkpoint inhibitors, through appropriate antibodies, to reverse immune evasion within tumors. Radiation can enhance this process if delivered in combination. We shall term such combination therapy "radioimmunotherapy" (RIT) throughout this review article. The underlying paradigm is that the radiation induced damage gives rise to the expression of immune stimulating damage markers such as calreticulin, HMGB1 or ATP, or causes a release of interferon by pathways such as cGAS/STING (4). These processes allow tumor cells to be recognized by their specific antigens and leads to attraction of antigen presenting cells that initiate the activation of effector cells that can eventually inactivate the tumor. The particular role of radiation is therefore thought to restore the visibility of

the tumor to the immune system, while the immune therapy antibodies efficiently attack the (now visible) tumor, as well as metastases throughout the body. Indeed, an abscopal effect, i.e. the shrinking or definite cure of metastatic lesions has been observed in situations where immune therapy or radiation therapy alone is likely to fail (5, 6).

The interplay of radiation with the immune system is remarkably versatile and has been readily acknowledged as one of the key aspects of radiation therapy (7): In RIT, radiation offers a systemic therapeutic potential, while classical radiotherapy acts targeted and restricted to the tumor region only. The interaction of radiation induced damage with the immune system is even visible when radiation alone is given: On the one hand, even when given alone radiation at high doses can act immunostimulating by supporting the activation of antigen presenting cells (8) and by increasing T-cell infiltration and the expression of MHC class 1 exploited for antigen presentation (9). However, at the same time the radiation action can suppress the immune system, e.g. by irradiation of draining lymph nodes, inhibiting effector cell activation (10–12). This eventually results in lymphopenia, which is known as a common side effect of radiation therapy (13–17) and associated with a worse prognosis. Likewise, radiation may cause upregulation of immune checkpoints, paving the way for a durable escape of the tumor from immune surveillance (18). Hence, from a mechanistic point of view, it is not clear under which circumstances radiation can really be supportive for immune therapy, and quantification of processes and effects are needed to approach this challenge.

Currently, RIT is used in several hundred clinical studies, and more than 50 of those are already in phase 3 (9). The investigations mostly focus on melanoma, non small cell lung cancer, head and neck squamous cell carcinoma and breast cancer. There are a number of FDA approved drugs that focus on inhibiting the immune checkpoints relevant for the lymphocyte activation (CTLA-4) and lymphocyte effects to the tumor (PD-1 or PD-L1). Current clinical strategy is to convert non-immunogenic 'cold' tumors into immunogenic, 'hot' ones, which allow the infiltration and action of immune effector cells, mostly CD8+ T-lymphocytes. Also here, the question for the optimal therapeutic setting arises, and a quantification of the optimum doses and schedules as well as of success rates are urgently needed.

This challenge is approached by radiobiological modeling, and the aim of the present work is to briefly review modeling approaches associated with aspects of RIT as well as to show potential future developments of this field of research. We thereby also update recent review articles (19, 20) that are partially concerned with the state of the art in modeling RIT as well.

MODEL APPROACHES

In the context of RIT some modeling approaches have been developed that either aim at simulating the outcome of such therapy, or to model specific underlying processes that impose a

rationale for RIT. In particular, five major model approaches describe RIT using checkpoint blockers. Other models focus on the immunomodulatory effect of either radiation or checkpoint blockers alone, without considering their combination. A further class of model simulates in detail pathway related aspects on the way to establish the radioimmune response.

Models for Radioimmunotherapy

At present (February 2021) to the knowledge of the authors there are only five consistent model approaches that attempt to simulate the full course of RIT published in peer reviewed journals. Typically, the models consist of a number of coupled differential or difference equations, each of which describes the dynamics of a key quantity such as the amount of lymphocytes or tumor cells. They differ in mathematical structure, level of detail, type of checkpoint blocker(s), and type of dose and concentration response function. **Table 1** gives an overview of the present models.

To describe the effects of RIT, Serre et al published the first encompassing model framework (21). In this pioneering work the authors modeled the immune system by the amount of effector cells, whose amount is determined by the expression level of tumor antigens. While radiation causes the expression of such antigens, aPD-1 is giving clearance for the effector cells to shrink the tumor mass. The authors attributed the role of aCTLA4 to the long term immune response, i.e. the memory effect, while neglecting its role in fostering effector cell activation even at early times after irradiation. Serre et al. formulated their model as a set of coupled time dependent difference equations. The dose of checkpoint blockers results in quite specifically chosen nonlinear relationships into tumor cell removal, while radiation is assumed to lead to tumor cell inactivation according to the well accepted linear quadratic formalism. The synergism between radiation and checkpoint blockers establishes via the radiation stimulated antigen expression that promotes the immune response, if checkpoints are blocked. Serre et al. solved their set of equations numerically and could describe nicely tumor growth curves of a preclinical experiment. In a later publication (26) they added more dynamical information by allowing time for the antigen release and immune response to establish. As those time scales may interfere with radiation

TABLE 1 | Models for RIT and general properties.

Publication	Blocked checkpoint(s)	Number of interacting quantities
Serre (21)	PD-1, CTLA-4	3
Chakwizira (22)	IDO (in context of glioblastoma therapy)	3
Poleszczuk (23)	Not specified, but applied to CTLA-4	4
Kosinsky (24)	PD-1	5
Byun (25)	PD-1, PD-L1	4

The models address different checkpoint blockers, as given in the second column. They establish the interactions of tumor cells, immune cells, and eventually signals such as antigens via coupled dynamic equations, and the third column indicates the number of these quantities and equations. As PD-1 and PD-L1 form an axis, models applicable to PD-1 blocking are applicable to PD-L1 blocking as well.

fractionation schemes they introduced the concept of immunologically effective dose (IED), which is the counterpart of the biologically effective dose (BED). BED and IED are the total radiation doses that would be delivered in infinitely many fractions to result in the same targeted and abscopal effect, respectively, as for a regimen with a given fractionation scheme.

Chakwizira et al. (22) simplified Serre's original model to explain the immune response of radiation in combination with a checkpoint blocker targeting IDO, which is used in the context of treating glioblastoma. They only considered the short time immune response and replaced the complicated response after PD-1 checkpoint blocking in Serre's model by a simplified dose response to IDO blockers. They succeeded to reproduce with their model experimentally determined survival times of rats with glioblastoma for different radiation doses alone or in combination with immune therapy. Using the model prospectively they predicted that hypofractionation without unusual long gaps (> 1d) maximizes the synergy between radiation and immune therapy.

Poleszczuk et al. (23) developed a model approach including simple, linear interaction terms reflecting immune cells affecting the tumor. They also include a continuously time delayed removal of tumor cells that are committed to death, and distinguish between immunogenic or radiation induced death. To simulate abscopal effects, they rely on their prior work for effector cell motion, explaining variations in transport to distant metastatic sites. Accelerated primary tumor growth appears in favor of abscopal effects due to detraction of immune cells. Interestingly, in that framework they predict a worse prognosis for treating a primary tumor in case an abscopal tumor is present, as the latter one would attract effector cells as well and thus stands in competition with the primary one.

In the model presented by Kosinsky et al. (24) a logistic tumor growth is modified by radiation essentially following the LQ formalism and by the presence of T cells. Here, the latter is amplified, triggered by cell death via an enhancement of the immune activation rate that depends on the PD-1 checkpoint blocker. While being similar to Serre's model, this approach is more versatile as both undifferentiated and differentiated T cell compartments in the tumor microenvironment are simulated, and there is an explicit dynamic formulation for the removal of dying cells. However, this is established at the expense of numerous parameters, which makes the model harder to validate. Nevertheless, the authors managed to mostly reproduce experimental findings in giving aPD-1 concomitantly or subsequently to radiation therapy.

The model of Byun et al. (25) provides an explicit simulation of both the PD-1 and the PD-L1 concentration, which mainly determine the interaction between tumor cells and T cells. They assume a decaying action strength of both radiation and administered drugs, and consider the binding kinetics of immune checkpoints, modified by checkpoint blocking antibodies. Their model is benchmarked at hand of one rich data set. The model properties are also investigated by a sensitivity analysis and by systematically inspecting model predictions depending on input parameters.

Models for the Immune Response After Either Irradiation or Checkpoint Blocking Alone

In the literature also a number of models can be found that consider the immunomodulatory action of radiation or of checkpoint blockers alone, without considering their combined action. Such a rather isolated consideration may be useful to inspect the individual agent based effects before considering their combination, which is expected to be more complicated due to additional synergistic mechanisms. A selection of models is compiled in **Table 2** and summarized below.

Alfonso et al. (27) suggested a model for the immune modulatory effect of fractionated radiation. It starts off from a quite detailed model of tumor growth dynamics, accounting for hypoxic avascular and potentially necrotic regions inside the tumor. The level of available effector cells in the tumor microenvironment is promoted by radiation, which is modeled via a reaction kinetics approach. The degree of effector cell infiltration is modeled empirically as well, and they account for a delayed shrinking of the tumor mass after irradiation. Their model suggests that the level of functional vascularization is an important determinant for therapy design rather than tumor size alone.

The work of Valentinuzzi (28) implemented Gompertzian tumor growth model and explicitly simulated modes of inhibition of the PD-1 – PD-L1 axis. They furthermore distinguish between unaffected tumor cells and tumor cells that are continuously being removed after immune cell attack.

Lai and Frieman (29) modeled the interaction of a tumor, several types of immune cells, DAMP release and PD-1 checkpoint blockers on a quite detailed level, including active transport and/or diffusion of these quantities. They also modeled vaccinations with drugs promoting tumor infiltration of T cells, and their model supports the belief that infiltration is a necessary precondition for successful immunotherapy.

Milberg et al. (30) used a physiologically based pharmacokinetic model for deriving the impact of checkpoint inhibition. They follow a quantitative systems pharmacology approach, describing the dynamics of many involved factors explicitly.

In the model of Radunskaya et al. (31) the authors investigated the immune cell dynamics within the spleen, the blood and the tumor. Modeling interaction between those

TABLE 2 | Selected models for immune response after radiation or immune therapy with checkpoint blockers alone.

Publication	Considered agent
Alfonso (27)	radiation
Valentinuzzi (28)	aPD-1, aPD-L1
Lai and Frieman (29)	aPD-1
Milberg (30)	aPD-1 and a-CTLA-4
Radunskaya (31)	aPD-L1
Nikolopoulu (32)	aPD-1
Butner (33)	Any checkpoint blocker
Wilkie (34)	Unspecified

compartments, their model allows to calculate the impact on tumor growth, and blocking of PD-L1 modifies these interactions.

The work of Nikolopoulo et al. (32) considers in particular the dynamics of PD-1. They present a stability analysis of the underlying equations in the case of no therapy, where they find an equilibrium between T cells and cancer cells. Including checkpoint blocking antibodies they present also a sensitivity analysis.

Butner et al. (33) presented a model approach that intends to describe the clinical outcome of immune therapy. Remarkably, they applied their model to clinical data and demonstrated its capability for discriminating between therapy responders and non-responders based on early assessments of tumor growth. The model uses methods of statistical physics, where the transport of drugs and cytokines are described by diffusion. They finally derive an approximate, but fairly simple formula, which is used for further evaluations.

Wilkie et al. (34) instead employed a logistic tumor growth model, which is modified by a predation mechanism reflecting immune cells, that themselves are promoted by the presence of tumor cells. They used their model to explain the phenomenon of transient tumor dormancy. Although the authors did not employ a specific mechanism for checkpoint blocking, the interaction function has been set up quite generally and can be easily gauged to contain such immune suppressing factors.

Models at the Level of Underlying Pathways

Modeling of immune responses at the pathway scale becomes rather difficult due to the complexity of the underlying protein networks, which are usually not completely known. Understanding at the pathway scale is, however, desirable for a number of reasons, for instance to identify mechanistic steps that can be targeted through intervention. Although the mechanisms are often understood qualitatively, the quantitative data required for model construction tends to be missing, mostly due to a lack of experimental accessibility. However, some models at this scale do exist, despite lack of data and resultant uncertainties, albeit primarily focused on modeling the immune response alone, discarding interactions with radiation.

Gregg et al. introduced a systems biology approach model of DNA sensing and interferon production (35), later expanding the model to describe the cGAS-STING pathway (36). The model describes the dynamics of the pathway through a series of "states", with ordinary differential equations determining transitions between states and enzyme reactions described through Michaelis Menten kinetics. In total the model uses 13 states giving rise to 34 model parameters; 13 describing cGAS, 11 describing JAK/STAT, and 10 describing degradation rate parameters (e.g. DNA degradation by TREX1). The model parameters are fit to experimental data where possible and unknown parameters are optimized (25 unknown in total, with all cGAS related parameters assumed to be unknown). The model calculates molecule concentrations within the cytosol as a function of time; including cGAS, STING, DNA, IFNβ, and

TREX1. The authors are able to reproduce findings such as drug inhibition of cGAS described through mass action kinetics. The detailed modeling approach allows for investigation of more potent drugs through the variation of association constant. The authors also performed a sensitivity analysis of their model and showed that IFNβ activity is highly robust to perturbations in TREX1 feedback, making the model less dependent on the particular choice of the corresponding input parameters. In the same way, the insensitivity of IFNβ production on TREX1 activity also provides a testable hypothesis. Whilst the model presented by Gregg et al. (36) was not specifically designed for the combined radiation action it is not difficult to foresee modifications that would accommodate this; for example, modifying the initial amount of cytosolic DNA as a function of radiation quality and dose.

The extent, and success, of an anti-tumor immune response is dependent on immune cell activation and signaling. To that end a number of mathematical models have been designed to probe these mechanisms. For example, Mesecke et al. (37) developed a mathematical model of natural killer (NK) cell activating/inhibitory signal receptors at the molecular level. The model is designed with "optional" modules to investigate mechanisms, giving rise to 72 individual models of NK activation and inhibition. Similarly, a number of mechanistic models have been developed to describe T-cell activation (38, 39).

Immune response modeling spans many scales, from the molecular level up to the patient level (40). Palsson et al. (41) developed a framework to integrate published subset models into a single multiscale model through parameterization, known as the Fully-integrated Immune Response Model (FIRM). In FIRM connectivity matrices are built between subset models to describe the global network structure. The model specifies antigen exposure over time and calculates antibody levels and cell concentrations. Although initially designed to simulate the immune response to tuberculosis infection FIRM is also capable of simulating the cellular response to tumor challenge.

Beyond these models, a number of tools are available to simplify and increase the accessibility of immune process modeling. Such tools as BioNetGen (42), Cell studio (43), NetLogo (44), and Simmune (45) may be helpful in simulating various aspects in a pathway oriented modeling of radioimmune response.

STATE OF THE ART IN MODELING RADIOIMMUNOTHERAPY

To summarize, there are numerous model approaches that cover aspects of RIT. These approaches can be distinguished, as used to structure the present review, by their level of applicability: Some models focus on specific pathways or on the general interaction between a tumor and the immune system, other approaches model the immunologic response to checkpoint blockers or radiation alone, and a few models even attempt to model RIT. On all these levels, models are found with different levels of detail.

As RIT approaches a standard treatment for some cancer types, such modeling is needed to interpret clinical outcome in a quantitative way. However, there are various gaps in our knowledge on biologic aspects of the immune response, and therefore these models accumulate open parameters. Furthermore, due to a lack of clinical experience a validation and benchmarking can only occur with preclinical experiments, where usually growth dynamics of implanted synthetic tumors has been investigated.

Comparing the five models for RIT summarized in **Table 1**, one finds a number of similarities. All models describe the dynamics of cancer cells, immune cells and eventually of signals leading to recruiting activated T cells (DAMPs, antigens, IFN release, e.g.) via rate equations, i.e. coupled differential or difference equations. They all include that dying cancer cells finally provoke lymphocyte presence, which is why radiation can trigger this process. Checkpoint blocking is included in all models as a key to admit lymphocyte action. It is worth to note that the complicated network of a variety of different immune cell types and multiple underlying processes like different modes of immune mediated cell inactivation is not reflected by any model. Models are rather kept simplified, working with effective quantities e.g. by ignoring different types of lymphocytes. For instance, most models do not distinguish between helper and cytotoxic T cells, because finally the amount of effector cells of whatever type are of interest, while other cell types may support their presence as mediators and are simulated implicitly, i.e. without explicitly appearing in equations. This level of abstraction is for a good reason: A corresponding model

to such detail would require a plethora of model parameters, thereby ruling out robust predictions.

The underlying paradigm including aCTLA-4 and aPD-1 as checkpoint blockers are visualized in **Figure 1** in a modeler's perspective, identifying three key quantities and three agents. The sequence of processes reflects the immunity cycle as suggested by Chen and Mellmann (46), where here radiation is the primary cause of cell death of tumor cells, which at the same time triggers a systemic antitumor response. With some modifications, a similar circle of dependencies could be established for the IDO checkpoint instead of the PD-1 and CTLA-4 checkpoints. Notably, there are many more molecules involved in the immune checkpoints than the ones the checkpoints are named after, and the expression of these molecules is a dynamic process that may be modified also by other agents than radiation, e.g. heat (47). Again, models tend here to simplify the situation and model effectively the onset of immune activation triggered by radiation induced cell death.

As a further similarity, all models follow the general idea of simulating the dynamics of T cells at the tumor site(s), eventually capable to predate tumor cells. This is performed by first defining initial conditions and then following tumor growth and its possible turnover into shrinkage by the synergism of radiation exposure and immunotherapy, as indicated in **Figure 2**.

The models, however, differ in many aspects as well: They use various tumor growth models without considering radiation or immune effects, which might be reasoned partially in the experimental data used for benchmarking. They differ further in the particular choice of interaction terms between immune
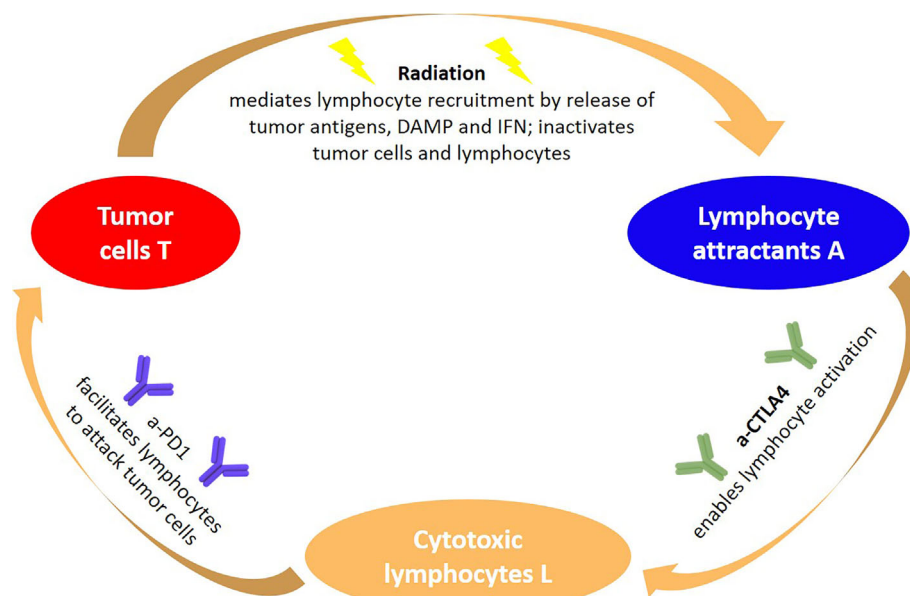
FIGURE 1 | General paradigm underlying RIT using immune checkpoint blockers from a modeler's perspective: The abundance of tumor cells, lymphocyte attracting signals and activated lymphocytes are three quantities that depend on each other, but are also impacted by external agents such as radiation and immune checkpoint blockers. The synergy of coupling radiation and immune therapy emerges, as radiation amplifies signals that are exploited for tumor cell recognition, which in combination with aCTLA-4 lead to an effective lymphocyte activation, resulting in a tumor cell predation driven by cytotoxic lymphocytes.

FIGURE 2 | Logic underlying the simulation of combined radiation and immunotherapy effects: In a first step, initial conditions are defined which characterize tumor growth and the immune system's capability (e.g., represented by the number of lymphocytes effectively taking part in tumor cell eradication) without therapy. In a second step the targeted radiation effects as well as checkpoint blocking is simulated, leading to a synergistic immune response. Finally, this results in an enhancement of cytotoxic T lymphocytes (CTL) in the tumor microenvironment (TME) of the irradiated and—if applicable—of an abscopal site. The T cells may eradicate tumor cells, which eventually leads to tumor control. If the therapy design is successful, typically within the therapy block or shortly after the tumor growth will turn into shrinkage as indicated by the color scale in the time arrow (green, no tumor; red, large tumor mass).

effector cells and tumor cells. They also vary in the selection of subclasses of tumor cells (hypoxic, inactivated but not yet removed…) and immune cells (CD4+, CD8+, dendritic cells, …) employed. Needless to say, as they are complex models they differ in the number of open parameters (i.e. degrees of freedom of the model), the knowledge about experimentally inspired fixed model parameters, and the associated numerical values. Model limitations are directly connected to the particular choice of modeled cell types, interaction processes and functional dependences and need to be investigated for each model separately.

As the models are established from authors with somewhat different background and perspective, they all use a different terminology and a different notation, making comparisons in view of their complexity quite tedious. Finally, they are validated against experimental data to different levels, while a comprehensive validation across multiple data sets has not been demonstrated so far at all. Nevertheless, all models managed to recover the experimentally observed amplification of immune response by radiation and allow investigation of impacting factors such as dosage, fractionation scheme and the drug administration schedule.

FUTURE PERSPECTIVES

Rather than only considering fully integrated models for predicting the outcome of RIT, the approaches at a lower level of applicability may be important to test and maybe reject underlying assumptions in comparison with experimental data. We would like to stress that also model approaches that attempt to model general functionality of the immune system or the interaction of a growing tumor with the immune system provoked many model based investigations (48–53), that may help to optimize model strategies.

Several differences between the models have been pointed out above. Although these may seem technical and a matter of proper implementation at the first glance, they may have a strong impact on the simulation outcome. These include the choice of the tumor growth model as well as the functional relationship expressed by the interaction terms. Here various assumptions need to be tested against available data, e.g., there is no unique answer on how many activated cytotoxic T-cells are needed to effectively remove a single tumor cell, and how tumor cells can be accessed by T cells due to space limitations.

Besides overcoming such open questions in current models, the following key questions appear to be most promising to be addressed by the following future model approaches, which shall be briefly discussed below:

- What does the therapy response to radiation and checkpoint blockers look like, and how can underlying *response times* be used to optimize scheduling?
- How do primary tumor and abscopal sites differ in *availability and accessibility of T cells*?
- What is the role of radiation induced *lymphocyte inactivation* in cases where the radiation field covers a large portion of vascularized tissue or lymph nodes?
- What is the potential role of *high LET radiation* in regard of the previous aspects?

Response times: A very important aspect that is rarely discussed is the time delay between involved biological steps. For instance, cells killed by radiation are not killed immediately. Rather cell death is a process, and therefore also DAMP signals will be elicited with some delay after irradiation. Likewise, the removal of cells will take place later, and T cell activation and recruitment also takes time. In some approaches tumor cells that are inactivated will be removed according to an ordinary decay differential equation, leading to an exponential removal. However, it would be much more plausible to introduce

peaked distribution functions with a support on a finite time interval (i.e. with a maximum value) for such delay times.

Availability and accessibility of T cells: Concerning the attempt to model the immune response in an abscopal tumor that is not irradiated at all, the crucial question is, what amount of radiation amplified T cells will migrate to this tumor site. It is unclear to what extent other draining lymph nodes except the one corresponding to the irradiation site contribute to the pool of activated lymphocytes. While models at the moment can only use assumptions, future dedicated experimental studies could provide more insight. Such studies might help to decide whether activated T cells in the microenvironment of the primary tumor, the abscopal tumor and in the blood need to be modeled separately, eventually including spatial aspects, or can be simply related, thereby reducing the number of degrees of freedom.

Lymphocyte inactivation: Another aspect not sufficiently included in models so far is suppression of the lymphocyte status by radiation. While models account for such suppression eventually in the tumor region, the lymphocyte pool can be largely inactivated, or, if lymph nodes are in the radiation field, the number of naïve T cells can be reduced so that a replenishment is strongly inhibited. This idea demonstrates that radiation has both an immune stimulating and immunosuppressive effect, and modeling could help to determine optimum doses, investigating the impact of dose rate and treatment modality etc. Indeed it is evident that patients with lymphopenia have a worse therapy prognosis (12–17). Experimental studies indicate that (i) lymph node irradiation is a crucial factor that should be avoided, if possible (10, 11), and that lymphocytes in general are quite radiosensitive and hence the blood pool is vulnerable by radiation (54–60). There are only few studies on the dose response of radiation induced lymphopenia (61–63), considering the dose distribution within the blood pool. Again, general models of lymphocyte dynamics (64) may contribute to further model developments.

High LET radiation: The role of proton and carbon ion therapy in the context of RIT is at the moment rather unexplored but appears to be quite promising (65, 66): With protons and carbon ions a very conformal irradiation of the target is achieved. In particular, for carbon ions, additional biological advantages result in an enhanced effect in the target region and allow for hypofractionated regimens (67, 68). In the context of RIT this promises at least a twofold advantage: First, sparing normal tissue allows for a tremendous reduction of effective field sizes and allows for less reduction of the lymphocyte pool. With an appropriate field design, lymph nodes could even be spared as well (66). If however lymph nodes are affected by metastases, they may be specifically treated by elective node irradiation using small treatment fields, although the benefit of such treatment remains debated in conventional therapy (69–71). With sufficiently conformal fields, surrounding organs at risk, but also circulatory lymphocytes and unaffected nodes can be spared. The precise conformal irradiation can be realized using ion beams (72, 73). Second, with carbon ions large doses as frequently applied in RIT can be generically realized with comparably tolerable side effects

to the normal tissue. This is ultimately reasoned in the high LET effects to cells and tissues, i.e. providing a large relative biological effectiveness and overcoming the resistance of cells in S/G2 phases or of hypoxic cells in the target region. One may conjecture that the damage complexity inflicted by high LET radiation gives rise to a third advantage: Overcoming the radioresistance of hypoxic cells and in general locally clustered DNA damage could lead to a larger level of immune stimulation. One may suspect about a more efficient activation of the cGAS/STING pathway or an enhanced release of DAMPs (74, 75). Considering the temporal pattern of the immune response, the time scales between irradiation and radiation effects are expected to be modified after high LET radiation, accounting for the more severe inflicted damage (76, 77). A faster manifestation of cell inactivation as compared to low-LET radiation suggests a more rapid immune activation and T cell recruitment, while at the same time providing a stronger delay in tumor growth. On the other hand, the immunosuppressive effects of radiation as PD-L1 upregulation may be modified and eventually amplified by the enormous energy concentration within high LET ion tracks. Also at the moment it is not clear whether or not high LET radiation will enhance the infiltration capability of T cells in the tumor microenvironment, or whether the latter will be modified in other aspects. First experimental results (78–80) do not show a clear picture yet, while the tissue sparing effect of particle irradiation indeed seems to be beneficial regarding lymphocyte deprivation (81). Thus the multiple perspectives and open questions associated with the use of high LET RIT warrant further preclinical experiments, which are able to answer the speculative and encouraging expectations presented above.

From the considerations regarding high LET radiation one might also expect that hypofractionated irradiation of small fields would be most suitable for RIT. For SBRT regimens, e.g. enough cells would be inactivated in the target area to set on the immune stimulating effect, while in the small entrance channels only a smaller fraction of lymphocytes in the blood stream would be affected (82). Indeed, early clinical experience using SBRT in combination with checkpoint blockers indicates therapeutic benefits (83).

The four radiobiological questions that have been identified and discussed above can be addressed both experimentally and theoretically. For theoretic model formulation it is an important aspect that the considered experimental data are comprehensive, i.e. self-consistent data sets where multiple observables (e.g. CD 8+ cell count, DAMP release and tumor masses) are simultaneously analyzed for various (many) treatment conditions. Such data sets are most profitable, as they can be directly used for comprehensive model gauging. This approach is complementary to applying models to multiple, independent data sets which is a rather convenient strategy for model testing, thereby supporting or falsifying the underlying mechanistic assumptions. More comprehensive data sets will therefore potentially allow to better assess distinct model approaches. For simplistic models the task is then to choose the most important key quantities that determine tumor mass dynamics, and for very detailed models following an ab-initio approach implementing OMICS data in immune response models (84)

may help to keep model uncertainties comparably low despite a high number of degrees of freedom.

Generally, to support the models' validity and to test their assumptions a broader benchmarking against experimental data is desirable. A fruitful strategy would be to apply one model with fixed model constants (except those characterizing a particular experiments) to multiple independent data sets. At the moment there exist quite a number of thoroughly analyzed experimental data sets (mainly tumor growth dynamics) of primary and abscopal tumors with various doses and fractionation schemes etc., e.g. (4, 10, 85–89). In that line, theoretic models may come up with specific predictions, to interpolate between the results, and identify interesting treatment scenarios to be investigated. Experiments will be able to answer these questions, thereby making our current understanding of the combined action of radiation and immunotherapy more precise. We would like to stress here, that there is still a lack of apparently basic experiments such as investigating interferon release in dependence of radiation quality and dose. Such systematic quantification experiments, although not directly related to current 'hot topics', would be very valuable to establish a consistent mechanistic understanding of interactions between radiation and the immune system. Also, experiments are not available where both radiation dose and checkpoint blocker drug concentration are varied systematically. Such experiments would be very valuable to quantify the expected synergism of radiation and checkpoint blocking. Generally, a dialogue of modelers, immunologists and oncologists will be needed to decide about the necessities and options to go for, aiming for a quantification of radio immune response.

Concerning the use in the clinics, the pivotal role of RIT modeling is to indicate factors to account for in treatment planning. This includes, for instance, the need to consider the entire vascular system and the blood pool as an organ at risk for lymphopenia (90). Degrees of freedom that need to be optimized are the radiation dose, the fractionation schedule, radiation type, geometry of the irradiation field(s), irradiation angles, antibody type, drug concentration and drug delivery schedule. This also includes exhibiting the role of emerging radiation therapy modalities such as FLASH or spatial fractionation, which may also spare the blood pool efficiently, but for which the interaction with the immune system is unclear at the moment (91).

Within therapy, the adaptive change or adjustment of initial treatment strategies may be aided or reasoned by model approaches. The advantage of mathematical models as compared to general perceptions is that they are quantitative in nature. At this moment models are quite successful in describing preclinical experiments. In near future, an emerging task will be to develop corresponding model description tailored to clinical situations. For integrated modeling in clinical practice, eventually involved in treatment planning, the step from preclinical experiments towards application in therapy of patients has to be thoroughly validated. In this regard, experience of RIT in patients will be of particular importance, and existing models may be supportive in finding interpretations that help to improve schedules and dosage, and in the same way eventually experience gradual validation.

Thus, benchmark data for such models will be generated within ongoing clinical studies, and hopefully models will acquire predictive power that finally can be used in decision making and treatment planning.

AUTHOR CONTRIBUTIONS

TF and NH designed and wrote the manuscript. MD contributed with input on the general outline and the potential capabilities of high LET radiation. All authors edited and proofread the manuscript. All authors contributed to the article and approved the submitted version.

FUNDING

ACKNOWLEDGMENTS

REFERENCES

1. Ko EC, Formenti SC. Radiation therapy to enhance tumor immunotherapy: a novel application for an established modality. *Int J Radiat Biol* (2019) 95:936–9. doi: 10.1080/09553002.2019.1623429

2. Frey B, Rückert M, Deloch L, Rühle PF, Derer A, Fietkau R, et al. Immunomodulation by ionizing radiation-impact for design of radio-immunotherapies and for treatment of inflammatory diseases. *Immunol Rev* (2017) 280(1):231–48. doi: 10.1111/imr.12572

3. Wang Y, Deng W, Li N, Neri S, Sharma A, Jiang W, et al. Combining Immunotherapy and Radiotherapy for Cancer Treatment: Current Challenges and Future Directions. *Front Pharmacol* (2018) 9:185. doi: 10.3389/fphar.2018.00185

4. Vanpouille-Box C, Alard A, Aryankalayil MJ, Sarfraz Y, Diamond JM, Schneider RJ, et al. DNA exonuclease Trex1 regulates radiotherapy-induced tumour immunogenicity. *Nat Commun* (2017) 8:15618. doi: 10.1038/ncomms15618

5. Formenti SC, Demaria S. Radiation therapy to convert the tumor into an in situ vaccine. *Int J Radiat Oncol Biol Phys* (2012) 84:879–80. doi: 10.1016/j.ijrobp.2012.06.020

6. Brix N, Tiefenthaller A, Anders H, Belka C, Lauber K. Abscopal, immunological effects of radiotherapy: Narrowing the gap between clinical and preclinical experiences. *Immunol Rev* (2017) 280(1):249–79. doi: 10.1111/imr.12573

7. Boustani J, Grapin M, Laurent PA, Apetoh L, Mirjolet C. The 6th R of Radiobiology: Reactivation of Anti-Tumor Immune Response. *Cancers (Basel)* (2019) 11:860. doi: 10.3390/cancers11060860

8. Gupta A, Probst HC, Vuong V, Landshammer A, Muth S, Yagita H, et al. Radiotherapy promotes tumor-specific effector CD8+ T cells via dendritic cell activation. *J Immunol* (2012) 189:558–66. doi: 10.4049/jimmunol.1200563

9. Jagodinsky JC, Harari PM, Morris ZS. The Promise of Combining Radiation Therapy With Immunotherapy. *Int J Radiat Oncol Biol Phys* (2020) 108:6–16. doi: 10.1016/j.ijrobp.2020.04.023

10. Marciscano AE, Ghasemzadeh A, Nirschl TR, Theodros D, Kochel CM, Francica BJ, et al. Elective Nodal Irradiation Attenuates the Combinatorial

Efficacy of Stereotactic Radiation Therapy and Immunotherapy. *Clin Cancer Res* (2018) 24:5058–71. doi: 10.1158/1078-0432.CCR-17-3427

11. Buchwald ZS, Nasti TH, Lee J, Eberhardt CS, Wieland A, Im SJ, et al. Tumor-draining lymph node is important for a robust abscopal effect stimulated by radiotherapy. *J Immunother Cancer* (2020) 8:e000867. doi: 10.1136/jitc-2020-000867

12. Davuluri R, Jiang W, Fang P, Xu C, Komaki R, Gomez DR, et al. Lymphocyte Nadir and Esophageal Cancer Survival Outcomes After Chemoradiation Therapy. *Int J Radiat Oncol Biol Phys* (2017) 99:128–35. doi: 10.1016/j.ijrobp.2017.05.037

13. Ray-Coquard I, Cropet C, Van Glabbeke M, Sebban C, Le Cesne A, Judson I, et al. European Organization for Research and Treatment of Cancer Soft Tissue and Bone Sarcoma Group. Lymphopenia as a prognostic factor for overall survival in advanced carcinomas, sarcomas, and lymphomas. *Cancer Res* (2009) 69:5383–91. doi: 10.1158/0008-5472.CAN-08-3845

14. Balmanoukian A, Ye X, Herman J, Laheru D, Grossman SA. The association between treatment-related lymphopenia and survival in newly diagnosed patients with resected adenocarcinoma of the pancreas. *Cancer Invest* (2012) 30:571–6. doi: 10.3109/07357907.2012.700987

15. Zhao Q, Chen G, Ye L, Shi S, Du S, Zeng Z, et al. Treatment-duration is related to changes in peripheral lymphocyte counts during definitive radiotherapy for unresectable stage III NSCLC. *Radiat Oncol* (2019) 14:86. doi: 10.1186/s13014-019-1287-z

16. Grossman SA, Ellsworth S, Campian J, Wild AT, Herman JM, Laheru D, et al. Survival in Patients With Severe Lymphopenia Following Treatment With Radiation and Chemotherapy for Newly Diagnosed Solid Tumors. *J Natl Compr Canc Netw* (2015) 13:1225–31. doi: 10.6004/jnccn.2015.0151

17. Venkatesulu BP, Mallick S, Lin SH, Krishnan S. A systematic review of the influence of radiation-induced lymphopenia on survival outcomes in solid tumors. *Crit Rev Oncol Hematol* (2018) 123:42–51. doi: 10.1016/j.critrevonc.2018.01.003

18. Wang Y, Kim TH, Fouladdel S, Zhang Z, Soni P, Qin A, et al. PD-L1 Expression in Circulating Tumor Cells Increases during Radio(chemo) therapy and Indicates Poor Prognosis in Non-small Cell Lung Cancer. *Sci Rep* (2019) 9:566. doi: 10.1038/s41598-018-36096-7

19. Peskov K, Azarov I, Chu L, Voronova V, Kosinsky Y, Helmlinger G. Quantitative Mechanistic Modeling in Support of Pharmacological Therapeutics Development in Immuno-Oncology. *Front Immunol* (2019) 10:924. doi: 10.3389/fimmu.2019.00924

20. Grassberger C, Ellsworth SG, Wilks MQ, Keane FK, Loeffler JS. Assessing the interactions between radiotherapy and antitumour immunity. *Nat Rev Clin Oncol* (2019) 16:729–45. doi: 10.1038/s41571-019-0238-9

21. Serre R, Benzekry S, Padovani L, Meille C, André N, Ciccolini J, et al. Mathematical Modeling of Cancer Immunotherapy and Its Synergy with Radiotherapy. *Cancer Res* (2016) 76:4931–40. doi: 10.1158/0008-5472.CAN-15-3567

22. Chakwizira A, Ahlstedt J, Nittby Redebrandt H, Ceberg C. Mathematical modelling of the synergistic combination of radiotherapy and indoleamine-2,3-dioxygenase (IDO) inhibitory immunotherapy against glioblastoma. *Br J Radiol* (2018) 91(1087):20170857. doi: 10.1259/bjr.20170857

23. Poleszczuk J, Enderling H. The Optimal Radiation Dose to Induce Robust Systemic Anti-Tumor Immunity. *Int J Mol Sci* (2018) 19:3377. doi: 10.3390/ijms19113377

24. Kosinsky Y, Dovedi SJ, Peskov K, Voronova V, Chu L, Tomkinson H, et al. Radiation and PD-(L)1 treatment combinations: immune response and dose optimization via a predictive systems model. *J Immunother Cancer* (2018) 6:17. doi: 10.1186/s40425-018-0327-9

25. Byun JH, Yoon IS, Jeong YD, Kim S, Jung IH. A Tumor-Immune Interaction Model for Synergistic Combinations of Anti PD-L1 and Ionizing Irradiation Treatment. *Pharmaceutics* (2020) 12(9):830. doi: 10.3390/pharmaceutics12090830

26. Serre R, Barlesi F, Muracciole X, Barbolosi D. Immunologically effective dose: a practical model for immuno-radiotherapy. *Oncotarget* (2018) 9:31812–9. doi: 10.18632/oncotarget.25746

27. Alfonso JCL, Papaxenopoulou LA, Mascheroni P, Meyer-Hermann M, Hatzikirou H. On the Immunological Consequences of Conventionally Fractionated Radiotherapy. *iScience* (2020) 23:100897. doi: 10.1016/j.isci.2020.100897

28. Valentinuzzi D, Simončič U, Uršič K, Vrankar M, Turk M, Jeraj R. Predicting tumour response to anti-PD-1 immunotherapy with computational modelling. *Phys Med Biol* (2019) 64:025017. doi: 10.1088/1361-6560/aaf96c

29. Lai X, Friedman A. Combination therapy of cancer with cancer vaccine and immune checkpoint inhibitors: A mathematical model. *PLoS One* (2017) 12:e0178479. doi: 10.1371/journal.pone.0178479

30. Milberg O, Gong C, Jafarnejad M, Bartelink IH, Wang B, Vicini P, et al. A QSP Model for Predicting Clinical Responses to Monotherapy, Combination and Sequential Therapy Following CTLA-4, PD-1, and PD-L1 Checkpoint Blockade. *Sci Rep* (2019) 9:11286. doi: 10.1038/s41598-019-47802-4

31. Radunskaya A, Kim R, Woods TII. Mathematical modeling of tumor immune interactions: A closer look at the role of a PD-L1 inhibitor in cancer immunotherapy. *Spora: A J Biomath* (2018) 4:25–41. doi: 10.30707/SPORA4.1Radunskaya

32. Nikolopoulou E, Johnson LR, Harris D, Nagy JD, Stites EC, Kuang Y. Tumour-immune dynamics with an immune checkpoint inhibitor. *Lett Biomath* (2018) 5(2):S137–59. doi: 10.1080/23737867.2018.1440978

33. Butner JD, Elganainy D, Wang CX, Wang Z, Chen SH, Esnaola NF, et al. Mathematical prediction of clinical outcomes in advanced cancer patients treated with checkpoint inhibitor immunotherapy. *Sci Adv* (2020) 6(18): eaay6298. doi: 10.1126/sciadv.aay6298

34. Wilkie KP, Hahnfeldt P. Tumor-immune dynamics regulated in the microenvironment inform the transient nature of immune-induced tumor dormancy. *Cancer Res* (2013) 73:3534–44. doi: 10.1158/0008-5472

35. Gregg RW, Sarkar S, Shoemaker JE. Examining Dynamic Emergent Properties of the DNA Sensing Pathway. *IFAC-PapersOnLine* (2018) 51:112–3. doi: 10.1016/j.ifacol.2018.09.017

36. Gregg RW, Sarkar SN, Shoemaker JE. Mathematical modeling of the cGAS pathway reveals robustness of DNA sensing to TREX1 feedback. *J Theor Biol* (2019) 462:148–57. doi: 10.1016/j.jtbi.2018.11.001

37. Mesecke S, Urlaub D, Busch H, Eils R, Watzl C. Integration of activating and inhibitory receptor signaling by regulated phosphorylation of Vav1 in immune cells. *Sci Signal* (2011) 4:1–10. doi: 10.1126/scisignal.2001325

38. Rohrs JA, Wang P, Finley SD. Understanding the Dynamics of T-Cell Activation in Health and Disease Through the Lens of Computational Modeling. *JCO Clin Cancer Inform* (2019) 3:1–8. doi: 10.1200/CCI.18.00057

39. Mahlbacher GE, Reihmer KC, Frieboes HB. Mathematical modeling of tumor-immune cell interactions. *J Theor Biol* (2019) 469:47–60. doi: 10.1016/j.jtbi.2019.03.002

40. Makaryan SZ, Cess CG, Finley SD. Modeling immune cell behavior across scales in cancer. *Wiley Interdisc Rev Syst Biol Med* (2020) 12:1–16. doi: 10.1002/wsbm.1484

41. Palsson S, Hickling TP, Bradshaw-Pierce EL, Zager M, Jooss K, O'Brien PJ, et al. The development of a fully-integrated immune response model (FIRM) simulator of the immune response through integration of multiple subset models. *BMC Syst Biol* (2013) 7:1. doi: 10.1186/1752-0509-7-95

42. Harris LA, Hogg JS, Tapia JJ, Sekar JAP, Gupta S, Korsunsky I, et al. BioNetGen 2.2: Advances in rule-based modeling. *Bioinformatics* (2016) 32:3366–8. doi: 10.1093/bioinformatics/btw469

43. Liberman A, Kario D, Mussel M, Brill J, Buetow K, Efroni S, et al. Cell studio: A platform for interactive, 3D graphical simulation of immunological processes. *APL Bioeng* (2018) 2:026107. doi: 10.1063/1.5039473

44. Shinde SB, Kurhekar MP. *Agent-Based Modeling of the Adaptive Immune System Using Netlogo Simulation Tool BT - Soft Computing for Problem Solving.* KN Das, JC Bansal, K Deep, AK Nagar, P Pathipooranam, RC Naidu, editors. Singapore: Springer Singapore (2020) p. 463–74.

45. Angermann BR, Meier-Schellersheim M. *Using Python for Spatially Resolved Modeling with Simmune BT - Modeling Biomolecular Site Dynamics: Methods and Protocols.* WS Hlavacek, editor. New York, NY: Springer New York (2019) p. 161–77. doi: 10.1007/978-1-4939-9102-0_7

46. Chen DS, Mellman I. Oncology meets immunology: the cancer-immunity cycle. *Immunity* (2013) 39:1–10. doi: 10.1016/j.immuni.2013.07.012

47. Hader M, Savcigil DP, Rosin A, Ponfick P, Gekle S, Wadepohl M, et al. Differences of the Immune Phenotype of Breast Cancer Cells after Ex Vivo Hyperthermia by Warm-Water or Microwave Radiation in a Closed-Loop System Alone or in Combination with Radiotherapy. *Cancers* (2020) 12 (5):1082. doi: 10.3390/cancers12051082

48. Eftimie R, Gillard JJ, Cantrell DA. Mathematical Models for Immunology: Current State of the Art and Future Research Directions. *Bull Math Biol* (2016) 78:2091–134. doi: 10.1007/s11538-016-0214-9

49. Li X-h, Wang Z-x, Lu T-y, Che X-j. Modelling Immune System: Principles, Models, Analysis and Perspectives. *J Bionic Eng* (2009) 6:77–85. doi: 10.1016/S1672-6529(08)60101-8

50. Sontag ED. A Dynamic Model of Immune Responses to Antigen Presentation Predicts Different Regions of Tumor or Pathogen Elimination. *Cell Syst* (2017) 4:231–41.e11. doi: 10.1016/j.cels.2016.12.003

51. Kim PS, Levy D, Lee PP. Chapter 4 - Modeling and Simulation of the Immune System as a Self-Regulating Network. Ed.: Michael L. Johnson, Ludwig Brand. *Methods Enzymol* (2009) 467:79–109. doi: 10.1016/S0076-6879(09)67004-X

52. de Pillis LG, Radunskaya AE, Wiseman CL. A validated mathematical model of cell-mediated immune respon1se to tumor growth. *Cancer Res* (2005) 65:7950–8. doi: 10.1158/0008-5472

53. Mpekris F, Voutouri C, Baish JW, Duda DG, Munn LL, Stylianopoulos T, et al. Combining microenvironment normalization strategies to improve cancer immunotherapy. *Proc Natl Acad Sci U S A* (2020) 117:3728–37. doi: 10.1073/pnas.1919764117

54. Yovino S, Kleinberg L, Grossman SA, Narayanan M, Ford E. The etiology of treatment-related lymphopenia in patients with malignant gliomas: modeling radiation dose to circulating lymphocytes explains clinical observations and suggests methods of modifying the impact of radiation on immune cells. *Cancer Invest* (2013) 31:140–4. doi: 10.3109/07357907.2012.762780

55. Nakamura N, Kusunoki Y, Akiyama M. Radiosensitivity of CD4 or CD8 positive human T-lymphocytes by an in vitro colony formation assay. *Radiat Res* (1990) 123:224–7. doi: 10.2307/3577549

56. Nakamura N, Sposto R, Kushiro J, Akiyama M. Is interindividual variation of cellular radiosensitivity real or artifactual? *Radiat Res* (1991) 125:326–30. doi: 10.2307/3578118

57. Elyan SA, West CM, Roberts SA, Hunter RD. Use of low-dose rate irradiation to measure the intrinsic radiosensitivity of human T-lymphocytes. *Int J Radiat Biol* (1993) 64:375–83. doi: 10.1080/09553009314551561

58. Geara FB, Peters LJ, Ang KK, Wike JL, Sivon SS, Guttenberger R, et al. Intrinsic radiosensitivity of normal human fibroblasts and lymphocytes after high- and low-dose-rate irradiation. *Cancer Res* (1992) 52:6348–52.

59. Durante M, Yamada S, Ando K, Furusawa Y, Kawata T, Majima H, et al. X-rays vs. carbon-ion tumor therapy: cytogenetic damage in lymphocytes. *Int J Radiat Oncol Biol Phys* (2000) 47:793–8. doi: 10.1016/s0360-3016(00)00455-7

60. Falcke SE, Rühle PF, Deloch L, Fietkau R, Frey B, Gaipl US. Clinically Relevant Radiation Exposure Differentially Impacts Forms of Cell Death in Human Cells of the Innate and Adaptive Immune System. *Int J Mol Sci* (2018) 19:3574. doi: 10.3390/ijms19113574

61. Basler L, Andratschke N, Ehrbar S, Guckenberger M, Tanadini-Lang S. Modelling the immunosuppressive effect of liver SBRT by simulating the dose to circulating lymphocytes: an in-silico planning study. *Radiat Oncol* (2018) 13:10. doi: 10.1186/s13014-018-0952-y

62. Hammi A, Paganetti H, Grassberger C. 4D blood flow model for dose calculation to circulating blood and lymphocytes. *Phys Med Biol* (2020) 65:055008. doi: 10.1088/1361-6560/ab6c41

63. Jin JY, Mereniuk T, Yalamanchali A, Wang W, Machtay M, Spring Kong FM, et al. A framework for modeling radiation induced lymphopenia in radiotherapy. *Radiother Oncol* (2020) 144:105–13. doi: 10.1016/j.radonc.2019.11.014

64. Stekel DJ, Parker CE, Nowak MA. A model of lymphocyte recirculation. *Immunol Today* (1997) 18:216–21. doi: 10.1016/s0167-5699(97)01036-0

65. Ebner DK, Tinganelli W, Helm A, Bisio A, Yamada S, Kamada T, et al. The Immunoregulatory Potential of Particle Radiation in Cancer Therapy. *Front Immunol* (2017) 8:99. doi: 10.3389/fimmu.2017.00099

66. Durante M, Formenti S. Harnessing radiation to improve immunotherapy: better with particles? *Br J Radiol* (2020) 93:20190224. doi: 10.1259/bjr.20190224

67. Durante M, Loeffler JS. Charged particles in radiation oncology. *Nat Rev Clin Oncol* (2010) 7:37–43. doi: 10.1038/nrclinonc.2009.183

68. Ebner DK, Kamada T. The Emerging Role of Carbon-Ion Radiotherapy. *Front Oncol* (2016) 6:140. doi: 10.3389/fonc.2016.00140

69. d'Alesio V, Pacelli R, Durante M, Canale Cama G, Cella L, Gialanella G, et al. Lymph nodes in the irradiated field influence the yield of radiation-induced chromosomal aberrations in lymphocytes from breast cancer patients. *Int J Radiat Oncol Biol Phys* (2003) 57:732–8. doi: 10.1016/s0360-3016(03)00664-3

70. Whelan TJ, Olivotto IA, Parulekar WR, Ackerman I, Chua BH, Nabid A, et al. Regional Nodal Irradiation in Early-Stage Breast Cancer. *N Engl J Med* (2015) 373:307–16. doi: 10.1056/NEJMoa1415340

71. Moreno AC, Lin YH, Bedrosian I, Shen Y, Stauder MC, Smith BD, et al. Use of regional nodal irradiation and its association with survival for women with high-risk, early stage breast cancer: A National Cancer Database analysis. *Adv Radiat Oncol* (2017) 2:291–300. doi: 10.1016/j.adro.2017.04.008

72. De Rose F, Cozzi L, Meattini I, Fogliata A, Franceschini D, Franzese C, et al. The Potential Role of Intensity-modulated Proton Therapy in the Regional Nodal Irradiation of Breast Cancer: A Treatment Planning Study. *Clin Oncol (R Coll Radiol)* (2020) 32:26–34. doi: 10.1016/j.clon.2019.07.016

73. Jimenez RB, Hickey S, DePauw N, Yeap BY, Batin E, Gadd MA, et al. Phase II Study of Proton Beam Radiation Therapy for Patients With Breast Cancer Requiring Regional Nodal Irradiation. *J Clin Oncol* (2019) 37:2778–85. doi: 10.1200/JCO.18.02366

74. Durante M, Brenner DJ, Formenti SC. Does Heavy Ion Therapy Work Through the Immune System? *Int J Radiat Oncol Biol Phys* (2016) 96(5):934–6. doi: 10.1016/j.ijrobp.2016.08.037

75. Durante M, Formenti SC. Radiation-Induced Chromosomal Aberrations and Immunotherapy: Micronuclei, Cytosolic DNA, and Interferon-Production Pathway. *Front Oncol* (2018) 8:192. doi: 10.3389/fonc.2018.00192

76. Böhrnsen G, Weber KJ, Scholz M. Measurement of biological effects of high-energy carbon ions at low doses using a semi-automated cell detection system. *Int J Radiat Biol* (2002) 78:259–66. doi: 10.1080/09553000110110293

77. Brownstein JM, Wisdom AJ, Castle KD, Mowery YM, Guida P, Lee CL, et al. Characterizing the Potency and Impact of Carbon Ion Therapy in a Primary Mouse Model of Soft Tissue Sarcoma. *Mol Cancer Ther* (2018) 17:858–68. doi: 10.1158/1535-7163.MCT-17-0965

78. Takahashi Y, Yasui T, Minami K, Tamari K, Hayashi K, Otani K, et al. Carbon ion irradiation enhances the antitumor efficacy of dual immune checkpoint blockade therapy both for local and distant sites in murine osteosarcoma. *Oncotarget* (2019) 10:633–46. doi: 10.18632/oncotarget.26551

79. Helm A, Tinganelli W, Simoniello P, Kurosawa F, Fournier C, Shimokawa T, et al. Reduction of Lung Metastases in a Mouse Osteosarcoma Model Treated With Carbon Ions and Immune Checkpoint Inhibitors. *Int J Radiat Oncol Biol Phys* (2020) 109(2):594–602. doi: 10.1016/j.ijrobp.2020.09.041

80. Hartmann L, Schröter P, Osen W, Baumann D, Offringa R, Moustafa M, et al. Photon versus carbon ion irradiation: immunomodulatory effects exerted on murine tumor cell lines. *Sci Rep* (2020) 10:21517. doi: 10.1038/s41598-020-78577-8

81. Shiraishi Y, Fang P, Xu C, Song J, Krishnan S, Koay EJ, et al. Severe lymphopenia during neoadjuvant chemoradiation for esophageal cancer: A propensity matched analysis of the relative risk of proton versus photon-based radiation therapy. *Radiother Oncol* (2018) 128:154–60. doi: 10.1016/j.radonc.2017.11.028

82. Wild AT, Herman JM, Dholakia AS, Moningi S, Lu Y, Rosati LM, et al. Lymphocyte-Sparing Effect of Stereotactic Body Radiation Therapy in Patients With Unresectable Pancreatic Cancer. *Int J Radiat Oncol Biol Phys* (2016) 94:571–9. doi: 10.1016/j.ijrobp.2015.11.026

83. Chen D, Patel RR, Verma V, Ramapriyan R, Barsoumian HB, Cortez MA, et al. Interaction between lymphopenia, radiotherapy technique, dosimetry, and survival outcomes in lung cancer patients receiving combined immunotherapy and radiotherapy. *Radiother Oncol* (2020) 150:114–20. doi: 10.1016/j.radonc.2020.05.051

84. Lazarou G, Chelliah V, Small BG, Walker M, van der Graaf PH, Kierzek AM. Integration of Omics Data Sources to Inform Mechanistic Modeling of Immune-Oncology Therapies: A Tutorial for Clinical Pharmacologists. *Clin Pharmacol Ther* (2020) 107:858–70. doi: 10.1002/cpt.1786

85. Dovedi SJ, Adlard AL, Lipowska-Bhalla G, McKenna C, Jones S, Cheadle EJ, et al. Acquired resistance to fractionated radiotherapy can be overcome by concurrent PD-L1 blockade. *Cancer Res* (2014) 74:5458–68. doi: 10.1158/0008-5472.CAN-14-1258

86. Dovedi SJ, Cheadle EJ, Popple AL, Poon E, Morrow M, Stewart R, et al. Fractionated Radiation Therapy Stimulates Antitumor Immunity Mediated by Both Resident and Infiltrating Polyclonal T-cell Populations when Combined

with PD-1 Blockade. *Clin Cancer Res* (2017) 23:5514–26. doi: 10.1158/1078-0432.CCR-16-1673

87. Demaria S, Kawashima N, Yang AM, Devitt ML, Babb JS, Allison JP, et al. Immune-mediated inhibition of metastases after treatment with local radiation and CTLA-4 blockade in a mouse model of breast cancer. *Clin Cancer Res* (2005) 11:728–34.

88. Dewan MZ, Galloway AE, Kawashima N, Dewyngaert JK, Babb JS, Formenti SC, et al. Fractionated but not single-dose radiotherapy induces an immune-mediated abscopal effect when combined with anti-CTLA-4 antibody. *Clin Cancer Res* (2009) 15:5379–88. doi: 10.1158/1078-0432.CCR-09-0265

89. Deng L, Liang H, Burnette B, Beckett M, Darga T, Weichselbaum RR, et al. Irradiation and anti-PD-L1 treatment synergistically promote antitumor immunity in mice. *J Clin Invest* (2014) 124:687–95. doi: 10.1172/JCI67313

90. Ellsworth SG. Field size effects on the risk and severity of treatment-induced lymphopenia in patients undergoing radiation therapy for solid tumors. *Adv Radiat Oncol* (2018) 3:512–9. doi: 10.1016/j.adro.2018.08.014

91. Griffin RJ, Ahmed MM, Amendola B, Belyakov O, Bentzen SM, Butterworth KT, et al. Understanding High-Dose, Ultra-High Dose Rate, and Spatially Fractionated Radiation Therapy. *Int J Radiat Oncol Biol Phys* (2020) 107 (4):766–78. doi: 10.1016/j.ijrobp.2020.03.028

Conflict of Interest: The authors declare that the research was conducted in the absence of any commercial or financial relationships that could be construed as a potential conflict of interest.

Progressive Study on the Non-thermal Effects of Magnetic Field Therapy in Oncology

Aoshu Xu[1,2], Qian Wang[1,2], Xin Lv[1,2] and Tingting Lin[1,2]*

[1] College of Instrumentation and Electrical Engineering, Jilin University, Changchun, China, [2] Key Laboratory of Geophysics Exploration Equipment, Ministry of Education of China, Changchun, China

Cancer is one of the most common causes of death worldwide. Although the existing therapies have made great progress and significantly improved the prognosis of patients, it is undeniable that these treatment measures still cause some serious side effects. In this context, a new treatment method is needed to address these shortcomings. In recent years, the magnetic fields have been proposed as a novel treatment method with the advantages of less side effects, high efficiency, wide applications, and low costs without forming scars. Previous studies reported that static magnetic fields (SMFs) and low-frequency magnetic fields (LF-MFs, frequency below 300 Hz) exert anti-tumor function, independent of thermal effects. Magnetic fields (MFs) could inhibit cell growth and proliferation; induce cell cycle arrest, apoptosis, autophagy, and differentiation; regulate the immune system; and suppress angiogenesis and metastasis *via* various signaling pathways. In addition, they are effective in combination therapies: MFs not only promote the absorption of chemotherapy drugs by producing small holes on the surface of cell membrane but also enhance the inhibitory effects by regulating apoptosis and cell cycle related proteins. At present, MFs can be used as drug delivery systems to target magnetic nanoparticles (MNPs) to tumors. This review aims to summarize and analyze the current knowledge of the pre-clinical studies of anti-tumor effects and their underlying mechanisms and discuss the prospects of the application of MF therapy in cancer prevention and treatment.

Keywords: magnetic fields, anti-tumor, molecular mechanism, static magnetic fields, low-frequency magnetic fields

INTRODUCTION

Cancer is a serious threat to human health and one of the leading causes of death worldwide. According to estimates with regard to morbidity and mortality for 36 kinds of cancers in 185 countries, about 18.1 million new cancer cases plus 9.6 million cancer-associated deaths happened in 2018 (1). Among these cancers, the highest incidence types are lung (11.6%), breast (11.6%), prostate (7.1%), and colorectal (6.1%) cancers. At present, the primary options for advanced cancer treatments, namely chemotherapy and radiotherapy, always have some limitations such as severe side effects and drug resistance (2–4). It is necessary to develop new therapies to address these disadvantages. In this context, more attention was paid for alternative treatments involving some non-invasive approaches like light, heat, electrical field, magnetic field (MFs), and ultrasound therapies (5–9), which are of high efficiency and incur low costs without inducing infections or

forming scars. Among them, the MF therapy has been studied a lot in recent years, as early as 1971, when Weber et al. (10) validated the inhibitory effects of MFs on tumor-bearing mice. Over the next few decades, many researchers have explored this phenomenon and put forward more evidence about the relevant mechanisms (11–13); at the same time, clinical trials demonstrated its advantage in relieving clinical symptoms, and improving the quality of life of patients with recurrent and rapidly progressing tumors (**Table 1**) (17). Early studies have shown that in the field of cancer treatment, MFs have potential application prospects with few side effects and wide applications. MFs could non-invasively induce the death of cancer cells, whereas lymphocytes showed little necrosis *in vitro* (18, 19). In other medical studies, the MF therapy has been reported to have beneficial results in peripheral nerve regeneration (20), osteo-necrosis (21), and injury-induced osteoporosis (22). MFs at frequencies above 100 kHz predominately show thermal effects; otherwise, they would exert non-thermal effects (23). Recently, non-thermal biological effects of MFs have been reported in many aspects, among which are studies on tumor treatment. The inhibitory effects of static magnetic fields (SMFs) and low-frequency magnetic fields (LF-MFs, with frequency below 300 Hz) have been studied against a wide variety of human cancer cell lines, such as leukemia (24–31), fibrosarcoma (32), colon carcinoma (32–34), and breast cancer (35–40). Furthermore, MFs suppress the growth of Lewis lung carcinoma (LLC) (41) and Ehrlich ascites carcinoma (42, 43) *in vivo*, and even prolong survival and improve the general symptoms of 21 patients with advanced gastric cancer (44). MFs have shown to exert anti-tumor action through various pathways and multiple molecular mechanisms, such as the inhibition of cell growth and proliferation; the induction of apoptosis, cell cycle arrest, and autophagy; participation in immune regulation as well as depression of angiogenesis, and metastasis; and promotion of differentiation. Of interest, they are effective in combination therapies with chemotherapeutic agents and magnetic nanoparticles (MNPs).

AIM AND SEARCHING CRITERIA

Thermal Effects and Non-thermal Effects by (MF) Therapy

Two conditions of the molecular mechanism, namely thermal effects and non-thermal effects, are involved in MF-induced biological effects (23). According to IEEE C95.1-2019, thermal effects are defined as "changes associated with heating of the whole body or an affected region sufficient to induce a biological effect." Electro-stimulation is the dominant effect at low frequencies and thermal effects dominate above radio frequencies. The International Commission on Non-Ionizing Radiation Protection (ICNIRP) gives a more detailed description of electro-magnetic fields at radio frequency (100 kHz—300 GHz), which could penetrate the body and cause a vibration of charged or polar molecules inside, resulting in friction and heat. Thermal effects lead to an increase in bulk temperature, which would thermally induce membrane depolarization, excitation,

TABLE 1 | Early research foundation of magnetic fields (MFs) in tumor suppression.

Year	Some important breakthroughs	Reference
1961	Mulay et al. discovered tumor cells exposed to MFs showed complete degeneration.	(14)
1971	Weber et al. confirmed that the non-homogeneous MF consistently prolonged the life spans and slowed down the growth of tumors in mice.	(10)
1971–1975	Mizushima and Degen et al. reported the anti-inflammatory effects of MFs.	(11, 15)
1999	Chakkalakal et al. found that the MFs had the potential to promote the effects of chemotherapeutic drugs and reduced the dosage and side effects.	(16)
2001	Tofani et al. demonstrated that static plus low-frequency magnetic fields (LF_MFs) induced the apoptosis of tumor cells.	(13)
	Douglas et. al. described the inhibitory effects of MFs on angiogenesis during tumor growth.	(12)
2010	Vasishta found MFs alleviated the clinical symptoms and improved the quality of the life of patients with anaplastic astrocytoma.	(17)

and breakdown and show a distinct side effect on the organisms (45). Non-thermal effects could be described as direct interactions of MF with biological cells that are not associated with any heating but are associated mainly with electro-stimulation (23, 46). Based on the physical mechanisms, extremely LF-MFs (<300 Hz) are regarded as non-thermal effects (47).

Aim and Scope

Magnetic fields are generally generated by permanent magnets or electric currents, and there are several classification methods for MFs. According to the mechanism of the generation of MFs, they are divided into permanent magnetic fields and electromagnetic fields. While the variation rate of the intensity of the MF with spatial displacement is equal to 0, it is a uniform MF; otherwise, it is a gradient magnetic field (GMF). Moreover, if the distribution of the MF changes with time, they are classified as SMFs and non-SMFs, such as alternating magnetic fields (AMFs), pulsed magnetic fields (PMFs), and rotating magnetic fields (RMFs). In consideration of their working frequency, the MF is classified into low frequency (LF) (<300 kHz), medium frequency (MF) (300 kHz—3 MHz), and high frequency (HF) (>3 MHz). According to the Regulations (2012) of the International Telecommunication Union (ITU), LF-MFs are further divided into tremendously LF(<3 Hz), extremely LF (3–30 Hz), super LF (30–300 Hz), ultra LF (300–3000 Hz), very LF (3–30 kHz), and LF (30–300 kHz) (48). Many studies have shown that SMFs and LF-MFs (f < 300 Hz) exerted anti-tumor effects, in which the temperature was maintained at around 37°C for cell culture *in vitro* and excluded thermal effects (30, 49, 50). To comprehend the non-thermal effects of the MF therapy on cancers, we focus on the abovementioned MF types in this review, aiming at describing the state of the art of MF therapy, discussing the current

understanding of the underlying anti-cancer mechanisms, and outlining future therapeutic perspectives in oncology. Common setups, types, exposure direction, and duration of the action are summarized in **Table 2**.

In this review, we focus on the non-thermal effects of SMFs and LF-MFs (<300 Hz) on cancer cells and their applications in cancer treatment. The review aims to highlight the critical areas regarding the uses of MF therapy, which are not fully understood and need to be investigated further.

Searching Criteria

The literature search was carried out with Scopus, Google Scholar, PubMed, Web of Sciences (ISI Web of Knowledge), Medline, and Wiley Online Library databases. Available publications (in English) in peer-reviewed journals on the biological effects of SMFs and LF-MFs between 2008 and 2019 were selected for analysis. We focus on SMF- and LF-MF-induced anti-tumor effects in *in vivo* and *in vitro* studies. The studies on the influence of SMFs and LF-MFs on other organs and systems were excluded from the literature. The keywords used for the literature research were "apoptosis," "cell cycle arrest," "autophagy," "angiogenesis," "immune," "inflammation," "differentiation" (as a combination with "low frequency electromagnetic fields" or "static magnetic fields," and "tumor" or "cancer" or "oncology").

THE EFFECTS OF MFS ON CELL PROLIFERATION, CELL CYCLE ARREST, CELL APOPTOSIS, AND AUTOPHAGY

Magnetic fields exert their function through various pathways and multiple targets. A large number of recent studies have shown that MFs have anti-tumor effects by inhibiting cell proliferation and inducing cell cycle arrest, apoptosis, and autophagy.

Cell Cycle Arrest

The cell cycle, which consists of the G1, S, G2, and M phases, is a very complex and delicate regulation process closely related to cell differentiation, growth, and death. Abnormal expressions of some cell cycle proteins could cause uncontrolled replication of cancer cells; so it is a promising therapy to target cyclins (58).

DNA integrity is critical to cells; common radiotherapy and most of the chemotherapies exert their function by damaging the cancer cells of DNA, which would inhibit proliferation at cell cycle checkpoints and lead to cell death (59). SMFs (8.8 mT, 12 h) enhanced the killing potency of cisplatin, adriamycin, and paclitaxel by triggering DNA damage, inducing cell ultrastructure alteration, and arresting K562 cells at the G2/M phase (27–29). RMFs (0.4 T, 7.5 Hz, 2 h/day) inhibited the growth of B16-F10 *in vitro*, elevated the survival rate, and inhibited the proliferation in the lung metastasis model mice, where an increase in the G2/M phase was detected (52). CDK1-cyclin B, also known as cell division control protein kinase 2-cyclin B (cdc2-cyclin B) functions at the G2/M phase of the cell cycle, to accelerate cell mitosis (60). SMFs (200 ± 60 mT, 48 ± 4 h) induced human
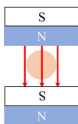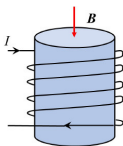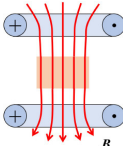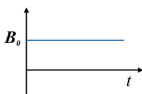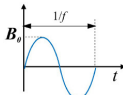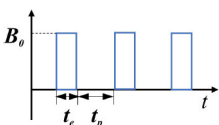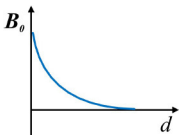
malignant glioblastomata, such as U87 and U251, to arrest the G2/M phase by downregulating the expressions of cyclin B1 and CDK1 (61). The p53 protein is a critical participant in the signal transduction pathway which mediated apoptosis and G1 cell cycle arrest in mammalian cells (62). LF-MFs significantly inhibited tumor growth, induced cell senescence, inhibited iron metabolism of the LLC murine model, and the *in vitro* induced G0/G1 phase arrest of A549 lung cancer cells *via* stabilizing p53 protein and activation of the P53-miR-34a-E2F1/E2F3 pathway (41). In addition, earlier experiments with high risk BE(2)-C neuroblastomas continuously exposed in 50 Hz, 1mT LF-MF for 72 h led to an enhanced cell response to ATRA, along with an increase in the levels of p21, Cdk-5, and G0/G1 population (63). A 24-h exposure of 50 Hz, 100 uT LF-MF exposure slowed down the progression of the cell cycle, which is associated with the regulation of p21 in early response (64). These data indicate that MFs are found to arrest cells at different stages, thus leading to anti-proliferation effects on cells by modulating cell cycle regulatory proteins, as summarized in **Figure 1**.

Apoptosis

Apoptosis, which is a form of programmed cell death as well as a target for anti-tumor therapies, plays an important role in cancer treatment (65). There are two main apoptosis pathways: one occurs through the mitochondrial pathway (intrinsic pathway) and another through the cell death receptor pathway (extrinsic pathway). The intracellular mitochondrial pathway is mainly regulated by B-cell lymphoma-2 family, which could promote the formation of channels in the extracellular membrane of mitochondria to change the permeability, release a variety of apoptosis-related proteins to activate caspase, and induce apoptosis (66, 67). Targeting some pro-apoptosis proteins, anti-apoptosis proteins, and mitochondrial membrane permeability are attractive for cancer therapy, by contributing to the occurrence of the intrinsic apoptosis pathway (68, 69).
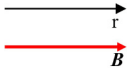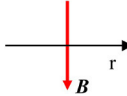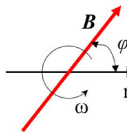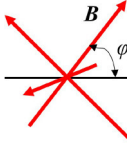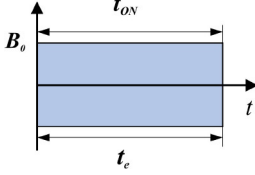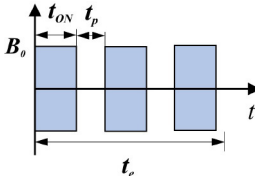
Magnetic fields have been shown to induce apoptosis in human tumor cells studied *in vitro*. A 50-Hz LF-MF (5.1 mT, 2 h/day) inhibited proliferation of nephroblastoma and neuroblastoma cells, induced apoptosis *in vitro*, and promoted the efficacy of cisplatin *in vivo* (49). Reactive oxygen species (ROS) and mitochondria play an important role in the induction of apoptosis (70), and an increase in ROS levels can lead to cytochrome c release and mitochondrial apoptosis (54). The MF treatment has been shown to promote the generation of ROS in many studies (31, 71, 72), with exposure within a 60 Hz sinusoidal MF for 48 h in induced human prostate cancer for DU145, PC3, and LNCaP apoptoses, associated with the accumulation of ROS in an intensity-dependent manner (73). Generally, apoptosis provoked by genotoxins is largely due to DNA damage (74), while DNA double-strand breaks (DSBs) are one of the most severe types of DNA lesions (75). Repetitive exposure to LF-MFs induced DNA damage and accumulation of DSBs and triggered apoptosis in Hela and MCF7 cell lines (35, 76). As p53 is a tumor suppressor gene that plays a pivotal role in apoptosis, PMFs could trigger apoptosis cell death by upregulating the p53 level and through the mitochondrial-dependent pathway (57). LF-MFs (300 mT, 6 Hz,

TABLE 2 | Common setups, types, exposure direction, and duration of the action of MFs used in anti-tumor studies.

Characteristics	Terminology	Graphic representation	Description	Reference
Common MF setups	Permanent magnet		One permanent magnet	(51)
	Permanent magnets		Two permanent magnets aligned in the same direction	(52)
	Solenoid coils		$B = u_0 \times (N/L) \times I$ N - turn ratio of coils; L - solenoid length	(27, 53)
	Uniform (Helmholtz geometry)		$B(x, y, z) \approx$ const grad $B \approx 0$	(54)
MF types	Static magnetic fields (SMFs)		$B = B_0 =$ const	(24, 51)
	Alternating magnetic fields (AMFs)		$B = B_0 \times \sin (2\pi ft)$ f - field change frequency;	(39)
	Pulsed-magnetic fields (PMFs)		t_e - field action duration t_p - pause duration	(35)
	Gradient magnetic fields (GMFs)		B is proportional to $1/d^2$ d - the distance away from the magnets	(55)

(Continued)

TABLE 2 | Continued

Characteristics	Terminology	Graphic representation	Description	Reference
Orientational	Parallel	r, B	B parallel to r r - the plane of cell culture dish	(26)
	Vertical	r, B	B perpendicular to r	(33)
	Rotating	B, φ, r, ω	$B =$ const $\varphi = \omega\, t$	(52)
	Random	B, φ, r	$B \sim$ variable $\varphi \sim$ variable	(40, 56)
Exposure	Continuous	t_{ON}, B_0, t, t_e	$t_{ON} = t_e$ t_{ON} - field action duration; t_e-exposure duration	(57)
	Intermittent	t_{ON} t_p, B_0, t, t_e	t_{ON}- pause duration $\sum t_{ON} < t_e$	(35)

24 h) also induced apoptosis by suppressing protein kinase B (Akt) signaling, activating p38 mitogen-activated protein kinase (MAPK) signaling, and caspase-9, which is the executor of the mitochondrial apoptosis pathway (77).

The findings of these studies have shown that MFs affect apoptosis in the cancer cell lines of various origins. However, at present, there are few studies in this area, and further studies are required for detailed mechanisms. The proposed mechanism involved in the effects of MFs on tumor cell apoptosis is shown in **Figure 1**.

Autophagy

Autophagy is thought to have a therapeutic potential to prevent cancer development, but whether to enhancing or inhibiting it will achieve the desired anti-tumor effects remains questionable (78). Autophagy could be ascertained by detecting LC3-II, a marker of autophagic vesicle accumulation (79). To date, miRNAs were proved to involve in the modulation of a wide range of biological processes, including apoptosis and autophagy (80). The expression of the autophagy marker, LC3-II, detected by Western blotting and GFP-LC3 puncta-formation assay examined by confocal microscopy, showed that RMFs (0.4T, 7.5 Hz, 4 h/day) induced autophagic cell death and suppressed cancer growth *in vitro* and *in vivo*. The main mechanism involved the upregulation of the expression level of miR-486, which was targeting BCAP, the inhibition of Akt/mechanistic target of rapamycin kinase (mTOR), and the induction of autophagy by RMF (81). These findings

FIGURE 1 | The effect of MFs on different signaling pathways and their molecular targets. MF, magnetic field; cdc, cell division control protein kinase; ERK, extracellular signal-regulated kinase; MAPK, mitogen-activated protein kinase; Akt, protein kinase B; Pi3k, phosphatidylinositol 3-kinase; mTOR, mechanistic target of rapamycin kinase; eEF2K, eukaryotic elongation factor 2 kinase; NF-κB, nuclear factor kappa B; IL, interleukin; TNF, tumor necrosis factor; VEGFR, vascular endothelial growth factor receptor.

showed the potential of MF in triggering the autophagic cell death.

THE EFFECTS OF MFS ON THE IMMUNE SYSTEM

The immune function in an organism exerts an essential role in the occurrence and metastasis of tumors. The RMF (0.4T, 7.5 Hz, 2 h/day) has the capacity to elevate the survival rate of tumor-bearing by modulating the immune response and functions of innate immune cells and adaptive immune cells, such as regulating cytokine production in mice serum, promoting T-cell polarization in the spleen, preventing the differentiation of the regulatory cells (Tregs), and increasing the expression of CD40 in dendritic cells (52). Furthermore, analogous results were discovered in mouse H22 hepatocellular carcinoma, with an enhanced anti-tumor immune response; the

inhibition of tumor growth; and the suppression of interleukin-6 (IL-6), granulocyte colony-stimulating factor (G-CSF), and keratinocyte-derived chemokine (KC). Meanwhile, the MF exposure was associated with the activation of macrophages and dendritic cells, enhancement of the profiles of CD4+T and CD8+T lymphocytes, the balance of Th17/Treg, and the reduction of the inhibitory function of Treg cells *in vivo* (82). A combination of SMF with AMF stimulated the production of tumor necrosis factor-α (TNF-α), interferon-gamma, IL-2, and IL-3 in healthy mouse cells, inhibited solid tumor growth, and enhanced the average lifespan, after daily exposure for 2 h within 14 days (83).

Inflammation is a key factor in the immune response to injury and infection; some studies have shown that the progression of various cancers may be closely related to chronic inflammation (84, 85). Exposure to PMF with an intensity of 40 Gauss and frequency below 30 Hz for 48 h decreased the production of the inflammation marker TNF-α and the transcription factor nuclear

factor kappa B (NF-κB). In RAW 264.7 macrophage-like cells, induced by LPS, this regulation process could be appropriately applied to patients with sepsis (86). The upregulation of A2A and A3ARs adenosine receptor mRNA levels by the PMF (1.5 ± 0.2 mT, 75 Hz, 24 h) mediated the anti-inflammation effect, induced the decrease of NF-κB expression, upregulated p53, and induced apoptosis in tumor cells (57). The GMF (6.39–513.69 mT, 24 h) significantly inhibited the release of pro-inflammatory cytokines, IL-6, IL-8, and TNF-α, from macrophages and assisted the production of anti-inflammatory cytokine, IL-10, when treate alone for 24 h and then combined with LPS (87). A similar response was induced by the PMF in N9 microglial cells (88). An *in vitro* study found that SMF (0.4 T, 6 h) could attenuate LPS-induced neuro-inflammatory responses in BV-2 cells, and this effect was associated with increased microglial membrane rigidity and downregulation of IL-6 release (89). MFs have the ability to enhance the immune response of the body to tumors by modulating the functions of immune cells and inhibiting chronic inflammation (**Figure 1**); while the regulation of the immune system is complex, further research is needed to explain the relationship.

THE EFFECTS OF MFS ON ANGIOGENESIS, METASTASIS, AND DIFFERENTIATION

Angiogenesis

Angiogenesis is a critical physiological and pathological process in embryo development, tumor development, and metastasis. The formation of new blood vessels gradually has become an essential therapeutic target in cancer treatment, ischemic diseases, and chronic inflammation (90). Vascular endothelial cell migration is an important part of the angiogenesis process of tumors, and vascular endothelial growth factor (VEGF-A, VEGF) and its receptor-2 (VEGFR-2) play an important role in tumor angiogenesis, which gradually becomes a target in anti-tumor therapy (91). The SMF (600 mT, 10 days) has been shown to inhibit angiogenesis by reducing vessel diameters, the functional vessel density (FVD), and red blood cell velocity to retard vessel maturation by *in vivo* tests (92). After 24-h exposure in the GMF (0.2–0.4 T, 2.09 T/m), the proliferation ability of human umbilical vein endothelial cells (HUVECs) was significantly inhibited. In the chick embryo chorioallantoic membrane (CAM) model, vascular numbers of continuously exposure treatment group (7–11 days) are fewer than those in the control group, which is consistent with the results in matrigel plugs models (55). Sinusoidal MF (1 mT, 50 Hz,72 h) inhibited the formation of tubule-like structures and downregulated the process and migration of HUVECs by reducing the expression and activation levels of VEGFR2 (93). A combination therapy of MF (0.04 T,50 Hz, 1 h) and saffron had synergic effects on VEGFR2 gene expression; they reduced the VEGFR-2 level by 36%, while MF alone only induced a 20% decline in human breast cancer cells (37). A therapeutic MF device, which could generate a defined 120 Hz semi sine wave signal with variable intensity (10–20 mT), was tested for the optimal intensity and

treatment period of MF therapy for breast cancer. Exposure to 20 mT for 10 min two times a day within 12 days was the most effective tumor suppressor; the MF treatment reduced the vascular (CD31 immuno-histochemically positive) volume fraction (94). These studies indicate that the MF therapy is a promising therapy that may target tumor angiogenesis through the pathways showed in **Figure 1**.

Metastasis

Tumor metastasis is the leading cause for death in patients with cancer, and up to 90% of cancer deaths occur due to metastasis. After intermittent treatment for several weeks, a therapeutic electromagnetic field (15 mT, 10 min/day) has proved to inhibit the metastatic spread in the nude mice injected with breast cancer cells, which might be associated with the decrease in volume density of blood vessels (95). Furthermore, the RMF (0.4 T, 7.5 Hz, 2 h) significantly suppressed the metastasis of melanoma and survival time of the mice injected with B16-F19 cells (52). Actin cytoskeleton plays a major role in the process of driving cellular protrusions, such as lamellipodia and filopodia, at the leading edge of the cell, which is necessary for cell migration (96). In the absence of the geomagnetic field, also known as hypomagnetic field environment, the SH-SY5Y neuroblastoma cell adhesion and migration ability were diminished. Geomagnetic field shielding decreased the irregularity and eccentricity of the cell shape; cells maintain a weakened adhesive morphology, thicker, smaller, and rounder, which may be associated with its negative regulation of actin assembly (97).
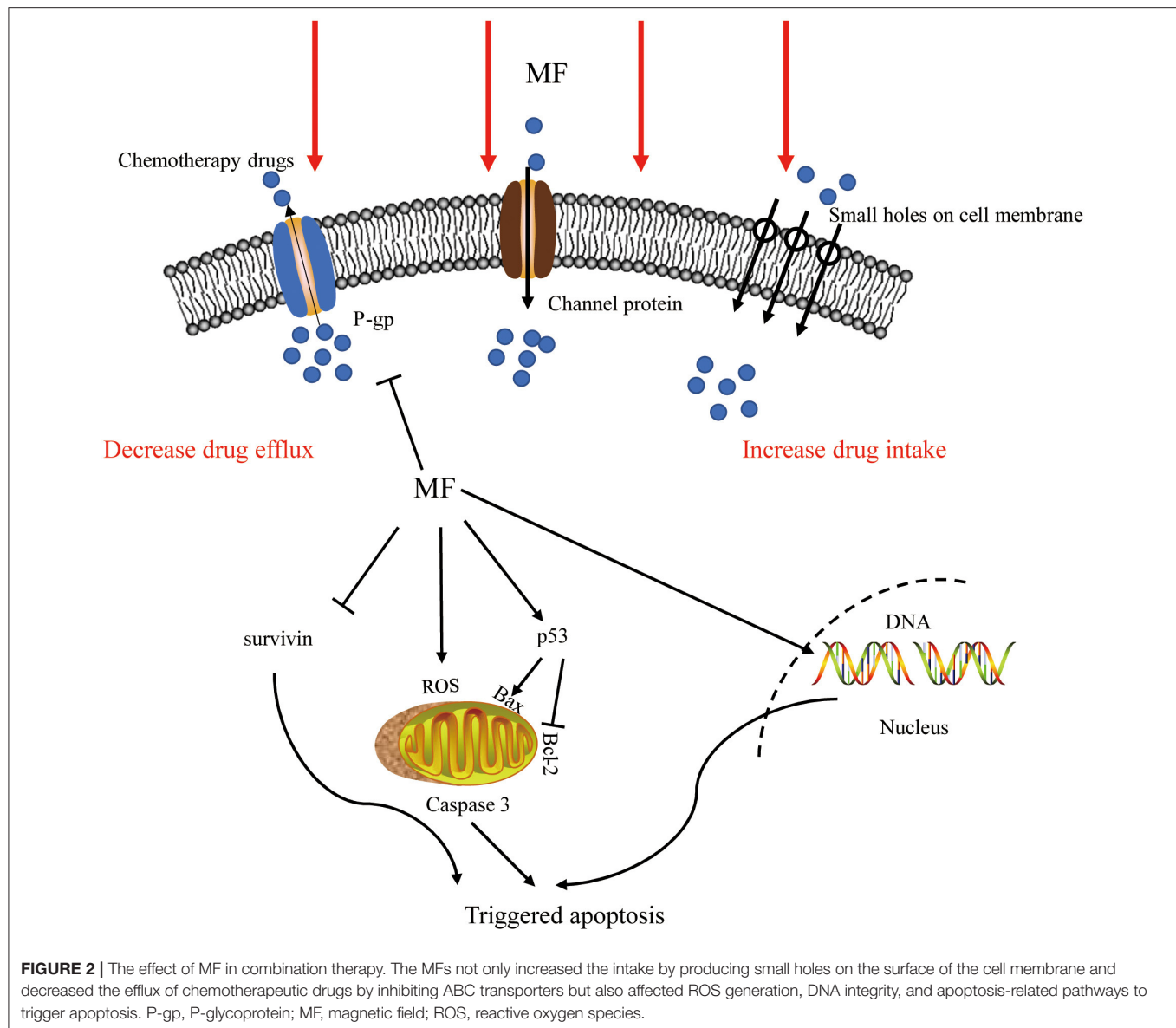
Differentiation

Moreover, the growth rate of tumors is closely related to the degree of tumor differentiation, which is an important reference index in cancer diagnosis and treatment. The LF-MF (5 mT, 50 Hz) was proved to cause an increase in 20% differentiation of hemin-induced K562 cells with a daily exposure of 1 h for 4 days (30). Another study found that the LF-MF (2 mT, 50 Hz, 96 h) exposure decreased the cellular proliferation potential and contributed to the ATRA-treated acute promyelocytic leukemia NB4 cell differentiation that varies with dose, where ROS and extracellular signal-regulated kinase (ERK) signaling pathways may be involved (31). These data suggested that MFs play promising roles as an assistant therapy in combination with other drugs to induce differentiation of leukemia cells. However, only a few studies have focused on the effects of MFs on the differentiation of cancer cells, and the mechanism involved might need a more detailed research.
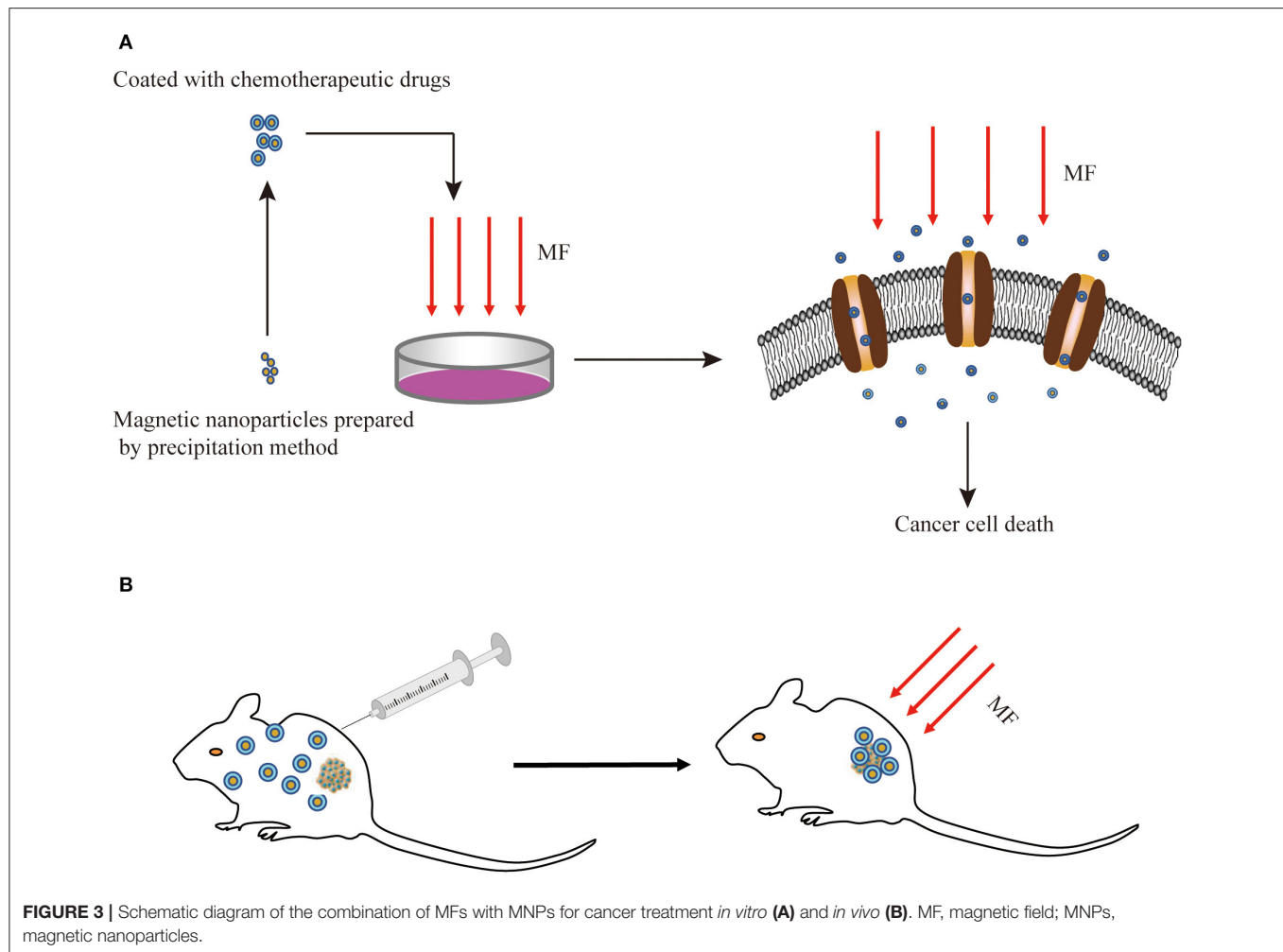
MFS IN COMBINATION THERAPIES

In Combination With Chemotherapy and Other Therapies

Chemotherapy always meets with increased toxicity and side effects caused by high dosage and drug resistance triggered by prolonged treatment, while combination therapy has obvious advantages by avoiding these. The co-treatment of SMF and cisplatin (10 ug/ml) for 12 h substantially suppressed the growth

FIGURE 2 | The effect of MF in combination therapy. The MFs not only increased the intake by producing small holes on the surface of the cell membrane and decreased the efflux of chemotherapeutic drugs by inhibiting ABC transporters but also affected ROS generation, DNA integrity, and apoptosis-related pathways to trigger apoptosis. P-gp, P-glycoprotein; MF, magnetic field; ROS, reactive oxygen species.

of K562 cells and augmented the chemosensitivity to cisplatin. This effect was correlated with the enhanced level of DNA damage and the arrest of the S-phase (27). Exposure to SMF with the intensity of 10 mT for 48 h led to a marked decrease in the viability percentage of cisplatin-treated HeLa cells through ROS accumulation (72). Appropriate SMF therapy increased the sensitivity of ovarian cancer cells, such as A2780 and A2780-CP, to cisplatin depending upon dose and exposure time, *via* producing small holes and large verrucous structures on the surface of the cell membrane (27, 98). The expression of P-glycoprotein is associated with multidrug resistance (MDR) in cancer cells, which is one of the main mechanisms of drug resistance in cancer cells (99). A combination with the SMF (8.8 m T, 12 h) decreased the expression of P-glycoprotein (P-gp) in K562 cancer cells, while adriamycin itself induced an increase (28). PMF (2 mT, 75 Hz, 1 h/day) coupled with temozolomide

could slow down the proliferation of chemo- and radio-resistant T98G glioblastoma cell line by epigenetically affecting the regulation of oncogenes and tumor suppressors (100). The LF-MF (10 mT, 100 Hz, 144 h) promoted the sensitization of human glioblastomata, namely U87 and T98G, to temozolomide, which led to an increased apoptosis rate, with the evidence of increasing the expression of p53 and Bax and decreasing the expression of Bcl-2 and cyclin D1 (54). Capsaicin is the major pungent ingredient of the hot chili peppers, which could bind to distinct cell surface receptors including transient receptor potential vanilloid 1 (TRPV1) ion channel to exert anti-tumor function. An increased apoptosis rate was realized through the mitochondria-dependent apoptosis pathway, and the conformational change of TRPV1 triggered by the SMF (0.5 T, 72 h) might be the reason for this enhancement effect (101). Pre-exposure to 50 Hz LF-MF for 12 h and treatement with 5-fluorouracil (5-FU) for

FIGURE 3 | Schematic diagram of the combination of MFs with MNPs for cancer treatment *in vitro* **(A)** and *in vivo* **(B)**. MF, magnetic field; MNPs, magnetic nanoparticles.

24 h significantly inhibited the proliferation of MCF7 cells. This phenomenon was explained by increased DNA synthesis and upregulated cyclin E and cyclin D1 by the the MF to accumulate cancer cells at the S phase, which was more sensitive to 5-FU (102). The MF also showed a potential to retard tumor growth, elevate survival improvement, and reduce side effects when combined with radiotherapy and bacteriolytic therapy (43, 103). Therefore, the results of these studies support the fact that the MFs can be used as an adjunctive treatment to enhance the effects of chemotherapeutic drugs by increasing the DNA damage, cell apoptosis, and arresting the cell cycle, as summarized in **Figure 2**.

Acting as a Drug Delivery System

Drug delivery systems (DDSs) were developed for targeting active biomolecules at the specific site of infection when treating patients with cancer, to improve the selectivity of the action sites of drugs, eliminate the side effects, and improve treatment efficiency. The MF targeting systems are always applied in combination with magnetic materials and anticancer drugs. Under the function of 100 Hz, 0.7 mT AMF, folic acid-modified magnetic nanoparticles (FA-MNPs) and alpha fetal protein monoclonal antibody-loaded MNPs (ATP-loaded MNPs) selectively induced the apoptosis of cancer cells and elevated the

cellular iron uptake in a dose-dependent manner but had slight toxic effects on healthy cells (104, 105). The growth-inhibitory effects induced by SMFs and RMFs were enhanced by pretreating the cells with MNPs, while regulating the type and parameters of MFs could affect anti-tumor effects (106). The SMF along with low-intensity pulsed ultrasound (LIPUS) plus methotrexate (MT) prevented the growth of cancer cells better than bare drugs and single DDS, without any inhibition on the healthy cells (107). The detailed *in vitro* experiment results were subsequently validated *via in vivo* experiments, and the LIPUS+SMF DDS therapy improved at least 40% of the treatment efficacy, therapy reducing the natural activities of the cancer cells by changing the permeability, the potential of the cell membrane, and ROS generation (108). These results indicate that the MF could act as a DDS to target solid tumors in combination with MNPs to inhibit proliferation (**Figure 3**).

CONCLUSION AND FUTURE PERSPECTIVE

Numerous studies have shown that a wide range of types of MFs could affect the tumor cells at different degrees, while the

dominant effects were associated with thermal or non-thermal mechanisms. The focus of this review is non-thermal effects, which were produced directly by the applied MFs themselves, instead of being produced indirectly as a result of heating. We summarized the performance, namely inhibiting cancer cell proliferation and inducing cell death in *in vitro* and *in vivo* models, of SMFs and LF-MFs in anti-tumor treatments. Also, co-treating with chemotherapy would achieve better therapeutic effects; meanwhile, the MF could serve as a DDS, targeting MNPs to the tumor, and the side effects are within the controllable range. Although various potential mechanisms of MFs against different cancer cell lines have been reported and discussed, few studies were performed on *in vivo* models. At present, most of these studies are confined to *in vitro* studies. Also, relevant clinical trials to test the safety and efficacy of MFs are not available. The limitations in these clinical studies might be due to their controversial roles in *in vitro* and *in vivo* studies, which are affected by some experimental variables such as the frequencies, intensities, or exposure duration of the MFs. Before clinical applications, there is still a demand for systematically exploring. Future studies should aim at finding optimum parameters at which these types of MFs will be most effective. Epidemiological studies have suggested that MFs at 50/60 Hz were also related to the development of depressive state anxiety, metabolic disturbance, poor sleep quality, and locomotor activity. However, according to ICNIRP, there is no sufficient scientific evidence for the association between MF exposure and these effects. Therefore, the most effective MF therapy should be tested further to guarantee its possible investigation in human. As for the MF devices, in consideration of the increasingly available clinical applications, the expectations should be portable and affordable. Future studies are expected to further determine the potential of the MF therapy in oncology.

AUTHOR CONTRIBUTIONS

FUNDING

REFERENCES

1. Bray F, Ferlay J, Soerjomataram I, Siegel RL, Torre LA, Jemal A. Global cancer statistics 2018: GLOBOCAN estimates of incidence and mortality worldwide for 36 cancers in 185 countries. *CA Cancer J Clin.* (2018) 68:394–424. doi: 10.3322/caac.21492

2. Baguley BC. Novel strategies for overcoming multidrug resistance in cancer. *Biodrugs.* (2002) 16:97–103. doi: 10.2165/00063030-200216020-00003

3. Wang J, Seebacher N, Shi H, Kan Q, Duan Z. Novel strategies to prevent the development of multidrug resistance (MDR) in cancer. *Oncotarget.* (2017) 8:84559–71. doi: 10.18632/oncotarget.19187

4. Christian Nicolaj A, Jan A. Genetic variants and normal tissue toxicity after radiotherapy: a systematic review. *Radiother Oncol.* (2009) 92:299–309. doi: 10.1016/j.radonc.2009.06.015

5. Dabrowski JM, Arnaut LG. Photodynamic therapy (PDT) of cancer: from local to systemic treatment. *Photochem Photobiol Sci.* (2015) 14:1765–80. doi: 10.1039/C5PP00132C

6. Zhang H, Liu K, Xue Z, Yin H, Dong H, Jin W, et al. High-voltage pulsed electric field plus photodynamic therapy kills breast cancer cells by triggering apoptosis. *Am J Transl Res.* (2018) 10:334–51.

7. Ibsen S, Schutt CE, Esener S. Microbubble-mediated ultrasound therapy: a review of its potential in cancer treatment. *Drug Des Devel Ther.* (2013) 7:375–88. doi: 10.2147/DDDT.S31564

8. Sengupta S, Balla VK. A review on the use of magnetic fields and ultrasound for non-invasive cancer treatment. *J Adv Res.* (2018) 14:97–111. doi: 10.1016/j.jare.2018.06.003

9. Macdonald IJ, Dougherty TJ. Basic principles of photodynamic therapy. *J Porphyr Phthalocyanines.* (2009) 05:105–29. doi: 10.1002/jpp.328

10. Weber T, Cerilli GJ. Inhibition of tumor growth by the use of non-homogeneous magnetic fields. *Cancer.* (1971) 28:340–3. doi: 10.1002/1097-0142(197108)28:2<340::AID-CNCR2820280213>3.0.CO;2-E

11. Mizushima Y, Akaoka I, Nishida Y. Effects of magnetic field on inflammation. *Experientia.* (1975) 31:1411–2. doi: 10.1007/BF01923216

12. Williams CD, Markov MS. Therapeutic electromagnetic field effects on angiogenesis during tumor growth: a pilot study in mice. *Electro Magnetobiol.* (2001) 20:323–9. doi: 10.1081/JBC-100108573

13. Tofani S, Barone D, Cintorino M, de Santi MM, Ferrara A, Orlassino R, et al. Static and ELF magnetic fields induce tumor growth inhibition and apoptosis. *Bioelectromagnetics.* (2001) 22:419–28. doi: 10.1002/bem.69

14. Mulay IL, Mulay LN. Effect of a magnetic field on sarcoma 37 ascites tumour cells. *Nature.* (1961) 190:1019. doi: 10.1038/1901019a0

15. Degen IL. Treatment of traumatic edema by a magnetic field. *J Trauma.* (1971) 11:979. doi: 10.1097/00005373-197111000-00015

16. Chakkalakal D, Mollner T Mr, Fritz E, Novak J, Mcguire M. Magnetic field induced inhibition of human osteosarcoma cells treated with adriamycin. *Canc Biochem Biophys.* (1999) 17:89–98.

17. Vasishta VG. Sequentially programmed magnetic field therapy in the management of recurrent anaplastic astrocytoma: a case report and literature review. *Case Rep Oncol.* (2010) 3:189–94. doi: 10.1159/000316358

18. Radeva M, Berg H. Differences in lethality between cancer cells and human lymphocytes caused by LF-electromagnetic fields. *Bioelectromagnetics.* (2004) 25:503. doi: 10.1002/bem.20023

19. Hisamitsu T, Narita K, Kasahara T, Seto A, Yu Y, Asano K. Induction of apoptosis in human leukemic cells by magnetic fields. *Jpn J Physiol.* (1997) 47:307–10. doi: 10.2170/jjphysiol.47.307

20. Suszyński K, Marcol W, Szajkowski S, Pietrucha-Dutczak M, Cieślar G, Sieroń A, et al. Variable spatial magnetic field influences peripheral nerves regeneration in rats. *Electromagn Biol Med.* (2014). doi: 10.3109/15368378.2013.801351

21. Ding S, Peng H, Fang HS, Zhou JL, Wang Z. Pulsed electromagnetic fields stimulation prevents steroid-induced osteonecrosis in rats. *BMC Musculoskelet Disord.* (2011) 12:215. doi: 10.1186/1471-2474-12-215

22. Manjhi J, Kumar S, Behari J, Mathur R. Effect of extremely low frequency magnetic field in prevention of spinal cord injury-induced osteoporosis. *J Rehabil Res Dev.* (2013) 50:17–30. doi: 10.1682/JRRD.2011.12.0248

23. Israel M, Zaryabova V, Ivanova M. Electromagnetic field occupational exposure: non-thermal vs. thermal effects. *Electromagnetic Biol Med.* (2013) 32:145–54. doi: 10.3109/15368378.2013.776349

24. Yang P, Hu L, Zhe W, Chong D, Wei Z, Qian A, et al. Inhibitory effects of moderate static magnetic field on leukemia. *IEEE Trans Magn.* (2009) 45:2136–9. doi: 10.1109/TMAG.2009.2012703

25. Gellrich D, Becker S, Strieth S. Static magnetic fields increase tumor microvessel leakiness and improve antitumoral efficacy in combination with paclitaxel. *Cancer Lett.* (2014) 343:107–14. doi: 10.1016/j.canlet.2013.09.021

26. Tian X, Wang D, Zha M, Yang X, Ji X, Zhang L, et al. Magnetic field direction differentially impacts the growth of different cell types. *Electromagn Biol Med.* (2018) 37:114–25. doi: 10.1080/15368378.2018.1458627

27. Chen WF, Qi H, Sun RG, Liu Y, Zhang K, Liu JQ. Static magnetic fields enhanced the potency of cisplatin on k562 cells. *Cancer Biother Radiopharm.* (2010) 25:401–8. doi: 10.1089/cbr.2009.0743

28. Hao Q, Wenfang C, Xia A, Qiang W, Ying L, Kun Z, et al. Effects of a moderate-intensity static magnetic field and adriamycin on K562 cells. *Bioelectromagnetics.* (2011) 32:191–9. doi: 10.1002/bem.20625

29. Sun RG, Chen WF, Qi H, Zhang K, Bu T, Liu Y, et al. Biologic effects of SMF and paclitaxel on K562 human leukemia cells. *Gen Physiol Biophys.* (2012) 31:1–10. doi: 10.4149/gpb_2012_002

30. Ayse IG, Zafer A, Sule O, Isil IT, Kalkan T. Differentiation of K562 cells under ELF-EMF applied at different time courses. *Electromagn Biol Med.* (2010) 29:122–30. doi: 10.3109/15368378.2010.502451

31. Errico Provenzano A, Amatori S, Nasoni MG, Persico G, Russo S, Mastrogiacomo AR, et al. Effects of fifty-hertz electromagnetic fields on granulocytic differentiation of atra-treated acute promyelocytic leukemia nb4 cells. *Cell Physiol Biochem.* (2018) 46:389–400. doi: 10.1159/000488473

32. Martino CF, Portelli L, McCabe K, Hernandez M, Barnes F. Reduction of the Earth's magnetic field inhibits growth rates of model cancer cell lines. *Bioelectromagnetics.* (2010) 31:649–55. doi: 10.1002/bem.20606

33. Destefanis M, Viano M, Leo C, Gervino G, Ponzetto A, Silvagno F. Extremely low frequency electromagnetic fields affect proliferation and mitochondrial activity of human cancer cell lines. *Int J Radiat Biol.* (2015) 91:964–72. doi: 10.3109/09553002.2015.1101648

34. Wang T, Nie Y, Zhao S, Han Y, Du Y, Hou Y. Involvement of midkine expression in the inhibitory effects of low-frequency magnetic fields on cancer cells. *Bioelectromagnetics.* (2011) 32:443–52. doi: 10.1002/bem.20654

35. Crocetti S, Beyer C, Schade G, Egli M, Frohlich J, Franco-Obregon A. Low intensity and frequency pulsed electromagnetic fields selectively impair breast cancer cell viability. *PLoS ONE.* (2013) 8:e72944. doi: 10.1371/journal.pone.0072944

36. Zhang L, Ji X, Yang X, Zhang X. Cell type- and density-dependent effect of 1 T static magnetic field on cell proliferation. *Oncotarget.* (2017) 8:13126–41. doi: 10.18632/oncotarget.14480

37. Marzieh M, Javad B, Khadijeh S. The synergic effects of *Crocus Sativus L.* and low frequency electromagnetic field on VEGFR2 gene expression in human breast cancer cells. *Avicenna J Med Biotechnol.* (2014) 6:123–7.

38. Buckner CA, Buckner AL, Koren SA, Persinger MA, Lafrenie RM. Inhibition of cancer cell growth by exposure to a specific time-varying electromagnetic field involves T-type calcium channels. *PLoS ONE.* (2015) 10:e0124136. doi: 10.1371/journal.pone.0124136

39. Filipovic N, Djukic T, Radovic M, Cvetkovic D, Curcic M, Markovic S, et al. Electromagnetic field investigation on different cancer cell lines. *Cancer Cell Int.* (2014) 14:84. doi: 10.1186/s12935-014-0084-x

40. Buckner CA, Buckner AL, Koren SA, Persinger MA, Lafrenie RM. Exposure to a specific time-varying electromagnetic field inhibits cell proliferation via cAMP and ERK signaling in cancer cells. *Bioelectromagnetics.* (2018) 39:217–30. doi: 10.1002/bem.22096

41. Ren J, Ding L, Xu Q, Shi G, Li X, Li X, et al. LF-MF inhibits iron metabolism and suppresses lung cancer through activation of P53-miR-34a-E2F1/E2F3 pathway. *Sci Rep.* (2017) 7:749. doi: 10.1038/s41598-017-00913-2

42. Novikov VV, Novikov GV, Fesenko EE. Effect of weak combined static and extremely low-frequency alternating magnetic fields on tumor growth in mice inoculated with the Ehrlich ascites carcinoma. *Bioelectromagnetics.* (2009) 30:343–51. doi: 10.1002/bem.20487

43. Ali FM, El-Gebaly RH, Hamad AM. Combination of bacteriolytic therapy with magnetic field for Ehrlich tumour treatment. *Gen Physiol Biophys.* (2017) 36:259–71. doi: 10.4149/gpb_2016051

44. Chen Z, Liu H, Wang H, Wu C, Feng H, Han J. Effect of low-frequency rotary magnetic fields on advanced gastric cancer: Survival and palliation of general symptoms. *J Cancer Res Ther.* (2018) 14:815–9. doi: 10.4103/jcrt.JCRT_991_17

45. Foster KR. Thermal and non-thermal mechanisms of interaction of radio-frequency energy with biological systems. *IEEE Trans Plasma Sci.* (2000) 28:15–23. doi: 10.1109/27.842819

46. Zakaria Z, Rahim RA, Lee PY, Mansor MSB, Muji SZM. Review on interaction between electromagnetic field and biological tissues. *Sens Transducers.* (2012) 143:60–70.

47. Engstrom S. Physical mechanisms of non-thermal extremely-low-frequency magnetic-field effects. *Ursi Radio Sci Bull.* (2004) 77:95–106. doi: 10.23919/URSIRSB.2004.7909638

48. Golovin YI, Klyachko NL, Majouga AG, Sokolsky M, Kabanov AV. Theranostic multimodal potential of magnetic nanoparticles actuated by non-heating low frequency magnetic field in the new-generation nanomedicine. *J Nanopart Res.* (2017) 19:63. doi: 10.1007/s11051-017-3746-5

49. Yuan LQ, Wang C, Zhu K, Li HM, Gu WZ, Zhou DM, et al. The antitumor effect of static and extremely low frequency magnetic fields against nephroblastoma and neuroblastoma. *Bioelectromagnetics.* (2018) 39:375–85. doi: 10.1002/bem.22124

50. Fan Z, Hu P, Xiang L, Liu Y, Lu T. A static magnetic field inhibits the migration and telomerase function of mouse breast cancer cells. *BioMed Res Int.* (2020) 2020:1–9. doi: 10.1155/2020/7472618

51. Zhang L, Yang X, Liu J, Luo Y, Li Z, Ji X, et al. 1T moderate intensity static magnetic field affects Akt/mTOR pathway and increases the antitumor efficacy of mTOR inhibitors in CNE-2Z cells. *Sci Bull.* (2015) 60:2120–8. doi: 10.1007/s11434-015-0950-5

52. Nie Y, Du L, Mou Y, Xu Z, Weng L, Du Y, et al. Effect of low frequency magnetic fields on melanoma: tumor inhibition and immune modulation. *BMC Cancer.* (2013) 13:582. doi: 10.1186/1471-2407-13-582

53. Ahmadianpour MR, Abdolmaleki P, Mowla SJ, Hosseinkhani S. Static magnetic field of 6 mT induces apoptosis and alters cell cycle in p53 mutant Jurkat cells. *Electromagn Biol Med.* (2013) 32:9–19. doi: 10.3109/15368378.2012.692748

54. Akbarnejad Z, Eskandary H, Dini L, Vergallo C, Nematollahi-Mahani SN, Farsinejad A, et al. Cytotoxicity of temozolomide on human glioblastoma cells is enhanced by the concomitant exposure to an extremely low-frequency electromagnetic field (100Hz, 100G). *Biomed Pharmacother.* (2017) 92:254–64. doi: 10.1016/j.biopha.2017.05.050

55. Wang Z, Yang P, Xu H, Qian A, Hu L, Shang P. Inhibitory effects of a gradient static magnetic field on normal angiogenesis. *Bioelectromagnetics.* (2009) 30:446–53. doi: 10.1002/bem.20501

56. Buckner CA, Buckner AL, Koren SA, Persinger MA, Lafrenie RM. The effects of electromagnetic fields on B16-BL6 cells are dependent on their spatial and temporal character. *Bioelectromagnetics.* (2017) 38:165–74. doi: 10.1002/bem.22031

57. Vincenzi F, Targa M, Corciulo C, Gessi S, Merighi S, Setti S, et al. The anti-tumor effect of A3 adenosine receptors is potentiated by pulsed electromagnetic fields in cultured neural cancer cells. *PLoS ONE.* (2012) 7:e39317. doi: 10.1371/journal.pone.0039317

58. Otto T, Sicinski P. Cell cycle proteins as promising targets in cancer therapy. *Nat Rev Cancer.* (2017) 17:93–115. doi: 10.1038/nrc.2016.138

59. Cheung-Ong K, Giaever G, Nislow C. DNA-damaging agents in cancer chemotherapy: serendipity and chemical biology. *Chem Biol.* (2013) 20:648–59. doi: 10.1016/j.chembiol.2013.04.007

60. Liu B, Liu L, Zang A, Song Z, Yang H, Wang Z, et al. Tanshinone IIA inhibits proliferation and induces apoptosis of human nasopharyngeal carcinoma cells via p53-cyclin B1/CDC2. *Oncol Lett.* (2019) 18:3317–22. doi: 10.3892/ol.2019.10658

61. Kim SC, Im W, Shim JY, Kim SK, Kim BJ. Static magnetic field controls cell cycle in cultured human glioblastoma cells. *Cytotechnology.* (2016) 68:2745–51. doi: 10.1007/s10616-016-9973-2

62. Canman CE, Wolff AC, Chen CY, Fornace AJ, Kastan MB. The p53-dependent G1 cell cycle checkpoint pathway and ataxia-telangiectasia. *Cancer Res.* (1994) 54:5054–8.

63. Marcantonio P, Del Re B, Franceschini A, Capri M, Lukas S, Bersani F, et al. Synergic effect of retinoic acid and extremely low frequency magnetic field exposure on human neuroblastoma cell line BE(2)C. *Bioelectromagnetics.* (2010) 31:425–33. doi: 10.1002/bem.20581

64. Luukkonen J, Hoyto A, Sokka M, Liimatainen A, Syvaoja J, Juutilainen J, et al. Modification of p21 level and cell cycle distribution by 50 Hz magnetic fields in human SH-SY5Y neuroblastoma cells. *Int J Radiat Biol.* (2017) 93:240–8. doi: 10.1080/09553002.2017.1235298

65. Mohammad RM, Muqbil I, Lowe L, Yedjou C, Hsu HY, Lin LT, et al. Broad targeting of resistance to apoptosis in cancer. *Semin Cancer Biol.* (2015) 35:S78–103. doi: 10.1016/j.semcancer.2015.03.001

66. Reubold TF, Eschenburg S. A molecular view on signal transduction by the apoptosome. *Cell Signal.* (2012) 24:1420–5. doi: 10.1016/j.cellsig.2012.03.007

67. Adrain C, Martin SJ. The mitochondrial apoptosome: a killer unleashed by the cytochrome seas. *Trends Biochem Sci.* (2001) 26:390–7. doi: 10.1016/S0968-0004(01)01844-8

68. Liam P, Grant N, Caitlin C, Matthew G, Greenwood MT. Anti-apoptosis and cell survival: a review. *Biochim Biophys Acta.* (2011) 1813:238–59. doi: 10.1016/j.bbamcr.2010.10.010

69. Jae-Kyun K, Kyoung-Han C, Zui P, Peihui L, Noah W, Chul-Woo K, et al. The tail-anchoring domain of Bfl1 and HCCS1 targets mitochondrial membrane permeability to induce apoptosis. *J Cell Sci.* (2007) 120(Pt. 16):2912–23. doi: 10.1242/jcs.006197

70. Simon HU, Haj-Yehia A, Levi-Schaffer F. Role of reactive oxygen species (ROS) in apoptosis induction. *Apoptosis.* (2000) 5:415–8. doi: 10.1023/A:1009616228304

71. Storch K, Dickreuter E, Artati A, Adamski J, Cordes N. BEMER electromagnetic field therapy reduces cancer cell radioresistance by enhanced ROS formation and induced DNA damage. *PLoS ONE.* (2016) 11:e0167931. doi: 10.1371/journal.pone.0167931

72. Kamalipooya S, Abdolmaleki P, Salemi Z, Javani Jouni F, Zafari J, Soleimani H. Simultaneous application of cisplatin and static magnetic field enhances oxidative stress in HeLa cell line. *In Vitro Cell Dev Biol Anim.* (2017) 53:783–90. doi: 10.1007/s11626-017-0148-z

73. Koh EK, Ryu BK, Jeong DY, Bang IS, Nam MH, Chae KS. A 60-Hz sinusoidal magnetic field induces apoptosis of prostate cancer cells through reactive oxygen species. *Int J Radiat Biol.* (2008) 84:945–55. doi: 10.1080/09553000802460206

74. Roos WP, Bernd K. DNA damage-induced cell death by apoptosis. *Trends Mol Med.* (2006) 12:440–50. doi: 10.1016/j.molmed.2006.07.007

75. Elisabetta C. Fine-tuning the ubiquitin code at DNA double-strand breaks: deubiquitinating enzymes at work. *Front Genet.* (2015) 6:282. doi: 10.3389/fgene.2015.00282

76. Kim J, Ha CS, Lee HJ, Song K. Repetitive exposure to a 60-Hz time-varying magnetic field induces DNA double-strand breaks and apoptosis in human cells. *Biochem Biophys Res Commun.* (2010) 400:739–44. doi: 10.1016/j.bbrc.2010.08.140

77. Lei H, Xu Y, Guan R, Li M, Hui Y, Gao Z, et al. Effect of gyromagnetic fields on human prostatic adenocarcinoma cells. *Onco Targets Ther.* (2015) 8:3489–97. doi: 10.2147/OTT.S95306

78. Yasuko K, Takao K, Raymond S, Seiji K. The role of autophagy in cancer development and response to therapy. *Nat Rev Cancer.* (2005) 5:726–34. doi: 10.1038/nrc1692

79. Boone BA, Zeh HJ III, Bahary N. Autophagy inhibition in pancreatic adenocarcinoma. *Clin Colorectal Cancer.* (2018) 17:25–31. doi: 10.1016/j.clcc.2017.10.013

80. Yu Y, Cao L, Yang L, Kang R, Lotze M, Tang D. microRNA 30A promotes autophagy in response to cancer therapy. *Autophagy.* (2012) 8:853–5. doi: 10.4161/auto.20053

81. Xu Y, Wang Y, Yao A, Xu Z, Dou H, Shen S, et al. Low frequency magnetic fields induce autophagy-associated cell death in lung cancer through miR-486-mediated inhibition of Akt/mTOR signaling pathway. *Sci Rep.* (2017) 7:11776. doi: 10.1038/s41598-017-10407-w

82. Nie Y, Chen Y, Mou Y, Weng L, Xu Z, Du Y, et al. Low frequency magnetic fields enhance antitumor immune response against mouse H22 hepatocellular carcinoma. *PLoS ONE.* (2013) 8:e72411. doi: 10.1371/journal.pone.0072411

83. Novoselova EG, Novikov VV, Lunin SM, Glushkova OV, Novoselova TV, Parfenyuk SB, et al. Effects of low-level combined static and weak low-frequency alternating magnetic fields on cytokine production

84. Zaalberg A, Moradi Tuchayi S, Ameri AH, Ngo KH, Cunningham TJ, Eliane JP, et al. Chronic inflammation promotes skin carcinogenesis in cancer-prone discoid lupus erythematosus. *J Invest Dermatol.* (2019) 139:62–70. doi: 10.1016/j.jid.2018.06.185

85. Demb J, Wei EK, Izano M, Kritchevsky S, Swede H, Newman AB, et al. Chronic inflammation and risk of lung cancer in older adults in the health, aging and body composition cohort study. *J Geriatr Oncol.* (2019) 10:265–71. doi: 10.1016/j.jgo.2018.07.008

86. Ross CL, Harrison BS. Effect of pulsed electromagnetic field on inflammatory pathway markers in RAW 264.7 murine macrophages. *J Inflamm Res.* (2013) 6:45–51. doi: 10.2147/JIR.S40269

87. Vergallo C, Dini L, Szamosvolgyi Z, Tenuzzo BA, Carata E, Panzarini E, et al. *In vitro* analysis of the anti-inflammatory effect of inhomogeneous static magnetic field-exposure on human macrophages and lymphocytes. *PLoS ONE.* (2013) 8:e72374. doi: 10.1371/journal.pone.0072374

88. Vincenzi F, Ravani A, Pasquini S, Merighi S, Gessi S, Setti S, et al. Pulsed electromagnetic field exposure reduces hypoxia and inflammation damage in neuron-like and microglial cells. *J Cell Physiol.* (2016) 232:1200–8. doi: 10.1002/jcp.25606

89. Shen LK, Huang HM, Yang PC, Huang YK, Wang PD, Leung TK, et al. A static magnetic field attenuates lipopolysaccharide-induced neuro-inflammatory response via IL-6-mediated pathway. *Electromagn Biol Med.* (2014) 33:132–8. doi: 10.3109/15368378.2013.794734

90. Harlozinska A. Progress in molecular mechanisms of tumor metastasis and angiogenesis. *Anticancer Res.* (2005) 25:3327–33.

91. Ferrara N, Gerber HJ. The biology of VEGF and its receptors. *Nat Med.* (2003) 9:669–76. doi: 10.1038/nm0603-669

92. Strelczyk D, Eichhorn ME, Luedemann S, Brix G, Dellian M, Berghaus A, et al. Static magnetic fields impair angiogenesis and growth of solid tumors *in vivo*. *Cancer Biol Ther.* (2014) 8:1756–62. doi: 10.4161/cbt.8.18.9294

93. Delle Monache S, Angelucci A, Sanita P, Iorio R, Bennato F, Mancini F, et al. Inhibition of angiogenesis mediated by extremely low-frequency magnetic fields (ELF-MFs). *PLoS ONE.* (2013) 8:e79309. doi: 10.1371/journal.pone.0079309

94. Cameron IL, Markov MS, Hardman WE. Optimization of a therapeutic electromagnetic field (EMF) to retard breast cancer tumor growth and vascularity. *Cancer cell Int.* (2014) 14:1–10. doi: 10.1186/s12935-014-0125-5

95. Cameron IL, Sun LZ, Short N, Hardman WE, Williams CD. Therapeutic electromagnetic field (TEMF) and gamma irradiation on human breast cancer xenograft growth, angiogenesis and metastasis. *Cancer Cell Int.* (2005) 5:23. doi: 10.1186/1475-2867-5-23

96. Le CC, Carlier MF. Regulation of actin assembly associated with protrusion and adhesion in cell migration. *Physiol Rev.* (2008) 88:489–513. doi: 10.1152/physrev.00021.2007

97. Mo WC, Zhang ZJ, Wang DL, Liu Y, Bartlett PF, He RQ. Shielding of the geomagnetic field alters actin assembly and inhibits cell motility in human neuroblastoma cells. *Sci Rep.* (2016) 6:22624. doi: 10.1038/srep32055

98. Jalali A, Zafari J, Jouni FJ, Abdolmaleki P, Shirazi FH, Khodayar MJ. Combination of static magnetic field and cisplatin in order to reduce drug resistance in cancer cell lines. *Int J Radiat Biol.* (2019) 95:1194–201. doi: 10.1080/09553002.2019.1589012

99. Zhang K, Chen W, Bu T, Qi H, Sun R, He X. Decreased P-glycoprotein is associated with the inhibitory effects of static magnetic fields and cisplatin on K562 cells. *Bioelectromagnetics.* (2014) 35:437–43. doi: 10.1002/bem.21863

100. Pasi F, Fassina L, Mognaschi ME, Lupo G, Corbella F, Nano R, et al. Pulsed electromagnetic field with temozolomide can elicit an epigenetic pro-apoptotic effect on glioblastoma T98G cells. *Anticancer Res.* (2016) 36:5821–6. doi: 10.21873/anticanres.11166

101. Chen WT, Lin GB, Lin SH, Lu CH, Hsieh CH, Ma BL, et al. Static magnetic field enhances the anticancer efficacy of capsaicin

on HepG2 cells via capsaicin receptor TRPV1. *PLoS ONE.* (2018) 13:e0191078. doi: 10.1371/journal.pone.0191078

102. Han Q, Chen R, Wang F, Chen S, Sun X, Guan X, et al. Pre-exposure to 50 Hz-electromagnetic fields enhanced the antiproliferative efficacy of 5-fluorouracil in breast cancer MCF-7 cells. *PLoS ONE.* (2018) 13:e0192888. doi: 10.1371/journal.pone.0192888

103. Wen J, Jiang S, Chen B. The effect of 100 Hz magnetic field combined with X-ray on hepatoma-implanted mice. *Bioelectromagnetics.* (2011) 32:322–4. doi: 10.1002/bem.20646

104. Wen J, Jiang S, Chen Z, Zhao W, Yi Y, Yang R, et al. Apoptosis selectively induced in BEL-7402 cells by folic acid-modified magnetic nanoparticles combined with 100 Hz magnetic field. *Int J Nanomed.* (2014) 9:2043–50. doi: 10.2147/IJN.S60457

105. Ju H, Cui Y, Chen Z, Fu Q, Sun M, Zhou Y. Effects of combined delivery of extremely low frequency electromagnetic field and magnetic Fe_3O_4 nanoparticles on hepatic cell lines. *Am J Transl Res.* (2016) 8:1838–47.

106. Spyridopoulou K, Makridis A, Maniotis N, Karypidou N, Myrovali E, Samaras T, et al. Effect of low frequency magnetic fields on the growth of MNP-treated HT29 colon cancer cells. *Nanotechnology.* (2018) 29:175101. doi: 10.1088/1361-6528/aaaea9

107. Sengupta S, Khatua C, Balla VK. *In vitro* carcinoma treatment using magnetic nanocarriers under ultrasound and magnetic fields. *ACS Omega.* (2018) 3:5459–69. doi: 10.1021/acsomega.8b00105

108. Sengupta S, Khatua C, Jana A, Balla VK. Use of ultrasound with magnetic field for enhanced *in vitro* drug delivery in colon cancer treatment. *J Mater Res.* (2018) 33:625–37. doi: 10.1557/jmr.2018.43

Inhibition of HSP90 as a Strategy to Radiosensitize Glioblastoma: Targeting the DNA Damage Response and Beyond

Michael Orth[1], Valerie Albrecht[1], Karin Seidl[1], Linda Kinzel[1], Kristian Unger[2], Julia Hess[2], Lisa Kreutzer[2], Na Sun[3], Benjamin Stegen[1,4,5], Alexander Nieto[1], Jessica Maas[1], Nicolas Winssinger[6], Anna A. Friedl[1], Axel K. Walch[3], Claus Belka[1,4,7], Horst Zitzelsberger[2,7], Maximilian Niyazi[1] and Kirsten Lauber[1,4,7]*

[1] Department of Radiation Oncology, University Hospital, LMU Munich, Munich, Germany, [2] Research Unit Radiation Cytogenetics, Helmholtz Center Munich, German Research Center for Environmental Health GmbH, Neuherberg, Germany, [3] Research Unit Analytical Pathology, Helmholtz Center Munich, German Research Center for Environmental Health GmbH, Neuherberg, Germany, [4] German Cancer Consortium, Munich, Germany, [5] German Cancer Research Center, Heidelberg, Germany, [6] Department of Organic Chemistry, NCCR Chemical Biology, University of Geneva, Geneva, Switzerland, [7] Clinical Cooperation Group Personalized Radiotherapy in Head and Neck Cancer, Helmholtz Center Munich, Neuherberg, Germany

Radiotherapy is an essential component of multi-modality treatment of glioblastoma (GBM). However, treatment failure and recurrence are frequent and give rise to the dismal prognosis of this aggressive type of primary brain tumor. A high level of inherent treatment resistance is considered to be the major underlying reason, stemming from constantly activated DNA damage response (DDR) mechanisms as a consequence of oncogene overexpression, persistent replicative stress, and other so far unknown reasons. The molecular chaperone heat shock protein 90 (HSP90) plays an important role in the establishment and maintenance of treatment resistance, since it crucially assists the folding and stabilization of various DDR regulators. Accordingly, inhibition of HSP90 represents a multi-target strategy to interfere with DDR function and to sensitize cancer cells to radiotherapy. Using NW457, a pochoxime-based HSP90 inhibitor with favorable brain pharmacokinetic profile, we show here that HSP90 inhibition at low concentrations with *per se* limited cytotoxicity leads to downregulation of various DNA damage response factors on the protein level, distinct transcriptomic alterations, impaired DNA damage repair, and reduced clonogenic survival in response to ionizing irradiation in glioblastoma cells *in vitro*. *In vivo*, HSP90 inhibition by NW457 improved the therapeutic outcome of fractionated CBCT-based irradiation in an orthotopic, syngeneic GBM mouse model, both in terms of tumor progression and survival. Nevertheless, in view of the promising *in vitro* results the *in vivo* efficacy was not as strong as expected, although apart from the radiosensitizing effects HSP90 inhibition also reduced irradiation-induced GBM cell migration and tumor invasiveness. Hence, our findings identify the combination of HSP90 inhibition and radiotherapy in principle as a promising strategy for GBM treatment whose performance needs to be further optimized by improved inhibitor substances, better formulations and/or administration routes, and fine-tuned treatment sequences.

Keywords: HSP90 inhibition, HSP90i, NW457, radiosensitization, glioblastoma, radiotherapy, hypermigration

INTRODUCTION

Glioblastoma (GBM) is the most aggressive type of primary brain tumor with a highly dismal prognosis and a 5-year overall survival of less than 5% (1). Standard treatment involves maximal safe resection—if possible—followed by radio(chemo)therapy, and maintenance chemotherapy according to the EORTC/NCIC protocol (2–5). However, treatment failure and recurrence are frequent, and the major underlying reason appears to be the high level of inherent resistance against both chemo- and radiotherapy which represents a central hallmark of this cancer entity (6–9). Moreover, recent data indicate that the degree of radioresistance further increases during therapy—particularly when radiotherapy is applied in classically fractionated regimens (10, 11). Adaptive processes and an overt upregulation of the DNA damage response (DDR) have been reported to be crucial driving forces in this scenario (12–16). Since alternative fractionation regimens of radiotherapy have not shown relevant improvements (17–19), and recurrence frequently occurs within the irradiated volume (20), the question arises if biological targeting of the DDR can contribute to break GBM radiation resistance. Intriguingly, the DDR relies on high molecular weight proteins and multi-protein complexes which essentially require folding assistance and stabilization by chaperones, such as heat shock protein 90 (HSP90) (21–23). Thus, HSP90 actively contributes to radio- and chemoresistance of GBM and other cancer cells and represents an attractive target for biologically targeted radiosensitization, because HSP90 inhibition (HSP90i) —at least in principle—can affect multiple DDR pathways simultaneously (24–26). This was the focus of the present study for which we made use of the pochoxime-based, second generation HSP90 inhibitor NW457 with documented radiosensitizing potential in other cancer entities (27–32). We observed that diverse DDR regulators are overexpressed in human GBM cells and that their protein levels decrease upon HSP90i at low nanomolar doses which *per se* exhibited only limited cytotoxicity. In HSP90i-treated GBM cells, DNA damage repair was clearly impaired translating into significantly reduced clonogenic survival upon irradiation *in vitro*. *In vivo*, HSP90i augmented the therapeutic efficacy of fractionated, conebeam CT (CBCT)-based irradiation in an orthotopic GBM mouse model, although less potently than expected. Interestingly, the invasive morphology of radiotherapy-treated tumors was reverted by additional HSP90i, and *in vitro* migration analyses confirmed that HSP90i does reduce irradiation-induced GBM hypermigration.

MATERIALS AND METHODS

Cell Lines and Reagents

The human GBM cell lines LN229 and T98G were obtained from ATCC (Manassas, VA, USA) and were cultured in Dulbecco's Modified Eagle medium (DMEM), supplemented with 10% heat-inactivated fetal calf serum, 100 U/ml penicillin, and 0.1 mg/ml streptomycin (all from ThermoScientific, Schwerte, Germany) at 37°C and 7.5% CO_2. The murine GBM cell line GL261 was obtained from the National Cancer Institute (NCI, Bethesda, MD,

U.S.A.) and was cultured under same conditions. All cell lines were screened to be free from mycoplasma infection, and identity of human cell lines was confirmed by short tandem repeat (STR) typing (service provided by DSMZ, Braunschweig, Germany).

The HSP90 inhibitor NW457 (*epi*-pochoxime F) was previously described (27–31). For *in vitro* experiments, a 10 mM stock solution was prepared in DMSO (Sigma-Aldrich, Taufkirchen, Germany) and was further diluted to 100 μM with DMSO before final concentrations were adjusted in cell culture medium. Respective amounts of DMSO served as controls. For *in vivo* purposes, NW457 was dissolved at 100 mg/ml in DMSO and was further diluted in 0.9% NaCl (37°C), supplemented with 5% Tween-20 (all from Sigma-Aldrich). The vehicle formulation was used as control.

X-Ray Treatment *In Vitro*

Irradiation of cells was done with an RS225 X-ray tube (200 kV and 10 mA, Thoreaus filter, 1 Gy in 63 s, Xstrahl, Camberley, Great Britain) as described (30).

Quantitative Real-Time PCR (qRT-PCR)

Profiling of mRNA expression levels was performed by quantitative realtime RT-PCR as described (32). Briefly, total RNA was extracted from cells by NucleoSpin RNA II extraction kit (Macherey & Nagel, Dueren, Germany). 500 ng of isolated RNA were mixed with 5 μM random hexamers, 5 μM Oligo(dT)$_{18}$, 500 μM dNTPs, 1 U/μl Ribolock RNase inhibitor, and 10 units/μl RevertAid transcriptase (all from ThermoScientific) and subjected to reverse transcription. Twenty nanograms of cDNA were employed for Realtime PCR runs with 300 nM primers in 1x Maxima SYBR Green qPCR Mastermix (ThermoScientific) on an LC480 qPCR platform (Roche Applied Science, Penzberg, Germany). Primer sequences are listed in **Supplementary Table 1**. Relative quantification was performed by the $\delta\delta C_T$ method. Results were normalized to a matrix of reference genes comprising 18S rRNA, δ-Aminolaevulinate-synthase (ALAS), and β2-Microglobulin (B2M) and calibrated to the relative expression levels measured in primary human astrocytes (BioCat, Heidelberg, Germany). Three replicates were analyzed per cell line, and heatmaps were generated using the matrix visualization software Morpheus (https://software.broadinstitute.org/morpheus).

Clonogenic Survival Assay

Clonogenic survival was assessed by colony formation assays as described before (30, 33). In brief, cells were detached by Trypsin/EDTA (ThermoScientific), counted with a Neubauer counting chamber, and seeded as single cell suspensions at defined numbers anticipating 20–100 colonies per well depending on the different irradiation doses into 6-well plates. Adherence was allowed for 4 h. LN229 and T98G cells were treated with 10 nM NW457 or DMSO for 24 h, irradiated, and incubated in the presence of 10 nM NW457 for 13 d. GL261 cells were treated in a similar fashion, except that NW457 was removed by medium exchange after the 24 h of pre-incubation. Colonies were stained with methylene blue (dissolved at 0.3% in 80% ethanol, both from Merck, Darmstadt, Germany), and all colonies containing more than 50 cells were counted under a Stemi 305 stereomicroscope

(Carl Zeiss, Oberkochen, Germany). The percentages of surviving cells were determined and calibrated to the corresponding plating efficiencies. Regression was performed according to the linear-quadratic model.

Viability Assay

Viability was determined by Alamar Blue assays (BioRad, Puchheim, Germany) as described (30). Briefly, 5,000 cells were seeded into 96-well plates, adherence was allowed for 4 h, and cells were treated with NW457 at the indicated doses. Upon incubation for 24–96 h, medium was replaced by fresh medium supplemented with 1/10 volume of Alamar Blue reagent, and Resazurin conversion was allowed at 37°C and 7.5% CO_2 for 2–6 h. Resorufin fluorescence was measured on a Synergy Mx microplate reader platform (BioTek, Bad Friedrichshall, Germany), and results were calibrated to untreated controls.

Quantitative Fluorescence Microscopy

DNA damage repair was examined by immunofluorescence staining of phosphorylated histone variant H2AX (γH2AX) and p53-binding protein 1 (53BP1), followed by quantitative fluorescence microscopy as described (32). Cells were seeded into 24-well plates supplemented with coverslips, allowed to adhere overnight, and treated with 10 nM NW457 or DMSO for 24 h before being irradiated at 2 Gy. At the indicated time points, cells were fixed with 3.7% isotonic paraformaldehyde (Merck), containing 0.1% Triton X-100 (v/v Sigma-Aldrich) for 10 min before being permeabilized with 0.5% isotonic Triton X-100 for 5 min. Unspecific binding sites were blocked with 3% isotonic bovine serum albumin (w/v, Sigma-Aldrich) and 0.1% Triton X-100 at 4°C overnight. Cells were stained with monoclonal mouse anti-γH2AX (Merck Millipore) and polyclonal rabbit anti-53BP1 (Bio-Techne, Wiesbaden, Germany) antibodies diluted in 3% isotonic bovine serum albumin and 0.1% Triton X-100 for 2 h at room temperature. After extensive washing with PBS plus 0.1% Triton X-100, cells were stained with Alexa488-coupled goat-anti-mouse IgG and Alexa568-coupled goat-anti-rabbit IgG (both from ThermoScientific) for 1 h. DNA was stained with 2 µg/ml Hoechst 33342 (Sigma Aldrich) for 10 min. Upon several washing steps with PBS plus 0.1% Triton X-100, coverslips were mounted with 4 µl mounting medium (Sigma-Aldrich) onto object slides. Microscopic analysis was performed with a Zeiss AxioObserver Z1 inverted microscope, equipped with an LCI Plan-Neofluar 63x/1.3 glycerol objective, an AxioCam MR Rev3 camera, and ZEN 2.3 software (all from Carl Zeiss). For image acquisition, 31 z-stacks with 250 nm interstack distance were captured, and deconvolution was performed with ZEN 2.3 software. For quantification of DNA damage repair, γH2AX/53BP1 double-positive foci were used. At least 20 nuclei of non-deformed morphology were selected for each condition, and foci were counted by hand. Results are depicted as individual data points with superimposed means and 95% confidence intervals.

Live-Cell Microscopy of Cell Death Morphology

For live-cell imaging, a Zeiss AxioObserver Z1 inverted microscope, equipped with an AxioCam MR Rev3 camera, an XL multi S1 incubation chamber, and a PS1 compact heating unit (both from Pecon, Erbach, Germany) was used. Briefly, cells were seeded into Ibidi µ-slides (Ibidi GmbH, Martinsried, Germany) and allowed to adhere for 4 h before treatment with 10 nM NW457 or DMSO for 24 h and irradiation at 4 Gy. Live-cell imaging was initiated 1 h after irradiation and performed over 12 d. Images were captured in 12 min intervals, and movies were processed with Fiji software.

Wound Healing Assay

Migration of GBM cells was assessed by wound healing assays. Cells were seeded into Ibidi µ-slides supplemented with culture inserts (both from Ibidi) and allowed to adhere overnight. Cells were treated with 30 nM NW457 or DMSO for 24 h, irradiated at 3 Gy, and live-cell imaging was performed for 12 h. Images were captured in intervals of 3 min, and cell migration was analyzed using the manual tracking plugin tool (ImageJ) as previously described (31, 34). Migration was quantified in form of colonized area (four regions of interest per condition in three independent experiments) and accumulated distance per cell over time (at least 25 randomly picked cells per condition).

SDS-PAGE and Western Blot

Reducing gradient SDS-PAGE and western blot analyses of whole cell lysates (20–400 µg total protein per lane) were performed as described before (30, 35). Briefly, cells were lysed in lysis buffer (50 mM Tris-HCl pH 7.6, 150 mM NaCl, 1% Triton X-100 (v/v) (all from Sigma Aldrich), 1 x EDTA-free protease inhibitor cocktail (Roche)), protein concentrations were measured by Bradford assay (BioRad, Feldkirchen, Germany), and 20 - or 400 µg of total protein were subjected to gradient (4–15% or 6–15%) SDS-PAGE. Proteins were transferred onto PVDF Immobilon FL membranes (Merck Millipore), membranes were blocked with 5% low-fat milk powder (Carl Roth, Karlsruhe, Germany), dissolved in TBST buffer ((13 mM Tris-HCl pH 7.5, 150 mM NaCl, 0.02% Triton X-100 (v/v)), and incubated with primary antibodies at 4°C overnight. Primary antibodies used for western blot analyses were: Rabbit-anti-ATM, rabbit anti-ATR, rabbit-anti-FANCA, mouse-anti-RAD51 (Merck Millipore), mouse-anti-CHK1, mouse-anti-Vinculin, mouse-anti-α-tubulin (Sigma-Aldrich), rabbit-anti-KU70, rabbit-anti-XRCC3, rabbit-anti-MGMT (Biozol, Eching, Germany), mouse-anti-CHK2, mouse-anti-B-Raf (BD Transduction Laboratories, Heidelberg, Germany), rabbit-anti-RPA1, rabbit-anti-RBBP8 (Biomol, Hamburg, Germany), rabbit-anti-KU80, rabbit-anti-DNA2 (Thermo Scientific), rabbit-anti-p53 (Cell Signaling, Leiden, Netherlands), rabbit-anti-DNA-PKcs (Abcam, Berlin, Germany), mouse-anti-NHEJ1 (Santa Cruz, Heidelberg, Germany), rabbit-anti-LIG4 (Origene, Herford, Germany), and mouse-anti-HSP70 (BD Biosciences). Upon washing with TBST, membranes were incubated with IRDye800-conjugated secondary antibodies (LI-COR Biosciences, Bad Homburg, Germany) for 1 h at room temperature. Measurements and quantifications of IR800 dye fluorescence were performed with an ODYSSEY scanner (LI-COR Biosciences, Bad Homburg, Germany). Relative signal intensities were normalized to a matrix of vinculin and α-tubulin, calibrated to the untreated controls, and heatmaps were

visualized using the matrix visualization software Morpheus (https://software.broadinstitute.org/morpheus).

Transcriptome Analysis Via RNA Sequencing

Transcriptome profiling was performed by 3'-RNA sequencing. Prior to sequencing, RNA integrity was assessed using the Agilent Bioanalyzer RNA 6000 Nano Kit (Agilent Technologies, Waldbronn, Germany) by calculating the percentage of fragments > 200 nucleotides (DV200). Sequencing libraries were prepared with 100 ng total RNA using the QuantSeq 3'-RNA-Seq Library Prep Kit FWD for Illumina (Lexogen GmbH, Vienna, Austria) according to the manufacturer's instructions for single-indexing and good RNA quality. For library amplification, PCR cycles were determined using the PCR Add-on Kit for Illumina (Lexogen), and the individual libraries were amplified with 17 PCR cycles. Quantity and quality of sequencing libraries were assessed using the Quanti-iT PicoGreen dsDNA Assay Kit (ThermoScientific) and the Bioanalyzer High Sensitivity DNA Analysis Kit (Agilent Technologies). Libraries were sequenced in 150 bp paired-end mode on a HiSeq4000 sequencer (Illumina, Berlin, Germany). The pool of individually barcoded libraries was distributed across the lanes of the same flow-cell aiming for approximately ten million paired-end reads per sample.

For sequence data processing, adapter sequences were removed using BBDUk (https://jgi.doe.gov/data-and-tools/bbtools). Human fastq-files including forward-reads were subjected to alignment against the human genome reference genome (GRCh38) using STAR (36). Aligned reads were quantified *via* htseq-count employing appropriate transcriptome gtf-files (37). FastQC was utilized for analyzing quality of unaligned and aligned reads (https://www.bioinformatics.babraham.ac.uk/projects/fastqc/) followed by summarization *via* multiQC (https://multiqc.info). Genes with a raw read count (for the whole dataset) smaller than five times the total number of samples were excluded. Correlation heatmaps were employed to analyze data consistency and technical outlier detection, and shrinked (apeglm) log2 expression values were determined (38). Calculation of differentially expressed genes and geneset enrichment analyses (GSEAs) were performed on the basis of log2 expression values (39). Reactome functional interaction (FI) networks were constructed and analyzed in Cytoscape (40, 41). iRegulon was employed to identify potential transcriptional regulators (42).

Orthotopic Mouse Glioblastoma Model and Contrast-Enhanced, Conebeam CT-Based, Fractionated Radiotherapy

All animal experiments were performed in accordance with the FELASA guidelines and upon ethical approval by the *Regierung von Oberbayern*. Female C57BL/6 mice were obtained from Charles River (Sulzfeld, Germany), and housed in groups of maximally four animals in individually ventilated cages (GM500, Tecniplast, Hohenpeißenberg, Germany) in a specified, pathogen-free animal facility with a 12 h day/night cycle. Standard rodent feed (from Ssniff, Soest, Germany) and water were provided *ad libitum*. Animals were inspected on a daily

basis and sacrificed when reaching pre-defined health scores. Criteria for immediate sacrifice comprised the following: Strongly altered hygiene behavior, flattened breathing, body weight loss of ≥ 20%, ulcerating wounds, epileptic seizures or spasms, paralysis of extremities, bloody diarrhea, apathy, hunchbacked posture, self-mutilation, isolation from the group. In milder occurrence of these criteria, mice were sacrificed within 48 h. Intracranial implantation of GL261 cells was performed as described recently (43). Briefly, mice were medicated with 200 μg/g metamizol (WDT, Garbsen, Germany) and anesthetized by intraperitoneal injection of 100 μg/g ketamine and 10 μg/g xylazine (both from WDT). Mouse heads were mounted onto a stereotaxic frame (David Instruments, Tujanga, CA, USA), skulls were exposed by longitudinal skin incision, and a hole was drilled 1.5 mm laterally (right) and 1 mm anteriorly to the bregma using a pair of 23G and 21G microlances (BD Biosciences). Then, 90,000 GL261 cells (in 1 μl PBS) were slowly injected into the right striatum, using a stereotactically guided syringe (Hamilton, Bonaduz, Switzerland). Once the syringe was withdrawn, skin was closed with Ethibond Excel 5-0 suture material (Ethicon, Norderstedt, Germany), and mice were monitored until regaining consciousness. Starting at d7 after implantation, tumor growth was monitored by contrast-enhanced, conebeam computed tomography (CBCT) scans twice weekly using the small animal radiation research platform (SARRP, X-Strahl, Camberley, Great Britain) (44). For acquisition of CBCT scans, 360 projection images were captured (1° per image, x-ray tube settings: 60 kV, 0.8 mA, 1.0 mm aluminium filter). To enhance the contrast of soft tissue, 300 μl Imeron-300 (Bracco, Konstanz, Germany) were administered intravenously before CBCT scanning. Irradiation was performed at a weekdaily fractionation regimen of 2 Gy (2× 5× 2 Gy in total) with two contralateral beams (gantry positions − 90° and 90°) and 3× 9 mm^2 collimation (fixed nozzle, x-ray tube settings: 220 kV, 13 mA, 0.15mm copper filter) on d7-11 and d14–18. Isocenters were aligned to the centers of contrast enriching volumes, and treatment planning was executed with Muriplan software (X-Strahl). NW457 was administered intraperitoneally at 10 μg/g or 50 μg/g 24 h before irradiation. Tumor volumes were determined by Lx Wx H measurements of the 3 longest orthogonal axes as described (43), and 3D reconstructions were generated in 3D-Slicer (www.slicer.org/).

Histological Analyses

For histological analyses, mice were anesthetized by intraperitoneal injection of 50 μg/g pentobarbital (WDT), followed by cardial perfusion with 3.5% paraformaldehyde (Sigma-Aldrich) as described (43). Then, brains were explanted and fixed with 3.5% paraformaldehyde for 48 h at 4°C. Brains were dehydrated for 48 h in 30% sucrose (Sigma-Aldrich), embedded in NEG-50 frozen section medium (ThermoScientific) and stored until analysis at −80°C. Slices of 40 μm thickness were prepared with a Microm HM355S microtom (ThermoScientific), stored in cryopreserving solution (200 mM Na$_2$HPO$_4$, 200 mM KH$_2$PO$_4$, 25% ethylenglycol (v/v), 25% glycerol (v/v) (all from Sigma Aldrich)) at −20°C, before being stained with Mayer's hematoxylin and eosin (both from Merck) for 1 min each. After dehydration in 70, 96, and 100% ethanol, and xylene, slices were mounted onto microscope slides

using Entellan (Merck). Microscopic analysis was performed on an AxioLab A.1 microscope, equipped with an AxioCam Erc5s camera and AxioVision 4.9 software (all from Carl Zeiss).

Statistical Analyses

Statistical analyses were performed using OriginPro 9.1 software (OriginLab Ltd., Northhampton, MA, USA). Results are shown as individual data points of all replicates, means ± s.d., or means ± 95% confidence intervals as indicated. For group comparisons, two-sided Student's *t*-tests or ANOVAs (one-way or two-way) were employed as indicated. Survival analyses were performed according to Kaplan-Meier with log-rank testing.

RESULTS

HSP90 Inhibition by NW457 Leads to Downregulation of DNA Damage Response Factors on the Protein Level, Impaired DNA Damage Repair, and Reduced Clonogenic Survival in Response to Ionizing Irradiation in Glioblastoma Cells

A high degree of inherent radioresistance belongs to the signature hallmarks of GBM (6, 8). On the molecular level, GBM radioresistance is considered to derive from constantly activated DNA damage response (DDR) mechanisms driven by the overexpression of oncogenes, persistent replicative stress, and other so far unknown reasons (45, 46). Previous studies have shown that HSP90 plays an important role in DDR function *via* its crucial involvement in folding and stabilizing DDR proteins and/or multi-protein complexes (21, 22). Accordingly, the present study was designed to examine whether HSP90 inhibition (HSP90i) can efficiently sensitize experimental model systems of GBM to ionizing irradiation *in vitro* and *in vivo* as a multi-target approach of pharmacological interference with the DDR (26, 47, 48). For our study, we made use of two human and one mouse GBM cell line with distinct alterations in the loci of TP53, MGMT, CDKN2A, PTEN, and IDH1/2 as described for primary GBM (**Table 1**) (51, 52). Initial qRT-PCR profiling confirmed that the human GBM cell lines LN229 and T98G show a broad-range upregulation of diverse DDR regulators as compared to normal human astrocytes suggesting that DDR activity is indeed increased—irrespective of the O6-methylguanine-DNA-methyltransferase (MGMT) status (**Figure 1A** and **Supplementary Figure 1A**) (53). The highest levels of overexpression were detected for the replication and DDR-associated nucleases FEN1 and EXO1, members of the DNA double-strand break (DSB) detecting MRN complex (MRE11 and NBN), the DNA helicases BLM and PALB2, the single-strand binding protein RPA1, and members of the XRCC family which are involved in non-homologous end joining (XRCC4 and XRCC6) and alternative non-homologous end joining (XRCC1).

We then tested whether HSP90i can interfere with DDR overexpression and treated the cells with NW457, a pochxime-derived HSP90 inhibitor with documented radiosensitizing potential and improved pharmacokinetic profile (27–30, 32).

TABLE 1 | Characteristics of the GBM cell lines used in the present study.

Cell Line	LN229	T98G	GL261
Species	Human	Human	Mouse
Sex	Female	Male	No Y chromosome detectable
Age	60 years	61 years	–
MGMT status	Promoter methylated, mRNA not detectable	Promoter not methylated, mRNA detectable	mRNA weakly detectable
IDH1/2 status	Wildtype	Wildtype	Wildtype
TP53 status	P98L mutation Function unclear	M237I mutation Dominant negative	R153P mutation Dominant negative
CDKN2A status	Null	Null	Null
PTEN status	Wildtype	L42R	Wildtype

Data were compiled from Ishii et al. (49), Cellosaurus (50), ATCC, and own unpublished data.

Time course westernblot analyses of diverse DDR proteins revealed different clusters of responses in LN229 and T98G cells with several common motifs (**Figure 1B**). Whereas the protein levels of few individual DDR regulators, such as NBN and RBBP8, increased upon HSP90i by NW457, clearly more candidates were downregulated, including a core cluster of CHK1, RAD51, and DNA2 with a particularly strong decrease in protein levels. Other downregulated DDR proteins comprised NHEJ1, KU80, XRCC3, ATR, CHK2, LIG4, and RPA1, and for some candidates mixed responses were observed. Our findings confirm and complement previous reports showing the critical dependence of certain DDR regulators on HSP90 chaperoning function (54–56). However, our data disclose also several DDR factors with so far unknown HSP90 dependence, including DNA2, an end resecting DNase with important functions in replication and DSB repair (57–60), and NHEJ1, a scaffold protein that binds to and assists DNA ligase 4 (LIG4) in DSB repair (61). Overall, HSP90i affected proteins of various DDR pathways – at least in the GBM cell lines used in our study – thereby providing a strong rationale for combined modality approaches of HSP90i and radiotherapy. Importantly, downregulation of DDR proteins occurred already at very low concentrations of NW457 (10 nM) which *per se* exhibited only marginal cytotoxicity even during prolonged treatment—a characteristic which is of special interest for potential future clinical translation (**Supplementary Figure 1B**). These findings confirm the notion that DDR regulators, compared to other HSP90 client proteins, are particularly sensitive towards HSP90i (22).

In order to examine the consequences of HSP90i on DDR function, LN229 and T98G cells were pre-treated with NW457 for 24 h, irradiated at 2 Gy, and subjected to immunofluorescence staining for phosphorylated histone H2AX (γH2AX) and 53BP1. The kinetics of DNA damage foci formation and clearance was quantitatively analyzed (**Figures 1C, D**). HSP90i by NW457 resulted in significantly delayed clearance of γH2AX/53BP1 double-positive foci, indicating that DNA repair was obviously impaired. HSP90i also increased the overall numbers of foci as compared to the controls. This could either be due to false repair of irradiation-induced DNA damages, or irradiation-independent formation of damage sites. So far, our data show that HSP90i by

FIGURE 1 | HSP90i by NW457 leads to downregulation of DNA damage response factors, impaired DNA damage repair, and reduced clonogenic survival in response to ionizing irradiation in human glioblastoma cells. **(A)** Transcriptomic profiling of regulators of the DNA damage response (DDR) in LN229 and T98G cells. mRNA expression levels were determined by qRT-PCR, normalized to a matrix of 3 reference genes (18S rRNA, δ-amino-laevulinate-synthase, and β2-microglobulin), and calibrated to the results of untransformed human astrocytes. For both cell lines, three replicates were analyzed and are displayed as x-fold log2-values. **(B)** Time course analysis of DDR regulator protein expression in LN229 and T98G cells upon HSP90i by 10 nM NW457. Arrowheads indicate the bands that were used for quantification. Protein levels were normalized to a matrix comprising vinculin and α-tubulin and are depicted as x-fold log2-values compared to the 0 h controls. **(C)** Immunofluorescence microscopy of γH2AX and 53BP1 DNA damage repair foci in LN229 and T98G cells upon irradiation at 2 Gy ± HSP90i by NW457. Cells were treated with NW457 (10 nM) or DMSO for 24 h, irradiated, and fixed at the indicated times. Cells were stained for γH2AX, 53BP1, and DNA and subjected to deconvolution immunofluorescence microscopy. Scale bar depicts 10 μm. **(D)** Quantification of DNA damage repair kinetics from **(C)**. γH2AX and 53BP1 double-positive foci in at least 20 randomly picked nuclei were counted by hand. Individual data points with superimposed means ± 95% confidence intervals are displayed, and overall curve comparison was performed by two-way ANOVA. **(E)** Clonogenic survival of LN229 and T98G cells upon irradiation at 0–8 Gy ± HSP90i by NW457. Cells were pre-treated with 10 nM NW457 or DMSO for 24 h followed by irradiation at the indicated doses, and colony formation was allowed for 13 d ± continuous NW457 treatment. Individual data points of 4 independent experiments are shown, linear-quadratic regression lines are superimposed, and overall curve comparison was performed by two-way ANOVA.

low concentrations of NW457 leads to destabilization of DDR regulators in various pathways and reduced DNA damage repair capacity. In consequence, the question arises whether this also translates into reduced clonogenic survival of GBM cells upon irradiation. To this end, LN229 and T98G cells were pre-treated with NW457 for 24 h, irradiated at 0–8 Gy, and clonogenic survival

was analyzed after 13 d incubation in the presence of NW457. As suggested by its marginal cytotoxicity (**Supplementary Figure 1B**), the effect of HSP90i monotherapy on clonogenic survival was modest in LN229 cells. In T98G cells it was clearly stronger, and for both cell lines this was statistically significant (**Supplementary Figure 1C**). Importantly, HSP90i by NW457 significantly reduced

the clonogenic survival upon irradiation in both cell lines (**Figure 1E**), confirming our hypothesis that multi-target interference with DDR function by HSP90i at *per se* non-toxic doses suffices to sensitize resistant GBM cells to irradiation. Similar findings were very recently reported for other cancer entities (62, 63). Morphologically, the mode of cell death underlying reduced clonogenic survival upon HSP90i plus radiation was a highly disruptive, necrotic one which occurred after several rounds of aberrant mitosis and intermediate states of highly aneuploid cells with multiple and/or giant nuclei (**Supplementary Movie File 1**) (64).

HSP90 Inhibition by NW457 Stimulates a Compensatory Transcriptional Upregulation of Genes Involved in Protein Production Accompanied by Downregulation of Genes Engaged in Survival Signaling, Cell Stemness, and Integrin Signaling

Our results suggest—at first sight—that sensitization to radiotherapy upon HSP90i by NW457 derives from the downregulation of crucial DDR mediators on the protein level. Certainly, the immediate consequences of HSP90i affect the post-translational level where abortive chaperoning leads to proteasomal degradation of HSP90 client proteins (65). Nevertheless, it is feasible to assume that this broad-range protein catabolic remodeling can also stimulate complex responses on the transcriptome level which may contribute to radiosensitization as well. In order to address this question, we performed RNA sequencing analyses upon HSP90i by NW457 (10 nM) in LN229 and T98G cells. Differential gene expression analysis revealed an overt transcriptomic response in LN229 cells, and an attenuated but still detectable response in T98G cells (**Supplementary Figure 2A**). The overlap in up- or downregulated genes was rather small (**Supplementary Figure 2B**), possibly pointing towards a regulatory involvement of p53 (T98G have dominant negative p53^{M237I}, LN229 carry p53^{P98L} with unclear functionality but intact DNA binding domain, see **Table 1** and **Supplementary Table 2**). Construction of a functional interaction (FI) network of the upregulated intersect genes revealed a clear activation of the heat shock response, comprising many chaperones and members of the heat shock protein family (**Supplementary Figure 2C**). This FI network appeared to be predominantly controlled by heat shock factor 1 (HSF1) as suggested by iRegulon analysis (**Supplementary Figure 2D**). For the common downregulated genes shared by LN229 and T98G cells, a smaller FI network was constructed, basically comprising elements of DNA repair, mitosis regulation, NOTCH signaling, and protein folding (**Supplementary Figure 2E**). iRegulon analysis suggested a rather heterogenous pattern of transcriptional regulators, including EP300, JUND, BCL3, and others (**Supplementary Figure 2F**).

Further geneset enrichment analysis (GSEA) of the transcriptomic alterations in LN229 cells upon HSP90i revealed positive enrichment of distinct MSigDB hallmark genesets comprising targets of MYC and E2F, as well as regulators of the G2/M cell cycle checkpoint (**Supplementary Figure 3A**). The FI

network of the compiled leading edge genes allowed the conclusion that this was in principle a compensatory response to HSP90i treatment, because interaction clusters representing basic functions of RNA polymerase II transcription, mRNA processing and splicing, RNA transport, translation initiation, protein folding, rRNA processing, and ribosome biogenesis were identified. Moreover, clusters involved in cell cycle regulation (G2/M transition, G1/S transition, and mitosis) and DNA repair were observed among the leading edge genes. Without prior GSEA, the FI network of all significantly upregulated genes showed additional interaction clusters of transcription factor activation (AP1, GR, and p53), focal adhesion and organization of the extracellular matrix (ECM), the heat shock response, and signaling by small GTPases (RAS, RAP1, and RHO) (**Supplementary Table 2**).

In terms of transcriptional downregulation upon HSP90i, no significantly enriched MSigDB hallmark genesets (FDR < 0.1) were observed in LN229 cells. However, on the level of significantly downregulated individual genes FI network construction revealed several interaction clusters whose decreased expression may contribute to radiosensitization by HPS90i. As such, clusters involved in survival signaling (EGFR and IGF1 signaling, PI3K/AKT/mTOR signaling) and maintenance of cell stemness (NOTCH signaling) represent potential candidates, as well as clusters orchestrating integrin signaling, ECM receptor interaction, and ECM organization (**Supplementary Table 3**).

HSP90 Inhibition by NW457 Improves the Efficacy of Fractionated Radiotherapy in an Orthotopic, Syngeneic GBM Mouse Model

In the next step, we examined the performance of HSP90i plus radiotherapy *in vivo*. We made use of a syngeneic orthotopic mouse GBM transplantation model with *i.p.* injection of an *in vivo* NW457 formulation and contrast-enhanced, conebeam (CB)CT-based, fractionated radiotherapy (43) (**Figure 2**). Importantly, we first recapitulated the basic *in vitro* experiments with GL261 cells, the murine cell line that was used for transplantation. This cell line showed a particularly strong downregulation of DDR proteins upon HSP90i (**Supplementary Figures 4A, B**) and did not tolerate permanent NW457 incubation in colony formation assays so that NW457 needed to be removed after the 24 h pre-incubation time (**Supplementary Figures 4C, D**). Nevertheless, this treatment was already sufficient to facilitate radiosensitization of GL261 cells which have been described to exhibit particularly high levels of intrinsic treatment resistance (66).

Upon transplantation of GL261 cells into the right hemispheres of C57BL/6 mice, tumor progression was monitored by contrast-enhanced CBCT scans over time (**Figure 2A**). Starting at d7 after implantation, mice were subjected to CBCT-guided, fractionated radiotherapy with 2× 5× 2 Gy using two contralateral beams at 3× 9 mm^2 collimation (**Figure 2B**), and NW457 (or the vehicle control) was administered 24 h before each radiation treatment (10 or 50 μg/g *i.p.*). Tumor growth follow-up was accomplished by serial contrast-enhanced CBCT scans, and animals were sacrificed when reaching the pre-defined humane endpoints. Of note, d7 CBCT scans confirmed that tumor volumes were statistically not

significantly different across different treatment groups at the start of therapy (**Supplementary Figure 5A**).

Overall, the treatment was tolerated well, and no significant differences in body weight in response to the treatment were observed (**Supplementary Figure 5B**). Tumors of vehicle-treated animals grew exponentially, and monotherapy with HSP90i delayed tumor growth only marginally (**Figure 2C**). Fractionated radiotherapy exerted strong inhibitory effects on tumor growth, but responses were rather heterogeneous among the animals in this group. Additional HSP90i delayed tumor growth even further—yet compared to the effects observed *in vitro*, the *in vivo* performance was not as strong as expected. These findings basically mirrored the Kaplan-Meier survival analyses (**Figure 2D**). HSP90i in mono-agent settings had only minor impact on animal survival, although this reached statistical significance compared to the vehicle controls at 50 μg/g NW457. Upon radiotherapy alone, animals revealed clearly prolonged survival, albeit again with heterogenous responses. Survival times were further increased by additional HSP90i, although to a rather limited, yet statistically significant extent in case of 50 μg/g NW457. Interestingly, two animals of

the combined modality group (radiotherapy + 50 μ/g NW457) showed full tumor remission translating into persistent survival until the end of the experiment (**Supplementary Figure 5C**). In summary, these data indicate that HSP90i by NW457 can complement and improve the efficacy of fractionated radiotherapy in the used GBM *in vivo* model. Nevertheless, since the effects observed *in vitro* clearly outcompete the performance *in vivo*, further optimization of HSP90 inhibitor substances and/or treatment sequences would be needed.

HSP90i by NW457 Attenuates Irradiation-Induced Hypermigration and Invasiveness of GBM Cells *In Vitro* and *In Vivo*

Several previous studies have shown that non-lethal irradiation results in accelerated GBM cell migration—a phenomenon with implications for relapse and treatment failure (67, 68). We therefore examined, whether HSP90i by low-dose NW457 treatment does interfere with GBM cell migration. LN229 cells were treated with NW457 for 24 h, irradiated at 3 Gy, and their migratory behavior was analyzed in wound healing setups by
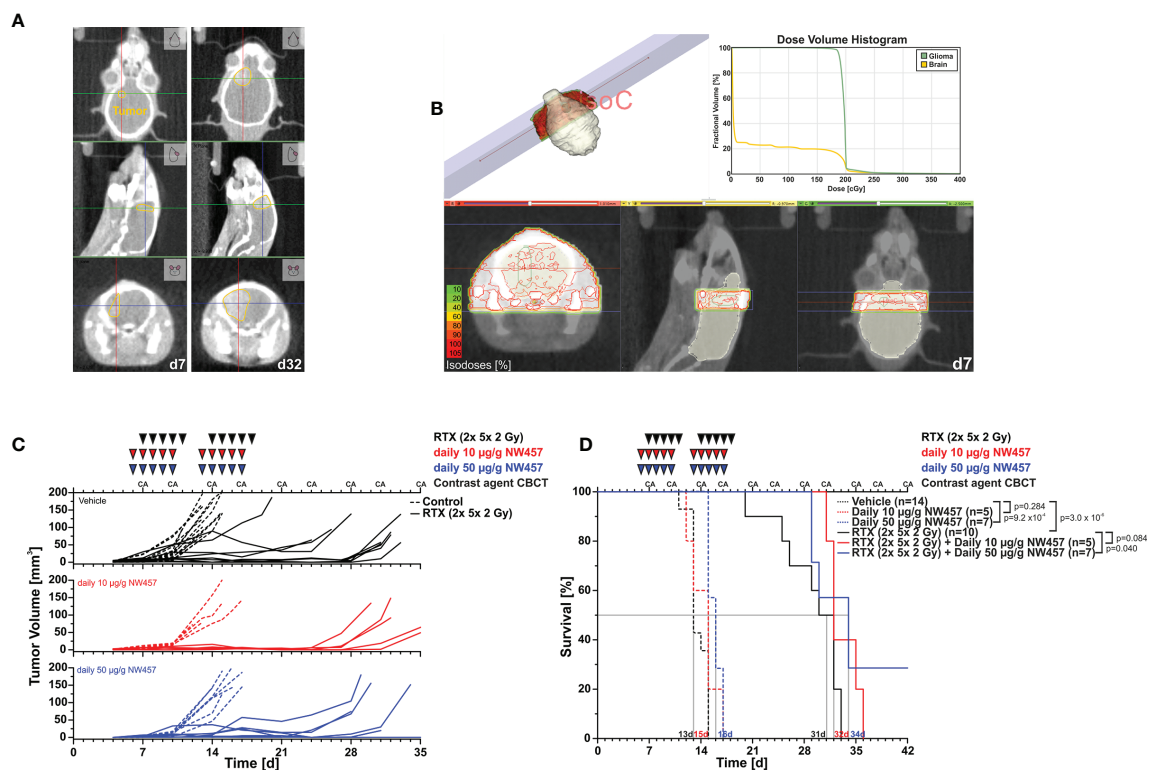
FIGURE 2 | HSP90i by NW457 improves the efficacy of fractionated radiotherapy in an orthotopic, syngeneic GBM mouse model. *In vivo* performance of NW457-mediated HSP90i in combination with fractionated radiotherapy in orthotopically transplanted GL261 tumors. **(A)** Tumor localization and growth monitoring of orthotopically implanted GL261 cells in C57BL/6 mice were performed by contrast-enhanced CBCT scans and manual contouring. **(B)** Treatment plan and dose volume histogram. Two contralateral beams with 3× 9 mm² collimation were used to administer 2× 5× 2 Gy. **(C)** Treatment schedule and tumor growth curves. Six days after orthotopic transplantation, mice were randomized into 6 groups (vehicle, 10 μg/g NW457, 50 μg/g NW457, 2× 5× 2 Gy + vehicle, 2× 5× 2 Gy + 10 μg/g NW457, 2× 5× 2 Gy + 50 μg/g NW457), and treatment was administered according to the indicated schedule. **(D)** Kaplan-Meier survival analysis of all treatment groups. Tumor-specific death was scored when mice showed pre-defined symptoms. p-values were obtained by log-rank test.

live-cell imaging (**Figure 3A** and **Supplementary Movies File 2**). Migration was quantitated by the colonized area and the accumulated distance per cell over time as determined by tracking of at least 25 randomly picked cells per condition (**Figures 3B–D**). With both approaches, the basal migratory activity of LN229 cells was observed to be significantly increased by radiation at 3 Gy, and this was almost completely reversed by pre-treatment with NW457. Thus, HSP90i, in addition to its radiosensitizing potential, does also efficiently counteract irradiation-induced hypermigration of GBM cells. In order to test whether this also holds true *in vivo*, we characterized the morphology of the tumors from our *in vivo* experiments. The aspect ratios of L axes (cranial-caudal, 90° to beam axes) and W axes (left-right, 0° to beam axes) were determined in contrast-enhanced CBCT scans of all mice at the day of sacrifice, and exemplary 3D reconstructions were generated (**Figures 4A–C**). Tumors of mice from the radiotherapy-only group showed significantly distorted aspect ratios and caudal-cranially stretched 3D reconstructions, implying tumor progress orthogonally to the irradiation field. This effect was fully reversed by additional NW457 treatment. Histologically, tumors from irradiated mice revealed clearly more invasive borders than tumors from vehicle or NW457-only-treated mice, and also more and larger areas of hemorrhage (**Figure 4D**). Intriguingly, this morphotype was also fully reversed upon co-treatment with NW457, indicating that HSP90i does not only improve the therapeutic efficacy of radiotherapy but also counteracts GBM cell migration and tumor invasiveness in
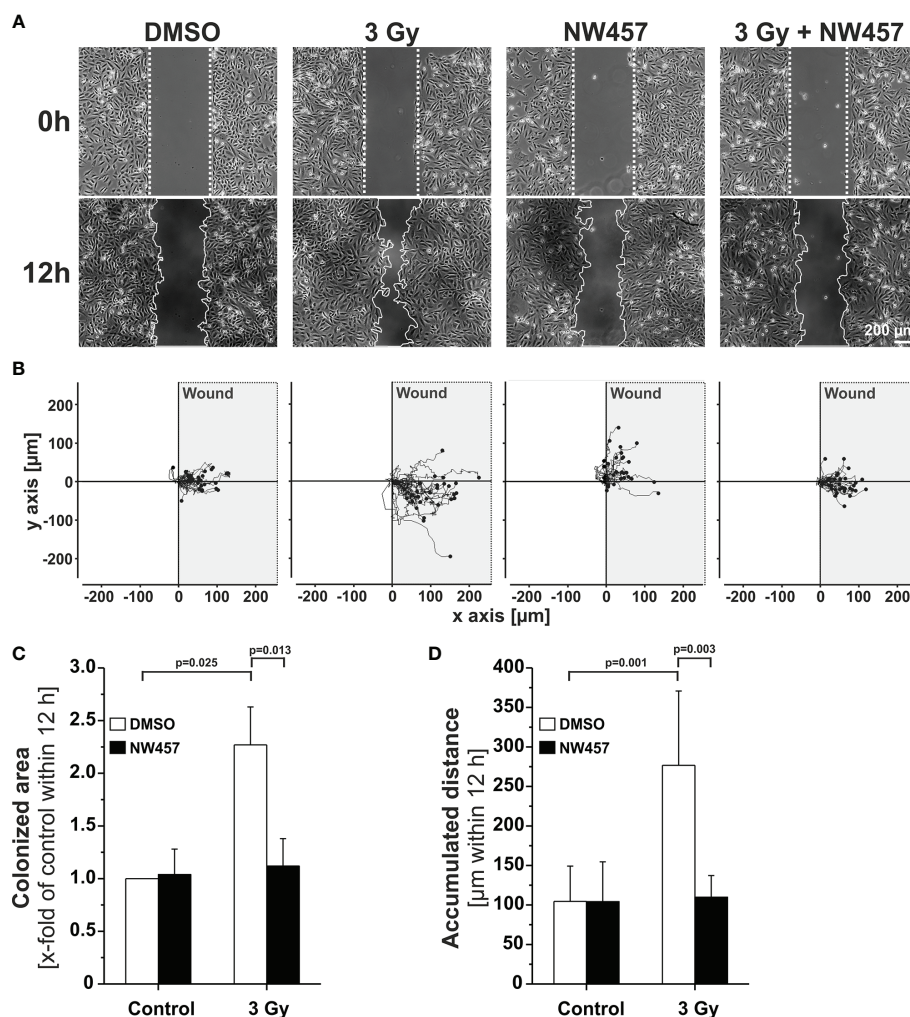
FIGURE 3 | HSP90i by NW457 counteracts GBM cell hypermigration in response to irradiation *in vitro*. **(A)** Live-cell imaging of the migratory behavior of GBM cells in wound healing assays. LN229 cells were seeded into Ibidi μ-slides with silicon "wound" inserts, pre-treated with 30 nM NW457 or DMSO for 24 h, irradiated at 3 Gy where indicated, and analyzed by live-cell microscopy for 12 h. "Wound" edges at the beginning and the end of the experiment are delineated by white dotted lines, and scale bar depicts 200 μm. **(B)** Trajectory plots showing the migratory paths of at least 25 randomly picked and manually tracked cells from **(A)**. **(C)** Relative quantification of the colonized area (depicted as x-fold values of controls) is shown as means ± s.d. of 3 independent experiments. Group comparisons were performed by Student's *t*-tests. **(D)** Relative quantification of accumulated distances per cell. Means ± s.d. of at least 25 randomly picked cells are shown. Group comparisons were performed by Student's *t*-tests.

DISCUSSION

Radiotherapy is a fundamental part of the standard of care for the treatment of glioblastoma (GBM) (69). However, treatment failure and (in-field) recurrence are frequent and form the basis for the dismal prognosis of this devastating disease (1). Significant advances in radiotherapy treatment and image-guidance technology as well as the addition of temozolomide (TMZ), a DNA alkylating chemotherapeutic drug, have led to modestly improved outcomes (2, 3), yet continued development remains urgently needed. GBM is characterized by a high level of inherent radioresistance which is considered to derive from overexpression of DNA damage response (DDR) genes and basally increased DDR activity (6, 8, 9, 45, 46). In this context, the molecular chaperone HSP90 is of particular interest and represents a promising target for radiosensitization approaches, since several key regulators of the DDR are known to crucially depend on HSP90 folding assistance (70–75). However, in single-agent settings administration of HSP90 inhibitors was frequently associated with side effects of relevant severity, including gastrointestinal toxicity and hepatoxicity, because the concentrations needed to achieve anti-tumor effects—despite the relative selectivity for cancer versus normal cells—were rather high, and the employed substances exhibited suboptimal toxicity profiles and poor pharmacokinetic features (76). Intriguingly, quantitative mass spectrometric analyses revealed that pathways of the DDR are among the most sensitive ones in cancer cells that are perturbed by HSP90i already at very low inhibitor concentrations (22). Furthermore, a recent study showed that administration of very low, non-toxic doses of an HSP90 inhibitor of the third generation results in DDR protein disintegration in HNSCC and pancreatic cancer cells, while this was not observed in non-transformed, normal cells (62). This would allow targeting DNA damage repair mechanisms in cancer cells while not affecting the normal tissue and—in combination with radiotherapy—would imply a kind of biologically driven increase in radiation dose selectively at the tumor. Given that treatment-associated radionecrosis represents a major dose limiting factor in GBM radiotherapy, targeted radiosensitization of the tumor by HSP90i appears specifically attractive for this cancer entity, ideally in combination with modern high precision, image-guided radiotherapy (69).

In the present study, we report that treatment with very low concentrations of the pochoxime-derived HSP90 inhibitor NW457 which *per se* exhibit only limited cytotoxicity leads to
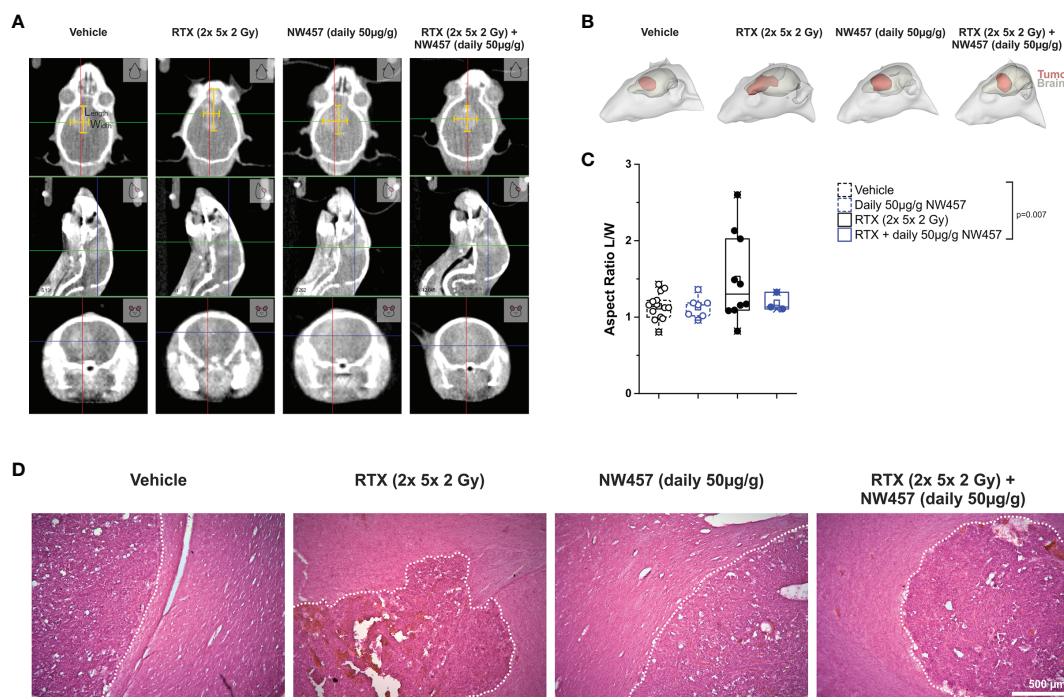
FIGURE 4 | HSP90i by NW457 attenuates GBM invasiveness in response to irradiation *in vivo*. Analysis of tumor morphology upon treatment at the time of animal sacrifice. **(A)** Contrast-enhanced CBCT scans of mice from different treatment groups. Tumor dimensions (width, length) are depicted by yellow bars in the coronal section (upper panels). **(B)** 3D reconstruction of tumors (red) and brains (grey) in mice from each treatment group as generated in 3D-Slicer. **(C)** Quantitative aspect ratio analysis of tumor length/width from each treatment group. p-value was calculated by one-way ANOVA (RTX vs. all other groups). **(D)** Hematoxylin/eosin (HE) stainings of tumors from all treatment groups. Tumor borders are highlighted by a dotted white line, and scale bar depicts 500 μm.

DDR protein disintegration in GBM cells. We observed several key regulators of the DDR to be affected by HSP90i, previously published HSP90 client proteins as well as DDR regulators with so far unknown HSP90 dependence (32, 54–56, 62). The cluster with the strongest decrease in protein levels upon HSP90i treatment in human and mouse GBM cell lines comprised CHK1, RAD51, DNA2, and NHEJ1. Accordingly, HSP90i represents a multi-target approach and affects various DDR pathways, including upstream checkpoint signaling (CHK1), double-strand break (DSB) repair by homologous recombination (RAD51), and non-homologous end-joining (NHEJ1), as well as crosslink repair and DNA replication (DNA2). This may explain why HSP90i is such a potent means of radiosensitization compared to mono-target approaches, for instance PARP inhibition (26, 77). Nevertheless, due to the correlative nature of our observations we cannot exclude that other mechanisms, such as the HSP90i-triggered proteasomal degradation of non-DDR proteins or the observed transcriptional downregulation of various genes, for instance genes involved in survival and/or integrin signaling, contribute to radiosensitization (78–81).

Functionally, degradation of DDR regulators upon HSP90i was accompanied by delayed DNA damage repair kinetics and significantly impaired clonogenic survival upon irradiation. In vivo, HSP90i by NW457 augmented the efficacy of fractionated radiotherapy in an orthotopic, syngeneic GBM mouse model, both in terms of tumor progression and survival. However, the observed effects were not as strong as expected from the convincing in vitro results. This may be due to limited GBM penetration by the inhibitor in vivo, although the family of pochoxime-derived HSP90 inhibitors has been shown to exhibit favorable brain pharmacokinetic profiles (82). Nevertheless, a very recent study with an orthotopic patient-derived GBM model reported similar therapeutic efficacy of a related pochoxime-derived HSP90 inhibitor in combination with whole brain irradiation (83). So, inhibitor substances with improved brain pharmacokinetic profiles, optimized formulations and/or administration routes, and/or fine-tuned treatment sequences may help to fully develop the synergistic potential of HSP90i and radiotherapy for the treatment of GBM.

In addition to its radiosensitizing effects, we observed that HSP90i by NW457 did reverse irradiation-induced GBM cell hypermigration in vitro and GBM invasiveness in vivo. This is of relevant interest, since GBM cells which survive radiotherapy and evade the target volume of radiotherapy may drive tumor relapse and dissemination. Our findings are in line with other reports showing that HSP90i efficiently decreases migration and invasion of human GBM cell lines (84–86). Although the detailed mechanisms of action remain elusive, we assume that the downregulation of migration regulating proteins is of importance in this scenario. On the protein level, mediators of protein (tyrosine) kinases have been reported to be particularly sensitive to HSP90i, and these are crucial regulators of migration-relevant signaling cascades (22). Additionally, our study shows that HSP90i stimulated the transcriptional downregulation of several interaction clusters involved in migratory processes, including integrin signaling, ECM receptor interaction, and signaling by small and large GTPases. HSP90i may thus offer a means to interfere with the highly infiltrative GBM phenotype which worsens with radiotherapy and represents another hallmark of this cancer entity contributing to its poor prognosis.

It should be noted, that HSP90i has also been shown to synergize with TMZ treatment in orthotopic models of GBM (87). This raises the question whether a triple combination of HSP90i and the current clinical standard of TMZ-based radiochemotherapy may improve the therapeutic outcome even further.

In conclusion, our study shows that HSP90i by low doses of NW457 potently interferes with the DDR in GBM cells leading to significant sensitization towards radiotherapy in vitro. The in vivo performance of this combined modality approach was less convincing than expected, although tumor growth was clearly delayed, survival was significantly prolonged, and radiation-induced invasive tumor morphology was reverted. Hence, our data reveal that the combination of HSP90i and radiotherapy is a promising strategy for GBM treatment whose performance needs to be further optimized by improved inhibitor substances, better formulations and/or administration routes, and fine-tuned treatment sequences.

DATA AVAILABILITY STATEMENT

The RNA sequencing datasets presented in this study can be found in online repositories. The names of the repository/repositories and accession number(s) can be found here: NCBI GEO: GSE164717. All other datasets are available from the corresponding author upon reasonable request.

ETHICS STATEMENT

The animal study was reviewed and approved by the Regierung von Oberbayern.

AUTHOR CONTRIBUTIONS

KL, MN, CB, AAF, HZ, KU, AKW and MO conceived and designed the experiments. MO, VA, KS, LKi, BS, AN, JM, LKr, NS, JH, KU and KL performed the experiments and analyzed the data. NW provided the HSP90i NW457. MO and KL wrote the manuscript with support from KU and JH. All authors discussed the results, commented on and revised the manuscript.

FUNDING

(INST 409/126-1 FUGG, INST 409/20-1 FUGG, and INST 409/22-1 FUGG), and the FoeFoLe Program of the Medical Faculty of the LMU Munich.

ACKNOWLEDGMENTS

SUPPLEMENTARY MATERIAL

The Supplementary Material for this article can be found online at: https://www.frontiersin.org/articles/10.3389/fonc.2021.612354/full#supplementary-material

REFERENCES

1. Fisher JL, Schwartzbaum JA, Wrensch M, Wiemels JL. Epidemiology of brain tumors. *Neurol Clin* (2007) 25:867–90, vii. doi: 10.1016/j.ncl.2007.07.002
2. Stupp R, Hegi ME, Mason WP, van den Bent MJ, Taphoorn MJ, Janzer RC, et al. Radiation Oncology, and G. National Cancer Institute of Canada Clinical Trials, Effects of radiotherapy with concomitant and adjuvant temozolomide versus radiotherapy alone on survival in glioblastoma in a randomised phase III study: 5-year analysis of the EORTC-NCIC trial. *Lancet Oncol* (2009) 10:459–66. doi: 10.1016/S1470-2045(09)70025-7
3. Stupp R, Mason WP, van den Bent MJ, Weller M, Fisher B, Taphoorn MJ, et al. Radiotherapy plus concomitant and adjuvant temozolomide for glioblastoma. *N Engl J Med* (2005) 352:987–96. doi: 10.1056/NEJMoa043330
4. Wilson TA, Karajannis MA, Harter DH. Glioblastoma multiforme: State of the art and future therapeutics. *Surg Neurol Int* (2014) 5:64. doi: 10.4103/2152-7806.132138
5. Davis ME. Glioblastoma: Overview of Disease and Treatment. *Clin J Oncol Nurs* (2016) 20:S2–8. doi: 10.1188/16.CJON.S1.2-8
6. Osuka S, Van Meir EG. Overcoming therapeutic resistance in glioblastoma: the way forward. *J Clin Invest* (2017) 127:415–26. doi: 10.1172/JCI89587
7. Taylor OG, Brzozowski JS, Skelding KA. Glioblastoma Multiforme: An Overview of Emerging Therapeutic Targets. *Front Oncol* (2019) 9:963. doi: 10.3389/fonc.2019.00963
8. Mannino M, Chalmers AJ. Radioresistance of glioma stem cells: intrinsic characteristic or property of the 'microenvironment-stem cell unit'? *Mol Oncol* (2011) 5:374–86. doi: 10.1016/j.molonc.2011.05.001
9. Han X, Xue X, Zhou H, Zhang G. A molecular view of the radioresistance of gliomas. *Oncotarget* (2017) 8:100931–41. doi: 10.18632/oncotarget.21753
10. Alhajala HS, Nguyen HS, Shabani S, Best B, Kaushal M, Al-Gizawiy MM, et al. Irradiation of pediatric glioblastoma cells promotes radioresistance and enhances glioma malignancy via genome-wide transcriptome changes. *Oncotarget* (2018) 9:34122–31. doi: 10.18632/oncotarget.26137
11. Stanzani E, Martinez-Soler F, Mateos TM, Vidal N, Villanueva A, Pujana MA, et al. Radioresistance of mesenchymal glioblastoma initiating cells correlates with patient outcome and is associated with activation of inflammatory program. *Oncotarget* (2017) 8:73640–53. doi: 10.18632/oncotarget.18363
12. Bao S, Wu Q, McLendon RE, Hao Y, Shi Q, Hjelmeland AB, et al. Glioma stem cells promote radioresistance by preferential activation of the DNA damage response. *Nature* (2006) 444:756–60. doi: 10.1038/nature05236
13. Bhat KPL, Balasubramaniyan V, Vaillant B, Ezhilarasan R, Hummelink K, Hollingsworth F, et al. Mesenchymal differentiation mediated by NF-kappaB promotes radiation resistance in glioblastoma. *Cancer Cell* (2013) 24:331–46. doi: 10.1016/j.ccr.2013.08.001
14. Segerman A, Niklasson M, Haglund C, Bergstrom T, Jarvius M, Xie Y, et al. Clonal Variation in Drug and Radiation Response among Glioma-Initiating Cells Is Linked to Proneural-Mesenchymal Transition. *Cell Rep* (2016) 17:2994–3009. doi: 10.1016/j.celrep.2016.11.056
15. Jeon HY, Ham SW, Kim JK, Jin X, Lee SY, Shin YJ, et al. Ly6G(+) inflammatory cells enable the conversion of cancer cells to cancer stem cells in an irradiated glioblastoma model. *Cell Death Differ* (2019) 26:2139–56. doi: 10.1038/s41418-019-0282-0
16. Otomo T, Hishii M, Arai H, Sato K, Sasai K. Microarray analysis of temporal gene responses to ionizing radiation in two glioblastoma cell lines: up-regulation of DNA repair genes. *J Radiat Res* (2004) 45:53–60. doi: 10.1269/jrr.45.53

17. Lewitzki V, Klement RJ, Kosmala R, Lisowski D, Flentje M, Polat B. Accelerated hyperfractionated radiochemotherapy with temozolomide is equivalent to normofractionated radiochemotherapy in a retrospective analysis of patients with glioblastoma. *Radiat Oncol* (2019) 14:227. doi: 10.1186/s13014-019-1427-5
18. Trone JC, Vallard A, Sotton S, Ben Mrad M, Jmour O, Magne N, et al. Survival after hypofractionation in glioblastoma: a systematic review and meta-analysis. *Radiat Oncol* (2020) 15:145. doi: 10.1186/s13014-020-01584-6
19. Liao G, Zhao Z, Yang H, Li X. Efficacy and Safety of Hypofractionated Radiotherapy for the Treatment of Newly Diagnosed Glioblastoma Multiforme: A Systematic Review and Meta-Analysis. *Front Oncol* (2019) 9:1017. doi: 10.3389/fonc.2019.01017
20. Sherriff J, Tamangani J, Senthil L, Cruickshank G, Spooner D, Jones B, et al. Patterns of relapse in glioblastoma multiforme following concomitant chemoradiotherapy with temozolomide. *Br J Radiol* (2013) 86:20120414. doi: 10.1259/bjr.20120414
21. Pennisi R, Ascenzi P, di Masi A. Hsp90: A New Player in DNA Repair? *Biomolecules* (2015) 5:2589–618. doi: 10.3390/biom5042589
22. Sharma K, Vabulas RM, Macek B, Pinkert S, Cox J, Mann M, et al. Quantitative proteomics reveals that Hsp90 inhibition preferentially targets kinases and the DNA damage response. *Mol Cell Proteomics* (2012) 11:M111 014654. doi: 10.1074/mcp.M111.014654
23. Knighton LE, Truman AW. Role of the Molecular Chaperones Hsp70 and Hsp90 in the DNA Damage Response. In: AAA Asea, P Kaur, editors. *Heat Shock Proteins in Signaling Pathways*. Cham: Springer International Publishing (2019). p. 345–58. doi: 10.1007/978-3-030-03952-3_18
24. Lu X, Xiao L, Wang L, Ruden DM. Hsp90 inhibitors and drug resistance in cancer: the potential benefits of combination therapies of Hsp90 inhibitors and other anti-cancer drugs. *Biochem Pharmacol* (2012) 83:995–1004. doi: 10.1016/j.bcp.2011.11.011
25. Combs SE, Schmid TE, Vaupel P, Multhoff G. Stress Response Leading to Resistance in Glioblastoma-The Need for Innovative Radiotherapy (iRT) Concepts. *Cancers (Basel)* (2016) 8(1):15. doi: 10.3390/cancers8010015
26. Biau J, Chautard E, Verrelle P, Dutreix M. Altering DNA Repair to Improve Radiation Therapy: Specific and Multiple Pathway Targeting. *Front Oncol* (2019) 9:1009. doi: 10.3389/fonc.2019.01009
27. Barluenga S, Wang C, Fontaine JG, Aouadi K, Beebe K, Tsutsumi S, et al. Divergent synthesis of a pochonin library targeting HSP90 and in vivo efficacy of an identified inhibitor. *Angew Chem Int Ed Engl* (2008) 47:4432–5. doi: 10.1002/anie.200800233
28. Karthikeyan G, Zambaldo C, Barluenga S, Zoete V, Karplus M, Winssinger N. Asymmetric synthesis of pochonin E and F, revision of their proposed structure, and their conversion to potent Hsp90 inhibitors. *Chemistry* (2012) 18:8978–86. doi: 10.1002/chem.201200546
29. Barluenga S, Fontaine JG, Wang C, Aouadi K, Chen R, Beebe K, et al. Inhibition of HSP90 with pochoximes: SAR and structure-based insights. *Chembiochem* (2009) 10:2753–9. doi: 10.1002/cbic.200900494
30. Kinzel L, Ernst A, Orth M, Albrecht V, Hennel R, Brix N, et al. A novel HSP90 inhibitor with reduced hepatotoxicity synergizes with radiotherapy to induce apoptosis, abrogate clonogenic survival, and improve tumor control in models of colorectal cancer. *Oncotarget* (2016) 7:43199–219. doi: 10.18632/oncotarget.9774
31. Ernst A, Hennel R, Krombach J, Kapfhammer H, Brix N, Zuchtriegel G, et al. Priming of anti-tumor immune mechanisms by radiotherapy is augmented by

inhibition of heat shock protein. *Front Oncol* (2020) 10:1668 doi: 10.3389/fonc.2020.01668

32. Ernst A, Anders H, Kapfhammer H, Orth M, Hennel R, Seidl K, et al. HSP90 inhibition as a means of radiosensitizing resistant, aggressive soft tissue sarcomas. *Cancer Lett* (2015) 365:211–22. doi: 10.1016/j.canlet.2015.05.024

33. Unkel S, Belka C, Lauber K. On the analysis of clonogenic survival data: Statistical alternatives to the linear-quadratic model. *Radiat Oncol* (2016) 11:11. doi: 10.1186/s13014-016-0584-z

34. Hennel R, Brix N, Seidl K, Ernst A, Scheithauer H, Belka C, et al. Release of monocyte migration signals by breast cancer cell lines after ablative and fractionated gamma-irradiation. *Radiat Oncol* (2014) 9:85. doi: 10.1186/1748-717X-9-85

35. Orth M, Unger K, Schoetz U, Belka C, Lauber K. Taxane-mediated radiosensitization derives from chromosomal missegregation on tripolar mitotic spindles orchestrated by AURKA and TPX2. *Oncogene* (2018) 37:52–62. doi: 10.1038/onc.2017.304

36. Dobin A, Davis CA, Schlesinger F, Drenkow J, Zaleski C, Jha S, et al. STAR: ultrafast universal RNA-seq aligner. *Bioinformatics* (2013) 29:15–21. doi: 10.1093/bioinformatics/bts635

37. Anders S, Pyl PT, Huber W. HTSeq–a Python framework to work with high-throughput sequencing data. *Bioinformatics* (2015) 31:166–9. doi: 10.1093/bioinformatics/btu638

38. Zhu A, Ibrahim JG, Love MI. Heavy-tailed prior distributions for sequence count data: removing the noise and preserving large differences. *Bioinformatics* (2019) 35:2084–92. doi: 10.1093/bioinformatics/bty895

39. Subramanian A, Tamayo P, Mootha VK, Mukherjee S, Ebert BL, Gillette MA, et al. Gene set enrichment analysis: a knowledge-based approach for interpreting genome-wide expression profiles. *Proc Natl Acad Sci USA* (2005) 102:15545–50. doi: 10.1073/pnas.0506580102

40. Shannon P, Markiel A, Ozier O, Baliga NS, Wang JT, Ramage D, et al. Cytoscape: a software environment for integrated models of biomolecular interaction networks. *Genome Res* (2003) 13:2498–504. doi: 10.1101/gr.1239303

41. Wu G, Haw R. Functional Interaction Network Construction and Analysis for Disease Discovery. *Methods Mol Biol* (2017) 1558:235–53. doi: 10.1007/978-1-4939-6783-4_11

42. Janky R, Verfaillie A, Imrichova H, Van de Sande B, Standaert L, Christiaens V, et al. iRegulon: from a gene list to a gene regulatory network using large motif and track collections. *PLoS Comput Biol* (2014) 10:e1003731. doi: 10.1371/journal.pcbi.1003731

43. Stegen B, Nieto A, Albrecht V, Maas J, Orth M, Neumaier K, et al. Contrast-enhanced, conebeam CT-based, fractionated radiotherapy and follow-up monitoring of orthotopic mouse glioblastoma: a proof-of-concept study. *Radiat Oncol* (2020) 15:19. doi: 10.1186/s13014-020-1470-2

44. Wong J, Armour E, Kazanzides P, Iordachita I, Tryggestad E, Deng H, et al. High-resolution, small animal radiation research platform with x-ray tomographic guidance capabilities. *Int J Radiat Oncol Biol Phys* (2008) 71:1591–9. doi: 10.1016/j.ijrobp.2008.04.025

45. Mukherjee B, McEllin B, Camacho CV, Tomimatsu N, Sirasanagandala S, Nannepaga S, et al. EGFRvIII and DNA double-strand break repair: a molecular mechanism for radioresistance in glioblastoma. *Cancer Res* (2009) 69:4252–9. doi: 10.1158/0008-5472.CAN-08-4853

46. Carruthers RD, Ahmed SU, Ramachandran S, Strathdee K, Kurian KM, Hedley A, et al. Replication Stress Drives Constitutive Activation of the DNA Damage Response and Radioresistance in Glioblastoma Stem-like Cells. *Cancer Res* (2018) 78:5060–71. doi: 10.1158/0008-5472.CAN-18-0569

47. Jackson SP, Bartek J. The DNA-damage response in human biology and disease. *Nature* (2009) 461:1071–8. doi: 10.1038/nature08467

48. Turgeon MO, Perry NJS, Poulogiannis G, Damage DNA. Repair, and Cancer Metabolism. *Front Oncol* (2018) 8:15. doi: 10.3389/fonc.2018.00015

49. Ishii N, Maier D, Merlo A, Tada M, Sawamura Y, Diserens AC, et al. Frequent co-alterations of TP53, p16/CDKN2A, p14ARF, PTEN tumor suppressor genes in human glioma cell lines. *Brain Pathol* (1999) 9:469–79. doi: 10.1111/j.1750-3639.1999.tb00536.x

50. Bairoch A. The Cellosaurus, a Cell-Line Knowledge Resource. *J Biomol Tech* (2018) 29:25–38. doi: 10.7171/jbt.18-2902-002

51. Verhaak RG, Hoadley KA, Purdom E, Wang V, Qi Y, Wilkerson MD, et al. Integrated genomic analysis identifies clinically relevant subtypes of glioblastoma characterized by abnormalities in PDGFRA, IDH1, EGFR, and NF1. *Cancer Cell* (2010) 17:98–110. doi: 10.1016/j.ccr.2009.12.020

52. Brennan CW, Verhaak RG, McKenna A, Campos B, Noushmehr H, Salama SR, et al. The somatic genomic landscape of glioblastoma. *Cell* (2013) 155:462–77. doi: 10.1016/j.cell.2013.09.034

53. Esteller M, Garcia-Foncillas J, Andion E, Goodman SN, Hidalgo OF, Vanaclocha V, et al. Inactivation of the DNA-repair gene MGMT and the clinical response of gliomas to alkylating agents. *N Engl J Med* (2000) 343:1350–4. doi: 10.1056/NEJM200011093431901

54. Dote H, Burgan WE, Camphausen K, Tofilon PJ. Inhibition of hsp90 compromises the DNA damage response to radiation. *Cancer Res* (2006) 66:9211–20. doi: 10.1158/0008-5472.CAN-06-2181

55. Dungey FA, Caldecott KW, Chalmers AJ. Enhanced radiosensitization of human glioma cells by combining inhibition of poly(ADP-ribose) polymerase with inhibition of heat shock protein 90. *Mol Cancer Ther* (2009) 8:2243–54. doi: 10.1158/1535-7163.MCT-09-0201

56. Arlander SJ, Eapen AK, Vroman BT, McDonald RJ, Toft DO, Karnitz LM. Hsp90 inhibition depletes Chk1 and sensitizes tumor cells to replication stress. *J Biol Chem* (2003) 278:52572–7. doi: 10.1074/jbc.M309054200

57. Zheng L, Meng Y, Campbell JL, Shen B. Multiple roles of DNA2 nuclease/helicase in DNA metabolism, genome stability and human diseases. *Nucleic Acids Res* (2020) 48:16–35. doi: 10.1093/nar/gkz1101

58. Pawlowska E, Szczepanska J, Blasiak J. DNA2-An Important Player in DNA Damage Response or Just Another DNA Maintenance Protein? *Int J Mol Sci* (2017) 18(7):1562. doi: 10.3390/ijms18071562

59. Kumar S, Peng X, Daley J, Yang L, Shen J, Nguyen N, et al. Inhibition of DNA2 nuclease as a therapeutic strategy targeting replication stress in cancer cells. *Oncogenesis* (2017) 6:e319. doi: 10.1038/oncsis.2017.15

60. Liu W, Zhou M, Li Z, Li H, Polaczek P, Dai H, et al. A Selective Small Molecule DNA2 Inhibitor for Sensitization of Human Cancer Cells to Chemotherapy. *EBioMedicine* (2016) 6:73–86. doi: 10.1016/j.ebiom.2016.02.043

61. Ochi T, Wu Q, Blundell TL. The spatial organization of non-homologous end joining: from bridging to end joining. *DNA Repair (Amst)* (2014) 17:98–109. doi: 10.1016/j.dnarep.2014.02.010

62. Mehta RK, Pal S, Kondapi K, Sitto M, Dewar C, Devasia T, et al. Low-Dose Hsp90 Inhibitor Selectively Radiosensitizes HNSCC and Pancreatic Xenografts. *Clin Cancer Res* (2020) 26(19):5246–57. doi: 10.1158/1078-0432.CCR-19-3102

63. Lai TH, Mitchell S, Wu PJ, Orwick S, Liu C, Ravikrishnan J, et al. HSP90 inhibition depletes DNA repair proteins to sensitize acute myelogenous leukemia to nucleoside analog chemotherapeutics. *Leuk Lymphoma* (2019) 60:2308–11. doi: 10.1080/10428194.2019.1571197

64. Lauber K, Ernst A, Orth M, Herrmann M, Belka C. Dying cell clearance and its impact on the outcome of tumor radiotherapy. *Front Oncol* (2012) 2:116. doi: 10.3389/fonc.2012.00116

65. Trepel J, Mollapour M, Giaccone G, Neckers L. Targeting the dynamic HSP90 complex in cancer. *Nat Rev Cancer* (2010) 10:537–49. doi: 10.1038/nrc2887

66. Newcomb EW, Lymberis SC, Lukyanov Y, Shao Y, Schnee T, Devitt M, et al. Radiation sensitivity of GL261 murine glioma model and enhanced radiation response by flavopiridol. *Cell Cycle* (2006) 5:93–9. doi: 10.4161/cc.5.1.2271

67. Wild-Bode C, Weller M, Rimner A, Dichgans J, Wick W. Sublethal irradiation promotes migration and invasiveness of glioma cells: implications for radiotherapy of human glioblastoma. *Cancer Res* (2001) 61:2744–50.

68. Kargiotis O, Geka A, Rao JS, Kyritsis AP. Effects of irradiation on tumor cell survival, invasion and angiogenesis. *J Neurooncol* (2010) 100:323–38. doi: 10.1007/s11060-010-0199-4

69. Mann J, Ramakrishna R, Magge R, Wernicke AG. Advances in Radiotherapy for Glioblastoma. *Front Neurol* (2017) 8:748. doi: 10.3389/fneur.2017.00748

70. Kabakov AE, Kudryavtsev VA, Gabai VL. Hsp90 inhibitors as promising agents for radiotherapy. *J Mol Med (Berl)* (2010) 88:241–7. doi: 10.1007/s00109-009-0562-0

71. Lauber K, Brix N, Ernst A, Hennel R, Krombach J, Anders H, et al. Targeting the heat shock response in combination with radiotherapy: Sensitizing cancer cells to irradiation-induced cell death and heating up their immunogenicity. *Cancer Lett* (2015) 368:209–29. doi: 10.1016/j.canlet.2015.02.047

72. Camphausen K, Tofilon PJ. Inhibition of Hsp90: a multitarget approach to radiosensitization. *Clin Cancer Res* (2007) 13:4326–30. doi: 10.1158/1078-0432.CCR-07-0632

73. Lomeli N, Bota DA. Targeting HSP90 in malignant gliomas: onalespib as a potential therapeutic. *Transl Cancer Res* (2018) 7:6215–26. doi: 10.21037/tcr.2018.03.05

74. van Ommeren R, Staudt MD, Xu H, Hebb MO. Advances in HSP27 and HSP90-targeting strategies for glioblastoma. *J Neurooncol* (2016) 127:209–19. doi: 10.1007/s11060-016-2070-8

75. Hintelmann K, Kriegs M, Rothkamm K, Rieckmann T. Improving the Efficacy of Tumor Radiosensitization Through Combined Molecular Targeting. *Front Oncol* (2020) 10:1260. doi: 10.3389/fonc.2020.01260

76. Butler LM, Ferraldeschi R, Armstrong HK, Centenera MM, Workman P. Maximizing the Therapeutic Potential of HSP90 Inhibitors. *Mol Cancer Res* (2015) 13:1445–51. doi: 10.1158/1541-7786.MCR-15-0234

77. Javle M, Curtin NJ. The role of PARP in DNA repair and its therapeutic exploitation. *Br J Cancer* (2011) 105:1114–22. doi: 10.1038/bjc.2011.382

78. Storch K, Sagerer A, Cordes N. Cytotoxic and radiosensitizing effects of FAK targeting in human glioblastoma cells in vitro. *Oncol Rep* (2015) 33:2009–16. doi: 10.3892/or.2015.3753

79. Toulany M, Dittmann K, Kruger M, Baumann M, Rodemann HP. Radioresistance of K-Ras mutated human tumor cells is mediated through EGFR-dependent activation of PI3K-AKT pathway. *Radiother Oncol* (2005) 76:143–50. doi: 10.1016/j.radonc.2005.06.024

80. Mohammadian Gol T, Rodemann HP, Dittmann K. Depletion of Akt1 and Akt2 Impairs the Repair of Radiation-Induced DNA Double Strand Breaks via Homologous Recombination. *Int J Mol Sci* (2019) 20(24):6316. doi: 10.3390/ijms20246316

81. Vehlow A, Klapproth E, Storch K, Dickreuter E, Seifert M, Dietrich A, et al. Adhesion- and stress-related adaptation of glioma radiochemoresistance is circumvented by beta1 integrin/JNK co-targeting. *Oncotarget* (2017) 8:49224–37. doi: 10.18632/oncotarget.17480

82. Cha JR, St Louis KJ, Tradewell ML, Gentil BJ, Minotti S, Jaffer ZM, et al. A novel small molecule HSP90 inhibitor, NXD30001, differentially induces heat shock proteins in nervous tissue in culture and in vivo. *Cell Stress Chaperones* (2014) 19:421–35. doi: 10.1007/s12192-013-0467-2

83. Chen H, Gong Y, Ma Y, Thompson RC, Wang J, Cheng Z, et al. A Brain-Penetrating Hsp90 Inhibitor NXD30001 Inhibits Glioblastoma as a Monotherapy or in Combination With Radiation. *Front Pharmacol* (2020) 11:974. doi: 10.3389/fphar.2020.00974

84. Annamalai B, Liu X, Gopal U, Isaacs JS. Hsp90 is an essential regulator of EphA2 receptor stability and signaling: implications for cancer cell migration and metastasis. *Mol Cancer Res* (2009) 7:1021–32. doi: 10.1158/1541-7786.MCR-08-0582

85. Kim MS, Kwak HJ, Lee JW, Kim HJ, Park MJ, Park JB, et al. 17-Allylamino-17-demethoxygeldanamycin down-regulates hyaluronic acid-induced glioma invasion by blocking matrix metalloproteinase-9 secretion. *Mol Cancer Res* (2008) 6:1657–65. doi: 10.1158/1541-7786.MCR-08-0034

86. Gopal U, Bohonowych JE, Lema-Tome C, Liu A, Garrett-Mayer E, Wang B, et al. A novel extracellular Hsp90 mediated co-receptor function for LRP1 regulates EphA2 dependent glioblastoma cell invasion. *PloS One* (2011) 6:e17649. doi: 10.1371/journal.pone.0017649

87. Canella A, Welker AM, Yoo JY, Xu J, Abas FS, Kesanakurti D, et al. Efficacy of Onalespib, a Long-Acting Second-Generation HSP90 Inhibitor, as a Single Agent and in Combination with Temozolomide against Malignant Gliomas. *Clin Cancer Res* (2017) 23:6215–26. doi: 10.1158/1078-0432.CCR-16-3151

GLOSSARY

53BP1	p53-binding protein 1
ATM	ataxia telangiectasia mutated
ATR	ataxia telangiectasia and Rad3 related
BLM	Bloom syndrome helicase
BRCA1	breast cancer gene 1
BRCA2	breast cancer gene 2
BRIP1	BRCA1-interacting protein 1
CBCT	conebeam computed tomography
CDKN1A	cyclin dependent kinase inhibitor 1A
CHK1	checkpoint kinase 1 (gene symbol CHEK1)
CHK2	checkpoint kinase 2 (gene symbol CHEK2)
DCLR1C	DNA cross-link repair protein 1C
DNA2	DNA replication ATP-dependent nuclease 2
DNA-PKcs	catalytic subunit of DNA-dependent protein kinase (gene symbol PRKDC)
DDR	DNA damage response
DMSO	dimethyl sulfoxide
DSB	double-strand break
EORTC	European Organization for Research and Treatment of Cancer
EXO1	exonuclease 1
FANCA	Fanconi anemia complementation group A
FEN1	Flap endonuclease 1
FCS	fetal calf serum
GBM	glioblastoma
γH2AX	phosphorylated histone variant 2AX (pS139)
HE	hematoxylin and eosin
HSP70	heat shock protein 70
HSP90	heat shock protein 90
HSP90i	heat shock protein 90 inhibition
KU70	ATP-dependent DNA helicase subunit KU70 (gene symbol XRCC6)
KU80	ATP-dependent DNA helicase subunit KU80 (gene symbol XRCC5)
LIG4	DNA-ligase 4
MGMT	O6-methylguanine-DNA-methyltransferase
MRE11	meiotic recombination protein 11
MRN	MRE11-RAD50-NBN
NBN	Nibrin
NCIC	national cancer information center
NHEJ1	non-homologous end joining protein 1
p21	cyclin-dependent kinase inhibitor p21 (gene symbol CDKN1A)
p53	tumor suppressing protein p53 (gene symbol TP53)
PALB2	partner and localizer of BRCA2
PARP1	poly(ADP-ribose)-polymerase 1
PARP2	poly(ADP-ribose)-polymerase 2
PS	pencillin/streptomycin
RAD50	DNA repair protein RAD50
RAD51	DNA repair protein RAD51
RAD52	DNA repair protein RAD52
RAD54	DNA repair protein RAD54
RBBP8	Retinoblastoma-binding protein 8
RPA1	replication protein A1
qRT-PCR	quantitative realtime reverse transcription polymerase chain reaction
RTX	radiotherapy
STR	short tandem repeat
TMZ	temozolomide
XRCC1-5	x-ray repair cross-complementing protein 1-5

A Comparison Between Chemo-Radiotherapy Combined With Immunotherapy and Chemo-Radiotherapy Alone for the Treatment of Newly Diagnosed Glioblastoma: A Systematic Review and Meta-Analysis

Montserrat Lara-Velazquez[1], Jack M. Shireman[1], Eric J. Lehrer[2], Kelsey M. Bowman[1], Henry Ruiz-Garcia[3], Mitchell J. Paukner[4], Richard J. Chappell[4] and Mahua Dey[1*]

[1] Department of Neurosurgery, University of Wisconsin School of Medicine & Public Health, UW Carbone Cancer Center, Madison, WI, United States, [2] Department of Radiation Oncology, Icahn School of Medicine at Mount Sinai, New York, NY, United States, [3] Department of Neurosurgery and Radiation Oncology, Mayo Clinic, Jacksonville, FL, United States, [4] Department of Statistics, Biostatistics and Medical Informatics, University of Wisconsin School of Medicine & Public Health, UW Carbone Cancer Center, Madison, WI, United States

Background: Immunotherapy for GBM is an emerging field which is increasingly being investigated in combination with standard of care treatment options with variable reported success rates.

Objective: To perform a systematic review of the available data to evaluate the safety and efficacy of combining immunotherapy with standard of care chemo-radiotherapy following surgical resection for the treatment of newly diagnosed GBM.

Methods: A literature search was performed for published clinical trials evaluating immunotherapy for GBM from January 1, 2000, to October 1, 2020, in PubMed and Cochrane using PICOS/PRISMA/MOOSE guidelines. Only clinical trials with two arms (combined therapy *vs.* control therapy) were included. Outcomes were then pooled using weighted random effects model for meta-analysis and compared using the Wald-type test. Primary outcomes included 1-year overall survival (OS) and progression-free survival (PFS), secondary outcomes included severe adverse events (SAE) grade 3 or higher.

Results: Nine randomized phase II and/or III clinical trials were included in the analysis, totaling 1,239 patients. The meta-analysis revealed no statistically significant differences in group's 1-year OS [80.6% (95% CI: 68.6%–90.2%) *vs.* 72.6% (95% CI: 65.7%–78.9%), p = 0.15] or in 1-year PFS [37% (95% CI: 26.4%–48.2%) *vs.* 30.4% (95% CI: 25.4%–35.6%) p = 0.17] when the immunotherapy in combination with the standard of care group (combined therapy) was compared to the standard of care group alone (control). Severe adverse events grade 3 to 5 were more common in the immunotherapy and standard of care group than in

the standard of care group (47.3%, 95% CI: 20.8–74.6%, *vs* 43.8%, 95% CI: 8.7–83.1, p = 0.81), but this effect also failed to reach statistical significance.

Conclusion: Our results suggests that immunotherapy can be safely combined with standard of care chemo-radiotherapy without significant increase in grade 3 to 5 SAE; however, there is no statistically significant increase in overall survival or progression free survival with the combination therapy.

INTRODUCTION

Glioblastoma (GBM) is the most common primary and dismal brain cancer in adults, this carries a poor prognosis and median overall survival (OS) (1). It is a highly aggressive and heterogeneous entity that survives even the most eradicative treatments (2–4). Current standard of care for GBM includes safe maximal tumor resection, followed by temozolomide (TMZ) chemotherapy (75 mg/m2/day for 6 weeks) and concomitant radiation (60 Gy in 30 fractions). TMZ is then followed by six continued maintenance cycles (150–200 mg/m2/day for the first 5 days of a 28-day cycle); accompanied by the antimitotic device tumor treating fields (TTF) (Optune, Novocure Inc) (4–6), which is continued once TMZ is completed. This standard of care with TTF included, achieves a median overall survival of 20.9 months, that is in contrast with the 16 months median survival obtained with surgery and chemo-radiotherapy alone (7). However, tumor recurrence happens in the majority of the patients despite the aggressive treatment regimen (8), highlighting a major treatment gap in GBM that has yet to be addressed (9–14). Multiple strategies are being developed with the goal of effectively treating GBM, however, one such strategy that has proven viable in other cancer domains and is currently being heavily investigated is immunotherapy (6, 15).

Immunotherapy, is an evolving field of medicine that enhances the activity of select cells in the immune system to recognize, attack, and kill cancer cells *via* targeted anti-tumor-cytotoxicity without harming the normal tissue (16, 17). The main promise of immunotherapy is not only to combat tumor growth by eliminating cancer cells, but to keep an army of memory cells to avoid tumor recurrence, a facet of treatment that will be crucial for GBM (18). The discovery of specific tumor associated peptides presented by major histocompatibility complexes (MHC) (19, 20); and inhibition of immune checkpoint molecules (cytotoxic T lymphocyte antigen 4 (CTLA4) and programmed cell death 1 (PD1) that regulate T cell activation; opened new doors for the treatment of cancer, by augmenting the natural functions of the immune system (17, 21–23). Biological options of immune-based therapies that have been developed include checkpoint inhibitors, cellular therapies, vaccines, engineered T cells, small peptide inhibitors of specific pathways, monoclonal antibodies, and cytokine therapy (24–26).

Currently there are no Food and Drug Administration (FDA) approved immunotherapy regimens for the treatment of GBM (16). Although there are several immune-based therapies currently being tested for GBM, the majority evaluate mainly tolerance and toxicity (16). Even while some immunotherapies have shown promising clinical results when evaluated as a monotherapy, their true impact when combined with, or given alongside of, standard of care is unknown (27). Moreover, only a few of these modalities have progressed to the phase II or III clinical trial setting to systematically test their impact on overall survival, progression of the disease, and severe adverse events when administered in combination with current standard of care (28). Because of this, little is known about the true clinical benefits and toxicity profile of immunotherapy given in combination with chemo-radiotherapy. Ongoing (unpublished) phase II or III clinical trials of immune checkpoint inhibitors used in combination with standard of care for newly diagnosed GBM failed to meet survival expectancy and PFS in MGMT methylated (CheckMate 548, NCT02667587) (29, 30) or un-methylated (CheckMate 498, NCT02617589) (31, 32) GBM patients. The randomized trial phase II/III NRG-BN007 evaluating ipilimumab and nivolumab versus temozolomide to radiotherapy in un-methylated GBM patients is also ongoing, and the results are awaited with high expectations (33). Unfortunately, most of the results with different immunotherapies in GBM have disappointed the medical community in regards of improving survival for these patients. However, these studies are essential to understand the benefits and the associated risks of immunotherapies in gliomas.

This gap in the knowledge could be masking the full potential of immunotherapy when used as an adjuvant treatment in GBM and can be limiting our ability to make fully informed decisions in regard to adding immunotherapy to the current standard of care for GBM. To address the knowledge gap in this area and to provide a scientific rationale about the possible synergistic effect that chemo-radiation and immunotherapy may have when used together, we performed a systematic review and meta-analysis. We analyzed and compared 1-year overall survival (OS), 1-year progression free survival (PFS) and grade 3 to 5 adverse events, in the immunotherapy plus chemo-radiotherapy regimen (defined as immunotherapy and standard of care or combined group), *versus* chemo-radiotherapy alone regimen (defined as standard of care or control group), in patients with newly diagnosed GBM.

MATERIALS AND METHODS

Study Selection Criteria

A search strategy was developed using the Population, Intervention, Comparison, Outcome, Study type (PICOS) question format: In newly-diagnosed glioblastoma patients (Population) that receive standard of care with or without immunotherapy (Intervention and Comparison), what are the overall survival, progression free survival and severe adverse events grades 3 to 5 (Study Type) based on results from phase II and III clinical trials (Study type) (**Supplementary Table 1**).

A literature search in PUBMED and Cochrane was performed by three independent reviewers according to the Preferred Reporting Items for Systematic Reviews and Meta-Analyses (PRISMA) (**Figure 1** and **Supplementary Table 2**) (34) and Meta-Analyses and Systematic Reviews of Observational Studies (MOOSE) (35) (**Supplementary Table 3**) guidelines. Our search included phase II and/or III clinical trials, published from January 1st 2000 to October 1st 2020. The terms used for literature search included "glioblastoma," OR "newly diagnosed glioblastoma," OR "malignant glioma," AND "radiation" AND "chemotherapy" OR "radio-chemotherapy," AND "immunotherapy". These terms were specifically used as follows in batch searches across both databases: glioblastoma and radio chemotherapy and immunotherapy, newly diagnosed glioblastoma and radio chemotherapy and immunotherapy, newly diagnosed glioblastoma and radio chemotherapy, newly diagnosed glioblastoma and immunotherapy, glioblastoma and immunotherapy, newly diagnosed glioblastoma and radiotherapy, newly diagnosed glioblastoma and chemotherapy and malignant glioma and radio chemotherapy and immunotherapy. Any disagreement was discussed and resolved by the reviewers and senior author. All the articles resulting from our initial search were analyzed for our inclusion and exclusion criteria (**Table 1**) and only articles that satisfied all our inclusion and exclusion criteria were selected for the final analysis.

Data Extraction

All data were extracted from the main manuscript and supplementary text, tables, and figures of the included articles. Our primary outcome of interest was clinical efficacy of combined therapy compared with control therapy in patients with newly diagnosed GBM; (as reflected by median and 1-year survival and PFS). Estimation of survival and PFS at 1 year was done by using the software Plot Digitizer® v.2.6.8 in those articles that did not report these parameters as such. OS and PFS were calculated from the data based on date of surgery until event (death or recurrence). The secondary outcome was toxicity, measure as the number and proportion of incidental grades 3 to 5 adverse events by the end of the study in the standard of care and immunotherapy group as compared with the standard of care group alone. Two independent investigators extracted the data (M.L.V and K.M.B), and confirmation of extracted data was done by two other independent reviewers (H.R.G and J.M.S).

Statistical Analysis

R Studio (36), Version 1.1.383 (Boston, MA) was used to perform the statistical analyses. Generation of random-effects meta-analyses, assessments of heterogeneity and publication bias, and generation of forest plots were conducted as previously described by Lehrer et al. (37) Study arms were compared using the Wald-type test, where the null-hypothesis was rejected for p<0.05.

Quality Evaluation of Clinical Trials

Publications accepted in the study were methodologically evaluated according to the revised Cochrane risk-of-bias tool for randomized trials (38). This system categorizes the studies in low, unclear or high risk of bias, according to the following parameters: random sequence generation, allocation concealment, blinding of participants and personnel, blinding of outcome assessment (self-reported outcomes and objective measures), incomplete outcome data, selective reporting and other bias. Buchroithner, Cho, Kong, Ursu, and Wakabayashi trials had unclear to high risk of bias in at least three different parameters evaluated, Wheeler and Sampson had high risk of bias in five parameters. Weller and Wen trials had unclear risk of bias in only one parameter, making them the trials with lower risk of bias in the entire study (**Supplementary Figure 1**).

We also evaluated the quality of the included trials with the Grading of Recommendations, Assessment, Development, and Evaluation (GRADE) system (GRADEpro). For the evaluated outcomes, 1-year OS and PFS were rated with moderate quality, whereas SAEs grades 3 to 5 were rated as low quality (**Supplementary Tables 4** and **5**).

RESULTS

Study Characteristics

Our initial search resulted in 1901 publications (1809 from PUBMED and 92 from Cochrane). Due to duplicity 213 articles were eliminated, while 1631 were eliminated after the title/abstract was screened based on our inclusion and exclusion criteria. A total of 57 papers met our initial screening of the eligibility criteria. The full text of those articles was analyzed and a total of nine articles met all our inclusion and exclusion criteria and were included for final analysis. Of the nine studies included, seven were phase II clinical trials (77.7%) and two were phase III (22.2%) (**Figure 1** and **Table 2**). Three studies were conducted in North America (39–41), two in Europe (42–44), three in Asia (45–47), and one in Europe and North America (48). Combining all the studies, a total of 1239 patients were included. There were 583 (47%) patients in the immunotherapy and standard of care group, and 656 (52.9%) in the standard of care group. Of the seven articles that described gender information of the included patients (40, 42–50), 619 (60.5%) were male and 403 (39.4%) were female; two articles did not include this information (39, 41). Average age of the patients ranged from 27 years to 72.2
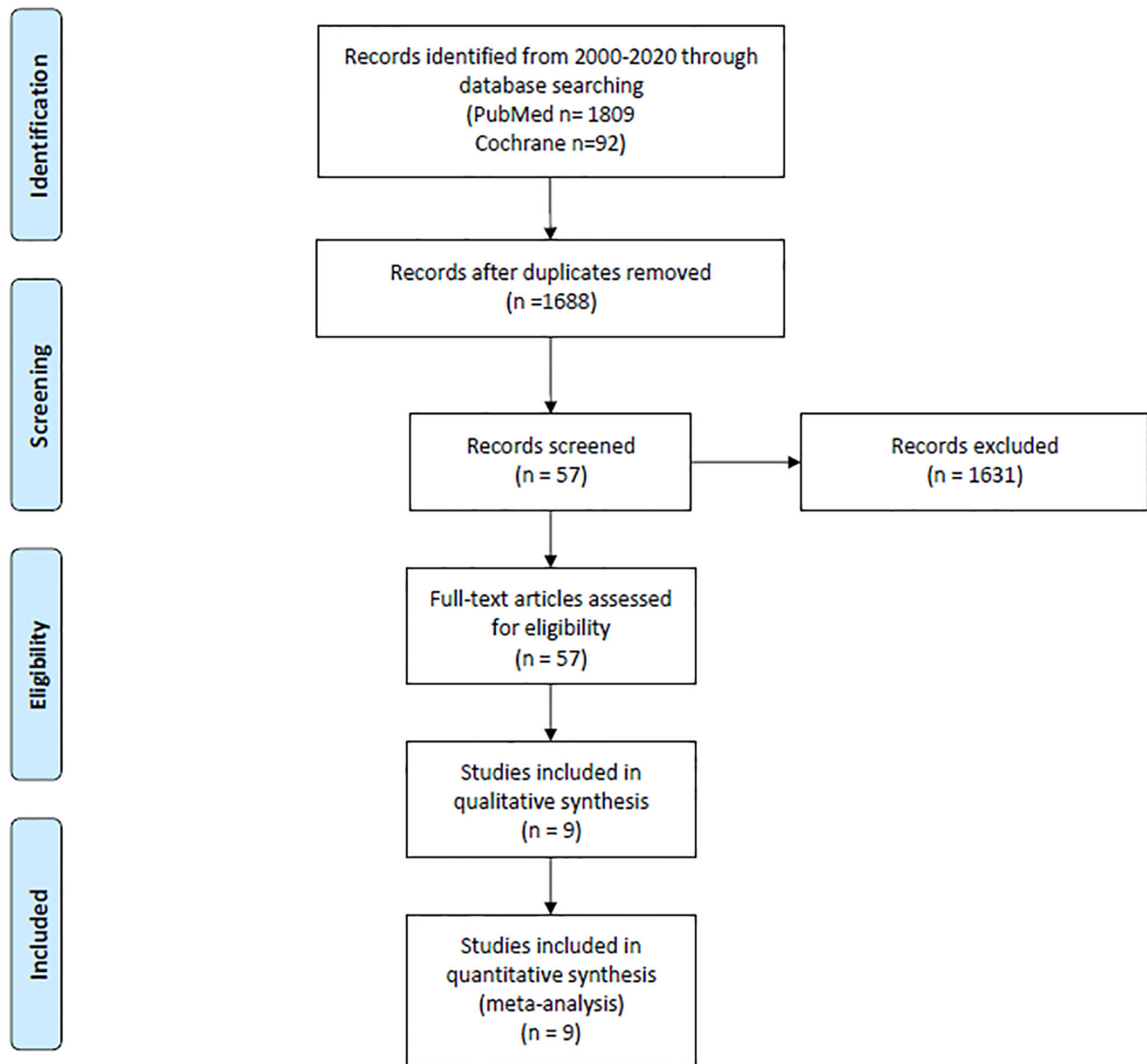
PRISMA 2009 Flow Diagram

FIGURE 1 | PRISMA diagram describing study design and selection (34).

years. Regarding the immunotherapy approach, four studies used cellular vaccines, two used peptide vaccines, one used immunostimulating oligodeoxynucleotides, one interferon β, and one gene-mediated cytotoxic immunotherapy. All trials combined one of these regimens in combination with chemoradiotherapy, while a chemoradiotherapy regimen alone group was used as control in all of them. Four immune based approaches were administered intravenously (44.4%), one cranially (11.1%), three intradermally (33.3%), and one intracranially, intravenously and/or orally (11.1%) (**Supplementary Table 6**).

TABLE 1 | Inclusion and exclusion criteria.

Inclusion	Exclusion
(1) patients with newly diagnosed GBM confirmed by pathology	(1) patients with recurrent GBM
(2) with no other neurological diseases	(2) with other neurological diseases
(3) study specifically described as clinical phase II or III	(3) study not specified as clinical phase II or III
(4) with two arm groups: control and combined	(4) with one arm group only
(5) published only in English	(5) published in other language different than English
(6) limited to human subjects	(6) not limited to human subjects

Finally, we analyzed the clinical trials that used the same immunotherapy strategy. The cellular vaccines subgroup was the only category with enough studies to perform a statistical analysis (four studies total: Buchroithner, Wen, Cho, and Kong) (40, 42, 45, 46).

Clinical Outcomes
Combined Therapy Was Not Associated With Significant Improvement in Overall Survival
The 1-year OS was 72.6% (95% CI: 65.7%–78.9%, I2: 71%) versus 80.6% (95% CI: 68.6%–90.2%, I2: 75%) for the control and combined therapy groups, respectively (p = 0.15). Publication bias was absent with p-values of 0.89 and 0.72, respectively. These results are shown in **Figure 2**. Median OS was 16.9 months in control group vs. 20.1 months in the combined therapy group (**Supplementary Table 7**).

In the cellular vaccine subgroup analysis, 1-year OS was 71.2% (95% CI: 62%.1–79.4%, I^2 = 0%) versus 76.5% (95% CI: 66.8%–85%, I^2 = 4%) for the standard of care and immunotherapy groups, respectively (p = 0.21). There was no publication bias with p-values of 0.82 and 0.36, respectively. These results are shown in **Figure 3**.

Combined Therapy Was Not Associated With Significant Improvement in Progression Free Survival
The estimated 1-year PFS was 37% (95% CI: 26.4–48.2, I^2 = 60%) versus 30.4% (95% CI: 25.4–35.6; I^2 = 0%) for the combined therapy and control groups, respectively (p = 0.17). Publication bias was absent with p-values of 0.13 and 0.63, respectively (**Figure 4**). Two clinical trials were not included in this analysis since they did not describe PFS information properly for GBM patients (35, 44). Median PFS were 8.5 months and 7.7 months in the combined therapy group and control group, respectively (**Supplementary Table 7**).

In the cellular vaccine subgroup analysis, 1-year PFS was 35% (95% CI: 18.2–53.9, I^2 = 62%) versus 26.2% (95% CI: 19.8–33.3, I^2 = 0%) in the combine therapy group and control group, respectively (p = 0.19). No publication bias was present in neither of both groups (p = 0.73 and p = 0.27, respectively) as described in **Figure 5**.

Combined Therapy Was Not Associated With Significant Increase in Incidence of Grade 3-5 Severe Adverse Events
Toxicity analysis was performed with data from four clinical trials that described SAE grades 3 to 5 appropriately (40, 42, 46,

48). SAE was 47.3% (95% CI: 20.8–74.6, I^2 = 95%) versus 43.8% (95% CI: 8.7–83.1, I^2 = 94%) in the combined therapy group and control group, respectively (p = 0.81). There were not bias associated with publication in these studies (p = 0.22 and p = 0.37, respectively). These results are depicted in **Figure 6**. Of the 1110 pooled patients included in this analysis, 184 (16.5%) in the control group versus 201 (18.1%) patients in combined therapy group had a SAE (**Supplementary Table 8**).

In the cellular vaccine subgroup analysis, one trial did not include a full description of SAE (45); thus, subgroup analysis was performed with the other three studies (40, 42, 46). SAEs analysis revealed higher occurrence in the vaccine and standard of care group (57.3%, 95% CI: 51.1–63.4, I^2 = 0%) when compared to standard of care group (49.6%, 95% CI: 0.2–99.8, I^2 = 94%), p = 0.68. Publication bias was absent with p-values of 0.19 and 0.78, respectively. These results are shown in **Figure 7**.
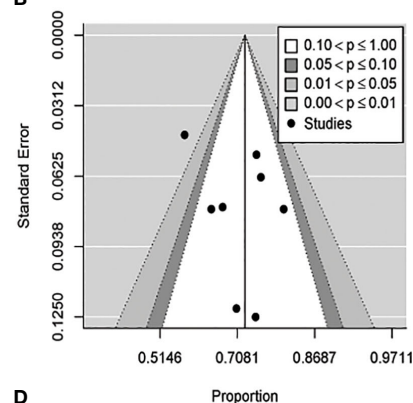
DISCUSSION

In this systematic review and meta-analysis, we objectively analyzed the survival, progression free survival, and toxicity profile of immunotherapy in combination with chemo-radiation versus chemo-radiotherapy alone in newly diagnosed GBM. In regard to overall survival and progression free survival we found that immunotherapy marginally prolonged both; however, this effect was not statistically significant. We also found that immunotherapy with standard of care does not increase grade 3 to 5 SAE in a statistically significant manner when compared to standard of care alone (**Table 3**).

As inherent in the nature of a meta-analysis, our overall analysis is limited by the individual limitations of each of the studies included in the analysis. The number of patients treated in each trial varied widely, from 34 patients (45) to 405 patients (48), between trials thus weighing differently on the overall analysis.

The immunotherapy was administered in different ways [intravenous, intradermal, oral (39, 40, 42, 45–48) and intracerebral (41, 44)] possibly limiting therapeutic distribution as well as immune cell recruitment and diminished effector function. Furthermore, the targeted dose, as well as the number of doses administered, varied among trials. Although most of the studies administered the immunotherapy agent at minimum two to five times, the total number of doses was patient specific and was dependent on clinical progression or death. There was also a variability in the follow-up period between trials, making the comparison between trials heterogeneous. The timing of when the immunotherapy was initiated varied between trials which could influence the overall toxicity profile of the combined strategy and finally determined the reported SAEs in the trials. Most of the trials used an early start of immunotherapy including: 1 to 2 weeks after chemoradiation (42, 48), at the same time as chemoradiation (46), preoperatively (41, 44), on alternate days during radiation (47), and between radiotherapy and at the beginning of temozolomide (40). While two studies showed a mid-late start of immunotherapy: within 6

TABLE 2 | Overall characteristics of the studies.

| First Author	Buchroithner	Cho	Kong	Sampson	Ursu	Wakabayashi	Weller	Wen	Wheeler	Total	Median
Year	2018	2011	2017	2010	2017	2018	2017	2019	2016		
Trial Phase	II	II	III	II	II	II	III	II	II		
Country of Publication	Austria	China	Korea	USA	France	Japan	Switzerland/ USA	USA	USA		
Age (low limit)	19	14	19	29	42	22	51	22	32		27
Age (high limit)	70	70	69	71	78	75	64	81	72		72.2
Patients Included (n)	76	34	180	35	81	122	405	124	182	1239	
Immunoteraphy group (n)	34	18	91	18	39	59	195	81	48	583	
Immunotherapy group (%)	44.73684211	52.94117647	50.55555556	51.42857143	48.14814815	48.36065574	48.14814815	65.32258065	26.37362637		47
Control group (n)	42	16	89	17	42	63	210	43	134	656	
Control group (%)	55.26315789	47.05882353	49.44444444	48.57142857	51.85185185	51.63934426	51.85185185	34.67741935	73.62637363		52.9
Immunotherapy type used	Tumor lysate-charfed autologous dendritic cells (Audencel)	Whole-cell lysate dendritic cell vaccine	Autologous cytokine-induced killer cells	PEPvIII vaccine (13-amino acid peptide w/ an additional terminal cystine that spans the EGFRvIII mutation)	Immunostimulating oligodeoxynucleotides containing unmethylated cytoside-guanosine motifs (CpG-ODN)	Interferon β	Rindopepimut	ICT-107 (autologous dendritic cells)	Aglatimagene besadenovec (AdV- tk) plus valcyclovir (gene-mediated cyottoxic immunotherapy)		
Male (n)	51	16	102	NA	48	73	254	75	NA	619	
Male %	67.10526	47.05882	56.66667	NA	59.25926	59.83607	62.71605	60.48387	NA		60.5
Female (n)	25	18	78	NA	33	49	151	49	NA	403	
Female %	32.89474	52.94118	43.33333	NA	40.74074	40.16393	37.28395	39.51613	NA		39.4
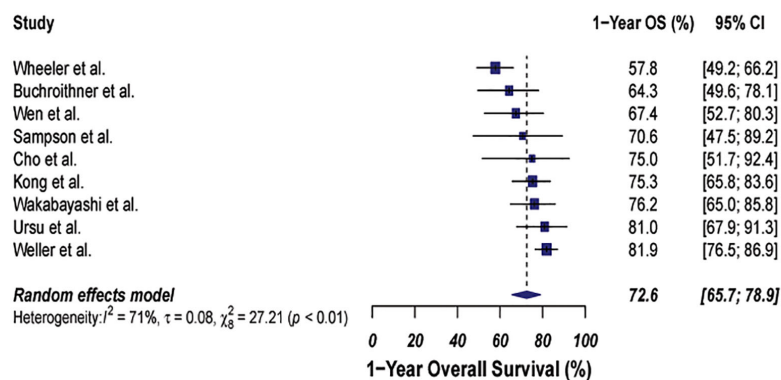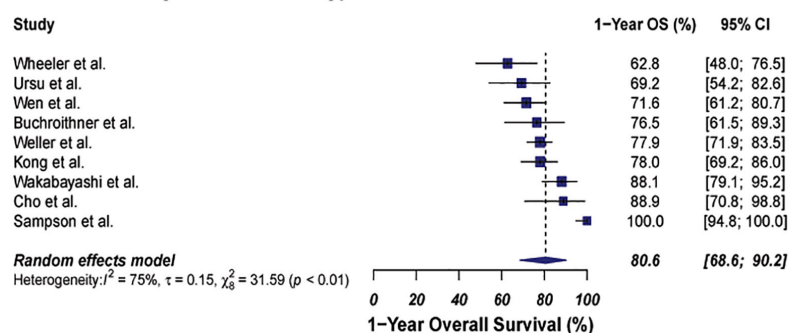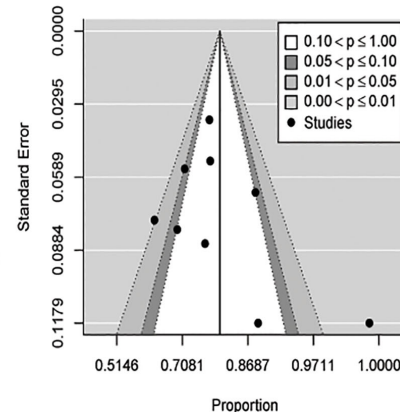
FIGURE 2 | Meta-analysis of 1-year OS in patients from all trials receiving standard of care or immunotherapy plus standard of care therapy. **(A, B)** 1-year OS forest and funnel plots of patients who received standard of care treatment [72.6% (95% CI: 65.7%–78.9%, I2: 71%)]. **(C, D)** 1-year OS forest and funnel plots of patients who received standard of care and immunotherapy treatment [80.6% (95% CI: 68.6%–90.2%, I2: 75%)] (p = 0.15). Funnel plots showing no significant publication bias found in the present meta-analysis in both groups with p-values of 0.89 and 0.72, in standard of care and immunotherapy treatment group respectively. In forest plots size of each square is proportional to its corresponding study's total sample size. The ends of the horizontal bars denote a 95% CI. The diamond gives the overall odds ratio for the combined results of all trials. The center denotes the odds ratio, and the extremities denote the 95% CI.

weeks of completing radiation (39), and 1 to 2 months postoperatively (45).

There was significant variation among concomitant and maintenance therapy regiments that can directly influence OS and PFS of the individual studies. While most of the studies (6/10) used the standardized dose of TMZ and radiation during concomitant treatment (radiation at a dose of 60 Gy and TMZ at a dose of 75 mg/m^2), two studies did not report doses (41, 44), and one study (45) used a higher TMZ dose (100 mg/m^2). During the maintenance phase, TMZ was the most used drug, with some variabilities in dosage (100 mg/m^2 to 200 mg/m^2) and treatment length. Other agents used as maintenance treatment were: bevacizumab, nitrosoureas, irinotecan, tumor-treating fields, other chemotherapy (not defined), investigational drugs, tyrosine kinase inhibitors and check-point inhibitors (42, 44). In addition, there is significant variation in the radiation therapy practices for GBM around the word in terms of radiation dose and treatment field (51–53). Since the clinical trials included in our analysis originated in several different countries this variability is built into

our model and is likely playing a critical role in the overall heterogeneity of the studies and overall outcome parameters being assessed.

Another known factor that significantly impacts patient's overall survival and PFS is the extent of resection (54, 55), which varied widely amongst the studies included in this meta-analysis. The variability in the total volume of tumor resected between studies is a limiting factor in evaluating the true response rate of immunotherapy. Patients were categorized under gross, subtotal, partial, and large resection, and in residual or non-residual disease. To make our analysis as consistent as possible, our calculations in the studies that considered those variables, were based on OS and PFS of total number of patients included without making distinctions in the surgical outcome. However, this almost certainly introduced some variability and noise into our data that could have been accounted for with a more consistently designed set of trials. Also, PFS assessment variability between studies has to be considered, since pseudo-progression is still a
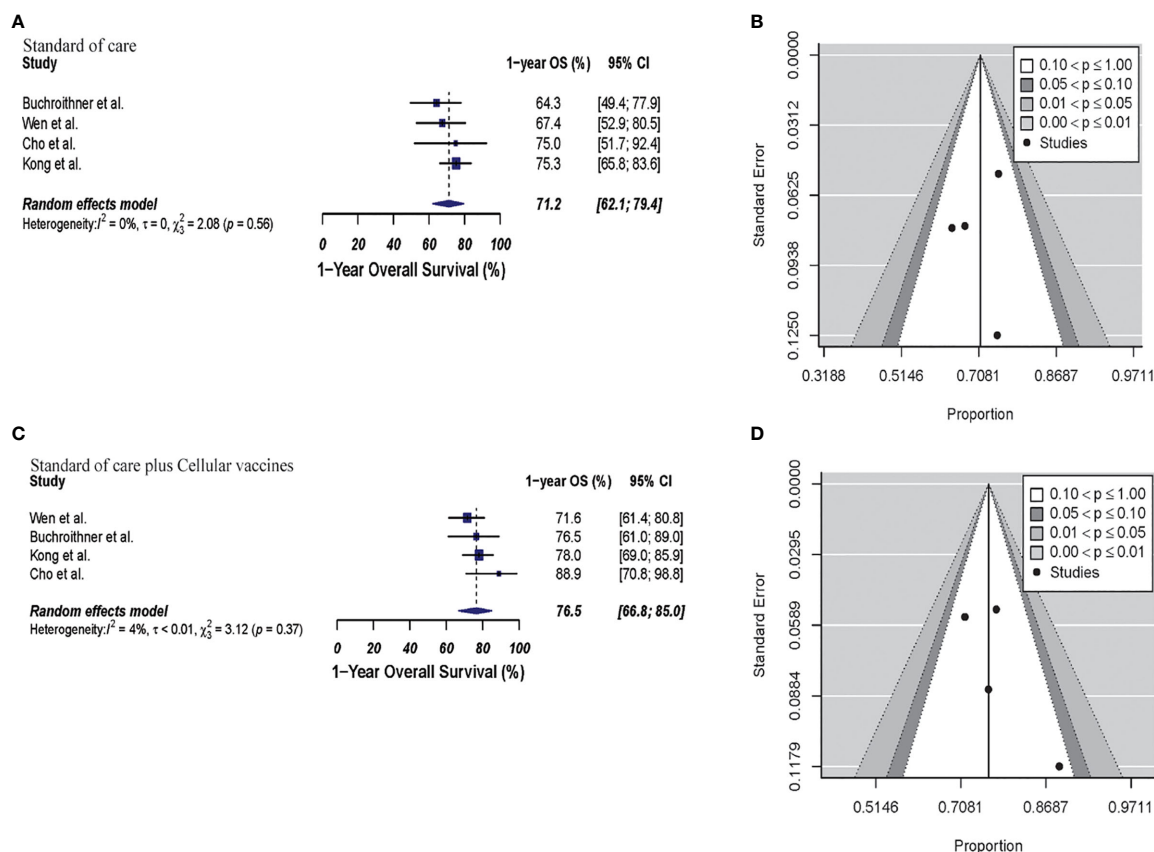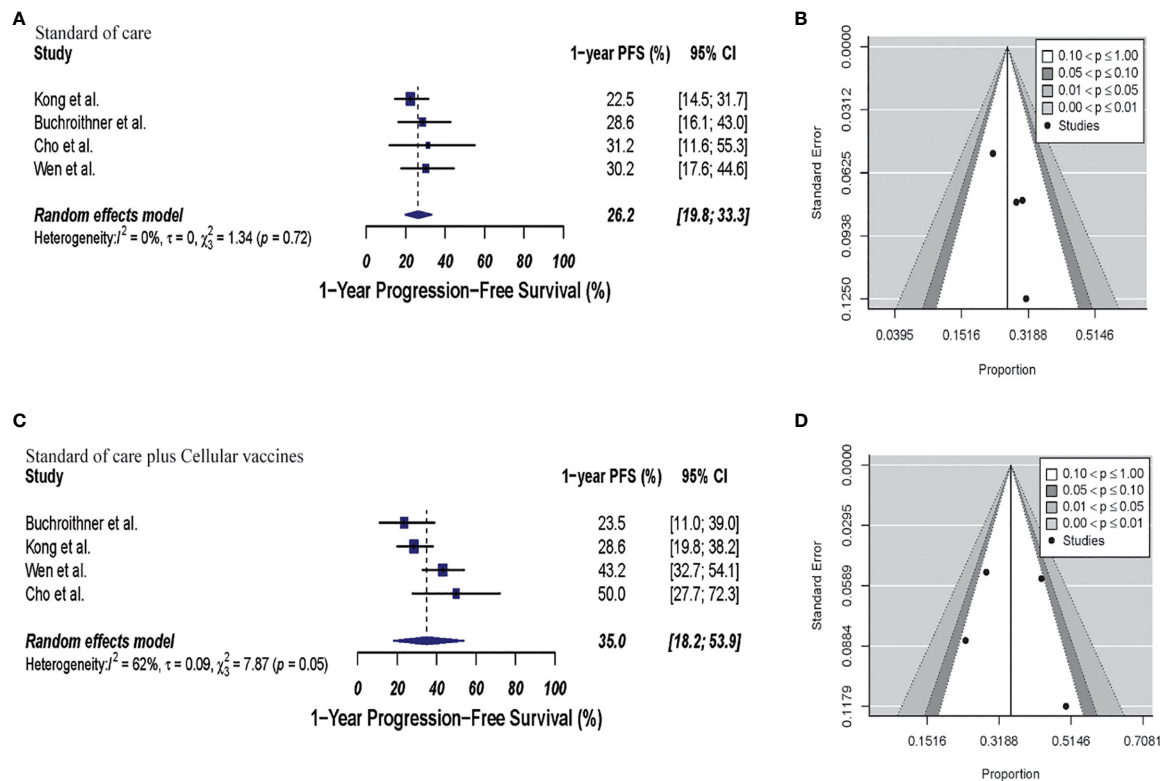
FIGURE 3 | Meta-analysis of 1-year OS in patients from trials receiving standard of care or cellular vaccine therapy plus standard of care therapy. **(A, B)** 1-year OS forest and funnel plots of patients who received standard of care treatment [71.2% (95% CI: 62.1–79.4, I^2 = 0%)]. **(C, D)** 1-year OS forest and funnel plots of patients who received standard of care and cellular vaccine treatment [76.5% (95% CI: 66.8%–85%, I^2 = 4%) (p = 0.21)]. Funnel plots showing no significant publication bias found in the present meta-analysis in both groups with p-values of 0.82 and 0.36, in standard of care and immunotherapy treatment group respectively. In forest plots size of each square is proportional to its corresponding study's total sample size. The ends of the horizontal bars denote a 95% CI. The diamond gives the overall odds ratio for the combined results of all trials. The center denotes the odds ratio, and the extremities denote the 95% CI.

controversial topic (56) that need to be addressed to ensure clear accountability of this parameter in response to immunotherapy. Although the Macdonald criteria for tumor response assessment was used by the majority of the studies, this classification has multiple limitations such as the presence of necrosis or residual changes secondary to tumor resection. As a result, a more comprehensive imaging criteria was defined for assessing response/progression by the Response Assessment in Neuro-Oncology (RANO) (57) and the immunotherapy response assessment for Neuro-oncology (iRANO). The RANO criteria is widely used in clinical trials in oncology for an accurate assessment of pseudo progression in response to temozolomide and radiotherapy in malignant gliomas during concomitant or maintenance regimens (58). RANO criteria does not suit properly the needs for response evaluation in patients treated with immune based therapies. Thus, the iRANO criteria was defined to assess clinical outcomes and tumor regression despite progression of the disease in the context of immunotherapy (59). It accounts for the differential mechanistic and imaging findings

elicited by immunotherapy to the ones by chemoradiation; such as enhancing lesions outside the main radiation field and delayed therapeutic efficacy, that with other criteria would be classified as disease progression (60). iRANO defines disease progression when tumor persistence is registered in a specific period of time, after an initial radiographical evidence of tumor progression in response to immunotherapy (60).

Finally, although for the purposes of this analysis, we combined the included studies into the broad umbrella of "immunotherapy" it is useful to examine the specific therapies in more detail to clearly understand the clinical immunotherapy landscape.

Cellular Vaccines

Our analysis included three phase II clinical trials (Buchroithner et al. with 76 patients, Cho et al. with 34 patients and Wen et al. with 124 patients), that used dendritic cells, and one phase III trial (Kong et al. with 180 patients) that used cytokine-induced
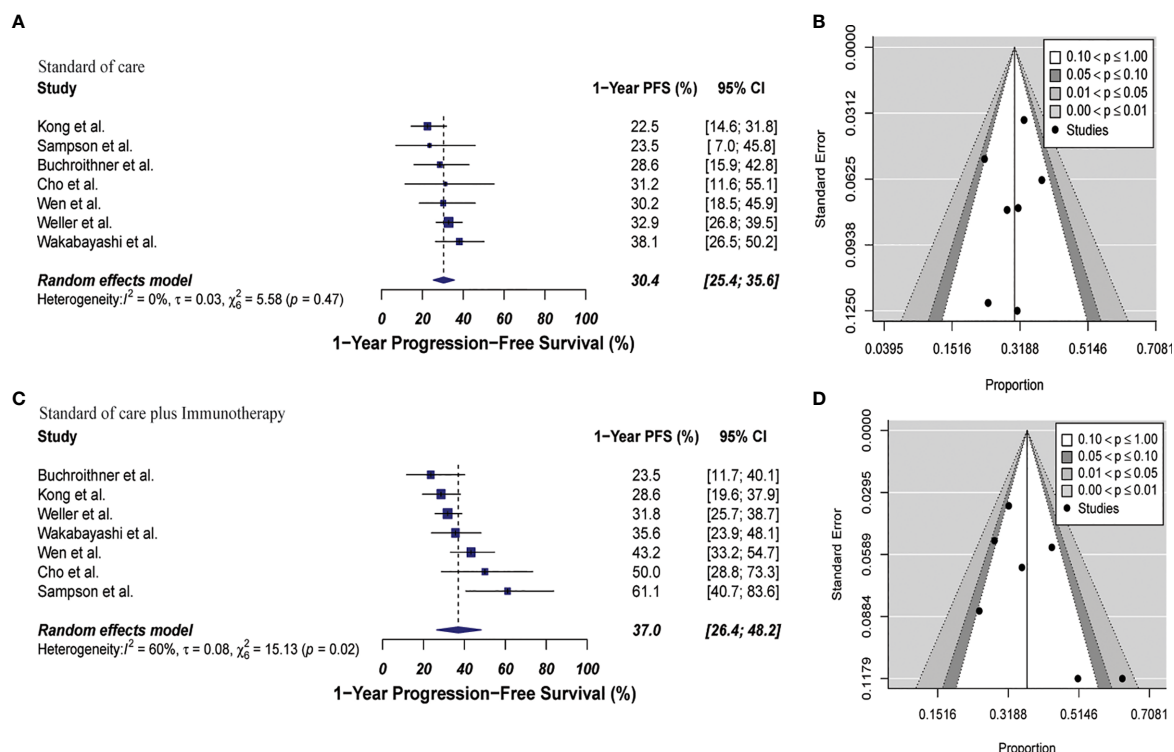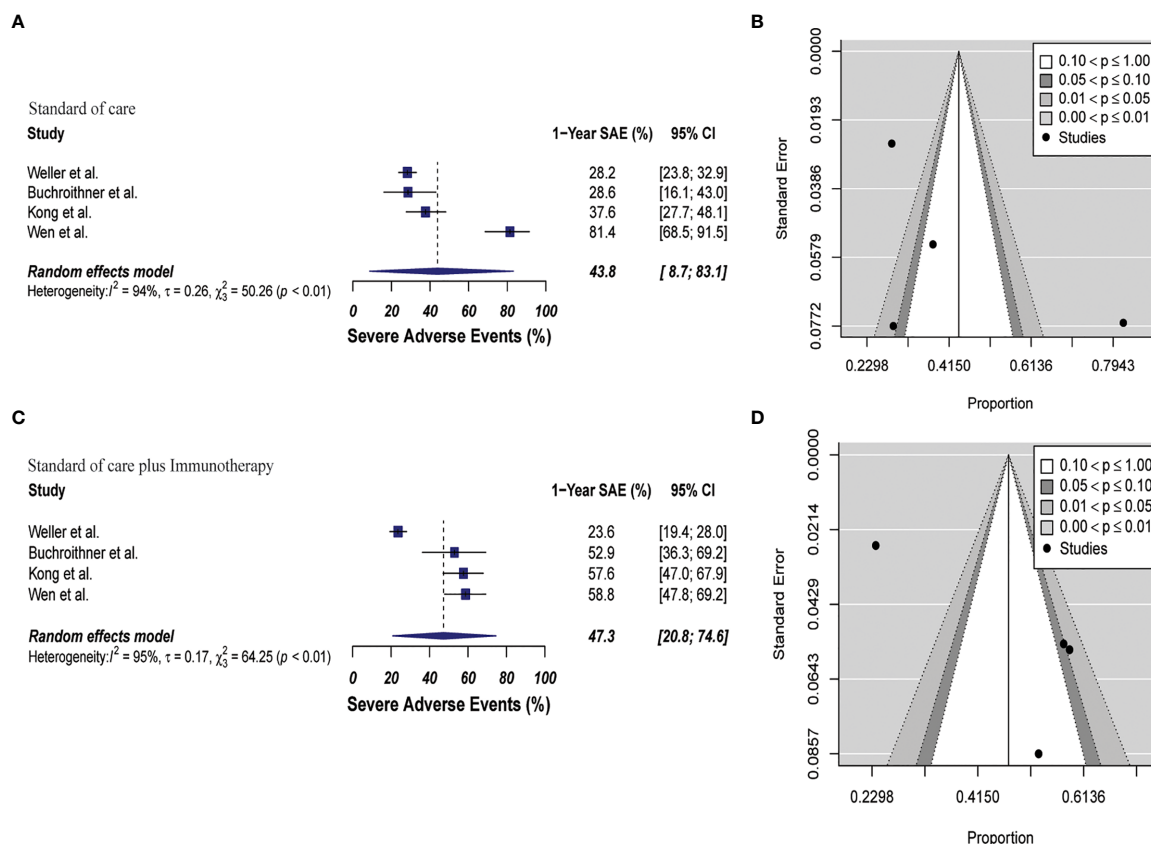
FIGURE 4 | Meta-analysis of 1-year PFS in patients from all trials receiving standard of care or immunotherapy plus standard of care therapy. **(A, B)** 1-year PFS forest and funnel plots of patients who received standard of care treatment [30.4% (95% CI: 25.4–35.6; I^2 = 0%)]. **(C, D)** 1-year PFS forest and funnel plots of patients who received standard of care and immunotherapy treatment [37% (95% CI: 26.4–48.2, I^2 = 60%) (p = 0.17)]. Funnel plots showing no significant publication bias found in the present meta-analysis in both groups with p-values of 0.63 and 0.13 in standard of care and immunotherapy treatment group respectively. In forest plots size of each square is proportional to its corresponding study's total sample size. The ends of the horizontal bars denote a 95% CI. The diamond gives the overall odds ratio for the combined results of all trials. The center denotes the odds ratio, and the extremities denote the 95% CI.

killer (CIK) cells with standard of care. Of these, the trial by Cho et al. showed the highest improvement in median and 1-year survival expectancy (median OS:15 *vs* 31.9 months, and 1-year OS: 75% *vs* 88.9%, in control *versus* combined therapy, respectively). This can be attributed primarily to two distinct features of the trial: 1) the strategy of using personalized DCs vaccines, where a diverse group of individualized highly immunogenic peptides educating the DCs, could potentially elicit a better tumor clearance by the immune system and 2) the adjuvant treatment strategy used upon tumor recurrence, defined by tumor size increase >20%, which included repeated surgical-intervention, chemotherapy or boost gamma knife radiosurgery. In addition, a reinforced dose of vaccination (made from recurrent tumor tissue) was given to patients that underwent a second surgery (6 of 18 patients).

Of the four trials in this category the trial by Kong et al. was a phase III trial that showed very modest effect with an extension of 5.6 months in median OS and 3% improvement at 1-year survival. The limited response in survival in this study could be mainly due to biodistribution of the cytokine induced lymphocytes and their ability to selectively home into the tumor microenvironment. Additionally, there was some

variability in the timing of the administration of the cells which most likely influenced the overall outcome of the trial.

Peptide Vaccines

EGFR (epidermal growth factor receptor) overexpression is one of the most prevalent mutations in GBM (60%) (61). 20% to 30% of these tumors, present a deletion of exons 2 to 7 in the EGFRvIII receptor (type III EGFR) (62). Sampson et al, phase II trial included 35 patients using EGFRvIII-targeted peptide vaccine and chemo-radiotherapy, showed an extension of approximately 9 months in median OS and PFS, extension of almost 30% at 1-year survival and 40.1% at 1-year PFS. However, in the phase III clinical trial that included 405 patients using this strategy, Weller et al, found no benefits in overall survival or PFS. (Median OS of ˜ 20 months in both groups, 1-year survival decreased by 4% with immunotherapy, improvement of 0.6 months in median PFS and 1% decrease at 1-year PFS, with combined treatment). Benefits in the trial by Sampson et al. could be due to an enhanced humoral and cellular immune response rate produced by the vaccine elicited with dose intensified TMZ regiment (100 mg/m^2 for first 21 days of 28 days cycle) in comparison with standard dosing (200 mg/m^2 for

FIGURE 5 | Meta-analysis of 1-year PFS in patients from trials receiving standard of care or cellular vaccine therapy plus standard of care. **(A, B)** 1-year PFS forest and funnel plots of patients who received standard of care treatment [26.2% (95% CI: 19.8–33.3, I² = 0%)]. **(C, D)** 1-year PFS forest and funnel plots of patients who received standard of care and cellular vaccine treatment [35% (95% CI: 18.2–53.9, I² = 62%) (p = 0.19)]. Funnel plots showing no significant publication bias found in the present meta-analysis in both groups p = 0.27 and p = 0.73, in standard of care and immunotherapy treatment group respectively. In forest plots size of each square is proportional to its corresponding study's total sample size. The ends of the horizontal bars denote a 95% CI. The diamond gives the overall odds ratio for the combined results of all trials. The center denotes the odds ratio, and the extremities denote the 95% CI.

first 5 days of 28 days cycle), that was significant despite chemotherapy-induced lymphopenia. In comparison the phase III trial by Weller et al. used only the standard TMZ protocol and did not have the dose intensified arm. It is well described that the patient selection criteria and overall health status of the patients enrolled heavily weighs on the overall outcome of the patients in clinical trial (63). The majority of the patients included in the Sampson et al. trial had KPS score of 100 whereas majority of the patients in the Weller et al. trial had RPA class IV or higher, which most likely influenced the overall outcome. Most importantly the trial by Sampson et al. used historical control group which might not truly capture the complexity of the trial group and hence does not represent a true control arm.

Other Immune-Based Therapies

Other forms of immunotherapy clinical trials included: a) intracerebral administration of CpG ODN (44), b) intravenous IFNβ (47) and c) gene-mediated cytotoxic immunotherapy (aglatimagene besadenovec (AdV-tk), an adenoviral vector containing the herpes simplex virus thymidine kinase gene, followed by an antiherpetic prodrug such as valacyclovir) (41).

The phase II trial by Ursu et al. included 81 patients, showed no improvement in median and 1-year survival or median PFS with intracerebral administration of CpG ODN and chemo-radiation. (median OS ˜ 18 months and median PFS ˜ 9 months in both groups, and 1-year survival decreased by 10%). The results of this trial again highlight the difficulties surrounding the issue of drug delivery and penetration in the context of GBM. In this trial CpG ODN was injected by needles in the resection cavity which restricted the amount of drug that penetrated beyond a small perimeter. Most local drug delivery studies report reliable penetration only few millimeters from the site of injection (50), whereas studies with convention enhanced delivery have reported a diffusion in centimeters (64, 65), still any tumor cells beyond that margin will not be affected by this treatment strategy.

The phase II clinical trial by Wakabayashi et al. included 122 patients and evaluated IFNβ in combination with standard of care for newly diagnosed GBMs and found an extended median OS of almost 4 months (1-year survival rate improved by 11%) with combination therapy but a decrease in PFS by 1.6 months (1-year PFS decreased by 2.5%). IFNβ was used as a
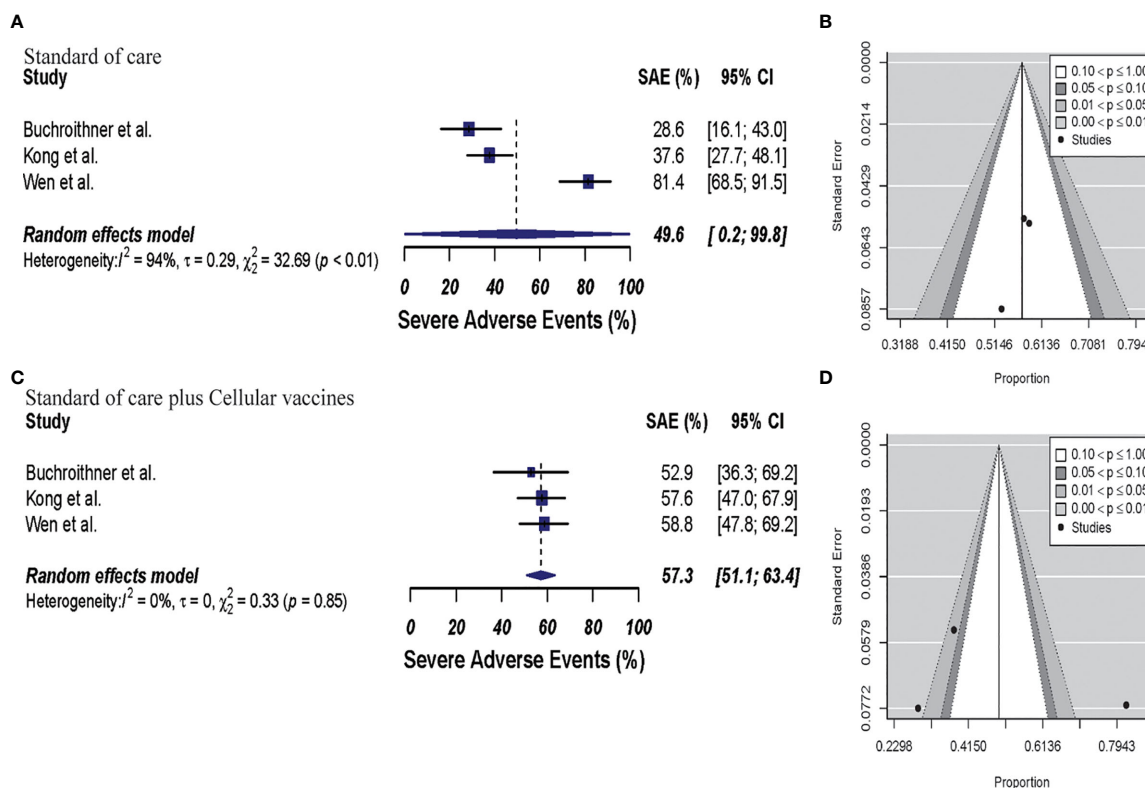
FIGURE 6 | Meta-analysis of SAEs grade 3 to 5 in patients from trials receiving standard of care or immunotherapy plus standard of care therapy. **(A, B)** SAEs forest and funnel plots of patients who received standard of care treatment [43.8% (95% CI: 8.7–83.1, I² = 94%)]. **(C, D)** SAEs forest and funnel plots of patients who received standard of care and immunotherapy treatment [47.3% (95% CI: 20.8–74.6, I² = 95%) (p = 0.81)]. Funnel plots showing no significant publication bias found in the present meta-analysis in both groups p = 0.37 and p = 0.22, in standard of care and immunotherapy treatment group respectively. In forest plots size of each square is proportional to its corresponding study's total sample size. The ends of the horizontal bars denote a 95% CI. The diamond gives the overall odds ratio for the combined results of all trials. The center denotes the odds ratio, and the extremities denote the 95% CI.

chemosensitizer that enhances the toxicity of chemotherapeutic agents such as TMZ. Thus, it is not surprising that the combination therapy arm had significantly higher rate of hematological as well as non-hematological toxicities. Higher toxicity also negatively impacted treatment compliance to the point that a high number of patients terminated the treatment protocol prematurely, which most likely played a role in the poor overall survival.

The Wheeler et al. phase II trial included 182 patients total and tested gene-mediated cytotoxic (GMC) immunotherapy in combination with standard of care. This trial did not yield survival benefits either, GBM data sub analysis showed 3-month prolonged median OS and 1-year survival rate improved by 5% that were not statistically significant. Efficacy and biodistribution of the virus delivery by local injection in the resection cavity is limited by the previously outlined constrains of drug or biological agents penetration issues in the CNS microenvironment. In addition, virus particles induce prompt and effective anti-virus immune response which accelerates the

clearance of virus further limiting its penetration in the tumor microenvironment (66). If the issue of immune mediated virus clearance is not weighted in properly into the timing of administration of the activating pro-drug there will be no effective immune response. Extent of resection is also important when assessing the likelihood of overall success of immunotherapy since immunosuppressive features such as expression of PD-L1, presence of regulatory cells etc. in the residual tumors decreases the overall efficacy of the immunotherapy (67).

In summary, upon closer evaluation of the individual immunotherapies across the trials analyzed in this study, it becomes clear that there is a large amount of variability in patient response within the trials and across the trials. This highlights the often-seen tail phenomenon of GBM patients in immunotherapy trials where there are small groups of patients who do respond and do while even if the majority of patients in cohort may not benefit resulting in an overall negative trial (16). This data points toward the need for better design of

FIGURE 7 | Meta-analysis of SAEs grade 3 to 5 in patients from trials receiving standard of care or cellular vaccine therapy plus standard of care. **(A, B)** SAEs forest and funnel plots of patients who received standard of care treatment [49.6% (95% CI: 0.2–99.8, I^2 = 94%)]. **(C, D)** SAEs forest and funnel plots of patients who received standard of care plus cellular vaccine treatment [57.3% (95% CI: 51.1–63.4, I^2 = 0%) (p = 0.68)]. Funnel plots showing no significant publication bias in both groups with p-values of 0.78 and 0.19 in standard of care and immunotherapy treatment group respectively. In forest plots size of each square is proportional to its corresponding study's total sample size. The ends of the horizontal bars denote a 95% CI. The diamond gives the overall odds ratio for the combined results of all trials. The center denotes the odds ratio, and the extremities denote the 95% CI.

TABLE 3 | Summarized results for 1-year OS and PFS, and SAEs in standard of care and standard of care and immunotherapy groups, and for trials that used cellular vaccines only.

Group	Outcome	Wald Test	Peter's Test
Control	1y OS	Ref	0.89
Combined	1y OS	0.15	0.72
Control (Vaccine Only)	1y OS	Ref	0.82
Combined (Vaccine Only)	1y OS	0.21	0.36
Control	1y PFS	Ref	0.63
Combined	1y PFS	0.17	0.13
Control (Vaccine Only)	1y PFS	Ref	0.27
Combined (Vaccine Only)	1y PFS	0.19	0.73
Control	SAE	Ref	0.37
Combined	SAE	0.81	0.22
Control (Vaccine Only)	SAE	Ref	0.78
Combined (Vaccine Only)	SAE	0.68	0.19

immunotherapy clinical trials that include potential responders using synergistic combination therapy that boosts the overall function of the immune system in addition to tumor specific immune response.

Severe Adverse Events in Immunotherapy

SAEs in clinical trials are considered as complications/toxicity, morbidity or mortality as a result of a tested treatment (68). They can be symptomatic (reported by the patient) or asymptomatic (detected during a physical examination, laboratory results or imaging reports) (69). Grade 1 and 2 events are mild or moderate, or even asymptomatic symptoms that can be managed with outpatient medication. Grade 3 events are severe non-immediately-life threatening symptoms that can be controlled usually during inpatient treatment or prolonged hospitalization (parental administration of drugs or surgical intervention). Grade 4 events put the life of the person at risk, and can result in disabilities and organ dysfunctions, whereas grade 5 events are deadly (69, 70).

There was significant heterogeneity in the SAE reporting criteria used by each of the clinical trials included in this meta-analysis. Criteria used for the grading and defining grade 3 to 5 SAEs in the studies included in this analysis were the National Cancer Institute (NCI) Common Terminology Criteria for Adverse Events (CTCAE) version 3.0 by Wheeler et al, Wakabayashi et al, and by Kong et al, and version 4.0 by

Weller et al. The precursor of this classification, the NCI Common Toxicity Criteria (CTC) version 2.0 was used by Sampson et al, version 3.0 by Ursu, version 4.0 by Buchroithner, and 4.03 by Wen. Cho's trial did not specify the classification used. Analysis of SAEs grade 3 to 5 in Cho, Sampson, Ursu, Wakabayashi and Wheeler's trials were not possible due to the presentation of the data. (ie, grades 2 and 3 events reported combined, events non-separated by grade, and events reported separately during concomitant and/or maintenance treatment).

We only used four out of the nine studies for the grade 3 to 5 SAE analysis (40, 42, 46, 48). Our analysis showed an increased occurrence of grade 3 to 5 SAEs associated with immunotherapy in combination with chemo-radiation compared to chemo and radiation but the effect failed to reach statistical significance. Although some of these events may be expected due to the immune nature of the therapies and the known effects of chemoradiation, the majority of these were severe non-immediately-life threatening SAEs controlled with inpatient medication or hospitalization. The only two deadly events found with our analysis was with the immunotherapy CpG in the study by Ursu et al. (secondary to reactivation of hepatitis B infection) and the peptide vaccine in Sampson's trial (due to pulmonary embolism). Among immunotherapy approaches, the most common SAEs were: headache, nausea, vomiting, seizures, constipation, diarrhea, weakness, anorexia, pyrexia, increase transaminases, increase lipases, increase intracranial pressure, and rash/allergic reactions. Hematological toxicities frequently seen after immunotherapy and standard of care were: lymphopenia, thrombocytopenia and neutropenia (For grading criteria of the most common grade 3 to 5 SAEs found among trials go to **Supplementary Table 9**).

Pneumonia and acute-renal failure were specifically described in one trial using cellular vaccines (46). Peptide vaccines were specifically linked with brain edema, and one deadly event due to pulmonary thromboembolism (48). CpG ODN and chemo-radiation was related with post-surgical hematoma, seizures (probably secondary to the intracerebral administration of the agent), and with one death related with reactivation of hepatitis B infection (although a full analysis of SAEs was not possible due to the format used for data presentation). Gene-mediated cytotoxicity therapy was related with hemiparesis (motor neuropathy), speech impairment, insomnia, and wound complication (specific analysis of SAEs 3 to 5 was not possible due to how the data was presented).

Taken together, this evidence demonstrates that although adverse events grade 3 to 5 are more frequent in the immunotherapy and chemo-radiation treatment when compared with chemo-radiation only, they are mostly non-deadly toxicities that can be managed during an inpatient encounter or hospitalization. Importantly, our findings are in accordance with the data described in the retrospective study of 22 trials done by Magee and colleagues in 2020, where the risk of an adverse event grade 3 or higher was increased in the immunotherapy arm compared with the chemotherapy arm alone for solid tumors (71). Nonetheless, our data show that

this trend in increased toxicity in immunotherapy was not statistically significant.

STRENGTHS AND LIMITATIONS

The strength of our study lies in the strict inclusion and exclusion criteria used for article selection. We used a clearly defined list formed by several characteristics allowing us to compare control versus combined therapy in newly diagnosed GBM patients. This eliminated the potential of patients having received prior treatment. Additionally, we included phase II and III clinical trials that evaluated survival benefits (OS and PFS), as well as toxicity (SAEs) secondary to treatment. By doing so, we were able to perform a more reliable comparison of the results in the control and combined groups for each study. Moreover, we attempted to reduce heterogeneity by excluding trials that were not specifically described as phase II or III, even if they described OS, PFS, or adverse events related with immunotherapy.

Our study also has significant limitations, with inherent variabilities between studies, such as sample size and different statistical methods (HR, CIs) as well as variable modalities of immunotherapies, radiation and chemotherapy doses. Also, in GBM the response to chemo-radiotherapy is significantly affected by the genetic makeup of the tumor (72) and through analysis of biological confounding variables, such as IDH mutations, 1p19q co-deletion, MGMT status etc, could not be done since many trials did not include this information. Importantly, the lack of similarity in treatment modalities and schemes used in these studies limits a truly fair comparison of the possible benefit of immunotherapy. Another limitation in our study is the selection of clinical trials phase II and III, that might bias the results due to the often benefit seen in clinical studies phase II, that do not demonstrate benefits when tested in multiple centers in larger cohorts during phase III trials. Our intention is not to overestimate (or vice versa) the effect of immunotherapy in GBM, but to demonstrate that more clinical trials accounting for dependent and independent-patient variables are needed to truly understand the full potential of immunotherapy in combination with current standard of care.

CONCLUSION

In summary, our results demonstrated that the combination of immunotherapy with standard of care chemotherapy and radiation produced no significant survival benefit in patients. Furthermore, the combination was not significantly associated with an increased incidence of grade 3 to 5 SAEs, despite the observed trend. Most of these SAEs were successfully managed clinically, which allow us to conclude that the integration of immunotherapy into the standard of care for GBM is relatively safe. We believe, standardization of clinical trials in regard to immunotherapy and chemo-radiation treatment schemes for GBM treatment is necessary for a more accurate comparison

and analysis of these combined treatments and is warranted to fully explore the potential benefits of this therapeutic combination.

DATA AVAILABILITY STATEMENT

The original contributions presented in the study are included in the article/**Supplementary Material**. Further inquiries can be directed to the corresponding author.

AUTHOR CONTRIBUTIONS

ML-V, JS, MD, and HR-G wrote the manuscript. ML-V, KB, HR-G, and JS collected the data. EJL, MP, and RC analyzed the data.

SUPPLEMENTARY MATERIAL

The Supplementary Material for this article can be found online at: https://www.frontiersin.org/articles/10.3389/fonc.2021.662302/full#supplementary-material

REFERENCES

1. Jang HS, Shin WJ, Lee JE, Do JT. Cpg and Non-CpG Methylation in Epigenetic Gene Regulation and Brain Function. *Genes (Basel)* (2017) 8:148. doi: 10.3390/genes8060148

2. Davis ME. Glioblastoma: Overview of Disease and Treatment. *Clin J Oncol Nurs* (2016) 20:S2–8. doi: 10.1188/16.CJON.S1.2-8

3. Nabors LB, Portnow J, Ahluwalia M, Baehring J, Brem H, Brem S, et al. Central Nervous System Cancers, Version 3.2020, NCCN Clinical Practice Guidelines in Oncology. *J Natl Compr Canc Netw* (2020) 18:1537–70. doi: 10.6004/jnccn.2020.0052

4. Stupp R, Mason WP, van den Bent MJ, Weller M, Fisher B, Taphoorn MJB, et al. Radiotherapy Plus Concomitant and Adjuvant Temozolomide for Glioblastoma. *N Engl J Med* (2005) 352:987–96. doi: 10.1056/NEJMoa043330

5. Lara-Velazquez M, Al-Kharboosh R, Jeanneret S, Vazquez-Ramos C, Mahato D, Tavanaiepour D, et al. Advances in Brain Tumor Surgery for Glioblastoma in Adults. *Brain Sci* (2017) 7(10):1100–8. doi: 10.3390/brainsci7120166

6. Fernandes C, Costa A, Osório L, Costa Lago R, Linhares P, Carvalho B, et al. Current Standards of Care in Glioblastoma Therapy. In: S De Vleeschouwer, editor. *Glioblastoma*. Brisbane (AU: Codon Publications Copyright: The Authors (2017).

7. Stupp R, Taillibert S, Kanner AA, Kesari S, Steinberg DM, Toms SA, et al. Maintenance Therapy With Tumor-Treating Fields Plus Temozolomide vs Temozolomide Alone for Glioblastoma: A Randomized Clinical Trial. *JAMA* (2015) 314:2535–43. doi: 10.1001/jama.2015.16669

8. Mallick S, Benson R, Hakim A, Rath GK. Management of Glioblastoma After Recurrence: A Changing Paradigm. *J Egypt Natl Canc Inst* (2016) 28:199–210. doi: 10.1016/j.jnci.2016.07.001

9. Gandhi L, Rodriguez-Abreu D, Gadgeel S, Esteban E, Felip E, De Angelis F, et al. Pembrolizumab Plus Chemotherapy in Metastatic non-Small-Cell Lung Cancer. *N Engl J Med* (2018) 378:2078–92. doi: 10.1056/NEJMoa1801005

10. Lehrer EJ, McGee HM, Peterson JL, Vallow L, Ruiz-Garcia HG, Zaorsky N, et al. Stereotactic Radiosurgery and Immune Checkpoint Inhibitors in the Management of Brain Metastases. *Int J Mol Sci* (2018) 19(10):3054. doi: 10.3390/ijms19103054

11. Lehrer EJ, McGee HM, Sheehan JP, Trifiletti DM. Integration of Immuno-Oncology With Stereotactic Radiosurgery in the Management of Brain Metastases. *J Neurooncol* (2021) 151:75–84. doi: 10.1007/s11060-020-03427-6

12. Lehrer EJ, Peterson J, Brown PD, Sheehan JP, Quiñones-Hinojosa A, Zaorsky NG, et al. Treatment of Brain Metastases With Stereotactic Radiosurgery and Immune Checkpoint Inhibitors: An International Meta-Analysis of Individual Patient Data. *Radiother Oncol* (2019) 130:104–12. doi: 10.1016/j.radonc.2018.08.025

13. Reck M, Rodriguez-Abreu D, Robinson AG, Hui R, Csőszi T, Fülöp A, et al. Pembrolizumab Versus Chemotherapy for PD-L1-Positive non-Small-Cell Lung Cancer. *N Engl J Med* (2016) 375:1823–33. doi: 10.1056/NEJMoa1606774

14. Tan AC, Ashley DM, López GY, Malinzak M, Friedman HS, Khasraw M, et al. Management of glioblastoma: State of the art and future directions. *CA Cancer J Clin* (2020) 70:299–312. doi: 10.3322/caac.21613

15. Kamiya-Matsuoka C, Gilbert MR. Treating Recurrent Glioblastoma: An Update. *CNS Oncol* (2015) 4:91–104. doi: 10.2217/cns.14.55

16. McGranahan T, Therkelsen KE, Ahmad S, Nagpal S. Current State of Immunotherapy for Treatment of Glioblastoma. *Curr Treat Options Oncol* (2019) 20:24. doi: 10.1007/s11864-019-0619-4

17. Wahid B, Ali A, Rafique S, Waqar M, ad Wasim M, Wahid K, et al. An Overview of Cancer Immunotherapeutic Strategies. *Immunotherapy* (2018) 10:999–1010. doi: 10.2217/imt-2018-0002

18. Yang Y. Cancer Immunotherapy: Harnessing the Immune System to Battle Cancer. *J Clin Invest* (2015) 125:3335–7. doi: 10.1172/JCI83871

19. Johanns TM, Bowman-Kirigin JA, Liu C, Dunn GP. Targeting Neoantigens in Glioblastoma: An Overview of Cancer Immunogenomics and Translational Implications. *Neurosurgery* (2017) 64:165–76. doi: 10.1093/neuros/nyx321

20. Raucher D. Tumor Targeting Peptides: Novel Therapeutic Strategies in Glioblastoma. *Curr Opin Pharmacol* (2019) 47:14–9. doi: 10.1016/j.coph.2019.01.006

21. Koury J, Lucero M, Cato C, Chang L, Geiger J, Henry H, et al. Immunotherapies: Exploiting the Immune System for Cancer Treatment. *J Immunol Res* (2018) 2018:9585614. doi: 10.1155/2018/9585614

22. Waldman AD, Fritz JM, Lenardo MJ. A Guide to Cancer Immunotherapy: From T Cell Basic Science to Clinical Practice. *Nat Rev Immunol* (2020) 20:651–68. doi: 10.1038/s41577-020-0306-5

23. Al-Kharboosh R, ReFaey K, Lara-Velazquez M, Grewal SS, Imitola J, Quiñones-Hinojosa A. Inflammatory Mediators in Glioma Microenvironment Play a Dual Role in Gliomagenesis and Mesenchymal Stem Cell Homing: Implication for Cellular Therapy. *Mayo Clin Proc Innov Qual Outcomes* (2020) 4:443–59. doi: 10.1016/j.mayocpiqo.2020.04.006

24. Choi BD, Maus MV, June CH, Sampson JH. Immunotherapy for Glioblastoma: Adoptive T-cell Strategies. *Clin Cancer Res* (2019) 25:2042–8. doi: 10.1158/1078-0432.CCR-18-1625

25. Sampson JH, Maus MV, June CH. Immunotherapy for Brain Tumors. *J Clin Oncol* (2017) 35:2450–6. doi: 10.1200/JCO.2017.72.8089

26. Akhavan D, Alizadeh D, Wang D, Weist MR, Shepphird JK, Brown CE. Car T Cells for Brain Tumors: Lessons Learned and Road Ahead. *Immunol Rev* (2019) 290:60–84. doi: 10.1111/imr.12773

27. Weenink B, French PJ, Sillevis Smitt PAE, Debets R, Geurts M. Immunotherapy in Glioblastoma: Current Shortcomings and Future Perspectives. *Cancers (Basel)* (2020) 12:1–20. doi: 10.3390/cancers12030751

28. Farber SH, Elsamadicy AA, Atik AF, Suryadevara CM, Chongsathidkiet P, Fecci PE, et al. The Safety of Available Immunotherapy for the Treatment of Glioblastoma. *Expert Opin Drug Saf* (2017) 16:277–87. doi: 10.1080/14740338.2017.1273898

29. Available at: https://www.targetedonc.com/view/upfront-nivolumab-not-additive-in-phase-iii-trial-of-mgmtmethylated-gbm.

30. Available at: https://clinicaltrials.gov/ct2/show/results/NCT02667587?term=NCT02667587&draw=2&rank=1.

31. Available at: https://news.bms.com/news/details/2019/Bristol-Myers-Squibb-Announces-Phase-3-CheckMate–498-Study-Did-Not-Meet-Primary-Endpoint-of-Overall-Survival-with-Opdivo-nivolumab-Plus-Radiation-in-

Patients-with-Newly-Diagnosed-MGMT-Unmethylated-Glioblastoma-Multiforme/default.aspx.

32. Available at: https://clinicaltrials.gov/ct2/show/NCT02617589?term=NCT02617589&draw=2&rank=1.

33. Available at: https://clinicaltrials.gov/ct2/show/NCT04396860.

34. Moher D, Liberati A, Tetzlaff J, Altman D. Preferred Reporting Items for Systematic Reviews and Meta-Analyses: The PRISMA Statement. *PloS Med* (2009) 6:e1000097. doi: 10.1371/journal.pmed.1000097

35. Stroup DF, Berlin JA, Morton SC, Olkin I, Williamson GD, Rennie D, et al. Meta-Analysis of Observational Studies in Epidemiology: A Proposal for Reporting. *Meta-analysis Of Observational Stud Epidemiol (MOOSE) Group JAMA* (2000) 283:2008–12. doi: 10.1001/jama.283.15.2008

36. Team R. *Rstudio: Integrated Development Environment for R.* Boston, MA: RStudio, PBC (2015). Available at: http://www.rstudio.com/.

37. Lehrer EJ, Singh R, Wang M, Chinchilli VM, Trifiletti DM, Ost P, et al. Safety and Survival Rates Associated With Ablative Stereotactic Radiotherapy for Patients With Oligometastatic Cancer: A Systematic Review and Meta-Analysis. *JAMA Oncol* (2021) 7:92–106. doi: 10.1001/jamaoncol.2020.6146

38. Minozzi S, Cinquini M, Gianola S, Gonzalez-Lorenzo M, Banzi R. The Revised Cochrane Risk of Bias Tool for Randomized Trials (Rob 2) Showed Low Interrater Reliability and Challenges in its Application. *J Clin Epidemiol* (2020) 126:37–44. doi: 10.1016/j.jclinepi.2020.06.015

39. Sampson JH, Aldape KD, Archer GE, Coan A, Desjardins A, Friedman AH, et al. Greater Chemotherapy-Induced Lymphopenia Enhances Tumor-Specific Immune Responses That Eliminate EGFRvIII-expressing Tumor Cells in Patients With Glioblastoma. *Neuro-Oncology* (2010) 13:324–33. doi: 10.1093/neuonc/noq157

40. Wen PY, Reardon DA, Armstrong TS, Phuphanich S, Aiken RD, Landolfi JC, et al. A Randomized Double-Blind Placebo-Controlled Phase II Trial of Dendritic Cell Vaccine Ict-107 in Newly Diagnosed Patients With Glioblastoma. *Clin Cancer Res* (2019) 25:5799–807. doi: 10.1158/1078-0432.CCR-19-0261

41. Wheeler LA, Manzanera AG, Bell SD, Cavaliere R, McGregor JM, Grecula JC, et al. Phase II Multicenter Study of Gene-Mediated Cytotoxic Immunotherapy as Adjuvant to Surgical Resection for Newly Diagnosed Malignant Glioma. *Neuro-Oncology* (2016) 18:1137–45. doi: 10.1093/neuonc/now002

42. Buchroithner J, Erhart F, Pichler J, Widhalm G, Preusser M, Stockhammer G, et al. Audencel Immunotherapy Based on Dendritic Cells Has No Effect on Overall and Progression-Free Survival in Newly Diagnosed Glioblastoma: A Phase II Randomized Trial. *Cancers (Basel)* (2018) 10(10):372. doi: 10.3390/cancers10100372

43. Stupp R, Hegi ME, Gorlia T, Erridge SC, Perry J, Hong Y, et al. Cilengitide Combined With Standard Treatment for Patients With Newly Diagnosed Glioblastoma With Methylated MGMT Promoter (CENTRIC EORTC 26071-22072 Study): A Multicentre, Randomised, Open-Label, Phase 3 Trial. *Lancet Oncol* (2014) 15:1100–8. doi: 10.1016/S1470-2045(14)70379-1

44. Ursu R, Carpentier A, Metellus P, Chinot O, Lambert J, Carpentier AF, et al. Intracerebral Injection of CpG Oligonucleotide for Patients With De Novo Glioblastoma-a Phase II Multicentric, Randomised Study. *Eur J Cancer* (2017) 73:30–7. doi: 10.1016/j.ejca.2016.12.003

45. Cho D-Y, Yang W-K, Lee H-C, MeiHsu D, LinLin H, Zong Lin S, et al. Adjuvant Immunotherapy With Whole-Cell Lysate Dendritic Cells Vaccine for Glioblastoma Multiforme: A Phase II Clinical Trial. *World Neurosurg* (2012) 77:736–44. doi: 10.1016/j.wneu.2011.08.020

46. Kong DS, Nam DH, Kang SH, Lee JW, Chang JH, Kim J, et al. Phase III Randomized Trial of Autologous Cytokine-Induced Killer Cell Immunotherapy for Newly Diagnosed Glioblastoma in Korea. *Oncotarget* (2017) 8:7003–13. doi: 10.18632/oncotarget.12273

47. Wakabayashi T, Natsume A, Mizusawa J, Katayama H, Fukuda H, Sumi M, et al. Jcog0911 INTEGRA Study: A Randomized Screening Phase II Trial of Interferonβ Plus Temozolomide in Comparison With Temozolomide Alone for Newly Diagnosed Glioblastoma. *J Neurooncol* (2018) 138:627–36. doi: 10.1007/s11060-018-2831-7

48. Weller M, Butowski N, Tran DD, Recht LD, Lim M, Hirte H, et al. Rindopepimut With Temozolomide for Patients With Newly Diagnosed, EGFRvIII-expressing Glioblastoma (ACT IV): A Randomised, Double-Blind, International Phase 3 Trial. *Lancet Oncol* (2017) 18:1373–85. doi: 10.1016/S1470-2045(17)30517-X

49. Chinnaiyan P, Won M, Wen PY, Rojiani AM, Werner-Wasik M, Shih HA, et al. A Randomized Phase II Study of Everolimus in Combination With Chemoradiation in Newly Diagnosed Glioblastoma: Results of NRG Oncology RTOG 0913. *Neuro Oncol* (2018) 20:666–73. doi: 10.1093/neuonc/nox209

50. Lee EQ, Kaley TJ, Duda DG, Schiff D, Lassman AB, Wong ET, et al. A Multicenter, Phase II, Randomized, Noncomparative Clinical Trial of Radiation and Temozolomide With or Without Vandetanib in Newly Diagnosed Glioblastoma Patients. *Clin Cancer Res* (2015) 21:3610–8. doi: 10.1158/1078-0432.CCR-14-3220

51. Cabrera AR, Kirkpatrick JP, Fiveash JB, Chakravarti A, Wen PY, Chang E, et al. Radiation Therapy for Glioblastoma: Executive Summary of an American Society for Radiation Oncology Evidence-Based Clinical Practice Guideline. *Pract Radiat Oncol* (2016) 6:217–25. doi: 10.1016/j.prro.2016.03.007

52. Palmer JD, Gamez ME, Ranta K, Ruiz-Garcia H, Peterson JL, Blakaj DM, et al. Radiation Therapy Strategies for Skull-Base Malignancies. *J Neurooncol* (2020) 150:445–62. doi: 10.1007/s11060-020-03569-7

53. Trifiletti DM, Ruiz-Garcia H, Quinones-Hinojosa A, Ramakrishna R, Sheehan JP. The Evolution of Stereotactic Radiosurgery in Neurosurgical Practice. *J Neurooncol* (2021) 151:451–9. doi: 10.1007/s11060-020-03392-0

54. ALA-Glioma Study Group. Extent of Resection and Survival in Glioblastoma Multiforme: Identification of and Adjustment for Bias. *Neurosurgery* (2008) 62:564–76; discussion -76. doi: 10.1227/01.neu.0000317304.31579.17

55. Suarez-Meade P, Marenco-Hillembrand L, Prevatt C, Murguia-Fuentes R, Mohamed A, Alsaeed T, et al. Awake vs. Asleep Motor Mapping for Glioma Resection: A Systematic Review and Meta-Analysis. *Acta Neurochir (Wien)* (2020) 162:1709–20. doi: 10.1007/s00701-020-04357-y

56. Ellingson BM, Chung C, Pope WB, Boxerman JL, Kaufmann TJ. Pseudoprogression, Radionecrosis, Inflammation or True Tumor Progression? Challenges Associated With Glioblastoma Response Assessment in an Evolving Therapeutic Landscape. *J Neurooncol* (2017) 134:495–504. doi: 10.1007/s11060-017-2375-2

57. Vogelbaum MA, Jost S, Aghi MK, Heimberger AB, Sampson JH, Wen PY, et al. Application of Novel Response/Progression Measures for Surgically Delivered Therapies for Gliomas: Response Assessment in Neuro-Oncology (Rano) Working Group. *Neurosurgery* (2012) 70:234–44. doi: 10.1227/NEU.0b013e318223f5a7

58. Chukwueke UN, Wen PY. Use of the Response Assessment in Neuro-Oncology (RANO) Criteria in Clinical Trials and Clinical Practice. *CNS Oncol* (2019) 8:CNS28–CNS. doi: 10.2217/cns-2018-0007

59. Okada H, Downey KM, Reardon DA. Chapter 59 - Immunotherapy Response Assessment in Neuro-Oncology (Irano). In: HB Newton, editor. *Handbook of Brain Tumor Chemotherapy, Molecular Therapeutics, and Immunotherapy, 2nd ed.* United States: Academic Press (2018). p. 761–6. doi: 10.1016/B978-0-12-812100-9.00060-7

60. Okada H, Weller M, Huang R, Finocchiaro G, Gilbert MR, Wick W, et al. Immunotherapy Response Assessment in Neuro-Oncology: A Report of the RANO Working Group. *Lancet Oncol* (2015) 16:e534–42. doi: 10.1016/S1470-2045(15)00088-1

61. Moscatello DK, Ramirez G, Wong AJ. A Naturally Occurring Mutant Human Epidermal Growth Factor Receptor as a Target for Peptide Vaccine Immunotherapy of Tumors. *Cancer Res* (1997) 57:1419–24.

62. Heimberger AB, Suki D, Yang D, Shi W, Aldape K. The Natural History of EGFR and EGFRvIII in Glioblastoma Patients. *J Transl Med* (2005) 3:38. doi: 10.1186/1479-5876-3-38

63. Lawrence W Jr. Patient Selection for Clinical Trials. Risks Versus Benefits and Quality of Life Issues. *Cancer* (1993) 72:2798–800. doi: 10.1002/1097-0142(19931101)72:9+<2798::AID-CNCR2820721504>3.0.CO;2-#

64. Morrison PF, Laske DW, Bobo H, Oldfield EH, Dedrick RL. High-Flow Microinfusion: Tissue Penetration and Pharmacodynamics. *Am J Physiol* (1994) 266:R292–305. doi: 10.1152/ajpregu.1994.266.1.R292

65. Fiandaca MS, Berger MS, Bankiewicz KS. The Use of Convection-Enhanced Delivery With Liposomal Toxins in Neurooncology. *Toxins (Basel)* (2011) 3:369–97. doi: 10.3390/toxins3040369

66. Hulou MM, Cho C-F, Chiocca EA, Bjerkvig R. Chapter 11 - Experimental therapies: gene therapies and oncolytic viruses. *Handb Clin Neurol* (2016) 134:183–97. doi: 10.1016/B978-0-12-802997-8.00011-6

67. Bakos O, Lawson C, Rouleau S, Tai L-H. Combining Surgery and Immunotherapy: Turning an Immunosuppressive Effect Into a Therapeutic Opportunity. *J ImmunoTher Cancer* (2018) 6:86. doi: 10.1186/s40425-018-0398-7

68. George GC, Barata PC, Campbell A, Yap TA, Cleeland CS, Hong DS, et al. Improving Attribution of Adverse Events in Oncology Clinical Trials. *Cancer Treat Rev* (2019) 76:33–40. doi: 10.1016/j.ctrv.2019.04.004

69. Kennedy LB. Salama Aks. A Review of Cancer Immunotherapy Toxicity. *CA Cancer J Clin* (2020) 70:86–104. doi: 10.3322/caac.21596

70. Sivendran S, Latif A, McBride RB, Stensland KD, Wisnivesky J, Haines L, et al. Adverse Event Reporting in Cancer Clinical Trial Publications. *J Clin Oncol* (2014) 32:83–9. doi: 10.1200/JCO.2013.52.2219

71. Magee DE, Hird AE, Klaassen Z, Sridhar SS, Nam RK, Wallis CJD, et al. Adverse Event Profile for Immunotherapy Agents Compared With Chemotherapy in Solid Organ Tumors: A Systematic Review and Meta-Analysis of Randomized Clinical Trials. *Ann Oncol* (2020) 31:50–60. doi: 10.1016/j.annonc.2019.10.008

72. Liu A, Hou C, Chen H, Zong X, Zong P. Genetics and Epigenetics of Glioblastoma: Applications and Overall Incidence of IDH1 Mutation. *Front Oncol* (2016) 6:16. doi: 10.3389/fonc.2016.00016

Valproic Acid-Like Compounds Enhance and Prolong the Radiotherapy Effect on Breast Cancer by Activating and Maintaining Anti-Tumor Immune Function

Zuchao Cai[1], David Lim[2,3], Guochao Liu[1], Chen Chen[1], Liya Jin[1], Wenhua Duan[1], Chenxia Ding[1], Qingjie Sun[1], Junxuan Peng[1], Chao Dong[1], Fengmei Zhang[1] and Zhihui Feng[1]*

[1] Department of Occupational Health and Occupational Medicine, School of Public Health, Cheeloo College of Medicine, Shandong University, Jinan, China, [2] School of Health Sciences, Western Sydney University, Campbelltown, NSW, Australia, [3] College of Medicine and Public Health, Flinders University, Bedford Park, SA, Australia

Inadequate sustained immune activation and tumor recurrence are major limitations of radiotherapy (RT), sustained and targeted activation of the tumor microenvironment can overcome this obstacle. Here, by two models of a primary rat breast cancer and cell co-culture, we demonstrated that valproic acid (VPA) and its derivative (HPTA) are effective immune activators for RT to inhibit tumor growth by inducing myeloid-derived macrophages and polarizing them toward the M1 phenotype, thus elevate the expression of cytokines such as IL-12, IL-6, IFN-γ and TNF-α during the early stage of the combination treatment. Meanwhile, activated CD8^{+} T cells increased, angiogenesis of tumors is inhibited, and the vasculature becomes sparse. Furthermore, it was suggested that VPA/HPTA can enhance the effects of RT *via* macrophage-mediated and macrophage-CD8^{+} T cell-mediated anti-tumor immunity. The combination of VPA/HPTA and RT treatment slowed the growth of tumors and prolong the anti-tumor effect by continuously maintaining the activated immune response. These are promising findings for the development of new effective, low-cost concurrent cancer therapy.

Keywords: VPA-like compounds, radiotherapy, breast cancer, TAMs, M1-like macrophages, CD8^{+} T, vasculature

Abbreviations: VPA, valproic acid; HPTA, 2-hexyl-4-pentynoic acid; DAB, 3,3'-diaminobenzidine; DMBA, 7,12-dimethylbenz[a]anthracene; FBS, fetal bovine serum; HDACi, histone deacetylase inhibitor; BrdU, 5-Bromo-2′-deoxyuridine; HE, hematoxylin and eosin; IHC, immunohistochemistry; SD, Sprague–Dawley; TBS, Tris-Buffered Saline; TAMs, tumor-associated macrophages; CTLs, cytotoxic T lymphocytes; PD1, programmed cell death protein 1; EMT, Epithelial–mesenchymal transition; PBMCs, Peripheral blood mononuclear cells; MDSCs, Myeloid-derived suppressor cells; Tregs, Regulatory cells; CTLA-4, Cytotoxic T-lymphocyte-associated protein 4.

INTRODUCTION

Breast cancer is one of the most common types of tumors in women, and radiotherapy (RT) is a mainstay of oncology treatment. In addition to the direct cytoreductive effect of RT in breast cancer, emerging evidence suggests that the generation of an anti-tumor immune response also plays an important role in the effectiveness of this treatment modality (1, 2).

A variety of different cell types within tumors have been described to undergo apoptosis after local irradiation, these include T cells, stromal cells, and vascular endothelial cells, which limited the therapeutic effect to some extent and increased the possibility of immune escape (2). At the same time, RT paradoxically promotes metastasis and invasion of cancer cells by inducing the epithelial–mesenchymal transition (EMT), and can even cause tumor recurrence (3), which are the main obstacles to the successful treatment of cancer, and remains the important cause of mortality in patients receiving RT (4). New therapeutic strategies, such as combining immunotherapy with RT are being trialed (5).

Breast cancer has a complex microenvironment consisting of malignant cells, resident histiocytes such as adipocytes and recruited cell types, which play an important role in the progression of breast cancer to malignancy and resistance to treatments (6). Among them, macrophages play a pivotal role. Tumor-associated macrophages (TAMs), one of the main types of immunosuppressive cells in the tumor microenvironment, are key players in tumor immune escape, a major obstacle to cancer immunotherapy (7, 8). In the overwhelming majority of tumors, TAMs stimulate tumor cell migration, invasion, intravasation as well as the angiogenic response required for tumor growth (9–11). Clinicopathological studies have suggested that TAMs accumulation in tumors is correlated with a poorer clinical outcome (12). In human breast carcinomas, high TAMs density is correlated with poorer prognosis (13). Depending on the microenvironmental presence, macrophages are polarized into two distinct phenotypes, the classically activated (M1) or the alternative activated (M2) macrophages. TAMs closely resemble the M2-polarized phenotype (14). Recent studies have shown that polarizing TAMs toward M1 phenotype can effectively treat tumors (15–19). This suggests that macrophages have plasticity, which can restore the anti-tumor properties of TAMs for the treatment of tumors (20). Therefore, TAMs are considered as one of the important therapeutic targets to improve the efficacy of immunotherapy, and the search for novel drugs that can modulate the TAMs phenotype holds promise for safer and more effective oncology treatment.

On the other hand, activation and recruitment of cytotoxic lymphocytes (CTLs) have been recognized as key to effective immunotherapy for solid tumors. Among them, CD8^{+} T cells are essential to inhibit the occurrence and development of solid tumors, because once these cells exert full cytotoxicity, they can eliminate tumor cells (21). Most solid tumors include a variety of immune cells, such as regulatory T cells and TAMs, which can inhibit CTLs function (22, 23). It was reported that the depletion of TAMs enhances CD8^{+} T cell-mediated anti-tumor immunity in a mouse model of breast cancer (24). Therefore, therapies targeting the immune system hold great promise for the treatment of cancer (25, 26).

In recent years, some scholars have reported that a histone deacetylase inhibitor (HDACi), TMP195 can switch the major macrophage type in tumors from TAMs to the high phagocytic macrophages in mice mammary tumors (27). In this model, TMP195 activates immune pathways, and synergistic anti-PD1 antibodies and chemotherapy significantly inhibited tumor development. This HDACi, which has a stable and effective regulatory effect on the immune system, hold great potential as it targets specifically immune cells, resistance to treatment is rare as compared with those agents which directly act on the tumor cells (28, 29). The other HDACi, valproic acid (VPA), a well-tolerated anti-epileptic agent used since the 1970s, has also received attention recently as a possible concurrent therapy to RT. Many researchers have demonstrated that VPA-like compounds can kill a variety of tumor cells, including glioma (30), breast cancer (31), prostate cancer (32), while sensitizing tumor cells to RT or chemotherapy through its effect on DNA repair (33–35). It was not clear whether VPA and VPA-like compounds reported sensitization of tumor cells to RT or chemotherapy was associated with the regulation of immune function.

Therefore, in our study, we used a well-established animal model of breast cancer that does not affect tumor immune function (36) to explore whether VPA and VPA-like compounds may also have the ability to activate immune pathways, and when co-administered with RT can better inhibit the development of tumors.

METHODS AND MATERIALS

Establishment of a Breast Cancer Model

Detailed steps are reported in our previous article (35). In brief, female Sprague–Dawley (SD) rats were purchased from Peng Yue Laboratory Animal Co. Ltd., Jinan, China. The studies of animal tissue were performed in accordance with the requirements of the Shandong University Human and Animal Ethics Research Committee (project identification code 81472800, approved 3 March 2014). A single dose of 1 ml 7,12-dimethylbenz[α]anthracene (DMBA) oil was administered to 50-day-old SD rats through intragastric gavage (37, 38). At 40–60 days after gavage, primary tumors could be detected through palpation around the breast. The tumor size, location and appearance were recorded weekly and measured with Vernier Caliper. Tumor volume was calculated according to the clinical standard formula "Volume (V; mm^3) = Length (L) ∗ Width (W)^2 ∗ 0.5".

Drug Treatment and Radiotherapy in Rats

The tumor-bearing rats were given an intraperitoneal injection of saline, VPA (BP452, Sigma) or HPTA (H0964, TCI) twice a day for 6 consecutive days. RT was applied to rats by using X-ray Irradiator (X-RAD225 OptiMAX, Pxi) as shown in **Figure S1**. Four fractionated doses of 2 Gy were utilized in our study. The specific methods are as follows: When irradiating, we fixed the

rat and placed it on the round plate. And the hollow cylinder indicated by the red arrow is used for the precise irradiation of the tumor. The inside diameter of the hollow cylinder is 2 cm, and the tumor was exposed to radiation here (as indicated by the red arrow). And the X-ray aperture was selected to match the diameter of the tumor. The cylinder is made of solid copper, allowing full protection of the rest of the body.

BrdU Incorporation and HE Staining

5-Bromo-2′-deoxyuridine (BrdU) (B5002, Sigma) was injected intraperitoneally at a dose of 100 mg/kg 24 h before tissue harvest. Tumor tissues and normal breast were fixed overnight in 4% paraformaldehyde solution, embedded in paraffin and serially sectioned 5 μm thick for hematoxylin and eosin (HE) staining according to the manufacture's procedures guideline.

Immunohistochemistry (IHC)

The avidin–biotin immunoperoxidase method was used for deparaffinized zinc formalin-fixed, paraffin-embedded sections. Specific methods are detailed in our previous article (27). The primary antibodies including CD11b (1:5,000, ab133357, Abcam), F4/80 (1:200, 123101, BioLegend), CD68 (1:500, GB11067, Servicebio), Cleaved caspase-3 (1:300, 9661, Cell Signaling), BrdU (1:50, B44, BD), Ki67 (1:400, 12202, Cell Signaling), CD8 (1:500, GB11068, Servicebio), granzyme-B (1:200, sc-8002, Santa Cruz), followed by incubation with secondary antibodies: biotinylated goat anti-mouse IgG (1:300, BA-9200, Vector), biotinylated goat anti-rat IgG (1:300, BA-9400, Vector) and biotinylated goat anti-rabbit IgG (1:300, BA-1000, Vector). Images were taken through a light microscope (Olympus).

Immunofluorescence

Specific methods are detailed elsewhere (33, 39). The primary antibodies including CD11b (1:1,000, ab133357, Abcam), F4/80 (1:200, 123101, BioLegend), EpCAM (1:200, sc-66020, Santa Cruz), CD31 (1:200, GB12063, Servicebio), followed by staining with Alexa Fluor® 594 goat anti-mouse IgG(H+L) (1:300; A11032, Molecular probes), Alexa Fluor® 488 chicken anti-rabbit IgG(H+L) (1:300; A21441, Molecular probes). Images were taken using Zeiss 880 Confocal Microscope and analyzed on Leica Microsystems imaging software. Composite images and pseudo-colored images were generated using Fiji software and images were captured using a laser confocal microscope.

Real-Time Quantitative Reverse Transcriptase PCR (qRT-PCR)

The tumors were rapidly extracted after the tissues were harvested, snap-frozen in liquid nitrogen, and stored at −80°C before being used for qRT-PCR analysis. The RNA was extracted from whole tumor tissue according to the RNA prep Pure Tissue Kit (Tiangen) protocol. For the cellular experiment, we extracted RNA according to the FastPure Cell/Tissue Total RNA Isolation Kit (vazyme) and the isolated RNA was quantified by NanoDrop ND-2000 spectrophotometer (Nadro Drop Technologies, Wilmington, DE, USA). cDNA synthesis was performed using the ReverAid First Strand cDNA Synthesis Kit (Thermo). Finally,

specific primers and Maxima SYBR Green (Thermo) were used, and qRT-PCR analysis was performed on Light Cycler® 480II (Roche Applied Science, Indianapolis, IN, USA) using 1 μL of each primer and 1 μL of cDNA. The levels of the relative genes and the internal reference gene (GAPDH) expressed were measured, and the C_t values (threshold cycle number) of the target gene and the reference gene were calculated according to the Light Cycler® 480 Software release 1.5.0 SP4 software, use $2^{-\Delta\Delta}C_t$ method. Sample from the DMBA-induced breast cancer was used as control sample, and the expression of the target gene of each group was compared. $\Delta\Delta C_t$ = experimental group ΔC_t − control group ΔC_t, ΔC_t = (average C_t of the target gene of the control sample - average C_t of the control sample GAPDH) (40, 41). The primer sequences used in this study are listed in **Table S1**.

Cell Culture

MCF7 and RAW264.7 cell lines were purchased from American Type Culture Collection (ATCC) and maintained in DMEM (12100046, Gibco) medium with 10% Fetal Bovine Serum (10270106, Gibco) and 1% Penicillin-Streptomycin (V900929, Sigma). All cells were confirmed to be mycoplasma-free, and maintained at 37°C and 5% CO_2.

Cytokine Detection in Macrophage Lysate

MCF7 cells were seeded in P60 dishes followed by 500μM VPA, 15μM HPTA and 100 ng/ml LPS (L8880, Solarbio) treatment for 24 h. The culture was centrifuged to collect the medium supernatant, which is subsequently added to the P35 dishes seeded with RAW264.7 cells. After 24hrs, RAW264.7 cells were lysed by repeated freeze-thawing in PBS, and lysates were collected. Cytokines detection (IL-12, IL-10, TNF-α, IFN-γ) were performed using ELISA kits (1211232, 1211002, 1217202, 1210002, DAKEWE, China).

Primary Culture and Stimulation of Human Peripheral Blood Mononuclear Cells (PBMCs)

Whole blood samples were collected from healthy donors after obtaining informed consent in accordance with the National Regulations on the Administration of Human Genetic Resources, China. The ethics for this part of the study was approved by the Shandong University Human and Animal Ethics Research Committee's requirements (project identification code 81472800, approved on 3 March 2014). PBMCs were isolated from whole blood using Lymphocyte Isolate (LTS1007-1, TBDScience, China) density gradient centrifugation. The PBMCs were maintained in RPMI 1640 (12633012, Gibco) medium with 10% Fetal Bovine Serum (10270106, Gibco) and 1% Penicillin–Streptomycin (V900929, Sigma).

PBMCs were isolated, and cells were seeded at 5×10^5 in 24-well plate coated with CD3 (5 μg/ml) (B287689, BioLegend) at 4°C overnight, 500 μl/well, and added to CD28 (1 μg/ml) (B281555, BioLegend) with IL-2 (10 ng/ml) (031612, PEPROTECH) and maintained at 37°C and 5% CO_2 for 3 days. Subsequent experiments were performed after sufficient cells were reached.

Flow Cytometry

Lysates were extracted following the macrophage factor detection step and added to the already activated PBMC cells at a 1:3 of medium volume ratio for 5 days in culture. Then PBMCs were collected, washed three times with PBS, incubated with the CD3 (B278047, BioLegend), CD4 (B310677, BioLegend) and CD8 (B311544, BioLegend), and centrifuged to collect cells. Cells were washed three more times with PBS and resuspended as a single cell suspension for flow cytometry.

Co-Culture of Tumor Cells With PBMCs

Lysates were extracted following the macrophage factor detection step and added to the already activated PBMC cells at a 1:3 of medium volume ratio for 5 days in culture. 4×10^5 MCF7 cells were seeded on the lower chamber of the transwell (Corning #3412, 24 mm Transwell® with 0.4 µm Pore Polycarbonate Membrane Insert), and 2 Gy irradiation treatment was administered after the cells had fully adherent growth. At the end of irradiation, 2×10^5 PBMC cells cultured for 5 days were transferred to the upper chamber of the transwell for co-cultured for 24 h. The tumor cells in the lower chamber were subjected to MTT to detect the number of viable cells.

MTT

MCF7 cells were seeded in lower chamber of a 6-well transwell at a density of 4×10^5 cells per well. Following treatments, MTT solution (5 mg/ml, Sigma) was added to the treated cells and incubated for 4 h at 37°C. Then the medium was replaced with dimethyl sulfoxide. After mixing, 120 µl was added to each well in a 96-well plate. The absorbance of the solution was measured using an enzyme immunoassay analyzer at 540 nm.

To determinate the effect of IR on the growth of macrophage, RAW264.7 were seeded at a density of 2×10^3 cells per well in 96-well plate, and treated with 4 and 8 Gy after the cells had attached, and the growth of the cells observed by MTT assay after 72 h.

Statistical Analysis

All statistical analyses were performed with Student's t-test on SPSS Statistics for Windows, version 23.0 (Armonk, NY: IBM Corp; licensed to Shandong University) and represented as mean ± SD. The P values were designated as: *, $P <0.05$; **, $P <0.01$, indicating a statistically significant difference.

RESULTS

VPA/HPTA Enhanced Radiotherapy Effect to Inhibit Tumor Growth in Rats With Breast Cancer

To study whether VPA/HPTA can enhance the effect of radiotherapy *in vivo*, we used the primary breast cancer model in rats induced by the environmental carcinogen DMBA, which was previously described and employed in related studies (33, 35, 36). In brief, around 40 days after DMBA gavage to female SD rats, lumps in the breast sites were found. The shape of lumps in the location of mammary glands was irregular (**Figure 1A**).

By HE staining, when compared with the normal breast tissue, a monotonous population of cells, poorly circumscribed, infiltrating the surrounding soft and adipose tissues, cords and nodules of atypical epithelial cells, with some duct or gland formation, indicating that breast cancer in rats was successfully induced. Next, the dose of VPA/HPTA and radiotherapy were determined for the tumor treatment in this animal model. Reported studies of VPA on glioblastoma utilized intraperitoneal injection of VPA in the range from 150 to 600 mg/kg (42), here, we choose 200 mg/kg as the treatment dose of VPA, which was the same as that used to treat the cells (0.5 mM) in our working system (33, 35). 20 mg/kg HPTA was adopted as this is closest to the 200 mg/kg VPA previously utilized in cell culture (0.015 mM) (34). Four fractionated doses of 2 Gy, based on previous studies, were utilized (43, 44). The workflow of our experimental design is detailed in **Figure 1B** upper.

During the early observation, the growth of tumors in VPA/HPTA-treated rats was inhibited ($P <0.05$). Compared with the RT-alone group, the reduction of breast cancer volume in the VPA/HTPA treatment groups was significantly more ($P <0.01$). On the 10th day post-treatment, the morphological structure of tumors was observed by HE staining (**Figure 1C**). The VPA/HPTA treatment led to vacuole structures formation in the breast cancer tissue as compared with the untreated control group; there were more vacuoles structures and number of necrotic cells after the RT, and larger necrotic areas and cells were seen in the tissues in the combination treatment groups. The morphological results are consistent with the above findings. The results demonstrated that 200 mg/kg VPA or 20 mg/kg HPTA can effectively enhance RT for breast cancer in our rat working model.

We next tested the cell proliferation ability in the tumor using both BrdU and Ki67 markers. BrdU IHC staining results showed that VPA/HPTA treatment significantly reduced the proliferation of tumor cells, the reduction was significantly greater in the combination treatment groups ($P <0.01$, **Figure 1D**). Similar results were noted with the Ki67 proliferation marker ($P <0.01$, **Figure S1A**). The IHC findings were consistent with the gross observation and measurement. In conclusion, we highlight that the combination of both treatment modalities is superior to each treatment modality alone.

VPA/HPTA Activates the Macrophages and Reprograms TAMs Polarization Towards M1 Phenotype in Irradiated Breast Tumor at the Early Stage of the Treatment

Other scholars had reported that TMP195 has a macrophage-mediated immune effect (27), so we next studied the macrophages in the tumor microenvironment to investigate whether VPA and VPA-like compound (HPTA) may have a similar effect during RT treatment in our working model.

We used the macrophage marker F4/80 for IHC staining (**Figure 2A**) and found that after VPA/HPTA treatment, the macrophages increased significantly in the tumor, while in the combination treatment groups, there were a further substantial increased ($P <0.01$). Similar results were observed for the other
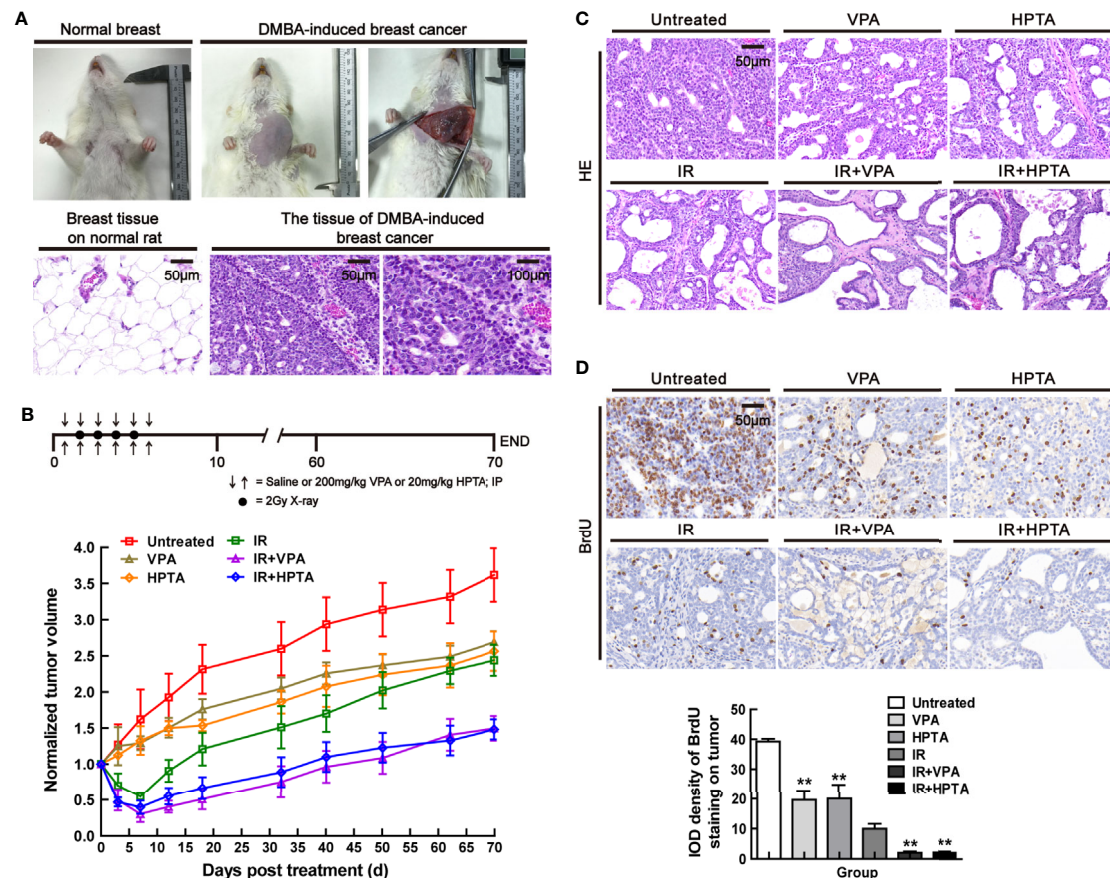
FIGURE 1 | VPA/HPTA enhanced radiotherapy effect to inhibit tumor growth in rats with breast cancer **(A)** Normal breast and DMBA-induced breast cancer of rats under gross observation. HE staining for the morphology of normal tissue and DMBA-induced breast cancer. **(B)** The tumor-bearing rats were given intraperitoneal injection of saline, 200 mg/kg of VPA or 20 mg/kg of HPTA twice a day for 6 consecutive days in combination with 2Gy of radiotherapy once a day for 4 consecutive days. The change in tumor volumes in different groups after treatment, which was normalized by untreated group. **(C)** HE staining for the morphology of tumors in different groups. **(D)** IHC was performed on tumor sections with BrdU, a marker of proliferation. Quantitation as a percentage of total tissue is shown to the right of representative images. Each data point in the graphs was from three independent experiments (mean ± SD). *P*-values were calculated by Student's t-test (*$P < 0.05$, **$P < 0.01$).

macrophage marker, CD68 (*P* <0.01, **Figure S2**). The data indicate that the immune system is activated by VPA/HPTA in response to RT.

TAMs, being a M2 macrophage, play a key role in cancer immune escape. We next investigate whether VPA/HPTA treatment may be able to switch the polarization of macrophages to the pro-inflammatory M1 phenotype. As shown in **Figure 2B**, VPA/HPTA treatment alone significantly promoted an increase in the cell population expressing M1 marker (CD86; *P* <0.01) and M1 function markers (IL-12, IL-6, MHC-II, IFN-γ and TNF-α; *P* <0.01) at the transcriptional level in the tumor. The M2 macrophage marker (CD209 and CD163) and the function marker (IL-10) also had no significant change. For the RT-alone group, M2 macrophages, but not M1 macrophages, were significantly increased compared with the untreated control group. Meanwhile, in the combination treatment groups, the increase in M1 marker and function markers and decrease in M2 marker (CD209 and CD163) and function marker (IL-10) was

further amplified (*P* <0.01). The data suggest that VPA/HPTA can reverse and further activate the RT-induced immune pathway at the early stage after the RT treatment.
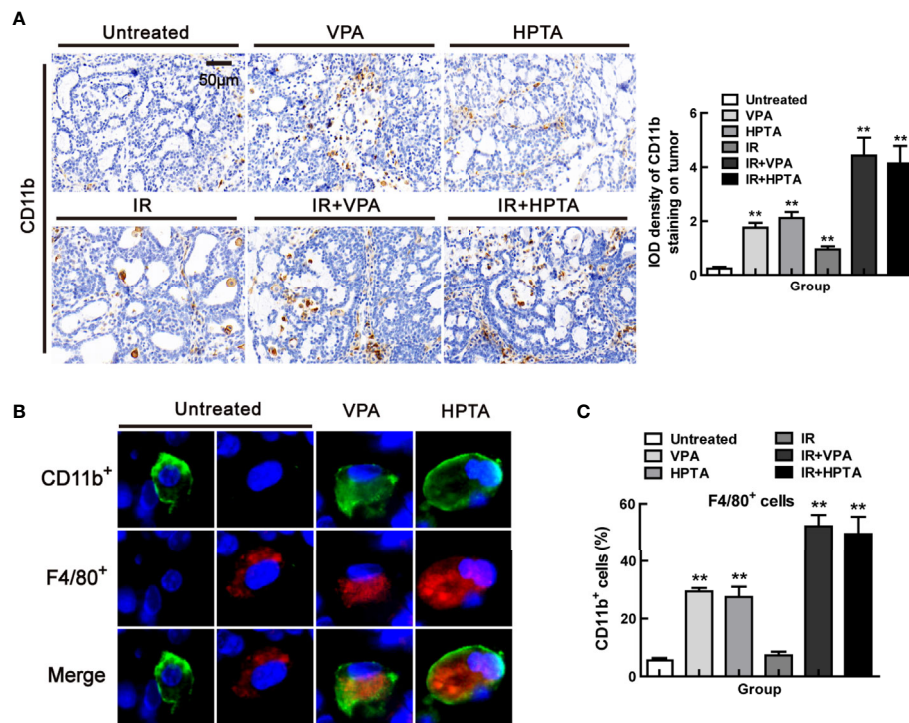
VPA/HPTA Regulates Myeloid-Derived Macrophages to Enhance Radiotherapy Effect in Breast Cancer at the Early Stage of Treatment *In Vivo*

We next explore the origin of the macrophages which were recruited into the tumor microenvironment by VPA/HPTA. Some scholars have reported that CD11b, a marker of myeloid-derived differentiated cells, can promote bone marrow cells to develop into macrophages and then inhibit tumor growth (45). Therefore, we performed IHC analysis of tumor tissues in each group with CD11b, the results showed that CD11b^{+} cells were significantly increased after VPA/HPTA treatment (1.76 ± 0.24/2.11 ± 0.31) (*P* <0.01, **Figure 3A**), there was a small increase after RT-alone (0.95 ± 0.15, *P* <0.05). We noticed a substantial
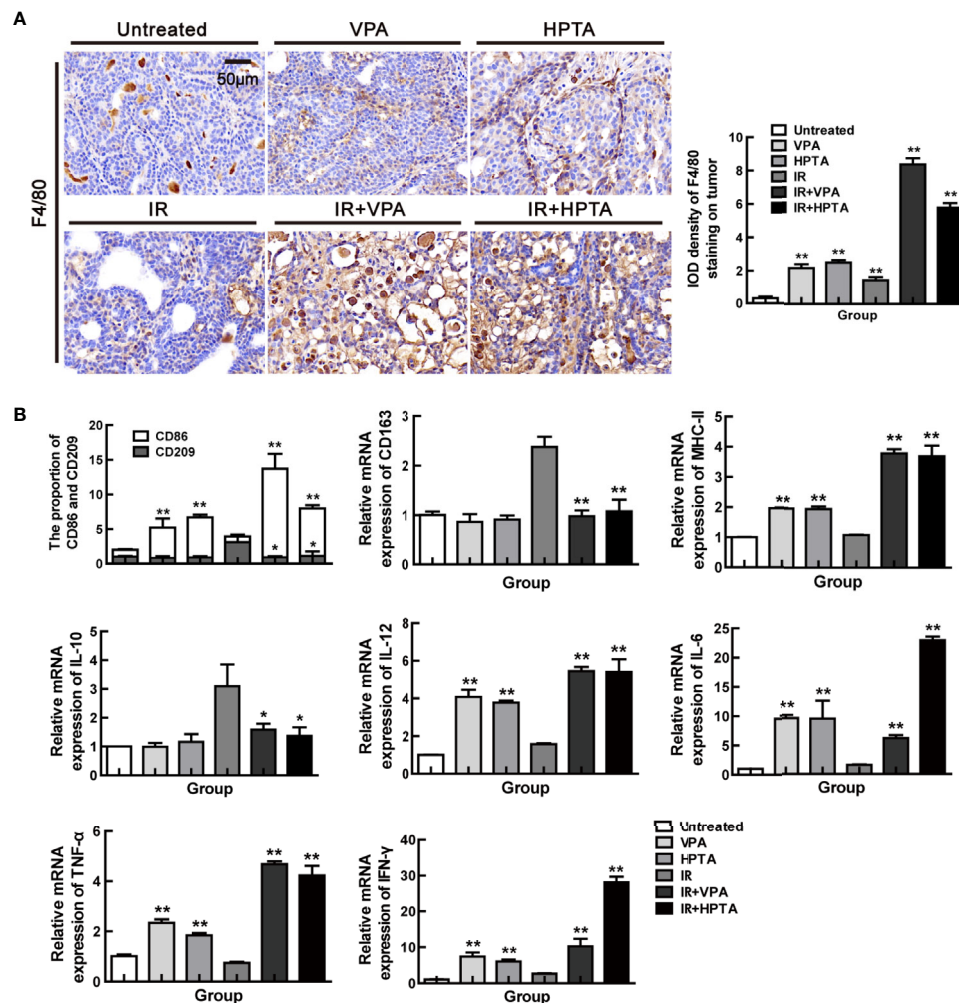
FIGURE 2 | VPA/HPTA activates the macrophages and reprograms TAMs polarization towards M1 phenotype in irradiated breast tumor at the early stage of the treatment **(A)** IHC was performed on tumor sections with the macrophage-specific marker F4/80 to assess infiltration of macrophages, and representative quantitation and images are shown. **(B)** The mRNA expression levels of CD86, CD209, CD163, MHC-II, IL-10, TNF-α, IFN-γ, IL-6 and IL-12 in DMBA-induced breast tumors in rats were determined by real-time PCR. Data were normalized to untreated group. Each data point in the graphs was from three independent experiments (mean ± SD). P-values were calculated by Student's t-test (*$P < 0.05$, **$P < 0.01$).

increase in CD11b$^+$ cells with the combination treatment (4.42 ± 0.94/4.14 ± 0.91) ($P <0.01$). The data demonstrate that VPA/HPTA can induce an increase in CD11b$^+$ cells in the tumor.

Next, to verify the source of VPA/HPTA-induced macrophages, we employed co-localization staining of CD11b and F4/80 markers. As shown in **Figure 3B**, all F4/80$^+$ cells co-localized with CD11b, and the proportion of the cells (CD11b$^+$, F4/80$^+$) increased significantly after VPA/HPTA treatment (29.4%/27.5%) ($P <0.01$, **Figures 3C** and **S3A**). This proportion was further increased in the combination treatment groups (52.2%/49.4%) ($P <0.01$), but not in the RT-alone group ($P >0.05$). The data demonstrate that the increased macrophages in the tumor may be of myeloid origin, which can be recruited into the tumor microenvironment by VPA/HPTA.

To distinguish whether the increased macrophage population were the resident macrophages in the tumor, the ability of

RAW264.7 macrophages was tested after IR and VPA/HPTA combination treatment by MTT assay *in vitro*. We found that the ability of the macrophages irradiated with 4 and 8Gy was significantly decreased (**Figure S3B**, $P <0.01$); however, VPA/HPTA treatment did not cause a further decrease in the cell ability ($P >0.05$). We concluded that the previously observed increased macrophage population is likely from non-tumor resident macrophages, the myeloid-derived macrophages may be recruited from other tissues.

VPA/HPTA-Activated Macrophages Are Highly Phagocytic in Breast Tumors at the Early Stage of Treatment *In Vivo*

To determine the effect of VPA/HPTA-activated macrophages on tumors, we found that the proportion of apoptotic cells (Cleaved caspase-3$^+$) was increased after VPA/HPTA

FIGURE 3 | VPA/HPTA regulates myeloid-derived macrophages to enhance radiotherapy effect in breast cancer at the early stage of treatment *in vivo* **(A)** IHC was performed on tumor sections with the myeloid marker CD11b to assess infiltration, representative quantitation and images are shown. Immunofluorescence co-staining of myeloid derived cells (CD11b+: green) and macrophages (F4/80+: red), and representative images **(B)** and quantitation **(C)** are shown. Each data point in the graphs was from three independent experiments (mean ± SD). *P*-values were calculated by Student's t-test (*$P < 0.05$, **$P < 0.01$).

treatment and RT-alone treatment, this was further increased after the combined treatment ($2.03 \pm 0.43/1.90 \pm 0.41$, $P < 0.01$, **Figure 4A**), suggesting that the combination treatment promoted the apoptosis of tumor cells.

Phagocytosis of breast tumor cells was quantified as the proportion of F4/80+ macrophages that contain intracellular EpCAM, a marker of breast tumor cells. By co-localization staining with F4/80 and EpCAM markers (**Figure 4B**), we found that the proportion was increased significantly both in the VPA/HPTA-alone and the combination treatment groups (89.61%/87.73%) ($P < 0.01$, **Figures 4C** and **S4**). Thus, the macrophages induced by VPA/HPTA are highly phagocytic, which we concluded is helpful to enhance the RT effect in eliminating tumor cells.

VPA/HPTA Reinforces the Anti-Tumor Effect of Radiotherapy by Activating CD8+ T Cell-Dependent Anti-Tumor Response and Inducing Vascular Normalization *In Vivo* at the Early Stage of the Treatment

TAMs can target CD8+ T cells and inhibit immune rejection of tumor cells through various mechanisms (46), while IL-12 secreted by M1 cells can activate CD8+ T cells to stimulate an anti-tumor response in solid tumor models (47, 48). CD8+ T cells mediate the most important anti-tumor immune response *in vivo*, and most cancer immunotherapy approaches aim to evoke,

promote and enhance the specific anti-tumor activity of CD8+ T cells (49). Since we found that VPA/HPTA promoted pro-inflammatory M1 phenotype and increased IL-12 expression in our study, we next examined whether VPA/HPTA can activate CD8+ T cells to be involved in the anti-tumor response. The results in **Figure 5A** showed that VPA/HPTA treatment induced an increase in CD8+ T cells population ($P < 0.01$), which was also modestly increased in the RT-alone treatment group ($P < 0.05$). The combination treatment further significantly increased the CD8+ T cells population ($19.85 \pm 5.61/20.00 \pm 5.43$) ($P < 0.01$). Granzyme-B, the functional marker of CD8+ T cells, was also increased in the combination treatment groups (**Figure 5B**), indicating that VPA/HPTA activated the CD8+ T cells and thus enhanced the RT effect in the tumor, which may be associated with IL-12 secreted by anti-tumor M1-type macrophages.

The tumor-promoting TAMs contribute to abnormalities in tumor vasculature (9, 50–52), while anti-tumor M1 macrophages are associated with anti-angiogenic effects including vascular pruning and normalization (53). Studies have shown that IFN-γ can interfere with the integrity of blood vessels and affect the progression of tumors (27, 39). Since we discovered that VPA/HPTA increased mRNA level of IFN-γ of M1 function markers in our study, we next examine whether VPA/HPTA can influence angiogenesis in the tumor. The results of CD31, the markers of endothelial blood vessel, demonstrated that VPA/HPTA treatment, as well as the RT-alone treatment, reduced the size,
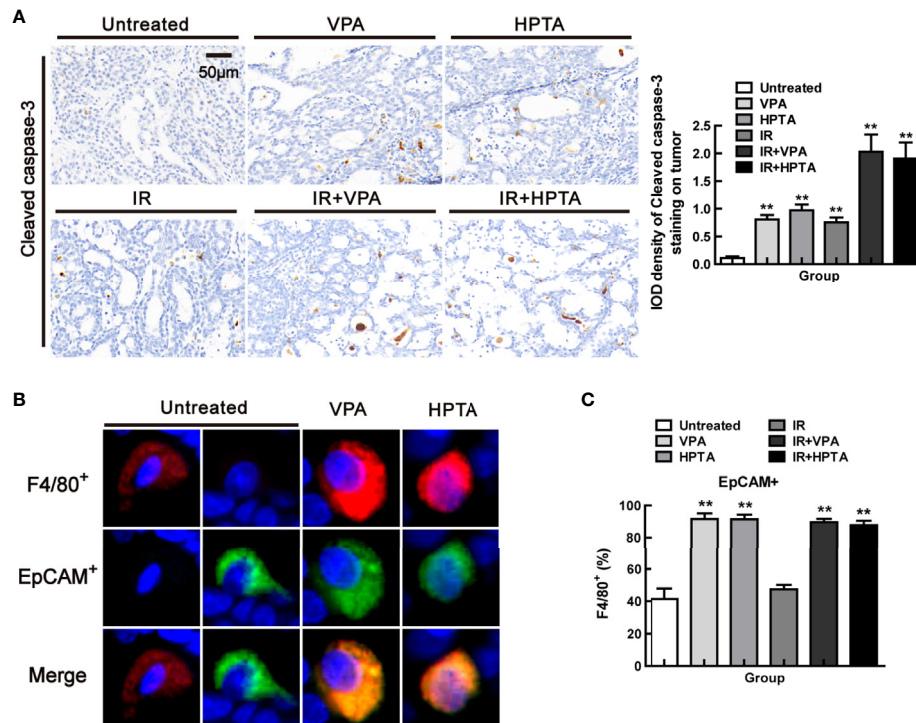
FIGURE 4 | VPA/HPTA-activated macrophages are highly phagocytic in breast tumors at the early stage of treatment *in vivo* **(A)** IHC was performed using the cleaved caspase-3 to identify apoptotic bodies within macrophages, representative images and quantitation are shown. Phagocytosis of breast tumor cells was quantified as the proportion of F4/80+ macrophages (red) that contain intracellular EpCAM+ (green), a marker of breast tumor cells by immunofluorescence, representative images **(B)** and quantitation **(C)** are shown. Data were normalized to untreated group. Each data point in the graphs was from three independent experiments (mean ± SD). *P*-values were calculated by Student's t-test (*$P < 0.05$, **$P < 0.01$).

density and aberrantly branches of the vasculature, and the effect was augmented in the combination treatment groups (**Figure 5C**). These findings suggest that VPA/HPTA combined with radiotherapy can inhibit tumor neovascularization, such action is associated with IFN-γ secreted by anti-tumor M1 macrophages exhibiting anti-angiogenic properties.

VPA/HPTA Prolong the Radiotherapy Effect of Breast Cancer *via* Maintaining the Durability of Anti-Tumor Immune Response *In Vivo*

Our results on the tumor growth revealed an interesting phenomenon. As shown in **Figure 1B**, the tumor volume significantly decreased in the first week after the RT-alone treatment, and then started to increase after that. At the end of the observation period (70 days), the tumor volume elevated to about 2.5 times than that before RT treatment. Surprisingly, for the combination treatment groups, the tumor volume grew slowly after an initial decrease in the first week, and subsequently the tumor volume was increased about 0.5 times than that before the treatment at the end of the observation period, indicating that both VPA and HPTA could significantly prolong the RT effect in inhibiting tumor growth. We speculated that this effect may be associated with anti-tumor immune response activated at the early stage of the treatment, so we

further analyzed the immune state in the tumor at 70 days after treatment.

Firstly, HE staining showed that there were still large necrotic areas and cells in the combination treatment groups (**Figure S5A**). The results of BrdU showed that the cells in the untreated group were still high-proliferative, the proliferative capacity in the RT-alone group was the same as in the VPA/HPTA-alone groups, which was consistent with the tumor growth (**Figure 1B**), but was lower than that in the untreated control group ($P < 0.01$). While, the combination treatment groups still showed much lower proliferative capacity ($P < 0.01$, **Figures 5B** and **6A**). Similar findings were noted with Ki67 ($P < 0.01$, **Figure S5C**). The data indicate that the tumor growth was inhibited in the combination treatment at the later stage of RT treatment.

Subsequently, F4/80 IHC results suggested that macrophages were still active in the combination treatment group ($P < 0.01$, **Figures 6B** and **S5D**), although not as evident as in the early stage, as can be seen largely by the CD68 staining ($P < 0.01$, **Figure S5E**). We further analyzed the macrophage phenotype and its function. The increase of CD86+ M1-type population ($P < 0.01$) and mRNA level of M1 function markers (IL-12, IL-6, MHC-II, IFN-γ and TNF-α; $P < 0.01$) and the decrease of CD209+/CD163+ M2-type population ($P < 0.05$) and mRNA level of M2 function marker (IL-10; $P < 0.01$) were also observed in the combination treatment groups but not in RT-alone group (**Figure 6C**). Such effects are not
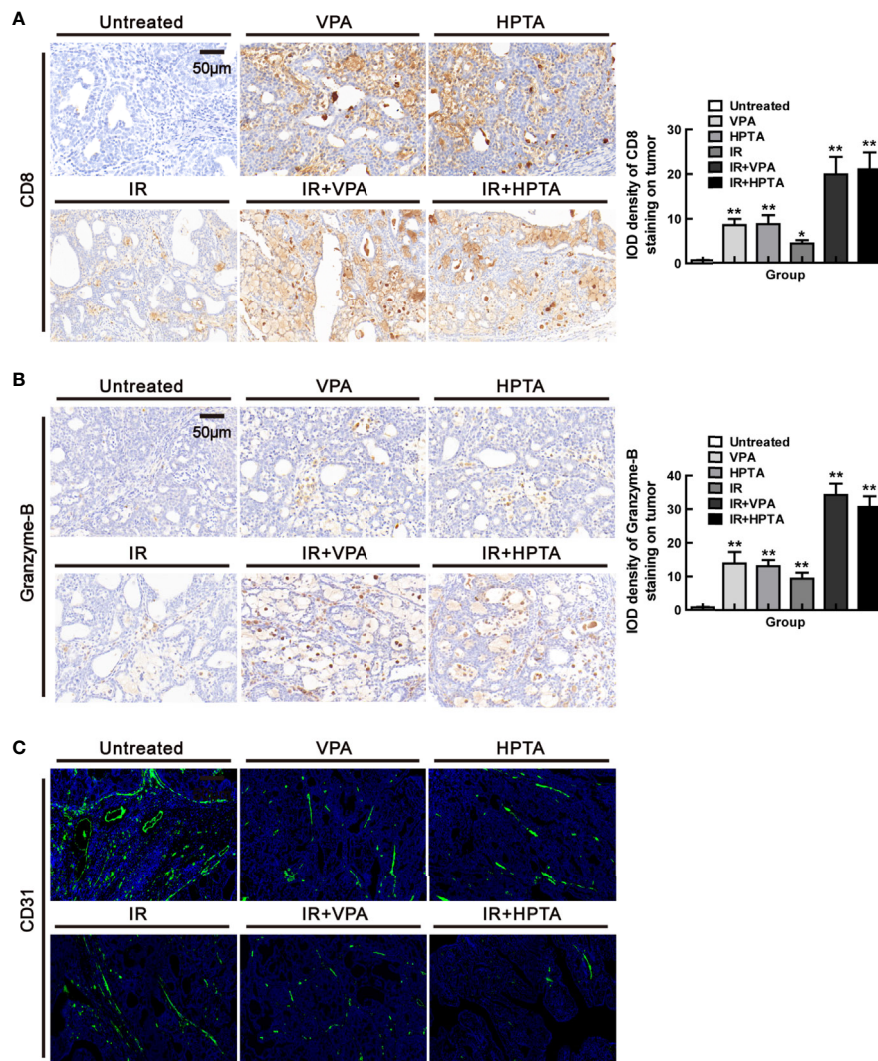
FIGURE 5 | VPA/HPTA reinforces the anti-tumor effect of radiotherapy by activating CD8+ T cell-dependent anti-tumor response and inducing vascular normalization in vivo at an early stage of the treatment. **(A)** IHC was performed on tumor sections for the marker CD8. Quantitation as a percentage of total tissue is shown to the right of representative images. **(B)** IHC was performed on tumor sections with the marker granzyme-B. Quantitation as a percentage of total tissue is shown to the right of representative images. **(C)** Immunofluorescence staining of tumor vessels (CD31+: green) and representative images are shown. Each data point in the graphs was from three independent experiments (mean ± SD). P-values were calculated by Student's t-test (*$P < 0.05$, **$P < 0.01$).

as strong as in the early stage of the treatment (**Figure 2B**). The increased of CD8$^+$ T cell population (**Figure 6D**) with higher expression of granzyme-B (**Figure 6E**) and a reduction in vascular (**Figure 6F**), under the combination treatment were also observed, supporting the hypothesis that VPA/HPTA prolonged the RT effect by maintaining anti-tumor immune response through the later stage of treatment.

VPA/HPTA Can Directly Promote M1 Polarization of Macrophages to Activate Anti-Tumor Response of CD8$^+$ T Cells *In Vitro*

To verify VPA-like compounds can directly reprogram M1 polarization and activate anti-tumor response, the conditional

medium experiment was employed for this study. Firstly, to manipulate the environment for tumor cell growth, the conditional medium, which was from the culturing breast cancer cell line MCF7, was used to incubate the macrophage cells, RAW264.7, thus to investigate the effect of VPA/HPTA on RAW264.7 polarization. The experiment design was shown in **Figure 7A**. As a negative control, regular medium was used. Both the qRT-PCR and ELISA experiments demonstrated a significant decreased in the level of the M1 marker CD86 and its secreted cytokines (IL-12, IFN-γ, and TNF-α), and a significant increase in M2 secreted cytokine IL-10 were observed after VPA/HPTA treatment ($P < 0.01$), although the significant changes in the level of the M2 marker CD209 were not observed (**Figures 7B, C**). The results indicate that VPA/HPTA
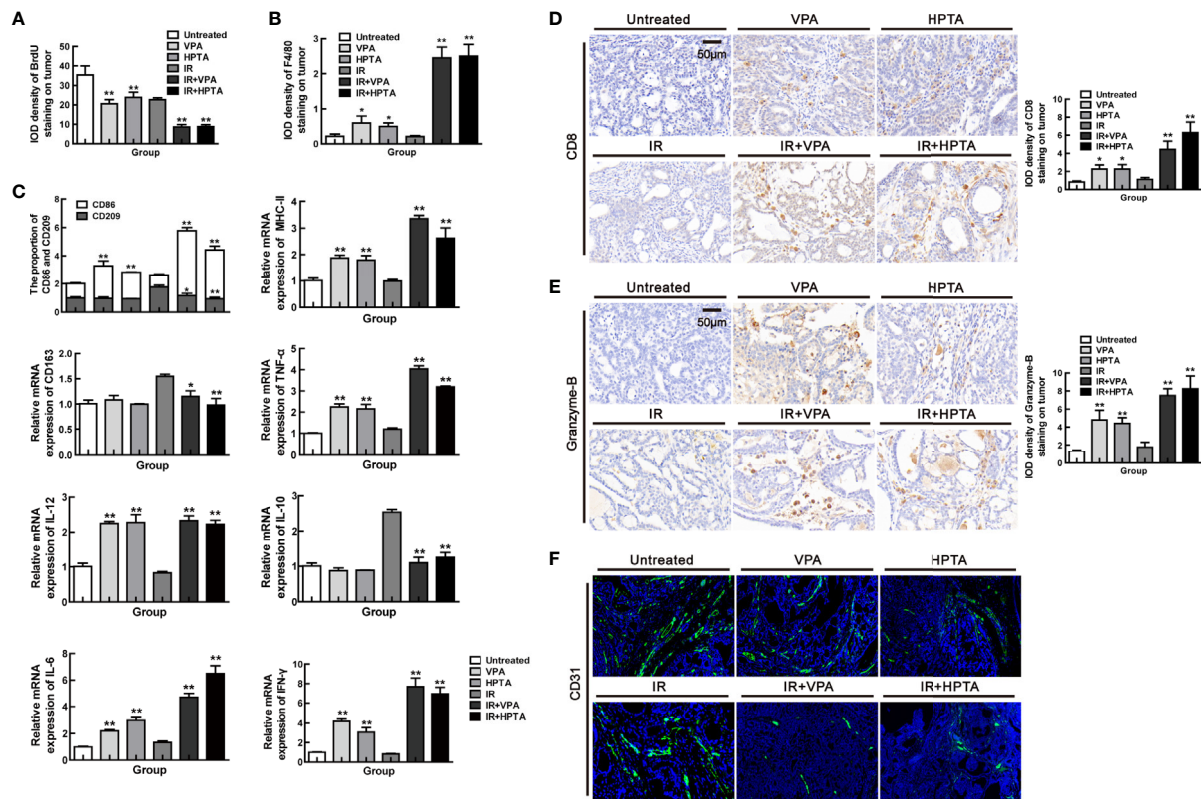
FIGURE 6 | VPA/HPTA prolong the radiotherapy effect of breast cancer via maintaining the durability of anti-tumor immune response *in vivo* Tumor tissues were analyzed 70 days after treatment. Quantitative analysis of BrdU **(A)** and F4/80 **(B)** immunohistochemistry. **(C)** The mRNA expression levels of CD86, CD209, CD163, MHC-II, IL-10, TNF-α, IFN-γ, IL-6 and IL-12 in DMBA-induced breast tumors in rats were determined by real-time PCR. Data were normalized to the untreated group. **(D)** IHC was performed on tumor sections for the marker CD8. Quantitation as a percentage of total tissue is shown to the right of representative images. **(E)** IHC was performed on tumor sections for the marker granzyme-B. Quantitation as a percentage of total tissue is shown to the right of representative images. **(F)** Immunofluorescence staining of tumor vessels (CD31+: green) and representative images are shown. Each data point in the graphs was from three independent experiments (mean ± SD). *P*-values were calculated by Student's t-test (**P* < 0.05, ***P* < 0.01).

can induce M2 polarization of macrophages under a normal culture environment.

With the conditional medium, through both qRT-PCR and ELISA, a significant elevation of the level of CD86 and the cytokines (IL-12, IFN-γ, and TNF-α) (*P* <0.01) and a significant decrease of the level of CD209 and IL-10 were found after VPA/HPTA treatment (*P* <0.01). The results indicate that VPA/HPTA can directly promote M1 polarization under tumor cell growth environment (**Figures 7B, C**).

We also used LPS as a positive control for this study. The results indicated that LPS can induce M1 polarization of macrophages under regular medium and conditional medium (**Figures 7B, C**), consistent with other reports (54, 55), suggesting that our experimental design was reliable.

Cell lysate from the macrophages was further used to incubate MCF7 cells to test for cell viability (**Figure 7D**). We found that the relative survival fraction of VPA/HPTA-alone was comparable to RT-alone treatment. The combination treatment resulted in further inhibited cell growth (*P* <0.01).

We concluded from the above results that VPA/HPTA can directly induce macrophage M1 polarization in the tumor

environment, and activate macrophage-mediated anti-tumor immunity for enhancing the effects of radiotherapy to tumor.

Since VPA/HPTA can directly induce M1 polarization and result in the increase of IL-12 level, we next test the effect of VPA/HPTA-induced M1 polarization on CD8+ T cells *in vitro*. The cell lysate from the VPA/HPTA-treated macrophage RAW264.7 was used to treat isolated mononuclear cells extracted from venous blood from healthy donors, at the same time the isolated mononuclear cells were activated with anti-CD3/CD28. The experimental design was shown in **Figure 7E**. After treatment for 5 days, the mononuclear cells were labeled with the antibodies of CD3 and CD8 for isolating CD8+ T cells by flow analysis. The results showed that VPA/HPTA significantly increased the number of CD3+CD8+ T lymphocytes (**Figure 7F**, *P* <0.05), indicating that VPA/HPTA-induced M1 polarization can promote the proliferation of CD8+ T cells. Next, to further illustrate the effect of activated CD8+ T cells on the growth of tumor cell MCF7 (**Figure 7G**), the PBMCs treated by VPA/HPTA-treated macrophage lysate were co-cultured with MCF7 cells for 48 h. We found the viability of MCF7 cells was inhibited by VPA/HPTA-alone and RT-alone treatment (*P* <0.05), this was further
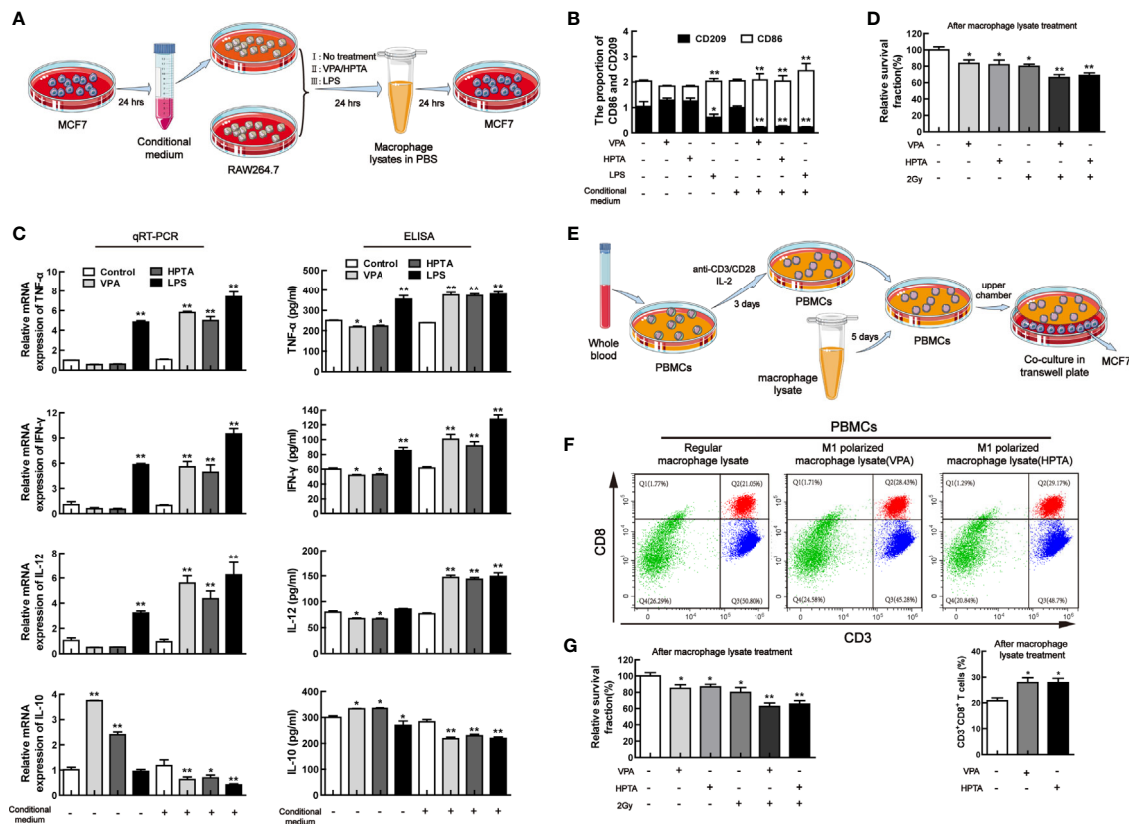
FIGURE 7 | VPA/HPTA can directly promote M1 polarization of macrophages to activate anti-tumor response of CD8+ T cells in vitro **(A)** Protocol for MCF7 conditional medium and macrophage polarization experiment. **(B)** qRT-PCR analysis of markers (CD86 and CD209) of reprogrammed RAW264.7 macrophages under different treatment conditions. **(C)** qRT-PCR and ELISA analysis of cytokines (TNF-α, IFN-γ, IL-10 and IL-12) of reprogrammed RAW264.7 macrophages under different treatment conditions. **(D)** The survival of MCF7 cells treated with macrophage lysate was detected by MTT assay. **(E)** Protocol for extraction and activation of PBMCs and the co-culture with MCF7 cells. **(F)** Flow cytometric analysis of the effect of macrophage lysates on CD8$^+$ T lymphocytes. **(G)** MTT results of survival of MCF7 cells after co-culture. Each data point in the graphs was from three independent experiments (mean ± SD). P-values were calculated by Student's t-test (*$P < 0.05$, **$P < 0.01$).

reduced in the combination treatment groups ($P < 0.01$). The results suggested that VPA/HPTA not only can activate macrophage-mediated anti-tumor immunity but also can activate macrophage-CD8$^+$ T cell-mediated anti-tumor immunity to enhance the effects of RT to tumor, thus supported the earlier *in vivo* results.

DISCUSSION

In this study, we demonstrate that VPA/HPTA evokes immune activation by mobilizing myeloid-derived macrophages and triggering M1 polarization in a DMBA-induced rat breast cancer model. These reprogrammed macrophages led to subsequent T cell recruitment and activation, vascular normalization, and tumor suppression (**Figure 8**). Our findings support the proposition of VPA/HPTA as an adjuvant therapy to low-dose radiotherapy in breast cancer; VPA/HPTA enhances and prolongs the RT effect on breast cancer by activating and maintaining the anti-tumor immune function.

Persistent Immune Activation Is the Key to Prevent Tumor Recurrence

RT has been the mainstay of oncological treatment of breast cancer since the 1900s; today, about 50–60% of cancer patients continue to receive this treatment modality. However, the resistance of tumor cells to RT and high cancer recurrence rate has been reported (56). Understanding the mechanism of radiation resistance in breast cancer is of clinical importance. The tumor microenvironment has been known to influence the response to RT, specifically lymphocytes, monocytes and macrophages are particularly radiosensitive. Furthermore, ionizing radiation has an effect on the vascular endothelium and affects the recruitment of anti-tumor T cells into the tumor site, as well as initiating adaptive and innate immune responses that can result in systemic anti-tumorigenic effects both inside and outside of the irradiation field.

Studies have shown that cancer immunotherapy achieves a durable clinical response in patients with advanced cancer, who are refractory to conventional treatment (57). While RT can also activate the immune system to some extent (58), it is limited by the dose and frequency of RT. Such RT-induced immune
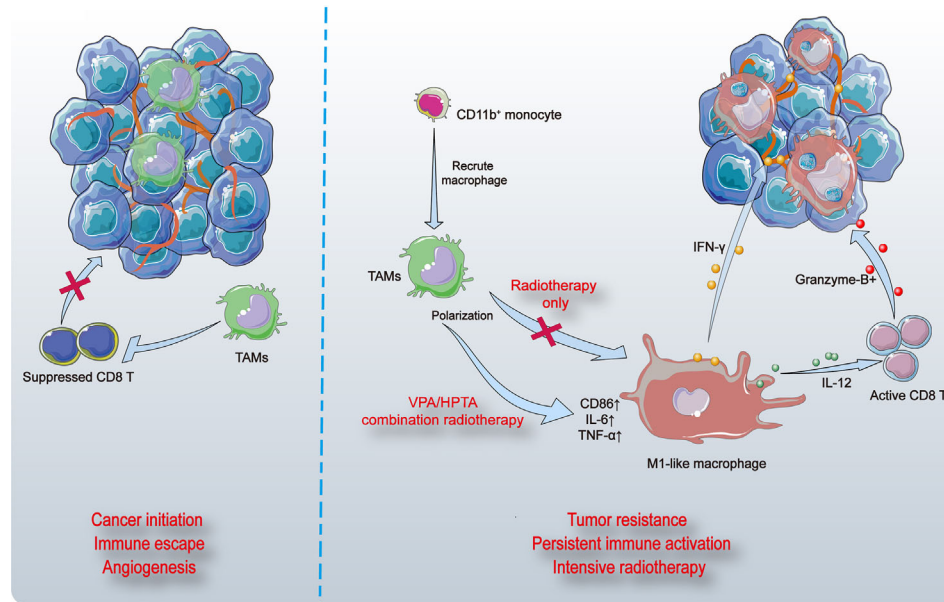
FIGURE 8 | The model of VPA/HPTA to enhance and prolong the radiotherapy effect by activating and maintaining anti-tumor immune response. Breast tumors in rats induced by DMBA contain abundant vasculature and pro-tumor macrophages (TAMs) that suppress the function of CD8+ T cells (left). Myeloid-derived cells are recruited to tumor sites, differentiate into macrophages, and further polarize toward M1 phenotype, thus promote inflammatory response. CD8+ T cells are activated, granzyme-B is secreted possibly through the IL-12 pathway, thereby killing tumors. The vasculature of tumors becomes sparse, possibly due to stimulation by IFN-γ. At the same time, the combination treatment not only effectively improve the effect of radiotherapy during the immediate exposure, the concurrent therapy also delay the growth of tumors and prolong the anti-tumor effect by continuously activating the immune response to compensate for recurrence after radiotherapy.

activation is short-lived and tumors are prone to recurrence. Therefore, safer and more effective immune activators are needed to supplement and complement RT.

VPA-Like Compounds Are Ideal Immune Activators, Which Can Activate the Anti-Tumor Response of CD8⁺ T Cells and Enhance and Prolong the Curative Effect of Radiotherapy

The microenvironment plays an important role in the progress of breast cancer and its resistance to treatment (36). Most solid tumor microenvironments tend to have a certain amount of TAMs and are associated with tumor invasion and poor prognosis (17–19, 59). TAMs were found to enhance malignancy by stimulating angiogenesis, inducing tumor cell migration, invasion and infiltration, and inhibiting anti-tumor immunity in mouse models (60). In our working model, VPA/HPTA induces an increase in myeloid-derived macrophages and activates polarization toward a M1 phenotype that is pro-inflammatory and has phagocytic capacity.

Analysis of breast cancer patients indicates that a low ratio of macrophages to CD8⁺ T cells is associated with poorer survival, suggesting that macrophages may play a major role in suppressing T cell activity against tumors (61). CD8⁺ T cells play a key role in anti-tumor immunity, but their activity is inhibited in the tumor microenvironment, therefore tumors can escape immune attack by various mechanisms of immunosuppression (62–65). The

cytotoxicity of reactivated CD8⁺ T cells has important clinical significance in cancer immunotherapy. Here, we explored a novel combination treatment modality that activates the anti-tumor CD8⁺ T cells through regulation of the tumor microenvironment to enhance the efficacy of RT. We demonstrate that VPA/HPTA can reprogram macrophages in tumors, activate CD8⁺ T cell-mediated anti-tumor immune response, and enhance radiotherapy efficacy.

Additional Implementation of Immune Checkpoint Inhibitors May Have a Further Positive Impact on the Treatment Efficacy in Our Model

Immune checkpoints are immunosuppressive pathways that maintain self-tolerance and protect surrounding tissues by modulating immune responses, a property that tumor cells exploit to evade attack by immune cells. Currently, two of the most extensively studied immune checkpoint targets in tumors are Cytotoxic T lymphocyte associated antigen 4 (CTLA-4) and the PD-1 receptor. Immune checkpoint inhibitors release the "immune brakes" in the tumor microenvironment, reactivate the immune response effect of T cells on tumors, thereby achieving anti-tumor effects. It is also of interest whether immune checkpoint inhibition and other immunotherapies can be combined to better exert anti-tumor effects.

Studies have reported that the triple combination of anti-CTLA-4, anti-PD-1, and G47Δ-mIL12 was able to cure most

mice of glioma (66, 67). This treatment was associated with macrophage influx and M1-like polarization, along with increased T effector to T regulatory cell ratios. Among them, G47Δ-mIL12 induces M1-like polarization in TAMs. This synergy may permit low dose of the immune checkpoint inhibitors to reduce potential adverse effects (67). In our study, VPA/HPTA seems to act similarly to G47Δ-mIL12 by mobilizing macrophages to recruit and trigger M1 polarization, suggesting that administration of immune checkpoint inhibition (anti-CTLA-4, anti-PD-1) in our model may potentially achieve better therapeutic outcomes. Furthermore, VPA has been used clinically for decades and is a low-cost alternative to the currently available immune checkpoint inhibitor such as ipilimumab, pembrolizumab and nivolumab, especially so for resource-constraint countries.

It was previously shown that the combination of RT, anti-CTLA4, and anti-PD-L1 promotes immunity through distinct mechanisms. Anti-CTLA4 predominantly inhibits T regulatory cells (Tregs) to increase the CD8 T cell to Treg (CD8/Treg) ratio. RT enhances the diversity of the T cell receptor (TCR) repertoire of intratumoral T cells. Together, anti-CTLA4 promotes expansion of T cells, while RT shapes the TCR repertoire of the expanded peripheral clones. PD-L1 blockade reverses T cell exhaustion and attenuates the decrease in the CD8/Treg ratio, further encourages oligo-clonal T cell expansion (68). This suggests that the combination of RT with immune checkpoint inhibitor can improve tumor immunotherapy efficacy. Thus, we speculate that the addition of immune checkpoint inhibitor to existing treatment modalities may have a further positive impact on treatment efficacy.

The Specific Immune Activation Mechanism and More Reasonable Strategies of VPA-Like Substances Need to Be Further Explored

We found that CD11b^{+} cells infiltrate tumors, but did not determine which stimuli and receptors were involved in this recruitment. There are several possibilities for the exact source of recruitment of CD11b^{+} cells and we cannot completely exclude the presence of CD11b^{+} MDSCs (Myeloid-derived suppressor cells). However, MDSCs, as immunosuppressive cells, induce the generation of Tregs (Regulatory cells) (69), promote the transformation of macrophages from M1 to M2 phenotype (70), thus leading to increased TAMs differentiation and vascular endothelial cells (71) as well as inhibiting the killing of tumor cells by T cells (72) to achieve anti-tumor immunosuppression. In our study, TAMs were polarized from M2 phenotype to M1 with VPA/HPTA-alone treatment as well as in combination with RT. Meanwhile, CD8^{+} T cells were induced to secrete granzyme B to restrain tumor, and CD31 immunofluorescence staining also indicated that the tumor vessels became sparse. These findings all confirmed that the recruited CD11b^{+} cells were not MDSCs; if any, minimal. Study has reported additional roles for CD11b (45): CD11b activation promotes pro-inflammatory macrophage polarization by stimulating the expression of microRNA *Let7a*. In contrast, inhibition of CD11b prevents *Let7a* expression and induces cMyc expression, leading to immune suppressive macrophage

polarization, vascular maturation, and accelerated tumor growth. This suggests that CD11b may serve as a positive regulator of immune activation and a target for cancer immunotherapy.

At the same time, we also found that although the growth of tumor volume was inhibited after the combination treatment as compared with radiotherapy alone, the tumor nonetheless continued to grow abide at a much slower growth rate, suggesting that rebound effect may nonetheless occur after stopping combination treatment (73). If we are to extend the duration of VPA/HPTA treatment, the stability of reprogramming phenotype and toxicology would warrant further exploration.

The strikingly different effects of VPA/HPTA on macrophage polarization demonstrated in the cell model *in vitro*, with and without the tumor cell medium environment, allow us to make bold speculation that in the animal model, in addition to promoting M1 polarization of macrophages to activate anti-tumor response of CD8^{+} T cells, VPA/HPTA may also exhibit protection against the injury of distant normal tissues induced by RT, as it is possible to mediate anti-inflammatory effects *via* macrophage M2 type polarization.

As for how CD8^{+} T cells may kill the tumor cells, the perforin/granzyme-B apoptosis pathway is a likely candidate (74), but there are also reports that T cell-promoted tumor ferroptosis is an anti-tumor mechanism (75), which needs further exploration.

Regardless of these hitherto untested possibilities, VPA/HPTA interventions are safe and effective options for the treatment of breast cancer: persistent immune activation and intensive radiotherapy. Our study may provide a more rational and long-term strategy for breast cancer treatment in clinic.

DATA AVAILABILITY STATEMENT

The original contributions presented in the study are included in the article/**Supplementary Material**. Further inquiries can be directed to the corresponding author.

ETHICS STATEMENT

The studies involving human participants were reviewed and approved by Shandong University Human and Animal Ethics Research Committee (81472800, approved March 2014). The patients/participants provided their written informed consent to participate in this study. The animal study was reviewed and approved by Shandong University Human and Animal Ethics Research Committee (81472800, approved March 2014).

AUTHOR CONTRIBUTIONS

ZC, DL and ZF designed the study, analyzed the data, and wrote the manuscript. ZC performed most of the experiments. GL, CC, LJ, WD, CDi, QS and JP finished the rest part of the experiments in this study, and they analyzed the data and designed the figures.

SUPPLEMENTARY MATERIAL

The Supplementary Material for this article can be found online at: https://www.frontiersin.org/articles/10.3389/fimmu.2021.646384/full#supplementary-material

REFERENCES

1. Lee Y, Auh SL, Wang Y, Burnette B, Wang Y, Meng Y, et al. Therapeutic Effects of Ablative Radiation on Local Tumor Require CD8+ T Cells: Changing Strategies for Cancer Treatment. *Blood* (2009) 114(3):589–95. doi: 10.1182/blood-2009-02-206870

2. Lugade AA, Moran JP, Gerber SA, Rose RC, Frelinger JG, Lord EM. Local Radiation Therapy of B16 Melanoma Tumors Increases the Generation of Tumor Antigen-Specific Effector Cells That Traffic to the Tumor. *J Immunol* (2005) 174(12):7516–23. doi: 10.4049/jimmunol.174.12.7516

3. Lee SY, Jeong EK, Ju MK, Jeon HM, Kim MY, Kim CH, et al. Induction of Metastasis, Cancer Stem Cell Phenotype, and Oncogenic Metabolism in Cancer Cells by Ionizing Radiation. *Mol Cancer* (2017) 16(1):10. doi: 10.1186/s12943-016-0577-4

4. Cummings B, Keane T, Pintilie M, Warde P, Waldron J, Payne D, et al. Five Year Results of a Randomized Trial Comparing Hyperfractionated to Conventional Radiotherapy Over Four Weeks in Locally Advanced Head and Neck Cancer. *Radiother Oncol* (2007) 85(1):7–16. doi: 10.1016/j.radonc.2007.09.010

5. Spaas M, Lievens Y. Is the Combination of Immunotherapy and Radiotherapy in Non-small Cell Lung Cancer a Feasible and Effective Approach? *Front Med (Lausanne)* (2019) 6:244. doi: 10.3389/fmed.2019.00244

6. Noy R, Pollard JW. Tumor-Associated Macrophages: From Mechanisms to Therapy. *Immunity* (2014) 41(1):49–61. doi: 10.1016/j.immuni.2014.06.010

7. Chanmee T, Ontong P, Konno K, Itano N. Tumor-Associated Macrophages as Major Players in the Tumor Microenvironment. *Cancers (Basel)* (2014) 6(3):1670–90. doi: 10.3390/cancers6031670

8. Devaud C, Westwood JA, Teng MW, John LB, Yong CS, Duong CP, et al. Differential Potency of Regulatory T Cell-Mediated Immunosuppression in Kidney Tumors Compared to Subcutaneous Tumors. *Oncoimmunology* (2014) 3(11):e963395. doi: 10.4161/21624011.2014.963395

9. Qian BZ, Pollard JW. Macrophage Diversity Enhances Tumor Progression and Metastasis. *Cell* (2010) 141(1):39–51. doi: 10.1016/j.cell.2010.03.014

10. DeNardo DG, Andreu P, Coussens LM. Interactions Between Lymphocytes and Myeloid Cells Regulate Pro- Versus Anti-Tumor Immunity. *Cancer Metastasis Rev* (2010) 29(2):309–16. doi: 10.1007/s10555-010-9223-6

11. Hanahan D, Coussens LM. Accessories to the Crime: Functions of Cells Recruited to the Tumor Microenvironment. *Cancer Cell* (2012) 21(3):309–22. doi: 10.1016/j.ccr.2012.02.022

12. Choi J, Gyamfi J, Jang H, Koo JS. The Role of Tumor-Associated Macrophage in Breast Cancer Biology. *Histol Histopathol* (2018) 33(2):133–45. doi: 10.14670/HH-11-916

13. Wynn TA, Chawla A, Pollard JW. Macrophage Biology in Development, Homeostasis and Disease. *Nature* (2013) 496(7446):445–55. doi: 10.1038/nature12034

14. Zhou K, Cheng T, Zhan J, Peng X, Zhang Y, Wen J, et al. Targeting Tumor-Associated Macrophages in the Tumor Microenvironment. *Oncol Lett* (2020) 20(5):234. doi: 10.3892/ol.2020.12097

15. Yan H, Zhang Y, Zeng B, Yin G, Zhang X, Ji Y, et al. Genetic Diversity and Association of EST-SSR and SCoT Markers With Rust Traits in Orchardgrass (Dactylis Glomerata L.). *Molecules* (2016) 21(1):66. doi: 10.3390/molecules21010066

16. Ni YH, Ding L, Huang XF, Dong YC, Hu QG, Hou YY. Microlocalization of CD68+ Tumor-Associated Macrophages in Tumor Stroma Correlated With Poor Clinical Outcomes in Oral Squamous Cell Carcinoma Patients. *Tumour Biol* (2015) 36(7):5291–8. doi: 10.1007/s13277-015-3189-5

17. Chaudhary B, Elkord E. Regulatory T Cells in the Tumor Microenvironment and Cancer Progression: Role and Therapeutic Targeting. *Vaccines (Basel)* (2016) 4(3):28. doi: 10.3390/vaccines4030028

18. Caetano MS, Zhang H, Cumpian AM, Gong L, Unver N, Ostrin EJ, et al. IL6 Blockade Reprograms the Lung Tumor Microenvironment to Limit the Development and Progression of K-ras-Mutant Lung Cancer. *Cancer Res* (2016) 76(11):3189–99. doi: 10.1158/0008-5472.CAN-15-2840

19. Liu M, Luo F, Ding C, Albeituni S, Hu X, Ma Y, et al. Dectin-1 Activation by a Natural Product Beta-Glucan Converts Immunosuppressive Macrophages Into an M1-like Phenotype. *J Immunol* (2015) 195(10):5055–65. doi: 10.4049/jimmunol.1501158

20. Williams CB, Yeh ES, Soloff AC. Tumor-Associated Macrophages: Unwitting Accomplices in Breast Cancer Malignancy. *NPJ Breast Cancer* (2016) 2:15205. doi: 10.1038/npjbcancer.2015.25

21. Dunn GP, Old LJ, Schreiber RD. The Immunobiology of Cancer Immunosurveillance and Immunoediting. *Immunity* (2004) 21(2):137–48. doi: 10.1016/j.immuni.2004.07.017

22. Smyth MJ, Ngiow SF, Ribas A, Teng MW. Combination Cancer Immunotherapies Tailored to the Tumour Microenvironment. *Nat Rev Clin Oncol* (2016) 13(3):143–58. doi: 10.1038/nrclinonc.2015.209

23. Sharma P, Hu-Lieskovan S, Wargo JA, Ribas A. Primary, Adaptive, and Acquired Resistance to Cancer Immunotherapy. *Cell* (2017) 168(4):707–23. doi: 10.1016/j.cell.2017.01.017

24. DeNardo DG, Brennan DJ, Rexhepaj E, Ruffell B, Shiao SL, Madden SF, et al. Leukocyte Complexity Predicts Breast Cancer Survival and Functionally Regulates Response to Chemotherapy. *Cancer Discov* (2011) 1(1):54–67. doi: 10.1158/2159-8274.CD-10-0028

25. Sharma P, Allison JP. The Future of Immune Checkpoint Therapy. *Science* (2015) 348(6230):56–61. doi: 10.1126/science.aaa8172

26. Anguille S, Smits EL, Lion E, van Tendeloo VF, Berneman ZN. Clinical Use of Dendritic Cells for Cancer Therapy. *Lancet Oncol* (2014) 15(7):e257–267. doi: 10.1016/S1470-2045(13)70585-0

27. Guerriero JL, Sotayo A, Ponichtera HE, Castrillon JA, Pourzia AL, Schad S, et al. Class IIa HDAC Inhibition Reduces Breast Tumours and Metastases Through Anti-Tumour Macrophages. *Nature* (2017) 543(7645):428–32. doi: 10.1038/nature21409

28. Sierra JR, Cepero V, Giordano S. Molecular Mechanisms of Acquired Resistance to Tyrosine Kinase Targeted Therapy. *Mol Cancer* (2010) 9:75. doi: 10.1186/1476-4598-9-75

29. Vesely MD, Kershaw MH, Schreiber RD, Smyth MJ. Natural Innate and Adaptive Immunity to Cancer. *Annu Rev Immunol* (2011) 29:235–71. doi: 10.1146/annurev-immunol-031210-101324

30. Li C, Chen H, Tan Q, Xie C, Zhan W, Sharma A, et al. The Therapeutic and Neuroprotective Effects of an Antiepileptic Drug Valproic Acid in Glioma Patients. *Prog Brain Res* (2020) 258:369–79. doi: 10.1016/bs.pbr.2020.09.008

31. Zhang S, Tang Z, Qing B, Tang R, Duan Q, Ding S, et al. Valproic Acid Promotes the Epithelial-to-Mesenchymal Transition of Breast Cancer Cells Through Stabilization of Snail and Transcriptional Upregulation of Zeb1. *Eur J Pharmacol* (2019) 865:172745. doi: 10.1016/j.ejphar.2019.172745

32. Tran LNK, Kichenadasse G, Morel KL, Lavranos TC, Klebe S, Lower KM, et al. The Combination of Metformin and Valproic Acid Has a Greater Anti-

Tumoral Effect on Prostate Cancer Growth in Vivo Than Either Drug Alone. *In Vivo* (2019) 33(1):99–108. doi: 10.21873/invivo.11445

33. Tian Y, Liu G, Wang H, Tian Z, Cai Z, Zhang F, et al. Valproic Acid Sensitizes Breast Cancer Cells to Hydroxyurea Through Inhibiting RPA2 Hyperphosphorylation-Mediated DNA Repair Pathway. *DNA Repair (Amst)* (2017) 58:1–12. doi: 10.1016/j.dnarep.2017.08.002

34. Ding W, Lim D, Wang Z, Cai Z, Liu G, Zhang F, et al. 2-hexyl-4-pentynoic Acid, a Potential Therapeutic for Breast Carcinoma by Influencing RPA2 Hyperphosphorylation-Mediated DNA Repair. *DNA Repair (Amst)* (2020) 95:102940. doi: 10.1016/j.dnarep.2020.102940

35. Liu G, Wang H, Zhang F, Tian Y, Tian Z, Cai Z, et al. The Effect of VPA on Increasing Radiosensitivity in Osteosarcoma Cells and Primary-Culture Cells From Chemical Carcinogen-Induced Breast Cancer in Rats. *Int J Mol Sci* (2017) 18(5):1027. doi: 10.3390/ijms18051027

36. Buque A, Bloy N, Perez-Lanzon M, Iribarren K, Humeau J, Pol JG, et al. Immunoprophylactic and Immunotherapeutic Control of Hormone Receptor-Positive Breast Cancer. *Nat Commun* (2020) 11(1):3819. doi: 10.1038/s41467-020-17644-0

37. Wang F, Ma Z, Wang F, Fu Q, Fang Y, Zhang Q, et al. Establishment of Novel Rat Models for Premalignant Breast Disease. *Chin Med J (Engl)* (2014) 127 (11):2147–52. doi: 10.3760/cma.j.issn.0366-6999.20130276

38. Feng M, Feng C, Yu Z, Fu Q, Ma Z, Wang F, et al. Histopathological Alterations During Breast Carcinogenesis in a Rat Model Induced by 7,12-Dimethylbenz (a) Anthracene and Estrogen-Progestogen Combinations. *Int J Clin Exp Med* (2015) 8(1):346–57.

39. He W, Zhu Y, Mu R, Xu J, Zhang X, Wang C, et al. A Jak2-selective Inhibitor Potently Reverses the Immune Suppression by Modulating the Tumor Microenvironment for Cancer Immunotherapy. *Biochem Pharmacol* (2017) 145:132–46. doi: 10.1016/j.bcp.2017.08.019

40. Aoyama K, Komatsu Y, Yoneda M, Nakano S, Ashikawa S, Kawai Y, et al. Alleviation of Salt-Induced Exacerbation of Cardiac, Renal, and Visceral Fat Pathology in Rats With Metabolic Syndrome by Surgical Removal of Subcutaneous Fat. *Nutr Diabetes* (2020) 10(1):28. doi: 10.1038/s41387-020-00132-1

41. Pfaffl MW. A New Mathematical Model for Relative Quantification in Real-Time RT-PCR. *Nucleic Acids Res* (2001) 29(9):e45. doi: 10.1093/nar/29.9.e45

42. Zhou Y, Niu J, Li S, Hou H, Xu Y, Zhang W, et al. Radioprotective Effects of Valproic Acid, a Histone Deacetylase Inhibitor, in the Rat Brain. *BioMed Rep* (2015) 3(1):63–9. doi: 10.3892/br.2014.367

43. Dovedi SJ, Adlard AL, Lipowska-Bhalla G, McKenna C, Jones S, Cheadle EJ, et al. Acquired Resistance to Fractionated Radiotherapy can be Overcome by Concurrent PD-L1 Blockade. *Cancer Res* (2014) 74(19):5458–68. doi: 10.1158/0008-5472.CAN-14-1258

44. Rudqvist NP, Pilones KA, Lhuillier C, Wennerberg E, Sidhom JW, Emerson RO, et al. Radiotherapy and CTLA-4 Blockade Shape the TCR Repertoire of Tumor-Infiltrating T Cells. *Cancer Immunol Res* (2018) 6(2):139–50. doi: 10.1158/2326-6066.CIR-17-0134

45. Schmid MC, Khan SQ, Kaneda MM, Pathria P, Shepard R, Louis TL, et al. Integrin CD11b Activation Drives Anti-Tumor Innate Immunity. *Nat Commun* (2018) 9(1):5379. doi: 10.1038/s41467-018-07387-4

46. Ruffell B, Chang-Strachan D, Chan V, Rosenbusch A, Ho CM, Pryer N, et al. Macrophage IL-10 Blocks CD8+ T Cell-Dependent Responses to Chemotherapy by Suppressing IL-12 Expression in Intratumoral Dendritic Cells. *Cancer Cell* (2014) 26(5):623–37. doi: 10.1016/j.ccell.2014.09.006

47. Harbeck N, Penault-Llorca F, Cortes J, Gnant M, Houssami N, Poortmans P, et al. Breast Cancer. *Nat Rev Dis Primers* (2019) 5(1):66. doi: 10.1038/s41572-019-0111-2

48. Kanemaru H, Yamane F, Fukushima K, Matsuki T, Kawasaki T, Ebina I, et al. Antitumor Effect of Batf2 Through IL-12 p40 Up-Regulation in Tumor-Associated Macrophages. *Proc Natl Acad Sci USA* (2017) 114(35):E7331–40. doi: 10.1073/pnas.1708598114

49. Cassetta L, Pollard JW. Repolarizing Macrophages Improves Breast Cancer Therapy. *Cell Res* (2017) 27(8):963–4. doi: 10.1038/cr.2017.63

50. Hanahan D, Folkman J. Patterns and Emerging Mechanisms of the Angiogenic Switch During Tumorigenesis. *Cell* (1996) 86(3):353–64. doi: 10.1016/S0092-8674(00)80108-7

51. Heldin CH, Rubin K, Pietras K, Ostman A. High Interstitial Fluid Pressure - an Obstacle in Cancer Therapy. *Nat Rev Cancer* (2004) 4(10):806–13. doi: 10.1038/nrc1456

52. Tredan O, Galmarini CM, Patel K, Tannock IF. Drug Resistance and the Solid Tumor Microenvironment. *J Natl Cancer Inst* (2007) 99(19):1441–54. doi: 10.1093/jnci/djm135

53. Jain RK. Antiangiogenesis Strategies Revisited: From Starving Tumors to Alleviating Hypoxia. *Cancer Cell* (2014) 26(5):605–22. doi: 10.1016/j.ccell.2014.10.006

54. Wu C, Li A, Leng Y, Li Y, Kang J. Histone Deacetylase Inhibition by Sodium Valproate Regulates Polarization of Macrophage Subsets. *DNA Cell Biol* (2012) 31(4):592–9. doi: 10.1089/dna.2011.1401

55. Venosa A, Gow JG, Hall L, Malaviya R, Gow AJ, Laskin JD, et al. Regulation of Nitrogen Mustard-Induced Lung Macrophage Activation by Valproic Acid, a Histone Deacetylase Inhibitor. *Toxicol Sci* (2017) 157(1):222–34. doi: 10.1093/toxsci/kfx032

56. Siegel RL, Miller KD, Jemal A. Cancer Statistics, 2017. *CA Cancer J Clin* (2017) 67(1):7–30. doi: 10.3322/caac.21387

57. Kaufman HL, Russell J, Hamid O, Bhatia S, Terheyden P, D'Angelo SP, et al. Avelumab in Patients With Chemotherapy-Refractory Metastatic Merkel Cell Carcinoma: A Multicentre, Single-Group, Open-Label, Phase 2 Trial. *Lancet Oncol* (2016) 17(10):1374–85. doi: 10.1016/S1470-2045(16)30364-3

58. Klug F, Prakash H, Huber PE, Seibel T, Bender N, Halama N, et al. Low-Dose Irradiation Programs Macrophage Differentiation to an iNOS(+)/M1 Phenotype That Orchestrates Effective T Cell Immunotherapy. *Cancer Cell* (2013) 24(5):589–602. doi: 10.1016/j.ccr.2013.09.014

59. Gentles AJ, Newman AM, Liu CL, Bratman SV, Feng W, Kim D, et al. The Prognostic Landscape of Genes and Infiltrating Immune Cells Across Human Cancers. *Nat Med* (2015) 21(8):938–45. doi: 10.1038/nm.3909

60. Kitamura T, Qian BZ, Pollard JW. Immune Cell Promotion of Metastasis. *Nat Rev Immunol* (2015) 15(2):73–86. doi: 10.1038/nri3789

61. Ruffell B, Au A, Rugo HS, Esserman LJ, Hwang ES, Coussens LM. Leukocyte Composition of Human Breast Cancer. *Proc Natl Acad Sci USA* (2012) 109 (8):2796–801. doi: 10.1073/pnas.1104303108

62. Fridman WH, Pages F, Sautes-Fridman C, Galon J. The Immune Contexture in Human Tumours: Impact on Clinical Outcome. *Nat Rev Cancer* (2012) 12 (4):298–306. doi: 10.1038/nrc3245

63. Tumeh PC, Harview CL, Yearley JH, Shintaku IP, Taylor EJ, Robert L, et al. PD-1 Blockade Induces Responses by Inhibiting Adaptive Immune Resistance. *Nature* (2014) 515(7528):568–71. doi: 10.1038/nature13954

64. Mellman I, Coukos G, Dranoff G. Cancer Immunotherapy Comes of Age. *Nature* (2011) 480(7378):480–9. doi: 10.1038/nature10673

65. Joyce JA, Fearon DT. T Cell Exclusion, Immune Privilege, and the Tumor Microenvironment. *Science* (2015) 348(6230):74–80. doi: 10.1126/science.aaa6204

66. Cheema TA, Wakimoto H, Fecci PE, Ning J, Kuroda T, Jeyaretna DS, et al. Multifaceted Oncolytic Virus Therapy for Glioblastoma in an Immunocompetent Cancer Stem Cell Model. *Proc Natl Acad Sci USA* (2013) 110(29):12006–11. doi: 10.1073/pnas.1307935110

67. Saha D, Martuza RL, Rabkin SD. Macrophage Polarization Contributes to Glioblastoma Eradication by Combination Immunovirotherapy and Immune Checkpoint Blockade. *Cancer Cell* (2017) 32(2):253–267 e255. doi: 10.1016/j.ccell.2017.07.006

68. Twyman-Saint Victor C, Rech AJ, Maity A, Rengan R, Pauken KE, Stelekati E, et al. Radiation and Dual Checkpoint Blockade Activate non-Redundant Immune Mechanisms in Cancer. *Nature* (2015) 520(7547):373–7. doi: 10.1038/nature14292

69. Li F, Zhao Y, Wei L, Li S, Liu J. Tumor-Infiltrating Treg, MDSC, and IDO Expression Associated With Outcomes of Neoadjuvant Chemotherapy of Breast Cancer. *Cancer Biol Ther* (2018) 19(8):695–705. doi: 10.1080/15384047.2018.1450116

70. Uehara T, Eikawa S, Nishida M, Kunisada Y, Yoshida A, Fujiwara T, et al. Metformin Induces CD11b+-cell-mediated Growth Inhibition of an Osteosarcoma: Implications for Metabolic Reprogramming of Myeloid Cells and Anti-Tumor Effects. *Int Immunol* (2019) 31(4):187–98. doi: 10.1093/intimm/dxy079

71. Frontiers Editorial Office. Retraction: Targeting and Therapy of Glioblastoma in a Mouse Model Using Exosomes Derived From Natural Killer Cells. *Front Immunol* (2019) 10:1770. doi: 10.3389/fimmu.2019.01770

72. Emoto M, Emoto Y, Yoshizawa I, Kita E, Shimizu T, Hurwitz R, et al. Retraction: alpha-GalCer Ameliorates Listeriosis by Accelerating Infiltration

of Gr-1(+) Cells Into the Liver. *Eur J Immunol* (2020) 50(9):1415. doi: 10.1002/eji.202070200

73. Bonapace L, Coissieux MM, Wyckoff J, Mertz KD, Varga Z, Junt T, et al. Cessation of CCL2 Inhibition Accelerates Breast Cancer Metastasis by Promoting Angiogenesis. *Nature* (2014) 515(7525):130–3. doi: 10.1038/nature13862

74. Golstein P, Griffiths GM. An Early History of T Cell-Mediated Cytotoxicity. *Nat Rev Immunol* (2018) 18(8):527–35. doi: 10.1038/s41577-018-0009-3

75. Wang W, Green M, Choi JE, Gijon M, Kennedy PD, Johnson JK, et al. CD8(+) T Cells Regulate Tumour Ferroptosis During Cancer Immunotherapy. *Nature* (2019) 569(7755):270–4. doi: 10.1038/s41586-019-1170-y

Combined Radiochemotherapy: Metalloproteinases Revisited

Verena Waller and Martin Pruschy [*]

Laboratory for Applied Radiobiology, Department of Radiation Oncology, University Hospital Zurich, University of Zurich, Zurich, Switzerland

Besides cytotoxic DNA damage irradiation of tumor cells triggers multiple intra- and intercellular signaling processes, that are part of a multilayered, treatment-induced stress response at the unicellular and tumor pathophysiological level. These processes are intertwined with intrinsic and acquired resistance mechanisms to the toxic effects of ionizing radiation and thereby co-determine the tumor response to radiotherapy. Proteolysis of structural elements and bioactive signaling moieties represents a major class of posttranslational modifications regulating intra- and intercellular communication. Plasma membrane-located and secreted metalloproteinases comprise a family of metal-, usually zinc-, dependent endopeptidases and sheddases with a broad variety of substrates including components of the extracellular matrix, cyto- and chemokines, growth and pro-angiogenic factors. Thereby, metalloproteinases play an important role in matrix remodeling and auto- and paracrine intercellular communication regulating tumor growth, angiogenesis, immune cell infiltration, tumor cell dissemination, and subsequently the response to cancer treatment. While metalloproteinases have long been identified as promising target structures for anti-cancer agents, previous pharmaceutical approaches mostly failed due to unwanted side effects related to the structural similarities among the multiple family members. Nevertheless, targeting of metalloproteinases still represents an interesting rationale alone and in combination with other treatment modalities. Here, we will give an overview on the role of metalloproteinases in the irradiated tumor microenvironment and discuss the therapeutic potential of using more specific metalloproteinase inhibitors in combination with radiotherapy.

Keywords: ionizing radiation (IR), metalloproteinases, combined treatment modalities, tumor microenvironment, radiotherapy

INTRODUCTION

History of medicine assigns the first oncologic treatment with ionizing radiation to Emil H. Grubbe exposing the mammary carcinoma of Mrs. Rose Lee to X-rays in January 1896. Thereby the first milestone for a radiation-based treatment strategy was defined, which is indispensable nowadays for cancer therapy (1). Starting from low energy treatments of superficial melanomas towards high

energy X-ray beams for the treatment of deeply located tumors in the early 20th century, the therapeutic use of radiotherapy (RT) has rapidly improved (2–4). Today, up to 50% of all cancer patients receive radiotherapy either alone, or in combination with surgery or systematic therapies (5, 6). The main rationale of radiotherapy is to achieve local tumor control by delivering a high dose of ionizing radiation to the tumor, while sparing the surrounding tissue and keeping the adjacent organs functionally intact.

Advances in intensity-modulated radiation therapy (IMRT) and image-guided radiation therapy (IGRT) paved the way towards better treatment planning and enhanced therapeutic efficacy (7). Despite being a highly localized treatment regimen with the ability to diminish tumors on a microscopic level, radiotherapy alone still fails to achieve tumor control for multiple tumor entities with many patients suffering from high tumor recurrence rates. Although overlooked for a long time, early studies already showed that tumor cells could exhibit intrinsic or acquired resistance mechanisms to ionizing radiation (IR), which are either due to the mutational status of the tumor or due to cellular and tumor pathophysiological processes induced by irradiation itself (8, 9). Tumors do not only consist of one malignant cancer cell population, but of a variety of different cell types and their sub-populations, which constitute the tumor microenvironment (TME). Only the deeper understanding of the heterogeneous architecture of the TME and its tight interplay with the tumor cells will lead us to the identification of related resistance mechanisms and novel treatment targets for a combined treatment strategy of radiotherapy with pharmacological agents (10).

In addition to DNA damage, IR also affects intra- and intercellular processes that trigger a multilayered stress response and co-determine the tumor response to RT. In this context, various signal transduction pathways are hijacked by the tumor for its cellular protection and are even further upregulated in response to irradiation. Among others, the MAPK axis represents one of the main signaling pathways controlling the majority of hallmarks of cancer, such as proliferative signaling, angiogenesis, inflammation and cell death evasion (11–13). Hence, upregulated kinase activity along those cascades leads to a proliferative advantage and cell survival upon IR. The basal phosphorylation status of a substrate is tightly regulated by the dynamic interplay between phosphatases and kinases. This interplay can be disturbed by reactive oxygen species (ROS) induced by IR. ROS oxidize critical cysteine residues in the conserved catalytic centers of phosphatases, thus impairing their function and shifting the balance towards a more phosphorylated and active state of the substrate (14, 15). Besides this ligand-independent activation of intracellular signal transduction cascades, ionizing radiation induces the secretion of growth factors and cytokines, thereby mediating intercellular communication via auto- and paracrine signaling through a wide range of soluble signaling molecules. Consequently, irradiation-induced secretion of pro-survival factors into the tumor environment also co-determines radiation resistance, as reported for multiple tumor entities including non-small cell lung cancer (NSCLC) and breast

cancer (16, 17). In this review we will discuss the interplay between ionizing radiation and Zn-metalloproteinases, which represent the major class of proteases responsible for the processing of these secreted factors.

Biochemistry of Metalloproteinases

Metalloproteinases are metal-, usually zinc-, dependent endopeptidases (metzincins) that play versatile roles in intercellular signaling pathways and tissue remodeling. The human superfamily comprises three subfamilies: matrixins (MMPs), astacins and adamalysins (18). Based on functional and structural properties, adamalysins can be further subdivided into a disintegrin and metalloproteinase (ADAM) and ADAM with thrombospondin motif (ADAMTS) (18).

Structurally the metzincins superfamily was defined by Bode et al. based on two properties which appear to be almost identical among all the members (19, 20). They reported an extended Zn^{2+} binding motif HEXXHXXGXXH in the catalytic site for the ligation of three zinc ions as well as a conserved methionine containing segment downstream of the third Zn^{2+}-binding histidine, that supports the formation of a β-turn and therefore participates in the structural integrity of the catalytic domain (the Met-turn) (19, 21).

Besides those common features, the core structures among the subgroups are varying, depending on their function. While MMPs and ADAMTS are mainly involved in the remodeling of the extracellular matrix (ECM), most of the members of the ADAM family are actively associated with the process of proteolytic 'shedding' of membrane-bound proteins, hence the rapid modulation of key signals in the TME (22). Thus, MMPs and ADAMTS are mainly present as secreted enzymes within the ECM, while ADAMs typically remain membrane-associated (**Figure 1**).

In order to prevent dispensable protein degradation, most proteinases, hence also metalloproteinases, are synthesized as latent zymogens. The autoinhibitory propeptide harbors a seven amino acid long motif (PRCGXPD), with the thiol of the cysteine chelating with the active Zn^{2+} site of the catalytic domain of the protein, keeping it inactivated (23). Crucial for the activation of the latent proenzymes is the "cysteine switch", a process describing the disruption of the thiol–zinc interaction (with or without cleavage of the propeptide) (24). This can be induced by the cleavage through other (metallo-) proteinases and allosteric disruption, or most commonly for the membrane-bound members of the metzincins, via proteolysis by the proprotein convertase furin (25).

Tissue Inhibitors of Metalloproteinases (TIMP)

Keeping the balance between an active and a latent state of metalloproteinases, four endogenous TIMPs (tissue inhibitors of metalloproteinases 1–4) are known to inhibit the active enzymes in mammalian tissue. Structurally, the small inhibitory molecules are highly conserved enabling them to inhibit all members of the metzincin family, but with different affinities and increased preference towards ADAMs and ADAMTS (26). TIMPs consist of two functional domains (stabilized via six disulfide bridges), that act independently from each other, pointing towards separate
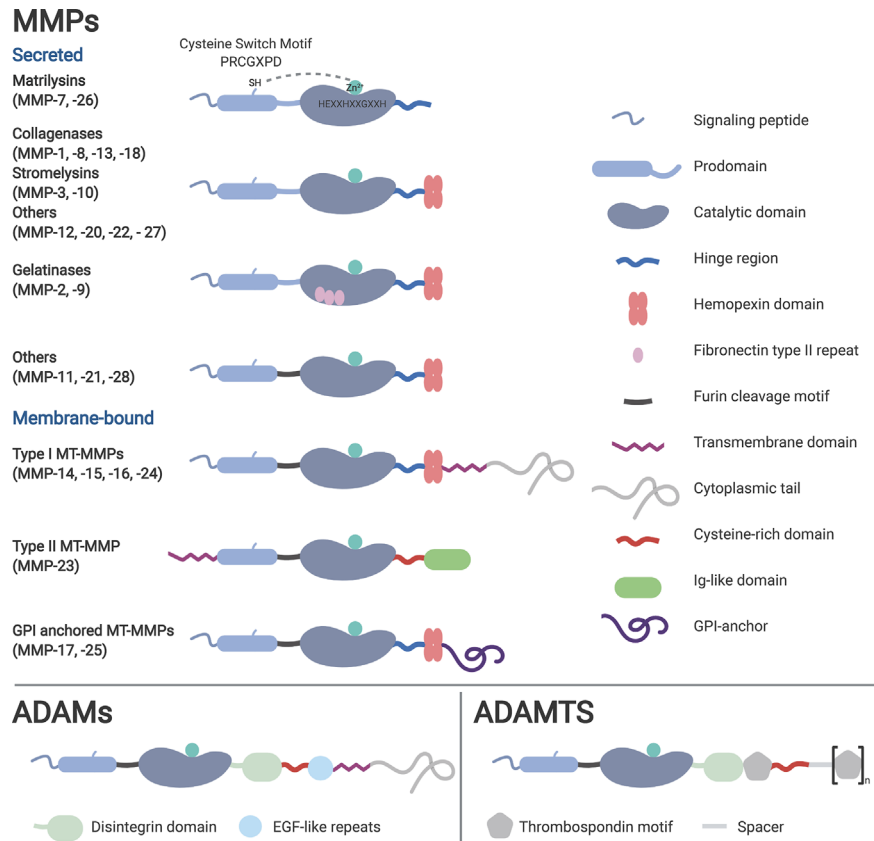
FIGURE 1 | Classification of the metzincins based on their structure and function. Typical for metzincins is their signal peptide, the prodomain, the catalytic domain containing the zinc motif, followed by the linker (hinge) region. Membrane-associated metalloproteinases typically harbor a transmembrane and cytosolic domain, lacking in the secreted family members. Depending on their mode of activation, several metalloproteinases have a furin recognition sequence. Distinctive for many MMPs is the hemopexin (PEX) domain, which facilitates substrate specificity and TIMP interaction.

evolution (27). Most of the inhibitory capacity lies within the large amino terminus, whereas the role of the smaller carboxy tail is not well understood. Inhibition of the target takes place at the very end of the N-terminus (Cys1-Pro5) of mature TIMPs. This short peptide sequence forms five intermolecular hydrogen bonds within the active-site cleft, binding to the metalloproteinase in an almost substrate-like manner (28). The only known function of the carboxy-terminus is the formation of a non-covalent 1:1 complex with the hemopexin domain of proMMP-2/-9. Secreted as such, the complex remains stable and protected from degradation, while the amino terminus can still exhibit its inhibitory function on other MMPs (29).

MATRIX METALLOPROTEINASES IN THE IRRADIATED TUMOR MICROENVIRONMENT

Already during the identification of the first matrix metalloproteinases a clear association with tumor progression

was drawn, as various MMPs were found to be upregulated in human tumors (30). MMPs are mainly acting on the processing of extracellular matrix components, such as collagen, glycoproteins, and proteoglycans, and are highly distributed among different cell types and tissues. In terms of cancer progression, the increased abundance of active MMPs results in the disruption of the matrix barrier, enabling tumor cells to invade into the surrounding tissues and blood vessels. MMPs are therefore mainly discussed in the context of tumor dissemination. However, recent studies revisited the role of different MMPs, differentiating their mode of action into ECM processing versus non-matrix acting, leading to an increased focus on the MMP-regulated intercellular communication via the secretion of cyto- and chemokines, growth and pro-angiogenic factors (30, 31). The fine-tuned balance between MMP and TIMP activation controls this proteolytic shedding, which can be deregulated during cancer progression and in response to exogenous stress, such as ionizing irradiation. MMP maturation is a tightly regulated process in which RT can interfere on many levels. Besides direct cell killing, RT induces cellular and molecular changes within the TME that

can activate MMPs. Overlooked for decades, immunologists have started to understand the immense ability of RT to induce a pro-inflammatory environment, susceptible for immune cell infiltration. No less important, the release of growth factors, chemo- and cytokines also has a direct impact on tumor stimulating MMP gene expression (32, 33). At the same time RT also increases furin gene expression, which results in increased furin-mediated posttranslational conversion of the proform and subsequent activation of many MMPs and all ADAMs/ADAMTS in response to irradiation (16, 25, 34). Furthermore, irradiation generates cellular reactive oxygen species, which also directly interact with biomolecules such as metalloproteinases. Metalloproteinase zymogens are regulated by the interaction of a cysteine amino acid residue in their prodomain and the Zn^{2+} site in the catalytic region. IR-induced oxidation of these critical cysteine sites leads to disruption of the inhibitory conformation and subsequent activation of the metalloproteinases (35, 36).

The diverse mechanisms by which irradiation influences the status of MMP activity in the irradiated TME renders this class of enzymes into an important family for the design of novel treatment strategies.

Role of MMP-2 and MMP-9 for the Radiation Response

MMP-2 and -9 play crucial roles in ECM remodeling and cleavage of membrane substrates and have therefore been associated with several hallmarks of cancer such as angiogenesis, tumor invasion, and metastasis (37–41). Clinical studies identified MMP-9 as a potential prognostic biomarker for various tumor entities such as NSCLC (42), cervical cancer (43, 44), pancreatic cancer (45), and osteosarcoma (46). In many cases, elevated MMP-9 levels were associated with poor prognosis and decreased overall survival. In 2014, Yousef et al. also detected differential expression of MMP-9 in the different molecular subtypes of breast cancer. Importantly, MMP-9 overexpression was found to be an important endpoint for the more aggressive subtypes, triple-negative and HER2-positive breast cancers (41, 47).

Several studies reported irradiation-induced upregulation of MMP-9, which highly correlates with enhanced metastasis and cell invasiveness *in vitro* and *in vivo* and influences treatment outcome (48–51). Confirming increased MMP-9 levels upon sublethal irradiation of Lewis lung carcinoma, Chou et al. observed enhanced cell invasion *in vivo* that resulted in RT-induced acceleration of pulmonary metastases in their C57BL/6 mouse model. This effect could be inhibited by pre-treatment with zoledronic acid, a prototypical MMP-9 inhibitor. Interestingly, high-dose treatment (30 Gy) of the primary tumor decreased MMP-9 serum levels, improved tumor control and eliminated the amount of disseminating cells (48). In NSCLC cells (49) and hepatocellular carcinoma (50), irradiation enhanced MMP-9 expression via the PI3K/AKT/NF-κB and the PI3K/AKT/MAPK pathway, respectively, leading to enhanced tumor cell invasiveness. Investigating drivers of radioresistance, Ko et al. observed increased MMP-9

activity and elevated EMT protein levels in their RT-resistant breast cancer cell line (51). Thus, MMP-9 activity should be carefully probed as biomarker for putative irradiation-induced cell dissemination.

Interestingly, the relevance for potent MMP-9 inhibition as part of a combined treatment modality with RT has also been demonstrated on the systemic level. MMP-9 activity from bone marrow-derived CD11b-positive myelomonocytic cells was most relevant for the process of tumor vasculogenesis. Ahn et al. demonstrated that not endothelial progenitor cells but primarily tumor-site infiltrating CD11b+ myelomonocytic cells are involved in remodeling of the extracellular matrix in the irradiated tumor bed, in promoting vasculogenesis (instead of angiogenesis). They thereby represent a risk for local recurrences (52). Of note, genetic depletion of the respective metalloproteinase activity prevented tumor growth in these pre-irradiated areas. Eventually, these insights resulted in the promising development of anti-vasculogenesis strategies in combination with radiotherapy (53, 54).

In terms of clinical relevance, MMP-9 has been proposed as a predictive marker for the efficacy of radiotherapy in NSCLC. Serum of patients with intermediate and advanced stages of NSCLC were tested prior and after treatment [prescribed dose of planning target volume (50–66 Gy)] which was given in fractions of 1.8–2.0 Gy/day. Only in responders, the MMP-9 serum levels were significantly reduced at 1–5 weeks after treatment, whereas for patients with stable disease (SD) and progressive disease (PD) stage no changes in serum MMP-9 could be detected (55). An additional study on rectal cancer identified alterations in MMP-9 levels at different stages of treatment. Circulating MMP-9 levels were significantly reduced after induction neoadjuvant chemotherapy (NACT), gradually increased after sequential radiochemotherapy (RCT) and almost recovered to baseline 4 weeks after treatment. Notably, progression free survival (PFS) correlated with the initial drop of MMP-9 levels after NACT and RCT (56). One clinical study focused on the impact of radiotherapy-induced MMP-9 activation in the healthy tissue surrounding the targeted tumor. After neoadjuvant RCT of esophageal cancer patients MMP-9 levels increased in the proximal and even distal healthy esophageal tissue, which could be associated with post-operative complications such as anastomotic leakage, and could potentially be avoided by MMP-9 inhibition (57).

Due to their structural and functional similarities, it is not surprising that multiple studies report co-upregulation of MMP-9 and MMP-2 upon irradiation, leading to increased tumor cell invasiveness, metastasis, and angiogenesis. MMP-2, which belongs to the same gelatinase family as MMP-9, is also highly associated with various tumor entities such as prostate cancer (58), gastrointestinal carcinomas (59, 60), and cervical cancer (44, 61). Similar to MMP-9, IR also induces upregulation of MMP-2 resulting in enhanced tumor growth and cell invasiveness. Moreover, MMP-2 activity is required for the angiogenic switch during tumor development and has, together with MMP-9, been implicated in the regulation of expression and release of vascular endothelial growth factor (VEGF) (62–65). Combining RT with

inhibition of MMP-2 activity impaired cancer cell invasion, reduced VEGF secretion and hindered radiation-induced capillary tube formation *in vivo*, expanding its role to an important regulator of angiogenesis (63, 64).

Bidirectional activation between MMP-2 and the pro-survival transcription factor FoxM1 influenced cell cycle progression and thereby impacted the treatment outcome of DNA damaging agents. Inhibition of MMP-2 abrogated IR-induced FoxM1 expression to overcome G2/M cell cycle arrest, thereby driving cells into apoptosis (66).

Genotyping of patients with advanced stages of NSCLC after RT revealed that carriers of selected functional MMP-2 polymorphism had significantly reduced PFS, proposing MMP-2 as prognostic marker (67). In glioma cells, RT-induced secretion of MMP-2/-9 enhanced tumor cell migration *in vitro* and dissemination *in vivo*. Conversely, TIMP-2 protein expression, which antagonizes MMP activation, was strongly reduced (68). In breast cancer and rectal cancer specimen, MMP-2/-9 activation was observed to be enhanced in the tumor site in comparison to the adjacent healthy tissue, and correlated with dissemination, cancer progression and treatment outcome (69–71). After radiotherapy, MMP-2/-9 levels increased drastically within the rectal adenocarcinoma indicating a role of MMP-2/-9 for radioresistance (71). Taken together, serum and even urine levels of circulating MMP-2/-9 can be used as good clinical markers for tumor incidence, cancer stages, and treatment prognosis or success (70, 72–74). At the same time, specific MMP-2/-9 inhibitors could be promising radiosensitizers in cancer therapy.

Versatile Roles of Other MMP Family Members

Even though MMP-2 and MMP-9 represent the most investigated MMPs in the context of radiotherapy, also other family members have been associated with the remodeling of the irradiated tumor microenvironment. Indeed, one of the first *in vivo* studies combining MMP inhibition with radiotherapy was conducted in 1992, with Sotomayor et al., detecting increased tumor growth control upon treatment with the collagenase (MMP-1) inhibitor minocycline in combination with RT (75). In addition to enhanced rates of cancer cell intravasation and dissemination, RT-induced MMP-activation (MMP-1/-2/-3/-9/-14) and subsequent degradation of the TME and the mucosal tissue adjacent to the irradiated tumor site, can induce strong normal tissue toxicities (76, 77). Elevated levels of secreted MMP-1/-2/-9 in the mucosa of rectal cancer patients after RT resulted in gut tissue toxicity increasing the risk for post-operative morbidity, wound infections as well as metastasis formation (78, 79). Interestingly, several studies also demonstrated an increase in MMP-7 gene expression after surgery and pre-operative high-dose RT in colorectal carcinoma cells but not in the adjacent mucosal tissue (80–82). Furthermore RT affected MMP-7 expression in a dose dependent way indicating that MMP-7 levels are very sensitive to different types of trauma, which can define treatment outcome and resistance (82). Hence,

different MMPs are responding in a differential way to radiotherapy and combining radiotherapy with specific MMP inhibitors could not only decrease the risk of local tumor recurrence but could also protect the healthy mucosa.

In oral squamous cell carcinoma patients, the MMP-13 expression levels highly correlated with different clinicopathological parameters, such as staging and grading of the tumor. Additionally, patients harboring less MMP-13 transcripts showed a better treatment response to radiotherapy in comparison to patients overexpressing MMP-13 (83). Similar results were obtained in a glioma patient study indicating its potential use as a predictive biomarker for RT, while another study determined MMP-13 as prognostic marker for tumor aggressiveness and recurrence in head and neck cancer patients (84, 85).

Among the six known membrane anchored matrix metalloproteinases, membrane type I matrix metalloproteinase MT1-MMP (MMP-14) is highly associated with cancer progression, angiogenesis, and immune response (86–89). Besides its original role as collagenase and MMP-2 activator, proteomics analysis of human melanoma cells revealed a broad influence of MT1-MMP on the tumor microenvironment, based on the shedding of a variety of adhesion molecules, receptor and transporter proteins (90). MT1-MMP accumulates on the migratory front of cells and facilitates the degradation of collagen, fibronectin and CD44. Disruption of the ECM barrier enables cell motility, and therefore MT1-MMP was considered as important protease for (tumor) cell migration and invasion (87, 91). Thus, MT1-MMP is an interesting target in combination with RT to mitigate cell migration and metastasis formation. In breast cancer models inhibition of MT1-MMP synergized with ionizing radiation and reduced cell migration (92–94). Investigating the invasiveness of triple-negative (TN) breast cancer cells after RT, MT1-MMP downregulation reduced the number of circulating tumor cells and lung metastases (93). Besides its pro-migratory effect, MT1-MMP has also been identified as an activator of the immune-suppressive cytokine transforming growth factor (TGF) β (95). Consistent with the decrease of TGF-β secretion, blockade of MT1-MMP with the antibody DX2400 polarized tumor-associated M2-like macrophages towards the anti-tumor M1-like population, contributing to tumor growth delay and reduced necrosis (94). In addition, MT1-MMP inhibition improved vessel perfusion and oxygenation of the tumor. Overcoming tumor hypoxia is one of the main challenges in the field of RT as hypoxic cells are radioresistant and negatively influence treatment outcome (96). Thus, MT1-MMP represents an interesting target in particular for the combined treatment of hypoxic tumors.

Moreover, an interesting study on intracellular signaling extended the effect of MT1-MMP beyond the tumor microenvironment and proposed its involvement in the DNA damage response along the MT1-MMP-integrinβ1 pathway (97). Inhibition of MT1-MMP reduced integrinβ1 signaling and sensitized TN breast cancer cells to radio-and chemotherapy by collapsing the replication machinery. Thus, combining RT with MT1-MMP inhibition could not only prevent cell dissemination but also enhance direct DNA damage.

Our own studies on increased MMP activities and invasiveness of irradiated tumor cells exemplify the complex network and regulation of metalloproteinase activities in response to stress. The IR-enhanced invasive capacity of fibrosarcoma and glioblastoma cells could mechanistically be linked to increased MMP activities, though irradiation only partially increased expression of MMP-2/-9/-14. On the other hand, irradiation specifically induced the secretion of TIMP-1/-2. Depending on the ratio of TIMPs and MMPs, TIMPs can not only inhibit but also activate MMPs, with TIMP-2 being relevant for processing of pro-MMP-2 (98). Interestingly, downregulation of TIMP-1/-2 not only reduced respective MMP-activities but also specifically blocked IR-induced invasiveness of these irradiated tumor cells. Cell invasion induced by low radiation doses (1.5–2.0 Gy) is of particular importance in the context of fractionated radiation schedules and sub-lethal irradiation of peripheral tumor cells of the radiotherapy treatment volume. Thus, a combined treatment modality reducing IR-upregulated MMP might reduce the potential risk for IR-induced (glioma) cell migration and dissemination.

ADAM-INDUCED SECRETOME IN THE IRRADIATED TUMOR MICROENVIRONMENT

In the past decades, the importance of the ADAM family members has shifted from embryonic development to versatile roles in disease including neurodegeneration, inflammation, and cancer in particular. ADAMs are recognized as important players in the ErbB1 (EGFR) signaling axis as ADAMs shed a large variety of (mitogenic) growth factors, growth factor receptors and cyto- and chemokines. The ErbB1 pathway is associated with cancer growth and progression and represents an attractive target for cancer therapy. However, targeting the pathway directly with tyrosine kinase inhibitors such as gefitinib has been challenging due to acquired pro-resistance mutations (99). The combination of RT with the ErbB1-directed monoclonal antibody cetuximab improved locoregional control and survival of patients suffering of advanced squamous-cell carcinoma of the head and neck, whereas the trimodal treatment with chemoradiotherapy and cetuximab showed no additive beneficial effect in stage III NSCLC patients (100, 101). Therefore, it could be of interest to inhibit not only ErbB1- but multiple ErbB (ErbB1–4), and other related receptor tyrosine kinases and signal transduction cascades, via inhibition of upstream sheddases such as ADAMs. ADAMs are upregulated in many cancer entities and have been associated with promotion of cell growth, survival, migration, and invasion (102). Similar to MMPs, ADAMs are activated in multiple ways, including gene expression, translocation to the cell membrane, posttranslational modifications on the cytoplasmic tail, zymogen activation via furin or their interplay with TIMPs (102, 103).

Among all ADAMs, ADAM10 and ADAM17 share the most structural and functional properties, being best known for their role in Notch signaling and the clinicopathology of Alzheimer's disease. ADAM17 represents the most intensively studied member of the ADAMs family and gained attention especially in the context of inflammatory disease due to its processing of TNF-α. Thus, ADAM17 is also known as TNF-alpha converting enzyme (TACE). As part of our own TME-oriented research we investigated how RT-induced secretion of para- and autocrine stress-response factors modulates cellular radiosensitivity, drives acquired rescue mechanisms and determines the overall radiation sensitivity of a tumor. We performed exhaustive large-scale secretome analysis using antibody arrays for a wide range of secretory factors (16). Secretion kinetics of selected factors were determined across different established tumor cells and in murine blood serum, derived from irradiated tumor xenograft-carrying mice. RT-induced expression and tumor cell secretion included top hits, such as amphiregulin, TGF-α and ALCAM. All these factors were secreted in a similar RT-induced time- and dose-dependent manner from several NSCLC cell lines (and other tumor entities), indicative of a common upstream mechanism without changes at the transcriptional level, pointing towards ADAM17. Interestingly, irradiation induced a dose-dependent increase in cleavage of the proform of ADAM17 by furin, which resulted in enhanced ADAM17 activity and correlated with subsequent substrate shedding. Pharmacological inhibition of ADAM17 with the small molecular inhibitor TMI-005 or siRNA-based targeting of ADAM17 suppressed RT-induced shedding of these factors, downregulated ErbB1-signaling in target cells and enhanced RT-induced cytotoxicity *in vitro* and *in vivo* (tumor xenograft model) even in tumors resistant to ErbB-targeting cancer therapeutics. *Ex vivo* substrate analysis of murine blood serum derived from irradiated tumor xenograft-carrying mice correlated with our *in vitro* results. Not surprisingly the supra-additive response to the combined treatment modality of RT and inhibition of ADAM17 on the *in vivo* level point towards multiple mechanisms of action, including tumor cell- and TME-oriented ionizing radiation-sensitive processes.

Cancer stem cell are often characterized by increased radiation resistance (104). Investigating the radioresistant and migratory phenotype of CD133+ liver cancer stem cell (CSC) Hong et al. observed next to increased MMP-9 and -2 expression also IR-enhanced ADAM17 activity in the CD133+ enriched cell population of hepatocellular carcinoma (HCC) (105). Of note inhibition of ADAM17 sensitized these CSCs to IR and disrupted their IR-induced metastatic potential. Overall, ADAM17 is gaining recognition in the field of combined treatment modalities with RT, in particular for aggressive tumor entities with high recurrence rates.

Even though ADAM10 and respective inhibitors are highly discussed as novel targets for cancer treatment, ADAM10 has not been very much investigated in combination with radiotherapy. As depicted by Sharma et al., while ADAM17 activity increased in an IR-dose-dependent manner, irradiation of NSCLC cells did not upregulate ADAM10 activity in these cells (16). However, IR-induced upregulation of these ADAM-isoforms might be tumor entity dependent. In a very recent report, Mueller et al.

demonstrated IR-increased ADAM10 expression in pancreatic tumor cells, which correlated with RT-induced fibrosis, tumor cell migration, and invasion. Targeting of ADAM10 sensitized orthotopic tumors to IR and prolonged mouse survival (106). Furthermore, a putative risk for cardiovascular damage exists as exposure of endothelial cells to irradiation increased the levels of active ADAM10 in those cells (107, 108). Subsequently ADAM10-mediated degradation of the endothelial specific adherens junction VE-Cadherin resulted in increased vascular permeability. Weakening the endothelial barriers facilitates transendothelial tumor cell migration and dissemination but also ischemic disease after RT. Thus, it is important to appreciate the vascular system as an organ of risk when irradiating solid tumors.

Most studies investigating the response of ADAMs to IR in cancer and adjacent endothelial tissues observed an upregulation of the metalloproteinases on the expression, total protein and/or activity level. However, studying radiation-induced renal dysfunction and tissue toxicity in healthy renal epithelial cells revealed the opposite effect. IR induced a downregulation of ADAM9/10/17 *in vitro* (mIMCD-3 cell line) as well as in kidney tissue derived from BALB/c mice. This phenotype directly correlated with decreased levels of the soluble anti-aging suppressor Klotho, a substrate of ADAM9/10/17. The clinical consequences are premature cellular senescence, nephropathy and even kidney failure as severe side effects after RT (109).

The reduction of the oxygen partial pressure below a critical physiological level represents a major radioresistance mechanism in tumors, due to the altered physico-chemical conditions but also due to biological adaptations. Tumor hypoxia renders tumor cells up to threefold more radioresistant than their normoxic counterparts. The hypoxia-inducible factor (HIF)-1α is stabilized under hypoxic conditions, accumulates and transactivates a large variety genes involved in the adaptive response of the tumor cells to hypoxia, including genes involved in metabolism, angiogenesis, cell proliferation, and also different metalloproteinases (110–112). Direct (through binding to the respective promotor region) and indirect mechanistic links were identified between HIF-1α accumulation and increased gene expression of MMP-1/-9/-13/-14 as well as ADAM10/17 (111–117) and correlated in most cancer cell types with increased aggressiveness and invasiveness (111–113). To ensure energy sustainability, hypoxic cancer cells shift their metabolism towards the glycolysis pathway (118), which generates high amounts of acidic end products. One important part of the pH-regulatory machinery plays the tumor-associated zinc-metalloenzyme carbonic anhydrase IX (CAIX) (118). Induced by HIF-1α, high levels of membrane-bound CAIX have been associated with cancer cell invasiveness and therapeutic resistance. Interestingly, hypoxia-stabilized HIF-1α also promotes increased ADAM17 expression (117), which recognizes CAIX on the cell surface as a substrate and releases the enzymatically active ectodomain of CAIX (119). However, the consequences of this specific altered extracellular proteome for the exact pro- and anti-tumorigenic responses have yet to be investigated (120).

Next to the release of immunosuppressive factors, a hypoxic tumor microenvironment also impairs anti-cancer immunity through HIF-1α-mediated upregulation of ADAM10. ADAM10 is required for shedding of MHC class I chain-related molecule A (MICA), which activates natural killer (NK) cell effector function and cell lysis. Decreased levels of MICA under hypoxic conditions subsequently lead to immune escape and tumor cell resistance to the cytolytic action of innate immune effectors (116). Due to their wide range of substrates, their importance for Notch signaling pathways and as attributes of almost every cell type of the immune system, ADAM10 and 17 have gained particular attention in recent years in immunology research (121). Furthermore, ADAM17 is considered the main protease to cleave the Fcγ receptor CD16A (FcγRIIIA) on NK cells, which is involved in antibody-dependent cell-mediated cytotoxicity (ADCC) (122, 123). Human NK cells exclusively recognize tumor-targeting therapeutic monoclonal antibodies via intact CD16A. Engagement with the target cell induces NK cell degranulation, followed by the release of cytolytic granules (124). Complementary to this, ADAM17 also cleaves CD62L (L-Selectin), an adhesion molecule that facilitates mobility and homing of lymphocytes, including NK cells (122). Furthermore, NKG2D ligands are also substrates of ADAM17, and as such ADAM17 plays a major role in the regulation of the innate immune system through direct cell killing (natural cytotoxity) (125, 126). Hence, inhibition of ADAM17 on tumor cells and NK cells could strongly enhance anti-tumor immunity alone and as part of combined treatment modalities with different targeting agents and immunogenic cell death inducers. Moreover, ADAM17-mediated shedding has also been investigated in CD8+ T-cells towards activation of proliferation but also as inducer of apoptosis (127, 128). CD62L shedding positively affected early clonal expansion of cytotoxic T-cells in virus-transfected mice suggesting ADAM17 as an important regulator of T-cell activation (127). Recent studies also identified the programmed death ligand 1 (PD-L1) as a novel substrate of ADAM17 (128, 129). Taken together, novel immunotherapeutic approaches should carefully consider the role of ADAMs as additional immune regulatory target and resistance mechanism to immune checkpoint inhibition, also when combined with radiotherapy.

The plethora of molecular interdependencies between tumor hypoxia, the immune system and radiotherapy is not within the scope of this review and is summarized elsewhere (130–133).

TARGETING METALLOPROTEINASES FOR CANCER TREATMENT

In addition to the use of metalloproteinases as diagnostic markers for tumor prognosis and treatment prediction, many efforts towards the development of potent MMP/ADAM inhibitors were pursued - unfortunately only with minimal success, which is primarily due to the lack of high specificity. Nevertheless, we will summarize the major developments on the

preclinical and clinical level and point towards combined treatment modalities with radiotherapy.

Small Molecular Inhibitors

The first generation of small molecular inhibitors comprised two functional groups: hydroxamic acid motifs that target the catalytic site of the MMPs by chelating the active zinc ion and a peptide derivate mimicking the collagen binding motif (**Figure 2**) (134). Binding to those peptidomimetics changes the conformation of the catalytic domain of metalloproteinases and disrupts the integrity of the enzyme. Batimastat (BB-94) was the first MMP-inhibitor to enter clinical trials (135). However, it could not be orally administered, thus, clinical testing was discontinued (136). The structurally related and orally bioavailable Marimastat (BB-2516) achieved promising results in early clinical trials (**Table 1**) (31). Nonetheless, in phase III clinical trials for different cancer entities Marimastat did not show added survival benefit and many treated patients suffered severe musculoskeletal side effects (31, 137). This high tissue toxicity is most probably due to the low selectivity of these broad-spectrum inhibitors towards different zinc-dependent proteases (137). Lessons from those early therapeutic efforts resulted in compounds targeting unique structural properties of MMPs. One structural characteristic that next generation of MMP inhibitors took advantage of was the variable S1' pocket of metalloproteinases. This pocket lies in close proximity to the Zn^{2+} binding site in the catalytic domain and defines binding and substrate specificity (134). Based on amino acid variation on this primed enzyme site MMPs can be classified into "deep pocket" and "shallow pocket" enzymes (134, 138). The majority of MMPs harbor a leucine that forms their S1'pocket, resulting in an open conformation, whereas the small pocket for MMP-1/-7/-11 is partially or entirely occluded by larger amino acid residues

(arginine, tyrosine, and glutamine, respectively) (134). The design of the nonpeptidic collagen-mimicking inhibitor Prinomastat (AG3340) was based on this rationale resulting in enhanced specificity for "deep pocket" MMP-2/-3/-9/-13. However, in phase III trials of advanced lung or prostate cancer Prinomastat did not improve clinical outcome when combined with chemotherapy, and further clinical studies were halted (31, 139).

TMI-005 (Apratastat), which shares structural similarities with Prinomastat, was originally designed for the treatment of rheumatoid arthritis due to its inhibitory potential of TNF-α release (140, 141). In contrast to previous clinical investigations with other small molecular inhibitors, TMI-005 showed very low tissue toxicity but the program with TMI-005 and other closely related derivatives was stopped due to lack of efficacy, related to constitutive activation of the TNF receptor on immunological cells, but not due to toxicity reasons (140). Based on its low toxicity profile and target relevance independent of TNF-α, TMI-005 and other new classes of ADAM17 inhibitors thus have a strong rationale for repurposing as drug in cancer therapy. After identifying ADAM17 as an important player for radiation resistance in NSCLC cells, our own studies demonstrated that pretreatment with TMI-005 sensitized NSCLC cell lines to RT and reduced secretion of ADAM17-specific substrates (16). Determining its efficacy in NSCLC cell-derived xenografts revealed supra-additive tumor control in combination with RT and defines its potential in cancer therapy.

Several other small molecular inhibitors have been designed to target members of the ADAM family with increased affinity towards ADAM10 and ADAM17. These two sheddases act upstream of multiple ErbB pathways, and interestingly their inhibition also synergized with therapeutics agents directly targeting the ErbB (1–3) pathways. Combining INCB3619,
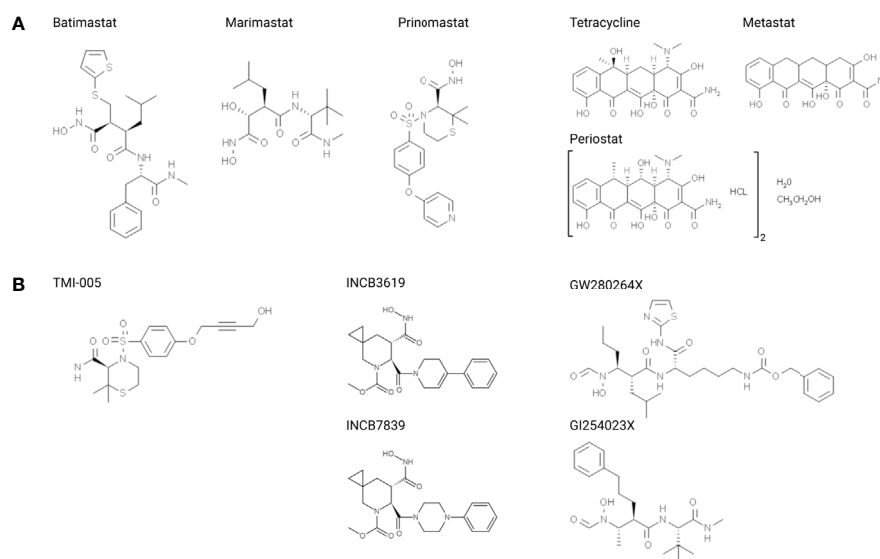

FIGURE 2 | Structural formulas of small molecular inhibitors discussed in this review, divided into **(A)** MMP-directed and **(B)** ADAM-directed inhibitors.

TABLE 1 | Summary of discussed metalloproteinase inhibitors in cancer-related clinical trials.

Name	Target	Tumor entity	Identifier
Marimastat (BB-2516)	Broad spectrum	SCLC	NCT00003011
		NSCLC	NCT00002911
		Breast cancer	NCT00003010
Prinomastat (AG3340)	MMP-2/-3/-9/-13	NSCLC	NCT00004199
		Brain and Central Nervous System Tumors plus RT	NCT00004200
		Prostate cancer	NCT00003343
Neovastat (AE-941)	MMP-2/-9/-12	NSCLC plus RT	NCT00005838
		Multiple Myeloma	NCT00022282
		Kidney cancer	NCT00005995
Metastat (Col-3, Incyclinide)	MMP-2, MMP-9	AIDS-Related Kaposi's Sarcoma	NCT00020683
		Advanced Solid Malignancies	NCT00003721
		Refractory metastatic cancer	NCT00001683
		Brain and Central Nervous System Tumors	NCT00004147
INCB7839 (Aderbasib)	ADAM10, ADAM17	Gliomas	NCT04295759
		Diffuse Large B Cell Non-Hodgkin Lymphoma	NCT02141451
		HER2+ metastatic Breast Cancer	NCT01254136
			NCT00864175
		Solid Tumors	NCT00820560
Andecaliximab (GS-5745)	MMP-9	Gastric or Gastroesophageal Junction Adenocarcinoma	NCT02864381
			NCT02545504
			NCT02862535
		Advanced solid tumors	NCT01803282
		Glioblastoma	NCT03631836

a dual inhibitor against ADAM10/17, with gefinitib or paclitaxel strongly downregulated proliferation of NSCLC cells, whereas other cell lines, which proliferate independently of ErbB-signaling, remained unaffected (142). Also in breast cancer models, selected sheddase inhibition mitigated the release of ErbB family ligands and enhanced the effect of ErbB-directed therapies *in vivo* (143, 144).The structurally related but pharmacokinetically improved inhibitor INCB7839 underwent clinical trials for the treatment of HER2 (ErbB2)-positive breast cancer patients with an interesting rationale to overcome trastuzumab-resistance. HER2 is a substrate of ADAM10 and the ADAM10 inhibitor INCB7839 reduced cleavage and release of the extracellular domain, thereby overcoming resistance to HER2-directed trastuzumab (145, 146). Indeed, administration of INCB7839 was well tolerated, decreased the plasma level of the extracellular domain of HER2. Future trials will show whether the promising combined treatment strategy will improve clinical outcome. HER2-mediated resistance mechanisms to other pharmacological therapies also exist in colorectal cancer cells and could also be related to upregulated ADAM10/17 (147, 148). As such treatment of colorectal cancer cells with the dual ADAM10/17 inhibitor GW280264X sensitized cells to chemotherapy (5-FU) (148).

Investigating the involvement of ADAM10/17 in the immunogenicity of glioblastoma-initiating cells, Wolpert et al. determined their role in regulating the NKG2D receptor-ligand system (among others MICA, MICB, ULBP2) (149). Inhibition of ADAM10/17 with GW280264X and the more specific ADAM10-directed compound GI254023X, increased cell surface abundance of ULBP2, which directly resulted in an increased immune response and susceptibility for NK cell mediated lysis. Studying the effect of ADAM10/17 inhibition on irradiation-induced cell permeability of endothelial cells,

GI254023X revealed the strong involvement of ADAM10 in VE-cadherin regulation and transendothelial migration (108). Overall, these mechanisms point towards the versatile function that ADAM10/17 exert in the tumor microenvironment.

Shortly after identifying shark cartilage as the first tissue with anti-angiogenic (anti-MMP-2/-9/-13) properties, the functionally active, naturally occurring compounds were extracted and developed as Neovastat (AE-941) (150). *In vivo*, treatment with Neovastat alone showed inhibited neovascularization and metastasis formation in a Lewis lung carcinoma model. Combination with cisplatin increased the therapeutic index showing strong anti-metastatic effects while protecting against cisplatin-induced myelosuppression (151). Being introduced to phase I/II trials, Neovastat was well tolerated and demonstrated increased median survival in patients with solid tumors, including renal, prostate and lung carcinoma (150). However, in patients with unresecetable stage III NSCLC, the treatment with Neovastat to did not improve efficacy of chemoradiotherapy and has not been recommended for further treatment of lung cancer (152).

Apart from their conventional role as antibiotics, tetracyclines are effective inhibitors of metalloproteinases in the treatment of malignant disease. Early studies suggested non-antimicrobial functions of synthetic tetracyclines as inhibitors of collagenase and gelatinase activity in periodontitis and anti-proliferative and anti-migratory effects migration in cancer cells (153–156). This new, promising function led to a wave in synthesis of improved chemically modified tetracyclines (CMT) with deletion of the anti-microbial functional group but enhancing their MMP-directed inhibitory potencies (157). The main mode of action is chelation of Zn^{2+} and Ca^{2+} ions, but also other mechanisms including regulation of gene expression and degradation of MMPs have been proposed (158). One of the most potent and promising compounds is Metastat (Col-3, Incyclinide) which

inhibited the expression and the activity of MMP-2 and reduced tumor growth and metastasis formation in pre-clinical tumor models (159). Interestingly, Metastat only minimally reduced tumor growth in the B16 melanoma model. However, the combined treatment modality with RT led to strong tumor growth delay and reduced angiogenesis (64). Four phase I/II clinical trials and pharmacokinetic studies were completed with Metastat in the treatment of patients with advanced solid malignancies, AIDS-related Kaposi's sarcoma, refractory metastatic cancer, and recurrent high-grade glioma (160–163). Metastat was well tolerated, but due to weak responses, no further clinical trials have been initiated. Notably Metastat was tested on the clinical level only as single treatment modality and not in combination with radio-/chemotherapy.

Interestingly, many other MMP inhibitors entered clinical trials with promising pre-clinical results to fail dramatically beyond Phase II (137, 158). Approved in 2001 for the treatment of chronic periodontitis, the doxycycline hyclate Periostat targeting collagenase activity in the gingival tissue represents the only FDA approved MMP inhibitor (153, 164, 165). Besides this sole success, decades of research have led us to reason that metalloproteinases do not represent suitable targets for cancer treatment (31, 137, 166, 167). Among many others, the major therapeutic challenge lies in the complexity of the protease network "protease web" as MMPs do not only act alone or in linear pathways, but are part of complex and dynamic amplification cascades or inter-regulatory circuits (166). Disease but also non-specific drugs perturb the order, adding higher spatio-temporal complexity to the network.

Therapeutic Antibodies

Targeting the catalytic domain of enzymes appears as an attractive therapeutic approach. However, these domains are highly conserved amongst different MMPs, leading to off-target effects and tissue toxicity. As MMPs act extracellularly they represent excellent targets for highly specific inhibitory monoclonal antibodies (mAb). Due to their versatile involvement in modulating the tumor microenvironment, inhibitory antibodies against MMP-9, MT1-MMP, and ADAM17 have recently been developed (168–175).

The strong influence of MT1-MMP on the tumor microenvironment renders it an attractive target for therapeutic strategies (90). Therefore, a range of antibodies have been designed that selectively block MT1-MMP, resulting in reduced tumor growth, angiogenesis, and dissemination in ovarian, breast, and melanoma tumor models (169, 172, 176–178). Discovered using phage display technology, DX-2400 blocked MT1-MMP with high potency and reduced tumor burden by inhibiting MMP-2 activation (94, 176). Subsequently, antibody treatment resulted in improved tissue perfusion leading to re-oxygenation of the tumor. This effect could be exploited by combined treatment with radiotherapy leading to additive tumor control in a murine mammary tumor model (94).

The challenge of selectively targeting MMP-9 lies in its structural similarity to MMP-2. The mAb REGA-3G12 solely binds to the catalytic domain of MMP-9, however and despite its strong binding affinity, REGA-3G12 only displays weak inhibitory activity (179, 180). Combining its target specificity with a small molecular MMP inhibitor, gave rise to an antibody-drug conjugate (ADC) consisting of REGA-3G12 and the broad spectrum inhibitor CGS27023A (181). *In vitro*, this ADC could bind to its target with high selectivity, while strongly inhibiting MMP-9 activity. It will be of interest to observe future validation and applications of this elegant approach of combining mAb with a small molecular inhibitor, alone and in combination with systemic chemotherapeutics and radiotherapy.

Selective inhibition of MMP-9 with the two monoclonal antibodies AB0041 and AB0046 reduced symptoms of DSS-induced ulcerative colitis and colorectal tumor burden in murine orthotopic tumor models (168). Given these encouraging results, AB0041 was humanized (GS-5745) towards clinic trials. This makes GS-5745/Andecaliximab the first anti-MMP antibody to currently undergo clinical investigation as monotherapy and as part of a combined treatment modality with chemotherapy (182–184).

Only in the last decade the first promising anti-human ADAM17 antibody D1(A12) was developed (171). Characteristic for this cross-domain antibody is its simultaneous recognition of catalytic as well as noncatalytic regions, acting as steric hindrance and allosteric inhibitor at the same time (171). D1 (A12) was shown to bind to ADAM17 in a subnanomolar range (K_D of 0.46 nM), reduced cleavage of ADAM17-specific substrates *in vitro* and *in vivo*, mitigated cell migration, and inhibited tumor growth with suitable pharmacokinetics (185–187). Two other antibodies, A9(B8) and MEDI3622, are currently undergoing pre-clinical investigation and demonstrate anti-tumor effects by inhibiting EGFR-dependent and -independent pathways (170, 174). Characteristic for MEDI3266 is its high site-specificity and target-sensitivity as it recognizes the surface loop sIVa-sIVb β-hairpin on the M-domain, unique for ADAM17 (188). MEDI3266 was shown to inhibit tumor growth of different tumor models. Combined treatment with EGFR-directed cetuximab led to complete tumor regression in the OE21 esophageal xenograft model and others (174). Furthermore, ADAM17-inhibition by MEDI3266 blocked CD16A cleavage from activated NK-cells (see above) and resulted in increased production of IFNγ in the presence of antibody-opsonized tumor cells (189). Several studies have investigated the consequences of CD16A blocking for antibody-dependent cellular cytotoxicity (ADCC), though with contradictory results (124). Hence, the precise ways on how ADAM17-inhibition leads to tumor reduction and the involvement of ADCC remains to determined. Nevertheless, based on their specificity, these ADAM17-directed antibodies represent ideal candidates for a combined treatment modality with RT.

DISCUSSION

Modern image-guided radiotherapy has reached a level of technical conformity that nowadays requires biological means to further increase the therapeutic window towards improved

treatment outcome e.g. as part of combined treatment modalities with highly potent pharmacological agents specifically sensitizing the tumor compartment to ionizing radiation. While radiotherapy combined with classic chemotherapeutic agents e.g. cisplatin for head and neck squamous cell carcinoma became standard clinical practice within the last twenty years, combined treatment with small molecular agents or inhibitory antibodies targeting specific signaling moieties are still considered exceptional. This might be due to the continuous development of new radiotherapeutic treatment regimens, from classic fractionated low dose to hypofractionated and stereotactic single high dose treatment regimens. Indeed, different radiotherapy regimens induce differential biological processes and thus require adaptations, also in the choice of a combined treatment modality. On the other hand, major resistance factors for successful radiotherapy, such as tumor hypoxia, cannot be linked to a specific signal transduction cascade or a defined genetic background, rendering personalized radiochemotherapeutic approaches very difficult. With the exception of immune checkpoint inhibitors targeting specific intercellular signaling moieties and their rapid integration into clinical radioimmunotherapy protocols within the last five years, the combined treatment modality of radiotherapy with molecularly defined targeting agents did not reach maturity.

Thus, the slow progress towards a clinically relevant combined treatment modality of ionizing radiation with inhibitors of metalloproteinases is not an exception and includes additional hurdles. The development of small molecular compounds targeting selected metalloproteinases with sufficient specificity has not been successful so far without inducing limiting toxicities on the clinical level. This might be further restricted by existing redundancies in between different metalloproteinases for relevant substrates and represents an intrinsic challenge even for therapeutic antibodies targeting

individual metalloproteinases with highest specificity. On the other hand, such inhibitory antibodies might be accompanied by reduced normal tissue toxicities. Recent advances e.g. with ADAM17-targeting antibodies demonstrate promising results on the preclinical level (see above) and are currently also probed in combination with radiotherapy.

Individual metalloproteinases have a plethora of different substrates thereby co-regulating multiple biological processes, hallmarks of cancer and thus putative intrinsic treatment-induced resistance mechanisms at the same time. Thereby inhibition of individual metalloproteinases might affect at the same time not only the composition of the extracellular matrix but also tumor growth, tumor angiogenesis and immune cell infiltration via reduced shedding of respective bioactive substrates, such as tumor growth and pro-angiogenic factors, chemo- and cytokines. Insofar our knowledge on the role and the complexity of metalloproteinases for tumorigenesis, tumor growth and dissemination is steadily increasing.

Interestingly, many of the aforementioned processes are also triggered by radiotherapy. The insult on the level of DNA is most important for the cytotoxicity of radiotherapy. However, ionizing radiation also affects multiple intra- and inter-cellular processes thereby determining the tumor response to radiotherapy and eventually treatment outcome. Irradiated tumor, stromal and endothelial cells release auto- and paracrine factors in response to radiotherapy-induced DNA damage and radiotherapy-activated intracellular stress-responses, which subsequently modulate the tumor microenvironment and the radiosensitivity of the respective target cells. We currently recognize that these intercellular processes are often mediated via basal and even more so ionizing radiation-induced metalloproteinase activities rendering metalloproteinases to become interesting targets in this context (**Figure 3**). Furthermore, the intratumoral bystander
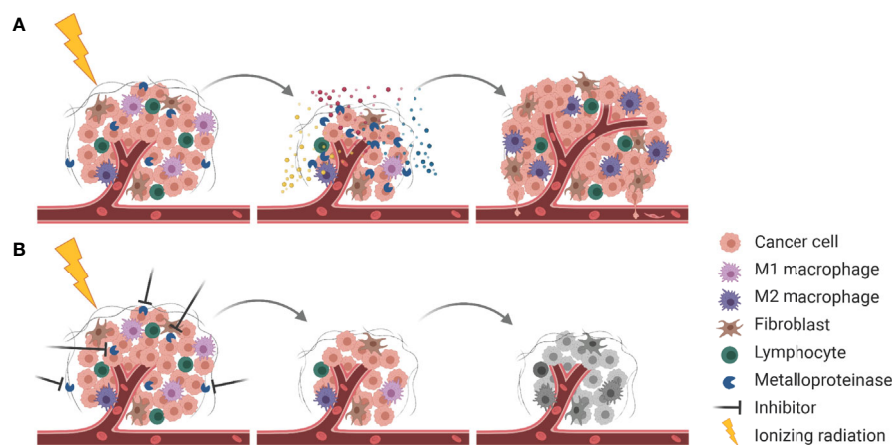

FIGURE 3 | Combining RT with metalloproteinase inhibitors for improved tumor control. **(A)** Next to cell killing and tumor shrinkage, RT activates metalloproteinases that release pro-survival factors (indicated in blue, red, and yellow) into the TME, resulting in tumor cell proliferation, enhanced tumor angiogenesis and pro-tumorigenic immune responses. At the same metalloproteinases disrupt the ECM barrier (gray), enabling tumor cell dissemination. **(B)** Combining RT with inhibition of metalloproteinases mitigates pro-survival signaling and results in more effective tumor cell killing.

effect induced by inhibition of extracellularly located metalloproteinase activities will conceptually also take advantage of and synergize with locoregionally applied ionizing radiation reaching each individual tumor cell. As such, targeting of specific metalloproteinases in combination with radiotherapy represents a highly promising treatment strategy; however, we still need to identify the best needle in the haystack.

AUTHOR CONTRIBUTIONS

VW performed literature search, drafted, and edited the manuscript. MP participated in conceptualization, revised, and finalized the manuscript. All authors contributed to the article and approved the submitted version.

REFERENCES

1. Grubbé EH. Priority in the Therapeutic Use of X-Rays. *Radiology* (1933) 21:156–62. doi: 10.1148/21.2.156
2. Gianfaldoni S, Gianfaldoni R, Wollina U, Lotti J, Tchernev G, Lotti T. An Overview on Radiotherapy: From Its History to Its Current Applications in Dermatology. *Open Access Maced J Med Sci* (2017) 5:521–5. doi: 10.3889/oamjms.2017.122
3. Lawrence EO, Livingston MS. The Production of High Speed Light Ions Without the Use of High Voltages. *Phys Rev* (1932) 40:19–35. doi: 10.1103/PhysRev.40.19
4. Connell PP, Hellman S. Advances in Radiotherapy and Implications for the Next Century: A Historical Perspective. *Cancer Res* (2009) 69:383–92. doi: 10.1158/0008-5472.CAN-07-6871
5. NCRI Clinical and Translational Radiotherapy Research Working Group, Harrington KJ, Billingham LJ, Brunner TB, Burnet NG, Chan CS, et al. Guidelines for Preclinical and Early Phase Clinical Assessment of Novel Radiosensitisers. *Br J Cancer* (2011) 105:628–39. doi: 10.1038/bjc.2011.240
6. Delaney G, Jacob S, Featherstone C, Barton M. The Role of Radiotherapy in Cancer Treatment: Estimating Optimal Utilization From a Review of Evidence-Based Clinical Guidelines. *Cancer* (2005) 104:1129–37. doi: 10.1002/cncr.21324
7. Elshaikh M, Ljungman M, Ten Haken R, Lichter AS. Advances in Radiation Oncology. *Annu Rev Med* (2006) 57:19–31. doi: 10.1146/annurev.med.57.121304.131431
8. Sato K, Shimokawa T, Imai T. Difference in Acquired Radioresistance Induction Between Repeated Photon and Particle Irradiation. *Front Oncol* (2019) 9:1213. doi: 10.3389/fonc.2019.01213
9. Willers H, Azzoli CG, Santivasi WL, Xia F. Basic Mechanisms of Therapeutic Resistance to Radiation and Chemotherapy in Lung Cancer. *Cancer J* (2013) 19:200–7. doi: 10.1097/PPO.0b013e318292e4e3
10. Barker HE, Paget JTE, Khan AA, Harrington KJ. The Tumour Microenvironment After Radiotherapy: Mechanisms of Resistance and Recurrence. *Nat Rev Cancer* (2015) 15:409–25. doi: 10.1038/nrc3958
11. Munshi A, Ramesh R. Mitogen-Activated Protein Kinases and Their Role in Radiation Response. *Genes Cancer* (2013) 4:401–8. doi: 10.1177/1947601913485414
12. Baskar R, Dai J, Wenlong N, Yeo R, Yeoh K-W. Biological Response of Cancer Cells to Radiation Treatment. *Front Mol Biosci* (2014) 1:24. doi: 10.3389/fmolb.2014.00024
13. Marampon F, Ciccarelli C, Zani BM. Biological Rationale for Targeting MEK/ERK Pathways in Anti-Cancer Therapy and to Potentiate Tumour Responses to Radiation. *Int J Mol Sci* (2019) 20:2530. doi: 10.3390/ijms20102530
14. Kim W, Youn H, Kang C, Youn B. Inflammation-Induced Radioresistance is Mediated by ROS-dependent Inactivation of Protein Phosphatase 1 in non-Small Cell Lung Cancer Cells. *Apoptosis* (2015) 20:1242–52. doi: 10.1007/s10495-015-1141-1

15. Kim HS, Song M-C, Kwak IH, Park TJ, Lim IK. Constitutive Induction of P-Erk1/2 Accompanied by Reduced Activities of Protein Phosphatases 1 and 2A and MKP3 Due to Reactive Oxygen Species During Cellular Senescence. *J Biol Chem* (2003) 278:37497–510. doi: 10.1074/jbc.M211739200
16. Sharma A, Bender S, Zimmermann M, Riesterer O, Broggini-Tenzer A, Pruschy MN. Secretome Signature Identifies ADAM17 as Novel Target for Radiosensitization of Non-Small Cell Lung Cancer. *Clin Cancer Res* (2016) 22:4428–39. doi: 10.1158/1078-0432.CCR-15-2449
17. Feys L, Descamps B, Vanhove C, Vral A, Veldeman L, Vermeulen S, et al. Radiation-Induced Lung Damage Promotes Breast Cancer Lung-Metastasis Through CXCR4 Signaling. *Oncotarget* (2015) 6:26615–32. doi: 10.18632/oncotarget.5666
18. Huxley-Jones J, Clarke T-K, Beck C, Toubaris G, Robertson DL, Boot-Handford RP. The Evolution of the Vertebrate Metzincins; Insights From Ciona Intestinalis and Danio Rerio. *BMC Evol Biol* (2007) 7:63. doi: 10.1186/1471-2148-7-63
19. Bode W, Gomis-Rüth F-X, Stöckler W. Astacins, Serralysins, Snake Venom and Matrix Metalloproteinases Exhibit Identical Zinc-Binding Environments (HEXXHXXGXXH and Met-turn) and Topologies and Should be Grouped Into a Common Family, the 'Metzincins'. *FEBS Lett* (1993) 331:134–40. doi: 10.1016/0014-5793(93)80312-I
20. Stöcker W, Bode W. Structural Features of a Superfamily of Zinc-Endopeptidases: The Metzincins. *Curr Opin Struct Biol* (1995) 5:383–90. doi: 10.1016/0959-440X(95)80101-4
21. Georgiadis D, Yiotakis A. Specific Targeting of Metzincin Family Members With Small-Molecule Inhibitors: Progress Toward a Multifarious Challenge. *Bioorg Med Chem* (2008) 16:8781–94. doi: 10.1016/j.bmc.2008.08.058
22. Seals DF. The ADAMs Family of Metalloproteases: Multidomain Proteins With Multiple Functions. *Genes Dev* (2003) 17:7–30. doi: 10.1101/gad.1039703
23. Cui N, Hu M, Khalil RA. Biochemical and Biological Attributes of Matrix Metalloproteinases. *Prog Mol Biol Transl Sci* (2017) 147:1–73. doi: 10.1016/bs.pmbts.2017.02.005
24. Van Wart HE, Birkedal-Hansen H. The Cysteine Switch: A Principle of Regulation of Metalloproteinase Activity With Potential Applicability to the Entire Matrix Metalloproteinase Gene Family. *Proc Natl Acad Sci* (1990) 87:5578–82. doi: 10.1073/pnas.87.14.5578
25. Ra H-J, Parks WC. Control of Matrix Metalloproteinase Catalytic Activity. *Matrix Biol* (2007) 26:587–96. doi: 10.1016/j.matbio.2007.07.001
26. Jackson HW, Defamie V, Waterhouse P, Khokha R. Timps: Versatile Extracellular Regulators in Cancer. *Nat Rev Cancer* (2017) 17:38–53. doi: 10.1038/nrc.2016.115
27. Nieuwesteeg MA, Willson JA, Cepeda M, Fox MA, Damjanovski S. Functional Characterization of Tissue Inhibitor of Metalloproteinase-1 (TIMP-1) N- and C-Terminal Domains During *Xenopus Laevis* Development. *Sci World J* (2014) 2014:1–10. doi: 10.1155/2014/467907
28. Bode W, Fernandez-Catalan C, Grams F, Gomis-Ruth F-X, Nagase H, Tschesche H, et al. Insights Into MMP-TIMP Interactions. *Ann N Y Acad Sci* (1999) 878:73–91. doi: 10.1111/j.1749-6632.1999.tb07675.x

29. Zucker S, Schmidt CE, Dufour A, Kaplan RC, Park HI, Jiang W. ProMMP-2:
TIMP-1 Complexes Identified in Plasma of Healthy Individuals. *Connect
Tissue Res* (2009) 50:223–31. doi: 10.1080/03008200802626970

30. Wojtowicz-Praga SM, Dickson RB, Hawkins MJ. Matrix Metalloproteinase
Inhibitors. *Invest New Drugs* (1997) 15:61–75. doi: 10.1023/A:1005722729132

31. Coussens LM. Matrix Metalloproteinase Inhibitors and Cancer–Trials and
Tribulations. *Science* (2002) 295:2387–92. doi: 10.1126/science.1067100

32. Mauviel A. Cytokine Regulation of Metalloproteinase Gene Expression.
J Cell Biochem (1993) 53:288–95. doi: 10.1002/jcb.240530404

33. McDonnell SE, Kerr LD, Matrisian LM. Epidermal Growth Factor
Stimulation of Stromelysin mRNA in Rat Fibroblasts Requires Induction
of Proto-Oncogenes C-Fos and C-Jun and Activation of Protein Kinase C.
Mol Cell Biol (1990) 10:4284–93. doi: 10.1128/mcb.10.8.4284

34. Lee M, Ryu CH, Chang HW, Kim GC, Kim SW, Kim SY. Radiotherapy-
Associated Furin Expression and Tumor Invasiveness in Recurrent Laryngeal
Cancer. *Anticancer Res* (2016) 36:5117–25. doi: 10.21873/anticanres.11081

35. Weiss S, Peppin G, Ortiz X, Ragsdale C, Test S. Oxidative Autoactivation of
Latent Collagenase by Human Neutrophils. *Science* (1985) 227:747–9.
doi: 10.1126/science.2982211

36. Yamamoto K, Murphy G, Troeberg L. Extracellular Regulation of
Metalloproteinases. *Matrix Biol* (2015) 44–46:255–63. doi: 10.1016/
j.matbio.2015.02.007

37. Webb AH, Gao BT, Goldsmith ZK, Irvine AS, Saleh N, Lee RP, et al.
Inhibition of MMP-2 and MMP-9 Decreases Cellular Migration, and
Angiogenesis in In Vitro Models of Retinoblastoma. *BMC Cancer* (2017)
17:434. doi: 10.1186/s12885-017-3418-y

38. Liu Y, Zhang H, Yan L, Du W, Zhang M, Chen H, et al. MMP-2 and MMP-9
Contribute to the Angiogenic Effect Produced by Hypoxia/15-HETE in
Pulmonary Endothelial Cells. *J Mol Cell Cardiol* (2018) 121:36–50.
doi: 10.1016/j.yjmcc.2018.06.006

39. Bruni-Cardoso A, Johnson LC, Vessella RL, Peterson TE, Lynch CC.
Osteoclast-Derived Matrix Metalloproteinase-9 Directly Affects
Angiogenesis in the Prostate Tumor-Bone Microenvironment. *Mol Cancer
Res* (2010) 8:459–70. doi: 10.1158/1541-7786.MCR-09-0445

40. Xu D, McKee CM, Cao Y, Ding Y, Kessler BM, Muschel RJ. Matrix
Metalloproteinase-9 Regulates Tumor Cell Invasion Through Cleavage of
Protease Nexin-1. *Cancer Res* (2010) 70:6988–98. doi: 10.1158/0008-
5472.CAN-10-0242

41. Mehner C, Hockla A, Miller E, Ran S, Radisky DC, Radisky ES. Tumor Cell-
Produced Matrix Metalloproteinase 9 (MMP-9) Drives Malignant
Progression and Metastasis of Basal-Like Triple Negative Breast Cancer.
Oncotarget (2014) 5:2736–49. doi: 10.18632/oncotarget.1932

42. Blanco-Prieto S, Barcia-Castro L, Páez de la Cadena M, Rodríguez-Berrocal
FJ, Vázquez-Iglesias L, Botana-Rial MI, et al. Relevance of Matrix
Metalloproteases in non-Small Cell Lung Cancer Diagnosis. *BMC Cancer*
(2017) 17:823. doi: 10.1186/s12885-017-3842-z

43. Li Y, Wu T, Zhang B, Yao Y, Yin G. Matrix Metalloproteinase-9 is a
Prognostic Marker for Patients With Cervical Cancer. *Med Oncol* (2012)
29:3394–9. doi: 10.1007/s12032-012-0283-z

44. Zhang H, Li G, Zhang Z, Wang S, Zhang S. MMP-2 and MMP-9 Gene
Polymorphisms Associated With Cervical Cancer Risk. *Int J Clin Exp Pathol*
(2017) 10:11760–5.

45. Tian M, Cui Y-Z, Song G-H, Zong M-J, Zhou X-Y, Chen Y, et al. Proteomic
Analysis Identifies MMP-9, DJ-1 and A1BG as Overexpressed Proteins in
Pancreatic Juice From Pancreatic Ductal Adenocarcinoma Patients. *BMC
Cancer* (2008) 8:241. doi: 10.1186/1471-2407-8-241

46. Wang J, Shi Q, Yuan T, Song Q, Zhang Y, Wei Q, et al. Matrix
Metalloproteinase 9 (MMP-9) in Osteosarcoma: Review and Meta-
Analysis. *Clin Chim Acta* (2014) 433:225–31. doi: 10.1016/j.cca.2014.03.023

47. Yousef EM, Tahir MR, St-Pierre Y, Gaboury LA. MMP-9 Expression Varies
According to Molecular Subtypes of Breast Cancer. *BMC Cancer* (2014)
14:609. doi: 10.1186/1471-2407-14-609

48. Chou CH, Teng C-M, Tzen K-Y, Chang Y-C, Chen J-H, Cheng JC-H. MMP-
9 From Sublethally Irradiated Tumor Promotes Lewis Lung Carcinoma Cell
Invasiveness and Pulmonary Metastasis. *Oncogene* (2012) 31:458–68.
doi: 10.1038/onc.2011.240

49. Gu Q, He Y, Ji J, Yao Y, Shen W, Luo J, et al. Hypoxia-Inducible Factor 1α
(Hif-1α) and Reactive Oxygen Species (ROS) Mediates Radiation-Induced

50. Cheng JC-H, Chou CH, Kuo ML, Hsieh C-Y. Radiation-Enhanced
Hepatocellular Carcinoma Cell Invasion With MMP-9 Expression
Through PI3K/Akt/NF-κB Signal Transduction Pathway. *Oncogene* (2006)
25:7009–18. doi: 10.1038/sj.onc.1209706

51. Ko Y, Jin H, Lee J, Park S, Chang K, Kang K, et al. Radioresistant Breast
Cancer Cells Exhibit Increased Resistance to Chemotherapy and Enhanced
Invasive Properties Due to Cancer Stem Cells. *Oncol Rep* (2018) 40:3752–
3762. doi: 10.3892/or.2018.6714

52. Ahn G-O, Brown JM. Matrix Metalloproteinase-9 is Required for Tumor
Vasculogenesis But Not for Angiogenesis: Role of Bone Marrow-Derived
Myelomonocytic Cells. *Cancer Cell* (2008) 13:193–205. doi: 10.1016/
j.ccr.2007.11.032

53. Kioi M, Vogel H, Schultz G, Hoffman RM, Harsh GR, Brown JM. Inhibition
of Vasculogenesis, But Not Angiogenesis, Prevents the Recurrence of
Glioblastoma After Irradiation in Mice. *J Clin Invest* (2010) 120:694–705.
doi: 10.1172/JCI40283

54. Brown JM. Vasculogenesis: A Crucial Player in the Resistance of Solid
Tumours to Radiotherapy. *Br J Radiol* (2014) 87:20130686. doi: 10.1259/
bjr.20130686

55. Ding G, Liu Y, Liang C. Efficacy of Radiotherapy on Intermediate and
Advanced Lung Cancer and its Effect on Dynamic Changes of Serum
Vascular Endothelial Growth Factor and Matrix Metalloproteinase–9.
Oncol Lett (2018) 16:219–224. doi: 10.3892/ol.2018.8622

56. Kalanxhi E, Hektoen HH, Meltzer S, Dueland S, Flatmark K, Ree AH.
Circulating Proteins in Response to Combined-Modality Therapy in Rectal
Cancer Identified by Antibody Array Screening. *BMC Cancer* (2016) 16:536.
doi: 10.1186/s12885-016-2601-x

57. Rieff EA, Hendriks T, Rutten HJT, Nieuwenhuijzen GAP, Gosens MJEM,
van den Brule AJC, et al. Neoadjuvant Radiochemotherapy Increases Matrix
Metalloproteinase Activity in Healthy Tissue in Esophageal Cancer Patients.
Ann Surg Oncol (2009) 16:1384–9. doi: 10.1245/s10434-009-0365-0

58. Xie T, Dong B, Yan Y, Hu G, Xu Y. Association Between MMP-2 Expression
and Prostate Cancer: A Meta-Analysis. *BioMed Rep* (2016) 4:241–5.
doi: 10.3892/br.2015.553

59. Deng J, Chen W, Du Y, Wang W, Zhang G, Tang Y, et al. Synergistic
Efficacy of Cullin1 and MMP-2 Expressions in Diagnosis and Prognosis of
Colorectal Cancer. *Cancer Biomark* (2017) 19:57–64. doi: 10.3233/CBM-
160341

60. Zhai L-L, Cai C-Y, Wu Y, Tang Z-G. Correlation and Prognostic
Significance of MMP-2 and TFPI-2 Differential Expression in Pancreatic
Carcinoma. *Int J Clin Exp Pathol* (2015) 8:682–91.

61. Nasr M, Ayyad SB, El-Lamie IKI, Mikhail MY. Expression of Matrix
Metalloproteinase-2 in Preinvasive and Invasive Carcinoma of the Uterine
Cervix. *Eur J Gynaecol Oncol* (2005) 26:199–202.

62. Fang J, Shing Y, Wiederschain D, Yan L, Butterfield C, Jackson G, et al.
Matrix Metalloproteinase-2 is Required for the Switch to the Angiogenic
Phenotype in a Tumor Model. *Proc Natl Acad Sci* (2000) 97:3884–9.
doi: 10.1073/pnas.97.8.3884

63. Kargiotis O, Chetty C, Gondi CS, Tsung AJ, Dinh DH, Gujrati M, et al.
Adenovirus-Mediated Transfer of siRNA Against MMP-2 mRNA Results in
Impaired Invasion and Tumor-Induced Angiogenesis, Induces Apoptosis In
Vitro and Inhibits Tumor Growth In Vivo in Glioblastoma. *Oncogene* (2008)
27:4830–40. doi: 10.1038/onc.2008.122

64. Kaliski A, Maggiorella L, Cengel KA, Mathe D, Rouffiac V, Opolon P, et al.
Angiogenesis and Tumor Growth Inhibition by a Matrix Metalloproteinase
Inhibitor Targeting Radiation-Induced Invasion. *Mol Cancer Ther* (2005)
4:1717–28. doi: 10.1158/1535-7163.MCT-05-0179

65. Belotti D, Paganoni P, Manenti L, Garofalo A, Marchini S, Taraboletti G,
et al. Matrix Metalloproteinases (MMP9 and MMP2) Induce the Release of
Vascular Endothelial Growth Factor (VEGF) by Ovarian Carcinoma Cells:
Implications for Ascites Formation. *Cancer Res* (2003) 63:5224–9.

66. Chetty C, Bhoopathi P, Rao JS, Lakka SS. Inhibition of Matrix
Metalloproteinase-2 Enhances Radiosensitivity by Abrogating Radiation-
Induced FoxM1-mediated G2/M Arrest in A549 Lung Cancer Cells. *Int J
Cancer* (2009) 124:2468–77. doi: 10.1002/ijc.24209

Invasiveness Through the SDF-1α/CXCR4 Pathway in non-Small Cell Lung
Carcinoma Cells. *Oncotarget* (2015) 6:10893–907. doi: 10.18632/
oncotarget.3535

67. Butkiewicz D, Krześniak M, Drosik A, Giglok M, Gdowicz-Kłosok A, Kosarewicz A, et al. The *VEGFR2* , *COX-2* and *MMP-2* Polymorphisms are Associated With Clinical Outcome of Patients With Inoperable non-Small Cell Lung Cancer: *VEGFR2*, *COX-2* and *MMP-2* Variants and NSCLC Prognosis. *Int J Cancer* (2015) 137:2332–42. doi: 10.1002/ijc.29605

68. Wild-Bode C, Weller M, Rimner A, Dichgans J, Wick W. Sublethal Irradiation Promotes Migration and Invasiveness of Glioma Cells: Implications for Radiotherapy of Human Glioblastoma. *Cancer Res* (2001) 61:2744–50.

69. Mehvar R, Gross ME, Kreamer RN. Pharmacokinetics of Atenolol Enantiomers in Humans and Rats. *J Pharm Sci* (1990) 79:881–5. doi: 10.1002/jps.2600791007

70. Li H, Qiu Z, Li F, Wang C. The Relationship Between MMP-2 and MMP-9 Expression Levels With Breast Cancer Incidence and Prognosis. *Oncol Lett* (2017) 14:5865–70. doi: 10.3892/ol.2017.6924

71. Kumar A, Collins HM, Scholefield JH, Watson SA. Increased type-IV Collagenase (MMP-2 and MMP-9) Activity Following Preoperative Radiotherapy in Rectal Cancer. *Br J Cancer* (2000) 82:960–5. doi: 10.1054/bjoc.1999.1025

72. Chan LW, Moses MA, Goley E, Sproull M, Muanza T, Coleman CN, et al. Urinary VEGF and MMP Levels As Predictive Markers of 1-Year Progression-Free Survival in Cancer Patients Treated With Radiation Therapy: A Longitudinal Study of Protein Kinetics Throughout Tumor Progression and Therapy. *J Clin Oncol* (2004) 22:499–506. doi: 10.1200/JCO.2004.07.022

73. Smith ER, Zurakowski D, Saad A, Scott RM, Moses MA. Urinary Biomarkers Predict Brain Tumor Presence and Response to Therapy. *Clin Cancer Res* (2008) 14:2378–86. doi: 10.1158/1078-0432.CCR-07-1253

74. Waas ET, Hendriks T, Lomme RMLM, Wobbes T. Plasma Levels of Matrix Metalloproteinase-2 and Tissue Inhibitor of Metalloproteinase-1 Correlate With Disease Stage and Survival in Colorectal Cancer Patients. *Dis Colon Rectum* (2005) 48:700–10. doi: 10.1007/s10350-004-0854-y

75. Sotomayor EA, Teicher BA, Schwartz GN, Holden SA, Menon K, Herman TS, et al. Minocycline in Combination With Chemotherapy or Radiation Therapy In Vitro and In Vivo. *Cancer Chemother Pharmacol* (1992) 30:377–84. doi: 10.1007/BF00689966

76. Stansborough RL, Al-Dasooqi N, Bateman EH, Bowen JM, Keefe DMK, Logan RM, et al. Matrix Metalloproteinase Expression is Altered in the Small and Large Intestine Following Fractionated Radiation In Vivo. *Support Care Cancer* (2018) 26:3873–82. doi: 10.1007/s00520-018-4255-5

77. Strup-Perrot C, Vozenin-Brotons M-C, Vandamme M, Benderitter M, Mathe D. Expression and Activation of MMP -2, -3, -9, -14 are Induced in Rat Colon After Abdominal X-Irradiation. *Scand J Gastroenterol* (2006) 41:60–70. doi: 10.1080/00365520510023963

78. Angenete E, Öresland T, Falk P, Breimer M, Hultborn R, Ivarsson M-L. Preoperative Radiotherapy and Extracellular Matrix Remodeling in Rectal Mucosa and Tumour Matrix Metalloproteinases and Plasminogen Components. *Acta Oncol* (2009) 48:1144–51. doi: 10.3109/02841860903150510

79. Angenete E, Langenskiöld M, Falk P, Ivarsson M-L. Matrix Metalloproteinases in Rectal Mucosa, Tumour and Plasma: Response After Preoperative Irradiation. *Int J Colorectal Dis* (2007) 22:667–74. doi: 10.1007/s00384-006-0225-3

80. Kumar A, Collins H, Van Tam J, Scholefield JH, Watson SA. Effect of Preoperative Radiotherapy on Matrilysin Gene Expression in Rectal Cancer. *Eur J Cancer* (2002) 38:505–10. doi: 10.1016/S0959-8049(01)00392-6

81. Zhang W, Li Y, Yang L, Zhou B, Chen K-L, Meng W-J, et al. Knockdown of MMP-7 Inhibits Cell Proliferation and Enhances Sensitivity to 5-Fluorouracil and X-ray Irradiation in Colon Cancer Cells. *Clin Exp Med* (2014) 14:99–106. doi: 10.1007/s10238-012-0212-7

82. Stene C, Polistena A, Gaber A, Nodin B, Ottochian B, Adawi D, et al. MMP7 Modulation by Short- and Long-term Radiotherapy in Patients With Rectal Cancer. *In Vivo* (2018) 32:133–8. doi: 10.21873/invivo.11215

83. Singh SS, Bhatt MLB, Kushwaha VS, Singh A, Kumar R, Gupta R, et al. Role of Matrix Metalloproteinase 13 Gene Expression in the Evaluation of Radiation Response in Oral Squamous Cell Carcinoma. *J Carcinog* (2017) 16:2. doi: 10.4103/jcar.JCar_5_16

84. Wang J, Li Y, Wang J, Li C, Yu K, Wang Q. Increased Expression of Matrix Metalloproteinase-13 in Glioma is Associated With Poor Overall Survival of Patients. *Med Oncol* (2012) 29:2432–7. doi: 10.1007/s12032-012-0181-4

85. Luukkaa M, Vihinen P, Kronqvist P, Vahlberg T, Pyrhönen S, Kähäri V-M, et al. Association Between High Collagenase-3 Expression Levels and Poor Prognosis in Patients With Head and Neck Cancer. *Head Neck* (2006) 28:225–34. doi: 10.1002/hed.20322

86. Quintero-Fabián S, Arreola R, Becerril-Villanueva E, Torres-Romero JC, Arana-Argáez V, Lara-Riegos J, et al. Role of Matrix Metalloproteinases in Angiogenesis and Cancer. *Front Oncol* (2019) 9:1370. doi: 10.3389/fonc.2019.01370

87. Seiki M. Membrane-Type 1 Matrix Metalloproteinase: A Key Enzyme for Tumor Invasion. *Cancer Lett* (2003) 194:1–11. doi: 10.1016/S0304-3835(02)00699-7

88. Liu G, Atteridge CL, Wang X, Lundgren AD, Wu JD. Cutting Edge: The Membrane Type Matrix Metalloproteinase MMP14 Mediates Constitutive Shedding of MHC Class I Chain-Related Molecule A Independent of A Disintegrin and Metalloproteinases. *J Immunol* (2010) 184:3346–50. doi: 10.4049/jimmunol.0903789

89. Thakur V, Bedogni B. The Membrane Tethered Matrix Metalloproteinase MT1-MMP At the Forefront of Melanoma Cell Invasion and Metastasis. *Pharmacol Res* (2016) 111:17–22. doi: 10.1016/j.phrs.2016.05.019

90. Tomari T, Koshikawa N, Uematsu T, Shinkawa T, Hoshino D, Egawa N, et al. High Throughput Analysis of Proteins Associating With a Proinvasive MT1-MMP in Human Malignant Melanoma A375 Cells. *Cancer Sci* (2009) 100:1284–90. doi: 10.1111/j.1349-7006.2009.01173.x

91. Kajita M, Itoh Y, Chiba T, Mori H, Okada A, Kinoh H, et al. Membrane-Type 1 Matrix Metalloproteinase Cleaves Cd44 and Promotes Cell Migration. *J Cell Biol* (2001) 153:893–904. doi: 10.1083/jcb.153.5.893

92. Paquette B, Therriault H, Desmarais G, Wagner R, Royer R, Bujold R. Radiation-Enhancement of MDA-MB-231 Breast Cancer Cell Invasion Prevented by a Cyclooxygenase-2 Inhibitor. *Br J Cancer* (2011) 105:534–41. doi: 10.1038/bjc.2011.260

93. Bouchard G, Therriault H, Geha S, Bujold R, Saucier C, Paquette B. Radiation-Induced Lung Metastasis Development is MT1-MMP-dependent in a Triple-Negative Breast Cancer Mouse Model. *Br J Cancer* (2017) 116:479–88. doi: 10.1038/bjc.2016.448

94. Ager EI, Kozin SV, Kirkpatrick ND, Seano G, Kodack DP, Askoxylakis V, et al. Blockade of MMP14 Activity in Murine Breast Carcinomas: Implications for Macrophages, Vessels, and Radiotherapy. *J Natl Cancer Inst* (2015) 107:djv017. doi: 10.1093/jnci/djv017

95. Mu D, Cambier S, Fjellbirkeland L, Baron JL, Munger JS, Kawakatsu H, et al. The Integrin αvβ8 Mediates Epithelial Homeostasis Through MT1-MMP–dependent Activation of TGF-β1. *J Cell Biol* (2002) 157:493–507. doi: 10.1083/jcb.200109100

96. Gray LH, Conger AD, Ebert M, Hornsey S, Scott OCA. The Concentration of Oxygen Dissolved in Tissues At the Time of Irradiation as a Factor in Radiotherapy. *Br J Radiol* (1953) 26:638–48. doi: 10.1259/0007-1285-26-312-638

97. Thakur V, Zhang K, Savadelis A, Zmina P, Aguila B, Welford SM, et al. The Membrane Tethered Matrix Metalloproteinase MT1-MMP Triggers an Outside-in DNA Damage Response That Impacts Chemo- and Radiotherapy Responses of Breast Cancer. *Cancer Lett* (2019) 443:115–24. doi: 10.1016/j.canlet.2018.11.031

98. Furmanova-Hollenstein P, Broggini-Tenzer A, Eggel M, Millard A-L, Pruschy M. The Microtubule Stabilizer Patupilone Counteracts Ionizing Radiation-Induced Matrix Metalloproteinase Activity and Tumor Cell Invasion. *Radiat Oncol Lond Engl* (2013) 8:105. doi: 10.1186/1748-717X-8-105

99. Giaccone G. EGFR Point Mutation Confers Resistance to Gefitinib in a Patient With non-Small-Cell Lung Cancer. *Nat Clin Pract Oncol* (2005) 2:296–7. doi: 10.1038/ncponc0200

100. Bonner JA, Harari PM, Giralt J, Azarnia N, Shin DM, Cohen RB, et al. Radiotherapy Plus Cetuximab for Squamous-Cell Carcinoma of the Head and Neck. *N Engl J Med* (2006) 354:567–78. doi: 10.1056/NEJMoa053422

101. Bradley JD, Paulus R, Komaki R, Masters G, Blumenschein G, Schild S, et al. Standard-Dose Versus High-Dose Conformal Radiotherapy With Concurrent and Consolidation Carboplatin Plus Paclitaxel With or Without Cetuximab for Patients With Stage IIIA or IIIB non-Small-Cell Lung Cancer (RTOG 0617): A Randomised, Two-by-Two Factorial Phase 3 Study. *Lancet Oncol* (2015) 16:187–99. doi: 10.1016/S1470-2045(14)71207-0

102. Mochizuki S, Okada Y. Adams in Cancer Cell Proliferation and Progression. *Cancer Sci* (2007) 98:621–8. doi: 10.1111/j.1349-7006.2007.00434.x

103. Kataoka H. EGFR Ligands and Their Signaling Scissors, ADAMs, as New Molecular Targets for Anticancer Treatments. *J Dermatol Sci* (2009) 56:148–53. doi: 10.1016/j.jdermsci.2009.10.002

104. Chang L, Graham P, Hao J, Ni J, Deng J, Bucci J, et al. Cancer Stem Cells and Signaling Pathways in Radioresistance. *Oncotarget* (2016) 7:11002–17. doi: 10.18632/oncotarget.6760

105. Hong SW, Hur W, Choi JE, Kim J-H, Hwang D, Yoon SK. Role of ADAM17 in Invasion and Migration of CD133-expressing Liver Cancer Stem Cells After Irradiation. *Oncotarget* (2016) 7:23482–97. doi: 10.18632/oncotarget.8112

106. Mueller AC, Piper M, Goodspeed A, Bhuvane S, Williams JS, Bhatia S, et al. Induction of ADAM10 by RT Drives Fibrosis, Resistance, and EMT in Pancreatic Cancer. *Cancer Res* (2021), canres.CAN–20-3892-A.2020. doi: 10.1158/0008-5472.CAN-20-3892

107. Kabacik S, Raj K. Ionising Radiation Increases Permeability of Endothelium Through ADAM10-mediated Cleavage of VE-Cadherin. *Oncotarget* (2017) 8:82049–63. doi: 10.18632/oncotarget.18282

108. Kouam PN, Rezniczek GA, Adamietz IA, Bühler H. Ionizing Radiation Increases the Endothelial Permeability and the Transendothelial Migration of Tumor Cells Through ADAM10-activation and Subsequent Degradation of VE-Cadherin. *BMC Cancer* (2019) 19:958. doi: 10.1186/s12885-019-6219-7

109. Kim D, Lee M, Kim E. Involvement of Klotho, TNF-α and ADAMs in Radiation–Induced Senescence of Renal Epithelial Cells. *Mol Med Rep* (2020) 23:1–1. doi: 10.3892/mmr.2020.11660

110. Masoud GN, Li W. HIF-1α Pathway: Role, Regulation and Intervention for Cancer Therapy. *Acta Pharm Sin B* (2015) 5:378–89. doi: 10.1016/j.apsb.2015.05.007

111. Choi JY, Jang YS, Min SY, Song JY. Overexpression of MMP-9 and HIF-1α in Breast Cancer Cells Under Hypoxic Conditions. *J Breast Cancer* (2011) 14:88. doi: 10.4048/jbc.2011.14.2.88

112. Shan Y, You B, Shi S, Shi W, Zhang Z, Zhang Q, et al. Hypoxia-Induced Matrix Metalloproteinase-13 Expression in Exosomes From Nasopharyngeal Carcinoma Enhances Metastases. *Cell Death Dis* (2018) 9:382. doi: 10.1038/s41419-018-0425-0

113. Shin DH, Dier U, Melendez JA, Hempel N. Regulation of MMP-1 Expression in Response to Hypoxia is Dependent on the Intracellular Redox Status of Metastatic Bladder Cancer Cells. *Biochim Biophys Acta* (2015) 1852:2593–602. doi: 10.1016/j.bbadis.2015.09.001

114. Chen J-Y, Lin C-H, Chen B-C. Hypoxia-Induced ADAM 17 Expression is Mediated by RSK1-dependent C/EBPβ Activation in Human Lung Fibroblasts. *Mol Immunol* (2017) 88:155–63. doi: 10.1016/j.molimm.2017.06.029

115. Noda K, Ishida S, Shinoda H, Koto T, Aoki T, Tsubota K, et al. Hypoxia Induces the Expression of Membrane-Type 1 Matrix Metalloproteinase in Retinal Glial Cells. *Invest Ophthalmol Vis Sci* (2005) 46:3817. doi: 10.1167/iovs.04-1528

116. Barsoum IB, Hamilton TK, Li X, Cotechini T, Miles EA, Siemens DR, et al. Hypoxia Induces Escape From Innate Immunity in Cancer Cells Via Increased Expression of ADAM10: Role of Nitric Oxide. *Cancer Res* (2011) 71:7433–41. doi: 10.1158/0008-5472.CAN-11-2104

117. Charbonneau M, Harper K, Grondin F, Pelmus M, McDonald PP, Dubois CM. Hypoxia-Inducible Factor Mediates Hypoxic and Tumor Necrosis Factor α-Induced Increases in Tumor Necrosis Factor-α Converting Enzyme/Adam17 Expression by Synovial Cells. *J Biol Chem* (2007) 282:33714–24. doi: 10.1074/jbc.M704041200

118. Pastorekova S, Gillies RJ. The Role of Carbonic Anhydrase IX in Cancer Development: Links to Hypoxia, Acidosis, and Beyond. *Cancer Metastasis Rev* (2019) 38:65–77. doi: 10.1007/s10555-019-09799-0

119. Zatovicova M, Sedlakova O, Svastova E, Ohradanova A, Ciampor F, Arribas J, et al. Ectodomain Shedding of the Hypoxia-Induced Carbonic Anhydrase IX is a Metalloprotease-Dependent Process Regulated by TACE/ADAM17. *Br J Cancer* (2005) 93:1267–76. doi: 10.1038/sj.bjc.6602861

120. Kajanova I, Zatovicova M, Jelenska L, Sedlakova O, Barathova M, Csaderova L, et al. Impairment of Carbonic Anhydrase IX Ectodomain Cleavage Reinforces Tumorigenic and Metastatic Phenotype of Cancer Cells. *Br J Cancer* (2020) 122:1590–603. doi: 10.1038/s41416-020-0804-z

121. Lambrecht BN, Vanderkerken M, Hammad H. The Emerging Role of ADAM Metalloproteinases in Immunity. *Nat Rev Immunol* (2018) 18:745–58. doi: 10.1038/s41577-018-0068-5

122. Romee R, Lenvik T, Wang Y, Walcheck B, Verneris MR, Miller JS. ADAM17, a Novel Metalloproteinase, Mediates CD16 and CD62L Shedding in Human Nk Cells and Modulates IFNγ Responses. *Blood* (2011) 118:2184–4. doi: 10.1182/blood.V118.21.2184.2184

123. Lajoie L, Congy-Jolivet N, Bolzec A, Gouilleux-Gruart V, Sicard E, Sung HC, et al. ADAM17-Mediated Shedding of FcγRIIIA on Human NK Cells: Identification of the Cleavage Site and Relationship With Activation. *J Immunol* (2014) 192:741–51. doi: 10.4049/jimmunol.1301024

124. Wu J, Mishra HK, Walcheck B. Role of ADAM17 as a Regulatory Checkpoint of CD16A in NK Cells and as a Potential Target for Cancer Immunotherapy. *J Leukoc Biol* (2019) 105:1297–303. doi: 10.1002/JLB.2MR1218-501R

125. Waldhauer I, Goehlsdorf D, Gieseke F, Weinschenk T, Wittenbrink M, Ludwig A, et al. Tumor-Associated MICA is Shed by ADAM Proteases. *Cancer Res* (2008) 68:6368–76. doi: 10.1158/0008-5472.CAN-07-6768

126. Boutet P, Agüera-González S, Atkinson S, Pennington CJ, Edwards DR, Murphy G, et al. Cutting Edge: The Metalloproteinase ADAM17/TNF-alpha-converting Enzyme Regulates Proteolytic Shedding of the MHC Class I-related Chain B Protein. *J Immunol Baltim Md 1950* (2009) 182:49–53. doi: 10.4049/jimmunol.182.1.49

127. Mohammed RN, Wehenkel SC, Galkina EV, Yates E-K, Preece G, Newman A, et al. ADAM17-Dependent Proteolysis of L-selectin Promotes Early Clonal Expansion of Cytotoxic T Cells. *Sci Rep* (2019) 9:5487. doi: 10.1038/s41598-019-41811-z

128. Orme JJ, Jazieh KA, Xie T, Harrington S, Liu X, Ball M, et al. ADAM10 and ADAM17 Cleave PD-L1 to Mediate PD-(L)1 Inhibitor Resistance. *Oncoimmunology* (2020) 9:1744980. doi: 10.1080/2162402X.2020.1744980

129. Romero Y, Wise R, Zolkiewska A. Proteolytic Processing of PD-L1 by ADAM Proteases in Breast Cancer Cells. *Cancer Immunol Immunother* (2020) 69:43–55. doi: 10.1007/s00262-019-02437-2

130. Sørensen BS, Horsman MR. Tumor Hypoxia: Impact on Radiation Therapy and Molecular Pathways. *Front Oncol* (2020) 10:562. doi: 10.3389/fonc.2020.00562

131. Colliez F, Gallez B, Jordan BF. Assessing Tumor Oxygenation for Predicting Outcome in Radiation Oncology: A Review of Studies Correlating Tumor Hypoxic Status and Outcome in the Preclinical and Clinical Settings. *Front Oncol* (2017) 7:10. doi: 10.3389/fonc.2017.00010

132. Noman MZ, Hasmim M, Messai Y, Terry S, Kieda C, Janji B, et al. Hypoxia: A Key Player in Antitumor Immune Response. A Review in the Theme: Cellular Responses to Hypoxia. *Am J Physiol Cell Physiol* (2015) 309:C569–79. doi: 10.1152/ajpcell.00207.2015

133. Eckert F, Zwirner K, Boeke S, Thorwarth D, Zips D, Huber SM. Rationale for Combining Radiotherapy and Immune Checkpoint Inhibition for Patients With Hypoxic Tumors. *Front Immunol* (2019) 10:407. doi: 10.3389/fimmu.2019.00407

134. Whittaker M, Floyd CD, Brown P, Gearing AJH. Design and Therapeutic Application of Matrix Metalloproteinase Inhibitors. *Chem Rev* (1999) 99:2735–76. doi: 10.1021/cr9804543

135. Rothenberg ML, Nelson AR, Hande KR. New Drugs on the Horizon: Matrix Metalloproteinase Inhibitors. *Stem Cells* (1999) 17:237–40. doi: 10.1002/stem.170237

136. Egeblad M, Werb Z. New Functions for the Matrix Metalloproteinases in Cancer Progression. *Nat Rev Cancer* (2002) 2:161–74. doi: 10.1038/nrc745

137. Fields GB. The Rebirth of Matrix Metalloproteinase Inhibitors: Moving Beyond the Dogma. *Cells* (2019) 8:984. doi: 10.3390/cells8090984

138. Jacobsen JA, Major Jourden JL, Miller MT, Cohen SM. To Bind Zinc or Not to Bind Zinc: An Examination of Innovative Approaches to Improved Metalloproteinase Inhibition. *Biochim Biophys Acta BBA - Mol Cell Res* (2010) 1803:72–94. doi: 10.1016/j.bbamcr.2009.08.006

139. Bissett D, O'Byrne KJ, von Pawel J, Gatzemeier U, Price A, Nicolson M, et al. Phase III Study of Matrix Metalloproteinase Inhibitor Prinomastat in Non–Small-Cell Lung Cancer. *J Clin Oncol* (2005) 23:842–9. doi: 10.1200/JCO.2005.03.170

140. Shu C, Zhou H, Afsharvand M, Duan L, Zhang H, Noveck R, et al. Pharmacokinetic-Pharmacodynamic Modeling of Apratastat: A Population-Based Approach. *J Clin Pharmacol* (2011) 51:472–81. doi: 10.1177/0091270010372389

141. Moss ML, Minond D. Recent Advances in ADAM17 Research: A Promising Target for Cancer and Inflammation. *Mediators Inflamm* (2017) 2017:1–21. doi: 10.1155/2017/9673537

142. Zhou B-BS, Peyton M, He B, Liu C, Girard L, Caudler E, et al. Targeting ADAM-mediated Ligand Cleavage to Inhibit HER3 and EGFR Pathways in non-Small Cell Lung Cancer. *Cancer Cell* (2006) 10:39–50. doi: 10.1016/j.ccr.2006.05.024

143. Fridman JS, Caulder E, Hansbury M, Liu X, Yang G, Wang Q, et al. Selective Inhibition of ADAM Metalloproteases as a Novel Approach for Modulating ErbB Pathways in Cancer. *Clin Cancer Res* (2007) 13:1892–902. doi: 10.1158/1078-0432.CCR-06-2116

144. Witters L, Scherle P, Friedman S, Fridman J, Caulder E, Newton R, et al. Synergistic Inhibition With a Dual Epidermal Growth Factor Receptor/HER-2/neu Tyrosine Kinase Inhibitor and a Disintegrin and Metalloprotease Inhibitor. *Cancer Res* (2008) 68:7083–9. doi: 10.1158/0008-5472.CAN-08-0739

145. Newton RC, Bradley EC, Levy RS, Doval D, Bondarde S, Sahoo TP, et al. Clinical Benefit of INCB7839, a Potent and Selective ADAM Inhibitor, in Combination With Trastuzumab in Patients With Metastatic HER2+ Breast Cancer. *J Clin Oncol* (2010) 28:3025–5. doi: 10.1200/jco.2010.28.15_suppl.3025

146. Feldinger K, Generali D, Kramer-Marek G, Gijsen M, Ng TB, Wong JH, et al. ADAM10 Mediates Trastuzumab Resistance and is Correlated With Survival in HER2 Positive Breast Cancer. *Oncotarget* (2014) 5:6633–46. doi: 10.18632/oncotarget.1955

147. Van Schaeybroeck S, Karaiskou-McCaul A, Kelly D, Longley D, Galligan L, Van Cutsem E, et al. Epidermal Growth Factor Receptor Activity Determines Response of Colorectal Cancer Cells to Gefitinib Alone and in Combination With Chemotherapy. *Clin Cancer Res* (2005) 11:7480–9. doi: 10.1158/1078-0432.CCR-05-0328

148. Kyula JN, Van Schaeybroeck S, Doherty J, Fenning CS, Longley DB, Johnston PG. Chemotherapy-Induced Activation of ADAM-17: A Novel Mechanism of Drug Resistance in Colorectal Cancer. *Clin Cancer Res* (2010) 16:3378–89. doi: 10.1158/1078-0432.CCR-10-0014

149. Wolpert F, Tritschler I, Steinle A, Weller M, Eisele G. A Disintegrin and Metalloproteinases 10 and 17 Modulate the Immunogenicity of Glioblastoma-Initiating Cells. *Neuro Oncol* (2014) 16:382–91. doi: 10.1093/neuonc/not232

150. Gingras D, Boivin D, Deckers C, Gendron S, Barthomeuf C, Béliveau R. Neovastat–a Novel Antiangiogenic Drug for Cancer Therapy. *Anticancer Drugs* (2003) 14:91–6. doi: 10.1097/00001813-200302000-00001

151. Dupont E, Falardeau P, Mousa SA, Dimitriadou V, Pepin M-C, Wang T, et al. Antiangiogenic and Antimetastatic Properties of Neovastat (AE-941), an Orally Active Extract Derived From Cartilage Tissue. *Clin Exp Metastasis* (2002) 19:145–53. doi: 10.1023/a:1014546909573

152. Lu C, Lee JJ, Komaki R, Herbst RS, Feng L, Evans WK, et al. Chemoradiotherapy With or Without AE-941 in Stage III Non-Small Cell Lung Cancer: A Randomized Phase III Trial. *J Natl Cancer Inst* (2010) 102:859–65. doi: 10.1093/jnci/djq179

153. Golub LM, Ciancio S, Ramamurthy NS, Leung M, McNamara TF. Low-Dose Doxycycline Therapy: Effect on Gingival and Crevicular Fluid Collagenase Activity in Humans. *J Periodontal Res* (1990) 25:321–30. doi: 10.1111/j.1600-0765.1990.tb00923.x

154. Fife RS, Sledge GW. Effects of Doxycycline on In Vitro Growth, Migration, and Gelatinase Activity of Breast Carcinoma Cells. *J Lab Clin Med* (1995) 125:407–11.

155. van den Bogert C, Dontje BH, Holtrop M, Melis TE, Romijn JC, van Dongen JW, et al. Arrest of the Proliferation of Renal and Prostate Carcinomas of Human Origin by Inhibition of Mitochondrial Protein Synthesis. *Cancer Res* (1986) 46:3283–9.

156. Fife RS, Rougraff BT, Proctor C, Sledge GW. Inhibition of Proliferation and Induction of Apoptosis by Doxycycline in Cultured Human Osteosarcoma Cells. *J Lab Clin Med* (1997) 130:530–4. doi: 10.1016/S0022-2143(97)90130-X

157. Yu Z, Leung MK, Ramamurthy NS, McNamara TF, Golub LM. HPLC Determination of a Chemically Modified Nonantimicrobial Tetracycline: Biological Implications. *Biochem Med Metab Biol* (1992) 47:10–20. doi: 10.1016/0885-4505(92)90003-H

158. Hidalgo M, Eckhardt SG. Development of Matrix Metalloproteinase Inhibitors in Cancer Therapy. *J Natl Cancer Inst* (2001) 93:178–93. doi: 10.1093/jnci/93.3.178

159. Acharya MR, Venitz J, Figg WD, Sparreboom A. Chemically Modified Tetracyclines as Inhibitors of Matrix Metalloproteinases. *Drug Resist Updat* (2004) 7:195–208. doi: 10.1016/j.drup.2004.04.002

160. Syed S, Takimoto C, Hidalgo M, Rizzo J, Kuhn JG, Hammond LA, et al. A Phase I and Pharmacokinetic Study of Col-3 (Metastat), an Oral Tetracycline Derivative With Potent Matrix Metalloproteinase and Antitumor Properties. *Clin Cancer Res* (2004) 10:6512–21. doi: 10.1158/1078-0432.CCR-04-0804

161. Cianfrocca M, Cooley TP, Lee JY, Rudek MA, Scadden DT, Ratner L, et al. Matrix Metalloproteinase Inhibitor COL-3 in the Treatment of AIDS-Related Kaposi's Sarcoma: A Phase I AIDS Malignancy Consortium Study. *J Clin Oncol* (2002) 20:153–9. doi: 10.1200/JCO.2002.20.1.153

162. Rudek MA, Figg WD, Dyer V, Dahut W, Turner ML, Steinberg SM, et al. Phase I Clinical Trial of Oral COL-3, a Matrix Metalloproteinase Inhibitor, in Patients With Refractory Metastatic Cancer. *J Clin Oncol* (2001) 19:584–92. doi: 10.1200/JCO.2001.19.2.584

163. Rudek MA, New P, Mikkelsen T, Phuphanich S, Alavi JB, Nabors LB, et al. Phase I and Pharmacokinetic Study of COL-3 in Patients With Recurrent High-Grade Gliomas. *J Neurooncol* (2011) 105:375–81. doi: 10.1007/s11060-011-0602-9

164. Golub LM, Sorsa T, Lee HM, Ciancio S, Sorbi D, Ramamurthy NS, et al. Doxycycline Inhibits Neutrophil (PMN)-Type Matrix Metalloproteinases in Human Adult Periodontitis Gingiva. *J Clin Periodontol* (1995) 22:100–9. doi: 10.1111/j.1600-051x.1995.tb00120.x

165. Periostat (Doxycycline 20mg). *Br Dent J* (2006) 200:115–5. doi: 10.1038/sj.bdj.4813235

166. Overall CM, Kleifeld O. Validating Matrix Metalloproteinases as Drug Targets and Anti-Targets for Cancer Therapy. *Nat Rev Cancer* (2006) 6:227–39. doi: 10.1038/nrc1821

167. Overall CM, López-Otín C. Strategies for MMP Inhibition in Cancer: Innovations for the Post-Trial Era. *Nat Rev Cancer* (2002) 2:657–72. doi: 10.1038/nrc884

168. Marshall DC, Lyman SK, McCauley S, Kovalenko M, Spangler R, Liu C, et al. Selective Allosteric Inhibition of MMP9 is Efficacious in Preclinical Models of Ulcerative Colitis and Colorectal Cancer. *PloS One* (2015) 10:e0127063. doi: 10.1371/journal.pone.0127063

169. Botkjaer KA, Kwok HF, Terp MG, Karatt-Vellatt A, Santamaria S, McCafferty J, et al. Development of a Specific Affinity-Matured Exosite Inhibitor to MT1-MMP That Efficiently Inhibits Tumor Cell Invasion *In Vitro* and Metastasis *In Vivo*. *Oncotarget* (2016) 7:16773–92. doi: 10.18632/oncotarget.7780

170. Yang Z, Chan KI, Kwok HF, Tam KY. Novel Therapeutic Anti-ADAM17 Antibody A9(B8) Enhances EGFR-TKI–Mediated Anticancer Activity in NSCLC. *Transl Oncol* (2019) 12:1516–24. doi: 10.1016/j.tranon.2019.08.003

171. Tape CJ, Willems SH, Dombernowsky SL, Stanley PL, Fogarasi M, Ouwehand W, et al. Cross-Domain Inhibition of TACE Ectodomain. *Proc Natl Acad Sci* (2011) 108:5578–83. doi: 10.1073/pnas.1017067108

172. Lopez T, Nam DH, Kaihara E, Mustafa Z, Ge X. Identification of Highly Selective MMP-14 Inhibitory Fabs by Deep Sequencing: Protease Inhibitory mAbs Discovered by Deep Sequencing. *Biotechnol Bioeng* (2017) 114:1140–50. doi: 10.1002/bit.26248

173. Nam DH, Fang K, Rodriguez C, Lopez T, Ge X. Generation of Inhibitory Monoclonal Antibodies Targeting Matrix metalloproteinase-14 by Motif Grafting and CDR Optimization. *Protein Eng Des Sel* (2017) 30:113–8. doi: 10.1093/protein/gzw070

174. Rios-Doria J, Sabol D, Chesebrough J, Stewart D, Xu L, Tammali R, et al. A Monoclonal Antibody to ADAM17 Inhibits Tumor Growth by Inhibiting EGFR and Non–EGFR-Mediated Pathways. *Mol Cancer Ther* (2015) 14:1637–49. doi: 10.1158/1535-7163.MCT-14-1040

175. Fischer T, Riedl R. Inhibitory Antibodies Designed for Matrix Metalloproteinase Modulation. *Molecules* (2019) 24:2265. doi: 10.3390/molecules24122265

176. Devy L, Huang L, Naa L, Yanamandra N, Pieters H, Frans N, et al. Selective Inhibition of Matrix Metalloproteinase-14 Blocks Tumor Growth, Invasion, and Angiogenesis. *Cancer Res* (2009) 69:1517–26. doi: 10.1158/0008-5472.CAN-08-3255

177. Remacle AG, Cieplak P, Nam DH, Shiryaev SA, Ge X, Strongin AY. Selective Function-Blocking Monoclonal Human Antibody Highlights the Important

Role of Membrane Type-1 Matrix Metalloproteinase (MT1-MMP) in Metastasis. *Oncotarget* (2017) 8:2781–99. doi: 10.18632/oncotarget.13157

178. Kaimal R, Aljumaily R, Tressel SL, Pradhan RV, Covic L, Kuliopulos A, et al. Selective Blockade of Matrix Metalloprotease-14 With a Monoclonal Antibody Abrogates Invasion, Angiogenesis, and Tumor Growth in Ovarian Cancer. *Cancer Res* (2013) 73:2457–67. doi: 10.1158/0008-5472.CAN-12-1426

179. Paemen L, Martens E, Masure S, Opdenakker G. Monoclonal Antibodies Specific for Natural Human Neutrophil Gelatinase B Used for Affinity Purification, Quantitation by Two-Site ELISA and Inhibition of Enzymatic Activity. *Eur J Biochem* (1995) 234:759–65. doi: 10.1111/j.1432-1033.1995.759_a.x

180. Martens E, Leyssen A, Van Aelst I, Fiten P, Piccard H, Hu J, et al. A Monoclonal Antibody Inhibits Gelatinase B/MMP-9 by Selective Binding to Part of the Catalytic Domain and Not to the Fibronectin or Zinc Binding Domains. *Biochim Biophys Acta BBA - Gen Subj* (2007) 1770:178–86. doi: 10.1016/j.bbagen.2006.10.012

181. Love EA, Sattikar A, Cook H, Gillen K, Large JM, Patel S, et al. Developing an Antibody–Drug Conjugate Approach to Selective Inhibition of an Extracellular Protein. *ChemBioChem* (2019) 20:754–8. doi: 10.1002/cbic.201800623

182. Shah MA, Metges J-P, Cunningham D, Shiu K-K, Wyrwicz L, Thai D, et al. A Phase II, Open-Label, Randomized Study to Evaluate the Efficacy and Safety of Andecaliximab Combined With Nivolumab Versus Nivolumab Alone in Subjects With Unresectable or Recurrent Gastric or Gastroesophageal Junction Adenocarcinoma. *J Clin Oncol* (2019) 37:75–5. doi: 10.1200/JCO.2019.37.4_suppl.75

183. Bendell JC, Starodub A, Huang X, Maltzman JD, Wainberg ZA, Shah MA. A Phase 3 Randomized, Double-Blind, Placebo-Controlled Study to Evaluate the Efficacy and Safety of GS-5745 Combined With mFOLFOX6 as First-Line Treatment in Patients With Advanced Gastric or Gastroesophageal Junction Adenocarcinoma. *J Clin Oncol* (2017) 35:TPS4139–TPS4139. doi: 10.1200/JCO.2017.35.15_suppl.TPS4139

184. Shah MA, Starodub A, Sharma S, Berlin J, Patel M, Wainberg ZA, et al. Andecaliximab/GS-5745 Alone and Combined With mFOLFOX6 in Advanced Gastric and Gastroesophageal Junction Adenocarcinoma: Results From a Phase I Study. *Clin Cancer Res* (2018) 24:3829–37. doi: 10.1158/1078-0432.CCR-17-2469

185. Richards FM, Tape CJ, Jodrell DI, Murphy G. Anti-Tumour Effects of a Specific Anti-ADAM17 Antibody in an Ovarian Cancer Model In Vivo. *PloS One* (2012) 7:e40597. doi: 10.1371/journal.pone.0040597

186. Caiazza F, McGowan PM, Mullooly M, Murray A, Synnott N, O'Donovan N, et al. Targeting ADAM-17 With an Inhibitory Monoclonal Antibody has Antitumour Effects in Triple-Negative Breast Cancer Cells. *Br J Cancer* (2015) 112:1895–903. doi: 10.1038/bjc.2015.163

187. Huang Y, Benaich N, Tape C, Kwok HF, Murphy G. Targeting the Sheddase Activity of ADAM17 by an Anti-ADAM17 Antibody D1(A12) Inhibits Head and Neck Squamous Cell Carcinoma Cell Proliferation and Motility Via Blockage of Bradykinin Induced HERs Transactivation. *Int J Biol Sci* (2014) 10:702–14. doi: 10.7150/ijbs.9326

188. Peng L, Cook K, Xu L, Cheng L, Damschroder M, Gao C, et al. Molecular Basis for the Mechanism of Action of an anti-TACE Antibody. *mAbs* (2016) 8:1598–605. doi: 10.1080/19420862.2016.1226716

189. Mishra HK, Pore N, Michelotti EF, Walcheck B. Anti-ADAM17 Monoclonal Antibody MEDI3622 Increases IFNγ Production by Human NK Cells in the Presence of Antibody-Bound Tumor Cells. *Cancer Immunol Immunother* (2018) 67:1407–16. doi: 10.1007/s00262-018-2193-1

frontiers
in Oncology

Exploiting Radiation Therapy to Restore Immune Reactivity of Glioblastoma

Mara De Martino[1], Oscar Padilla[2], Camille Daviaud[1], Cheng-Chia Wu[2,3], Robyn D. Gartrell[4] and Claire Vanpouille-Box[1,5]*

[1] Department of Radiation Oncology, Weill Cornell Medicine, New York, NY, United States, [2] Department of Radiation Oncology, Columbia University Irving Medical Center, New York, NY, United States, [3] Herbert Irving Comprehensive Cancer Center, New York, NY, United States, [4] Department of Pediatrics, Pediatric Hematology/Oncology/SCT, Columbia University Irving Medical Center, New York, NY, United States, [5] Sandra and Edward Meyer Cancer Center, New York, NY, United States

Glioblastoma (GBM) is among the most aggressive of brain tumors and confers a dismal prognosis despite advances in surgical technique, radiation delivery methods, chemotherapy, and tumor-treating fields. While immunotherapy (IT) has improved the care of several adult cancers with previously dismal prognoses, monotherapy with IT in GBM has shown minimal response in first recurrence. Recent discoveries in lymphatics and evaluation of blood brain barrier offer insight to improve the use of ITs and determine the best combinations of therapies, including radiation. We highlight important features of the tumor immune microenvironment in GBM and potential for combining radiation and immunotherapy to improve prognosis in this devastating disease.

Keywords: glioblastoma, radiotherapy, immunotherapy, antigenicity, adjuvanticity, immunosuppression

INTRODUCTION

Glioblastoma (GBM), a high-grade glial tumor, is the most frequent malignant primary brain tumor in adults (1). GBM prognosis remains dismal with a low 5-year survival rate of only 5.6% (1) and a median overall survival (OS) of approximately 18 months (2).

Immunotherapies (ITs) have long been overlooked for the treatment of central nervous system (CNS) malignancies presumably due to the long-held view of the brain as an immune-privileged compartment. However, the discovery of a dural lymphatic system (3, 4), the ability of some CNS-tissue resident cells to present antigen (5–9) and the functional characterization of the dural sinuses as an immune interface of the CNS (10) have introduced a paradigm shift whereby the brain possesses an immune-distinct tumor microenvironment (TME) that is still accessible for ITs (11–13). Since then, efforts have spurred in clinic to evaluate the efficacy of ITs in GBM (13), but the paucity of pre-existing T cells at diagnosis prevented the reactivation of anti-tumor immune responses (14–16). Notably, monotherapy with ITs have shown poor response rate in first GBM recurrence (17). In evaluation of responders to anti-PD1 monotherapy at first recurrence, patients are more likely to be Phosphatase and TENsin homolog (PTEN) wild type and have increased immune infiltration post anti-PD1 monotherapy compared to non-responders who are PTEN mutant and have low immune infiltrate both before and after IT (18). Consequently, it is critical to develop IT-based combinatorial approaches that both recruit and activate tumor-infiltrating lymphocytes (TILs).

Radiation therapy (RT) increases antigenicity and adjuvanticity of malignant cells (19), thus suggesting that RT could be used to coax T cells into GBM. Supporting this notion, several groups have reported synergism between RT and IT in preclinical models of GBM which have motivated the assessment of RT-based combinatorial approaches in Clinic (**Table 1**).

Here will we discuss the unique immune system of the central nervous system (CNS), the immunosuppressive TME of GBM and how RT can restore the sensitivity of GBM to modern IT by modulating systemic and local anti-tumor immunity.

THE UNIQUE IMMUNE SYSTEM OF THE CENTRAL NERVOUS SYSTEM

The traditional dogma of the brain as an immune-privileged organ was initiated by pioneer work from Murphy in the 1920s, demonstrating successful growth of mouse sarcoma after their implantation into the brain while rejection of these tumors was observed when transplanted in the periphery (20). Later on, these findings were confirmed with seminal work from Medawar, in the 1940s, which similarly demonstrate a high propensity of tumor engraftment in the brain parenchyma as opposed to tumor transplant in peripheral organs (21). Of notice, when first transplanted in peripheral organs before their implantation into the brain, these tumors were successfully rejected, thus suggesting that the activation of the immune system in the periphery can generate tumor rejection into the brain (21). Consequently, the fact that brains were unable to elicit anti-tumor immune responses by itself led to the concept of the immune privilege of the CNS.

Since then, studies have revealed that the immune privilege status of the CNS is overstated. Notably, the description of the afferent mechanism for CNS engagement in regional lymphatic (22–24) together with the discovery of the glymphatic (glial-lymphatic) system that links the parenchyma and the interstitium to the cerebrospinal fluid (CSF) spaces, started to challenge the concept of the brain as immunologically silenced.

Another breakthrough in the field of brain immunology was the identification of a functional meningeal lymphatic network that enables the drainage of immune cells, macromolecules and fluids from the CNS to the deep cervical lymph nodes (dcLN) (4, 25). This dural lymphatic system provides a physical connection for CSF-derived antigens to gain access to dcLN for priming and activation of T cells. Consequently, meningeal lymphatic vessels are critical regulators of drainage and immune surveillance, a notion that has been demonstrated in the context of GBM (26, 27). More recently, the dural sinuses were identified as a neuro-immune hub where circulating T cells can assess the brain and CSF-derived antigens to enable immune surveillance (10).

Given the complex lymphatic circuitry and the unique sites of neuro-interface of the CNS, the brain can no longer be perceived as an immune-privileged organ, but rather as an immune-distinct and highly immunosuppressive environment.

This concept is reinforced by the ongoing challenge of the efferent arm of CNS immunity. Indeed, the blood brain barrier (BBB), a structure composed of capillary tight junctions and astrocyte cell projections (aka astrocytic feet or "glia limitans") (28, 29), is thought to serve as a filter of the transit of molecules and immune cells between the brain and the systemic circulation. Some strategies to overcome the BBB have been explored, including the usage of nanoparticles, convection enhanced delivery, and non-invasive focused ultrasound and have achieved promising results in preclinical models (30–34). However, the recent demonstration of T cells infiltration and immune surveillance of the brain challenge the long-held view of BBB as an hermetic barrier to immune cell trafficking and suggest that the CNS is accessible to immune cells (35–37).

Aside distinct afferent and efferent circuits of CNS immunity, tissue-resident myeloid cells are another unique feature of brain immunity (38). This population is mainly composed of microglia (or tissue-resident macrophages) that originate from the yolk sac and migrate into the brain during embryonic development (39). The function of microglia is to assess the brain parenchyma and to maintain immunological homeostasis by responding to signals consistent with tissue damage, inflammation, or the presence of pathogens (40, 41). Such activation of the microglia leads to an increase capacity of antigen presenting functions as well as its phagocytic properties, suggesting that microglia serves as the resident antigen-presenting cells of the CNS (5, 9).

Thus, the unique features of the brain from its drainage to its tissue resident microglial cells (**Figure 1**) suggest that immune responses in the CNS are possible. However, the immune singularity of the brain calls for a better understanding of CNS immunity to optimally generate anti-tumor immunity against brain malignancies.

THE IMMUNE SUPPRESSIVE MICROENVIRONMENT OF GLIOBLASTOMA

A major obstacle to anti-tumor immune responses against GBM is its highly immunosuppressive TME (**Figure 1**).

Among key contributors to GBM immunosuppression, tumor-associated macrophages cells (TAMs) account for 30% to 50% of the tumor mass (42, 43). TAMs are usually pro-tumorigenic, and their accumulation correlate with tumor grade and poor prognosis (44–46). The recruitment and function of TAMs is modulated by GBM-secreted factors, such as the chemo-attractants stromal cell-derived factor 1 (SDF1) (47, 48), C–C motif chemokine ligand 2 (CCL2) (49, 50) and the colony-stimulation factor 1 (CSF1) (51). TAMs promote immunosuppression by the production of arginase, transforming growth factor-beta (TGFβ), interleukin (IL)-10 and IL-6, among others which collectively inhibit both the innate and adaptive immune systems with suppression of NK activity and T cell activation and proliferation (52–55).

Another mechanism responsible for immunosuppression and ultimately the lack of response of IT strategies in GBM patient is the low representation of T cells in the tumor. Studies have demonstrated that T cells influx in GBM is offset as a result of (1) reduced T cells production subsequent to thymic involution (56),

TABLE 1 | Combination of immunotherapy with radiation therapy in clinical development for glioblastoma.

| Target	Agent	New or Recurrent	Phase	Clinical Trial ID	Radiation regimen	Status	Notes
PD-1	Nivolumab	Newly diagnosed	III	NCT02617589	Standard fractionation	Active, not recruiting	Unmethylated MGMT; comparison anti-PD-1 versus TMZ each in combination with RT
PD-1	Nivolumab	Newly diagnosed	III	NCT02667587	Standard fractionation	Active, not recruiting	Methylated MGMT; TMZ plus RT combined with anti-PD-1
PD-1	Nivolumab	Newly diagnosed	I	NCT03576612	Standard fractionation	Recruiting	Neoadjuvant oncolytic adenovirus (GMCI) + TMZ
PD-1	Nivolumab	Recurrent	II	NCT03743662	Hypofractionated	Recruiting	Re-irradiation (6Gy x 5) +/- anti-PD-1 +/- Bevacizumab
PD-1	Nivolumab	Newly diagnosed	II	NCT04195139	Standard fractionation	Recruiting	Elderly patients; comparison RT+anti-PD-1 + TMZ versus standard treatment (RT+TMZ)
PD-1	Pembrolizumab	Newly diagnosed	II	NCT03018288	Standard fractionation	Recruiting	TMZ +/- heat shock protein (HSPPC-96)
PD-1	Pembrolizumab	Newly diagnosed	II	NCT03197506	Standard fractionation	Recruiting	Standard therapy (RT+TMZ) +/- anti-PD-1
PD-1	Pembrolizumab	Recurrent	I	NCT02313272	Standard fractionation	Active, not recruiting	Bevacizumab and RT (6Gy x 5) +/- anti-PD-1
PD-1	Pembrolizumab	Newly diagnosed	II	NCT03899857	Standard fractionation	Recruiting	standard treatment (RT+TMZ) + anti-PD-1
PD-1	Pembrolizumab	Newly diagnosed	I	NCT02287428	Standard fractionation	Recruiting	Unmethylated MGMT; RT+anti-PD-1+NeoAntigen Vaccine
PD-1	Pembrolizumab	Newly diagnosed	I	NCT03426891	Standard fractionation	Recruiting	Standard therapy (RT+TMZ) +/- HDAC inhibitor (Vorinostat) +/- anti-PD-1
PD-1	Pembrolizumab	Recurrent	II	NCT03661723	Hypofractionated	Recruiting	Re-irradiation (7Gy x 5) per week for 2 weeks +/- Bevacizumab
PD-1 and CTLA-4	Nivolumab and Ipilimumab	Newly diagnosed	II	NCT03367715	Hypofractionated	Recruiting	Unmethylated MGMT; RT (6Gy x 5) + anti-PD-1 + anti-CTLA4
PD-1 and CTLA-4	Nivolumab and Ipilimumab	Newly diagnosed	II/III	NCT04396860	Standard fractionation	Recruiting	Unmethylated MGMT; comparison standard treatment (RT+TMZ) versus RT+anti-PD-1+anti-CTLA-4
PD-1 and IDO	Nivolumab and BMS-986205	Newly diagnosed	I	NCT04047706	Standard fractionation	Recruiting	Standard treatment (RT+TMZ) +/- anti-PD-1 +/- IDO inhibitor
PD-L1	Durvalumab	Newly diagnosed and recurrent	II	NCT02336165	Standard fractionation	Active, not recruiting	Bevacizumab
PD-L1	Durvalumab	Recurrent	I/II	NCT02866747	Hypofractionated	Recruiting	RT (8Gy x 3)
PD-L1	Atezolizumab	Newly diagnosed	I/II	NCT03174197	Standard fractionation	Active, not recruiting	Standard treatment (RT+TMZ) +/− anti-PD-L1
PD-L1	Avelumab	Newly diagnosed	II	NCT02968940	Hypofractionated	Completed	IDH mutant; RT (6Gy x 5)
PD-L1	Avelumab	Newly diagnosed	II	NCT03047473	Standard fractionation	Active, not recruiting	Standard treatment (RT+TMZ) +/− anti-PD-L1
PD-L1	Avelumab	Recurrent	II	NCT03291314	Standard fractionation	Completed	Standard treatment (RT+TMZ) + anti-PD-L1 + tyrosine kinase inhibitor (axitinib)
GM-CSF	Sargranostim	Newly diagnosed	II	NCT02663440	Hypofractionated	Unknown	RT (regimen not specified) + TMZ + GM-CSF
GM-CSF and poly I:C	Sargranostim and Hiltonol	Recurrent	I	NCT03392545	Not specified	Recruiting	RT + GM-CSF and poly I:C
GM-CSF and tetanus-diphtheria toxoid (Td)	GM-CSF and Td	Newly diagnosed	II	NCT03927222	Standard fractionation	Recruiting	Unmethylated MGMT; Standard treatment (RT+TMZ) + Td + GM-CSF
TGF-β	Galunisertib	Newly diagnosed	I/II	NCT01220271	Standard fractionation	Completed	Standard treatment (RT+TMZ) +/− anti-TGF-β
IDO	Indoximod	Newly diagnosed	I/II	NCT02052648	Hypofractionated	Completed	TMZ +/− bevacizumab +/− IDO inhibitor +/− RT (5.5 × 5 Gy)
CXCR4	Plexirafor	Newly diagnosed	I/II	NCT01977677	Standard fractionation	Completed	Standard treatment (RT+TMZ) +/− CXCR4 inhibitor
CSF1R	Pexidartinib	Newly diagnosed	I/II	NCT01790503	Standard fractionation	Completed	Standard treatment (RT+TMZ) +/− CSF1R inhibitor
IGF-1R	IGV-001	Newly diagnosed	IIb	NCT04485949	Standard fractionation	Not yet recruiting	Standard treatment (RT+TMZ) +/− IGV-001 cell immunotherapy
PD-L1	Atezolizumab	Recurrent	II	NCT04729959	Hypofractionated	Not yet recruiting	IDH1 wild type; PD-L1 inhibitor; tocilizumab; RT
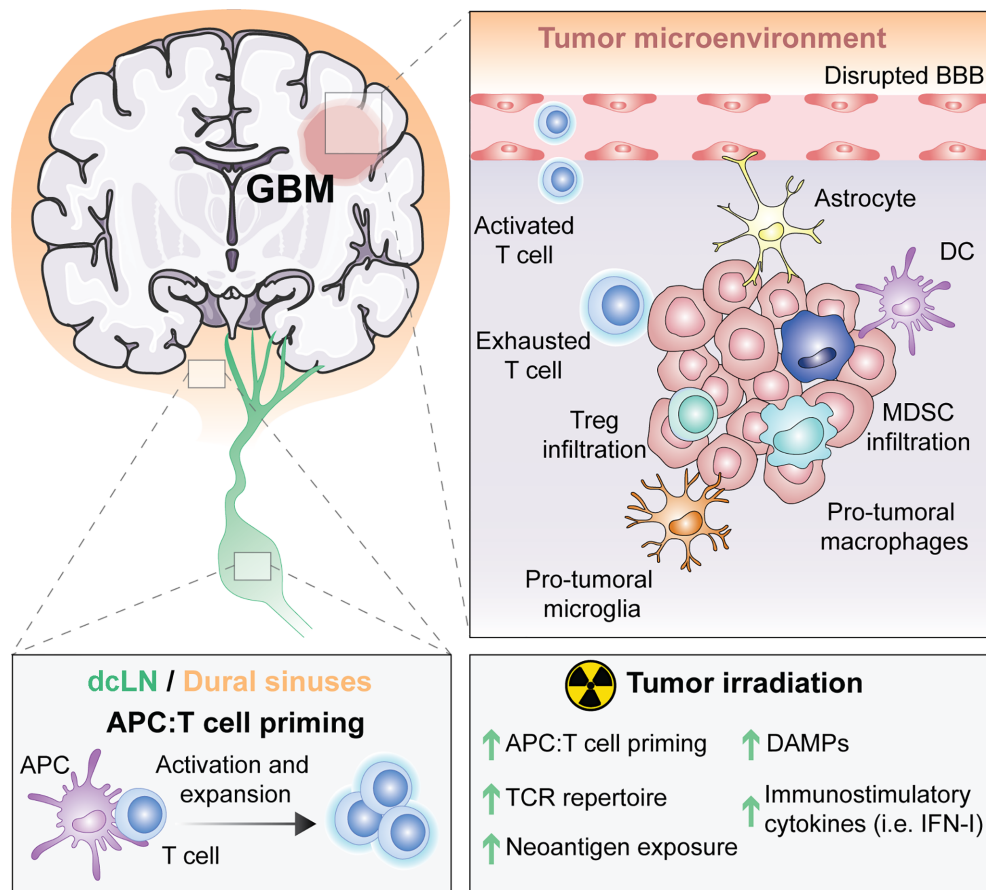
FIGURE 1 | The unique immune response in GBM and its modulation by RT. For many years, the central nervous system (CNS) was thought to be excluded from immune surveillance. However, it is now known that the CNS is not isolated from activated T cells and that CNS antigens can be presented locally or peripherally in the draining cervical lymph nodes or the dural sinuses. Diverse types of antigen presenting cells (APCs) exist within glioblastoma (GBM), including microglia, macrophages, astrocytes and classic APCs such as dendritic cells (DCs). APCs that have captured tumor antigens can present to naïve T cells, leading to their activation and expansion. Activated T cells migrate into the brain through a disrupted blood brain barrier (BBB), but once in the tumor microenvironment (TME) they differentiate into exhausted T cells. Within the TME, there are immunosuppressive regulatory T cells (Tregs), myeloid derived suppressor cells (MDSC), reactive astrocytes and pro-tumoral macrophages and microglia. Radiotherapy (RT), the standard of care for GBM, induces the exposure of tumor neoantigens and increases the T cell receptor (TCR) repertoire. Moreover, tumor irradiation promotes the release of danger associated molecular patterns (DAMPs) and type I interferon (IFN-I), which stimulate APCs cross-priming of T cells. All of these suggest that RT can be used to overcome GBM immunosuppression to optimally prime anti-tumor immunity.

(2) increased expression of the programmed death ligand-1 (PD-L1) (57), (3) loss of surface spingosine-1-phosphate receptor 1 (S1P1) in brain tumors to sequester T cells in the bone marrow (58) and (4) CD68+ microglia lose MHC-II (i.e. heterogeneity human leukocyte antigen (HLA)-DR isotype; HLA-DR) expression in a PTEN dependent fashion (18).

Despite these major obstacles, some T cells can successfully infiltrate intracranial tumors and have been shown post IT in patients who respond (18). However, infiltrating T cells are more likely to be dysfunctional and express markers of exhaustion like programmed cell death (PD-1), lymphocyte-activation gene 3 (LAG3) and T-cell immunoglobulin and mucin-domain containing-3 (TIM-3) (59–61). Importantly, a large proportion of T cells infiltrating GBM are regulatory T cells (Tregs) that co-expressed checkpoint inhibitors including cytotoxic T-lymphocyte-associated protein 4 (CTLA-4) and PD-1 (62). Treg is a subset of

CD4 T cells that express the transcription factor forkhead box protein3 (Foxp3) (63, 64). These cells suppress CD8 T cells activation by the secretion of immunosuppressive cytokines, namely TGFβ and IL-10 (65, 66). GBM attract Tregs from the periphery to the local TME by soluble factors, such as GBM-derived CCL22, CCL2, and TGFβ, to promote immunosuppression (66–69).

Overall, these findings underscore that not only do intracranial tumors display high infiltration of immunosuppressive cells but they also secrete factors that limit T cell responses against GBM.

The Cancer Genome Atlas (TCGA) has identified four subtypes of GBM (i.e. proneural, neural, classical, and mesenchymal), based on mutations that drive proliferation and survival of GBM (70). Consequently, the genetic heterogeneity of GBM predicts for a great mutational load, one of the favorable biomarkers for successful IT. However, GBM are characterized

by a relatively low mutational burden (71, 72), suggesting that GBM display limited somatic mutations for the T cells to target and ultimately lead to a restricted efficacy of IT when used as monotherapy.

Defects in the antigen presentation machinery, such as downregulation or loss of HLA class I, have also been reported in GBM patients (73). More specifically, microglia antigen-presenting cells (9, 74) present a downregulation of the major histocompatibility class I (MHC-I) due to immunosuppressive cytokines (e.g. TGFβ and IL-10) that emanate from the TME (75).

Therefore, low presence of antigens combined with defective presentation, represent an additional challenge to mount effective T cell responses against GBM.

Metabolic alterations of GBM is an emerging immune resistance mechanism (76). Notably, a recent study comparing the metabolic reprogramming of GBM patient samples with low-grade astrocytoma identified that variations in tryptophan, arginine, prostaglandin, and adenosine pathways might be responsible for the accumulation of Tregs and pro-tumorigenic TAMs in GBM (77). Moreover, activation of the mammalian target of rapamycin (mTOR) pathway in microglia promoted tumor growth and immune evasion in murine GBM (78). Therefore, targeting metabolic liabilities of intracranial tumors represents a promising strategy to overcome immunosuppression.

RADIOTHERAPY TO RESTORE THE SENSITIVITY OF GLIOBLASTOMA TO IMMUNOTHERAPY

The complexity of brain immunity combined with the immunosuppression exerted by the TME in brain tumors call for innovative approaches to break immune tolerance of brain malignancy.

One appealing strategy is to exploit the immuno-stimulatory properties of RT to generate an *in situ* tumor vaccine and the subsequent recruitment of effector T cells into GBM; a vital component for the efficacy of modern IT (**Figure 1**).

RT has been acknowledged as a potent immune adjuvant over the past two decades with major preclinical data demonstrating that RT promotes tumor specific T cell responses (79, 80). However, the concept of RT as an immune response modifier (IRM) was initiated forty years ago by Stone who demonstrated that responses to RT were impaired in the absence of T cells (81). While these findings were ignored for a long time, the breakthrough of ITs restimulated interest in exploiting the immunogenic properties of RT to expand the fraction of cancer patients that can benefit from IT. Since then, studies from experimental models have provided mechanistic insight pertaining to the ability of RT to stimulate the immune system. Notably, two main processes were found essential (but not mutually exclusive) to convey immunogenicity of an irradiated tumor: (1) the engagement of an immunogenic cell death (ICD) (82–85) and (2) the induction of type I interferon (IFN-I) (86–88). ICD is identified by the spatial and temporal occurrence of

three damage-associated molecular pattern (DAMPs) molecules, namely the pre-apoptotic exposure of calreticulin (CRT) on the cell surface (89), the active secretion of ATP (82, 83, 89–92) and the release of the non-histone nuclear protein High Mobolity Group Box 1 (HMGB1) (82).

Activation of IFN-I response is essential for T cell priming and is a consequence of the recognition of cytosolic double stranded (ds) DNA by the nucleic acid sensor (NAS) CGAS (i.e. cyclic GMP-AMP synthase) to engage stimulator of the interferon genes (STING) pathway in irradiated cells as well as in dendritic cells (DC) (87, 88, 93–98). The source of cytosolic DNA is currently being debated with reports indicating that micronuclei formed by mitotic defects (99–101) and/or the autophagy-dependent release of mitochondrial dsDNA (86).

Nevertheless, RT-induced IFN-I response is not restricted to cytoplasmic dsDNA sensing. Notably, recent studies have demonstrated that cytoplasmic recognition of dsRNA by the retinoic acid inducible gene I (RIG-I)-like receptors (RLRs) led to IFN-I post RT (102, 103). Cytosolic dsRNA sensing involves three RLR sensors, namely RIG-I, melanoma differentiation-associated gene 5 (MDA5), and laboratory of physiology and genetics 2 (LGP2 or DExH-box helicase 58; DHX58) (104, 105). A recent preclinical study, reported that host LGP2 was essential for optimal anti-tumor control of irradiated murine colorectal tumors (103). Consequently, the activation of RT-induced IFN-I is the result of DNA recognition by the CGAS-STING pathway but is also subsequent to RNA sensing by the RLR family. Whether these mechanisms are initiated in irradiated GBM remains unknown, but current data suggests that activation CGAS-STING in myeloid cells is important for anti-tumor immunity against this tumor type (106, 107).

Other major immunogenic features of RT is to shape the T cell receptor (TCR) repertoire of TILs (108–112) and to expose immunogenic mutations to the immune system (113). A detailed discussion describing the mechanisms responsible for the increase of antigenicity in irradiated tumors can be found elsewhere (114).

While the capacity of RT to generate similar mechanisms in the brain remains to be investigated, evidence of MHC-I upregulation and increase of antigen presentation from brain irradiation was described (115). More importantly, it was reported that personalized neoantigen vaccine generates intratumoral T cell responses in GBM patients, suggesting that RT-induced immunogenic mutation exposure is a promising strategy to treat intracranial tumors (116).

The impact of the isocitrate dehydrogenase 1 (IDH1) mutation together with the methylation status of O6-methylguanine-DNA methyltransferase (MGMT) on RT-induced anti-tumor immunity against GBM is unclear. However, the fact that neoantigen derived from mutant IDH1 can promote anti-tumor CD4+ T-cells and antibody responses in glioma together with the ability of RT to expose neoantigens, suggest that IDH1 mutated GBM patients might better respond to the RT-IT combinations as opposed to patients with wild-type IDH1 tumors (117).

Altogether, mechanistic insights pertaining to the immunogenic role and function of ionizing radiation elevated

the use of RT as a partner to IT in multiple cancer including GBM. Some RT-IT combination are already assessed in preclinical models of GBM as well as in clinic (**Table 1**). For instance, focal irradiation improved the survival of GBM-tumor bearing mice treated with anti-PD-1 (118, 119), anti-CTLA-4 + 4-1BB activation (120), dual TIM-3 and PD-1 blockade (121) and anti-GITR (glucocorticoid-induced TNFR family related gene) (122). Underscoring the potential of RT to promote GBM-targeted T cells responses, all of these studies reported an increase in T cell infiltration and some even documented long-lasting immune memory responses against GBM.

Importantly myeloid cells expressing the colony-stimulating factor-1 receptor (CSF-1R) (or TAM-CSF-1R+ cells) were recently found altered during the time-course of anti-GBM therapy. Notably, RT was described to promote recurrence-specific phenotypes in microglia and monocyte-derived macrophages (123). GBM tumor bearing mice treated with the combination of anti-CSF-1R with focal RT experienced increase in survival, thus indicating that CSF-1R targeting is a promising strategy for irradiated GBM (123).

Along similar lines, targeting PD-L1 expressing tumor associated myeloid cells in combination with dinaciclib, a cyclin-dependent kinase inhibitor, extended survival of mice bearing irradiated GBM tumors (124).

CLINICAL TRANSLATION AND CHALLENGES

A widespread interest of RT-based immuno-oncology combinations has spurred in Clinic due to the mounting evidence highlighting the role RT as an immune adjuvant. However, the clinic translation of experimental models turn out to be more challenging than anticipated due to several of host-responses to RT. Notably, mounting evidence highlight the critical aspect of the choice of radiation fractionation and regimen to elicit anti-tumor immunity. Consequently, the impact of RT planning and delivery must be considered including: absolute dose, dose-per-fraction, low dose spread, path of radiation delivery, and the effects of radiation cell kill. Radiation dose fractionation and dose per fraction has shown to differentially affect immune cells and the TME. For instance, radiation dose-dependent responses can be elicited on T-effector cells versus Tregs, macrophages, and TME regulation through TREX1-STING-IFN signaling (87, 125–128). The optimal radiation dose and regimen together with the best sequencing between IT and RT remains elusive (19, 129, 130).

Nevertheless, ongoing clinical trials assessing the combination of IT with either standard fractionation or hypofractionation regimen in CNS diseases (**Table 1**) may provide some indication on the optimal radiation regimen and sequencing of IT to generate GBM-targeted anti-tumor immune responses.

Another major limitation to RT-induced anti-tumor immunity is the activation of latent TGFβ that stem for the TME. TGFβ activation by RT promotes immunosuppression (131) and therefore represents a major challenge for the translation of RT-IT combinations. Nevertheless, cooperative effects of TGFβ blockade with focal RT has shown some promises in patients with metastatic breast cancer (132, 133), which underscore that blocking TGFβ in the context of RT might be required to elicit potent anti-tumor immunity.

There are many emerging ionizing radiation technologies that may further add to the immune modulatory effects including ultras-fast dose-rate radiotherapy (FLASH-RT) and particle therapy (proton and carbon ion therapy) (134). While preclinical studies hold great promises to generates anti-tumor immunity against FLASH-irradiated GBM (135), additional investigations are required to define the immunogenic properties of FLASH radiation, especially in the context of brain malignancies.

Overall, to achieve clinical translation for patient care, increase knowledge of the interplay between radiation responses of the host and immunosuppression must be investigated.

CONCLUSION

Although to date, the clinical trials assessing the efficacy of IT have been disappointing, the results from preclinical studies are very encouraging for the success of RT-IT combinations in treating GBM. Different strategies adapted from experimental models are currently being investigated to harness the immense potential of combining RT with IT (**Table 1**). As a scientific community, we strongly await the data from these ongoing clinical trials. Further efforts to understand the effect of RT in TME of GBM may uncover novel avenues to optimally combine RT with IT to generate an *in situ* vaccination against GBM. However, given the complexity of the brain immunity, together with the immunosuppression of GBM, it is likely that multiple targets will be required to eliminate irradiated GBM.

AUTHOR CONTRIBUTIONS

All authors (MD, OP, CD, C-CW, RG, and CV-B) contributed to article writing and editing. All authors contributed to the article and approved the submitted version.

FUNDING

REFERENCES

1. Ostrom QT, Gittleman H, Truitt G, Boscia A, Kruchko C, Barnholtz-Sloan JS. CBTRUS Statistical Report: Primary Brain and Other Central Nervous System Tumors Diagnosed in the United States in 2011-2015. *Neuro Oncol* (2018) 20(suppl_4):iv1–iv86. doi: 10.1093/neuonc/noy131

2. Stupp R, Taillibert S, Kanner A, Read W, Steinberg D, Lhermitte B, et al. Effect of Tumor-Treating Fields Plus Maintenance Temozolomide vs Maintenance Temozolomide Alone on Survival in Patients With Glioblastoma: A Randomized Clinical Trial. *JAMA* (2017) 318(23):2306–16. doi: 10.1001/jama.2017.18718

3. Louveau A, Harris TH, Kipnis J. Revisiting the Mechanisms of CNS Immune Privilege. *Trends Immunol* (2015) 36(10):569–77. doi: 10.1016/j.it.2015.08.006

4. Louveau A, Smirnov I, Keyes TJ, Eccles JD, Rouhani SJ, Peske JD, et al. Structural and Functional Features of Central Nervous System Lymphatic Vessels. *Nature* (2015) 523(7560):337–41. doi: 10.1038/nature14432

5. Aloisi F, Ria F, Adorini L. Regulation of T-Cell Responses by CNS Antigen-Presenting Cells: Different Roles for Microglia and Astrocytes. *Immunol Today* (2000) 21(3):141–7. doi: 10.1016/S0167-5699(99)01512-1

6. Beauvillain C, Donnou S, Jarry U, Scotet M, Gascan H, Delneste Y, et al. Neonatal and Adult Microglia Cross-Present Exogenous Antigens. *Glia* (2008) 56(1):69–77. doi: 10.1002/glia.20565

7. Becher B, Bechmann I, Greter M. Antigen Presentation in Autoimmunity and CNS Inflammation: How T Lymphocytes Recognize the Brain. *J Mol Med (Berl)* (2006) 84(7):532–43. doi: 10.1007/s00109-006-0065-1

8. Harris MG, Hulseberg P, Ling C, Karman J, Clarkson BD, Harding JS, et al. Immune Privilege of the CNS is Not the Consequence of Limited Antigen Sampling. *Sci Rep* (2014) 4:4422. doi: 10.1038/srep04422

9. Jarry U, Jeannin P, Pineau L, Donnou S, Delneste Y, Couez D. Efficiently Stimulated Adult Microglia Cross-Prime Naive CD8+ T Cells Injected in the Brain. *Eur J Immunol* (2013) 43(5):1173–84. doi: 10.1002/eji.201243040

10. Rustenhoven J, Drieu A, Mamuladze T, de Lima KA, Dykstra T, Wall M, et al. Functional Characterization of the Dural Sinuses as a Neuroimmune Interface. *Cell* (2021) 184(4):1000–31. doi: 10.1016/j.cell.2020.12.040

11. Preusser M, Lim M, Hafler DA, Reardon DA, Sampson JH. Prospects of Immune Checkpoint Modulators in the Treatment of Glioblastoma. *Nat Rev Neurol* (2015) 11(9):504–14. doi: 10.1038/nrneurol.2015.139

12. Wilcox JA, Ramakrishna R, Magge R. Immunotherapy in Glioblastoma. *World Neurosurg* (2018) 116:518–28. doi: 10.1016/j.wneu.2018.04.020

13. Lim M, Xia Y, Bettegowda C, Weller M. Current State of Immunotherapy for Glioblastoma. *Nat Rev Clin Oncol* (2018) 15(7):422–42. doi: 10.1038/s41571-018-0003-5

14. Liu Z, Meng Q, Bartek JJr., Poiret T, Persson O, Rane L, et al. Tumor-Infiltrating Lymphocytes (Tils) From Patients With Glioma. *Oncoimmunology* (2017) 6(2):e1252894. doi: 10.1080/2162402X.2016.1252894

15. Li B, Severson E, Pignon JC, Zhao H, Li T, Novak J, et al. Comprehensive Analyses of Tumor Immunity: Implications for Cancer Immunotherapy. *Genome Biol* (2016) 17(1):174. doi: 10.1186/s13059-016-1028-7

16. Reardon DA, Wen PY, Wucherpfennig KW, Sampson JH. Immunomodulation for Glioblastoma. *Curr Opin Neurol* (2017) 30(3):361–9. doi: 10.1097/WCO.0000000000000451

17. Omuro A, Vlahovic G, Lim M, Sahebjam S, Baehring J, Cloughesy T. Nivolumab With or Without Ipilimumab in Patients With Recurrent Glioblastoma: Results From Exploratory Phase I Cohorts of Checkmate 143. *Neuro Oncol* (2018) 20(5):674–86. doi: 10.1093/neuonc/nox208

18. Zhao J, Chen AX, Gartrell RD, Silverman AM, Aparicio L, Chu T, et al. Immune and Genomic Correlates of Response to Anti-PD-1 Immunotherapy in Glioblastoma. *Nat Med* (2019) 25(3):462–9. doi: 10.1038/s41591-019-0349-y

19. Rodriguez-Ruiz ME, Vanpouille-Box C, Melero I, Formenti SC, Demaria S. Immunological Mechanisms Responsible for Radiation-Induced Abscopal Effect. *Trends Immunol* (2018) 39(8):644–55. doi: 10.1016/j.it.2018.06.001

20. Murphy JB, Sturm E. Conditions Determining the Transplantability of Tissues in the Brain. *J Exp Med* (1923) 38(2):183–97. doi: 10.1084/jem.38.2.183

21. Medawar PB. Immunity to Homologous Grafted Skin; the Fate of Skin Homografts Transplanted to the Brain, to Subcutaneous Tissue, and to the Anterior Chamber of the Eye. *Br J Exp Pathol* (1948) 29(1):58–69.

22. Bradbury MW, Westrop RJ. Factors Influencing Exit of Substances From Cerebrospinal Fluid Into Deep Cervical Lymph of the Rabbit. *J Physiol* (1983) 339:519–34. doi: 10.1113/jphysiol.1983.sp014731

23. Cserr HF, Knopf PM. Cervical Lymphatics, the Blood-Brain Barrier and the Immunoreactivity of the Brain: A New View. *Immunol Today* (1992) 13(12):507–12. doi: 10.1016/0167-5699(92)90027-5

24. Goldmann J, Kwidzinski E, Brandt C, Mahlo J, Richter D, Bechmann I. T Cells Traffic From Brain to Cervical Lymph Nodes Via the Cribroid Plate and the Nasal Mucosa. *J Leukoc Biol* (2006) 80(4):797–801. doi: 10.1189/jlb.0306176

25. Aspelund A, Antila S, Proulx ST, Karlsen TV, Karaman S, Detmar M, et al. A Dural Lymphatic Vascular System That Drains Brain Interstitial Fluid and Macromolecules. *J Exp Med* (2015) 212(7):991–9. doi: 10.1084/jem.20142290

26. Song E, Mao T, Dong H, Boisserand LSB, Antila S, Bosenberg M, et al. VEGF-C-Driven Lymphatic Drainage Enables Immunosurveillance of Brain Tumours. *Nature* (2020) 577(7792):689–94. doi: 10.1038/s41586-019-1912-x

27. Hu X, Deng Q, Ma L, Li Q, Chen Y, Liao Y, et al. Meningeal Lymphatic Vessels Regulate Brain Tumor Drainage and Immunity. *Cell Res* (2020) 30(3):229–43. doi: 10.1038/s41422-020-0287-8

28. Tietz S, Engelhardt B. Brain Barriers: Crosstalk Between Complex Tight Junctions and Adherens Junctions. *J Cell Biol* (2015) 209(4):493–506. doi: 10.1083/jcb.201412147

29. Huber JD, Egleton RD, Davis TP. Molecular Physiology and Pathophysiology of Tight Junctions in the Blood-Brain Barrier. *Trends Neurosci* (2001) 24(12):719–25. doi: 10.1016/S0166-2236(00)02004-X

30. Taiarol L, Formicola B, Magro RD, Sesana S, Re F. An Update of Nanoparticle-Based Approaches for Glioblastoma Multiforme Immunotherapy. *Nanomed (Lond)* (2020) 15(19):1861–71. doi: 10.2217/nnm-2020-0132

31. Enriquez Perez J, Kopecky J, Visse E, Darabi A, Siesjo P. Convection-Enhanced Delivery of Temozolomide and Whole Cell Tumor Immunizations in GL261 and KR158 Experimental Mouse Gliomas. *BMC Cancer* (2020) 20(1):7. doi: 10.1186/s12885-019-6502-7

32. Sheybani ND, Breza VR, Paul S, McCauley KS, Berr SS, Miller GW, et al. Immunopet-Informed Sequence for Focused Ultrasound-Targeted Mcd47 Blockade Controls Glioma. *J Contr Rel* (2021) 331:19–29. doi: 10.1016/j.jconrel.2021.01.023

33. Yang FY, Wong TT, Teng MC, Liu RS, Lu M, Liang HF, et al. Focused Ultrasound and Interleukin-4 Receptor-Targeted Liposomal Doxorubicin for Enhanced Targeted Drug Delivery and Antitumor Effect in Glioblastoma Multiforme. *J Contr Rel* (2012) 160(3):652–8. doi: 10.1016/j.jconrel.2012.02.023

34. Vanpouille-Box C, Lacoeuille F, Belloche C, Lepareur N, Lemaire L, LeJeune JJ, et al. Tumor Eradication in Rat Glioma and Bypass of Immunosuppressive Barriers Using Internal Radiation With (188)Re-Lipid Nanocapsules. *Biomaterials* (2011) 32(28):6781–90. doi: 10.1016/j.biomaterials.2011.05.067

35. Schlager C, Korner H, Krueger M, Vidoli S, Haberl M, Mielke D, et al. Effector T-Cell Trafficking Between the Leptomeninges and the Cerebrospinal Fluid. *Nature* (2016) 530(7590):349–53. doi: 10.1038/nature16939

36. Engelhardt B, Ransohoff RM. The Ins and Outs of T-Lymphocyte Trafficking to the CNS: Anatomical Sites and Molecular Mechanisms. *Trends Immunol* (2005) 26(9):485–95. doi: 10.1016/j.it.2005.07.004

37. Korn T, Kallies A. T Cell Responses in the Central Nervous System. *Nat Rev Immunol* (2017) 17(3):179–94. doi: 10.1038/nri.2016.144

38. Li X, Ranjith-Kumar CT, Brooks MT, Dharmaiah S, Herr AB, Kao C, et al. The RIG-I-Like Receptor LGP2 Recognizes the Termini of Double-Stranded RNA. *J Biol Chem* (2009) 284(20):13881–91. doi: 10.1074/jbc.M900818200

39. Ginhoux F, Greter M, Leboeuf M, Nandi S, See P, Gokhan S, et al. Fate Mapping Analysis Reveals That Adult Microglia Derive From Primitive Macrophages. *Science* (2010) 330(6005):841–5. doi: 10.1126/science.1194637

40. Nimmerjahn A, Kirchhoff F, Helmchen F. Resting Microglial Cells are Highly Dynamic Surveillants of Brain Parenchyma In Vivo. *Science* (2005) 308(5726):1314–8. doi: 10.1126/science.1110647

41. Davalos D, Grutzendler J, Yang G, Kim JV, Zuo Y, Jung S, et al. ATP Mediates Rapid Microglial Response to Local Brain Injury In Vivo. *Nat Neurosci* (2005) 8(6):752–8. doi: 10.1038/nn1472

42. Quail DF, Joyce JA. The Microenvironmental Landscape of Brain Tumors. *Cancer Cell* (2017) 31(3):326–41. doi: 10.1016/j.ccell.2017.02.009

43. Graeber MB, Scheithauer BW, Kreutzberg GW. Microglia in Brain Tumors. *Glia* (2002) 40(2):252–9. doi: 10.1002/glia.10147

44. Komohara Y, Ohnishi K, Kuratsu J, Takeya M. Possible Involvement of the M2 Anti-Inflammatory Macrophage Phenotype in Growth of Human Gliomas. J Pathol (2008) 216(1):15–24. doi: 10.1002/path.2370

45. Hambardzumyan D, Gutmann DH, Kettenmann H. The Role of Microglia and Macrophages in Glioma Maintenance and Progression. Nat Neurosci (2016) 19(1):20–7. doi: 10.1038/nn.4185

46. Sorensen MD, Dahlrot RH, Boldt HB, Hansen S, Kristensen BW. Tumour-Associated Microglia/Macrophages Predict Poor Prognosis in High-Grade Gliomas and Correlate With an Aggressive Tumour Subtype. Neuropathol Appl Neurobiol (2018) 44(2):185–206. doi: 10.1111/nan.12428

47. Wang SC, Hong JH, Hsueh C, Chiang CS. Tumor-Secreted SDF-1 Promotes Glioma Invasiveness and TAM Tropism Toward Hypoxia in a Murine Astrocytoma Model. Lab Invest (2012) 92(1):151–62. doi: 10.1038/labinvest.2011.128

48. Kioi M, Vogel H, Schultz G, Hoffman RM, Harsh GR, Brown JM. Inhibition of Vasculogenesis, But Not Angiogenesis, Prevents the Recurrence of Glioblastoma After Irradiation in Mice. J Clin Invest (2010) 120(3):694–705. doi: 10.1172/JCI40283

49. Platten M, Kretz A, Naumann U, Aulwurm S, Egashira K, Isenmann S, et al. Monocyte Chemoattractant Protein-1 Increases Microglial Infiltration and Aggressiveness of Gliomas. Ann Neurol (2003) 54(3):388–92. doi: 10.1002/ana.10679

50. Takenaka MC, Gabriely G, Rothhammer V, Mascanfroni ID, Wheeler MA, Chao CC, et al. Control of Tumor-Associated Macrophages and T Cells in Glioblastoma Via AHR and CD39. Nat Neurosci (2019) 22(5):729–40. doi: 10.1038/s41593-019-0370-y

51. Pyonteck SM, Akkari L, Schuhmacher AJ, Bowman RL, Sevenich L, Quail DF, et al. CSF-1R Inhibition Alters Macrophage Polarization and Blocks Glioma Progression. Nat Med (2013) 19(10):1264–72. doi: 10.1038/nm.3337

52. Wang Q, He Z, Huang M, Liu T, Wang Y, Xu H, et al. Vascular Niche IL-6 Induces Alternative Macrophage Activation in Glioblastoma Through HIF-2alpha. Nat Commun (2018) 9(1):559. doi: 10.1038/s41467-018-03050-0

53. Bloch O, Crane CA, Kaur R, Safaee M, Rutkowski MJ, Parsa AT. Gliomas Promote Immunosuppression Through Induction of B7-H1 Expression in Tumor-Associated Macrophages. Clin Cancer Res (2013) 19(12):3165–75. doi: 10.1158/1078-0432.CCR-12-3314

54. Lamano JB, Lamano JB, Li YD, DiDomenico JD, Choy W, Veliceasa D, et al. Glioblastoma-Derived IL6 Induces Immunosuppressive Peripheral Myeloid Cell PD-L1 and Promotes Tumor Growth. Clin Cancer Res (2019) 25(12):3643–57. doi: 10.1158/1078-0432.CCR-18-2402

55. Gutmann DH, Kettenmann H. Microglia/Brain Macrophages as Central Drivers of Brain Tumor Pathobiology. Neuron (2019) 104(3):442–9. doi: 10.1016/j.neuron.2019.08.028

56. Andaloussi AE, Han Y, Lesniak MS. Progression of Intracranial Glioma Disrupts Thymic Homeostasis and Induces T-Cell Apoptosis In Vivo. Cancer Immunol Immunother (2008) 57(12):1807–16. doi: 10.1007/s00262-008-0508-3

57. Nduom EK, Wei J, Yaghi NK, Huang N, Kong LY, Gabrusiewicz K, et al. PD-L1 Expression and Prognostic Impact in Glioblastoma. Neuro Oncol (2016) 18(2):195–205. doi: 10.1093/neuonc/nov172

58. Chongsathidkiet P, Jackson C, Koyama S, Loebel F, Cui X, Farber SH, et al. Sequestration of T Cells in Bone Marrow in the Setting of Glioblastoma and Other Intracranial Tumors. Nat Med (2018) 24(9):1459–68. doi: 10.1038/s41591-018-0135-2

59. Mohme M, Schliffke S, Maire CL, Runger A, Glau L, Mende KC, et al. Immunophenotyping of Newly Diagnosed and Recurrent Glioblastoma Defines Distinct Immune Exhaustion Profiles in Peripheral and Tumor-Infiltrating Lymphocytes. Clin Cancer Res (2018) 24(17):4187–200. doi: 10.1158/1078-0432.CCR-17-2617

60. Woroniecka K, Chongsathidkiet P, Rhodin K, Kemeny H, Dechant C, Farber SH, et al. T-Cell Exhaustion Signatures Vary With Tumor Type and are Severe in Glioblastoma. Clin Cancer Res (2018) 24(17):4175–86. doi: 10.1158/1078-0432.CCR-17-1846

61. Park J, Kwon M, Kim KH, Kim TS, Hong SH, Kim CG, et al. Immune Checkpoint Inhibitor-Induced Reinvigoration of Tumor-Infiltrating CD8(+) T Cells is Determined by Their Differentiation Status in Glioblastoma. Clin Cancer Res (2019) 25(8):2549–59. doi: 10.1158/1078-0432.CCR-18-2564

62. Jacobs JF, Idema AJ, Bol KF, Nierkens S, Grauer OM, Wesseling P, et al. Regulatory T Cells and the PD-L1/PD-1 Pathway Mediate Immune Suppression in Malignant Human Brain Tumors. Neuro Oncol (2009) 11(4):394–402. doi: 10.1215/15228517-2008-104

63. El Andaloussi A, Lesniak MS. An Increase in CD4+CD25+FOXP3+ Regulatory T Cells in Tumor-Infiltrating Lymphocytes of Human Glioblastoma Multiforme. Neuro Oncol (2006) 8(3):234–43. doi: 10.1215/15228517-2006-006

64. Fecci PE, Mitchell DA, Whitesides JF, Xie W, Friedman AH, Archer GE, et al. Increased Regulatory T-Cell Fraction Amidst a Diminished CD4 Compartment Explains Cellular Immune Defects in Patients With Malignant Glioma. Cancer Res (2006) 66(6):3294–302. doi: 10.1158/0008-5472.CAN-05-3773

65. Iwata R, Hyoung Lee J, Hayashi M, Dianzani U, Ofune K, Maruyama M, et al. ICOSLG-Mediated Regulatory T-Cell Expansion and IL-10 Production Promote Progression of Glioblastoma. Neuro Oncol (2020) 22(3):333–44. doi: 10.1093/neuonc/noz204

66. Crane CA, Ahn BJ, Han SJ, Parsa AT. Soluble Factors Secreted by Glioblastoma Cell Lines Facilitate Recruitment, Survival, and Expansion of Regulatory T Cells: Implications for Immunotherapy. Neuro Oncol (2012) 14(5):584–95. doi: 10.1093/neuonc/nos014

67. Chang AL, Miska J, Wainwright DA, Dey M, Rivetta CV, Yu D, et al. CCL2 Produced by the Glioma Microenvironment is Essential for the Recruitment of Regulatory T Cells and Myeloid-Derived Suppressor Cells. Cancer Res (2016) 76(19):5671–82. doi: 10.1158/0008-5472.CAN-16-0144

68. Jordan JT, Sun W, Hussain SF, DeAngulo G, Prabhu SS, Heimberger AB. Preferential Migration of Regulatory T Cells Mediated by Glioma-Secreted Chemokines can be Blocked With Chemotherapy. Cancer Immunol Immunother (2008) 57(1):123–31. doi: 10.1007/s00262-007-0336-x

69. Ueda R, Fujita M, Zhu X, Sasaki K, Kastenhuber ER, Kohanbash G, et al. Systemic Inhibition of Transforming Growth Factor-Beta in Glioma-Bearing Mice Improves the Therapeutic Efficacy of Glioma-Associated Antigen Peptide Vaccines. Clin Cancer Res (2009) 15(21):6551–9. doi: 10.1158/1078-0432.CCR-09-1067

70. Verhaak RG, Hoadley KA, Purdom E, Wang V, Qi Y, Wilkerson MD, et al. Integrated Genomic Analysis Identifies Clinically Relevant Subtypes of Glioblastoma Characterized by Abnormalities in PDGFRA, IDH1, EGFR, and NF1. Cancer Cell (2010) 17(1):98–110. doi: 10.1016/j.ccr.2009.12.020

71. Hodges TR, Ott M, Xiu J, Gatalica Z, Swensen J, Zhou S, et al. Mutational Burden, Immune Checkpoint Expression, and Mismatch Repair in Glioma: Implications for Immune Checkpoint Immunotherapy. Neuro Oncol (2017) 19(8):1047–57. doi: 10.1093/neuonc/nox026

72. Bouffet E, Larouche V, Campbell BB, Merico D, de Borja R, Aronson M, et al. Immune Checkpoint Inhibition for Hypermutant Glioblastoma Multiforme Resulting From Germline Biallelic Mismatch Repair Deficiency. J Clin Oncol (2016) 34(19):2206–11. doi: 10.1200/JCO.2016.66.6552

73. Facoetti A, Nano R, Zelini P, Morbini P, Benericetti E, Ceroni M, et al. Human Leukocyte Antigen and Antigen Processing Machinery Component Defects in Astrocytic Tumors. Clin Cancer Res (2005) 11(23):8304–11. doi: 10.1158/1078-0432.CCR-04-2588

74. Moseman EA, Blanchard AC, Nayak D, McGavern DB. T Cell Engagement of Cross-Presenting Microglia Protects the Brain From a Nasal Virus Infection. Sci Immunol (2020) 5(48):eabb1817. doi: 10.1126/sciimmunol.abb1817

75. Roy LO, Poirier MB, Fortin D. Transforming Growth Factor-Beta and its Implication in the Malignancy of Gliomas. Target Oncol (2015) 10(1):1–14. doi: 10.1007/s11523-014-0308-y

76. Bi J, Chowdhry S, Wu S, Zhang W, Masui K, Mischel PS. Altered Cellular Metabolism in Gliomas - an Emerging Landscape of Actionable Co-Dependency Targets. Nat Rev Cancer (2020) 20(1):57–70. doi: 10.1038/s41568-019-0226-5

77. Kesarwani P, Prabhu A, Kant S, Chinnaiyan P. Metabolic Remodeling Contributes Towards an Immune-Suppressive Phenotype in Glioblastoma. Cancer Immunol Immunother (2019) 68(7):1107–20. doi: 10.1007/s00262-019-02347-3

78. Dumas AA, Pomella N, Rosser G, Guglielmi L, Vinel C, Millner TO, et al. Microglia Promote Glioblastoma Via Mtor-Mediated Immunosuppression of the Tumour Microenvironment. EMBO J (2020) 39(15):e103790. doi: 10.15252/embj.2019103790

79. Vanpouille-Box C, Formenti SC, Demaria S. Toward Precision Radiotherapy for Use With Immune Checkpoint Blockers. Clin Cancer Res (2018) 24(2):259–65. doi: 10.1158/1078-0432.CCR-16-0037

80. Krombach J, Hennel R, Brix N, Orth M, Schoetz U, Ernst A, et al. Priming Anti-Tumor Immunity by Radiotherapy: Dying Tumor Cell-Derived Damps Trigger Endothelial Cell Activation and Recruitment of Myeloid Cells. *Oncoimmunology* (2019) 8(1):e1523097. doi: 10.1080/2162402X.2018.1523097

81. Stone HB, Peters LJ, Milas L. Effect of Host Immune Capability on Radiocurability and Subsequent Transplantability of a Murine Fibrosarcoma. *J Natl Cancer Inst* (1979) 63(5):1229–35.

82. Apetoh L, Ghiringhelli F, Tesniere A, Obeid M, Ortiz C, Criollo A, et al. Toll-Like Receptor 4-Dependent Contribution of the Immune System to Anticancer Chemotherapy and Radiotherapy. *Nat Med* (2007) 13(9):1050–9. doi: 10.1038/nm1622

83. Golden EB, Frances D, Pelliccotta I, Demaria S, Helen Barcellos-Hoff M, Formenti SC. Radiation Fosters Dose-Dependent and Chemotherapy-Induced Immunogenic Cell Death. *Oncoimmunology* (2014) 3:e28518. doi: 10.4161/onci.28518

84. Dadey DYA, Kapoor V, Khudanyan A, Thotala D, Hallahan DE. PERK Regulates Glioblastoma Sensitivity to ER Stress Although Promoting Radiation Resistance. *Mol Cancer Res* (2018) 16(10):1447–53. doi: 10.1158/1541-7786.MCR-18-0224

85. Kim W, Lee S, Seo D, Kim D, Kim K, Kim E, et al. Cellular Stress Responses in Radiotherapy. *Cells* (2019) 8(9):1105. doi: 10.3390/cells8091105

86. Yamazaki T, Kirchmair A, Sato A, Buque A, Rybstein M, Petroni G, et al. Mitochondrial DNA Drives Abscopal Responses to Radiation That are Inhibited by Autophagy. *Nat Immunol* (2020) 21(10):1160–71. doi: 10.1038/s41590-020-0751-0

87. Vanpouille-Box C, Alard A, Aryankalayil MJ, Sarfraz Y, Diamond JM, Schneider RJ, et al. DNA Exonuclease Trex1 Regulates Radiotherapy-Induced Tumour Immunogenicity. *Nat Commun* (2017) 8:15618. doi: 10.1038/ncomms15618

88. Deng L, Liang H, Xu M, Yang X, Burnette B, Arina A, et al. STING-Dependent Cytosolic DNA Sensing Promotes Radiation-Induced Type I Interferon-Dependent Antitumor Immunity in Immunogenic Tumors. *Immunity* (2014) 41(5):843–52. doi: 10.1016/j.immuni.2014.10.019

89. Obeid M, Tesniere A, Ghiringhelli F, Fimia GM, Apetoh L, Perfettini JL, et al. Calreticulin Exposure Dictates the Immunogenicity of Cancer Cell Death. *Nat Med* (2007) 13(1):54–61. doi: 10.1038/nm1523

90. Galluzzi L, Vitale I, Aaronson SA, Abrams JM, Adam D, Agostinis P, et al. Molecular Mechanisms of Cell Death: Recommendations of the Nomenclature Committee on Cell Death 2018. *Cell Death Differ* (2018) 25(3):486–541. doi: 10.1038/s41418-018-0102-y

91. Ghiringhelli F, Apetoh L, Tesniere A, Aymeric L, Ma Y, Ortiz C, et al. Activation of the NLRP3 Inflammasome in Dendritic Cells Induces IL-1beta-Dependent Adaptive Immunity Against Tumors. *Nat Med* (2009) 15(10):1170–8. doi: 10.1038/nm.2028

92. Kepp O, Senovilla L, Vitale I, Vacchelli E, Adjemian S, Agostinis P, et al. Consensus Guidelines for the Detection of Immunogenic Cell Death. *Oncoimmunology* (2014) 3(9):e955691. doi: 10.4161/21624011.2014.955691

93. Gao P, Ascano M, Wu Y, Barchet W, Gaffney BL, Zillinger T, et al. Cyclic [G (2′,5′)Pa(3′,5′)P] is the Metazoan Second Messenger Produced by DNA-Activated Cyclic GMP-AMP Synthase. *Cell* (2013) 153(5):1094–107. doi: 10.1016/j.cell.2013.04.046

94. Mankan AK, Schmidt T, Chauhan D, Goldeck M, Honing K, Gaidt M, et al. Cytosolic RNA:DNA Hybrids Activate the Cgas-STING Axis. *EMBO J* (2014) 33(24):2937–46. doi: 10.15252/embj.201488726

95. Sun L, Wu J, Du F, Chen X, Chen ZJ. Cyclic GMP-AMP Synthase is a Cytosolic DNA Sensor That Activates the Type I Interferon Pathway. *Science* (2013) 339(6121):786–91. doi: 10.1126/science.1232458

96. Yoh SM, Schneider M, Seifried J, Soonthornvacharin S, Akleh RE, Olivieri KC, et al. PQBP1 is a Proximal Sensor of the Cgas-Dependent Innate Response to HIV-1. *Cell* (2015) 161(6):1293–305. doi: 10.1016/j.cell.2015.04.050

97. Ishikawa H, Barber GN. STING is an Endoplasmic Reticulum Adaptor That Facilitates Innate Immune Signalling. *Nature* (2008) 455(7213):674–8. doi: 10.1038/nature07317

98. Ishikawa H, Ma Z, Barber GN. STING Regulates Intracellular DNA-Mediated, Type I Interferon-Dependent Innate Immunity. *Nature* (2009) 461(7265):788–92. doi: 10.1038/nature08476

99. Bakhoum SF, Ngo B, Laughney AM, Cavallo JA, Murphy CJ, Ly P, et al. Chromosomal Instability Drives Metastasis Through a Cytosolic DNA Response. *Nature* (2018) 553(7689):467–72. doi: 10.1038/nature25432

100. Harding SM, Benci JL, Irianto J, Discher DE, Minn AJ, Greenberg RA. Mitotic Progression Following DNA Damage Enables Pattern Recognition Within Micronuclei. *Nature* (2017) 548(7668):466–70. doi: 10.1038/nature23470

101. Mackenzie KJ, Carroll P, Martin CA, Murina O, Fluteau A, Simpson DJ, et al. Cgas Surveillance of Micronuclei Links Genome Instability to Innate Immunity. *Nature* (2017) 548(7668):461–5. doi: 10.1038/nature23449

102. Widau RC, Parekh AD, Ranck MC, Golden DW, Kumar KA, Sood RF, et al. RIG-I-Like Receptor LGP2 Protects Tumor Cells From Ionizing Radiation. *Proc Natl Acad Sci USA* (2014) 111(4):E484–91. doi: 10.1073/pnas.1323253111

103. Zheng W, Ranoa DRE, Huang X, Hou Y, Yang K, Poli EC, et al. RIG-I-Like Receptor LGP2 is Required for Tumor Control by Radiotherapy. *Cancer Res* (2020) 80(24):5633–41. doi: 10.1158/0008-5472.CAN-20-2324

104. Reikine S, Nguyen JB, Modis Y. Pattern Recognition and Signaling Mechanisms of RIG-I and MDA5. *Front Immunol* (2014) 5:342. doi: 10.3389/fimmu.2014.00342

105. Chow KT, Gale MJr., Loo YM. RIG-I and Other RNA Sensors in Antiviral Immunity. *Annu Rev Immunol* (2018) 36:667–94. doi: 10.1146/annurev-immunol-042617-053309

106. Ohkuri T, Ghosh A, Kosaka A, Zhu J, Ikeura M, David M, et al. STING Contributes to Antiglioma Immunity Via Triggering Type I IFN Signals in the Tumor Microenvironment. *Cancer Immunol Res* (2014) 2(12):1199–208. doi: 10.1158/2326-6066.CIR-14-0099

107. von Roemeling CA, Wang Y, Qie Y, Yuan H, Zhao H, Liu X, et al. Therapeutic Modulation of Phagocytosis in Glioblastoma can Activate Both Innate and Adaptive Antitumour Immunity. *Nat Commun* (2020) 11(1):1508. doi: 10.1038/s41467-020-15129-8

108. Formenti SC, Rudqvist NP, Golden E, Cooper B, Wennerberg E, Lhuillier C, et al. Radiotherapy Induces Responses of Lung Cancer to CTLA-4 Blockade. *Nat Med* (2018) 24(12):1845–51. doi: 10.1038/s41591-018-0232-2

109. Rudqvist NP, Pilones KA, Lhuillier C, Wennerberg E, Sidhom JW, Emerson RO, et al. Radiotherapy and CTLA-4 Blockade Shape the TCR Repertoire of Tumor-Infiltrating T Cells. *Cancer Immunol Res* (2018) 6(2):139–50. doi: 10.1158/2326-6066.CIR-17-0134

110. Chow J, Hoffend NC, Abrams SI, Schwaab T, Singh AK, Muhitch JB. Radiation Induces Dynamic Changes to the T Cell Repertoire in Renal Cell Carcinoma Patients. *Proc Natl Acad Sci USA* (2020) 117(38):23721–9. doi: 10.1073/pnas.2001933117

111. Wieland A, Kamphorst AO, Adsay NV, Masor JJ, Sarmiento J, Nasti TH, et al. T Cell Receptor Sequencing of Activated CD8 T Cells in the Blood Identifies Tumor-Infiltrating Clones That Expand After PD-1 Therapy and Radiation in a Melanoma Patient. *Cancer Immunol Immunother* (2018) 67(11):1767–76. doi: 10.1007/s00262-018-2228-7

112. Cloughesy TF, Mochizuki AY, Orpilla JR, Hugo W, Lee AH, Davidson TB, et al. Neoadjuvant Anti-PD-1 Immunotherapy Promotes a Survival Benefit With Intratumoral and Systemic Immune Responses in Recurrent Glioblastoma. *Nat Med* (2019) 25(3):477–86. doi: 10.1038/s41591-018-0337-7

113. Lhuillier C, Rudqvist NP, Yamazaki T, Zhang T, Charpentier M, Galluzzi L, et al. Radiotherapy-Exposed CD8+ and CD4+ Neoantigens Enhance Tumor Control. *J Clin Invest* (2021) 131(5):e138740. doi: 10.1172/JCI138740

114. Lhuillier C, Rudqvist NP, Elemento O, Formenti SC, Demaria S. Radiation Therapy and Anti-Tumor Immunity: Exposing Immunogenic Mutations to the Immune System. *Genome Med* (2019) 11(1):40. doi: 10.1186/s13073-019-0653-7

115. Newcomb EW, Demaria S, Lukyanov Y, Shao Y, Schnee T, Kawashima N, et al. The Combination of Ionizing Radiation and Peripheral Vaccination Produces Long-Term Survival of Mice Bearing Established Invasive GL261 Gliomas. *Clin Cancer Res* (2006) 12(15):4730–7. doi: 10.1158/1078-0432.CCR-06-0593

116. Keskin DB, Anandappa AJ, Sun J, Tirosh I, Mathewson ND, Li S, et al. Neoantigen Vaccine Generates Intratumoral T Cell Responses in Phase Ib Glioblastoma Trial. *Nature* (2019) 565(7738):234–9. doi: 10.1038/s41586-018-0792-9

117. Schumacher T, Bunse L, Pusch S, Sahm F, Wiestler B, Quandt J, et al. A Vaccine Targeting Mutant IDH1 Induces Antitumour Immunity. *Nature* (2014) 512(7514):324–7. doi: 10.1038/nature13387

118. Zeng J, See AP, Phallen J, Jackson CM, Belcaid Z, Ruzevick J, et al. Anti-PD-1 Blockade and Stereotactic Radiation Produce Long-Term Survival in Mice With Intracranial Gliomas. *Int J Radiat Oncol Biol Phys* (2013) 86(2):343–9. doi: 10.1016/j.ijrobp.2012.12.025

119. Stessin AM, Clausi MG, Zhao Z, Lin H, Hou W, Jiang Z, et al. Repolarized Macrophages, Induced by Intermediate Stereotactic Dose Radiotherapy and Immune Checkpoint Blockade, Contribute to Long-Term Survival in Glioma-Bearing Mice. *J Neurooncol* (2020) 147(3):547–55. doi: 10.1007/s11060-020-03459-y

120. Belcaid Z, Phallen JA, Zeng J, See AP, Mathios D, Gottschalk C. Focal Radiation Therapy Combined With 4-1BB Activation and CTLA-4 Blockade Yields Long-Term Survival and a Protective Antigen-Specific Memory Response in a Murine Glioma Model. *PloS One* (2014) 9(7):e101764. doi: 10.1371/journal.pone.0101764

121. Kim JE, Patel MA, Mangraviti A, Kim ES, Theodros D, Velarde E, et al. Combination Therapy With Anti-PD-1, Anti-TIM-3, and Focal Radiation Results in Regression of Murine Gliomas. *Clin Cancer Res* (2017) 23(1):124–36. doi: 10.1158/1078-0432.CCR-15-1535

122. Patel MA, Kim JE, Theodros D, Tam A, Velarde E, Kochel CM, et al. Agonist Anti-GITR Monoclonal Antibody and Stereotactic Radiation Induce Immune-Mediated Survival Advantage in Murine Intracranial Glioma. *J Immunother Cancer* (2016) 4:28. doi: 10.1186/2051-1426-3-S2-P194

123. Akkari L, Bowman RL, Tessier J, Klemm F, Handgraaf SM, de Groot M, et al. Dynamic Changes in Glioma Macrophage Populations After Radiotherapy Reveal CSF-1R Inhibition as a Strategy to Overcome Resistance. *Sci Transl Med* (2020) 12(552):eaaw7843. doi: 10.1126/scitranslmed.aaw7843

124. Zhang P, Miska J, Lee-Chang C, Rashidi A, Panek WK, An S, et al. Therapeutic Targeting of Tumor-Associated Myeloid Cells Synergizes With Radiation Therapy for Glioblastoma. *Proc Natl Acad Sci USA* (2019) 116:23714–23. doi: 10.1073/pnas.1906346116

125. Cao M, Cabrera R, Xu Y, Liu C, Nelson D. Different Radiosensitivity of CD4 (+)CD25(+) Regulatory T Cells and Effector T Cells to Low Dose Gamma Irradiation In Vitro. *Int J Radiat Biol* (2011) 87(1):71–80. doi: 10.3109/09553002.2010.518208

126. Kachikwu EL, Iwamoto KS, Liao YP, DeMarco JJ, Agazaryan N, Economou JS, et al. Radiation Enhances Regulatory T Cell Representation. *Int J Radiat Oncol Biol Phys* (2011) 81(4):1128–35. doi: 10.1016/j.ijrobp.2010.09.034

127. Klug F, Prakash H, Huber PE, Seibel T, Bender N, Halama N, et al. Low-Dose Irradiation Programs Macrophage Differentiation to an Inos(+)/M1

128. Wang Y. Advances in Hypofractionated Irradiation-Induced Immunosuppression of Tumor Microenvironment. *Front Immunol* (2020) 11:612072. doi: 10.3389/fimmu.2020.612072

129. Gunderson AJ, Young KH. Exploring Optimal Sequencing of Radiation and Immunotherapy Combinations. *Adv Radiat Oncol* (2018) 3(4):494–505. doi: 10.1016/j.adro.2018.07.005

130. De Martino M, Daviaud C, Vanpouille-Box C. Radiotherapy: An Immune Response Modifier for Immuno-Oncology. *Semin Immunol* (2021) p:101474. doi: 10.1016/j.smim.2021.101474

131. Vanpouille-Box C, Diamond JM, Pilones KA, Zavadil J, Babb JS, Formenti SC, et al. Tgfbeta is a Master Regulator of Radiation Therapy-Induced Antitumor Immunity. *Cancer Res* (2015) 75(11):2232–42. doi: 10.1158/0008-5472.CAN-14-3511

132. Formenti SC, Lee P, Adams S, Goldberg JD, Li X, Xie MW, et al. Focal Irradiation and Systemic Tgfbeta Blockade in Metastatic Breast Cancer. *Clin Cancer Res* (2018) 24(11):2493–504. doi: 10.1158/1078-0432.CCR-17-3322

133. Formenti SC, Hawtin RE, Dixit N, Evensen E, Lee P, Goldberg JD, et al. Baseline T Cell Dysfunction by Single Cell Network Profiling in Metastatic Breast Cancer Patients. *J Immunother Cancer* (2019) 7(1):177. doi: 10.1186/s40425-019-0633-x

134. Rama N, Saha T, Shukla S, Goda C, Milewski D, Mascia AE, et al. Improved Tumor Control Through T-Cell Infiltration Modulated by Ultra-High Dose Rate Proton FLASH Using a Clinical Pencil Beam Scanning Proton System. *Int J Radiat Oncol Biol Phys* (2019) 105(1):S164–5. doi: 10.1016/j.ijrobp.2019.06.187

135. Montay-Gruel P, Acharya MM, Goncalves Jorge P, Petit B, Petridis IG, Fuchs P, et al. Hypofractionated FLASH-RT as an Effective Treatment Against Glioblastoma That Reduces Neurocognitive Side Effects in Mice. *Clin Cancer Res* (2021) 27(3):775–84. doi: 10.1158/1078-0432.CCR-20-0894

Involved Site Radiotherapy Extends Time to Premature Menopause in Infra-Diaphragmatic Female Hodgkin Lymphoma Patients – An Analysis of GHSG HD14- and HD17-Patients

Johannes Rosenbrock[1,2]*, Andrés Vásquez-Torres[1,2], Horst Mueller[3], Karolin Behringer[3,4], Matthias Zerth[1], Eren Celik[1,2], Jiaqi Fan[1,2], Maike Trommer[1,2], Philipp Linde[1,2], Michael Fuchs[3,4], Peter Borchmann[3,4], Andreas Engert[3,4], Simone Marnitz[1,2] and Christian Baues[1,2]

[1] Department of Radiation Oncology, CyberKnife and Radiation Therapy, Faculty of Medicine and University Hospital Cologne, University of Cologne, Cologne, Germany, [2] Radiation Therapy Reference Center of the German Hodgkin Study Group (GHSG), Faculty of Medicine and University Hospital Cologne, University of Cologne, Cologne, Germany, [3] German Hodgkin Study Group, Faculty of Medicine and University Hospital Cologne, University of Cologne, Cologne, Germany, [4] Department of Hematology and Oncology, Faculty of Medicine and University Hospital Cologne, University of Cologne, Cologne, Germany

Introduction: Consolidation radiotherapy in intermediate stage Hodgkin´s lymphoma (HL) has been the standard of care for many years as involved field radiotherapy (IFRT) after chemotherapy. It included initially involved region(s). Based on randomized studies, radiation volumes could be reduced and involved site radiation therapy (ISRT) became the new standard. ISRT includes the initially affected lymph nodes. In young adults suffering from HL, infertility and hypogonadism are major concerns. With regard to these questions, we analyzed the influence of modern radiotherapy concepts such as consolidating ISRT in infradiaphragmatic involvement of HL after polychemotherapy.

Patients and Methods: Five hundred twelve patients treated within German Hodgkin Study Group (GHSG) HD14 and HD17 trials were evaluated. We analyzed log-adjusted follicle-stimulating-hormone (FSH)- and luteinizing-hormone (LH)-levels of HD14-patients with infradiaphragmatic radiotherapy (IDRT) in comparison with HD14-patients, who had a supradiaphragmatic radiotherapy (SDRT). In a second step, we compared IFRT with ISRT of female HD17 patients regarding the effects on ovarian function and premature menopause.

Results: We analyzed FSH- and LH-levels of 258 female and 241 male patients, all treated with IFRT. Of these 499 patients, 478 patients had SDRT and 21 patients had IDRT. In a multiple regression model, we could show that log-adjusted FSH (p=0.0006) and LH values (p=0.0127) were significantly higher after IDRT than after SDRT. The effect of IDRT on gonadal function was comparable to two cycles of escalated bleomycin, etoposide, doxorubicin, cyclophosphamide, vincristine, procarbazine, and prednisone

(BEACOPPesc). We compared the effect of IFRT with ISRT in thirteen female HD17 patients with infradiaphragmatic (ID) involvement. The mean ovarian dose after ISRT was significantly lower than after IFRT. The calculated proportion of surviving non-growing follicles (NGFs) increased significantly from 11.87% to 24.48% in ISRT compared to IFRT, resulting in a significantly longer calculated time to menopause. The younger the age at therapy, the greater the absolute time gain until menopause.

Conclusion: Infradiaphragmatic IFRT impairs gonadal function to a similar extent as two cycles of BEACOPPesc. In comparison, the use of ISRT target volume definition significantly reduced radiation dose to the ovaries and significantly extends the time interval from treatment to premature menopause.

INTRODUCTION

Nowadays Hodgkin´s Lymphoma (HL) is a very well curable disease. Due to improved overall survival of more than 90% after 5 years for early stage HL (1–4) and even advanced stages (5, 6), reduction of long-term side effects became more and more important. Therefore, recent studies focused on de-escalation of both treatment modalities- radiotherapy (RT) and chemotherapy (1, 3). In the young adult population suffering from HL, infertility and hypogonadism are major concerns, which affect quality of life as well as life planning, desire to have children, and parenthood. Several studies have investigated the effects of chemotherapy and RT on infertility and hypogonadism in HL patients. However, whereas there are studies on current chemotherapy regimens (7–9), the studies on RT date back to the extended field radiotherapy (EFRT) era (10–13).

For the last two decades, consolidating RT in intermediate stage HL was performed as involved field radiotherapy (IFRT) and no longer as EFRT as part of the combined modality treatment (14). It included one or more initially involved regions after completion of polychemotherapy with two cycles of escalated bleomycin, etoposide, doxorubicin, cyclophosphamide, vincristine, procarbazine, and prednisone (BEACOPPesc) and two cycles of doxorubicin, vinblastine, dacarbazine, and bleomycin (ABVD) (2). Based on the ILROG (international Lymphoma Radiation Oncology Group) guidelines for target volume definition in HL involved site radiotherapy (ISRT) has been established since 2014 as new standard (4, 15, 16). Instead of irradiating the initially affected areas, only the initially affected lymph nodes with a margin dependent on the uncertainty in contouring are included in the ISRT target volume (15), which reduces the planning target volume by about half - at least in the case of supradiaphragmatic radiotherapy (SDRT) (17).

The observation of cancer childhood survivors showed that the testis (18) and the ovaries are very sensitive to RT (19–21). The high radiation sensitivity of the gonads has also been detected in adult cancer survivors (10–13, 22, 23). In case of irradiation of the ovaries, a certain percentage of follicles will survive depending on the applied dose, so that the time until the onset of ovarian insufficiency depends not only on the applied dose but also on the pre-existing ovarian reserve of the patient (24). Wallace et al. developed a model to calculate the survival fraction of non-growing follicles (NGF) as a function of dose. He showed that the median lethal dose (LD50), which destroys 50% of the NGF, is < 2Gy (25). Ovarian failure causes not only infertility but also premature menopause. This in turn can lead to increased cardiovascular risk (26, 27), osteoporosis (28) with a risk of bone fracture (29), and reduced quality of life (30).

In this study, we investigate the effects of radiotherapy on Infertility and Hypogonadisms in HL patients and the chance of reducing this impact by using ISRT.

PATIENTS AND METHODS

To evaluate the effects of infradiaphragmatic involved-field radiotherapy (IDRT), we analyzed hormone levels of German Hodgkin Study Group (GHSG) HD14-patients (**Figure 1**). In a second step, we compared IFRT and ISRT of female HD17-patients with regard to premature menopause.

Hormone Levels

In the HD-14 trial 1,528 patients with early unfavorable HL were included. The treatment consisted of either 4xABVD or 2xBEACOPPesc + 2xABVD (2 + 2-regime) followed by 30 Gy IFRT (2). Behringer et al. determined FSH, LH and AMH/Inhibin B-values of 1,323 patients, who had participated in the HD13-15-trials and had finished chemotherapy at least one year before. They included female patients who were younger than 40 years at the time of diagnosis and male patients who were younger than 50 years at the time of diagnosis but were still in remission and receiving no therapy other than the study medication (7).

To evaluate the effects of RT on gonadal function we compared FSH and LH values of HD-14 patients from this collective who received IDRT with the values of the patients
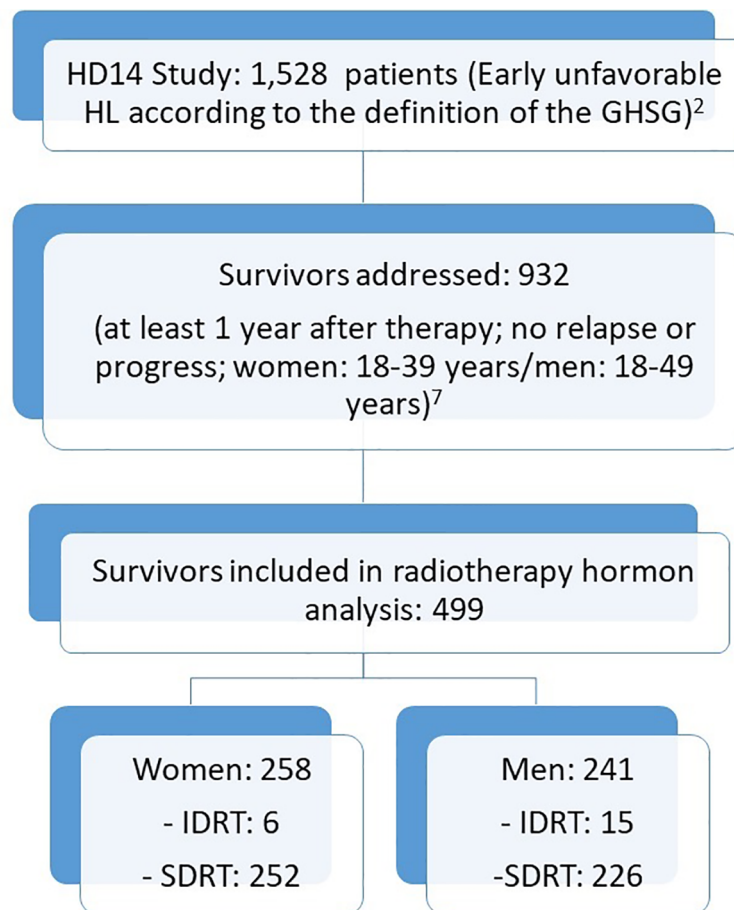
FIGURE 1 | Consort Diagram: hormone analysis.

radiated with SDRT. Patients from whom the information on irradiation, FSH and LH levels were available were considered.

Hormone Levels - Statistics

To achieve a normalized distribution of FSH and LH we took the natural logarithm of the hormone levels. We analyzed the effects of IDRT versus SDRT on log-transformed FSH value. For the analysis, we used a multiple regression model with adjustment for age, gender and chemotherapy (ABVD versus 2 + 2-regime) and computed best linear unbiased estimates to account additionally for the interaction between age and gender. We set the level of significance to 0.05, computed two-sided p values and used SAS 9.4 for the statistical analysis of hormones.

Comparison IFRT and ISRT

In the subsequent HD17-trial for early unfavorable HL, patients receive 2xBEACOPPesc + 2xABVD. After a post-chemotherapy PET-CT, patients were treated with IFRT in the standard am regardless of the PET-CT result. In the experimental arm, INRT was performed if the patient was PET-CT positive. If the PET-CT was negative, radiotherapy was omitted.

For our analysis, we chose female patients, who had provided us with both initial CT-Scans, pre-radiotherapy-CT-Scans, and who had no oophorectomy. For each patient we contoured an IFRT Planning Target Volume (PTV) in accordance with the definition of the GHSG and an ISRT-PTV according to the ILROG. We chose ISRT and not INRT due to the higher clinical relevance after the implementation of ISRT in several guidelines (15). We calculated for both PTVs a Volumetric Arc Therapy (VMAT)- plan with VARIAN Eclipse 13.6 and analyzed ovaries, uterus, small bowl, rectum, bladder, spinal cord and femoral heads as organs at risk (OAR).

Comparison IFRT and ISRT – Influence on Premature Menopause

Using Wallace's surviving percentage function (24) $log_{10} (g(z)) =$ $2–0.15z$, we calculated for each patient the percentage of NGF surviving the IFRT and ISRT (g = surviving NGF in %; z dose in Gray). For this, the dose-volume histograms (DVHs) of both ovaries together were analyzed with an interval width of 0.1 Gray and Wallace's survival function was applied to the resulting data:

$$g = \sum_{i=1}^{d_{max}} \left(10^{2-0.15 * \left(1/2 * (d_i + d_{i+1}) \right)} * \frac{v_i}{v_{both\ ovaries}} \right)$$

Based on a theoretical age at the beginning of therapy of 18 to 48 years in two-year steps, we calculated the expected time to menopause for each age and each resulting percentage of NGF. For this, we used Hansen's model (31) $log_{10}(n) = (-0.00019)*$ $(age\ in\ years)^{2.452} + 5.717$ to calculate an initial value for NGF for each age between 18 and 48 years. For each patient, we multiplied this baseline with the calculated percentage of surviving follicles after IFRT and ISRT to calculate the reproductive age using the Hansen model. According to Wallace (24), the time of menopause was determined by subtracting reproductive age of 50.4 years.

Comparison IRT and ISRT - Statistics

We compared the mean dose of the OARs, the mean of surviving NGFs and the mean of the time to menopause. Since the mean values of the examined parameters were not normally distributed and not symmetrically distributed, we used a sign test.

RESULTS

Hormone Levels

We analyzed FSH and LH levels of 258 female and 241 male HD-14 patients. Of 258 female patients, six women were treated with IDRT and 252 women with SDRT. Of 241 male patients, 15 men had been radiated with IDRT and 226 men with SDRT (**Table 1**).

Hormone levels were taken in mean at 41.4 months (Standard deviation 19.2 months) after RT was performed. **Tables 2A** and **2B** show FSH and LH values stratified by irradiation type and age.

Using a multiple regression model we found that the adjusted log values of FSH (FSH p= 0.0006) and LH (p= 0.0127) were significantly higher after IDRT than after SDRT. Apart from radiotherapy, type of chemotherapy, age and interaction of age and gender influenced hormone levels significantly (**Table 3**).

As the consequences of the multiple regression model in **Table 3** and especially the observed interaction effect are difficult to understand, we used the R package visreg (https://cran.r-project.org/web/packages/visreg/visreg.pdf) to visualize the consequences of the model for FSH levels (**Figure 2**). As shown in **Figure 2**, increased FSH values were present after IDRT and especially women were negatively affected. As the effects of infradiaphragmatic RT versus supradiaphragmatic RT and 2 + 2 versus ABVD were statistically coded in the same way, the similar regression coefficients (0.634 and 0.598) in **Table 3** correspond to comparable effect sizes. The combination of infradiaphragmatic RT and 2 + 2 causes significantly increased FSH values even in younger women. At the other side, males and their FSH levels are clearly less affected, even if heavily treated with 2 + 2, IDRT and in higher age.

TABLE 1 | Frequency of IDRT/SDRT.

	Female		Male		Total	
	N	%	N	%	N	%
IDRT	6	2.3	15	6.2	21	4.2
SDRT	252	97.7	226	93.8	478	95.8
Total	258	100.0	241	100.0	499	100.0

**TABLE 2A** | Hormone statistics in HD14 according to age group; Standard deviation (Std Dev).

	Original units, U/l				Log Transformed			
	Age < 30 years		Age ≥ 30 years		Age < 30 years		Age ≥ 30 years	
	Mean	Std Dev	Mean	Std Dev	Mean	Std Dev	Mean	Std Dev
FSH fem	6.0	4.6	16.1	23.7	1.3	1.2	1.9	1.5
FSH male	7.1	8.0	8.7	8.1	1.6	0.8	1.9	0.8
LH fem	6.0	7.9	11.1	13.5	1.0	1.6	1.6	1.6
LH male	5.3	3.0	5.4	3.5	1.5	0.5	1.5	0.6

TABLE 2B | Hormone statistics in HD14 according to SDRT vs. IDRT; Standard deviation (Std Dev).

	Original units, U/l				Log Transformed			
	SDRT		IDRT		SDRT		IDRT	
	Mean	Std Dev	Mean	Std Dev	Mean	Std Dev	Mean	Std Dev
FSH fem	11.9	19.3	17.3	10.0	1.7	1.4	2.5	1.1
FSH male	7.9	8.0	14.3	8.6	1.7	0.8	2.4	0.7
LH fem	8.9	11.9	11.9	8.4	1.4	1.6	2.2	0.9
LH male	5.2	3.4	7.1	3.2	1.5	0.6	1.9	0.5

TABLE 3 | Multiple regression model of log. FSH and log. LH (weighted least squares, 258 females and 241 males, best linear unbiased estimators).

	Log FSH		Log LH	
	regression coefficient	p-value	regression coefficient	p-value
Intercept	2.069	<.0001	1.624	<.0001
Age(z)	0.039	<.0001	0.033	<.0001
Sex(z)	0.101	0.0816	-0.036	0.7455
Age*Sex(z)	-0.040	0.0027	-0.056	0.0002
ABVD (vs. 2 + 2)	-0.634	<.0001	-0.243	0.0002
Infra- diaphragmatic RT fields (vs. upper fields)	0.598	0.0006	0.349	0.0127
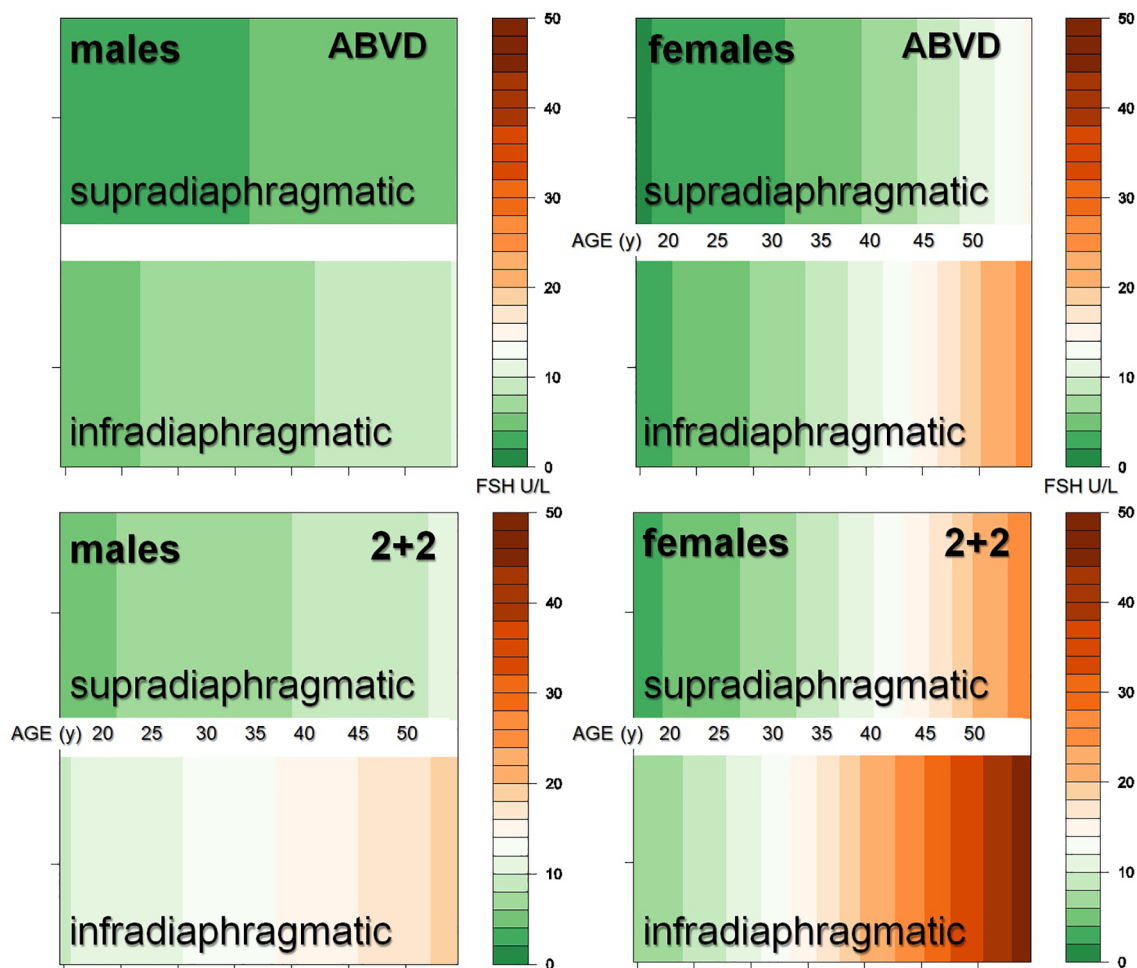
FIGURE 2 | FSH by RT-Field, chemotherapy, gender, and age as estimated in the multiple regression model of Table 3.

Comparison IFRT and ISRT

The imaging required for analysis was available for 13 HD17-patients, so that we were able to include these patients in the plan comparison. The initial involvement of the patients is shown in **Table 4**. We could show that in comparison with IFRT the use of ISRT significantly reduced the mean ovarian dose from 15.13 Gy to 7.44 Gy (**Table 5**).

The mean dose exposure in uterus decreased significantly from 14.51 Gy to 8.94 Gy. The mean dose in all other risk organs studied was also significantly lower with ISRT than with IFRT.

The proportion of surviving NGF increased significantly from 11,87% after IFRT to 24,48% using ISRT. Up to an age of 44 years, the calculated premature menopause occurs significantly

TABLE 4 | Initial nodal involvement.

Nodal involvement	N	%
Iliacal right	4	30.8
Inguinal right	4	30.8
Iliacal left	11	84.6
Inguinal left	10	76.9
paraaortic	9	69.2
Celiac	2	15.4
Mesenteric	4	30.8
Liver	0	0.0
Hepatic hilum	1	7.7
Spleen	0	0.0
Splenic hilum	0	0.0

later after ISRT than after IFRT (**Table 6** and **Figure 3**). After 44 years this difference is no longer significant.

DISCUSSION

By intensifying chemotherapy over the years, the HL specific mortality decreased. Current therapeutic strategies lead to 5-years OS-rates above 90-95% for early-stage favorable and unfavorable HL (1–4). Considering this, the toxicity of the combined modality treatment plays a crucial role and researcher are trying to reducing these long-term effects. An important step in the reduction of side effects in the context of radiotherapy, was the change from EFRT to IFRT and finally to ISRT. This gradual reduction of the RT fields led to a consecutive reduction of the irradiated volume and a lower exposure of the organs at risk. Especially in young HL-patients, hypogonadism and infertility are particularly important issues, which can be caused by chemotherapy or radiotherapy. The use of ISRT could help to reduce this particularly relevant toxicity.

We could show that log-adjusted FSH and LH values were significantly higher after infradiaphragmatic IFRT than after supradiaphragmatic IFRT. The negative effect of infra-diaphragmatic IFRT on gonadal function was comparable to the effect of two cycles of BEACOPPesc. Our comparison between IFRT and ISRT indicated that the mean ovarian dose was significantly lower and the calculated time to menopause was significantly longer after infradiaphragmatic ISRT than after

infradiaphragmatic IFRT. The younger the age at therapy, the greater the absolute time gain until menopause.

Our evaluation of the hormone levels of infradiaphragmatic IFRT treated HD14 patients confirms that women in particular have a high risk of premature onset of hypogonadism and the effect is comparable to the effect of 2 cycles of BEACOPPesc. These results correspond with the outcome of other groups. Van der Kaaij analyzed 460 female HL-survivors. Forty-one percent (11/27) of the patients treated with iliacal RT suffered from premature ovarian failure. However, all of them had also been treated with alkylating chemotherapy (10). De Bruin et al. calculated the cumulative risk for menopause at the age of 40 years by examining a collective of 549 women after HL-Therapy. Thirty-one women had been treated with RT only, which included the ovaries. Thirteen of these 31 patients developed a menopause before they had reached the age of 40 years (12). Moreover, our results fit well with the model designed by Wallace, in which the ovarian reserve after RT depends on two independent factors: dose and age (24).

A weakness of our analysis is the small number of patients who were irradiated infradiaphragmatic. On the other hand, the studies described in the literature are also based on very few patients, so that they were not statistically analyzed (10–13). Since we examined a well-defined collective of a clinical study, we were able to demonstrate a highly significant difference independent of the chemotherapy used, despite the small number of patients. Furthermore, our study is - to our knowledge - the first to investigate the effect of infra-diaphragmatic IFRT on gonadal function in post EFRT era.

Due to the proven high gonadal toxicity of infra-diaphragmatic IFRT, it is important to find ways to reduce it. Planning studies show that with supradiaphragmatic INRT/ISRT (17, 32, 33) and infradiaphragmatic ISRT (33) second malignancy risk is significantly lower than with IFRT. To date, however, no studies have investigated the effect of infra-diaphragmatic ISRT/INRT on fertility. Knowing the high gonadal toxicity of infradiaphragmatic IFRT in women, the evaluation of ISRT is of high importance.

To our knowledge, our study is the first, which investigated the opportunity of reducing gonadal toxicity by using ISRT for infradiaphragmatic HL involvement. Our results show that the mean dose in the ovaries is significantly lower

TABLE 5 | Organs at risk.

	Involved Field		Involved Site		p-value
	Mean	Standard deviation	Mean	Standard deviation	
Small bowel (D_{mean} in Gy)	13,29	1,52	7,88	2,65	<0.001
Bladder (D_{mean} in Gy)	11,67	3,56	8,74	3,36	0.003
Femoral head left (D_{mean} in Gy)	17,51	4,10	14,47	4,89	0.022
Femoral head right (D_{mean} in Gy)	9,40	7,23	5,02	5,13	<0.001
Rectum (D_{mean} in Gy)	10,03	4,01	6,44	3,48	<0.001
Spinal cord (D_{max} in Gy)	18.88	1.43	15.06	2.85	<0.001
Uterus (D_{mean} in Gy)	14,51	5,41	8,94	4,43	<0.001
Ovaries (D_{mean} in Gy)	15,13	6,34	7,44	5,64	<0.001
Surviving NGF (in %)	11,87	13,01	24,48	12,69	<0.001

TABLE 6 | Time to menopause.

Age, years	Involved Field Radiotherapy – time to menopause		Involved Site Radiotherapy – time to menopause		Time-Difference of Involved Field and Involved Site radiotherapy		p-value
	Mean, years	Standard deviation, years	Mean, years	Standard deviation, years	Mean, years	Standard deviation, years	
18	12.86	6.82	19.16	3.49	6.30	5.35	<0.001
20	12.13	6.56	18.19	3.33	6.06	5.18	<0.001
22	11.34	6.21	17.13	3.18	5.79	4.91	<0.001
24	10.49	5.82	15.97	3.03	5.48	4.57	<0.001
26	9.57	5.40	14.73	2.88	5.16	4.21	<0.001
28	8.59	4.96	13.42	2.73	4.83	3.84	<0.001
30	7.55	4.51	12.04	2.59	4.49	3.44	<0.001
32	6.45	4.06	10.60	2.46	4.15	3.05	<0.001
34	5.31	3.61	9.11	2.33	3.80	2.66	<0.001
36	4.12	3.18	7.57	2.21	3.45	2.30	<0.001
38	2.89	2.79	5.99	2.10	3.10	2.00	<0.001
40	1.72	2.38	4.37	2.00	2.65	1.68	<0.001
42	0.95	1.75	2.81	1.71	1.87	1.23	0.001
44	0.46	1.14	1.37	1.27	0.90	0.71	0.001
46	0.19	0.47	0.33	0.71	0.15	0.27	0.125
48	0.00	0.00	0.02	0.06	0.02	0.06	1.000

with ISRT than with IFRT and furthermore, the predicted percentage of surviving NGFs is significantly higher after ISRT. This is reflected in the clinically relevant time to premature menopause after RT. Using Wallace's survival model for NGFs (24) and Hansen's NGF model for age (31) we could demonstrate that the time to menopause is significantly longer after ISRT than after IFRT. This is particularly evident in younger women.

A limitation of our analysis is that we performed a plan comparison in only 13 patients. However, small numbers of patients are common in planning studies. Furthermore, we were able to demonstrate an advantage for ISRT in every single patient. A hormonal analysis of patients with IFRT versus

FIGURE 3 | Time to menopause by age and RT-Field; Boxplot (minimum, first quartile, median, third quartile, and maximum; Dots represent outliers greater or less than the 1.5 x interquartile range).

ISRT in a prospective study would certainly be preferable. However, since ISRT has meanwhile replaced IFRT as the standard, this would be difficult to realize.

A further weakness of our analyzed patient cohort was that patients had not received ovarian transposition prior to radiotherapy. Some studies have shown that oophoropexy can preserve ovarian function despite large-volume IDRT (34–36). However, in other publications, premature menopause could not be prevented by ovarian transposition (37, 38). One reason for this was possibly the scattered radiation, which in the case of paraaortic RT probably resulted in a relevant dose exposure to the ovaries despite oophoropexy. This is especially true for modern irradiation techniques such as VMAT, as the irradiation is not strictly appa oriented. This results in optimized dose coverage of the target volume, but at the cost of some low-dose exposure in the area of the organs at risk, and in this case, the ovaries. Therefore, the combination of ISRT and oophoropexy may lead to the necessary reduction of the ovarian dose.

Furthermore, the use of ISRT reduced significantly the mean dose of the uterus. Studies of childhood cancer survivors have reported that radiation of the uterus in childhood can lead to severe dysfunction (39, 40). In adults, pregnancies following pelvic radiation are very rare and only few case of successful pregnancies after RT have been reported (41). Accordingly, a premenopausal irradiated uterus presents on MRI imaging similar to a postmenopausal uterus (42). Overall, it is assumed that irradiation of the uterus can lead to infertility, miscarriages, premature births, and low birth weight even in adult women (43). This is caused by damage to the endometrium, which impedes implantation of the ovum, damage to the uterine vessels and fibrosis of the myometrium, which cause growth retardation and thus early abortion (43). Besides the low ovarian dose, the significant reduction of the uterine dose makes pregnancy more likely after ISRT compared to IFRT.
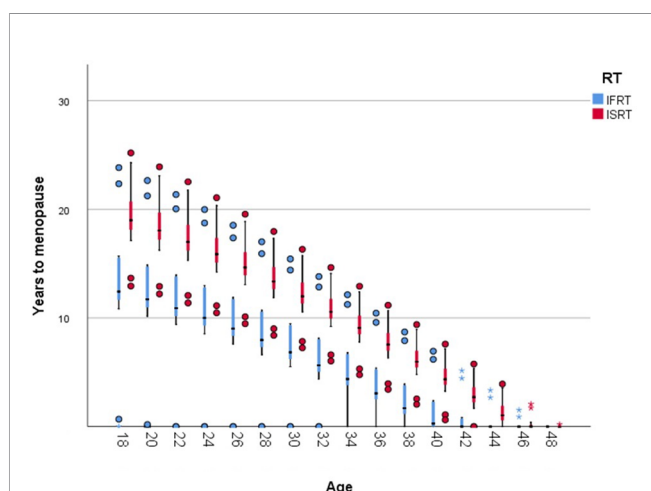
Therefore, we assume that the positive effect of oophoropexy on fertility can be further enhanced by ISRT.

In summary, the use of ISRT prolongs the time to early menopause. Since premature menopause can lead to increased cardiovascular risk (26, 27) and osteoporosis (28, 29), it can be supposed that these effects can be reduced by the use of ISRT. Furthermore, due to the less reduced ovarian reserve and the lower uterine dose, it can be assumed that the probability of pregnancy after infradiaphragmatic ISRT is clinically relevant higher than after infradiaphragmatic IFRT.

Another point to be discussed is the early onset of menopause in many women after chemotherapy. This could be an indication that the sparing of the ovaries during radiation may not seem to be so relevant. However, Behringer et al. reported that compared to 6-8 cycles of BEACOPPesc after the 2 + 2-regime and especially after ABVD, there are fewer limitations of gonadal function (7). In another analysis by Behringer et al, the 2 + 2 regimen and ABVD did not differ in terms of pregnancies, offspring, amenorrhea, and menopausal symptoms. After adjustment for age, there was no difference between the patients analyzed and the general German population in terms of motherhood rates (8). Nevertheless, we could show that especially the combination of the 2 + 2 regimen and infradiaphragmatic IFRT leads to a significant reduction of ovarian reserve even in young women. Therefore, especially in the early favorable and early unfavorable stage, ovarian sparing should be aimed at.

In conclusion, we demonstrated that the long-term effects of infradiaphragmatic IFRT on ovarian function are comparable to the effects of BEACOPP$_{esc}$ in the 2 + 2 regimen and the combination of both causes early menopause even in young women. Therefore, optimal sparing of the ovaries should always be performed in the combined modality treatment. In addition, we have been able to report how large the effect of an optimized target volume definition is. By using ISRT, a significant reduction of the radiotherapy volume can be achieved, which plays a crucial role with regard to the improved sparing of the ovaries and the consecutive ovarian function. It is assumed that in the future immunotherapy will play a greater role in the primary therapy of HL and this will lead to reduced toxicity of systemic therapy while maintaining the prognosis in early and intermediate stages of HL. Therefore, in the future, even more attention should be paid to the protection of the ovaries during consolidative radiotherapy.

DATA AVAILABILITY STATEMENT

The raw data supporting the conclusions of this article will be made available by the authors, without undue reservation.

ETHICS STATEMENT

The studies involving human participants were reviewed and approved by Ethikkommission Köln. The patients/participants provided their written informed consent to participate in this study.

AUTHOR CONTRIBUTIONS

JR and CB conceived and designed the study. JR, AV-T, CB, and MZ performed the data collection. HM and JR performed the statistical analysis. All authors wrote the manuscript. All authors contributed to the article and approved the submitted version.

FUNDING

REFERENCES

1. Fuchs M, Goergen H, Kobe C, Kuhnert G, Lohri A, Greil R, et al. Positron Emission Tomography–Guided Treatment in Early-Stage Favorable Hodgkin Lymphoma: Final Results of the International, Randomized Phase Iii HD16 Trial by the German Hodgkin Study Group. JCO (2019) 37:2835–45. doi: 10.1200/JCO.19.00964

2. von Tresckow B, Plütschow A, Fuchs M, Klimm B, Markova J, Lohri A, et al. Dose-Intensification in Early Unfavorable Hodgkin's Lymphoma: Final Analysis of the German Hodgkin Study Group HD14 Trial. JCO (2012) 30:907–13. doi: 10.1200/JCO.2011.38.5807

3. Behringer K, Goergen H, Hitz F, Zijlstra JM, Greil R, Markova J, et al. Omission of Dacarbazine or Bleomycin, or Both, From the ABVD Regimen in Treatment of Early-Stage Favourable Hodgkin's Lymphoma (GHSG HD13): An Open-Label, Randomised, non-Inferiority Trial. Lancet (2015) 385:1418–27. doi: 10.1016/S0140-6736(14)61469-0

4. André MPE, Girinsky T, Federico M, Reman O, Fortpied C, Gotti M, et al. Early Positron Emission Tomography Response–Adapted Treatment in Stage I and II Hodgkin Lymphoma: Final Results of the Randomized Eortc/Lysa/Fil H10 Trial. JCO (2017) 35:1786–94. doi: 10.1200/JCO.2016.68.6394

5. Engert A, Haverkamp H, Kobe C, Markova J, Renner C, Ho A, et al. Reduced-Intensity Chemotherapy and PET-guided Radiotherapy in Patients With Advanced Stage Hodgkin's Lymphoma (HD15 Trial): A Randomised, Open-Label, Phase 3 non-Inferiority Trial. Lancet (2012) 379:1791–9. doi: 10.1016/S0140-6736(11)61940-5

6. Borchmann P, Goergen H, Kobe C, Lohri A, Greil R, Eichenauer DA, et al. PET-Guided Treatment in Patients With Advanced-Stage Hodgkin's Lymphoma (HD18): Final Results of an Open-Label, International, Randomised Phase 3 Trial by the German Hodgkin Study Group. Lancet (2017) 390:2790–802. doi: 10.1016/S0140-6736(17)32134-7

7. Behringer K, Mueller H, Goergen H, Thielen I, Eibl AD, Stumpf V, et al. Gonadal Function and Fertility in Survivors After Hodgkin Lymphoma Treatment Within the German Hodgkin Study Group HD13 to HD15 Trials. JCO (2013) 31:231–9. doi: 10.1200/JCO.2012.44.3721

8. Behringer K, Thielen I, Mueller H, Goergen H, Eibl AD, Rosenbrock J, et al. Fertility and Gonadal Function in Female Survivors After Treatment of Early Unfavorable Hodgkin Lymphoma (HL) Within the German Hodgkin Study Group HD14 Trial. Ann Oncol (2012) 23:1818–25. doi: 10.1093/annonc/mdr575

9. Gaudio F, Nardelli C, Masciandaro P, Perrone T, Laddaga FE, Curci P, et al. Pregnancy Rate and Outcome of Pregnancies in Long-Term Survivors of

Hodgkin's Lymphoma. *Ann Hematol* (2019) 98:1947–52. doi: 10.1007/s00277-019-03684-0

10. van der Kaaij MAE, Heutte N, Meijnders P, Abeilard-Lemoisson E, Spina M, Moser EC, et al. Premature Ovarian Failure and Fertility in Long-Term Survivors of Hodgkin's Lymphoma: A European Organisation for Research and Treatment of Cancer Lymphoma Group and Groupe D'Étude Des Lymphomes De L'adulte Cohort Study. *JCO* (2012) 30:291–9. doi: 10.1200/JCO.2011.37.1989

11. Swerdlow AJ, Cooke R, Bates A, Cunningham D, Falk SJ, Gilson D, et al. Risk of Premature Menopause After Treatment for Hodgkin's Lymphoma. *JNCI: J Natl Cancer Inst* (2014) 106:dju207. doi: 10.1093/jnci/dju207

12. De Bruin ML, Huisbrink J, Hauptmann M, Kuenen MA, Ouwens GM, van't Veer MB, et al. Treatment-Related Risk Factors for Premature Menopause Following Hodgkin Lymphoma. *Blood* (2008) 111:101–8. doi: 10.1182/blood-2007-05-090225

13. Haukvik UKH, Dieset I, Bjøro T, Holte H, Fosså SD. Treatment-Related Premature Ovarian Failure as a Long-Term Complication After Hodgkin's Lymphoma. *Ann Oncol* (2006) 17:1428–33. doi: 10.1093/annonc/mdl149

14. Engert A, Schiller P, Josting A, Herrmann R, Koch P, Sieber M, et al. Involved-Field Radiotherapy is Equally Effective and Less Toxic Compared With Extended-Field Radiotherapy After Four Cycles of Chemotherapy in Patients With Early-Stage Unfavorable Hodgkin's Lymphoma: Results of the HD8 Trial of the German Hodgkin's Lymphoma Study Group. *JCO* (2003) 21:3601–8. doi: 10.1200/JCO.2003.03.023

15. Specht L, Yahalom J, Illidge T, Berthelsen AK, Constine LS, Eich HT, et al. Modern Radiation Therapy for Hodgkin Lymphoma: Field and Dose Guidelines From the International Lymphoma Radiation Oncology Group (Ilrog). *Int J Radiat Oncol Biol Phys* (2014) 89:854–62. doi: 10.1016/j.ijrobp.2013.05.005

16. Maraldo MV, Aznar MC, Vogelius IR, Petersen PM, Specht L. Involved Node Radiation Therapy: An Effective Alternative in Early-Stage Hodgkin Lymphoma. *Int J Radiat Oncol Biol Phys* (2013) 85:1057–65. doi: 10.1016/j.ijrobp.2012.08.041

17. Murray L, Sethugavalar B, Robertshaw H, Bayman E, Thomas E, Gilson D, et al. Involved Node, Site, Field and Residual Volume Radiotherapy for Lymphoma: A Comparison of Organ at Risk Dosimetry and Second Malignancy Risks. *Clin Oncol* (2015) 27:401–10. doi: 10.1016/j.clon.2015.03.005

18. Sklar CA, Robison LL, Nesbit ME, Sather HN, Meadows AT, Ortega JA, et al. Effects of Radiation on Testicular Function in Long-Term Survivors of Childhood Acute Lymphoblastic Leukemia: A Report From the Children Cancer Study Group. *J Clin Oncol* (1990) 8:1981–7. doi: 10.1200/JCO.1990.8.12.1981

19. Wallace WHB, Shalet SM, Crowne EC, Morris-Jones PH, Gattamaneni HR. Ovarian Failure Following Abdominal Irradiation in Childhood: Natural History and Prognosis. *Clin Oncol* (1989) 1:75–9. doi: 10.1016/S0936-6555(89)80039-1

20. Hamre MR, Robison LL, Nesbit ME, Sather HN, Meadows AT, Ortega JA, et al. Effects of Radiation on Ovarian Function in Long-Term Survivors of Childhood Acute Lymphoblastic Leukemia: A Report From the Childrens Cancer Study Group. *JCO* (1987) 5:1759–65. doi: 10.1200/JCO.1987.5.11.1759

21. Thibaud E, Rodriguez-Macias K, Trivin C, Espérou H, Michon J, Brauner R. Ovarian Function After Bone Marrow Transplantation During Childhood. *Bone Marrow Transplant* (1998) 21:287–90. doi: 10.1038/sj.bmt.1701075

22. Yau I, Vuong T, Garant A, Ducruet T, Doran P, Faria S, et al. Risk of Hypogonadism From Scatter Radiation During Pelvic Radiation in Male Patients With Rectal Cancer. *Int J Radiat Oncol Biol Phys* (2009) 74:1481–6. doi: 10.1016/j.ijrobp.2008.10.011

23. Dueland S, Grønlie Guren M, Rune Olsen D, Poulsen JP, Magne Tveit K. Radiation Therapy Induced Changes in Male Sex Hormone Levels in Rectal Cancer Patients. *Radiother Oncol* (2003) 68:249–53. doi: 10.1016/S0167-8140(03)00120-8

24. Wallace WHB, Thomson AB, Saran F, Kelsey TW. Predicting Age of Ovarian Failure After Radiation to a Field That Includes the Ovaries. *Int J Radiat Oncol Biol Phys* (2005) 62:738–44. doi: 10.1016/j.ijrobp.2004.11.038

25. Wallace WHB, Thomson AB, Kelsey TW. The Radiosensitivity of the Human Oocyte. *Hum Reprod* (2003) 18:117–21. doi: 10.1093/humrep/deg016

26. Lobo RA. Surgical Menopause and Cardiovascular Risks. *Menopause* (2007) 14:562–6. doi: 10.1097/gme.0b013e318038d333

27. Roeters van Lennep JE, Heida KY, Bots ML, Hoek A. On Behalf of the Collaborators of the Dutch Multidisciplinary Guideline Development Group on Cardiovascular Risk Management After Reproductive Disorders. Cardiovascular Disease Risk in Women With Premature Ovarian Insufficiency: A Systematic Review and Meta-Analysis. *Eur J Prev Cardiolog* (2016) 23:178–86. doi: 10.1177/2047487314556004

28. Hadjidakis DJ, Kokkinakis EP, Sfakianakis ME, Raptis SA. Bone Density Patterns After Normal and Premature Menopause. *Maturitas* (2003) 44:279–86. doi: 10.1016/S0378-5122(03)00040-9

29. Gallagher JC. Effect of Early Menopause on Bone Mineral Density and Fractures. *Menopause* (2007) 14:567–71. doi: 10.1097/gme.0b013e31804c793d

30. Liao KLM, Wood N, Conway GS. Premature Menopause and Psychological Well-Being. *J Psychosom Obstet Gynecol* (2000) 21:167–74. doi: 10.3109/01674820009075624

31. Hansen KR, Knowlton NS, Thyer AC, Charleston JS, Soules MR, Klein NA. A New Model of Reproductive Aging: The Decline in Ovarian Non-Growing Follicle Number From Birth to Menopause. *Hum Reprod* (2008) 23:699–708. doi: 10.1093/humrep/dem408

32. Mazonakis M, Lyraraki E, Damilakis J. Second Cancer Risk Assessments After Involved-Site Radiotherapy for Mediastinal Hodgkin Lymphoma. *Med Phys* (2017) 44:3866–74. doi: 10.1002/mp.12327

33. Kourinou KM, Mazonakis M, Lyraraki E, Papadaki Hα, Damilakis J. Probability of Carcinogenesis Due to Involved Field and Involved Site Radiation Therapy Techniques for Supra- and Infradiaphragmatic Hodgkin's Disease. *Physica Med* (2019) 57:100–6. doi: 10.1016/j.ejmp.2018.12.036

34. Le Floch O, Donaldson SS, Kaplan HS. Pregnancy Following Oophoropexy and Total Nodal Irradiation in Women With Hodgkin's Disease. *Cancer* (1976) 38:2263–8. doi: 10.1002/1097-0142(197612)38:6<2263::aid-cncr2820380612>3.0.co;2-s

35. Clough KB, Goffinet F, Labib A, Renolleau C, Campana F, de la Rochefordiere A, et al. Laparoscopic Unilateral Ovarian Transposition Prior to Irradiation: Prospective Study of 20 Cases. *Cancer* (1996) 77:2638–45. doi: 10.1002/(SICI)1097-0142(19960615)77:12<2638::AID-CNCR30>3.0.CO;2-R

36. Al-Badawi IA, Al-Aker M, AlSubhi J, Salem H, Abduljabbar A, Balaraj K, et al. Laparoscopic Ovarian Transposition Before Pelvic Irradiation: A Saudi Tertiary Center Experience. *Int J Gynecol Cancer* (2010) 20:1082–6. doi: 10.1111/IGC.0b013e3181e2ace5

37. Fernandez-Pineda I, Davidoff AM, Lu L, Rao BN, Wilson CL, Srivastava DK, et al. Impact of Ovarian Transposition Before Pelvic Irradiation on Ovarian Function Among Long-Term Survivors of Childhood Hodgkin Lymphoma: A Report From the St. Jude Lifetime Cohort Study. *Pediatr Blood Cancer* (2018) 65:e27232. doi: 10.1002/pbc.27232

38. Thomas PR, Winstanly D, Peckham MJ, Austin DE, Murray MA, Jacobs HS. Reproductive and Endocrine Function in Patients With Hodgkin's Disease: Effects of Oophoropexy and Irradiation. *Br J Cancer* (1976) 33:226–31. doi: 10.1038/bjc.1976.29

39. Larsen EC, Schmiegelow K, Rechnitzer C, Loft A, Müller J, Nyboe Andersen A. Radiotherapy at a Young Age Reduces Uterine Volume of Childhood Cancer Survivors: Uterine Size in Childhood Cancer Survivors. *Acta Obstetricia Gynecol Scand* (2004) 83:96–102. doi: 10.1111/j.1600-0412.2004.00332.x

40. Signorello LB, Cohen SS, Bosetti C, Stovall M, Kasper CE, Weathers RE, et al. Female Survivors of Childhood Cancer: Preterm Birth and Low Birth Weight Among Their Children. *JNCI: J Natl Cancer Inst* (2006) 98:1453–61. doi: 10.1093/jnci/djj394

41. Köhler C, Marnitz S, Biel P, Cordes T. Successful Delivery in a 39-Year-Old Patient With Anal Cancer After Fertility-Preserving Surgery Followed by Primary Chemoradiation and Low Anti-Mullerian Hormone Level. *Oncology* (2016) 91:295–8. doi: 10.1159/000449416

42. Arrivé L, Chang YC, Hricak H, Brescia RJ, Auffermann W, Quivey JM. Radiation-Induced Uterine Changes: MR Imaging. *Radiology* (1989) 170:55–8. doi: 10.1148/radiology.170.1.2909120

43. Teh WT, Stern C, Chander S, Hickey M. The Impact of Uterine Radiation on Subsequent Fertility and Pregnancy Outcomes. *BioMed Res Int* (2014) 2014:1–8. doi: 10.1155/2014/482968

Graphene-Induced Hyperthermia (GIHT) Combined With Radiotherapy Fosters Immunogenic Cell Death

Malgorzata J. Podolska[1,2], Xiaomei Shan[1,2], Christina Janko[3], Rabah Boukherroub[4], Udo S. Gaipl[5], Sabine Szunerits[4], Benjamin Frey[5] and Luis E. Muñoz[1,2]*

[1] Department of Internal Medicine 3 - Rheumatology and Immunology, Friedrich-Alexander-University of Erlangen-Nürnberg (FAU), Universitätsklinikum Erlangen, Erlangen, Germany, [2] Deutsches Zentrum für Immuntherapie (DZI), Friedrich-Alexander-University Erlangen-Nürnberg and Universitätsklinikum Erlangen, Erlangen, Germany, [3] Department of Otorhinolaryngology, Head and Neck Surgery, Section of Experimental Oncology and Nanomedicine (SEON), Else Kröner-Fresenius-Stiftung Professorship, Universitätsklinikum Erlangen, Erlangen, Germany, [4] Univ. Lille, CNRS, Centrale Lille, Univ. Polytechnique Hauts-de-France, UMR 8520-IEMN, Lille, France, [5] Translational Radiobiology, Department of Radiation Oncology, Universitätsklinikum Erlangen, Friedrich-Alexander-Universität Erlangen-Nürnberg (FAU), Erlangen, Germany

Radiotherapy and chemotherapy are the standard interventions for cancer patients, although cancer cells often develop radio- and/or chemoresistance. Hyperthermia reduces tumor resistance and induces immune responses resulting in a better prognosis. We have previously described a method to induce tumor cell death by local hyperthermia employing pegylated reduced graphene oxide nanosheets and near infrared light (graphene-induced hyperthermia, GIHT). The spatiotemporal exposure/release of heat shock proteins (HSP), high group mobility box 1 protein (HMGB1), and adenosine triphosphate (ATP) are reported key inducers of immunogenic cell death (ICD). We hypothesize that GIHT decisively contributes to induce ICD in irradiated melanoma B16F10 cells, especially in combination with radiotherapy. Therefore, we investigated the immunogenicity of GIHT alone or in combination with radiotherapy in melanoma B16F10 cells. Tumor cell death *in vitro* revealed features of apoptosis that is progressing fast into secondary necrosis. Both HSP70 and HMGB1/DNA complexes were detected 18 hours post GIHT treatment, whereas the simultaneous release of ATP and HMGB1/DNA was observed only 24 hours post combined treatment. We further confirmed the adjuvant potential of these released DAMPs by immunization/challenge experiments. The inoculation of supernatants of cells exposed to sole GIHT resulted in tumor growth at the site of inoculation. The immunization with cells exposed to sole radiotherapy rather fostered the growth of secondary tumors *in vivo*. Contrarily, a discreet reduction of secondary tumor volumes was observed in mice immunized with a single dose of cells and supernatants treated with the combination of GIHT and irradiation. We propose the simultaneous release of several DAMPs as a potential mechanism fostering anti-tumor immunity against previously irradiated cancer cells.

Keywords: reduced graphene oxide, immunogenic cell death, hyperthermia, multimodal, radiotherapy, melanoma

INTRODUCTION

Every anti-tumor therapy aims to induce immunogenic cell death (ICD), which favors the development of specific anti-tumor responses. The spatiotemporal exposure of calreticulin on the outer leaflet of the plasma membrane (1, 2), the secretion of ATP (3, 4), and the release of DAMPs such as HMGB1 (4–6), heat shock protein 70 (HSP70) (7, 8) and HSP90 (4, 9) are essential organic adjuvants required to induce ICD. These signals are recognized by various pattern recognition receptors on antigen presenting cells facilitating their activation and migration to draining lymph nodes followed by induction of potent adaptive immune response (10). The presence of one of the organic adjuvants is not sufficient to induce proper immune reactions and must be accompanied by additional signals. We have postulated that the release from dead cells of both 'find-me' (ATP) and danger signals (HMGB1 and HSP90) is enough to support robust immune responses, whereas when only one of the adjuvants concurs, anti-tumor immunity fails (4). Some mediators released by dying cells, such as Prostaglandin E2 or adenosine, show immunosuppressive features contributing to the tolerance (11, 12) and growth of tumor cells (13).

Besides sensitizing tumor cells to radio- and chemotherapy (14), hyperthermia has been demonstrated to have a direct cell killing effect (apoptosis or necrosis) in both *in vitro* and *in vivo* conditions (15–17). This is achieved by the denaturation and aggregation of intracellular proteins that are not seen in the case of radio- or chemotherapies (18–22). Temperatures above 44°C cause extensive cell damage due to sudden protein aggregation and result in necrosis, whereas apoptosis is usually elicited in the case of moderate hyperthermia (i.e., 41.5°C) (23, 24). There are hints that the mode of action inducing the heat has a decisive effect on the cell death (25). Nuclear proteins and components of the Mre11-Rad50-Nbs1 complex orchestrating the repair of double strand breaks in DNA are the most prone to heat-induced degradation (26–29). Hence, the energy dose (temperature) and time jointly orchestrate the systemic outcome. This means that the generation and control of the heat are essential parameters to be modulated. With the lack of instruments assuring homogenous heat dispersion, profound damage can be induced to the surrounding tissues. The prevention of the latter and targeting invisible metastasis are the main challenges of this field and are still under development. Although shrinking tumors, sole hyperthermia cannot substitute any actual therapy (30). Nevertheless, hyperthermia is undoubtedly sensitizing tumor cells for further treatments (25, 31–33).

Gamma irradiation induces irreversible double-strand DNA breaks leading to apoptotic cell death. Dying tumor cells *in vivo* are sensed by the immune system propagating predominantly tolerogenic messages (34–36). Whether hyperthermia complementing radiotherapy results in ICD has not been investigated in-depth yet. We have recently shown that PEGylated reduced graphene oxide nanosheets (rGO-PEG) are biocompatible, non-toxic, and can be used for intravenous application to induce fine-tuned localized hyperthermia by application of near infrared radiation (37). We demonstrate herein that tumor cells killed by the combination of gamma irradiation and hyperthermia release several DAMPs in a fashion that renders dead B16F10 melanoma cells immunogenic.

MATERIALS AND METHODS

Gamma Irradiation (X rays)

B16F10 melanoma cells derived from the C57BL/6 mouse (ATCC, #CRL-6475) were exposed to ionizing irradiation (20 Gy, 120 kV, 22.7 mA; GE Inspection Technologies, Germany).

Graphene-Induced Hyperthermia (GIHT)

B16F10 melanoma cells were exposed to GIHT as described before (37). The cells were seeded in 24-well flat-bottom culture plates (2×10^5 cells/well). Next, graphene nanosheets (50 µg/ml) were placed in transwell inserts (0.4 µm pores) in close proximity to the cells, and plates were exposed to near-infrared irradiation (NIR, 960 nm, 1 hour, 2 W/cm^2) applied by Hydrosun®750 (Hydrosun Medizintechnik, Müllheim, Germany). The lower compartment's temperature was registered every 10 s with a Voltcraft K204 Thermometer (Voltcraft, Wollerau, Switzerland) and a high sensitive "in-well" temperature probe.

Flow Cytometric Analysis of Cell Death

The supernatants (SNs) containing detached B16F10 melanoma cells treated with X-ray irradiation, GIHT, or a combination of both were collected 24 hours post treatment into polypropylene tubes. Remaining adherent cells were exposed to trypsin-EDTA solution for 5 min at room temperature (RT), and detached cells were added to their corresponding SN fractions. Cells kept at 37°C and 5% CO_2 served as control of cell death and normal cell turnover. Harvested cells were centrifuged at 300×g for 5 min, and a morpho-physiological characterization of cell death by flow cytometry measurement was performed as described before (38). Briefly, the cells were resuspended in a four-color staining solution containing 1 µg/ml of Annexin A5 (AxA5)-FITC (ImmunoTools, Friesoythe, Germany), 100 ng/ml of PI (Sigma-Aldrich, Taufkirchen, Germany), 10 nM 1,1′,3,3,3′,3′-hexamethylindodicarbo - cyanine iodide (DiIc1(5), Enzo Life Sciences, Lörrach, Germany), 1 µg/ml of Hoechst 33342 (Thermo Fisher Scientific Inc., Waltham, USA) in Ringer's solution for 30 min at RT followed by acquisition on Gallios flow cytometer and analysis with the software Kaluza 2.1.

Detection of Danger Signals

Plates containing treated B16F10 melanoma cells and specified controls were centrifuged at 300xg for 5 min at the indicated time points, and the SNs were collected. The release of ATP from B16F10 melanoma cells was detected with the 'Luminescent ATP Detection Assay Kit' (Abcam, Cambridge, UK). ATP degradation was prevented by the provided lysis buffer. Luminescence measurements were performed on a Centro LB960 luminometer. HMGB1 and HSP70 were detected with the HMGB1 ELISA Kit II (IBL International, Hamburg, Germany) and DuoSet IC Kit (R&D Systems (Minneapolis, USA), respectively, according to the manufacturer's instructions. For the measurement of absorbance, an ELISA Microplate Reader and the software Magellan 7.1 SP1 were used.

Splenocytes Isolation and Staining

Briefly, Balb/c mice were sacrificed, and dissected spleens were pressed through a 70 μm cell strainer washed with ice-cold PBS. Collected cells were centrifuged at 300xg for 5 min at 4°C. Erythrocytes were lysed with erythrocytes lysis buffer for 2 min, followed by centrifugation at 300xg for 5 min at 4°C. Splenocytes proliferation was detected with the CellTrace™ CFSE Cell Proliferation Kit (Thermo Fisher Scientific, Rockford, USA) employed according to the manufacturer's instructions. In brief, splenocytes (10e6 cells/ml) were incubated in 5 μM staining solution for 20 min at RT. Excessive dye was removed by adding the medium with 10% serum for 5 min at RT. Next, labeled cells were centrifuged at 300xg for 5 min and were employed in further experiments.

Dendritic Cell Generation and Activation

Femora and tibia bones from sacrificed C57BL/6 mice were sterilized in 70% ethanol. Next, bone marrow was washed out with a needle (0.4 mm x 19 mm) into ice-cold medium. Collected cells were filtered through a 70 μm cell strainer and centrifuged at 300xg for 5 min at 4°C. Bone marrow-derived cells were differentiated with a complete cell culture medium containing 4 ng/ml of GM-CSF (ImmunoTools, Friesoythe, Germany) and 10 ng/ml IL-4 (ImmunoTools, Friesoythe, Germany) for 7 days. On days 3 and 5, a fresh DCs medium was added. DC cultures were treated with 100 μl of SNs from B16F10 melanoma cells treated with X-ray irradiation, GIHT, or a combination of both for 24 hours at 37°C and 5% CO_2. The expression of co-stimulatory molecules on DCs was confirmed after the conditioning treatment by flow cytometry using the following antibodies anti-mouse MHC II (1:600, Biolegend, San Diego, USA), anti-mouse CD11c (1:800, Biolegend, San Diego, USA), CD40 (1:800, Biolegend, San Diego, USA), CD86 (1:400, Biolegend, San Diego, USA).

T Cell Activation and Proliferation

Conditioned DCs were irradiated (20 Gy) and co-incubated with CFSE-stained splenocytes for four days, at 37°C and 5% CO_2. After 4 days splenocytes were stained with anti-mouse CD3 (1:400, Thermo Fisher Scientific, Rockford, USA), anti-mouse CD4 (1:600, Biolegend, San Diego, USA), and anti-mouse CD8 (1:800, Biolegend, San Diego, USA) antibodies added for 30 min at RT in the dark and analyzed with Gallios flow cytometer and the software Kaluza 2.1. The mean fluorescence intensity (MFI) of T cells exposed to unprimed DCs was used as the maximal signal to calculate the dilution of the dye induced by proliferation. The average number of divisions (division index) was obtained by dividing the maximal MFI signal by the signal obtained from T cells exposed to DCs pre-incubated with the indicated conditions.

Mice

All mice experiments were conducted in full agreement with institutional guidelines on animal welfare and with the approval of the local Animal Care and Use Committees of the University Erlangen-Nürnberg and the 'Regierung von Unterfranken' [Allowance numbers TS-12/2015 (bone marrow cells and splenocytes); 55.2 DMS-2532-2-103 (airpouch model); 54-2532.1-6/12 (tumor growth)].

Air-Pouch Model

Briefly, 5 mL of sterile air was injected subcutaneously in the back of previously anesthetized mice (isofluorane). The air formed a cavity between the skin and the fascia of the back of the thorax. This cavity was stabilized with 3 ml of sterile air after three days. After five days the cellular membrane formed allows the study and quantification of infiltrating leukocytes. On day five, 5 mL of supernatants collected 24 hours post-treatment from B16F10 melanoma cells treated with X-ray irradiation, GIHT, or a combination of both were injected into airpouches. After 24 hours, the mice were sacrificed, and the lavage of pouches was collected. Lavages were centrifuged for 5 min at 300x g and stained for 30 min at room temperature in the dark with the following antibodies: α-ms CD45 (Biolegend, San Diego, USA), α-ms CCR3 (Biolegend, San Diego, USA), α-ms CD11b (Thermo Fisher Scientific, Rockford, USA), α-ms Ly-6C (Biolegend, San Diego, USA), α-ms Ly-6G (Biolegend, San Diego, USA), α-ms CD170 (Siglec-F) (Biolegend, San Diego, USA), α-ms CD115 (Biolegend, San Diego, USA), α-ms F4/80 (Biolegend, San Diego, USA). Fluorescence was measured on a Gallios cytofluorometer, and data analysis was performed with the software Kaluza 2.1 Following populations were distinguished: inflammatory monocytes (CD45pos CD11bpos Ly6Chigh Ly6Gneg CCR3neg SiglecFneg), anti-inflammatory monocytes (CD45pos CD11bpos Ly6Clow Ly6Gneg CCR3neg SiglecFneg), macrophages (CD45pos CD11bpos CD115pos F4/80pos), neutrophils (CD45pos CD11bpos Ly6Cpos Ly6Gpos CCR3neg SiglecFneg).

Evaluation of the Efficiency of the Killing Method

In order to determine whether supernatants of treated cells contained surviving cells that might preclude their use as immunization agent, supernatants containing detached dead and dying cells were transferred to a new culture flask containing fresh DMEM supplemented with 10% (v/v) FBS and penicillin–streptomycin and cultured at 37°C in a 5% CO_2 atmosphere. Cell survival and ability to form colonies were investigated 7 days post-transfer. Microphotographs were taken on Microscope Axiovert 25 by a Nikon D700 reflex camera. Images were processed using Adobe Photoshop CS5. Also C57BL/6 mice were injected intraperitoneally (i.p.) with supernatants of treated cells. Mice were sacrificed once tumor growth in the peritoneal cavity was detected by simple inspection and palpation. The experiment ended at 32 days, and surviving mice were sacrificed. Results are presented as Kaplan-Meier survival curves (**Figure 2**).

Anti-Tumor Immunization

A syngeneic anti-tumor immunization model was used. Mice (C57BL/6, MHC haplotype H2b) were immunized i.p. with supernatants containing detached dead and dying cells harvested 24 hours post-treatment from B16F10 melanoma cells (carriers of the MHC haplotype H2b). SNs from cells treated with gamma irradiation or the combination of GIHT and gamma irradiation were used in this experiment. GIHT alone was not used as immunization since the inoculum

contained surviving cells and was not suitable as an immunization agent (**Figure 2**). After 14 days, the mice were challenged subcutaneously (s.c.) in the back with viable B16F10 melanoma cells (1×10^6). The width, height, and depth of subcutaneous tumors were measured with a caliper and recorded for a maximum 16 days.

Statistics

Statistical analysis was performed by GraphPad Prism (version 7.0) software. As statistically significant, the p-values ≤ 0.05 were considered.

RESULTS

GIHT Triggers Apoptosis Rapidly Followed by Secondary Necrosis

Anti-tumor therapies induce various types of cell death that might result either in the activation or in the inhibition of specific anti-tumor immune responses. For example, the survival of cancer patients has been negatively correlated with tolerogenic apoptosis (39), and primary necrosis was shown to lack of immunogenicity (4). Therefore, we first evaluated the type of cell death induced by GIHT, gamma irradiation and its combination *in vitro* employing a flow cytometry-based six-parameter classification protocol (**Supplementary Figures 1, 2**) (38). Untreated cells display a high proportion of viable cells (**Figure 1**). The exposure of B16F10 melanoma cells to gamma irradiation alone results mainly in primary necrosis independently of GIHT (**Figure 1**). NIR exposure caused hyperthermia and rapid progression to secondary necrosis when rGO or rGO-PEG were present (GIHT, **Supplementary Figure 2**) (37). This phenotype persisted after the combined action of gamma-irradiation and GIHT (**Figure 1**).

Surviving Cells Are Present in Supernatants of Dead and Dying Cells

The stimulation of proliferation of few surviving cells by bystander dead cells has been confirmed for melanoma cells, fibroblasts, and primary synoviocytes (13) and it might contribute considerably to relapses after radio- or chemotherapy (40–42). In order to determine the suitability of dying tumor cells supernatants as immunization adjuvants, we further cultured supernatants containing detached dead and dying cells in culture flasks and in the peritoneal cavity of C57Bl/6 mice. The supernatants of untreated cells and those treated with GIHT contained surviving cells that generated colonies after 7 days of cultures *in vitro* and tumors in the peritoneal cavity of mice, respectively (**Figure 2**). Contrarily, supernatants of cells treated with gamma irradiation and with the combination of irradiation and GIHT did not generate colonies *in vitro* or peritoneal tumors *in vivo* (**Figure 2**). This indicates that killing of B16F10 melanoma cells by hyperthermia alone might cause the release of growth and survival factors that support the growth of tumors at the site of injection of supernatants. This precludes the use of cells treated with hyperthermia alone in immunization protocols.
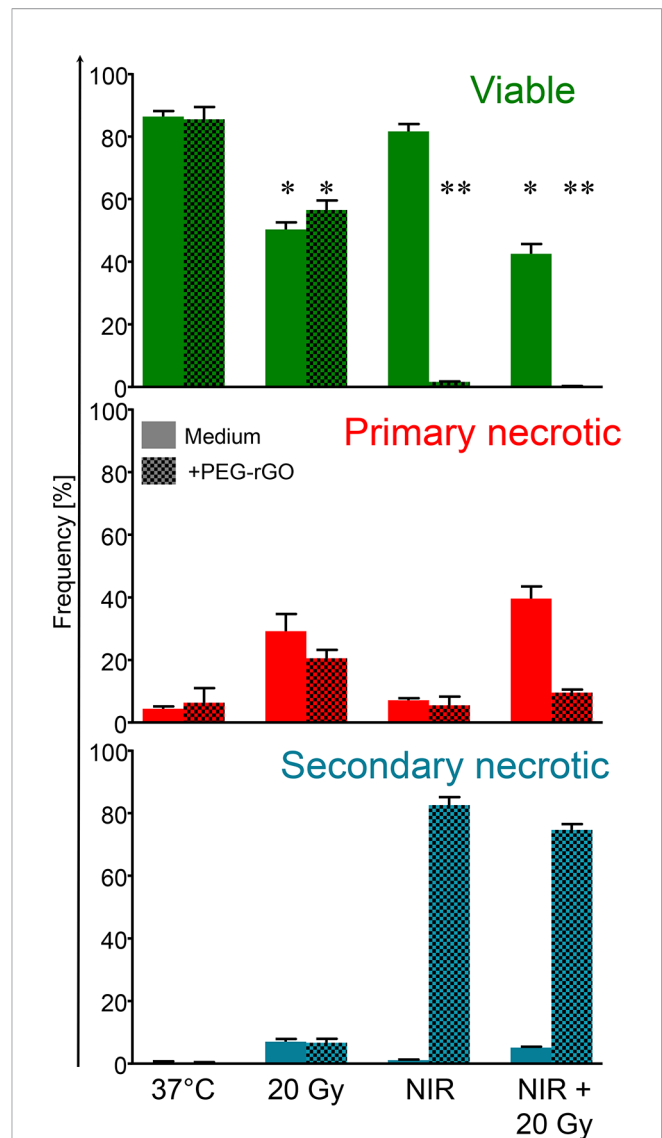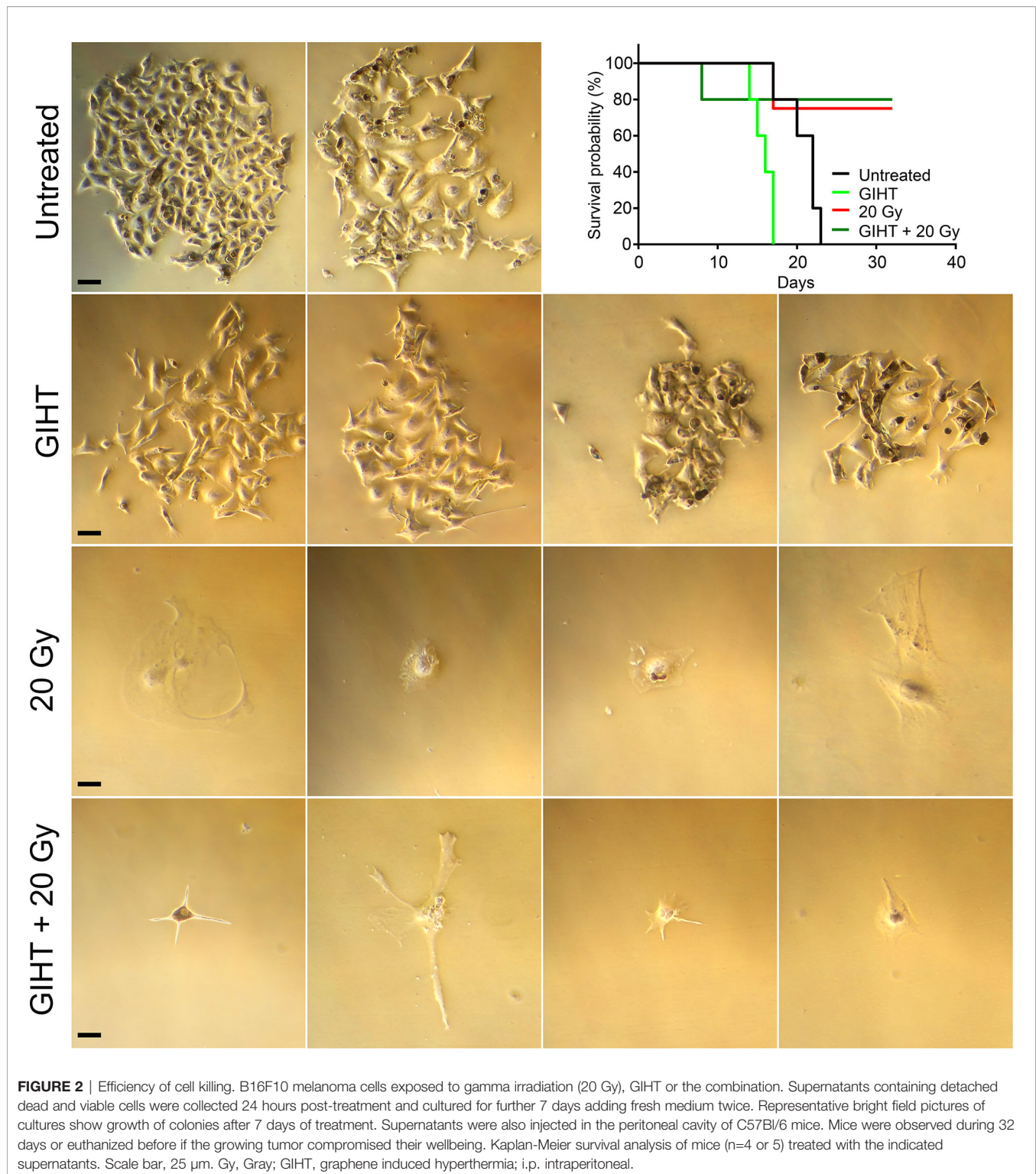

FIGURE 1 | Frequencies of subpopulations of dead and dying cells. B16F10 melanoma cells exposed to gamma irradiation (20 Gy), graphene induced hyperthermia (GITH) or the combination were classified by flow cytometry employing multiparametric cell staining after 24 hours. Viable cells, green, negative for PI and AxA5. Primary necrotic cells, red, positive for PI and AxA5 with high DNA content (Hoechst). Secondary necrotic cells, blue, positive for PI and AxA5 with low DNA content (Hoechst). NIR, near infrared irradiation; Gy, Gray; PI, propidium iodide; AxA5, annexin A5. *p < 0.05; **p < 0.01.

Dying Cells Killed by GIHT Combined With Gamma Irradiation Induce Inflammatory Cell Infiltration in the Site of Injection

Employing the *in vivo* airpouch model, we investigated the pro-inflammatory potential of mediators released by dead cells induced by GIHT alone or in the combination with gamma irradiation (**Figure 3**). Supernatants of dead and dying cells were injected into established sterile airpouches. We observed a significant increase in the infiltration of inflammatory

FIGURE 2 | Efficiency of cell killing. B16F10 melanoma cells exposed to gamma irradiation (20 Gy), GIHT or the combination. Supernatants containing detached dead and viable cells were collected 24 hours post-treatment and cultured for further 7 days adding fresh medium twice. Representative bright field pictures of cultures show growth of colonies after 7 days of treatment. Supernatants were also injected in the peritoneal cavity of C57Bl/6 mice. Mice were observed during 32 days or euthanized before if the growing tumor compromised their wellbeing. Kaplan-Meier survival analysis of mice (n=4 or 5) treated with the indicated supernatants. Scale bar, 25 µm. Gy, Gray; GIHT, graphene induced hyperthermia; i.p. intraperitoneal.

neutrophils into airpouches supernatants induced by the combination of therapies accompanied by a significantly decreased proportion of anti-inflammatory monocytes and macrophages. Supernatants of irradiated cells caused a moderate elevation of inflammatory monocytes (**Figure 3**).

GIHT Combined With Gamma Irradiation Elicits the Release of Organic Adjuvants With a Specific Spatiotemporal Pattern

We further analyzed the presence of organic adjuvants released by dead and dying B16F10 melanoma cells after GIHT (37)

(**Figure 4**). We observed an early (t0) and late (t24) release of ATP in the case of GIHT applied alone or in combination with gamma irradiation (**Figure 4A**). Also, both treatments induced late release of HSP-70 (**Figure 4B**). However, only the combination of GIHT and 20 Gy was associated with a late secretion of HMGB-1 (**Figure 4C**), suggesting the release of nucleosome-bound HMGB-1 as reported for secondary necrotic cells (43).

Dying Cells Treated With GIHT and X-Rays Induce the Proliferation of Naive T Cells *In Vitro*

After confirming the presence of released organic adjuvants and testing its inflammatory potential, we aimed to investigate whether these adjuvants contribute to the activation of DCs. The supernatants of all treatments caused a significant upregulation of the activation markers CD80, CD86, MHC-II and CD40 on bone marrow derived DCs (**Supplementary Figure 3**). These conditionally activated DCs were used in a modified mixed lymphocyte reaction (MLR) to activate naive allogeneic T cells to proliferate (**Figures 5A, B**). The allogeneic

major histocompatibility complex (MHC) molecules induced so-called background stimulation of T cells proliferation (**Figures 5A, B**, UNT). We observed that the proliferation of CD4+ T cells but not CD8+ T cells were significantly increased in response to SN from tumor cells exposed to GIHT alone or in combination with gamma irradiation (**Figures 5A, B**).

Dying Cells Killed by GIHT Combined With Gamma Irradiation Elicit Specific Anti-Tumor Immune Responses *In Vivo*

Once we observed that innate and adaptive immune activation was induced by the SN from tumor cells killed by the combination of hyperthermia and gamma irradiation, we sought to determine whether these SN are able to support specific anti-tumor responses if inoculated together with dead tumor cells in an immunization/challenge experiment. For this experiment we used the SN from untreated (containing no viable tumor cells), gamma irradiated alone (containing dead tumor cells) and in combination with GITH (containing dead tumor cells) as a single immunization dose. Mice were challenged with viable tumor cells after 14 days, and tumor growth was
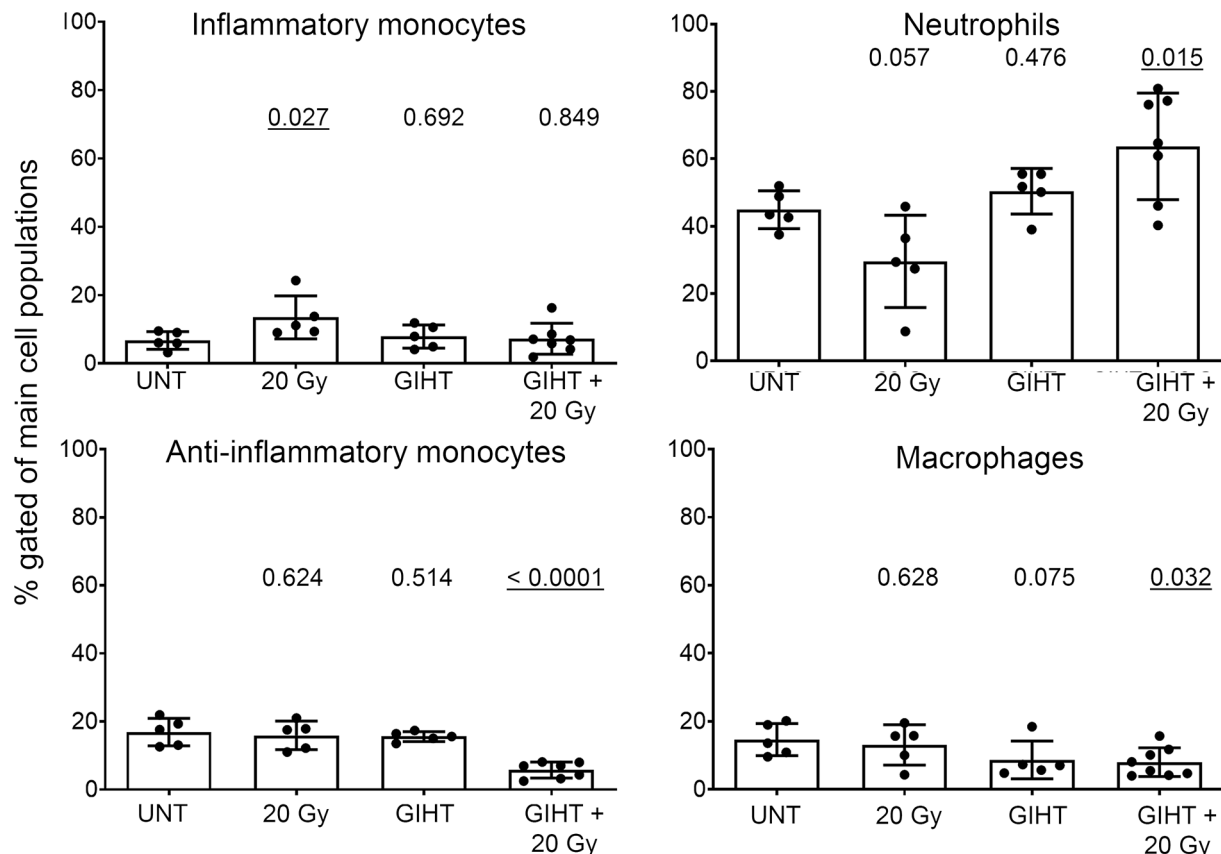
FIGURE 3 | Inflammatory cell infiltration to the site of cell death. SNs of dying B16F10 melanoma cells (24h) were injected into air pouches of mice and the infiltrating cells were quantified by flow cytometry. The infiltration caused by supernatants of untreated cells was used as a baseline. The main four myeloid populations are shown. One-way analysis of variances of five mice with Tukey's multiple comparison test is shown. Values of p < 0.05 considered as significant are underlined. UNT, untreated; Gy, Gray; GIHT, graphene-induced hyperthermia.
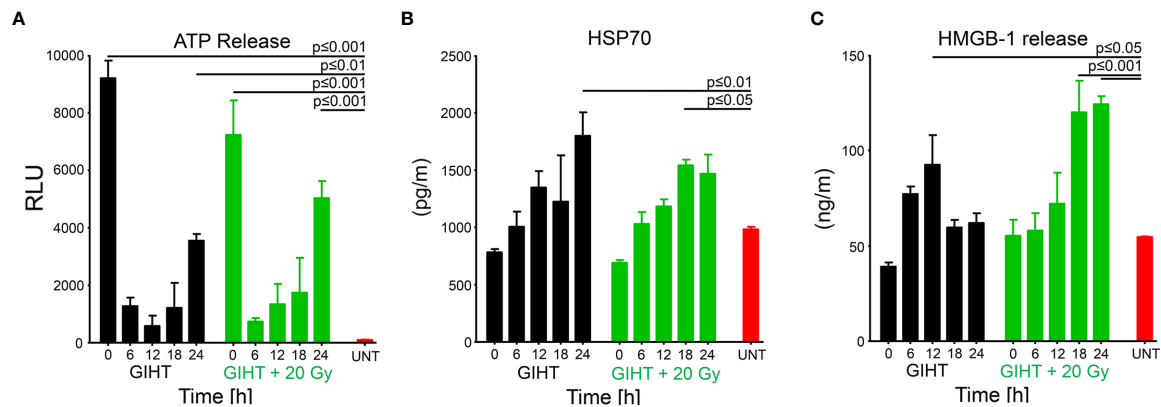
FIGURE 4 | Organic adjuvants released from GIHT treated B16F10 melanoma cells. **(A)** Time kinetic of the levels of ATP, **(B)** HSP70, and **(C)** HMGB-1 detected in supernatants after the application of the treatment. Supernatants from untreated cells (UNT) represent basal concentrations of DAMPs. The two-way analyses of variance with Bonferonni posttest was employed. Values of $p < 0.05$ were considered as significant. Means with the standard error of the mean (SEM) are shown. GIHT, graphene induced hyperthermia; UNT, untreated; ATP, adenosine triphosphate; HSP70, heat shock protein 70; HMGB1, high mobility group box 1 protein.

monitored for 32 days. The SN of cells exposed to the single treatment modality of gamma irradiation fostered the growth of secondary tumors while the combination of gamma irradiation and GITH resulted in a discreet reduction of the tumor volume of secondary tumors (**Figures 5C–F** and **Supplementary Table 1**).

DISCUSSION

Radiotherapy is an essential treatment option for the majority of patients bearing tumors (44). However, radioresistance of some cancer cells results in the failure of this therapy (45). Hyperthermia was demonstrated to radiosensitize tumor cells (46, 47). The effect of GIHT administered before radiation on the progression of cell death of the poorly immunogenic B16F10 melanoma cells was investigated. Twenty Gy resemble the two weeks cumulative dose of X-rays that patients receive when undergo radiotherapy (31).

We have observed that rGO and rGO-PEG exhibit the best photothermal conversion efficacy (37). The hyperthermia (42-43°C) induced by rGO and rGO-PEG alone or in combination with gamma irradiation led to significantly increased cell death. When GIHT was administered alone or in combination with gamma irradiation, melanoma cells mainly followed apoptotic cell death patterns with fast progression to secondary necrosis. The decision taken by the dying cell is orchestrated by multiple factors, such as the severity of the damage, energy availability, the presence/absence of ligands of cell death/dependent receptors, or inhibitors of specific pathways. The outcome has profound effects on the subsequent immune response (48). Necrotic cell death does not always induce robust immune responses (4), and the activation of apoptosis might result as a double edge sword with features of immunogenic (4, 49, 50) or tolerogenic (36) (40) cellular demise. Necroptotic cells, for example, although releasing 'find me' signals, may be engulfed without activating the immune system (51). Therefore, determining the precise

death pathway and delineating its immunological consequences results of major importance while designing novel anti-cancer therapies.

When apoptotic cells are not cleared in an efficient and timely manner, they become secondary necrotic (52). *In vivo*, the complete apoptotic program's execution is usually interfered by rapid phagocytosis (53). However, in the case of large amounts of cell demise that challenges the capacity of phagocytes to efficiently clear cellular debris (54) or when the clearance capacity is itself reduced (35, 55), apoptotic cells lose their plasma membrane integrity and release immune stimulators (56, 57). Secondary necrosis *in vivo* is linked to multiple inflammatory and autoimmune disorders (35, 58, 59). Based on our observations, we suggest that when GIHT is applied in combination with gamma irradiation, a large number of apoptotically modified tumor-derived antigens along with an appropriate cocktail of mediators are released and can stimulate DCs. This is possible due to the high frequency of secondarily necrotic cells observed with the multimodal therapy.

The efficiency of anti-cancer therapies rely on many factors. One of them is the microenvironment resulting directly after therapy. Massive cell death of solid tumors changes dramatically the tumor microenvironment and triggers biological reactions in the host and tumor. Inosine released by dead and dying cells mediates proliferation of surviving cells *via* purinergic receptors (13) and this might support the appearance of relapses (40, 42). The treatment with GITH alone was inefficient and fostered the rapid proliferation of surviving cells in our *in vitro* and *in vivo* settings.

It was demonstrated that the spatiotemporal appearance of organic adjuvants such as ATP (3, 4), HMGB1 (4–6), HSP70 (7, 8, 60, 61) and HSP90 (4, 9) decides about the consequences of cell demise. In line with this, we previously proposed that the sole presence of ATP leads to the silent removal of dead cells, whereas the presence of ATP together with HMGB1 or HSP90 induces the robust anti-tumor immune responses (4).
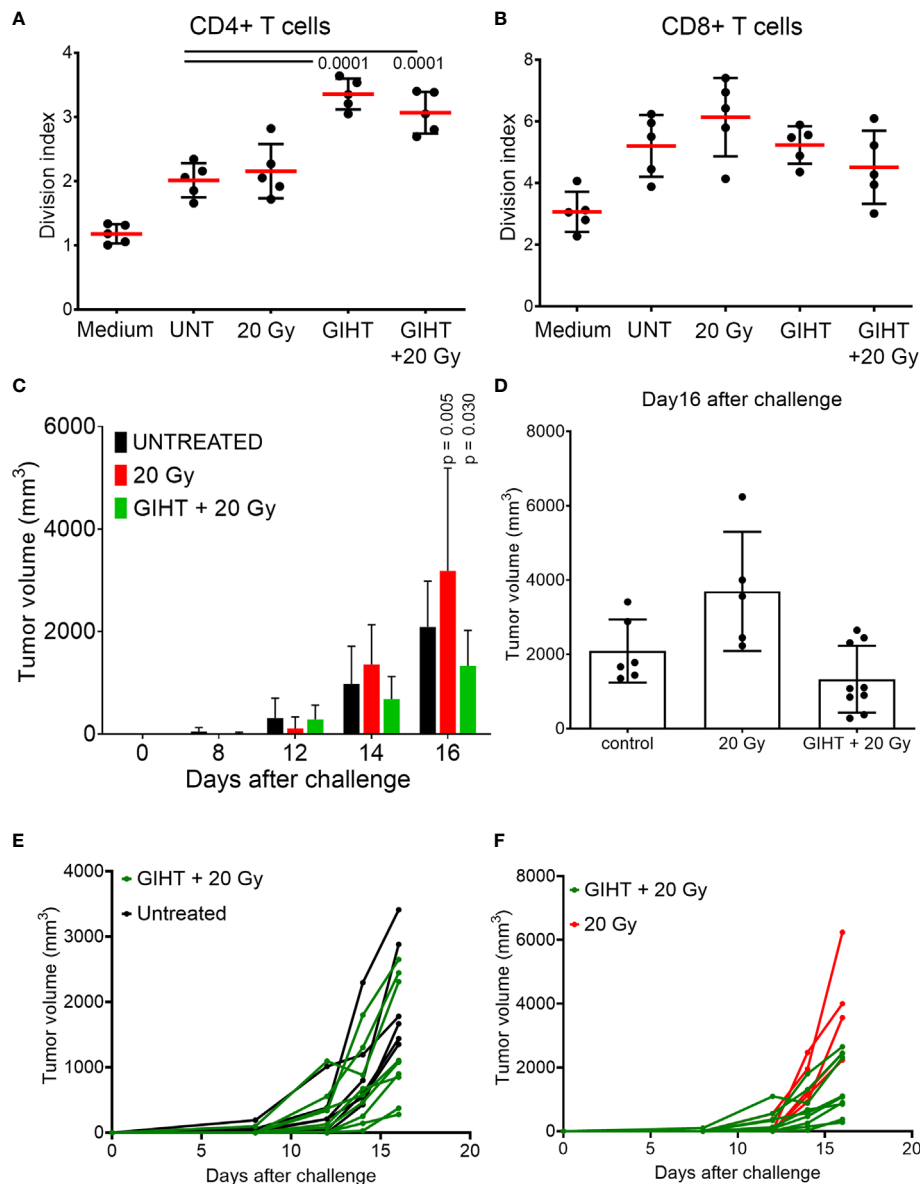
FIGURE 5 | Induction of specific anti-tumor immune responses. T cells proliferation induced by conditioned DCs. DCs were co-incubated for 24 hours with SN collected from B16F10 melanoma cells exposed to indicated treatments. CSFE-labelled T cells were co-cultured with DCs for 4 days. To show bottom-line proliferation, DCs were conditioned with fresh medium. Division index of CD4 positive T cells **(A)** and CD8 positive T cells **(B)** is shown. Kruskal-Wallis test with Dunn's multiple comparison test was employed. Values of p < 0.05 were considered as significant. **(C)** Tumor growth after challenge of immunized mice. Immunization was performed with a single i.p. dosis of detached B16F10 melanoma cells including their supernatants. Fourteen days after the immunization, mice were challenged with viable B16F10 melanoma cells injected subcutaneously in the back. Two-way ANOVA was used to compare the means at each time point. Values of p < 0.05 after Tukey's multiple comparison test were considered as significant and depicted. **(D)** Tumor volume of immunized mice at day16 after the challenge with viable B16F10 melanoma cells. One way ANOVA was applied to evaluate the means at day 16 after challenge. **(E, F)** Tumor growth of single mice of the experiment shown in **(C)**. P values of Fisher's least significant differences are depicted. Gy, Gray; GIHT, graphene-induced hyperthermia.

We detected significantly increased ATP release levels into the extracellular space mostly due to a temporal heat-induced permeability of membranes (62, 63), including mitochondrial envelopes. Notably, the recovery of plasma membranes occurs in the latest 40 minutes after the treatment since most of the cells are PI negative by this time

point. The progression towards secondary necrosis was then responsible for the releases of further intracellular contents later on (24 hours).

We detected significantly increased secretion of HSP70 at 24 and 12 hours post administration of GIHT alone or combined with gamma irradiation, respectively. Exposure to

elevated temperatures leads to the increased expression of intracellular HSP. Colorectal adenocarcinoma cells exposed to 41.5°C for 1-hour show significantly decreased cell death orchestrated probably by the Thermo protection effect of HSP (64). In terms of ICD, when HSP proteins are presented on the plasma membrane's outer leaflet or are released in the extracellular milieu, they gain immune stimulatory properties (7, 8, 60, 61). In other studies, hyperthermia (41.5°C, 1 hour) administered alone or in combination with radiation (2 Gy) was demonstrated to trigger the release of both proteins HSP70 and HMGB1 by dead and dying B16F10 melanoma cells (65). HSP70 secreted after the treatment elicits the maturation of DC and promotes the release of pro-inflammatory cytokines (64).

Chronic persistent inflammation is linked to tumorigenesis, and extracellular HMGB1 is perceived as a pro-inflammatory cytokine inducing the expression of other inflammatory factors (66–68). Besides that, HMGB1 leads to the secretion of other pro-inflammatory cytokines (i.e., TNF, IL-1, or IL-6) by resident or migrated leukocytes (69). In this manner, HMGB1 further fosters a vicious cycle of inflammation and manipulation of the immune system. The plethora of actions of HMGB1 can be explained by its redox status, the type of affected cell, and available receptors (70), as well as by its interaction with DNA. Free reduced HMGB1 protein was shown to be passively released by primary necrotic cells, whereas the oxidized form, which is additionally bound to the nucleosome, was observed in secondary necrotic cells (43, 71). It was reported that during apoptosis, cysteine residues of HMGB1 are oxidized by mitochondrial ROS produced in a caspase-dependent manner. This fosters immunological tolerance. Immunogenicity was then recovered by blocking its oxidation (72). Furthermore, apoptotic cell death accompanied by elevated intracellular levels of ROS exhibited higher immunogenicity *in vivo* when compared to the death developing in the absence of ROS (71).

In the death induced by GIHT alone, the release of danger signals was significantly increased at the earlier time points (HMGB1/DNA, 12 hours) when ATP was still absent. In the case of the combined treatments, we detected significant concentrations of extracellular DAMPs, HSP70, and HMGB1/DNA, 18 hours post treatment. The combinational therapy was then characterized by the simultaneous increase of ATP and HMGB1/DNA released 24 hours post treatment. We have previously observed that dying cells are less potent stimulators when ATP is released without other DAMPs (4). The presence of only one of the organic adjuvants is not enough to provide sufficient stimulation of the immune system. Werthmöller et al. reported that the simultaneous presence of HSP70 and HMGB1 was linked to the increased immunogenic potential of cellular demise (65). This suggests that the DAMPs detected 18 hours post combinational treatment can stimulate the immune system. The additional presence of ATP further fosters the activation.

At the site of inoculation of supernatants, we observed significant infiltration of neutrophils and significantly decreased levels of anti-inflammatory monocytes in response to cells treated with GIHT combined with gamma irradiation. Single treatments affected less the composition of early infiltrates. It was demonstrated that dying cancer cells secrete specific chemokines to recruit cells of the immune system (11, 73). IL-1α and IL-1β were reported to attract neutrophils (initial phase) and macrophages (late phase) during sterile inflammation, respectively (74). Additionally, IL-1α was shown to sustain chronic infiltration of neutrophils (75). After migration to the site of inflammation, exposure of neutrophils to 'eat me' signals, such as PS and calreticulin, results in the polarization to pro-inflammatory phenotype and, consequently, to cytotoxicity towards remaining cancer cells that survived the therapy (11). Therefore, we speculate that the observed infiltration of neutrophils might further support our multimodal therapy's anti-tumor potential.

Finally, we demonstrated that cell death induced by GIHT alone or in combination with gamma irradiation resulted in the activation of DCs, which stimulated the proliferation of CD4+ T cells *in vitro*. This suggests that released ATP and HMGB1-DNA complexes are potent supporters of T cell activation. Employing dead and dying cells in an immunization/challenge experiment, we observed a decreased tumor volume in the group of mice immunized with the combined treatment. Contrarily, gamma irradiation alone fails to induce protection against tumor growth. We suggest that the significant release of several DAMPs significantly contributes to increased immunogenicity of B16F10 melanoma cells. Therefore, GIHT could be implemented in multimodal therapies since it may take advantage of radio sensitization of tumor cells by inducing the timely release of ATP and HMGB1-DNA complexes during the progress of cell death.

The melanoma B16F10 clone implanted in immunocompetent syngeneic mice allows the study of tumor growth preserving the interactions between cancer cells and the microenvironment (76–78). However, this clone has the disadvantage to have a high proliferative and metastasizing capability (79) that precludes the use of viable cells for immunization. Therefore, the antigenic load at the immunization site might be insufficient to trigger immune responses that resulted in tumor free mice after the challenge. Nevertheless, our observations are significant enough to propose the study of the principle of radiosensation using nanosheets-targeted hyperthermia in other solid tumors models in future research. When biocompatible rGO-PEG nanosheets are applied intravenously, they become enriched in well-vascularized tumors by the enhanced permeability and retention effect. These nanosheets can be then stimulated with deep penetrating NIR irradiation to achieve fine-tuned localized hyperthermia (GITH) in solid tumors.

DATA AVAILABILITY STATEMENT

The raw data supporting the conclusions of this article will be made available by the authors, without undue reservation.

ETHICS STATEMENT

The animal study was reviewed and approved by Animal Care and Use Committees of the University Erlangen-Nürnberg and the 'Regierung von Unterfranken'.

AUTHOR CONTRIBUTIONS

Conceptualization, MP, CJ, BF, SS, and LM. Methodology, MP, XS, CJ, BF, and RB. Software, MP, XS, and CJ. Validation, MP, CJ, SS, and LM. Formal analysis, MP, XS, CJ, BF, UG, and LM. Investigation, MP, CJ, BF, and LM. Resources, RB, UG, SS, and LM. Data curation, MP, BF, UG, RB, CJ, and LM. Writing and original draft preparation, MP and LM. Writing—review and editing, MP, BF, UG, RB, SS, CJ, and LM. Visualization, MP, BF, CJ, and LM. Supervision, BF, SS, and LM. Funding acquisition, BF, SS, and LM. All authors contributed to the article and approved the submitted version.

SUPPLEMENTARY MATERIAL

The Supplementary Material for this article can be found online at: https://www.frontiersin.org/articles/10.3389/fonc.2021.664615/full#supplementary-material

REFERENCES

1. Obeid M, Panaretakis T, Joza N, Tufi R, Tesniere A, van Endert P, et al. Calreticulin Exposure is Required for the Immunogenicity of Gamma-Irradiation and UVC Light-Induced Apoptosis. *Cell Death Differentiation* (2007) 14:1848–50. doi: 10.1038/sj.cdd.4402201

2. Gardai SJ, McPhillips KA, Frasch SC, Janssen WJ, Starefeldt A, Murphy-Ullrich JE, et al. Cell-Surface Calreticulin Initiates Clearance of Viable or Apoptotic Cells Through Trans-Activation of LRP on the Phagocyte. *Cell* (2005) 123:321–34. doi: 10.1016/j.cell.2005.08.032

3. Elliott MR, Chekeni FB, Trampont PC, Lazarowski ER, Kadl A, Walk SF, et al. Nucleotides Released by Apoptotic Cells Act as a Find-Me Signal to Promote Phagocytic Clearance. *Nature* (2009) 461:282–6. doi: 10.1038/nature08296

4. Maueroder C, Chaurio RA, Dumych T, Podolska M, Lootsik MD, Culemann S, et al. A Blast Without Power - Cell Death Induced by the Tuberculosis-Necrotizing Toxin Fails to Elicit Adequate Immune Responses. *Cell Death Differentiation* (2016) 23:1016–25. doi: 10.1038/cdd.2016.4

5. Apetoh L, Ghiringhelli F, Tesniere A, Obeid M, Ortiz C, Criollo A, et al. Toll-Like Receptor 4-Dependent Contribution of the Immune System to Anticancer Chemotherapy and Radiotherapy. *Nat Med* (2007) 13:1050–9. doi: 10.1038/nm1622

6. Scaffidi P, Misteli T, Bianchi ME. Release of Chromatin Protein HMGB1 by Necrotic Cells Triggers Inflammation. *Nature* (2002) 418:191–5. doi: 10.1038/nature00858

7. Schildkopf P, Frey B, Ott OJ, Rubner Y, Multhoff G, Sauer R, et al. Radiation Combined With Hyperthermia Induces HSP70-Dependent Maturation of Dendritic Cells and Release of Pro-Inflammatory Cytokines by Dendritic Cells and Macrophages. *Radiotherapy Oncol* (2011) 101:109–15. doi: 10.1016/j.radonc.2011.05.056

8. Song S, Zhou F, Chen WR, Xing D. PDT-Induced HSP70 Externalization Up-Regulates NO Production *via* TLR2 Signal Pathway in Macrophages. *FEBS Lett* (2013) 587:128–35. doi: 10.1016/j.febslet.2012.11.026

9. Spisek R, Charalambous A, Mazumder A, Vesole DH, Jagannath S, Dhodapkar MV. Bortezomib Enhances Dendritic Cell (DC)-Mediated Induction of Immunity to Human Myeloma *via* Exposure of Cell Surface Heat Shock Protein 90 on Dying Tumor Cells: Therapeutic Implications. *Blood* (2007) 109:4839–45. doi: 10.1182/blood-2006-10-054221

10. Chen X, Li W, Ren J, Huang D, He WT, Song Y, et al. Translocation of Mixed Lineage Kinase Domain-Like Protein to Plasma Membrane Leads to Necrotic Cell Death. *Cell Res* (2014) 24:105–21. doi: 10.1038/cr.2013.171

11. Garg AD, Agostinis P. Cell Death and Immunity in Cancer: From Danger Signals to Mimicry of Pathogen Defense Responses. *Immunol Rev* (2017) 280:126–48. doi: 10.1111/imr.12574

12. Galluzzi L, Bravo-San Pedro JM, Demaria S, Formenti SC, Kroemer G. Activating Autophagy to Potentiate Immunogenic Chemotherapy and Radiation Therapy. *Nat Rev Clin Oncol* (2017) 14:247–58. doi: 10.1038/nrclinonc.2016.183

13. Chen J, Chaurio RA, Maueroder C, Derer A, Rauh M, Kost A, et al. Inosine Released From Dying or Dead Cells Stimulates Cell Proliferation *via* Adenosine Receptors. *Front Immunol* (2017) 8:504. doi: 10.3389/fimmu.2017.00504

14. Hildebrandt B, Wust P, Ahlers O, Dieing A, Sreenivasa G, Kerner T, et al. The Cellular and Molecular Basis of Hyperthermia. *Crit Rev Oncol/Hematol* (2002) 43:33–56. doi: 10.1016/s1040-8428(01)00179-2

15. Dewey WC. Arrhenius Relationships From the Molecule and Cell to the Clinic. *Int J Hyperthermia* (2009) 25:3–20. doi: 10.1080/02656730902747919

16. Dewhirst MW, Prosnitz L, Thrall D, Prescott D, Clegg S, Charles C, et al. Hyperthermic Treatment of Malignant Diseases: Current Status and a View Toward the Future. *Semin Oncol* (1997) 24:616–25.

17. Urano M, Kuroda M, Nishimura Y. For the Clinical Application of Thermochemotherapy Given at Mild Temperatures. *Int J Hyperthermia* (1999) 15:79–107. doi: 10.1080/026567399285765

18. Dewey WC, Thrall DE, Gillette EL. Hyperthermia and Radiation–a Selective Thermal Effect on Chronically Hypoxic Tumor Cells In Vivo. *Int J Radiat Oncol Biol Phys* (1977) 2:99–103. doi: 10.1016/0360-3016(77)90013-X

19. Westra A, Dewey WC. Variation in Sensitivity to Heat Shock During the Cell-Cycle of Chinese Hamster Cells In Vitro. *Int J Radiat Biol Related Stud Physics Chemistry Med* (1971) 19:467–77. doi: 10.1080/09553007114550601

20. Overgaard J, Suit HD. Time-Temperature Relationship Th Hyperthermic Treatment of Malignant and Normal Tissue In Vivo. *Cancer Res* (1979) 39:3248–53.

21. Sapareto SA, Raaphorst GP, Dewey WC. Cell Killing and the Sequencing of Hyperthermia and Radiation. *Int J Radiat Oncol Biol Phys* (1979) 5:343–7. doi: 10.1016/0360-3016(79)91214-8

22. Dewhirst MW, Vujaskovic Z, Jones E, Thrall D. Re-Setting the Biologic Rationale for Thermal Therapy. *Int J Hyperthermia* (2005) 21:779–90. doi: 10.1080/02656730500271668

23. Sakaguchi Y, Stephens LC, Makino M, Kaneko T, Strebel FR, Danhauser LL, et al. Apoptosis in Tumors and Normal Tissues Induced by Whole Body Hyperthermia in Rats. *Cancer Res* (1995) 55:5459–64.

24. Alekseenko LL, Zemelko VI, Zenin VV, Pugovkina NA, Kozhukharova IV, Kovaleva ZV, et al. Heat Shock Induces Apoptosis in Human Embryonic Stem Cells But a Premature Senescence Phenotype in Their Differentiated Progeny. *Cell Cycle* (2012) 11:3260–9. doi: 10.4161/cc.21595

25. Hader M, Frey B, Fietkau R, Hecht M, Gaipl US. Immune Biological Rationales for the Design of Combined Radio- and Immunotherapies. *Cancer Immunol Immunother* (2020) 69:293–306. doi: 10.1007/s00262-019-02460-3

26. Lepock JR, Frey HE, Heynen ML, Senisterra GA, Warters RL. The Nuclear Matrix is a Thermolabile Cellular Structure. *Cell Stress Chaperones* (2001) 6:136–47. doi: 10.1379/1466-1268(2001)006<0136:TNMIAT>2.0.CO;2

27. Lepock JR. Role of Nuclear Protein Denaturation and Aggregation in Thermal Radiosensitization. *Int J Hyperthermia* (2004) 20:115–30. doi: 10.1080/02656730310001637334

28. Roti Roti JL. Cellular Responses to Hyperthermia (40-46 Degrees C): Cell Killing and Molecular Events. *Int J Hyperthermia* (2008) 24:3–15. doi: 10.1080/02656730701769841

29. Vidair CA, Dewey WC. Division-Associated and Division-Independent Hyperthermic Cell Death: Comparison With Other Cytotoxic Agents. *Int J Hyperthermia* (1991) 7:51–60. doi: 10.3109/02656739109004976

30. Wust P, Hildebrandt B, Sreenivasa G, Rau B, Gellermann J, Riess H, et al. Hyperthermia in Combined Treatment of Cancer. *Lancet Oncol* (2002) 3:487–97. doi: 10.1016/S1470-2045(02)00818-5

31. Schildkopf P, Frey B, Mantel F, Ott OJ, Weiss E-M, Sieber R, et al. Application of Hyperthermia in Addition to Ionizing Irradiation Fosters Necrotic Cell Death and HMGB1 Release of Colorectal Tumor Cells. *Biochem Biophys Res Commun* (2010) 391:1014–20. doi: 10.1016/j.bbrc.2009.12.008

32. Issels RD. Hyperthermia Adds to Chemotherapy. *Eur J Cancer* (2008) 44:2546–54. doi: 10.1016/j.ejca.2008.07.038

33. Horsman MR, Overgaard J. Hyperthermia: A Potent Enhancer of Radiotherapy. *Clin Oncol (R Coll Radiol)* (2007) 19:418–26. doi: 10.1016/j.clon.2007.03.015

34. Elliott MR, Ravichandran KS. Clearance of Apoptotic Cells: Implications in Health and Disease. *J Cell Biol* (2010) 189:1059–70. doi: 10.1083/jcb.201004096

35. Gaipl US, Munoz LE, Grossmayer G, Lauber K, Franz S, Sarter K, et al. Clearance Deficiency and Systemic Lupus Erythematosus (SLE). *J Autoimmun* (2007) 28:114–21. doi: 10.1016/j.jaut.2007.02.005

36. Voll RE, Herrmann M, Roth EA, Stach C, Kalden JR, Girkontaite I. Immunosuppressive Effects of Apoptotic Cells. *Nature* (1997) 390:350–1. doi: 10.1038/37022

37. Podolska MJ, Barras A, Alexiou C, Frey B, Gaipl U, Boukherroub R, et al. Graphene Oxide Nanosheets for Localized Hyperthermia-Physicochemical Characterization, Biocompatibility, and Induction of Tumor Cell Death. *Cells* (2020) 9(3):776. doi: 10.3390/cells9030776

38. Munoz LE, Maueroder C, Chaurio R, Berens C, Herrmann M, Janko C. Colourful Death: Six-Parameter Classification of Cell Death by Flow Cytometry–Dead Cells Tell Tales. *Autoimmunity* (2013) 46:336–41. doi: 10.3109/08916934.2012.755960

39. Gregory CD, Pound JD. Cell Death in the Neighbourhood: Direct Microenvironmental Effects of Apoptosis in Normal and Neoplastic Tissues. *J Pathol* (2011) 223:177–94. doi: 10.1002/path.2792

40. Chaurio R, Janko C, Schorn C, Maueroder C, Bilyy R, Gaipl U, et al. UVB-Irradiated Apoptotic Cells Induce Accelerated Growth of Co-Implanted Viable Tumor Cells in Immune Competent Mice. *Autoimmunity* (2013) 46:317–22. doi: 10.3109/08916934.2012.754433

41. Cheng J, He S, Wang M, Zhou L, Zhang Z, Feng X, et al. The Caspase-3/Pkcdelta/Akt/VEGF-a Signaling Pathway Mediates Tumor Repopulation During Radiotherapy. *Clin Cancer Res* (2019) 25:3732–43. doi: 10.1158/1078-0432.CCR-18-3001

42. Huang Q, Li F, Liu X, Li W, Shi W, Liu FF, et al. Caspase 3-Mediated Stimulation of Tumor Cell Repopulation During Cancer Radiotherapy. *Nat Med* (2011) 17:860–6. doi: 10.1038/nm.2385

43. Urbonaviciute V, Furnrohr BG, Meister S, Munoz L, Heyder P, De Marchis F, et al. Induction of Inflammatory and Immune Responses by HMGB1-Nucleosome Complexes: Implications for the Pathogenesis of SLE. *J Exp Med* (2008) 205:3007–18. doi: 10.1084/jem.20081165

44. Ruckert M, Deloch L, Fietkau R, Frey B, Hecht M, Gaipl US. Immune Modulatory Effects of Radiotherapy as Basis for Well-Reasoned Radioimmunotherapies. *Strahlenther Onkol* (2018) 194:509–19. doi: 10.1007/s00066-018-1287-1

45. Gorayski P, Burmeister B, Foote M. Radiotherapy for Cutaneous Melanoma: Current and Future Applications. *Future Oncol* (2015) 11:525–34. doi: 10.2217/fon.14.300

46. Orth M, Lauber K, Niyazi M, Friedl AA, Li M, Maihofer C, et al. Current Concepts in Clinical Radiation Oncology. *Radiat Environ Biophys* (2014) 53:1–29. doi: 10.1007/s00411-013-0497-2

47. Triantopoulou S, Efstathopoulos E, Platoni K, Uzunoglou N, Kelekis N, Kouloulias V. Radiotherapy in Conjunction With Superficial and Intracavitary Hyperthermia for the Treatment of Solid Tumors: Survival and Thermal Parameters. *Clin Transl Oncol* (2013) 15:95–105. doi: 10.1007/s12094-012-0947-3

48. Maueroder C, Munoz LE, Chaurio RA, Herrmann M, Schett G, Berens C. Tumor Immunotherapy: Lessons From Autoimmunity. *Front Immunol* (2014) 5:212. doi: 10.3389/fimmu.2014.00212

49. Obeid M, Tesniere A, Ghiringhelli F, Fimia GM, Apetoh L, Perfettini JL, et al. Calreticulin Exposure Dictates the Immunogenicity of Cancer Cell Death. *Nat Med* (2007) 13:54–61. doi: 10.1038/nm1523

50. Zitvogel L, Casares N, Pequignot MO, Chaput N, Albert ML, Kroemer G. Immune Response Against Dying Tumor Cells. *Adv Immunol* (2004) 84:131–79. doi: 10.1016/S0065-2776(04)84004-5

51. Wang Q, Ju X, Zhou Y, Chen K. Necroptotic Cells Release Find-Me Signal and are Engulfed Without Proinflammatory Cytokine Production. *In Vitro Cell Dev Biol Anim* (2015) 51:1033–9. doi: 10.1007/s11626-015-9926-7

52. Wyllie AH, Kerr JF, Currie AR. Cell Death: The Significance of Apoptosis. *Int Rev Cytol* (1980) 68:251–306. doi: 10.1016/S0074-7696(08)62312-8

53. Butkevich OM, Vinogradova TL. [Clinical Aspects and Diagnosis of Infectious Endocarditis]. *Kardiologiia* (1990) 30:96–100.

54. Garg AD, Romano E, Rufo N, Agostinis P. Immunogenic Versus Tolerogenic Phagocytosis During Anticancer Therapy: Mechanisms and Clinical Translation. *Cell Death Differentiation* (2016) 23:938–51. doi: 10.1038/cdd.2016.5

55. Munoz LE, Gaipl US, Franz S, Sheriff A, Voll RE, Kalden JR, et al. SLE–a Disease of Clearance Deficiency? *Rheumatol (Oxford)* (2005) 44:1101–7. doi: 10.1093/rheumatology/keh693

56. Gaipl US, Kuenkele S, Voll RE, Beyer TD, Kolowos W, Heyder P, et al. Complement Binding is an Early Feature of Necrotic and a Rather Late Event During Apoptotic Cell Death. *Cell Death Differentiation* (2001) 8:327–34. doi: 10.1038/sj.cdd.4400826

57. Matzinger P. The Danger Model: A Renewed Sense of Self. *Science* (2002) 296:301–5. doi: 10.1126/science.1071059

58. Munoz LE, Lauber K, Schiller M, Manfredi AA, Herrmann M. The Role of Defective Clearance of Apoptotic Cells in Systemic Autoimmunity. *Nat Rev Rheumatol* (2010) 6:280–9. doi: 10.1038/nrrheum.2010.46

59. Munoz LE, Janko C, Grossmayer GE, Frey B, Voll RE, Kern P, et al. Remnants of Secondarily Necrotic Cells Fuel Inflammation in Systemic Lupus Erythematosus. *Arthritis Rheumatism* (2009) 60:1733–42. doi: 10.1002/art.24535

60. Pei Q, Pan J, Zhu H, Ding X, Liu W, Lv Y, et al. Gemcitabine-Treated Pancreatic Cancer Cell Medium Induces the Specific CTL Antitumor Activity by Stimulating the Maturation of Dendritic Cells. *Int Immunopharmacol* (2014) 19:10–6. doi: 10.1016/j.intimp.2013.12.022

61. Lin TJ, Lin HT, Chang WT, Mitapalli SP, Hsiao PW, Yin SY, et al. Shikonin-Enhanced Cell Immunogenicity of Tumor Vaccine is Mediated by the Differential Effects of DAMP Components. *Mol Cancer* (2015) 14:174. doi: 10.1186/s12943-015-0435-9

62. Dickerson EB, Dreaden EC, Huang X, El-Sayed IH, Chu H, Pushpanketh S, et al. Gold Nanorod Assisted Near-Infrared Plasmonic Photothermal Therapy (PPTT) of Squamous Cell Carcinoma in Mice. *Cancer Lett* (2008) 269:57–66. doi: 10.1016/j.canlet.2008.04.026

63. Dreaden EC, Mackey MA, Huang X, Kang B, El-Sayed MA. Beating Cancer in Multiple Ways Using Nanogold. *Chem Soc Rev* (2011) 40:3391–404. doi: 10.1039/c0cs00180e

64. Schildkopf P, Holmer R, Sieber R, Ott OJ, Janko C, Mantel F, et al. Hyperthermia in Combination With X-Irradiation Induces Inflammatory Forms of Cell Death. *Autoimmunity* (2009) 42:311–3. doi: 10.1080/08916930902832041

65. Werthmoller N, Frey B, Ruckert M, Lotter M, Fietkau R, Gaipl US. Combination of Ionising Radiation With Hyperthermia Increases the Immunogenic Potential of B16-F10 Melanoma Cells *In Vitro* and In Vivo. *Int J Hyperthermia* (2016) 32:23–30. doi: 10.3109/02656736.2015.1106011

66. Tadie JM, Bae HB, Deshane JS, Bell CP, Lazarowski ER, Chaplin DD, et al. Toll-Like Receptor 4 Engagement Inhibits Adenosine 5'-Monophosphate-Activated Protein Kinase Activation Through a High Mobility Group Box 1 Protein-Dependent Mechanism. *Mol Med* (2012) 18:659–68. doi: 10.2119/molmed.2011.00401

67. Weng H, Deng Y, Xie Y, Liu H, Gong F. Expression and Significance of HMGB1, TLR4 and NF-Kappab P65 in Human Epidermal Tumors. *BMC Cancer* (2013) 13:311. doi: 10.1186/1471-2407-13-311

68. Yan HX, Wu HP, Zhang HL, Ashton C, Tong C, Wu H, et al. P53 Promotes Inflammation-Associated Hepatocarcinogenesis by Inducing HMGB1 Release. *J Hepatol* (2013) 59:762–8. doi: 10.1016/j.jhep.2013.05.029

69. Yang H, Hreggvidsdottir HS, Palmblad K, Wang H, Ochani M, Li J, et al. A Critical Cysteine Is Required for HMGB1 Binding to Toll-Like Receptor 4 and Activation of Macrophage Cytokine Release. *Proc Natl Acad Sci U S A* (2010) 107:11942–7. doi: 10.1073/pnas.1003893107

70. Kang R, Zhang Q, Zeh HJ3rd, Lotze MT, Tang D. HMGB1 in Cancer: Good, Bad, or Both? *Clin Cancer Res* (2013) 19:4046–57. doi: 10.1158/1078-0432.CCR-13-0495

71. Chaurio RA, Munoz LE, Maueroder C, Janko C, Harrer T, Furnrohr BG, et al. The Progression of Cell Death Affects the Rejection of Allogeneic Tumors in Immune-Competent Mice - Implications for Cancer Therapy. *Front Immunol* (2014) 5:560. doi: 10.3389/fimmu.2014.00560

72. Kazama H, Ricci JE, Herndon JM, Hoppe G, Green DR, Ferguson TA. Induction of Immunological Tolerance by Apoptotic Cells Requires Caspase-Dependent Oxidation of High-Mobility Group Box-1 Protein. *Immunity* (2008) 29:21–32. doi: 10.1016/j.immuni.2008.05.013

73. Kolaczkowska E, Kubes P. Neutrophil Recruitment and Function in Health and Inflammation. *Nat Rev Immunol* (2013) 13:159–75. doi: 10.1038/nri3399

74. Rider P, Carmi Y, Guttman O, Braiman A, Cohen I, Voronov E, et al. IL-1alpha and IL-1beta Recruit Different Myeloid Cells and Promote Different Stages of Sterile Inflammation. *J Immunol* (2011) 187:4835–43. doi: 10.4049/jimmunol.1102048

75. Lee PY, Kumagai Y, Xu Y, Li Y, Barker T, Liu C, et al. IL-1alpha Modulates Neutrophil Recruitment in Chronic Inflammation Induced by Hydrocarbon Oil. *J Immunol* (2011) 186:1747–54. doi: 10.4049/jimmunol.1001328

76. Hart IR. The Selection and Characterization of an Invasive Variant of the B16 Melanoma. *Am J Pathol* (1979) 97:587–600.

77. Danciu C, Falamas A, Dehelean C, Soica C, Radeke H, Barbu-Tudoran L, et al. A Characterization of Four B16 Murine Melanoma Cell Sublines Molecular Fingerprint and Proliferation Behavior. *Cancer Cell Int* (2013) 13:75. doi: 10.1186/1475-2867-13-75

78. Barutello G, Rolih V, Arigoni M, Tarone L, Conti L, Quaglino E, et al. Strengths and Weaknesses of Pre-Clinical Models for Human Melanoma Treatment: Dawn of Dogs' Revolution for Immunotherapy. *Int J Mol Sci* (2018) 19(3):799. doi: 10.3390/ijms19030799

79. Saleh J. Murine Models of Melanoma. *Pathol Res Pract* (2018) 214:1235–8. doi: 10.1016/j.prp.2018.07.008

Conflict of Interest: The authors declare that the research was conducted in the absence of any commercial or financial relationships that could be construed as a potential conflict of interest.

Publisher's Note: All claims expressed in this article are solely those of the authors and do not necessarily represent those of their affiliated organizations, or those of the publisher, the editors and the reviewers. Any product that may be evaluated in this article, or claim that may be made by its manufacturer, is not guaranteed or endorsed by the publisher.

MMS22L Expression as a Predictive Biomarker for the Efficacy of Neoadjuvant Chemoradiotherapy in Oesophageal Squamous Cell Carcinoma

Qiyu Luo[1,2†], Wenwu He[3†], Tianqin Mao[1], Xuefeng Leng[3], Hong Wu[4], Wen Li[4], Xuyang Deng[3], Tingci Zhao[5], Ming Shi[6], Chuan Xu[4*] and Yongtao Han[3*]

[1] School of Medicine, University of Electronic Science and Technology of China (UESTC), Chengdu, China, [2] Department of Thoracic Surgery, Second Affiliated Hospital of Chengdu Medical College (China National Nuclear Corporation 416 Hospital), Chengdu, China, [3] Department of Thoracic Surgery, Sichuan Cancer Hospital & Research Institute, School of Medicine, University of Electronic Science and Technology of China (UESTC), Chengdu, China, [4] Integrative Cancer Center & Cancer Clinical Research Center, Sichuan Cancer Hospital & Institute Sichuan Cancer Center, School of Medicine, University of Electronic Science and Technology of China, Chengdu, China, [5] Department of International Medical Center/Ward of General Practice, West China Hospital, Sichuan University, Chengdu, China, [6] Department of Pathology, Sichuan Cancer Hospital & Research Institute, School of Medicine, University of Electronic Science and Technology of China (UESTC), Chengdu, China

Long-term survival in oesophageal squamous cell carcinoma (ESCC) is related with pathological response after neoadjuvant chemoradiotherapy (NCRT) followed by surgery. However, effective biomarkers to predict the pathologic response are still lacking. Therefore, a systematic analysis focusing on genes associated with the efficacy of chemoradiotherapy in ESCC will provide valuable insights into the regulation of molecular processes. By screening publications deposited in PubMed, we collected genes associated with the efficacy of chemoradiotherapy. A specific subnetwork was constructed using the Steiner minimum tree algorithm. Survival analysis in Kaplan-Meier Plotter online resources was performed to explore the relationship between gene mRNA expression and the prognosis of patients with ESCC. Quantitative real-time polymerase chain reaction (qRT-PCR), Western blotting, and immunohistochemical staining (IHC) were used to evaluate the expression of key genes in cell lines and human samples. The areas under the receiver operating characteristic (ROC) curves (AUCs) were used to describe performance and accuracy. Transwell assays assessed cell migration, and cell viability was detected using the Cytotoxicity Assay. Finally, we identified 101 genes associated with efficacy of chemoradiotherapy. Additionally, specific molecular networks included some potential related genes, such as *CUL3*, *MUC13*, *MMS22L*, *MME*, *UBC*, *VAPA*, *CYP1B1*, and *UGDH*. The *MMS22L* mRNA expression level showed the most significant association with the ESCC patient outcome (p < 0.01). Furthermore, *MMS22L* was downregulated at both the mRNA (p < 0.001) and protein levels in tumour tissues

compared with that in normal tissues. Lymph node metastasis was significantly associated with low *MMS22L* expression ($p < 0.01$). *MMS22L* levels were inversely correlated with the NCRT response in ESCC ($p < 0.01$). The resulting area under the ROC curve was 0.847 (95% CI: 0.7232 to 0.9703; $p < 0.01$). In conclusion, low expression of *MMS22L* is associated with poor response to NCRT, worse survival, lymph node metastasis, and enhanced migration of tumour cells in ESCC.

Keywords: oesophageal squamous cell carcinoma, *MMS22L*, bioinformatics analysis, neoadjuvant chemoradiotherapy, lymph node metastasis, migration

INTRODUCTION

According to the 2018 Global Cancer Statistics report, oesophageal cancer is among the 10 most frequent carcinomas globally (1). Squamous cell carcinoma (SCC) and adenocarcinoma are the major histologic types of oesophageal carcinoma, and SCC is the main histological type in China (1, 2). Despite advances in surgery, radiotherapy, and chemotherapy, the 5-year survival rate for patients with oesophageal squamous cell carcinoma (ESCC) remains markedly poor because of an advanced stage at diagnosis, the presence of tumour heterogeneity, and insufficient tumour prognostic factors (3, 4). Regarding ESCC at moderate-to-advanced stages, both effective preoperative chemotherapy and chemoradiotherapy have been widely used to shrink tumour size, repress tumour growth or metastasis, increase the R0 resection rate, and reduce the local recurrence rate of ESCC, to improve overall survival compared with surgery alone (5–8). No significant benefits were found in patients who did not respond to the conventional therapy because of toxicity from neoadjuvant chemoradiation therapy (NCRT); they might miss the best timing of treatment and obtain worse prognosis (9–11).

Tumour heterogeneity presents a challenge to successfully treat cancer using chemoradiotherapy, and it is a major factor in chemoradiotherapy failure (12, 13). To enable individualised treatment, screening out response cases and avoiding overtreatment of patients who would not benefit from the inclusion of chemotherapy with sensitive biomarkers are critical. In recent years, although some studies have attempted to reveal the biomarkers that predict responses to chemoradiotherapy, no reliable biomarkers have been identified to assess the efficacy of NCRT in ESCC. Therefore, large amount of studies are needed to further refine the biomarkers for easy use and validate them as biomarkers for future clinical trials.

Identifying new biomarkers is warranted to assist in screening patients who can benefit from chemotherapy and chemoradiotherapy based on bioinformatics analysis, offering consolidated validation for the individual candidate genes. In this study, we collected genes potentially associated with efficacy of chemoradiotherapy to infer specific molecular networks associated with the efficacy of chemoradiotherapy, and some potential related genes were identified. Additionally, the primary aim of the study was to measure potential related gene expression levels in ESCC tissues and evaluate their value as potential predictive biomarkers for the NCRT response in ESCC.

MATERIALS AND METHODS

Candidate Gene Set Approach

As reported previously (4), the efficacy of chemoradiotherapy in patients with ESCC is associated with multiple genes. In the present study, all the genes were obtained by systematic analysis of the human genetic association studies deposited in PubMed (https://www.ncbi.nlm.nih.gov/pubmed). Briefly, with reference to published studies, the search terms were: "(chemotherapy OR radiotherapy OR chemoradiotherapy) AND (cancer OR carcinoma OR neoplasm OR tumour) AND (esophagus OR gastroesophageal) AND (genetic polymorphism OR genes)", and the date of the last search was September 15, 2019. In total, 217 abstracts were identified by the final electronic searches in PubMed. We included abstracts with sufficient evaluation data, including the methodology, the definition of outcomes, and an appropriate evaluation matrix. Studies without any kind of validation (external validation or internal validation) were excluded. We excluded reviews, editorials, nonhuman studies, and letters without sufficient data. In total, 138 studies were excluded because they failed to meet the above criteria, and 79 articles met the prespecified inclusion criteria. The publications used and the discarded publications can be found in the supplementary documentation (**Supplementary Table S1**). Two reviewers (QL and MT) independently screened the full text and extracted the following information from each study: patient race, number of positive cases, interventions, histological type, the origin of specimens, and genes. Finally, we assembled the purpose genes associated with the response to chemoradiotherapy in ESCC histological type or cell lines.

Functional Enrichment Analysis

Gene Ontology (GO) and Kyoto Encyclopedia of Genes and Genomes (KEGG) functional enrichment analyses were performed using the R package "cluster Profiler" (14). For the GO and pathway enrichment analysis results, the p-value and q-values were calculated using Fisher's exact test and the R package (p-value <0.05 and q-value <0.05).

Construction of the Protein Subnetwork

In the context of a human protein-protein interaction (PPI) data set obtained from Protein Interaction Network Analysis platform (PINA) (15), we applied the Steiner minimum tree algorithm implemented in our software framework GenRev to construct

aspecific subnetwork by using the candidate gene set as seeds (16). A PPI network was built using the Search Tool for the Retrieval of Interacting Genes (STRING) database (version 11.0; https://string-db.org/) (17) and visualised by Cytoscape (an open-source software platform) (18).

Survival Analysis of New Genes Based on mRNA Expression

The prognostic value of the expression of new gene mRNAs was evaluated using publicly available miRNA expression datasets (Pan-cancer RNA-seq) in Kaplan-Meier plotter (http://kmplot. com/analysis/), an online database including gene expression data and clinical data (19, 20). To assess the prognostic value of a specific gene, the patient samples were divided into two cohorts (high and low expression groups) according to the median mRNA expression of the gene. We analysed the overall survival (OS) of ESCC patients by using a Kaplan-Meier survival plot. Briefly, eight genes (*CUL3*, *MUC13*, *MMS22L*, *MME*, *UBC*, *VAPA*, *CYP1B1*, and *UGDH*) were uploaded into the database respectively to obtain the Kaplan-Meier survival plots, in which the number-at-risk is shown below the main plot. Log rank *p*-value and hazard ratio (HR) with 95% confidence intervals were calculated and displayed on the picture. A *p*-value <0.05 was considered statistically significant.

Patients and Tumour Samples

Sixty-one ESCC tissues were obtained from the Department of Thoracic Surgery of Sichuan Cancer Hospital (Chengdu, China) from Jan 2018 to Sept 2019 in this study, and all the samples were histologically confirmed to be ESCC tissues by a postoperative pathologist. Twenty-three paired human ESCC cancer tissues and matched adjacent normal tissues (located at least 5 cm from the tumour border, **Supplementary Figure S1**) from 23 patients with surgery alone were snap frozen after they were taken from surgery and then stored in liquid nitrogen for quantitative real-time PCR and Western blotting. Another 38 ESCC biopsy specimens from the gastroscopies were paraffin embedded for immunohistochemical staining analysis before patients received NCRT. The samples used in the study were approved by the Ethical Committee of the Sichuan Cancer Hospital (No. SCCHEC-02-2017-043), and the patients provided written informed consent to participants.

Cell Culture

The human ESCC cell lines TE-1, Kyse150, and Eca109 and the human normal oesophageal cell line HEEC were provided by the Shanghai Institute of Cell Biology, Chinese Academy of Sciences. All the cell lines were maintained in RPMI-1640 (HyClone, USA) supplemented with 100 U/ml of penicillin-streptomycin (HyClone, USA) and 10% foetal bovine serum (FBS; Gibco, USA) at 37°C with 5% CO_2 in a humidified atmosphere.

Quantitative Real-Time PCR

The mRNA expression of *MMS22L* was measured by quantitative real-time polymerase chain reaction (qRT-PCR). The above cell clines and 23 paired human ESCC cancer tissues and matched adjacent normal tissues were individually

homogenised in liquid nitrogen, and total RNA was extracted from cells and tissues using TRIzol reagent (Invitrogen, Waltham, MA, USA). The total RNA products were immediately transcribed into cDNA using a cDNA synthesis kit (Takara, Kyoto, Japan) following the manufacturer's instructions. Complementary DNA was amplified using TB Green™ Advantage® qPCR Premix (Takara, Kyoto, Japan) on the CFX-Connect Real-Time PCR Detection System (Bio-Rad, Hercules, CA, USA). The *MMS22L* primers were as follows: forward 5′-CAGAGAATGTCACAGGTAGTGCC-3′; reverse 5′-TCTGATGGAGCTGTGCTTGGCA-3′. The conditions for qRT-PCR were as follows: initial denaturation at 95°C for 2 min, followed by 40 cycles of 95°C for 5 s and 55°C–57°C for 30 s, and melting curves were generated by heating from 55°C to 95°C with 0.5°C increments each cycle. The results were normalised to β-actin using the $2^{-\Delta\Delta Ct}$ method (21), the forward primer: 5′-CTTAGTTGCGTTACACCCTTTCTTG-3′ and reverse primer 3′-ACTGCTGTCACCTTCACCGTTC-5′. All the experiments were performed in triplicate.

Western Blotting

The Total proteins of tissues and cells were extracted using RIPA buffer with protease inhibitors (Biyuntian, China). The protein concentrations were measured using the bicinchoninic acid (BCA) Protein Assay Kit (Beijing Suolabao Biotech, China). The *MMS22L* protein levels in cancer tissue and adjacent tissue were evaluated by Western blotting (WB). Briefly, equal amounts of total protein extract were first separated in an 8% SDS-PAGE gel and transferred onto PVDF membranes (Millipore, Billerica, MA, USA). Next, the membranes were blocked for 2 h with PBST and 5% milk at room temperature, incubated with primary antibody overnight at 4°C and then with secondary antibody for 2 h at room temperature. Protein expression was detected using an anti-*MMS22L* (*C6orf167*) antibody (ab181047, 1:1,000, Abcam, Cambridge, MA, USA) and a β-actin polyclonal antibody (1:1,000 CST, Danvers, MA, USA). Protein bands were detected using an Immobilon® Western system (Millipore; #WBKLS0100) and imaged on the Minichemi machine (Sage Creation, Beijing, China).

Immunohistochemical Staining and Image Analysis

Tissues from paraffin-embedded blocks were sectioned at 5-μm thickness. Immunohistochemical staining (IHC) was performed using DAB kit (Zhongshan Golden Bridge, Beijing, China) following the manufacturer's protocol. The anti-*MMS22L* antibody (bs17689R) used for IHC was purchased from Bioss (Beijing, China). To quantify *MMS22L* staining, five randomly chosen fields per section were evaluated at ×200 magnification for each sample. Image-Pro Plus 6.0 was used to determine integrated optical density (IOD) values, and the IOD per unit area (mean density) represented the relative *MMS22L* expression level.

Cell Transfection

Two target small hairpin RNA (shRNA) lentiviruses of the *MMS22L* gene, sh147 and sh148 and a negative control shRNA lentivirus con077 were designed and synthesised by Shanghai Ji

Kai Gene Technology Co., Ltd. (Shanghai, China). TE-1 cells were infected with lentivirus at an MOI of 10 PFU per cell. Stable transformants were selected with 2 µg/ml of puromycin. The knockdown efficiency was detected by qRT-PCR and Western blotting.

Transswell Assay

Transwell migration assays were performed using plates (Corning, Corning, NY, USA) with 8-µm-pore size membranes. Briefly, 2×10^4 cells were suspended in 200 µl of FBS-free RPMI-1640 medium and added to the upper chambers of Transwell plates. RPMI-1640 medium (500 µl) supplemented with 5% FBS was seeded into the lower chamber. After a 24-h incubation period at 37°C and 5% CO_2, the migrated cells were fixed with 4% paraformaldehyde (in $1 \times$ PBS) for 20 min at room temperature and then were stained with crystal violet.

Cytotoxicity Assay

Cytotoxicity was assayed using cell counting kit (CCK8; Hanheng, Shanghai, China) following the manufacturer's instructions. Briefly, cells were seeded on 96-well plates at a density of 2.0×10^3 per well. After cells were treated with 5-FU (Selleck, Houston, TX, USA) at concentrations of 0, 0.1, 1, 5, 10, and 100 µM for 72 h, the medium containing 5-FU was exchanged for 100 µl of RPMI-1640, and 10 µl of CCK8 reagent was added. Two hours later, absorbance at 450 nm was measured using a microplate reader. Each group had three repeats, and the experiment was repeated three times.

Statistical Analysis

All the data were obtained from at least three independent measurements and were shown as means ± SEM. Student's t-test, Mann-Whitney tests, and receiver and IC_{50} operating characteristic (ROC) curves were performed using GraphPad Prism 7 software (GraphPad Software Inc., San Diego, CA, USA). One-way analysis of variance (ANOVA) followed by Tukey's *post-hoc* test was used for data analysis among three or more groups. Statistical analysis was conducted, and statistical significance was set at $p < 0.05$.

RESULTS

Candidate Gene Sets and Functional Enrichment

As described in the *Materials and Methods* section, 101 candidate genes associated with the efficacy of chemoradiotherapy in patients with ESCC were assembled after removing duplicates. The GO annotations were classified as biological process, cellular component, and molecular function ($p < 0.05$), and the top 10 GO terms are shown in **Figures 1A–C**, respectively. The top biological process GO enrichment terms were cotranslational protein targeting the membrane, targeting the ER, and establishment of protein localisation to endoplasmic reticulum. Ribosome component was the most enriched cellular component GO term. Additionally, we found several enriched molecular functions such

as structural constituent of ribosome, damaged DNA binding, antigen binding, single-stranded DNA binding, and ubiquitin protein ligase binding. Furthermore, the KEGG pathways in which 101 candidate genes were mostly enriched were ribosome, followed by human T-cell leukaemia virus 1 infection, platinum drug resistance, human cytomegalovirus infection, proteoglycans in cancer, etc. (**Figure 1D**).

Construction of the Protein Subnetwork

The protein subnetwork comprised 105 nodes and 379 edges (interactions), and 97 of 101 candidate genes were included in the subnetwork, accounting for 92.38% of 105 genes in the network and 96% of 101 candidate genes, and demonstrating a high coverage of the candidate genes set in the subnetwork (**Figure 2**). Additionally, eight genes in the subnetwork outside of the candidate gene set were obtained (**Table 1**).

Prognostic Value of mRNA Expression of Eight New Genes in ESCC

Using the Kaplan-Meier plotter database, the prognostic value of the eight novel genes was evaluated in ESCC patients. We found that higher and lower expression of five biomarkers was significantly associated with overall survival. ESCC patients with higher mRNA levels of *MMS22L* (HR = 0.33; CI: 0.14–0.75; logrank $p = 0.0052$) and *MUC13* (HR = 0.37; CI: 0.14–0.96; logrank $p = 0.033$) had higher OS (**Figures 3A, B**), and ESCC patients with lower mRNA levels of *VAPA* (HR = 2.32; CI: 1.04 −5.17; logrank $p = 0.035$), *CYP1B1* (HR = 2.67; CI: 1.02–6.97; logrank $p = 0.039$), and *UBC* (HR = 2.26; CI: 1.03−4.96; logrank $p = 0.038$) had higher OS (**Figures 3C–E**), while the mRNA expression of *UGDH, MME* and *CUL13* were not associated with ESCC patient survival (**Figures 3F–H**).

Expression of the *MMS22L* Genes in Cancer and Adjacent Normal Tissues

MMS22L is not a well-studied protein, and information about this gene product is very limited. As described above, the expression of *MMS22L* had the most significant association with ESCC patient outcome. Cellular components associated with the function of *MMS22L* were significantly enriched, such as damaged DNA binding and ubiquitin protein ligase binding. Therefore, we further detected the expression level of the *MMS22L* gene in ESCC tissues and adjacent normal tissues using quantitative real-time PCR and WB. MM*S22L* mRNA expression was significantly decreased in ESCC tissue compared with that in adjacent normal tissues ($p < 0.05$) (**Figure 4A**), and WB results were consistent with the RT-qPCR (**Figure 4B**). *MMS22L* protein expression was significantly reduced in seven tumour tissues compared with that in normal adjacent tissues.

Predictive Value of *MMS22L* for NCRT Efficacy in Patients With ESCC

According to the RECIST 1.1 criteria (22), the response to NCRT was defined as complete response (CR), partial response (PR), stable disease, (SD), and progressive disease (PD), and the 38 patients receiving NCRT were divided into the responding group
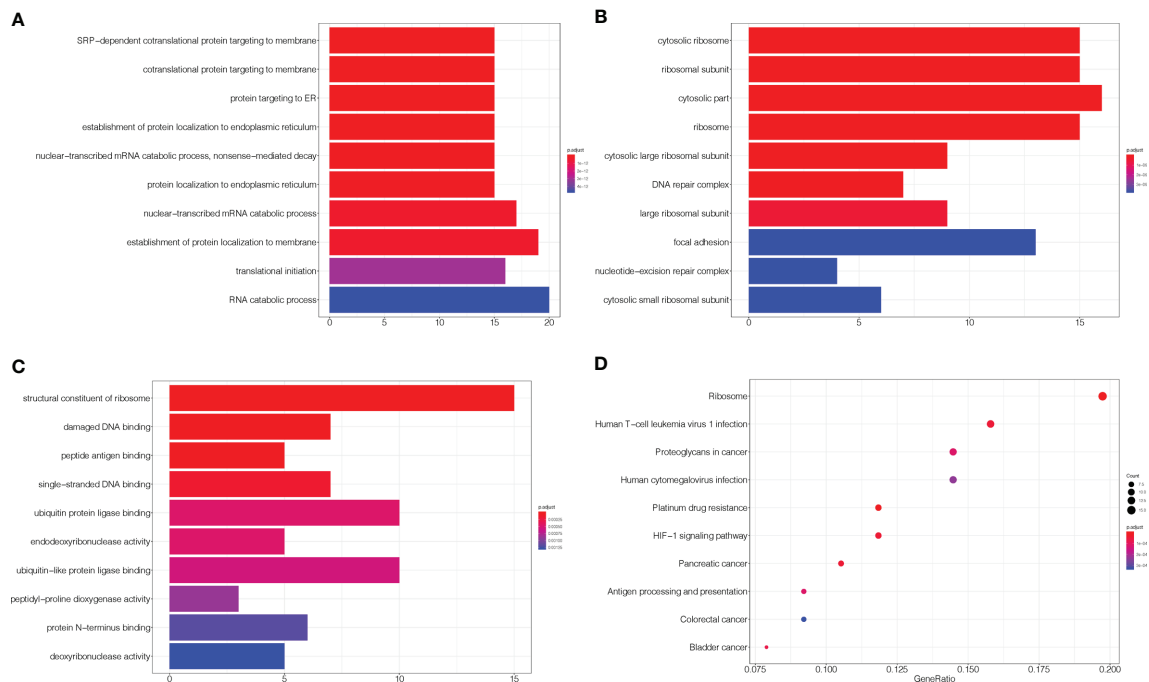
FIGURE 1 | GO and KEGG enrichment of related genes. **(A–C)** The top 10 GO terms in biological process, cellular component, and molecular function, respectively. **(D)** KEGG pathways were analysed, and the top 10 pathways are shown. The x-axis shows the GeneRatio, whereby a higher value indicates more genes enriched in the pathway; the y-axis shows the enriched pathways, and the redder the dot is, the more significant is the pathway.

(CR plus PR, 29 patients) and nonresponding group (SD, nine patients) according to the response to NCRT in this study. *MMS22L* IHC in representative tumour tissues are shown in **Figure 5A**. The *MMS22L* protein in the responding group was significantly higher than that in the nonresponding groups ($p <$ 0.01, **Figure 5B**). This result indicated that the *MMS22L* expression significantly predicted a response to NACRT. ROC curve analyses revealed that *MMS22L* was a valuable biomarker for differentiating responding from nonresponding for NCRT. *MMS22L* yielded an AUC of 0.847 (95% CI: 0.7232 to 0.9703; $p <$ 0.01; **Figure 5C**) with 100% sensitivity and 65.52% specificity in predicting the efficacy of NCRT in ESCC. Additionally, among the various clinicopathological characteristics evaluated, no significant associations were found between the *MMS22L* expression level and age, sex, differentiation, location, depth of invasion, or TNM clinical stage, but a low expression level of *MMS22L* was markedly associated with lymph node metastasis ($p <$ 0.01; **Table 2**).

MMS22L Inhibits Migration and Modulates 5-FU Sensitivity in TE-1 Cells

To assess *MMS22L* expression in human ESCC cells, we detected the mRNA and protein expression of *MMS22L* in HEEC cells and three human ESCC cell lines (TE-1, Kyse150, and Eca109) by qRT-PCR and WB, respectively. The expression of *MMS22L* was lower in TE-1, Kyse150, and Eca109 cells than in HEEC cells (**Figure 6A**). TE-1 cells showed the highest *MMS22L* expression in three human ESCC cell lines. Thus, TE-1 cells were selected

for subsequent assays. After targeting *MMS22L* with two different shRNAs, the knockdown efficiency was detected (**Figure 6B**). We performed Transwell migration assays to analyse whether *MMS22L* inhibits the migration ability of TE-1 cells. *MMS22L* inhibited the migration of TE-1 cells (**Figure 6C**). Different TE-1 cells were determined by CCK8 assays with different doses of 5-FU to calculate the IC_{50} and were performed in triplicate. The IC_{50} value decreased significantly after *MMS22L* knockout (**Figure 6D**). These results from *in vitro* experiments indicated that the knockdown of *MMS22L* in the TE-1 cell line is associated with enhanced migration and resistance to 5-FU.

DISCUSSION

According to published statistics, approximately 572,034 new oesophageal cancer cases (3.2%) and an estimated 508,585 related deaths (5.3%) occurred [1]. With the development of comprehensive treatment strategies, patients with ESCC benefit from NCRT [5]. However, the postoperative pathological complete response rate was only 43.2% according to a phase III, multicentre, randomised open-label clinical trial (NEOCRTEC5010) [23]. Therefore, further understanding of NCRT resistance-related genes as novel prognostic biomarkers in ESCC is necessary. Recently, an increasing number of potential genes have been found to be associated with chemoradiotherapy efficacy and prognosis in patients with cancer. However, a few of these predicted genes have
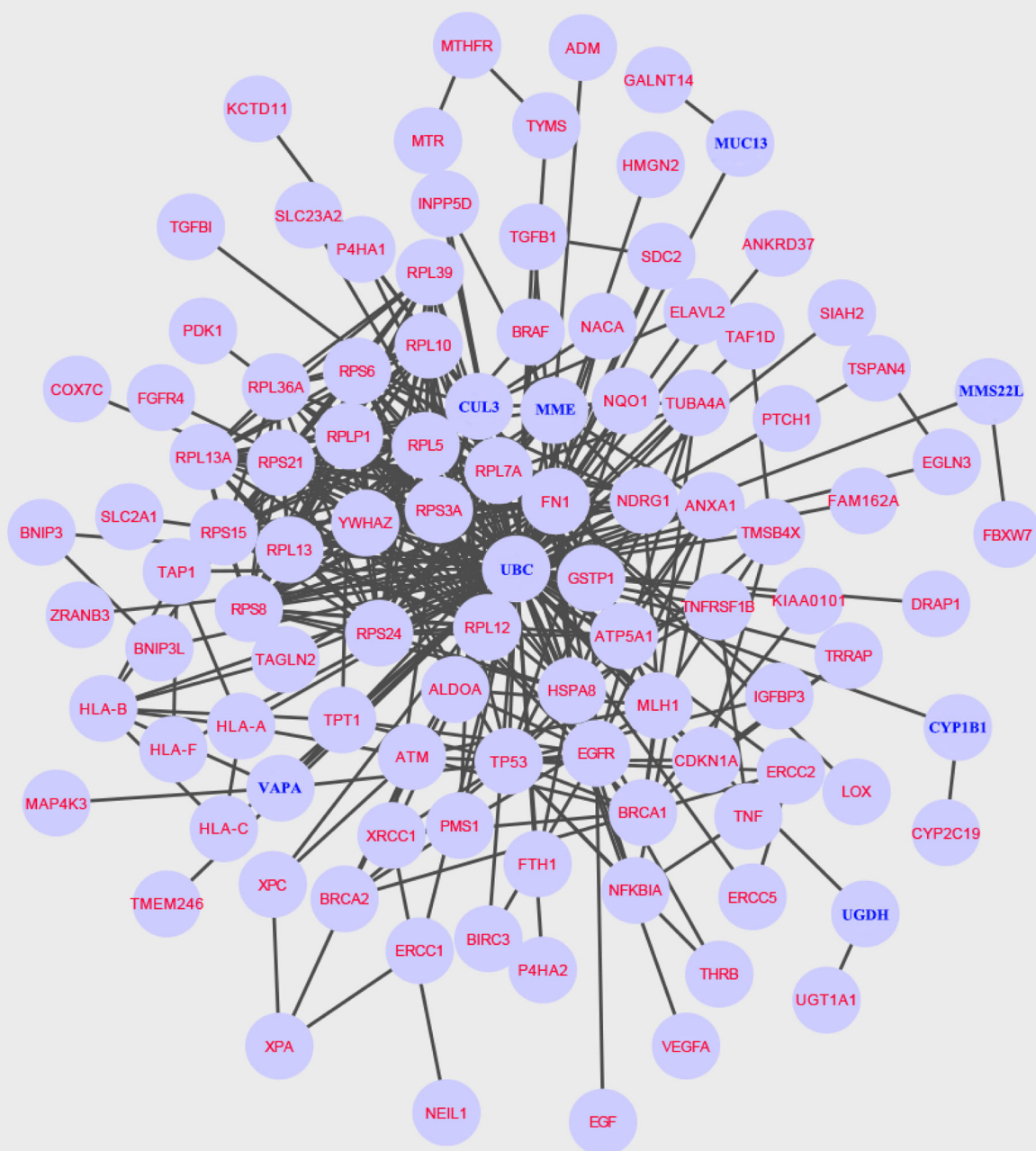
FIGURE 2 | A specific protein network associated with NCRT efficacy is built using the Steiner minimal tree algorithm, including 105 nodes and 379 edges. Additionally, eight new genes are labelled in blue.

been identified in ESCC, and a few biomarkers are available for clinical monitoring.

In our study, we applied the Steiner minimum tree algorithm to explore novel biomarkers in the context of a human PPI

background. First, a list of 101 candidate genes associated with the efficacy of chemoradiotherapy in patients with ESCC was assembled in 79 relevant articles. Simultaneously, to better understand the function of these genes in ESCC, we performed

Gene symbol	Gene ID	Map location	Description
UGDH	7358	4p14	UDP-glucose 6-dehydrogenase
MME	4311	3q25.2	Membrane metalloendopeptidase
VAPA	9218	18p11.22	VAMP-associated protein A
CUL3	8452	2q36.2	Cullin 3
UBC	7316	12q24.31	Ubiquitin C
CYP1B1	1545	2p22.2	Cytochrome P450 family 1 subfamily B member 1
MUC13	56667	3q21.2	Mucin 13, cell surface associated
MMS22L	253714	6q16.1	MMS22 like, DNA repair protein

GO and KEGG analyses. Notably, KEGG analysis revealed that the pathways in which these genes are mainly enriched are ribosome, human T-cell leukaemia virus 1 infection, platinum drug resistance, human cytomegalovirus infection, and proteoglycans in cancer. Second, we obtained eight novel genes associated with linking genes potentially related to chemoradiotherapy efficacy in ESCC outside the candidate gene set. Referring to published studies, the findings of our study validate previous reported outcomes because different functions of these genes have been identified to be associated with ESCC. *MUC13* is a potential biomarker to predict the efficacy of neoadjuvant chemotherapy in ESCC patients (24, 25). Moghadam et al. suggest a relationship between the *CYP1B1*-rs1056836 genetic
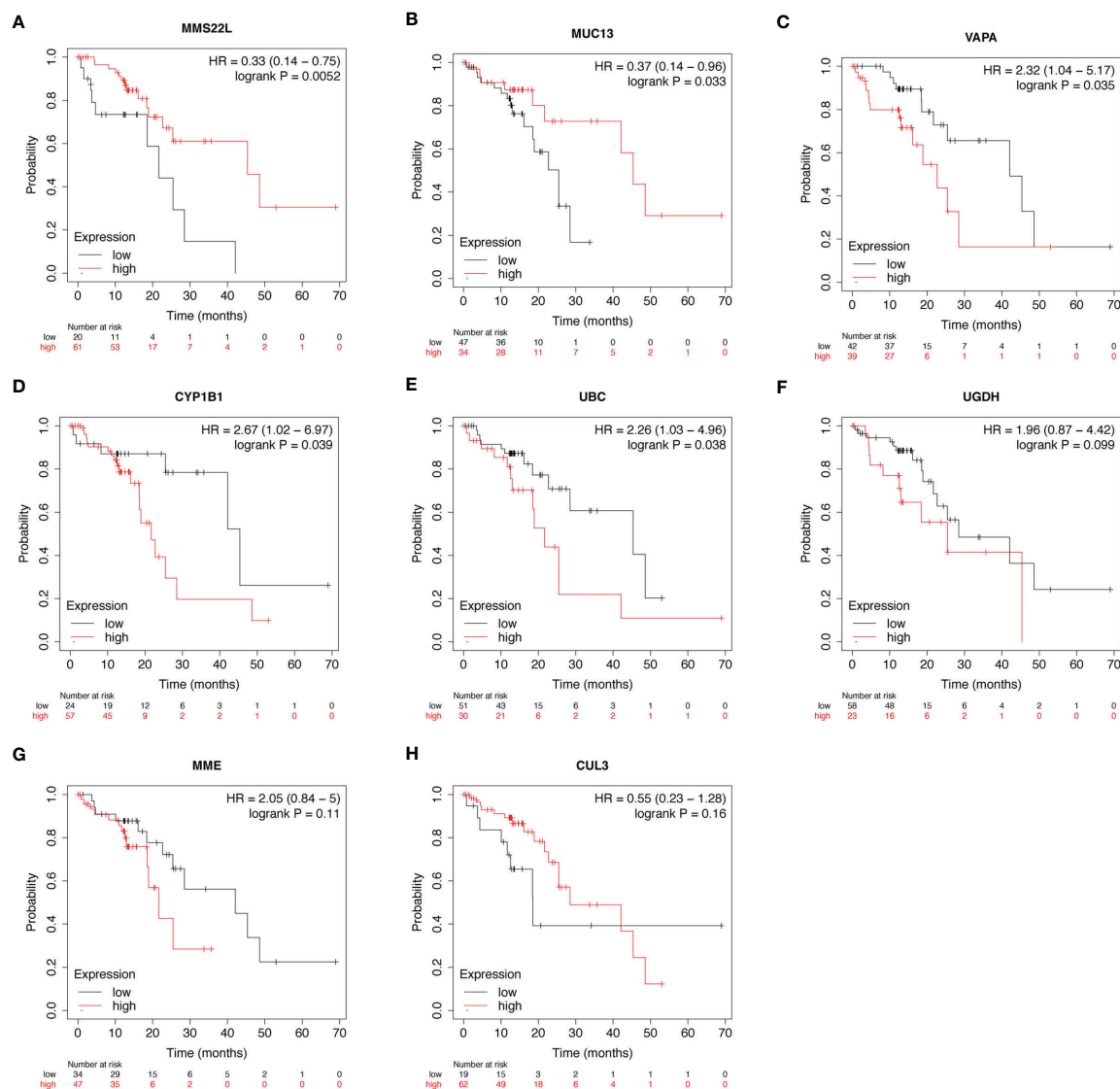
FIGURE 3 | Prognostic value of mRNA expression of eight genes in patients with ESCC. **(A–H)** Overall Survival curves of MMS22L **(A)**, MUC13 **(B)**, VAPA **(C)**, CYP1B1 **(D)**, UBC **(E)**, UGDH **(F)**, MME **(G)**, and CUL13 **(H)** were plotted in Kaplan-Meier plotter. "Probability" on the y-axis represents the survival rates, the red line represents the patients with mRNA expression above the median, and the black line represents the patients with mRNA expression below the median. ESCC, Oesophageal squamous cell carcinoma; HR, hazard ratio.
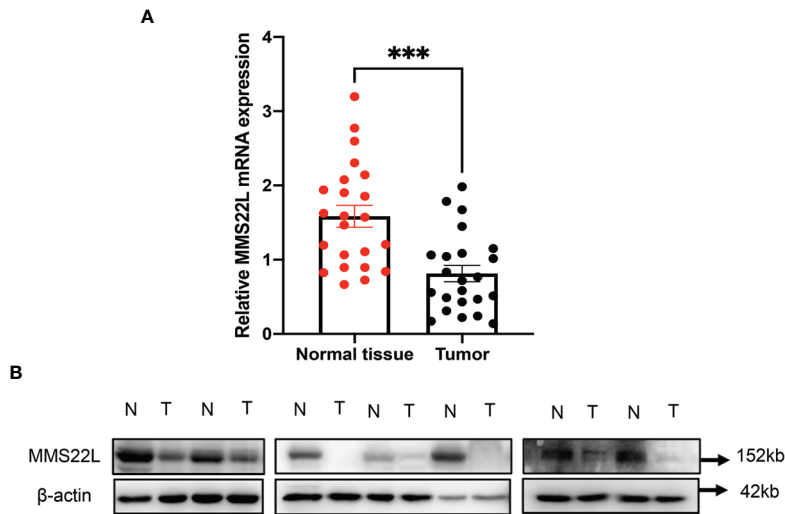
FIGURE 4 | The *MMS22L* mRNA and protein levels are significantly lower in cancerous tissues than in normal adjacent tissues. **(A)** *MMS22L* mRNA was detected by qRT-PCR, and relative quantification analysis was normalised to *β-actin* mRNA (***$p < 0.001$). **(B)** *MMS22L* protein expression was detected in randomly selected seven ESCC tissues and adjacent normal tissues using Western blotting. T, tumour tissues; N, normal adjacent tissues.

Groups	Case	Mean density	SEM
Responding	29	0.04261	0.003004
Non-responding	9	0.02430	0.002326

Cut-off value	0.03496
Sensitivity	100%
Specificity	65.52%
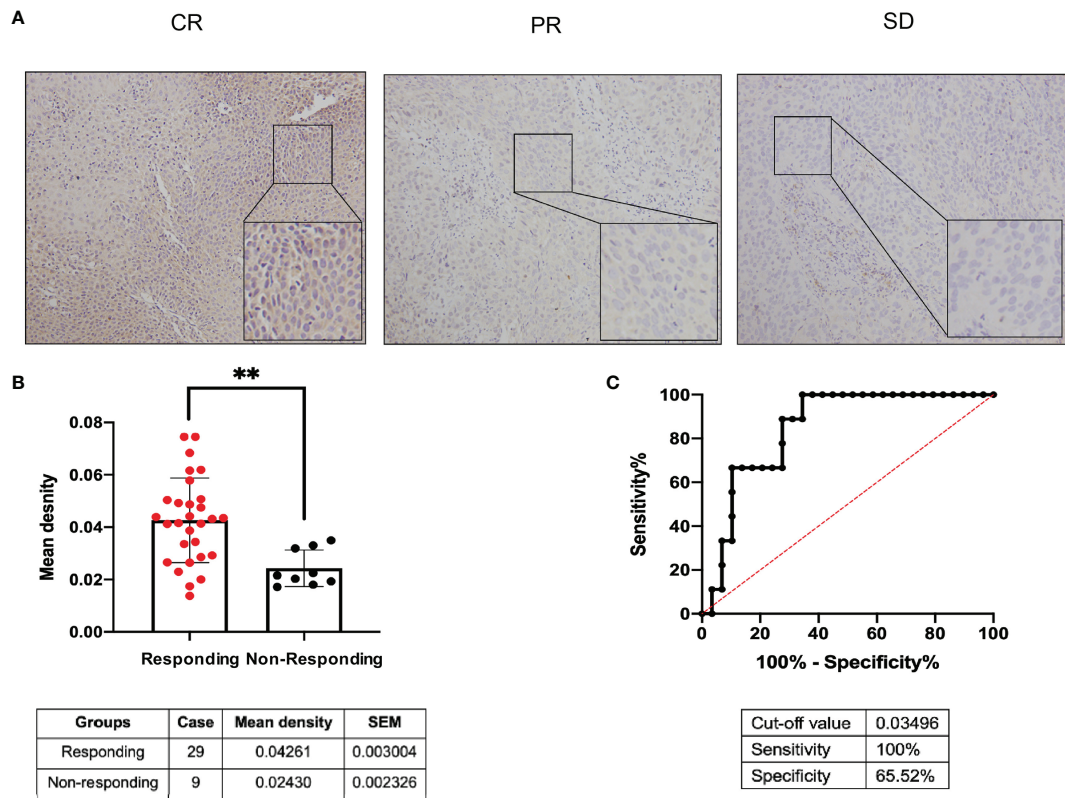
FIGURE 5 | Predictive value of *MMS22L* for different responses to NCRT in patients with ESCC. **(A)** *MMS22L* IHC in representative tumour tissues. **(B)** The mean density of the responding group and nonresponding group from all 38 cases who received NCRT is summarised in the table below. **(C)** ROC curve for evaluating the predictive value of *MMS22L* for ESCC patients with NCRT. The AUC was 0.847, the sensitivity was 100%, the specificity was 65.52%, and the cutoff value was 0.03495 (**$p < 0.01$). NCRT, neoadjuvant chemoradiotherapy; AUC, area under the ROC curve; ROC, receiver operating characteristic.

TABLE 2 | Association of *MMS22L* expression in the biopsy specimens with clinicopathological parameters.

Variable	N	Mean density ± SEM	p-Value
Age (year)			
≥60	24	0.03872 ± 0.003568	0.9366
<60	14	0.03698 ± 0.003682	
Sex			
Male	33	0.03859 ± 0.002842	0.7376
Female	5	0.03618 ± 0.008554	
Differentiation			
G1/Gx	24	0.04380 ± 0.003507	0.2028
G2	6	0.04526 ± 0.01146	
G3	8	0.02946 ± 0.004677	
Location			
Upper	8	0.03477 ± 0.005017	0.8406
Moderate	19	0.03978 ± 0.004123	
Lower	11	0.03901 ± 0.005607	
Depth of invasion			
cT1-T2	13	0.04069 ± 0.003240	0.2587
cT3-T4	25	0.03790 ± 0.003948	
Lymph node metastasis			
cN0	27	0.04188 ± 0.002912	0.0095
cN+	11	0.02942 ± 0.005090	
Stage			
cI-II	13	0.03962 ± 0.003136	0.3449
cIII-IV	25	0.03757 ± 0.003753	

The mean density represents the relative MMS22L expression level.

polymorphism and clinical features of ESCC (26). Therefore, the results of the present study are considered to be reliable.

To further identify effective biomarkers with diagnostic and prognostic value, we evaluated the effects of the eight novel genes on the survival of ESCC patients using the online Kaplan-Meier plotter. ESCC patients with higher mRNA levels of *MMS22L* and *MUC13* had higher OS. Additionally, ESCC patients with lower mRNA levels of *VAPA*, *CYP1B1*, and *UBC* had higher OS. As shown in the Kaplan-Meier plotter, *MMS22L* expression was the most likely candidate gene among many novel genes. The *MMS22L* gene is mapped to chromosome 6 open-reading frame 167, also known as *C6orf167*. In our study, *MMS22L* expression in 23 ESCC tissues was notably lower than that in their para-carcinoma tissues, and this trend was consistently observed across the ESCC cell lines and the human normal oesophageal cell line. Thus, *MMS22L* may be a tumour suppressor gene in ESCC. In contrast to our findings, a previous study found that *MMS22L* expression was upregulated in lung and oesophageal cancer tissues compared with that in adjacent normal lung and oesophageal tissues, and *MMS22L* was identified as an oncogene (27). This discrepancy may arise from the inadequate sample size and unknown oesophageal cancer histologic type in their study. Many genes play both tumour suppressor or oncogenic roles in different tissues, tumour types, or cellular contexts (28).
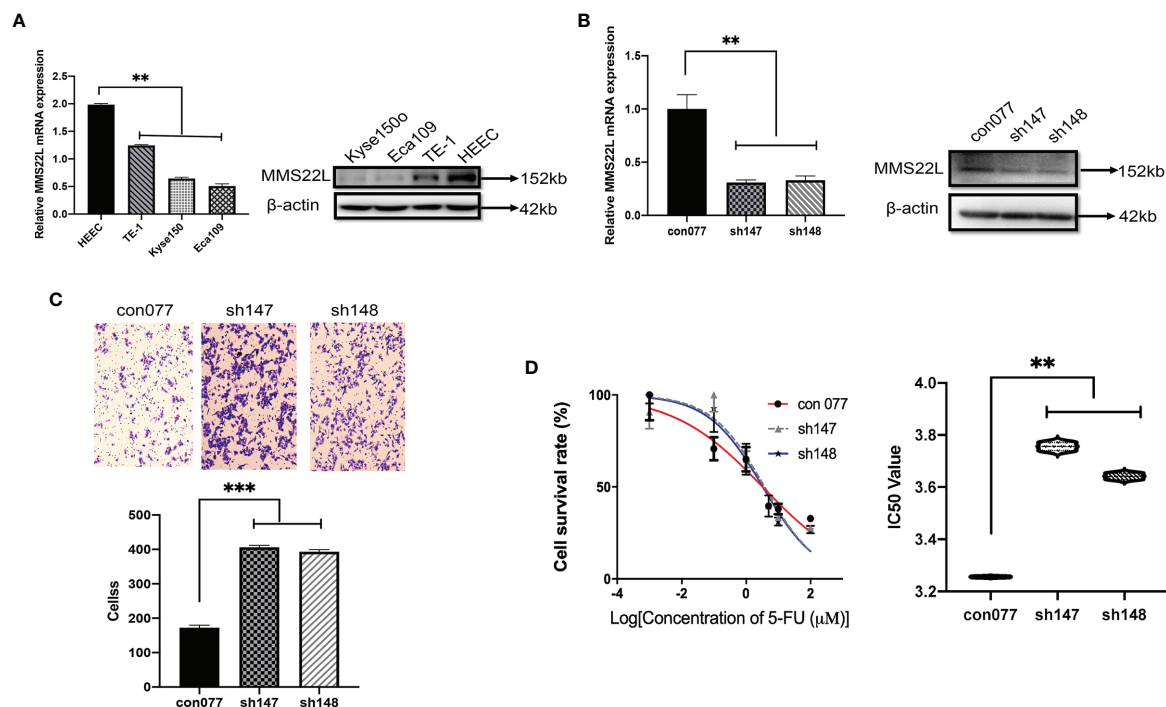
FIGURE 6 | Lower expression of *MMS22L* increases the migration capabilities and the 5-FU resistance of TE-1 cells. **(A)** *MMS22L* expression in a human normal oesophageal cell line (HEEC) and human ESCC cell lines. **(B)** The transfection efficiency was measured after 48 h. **(C)** In the shRNA groups, the migration capabilities increased and the number of migrating cells increased compared with those in the con077 group. **(D)** IC_{50} values of TE-1 cells to 5-FU were detected *via* the CCK8 assay after transfection (**$p < 0.01$; ***$p < 0.001$). CCK8, cell counting kit; IC_{50}, half-maximal inhibitory concentration; 5-FU, 5-fluorouracil.

Previous studies have shown that *MMS22L* plays critical roles in the DNA damage response and repair, affecting the response of tumour cells to DNA-damaging agents, such as camptothecin (CPT), ionising radiation (IR), hydroxyurea (HU), and methyl methanesulfonate (MMS) (29–32). According to previous reports, knocking down *MMS22L* promoted apoptosis by activating caspase-3 and downregulating *Bcl-XL* (29), an inhibitor of apoptosis. Importantly, Duro et al. found that tumour cells lacking *MMS22L* were resistant to HU, cisplatin, and IR. However, this finding is inconsistent with that reported by O'Connell et al. who found that Hela cells lacking *MMS22L* were sensitive to IR, CPT, and MMS (30). Additionally, downregulation of *MMS22L* is associated the bone metastasis in breast cancer (33). Previous controversial results have generated considerable interest regarding the function of *MMS22L* in ESCC. In the present study, we found that low *MMS22L* expression, immunohistochemically stained and analysed semiquantitatively in ESCC samples, was a useful predictor of worse responses to NCRT and lymph node metastasis, and enhanced migration and resistance to 5-FU in the TE-1 cell line. These findings were corroborated by *in vitro* studies showing that the knockdown of *MMS22L* in the TE-1 cell line was associated with enhanced migration and resistance to 5-FU.

Proteins associated with each other in the String Protein-Protein Interaction Network have related functions, and *FBXW7* is most closely related to *MMS22L*. *FBXW7* is an F-box protein that binds to key regulators of cell division and growth, including cyclin E, *MYC*, *JUN*, and Notch (34). *FBXW7* is a critical tumour suppressor involved in the ubiquitin-proteasome system in human cancer, and loss of *FBXW7* function leads to chromosomal instability (34, 35). *FBXW7* expression is downregulated in ESCC tissues and correlates with the TNM stage, the degree of differentiation, the invasion depth, the lymph node metastasis, and a worse prognosis in ESCC (36, 37). Mutations in *FBXW7* are associated with metastasis and correlates with increased expression of T-cell proliferation and antigen presentation functions (38). These results may suggest that an indirect or direct regulatory function between *MMS22L* and *FBXW7* will contribute to tumour progression and metastasis through immunological effects or the tumour microenvironment. However, this interpretation of these data remains speculative at this point and will require further cell biological studies.

In conclusion, network analysis based on molecular aspects associated with the efficacy of chemoradiotherapy in ESCC may facilitate identification of novel biomarkers and a deeper understanding of the mechanisms. Our approach presents interesting approaches for future studies. Additionally, our data indicate that low *MMS22L* expression status in biopsy specimens is a predictive factor for the unfavourable efficacy of NACRT in ESCC. Therefore, patients with ESCC receiving NCRT are likely to fail when *MMS22L* downregulation is observed on a biopsy specimen. However, a larger sample size will be needed to validate and possibly extend these findings.

DATA AVAILABILITY STATEMENT

The original contributions presented in the study are included in the article/**Supplementary Material**. Further inquiries can be directed to the corresponding authors.

ETHICS STATEMENT

The studies involving human participants were reviewed and approved by the Ethical Committee of the Sichuan Cancer Hospital (No. SCCHEC-02-2017-043). The patients/participants and legal guardian/next of kin provided written informed consent to participate in this study.

AUTHOR CONTRIBUTIONS

Conception and design: YH and CX. Acquisition of data: QL and WH. Analysis and interpretation of data: TM and XL. Drafting of the manuscript: QL and WH. Critical revision of the manuscript for important intellectual content: YH and CX. Harvesting of the specimen: XD and MS. Administrative, technical, or material support: HW, WL, and TZ. All authors contributed to the article and approved the submitted version.

SUPPLEMENTARY MATERIAL

The Supplementary Material for this article can be found online at: https://www.frontiersin.org/articles/10.3389/fonc.2021.711642/full#supplementary-material

REFERENCES

1. Bray F, Ferlay J, Soerjomataram I, Siegel RL, Torre LA, Jemal A. Global Cancer Statistics 2018: GLOBOCAN Estimates of Incidence and Mortality Worldwide for 36 Cancers in 185 Countries. *CA Cancer J Clin* (2018) 68 (6):394–424. doi: 10.3322/caac.21492

2. Liang H, Fan JH, Qiao YL. Epidemiology, Etiology, and Prevention of Esophageal Squamous Cell Carcinoma in China. *Cancer Biol Med* (2017) 14(1):33–41. doi: 10.20892/j.issn.2095-3941.2016.0093

3. Liu M, He Z, Guo C, Xu R, Li F, Ning T, et al. Effectiveness of Intensive Endoscopic Screening for Esophageal Cancer in China: A Community-Based Study. *Am J Epidemiol* (2019) 188(4):776–84. doi: 10.1093/aje/kwy291

4. Gusella M, Pezzolo E, Modena Y, Barile C, Menon D, Crepaldi G, et al. Predictive Genetic Markers in Neoadjuvant Chemoradiotherapy for Locally Advanced Esophageal Cancer: A Long Way to Go. Review of the Literature. *Pharmacogenomics J* (2018) 18(1):14–22. doi: 10.1038/tpj.2017.25

5. Shapiro J, van Lanschot JJB, Hulshof M, van Hagen P, van Berge Henegouwen MI, Wijnhoven BPL, et al. Neoadjuvant Chemoradiotherapy Plus Surgery *Versus* Surgery Alone for Oesophageal or Junctional Cancer (CROSS): Long-Term Results of a Randomised Controlled Trial. *Lancet Oncol* (2015) 16 (9):1090–8. doi: 10.1016/s1470-2045(15)00040-6

6. van Hagen P, Hulshof MC, van Lanschot JJ, Steyerberg EW, van Berge Henegouwen MI, Wijnhoven BP, et al. Preoperative Chemoradiotherapy for Esophageal or Junctional Cancer. *New Engl J Med* (2012) 366(22):2074–84. doi: 10.1056/NEJMoa1112088

7. Meredith KL, Weber JM, Turaga KK, Siegel EM, McLoughlin J, Hoffe S, et al. Pathologic Response After Neoadjuvant Therapy is the Major Determinant of Survival in Patients With Esophageal Cancer. *Ann Surg Oncol* (2010) 17 (4):1159–67. doi: 10.1245/s10434-009-0862-1

8. Oppedijk V, van der Gaast A, van Lanschot JJ, van Hagen P, van Os R, van Rij CM, et al. Patterns of Recurrence After Surgery Alone *Versus* Preoperative Chemoradiotherapy and Surgery in the CROSS Trials. *J Clin oncology: Off J Am Soc Clin Oncol* (2014) 32(5):385–91. doi: 10.1200/jco.2013.51.2186

9. Dittrick GW, Weber JM, Shridhar R, Hoffe S, Melis M, Almhanna K, et al. Pathologic Nonresponders After Neoadjuvant Chemoradiation for Esophageal Cancer Demonstrate No Survival Benefit Compared With Patients Treated With Primary Esophagectomy. *Ann Surg Oncol* (2012) 19 (5):1678–84. doi: 10.1245/s10434-011-2078-4

10. Donahue JM, Nichols FC, Li Z, Schomas DA, Allen MS, Cassivi SD, et al. Complete Pathologic Response After Neoadjuvant Chemoradiotherapy for Esophageal Cancer Is Associated With Enhanced Survival. *Ann Thorac Surg* (2009) 87(2):392–8; discussion 8-9. doi: 10.1016/j.athoracsur.2008.11.001

11. Pasini F, de Manzoni G, Zanoni A, Grandinetti A, Capirci C, Pavarana M, et al. Neoadjuvant Therapy With Weekly Docetaxel and Cisplatin, 5-Fluorouracil Continuous Infusion, and Concurrent Radiotherapy in Patients With Locally Advanced Esophageal Cancer Produced a High Percentage of Long-Lasting Pathological Complete Response: A Phase 2 Study. *Cancer* (2013) 119(5):939–45. doi: 10.1002/cncr.27822

12. Gerlinger M, Rowan AJ, Horswell S, Math M, Larkin J, Endesfelder D, et al. Intratumor Heterogeneity and Branched Evolution Revealed by Multiregion Sequencing. *New Engl J Med* (2012) 366(10):883–92. doi: 10.1056/NEJMoa1113205

13. Wu D, Wang DC, Cheng Y, Qian M, Zhang M, Shen Q, et al. Roles of Tumor Heterogeneity in the Development of Drug Resistance: A Call for Precision Therapy. *Semin Cancer Biol* (2017) 42:13–9. doi: 10.1016/j.semcancer.2016.11.006

14. Yu G, Wang LG, Han Y, He QY. Clusterprofiler: An R Package for Comparing Biological Themes Among Gene Clusters. *Omics* (2012) 16(5):284–7. doi: 10.1089/omi.2011.0118

15. Wu J, Vallenius T, Ovaska K, Westermarck J, Mäkelä TP, Hautaniemi S. Integrated Network Analysis Platform for Protein-Protein Interactions. *Nat Methods* (2009) 6(1):75–7. doi: 10.1038/nmeth.1282

16. Zheng S, Zhao Z. Genrev: Exploring Functional Relevance of Genes in Molecular Networks. *Genomics* (2012) 99(3):183–8. doi: 10.1016/j.ygeno.2011.12.005

17. Szklarczyk D, Gable AL, Lyon D, Junge A, Wyder S, Huerta-Cepas J, et al. STRING V11: Protein-Protein Association Networks With Increased Coverage, Supporting Functional Discovery in Genome-Wide Experimental Datasets. *Nucleic Acids Res* (2019) 47(D1):D607–d13. doi: 10.1093/nar/gky1131

18. Wiredja D, Bebek G. Identifying Gene Interaction Networks. *Methods Mol Biol* (2017) 1666:539–56. doi: 10.1007/978-1-4939-7274-6_27

19. Madamsetty VS, Pal K, Dutta SK, Wang E, Mukhopadhyay D. Targeted Dual Intervention-Oriented Drug-Encapsulated (DIODE) Nanoformulations for Improved Treatment of Pancreatic Cancer. *Cancers (Basel)* (2020) 12 (5):1189–208. doi: 10.3390/cancers12051189

20. Quiñones-Díaz BI, Reyes-González JM, Sánchez-Guzmán V, Conde-Del Moral I, Valiyeva F, Santiago-Sánchez GS, et al. MicroRNA-18a-5p Suppresses Tumor

21. Livak KJ, Schmittgen TD. Analysis of Relative Gene Expression Data Using Real-Time Quantitative PCR and the 2(-Delta Delta C(T)) Method. *Methods* (2001) 25(4):402–8. doi: 10.1006/meth.2001.1262

22. Eisenhauer EA, Therasse P, Bogaerts J, Schwartz LH, Sargent D, Ford R, et al. New Response Evaluation Criteria in Solid Tumours: Revised RECIST Guideline (Version 1.1). *Eur J Cancer* (2009) 45(2):228–47. doi: 10.1016/j.ejca.2008.10.026

23. Yang H, Liu H, Chen Y, Zhu C, Fang W, Yu Z, et al. Neoadjuvant Chemoradiotherapy Followed by Surgery *Versus* Surgery Alone for Locally Advanced Squamous Cell Carcinoma of the Esophagus (NEOCRTEC5010): A Phase III Multicenter, Randomized, Open-Label Clinical Trial. *J Clin Oncol* (2018) 36(27):2796–803. doi: 10.1200/jco.2018.79.1483

24. Shen LY, Wang H, Dong B, Yan WP, Lin Y, Shi Q, et al. Possible Prediction of the Response of Esophageal Squamous Cell Carcinoma to Neoadjuvant Chemotherapy Based on Gene Expression Profiling. *Oncotarget* (2016) 7 (4):4531–41. doi: 10.18632/oncotarget.6554

25. Wang H, Shen L, Lin Y, Shi Q, Yang Y, Chen K. The Expression and Prognostic Significance of Mucin 13 and Mucin 20 in Esophageal Squamous Cell Carcinoma. *J Cancer Res Ther* (2015) 11 Suppl 1:C74–9. doi: 10.4103/0973-1482.163846

26. Moghadam AR, Mehramiz M, Entezari M, Aboutalebi H, Kohansal F, Dadjoo P, et al. A Genetic Polymorphism in the CYP1B1 Gene in Patients With Squamous Cell Carcinoma of the Esophagus: An Iranian Mashhad Cohort Study Recruited Over 10 Years. *Pharmacogenomics* (2018) 19(6):539–46. doi: 10.2217/pgs-2018-0197

27. Nguyen MH, Ueda K, Nakamura Y, Daigo Y. Identification of a Novel Oncogene, MMS22L, Involved in Lung and Esophageal Carcinogenesis. *Int J Oncol* (2012) 41(4):1285–96. doi: 10.3892/ijo.2012.1589

28. Stepanenko AA, Vassetzky YS, Kavsan VM. Antagonistic Functional Duality of Cancer Genes. *Gene* (2013) 529(2):199–207. doi: 10.1016/j.gene.2013.07.047

29. Duro E, Lundin C, Ask K, Sanchez-Pulido L, MacArtney TJ, Toth R, et al. Identification of the MMS22L-TONSL Complex That Promotes Homologous Recombination. *Mol Cell* (2010) 40(4):632–44. doi: 10.1016/j.molcel.2010.10.023

30. O'Connell BC, Adamson B, Lydeard JR, Sowa ME, Ciccia A, Bredemeyer AL, et al. A Genome-Wide Camptothecin Sensitivity Screen Identifies a Mammalian MMS22L-NFKBIL2 Complex Required for Genomic Stability. *Mol Cell* (2010) 40(4):645–57. doi: 10.1016/j.molcel.2010.10.022

31. O'Donnell L, Panier S, Wildenhain J, Tkach JM, Al-Hakim A, Landry MC, et al. The MMS22L-TONSL Complex Mediates Recovery From Replication Stress and Homologous Recombination. *Mol Cell* (2010) 40(4):619–31. doi: 10.1016/j.molcel.2010.10.024

32. Piwko W, Olma MH, Held M, Bianco JN, Pedrioli PG, Hofmann K, et al. Rnai-Based Screening Identifies the Mms22L-Nfkbil2 Complex as a Novel Regulator of DNA Replication in Human Cells. *EMBO J* (2010) 29(24):4210–22. doi: 10.1038/emboj.2010.304

33. Savci-Heijink CD, Halfwerk H, Koster J, van de Vijver MJ. A Novel Gene Expression Signature for Bone Metastasis in Breast Carcinomas. *Breast Cancer Res Treat* (2016) 156(2):249–59. doi: 10.1007/s10549-016-3741-z

34. Welcker M, Clurman BE. FBW7 Ubiquitin Ligase: A Tumour Suppressor at the Crossroads of Cell Division, Growth and Differentiation. *Nat Rev Cancer* (2008) 8(2):83–93. doi: 10.1038/nrc2290

35. Lin PC, Yeh YM, Lin BW, Lin SC, Chan RH, Chen PC, et al. Intratumor Heterogeneity of MYO18A and FBXW7 Variants Impact the Clinical Outcome of Stage III Colorectal Cancer. *Front Oncol* (2020) 10:588557. doi: 10.3389/fonc.2020.588557

36. Yu H, Ling T, Shi R, Shu Q, Li Y, Tan Z. [Expression of FBXW7 in Esophageal Squamous Cell Carcinoma and Its Clinical Significance]. *Zhonghua Zhong Liu Za Zhi* (2015) 37(5):347–51.

37. Yokobori T, Mimori K, Iwatsuki M, Ishii H, Tanaka F, Sato T, et al. Copy Number Loss of FBXW7 is Related to Gene Expression and Poor Prognosis in Esophageal Squamous Cell Carcinoma. *Int J Oncol* (2012) 41(1):253–9. doi: 10.3892/ijo.2012.1436

38. Mlecnik B, Bindea G, Kirilovsky A, Angell HK, Obenauf AC, Tosolini M, et al. The Tumor Microenvironment and Immunoscore Are Critical Determinants

Growth *via* Targeting Matrix Metalloproteinase-3 in Cisplatin-Resistant Ovarian Cancer. *Front Oncol* (2020) 10:602670. doi: 10.3389/fonc.2020.602670

of Dissemination to Distant Metastasis. *Sci Transl Med* (2016) 8(327):327ra26. doi: 10.1126/scitranslmed.aad6352

Conflict of Interest: The authors declare that the research was conducted in the absence of any commercial or financial relationships that could be construed as a potential conflict of interest.

Publisher's Note: All claims expressed in this article are solely those of the authors and do not necessarily represent those of their affiliated organizations, or those of the publisher, the editors and the reviewers. Any product that may be evaluated in this article, or claim that may be made by its manufacturer, is not guaranteed or endorsed by the publisher.

Palbociclib Induces Senescence in Melanoma and Breast Cancer Cells and Leads to Additive Growth Arrest in Combination With Irradiation

Tina Jost[1,2]*, Lucie Heinzerling[3], Rainer Fietkau[1,2], Markus Hecht[1,2†] and Luitpold V. Distel[1,2†]

[1] Department of Radiation Oncology, University Hospital of Erlangen, Friedrich-Alexander University Erlangen-Nürnberg, Erlangen, Germany, [2] Comprehensive Cancer Center Erlangen-EMN, Erlangen, Germany, [3] Department of Dermatology, University Hospital of Munich, Ludwig-Maximilian University Munich (LMU), Munich, Germany

Introduction: Several kinase inhibitors (KI) bear the potential to act as radiosensitizers. Little is known of the radiosensitizing effects of a wide range of other KI like palbociclib, which is approved in ER+/HER2- metastatic breast cancer.

Method: In our study, we used healthy donor fibroblasts and breast cancer and skin cancer cells to investigate the influence of a concomitant KI + radiation therapy. Cell death and cell cycle distribution were studied by flow cytometry after Annexin-V/7-AAD and Hoechst staining. Cellular growth arrest was studied in colony-forming assays. Furthermore, we used C12-FDG staining (senescence) and mRNA expression analysis (qPCR) to clarify cellular mechanisms.

Results: The CDK4/6 inhibitor palbociclib induced a cell cycle arrest in the G0/G1 phase. Cellular toxicity (cell death) was only slightly increased by palbociclib and not enhanced by additional radiotherapy. As the main outcome of the colony formation assays, we found that cellular growth arrest was induced by palbociclib and improved by radiotherapy in an additive manner. Noticeably, palbociclib treatment clearly induced senescence not only in breast cancer and partly in melanoma cells, but also in healthy fibroblasts. According to these findings, the downregulation of senescence-related FOXM1 might be an involved mechanism of the senescence-induction potential of palbociclib.

Conclusion: The effect on cellular growth arrest of palbociclib and radiotherapy is additive. Palbociclib induces permanent G0/G1 cell cycle arrest by inducing senescence in fibroblasts, breast cancer, and melanoma cells. Direct cell death induction is only a minor secondary mechanism of action. Concomitant KI and radiotherapy is a strategy worth studying in clinical trials.

Keywords: senescence, kinase inhibitor, radiotherapy, palbociclib, breast cancer, melanoma

Influence of Kinase Inhibitor Palbociclib on Ionizing Radiation
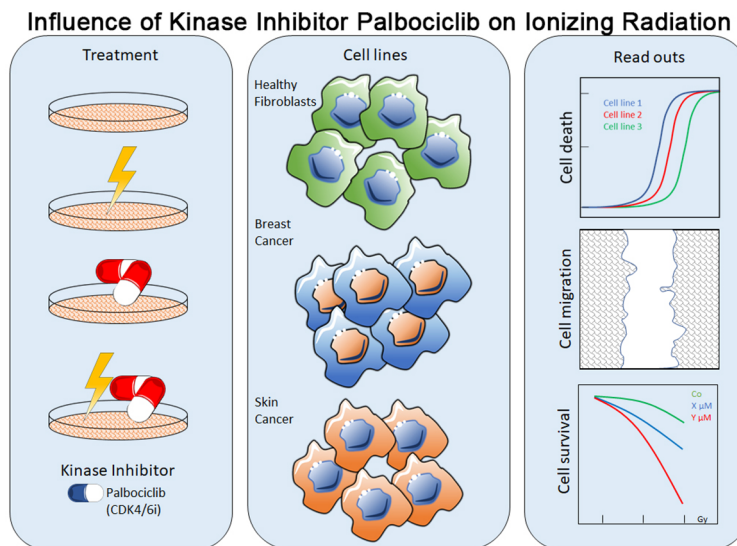
GRAPHICAL ABSTRACT |

INTRODUCTION

Female breast cancer is the most commonly diagnosed cancer. Citing the European Cancer Information System (ECIS), over 355,000 women in the EU-27 are estimated to be diagnosed with breast cancer in 2020 (1). This represents 13.3% of all cancer diagnoses. Between 2015 and 2017, approximately 13% of all female patients were treated with palbociclib (2). Palbociclib is a kinase inhibitor (KI) that blocks the cell cycle by inhibiting the phosphorylation of the Rb protein and was approved by the European Medicines Agency (EMA) in 2016 for ER+ and HER2- metastatic breast cancer (3). In essence, kinase inhibitors targeting different proteins in important cellular pathways are gaining more and more attention in the treatment of cancer patients. Moreover, the question of combining different therapy options like concomitant radiotherapy (RT) with focus on radiosensitization arises (4), especially in the metastatic situation, since metastases are commonly treated with irradiation (5).

Previous studies showed that kinase inhibitors are able to act as a radiosensitizer and therefore can enhance tumor control (6, 7), but have side effects on healthy tissue too. Radiosensitizing potential was found for BRaf V600E inhibitors vemurafenib and dabrafenib (8, 9). Consequently, a hold of KI treatment more than 3 days before and

after fractionated RT and hold of more than 1 day pre- and post-stereotactic radio surgery (SRS) are recommended by the Eastern Cooperative Oncology Group (ECOG) (10). Nevertheless, current data indicate an enhancement of local tumor control when KI therapy is combined with intracranial stereotactic RT without an increase of radionecrosis (11).

To enhance the treatment of cancer patients, a combination of KI and IR could be beneficial. However, the possible radiosensitizing effects of the cyclin-dependent kinase 4 (CDK4) and cyclin-dependent kinase 6 (CDK6) inhibitor palbociclib are not limited to tumor cells alone, but can also affect healthy cells. Additionally, healthy tissue like the skin is always affected during irradiation. Keeping these mechanisms of action in mind, our study focused on cellular response of tumor and healthy donor cells regarding cell death, cell cycle regulation, and senescence. Just few is known on the ability of palbociclib to trigger senescence. Nevertheless, this type of replicative G1-arrest is a main cellular outcome of radiation, since a fraction of the induced highly complex DNA damage cannot be repaired (12). Remarkably, the dependency of CDK4/6 in not limited to breast cancer alone, but to a wide range of entities like hepatocellular carcinoma, bronchial carcinoma, and head and neck squamous cell carcinoma (13–15). Increased CDK4 activity was also found in melanomas (16). This supports our intention of studying the effects of concomitant kinase inhibitor and RT not only in breast cancer cells, but also in skin cancer cells.

MATERIALS AND METHODS

Cell Lines and Kinase Inhibitor

Human skin fibroblasts SBLF7 and SBLF9 derived from different healthy donors; melanoma cells LIWE, HV18MK, ICNI, RERO,

ARPA, and ANST derived from different malign melanoma patients; and breast cancer cell lines MDA-MB-231 (TNBC) and MCF-7 (ER+, PR+) were used. MDA-MB-231 and MCF-7 were purchased by CLS cell lines service (Eppelheim, Germany). Primary human melanoma cells (from primary tumors) were collected in the Department of Dermatology of the Universitätsklinikum Erlangen following approval by the institutional review board (Ethic approval no. 204 17 BC). Single-cell suspensions were generated by digesting tissue samples with collagenase (Sigma Aldrich, München, Germany), hyaluronidase (Sigma Aldrich, München, Germany), and DNase (Roche, Mannheim, Germany) (17). The primary human fibroblasts SBLF7 and SBLF9 were isolated *via* skin biopsy of the cutis and subcutis after local anesthesia as described previously (18). Briefly, each biopsy was dissected in small pieces, placed in tissue culture flasks, and each covered with a drop of F-12 medium (Gibco, Waltham, USA) supplemented with 40% fetal bovine serum (FBS) (Merck, Darmstadt, Germany). After the skin pieces had attached to the culture flasks and the first fibroblasts had grown out, they were covered with F-12 medium supplemented with 12% FBS, 2% non-essential amino acids (NEA) (Merck, Darmstadt, Germany), and 1% penicillin/streptomycin (Gibco, Waltham, USA). When the primary cells were approximately 80% confluent, they were detached with 0.5% Trypsin (Gibco, Waltham, USA) and further cultured in the medium mentioned above. For continuous cell culture, fibroblasts were cultured in F-12 medium, supplemented with 15% FBS, 2% NEA, and 1% penicillin/streptomycin. Melanoma cells were cultured in RPMI-1640 (Sigma Aldrich, München, Germany), supplemented with 20% FBS (Merck, Darmstadt, Germany), 1% NEA (Merck, Darmstadt, Germany), 1% Pyruvate solution (Gibco, Waltham, USA), 1% L-Glutamine (Merck, Darmstadt, Germany), 1% HEPES (Merck, Darmstadt, Germany), and 0.05% Gentamicin (Merck, Darmstadt, Germany). Breast cancer cell lines were cultured in DMEM (PAN biotech, Aidenbach, Germany), supplemented with 10% FBS and 1% penicillin/streptomycin. All cells were incubated at 37°C in a humidified 5% CO_2 atmosphere. Cells were cultured 50 passages maximum. Palbociclib isethionate (MW 573.7 g/mol) (Selleck Chemicals LLC, Huston, USA) was prepared as stock solution in aqua bidest and stored at –80°C with a concentration of 1 mmol/L. The drug was diluted for experiments in dimethyl sulfoxide (DMSO) (Roth, Karlsruhe, Germany). Required aliquots were thawed freshly prior to each experiment.

Cell Death Analysis—FACS
Cells were washed with PBS (Sigma Aldrich, St. Louis, USA) and incubated with Trypsin/EDTA (Gibco, Waltham, USA) to detach the cells from cell culture flask to prepare a single-cell suspension. To reach a confluence of 50% up to 80% in 24 h up to 72 h, cells were seeded in an appropriate concentration. To reduce analytical interference and avoid an artificial increase of possible effects of our treatment through stimulation of cell proliferation (19–21), medium was exchanged for the experiments by serum-reduced cell culture medium (2% FBS) including 10 μl of various palbociclib concentrations. Previously,

we checked if serum starvation influences our cell death analysis (data shown in **Supplementary Figure S1**). We diluted palbociclib in a certain manner so that we always had to add 10 μl of dilution per 1 μM and 2 μM and 10 μl of pure DMSO (Roth, Karlsruhe, Germany) to the control. Finally, we had a DMSO concentration of less than or equal to 1%. We compared this DMSO concentration with controls and found no effect (data shown in **Supplementary Figure S2**), which is similar to other findings (22).

Cells were incubated in the presence of the inhibitor for 48 h at 37°C. Additionally, half of the cells were irradiated with 2 Gy ionizing radiation (IR) by an ISOVOLT Titan X-ray generator (GE, Ahrensburg, Germany) 3 h after addition of inhibitor. Supernatant was collated and treated cells were harvested by trypsination. After washing, cells were resuspended in 200 μl of Ringer solution and stained with Annexin V-APC (BD, Heidelberg, Germany) and 7-amino-actinomycin D (BD, Heidelberg, Germany) for 30 min on ice. To analyze apoptotic and necrotic cells using flow cytometry (Cytoflex, Beckman Coulter, Brea, USA), cell suspension was transferred to 96-well plates. Excitation at 660/10 nm (Annexin V-APC) and 546 nm (7-AAD) was used to measure stained cells. Double-negative (Ann-7AAD-) cells were defined as alive, Ann+7AAD- cells as apoptotic, and Ann+7AAD+ cells as necrotic.

Cell Cycle Analysis—FACS
After harvesting, cells were fixed in 10 ml of 70% ethanol (Roth, Karlsruhe, Germany) and 1 ml of serum-reduced cell culture medium for a minimum of 12 h at + 4°C and then stained with Hoechst 33342 (Invitrogen, Eugene, USA) for 60 min on ice. Because Hoechst 33342 is highly DNA-specific (preferentially binds to A-T base pairs), no RNA-digest is needed (Technical data sheet, BD Pharmingen). Cells were analyzed in the Cytoflex flow cytometer. In general, cells need approximately 24 h to go through cell cycle (Cooper, The cell—a molecular approach, 2nd Edition, 2000). To clearly identify any changes in cell cycle distribution, like G0/G1 or G2/M arrest, treatment of 48 h could be advisable. To test whether 24 h or 48 h of treatment should be done, we tested three cell lines previously (data shown in **Supplementary Figure S3**) and performed all experiments later on with 48 h of treatment.

Colony-Forming Assay
Cells were seeded in six-well plates with a density of 100–2,000 cells per well. Cells were treated with different concentrations of inhibitor and irradiated after 3 h with a 0- or 2-Gy dose. After another incubation phase of 24 h, medium was exchanged by fresh standard medium without any drug and the inhibitor was washed out. Plates were incubated for 10 to 14 days until colonies of minimum 50 cells were developed. Colonies were stained with methylene blue (Sigma Aldrich, München, Germany) for 30 min at room temperature and counted when dry.

C12-FDG Staining—Senescence
To investigate evolving senescence during KI or irradiation treatment, we seeded cells at low confluence in cell culture flasks. After 24 h of settlement, cells were treated with either

kinase inhibitor, irradiation, or combination of both. As a control, cells were treated with DMSO only. On day 6 after treatment, medium was exchanged including DMSO or kinase inhibitor again. After 10 days of treatment, cells were collected and stained as previously published (23). Briefly, cells were treated with 100 nM Bafilomycin A1 (Merck, Darmstadt, Germany) for 30 min (37°C). Afterwards, Hoechst dye was added for another 30 min (37°C) and finally cells were treated with C12-FDG for 60 min (37°C). After centrifugation cells were resuspended in Ringer solution and stained with Annexin V-APC and 7-AAD (BD, Heidelberg, Germany) for 30 min on ice. Finally, C12-FDG positive cells were measured using flow cytometry (Cytoflex S, Beckman Coulter, Brea, CA, USA).

Quantitative PCR—mRNA Expression Analysis

For analysis of mRNA expression after KI treatment, irradiation or the combination of both qRT-PCR was used as described previously (24). Briefly, cells were seeded in six-well-plates, treated with 2 μM palbociclib, 2 Gy dose, or the combination of both (2 μM + 2 Gy) and harvested 48 h after treatment. Cells were harvested by lysis with Trizol (peqlab, Darmstadt, Germany) and frozen (−80°C) immediately. RNA isolation was done with phenol-chloroform extraction and isolated RNA was frozen again. Genomic DNA was digested with DNase I Kit (Thermo Fisher Scientific, Waltham, USA) at 37°C for 30 min (Thermocycler, BIO-RAD, Hercules, CA, USA). RNA was transferred into cDNA *via* High-capacity RT kit (Thermo Fisher Scientific, Waltham, USA) and cDNA was diluted with water and Yellow dye (Thermo Fisher Scientific, Waltham, MA, USA). qRT-PCR was run using DyNAmo ColorFlash SYBR Green qPCR Kit (Thermo Fisher Scientific, Waltham, MA, USA). Bio-Rad primers (**Tables 1**, **2**, Bio-Rad Laboratories, Inc., Hercules, CA, USA) were used according to the manufacturer's instructions. Two technical replicates (duplicate wells) from one RNA/cDNA preparation (one biological sample) were measured.

Statistical Analysis

GraphPad prism 9 software (San Diego, CA, USA) was used to perform statistical analysis. Non-parametric, unpaired one-tailed Mann–Whitney *U* test was used to analyze data, based on the minimum number of *n* = 3 experiments. *p*-value ≤ 0.05 was determined as significant. Graphs were also generated using GraphPad Prism 9 software.

Ethics Approval and Consent to Participate

Ethical approval was obtained in the Department of Dermatology, Universitätsklinikum Erlangen following approval by the institutional review board (Ethik-Kommission der Friedrich-Alexander-Universität Erlangen-Nürnberg, approval No. 204_17 Bc). The patients provided written informed consent.

TABLE 1 | Primer for target genes.

Gene	Primer	Unique Assay ID	Application
cyclin D1	CCND1	qHsaCID0013833	Inhibits autophagy
forkhead box M1	FOXM1	qHsaCED0004022	Inhibits senescence
myristoylated alanine-rich protein kinase C substrate	MARCKKS	qHsaCED0045667	Promotes migration, invasion
p16 (Cyclin-dependent kinase inhibitor 2A)	CDKN2A	qHsaCED0056722	CKD4 inhibitor
regulatory associated protein of MTOR, complex 1	RPTOR	qHsaCID0016865	Promotes autophagy
RPTOR independent companion of MTOR, complex 2	RICTOR	qHsaCID0007506	Promotes autophagy
SMAD family member 3	SMAD3	qHsaCID0008503	Inhibits G1/S-progression
v-myc myelocytomatosis viral oncogene homolog (avian)	MYC	qHsaCID0012921	Inhibits apoptosis

TABLE 2 | Primer for housekeeper genes.

Gene	Primer	Unique Assay ID	Application
hydroxymethylbilane synthase	HMBS	qHsaCID0038839	Housekeeper
ribosomal protein L30	RPL30	qHsaCED0038096	Housekeeper
ubiquitin C	UBC	qHsaCED0023867	Housekeeper

RESULTS

Cell Death Is a Minor Way of Action in Palbociclib Treatment

To analyze the influence of kinase inhibitor palbociclib on RT, we investigated two fibroblast cell lines, as healthy controls, and two breast cancer and six skin cancer cell lines. First of all, cell death was measured by Annexin-7AAD staining using flow cytometry (**Figure 1**). The first dose escalation study (**Figure 1A**) showed IC50 values of 8 μM for the skin cancer cell line ICNI and 10 μM for the healthy fibroblasts SBLF7. Concerning the pharmacokinetics of palbociclib, we proceeded with physiologically achievable concentrations of 1 μM and 2 μM (25). Annexin-7AAD- cells were defined as "alive", Annexin+7AAD- cells as "apoptotic", and Annexin+7AAD+ cells as "necrotic" (**Figure 1B**).

Regarding our clinical context of the radiation oncology, we compared irradiation (IR) to the combination therapy (KI + IR), since KI can act as radiosensitizer and enhance the effect of IR in healthy tissue (side effects) and in tumor tissue leading to improve tumor control. The clinically most frequently used single dose of 2 Gy was chosen. Healthy fibroblasts did not show significant changes in apoptosis and necrosis (**Figure 1C**). Breast cancer cell line MCF-7 showed significant increase of apoptosis and total cell death after combination therapy with 2 μM and 2 Gy IR respectively (*p* = 0.05). The group of our tested skin cancer cell lines seemed to show diverse behavior, regarding strong tendencies, but not significant response in ARPA, and slight treatment-related response in RERO. HV18MK, ICNI, and LIWE did not respond in a treatment-related manner.
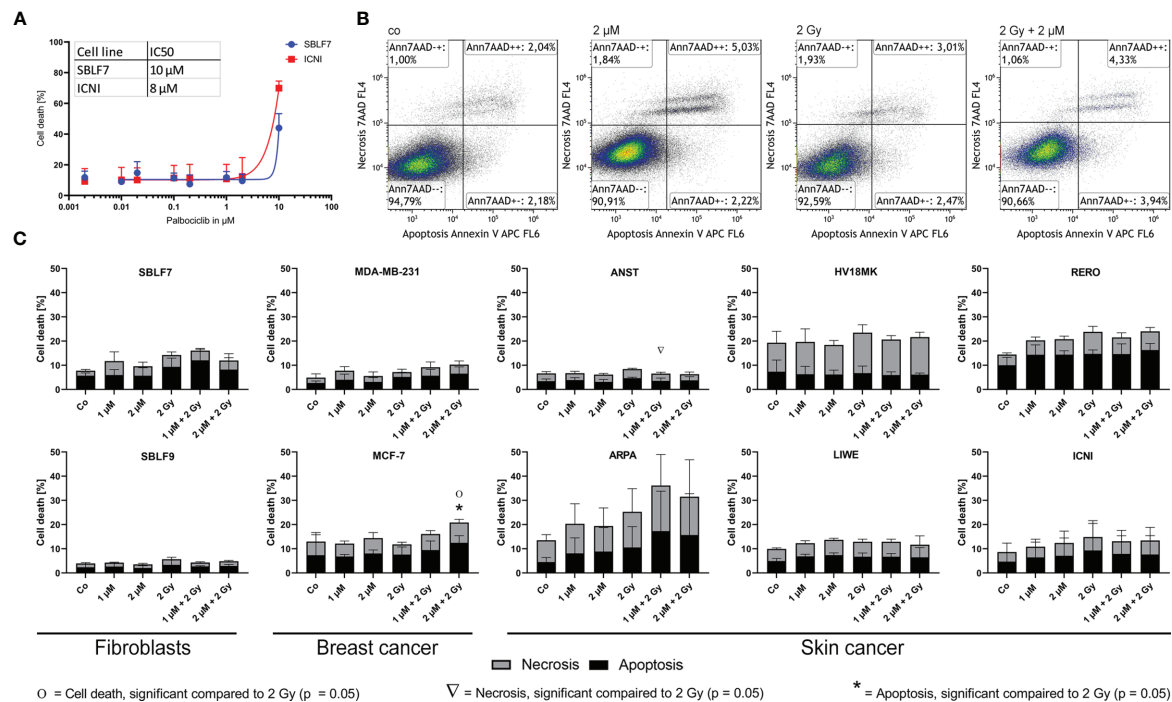
FIGURE 1 | Cell death analysis of different non-malign and malign cell lines. **(A)** Dose escalation study of the kinase inhibitor palbociclib in healthy fibroblasts and skin cancer cells [dose–response curve fitting by non-linear regression of log(agonist) vs. response based on Graph Pad Prism]. **(B)** Gating strategy of the Annexin-7AAD (cell death) staining of skin cancer cells RERO after KI treatment, irradiation, and combi therapy. **(C)** Necrotic and apoptotic populations in 10 different cell lines (healthy fibroblast SBLF7 and SBLF9, breast cancer MDA-MB-231 and MCF-7, and skin cancer ANST, ARPA, HV18MK, LIWE, RERO, and ICNI cells) after 48 h of treatment. Each value represents mean ± SD (n = 3). Significance was determined by one-tailed Mann–Whitney U test O/Δ/* p ≤ 0.05.

Interestingly, in the skin cancer cell line ANST, necrosis was significantly reduced in combination of KI and IR (*p* = 0.05).

Palbociclib and IR Influence Clonogenicity and Cell Survival in an Additive Manner

As a gold standard in radiation biology, colony-forming assays were used to investigate the interaction of palbociclib and irradiation within healthy and cancer cells (**Figure 2**). Both healthy fibroblasts decreased clonogenicity in a significant manner comparing combinatory therapy to irradiation alone (*p* = 0.05) in an additive manner. SBLF7 cells showed the most dramatic fall of survival in total. Breast cancer cell lines and three of six skin cancer cell lines decreased their colony-forming ability significantly (*p* = 0.05) in an additive manner. Additionally, we normalized our data to get a better understanding of antagonistic, additive, or synergistic effects. No significance could be detected in all tested cell lines.

Palbociclib Induces Senescence

Beside a wide range of effects like clonogenicity, survival, and cell death, colony-forming assay can also act as an indicator for senescence. We analyzed our malign and non-malign cell lines more deeply using a C12-FDG staining. Since senescence is a time-dependent process, we observed C12-FDG positivity initially of one healthy and one cancer cell line on days 3, 6,

and 10 (**Supplementary Figure S4**). The effect was best detectable on day 10. Subsequently, all cell lines were tested at day 10 after treatment (**Figure 3**). Healthy fibroblasts did not increase C12-FDG positive cells significantly after combination treatment, but SBLF9 with monotherapy palbociclib (*p* = 0.05). One breast cancer and two out of six skin cancer cell lines raised the amount of C12-FDG positive cells at day 10 after concomitant KI + IR therapy. Noticeably, palbociclib treatment alone already raises C12-FDG positive proportion of cells in five out of eight cancer cell lines (*p* = 0.05).

Additionally, as a first step of deeper analysis of interactions and outcomes of kinase inhibitors and concomitant irradiation, we analyzed cells after 48 h of treatment. We investigated mRNA expression levels of Cyclin D1, RPTOR, Myc, SMAD3, MARCKS, RICTOR, p16, and FOXM1, which are related to CDK4/6 as, e.g., cellular inhibitor, binding partner, or central proteins of downstream pathways in our 10 cell lines including healthy fibroblasts, breast cancer, and skin cancer cells. Expression was normalized to housekeeping genes HMBS, RPL30, and UBC. Additionally, expression of treated samples was normalized to the corresponding untreated control to verify down- or upregulation plotted in the heatmaps (**Supplementary Figures S5A–H**).

Noticeable, relevant downregulation of senescence-inhibiting FOXM1 was found after combination therapy in all cell lines and in almost all sample of single therapy treatment (**Supplementary**
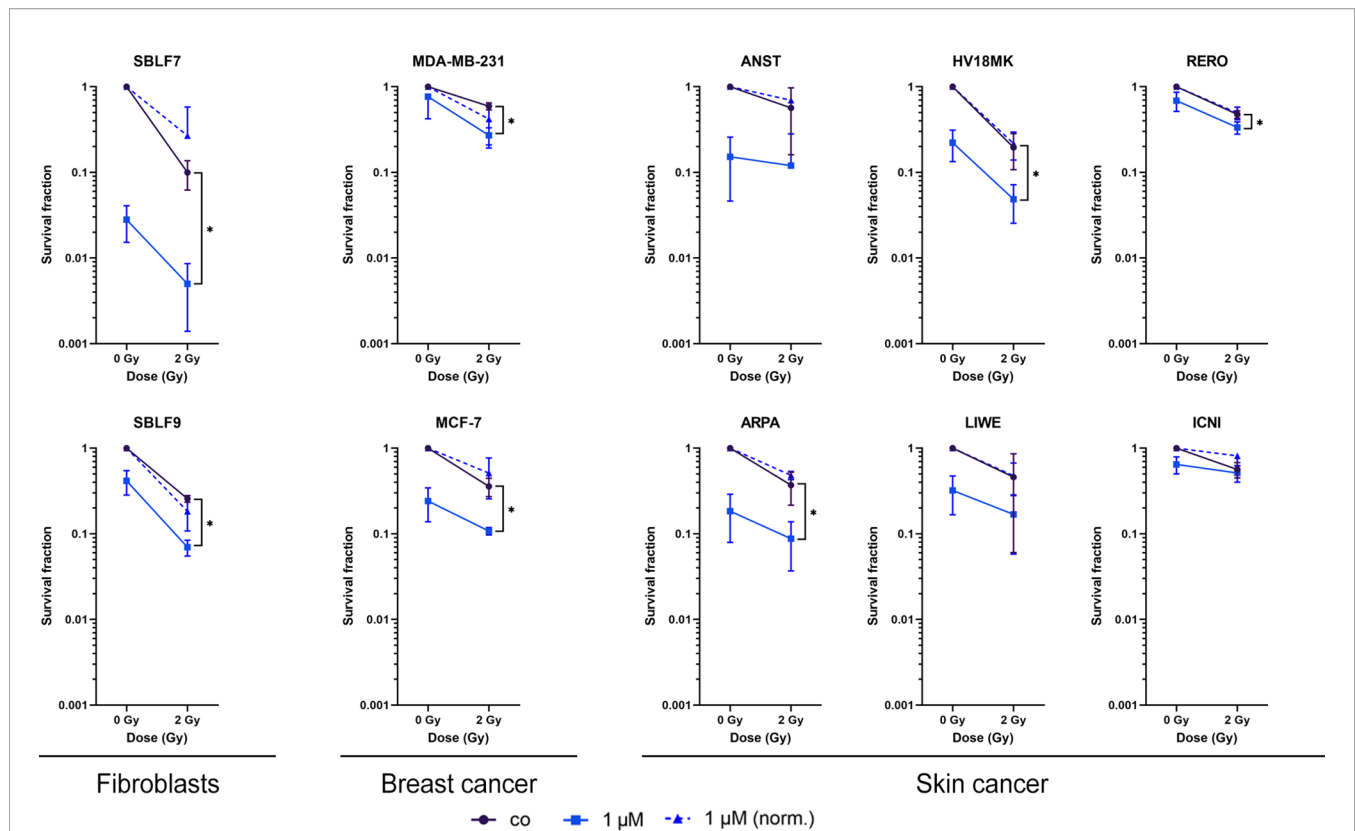
FIGURE 2 | Survival fractions of healthy fibroblasts and breast cancer and skin cancer cells. Clonogenicity of two healthy fibroblasts and two breast cancer and six skin cancer cell lines. Cells were treated with 1 µM palbociclib w/o 2 Gy. Values were normalized to the irradiated control fraction (blue dashed line). Each value represents mean ± SD ($n = 3$). Significance was determined by one-tailed Mann–Whitney U test *$p \leq 0.05$.
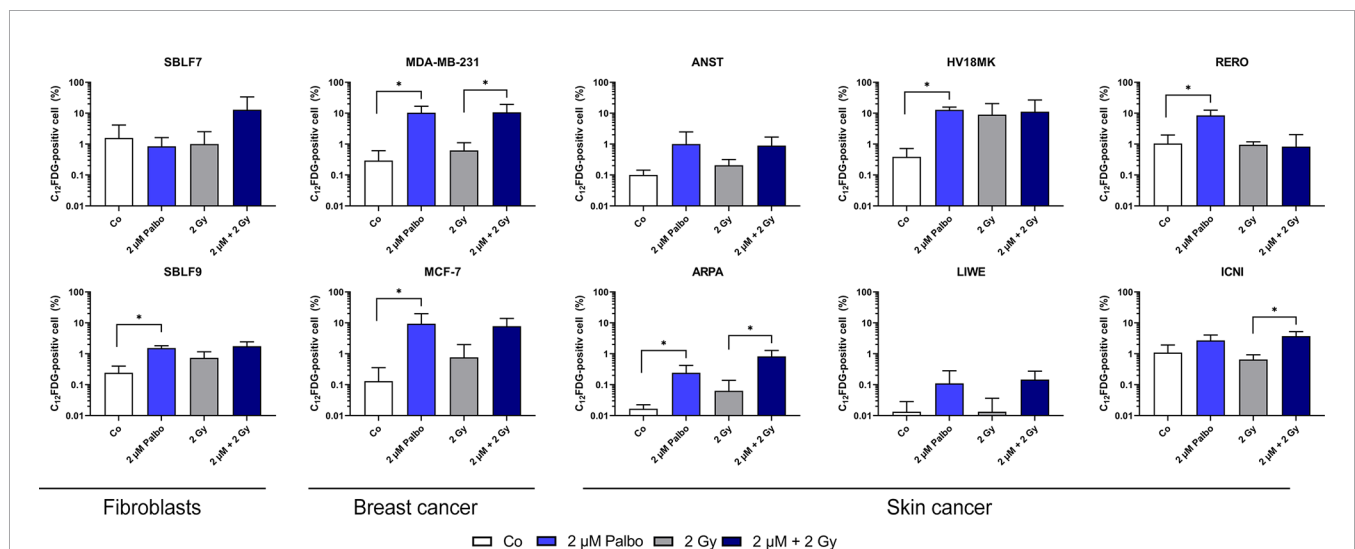

FIGURE 3 | C12-FDG staining as indicator of cellular senescence. Proportion of C12-FDG-positive cells after 10 days of incubation in 10 different cell lines (healthy fibroblast SBLF7 and SBLF9, breast cancer MDA-MB-231 and MCF-7, and skin cancer ANST, ARPA, HV18MK, LIWE, RERO, and ICNI cells). Cells were treated for 24 h and irradiated with a single dose of 2 Gy. Each value represents mean ± SD ($n = 3$). Significance was determined by one-tailed Mann–Whitney U test *$p \leq 0.05$.

Figure S5H). Furthermore, downregulation of p16 mRNA was found after IR in seven of eight and after combination therapy in five out of eight cancer cell lines (**Supplementary Figure S5G**). Interestingly, skin cancer cell line ANST showed overall diverse behavior, regarding downregulation of Cyclin D1, Myc, and SMAD3 as well as upregulation of MARCKS and RICTOR, compared to all other tested cell lines. Another special case seems to be skin cancer cell line LIWE, which showed downregulation after monotherapy (KI or IR) of Cyclin D1, RPTOR, and Myc in obvious contrast to the upregulation after combination of KI and IR. Overall, our mRNA expression data showed slight regulations in healthy fibroblasts compared to the wide-ranging behavior of the tested malign cancer cells. Nonetheless, these preliminary data should be held as first screening of mRNA expression and will lead to further analysis of the most interesting regulated genes of interest (GOI) in depth.

Palbociclib Induces a Cell Cycle Block

In general, palbociclib binds to CDK4 and 6, which are central proteins involved in controlling progression through the G1

phase of the cell cycle (**Figures 4A, B**) (26). Furthermore, the cell cycle status of cancer cells is relevant for irradiation therapy since the G2 phase is known to be more prone to IR (27). In healthy fibroblasts, no changes were detectable treating cells with palbociclib and irradiation (**Figure 4C**). In one of both breast cancer cell lines and four out of six skin cancer cell lines, the cell population in the G2/M phase decreased significantly after combination treatment compared to IR alone (ANST, RERO: $p = 0.05$; HV18MK, ARPA: $p = 0.01$), whereas the G0/G1 phase increased. Unexpectedly, we found in the skin cancer cell line LIWE an increase of cells in the G2/M phase of cell cycle ($p = 0.01$). To study if this cell cycle block is transient or durable, the effect on markers of cellular senescence was studied.

DISCUSSION

Flow cytometric analysis of cell death in cancer and healthy tissue cell lines indicated tendencies regarding that palbociclib influences apoptosis and necrosis in a cell line-specific manner but rarely significant. Healthy cells seem to be less affected than
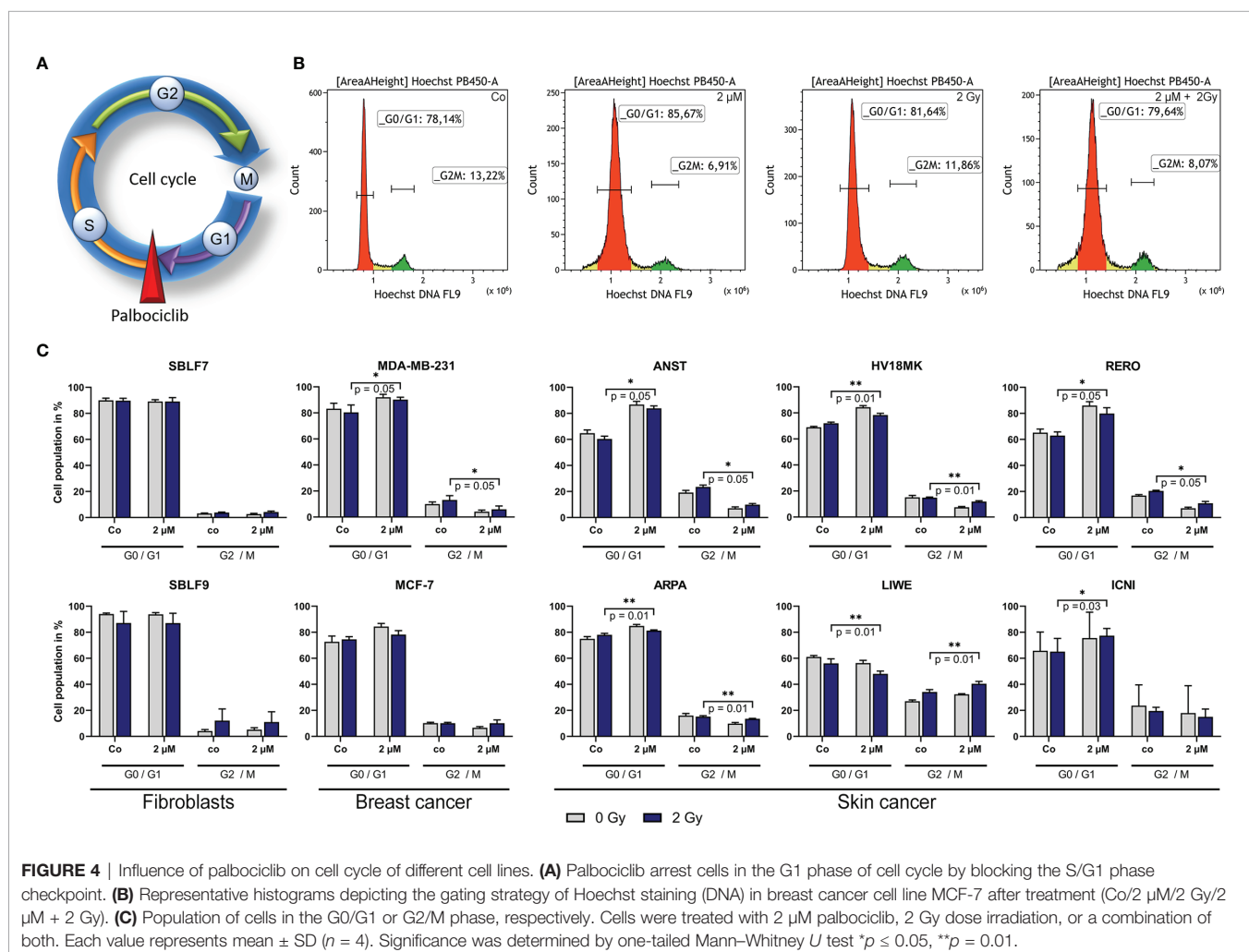

FIGURE 4 | Influence of palbociclib on cell cycle of different cell lines. **(A)** Palbociclib arrest cells in the G1 phase of cell cycle by blocking the S/G1 phase checkpoint. **(B)** Representative histograms depicting the gating strategy of Hoechst staining (DNA) in breast cancer cell line MCF-7 after treatment (Co/2 μM/2 Gy/2 μM + 2 Gy). **(C)** Population of cells in the G0/G1 or G2/M phase, respectively. Cells were treated with 2 μM palbociclib, 2 Gy dose irradiation, or a combination of both. Each value represents mean ± SD ($n = 4$). Significance was determined by one-tailed Mann–Whitney U test *$p \leq 0.05$, **$p = 0.01$.

tumor cells, but we assume that cell death is not the main mechanism of action of the CKD4/6 inhibitor palbociclib. The obvious intercellular differences might be explained by a heterogeneous mutation profile of our different cell lines. According to the distribution of cancer patients into different entities and subtypes (e.g., breast and lung cancer), it is known that every patient shows different mutations in depth. Our patient-derived skin cancer cell lines, which are harboring a more primary character, are used to represent a wider range of patient-specific mutations. Additionally, there is evidence that status of p53 and DNA damage repair proteins like ATM influences the outcome of palbociclib treatment in the context of irradiation (14).

Palbociclib plays an important role in cell cycle regulation as inhibitor of CDK4 and CDK6. Since the distribution of cell cycle phases is of relevant matter in radiation biology, we investigated the distribution of cell in the G0/G1 and G2/M phase. The G2 phase is known to be more sensitive to radiation (27). Healthy fibroblasts, representing normal tissue, were not affected by palbociclib significantly. Cancer cells responded controversially, as four out of six cell lines decreased G2/M populations. Interestingly, we also found one cell line that increased population of cells in the G2/M phase. This might be beneficial for radiosensitivity regarding improved local tumor control. However, our data suggest that blocking the cell cycle permanently could lead to senescence as the main mechanism of palbociclib treatment.

Regarding the results of our colony-forming assays, clear evidence is found for the higher effect of palbociclib on clonogenicity, survival, and senescence, since palbociclib blocks the cell cycle, but does not lead to cell death (28). Senescence can be triggered by, e.g., cellular stress like DNA damage or aging processes and could lead to irreversible growth arrest called stress-induced or replicative senescence, respectively (29). A senescent phenotype is also relevant in cancer and overexpression of senescence markers can be found in malign cells and tissues (30). Noticeable, colony forming was strongest decreased in healthy control cell line SBLF7. Nevertheless, all malign cell lines showed clear trends to lower cell survival rates after combination therapy compared to irradiation alone. Since irradiation is known to induce senescence as well, the combination therapy was assumed to increase this non-proliferating phenotype more efficiently (31). Additionally, effective combination of palbociclib and IR was previously described in glioblastoma multiforme intracranial xenografts (32). In our setting, we did not detect synergistic effects of simultaneous KI and IR therapy on senescence. However, this study leads us to the assumption that tumor control can be improved by combination therapy in an additive manner. To study the ability of palbociclib to induce senescence, further analysis of C12-FDG status was performed. Palbociclib clearly induced senescence in breast cancer cells. The melanoma cell lines responded very diversely. This probably indicates the inter-individual differences between every single cancer patient, according to our cell death analysis.

The preliminary analysis of mRNA expression under kinase inhibitor, irradiation, or combination therapy showed again a wide range of effects in different cancer cell lines. Eight CDK4/6 related targets were chosen to verify different ways of action of CDK4/6 blocking including, e.g., autophagy, apoptosis, migration, and senescence (33). FOXM1 was downregulated in all cell lines after combination therapy. Strong downregulation correlated with a significant increase of C12-FDG positive cells after combination therapy in, e.g., ARPA and ICNI cells. Unfortunately, for the unexpected behavior regarding upregulation of FOXM1 after palbociclib compared to significant enhancement of C12-FDG in HV18MK and RERO, we lack an appropriate explanation. Further analysis of the mutational profile of our patient-derived cell lines could help to overcome this point. Palbociclib does not lead to cell death itself, but induces senescence while blocking the cell cycle in G0/G1. As FOXM1 is known to inhibit senescence (33, 34) and, more importantly, is known to be reduced throughout palbociclib treatment (35), the decreased expression supports this idea. Unexpectedly, even after IR, downregulation of FOXM1 could be detected, an effect Li et al. (2019) published as a mechanism of pulmonary fibrosis (36). Additionally, the expression of p16, which is known as intracellular CDK4 and CDK6 inhibitor, was downregulated in five out of eight cancer cell lines after combination treatment, but might be triggered mainly by IR. Blocking the cell cycle with palbociclib may lead to less CKD4/6 and less p16 expression as a feedback loop (37). Overall, treatment with palbociclib or a combination with irradiation seems to induce senescence, but not cell death. Cellular processes like migration or autophagy may be involved, but further analyses will be necessary to understand how palbociclib influences these pathways.

Taken together, our data give evidence of inducing senescence as a main mechanism of palbociclib. However, there are some limitations, which should be considered for further research. Using patient-derived cell lines enables us to more real-life models than commercially available cell lines, which are long-term adapted to flasks and incubators. Characterization of the mutation profile of standard tumor suppressor and oncogenes might be a future strategy to explain the diverse response. Particularly, the p53 status should always be analyzed in future analyses focusing on cellular mechanisms of palbociclib. Melanoma show a high frequency of mutations in the CDK4 pathway and CDK4/6 inhibitors have been beneficial in breaking resistance (38). Thus, CDK4/6 inhibitors are potential candidates for therapy of melanoma especially as our data show in combination with RT.

CONCLUSION

Palbociclib induces cellular senescence in healthy skin fibroblasts, breast cancer, and melanoma cells. Cell death is only a secondary mechanism of action of palbociclib treatment. Concomitant RT leads to an increased cellular growth arrest in an additive manner. Since CDK4/6 is known to promote cancer progression in many entities (13–16), palbociclib has been approved for therapy of breast cancer. Its efficacy should also be studied in combination with RT.

DATA AVAILABILITY STATEMENT

The original contributions presented in the study are included in the article/**Supplementary Material**. Further inquiries can be directed to the corresponding author.

ETHICS STATEMENT

AUTHOR CONTRIBUTIONS

TJ, MH, and LD contributed to conception and design of the study. TJ performed all analysis. TJ organized the database. TJ performed the statistical analysis. TJ wrote the first draft of the manuscript. RF, LH, and LD provided the resources. All authors contributed to manuscript revision, read, and approved the submitted version.

ACKNOWLEDGMENTS

SUPPLEMENTARY MATERIAL

The Supplementary Material for this article can be found online at: https://www.frontiersin.org/articles/10.3389/fonc.2021.740002/full#supplementary-material

REFERENCES

1. Ferlay J, Colombet M, Soerjomataram I, Dyba T, Randi G, Bettio M, et al. Cancer Incidence and Mortality Patterns in Europe: Estimates for 40 Countries and 25 Major Cancers in 2018. *Eur J Cancer* (2018) 103:356–87. doi: 10.1016/j.ejca.2018.07.005

2. Kish JK, Ward MA, Garofalo D, Ahmed HV, McRoy L, Laney J, et al. Real-World Evidence Analysis of Palbociclib Prescribing Patterns for Patients With Advanced/Metastatic Breast Cancer Treated in Community Oncology Practice in the USA One Year Post Approval. *Breast Cancer Res* (2018) 20 (1):37. doi: 10.1186/s13058-018-0958-2

3. Saab R, Bills JL, Miceli AP, Anderson CM, Khoury JD, Fry DW, et al. Pharmacologic Inhibition of Cyclin-Dependent Kinase 4/6 Activity Arrests Proliferation in Myoblasts and Rhabdomyosarcoma-Derived Cells. *Mol Cancer Ther* (2006) 5(5):1299–308. doi: 10.1158/1535-7163.MCT-05-0383

4. Hashizume R, Zhang A, Mueller S, Prados MD, Lulla RR, Goldman S, et al. Inhibition of DNA Damage Repair by the CDK4/6 Inhibitor Palbociclib Delays Irradiated Intracranial Atypical Teratoid Rhabdoid Tumor and Glioblastoma Xenograft Regrowth. *Neuro Oncol* (2016) 18(11):1519–28. doi: 10.1093/neuonc/now106

5. O'Shaughnessy J. Extending Survival With Chemotherapy in Metastatic Breast Cancer. *Oncologist* (2005) 10(Suppl 3):20–9. doi: 10.1634/theoncologist.10-90003-20

6. Mohamed AA, Thomsen A, Follo M, Zamboglou C, Bronsert P, Mostafa H, et al. FAK Inhibition Radiosensitizes Pancreatic Ductal Adenocarcinoma Cells In Vitro. *Strahlenther Onkol* (2021) 197(1):27–38. doi: 10.1007/s00066-020-01666-0

7. Chen Y, Jin Y, Ying H, Zhang P, Chen M, Hu X. Synergistic Effect of PAF Inhibition and X-Ray Irradiation in non-Small Cell Lung Cancer Cells. *Strahlenther Onkol* (2020) 197(4):343–52. doi: 10.1007/s00066-020-01708-7

8. Hecht M, Zimmer L, Loquai C, Weishaupt C, Gutzmer R, Schuster B, et al. Radiosensitization by BRAF Inhibitor Therapy-Mechanism and Frequency of Toxicity in Melanoma Patients. *Ann Oncol* (2015) 26(6):1238–44. doi: 10.1093/annonc/mdv139

9. Hecht M, Meier F, Zimmer L, Polat B, Loquai C, Weishaupt C, et al. Clinical Outcome of Concomitant vs Interrupted BRAF Inhibitor Therapy During Radiotherapy in Melanoma Patients. *Br J Cancer* (2018) 118(6):785–92. doi: 10.1038/bjc.2017.489

10. Anker CJ, Grossmann KF, Atkins MB, Suneja G, Tarhini AA, Kirkwood JM. Avoiding Severe Toxicity From Combined BRAF Inhibitor and Radiation Treatment: Consensus Guidelines From the Eastern Cooperative Oncology Group (ECOG). *Int J Radiat Oncol Biol Phys* (2016) 95(2):632–46. doi: 10.1016/j.ijrobp.2016.01.038

11. Hadi I, Roengvoraphoj O, Bodensohn R, Hofmaier J, Niyazi M, Belka C, et al. Stereotactic Radiosurgery Combined With Targeted/ Immunotherapy in Patients With Melanoma Brain Metastasis. *Radiat Oncol* (2020) 15(1):37. doi: 10.1186/s13014-020-1485-8

12. Maier P, Hartmann L, Wenz F, Herskind C. Cellular Pathways in Response to Ionizing Radiation and Their Targetability for Tumor Radiosensitization. *Int J Mol Sci* (2016) 17(1):102. doi: 10.3390/ijms17010102

13. Huang CY, Hsieh FS, Wang CY, Chen LJ, Chang SS, Tsai MH, et al. Palbociclib Enhances Radiosensitivity of Hepatocellular Carcinoma and Cholangiocarcinoma via Inhibiting Ataxia Telangiectasia-Mutated Kinase-Mediated DNA Damage Response. *Eur J Cancer* (2018) 102:10–22. doi: 10.1016/j.ejca.2018.07.010

14. Fernandez-Aroca DM, Roche O, Sabater S, Pascual-Serra R, Ortega-Muelas M, Sánchez Pérez I, et al. P53 Pathway is a Major Determinant in the Radiosensitizing Effect of Palbociclib: Implication in Cancer Therapy. *Cancer Lett* (2019) 451:23–33. doi: 10.1016/j.canlet.2019.02.049

15. Gottgens EL, Bussink J, Leszczynska KB, Peters H, Span PN, Hammond EM. Inhibition of CDK4/CDK6 Enhances Radiosensitivity of HPV Negative Head and Neck Squamous Cell Carcinomas. *Int J Radiat Oncol Biol Phys* (2019) 105 (3):548–58. doi: 10.1016/j.ijrobp.2019.06.2531

16. Martin CA, Cullinane C, Kirby L, Abuhammad S, Lelliott EJ, Waldeck K, et al. Palbociclib Synergizes With BRAF and MEK Inhibitors in Treatment Naive Melanoma But Not After the Development of BRAF Inhibitor Resistance. *Int J Cancer* (2018) 142(10):2139–52. doi: 10.1002/ijc.31220

17. Walter L, Heinzerling L. BRAF Inhibitors and Radiation Do Not Act Synergistically to Inhibit WT and V600E BRAF Human Melanoma. *Anticancer Res* (2018) 38(3):1335–41. doi: 10.21873/anticanres.12356

18. Hecht M, Harrer T, Körber V, Sarpong EO, Moser F, Fiebig N, et al. Cytotoxic Effect of Efavirenz in BxPC-3 Pancreatic Cancer Cells is Based on Oxidative Stress and is Synergistic With Ionizing Radiation. *Oncol Lett* (2018) 15 (2):1728–36. doi: 10.3892/ol.2017.7523

19. Colzani M, Waridel P, Laurent J, Faes E, Rüegg C, Quadroni M. Metabolic Labeling and Protein Linearization Technology Allow the Study of Proteins Secreted by Cultured Cells in Serum-Containing Media. *J Proteome Res* (2009) 8(10):4779–88. doi: 10.1021/pr900476b

20. Kramer DK, Bouzakri K, Holmqvist O, Al-Khalili L, Krook A. Effect of Serum Replacement With Plysate on Cell Growth and Metabolismin Primary Cultures of Human Skeletal Muscle. *Cytotechnology* (2005) 48(1-3):89–95. doi: 10.1007/s10616-005-4074-7

21. Mannello F, Tonti GA. Concise Review: No Breakthroughs for Human Mesenchymal and Embryonic Stem Cell Culture: Conditioned Medium, Feeder Layer, or Feeder-Free; Medium With Fetal Calf Serum, Human Serum, or Enriched Plasma; Serum-Free, Serum Replacement

Nonconditioned Medium, or Ad Hoc Formula? All That Glitters is Not Gold! *Stem Cells* (2007) 25(7):1603–9. doi: 10.1634/stemcells.2007-0127

22. de Abreu Costa L, Henrique Fernandes Ottoni M, Dos Santos MG, Meireles AB, Gomes de Almeida V, de Fátima Pereira W, et al. Dimethyl Sulfoxide (DMSO) Decreases Cell Proliferation and TNF-Alpha, IFN-Gamma, and IL-2 Cytokines Production in Cultures of Peripheral Blood Lymphocytes. *Molecules* (2017) 22(11):1789. doi: 10.3390/molecules22111789

23. Dobler C, Jost T, Hecht M, Fietkau R, Distel L. Senescence Induction by Combined Ionizing Radiation and DNA Damage Response Inhibitors in Head and Neck Squamous Cell Carcinoma Cells. *Cells* (2020) 9(9):2012. doi: 10.3390/cells9092012

24. Deloch L, Fuchs J, Rückert M, Fietkau R, Frey B, Gaipl US. Low-Dose Irradiation Differentially Impacts Macrophage Phenotype in Dependence of Fibroblast-Like Synoviocytes and Radiation Dose. *J Immunol Res* (2019) 2019:3161750. doi: 10.1155/2019/3161750

25. Tamura K, Mukai H, Naito Y, Yonemori K, Kodaira M, Tanabe Y, et al. Phase I Study of Palbociclib, a Cyclin-Dependent Kinase 4/6 Inhibitor, in Japanese Patients. *Cancer Sci* (2016) 107(6):755–63. doi: 10.1111/cas.12932

26. Fry DW, Harvey PJ, Keller PR, Elliott WL, Meade M, Trachet E, et al. Specific Inhibition of Cyclin-Dependent Kinase 4/6 by PD 0332991 and Associated Antitumor Activity in Human Tumor Xenografts. *Mol Cancer Ther* (2004) 3 (11):1427–38.

27. Sinclair WK. Cyclic X-Ray Responses in Mammalian Cells In Vitro. *Radiat Res* (1968) 33(3):620–43. doi: 10.2307/3572419

28. Wang TH, Chen CC, Leu YL, Lee YS, Lian JH, Hsieh HL. Palbociclib Induces DNA Damage and Inhibits DNA Repair to Induce Cellular Senescence and Apoptosis in Oral Squamous Cell Carcinoma. *J Formos Med Assoc* (2020) 120 (9):1695–705. doi: 10.1016/j.jfma.2020.12.009

29. Di Micco R, Krizhanovsky V, Baker D, d'Adda di Fagagna F. Cellular Senescence in Ageing: From Mechanisms to Therapeutic Opportunities. *Nat Rev Mol Cell Biol* (2021) 22(2):75–95. doi: 10.1038/s41580-020-00314-w

30. Collado M, Gil J, Efeyan A, Guerra C, Schuhmacher AJ, Barradas M, et al. Tumour Biology: Senescence in Premalignant Tumours. *Nature* (2005) 436 (7051):642. doi: 10.1038/436642a

31. Rodier F, Coppé JP, Patil CK, Hoeijmakers WA, Muñoz DP, Raza SR, et al. Persistent DNA Damage Signalling Triggers Senescence-Associated Inflammatory Cytokine Secretion. *Nat Cell Biol* (2009) 11(8):973–9. doi: 10.1038/ncb1909

32. Michaud K, Solomon DA, Oermann E, Kim JS, Zhong WZ, Prados MD, et al. Pharmacologic Inhibition of Cyclin-Dependent Kinases 4 and 6 Arrests the Growth of Glioblastoma Multiforme Intracranial Xenografts. *Cancer Res* (2010) 70(8):3228–38. doi: 10.1158/0008-5472.CAN-09-4559

33. Sheppard KE, McArthur GA. The Cell-Cycle Regulator CDK4: An Emerging Therapeutic Target in Melanoma. *Clin Cancer Res* (2013) 19(19):5320–8. doi: 10.1158/1078-0432.CCR-13-0259

34. Yao S, Fan LY, Lam EW. The FOXO3-FOXM1 Axis: A Key Cancer Drug Target and a Modulator of Cancer Drug Resistance. *Semin Cancer Biol* (2018) 50:77–89. doi: 10.1016/j.semcancer.2017.11.018

35. Anders L, Ke N, Hydbring P, Choi YJ, Widlund HR, Chick JM, et al. A Systematic Screen for CDK4/6 Substrates Links FOXM1 Phosphorylation to Senescence Suppression in Cancer Cells. *Cancer Cell* (2011) 20(5):620–34. doi: 10.1016/j.ccr.2011.10.001

36. Li Y, Wu F, Tan Q, Guo M, Ma P, Wang X, et al. The Multifaceted Roles of FOXM1 in Pulmonary Disease. *Cell Commun Signal* (2019) 17(1):35. doi: 10.1186/s12964-019-0347-1

37. Harland M. CDKN2A. In: M Schwab, editor. *Encyclopedia of Cancer*. Berlin, Heidelberg: Springer Berlin Heidelberg (2017). p. 858–65.

38. Garutti M, Targato G, Buriolla S, Palmero L, Minisini AM, Puglisi F. CDK4/6 Inhibitors in Melanoma: A Comprehensive Review. *Cells* (2021) 10(6):1334. doi: 10.3390/cells10061334

Publisher's Note: All claims expressed in this article are solely those of the authors and do not necessarily represent those of their affiliated organizations, or those of the publisher, the editors and the reviewers. Any product that may be evaluated in this article, or claim that may be made by its manufacturer, is not guaranteed or endorsed by the publisher.

Advantages of publishing in Frontiers

OPEN ACCESS
Articles are free to read for greatest visibility and readership

FAST PUBLICATION
Around 90 days from submission to decision

HIGH QUALITY PEER-REVIEW
Rigorous, collaborative, and constructive peer-review

TRANSPARENT PEER-REVIEW
Editors and reviewers acknowledged by name on published articles

Frontiers
Avenue du Tribunal-Fédéral 34
1005 Lausanne | Switzerland

Visit us: www.frontiersin.org
Contact us: frontiersin.org/about/contact

REPRODUCIBILITY OF RESEARCH
Support open data and methods to enhance research reproducibility

DIGITAL PUBLISHING
Articles designed for optimal readership across devices

FOLLOW US
@frontiersin

IMPACT METRICS
Advanced article metrics track visibility across digital media

EXTENSIVE PROMOTION
Marketing and promotion of impactful research

LOOP RESEARCH NETWORK
Our network increases your article's readership